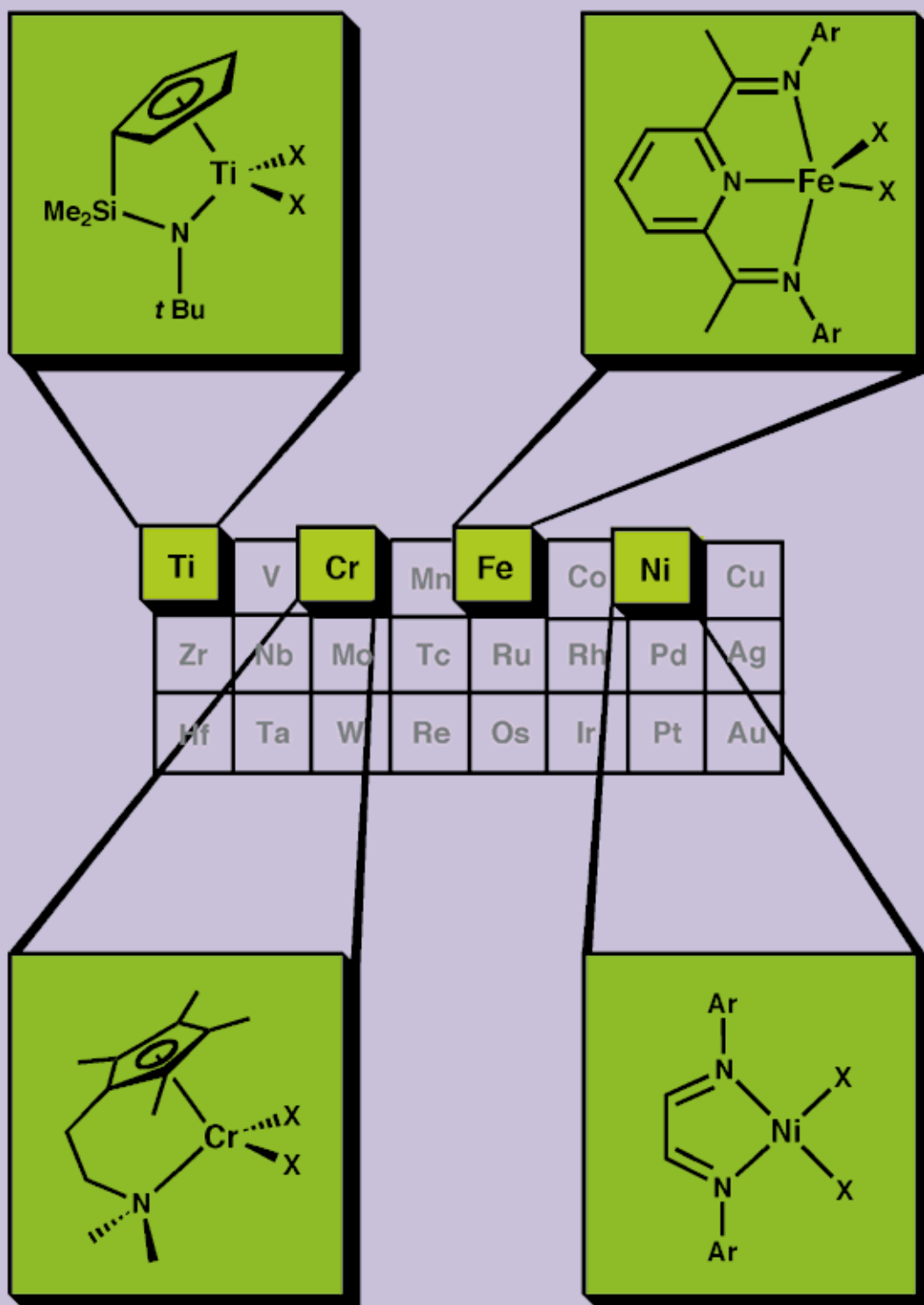


Examples of highly active non-metallocene olefin polymerization catalysts across the transition series



The Search for New-Generation Olefin Polymerization Catalysts: Life beyond Metallocenes

George J. P. Britovsek, Vernon C. Gibson,* and Duncan F. Wass

The introduction of well-defined, single-site organotransition metal olefin polymerization catalysts in the early 1980s highlighted the possibilities for controlling and dramatically improving the properties of commodity polymer products such as polyethylene and polypropylene. Group 4 metallocenes and half-sandwich titanium–amide complexes (constrained-geometry catalysts) have been at the forefront of these developments, and, as we approach the late 1990s, these catalysts are increasingly finding their way into commercial operations. However, it is

generally acknowledged that no single class of catalyst will be capable of controlling all of the macromolecular parameters relevant to a wide and varied range of polyolefinic products. Over the past few years, an intense search has therefore developed, in both academic and industrial research laboratories, for new-generation catalysts. Some of the most significant recent developments have occurred with late transition metal systems. Particularly, the discovery of exceptionally active catalysts based on iron, a metal that had no previous track

record of being applied in this way, has signposted the way for further technologically significant advances in the field. In this review, we highlight the key advances that have occurred in the discovery and development of non-Group 4 metallocene catalysts, amply demonstrating that there are significant signs of life beyond the Group 4 metallocenes.

Keywords: homogeneous catalysis • olefins • polymerizations • transition metals

1. Introduction

1.1. Background

The past 15 years have witnessed tremendous advances in the design and application of organometallic complexes as α -olefin polymerization catalysts; many are now reaching the early stages of commercialization. These developments have grown out of an increased understanding of the factors that are important for stabilizing polymerization-active metal centers and controlling their activity and selectivity, combined with the industrially important discovery that methylalumoxane (MAO) cocatalysts afford highly active and long-lived catalyst systems. To date, Group 4 metallocenes (**A**, Scheme 1) and related catalyst systems such as the half-sandwich amide or constrained-geometry catalysts (**B**) have been at the forefront of these developments.

However, the search for new catalysts would appear to be far from over. Driven by industry's desire to obtain ever



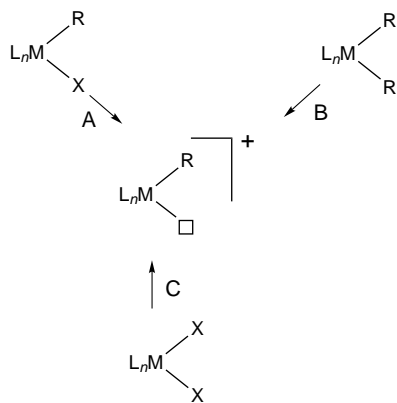
Scheme 1. Group 4 metallocenes (**A**) and constrained-geometry catalysts (**B**).

greater control over the properties of the resultant polymers and to extend the family of products to new monomer combinations, the search is gathering apace for yet new highly active, selective catalyst families that tolerate a variety of functional groups. In this review we shall highlight recent advances in the search for new catalysts, focusing primarily on ligand–metal complex design and catalyst activity rather than the properties of the resultant polymeric materials. A simple classification scheme is outlined that allows ligand–metal combinations for active catalysts to be charted. Variations on Group 4 metallocene catalyst systems will not be discussed in any detail here since they have been reviewed extensively elsewhere.^[1–7]

[*] Prof. Dr. V. C. Gibson, Dr. G. J. P. Britovsek, D. F. Wass
Department of Chemistry
Imperial College of Science, Technology and Medicine
Exhibition Road, South Kensington, London SW7 2AY (UK)
Fax: (+44) 171-5945810
E-mail: v.gibson@ic.ac.uk

1.2. The Active Site

It is generally agreed that the catalytically active species in olefin polymerization is a coordinatively unsaturated cationic alkyl complex $[L_nMR]^+$ that is stabilized by several ligands L (Scheme 2). To generate such species several methods can be employed; three different routes (A, B, and C) are shown in Scheme 2.



Scheme 2. Three different routes to the catalytically active species $[L_nMR]^+$ (see text for details). \square represents the site of coordinative unsaturation.

Route A involves the abstraction of an anionic ligand (e.g. a halide) and its substitution for a “noncoordinating” anion by a salt elimination. Common reagents are

$\text{Na}[\text{B}\{3,5-(\text{CF}_3)_2\text{C}_6\text{H}_3\}_4]^{[8]}$ or silver salts such as AgBF_4 or $\text{AgOSO}_2\text{CF}_3$ (AgOTf) for the later transition metals. Route B involves the abstraction of an alkyl ligand or, more strictly, an alkyl anion. Reagents used for these ligands are, for example, $[\text{Ph}_3\text{C}][\text{B}(\text{C}_6\text{F}_5)_4]$, $[\text{PhNHMe}_2][\text{B}(\text{C}_6\text{F}_5)_4]$, $[\text{H}(\text{OEt}_2)_2][\text{B}\{3,5-(\text{CF}_3)_2\text{C}_6\text{H}_3\}_4]^{[8]}$ or $\text{B}(\text{C}_6\text{F}_5)_3$. Whereas the trityl reagent is an abstracting agent, the anilinium salt and the acid remove the alkyl ligand by protonation. In the case of $\text{B}(\text{C}_6\text{F}_5)_3$ the alkyl ligand is only partly abstracted leading to “cation-like” catalytic species.^[9, 10] The applications of perfluorophenyl-substituted boranes and borates as cocatalysts have been recently reviewed.^[11]

Route C is a combined alkylation and abstraction process, which can be achieved by treating a dihalide procatalyst first with an alkylating species and then with one of the aforementioned alkyl-abstracting agents, for example a trialkylaluminum compound followed by $\text{B}(\text{C}_6\text{F}_5)_3$. Some reagents can perform both processes, for example, alkylaluminum halides and especially alumoxanes such as methylaluminoxane (MAO). Albeit the structure of MAO is still largely unknown, the high activities and long catalyst lifetimes it affords are well documented and still the subject of ongoing study.^[12–15]

Besides these classical activation methods, an alternative strategy for the generation of a catalytic active species has been introduced by Erker et al.^[16] Treatment of a $[\text{Cp}_2\text{Zr}(\text{butadiene})]$ complex (C) with $\text{B}(\text{C}_6\text{F}_5)_3$ results in a metallocene-borate-betaine system (D), which is highly active in olefin polymerization (Scheme 3).^[17, 18] In these systems the cationic and anionic parts are combined within the same molecules, “zwitterionic metallocenes”.^[19]

Vernon C. Gibson, born in 1958 in Grantham, England, studied chemistry at the University of Sheffield before moving to the University of Oxford, where he was awarded a D. Phil. in 1983 for work on the coordination and organometallic chemistry of the early transition metals carried out in the group of M. L. H. Green. He then spent two years as a NATO postdoctoral researcher at the California Institute of Technology with J. E. Bertozzi before returning to England to take up a lectureship in chemistry at Durham University in 1986. He was appointed to a Chair of Chemistry at Durham sponsored by BP Chemicals in 1993. In 1995 he and his group moved to Imperial College, London, where he is Head of the Centre for Catalysis and Advanced Materials.



V. C. Gibson



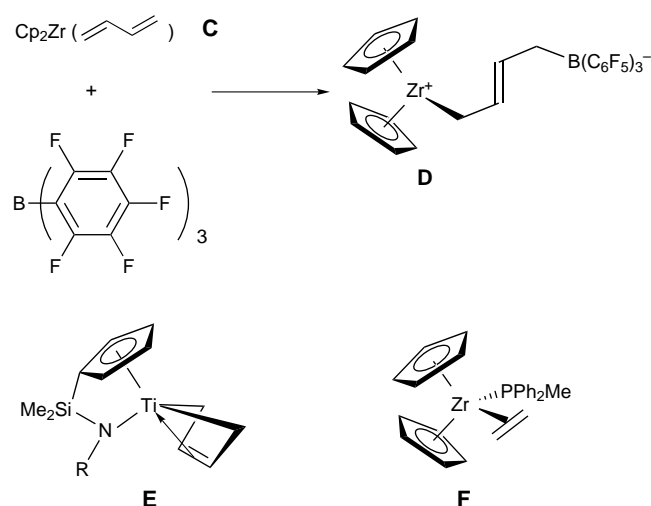
G. J. P. Britovsek



D. F. Wass

George J. P. Britovsek, born in 1966 in Heerlen, The Netherlands, studied chemistry at the Technische Universität Aachen (Germany). In 1993 he earned his doctorate from this university under the direction of W. Keim. He then spent two years as a postdoctoral researcher at the University of Tasmania (Australia) with K. J. Cavell, before joining the group of V. C. Gibson at Imperial College in London in 1996.

Duncan F. Wass was born in Leicester, England, in 1973. After studying chemistry at Durham University, he moved to Imperial College in 1995 where he is working for his Ph.D. under the supervision of V. C. Gibson.



Scheme 3. The zwitterionic approach to active polymerization catalysts.

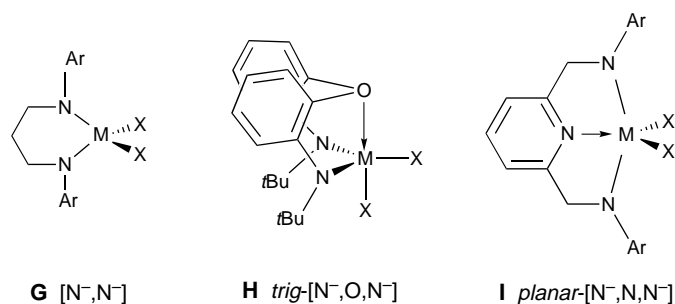
Similarly Devore and co-workers independently demonstrated the same principles for constrained-geometry titanium complexes **E**.^[20] Piers and co-workers have shown recently that simple alkenes, for example coordinated ethylene in $[\text{Cp}_2\text{Zr}^{\text{II}}(\text{C}_2\text{H}_4)(\text{PPh}_2\text{Me})]$ (**F**), also react with $\text{B}(\text{C}_6\text{F}_5)_3$ to form a zwitterionic metallocene capable of initiating olefin polymerization.^[21]

In this review, except for those cases where well-defined catalysts are reported, we have not considered in any detail the method of activation employed. By far the most common approach has been activation of a dialkyl or dihalide precursor with MAO. In these cases the alkyl or halide group are referred to as a generic group X.

1.3. Ligands

The attendant ligands in polymerization-active metal complexes have four important roles: 1) control over the metal coordination number, 2) control over the metal coordination geometry, 3) control over the formal oxidation state of the metal, and 4) steric protection of the active site and influence over (stereo)selectivity. To assist the reader in categorizing polymerization-active metal–ligand combinations and thereby illuminate possible ways forward for future catalyst design, we have used a simple classification system that allows the ligands to be categorized according to the number and nature of the donor atoms and also the ligand charge, including an indication of which metal-attached ligand atoms bear the formal charge.

By way of example, consider the series of active zirconium procatalysts **G–I** (Scheme 4). The choice of chelating dianionic diamide ligands allows zirconium(IV) dichloro fragments to be stabilized either in a pseudo-tetrahedral environment for **G** or in distorted trigonal-bipyramidal environments for **H** and **I**. Moreover, the choice of an ether or pyridyl bridge influences the relative dispositions of the metal-attached atoms. In the case of **H** there is a trigonal arrangement of the N,O,N atoms of the ligand with the oxygen occupying the axial



Scheme 4. Examples of zirconium(IV) procatalysts to illustrate the ligand classifications.

site of the trigonal bipyramid, while in the case of **I** the N,N,N tridentate chelating ligand binds in a planar arrangement, thereby leaving the chloro ligands to occupy the equatorial sites of the trigonal bipyramid. The ligands present in **G**, **H**, and **I** may be represented as $[\text{N}^-, \text{N}^-]$, $\text{trig}[\text{N}^-, \text{O}, \text{N}^-]$, and $\text{planar}[\text{N}^-, \text{N}, \text{N}^-]$, respectively. A description of this kind will be found adjacent to the pictorial representations of the procatalysts under discussion here, but will not be elaborated upon.

1.4. Catalyst Activities

The main focus of this review is catalyst performance for ethylene polymerization, though reference to other α -olefins is included wherever they have been reported. A “health warning” has to be applied when comparing catalyst activities reported by different groups of researchers, since experimentally determined values are highly dependent upon the precise reaction conditions, including stirring rate and the configuration of the reactor. Also, often little or no information is given about the kinetic profile or lifetime of the catalyst, with the consequence that a short polymerization run with a catalyst that is active only for 30 seconds before dying may give an “inflated” figure of merit compared to an activity reported for a one-hour run. Information about the catalyst’s kinetic profile is very useful in allowing the most appropriate operating conditions to be chosen. For example, solution-phase catalysts generally require shorter reactor residence times than for a supported gas-phase catalyst.

To give the reader some feeling for how active a particular catalyst is compared to other systems, we have converted the activity figures available in the literature to units of $\text{g mmol}^{-1} \text{h}^{-1} \text{bar}^{-1}$ and placed the catalyst on a scale of merit ranging from very low to very high, as shown in Table 1.

Table 1. Rating of the effectiveness of a catalyst based on its activity.

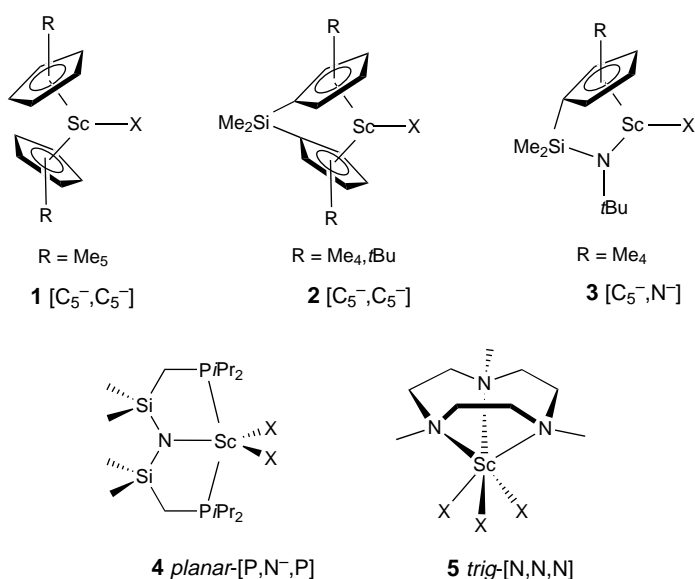
Rating	Activity [$\text{g mmol}^{-1} \text{h}^{-1} \text{bar}^{-1}$]
very low	< 1
low	1–10
moderate	10–100
high	100–1000
very high	> 1000

2. Catalysts with Group 3 and Rare Earth Metals

2.1. Group 3 Metal Catalysts

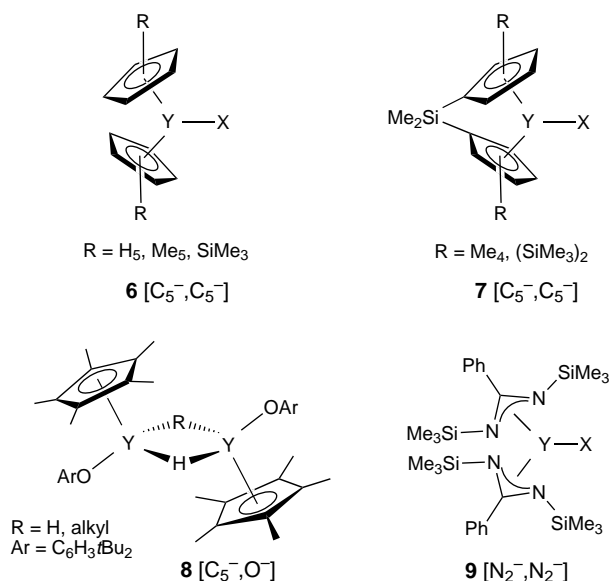
Neutral Group 3 alkyl complexes of scandium and yttrium are isoelectronic with Group 4 cationic alkyl complexes; compare, for example, $[\text{Cp}_2\text{ScR}]$ and $[\text{Cp}_2\text{ZrR}]^+$. This analogy has been used in the design of Group 3 olefin polymerization catalysts, as exemplified by the complexes shown in Schemes 5 and 6.

A potentially significant advantage of Group 3 catalysts is that they are single-component catalysts; no cocatalyst is needed. Commonly the neutral alkyl complexes, $[\text{L}_2\text{MR}]_2$, are dimeric in the solid state and in solution, and react with H_2 under mild conditions to yield the corresponding hydrides, $[\text{L}_2\text{MH}]_2$. Monomeric complexes have been obtained through the use of very bulky ligands or the addition of a donor ligand. The general low olefin polymerization activity of scandium complexes such as **1–3** (Scheme 5) has enabled detailed mechanistic investigations of the polymerization process.^[22–26] Mono(pentamethylcyclopentadienyl)alkoxy scandium compounds have not shown any polymerization activity, probably due to the formation of an oxygen-bridged complex;^[27] this is in contrast to observations made for analogous yttrium complexes (see below).^[28] An anionic scandium complex with a dianionic dicarbollide ligand was found to be remarkably unreactive towards ethylene,^[29] similar to the analogous neutral Group 4 titanium complex.^[30] Most of the ligand systems used in Group 3 catalysts have followed from ligands that have been shown to be successful for Group 4 systems, although the Group 3 metals are generally much less well explored. Recently, scandium procatalysts containing tridentate ligands have been described, one containing a monoanionic *planar*-[P,N[−],P] amide-diphosphane ligand (**4**), the other a neutral *trig*-[N,N,N] triazacyclononane ligand (**5**). Both are capable of polymerizing ethylene, though no activity figures were given.^[31, 32]



Scheme 5. Scandium complexes used as olefin polymerization catalysts.

Ligand design for organoyttrium olefin polymerization catalysts has also been following the trends of Group 4 catalysts (Scheme 6). Bis(cyclopentadienyl) complexes **6** have been the first reported to show moderate activity as

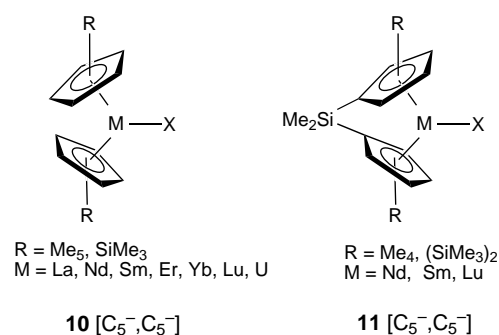


Scheme 6. Yttrium complexes used as olefin polymerization catalysts.

ethylene polymerization catalysts ($42 \text{ g mmol}^{-1} \text{ h}^{-1} \text{ bar}^{-1}$).^[33] ansa-Metallocene analogues **7** have been investigated by the groups of both Bercaw and Yasuda, the latter has reported high activities for the polymerization of ethylene ($584 \text{ g mmol}^{-1} \text{ h}^{-1} \text{ bar}^{-1}$).^[34–37] The reaction of hydrioyttrium complexes bearing bulky aryloxy ligands with ethylene has been reported to lead to the rapid formation of polyethylene. No quantitative data has been given, but valuable mechanistic information has been obtained from the reaction of the bridged hydride initiator **8** with olefins.^[28, 38, 39] Benzamidinate ligands (**9**) have been employed by Teuben and co-workers which have shown only very low ethylene polymerization activity.^[40, 41]

2.2. Rare Earth Metal Catalysts

Lanthanide- and actinide-based olefin polymerization catalysts (**10**, Scheme 7) have invariably been stabilized with substituted cyclopentadienyl ligands. The first reports on the application of organometallic complexes of rare earth metals in ethylene polymerization appeared in 1978. Ballard and co-workers at ICI reported moderate catalytic activities at 100°C ($82 \text{ g mmol}^{-1} \text{ h}^{-1} \text{ bar}^{-1}$) using an alkyl metallocene complex of erbium,^[33] and Marks et al. described bis(pentamethylcyclopentadienyl)uranium monochloride as a potent catalyst for ethylene polymerization.^[42] Mechanistic studies of the reversible insertion of propene into the Lu–H bond of $[(\text{C}_5\text{Me}_5)_2\text{LuH}]_2$ with subsequent competitive $\beta\text{-H}$ and $\beta\text{-Me}$ elimination were reported a few years later by Watson and co-workers at DuPont. They have also shown that alkyl metallocene complexes of lutetium are ethylene



Scheme 7. Lanthanide and actinide metallocenes investigated as olefin polymerization catalysts.

polymerization catalysts with moderate activity (66 gmmol^{−1} h^{−1} bar^{−1}).^[43–45] Studies by Schumann, Marks, and co-workers on hydride metallocene and ansa-metallocene complexes of lanthanum, neodymium, samarium, and lutetium (**11**) have shown remarkably high activities (146 400 gmmol^{−1} h^{−1} bar^{−1} for lanthanum). However, these figures are only initial activities, as polymerizations have been run only for a very short time (typically five seconds).^[46–48] The corresponding alkyl metallocene complexes (X = CH(SiMe₃)₂) of La, Nd, and Lu are reported to be inactive towards ethylene at room temperature.^[48] In contrast, alkyl metallocene complexes (X = CH(SiMe₃)₂) of samarium have shown moderate activities,^[37, 49] and the Nd complex has been reported to be a “good” catalyst at higher temperatures (160 °C).^[50]

3. Group 4 Metal Catalysts

In the search for new non-metallocene olefin polymerization catalysts, the vast majority of recent research effort has been directed towards the synthesis of alternative Group 4 catalysts. The wide variety of procatalysts that has been investigated necessitates a more systematic treatment of the differing ligand types. In Section 3.1 procatalysts of the type [L_nMX₂] which, when activated, give rise to cationic alkyl active sites [L_nMR]⁺ are described. This section is further divided according to carbon-, nitrogen-, and oxygen-based ligand types. Section 3.2 outlines applications of dianionic ligands ((L²)^{2−}) to generate neutral 14-electron complexes [L¹L²MR] (where L¹ is typically a monoanionic Cp ligand) as the active centers.

3.1. Cationic Group 4 Metal Complexes

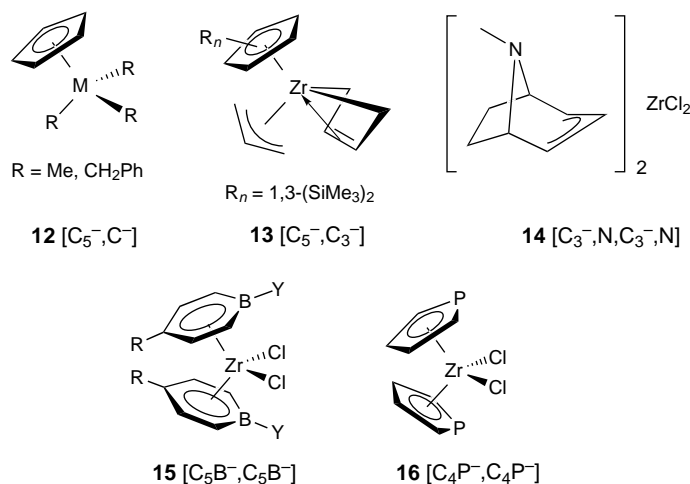
3.1.1. Carbon-Based Ligands

3.1.1.1. Alkyl Ligands [C[−]]

Simple homoleptic σ-hydrocarbyl complexes of Group 4 transition metals, for example [Ti(CH₂C₆H₅)₄] or [Zr(CH₂C₆H₅)₄], have produced active ethylene polymerization catalysts when activated with suitable Lewis acids such as MAO, [Me₂NHPh][B(C₆F₅)₄], [Ph₃C][B(C₆F₅)₄], or

B(C₆F₅)₃.^[51–54] Only moderate activities are obtained with these systems.

For monocyclopentadienyl trialkyl complexes **12** (Scheme 8), where the catalyst [Cp*TiMe₂]⁺ (Cp* = C₅Me₅) contains a ligand system that is a combination of a Cp ligand and an alkyl ligand [C[−], C₅[−]], moderate activities have been



Scheme 8. Group 4 procatalysts with alkyl [C[−]], allyl [C₃[−]], and modified Cp [C_nX[−]] ligands.

reported, both by Baird et al. (46 gmmol^{−1} h^{−1} bar^{−1})^[55–57] and by Zambelli et al. (80 gmmol^{−1} h^{−1} bar^{−1}).^[52, 58] Ethylene polymerization results obtained by Bochmann et al. have shown that the order of activity is [Cp₂ZrR]⁺ > [CpZrR₂]⁺ > [ZrR₃]⁺.^[53] One Cp–aryl combination, where aryl = C₆F₅, has been reported by Baird and co-workers to give moderate activity for ethylene polymerization (16 gmmol^{−1} h^{−1} bar^{−1}).^[57]

3.1.1.2. Allyl Ligands [C₃[−]]

Compared to alkyl ligands (two-electron donor) and a cyclopentadienyl ligand (six-electron donor) the intermediate allyl ligands (four-electron donor) have received little attention as spectator ligands in olefin polymerization catalysis. This may be due to the intrinsic higher reactivity of the allyl ligand compared to the cyclopentadienyl ligand. One report has described the use of a [Cp(allyl)Zr(dienyl)] complex (**13**, Scheme 8) which can be activated with B(C₆F₅)₃ (the method described by Erker et al.^[16]) to a zwitterionic diallyl zirconium complex. Moderate polymerization activities are observed for this system (98 gmmol^{−1} h^{−1} bar^{−1}), but the broad molecular weight distributions suggest the loss of active site uniformity.^[59] Bergman and Lavoie have shown recently that allyl ligands with an additional donor [C₃[−], N] are suitable ligand systems to generate zirconium complexes **14** with moderate ethylene polymerization activity (17 gmmol^{−1} h^{−1} bar^{−1}).^[60]

3.1.1.3. Cp Analogues [C₅X[−]] and [C₄X[−]]

One modification of a Cp ligand is formally obtained by the insertion of a BY unit into the Cp ring, resulting in a

boratabenzene [C_5B^-] ligand. Zirconium complexes using boratabenzene ligands **15** (Scheme 8) have been reported by Bazan et al., and high polymerization activities are observed ($105 \text{ g mmol}^{-1} \text{ h}^{-1} \text{ bar}^{-1}$) when it is used in combination with MAO.^[61, 62] Interestingly, changing the Y substituent on boron from diisopropylamine to phenyl or ethoxide increases the rate of β -elimination, which results in the formation of lower molecular weight oligomers instead of polymer.^[63] In combination with a constrained-geometry titanium catalyst, branched polyethylene has been produced.^[64]

Another Cp analogue is obtained by the substitution of a CH unit for a P atom, resulting in phosphacyclopentadienyl ligands [C_4P^-] (**16**, Scheme 8), which have been investigated by a number of research groups.^[65–68] These catalysts generally afford very high activities, comparable to that of zirconocene dichloride.

3.1.2. Nitrogen-Based Ligands

3.1.2.1. Amide Ligands [N^-]

During the past ten years it has emerged that Group 4 metal complexes containing amide ligands are promising systems for applications in olefin polymerization catalysis. A formal lower electron count ($[(R_2N)_2ZrR]^+$ is a 10-electron species; compared with 14-electrons for $[Cp_2ZrR^+]$) is likely to result in a more electrophilic and therefore potentially more active catalyst fragment.

A few reports on the use of monodentate amide ligands have appeared, featuring either trimethylsilyl or bulky aryl substituents on nitrogen.^[69, 70] Moderate activities ($13 \text{ g mmol}^{-1} \text{ h}^{-1} \text{ bar}^{-1}$) are reported for zirconium complex **17** (Scheme 9) using MAO as a cocatalyst. In contrast, bis(amido) complexes containing a bidentate [N^-, N^-] ligand system have received quite a lot of attention during the past two years. The different catalyst precursors are shown in Scheme 9.

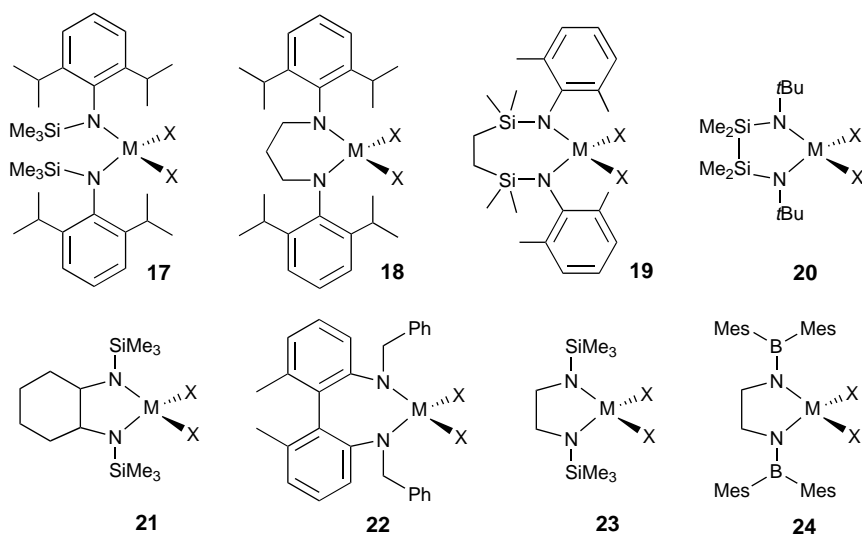
Olefin polymerization activities obtained with these complexes vary significantly and decrease in the order from **18** to

24. Activities are very low to low in the case of complexes **23**^[73] and **24**.^[71, 72] Moderate activity ($13 \text{ g mmol}^{-1} \text{ h}^{-1} \text{ bar}^{-1}$) is observed with the biphenyl derivative **22** investigated by Cloke et al.^[74] Zirconium compounds of type **21** have shown moderate activities ($50 \text{ g mmol}^{-1} \text{ h}^{-1} \text{ bar}^{-1}$);^[75] no polymerization activity data has been given for the titanium analogue.^[76] Complex **20**, containing a silicon backbone, was found to be considerably more active ($100 \text{ g mmol}^{-1} \text{ h}^{-1} \text{ bar}^{-1}$) than its carbon backbone analogue **23**. A lowering of the electron density on the metal center and an overall stabilizing effect are believed to be the reasons for this “silicon effect”.^[77] For the diamide system **18**, developed by McConville and co-workers, no activity data on ethylene polymerization is disclosed, but α -olefin polymerization results indicate very high activity.^[78–81] For the titanium complexes, living polymerization of 1-hexene has been reported.^[79] The silicon-bridged diamide complexes **19** developed in our laboratory also form highly active ethylene polymerization catalysts ($990 \text{ g mmol}^{-1} \text{ h}^{-1} \text{ bar}^{-1}$). Polymerization activity and kinetic profile are dramatically influenced by the chelate ring size.^[82] Both systems contain bulky aryl substituents on the nitrogen donors which probably provide steric protection to avoid attack of the cocatalyst (MAO) on the amide ligand. Such an attack may cause catalyst deactivation either by complete loss of the ligand, as observed by Eisen and Mack,^[83] or by intramolecular C–H activation; as observed by Horton and de With.^[84] In both cases the resulting complexes still give an active catalytic system, but for reasons other than those intended.

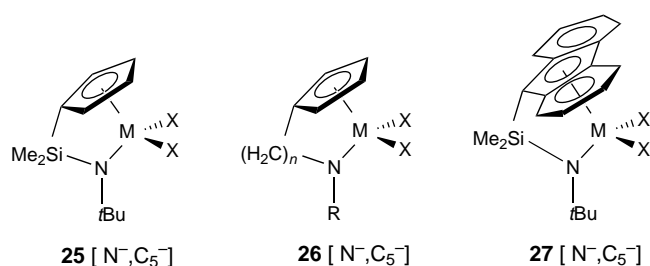
3.1.2.2. Combinations of an Amide Ligand with Other Ligands

With Cp Ligands [N^-, C_5^-]

An important class of olefin polymerization catalysts has been developed at Dow and Exxon, by combining Cp ligands with an amide functionality [N^-, C_5^-] to form a hybrid “half-metallocene”, the “constrained-geometry catalysts” (CGC; **25**, Scheme 10).^[70, 85, 86] These catalyst systems are highly active ($1500 \text{ g mmol}^{-1} \text{ h}^{-1} \text{ bar}^{-1}$) and are under development for commercial exploitation. The titanium complex **25** ($M = \text{Ti}$, $X = \text{benzyl}$), when activated with MAO, gives good incorporation of 1-hexene comonomer.^[86] More recently, variations on this theme have been reported in the academic literature. Teuben et al. and Green and co-workers have used a carbon linkage instead of silicon (**26**),^[87–89] and Okuda et al. have investigated a series of different Cp analogues (**27**).^[90] The copolymerization of ethylene and styrene has also been reported.^[91] Like metallocenes, these constrained-geometry catalysts have been the subject of several theoretical studies.^[92–95]



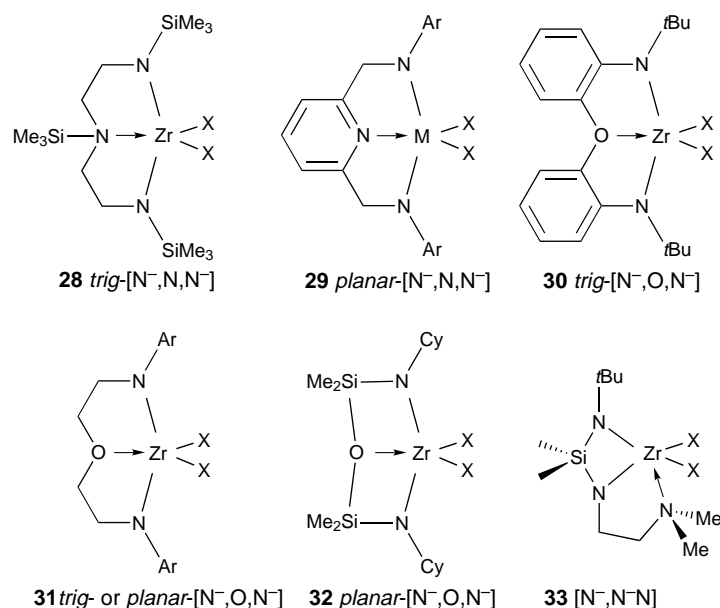
Scheme 9. Group 4 procatalysts containing diamide [N^-, N^-] ligands. Mes = 2,4,6-trimethylphenyl.



Scheme 10. Group 4 procatalysts with half-sandwich amide [N^-, C_5^-] ligands.

With Additional Donors [N^-, Y, N^-]

Three different systems have been reported to date of a Group 4 bis(amido) complex with an additional donor Y —that is, an amine, pyridyl, or ether donor—incorporated in the ligand system. The ligand systems *trig*-[N^-, N, N^-] (complex **28**, Scheme 11) developed by Horton et al.^[96] and *planar*-[N^-, O, N^-] (complex **32**) developed by Bochmann and co-workers^[75] have given moderate activities in the polymerization of ethylene (46 and 40 gmmol⁻¹ h⁻¹ bar⁻¹ respectively). The ethylene-bridged [N^-, O, N^-] system **31** has been shown to adopt both planar coordination (for $X = \text{Me}$) as well as the trigonal coordination mode (for $X = \text{benzyl}$); no details of ethylene polymerization have been given.^[97] The analogous aryl-bridged ligand *trig*-[N^-, O, N^-] (**30**) has shown moderate activities (100 gmmol⁻¹ h⁻¹ bar⁻¹).^[98] Interestingly, an additional pyridyl donor between the amide groups (**29**) affords very high activities (1500 gmmol⁻¹ h⁻¹ bar⁻¹),^[99] in contrast, the titanium analogue has shown only very low activities for the polymerization of ethylene, possibly due to reduction to titanium(III).^[100] Again bulky aryl substituents feature in this system, as in the [N^-, N^-] bis(amido) complexes (Scheme 9). A recent example of a zirconium complex containing a [N^-, N^-, N] type ligand (**33**), synthesised by Schrock and co-

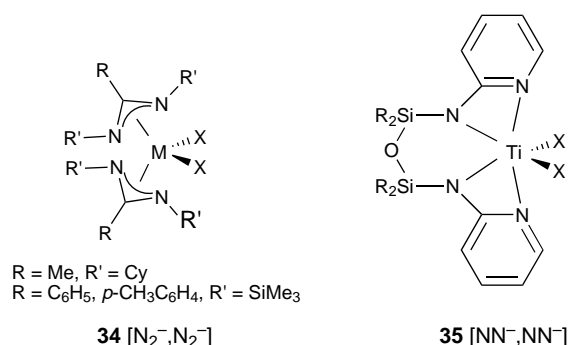


Scheme 11. Group 4 complexes with diamide ligands that contain an additional donor (the ligand connectivity only is depicted). Cy = cyclohexyl.

workers, has been shown to be inactive in the polymerization of 1-hexene,^[101] leading to the conclusion that the donor group should ideally be positioned between the amido functionalities.

3.1.2.3. Amidinate Ligands [N_2^-]

An amidinate ligand, a monoanionic six-electron ligand, can formally be regarded as a combination of an amido and an imine donor. Only a few examples have been studied, either with a methyl substituent in the backbone and cyclohexyl groups at nitrogen^[102] or with a phenyl or *p*-tolyl (*p*-CH₃C₆H₄) group in the backbone and SiMe₃ groups at nitrogen (**34**, Scheme 12).^[103–106] Thus far only moderate activities have



Scheme 12. Group 4 bis(amidinate) procatalysts.

been obtained. Polymerization of styrene with these complexes has also been reported.^[107] The imine moiety of the amidinate ligand can also be part of an aromatic system, for example a pyridine or pyrimidine ligand, giving aminopyridinato ligands (**35**). The complexes containing these ligands, however, have shown only low activity.^[108]

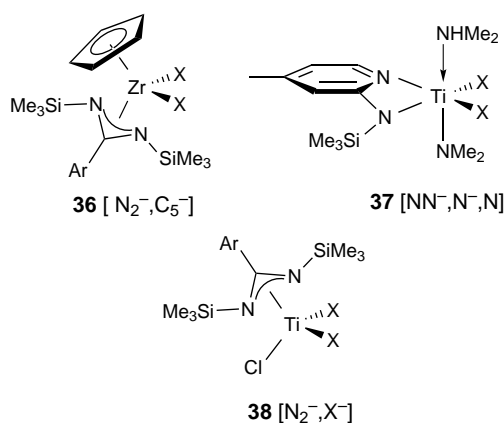
3.1.2.4. Combinations of an Amidinate Ligand with Other Ligands

With Cp Ligands [N_2^-, C_5^-]

Electronically related to the constrained-geometry catalysts—that is, a combination of a Cp and an amide ligand—combinations of Cp with amidinate ligands (**36**, Scheme 13) have been explored by Green, Teuben, and co-workers. Moderate activities have been obtained, using either the dihalide precursor in combination with MAO^[109, 110] or the dimethyl precursor with B(C₆F₅)₃.^[111]

With Amide Ligands [N_2^-, N^-]

One report by Kempe et al. appeared in 1996 on the combined use of an amidinate-type ligand (aminopyridinato ligand) and an amide ligand in titanium and zirconium complexes (e.g. **37**, Scheme 13). No ethylene polymerization data has been reported, but polymerization results for propene and 1-butene show remarkably high activities.^[112]



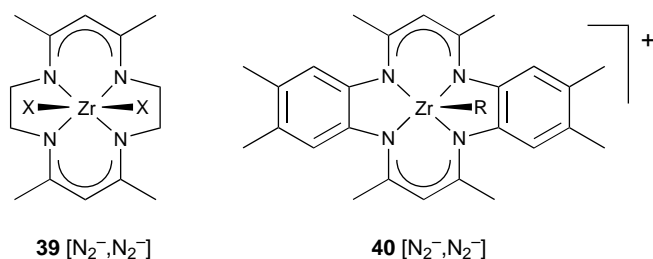
Scheme 13. Group 4 mono(amidinate) complexes with other ancillary ligands.

With Halide Ligands [N_2^-, X^-]

Monoamidinate trihalide complexes (**38**, Scheme 13) can be viewed as containing a combination of an amidinate ligand and a halide ligand, in analogy to monocyclopentadienyl trihalide complexes. Titanium complexes of this type have shown moderate activity ($80 \text{ gmmol}^{-1} \text{ h}^{-1} \text{ bar}^{-1}$),^[113] whereas the analogous zirconium complexes are reported to give only very low activity as ethylene polymerization catalysts.^[104]

3.1.2.5. β -Diketimate Ligands [N_2^-]

In 1993 Jordan and co-workers reported the synthesis of cationic d^0 Group 4 metal alkyl complexes incorporating tetraaza macrocyclic ligands and their application as olefin polymerization catalysts.^[114] These β -diketimates can be regarded as higher homologues of amidinate ligands, as depicted in Scheme 14. The corresponding Zr complexes **39** are about 30 times less active than $[Cp_2ZrCl_2]$, thereby falling in the category of moderately active catalysts. Well-defined cationic complexes of type **40** have been reported recently, which exhibited only very low activity for the polymerization of ethylene.^[115]



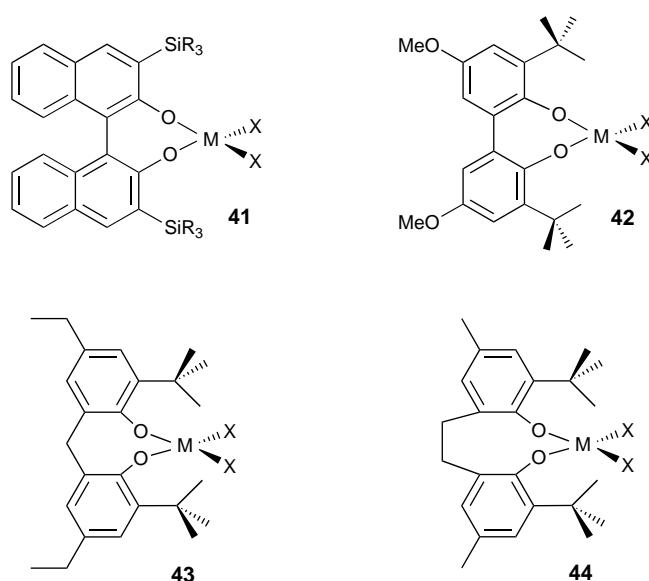
Scheme 14. Group 4 precatalysts with bis(diketimate) ligands.

Porphyrins have also been used as ancillary ligands to support zirconium- and hafnium-alkyl complexes.^[116] However, these complexes proved unreactive towards ethylene.

3.1.3. Oxygen-Based Ligands

3.1.3.1. Alkoxide Ligands [O^-]

Terminal oxygen donors such as phenoxide ligands have been used successfully in olefin polymerization catalysis. In 1995 Schaverien et al. presented a study using various sterically hindered chelating phenoxide complexes of titanium and zirconium as olefin polymerization catalysts.^[117] Ethylene polymerization tests with complexes **41** or **42** (Scheme 15) have shown only moderate activities, whereas complex **43**, with a methylene bridge, has given higher activity ($130 \text{ gmmol}^{-1} \text{ h}^{-1} \text{ bar}^{-1}$). Okuda et al. have used ethylene-bridged bis(alkoxide) complexes **44** successfully in the copolymerization of ethylene with styrene, but no homopolymerization results have been reported.^[118, 119] Theoretical calculations on these systems have been performed by Morokuma and co-workers.^[120]

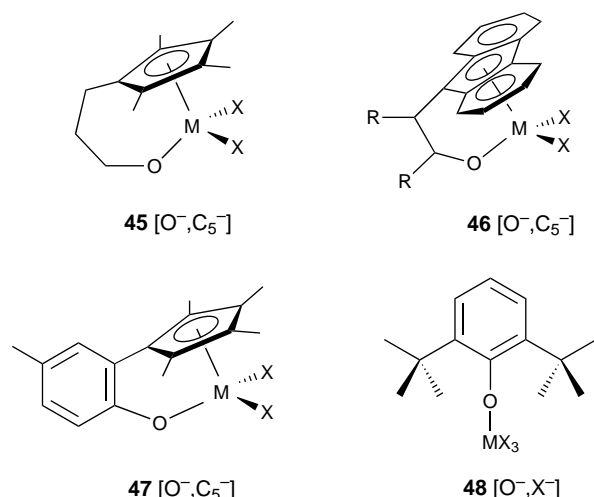


Scheme 15. Group 4 metal complexes bearing bidentate alkoxide [O^-, O^-] ligands.

3.1.3.2. Combinations of Alkoxides and Other Ligands

With Cp Ligands [O^-, C_5^-]

Though various reports on the synthesis of Group 4 metal complexes using Cp-alkoxide ligands [O^-, C_5^-] have appeared, only a few applications as olefin polymerization catalysts have been mentioned (Scheme 16). Hessen and co-workers have reported on the polymerization of propylene using well-defined Cp-alkoxide titanium complexes (**45**).^[121] Rieger has shown that a fluorenyl alkoxide zirconium dichloride complex (**46**) can be activated with MAO to give an active olefin polymerization catalyst.^[122] Marks et al. have shown that the combination of a Cp ligand and an aryloxy ligand (**47**) leads to a highly active polymerization catalyst for ethylene ($2100 \text{ gmmol}^{-1} \text{ h}^{-1} \text{ bar}^{-1}$), propylene, and also styrene.^[123] Furthermore, Baird et al. have reported on successful efforts utilizing monoalkoxide-Cp complexes as olefin polymerization catalysts, though no details have been given.^[124]



Scheme 16. Group 4 procatalysts with an alkoxide ligand and another ancillary ligand.

With Halide Ligands $[O^-, X^-]$

Another system worth mentioning in this context is a monoalkoxide titanium complex (**48**, Scheme 16) as an olefin polymerization catalyst. This complex can be regarded as a combination of an alkoxide and a halide ligand, $[O^-, X^-]$. The catalytic activity of this complex was studied for the copolymerization of ethylene and styrene. However, a mixture of polyethylene and polystyrene and not a copolymer was obtained.^[125]

3.1.3.3. Bis(alkoxides) with Additional Donors

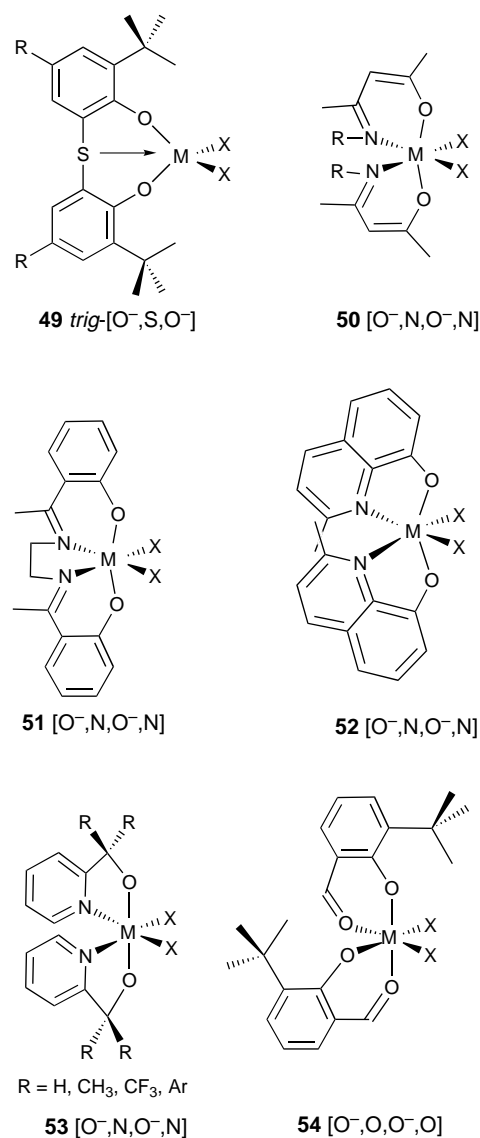
Monoanionic alkoxide ligands, being isonumeral^[126] and isolobal with Cp^- , can bind to a metal using one σ and two π orbitals. They can potentially donate up to six electrons to the metal center, which would result in a cationic 14-electron species $[L_2MR]^+$. However, due to the higher electronegativity of oxygen, the alkoxide moiety is normally regarded as a four-electron ligand. This leaves the opportunity to add additional donors to generate a cationic 14-electron species.

Bis(alkoxides) with One Additional Donor $[O^-, Y, O^-]$

It has been shown in several reports that the activity of bis(alkoxide) Group 4 metal catalysts is dramatically improved by having an additional donor in the ligand backbone (Scheme 17). First reports appeared in 1989 by Kakugo et al. on a chelating phenoxide titanium complex (**49**).^[127, 128] Further work by Schaverien et al.^[117] and Okuda et al. have shown the importance of the additional intramolecular sulfur donor for high catalytic activity.^[118, 129] Although the sulfur–titanium interaction is weak, it is likely to be of importance in stabilizing the active cationic species.^[130]

Bis(alkoxides) with Two Additional Donors $[O^-, Y, O^-, Y]$

The application of N,O chelating ligands in Group 4 olefin polymerization catalysts has been studied by Jordan et al. Acen-type ligands (**50**, Scheme 17) were first investigated, but showed only moderate activity, probably due to the planar



Scheme 17. Group 4 procatalysts that contain alkoxide ligands with other donors.

coordination geometry often observed for these ligands.^[131, 132] Cavell et al. have shown that these compounds can also act as highly active oligomerization catalysts.^[133] Salen-type complexes (**51**), which fall in this category, have given high activities ($600 \text{ g mmol}^{-1} \text{ h}^{-1} \text{ bar}^{-1}$, supported on SiO_2).^[134]

Alkoxide ligands with a different nitrogen donor, for example pyridine (**52**, **53**), have been investigated by Jordan et al. In the case of **53**, for $R = \text{CF}_3$ moderate activities are reported ($56 \text{ g mmol}^{-1} \text{ h}^{-1} \text{ bar}^{-1}$), whereas the complex with $R = \text{CH}_3$ shows no activity.^[135, 136] It is noteworthy that for $R = p\text{-tert-butylphenyl}$ the activity is significantly increased ($280 \text{ g mmol}^{-1} \text{ h}^{-1} \text{ bar}^{-1}$).^[137]

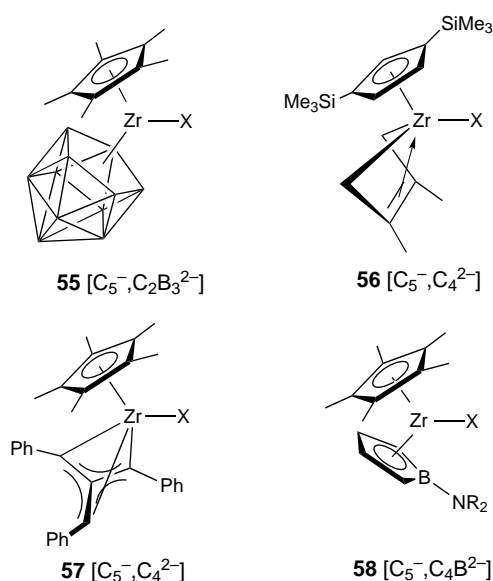
Finally, the use of additional oxygen donors (**54**) has been investigated by Matilainen and co-workers. In the presence of MAO, high catalytic activity is reported ($400 \text{ g mmol}^{-1} \text{ h}^{-1} \text{ bar}^{-1}$), affording high molecular weight polyethylene with a broad molecular weight distribution.^[138]

3.1.4. Halide Ligands [X⁻]

The use of simple halide ligands, as in ZrCl₄, together with a cocatalyst goes back to the early discoveries by Ziegler. Combinations of halides X⁻ with other ligands have been discussed above, except for the combination with Cp ligands, [X⁻, C₅⁻]. Monocyclopentadienyl titanium trichloride in combination with alkylaluminum cocatalysts is virtually inactive in olefin polymerization because of a fast reduction of the titanium center. Cyclopentadienyl ligands with pendant donors, for example amines, have shown increased stability and polymerization activity.^[139] [CpZrCl₃] gives moderate ethylene polymerization activities.^[140]

3.2. Neutral Group 4 Metal Complexes

The formal replacement of a monoanionic Cp⁻ ligand in [Cp₂MR]⁺ by isolobal, dianionic ligands reduces the overall charge by one unit, but leaves the gross structural and metal frontier orbital properties unchanged. Several dianionic ligands have been synthesized and converted into the corresponding monocyclopentadienyl zirconium complexes (Scheme 18). The complexes where X = Cl are commonly isolated as LiCl adducts, whereas the monoalkyl derivatives (X = alkyl) are stabilized by coordinated solvent.



Scheme 18. Group 4 procatalysts containing one dianionic ligand.

Interestingly, these neutral catalysts offer an attractive alternative to metallocene catalysts as no cocatalyst should be needed. However, it has been proposed that the neutral charge on the active species may facilitate β-H elimination by weakening the M–C bond.^[30] Moderate activity (70 g mmol⁻¹ h⁻¹ bar⁻¹) has been reported for the Cp–carborane zirconium complex **55**,^[141] whereas the analogous titanium complex slowly dimerizes ethylene to butene.^[30] The Cp–diene complex **56** reported by Bochmann and co-workers has given slightly higher activities (120 g mmol⁻¹ h⁻¹ bar⁻¹).^[142] Analysis of the oligomers produced by a Cp–dienyl complex

has shown that these catalysts behave as living polymerization catalysts.^[143] Trimethylenemethane-based catalysts (**57**) described by Bazan and Rodriguez^[144, 145] have shown high activities (400 g mmol⁻¹ h⁻¹ bar⁻¹). For the borollide complex **58** no quantitative data on the polymerization have been reported.^[146]

4. Group 5 Metal Catalysts

The most common approach to the design of Group 5 catalysts has been to exploit relationships between the monoanionic Cp ligand and isolobal dianionic fragments, similar to the approach outlined for neutral Group 4 catalysts in the previous section. Substitution of one Cp ligand from a Group 4 metallocene for an isolobal dianionic ligand and replacement of the metal by one from Group 5 gives access to high-valent 14-electron cationic alkyl species that may be expected to have metallocene-like reactivity. Complexes supported by a variety of such dianionic ligands have been investigated, although activities are generally disappointing compared to their Group 4 analogues.

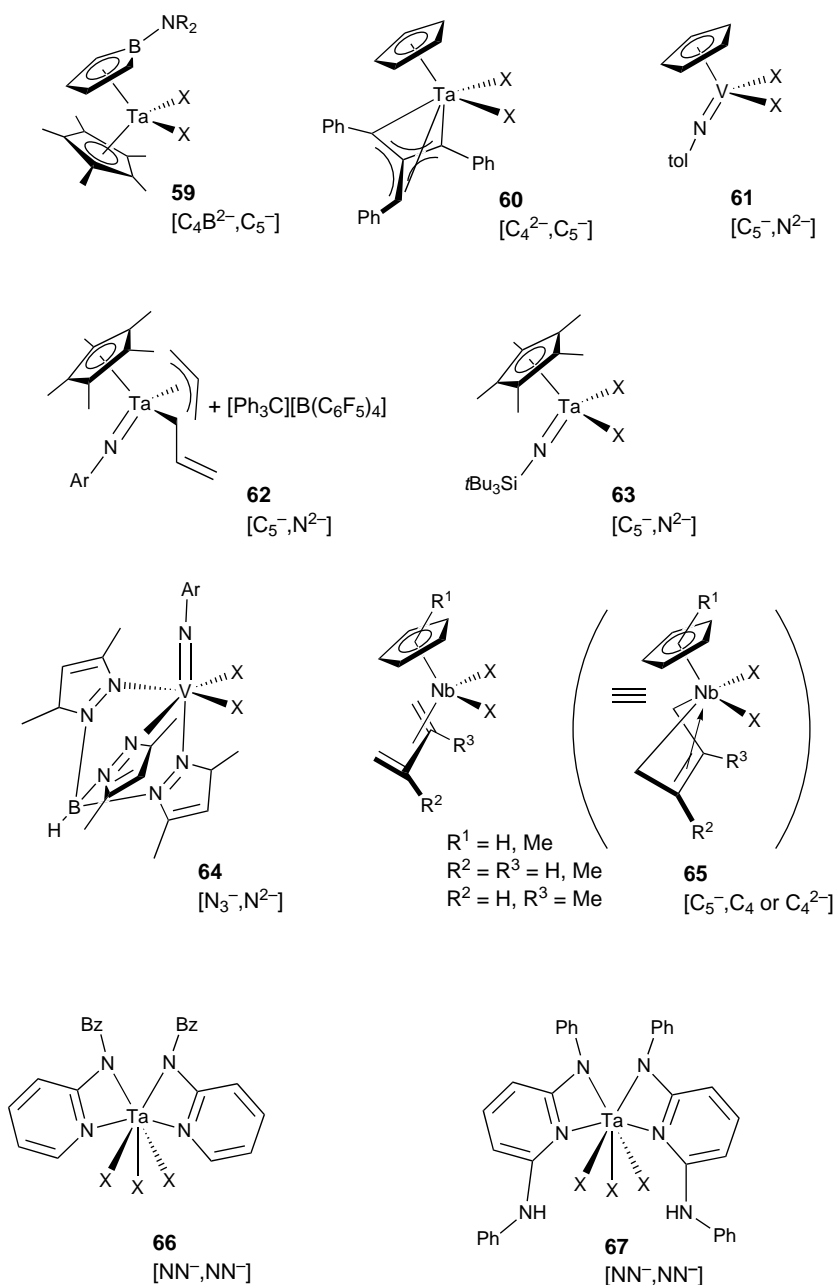
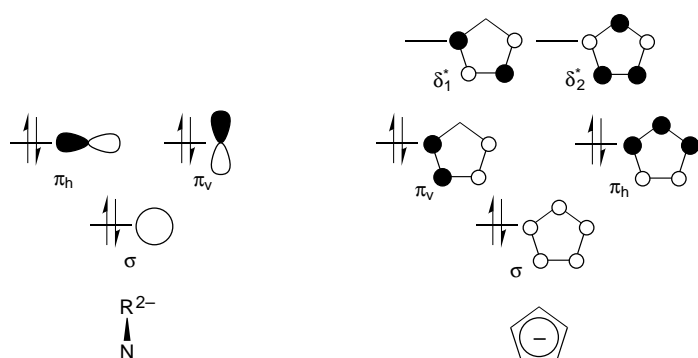
Substitution of a CH unit for a BNR₂ unit in a Cp ring gives the dianionic borollide ligand. Tantalum complex **59** (Scheme 19) is supported by this ligand and shows low ethylene polymerization activity.^[147] It is believed the reactivity of this [Cp*Ta^V(η⁵-borollide)Cl₂] complex may be affected by a resonance contribution from [Cp*Ta^{III}(η⁴-diene)Cl₂]. Complex **60** exploits the isolobal relationship between [C(CH₂Ph)₃]²⁻ and Cp⁻ moieties.^[145] Moderate polymerization activity of 40 g mmol⁻¹ h⁻¹ bar⁻¹ is found.

An isolobal analogy between terminal imido and Cp groups can be drawn;^[126] both groups donate electron density to a metal center through a σ and two π interactions (Scheme 20). The higher energy δ* orbitals of the Cp ligand can be neglected since they are not likely to make a significant contribution to the metal–Cp bonding at a d⁰ metal center. A half-sandwich Group 5 Cp–imido fragment can therefore be considered isolobal with a Group 4 metallocene.

Half-sandwich vanadium compound **61** (Scheme 19) has a moderate activity (27 g mmol⁻¹ h⁻¹ bar⁻¹) when treated with MAO.^[148] The analogous niobium system, although isolobal with zirconocene, is much less active.

Treatment of η¹,η³-diallyl tantalum complex **62** with a trityl fluoroborate salt affords a catalytic system with low ethylene polymerization activity. The allyl substitution pattern is required for complex stability and, although the active catalyst may be considered a single-site allyl or alkyl cation, a high molecular weight material with broad polydispersity is formed.^[149] The related compound **63** is supported by a very bulky silyl imido ligand and has moderate activity of 14 g mmol⁻¹ h⁻¹ bar⁻¹ when treated with MAO. A material of similar molecular weight but narrower polydispersity is formed.^[149]

Compound **64** not only exploits the isolobal relationship between Cp and the dianionic imido group but also that of Cp with the monoanionic trispyrazolylborate ligand. Moderate activity of 14 g mmol⁻¹ h⁻¹ bar⁻¹ for ethylene polymerization is

Scheme 19. Group 5 metal precatalysts. tol = *p*-CH₃C₆H₄.

Scheme 20. Orbital diagram showing the isolobal relationship between cyclopentadienide and imide groups.

shown, and propylene is also polymerized to a low molecular weight material.^[150]

The niobium complexes **65** can be considered to contain either a neutral butadiene (C₄) ligand and a niobium(III) metal center or a dianionic butadienide (C₄²⁻) ligand and a niobium(V) center. Polymerization activity is moderate at 39 gmmol⁻¹ h⁻¹ bar⁻¹, giving polyethylene with a molecular weight over 100 000.^[151–153] Polydispersities are very narrow when these catalysts are used, especially at reduced temperature where values as low as 1.05 have been obtained. These values are among the lowest for any polyethylene catalyst and suggest living polymerization may be occurring. Analogous tantalum catalysts have also been reported and show low activity.^[152]

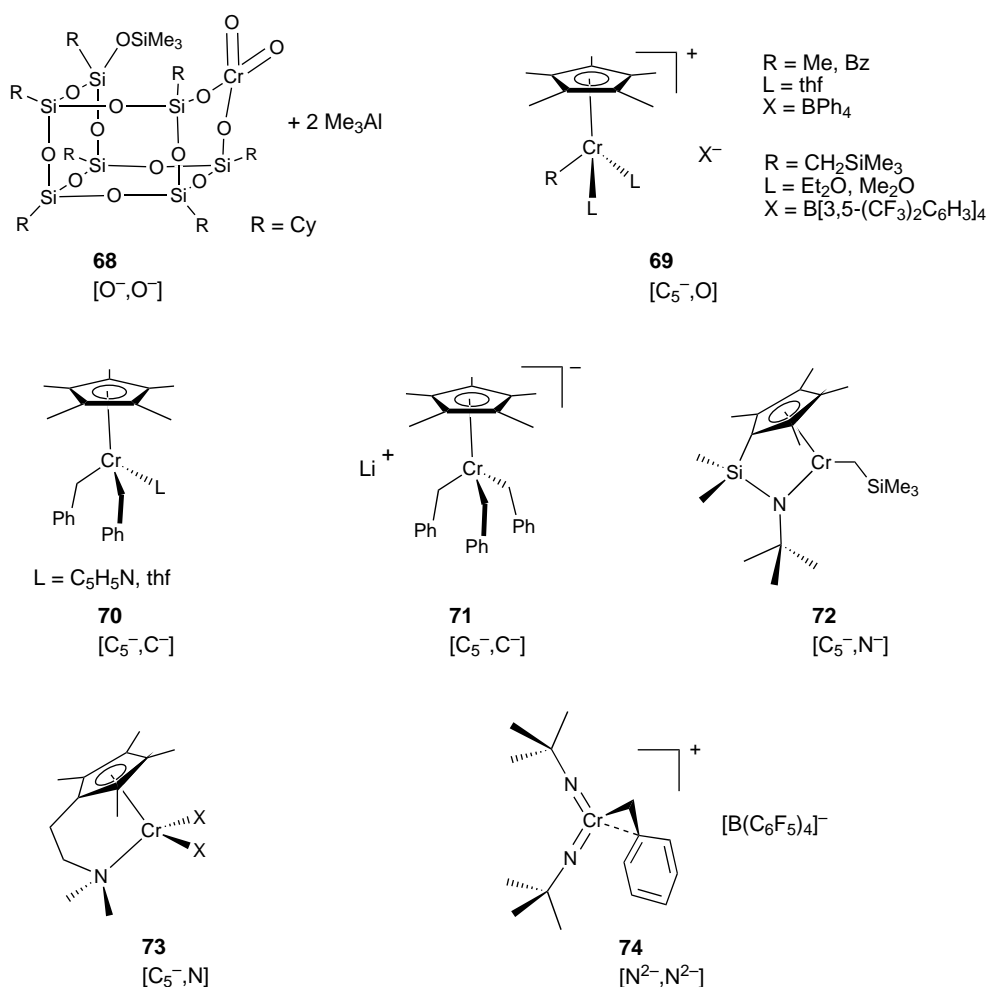
The most active Group 5 catalysts reported are compounds **66** and **67**.^[154] These show very high activity, up to 4780 gmmol⁻¹ h⁻¹ bar⁻¹ at 80 °C and 5 bar of ethylene pressure. At lower temperatures activity is considerably reduced. A range of polymer molecular weights are obtained depending upon the polymerization temperature, and polydispersities are narrow. MAO is used as a cocatalyst with the trihalide precursors, but no information regarding the nature of the active species is reported.

5. Group 6 Metal Catalysts

Group 6 heterogeneous catalysts play a central role in the commercial production of polyethylene. The Phillips catalyst, discovered as early as 1958 by Hogan and Banks,^[155, 156] uses a silica support treated with CrO₃, subsequently reduced to a low-valent species that is the active catalyst. By contrast, the Union Carbide catalyst uses

silica treated with divalent chromocene. Both systems are highly active and offer the advantage of not requiring any cocatalyst. The precise nature of the active sites of these systems is still to be elucidated. Perhaps for this reason—or the analytical problems associated with studying paramagnetic, low-valent chromium species—homogeneous analogues of these catalysts that parallel the discoveries in Group 4 metallocene/MAO systems have taken longer to be developed. Homogeneous chromium polymerization catalysts have been reviewed recently.^[157, 158]

Many Group 6 catalysts are based on low-valent chromium species as models for heterogeneous catalysts. Perhaps the closest model is compound **68** (Scheme 21) reported by Feher et al.,^[159, 160] which contains a chromyl fragment supported by two vicinal siloxy groups of a polyhedral oligosilsesquioxane.



Scheme 21. Group 6 metal precatalysts.

Although this precatalyst contains chromium(vi) sites, an active catalyst is formed after treatment with Me₃Al, which is believed to reduce the metal center to chromium(III).

Theopold and co-workers have reported a number of catalysts based on chromium(III) supported by the pentamethylcyclopentadienyl ligand.^[161–164] The most active system is the cationic compound **69**, which shows a moderate activity of 56 gmmol⁻¹ h⁻¹ bar⁻¹ when noncoordinating anions are employed.^[164] The active species is believed to be formed by dissociation of one labile tetrahydrofuran ligand, thus forming a [C₅⁻, O] donor set and enabling coordination of ethylene to the electrophilic metal center. Polyethylene materials are obtained with a range of molecular weights depending on the catalyst and conditions used, and the oligomerization of higher α -olefins is also reported. Theoretical calculations using [Cr(H₂O)ClMe]⁺ as a model catalyst for these systems have been performed.^[165]

The neutral complexes **70** show low activity.^[161] Again the active catalyst is formed by the loss of the labile ligand L. The related anionic compound **71** shows low activity,^[161] but the active species in this case is believed to be identical to that of the neutral complex **70** and is formed by the loss of LiBz. This is supported by the inhibiting effect of added LiBz. Compound **72** is based on a Cp–amido constrained-geometry catalyst.^[166] The activity reported is very low, and higher α -

olefins are only oligomerized or isomerized. Attempted copolymerization of ethylene with higher α -olefins, in contrast to the use of Group 4 constrained-geometry catalysts,^[70, 85, 86] results in no comonomer incorporation.

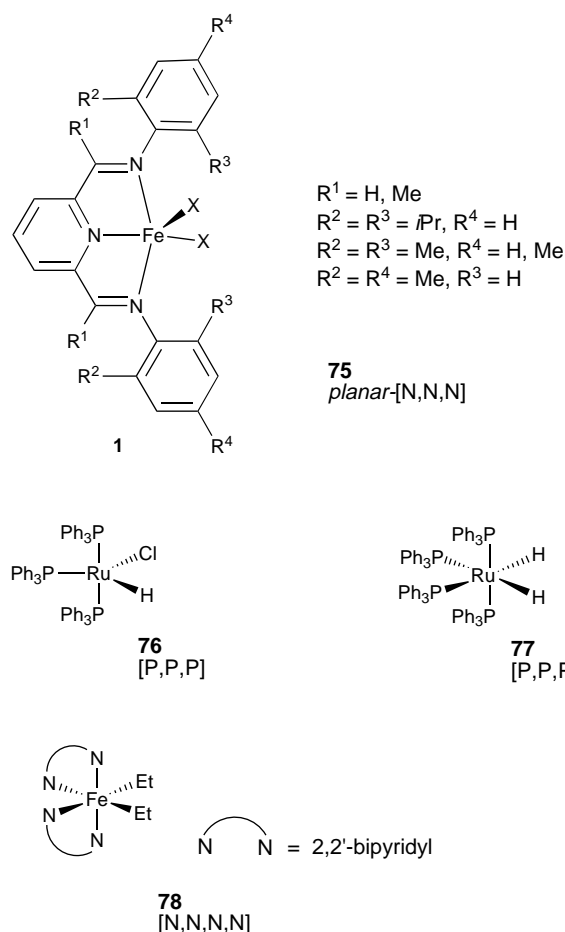
A very active catalyst is formed by treatment of **73** with as few as 100 equivalents of MAO.^[167, 168] Activities as high as 8300 gmmol⁻¹ h⁻¹ bar⁻¹ are reported. These complexes are related to constrained-geometry systems, being based on linked Cp–amine [C₅⁻, N] ligands, and have been studied as models for the trimerization of ethylene to 1-hexene. Propylene is also polymerized, and ethylene and norbornene are copolymerized to an alternating copolymer.

An alternative approach to the development of Group 6 catalysts has been to extend the principles of isolobality exploited for the Group 5 metals. Replacement of both Cp groups of a Group 4 metallocene with isolobal, dianionic imido ligands enables

high-valent chromium(vi) compounds with metallocene-like characteristics to be accessed. This extended isolobal relationship has been exploited in our group to develop the well-defined catalyst **74**.^[169] Moderate ethylene polymerization activity of up to 65 gmmol⁻¹ h⁻¹ bar⁻¹ is found.

6. Group 8 Metal Catalysts

One of the most recent additions to the small but growing number of highly active non-metallocene polymerization catalysts are the iron(II) complexes shown in Scheme 22.^[170, 171] Complex **75** is based on a five-coordinate iron center supported by a neutral tridentate 2,6-bis(imino)pyridine ligand and, when activated with MAO, shows exceptionally high activity. Activity figures in many cases are comparable or even higher than those found for Group 4 metallocenes under analogous conditions. The molecular weight of the polyethylene material generated shows a marked dependency upon the aryl substitution pattern. Aryl substituents with only one small *ortho* substituent give highly active oligomerization catalysts with exceptionally high selectivities for the production of α -olefins.^[170, 172] Increasing the size of this substituent to



Scheme 22. Group 8 metal precatalysts.

a *t*Bu group, or placing substituents in both of the *ortho* positions, results in the formation of high molecular weight polyethylene. ^{13}C NMR analysis of these polymers reveals saturated end groups in addition to low levels of vinyl unsaturation. This is consistent with a termination mechanism involving alkyl group transfer to the aluminum cocatalyst in addition to β -H transfer. Thus, by judicious choice of ligand substituents and polymerization conditions, a range of materials from α -olefins to polyethylenes can be obtained.

Only one other Group 8 ethylene polymerization catalyst has been reported to date.^[173] The ruthenium complex **76** shows very low activity for the polymerization of ethylene. The kinetics of polymerization using this catalyst have been extensively studied. A branched polyethylene is reported to be produced.

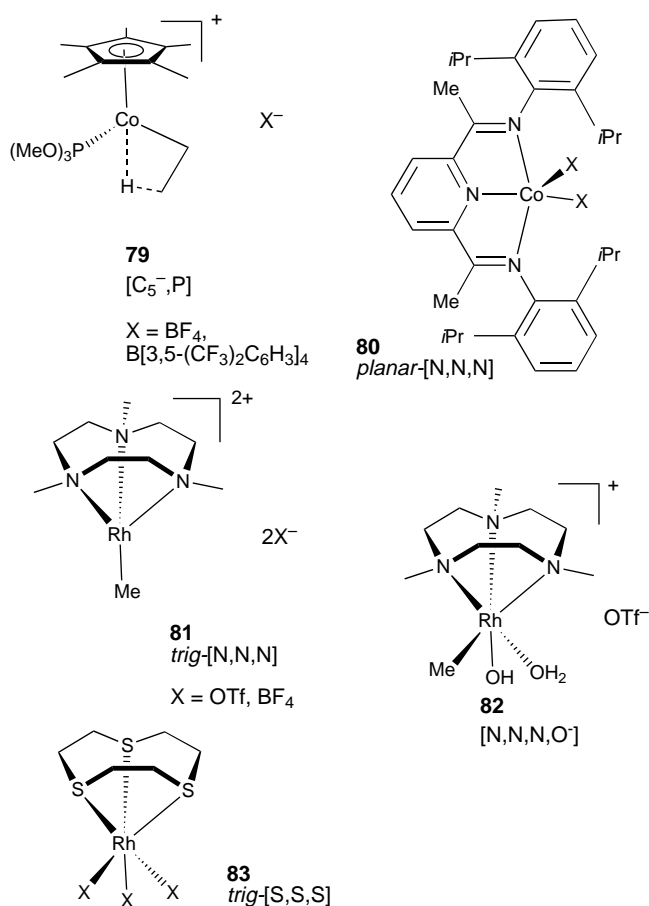
A series of papers by Yamamoto and co-workers report the polymerization of functionalized vinyl monomers by iron and ruthenium complexes.^[174–176] For example, complex **77**, although related to complex **76**, does not show any ethylene polymerization activity. Acrylonitrile, however, is polymerized with 57% conversion in five minutes.^[176]

Complex **78** is reported to polymerize a range of monomers including methyl methacrylate, acrolein, methyl vinyl ketone, and acrylonitrile.^[174] Conversion rates are low and ethylene is not polymerized. The mechanism for polymerization is

proposed to be by a coordinative pathway involving the partial dissociation of one 2,2'-bipyridyl ligand.^[175]

7. Group 9 Metal Catalysts

The most extensively studied example of the Group 9 catalysts is the cobalt(III) complex **79** (Scheme 23).^[8, 177–181] This cationic compound shows a β -agostic interaction and inserts ethylene in a living fashion to form high molecular weight polymers with narrow polydispersity. Activities are low, the most active catalyst being obtained when noncoordinating counterions are employed. Higher α -olefins are only oligomerized, but end-functionalized polyethylene materials have been successfully synthesised with this system.



Scheme 23. Group 9 metal precatalysts.

The cobalt(II) complex **80** shows an activity of 460 gmmol⁻¹h⁻¹bar⁻¹ when treated with MAO.^[170, 171] Although this figure of merit represents the highest activity reported for a Group 9 system, it is an order of magnitude lower than for the analogous iron catalyst **75** (Scheme 22). The polyethylene obtained is end-capped with a vinyl group, an observation consistent with β -H elimination being the predominant chain-termination process.

The dicationic rhodium(III) complex **81**, containing the hard triamine donor triazacyclononane, is reported to be an active ethylene polymerization catalyst^[182] although no activity

figure is given. The supporting ligand in this case is considered a *trig*-[N,N,N] donor, in contrast to the *planar*-[N,N,N] ligands of the highly active catalysts **75** and **80**. This system is the first example of a catalyst capable of polymerizing ethylene in water.^[183] The active species in aqueous solution is believed to be formed by the dissociation of the bound water molecule from **82**. Activity is extremely low, corresponding to only one turnover per day at 60 bar. Catalysis is also found to be sensitive to the pH value because of the equilibrium of species present in aqueous solution.

Related *trig*-[S,S,S] trithiacyclononane derivatives have recently been synthesized. The neutral procatalyst **83** has shown low activity for ethylene polymerization with MAO as cocatalyst.^[184]

8. Group 10 Metal Catalysts

Group 10 compounds with anionic P,O ligands are well known to oligomerize ethylene, playing a central role in the Shell Higher Olefin Process (SHOP). There have also been reports that SHOP-type oligomerization catalysts can polymerize ethylene under certain conditions.^[185–192] Compound **84** (Scheme 24), for example where L = PPh₃, shows very high polymerization activity, giving materials with molecular weights over 100 000.^[186, 187] Crucial to the formation of high molecular weight polymers rather than oligomers is the removal of L with phosphane scavengers such as [Ni(cod)₂]

(cod = 1,5-cyclooctadiene), or the use of more labile groups for L, such as pyridine or ylides. These catalysts have also been shown to be active for the copolymerization of ethylene with higher α -olefins or ω -functionalized α -olefins.^[186] An alternative approach has been to support such catalysts on organic polymers.^[185] Polyethylene is produced by these heterogeneous systems with very high activity.

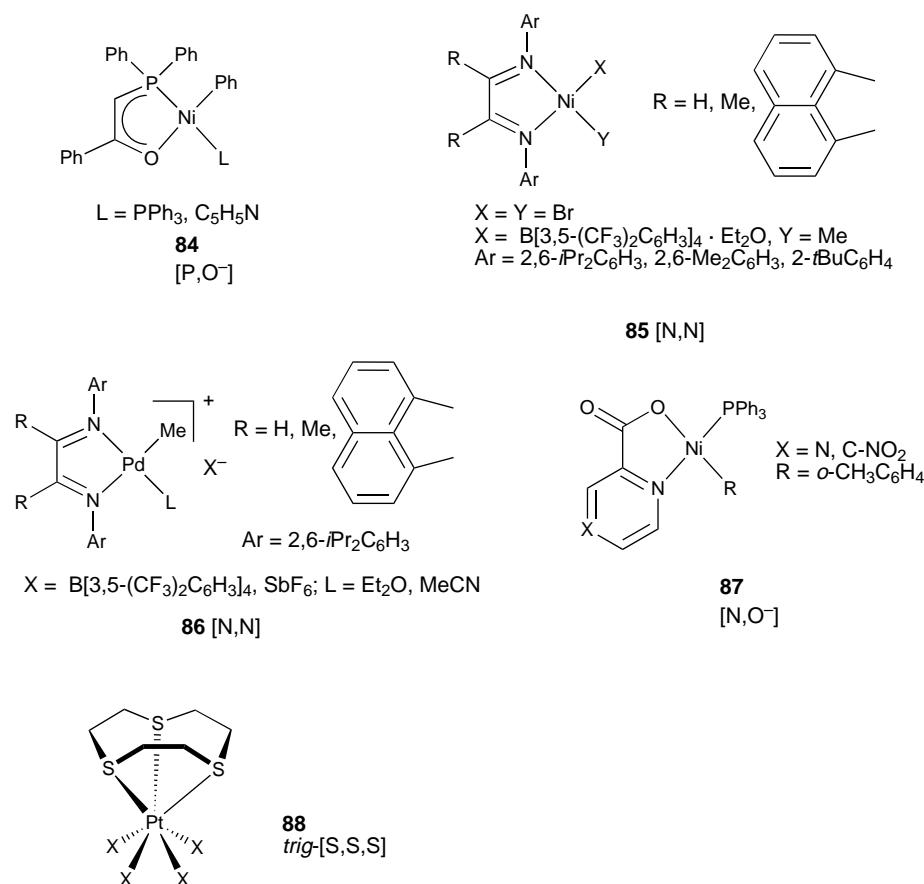
Complex **87**, based on mixed N,O donor chelates, shows low polymerization activity.^[193] Interestingly, the use of electron-withdrawing substituents or pyrazine donors is essential for polymerization to occur. Incorporation of simple pyridine donors result only in oligomerization.

The nickel(II) and palladium(II) systems reported by Brookhart and co-workers,^[194, 195] based on square-planar cationic alkyl compounds supported by bulky diimine [N,N] ligands, were the first examples of late transition metal catalysts capable of polymerizing higher α -olefins as well as ethylene to high molecular weight polymers.

When treated with MAO, the nickel dibromide derivative of compound **85** shows very high activity, up to 11 000 g mmol⁻¹ h⁻¹ bar⁻¹.^[195] The well-defined cationic alkyl species is also active. β -Elimination from the growing polymer chain leads to chain branching or chain transfer. The formation of high molecular weight polymers is possible because the steric protection of the vacant axial coordination sites reduces the rate of associative displacement from β -eliminated olefin-hydride complexes and thus reduces chain transfer rates. A range of polyethylene materials with

molecular weights up to 1×10^6 and degrees of branching from linear to over 70 branches per 1000 carbon atoms is accessible by simple variation of temperature, pressure, and ligand architecture. At low temperature, the polymerization is living, and di- and triblock ethylene/ α -olefin copolymers can be synthesized.^[196] Also at low temperature, propylene is polymerized to syndiotactic polypropylene by chain-end control.^[197] At higher temperatures, α -olefins are polymerized to give more linear materials than expected because of β -elimination and reinsertion mechanisms leading to chain straightening.

The analogous palladium(II) compounds **86** (Scheme 24) show more moderate activity to produce very highly branched amorphous polyethylene, with a range of molecular weights and up to 100 branches per 1000 carbon atoms. The mechanism of polymerization with these catalysts has been studied and the alkyl-olefin catalyst resting states characterized by NMR techniques. These catalysts are able to copolymerize α -olefins with functionalized



Scheme 24. Group 10 metal procatalysts.

comonomers such as methyl acrylate, resulting in highly branched random copolymers with ester groups on some chain ends.^[198, 199] The mechanism for copolymerization is by 2,1-insertion of acrylate and chelate ring expansion, followed by insertion of ethylene units. Activities, however, are found to be much lower than for homopolymerization.

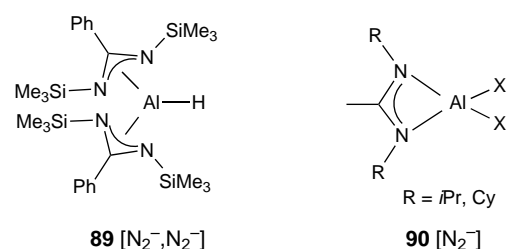
Calculations have been performed on both nickel and palladium systems.^[200–203] These studies corroborate the crucial role of axial steric protection in the formation of high molecular weight polymers.^[200] The development of these catalysts, both in terms of ligand modification and new activation pathways, continues apace.^[204, 205]

One example of a platinum(IV) catalyst has been reported.^[184] Trithiacyclononane-supported complex **88** shows a moderate activity of $12 \text{ gmmol}^{-1} \text{ h}^{-1} \text{ bar}^{-1}$ for the polymerization of ethylene with MAO activation. As with the related rhodium species **83**, no information as to the nature of the active catalytic species is reported.

9. Group 13 Metal Catalysts

Almost 40 years ago Ziegler et al. reported on “reactions of the aluminum–carbon bond with olefins”. The “aufbau” reaction—that is, the stepwise addition of the Al–C bond of a trialkylaluminum compound to ethylene—yielded α -olefins under high pressure and temperature.^[206] Activities of these trialkylaluminum compounds to form solid polyethylene have been extremely low.^[207]

More recently, two reports have appeared in the literature describing homogeneous aluminum compounds that are able to polymerize ethylene under mild conditions. One system, reported by Teuben and co-workers,^[208] features an aluminum hydride complex **89** (Scheme 25) containing two benzamidinate ligands. With ethylene, under moderate conditions (4 atm, 40 °C, 2 h), a small amount of polyethylene was obtained. No quantitative data have been reported.



Scheme 25. Aluminum complexes used as olefin polymerization catalysts.

Another aluminum catalyst was reported recently by Coles and Jordan.^[209] The neutral dialkylaluminum complex **90**, supported by only one benzamidinate ligand, is activated in an analogous fashion to many transition metal systems, by conversion into a cationic monoalkyl species. For example, activation of complex **90** with $[\text{Ph}_3\text{C}][\text{B}(\text{C}_6\text{F}_5)_4]$ in toluene has given an activity of $3 \text{ gmmol}^{-1} \text{ h}^{-1} \text{ bar}^{-1}$ under moderate conditions (2 atm, 85 °C). Although polymerization activities

obtained thus far are low, these catalysts are significant as they represent the first examples of well-defined main group complexes acting as ethylene polymerization catalysts.

10. Summary

To help the reader to categorize the large array of olefin polymerization catalysts presented in this review, a summary of all catalysts discussed is given in Table 2. The catalysts are

Table 2. Overview of catalysts discussed in this review and their ranking according to their activity.

Group	Activity ^[a]				
	very low < 1	low 1–10	moderate 10–100	high 100–1000	very high > 1000
3	Y: 9	Sc: 1–3	Y: 6 RE: ^[b] 10	Y: 7	RE: ^[b] 11
4	Ti: 24 Zr: 24 , 38, 40	Ti: 23, 35	Ti: 12, 34, 38 , 41, 42 Zr: 13, 14, 17 , 21, 22, 28, 30 , 32, 34, 36, 39 , 41, 42, 50	Ti: 20, 43, 49 , 54 Zr: 15, 53, 55 , 56, 57	Ti: 18, 25 , 37, 47 Zr: 16, 18 , 19, 25, 29
5		Ta: 59, 62	V: 61, 64 Nb: 65 Ta: 60, 63		Ta: 66, 67
6	Cr: 72	Cr: 70	Cr: 69, 74		Cr: 73
8	Ru: 76				Fe: 75
9	Rh: 82	Co: 79 Rh: 83		Co: 80	
10		Ni: 87	Pd: 86 Pt: 88		Ni: 84, 85
13	Al: 89	Al: 90			

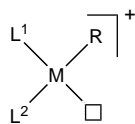
[a] Values given in units of $\text{gmmol}^{-1} \text{ h}^{-1} \text{ bar}^{-1}$; [b] RE = rare earth metals.

collected together according to the group in the periodic table within the activity ranges outlined in Table 1. Table 2 should be used as an indicator of activity trends, rather than an absolute measure of catalyst performance, since the activities are subject to polymerization conditions that may not have been optimized.

Having reviewed some of the key developments in the search for new olefin polymerization catalysts, it is appropriate to examine more closely the factors that are important for the generation of high-activity catalysts. Three features are essential: 1) electron deficiency—all known catalysts are electron-deficient species. With the exceptions of a few 15- and 16-electron species, they mostly contain 14 or fewer electrons. 2) The active center must have a vacant coordination site adjacent to the growing polymer chain. 3) The active catalyst should preferentially bear a positively charged metal center which enhances the electrophilicity of the active site and also helps to inhibit certain deactivation pathways such as dimerization, for example as seen in certain neutral catalysts such as $[(\text{Cp}_2\text{ScH})_2]$. It has also become increasingly clear, especially since the development of highly active late transition metal catalysts, that a fourth feature, steric protection, plays a crucial part in the stabilization of the active site

once formed, its selectivity towards olefin substrates, and control over the molecular weight parameters of the resultant polymers.

These guiding features can be used to construct a chart of metal–ligand combinations that afford polymerization active metal centers. Active cationic catalysts may be represented by the general formula shown in Scheme 26, where L^1 and L^2



Scheme 26. Generic structure of a cationic olefin polymerization catalyst (see text for details). □ represents the site of coordinative unsaturation.

represent coordinated ligands, and R may be either a simple alkyl group in an initiating species or the extended alkyl chain of the growing polymer.

For the purpose of this exercise, the electron-counting formalism with charged ligands is employed, and the ligands are considered to donate their maximum available number of electrons; for example, the cyclopentadienyl group is a monoanionic Cp^- unit donating six electrons to the metal center ($6e, -1$), an imido moiety is a dianionic RN^{2-} unit contributing a maximum of six electrons in its linear bonding mode ($6e, -2$). The growing polymer chain is a monoanionic R^- unit contributing two electrons. The charged formalism lends itself readily to assignment of the oxidation state of the metal center and allows a matrix for cationic 14-electron complexes to be constructed according to metal oxidation state (Table 3).

It can be seen from Table 3 that, in addition to well-established active catalyst families such as the metallocenes and nickel- and chromium-based systems, the matrix allows other metal–ligand combinations to be identified that afford 14-electron cationic alkyl species, thereby highlighting potential new catalyst targets. Examples of some of the most active catalyst systems discovered to date in this class are shown in boldface.

One example of a recently discovered 14-electron cationic alkyl catalyst system highlighted in Table 3 is the $[[bis(imino)pyridine]FeCl_2]$ system **75** (Scheme 22).^[170, 171] Iron(II) requires a neutral two-electron donor ligand and a neutral four-electron donor ligand (corresponding overall to three two-electron donor ligands). The tridentate pyridyldiimine ligand is found to meet these requirements perfectly, and activation of the complex with MAO affords a highly active ethylene polymerization catalyst.

Finally, it should be recognized that not all olefin polymerization catalysts are 14-electron species, and not all are cationic either. In general, active catalysts have to be

coordinatively unsaturated—that is, 16 electrons or less—and they may be cationic or neutral. For example, cationic 13-electron chromium(III),^[157] dicationic 14-electron rhodium(III),^[182] and neutral 15-electron chromium(III)^[166] systems are known. Related charts can be drawn up for species with different electron counts, both neutral and charged, and these too may serve to help identify new catalyst families.

11. Outlook

The field of α -olefin polymerization catalysis has developed dramatically over the past five years or so, with some of the most significant recent advances occurring for late transition metal systems. The discovery of a highly active family of catalysts based on iron, a metal that had no previous track record in this field, has highlighted the possibilities for further new catalyst discoveries. No longer need the search for new catalysts be restricted to metals that have a history of giving polymerization-active centers. The speed of catalyst discovery is likely to be limited only by the flair and imagination of the synthetic organometallic and coordination chemist for ligand design. The late transition metals especially are likely to provide fertile ground for future development, and the greater functional group tolerance of the late transition metals also offers the attractive prospect of polar comonomer incorporation. A relatively small amount of functionality can dramatically transform the adhesion and wettability properties of polyolefins; more heavily functionalized products offer the prospect of materials with totally new properties and performance parameters. It is clear that, for olefin polymerization catalysis, the process of catalyst discovery and development is far from over.

Received: May 26, 1998 [A 283 IE]

German version: *Angew. Chem.* **1999**, *111*, 448–468

- [1] M. Bochmann, *J. Chem. Soc. Dalton Trans.* **1996**, 255–270.
- [2] H. H. Brintzinger, D. Fischer, R. Mülhaupt, B. Rieger, R. M. Waymouth, *Angew. Chem.* **1995**, *107*, 1255–1283; *Angew. Chem. Int. Ed. Engl.* **1995**, *34*, 1143–1170.
- [3] P. C. Möhring, N. J. Coville, *J. Organomet. Chem.* **1994**, *479*, 1–29.
- [4] V. K. Gupta, S. Satish, I. S. Bhardwaj, *Rev. Macromol. Chem. Phys. C* **1994**, *34*, 439–514.
- [5] W. Kaminsky, *J. Chem. Soc. Dalton Trans.* **1998**, 1413–1418.
- [6] K. Soga, T. Shiono, *Prog. Polym. Sci.* **1997**, *22*, 1503–1546.
- [7] R. F. Jordan, *Adv. Organomet. Chem.* **1991**, *32*, 325–387.
- [8] M. Brookhart, B. Grant, A. F. Volpe, *Organometallics* **1992**, *11*, 3920.

Table 3. A matrix of metal–ligand combinations that give cationic 14-electron complexes.^[a]

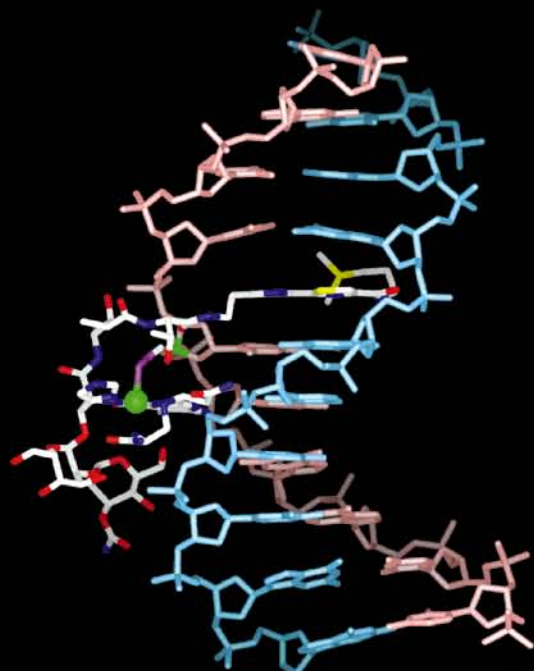
	2, 0	2, –1	4, 0	4, –1	4, –2	6, 0	6, –1	6, –2
2, 0	Ni^{II}, Pd^{II}	Au ^{III}	Fe^{II}, Ru^{II}	Co ^{III} , Rh ^{III}	Pd ^{IV} , Pt ^{IV}	Cr ^{II} , Mo ^{II}	Mn ^{III} , Re ^{III}	Fe ^{IV} , Ru ^{IV}
2, –1			Co ^{III} , Rh ^{III}	Pd ^{IV} , Pt ^{IV}		Mn ^{III} , Re ^{III}	Fe ^{IV} , Ru ^{IV}	
4, 0			Cr ^{II} , Mo ^{II}	Mn ^{III} , Re ^{III}	Fe ^{II} , Ru ^{IV}	Ti ^{II} , Zr ^{II}	V ^{III} , Nb ^{III}	Cr ^{IV} , Mo ^{IV}
4, –1				Fe ^{IV} , Ru ^{IV}		V ^{III} , Nb ^{III}	Cr ^{IV} , Mo ^{IV}	Mn ^V , Re ^V
4, –2						Cr ^{IV} , Mo ^{IV}	Mn ^V , Re ^V	
6, 0						Mg ^{II} , Ca ^{II}	Sc ^{III} , Y ^{III}	Ti ^{IV} , Zr ^{IV}
6, –1							Ti^{IV}, Zr^{IV}	V^V, Nb^V, Ta^V
6, –2								Cr^{VI}, Mo^{VI}

[a] The coordinated ligands L^1 and L^2 (Scheme 26) are represented by the designation (x, y), where x is the maximum available number of electrons and y is the charge.

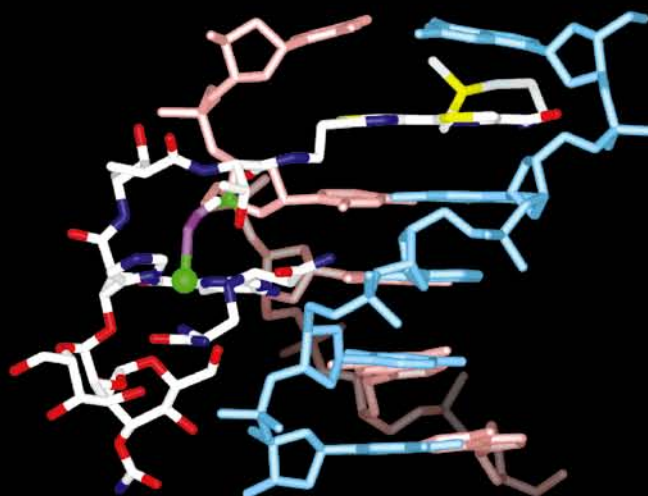
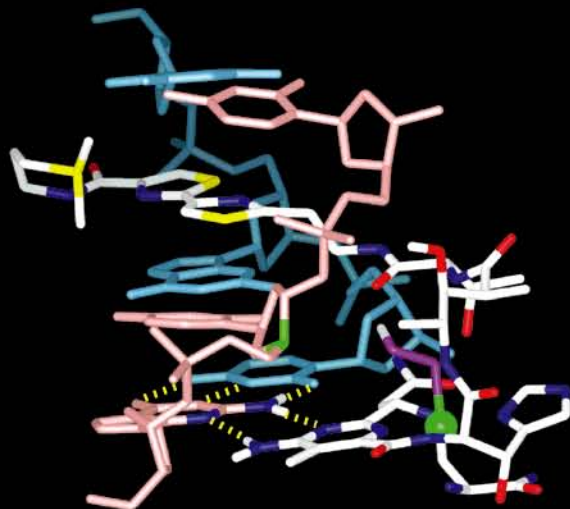
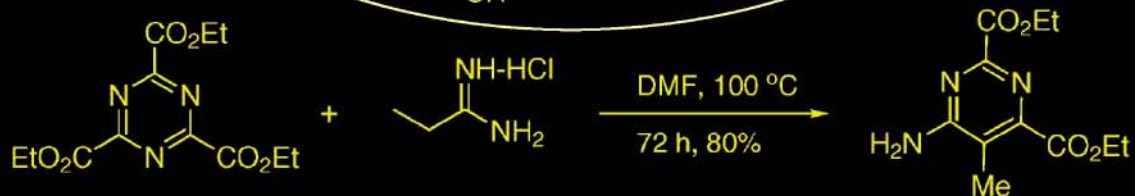
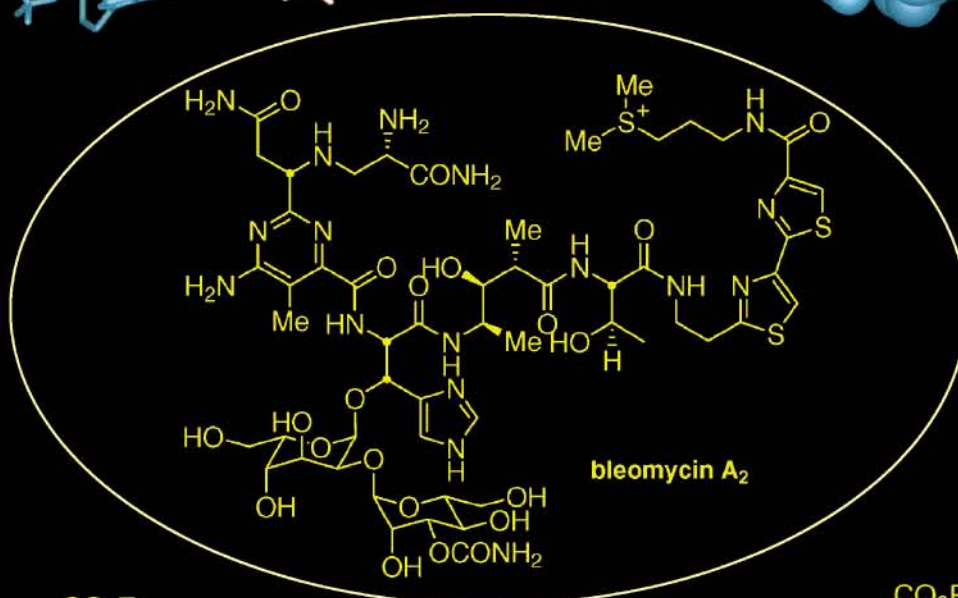
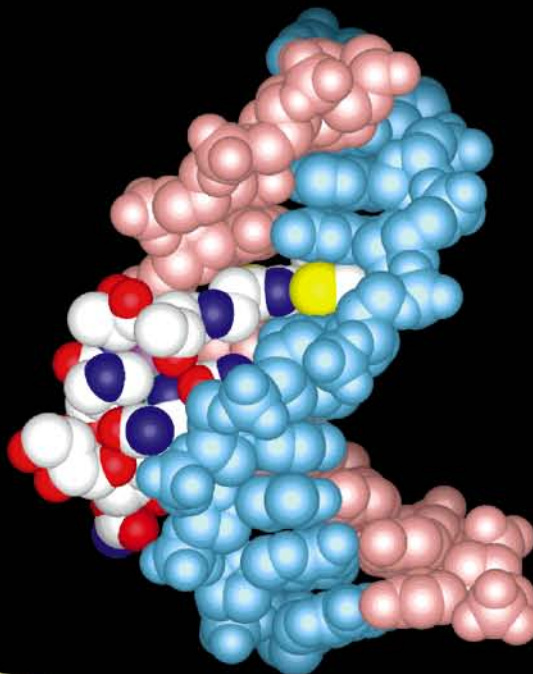
- [9] X. Yang, C. L. Stern, T. J. Marks, *J. Am. Chem. Soc.* **1991**, *113*, 3623–3625.
- [10] X. Yang, C. L. Stern, T. J. Marks, *J. Am. Chem. Soc.* **1994**, *116*, 10015–10031.
- [11] W. E. Piers, T. Chivers, *Chem. Soc. Rev.* **1997**, *26*, 345–354.
- [12] W. Kaminsky, *Macromol. Chem. Phys.* **1996**, *197*, 3907–3945.
- [13] S. Pasynkiewicz, *Polyhedron* **1990**, *9*, 429–453.
- [14] S. Pasynkiewicz, *Macromol. Symp.* **1995**, *97*, 1–13.
- [15] A. R. Barron, *Macromol. Symp.* **1995**, *97*, 15–25.
- [16] B. Temme, G. Erker, J. Karl, H. Luftmann, R. Fröhlich, S. Kotila, *Angew. Chem.* **1995**, *107*, 1867–1869; *Angew. Chem. Int. Ed. Engl.* **1995**, *34*, 1755–1757.
- [17] B. Temme, J. Karl, G. Erker, *Chem. Eur. J.* **1996**, *2*, 919.
- [18] J. Karl, G. Erker, *Chem. Ber.* **1997**, *130*, 1261–1267.
- [19] W. E. Piers, *Chem. Eur. J.* **1998**, *4*, 13–18.
- [20] D. D. Devore, F. J. Timmers, D. L. Hasha, R. K. Rosen, T. J. Marks, P. A. Deck, C. L. Stern, *J. Am. Chem. Soc.* **1995**, *117*, 3132–3134.
- [21] Y. Sun, W. E. Piers, S. J. Rettig, *Chem. Commun.* **1998**, 127–128.
- [22] P. J. Shapiro, W. D. Cotter, W. P. Schaefer, J. A. Labinger, J. E. Bercaw, *J. Am. Chem. Soc.* **1994**, *116*, 4623–4640.
- [23] P. J. Shapiro, E. E. Bunel, W. P. Schaefer, J. E. Bercaw, *Organometallics* **1990**, *9*, 867–869.
- [24] B. J. Burger, M. E. Thompson, W. D. Cotter, J. E. Bercaw, *J. Am. Chem. Soc.* **1990**, *112*, 1566–1577.
- [25] S. Hajela, J. E. Bercaw, *Organometallics* **1994**, *13*, 1147–1154.
- [26] W. E. Piers, P. J. Shapiro, E. E. Bunel, J. E. Bercaw, *Synlett* **1990**, 74–84.
- [27] W. E. Piers, E. E. Bunel, J. E. Bercaw, *J. Organomet. Chem.* **1991**, *407*, 51–60.
- [28] C. J. Schaverien, *J. Mol. Catal.* **1994**, *90*, 177–183.
- [29] G. C. Bazan, W. P. Schaeffer, J. E. Bercaw, *Organometallics* **1993**, *12*, 2126–2130.
- [30] C. Kreuder, R. F. Jordan, H. Zhang, *Organometallics* **1995**, *14*, 2993–3001.
- [31] M. D. Fryzuk, G. Giesbrecht, S. J. Rettig, *Organometallics* **1996**, *15*, 3329–3336.
- [32] S. Hajela, W. P. Schaefer, J. E. Bercaw, *J. Organomet. Chem.* **1997**, *532*, 45–53.
- [33] D. G. H. Ballard, A. Courtis, J. Holton, J. McMeeking, R. Pearce, *J. Chem. Soc. Chem. Commun.* **1978**, 994–995.
- [34] J. P. Mitchell, S. Hajela, S. K. Brookhart, K. I. Hardcastle, L. M. Henling, J. E. Bercaw, *J. Am. Chem. Soc.* **1996**, *118*, 1045–1053.
- [35] E. B. Coughlin, J. E. Bercaw, *J. Am. Chem. Soc.* **1992**, *114*, 7606–7607.
- [36] H. Yasuda, E. Ihara, *Tetrahedron* **1995**, *51*, 4563–4570.
- [37] H. Yasuda, E. Ihara, M. Morimoto, M. Nodono, S. Yoshioka, M. Furo, *Macromol. Symp.* **1995**, *95*, 203–216.
- [38] C. J. Schaverien, *J. Chem. Soc. Chem. Commun.* **1992**, 11–13.
- [39] C. J. Schaverien, *Organometallics* **1994**, *13*, 69–82.
- [40] R. Duchateau, C. T. van Wee, A. Meetsma, J. H. Teuben, *J. Am. Chem. Soc.* **1993**, *115*, 4931–4932.
- [41] R. Duchateau, C. T. van Wee, J. H. Teuben, *Organometallics* **1996**, *15*, 2291–2302.
- [42] *Chem. Eng. News* **1978**, 56(31), 24.
- [43] P. L. Watson, *J. Am. Chem. Soc.* **1982**, *104*, 337–339.
- [44] P. L. Watson, D. C. Roe, *J. Am. Chem. Soc.* **1982**, *104*, 6471–6473.
- [45] P. L. Watson, G. W. Parshall, *Acc. Chem. Res.* **1985**, *18*, 51–56.
- [46] D. Stern, M. Sabat, T. J. Marks, *J. Am. Chem. Soc.* **1990**, *112*, 9558–9575.
- [47] G. Jeske, L. E. Schock, P. N. Swepston, H. Schumann, T. J. Marks, *J. Am. Chem. Soc.* **1985**, *107*, 8103–8110.
- [48] G. Jeske, H. Lauke, H. Mauermann, P. N. Swepston, H. Schumann, T. J. Marks, *J. Am. Chem. Soc.* **1985**, *107*, 8091–8103.
- [49] W. J. Evans, K. J. Forrestal, J. W. Ziller, *Angew. Chem.* **1997**, *109*, 798–799; *Angew. Chem. Int. Ed. Engl.* **1997**, *36*, 774–776.
- [50] J. F. Pelletier, A. Mortreux, F. Petit, X. Olonde, K. Bujadoux, *Stud. Surf. Sci. Catal.* **1994**, *89*, 249.
- [51] C. Pellecchia, A. Proto, P. Longo, A. Zambelli, *Macromol. Chem. Rapid Commun.* **1991**, *12*, 663–667.
- [52] C. Pellecchia, A. Proto, P. Longo, A. Zambelli, *Macromol. Chem. Rapid Commun.* **1992**, *13*, 277–281.
- [53] M. Bochmann, S. J. Lancaster, *Organometallics* **1993**, *12*, 633–640.
- [54] C. Pellecchia, A. Grassi, A. Immirzi, *J. Am. Chem. Soc.* **1993**, *115*, 1160–1162.
- [55] R. Quyoum, Q. Wang, M.-J. Tudoret, M. C. Baird, *J. Am. Chem. Soc.* **1994**, *116*, 6435–6436.
- [56] Q. Wang, R. Quyoum, D. J. Gillis, M.-J. Tudoret, D. Jeremic, B. K. Hunter, M. C. Baird, *Organometallics* **1996**, *15*, 693–703.
- [57] S. W. Ewart, M. J. Sarsfield, D. Jeremic, T. L. Tremblay, E. F. Williams, M. C. Baird, *Organometallics* **1998**, *17*, 1502–1510.
- [58] C. Pellecchia, A. Immirzi, A. Grassi, A. Zambelli, *Organometallics* **1993**, *12*, 4473–4478.
- [59] G. Jiménez Pindado, M. Thornton-Pett, M. Bouwkamp, A. Meetsma, B. Hessen, M. Bochmann, *Angew. Chem.* **1997**, *109*, 2457–2460; *Angew. Chem. Int. Ed. Engl.* **1997**, *36*, 2358–2361.
- [60] G. G. Lavoie, R. G. Bergman, *Angew. Chem.* **1997**, *109*, 2555–2558; *Angew. Chem. Int. Ed. Engl.* **1997**, *36*, 2450–2452.
- [61] G. C. Bazan, G. Rodriguez, A. J. Ashe III, S. Al-Ahmad, C. Müller, *J. Am. Chem. Soc.* **1996**, *118*, 2291–2292.
- [62] G. C. Bazan, G. Rodriguez, *Organometallics* **1997**, *16*, 2492–2494.
- [63] J. S. Rogers, G. C. Bazan, C. K. Sperry, *J. Am. Chem. Soc.* **1997**, *119*, 9305–9306.
- [64] R. W. Barnhart, G. C. Bazan, T. Mourey, *J. Am. Chem. Soc.* **1998**, *120*, 1082–1083.
- [65] T. Wada, T. Tsukahara, T. Sugano, T. Takahama, H. Kurokawa (Mitsubishi Kagaku Kk), Jpn. Kokai Tokkyo Koho JP-A 07,188,335, **1995** [*Chem. Abstr.* **1995**, *123*, 199705v].
- [66] C. Janiak, K. C. H. Lange, U. Versteeg, D. Lentz, P. H. M. Budzelaar, *Chem. Ber.* **1996**, *129*, 1517–1529.
- [67] E. J. M. De Boer, H. J. Heeres, H. J. R. De Boer (Shell), EP-B 638,593, **1995** [*Chem. Abstr.* **1995**, *123*, 199670e].
- [68] T. Tsukahara, T. Wada, T. Sugano, T. Takahama, K. Yamamoto (Mitsubishi Kagaku Kk), Jpn. Kokai Tokkyo Koho JP-A 07,188,319, **1995** [*Chem. Abstr.* **1995**, *123*, 199704u].
- [69] S. A. A. Shah, H. Dorn, A. Voigt, H. W. Roesky, E. Parisini, H.-G. Schmidt, M. Noltemeyer, *Organometallics* **1996**, *15*, 3176–3181.
- [70] J. A. M. Canich, H. W. Turner (Exxon), WO-A 92/12162, **1992** [*Chem. Abstr.* **1993**, *118*, 81615j].
- [71] T. W. Warren, R. R. Schrock, W. M. Davis, *Organometallics* **1996**, *15*, 562–569.
- [72] T. H. Warren, R. R. Schrock, W. M. Davis, *Organometallics* **1998**, *17*, 308–321.
- [73] S. Tinkler, R. J. Deeth, D. J. Duncalf, A. McCamley, *Chem. Commun.* **1996**, 2623.
- [74] F. G. N. Cloke, T. J. Geldbach, P. B. Hitchcock, J. B. Love, *J. Organomet. Chem.* **1996**, *506*, 343–345.
- [75] N. A. H. Male, M. Thornton-Pett, M. Bochmann, *J. Chem. Soc. Dalton Trans.* **1997**, 2487–2494.
- [76] B. Tsui, D. C. Swenson, R. F. Jordan, *Organometallics* **1997**, *16*, 1392–1400.
- [77] F. Jäger, H. W. Roesky, H. Dorn, S. Shah, M. Noltemeyer, H.-G. Schmidt, *Chem. Ber.* **1997**, *130*, 399–403.
- [78] J. D. Scollard, D. H. McConville, N. C. Payne, J. J. Vittal, *Macromol.* **1996**, *29*, 5241–5243.
- [79] J. D. Scollard, D. H. McConville, *J. Am. Chem. Soc.* **1996**, *118*, 10008–10009.
- [80] J. D. Scollard, D. H. McConville, S. J. Rettig, *Organometallics* **1997**, *16*, 1810–1812.
- [81] J. D. Scollard, D. H. McConville, J. J. Vittal, *Organometallics* **1997**, *16*, 4415–4420.
- [82] V. C. Gibson, B. S. Kimberley, A. J. P. White, D. J. Williams, P. Howard, *Chem. Commun.* **1998**, 313–314.
- [83] H. Mack, M. S. Eisen, *J. Organomet. Chem.* **1996**, *525*, 81–87.
- [84] A. D. Horton, J. de With, *Chem. Commun.* **1996**, 1375–1376.
- [85] J. C. Stevens, F. J. Timmers, D. R. Wilson, G. F. Schmidt, P. N. Nickias, R. K. Rosen, G. W. Knight, S.-Y. Lai (Dow Chemical Co.), EP-B 0416815, **1990** [*Chem. Abstr.* **1991**, *115*, 93163m].
- [86] Y.-X. Chen, T. J. Marks, *Organometallics* **1997**, *16*, 3649–3657.
- [87] P. J. Sinnema, K. Liekelema, A. Meetsma, B. Hessen, J. H. Teuben, *Abstr. Pap. 213th ACS National Meeting* (San Francisco, CA) **1997**, INOR-285.
- [88] P.-J. Sinnema, L. van der Veen, A. L. Spek, N. Veldman, J. H. Teuben, *Organometallics* **1997**, *16*, 4245–4247.

- [89] P. T. Gomes, M. L. H. Green, A. M. Martins, P. Mountford, *J. Organomet. Chem.* **1997**, *541*, 121–125.
- [90] J. Okuda, F. Schattenmann, S. Wocadlo, W. Massa, *Organometallics* **1995**, *14*, 789–795.
- [91] F. G. Sernetz, R. Mülhaupt, F. Amor, T. Eberle, J. Okuda, *J. Poly. Sci. A* **1997**, *35*, 1571–1578.
- [92] T. K. Woo, L. Fan, T. Ziegler, *Organometallics* **1994**, *13*, 2252–2261.
- [93] T. K. Woo, L. Fan, T. Ziegler, *Organometallics* **1994**, *13*, 432–433.
- [94] L. Fan, D. Harrison, T. K. Woo, T. Ziegler, *Organometallics* **1995**, *14*, 2018–2026.
- [95] T. K. Woo, P. M. Margl, T. Ziegler, P. E. Blöchl, *Organometallics* **1997**, *16*, 3454–3468.
- [96] A. D. Horton, J. de With, A. J. van der Linden, H. van de Weg, *Organometallics* **1996**, *15*, 2672–2674.
- [97] R. R. Schrock, F. Schattenmann, M. Aizenberg, W. M. Davis, *Chem. Commun.* **1998**, 199.
- [98] R. Baumann, W. M. Davis, R. R. Schrock, *J. Am. Chem. Soc.* **1997**, *119*, 3830–3831.
- [99] F. Guérin, D. H. McConville, J. J. Vittal, *Organometallics* **1996**, *15*, 5586–5590.
- [100] F. Guérin, D. H. McConville, N. C. Payne, *Organometallics* **1996**, *15*, 5085–5089.
- [101] F. J. Schattenmann, R. R. Schrock, W. M. Davis, *Organometallics* **1998**, *17*, 989–992.
- [102] A. Littke, N. Sleiman, C. Bensimon, D. S. Richeson, G. P. A. Yap, S. J. Brown, *Organometallics* **1998**, *17*, 446–451.
- [103] D. Herskovics-Korine, M. S. Eisen, *J. Organomet. Chem.* **1995**, *503*, 307–314.
- [104] D. Walther, R. Fischer, H. Görls, J. Koch, B. Schweder, *J. Organomet. Chem.* **1996**, *508*, 13–22.
- [105] R. Schlund, M. Lux, F. Edelmann, U. Reissmann, W. Rohde (BASF), EP-B 687,693, **1995** [*Chem. Abstr.* **1996**, *124*, 147160q].
- [106] J. R. Hagadorn, J. Arnold, *J. Chem. Soc. Dalton Trans.* **1997**, 3087–3096.
- [107] J. C. Flores, J. C. W. Chien, M. D. Rausch, *Organometallics* **1995**, *14*, 1827–1833.
- [108] M. Oberthür, P. Arndt, R. Kempe, *Chem. Ber.* **1996**, *129*, 1087–1091.
- [109] A. N. Chernega, R. Gómez, M. L. H. Green, *J. Chem. Soc. Chem. Commun.* **1993**, 1415.
- [110] R. Gómez, R. Duchateau, A. N. Chernega, J. H. Teuben, F. T. Edelmann, M. L. H. Green, *J. Organomet. Chem.* **1995**, *491*, 153–158.
- [111] R. Gómez, M. L. H. Green, J. Haggitt, *J. Chem. Soc. Chem. Commun.* **1994**, 2607.
- [112] H. Fuhrmann, S. Brenner, P. Arndt, R. Kempe, *Inorg. Chem.* **1996**, *35*, 6742–6745.
- [113] J. C. Flores, J. C. W. Chien, M. D. Rausch, *Organometallics* **1995**, *14*, 2106–2108.
- [114] R. Uhrhammer, D. G. Black, T. G. Gardner, J. D. Olsen, R. F. Jordan, *J. Am. Chem. Soc.* **1993**, *115*, 8493–8494.
- [115] A. Martin, R. Uhrhammer, T. G. Gardner, R. F. Jordan, *Organometallics* **1998**, *17*, 382–397.
- [116] H. Brand, J. A. Capriotti, J. Arnold, *Organometallics* **1994**, *13*, 4469–4473.
- [117] A. van der Linden, C. J. Schaverien, N. Meijboom, C. Ganter, A. G. Orpen, *J. Am. Chem. Soc.* **1995**, *117*, 3008–3021.
- [118] F. G. Sernetz, R. Mülhaupt, S. Fokken, J. Okuda, *Macromol.* **1997**, *30*, 1562–1569.
- [119] S. Fokken, T. P. Spaniol, J. Okuda, F. G. Sernetz, R. Mülhaupt, *Organometallics* **1997**, *16*, 4240–4242.
- [120] R. D. J. Froese, D. G. Musaev, T. Matsubara, K. Morokuma, *J. Am. Chem. Soc.* **1997**, *119*, 7190–7196.
- [121] E. E. C. G. Gielens, J. Y. Tiesnitsch, B. Hessen, J. H. Teuben, *Organometallics* **1998**, *17*, 1652–1654.
- [122] B. Rieger, *J. Organomet. Chem.* **1991**, *420*, C17–C20.
- [123] Y.-X. Chen, P.-F. Fu, C. L. Stern, T. J. Marks, *Organometallics* **1997**, *16*, 5958–5963.
- [124] M. J. Sarsfield, S. W. Ewart, T. L. Tremblay, A. W. Roszak, M. C. Baird, *J. Chem. Soc. Dalton Trans.* **1997**, 3097–3104.
- [125] P. Aaltonen, J. Seppälä, L. Matilainen, M. Leskelä, *Macromol.* **1994**, *27*, 3136–3138.
- [126] V. C. Gibson, *J. Chem. Soc. Dalton Trans.* **1994**, 1607.
- [127] T. Miyatake, K. Mizunuma, Y. Seki, M. Kakugo, *Macromol. Chem. Rapid Commun.* **1989**, *10*, 349–352.
- [128] T. Miyatake, K. Mizunuma, M. Kakugo, *Macromol. Chem. Macromol. Symp.* **1993**, *66*, 203–214.
- [129] S. Fokken, T. P. Spaniol, H.-C. Kang, W. Massa, J. Okuda, *Organometallics* **1996**, *15*, 5069.
- [130] L. Porri, A. Ripa, P. Colombo, E. Miano, S. Capelli, S. V. Meille, *J. Organomet. Chem.* **1996**, *514*, 213–217.
- [131] E. B. Tjaden, D. C. Swenson, R. F. Jordan, J. L. Petersen, *Organometallics* **1995**, *14*, 371–386.
- [132] E. B. Tjaden, R. F. Jordan, *Macromol. Symp.* **1995**, *89*, 231–235.
- [133] D. Jones, A. Roberts, K. Cavell, W. Keim, U. Englert, B. W. Skelton, A. H. White, *J. Chem. Soc. Dalton Trans.* **1998**, 255–262.
- [134] T. Repo, M. Klinga, P. Pietikäinen, M. Leskelä, A.-M. Uusitalo, T. Pakkanen, K. Hakala, P. Aaltonen, B. Löfgren, *Macromol.* **1997**, *30*, 171–175.
- [135] X. Bei, D. C. Swenson, R. F. Jordan, *Organometallics* **1997**, *16*, 3282–3302.
- [136] T. Tsukahara, D. C. Swenson, R. F. Jordan, *Organometallics* **1997**, *16*, 3303–3313.
- [137] I. Kim, Y. Nishihara, R. F. Jordan, R. D. Rogers, A. L. Rheingold, G. P. A. Yap, *Organometallics* **1997**, *16*, 3314–3323.
- [138] L. Matilainen, M. Klinga, M. Leskelä, *J. Chem. Soc. Dalton Trans.* **1996**, 219–225.
- [139] J. C. Flores, J. C. W. Chien, M. D. Rausch, *Organometallics* **1994**, *13*, 4140–4142.
- [140] J. C. W. Chien, B.-P. Wang, *J. Poly. Sci. A* **1990**, *28*, 15–38.
- [141] D. J. Crowther, N. C. Baenziger, R. F. Jordan, *J. Am. Chem. Soc.* **1991**, *113*, 1455–1457.
- [142] G. Jiménez Pindado, M. Thornton-Pett, M. Bochmann, *J. Chem. Soc. Dalton Trans.* **1997**, 3115–3127.
- [143] B. Hessen, H. van der Heijden, *J. Am. Chem. Soc.* **1996**, *118*, 11670–11671.
- [144] G. Rodriguez, G. C. Bazan, *J. Am. Chem. Soc.* **1997**, *119*, 343–352.
- [145] G. Rodriguez, G. C. Bazan, *J. Am. Chem. Soc.* **1995**, *117*, 10155–10156.
- [146] A. Pastor, A. F. Kiely, L. M. Henling, M. W. Day, J. E. Bercaw, *J. Organomet. Chem.* **1997**, *528*, 65–75.
- [147] G. C. Bazan, S. J. Donnelly, G. Rodriguez, *J. Am. Chem. Soc.* **1995**, *117*, 2671–2672.
- [148] M. P. Coles, V. C. Gibson, *Polym. Bull.* **1994**, *33*, 529–533.
- [149] D. M. Antonelli, A. Leins, J. M. Stryker, *Organometallics* **1997**, *16*, 2500–2502.
- [150] S. Scheuer, J. Fischer, J. Kress, *Organometallics* **1995**, *14*, 2627–2629.
- [151] K. Mashima, S. Fujikawa, H. Urata, E. Tanaka, A. Nakamura, *J. Chem. Soc. Chem. Commun.* **1994**, 1623.
- [152] K. Mashima, S. Fujikawa, Y. Tanaka, H. Urata, T. Oshiki, E. Tanaka, A. Nakamura, *Organometallics* **1995**, *14*, 2633–2640.
- [153] K. Mashima, Y. Tanaka, M. Kaidzu, A. Nakamura, *Organometallics* **1996**, *15*, 2431–2433.
- [154] K. Hakala, B. Löfgren, *Macromol. Chem. Rapid Commun.* **1997**, *18*, 635–638.
- [155] J. P. Hogan, R. L. Banks (Phillips Petroleum Co.), US-A 2,825,721, **1958** [*Chem. Abstr.* **1958**, *52*, 8621h].
- [156] J. P. Hogan, *J. Poly. Sci. A* **1970**, *8*, 2637.
- [157] K. H. Theopold, *Eur. J. Inorg. Chem.* **1998**, 15.
- [158] K. H. Theopold, *CHEMTECH* **1997**, *27*(10), 26–32.
- [159] F. J. Feher, R. L. Blanski, *J. Chem. Soc. Chem. Commun.* **1990**, 1614.
- [160] F. J. Feher, R. L. Blanski, *J. Am. Chem. Soc.* **1992**, *114*, 5886.
- [161] G. Bhandari, Y. Kim, J. M. McFarland, A. L. Rheingold, K. H. Theopold, *Organometallics* **1995**, *14*, 738–745.
- [162] B. J. Thomas, K. H. Theopold, *J. Am. Chem. Soc.* **1988**, *110*, 5902–5903.
- [163] B. J. Thomas, S. Kyun Noh, G. K. Schulte, S. C. Sendlinger, K. H. Theopold, *J. Am. Chem. Soc.* **1991**, *113*, 893–902.
- [164] P. A. White, J. Calabrese, K. H. Theopold, *Organometallics* **1996**, *15*, 5473–5475.
- [165] V. R. Jensen, K. J. Borge, *Organometallics* **1997**, *16*, 2514–2522.
- [166] Y. Liang, G. P. A. Yap, A. L. Rheingold, K. H. Theopold, *Organometallics* **1996**, *15*, 5284–5286.
- [167] R. Emrich, O. Heinemann, P. W. Jolly, C. Krüger, G. P. J. Verhovnik, *Organometallics* **1997**, *16*, 1511.

- [168] P. W. Jolly, K. Jonas, G. P. J. Verhovnik, A. Dohring, J. Gohre, J. C. Weber (Studiengesellschaft Kohle m.b.H.), WO-A 98/04570, **1998** [*Chem. Abstr.* **1998**, 128, 167817v].
- [169] M. P. Coles, C. I. Dalby, V. C. Gibson, W. Clegg, M. R. J. Elsegood, *J. Chem. Soc. Chem. Commun.* **1995**, 1709.
- [170] G. J. P. Britovsek, V. C. Gibson, B. S. Kimberley, P. J. Maddox, S. J. McTavish, G. A. Solan, A. J. P. White, D. J. Williams, *Chem. Commun.* **1998**, 849–850.
- [171] B. L. Small, M. Brookhart, A. M. A. Bennett, *J. Am. Chem. Soc.* **1998**, 120, 4049.
- [172] B. L. Small, M. Brookhart, *J. Am. Chem. Soc.* **1998**, 120, 7143–7144.
- [173] B. R. James, L. D. Markham, *J. Catal.* **1972**, 27, 442–451.
- [174] T. Yamamoto, A. Yamamoto, S. Ikeda, *Bull. Chem. Soc. Jpn.* **1972**, 45, 1104.
- [175] T. Yamamoto, A. Yamamoto, S. Ikeda, *Bull. Chem. Soc. Jpn.* **1972**, 45, 1111.
- [176] T. Yamamoto, A. Yamamoto, S. Ikeda, *Bull. Chem. Soc. Jpn.* **1975**, 48, 101.
- [177] G. F. Schmidt, M. Brookhart, *J. Am. Chem. Soc.* **1985**, 107, 1433–1444.
- [178] M. J. Tanner, M. Brookhart, J. M. DeSimone, *J. Am. Chem. Soc.* **1997**, 119, 7617–7618.
- [179] M. Brookhart, D. M. Lincoln, *J. Am. Chem. Soc.* **1988**, 110, 8719–8720.
- [180] M. Brookhart, A. F. J. Volpe, D. M. Lincoln, I. T. Horvath, J. M. Millar, *J. Am. Chem. Soc.* **1990**, 112, 5634–5636.
- [181] M. Brookhart, J. M. DeSimone, B. E. Grant, M. J. Tanner, *Macromol.* **1995**, 28, 5378–5380.
- [182] L. Wang, T. C. Flood, *J. Am. Chem. Soc.* **1992**, 114, 3169–3170.
- [183] L. Wang, R. S. Lu, R. Bau, T. C. Flood, *J. Am. Chem. Soc.* **1993**, 115, 6999–7000.
- [184] S. Timonen, T. T. Pakkanen, T. A. Pakkanen, *J. Mol. Catal.* **1996**, 111, 267–272.
- [185] G. Braca, A. M. Raspolli Galletti, M. Di Girolamo, G. Sbrana, R. Silla, P. Ferrarini, *J. Mol. Catal.* **1995**, 96, 203–213.
- [186] U. Klabunde, S. D. Ittel, *J. Mol. Catal.* **1987**, 41, 123–134.
- [187] U. Klabunde, R. Mülhaupt, T. Herskovitz, A. H. Janowicz, J. Calabrese, S. D. Ittel, *J. Poly. Sci. A* **1987**, 1989–2003.
- [188] W. Keim, F. H. Kowaldt, R. Goddard, C. Krüger, *Angew. Chem.* **1978**, 90, 493; *Angew. Chem. Int. Ed. Engl.* **1978**, 17, 466–467.
- [189] G. Wilke, *Angew. Chem.* **1988**, 100, 189; *Angew. Chem. Int. Ed. Engl.* **1988**, 27, 185–206.
- [190] W. Keim, R. Appel, A. Storeck, C. Krüger, R. Goddard, *Angew. Chem.* **1981**, 93, 91; *Angew. Chem. Int. Ed. Engl.* **1981**, 20, 116–117.
- [191] W. Keim, R. Appel, S. Gruppe, F. Knoch, *Angew. Chem.* **1987**, 99, 1042; *Angew. Chem. Int. Ed. Engl.* **1987**, 26, 1012–1013.
- [192] K. A. Ostoja Starzewski, J. Witte, *Angew. Chem.* **1985**, 97, 610; *Angew. Chem. Int. Ed. Engl.* **1985**, 24, 599–601.
- [193] S. Y. Desjardins, K. J. Cavell, J. L. Hoare, B. W. Skelton, A. N. Sobolev, A. H. White, W. Keim, *J. Organomet. Chem.* **1997**, 544, 163.
- [194] L. K. Johnson, C. M. Killian, S. D. Arthur, J. Feldman, E. F. McCord, S. J. McLain, K. A. Kreutzer, M. A. Bennett, E. B. Coughlin, S. D. Ittel, A. Parthasarathy, D. J. Tempel, M. S. Brookhart (DuPont), WO-A 96/23010, **1996** [*Chem. Abstr.* **1996**, 125, 222773t].
- [195] L. K. Johnson, C. M. Killian, M. Brookhart, *J. Am. Chem. Soc.* **1995**, 117, 6414–6415.
- [196] C. M. Killian, D. J. Tempel, L. K. Johnson, M. Brookhart, *J. Am. Chem. Soc.* **1996**, 118, 11664.
- [197] C. Pellicchia, Zambelli, A., *Macromol. Chem. Rapid Commun.* **1996**, 17, 333.
- [198] S. Mecking, L. K. Johnson, L. Wang, M. Brookhart, *J. Am. Chem. Soc.* **1998**, 120, 888.
- [199] L. K. Johnson, S. Mecking, M. Brookhart, *J. Am. Chem. Soc.* **1996**, 118, 267–268.
- [200] L. Deng, T. K. Woo, L. Cavallo, P. M. Margl, T. Ziegler, *J. Am. Chem. Soc.* **1997**, 119, 6177.
- [201] L. Deng, P. M. Margl, T. Ziegler, *J. Am. Chem. Soc.* **1997**, 119, 1094.
- [202] D. G. Musaev, M. Svensson, K. Morokuma, S. Strömberg, K. Zetterberg, P. E. M. Siegbahn, *Organometallics* **1997**, 16, 1933–1945.
- [203] D. G. Musaev, R. D. J. Froese, M. Svensson, K. Morokuma, *J. Am. Chem. Soc.* **1997**, 119, 367.
- [204] J. Feldman, S. J. McLain, A. Parthasarathy, W. J. Marshall, J. C. Calabrese, S. D. Arthur, *Organometallics* **1997**, 16, 1514.
- [205] R. F. de Souza, R. S. Mauler, L. C. Simon, F. F. Nunes, D. V. S. Vescia, A. Cavagnoli, *Macromol. Chem. Rapid Commun.* **1997**, 18, 795.
- [206] K. Ziegler, H.-G. Gellert, K. Zosel, E. Holzkamp, J. Schneider, M. Söll, W.-R. Kroll, *Liebigs Ann. Chem.* **1960**, 629, 121.
- [207] H. Martin, H. Bretinger, *Makromol. Chem.* **1992**, 193, 1283–1288.
- [208] R. Duchateau, A. Meetsma, J. H. Teuben, *Chem. Commun.* **1996**, 223–224.
- [209] M. P. Coles, R. F. Jordan, *J. Am. Chem. Soc.* **1997**, 119, 8125–8126.



3' 5'
 G C
 G C
 T A
 C G
 C G
 G C
 G C
 A T
 C G
 C G



Bleomycin: Synthetic and Mechanistic Studies

Dale L. Boger* and Hui Cai

Bleomycin A₂ is a clinically employed antitumor agent that derives its properties through the sequence-selective cleavage of DNA in a process that is both metal-ion and O₂ dependent. Highlights of the evolution of a modular total synthesis of bleomycin A₂ amenable to the preparation of an

extensive series of analogues are detailed. The implementation of this technology in the preparation of nearly 50 analogues is summarized in efforts that clarify the functional roles of the individual subunits and their substituents. These studies, in conjunction with emerging structural models, define a

remarkable combination of functional, structural, and conformational properties embodied in the natural product.

Keywords: antitumor agent • bioorganic chemistry • bleomycin • DNA cleavage • total synthesis

1. Introduction

The bleomycins are a class of glycopeptide antitumor antibiotics that were isolated by Umezawa and co-workers from *Streptomyces verticellus* over 30 years ago (Figure 1).^[1] Bleomycin A₂ (**1**), which differs from other naturally occurring bleomycins only in the cationic C-terminus, is the major component (70%) of the clinical anticancer drug Blenoxane, which is used for the treatment of Hodgkin's lymphoma, carcinomas of the skin, head and neck, and testicular cancers.^[2–15] Through a series of now classic chemical degradation studies coupled with X-ray crystallographic identification of the products, Umezawa and co-workers established the structure of bleomycin A₂, complete with the assignment of its relative and absolute stereochemistry.^[16] The only exception to the X-ray structure determination of the degradation products was the N-terminus. Its early structural assignment, which contained a β -lactam, was revised to its correct structure in 1978^[17] and its spectroscopically-derived absolute configuration was confirmed in our synthetic efforts.^[18]

Bleomycin A₂ is thought to exert its biological effects through DNA binding and degradation, a process that is metal-ion and oxygen dependent.^[19–26] It cleaves double-strand DNA selectively at 5'-GC or 5'-GT sites by minor groove C4'-H atom abstraction and subsequent fragmentation of the deoxyribose backbone (Scheme 1 and Figure 2).^[27–32]

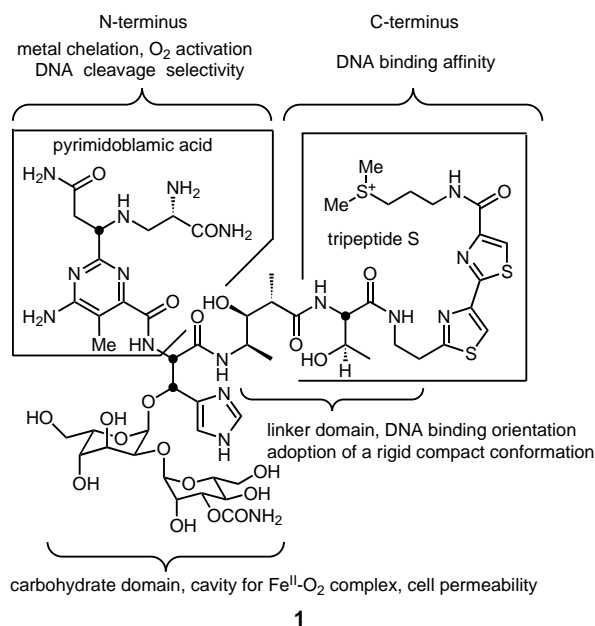
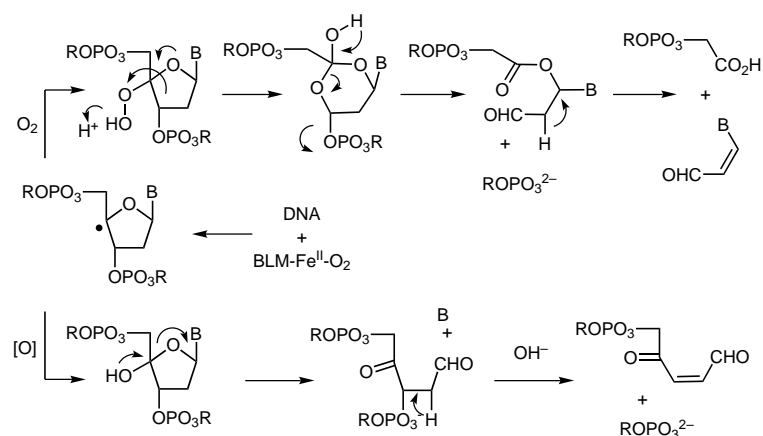


Figure 1. Structure of bleomycin A₂ (**1**) and functional roles of its subunits.

While both single- and double-strand cleavage are observed, the latter has been regarded by many as the biologically more important event.^[10b, 33–41] More recently, bleomycin A₂ has been shown to cleave RNA^[42, 43] as well as DNA-RNA hybrids,^[44] which provide additional nucleic acid targets potentially related to its biological properties.

Each structural unit of bleomycin A₂ contributes importantly to its biological activity (Figure 1). Early and extensive structural,^[45–65] biophysical,^[66–71] chemical,^[6, 72–75] and biological^[76, 77] studies on bleomycin A₂ and its derivatives defined the N-terminal pyrimidine, including its β -aminoalanine

[*] Prof. D. L. Boger, H. Cai
Department of Chemistry and
The Skaggs Institute for Chemical Biology
The Scripps Research Institute
10550 North Torrey Pines Road, La Jolla, CA 92037 (USA)
Fax: (+1) 619-784-7550
E-mail: boger@scripps.edu



Scheme 1. Primary mechanisms for DNA cleavage induced by bleomycin A₂. B = nucleobase, BLM = bleomycin A₂.

amide side chain and the linked β -hydroxy-L-histidine, as the metal binding domain, and demonstrated that the majority of the DNA binding affinity originates from the C-terminus with the bithiazole and the positively charged sulfonium salt. The role of the carbohydrate domain has been less extensively examined although it is known to enhance biological potency and efficacy;^[45, 76, 78, 79] while it does not influence the DNA cleavage selectivity, it does enhance cleavage efficiency. It has also been suggested that the carbohydrate domain facilitates cellular uptake. Although a crystal structure of bleomycin A₂ bound to DNA has not yet become available, several models based on solution structures determined by NMR spectroscopy have been advanced to elucidate the molecular basis of its metal chelation, DNA binding, and cleavage.^[52, 53]

Despite efforts over the past three decades, many key questions remained unanswered at the onset of our inves-

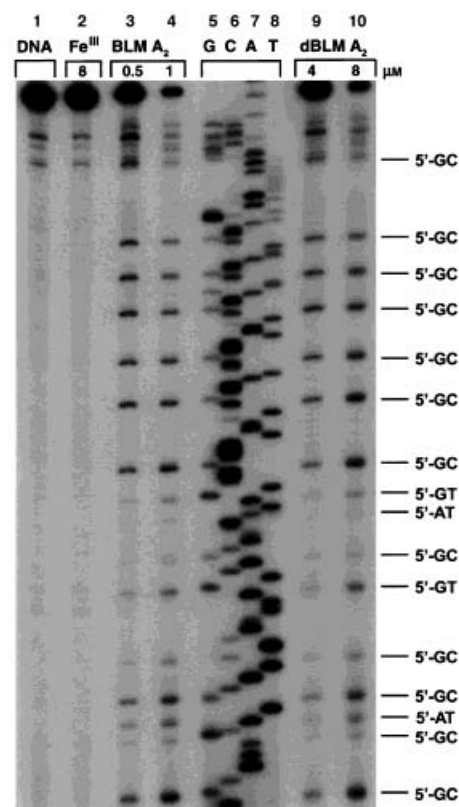


Figure 2. Sequence selective DNA cleavage by bleomycin A₂ (BLM A₂, **1**) and deglycobleomycin A₂ (dBLM A₂, **41**). The products were separated on a polyacrylamide gel by electrophoresis and detected autoradiographically. The untreated DNA was used as a control (lane 1), and its sequence is shown in lanes 5–8. No cleavage was observed on incubation with Fe^{III} ions alone (lane 2). The DNA was cleaved on incubation with BLM A₂ and dBLM A₂ in the presence of Fe^{III} ions (lanes 3 and 4, and 9 and 10, respectively), with the cleavage occurring at the sites labeled and at the concentrations indicated.

Dale L. Boger was born August 22, 1953, received his BSc in chemistry from the University of Kansas (1975) and PhD in chemistry from Harvard University (1980). Immediately after graduate school, he returned to the University of Kansas as a member of the faculty in the Department of Medicinal Chemistry (1979–1985), moved to the Department of Chemistry at Purdue University (1985–1991), and joined the faculty at The Scripps Research Institute (1991 to present) as the Richard and Alice Cramer Professor of Chemistry. His research interests span the fields of organic and bioorganic chemistry and include the development of synthetic methodology, the total synthesis of natural products, heterocyclic chemistry, bioorganic chemistry, medicinal chemistry, the study of DNA–agent and protein–ligand interactions, and antitumor agents.



D. L. Boger



H. Cai

Hui Cai was born April 6, 1968 in Yiyang, Hunan (P.R. China). She received her BSc in chemistry (1989) from Peking University where she also obtained her MSc in polymer chemistry (1992) with Professor Fumian Li. She is presently a PhD graduate student in chemistry at The Scripps Research Institute working on the synthesis and evaluation of enzyme inhibitors and DNA cleaving agents under the guidance of Professor D. L. Boger. Her research interests focus on the design and synthesis of novel molecules as potential antitumor drugs.

tigations. Among them was the nature of the metal-binding ligands and their arrangement in the metal complexes. The possible functional roles of the linker domain and its substituents as well as the disaccharide were untested and even the origin of the sequence selectivity of the DNA cleavage and mechanistic aspects of its double-strand (ds) cleavage remained elusive and controversial. Both the C-terminus bithiazole^[26, 80a] and the N-terminus metal-binding domain^[68, 72, 80b] have been proposed to control the cleavage selectivity, and both bithiazole minor groove binding^[26, 80a] or intercalation^[66, 67c, 77a, 81, 94] have been advanced. Efforts to address these questions were limited by the accessibility of structural analogues because of the inherent complexity of bleomycins. It was in this context that we initiated a program on bleomycin A₂, which has led to the development of an efficient total synthesis and its application in the subsequent design, synthesis, and evaluation of nearly 50 key analogues. The results of our studies are summarized herein.

2. Total Synthesis of (+)-P-3A and Bleomycin A₂

Preceding our efforts, both Umezawa, Ohno et al.^[82] and Hecht et al.^[83] detailed pioneering total syntheses of deglyco-bleomycin A₂ and bleomycin A₂. These efforts have been reviewed elsewhere^[6] and served to confirm the structure of the natural product and define challenges associated with its synthesis. Both were unable to control the stereochemistry at the C2 benzylic center of pyrimidoblastic acid and the diastereomer assignment was accomplished by correlation with the natural product, which precluded confirmation of the original assignment. By virtue of its highly substituted and functionalized nature, even the pyrimidoblastic acid preparation proved challenging and overall yields for the approaches were low. Assemblage and introduction of the disaccharide unit proved problematic and glycosidation of a protected β -hydroxy-L-histidine proved modest (ca. 20%) and proceeded with a lack of diastereoselection at the newly introduced anomeric center. Competitive reactions of the highly functionalized intermediates were addressed with the introduction of protecting groups, which added to the length and complexity of the synthesis. These challenges precluded the extrapolation of the studies to the preparation of a large number of key analogues of the natural product. In the intervening period since the disclosures of Umezawa, Ohno et al. and Hecht et al. that culminated in the total syntheses in 1982, advances in synthetic chemistry provided the opportunity to readdress these challenges and develop an approach amenable to analogue synthesis. Key elements of our approach include a concise and diastereoselective preparation of the fully substituted pyrimidine core, the use of recent advances in acyclic stereocontrol for direct introduction of eight of the acyclic stereogenic centers, a convergent assembly of the C-terminus, and a diastereoselective introduction of the disaccharide by enlisting recent advances in glycosidation methodology.

2.1. Construction of the Pyrimidine Core and Total Synthesis of (+)-P-3A^[18b, 84]

Central to the efforts was the preparation of the pyrimidine core and its attached side chains that constitute the metal binding domain. In this regard, (+)-P-3A (**2**) served as an appropriate initial synthetic target. It is a microbial product isolated in biosynthetic studies of the bleomycins, whose structure was established in an X-ray structure determination of its Cu^{II} complex **2a** (Figure 3).^[85] With the exception of the

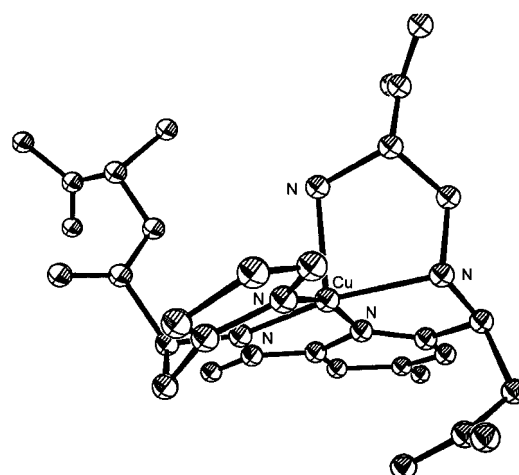
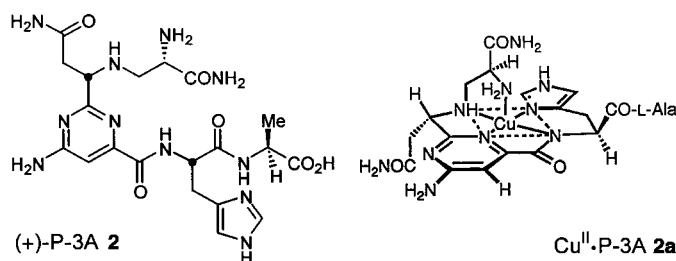


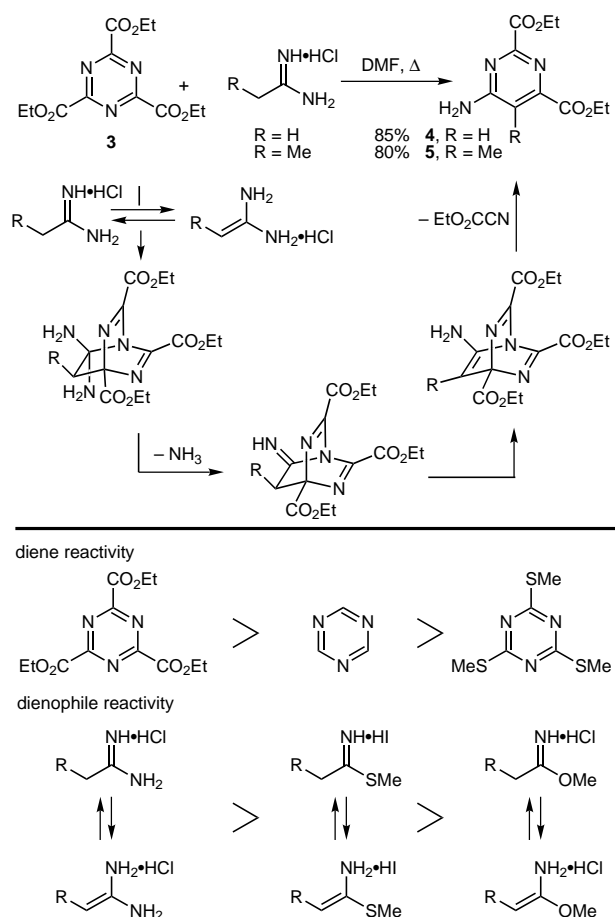
Figure 3. ORTEP representation of the X-ray structure of Cu^{II}·P-3A.

C5 methyl group, **2** contains the functionalized pyrimidine core of bleomycin A₂ and represents the simplest member of this class of agents. Although still an unresolved matter, the



Cu^{II} complex of P-3A is taken to represent the metal-ligated atoms of the iron and copper complexes of bleomycin A₂ and their activated intermediates. Presumably, oxygen complexation and activation occurs *trans* to the axial amine of the distorted square-planar metal complex. Since the disclosure of the X-ray structure in 1978 by Umezawa, spectroscopic studies of various metal complexes as well as those of simple models have been described.^[31a, 68, 73, 74] While most, including model Co^{III}-OOH metal complexes,^[52] support the ligated atoms observed with Cu^{II}-P-3A, alternatives have been advanced for bleomycin A₂. The potential for the disaccharide carbamoyl group to replace the axial amine as a ligand has been implicated in studies of Zn^{II}^[53, 60a, 61a] and Fe^{II}-(CO)^[60b] metal complexes, and the complexation of the deprotonated amide had been questioned.^[61a, b]

Key to the synthesis of **2** was the preparation of a fully substituted pyrimidine at the core of the structure. An effective one-step approach was devised based on an inverse electron demand Diels–Alder reaction of 1,3,5-triazines^[86] (Scheme 2). The in-situ thermal reaction of amidines with symmetrical 1,3,5-triazines^[87] provides substituted 4-amino-pyrimidines in excellent yields; the reaction proceeds with an amidine to 1,1-diaminoethene tautomerization, [4+2] cycloaddition with the 1,3,5-triazine, loss of ammonia from the Diels–Alder adduct, imine to enamine tautomerization, and

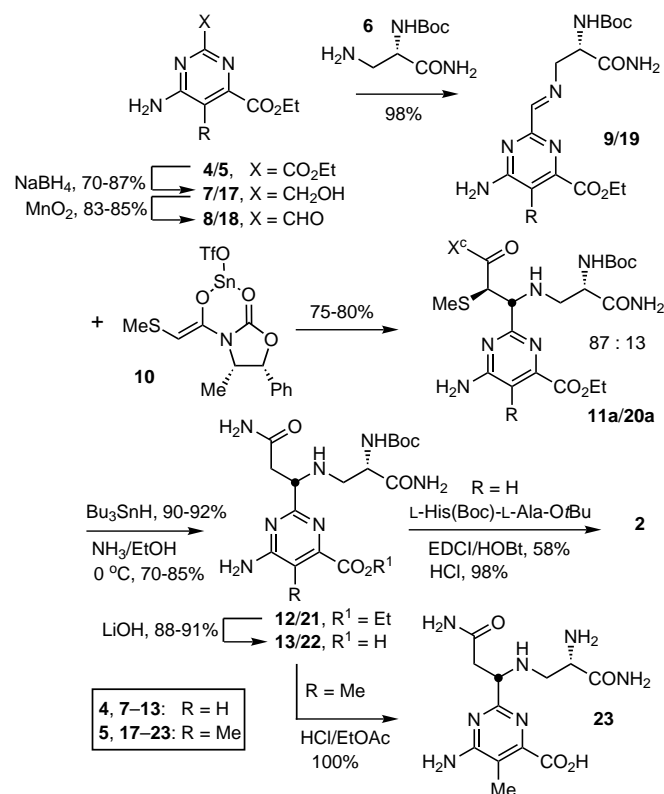


Scheme 2. Diels–Alder reaction of 1,3,5-triazine with amidine. DMF = dimethylformamide.

loss of ethyl cyanofornate through a retro Diels–Alder reaction. A comparative examination of amidines, thioimides, and imides revealed that amidines are uniquely suited for use in this reaction cascade. The reaction proceeds best with the amidine hydrochloride salts at intermediate reaction temperatures in polar, aprotic solvents. The reaction is invariant to the ratio of dienophile–diene used, and it is subject to triazine substituent effects, which are characteristic of an inverse electron demand Diels–Alder reaction.^[87]

Based on this cyclization, 2,4,6-triethoxycarbonyl-1,3,5-triazine (**3**) was treated with acetamidine hydrochloride to provide **4** (Scheme 2). A selective differentiation of the C2 and C4 ethyl esters was accomplished through low temperature NaBH₄ reduction of the more electrophilic C2 ester to

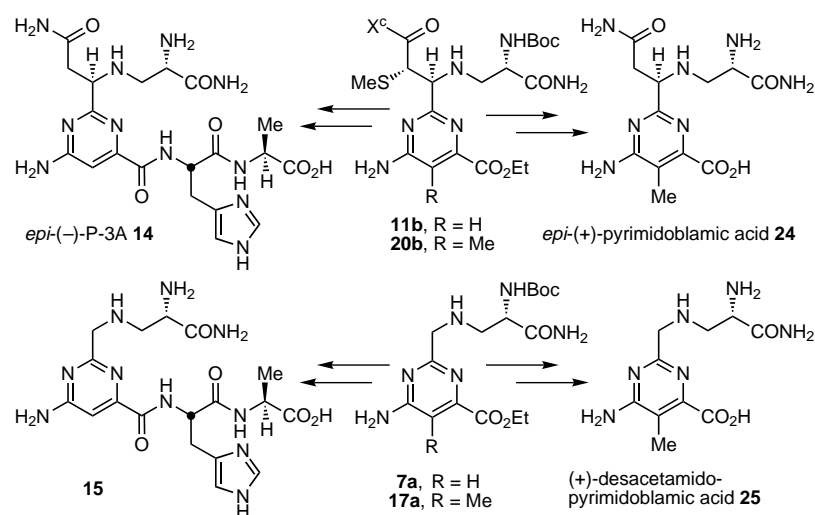
provide **7** (Scheme 3). The remaining strategic element was the stereocontrolled introduction of the C2-acetamido side chain. Previous studies employed nonselective approaches that required a separation of the resulting 1:1 mixture of diastereomers. In our studies, optically active *N*-acyloxazolidinones were found to provide a diastereoselective imine addition reaction suitable for the introduction of a C2-acetamido side chain.^[88] Thus, oxidation of **7** with MnO₂ followed by condensation of aldehyde **8** with *N*^α-Boc-β-amino-L-alanine amide (**6**) provided **9**. Treatment of imine **9**



Scheme 3. Total synthesis of (+)-P-3A (**2**) and (–)-pyrimidinoblastic acid (**23**). Boc = *tert*-butoxycarbonyl, EDCI = 1-(3-dimethylaminopropyl)-3-ethylcarbodiimide hydrochloride, HOBT = 1-hydroxy-1*H*-benzotriazole, Tf = trifluoromethanesulfonyl, X^c = chiral oxazolidinonyl.

with the stannous (*Z*)-enolate **10** provided the desired *anti* imine adduct **11a** accompanied by a small amount of the alternative and separable *anti* addition product **11b** (87:13). Reductive desulfurization of the major diastereomer **11a** and aminolysis afforded **12**. Ethyl ester hydrolysis and coupling of **13** with L-His(Boc)-L-Ala-OrBu provided the penultimate precursor in a reaction that was conveniently conducted without protection of the unreactive aryl amine or hindered secondary amine. A final acid-catalyzed deprotection provided (+)-P-3A (**2**).

The minor *anti* addition product that possesses the unnatural stereochemistry at the C2 benzylic center was converted to *epi*-(–)-P-3A (**14**)^[18b] and the product (**7a**) of the displacement of the primary tosylate derived from **7** with **6** was converted into (–)-desacetamido P-3A (**15**, Scheme 4).^[84]

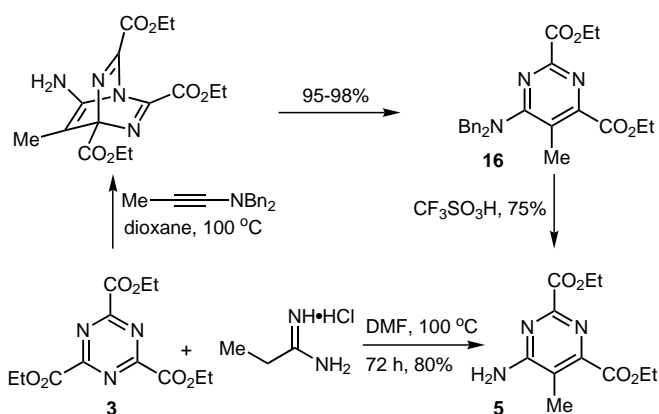


Scheme 4. Synthesis of *epi*-(-)-P-3A (**14**), (-)-desacetamido-P-3A (**15**), *epi*-(+)-pyrimidoblamic acid (**24**), and (+)-desacetamidopyrimidoblamic acid (**25**).

2.2. Synthesis of (-)-Pyrimidoblamic Acid^[18d]

The core structure of (-)-pyrimidoblamic acid was assembled through two complementary [4+2] cycloadditions of 2,4,6-triethoxycarbonyl-1,3,5-triazine (**3**) (Scheme 5). Thermal treatment of **3** with 1-(*N,N*-dibenzylamino)propyne and acid-catalyzed debenzylation of **16** provided **5**. Alternatively, **5** was derived more directly through the one-pot reaction cascade of an inverse electron demand Diels–Alder reaction between **3** and propionamidine hydrochloride.

Differentiation of the C2 and C4 esters was accomplished by selective reduction of the sterically more accessible and electronically more reactive C2 ester of **5** to provide **17**



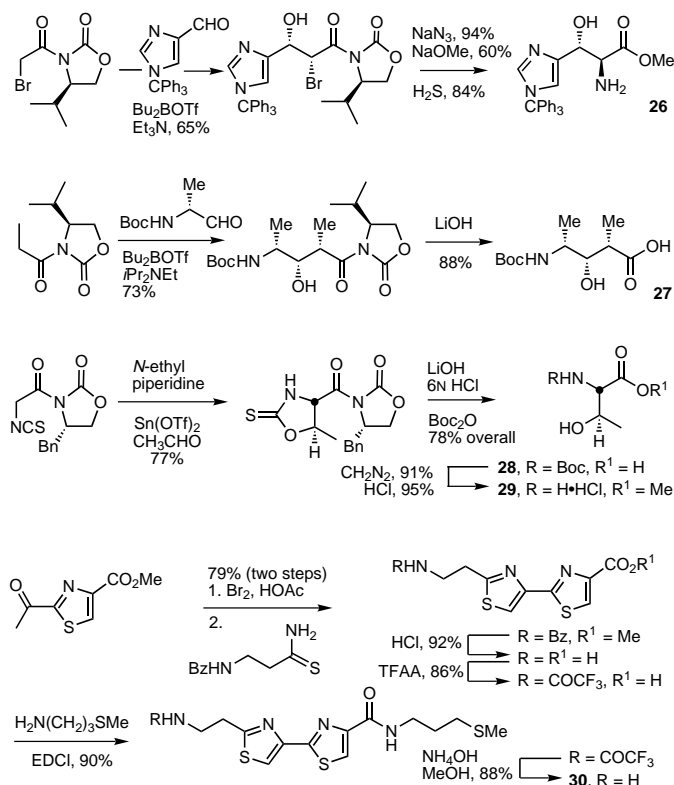
Scheme 5. Synthesis of the pyrimidine core. Bn = benzyl.

(Scheme 3). Diastereoselective addition of the stannous (*Z*)-enolate **10** with imine **19**, generated by MnO₂ oxidation and subsequent condensation of **18** with **6**, provided **20a** as the major *anti* addition product (87:13 diastereoselection). Reductive desulfurization, aminolysis, ester hydrolysis, and deprotection of the *N*-Boc group afforded (-)-pyrimidoblamic acid (**23**). An important ramification of these studies was the confirmation of Umezawa's spectroscopic assignment of the absolute configuration at the C2 benzylic center.

The minor *anti* diastereomer **20b** derived from the imine addition reaction was converted into *epi*-(+)-pyrimidoblamic acid (**24**). Displacement of the primary tosylate derived from **17** with **6** gave the substitution product **17a**, which was then used to prepare (+)-desacetamidopyrimidoblamic acid (**25**, Scheme 4).

2.3. Assembly of the C Terminus: Synthesis of Tri-, Tetra-, and Pentapeptide S^[18c, 89]

Concise diastereocontrolled syntheses of the C-terminus subunits **26**–**30**, which incorporated seven of the acyclic stereogenic centers were accomplished as described in Scheme 6. The *erythro*-β-hydroxy-L-histidine subunit **26** was prepared in four steps through adaptation of the approach of Ohno et al.^[90] with mod-



Scheme 6. Synthesis of the C-terminus subunits. Bz = benzoyl, TFAA = trifluoroacetic anhydride.

ifications in which the competitive retro aldol reaction was suppressed during the azide displacement reaction. The (2*S*,3*S*,4*R*)-4-amino-3-hydroxy-2-methylpentanoic acid subunit **27** was synthesized in two steps through a diastereoselective *syn* aldol addition of a boron-(*Z*)-enolate with *N*-Boc-D-amino-1-propanol followed by hydrolysis of the chiral auxiliary. Similarly, the L-threonine subunits **28** and **29** were prepared through diastereoselective *syn* aldol addition of a *N*-acyloxazolidinone stannous (*Z*)-enolate with acetaldehyde following a procedure detailed by Evans et al.^[91] The bithia-

Tripeptide S (**32**) was assembled by coupling **28** with **30** followed by S-methylation and N-Boc deprotection (Scheme 7). Complementary to a linear synthesis of tetrapeptide S based on the coupling of a tripeptide S precursor and **27** as detailed in the efforts of Umezawa et al. and Hecht et al.,^[82, 83] a convergent preparation was employed in our studies. Coupling of **27** with **29** (\rightarrow **33**) followed by methyl ester hydrolysis (\rightarrow **34**), further coupling with **30**, S-methylation, and N-Boc deprotection provided tetrapeptide S (**37**). While the introduction of the sulfonium salt was postponed to a latter stage in preceding efforts, its earlier introduction

One issue addressed with the C-terminus and its analogues was the role the linking chain and its substituents may play in the expression of the bleomycin A₂ properties. Central to any interpretation is their impact on the DNA binding affinity and selectivity. Consequently, the calf thymus DNA binding constants and the binding site size for bleomycin A₂, deglycobleomycin A₂, the Boc derivatives of di-, tri-, tetra-, pentapeptide S, and their analogues were determined through measurement of the quenching of the bithiazole fluorescence upon binding.^[18c] The Boc derivatives were selected for study rather than the free amines since they closely reflect the subunits as they are found in the natural product. Representative comparisons are summarized in Table 1 and over 15

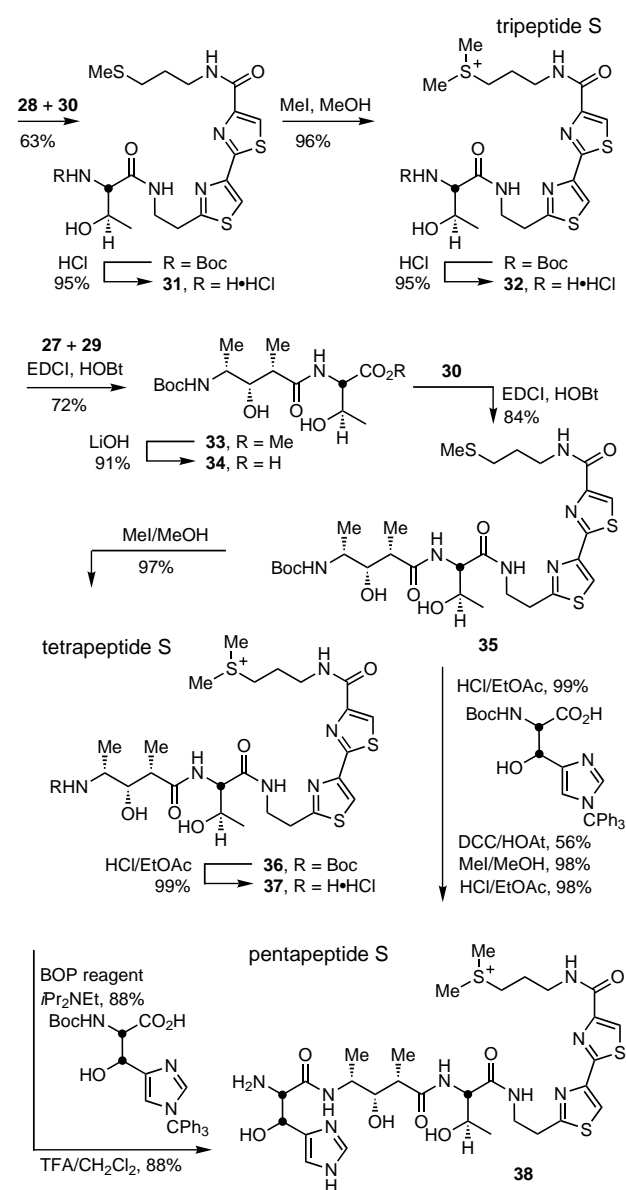
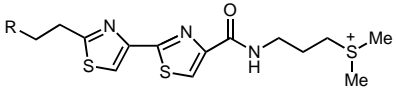
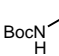
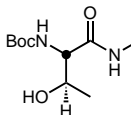
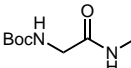
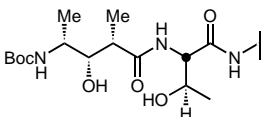
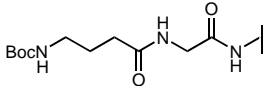
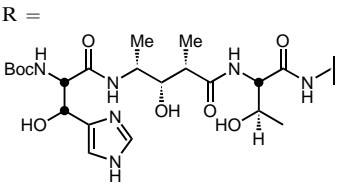


Table 1. Apparent DNA binding constants of bleomycin A₂ (**1**) and key partial structures to calf thymus DNA.

Agent	Formula	K_B [10^5 M^{-1}] ^[a]	L [bp] ^[b]
bleomycin A ₂	1	1.0	3.8
deglycobleomycin A ₂	41	1.1	3.9
			
dipeptide S	R = 	0.10	2.2
tripeptide S	R = 	0.26	3.6
	R = 	0.18	2.7
tetrapeptide S	R = 	0.21	3.7
	R = 	0.20	3.5
pentapeptide S	R = 	0.23	4.2

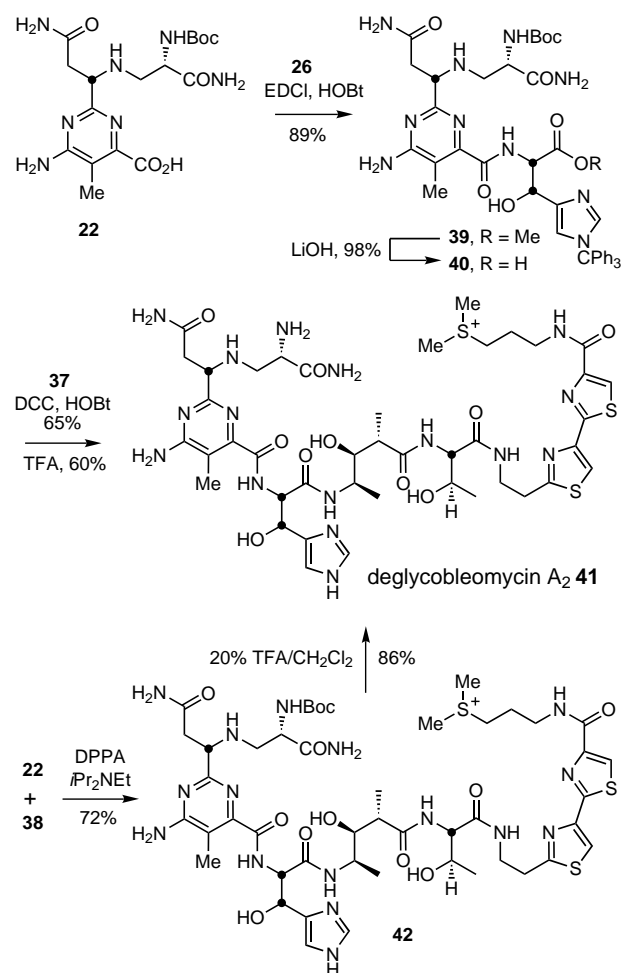
[a] K_B = apparent binding constant. [b] L = length of the binding site (base pairs) in DNA.

analogues of the C-terminus were examined, which complement and extend past studies.^[66, 77, 93, 94] *N*-Boc-tripeptide S, *N*-Boc-tetrapeptide S, and *N*-Boc-pentapeptide S exhibited near identical binding constants, which were greater than that of *N*-Boc-dipeptide S and only slightly lower than that of bleomycin A₂ or deglycobleomycin A₂. The comparisons indicate that the disaccharide is not contributing to the binding affinity, that the majority of the affinity is derived from tripeptide S, that the substituted pentanoic acid and β -hydroxy-L-histidine subunits are not contributing to DNA binding affinity, and infer that the N-terminus pyrimidoblastic acid subunit contributes the remaining affinity that is observed with deglycobleomycin A₂. The observation that removal of the hydroxyethyl substituent of tripeptide S lowers the binding affinity, while the removal of all the tetrapeptide S substituents does not, suggests that the L-threonine subunit productively interacts with DNA, that the L-threonine hydroxyethyl substituent may attenuate the binding, and that the remaining linking chain substituents do not contribute to binding. With the possible exception of the L-threonine substituent, this suggests that their effects on cleavage efficiency are not a consequence of stabilizing binding interactions with DNA. In addition, the binding site sizes corresponded nicely to the estimated size of bleomycin A₂ independently established by other techniques.^[66, 77, 93, 94] Consistent with conclusions drawn from the binding constants, the binding site sizes also suggested that the tripeptide S subunit is fully bound to DNA, that the L-threonine substituent may detectably affect the interaction with DNA, but that the remaining tetrapeptide S or pentapeptide S substituents do not substantially alter the binding site size or tripeptide S binding mode. Alternative substitutions of the pentanoic acid subunit had little effect on the binding affinity ($K_B = 0.18\text{--}0.23$ versus $0.21 \times 10^5 \text{ M}^{-1}$) or binding site size (3.5–3.9 versus 3.7 base pairs (bp)) and greater variations were observed with agents lacking the tripeptide S hydroxyethyl substituent.

Although these studies preceded recent NMR structural models,^[52, 53] the observations were interpreted to indicate that the significant reductions in the DNA-cleavage efficiencies observed with agents that incorporated modifications in the linking chain were not the result of an altered binding affinity or altered tripeptide S binding mode, but rather were related to conformational effects of the linking chain substituents and implicated a compact, DNA-bound conformation, which enlisted a turn at the threonine–valerate site.^[18c] With the availability of recent structural models, this may now be more definitively attributed to their role in the preorganization of bleomycin A₂ into such a compact conformation productive for DNA cleavage (see Section 3.3).

2.4. Total Syntheses of Deglycobleomycin A₂^[18a, c]

With the key intermediates available, the synthesis of deglycobleomycin A₂ was in hand. Coupling of *N*^α-Boc-pyrimidoblastic acid (22) with 26 provided 39 (Scheme 8). Hydrolysis of the ester and coupling of 40 with tetrapeptide S (37) that contained the intact sulfonium salt, followed by deprotection afforded deglycobleomycin A₂ (41). Alterna-



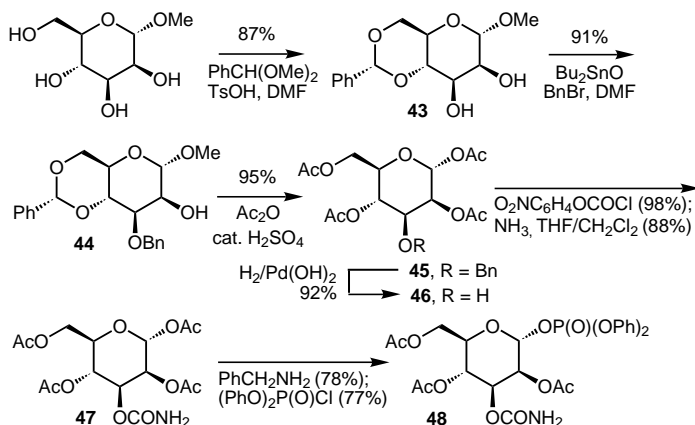
Scheme 8. Total syntheses of deglycobleomycin A₂. DPPA = diphenylphosphoryl azide.

tively, the coupling of pentapeptide S (38) with 22 proceeded smoothly to provide *N*^α-Boc-deglycobleomycin A₂ (42) when treated with DPPA.^[105] This was accomplished with the sulfonium salt installed, with only one protecting group in the reacting substrates, without deliberate protection of the imidazole, and without observation of competitive imidazole acylation. Acid-catalyzed deprotection of 42 provided deglycobleomycin A₂ (41). Typically, the more convergent synthesis with 40 has been employed in our preparation of deglycobleomycin A₂ analogues, while the approach that proceeds through 42 is especially convenient for those that incorporate changes in the pyrimidoblastic acid subunit.

2.5. Disaccharide Preparation and Total Synthesis of Bleomycin A₂^[18f]

The D-mannose subunit 48 was prepared from D-mannose itself through selective C3-functionalization. In addition, the intermediate 48, which serves as the mannose-derived glycosyl donor, was designed to use a C2 acetate to control the stereochemistry of the disaccharide glycosidation reaction. Alkylation of the 2,3-*O*-dibutylstannylene derived from the reaction of 43 with Bu₂SnO and benzyl bromide cleanly

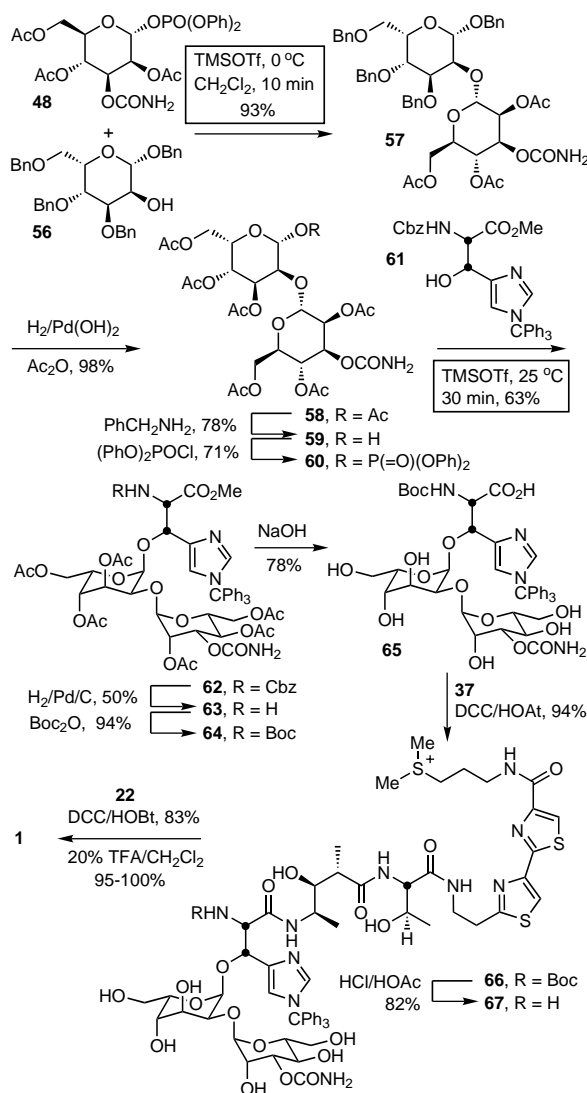
Scheme 10. Synthesis of the L-gulose subunit. Py = pyridine.



Scheme 9. Synthesis of the D-mannose subunit. Ts = toluene-4-sulfonyl.

Past efforts to prepare a suitably protected L-gulose derivative employed a six-step synthesis from the rare L-gulose (3–4% overall yield) or the successive head-to-tail inversion of α -D-glucofuranose with interconversion of the C1 and C6 oxidation states.^[82, 83] Our approach used a D-mannose precursor with the correct C1–C4 stereochemistry and a simple inversion of the C5 stereochemistry for interconversion of D-mannose to L-gulose. Thus, protection of the C4 and C6 hydroxyl groups of benzyl α -D-mannopyranoside to give acetal **49**, followed by selective equatorial C3 hydroxyl benzylation through alkylation of the intermediate 2,3-*O*-dibutylstannylene provided **50** (Scheme 10). Acetylation of the C2 alcohol followed by acetal hydrolysis and conversion of **51** into the corresponding primary iodide followed by HI elimination provided **53**. Rh^I-catalyzed hydroboration and oxidation of **53** cleanly provided **54**, with inversion of the C5 stereochemistry in a reaction that proceeded with a diastereoselection of $\geq 50:1$. Benzylation of **54** followed by acetate methanolysis provided **56** and a suitable L-gulose glycosyl acceptor for disaccharide coupling.

Disaccharide formation, with **56** serving as the glycosyl acceptor and **48** serving as the glycosyl donor, cleanly provided **57** (Scheme 11). The use of the diphenylphosphate **48** provided **57** under milder reaction conditions (0 versus 25 °C), in much shorter reaction times (10 min versus 10–36 h), and in higher conversions (94 versus 74–78 %) relative to the glycosyl bromide. Notably, the carbamoyl group could be taken through this glycosidation reaction without protection or competitive reactions. The exclusive retention of the α linkage may be attributed to neighboring group participation of the mannose C2' acetate group, which provides clean



Scheme 11. Final stages of total synthesis of bleomycin A₂ (**1**). Cbz = benzyloxycarbonyl, HOAt = 7-aza-1-hydroxy-1*H*-benzotriazole, TMS = trimethylsilyl.

retention of the C1' stereochemistry. Debenzylation of **57** followed by acetylation provided **58** in superb conversions, and activation as the α -glycosyl diphenylphosphate **60** was accomplished by sequential treatment with benzylamine and $(\text{PhO})_2\text{P}(\text{O})\text{Cl}$. The O-glycosidation reaction was conducted with **60** and *N*-Cbz- β -hydroxy-L-His(CPh₃) methyl ester (**61**) to provide adduct **62** under exceptionally mild conditions (25 °C, 30 min) in excellent conversion (63 %) as a greater than 13:1 mixture of the desired α and undesired β linked anomers. The initial approaches that enlisted glycosyl halide activation required prolonged reaction times, proceeded in much lower conversions, and produced a mixture of diastereomers. The high diastereoselectivity of this glycosidation reaction may be attributed to the low reactivity of the glycosyl acceptor, which favors formation of the most stable α anomer, and mechanistic characteristics of a glycosyl phosphate acceptor, which favor inversion of the stereochemistry at the reacting anomeric center. Selective Cbz deprotection without competitive hydrogenolysis of the trityl protecting group, *N*-Boc protection of the amine, and exhaustive ester hydrolysis provided **65** suitably protected for sequential couplings with tetrapeptide S and *N*^α-Boc-pyrimidoblastic acid.

The coupling of **65** with tetrapeptide S (**37**) provided **66** in superb yield without deliberate protection of the disaccharide or the hydroxyl groups of tetrapeptide S and was conducted with the sulfonium salt installed. Mild acid treatment of **66** under conditions defined by Sieber and Riniker^[95] cleanly provided **67** by removal of the Boc protecting group without deglycosidation or removal of the trityl protecting group. Subsequent coupling of **67** with *N*^α-Boc-pyrimidoblastic acid (**22**) and final acid-catalyzed deprotection provided bleomycin A₂ (**1**), identical in all respects with the natural material.

3. Probing the Functional Roles of the Bleomycin A₂ Subunits

The completion of a modular and convergent total synthesis of bleomycin A₂ provided a unique foundation upon which many analogues that contained single-point changes were prepared in efforts to answer key questions concerning metal chelation, oxygen activation, DNA binding, and the origin of sequence-selective DNA cleavage.

3.1. The Carbohydrate Domain

Of all the bleomycin A₂ subunits the role of the disaccharide is the most poorly understood. Although it is known not to impact on the cleavage selectivity (5'-GC, 5'-GT), it does account for subtle differences in the relative selectivity among the available sites.^[76, 96] It is also known to enhance biological potency and efficacy and make significant contributions to the DNA cleavage efficiency and ratio of ds to ss cleavage. Although there are many plausible explanations, the mannose C3-carbamoyl group had been implicated in the metal complexation that affected the structure and reactivity of the metal complexes.^[6, 45a, 61a,b] It had also been suggested that the bulky disaccharide serves the role, in conjunction with the

C2-acetamido side chain, of forming one side of a pocket to protect the reactive intermediates.^[45b, 73f, 78] To start addressing these questions, the impact of the individual disaccharide subunits was assessed through the synthesis and evaluation of three key analogues.

3.1.1. Demannosylbleomycin A₂^[97]

The analogue **77** lacks the terminal α -D-mannopyranoside unit and permits the establishment of its role, including that of the carbamoyl group, as a putative sixth ligand for metal complexation. To insure that the liberated L-gulose C2 alcohol would not affect the comparisons, it was capped as a methyl ether. The agent was prepared through diastereoselective O-glycosidation of **61** with the glycosyl diphenylphosphate of 3,4,6-tri-*O*-acetyl-2-*O*-methyl- β -L-gulopyranose (**70**), followed by adjustment or removal of the protecting groups and sequential couplings with tetrapeptide S and *N*^α-Boc-pyrimidoblastic acid (Scheme 12). The glycosidation reaction proceeded under exceptionally mild conditions (−15 °C, 30 min) in superb yield (65–72 %) with clean inversion of the stereochemistry at the glycosyl C1 position ($\geq 20:1 \alpha:\beta$) to provide **71**. Both the low reactivity of the glycosyl acceptor **61** and mechanistic features of a glycosyl phosphate donor, which favor inversion of the stereochemistry at the reacting center, account for the clean generation of **71**.

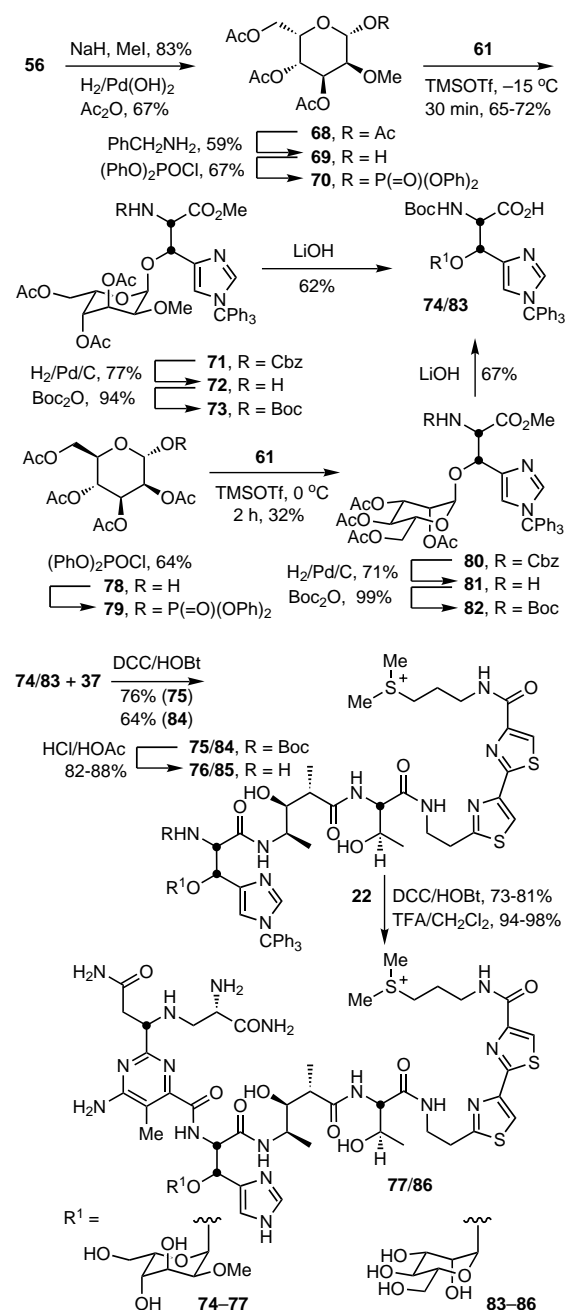
3.1.2. α -D-Mannopyranosyldeglycobleomycin A₂^[97]

The analogue **86** bears a monosaccharide in which the single C5 stereocenter of α -L-gulopyranoside has been inverted to provide a linked α -D-mannopyranoside. Glycosidation of **61** with the glycosyl diphenylphosphate of 2,3,4,6-tetra-*O*-acetyl- α -D-mannopyranose, which proceeded with net retention of the glycosyl C1 stereochemistry by virtue of participation of the neighboring C2 acetate group, provided **80** without detection of isomeric products (Scheme 12). Adjustment or removal of the protecting groups and sequential couplings with **37** and **22** provided **86**.

3.1.3. Deshydroxydeglycobleomycin A₂^[98]

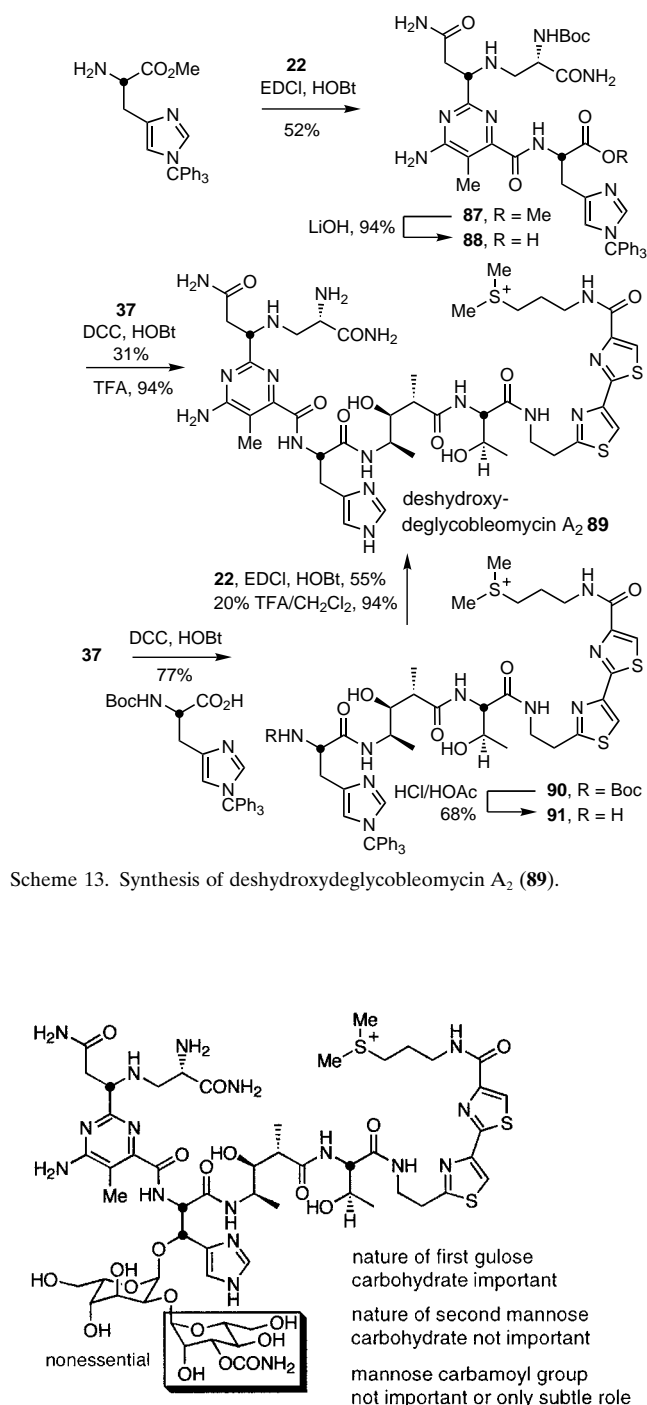
It was conceivable that the distinction between bleomycin A₂ and deglycobleomycin A₂ rested not with the removal of the disaccharide but rather with the liberation of the free alcohol of the β -hydroxy-L-histidine subunit. Therefore, deshydroxydeglycobleomycin A₂ (**89**), in which this alcohol was removed, was prepared for comparison (Scheme 13). Two approaches were used. The first was conducted by the coupling of **88** with tetrapeptide S and suffered partial racemization. Simply reversing the order of couplings such that the L-His carboxylate group was activated with a *N*-carbamoyl instead of the *N*-acyl group provided a more effective route to **89**.

The DNA cleavage efficiency, selectivity, and ds:ss cleavage ratio of demannosylbleomycin A₂ (**77**) proved similar or indistinguishable from bleomycin A₂ (**1**), which indicated that the terminal 2-*O*-(3-*O*-carbamoyl)- α -D-mannopyranoside, inclusive of the carbamoyl group, has little impact on the DNA



Scheme 12. Synthesis of demannosylbleomycin A₂ (77) and α-D-mannosyldeglycobleomycin A₂ (86).

cleavage properties (Figure 4). In contrast, the decreased efficiency of DNA cleavage and ds:ss cleavage ratio of **86**, which proved less effective than even deglycobleomycin A₂, indicate that the first carbohydrate of the disaccharide may greatly influence the properties. Similarly, deshydroxydeglycobleomycin A₂ (**89**) proved indistinguishable or slightly less effective than deglycobleomycin A₂, which indicates that it is the removal of the disaccharide and not the release of the L-histidine β-hydroxyl group that is responsible for its diminished DNA-cleavage properties. Importantly, these studies implicate the α-L-gulopyranoside and not the α-D-mannopyranoside inclusive of the carbamoyl group as the important disaccharide component required for full potentiation of the DNA-cleavage efficiency of bleomycin A₂.



Scheme 13. Synthesis of deshydroxydeglycobleomycin A₂ (89).

Agent	Efficiency	ds:ss	Selectivity
bleomycin A ₂ (1)	2 – 5	1 : 6	5'-GC, 5'-GT > 5'-GA
demannosyl bleomycin A ₂ (77)	2 – 4	1 : 7	5'-GC, 5'-GT > 5'-GA
α-D-mannosyl deglycobleomycin A ₂ (86)	0.6 – 1	1 : 20	5'-GC, 5'-GT > 5'-GA
deglycobleomycin A ₂ (41)	1	1 : 12	5'-GC, 5'-GT > 5'-GA
deshydroxy deglycobleomycin A ₂ (89)	0.75	1 : 12	5'-GC, 5'-GT > 5'-GA

Figure 4. DNA cleavage properties of bleomycin A₂ derivatives with modified disaccharide subunits. The results for bleomycin A₂ (**1**) and deglycobleomycin A₂ (**41**) show that the presence of the complete disaccharide subunit increases the cleavage efficiency two- to fivefold while the ratio of double strand to single strand cleavage doubles.

In support of the studies, recent structural studies from the Stubbe group completed subsequent to our studies demonstrated that the Co^{III} -OOH complexes of bleomycin A_2 and deglycobleomycin A_2 bind to an oligonucleotide cleavage site in identical manners, but **41** binds with a lower affinity ($30 \times$).^[52] The molecules adopt a compact conformation in the minor groove with partial intercalation of the bithiazole at the base pair 3' to the site of cleavage and with the metal-bound peroxide positioned in close proximity to the C4' hydrogen atom of the cleavage site. The disaccharide is located on the outer face of the minor groove and shields the complex from solvent (Figure 5). The primary amino group of the β -amino-

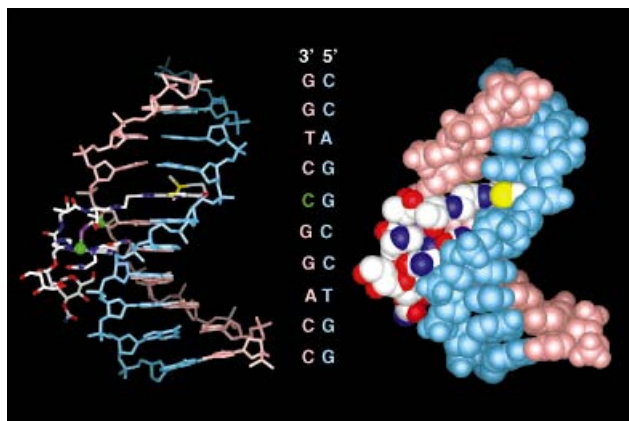


Figure 5. Model of Co^{III} -OOH bleomycin A_2 bound to DNA as determined by NMR spectroscopy.^[52]

alanineamido side chain of pyrimidoblastic acid but not the mannose C3-carbamoyl group is the axial ligand. These and related studies suggest that the mannose C3-carbamoyl group probably does not contribute to metal complexation, that the disaccharide may contribute protective stabilization and possibly enhanced facility for adoption of a productive DNA-bound conformation, and that deglycobleomycin A_2 may serve as a simplified model that provides relevant information on the interaction of bleomycin A_2 with DNA.

The observation that the Co^{III} -OOH complex of bleomycin A_2 bound 30 times more effectively than deglycobleomycin A_2 at a single oligonucleotide cleavage site was attributed to weak, nonselective contacts of the terminal mannose with the hydrophobic chain of the DNA backbone. The generality of such observations, which appear to contradict the effective properties of **77**, which lacks this terminal sugar, is under study.

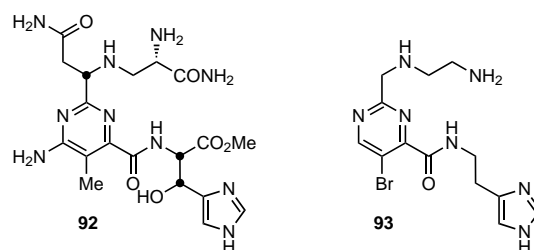
3.2. The Metal Binding Domain

Central to the properties of bleomycin A_2 is the metal chelation and subsequent O_2 activation. A commonly accepted depiction of the metal chelation is derived from the X-ray structure of Cu^{II} -P-3A, which shows the primary and secondary amine groups of the β -aminoalanineamide side chain, the N1 atom of the pyrimidine, the N3 atom of the imidazole from L-histidine, and its deprotonated amide are coordinated to the metal in a square-planar complex with the

primary amine occupying an axial coordination site^[85] (see Figure 3). NMR^[52–65] and related spectroscopic studies^[66–72] on a range of bleomycin A_2 metal complexes have contributed to the consensus that the pyrimidine, imidazole, and secondary amine are bound to the metal. While our studies together with those of others suggest that the mannose C3-carbamoyl group does not contribute to metal chelation and that the axial ligand is the primary amine of the β -aminoalanine, the additional metal ligand(s) remained ambiguous. In addition, the origin of the DNA cleavage selectivity remained unresolved at the start of our studies although the contribution that the metal binding domain makes to DNA binding affinity and polynucleotide recognition have been an active topic of investigation.^[68, 72, 80] Both the C-terminus^[26, 80a] and the N-terminus metal binding domain^[68, 72, 80b] has been suggested to be independently responsible for the 5'-GC/5'-GT cleavage selectivity. Consequently, a number of agents that directly address the issues of metal chelation and origin of DNA recognition have been examined.

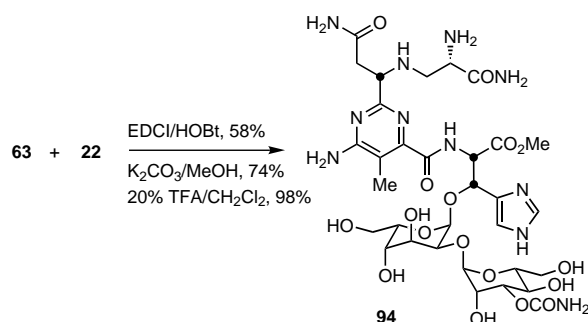
3.2.1. Full Metal Binding Domain^[100]

One important issue addressed in early studies was the DNA-cleavage properties of the metal binding domain itself. Although both Hecht et al.^[72] and later Mascharak et al.^[68] have advanced the proposal that the metal binding domain controls the DNA-cleavage selectivity, a structural origin of the polynucleotide recognition was not defined. Moreover, reports from Hecht et al.^[5b] that Fe complexes of **92**, the metal



binding domain alone, and related agents that constitute the N-terminus fail to cleave DNA above the background level of iron cleavage, while the simplified models including **93** described by Mascharak et al. produce a cleavage pattern similar, but not identical, to bleomycin A_2 remained unresolved.^[99] In efforts to address these issues and to assess the polynucleotide recognition features of the metal binding domain, the synthesis of the fully functionalized N-terminus metal binding domain complete with the linked 2-O-(3-O-carbamoyl- α -D-mannopyranosyl)- α -L-gulopyranosyl disaccharide (**94**), was conducted.^[100]

The synthesis is outlined in Scheme 14 from **22** and **63**, which were prepared in nine steps (20–25% overall) and seven steps (16–19% overall), respectively. Coupling of N^{α} -Boc-pyrimidoblastic acid (**22**) with **63**, followed by methanolysis of the six O acetate groups by treatment with powdered K_2CO_3 in CH_3OH , and acid-catalyzed deprotection provided **94**. For comparison, **92** was prepared by the acid-catalyzed deprotection of **39** (20% TFA/ CH_2Cl_2 , 95%).



Scheme 14. Synthesis of the full metal binding domain of bleomycin A₂ (**94**).

Unlike **92** the Fe^{II} complex of the full metal binding domain **94** was found to cleave DNA well above the background level of cleavage and only 10 times less efficiently than deglyco-bleomycin A₂, but to do so in a nonsequence-specific manner with a significantly reduced ds:ss cleavage ratio (Figure 6).^[100] Thus, although it may play a dominant role in determining the DNA cleavage selectivity when incorporated into the full natural product structure (see Section 3.2.8), the metal binding domain alone failed to exhibit the sequence selective DNA cleavage characteristic of bleomycin A₂.

Non-selective DNA cleavage by the metal binding domain

Agent	Efficiency	ds:ss	Selectivity
bleomycin A ₂ (1)	2–5	1 : 6	5'-GC, 5'-GT > 5'-GA
deglyco-bleomycin A ₂ (41)	1	1 : 12	5'-GC, 5'-GT > 5'-GA
94	0.1	1 : 48	none
92	<0.04	nd	none
Fe ^{III}	0.04	1 : 98	none

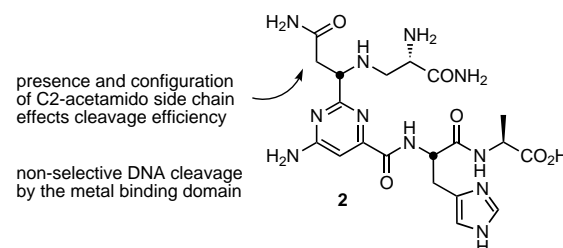
Figure 6. DNA cleavage properties of the metal binding domain. The complete metal binding domain alone exhibits no DNA cleavage selectivity. nd = not determined.

3.2.2. (+)-P-3A, *epi*-(–)-P-3A, and (–)-Desacetamido P-3A

Similarly, (+)-P-3A (**2**) along with *epi*-(–)-P-3A (**14**) and (–)-desacetamido-P-3A (**15**) were examined as being representative of the metal binding domain.^[18b, 84] (+)-P-3A (**2**) proved to be surprisingly effective at cleaving DNA, being even more effective than **92** or **94**. The Fe^{II} complexes of all three agents produced both ss and ds cleavage although with a decreased propensity for ds cleavage and no sequence selectivity (Figure 7). Fe^{II}·**2** proved to be only three to five times less efficient than deglyco-bleomycin A₂ and was three to five times more efficient than Fe^{II}·**14** and Fe^{II}·**15**. The results indicated not only that the metal binding domain is insufficient for sequence selective DNA cleavage, but also provided the first observation that the C2-acetamido side chain significantly effects cleavage efficiency although it is not involved in metal chelation.

3.2.3. L-Histidine Amide Replacements^[98]

Potentiometric titration of the bleomycin copper complex in Umezawa's studies indicated that one deprotonated functional group occupies a metal coordination site at pH values

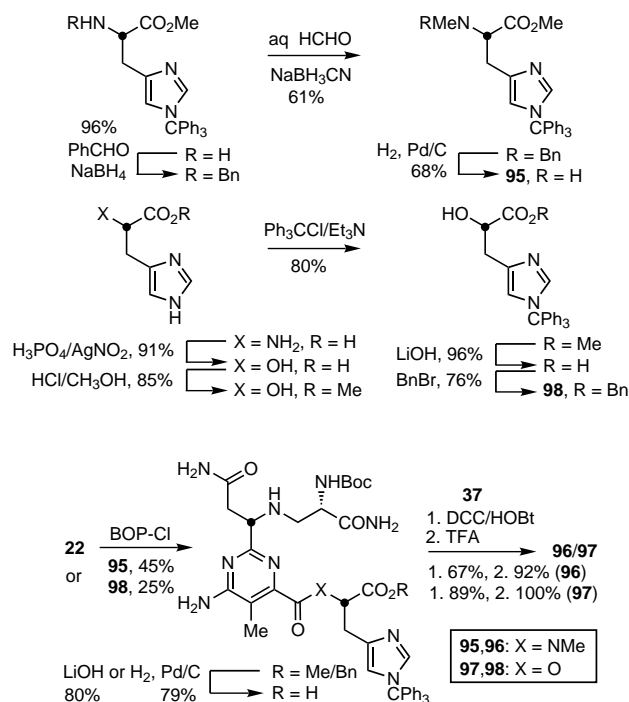


Agent	Efficiency	ds:ss	Selectivity
bleomycin A ₂ (1)	2–5	1 : 6	5'-GC, 5'-GT > 5'-GA
deglyco-bleomycin A ₂ (41)	1	1 : 12	5'-GC, 5'-GT > 5'-GA
(+)-P-3A (2)	0.3–0.2	1 : 30	none
<i>epi</i> -(–)-P-3A (14)	0.07	1 : 38	none
(–)-desacetamido P-3A (15)	0.07	1 : 40	none

Figure 7. DNA cleavage properties of (+)-P-3A and related agents.

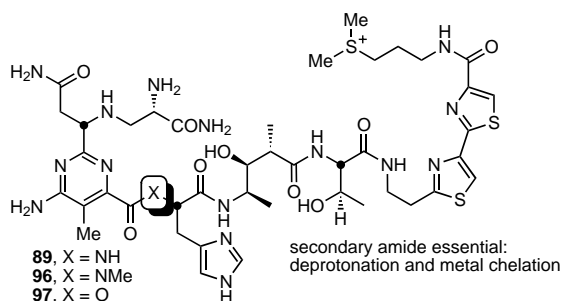
between 4 and 9.^[85] Since the amide group of the histidine unit is in a favorable position to coordinate to a metal center, it was inferred that the deprotonated amide nitrogen atom constituted one coordination site despite the relative pK_a of imidazole (14.4) and an amide (17) in the absence of a metal.^[85] This was supported by the X-ray crystal structure of Cu^{II}·P-3A (**2a**) and more recently by those of simple model complexes, which illustrate L-histidine imidazole N^π complexation and deprotonated amide N^σ complexation.^[68] While studies have addressed, and seem to confirm, this^[69b, c] related spectroscopic studies conducted on a range of metal complexes have also suggested that the histidine amide group may not always be involved and cast doubt on the site of the deprotonated metal ligand.^[61a, b] The evaluation of two amide replacement analogues was conducted in order to address the inferred importance of the secondary amide of L-histidine. The first analogue **96** incorporates a *N*-methylamide group. The *N*-methylamide is only capable of amide N^π complexation and is incapable of deprotonation and metal complexation through N^σ coordination. Similarly, the ester replacement in **97** is incapable of providing the deprotonated amide for metal coordination. The appropriately protected *N*-methyl-L-histidine methyl ester **95** for use in the synthesis of **96** was prepared from L-His(CPh₃)-OMe by sequential reductive benzylation and methylation followed by hydrogenolysis of the benzylamine group (Scheme 15). Coupling of **95** with N^α-Boc-pyrimidoblamic acid (**22**) led to introduction of the tertiary amide. Methyl ester hydrolysis, coupling with tetrapeptide S (**37**) and acid-catalyzed deprotection provided **96**. The synthesis of **97** required the selectively protected alcohol **98**, which could be deprotected after coupling with **22** without epimerization or competitive hydrolysis of the newly formed ester group. For this reason the benzyl ester **98** was selected and prepared from L-histidine (Scheme 15). Coupling of **98** with N^α-Boc-pyrimidoblamic acid (**22**) provided the linked ester, which was unusually sensitive to hydrolysis. Benzyl ester deprotection, coupling of the carboxylic acid with tetrapeptide S (**37**), and acid-catalyzed deprotection provided **97**.

The bleomycin analogues **96** and **97** that contain a *N*-methylamide and an ester group, respectively, in place of the secondary amide group of L-His were found to cleave DNA,



Scheme 15. Synthesis of bleomycin A₂ derivatives by replacement of the NH of the L-histidine amide group with *N*-Me or O. BOP-Cl = benzotriazolyloxytris(dimethylamino)phosphonium chloride.

but to do so in a nonsequence-selective fashion with a substantially reduced efficiency and a diminished ds:ss cleavage ratio that were only slightly greater than that of free Fe^{III} ions (Figure 8). These observations are consistent with the proposal that the deprotonated secondary amide of L-histidine is required for functional metal chelation and activity.



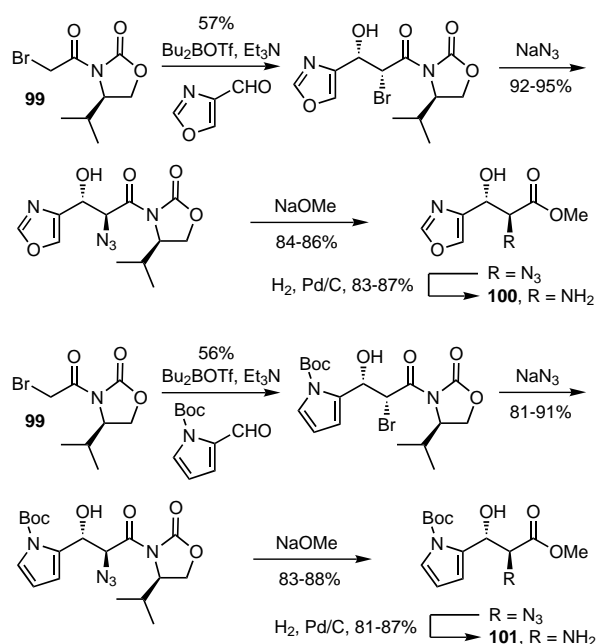
Agent	Efficiency	ds:ss	Selectivity
bleomycin A ₂ (1)	2 – 5	1 : 6	5'-GC, 5'-GT > 5'-GA
deglycobleomycin A ₂ (41)	1	1 : 12	5'-GC, 5'-GT > 5'-GA
89 , X = NH	0.75	1 : 12	5'-GC, 5'-GT > 5'-GA
96 , X = NMe	0.08	1 : 61	none
97 , X = O	0.13	1 : 49	none
Fe ^{III}	0.04	1 : 98	none

Figure 8. DNA cleavage properties of bleomycin analogues with modified amide groups on L-histidine. The results show that an unsubstituted amide group is essential.

3.2.4. Oxazole-, Pyrrole-, and Desimidazole-Deglycobleomycin A₂^[101]

The N3 atom of imidazole of the *erythro*- β -hydroxy-L-histidine subunit functions as a key ligand in the metal

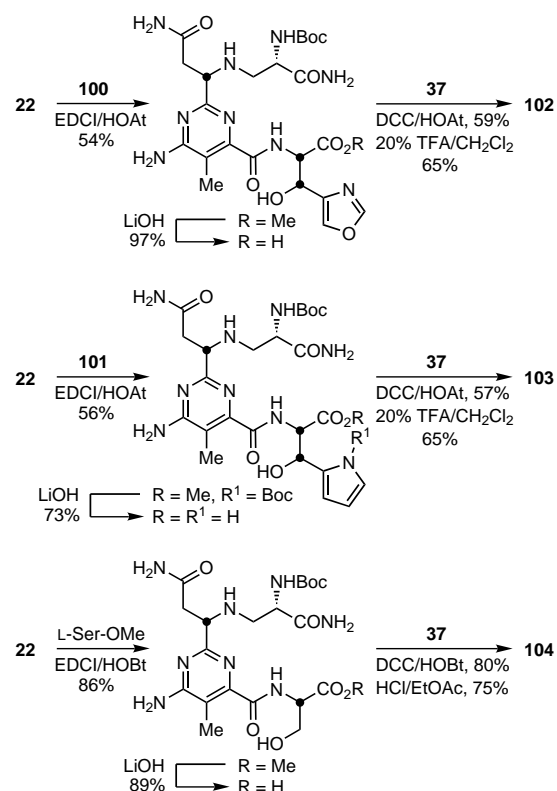
complexes and has been assumed to play a pivotal role in the oxygen-activation properties. In conjunction with our studies on the amide group of β -hydroxy-L-histidine, the issue of complexation of the N3 atom of the imidazole ring with either N^{σ} or N^{π} metal coordination was addressed with the evaluation of **102**–**104**. The oxazole analogue is only capable of N^{π} metal complexation through a form related to the N^1 -H imidazole tautomer of bleomycin A_2 , while the pyrrole analogue may mimic the N^{σ} metal complexation capabilities of the imidazole N^3 -H tautomer. The analogue **104**, which incorporates L-serine in place of the L-histidine subunit, lacks the imidazole group altogether. The synthesis of **102** and **103** required the protected *erythro*- β -hydroxy-L-histidine analogues **100** and **101**. Both were prepared according to the approach implemented for the authentic subunit by using the diastereoselective *syn* aldol addition of the optically active α -bromoacetylloxazolidinone **99** (Scheme 16).



Scheme 16. Preparation of the L-His subunit analogues.

Coupling of **100** with *N*^α-Boc-pyrimidoblamic acid (**22**) followed by methyl ester hydrolysis, coupling of the resulting carboxylic acid with tetrapeptide S (**37**) and acid-catalyzed deprotection provided **102**. The incorporation of **101** and L-Ser-OCH₃ into analogues **103** and **104** was accomplished similarly (Scheme 17).

The oxazole analogue **102**, which is incapable of N^{σ} metal chelation, was found to behave analogous to, and only slightly less effectively, than deglycobleomycin A_2 . The observation of sequence-selective cleavage confirmed that imidazole N^{π} metal chelation is sufficient for functional reactivity (Figure 9). The effective substitution of the O-1 oxazole atom for a N-1 histidine atom also illustrates that this group does not require deprotonation upon metal complexation, oxygen activation, or the ensuing oxidation reactions, that the functional bleomycin A_2 tautomer is the $\text{N}^1\text{-H}$ tautomer, and that the $\text{N}^1\text{-H}$ atom does not contribute to the polynucleotide



Scheme 17. Synthesis of bleomycin derivatives by replacement of imidazole group of the L-histidine subunit.

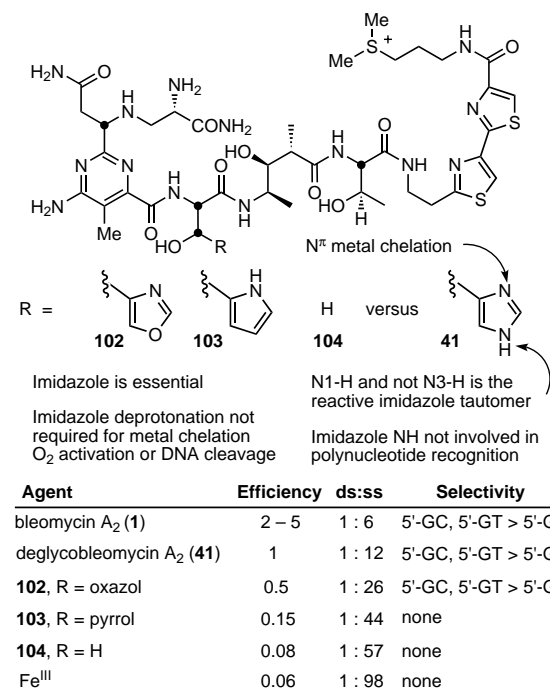


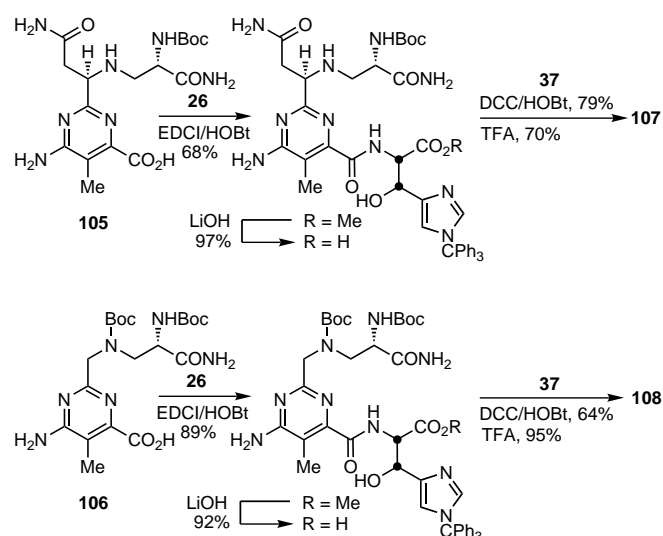
Figure 9. DNA cleavage properties of bleomycin derivatives with imidazole analogues of the histidine subunit. For further information see the text.

recognition through H-bonding to the phosphate backbone or nucleotide bases. In contrast, the pyrrole analogue **103**, which is incapable of N^π chelation and possesses the capabilities of functioning as a N^σ donor, was found to cleave DNA but did so in a nonsequence-selective fashion with a significantly reduced efficiency and ds:ss cleavage ratio, both only slightly

above background Fe itself. Similarly, **104** proved to be an ineffective agent, which confirmed the requirement for the imidazole group. The cleavage of DNA by **103**, like that of **104**, may be mediated through Fenton chemistry (H₂O₂ and a Fe(II) salt) with generation of diffusible oxidants including hydroxyl radicals. These observations support N^π, not N^σ, coordination through the N¹-H imidazole tautomer for the functional activity of bleomycin A₂. The more recent structural studies of Stubbe et al. conducted on the Co^{III}-OOH complex of bleomycin A₂ also illustrate, and would seem to confirm, the N^π complexation of the histidine imidazole group and the complexation from the deprotonated amide group.^[52]

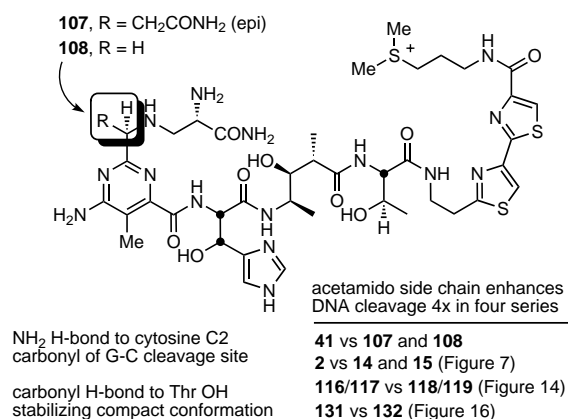
3.2.5. *epi*-Deglycobleomycin A₂ and Desacetamidodeglycobleomycin A₂^[18d,e, 102]

The C2-acetamido side chain is not intimately involved in the key metal chelation and subsequent oxygen activation and yet appears to be important to the natural product since *epi*-bleomycin A₂^[47] exhibits diminished biological activity and a reportedly altered DNA cleavage selectivity.^[96] Studies on (+)-P-3A and related agents also revealed a significant role for the C2-acetamido side chain in the DNA cleavage efficiency.^[84b, 102] Moreover, β-elimination of the β-amino-alanineamide activated by the C2-acetamido side chain may contribute to the inherent instability of bleomycin A₂. Thus, the removal of the C2-acetamido side chain could be anticipated to eliminate this degradation pathway and enhance the stability of the agent.^[48, 49] In efforts to address the role of the C2-acetamido side chain, *epi*-deglycobleomycin A₂ (**107**) and desacetamidodeglycobleomycin A₂ (**108**) were prepared. Coupling of **105**, epimeric with natural pyrimido-blamic acid at the C2-acetamido side chain center, and **106**, lacking the side chain altogether, with **26** followed by methyl ester hydrolysis, coupling with tetrapeptide S (**37**) and deprotection provided *epi*-deglycobleomycin A₂ (**107**) and desacetamidodeglycobleomycin A₂ (**108**), respectively (Scheme 18).



Scheme 18. Synthesis of bleomycin analogues with modifications in the C2-acetamido side chain.

$\text{Fe}^{\text{II}} \cdot \mathbf{107}$ and $\text{Fe}^{\text{II}} \cdot \mathbf{108}$ proved indistinguishable and both displayed a substantially diminished DNA cleavage efficiency and ds:ss cleavage ratio relative to deglycobleomycin \mathbf{A}_2 (Figure 10). The selectivity of the DNA cleavage was unaffected by the removal or epimerization of the C2-acetamido side chain. Since both $\mathbf{107}$ and $\mathbf{108}$ behave identically, it is not the unnatural configuration of $\mathbf{107}$ that diminishes cleavage efficiency. Rather, the results suggest a productive role for the natural C2-acetamido side chain that increases DNA cleavage



Agent	Efficiency	ds:ss	Selectivity
bleomycin \mathbf{A}_2 (1)	2–5	1 : 6	5'-GC, 5'-GT > 5'-GA
deglycobleomycin \mathbf{A}_2 (41)	1	1 : 12	5'-GC, 5'-GT > 5'-GA
107, R = CH_2CONH_2 (epi)	0.25	1 : 29	5'-GC, 5'-GT > 5'-GA
108, R = H	0.25	1 : 29	5'-GC, 5'-GT > 5'-GA

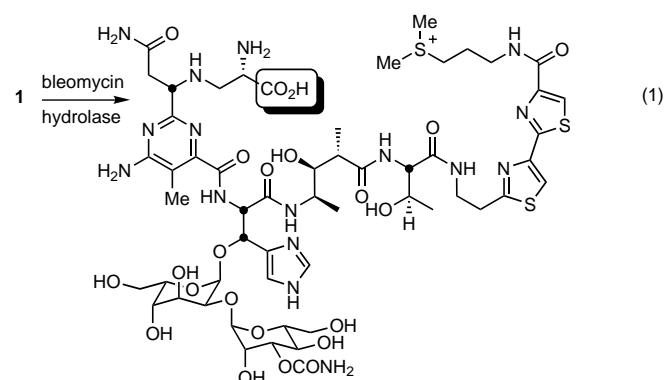
Figure 10. DNA cleavage by bleomycin derivatives containing C2-acetamido side chain modifications. The presence of the acetamido side chain enhances the DNA cleavage fourfold, as seen by a comparison of the data for **41** with those of **107** and **108**, those for **2** with those for **14** and **15** (Figure 7), those for **116/117** with those for **118/119** (Figure 14), as well as those for **131** with those for **132** (Figure 16).

efficiency and significantly increases the ratio of ds:ss DNA cleavage without affecting the cleavage selectivity. Although there are a number of attractive explanations for these observations, the trends are identical with those of (+)-P-3A (**2**), *epi*(-)-P-3A (**14**), and (-)-desacetamido-P-3A (**15**) where the agents were found to cleave DNA with no sequence selectivity. This observation suggests that the role of the C2-acetamido side chain may not be the result of a specific DNA interaction at a particular cleavage site. Rather, the observations would be consistent with a productive role in increasing DNA cleavage by stabilizing the activated metal complex, increasing its catalytic turnover, or diminishing decomposition perhaps through protecting the activated metal complex from solvent. However, the structural studies of Stubbe et al. on the Co^{III} -OOH complex of deglycobleomycin \mathbf{A}_2 suggest an additional provocative explanation.^[52] In this model, a highly organized H-bond network that involves the threonine NH, carbonyl, and hydroxyl group with the metal-bound hydroperoxide and the metal binding domain is observed. Both the C2-acetamido side chain carbonyl and the metal coordinated β -amino group of the pyrimidoblastic acid side chain are H-bonded to the threonine hydroxyl group and potentially contribute to the stability of a compact DNA-bound conformation. This could enhance cleavage efficiency

by either stabilization of the activated metal complex or by enhancing the adoption of a conformation productive for DNA cleavage (see Figures 13 and 19). In addition, the carboxamide NH_2 group of the C2-acetamido side chain may be H bonded to the C2 carbonyl group of the cytosine that is base paired with the guanine at the cleavage site. In principle, this provides a third H bond between the metal binding domain and the cleavage site GC base pair. The loss of this H bond could also account for the diminished cleavage efficiency but the results of our studies would indicate that it is not intimately required for recognition of the GC pair (see Section 3.2.8).

3.2.6. Descarboxamidodeglycobleomycin \mathbf{A}_2 ^[18e]

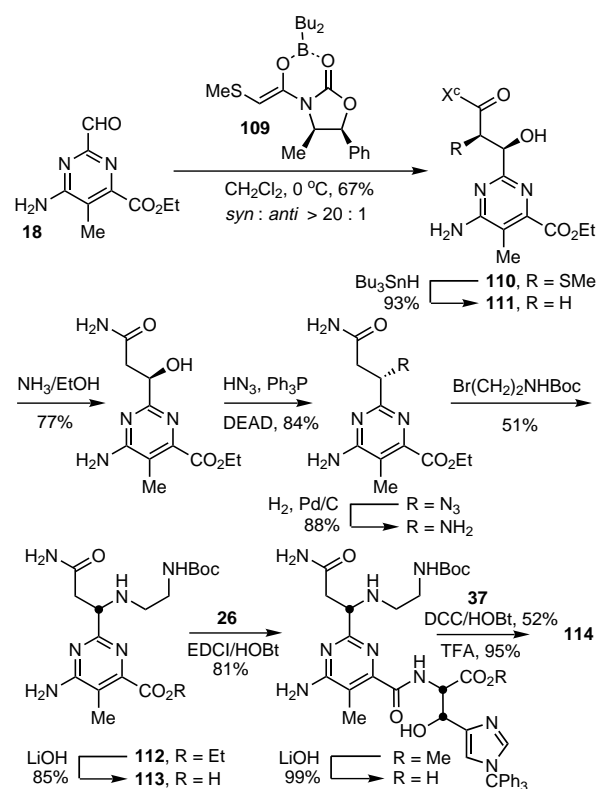
The terminal α -carboxamide found in the pyrimidoblastic acid side chain has long been suggested not to be involved in metal chelation and has no obvious role in the oxygen activation and DNA cleavage reactions. It does, however, undergo a rapid in-vivo hydrolysis that is catalyzed by bleomycin hydrolase [Eq. (1)].^[48, 103, 104] The resulting



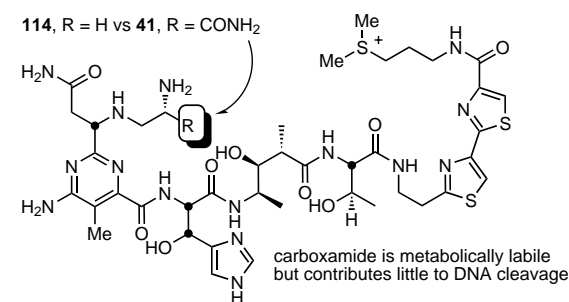
carboxylic acid displaces the metal-bound primary amine to serve as one tightly bound ligand of the inactivated metal complex. To determine if there was an unappreciated role for the metabolically labile carboxamide group, **114** was prepared for evaluation.

A modified approach was devised to prepare the pyrimidoblastic acid analogue **113** that lacked the carboxamide group. Treatment of **18** with the di-*n*-butylboronyl-(*Z*)-enolate **109** provided (2*R*,3*S*)-*syn*-**110** as the only detectable product (67 %, > 20:1; Scheme 19). Reductive desulfurization effected by Bu_3SnH (93 %), aminolysis (77 %), and Mitsunobu activation of the alcohol and azide displacement with inversion of the stereochemistry proceeded in excellent yield (84 %) with no loss of stereochemical integrity at the reaction center. The reverse order of Mitsunobu activation and azide displacement of the alcohol followed by aminolysis of the *N*-acyloxazolidinone also proceeded well but in lower conversions (51 and 40 %, respectively). Reduction of the azide, alkylation with *N*-Boc-2-bromoethylamine, and hydrolysis provided **113**. Coupling of **113** with **26**, methyl ester hydrolysis, coupling with tetrapeptide **S** (**37**), and deprotection provided **114**.

The comparison of **114** with deglycobleomycin \mathbf{A}_2 proved interesting. The analogue was only 1.6 times less effective at cleaving DNA, only slightly less effective at producing ds



Scheme 19. Synthesis of descarboxamidodeglycbleomycin A₂ (**114**). DEAD = diethylazodicarboxylate, X^c = oxazolidinonyl.



Agent	Efficiency	ds:ss	Selectivity
bleomycin A ₂ (1)	2–5	1 : 6	5'-GC, 5'-GT > 5'-GA
deglycbleomycin A ₂ (41)	1	1 : 12	5'-GC, 5'-GT > 5'-GA
114 , R = H	0.6	1 : 18	5'-GC, 5'-GT > 5'-GA

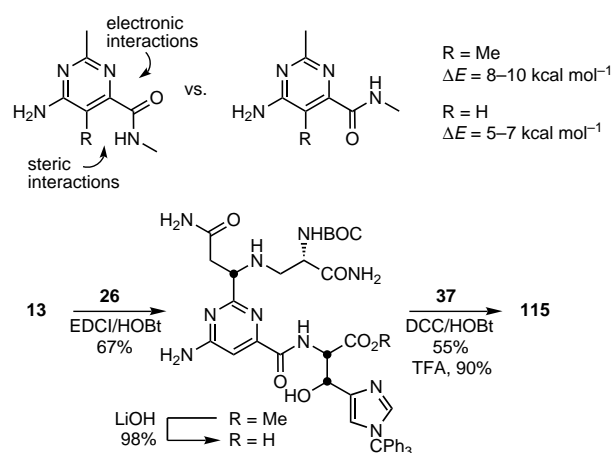
Figure 11. DNA cleavage by descarboxamidodeglycbleomycin A₂ (**114**).

versus ss cleavage, and no differences in the cleavage selectivity were observed (Figure 11). These small distinctions suggest analogues that lack the carboxamide group might represent more potent, more efficacious, or longer acting agents as a result of their increased stability toward bleomycin hydrolase inactivation.

3.2.7. C5-desmethyldeglycbleomycin A₂^[18e]

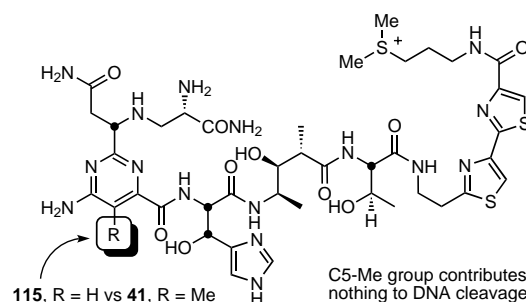
The C5-desmethyldeglycbleomycin A₂ (**115**) was prepared to assess the role of the methyl substituent on the pyrimidine ring. A steric interaction of the methyl group with the *ortho* carboxamide group may favor a conformation that enhances metal coordination, oxygen activation, and DNA cleavage. However, the inherent electronic destabilization of the *syn*

conformation derived from lone pair–lone pair repulsion coupled with an inherent destabilizing steric interaction between a NHR group and a H atom of the *syn* conformation of **115** should ensure that it adopts the *anti* conformation ($\Delta E = 5.4–7.2$ kcal mol^{−1}; Scheme 20). Consequently, the C5-methyl substituent was anticipated to be unnecessary. This was easily addressed with the use of **13**, which was available from our synthesis of P-3A. Thus, the coupling of **13** with **26**, methyl ester hydrolysis, coupling with tetrapeptide S (**37**), and acid-catalyzed deprotection provided **115**.



Scheme 20. Synthesis of C5-desmethyldeglycbleomycin A₂ (**115**).

The comparison of **115** with **41** proved exceptionally good (Figure 12). The two agents were indistinguishable and exhibited the same DNA cleavage efficiency, nearly the same ratio of ds:ss cleavage, and the same cleavage selectivity, which indicated that the C5-methyl substituent does not contribute productively to the properties of bleomycin A₂.



Agent	Efficiency	ds:ss	Selectivity
bleomycin A ₂ (1)	2–5	1 : 6	5'-GC, 5'-GT > 5'-GA
deglycbleomycin A ₂ (41)	1	1 : 12	5'-GC, 5'-GT > 5'-GA
115 , R = H	1	1 : 18	5'-GC, 5'-GT > 5'-GA

Figure 12. DNA cleavage by C5-desmethyldeglycbleomycin A₂ (**115**).

3.2.8. Dimethylamino- and Desaminodeglycbleomycin A₂: Confirmation of the Origin of Sequence Selective DNA Cleavage^[105]

The role of the C4 amino group of pyrimidine was probed through the synthesis and evaluation of **116** and **117** as well as their epimers **118** and **119** in which the amine was replaced

with a tertiary *N,N*-dimethylamine or removed altogether. In addition to the impact this may have on the metal chelation and oxygen-activation properties, their examination allowed the assessment of a potential key H bond from this primary C4 amine to the guanine N3 atom defined in the beautiful structural studies of Stubbe et al.^[52] These studies highlighted two previously unrecognized H bonds between the pyrimidine ring of the metal binding domain of bleomycin A₂ and guanine of the 5'-GC/5'-GT cleavage sites. The N3 atom of pyrimidoblastic acid was found to be H bonded to the nonbase pairing hydrogen atom of the C2-amine group of guanine and one of its C4-amine hydrogen atoms was H bonded to the N3 atom of guanine to provide a triplex-like recognition interaction in the minor groove (Figure 13). This interaction potentially provides the basis for the sequence selective cleavage of DNA and explains the requirement for the guanine C2-amine group for 5'-GC/5'-GT cleavage.^[26b, 44c, 76c, 76d, 106]

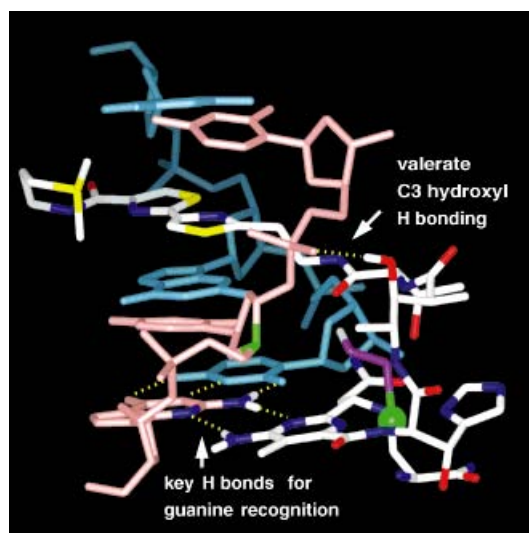
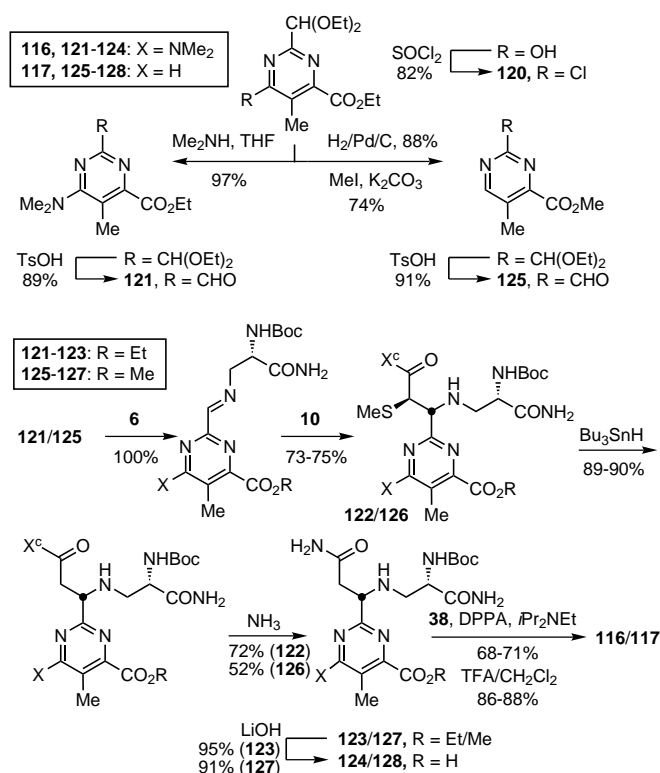


Figure 13. Expanded view of the complex structure determined by NMR spectroscopy (see Figure 5) illustrating the two H bonds between pyrimidoblastic acid (C4 amino group and N3 atom) and the guanine at the cleavage site. Also highlighted are the H bond between the valerate C3-OH subunit to DNA, the C4'-H abstraction site (green), the Co^{III}·OOH subunit (green ball and violet stick), and the rigid, compact conformation of the linker domain. For clarity, the disaccharide subunit is not shown.

The synthesis of **116** from an appropriately substituted pyrimidine was addressed after unsuccessful efforts to prepare **123** by reductive methylation or alkylation of the ethyl ester of *N*^α-Boc-pyrimidoblastic acid. Thus, dimethylamine displacement of the 4-chloro substituent of **120** provided cleanly the corresponding 4-dimethylaminopyrimidine, and subsequent acetal hydrolysis afforded the aldehyde **121** as a key intermediate for diastereoselective introduction of the side chain (Scheme 21). Condensation with **6** followed by addition of the stannous (*Z*)-enolate **10** provided **122** (87:13 diastereoselection). Reductive removal of the thiomethyl group, aminolysis of the *N*-acyloxazolidinone, followed by ester hydrolysis provided **124**. Coupling of **124** with pentapeptide S (**38**) and acid-catalyzed deprotection of the single *N*-Boc protecting group provided **116**.

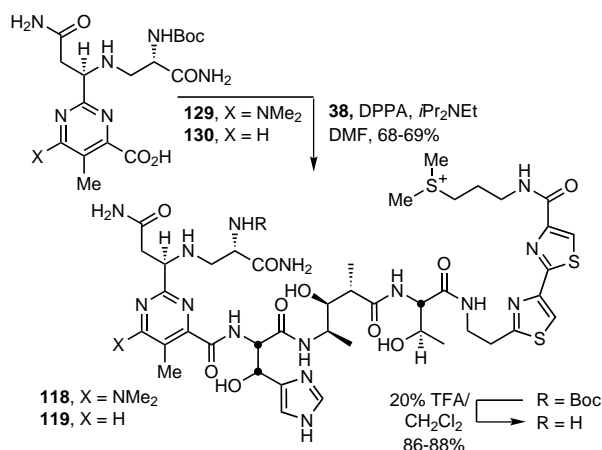


Scheme 21. Synthesis of dimethylaminodeglycobleomycin A₂ (**116**) and desaminodeglycobleomycin A₂ (**117**). X^C = oxazolidonyl.

The synthesis of **128** and its incorporation into **117** was accomplished after unsuccessful efforts at reductive deamination of a pyrimidoblastic acid precursor (Scheme 21). Reductive dechlorination of **120** under conditions that resulted in ethyl ester hydrolysis followed by reesterification and acetal hydrolysis provided the key aldehyde intermediate **125**. Condensation with **6** followed by addition of the stannous (*Z*)-enolate **10** provided **126** (89:11 diastereoselection). Reductive desulfurization, aminolysis, and ester hydrolysis afforded **128**. Coupling of **128** with pentapeptide S (**38**) and acid-catalyzed deprotection provided **117**.

Complementary to these efforts the minor diastereomers derived from the imine addition reactions, which possess the unnatural stereochemistry at the C2-acetamido side chain, were converted into **129** and **130** and incorporated into the epimeric analogues **118** and **119** (Scheme 22).

In initial efforts to characterize the properties of the agents, the ability of their Fe^{III} complexes to mediate the oxidation of styrene was investigated.^[72b, 107] Although the pyrimidine C4-amine group of bleomycin A₂ is not directly engaged in the metal chelation, the electronic character of C4 substituents has been shown to affect the O₂-activation properties.^[6, 68b, 73] The examination of **116** and **117** and their epimers revealed the same product distribution with all analogues and deglycobleomycin A₂, which indicates that all give rise to competent iron-oxo intermediates (Table 2). The relative efficiencies of the two dimethylamino analogues (**116** and **118**) were nearly indistinguishable from **41** itself, while those of the desamino analogues (**117** and **118**) were slightly lower. This is consistent with expectations that an electron-donating C4

Scheme 22. Synthesis of the epimeric analogues **118** and **119**.Table 2. Styrene oxidation by Fe^{III} complexes of bleomycin A₂ analogues.^[a]

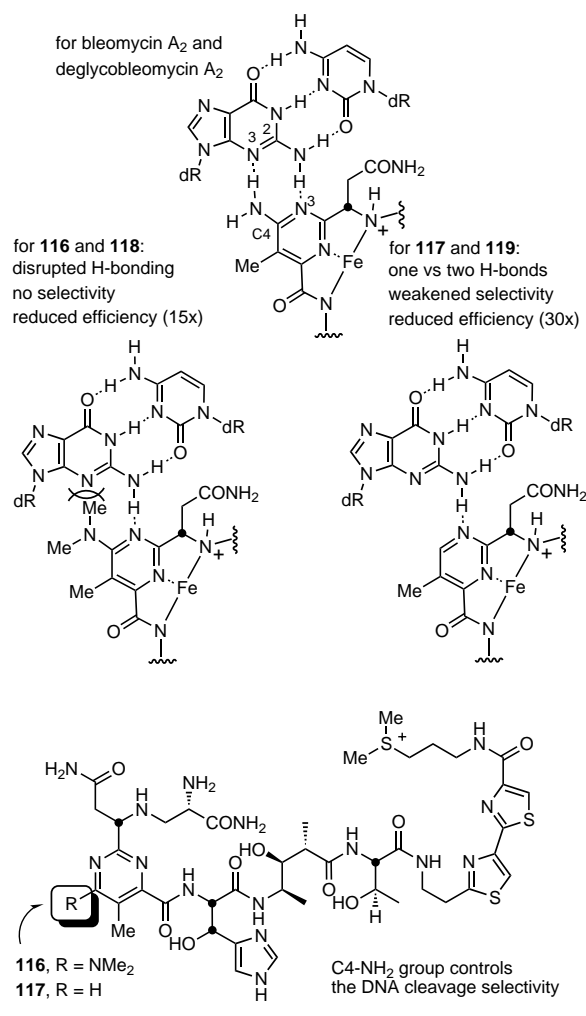
Agent	c(styrene oxide) [mm]	c(phenylacetaldehyde) [mm]	Ratio	c(total product) [mm]	Relative efficiency
Fe ^{III} · 41	1.80	1.32	1.36	3.12	1.0
Fe ^{III} · 116	1.67	1.21	1.38	2.88	0.92
Fe ^{III} · 117	1.11	0.88	1.26	1.99	0.64
Fe ^{III} · 118	1.55	1.00	1.55	2.55	0.82
Fe ^{III} · 119	1.07	0.79	1.35	1.86	0.59
Fe ^{III} [b]	0	0	–	0	0
Fe ^{III} · 41 [c]	0	0	–	0	0

[a] 500 μM Fe^{III}-agent, 50 mM styrene, 30 mM H₂O₂, 0 °C, 1.5 h, 80% CH₃OH in H₂O. [b] 500 μM Fe^{III} under identical conditions as [a] and with H₂O₂ present. [c] Same as in [a], but without H₂O₂.

substituent on pyrimidine would improve the O₂-activation properties of the metal complexes. However, all were effective and provided roughly 4–6 oxidations per Fe^{III} complex.

The DNA cleavage properties of the agents were especially revealing. The analogue **116** and its epimer **118** with a dimethylamino substituent exhibited a substantially diminished DNA cleavage efficiency (10–15 ×), reduced ratio of ds versus ss cleavage, and a complete loss of cleavage selectivity (Figure 14). These observations indicate that substitution with the C4 dimethylamino group not only precludes the formation of a H bond between the C4-amino group and the guanine N3 atom but also sterically prevents formation of the remaining H bond between the guanine C2 amino group and the pyrimidine N3 atom, which destroys both the cleavage efficiency and selectivity of the agent.

The analogues **117** and **119** exhibited an even greater diminished DNA cleavage efficiency (30 ×) with altered and sometimes lost sequence selectivity. Even in the instances where the selectivity was not substantially altered, its detection required assay conditions of 4 °C instead of the usual 25–37 °C. In addition, the cleavage at minor 5'-AT sites essentially disappeared. This suggests a reduced binding interaction and is consistent with the participation of the C4 amino group of pyrimidine in the formation of one of the two critical H bonds of the minor groove triplex-like recognition.



Agent	Efficiency	ds:ss	Selectivity
bleomycin A ₂ (1)	2–5	1 : 6	5'-GC, 5'-GT > 5'-GA
deglycobleomycin A ₂ (41)	1	1 : 12	5'-GC, 5'-GT > 5'-GA
	0.08	1 : 53	none
	0.06	1 : 45	5'-GC, 5'-GT > 5'-GA (weak)
118 , R = NMe ₂ (epi)	0.04	1 : 61	none
119 , R = H (epi)	0.03	1 : 48	5'-GC, 5'-GT > 5'-GA (weak)

Figure 14. DNA cleavage by bleomycin A₂ analogues with modified pyrimidine C4-amino groups. The results show that this group is essential to control the selectivity of the DNA cleavage.

Both these observations are consistent with the involvement of the C4 amino group in a pair of H bonds in a triplex-like recognition of the guanine at the cleavage site and provide direct evidence for its critical role in the polynucleotide recognition. In addition, these observations have further implications on the inherent DNA cleavage selectivity of bleomycin A₂ itself. Bleomycin A₂ not only cleaves essentially all 5'-GT, 5'-GC sites in DNA, but also cleaves 5'-AT, 5'-AC sites albeit less effectively (25–40% versus 100%) and does so with a weaker efficiency (Figure 15). Although the statistically minor cleavage sites compiled in Figure 15 could result from ds cleavage that originates from primary sites on the complementary strand, the more general cleavage preference of 5'-GPy > 5'-APy (Py = pyrimidine base) may be attributed

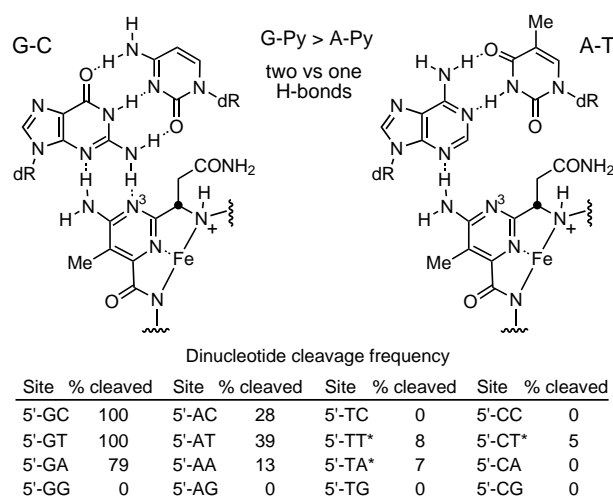


Figure 15. Further implications for bleomycin A_2 cleavage selectivity. The frequency of the cleavage of the dinucleotides is shown. The sites marked with a star are secondary ds-DNA cleavage sites.

to an analogous reduced binding affinity at the 5'-APy sites that result from one versus two triplex-like H bonds to adenine (Figure 15). Thus, although the properties of **117** might have been unanticipated based on the triplex-like H bond model, its behavior shed further light on the origin of the inherent 5'-GPy > 5'-APy cleavage selectivity of bleomycin A_2 itself. These results complement the studies where Waring and co-workers showed that the cleavage is diminished but not lost when guanine is replaced with inosine and that adenine cleavage is greatly increased when it is replaced with 2-aminoadenine.^[76] Both of these single site changes in the DNA also support the basis of the H-bonding specificity.

3.3. The Linker Domain

At the onset of our efforts the full role of the linker region joining the bithiazole C terminus and the N-terminus pyrimidoblastic acid was poorly understood. The importance of the presence and absolute stereochemistry of the C4 methyl group was first disclosed in the studies of Umezawa, Ohno, and co-workers on the DNA cleavage efficiency of a select set of bleomycin A_2 analogues.^[6, 73] Similarly, Hecht and co-workers have shown that the L-threonine subunit and its backbone substituents are not important to the cleavage selectivity although they appeared to have an impact on the cleavage efficiency.^[24d, 42b] In studies conducted concurrent with our synthesis of deglycobleomycin A_2 , **131** and **132** were prepared in which all the linker substituents had been removed.^[18e, 108] Their examination revealed that the substituents do not adversely affect the DNA binding affinity (calf thymus DNA $K_B = 2.4 \times 10^5 \text{ M}^{-1}$ versus $1-1.1 \times 10^5 \text{ M}^{-1}$ for **1** and **41**) or cleavage selectivity, but that the cleavage efficiency (ca. 10–100 times) and the ds:ss cleavage ratio were substantially reduced (Figure 16).^[18e] Such observations are consistent with our early proposal that the chain substituents of the linker facilitate the adoption of a compact bound conformation with at least one turn at the tripeptide S/

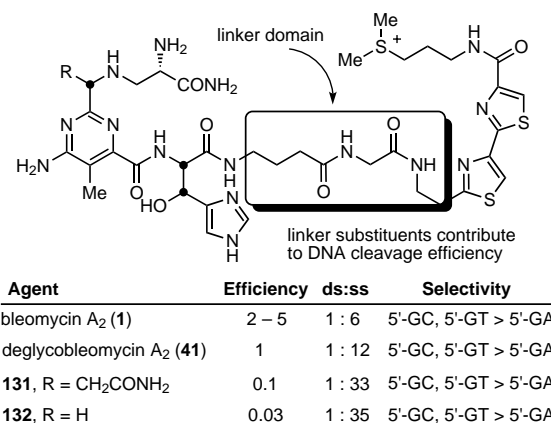


Figure 16. Cumulative effect of the substituents in the linker domain. These contribute to the efficiency of DNA cleavage.

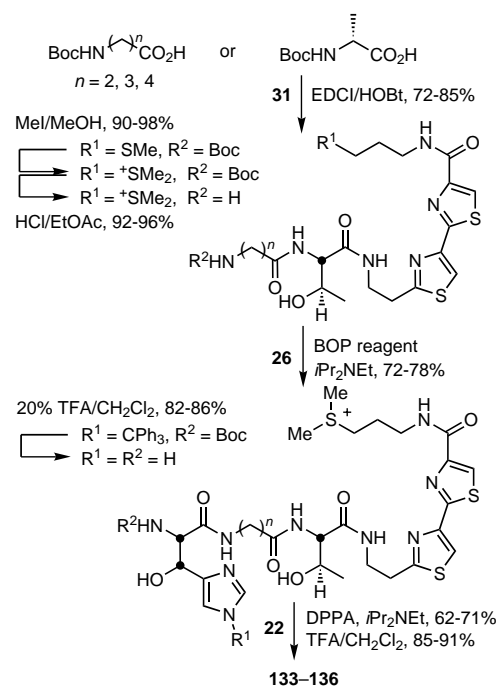
tetrapeptide S juncture. In efforts to address the contribution of the individual substituents of the linker domain and accurately define the effects, an extensive series of linker analogues was examined.

3.3.1. Valerate Subunit

3.3.1.1. Effect of Linker Length^[109]

The analogues **133–136** that incorporate 2–5 carbon linkers in place of the valerate subunit were prepared as outlined in Scheme 23. Their examination permitted an assessment of the impact of the length of the valerate subunit.

DNA cleavage studies revealed a well-defined relationship of C4 > C5, C3 > C2 where the length of the natural valerate linker was established to be best (Figure 17). This is consistent



Scheme 23. Synthesis of bleomycin A_2 analogues with variable linker lengths.

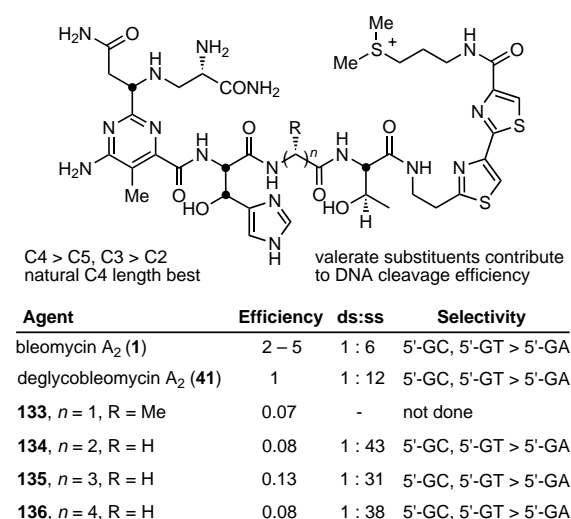
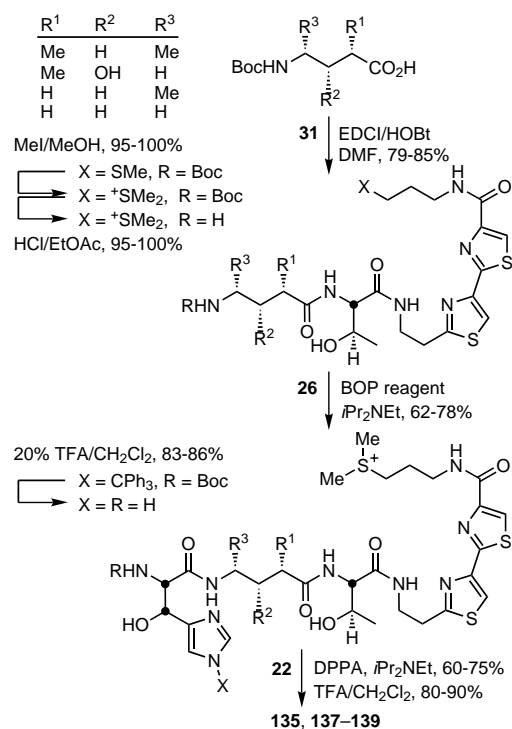


Figure 17. DNA cleavage by bleomycin A₂ analogues with various lengths of the valerate subunit.

with the adoption of a well-defined DNA-bound conformation where those agents that possess a valerate substitute shorter than four carbon atoms may have progressively more difficulty in adopting conformations that span the linker region. In turn, those longer than four carbon atoms possess greater flexibility and less opportunity to adopt the productive conformation required for selective cleavage.

3.3.1.2. Substituent Effects^[109]

Examination of **137**–**139** along with **135** allowed for a clear definition of the substituent effects. Analogue **137** permitted the assessment of the valerate C3-hydroxyl group. The



Scheme 24. Synthesis of bleomycin A₂ analogues containing the key valerate substituents.

examination of **138**–**139** was anticipated to clarify the role of the C2 and C4 methyl substituents, which had been identified as important in our previous studies.^[109] The analogues were prepared through the coupling of the pentapeptide S analogues with the modified valerate subunits with *N*^α-Boc-pyrimidoblastic acid (Scheme 24).

The DNA cleavage properties of the valerate substituent analogues are summarized in Figure 18. Analogue **137** was only slightly less effective (0.8 ×) than deglycobleomycin A₂ at cleaving DNA, while **138** was substantially less efficient (0.4 ×). Thus, removal of the C4 methyl group had a more significant impact than the C3 hydroxyl group. Removal of the C2 methyl and C3 hydroxyl group in **139** led to an even greater (fivefold) reduction, which indicated that the C4 methyl group alone cannot account for the cleavage efficiency induced by the substituents. Further removal of the remaining C4 methyl substituent with **135** resulted in a still greater reduction in the cleavage efficiency (0.13 ×). Analogous comparisons were made in a glycine versus threonine series where in addition to highlighting the significant effect of the threonine side chain, which is described in the following section, the same trends for the valerate substituents were observed (Figure 18).

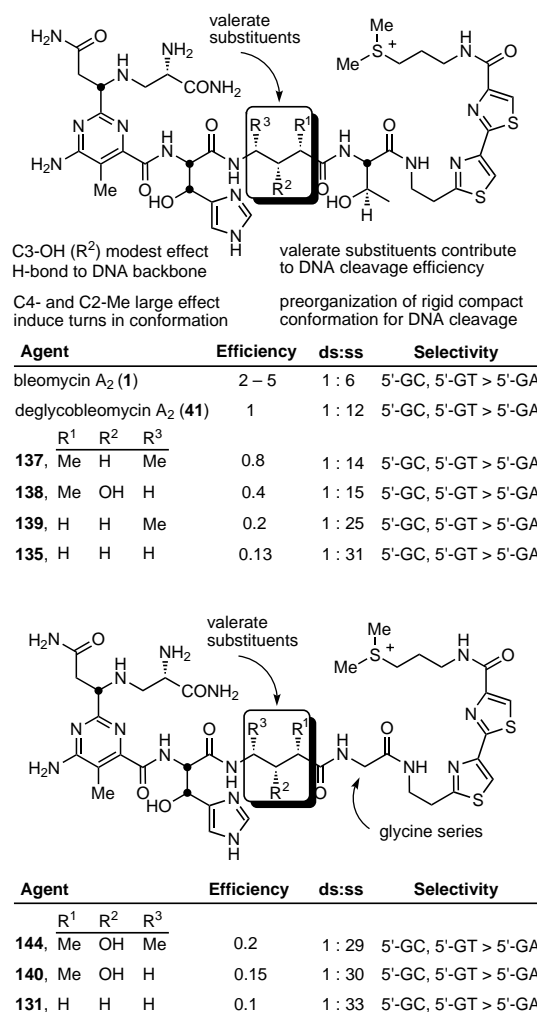


Figure 18. DNA cleavage by bleomycin A₂ analogues with modified valeric acid subunits. The valerate substituents contribute to the efficiency of the DNA cleavage.

The cumulative substituent effects are substantial and highlight an unappreciated role they play in the preorganization of bleomycin A₂ into a rigid, compact conformation suitable for DNA cleavage. The valerate subunit of both free and DNA-bound Co^{III}-OOH bleomycin A₂ and deglycobleomycin A₂ adopts an identical, well-defined, and rigid conformation (Figure 19). Important characteristics of this conformation are two turns, one at the C2 center and one at the C4 center. Diagnostic of this conformation is the small coupling constant for C2-H/C3-H ($J = 1.8 \pm 1.2$ Hz) and the large coupling constant for C3-H/C4-H ($J = 9.5 \pm 1.2$ Hz).^[52]

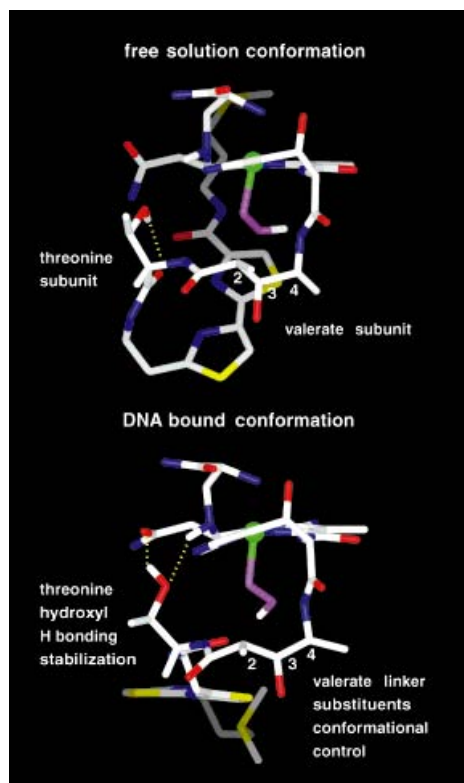


Figure 19. Models of the linker domain taken from the structures determined by NMR spectroscopy of free and DNA-bound Co^{III}-OOH bleomycin A₂.^[52]

The C2 site within the valerate could adopt two accessible conformations (Figure 20). The eclipsed conformation between the carbonyl and the C2 methyl group was found to be favored, presumably through adoption of H bonds from the valerate NH and the threonine NH to the metal-bound hydroperoxide (1.8 Å, 155° and 1.9 Å, 152°, respectively). This is further reinforced for the DNA-bound agents by a H bond from the C3 hydroxyl group to the DNA phosphate backbone (see Figure 13).^[52] Alternative conformations about the C3 (≥ 2.65 –3.35 kcal mol⁻¹) or C4 centers (> 2.4 –2.65 kcal mol⁻¹) are much less stable and constitute non-contributing conformations. The C4 methyl substituent when combined with the presence of the C2 methyl group, must adopt the extended orientation to induce a second turn in the valerate subunit at the amide bond that links the histidine

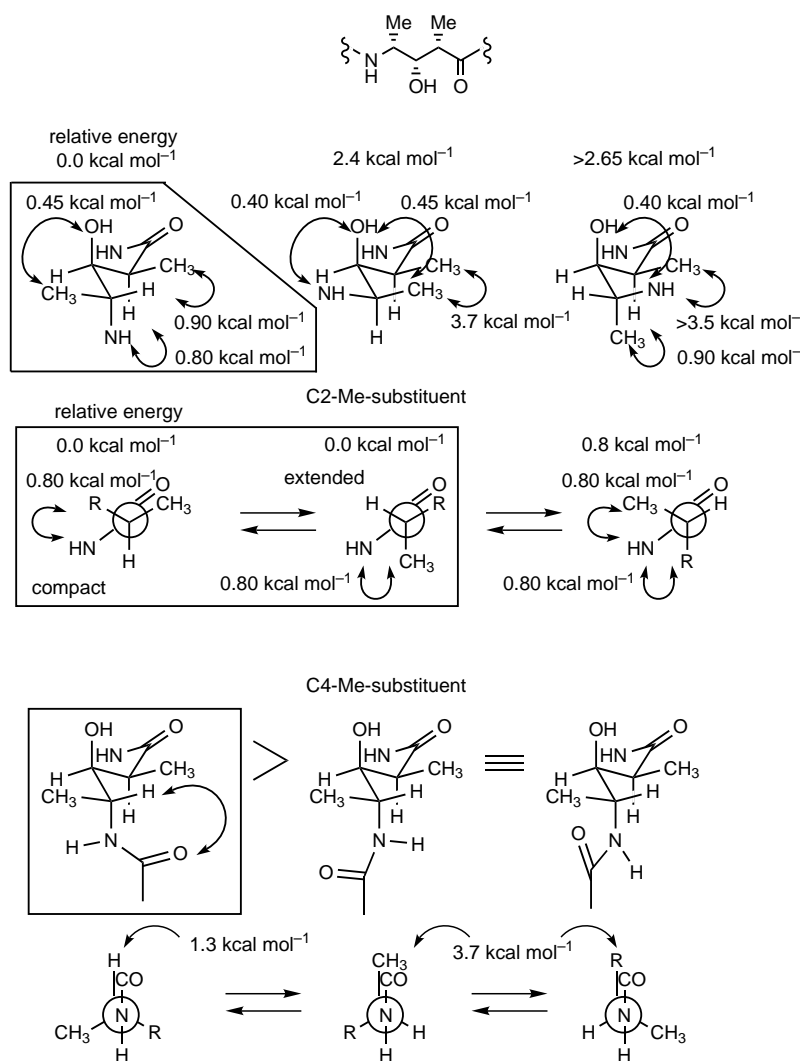


Figure 20. Conformational effects of the valerate substituents.

subunit (≥ 2.4 –2.65 kcal mol⁻¹). Just as important as this turn is the placement of the amide group, the conformation in which its carbonyl group eclipses the H atom is also preferred (ΔE ca. 2.4 kcal mol⁻¹) and sets a defined orientation for the histidine subunit and the entire metal binding domain. In total, this provides the rigid core structure about which the DNA binding domain and the metal chelation domain are linked.

The C3 hydroxyl group is engaged in a H bond with a DNA backbone phosphate group that spans the intercalation site, which may contribute to the affinity and alignment of the DNA-bound agent. Its removal has little effect on the conformation about the C3 center ($\Delta E_{\text{alternatives}} = 2.25$ –2.45 kcal mol⁻¹) or the C4 center ($\Delta E_{\text{alternatives}} = 2.0$ –2.7 kcal mol⁻¹), and it is the lost intermolecular H bond with the nonbridging oxygen atom of the phosphate backbone that may account for the modest decrease in the cleavage efficiency with **137** (0.8 ×). With the exception of this effect, the remainder of the results correlate remarkably well with the ability of the agents to adopt the compact conformation implicated in the structural studies of Stubbe et al. (Table 3). The cumulative effect is substantial and suggests that an important functional role of the valerate substituents is to

Table 3. Effects of the valerate substituents.

Agent	R ¹	R ²	R ³	$\Delta E_{\text{rel.}}^{\text{[a]}}$ [kcal mol ⁻¹]	Z ^[b]
41	Me	OH	Me	0.0	1.0
137	Me	H	Me	0.0 ^[c]	0.8 ^[c]
138	Me	OH	H	0.4 ^[d]	0.4 ^[d]
139	H	H	Me	0.8	0.2
135	H	H	H	1.6	0.13

[a] $\Delta E_{\text{rel.}} = E(\text{low energy conformation}) - E(\text{DNA-bound conformation adopted by Co}^{\text{III}}\text{-OOH BLM A}_2\text{})$. [b] Z is the relative DNA cleavage efficiency. [c] Lacks the capability for a intermolecular H bond from C3-OH to the DNA phosphate group (see text). [d] Possesses two equivalent amide orientations of the L-histidine subunit in which the H atoms are in eclipsed positions versus one which contributes further to a reduction in the cleavage efficiency (see text).

preorganize bleomycin A₂ into a rigid, compact conformation productive for DNA cleavage.

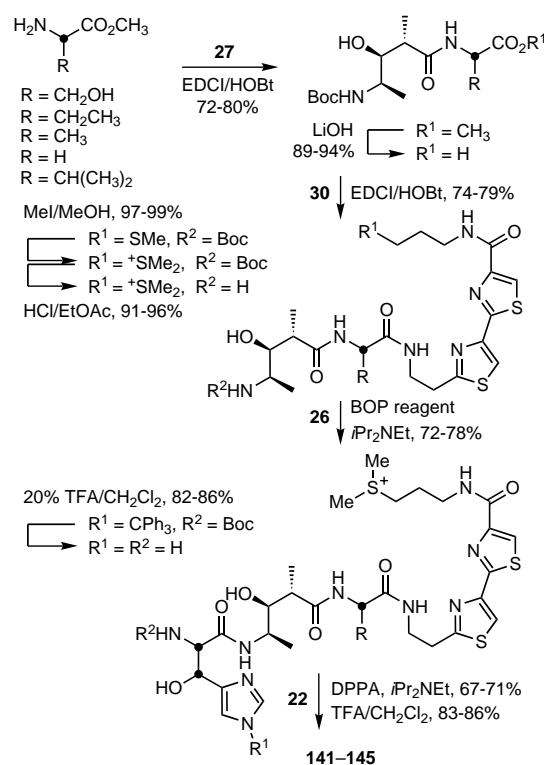
3.3.2. The Threonine Subunit

3.3.2.1. Substituent Effects^[109, 110]

In our efforts to understand the role of the linker domain and following initial studies that indicated that the L-threonine side chain contributed substantially to the cleavage efficiency, a complete series of side-chain analogues (**141**–**145**) was examined to systematically dissect the subtle contributions of this subunit. In part, this was assumed to be a consequence of conformational effects imposed by the side chain that induced a turn at the threonine–valerate junction and facilitated the adoption of a compact conformation. In addition, the threonine carbonyl group of the DNA bound conformation, but not the free solution conformation, of the bleomycin Co^{III}-OOH complex was found to be positioned to accept a H bond from the terminal oxygen atom of the hydroperoxide ligand in the structural model of Stubbe et al., which implicated additional roles for the L-threonine subunit. Similarly, the threonine hydroxyl group was engaged in a network of H bonding with the metal binding domain, which further contributes to the stabilization of the compact conformation. The approach to **141**–**145** entailed the synthesis of the pentapeptide S analogues with five altered side chains and a final coupling with N⁶-Boc-pyrimidoblamic acid (Scheme 25).

DNA cleavage studies revealed that variations in the L-threonine subunit substituents had no impact on the cleavage selectivity, but did have a large effect on the cleavage efficiency (Figure 21). This was consistent with our initial studies that indicated that the effect was both substantial and general when threonine was replaced with glycine (see Figures 16 and 18). In addition, the glycine analogue **144** was shown to oxidize styrene nearly as effectively as deglycobleomycin A₂ (0.5 ×) at an initial rate that was not distinguishable, albeit with twofold fewer turnovers in the catalytic reaction.

The studies defined a clear potentiating role for the L-threonine hydroxyl group, highlighted the importance of the presence of a substituent on the L-threonine subunit (R ≠ H), and suggested the effect is unusually sensitive to the size of the



Scheme 25. Preparation of bleomycin A₂ analogues with threonine subunit modifications.

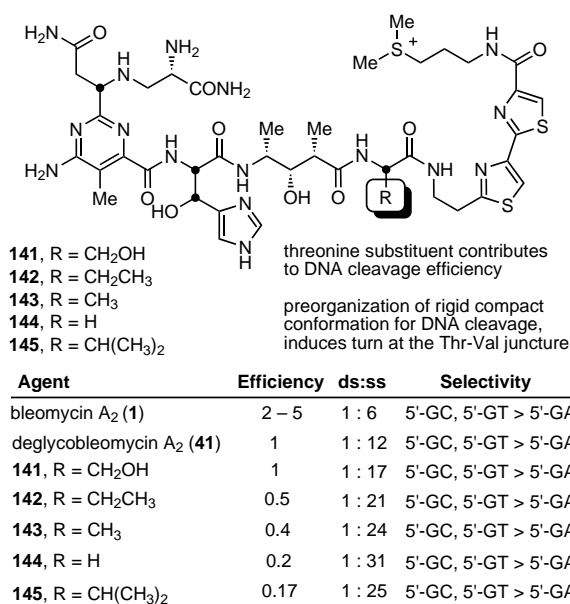


Figure 21. DNA cleavage of bleomycin A₂ analogues with threonine subunits modifications.

substituent (R = CH₃ ≅ Et > iPr). A remarkably good correlation was observed between the cleavage efficiencies and the calculated Boltzmann probabilities^[111] of adopting the L-threonine subunit local conformation observed with free Co^{III}-OOH bleomycin A₂ and, with the exception of valine, with the total distribution within the free and DNA-bound conformations of Co^{III}-OOH bleomycin A₂ (Table 4). This suggests that the L-threonine substituent facilitates preorga-

Table 4. Effects of substituents on the threonine subunit.

Agent	$Z^{[a]}$	$P_B^{[b]}$	$P_B^{[b]}$	$P_B^{[b]}$
		$\Psi = 20$ to 130°	$\Psi = 130$ to -140°	(total)
Thr, R = CH(OH)CH ₃	1.0	0.798	0.153	0.951
Ser, R = CH ₂ OH	1–0.9	0.776	0.087	0.863
Abu, R = Et	0.50	0.605	0.191	0.796
Ala, R = CH ₃	0.45	0.589	0.138	0.727
Gly, R = H	0.20	0.425	0.049	0.474
Val, R = <i>i</i> Pr	0.17	0.390	0.335	0.725

[a] Z is the relative DNA cleavage efficiency. [b] P_B = Boltzmann probability of having the peptide binding angle Ψ (taken from ref. [111], for AcN-X-NHMe). Free Co^{III}-OOH BLM A₂ ($\Phi = -121.5^\circ$, $\Psi = 120.4^\circ$). DNA-bound Co^{III}-OOH BLM A₂ ($\Phi = -145.5^\circ$, $\Psi = 173.9^\circ$).

nization of bleomycin A₂ into a compact conformation productive for DNA cleavage (see Figure 19). The additional important role of the hydroxyl group may be attributed to either intramolecular H bonding to the threonine carbonyl group or, more provocatively, to the distal carbonyl group of the C2-acetamido side chain of pyrimidoblastic acid to stabilize a preorganized conformation of activated bleomycin productive for DNA cleavage (see Figure 19). This could, in part, also explain the potentiating role of the acetamide side chain (ca. $4 \times$, see Figure 10). However, we cannot rule out an intermolecular H bond with DNA itself, although structural models to date have not provided evidence for such an interaction.

The simpler effect of the presence of a substituent is consistent with an important role in restricting the available conformations accessible to the agent (Figure 22). In the presence of a substituent ($R \neq H$), a dominant effect of restricting the valerate–threonine amide group to a single orientation ($\Phi = -120^\circ$) induces a turn in the linker domain. Removal of this substituent ($R = H$) results in five accessible conformations, at least three of which may be nonproductive for DNA cleavage. Moreover, as the size of the substituent increases, the conformations nonproductive for DNA cleavage become increasingly favored and result in diminished cleavage ($R = \text{Me} \cong \text{Et} > i\text{Pr}$).

3.3.2.2. Replacement of the Threonine Amide Group^[112]

The NMR studies of the Co^{III}-OOH complex of both free and DNA-bound bleomycin revealed that they may benefit from a H bond from the threonine NH group to the proximal oxygen atom of the metal-bound hydroperoxide (Figure 23).^[52] This H bond could stabilize the productive bound conformation of the activated agent, fix the position of the reacting Fe-oxo intermediate for abstraction of the C4' hydrogen atom, stabilize the metal-bound hydroperoxide, or contribute to catalysis of the reaction by assisting homolytic oxygen–oxygen bond cleavage. In light of this interaction of the threonine NH group, we examined **146** and its epimer **147** in which the threonine amide group was replaced with a *N*-methyl amide group. The synthesis of **146** was accomplished through preparation of the tetrapeptide **152** with the *N*-methyl-L-threonine subunit (Scheme 26). NMe-Thr-OMe was prepared from L-Thr-OMe by sequential reductive benzylation and methylation followed by reductive debenylation. Its

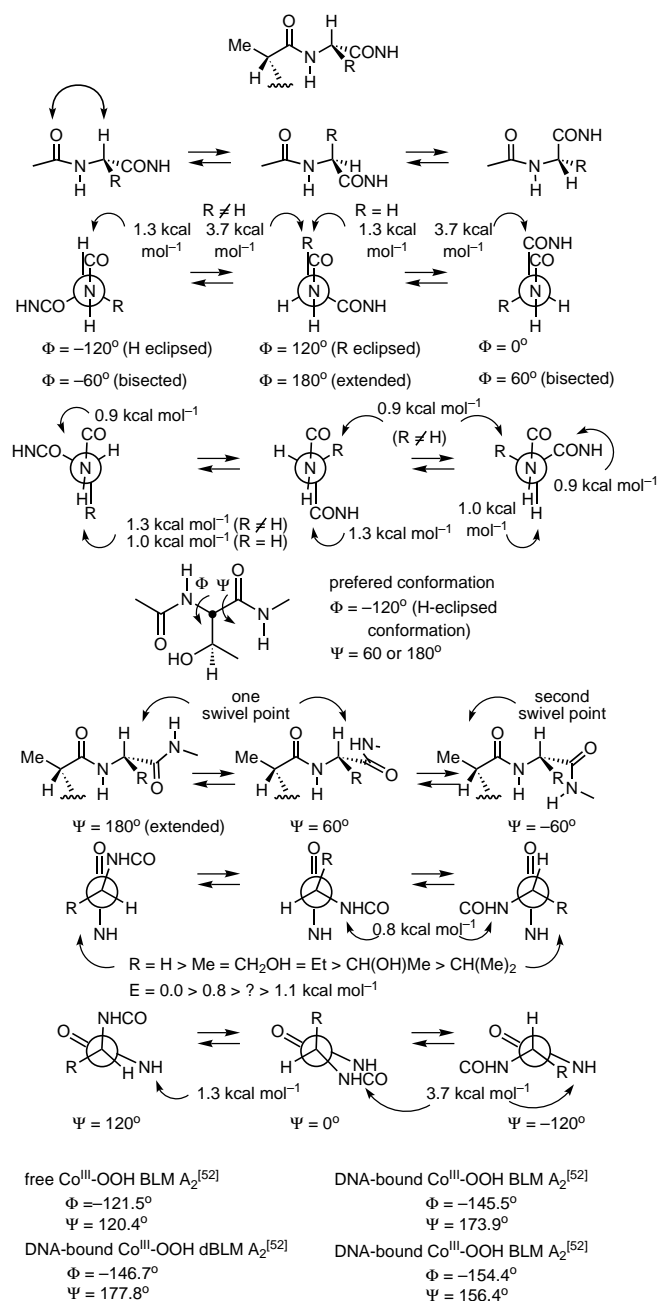
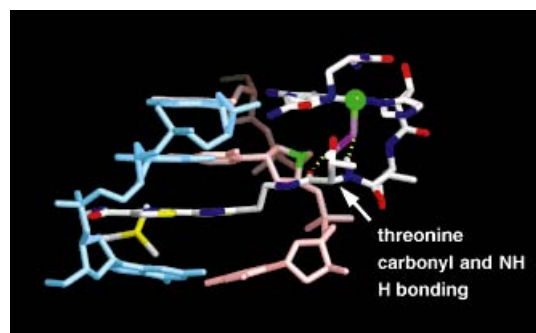
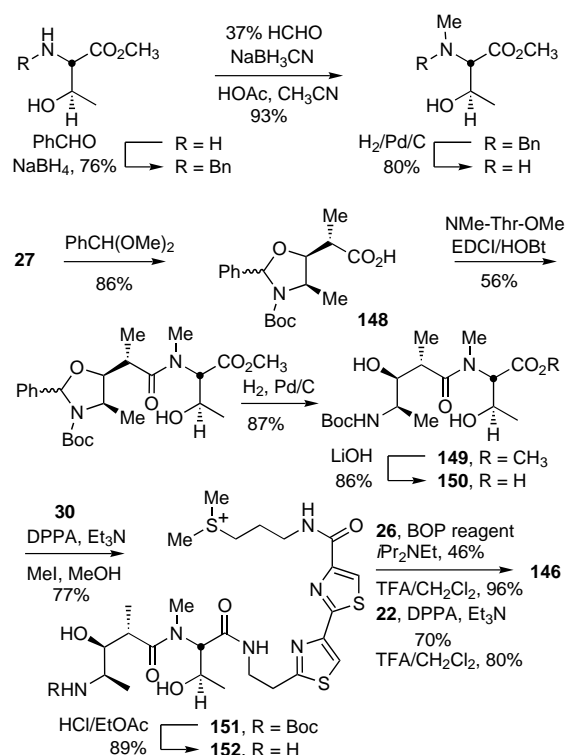


Figure 22. Conformational effects of the threonine subunit.

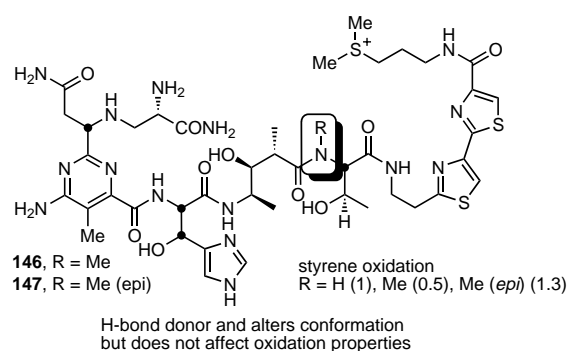
Figure 23. Model derived from ¹H NMR spectroscopy highlighting the threonine NH and carbonyl H bonds to the metal-bound hydroperoxide of Co^{III}-OOH bleomycin A₂.^[52]



Scheme 26. Synthesis of bleomycin A_2 analogues with *N*-methyl substituted threonine amide groups.

coupling with **27** failed to provide a useful approach to **149**, and **27** preferentially closed to the corresponding five-membered *N*-Boc lactam. Consequently, the coupling was accomplished with the cyclic N,O-acetal **148** prepared by treatment of **27** with benzaldehyde dimethyl acetal. Coupling of **148** with NMe-Thr-OMe after cleavage of the N,O-acetal provided the key dipeptide **149**. Methyl ester hydrolysis followed by coupling with **30** provided **151** and small amounts of the separable diastereomer. The analogue **146** was assembled by sequential couplings to introduce the *erythro*- β -hydroxy-L-histidine and pyrimidoblamic acid subunits after formation of the sulfonium salt. Conducting the same sequence on the minor diastereomer of **152** provided **147** in comparable conversions.

DNA cleavage studies revealed that *N*-methylation of the threonine amide group dramatically reduced the DNA cleavage efficiency (10–15 \times), weakened and nearly abolished the inherent DNA cleavage selectivity, but had little effect on the inherent oxidation capabilities of the activated Fe^{III} complexes (Figure 24). These results along with those in the preceding section not only suggest that the unsubstituted amide group is essential, but that the conformational or stabilization effects of the H bond of the threonine NH group account for the observations rather than a role related to oxidation catalysis. This is consistent with a previously unrecognized prominent role for the threonine NH group and suggests a potential importance for the H bond to the Fe^{III} -OOH complex of bleomycin or a subsequent Fe-oxo intermediate implicated the structural models of Stubbe et al.^[52]



Agent	Efficiency	ds:ss	Selectivity
bleomycin A_2 (1)	2–5	1 : 6	5'-GC, 5'-GT > 5'-GA
deglycobleomycin A_2 (41)	1	1 : 12	5'-GC, 5'-GT > 5'-GA
146 , R = Me	0.08	1 : 58	5'-GC, 5'-GT > 5'-GA
147 , R = Me (epi)	0.08	1 : 53	none
Fe^{III}	0.04	1 : 98	none

Figure 24. DNA cleavage properties of bleomycin A_2 with modified L-Thr amide groups.

3.4. The C-Terminus DNA Binding Domain

The importance of the C-terminus cation and its electrostatic contribution to DNA binding is well recognized from studies of *S*-desmethyldeglycobleomycin A_2 ^[24d, 72a] (**153**) and bleomycinic acid,^[96] both of which lack the terminal sulfonium salt. To assess the relative impact of the substitution of a sulfoxide for the sulfonium salt deglycobleomycin A_1 (**154**), the aglycone of a naturally occurring bleomycin, was prepared and evaluated. Despite the importance of this comparison, especially in light of the reported altered DNA cleavage selectivity of bleomycinic acid, neither synthetic nor naturally derived deglycobleomycin A_1 had been described previously.

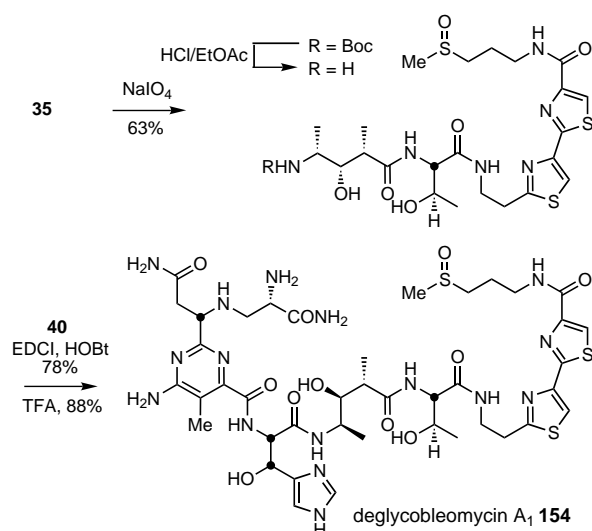
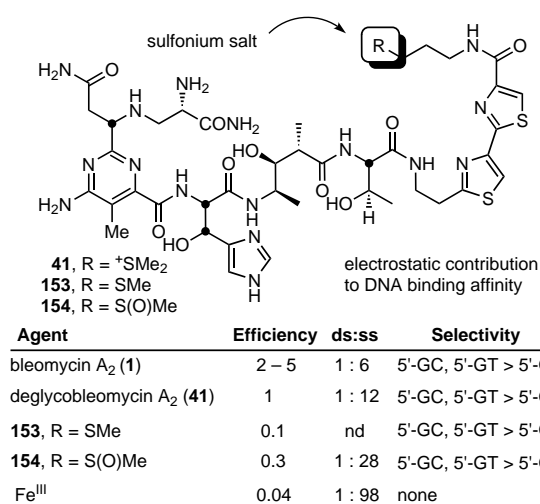
3.4.1. Deglycobleomycin A_1 ^[18e]

Deliberate oxidation of the tetrapeptide S precursor **35** proceeded cleanly to provide the sulfoxide (Scheme 27). Acid-catalyzed deprotection, coupling with **40**, and acid-catalyzed deprotection provided deglycobleomycin A_1 (**154**).

The DNA cleavage studies demonstrated an important, productive role for the terminal sulfoxide or sulfonium salt (Figure 25). Removal of the positive charge resulted in a tenfold decrease in DNA cleavage efficiency although the sequence selectivity was not altered. Introduction of the sulfoxide group reestablished some but not all of the cleavage efficiency. In the structural model of Stubbe et al. the cation threads through the base pairs into the major groove with the perpendicular intercalation of the bithiazole unit, and is in electrostatic contact with the negatively charged phosphate backbone.

4. Summary and Outlook

Our studies have focused on the elucidation of the functional roles of bleomycin subunits through the synthesis and

Scheme 27. Total synthesis of deglycobleomycin A₁ (**154**).Figure 25. DNA cleavage properties of bleomycin A₂ analogues with modified sulfonium groups.

evaluation of key structural analogues. These studies demonstrated the essential roles of the amide nitrogen atom of β -hydroxy-L-histidine and the imidazole N⁺ atom in metal chelation, the important role of tripeptide S and the C-terminus sulfonium cation in providing the majority of the binding affinity, and the unrecognized subtle substituent and conformational effects of the linker domain in preorganization and stabilization of a compact conformation implicated in DNA cleavage. Detailed assessments of the pyrimidoblastic acid substituents and side chains established little or no role for the C5 methyl and terminal α -carboxamide group, and an important subtle role for the C2-acetamide side chain. This latter role potentially involves H bonding of the carboxamide NH₂ group to the C2 carbonyl group of cytosine that is base paired with the guanine at the cleavage site, and H bonding of the carbonyl group to the threonine hydroxyl group. The former would contribute to the stability of the binding at a cleavage site while the latter reinforces adoption of a compact conformation productive for DNA cleavage. Most important was the demonstration of the C4 amine group on pyrimidine

in H bonding, DNA recognition, and as the source of the DNA cleavage selectivity. Based on these studies, new or rigid analogues of bleomycin A₂ that can potentially effect the preorganization of the productive bound conformation, affect or alter the sequence selectivity of the DNA cleavage, or affect the double strand versus single strand DNA cleavage events are being pursued in our laboratories. The integral details of the role of the disaccharide subunit remain to be established and a systematic examination of the intercalating bithiazole group have not yet been conducted. Specifically labeled materials (for example, N¹⁵) are being pursued in efforts to unambiguously define the metal chelation. Finally, details of the second cleavage reaction of double-strand DNA, as well as knowledge of the subtle details of the catalytic activation and degradation of bleomycin, would assist in the design of more effective agents.

The work detailed herein was carried out by a small but spirited group of students: Dr. S. L. Colletti, Dr. T. Honda, S. Teramoto, Hui Cai, Dr. Tim Ramsey, and Royce Menezes with the more recent investigations carried out in collaboration with Prof. J. Stubbe (MIT) and her group. The work was supported financially by the National Institutes of Health (CA42056) and the Skaggs Institute for Chemical Biology.

Received: December 29, 1997

Revised edition: April 14, 1998 [A267IE]

German version: *Angew. Chem.* **1999**, *111*, 470–500

- [1] H. Umezawa, K. Maeda, T. Takeuchi, Y. Okami, *J. Antibiot.* **1966**, *19*, 200–209.
- [2] *Bleomycin: Current Status and New Developments* (Eds.: S. K. Carter, S. T. Crooke, H. Umezawa), Academic Press, New York, **1978**.
- [3] *Bleomycin: Chemical, Biochemical and Biological Aspects* (Ed.: S. M. Hecht), Springer, New York, **1979**.
- [4] *Bleomycin Chemotherapy* (Eds.: B. I. Sikic, M. Rozenzweig, S. K. Carter), Academic Press, Orlando, **1985**.
- [5] a) A. Natrajan, S. M. Hecht in *Molecular Aspects of Anticancer Drug-DNA Interactions, Vol. 2* (Eds.: S. Neidle, M. J. Waring), CRC, Boca Raton, **1994**, pp. 197–242; b) S. A. Kane, S. M. Hecht, *Prog. Nucleic Acids Res. Mol. Biol.* **1994**, *49*, 313–352.
- [6] M. Ohno, M. Otsuka in *Recent Progress in the Chemical Synthesis of Antibiotics* (Eds.: G. Lukacs, M. Ohno), Springer, New York, **1990**, pp. 387–414.
- [7] L. F. Povirk in *Molecular Aspects of Anti-Cancer Drug Action* (Eds.: S. Neidle, M. J. Waring), MacMillan, London, **1983**, pp. 157–181.
- [8] J. S. Lazo, B. A. Chabner in *Cancer Chemotherapy and Biotherapy: Principles and Practice*, 2nd ed. (Eds.: B. A. Chabner, D. L. Longo), Lippincott-Raven, Philadelphia, **1996**, pp. 379–393.
- [9] J. C. Dabrowiak, *Adv. Inorg. Chem.* **1982**, *4*, 69–113.
- [10] a) J. Stubbe, J. W. Kozarich, *Chem. Rev.* **1987**, *87*, 1107–1136; b) J. Stubbe, J. W. Kozarich, W. Wu, D. E. Vanderwall, *Acc. Chem. Res.* **1996**, *29*, 322–330.
- [11] S. M. Hecht, *Acc. Chem. Res.* **1986**, *19*, 383–391.
- [12] P. C. Dedon, I. H. Goldberg, *Chem. Res. Toxicol.* **1992**, *5*, 311–332.
- [13] D. H. Petering, R. W. Byrnes, W. E. Antholine, *Chem. Biol. Interact.* **1990**, *73*, 133–182.
- [14] Y. Sugiura, T. Takita, H. Umezawa, *Met. Ions Biol. Syst.* **1985**, *19*, 81–108.
- [15] P. R. Twentyman, *Pharmacol. Ther.* **1984**, *23*, 417–441.
- [16] a) H. Umezawa, *Pure Appl. Chem.* **1971**, *28*, 665–680; b) T. Takita, Y. Muraoka, T. Yoshioka, A. Fujii, K. Maeda, H. Umezawa, *J. Antibiot.*

- 1972**, 25, 755–758; b) Y. Muraoka, A. Fujii, T. Yoshioka, T. Takita, H. Umezawa, *J. Antibiot.* **1977**, 30, 178–181.
- [17] a) T. Takita, Y. Muraoka, T. Nakatani, A. Fujii, Y. Umezawa, H. Naganawa, H. Umezawa, *J. Antibiot.* **1978**, 31, 801–804; b) T. Fukuoka, Y. Muraoka, A. Fujii, H. Naganawa, T. Kakita, H. Umezawa, *J. Antibiot.* **1980**, 33, 114–117.
- [18] a) D. L. Boger, R. F. Menezes, T. Honda, *Angew. Chem.* **1993**, 105, 310–311; *Angew. Chem. Int. Ed. Engl.* **1993**, 32, 273–275; b) D. L. Boger, T. Honda, R. F. Menezes, S. L. Colletti, Q. Dang, W. Yang, *J. Am. Chem. Soc.* **1994**, 116, 82–92; c) D. L. Boger, S. L. Colletti, T. Honda, R. F. Menezes, *J. Am. Chem. Soc.* **1994**, 116, 5607–5618; d) D. L. Boger, T. Honda, Q. Dang, *J. Am. Chem. Soc.* **1994**, 116, 5619–5630; e) D. L. Boger, T. Honda, R. F. Menezes, S. L. Colletti, *J. Am. Chem. Soc.* **1994**, 116, 5631–5646; f) D. L. Boger, T. Honda, *J. Am. Chem. Soc.* **1994**, 116, 5647–5656.
- [19] R. Ishida, T. Takahashi, *Biochem. Biophys. Res. Commun.* **1975**, 66, 1432–1438.
- [20] a) E. A. Sausville, J. Peisach, S. B. Horwitz, *Biochem. Biophys. Res. Commun.* **1976**, 73, 814–822; b) E. A. Sausville, R. W. Stein, J. Peisach, S. B. Horwitz, *Biochemistry* **1978**, 17, 2740–2746; c) R. M. Burger, J. Peisach, S. B. Horwitz, *J. Biol. Chem.* **1981**, 256, 11633–11644; d) R. M. Burger, T. A. Kent, S. B. Horwitz, E. Munck, J. Peisach, *J. Biol. Chem.* **1983**, 258, 1559–1564.
- [21] R. M. Burger, G. Tian, K. Drlica, *J. Am. Chem. Soc.* **1995**, 117, 1167–1168.
- [22] A. D. D'Andrea, W. A. Haseltine, *Proc. Natl. Acad. Sci. USA* **1978**, 75, 3608–3612.
- [23] M. Takeshita, A. P. Grollman, E. Ohtsubo, H. Ohtsubo, *Proc. Natl. Acad. Sci. USA* **1978**, 75, 5983–5987.
- [24] a) G. M. Ehrenfeld, J. B. Shipley, D. C. Heimbrook, H. Sugiyama, E. C. Long, J. H. van Boom, G. A. van der Marcel, N. J. Oppenheimer, S. M. Hecht, *Biochemistry* **1987**, 26, 931–942; b) A. Natrajan, S. M. Hecht, G. A. van der Marcel, J. H. van Boom, *J. Am. Chem. Soc.* **1990**, 112, 3997–4002; c) E. C. Long, S. M. Hecht, G. A. van der Marcel, J. H. van Boom, *J. Am. Chem. Soc.* **1990**, 112, 5272–5276; d) B. J. Carter, K. S. Reddy, S. M. Hecht, *Tetrahedron* **1991**, 47, 2463–2474.
- [25] L. F. Povirk, *Biochemistry* **1979**, 18, 3989–3995.
- [26] a) Y. Sugiura, T. Suzuki, *J. Biol. Chem.* **1982**, 257, 10544–10546; b) J. Kuwahara, Y. Sugiura, *Proc. Natl. Acad. Sci. USA* **1988**, 85, 2459–2463.
- [27] J. W. Sam, X.-J. Tang, J. Peisach, *J. Am. Chem. Soc.* **1994**, 116, 5250–5256.
- [28] T. E. Westre, K. E. Loeb, J. M. Zaleski, B. Hedman, K. O. Hodgson, E. I. Solomon, *J. Am. Chem. Soc.* **1995**, 117, 1309–1313.
- [29] a) H. Sugiyama, T. Tashiro, Y. Dannoue, T. Miwa, T. Matsuura, I. Saito, *Tetrahedron Lett.* **1989**, 30, 7213–7216; b) H. Sugiyama, H. Kawabata, T. Fujiwara, Y. Dannoue, I. Saito, *J. Am. Chem. Soc.* **1990**, 112, 5252–5257; c) H. Sugiyama, T. Sera, Y. Dannoue, R. Marumoto, I. Saito, *J. Am. Chem. Soc.* **1991**, 113, 2290–2295; d) H. Sugiyama, K. Ohmori, I. Saito, *J. Am. Chem. Soc.* **1994**, 116, 10326–10327.
- [30] a) J. C. Wu, J. W. Kozarich, J. Stubbe, *Biochemistry* **1985**, 24, 7562–7568; b) J. C. Wu, J. Stubbe, J. W. Kozarich, *Biochemistry* **1985**, 24, 7569–7573; c) J. W. Kozarich, L. Worth, Jr., B. L. Frank, D. F. Christner, D. E. Vanderwall, J. Stubbe, *Science* **1989**, 245, 1396–1399; d) L. E. Rabow, J. Stubbe, J. W. Kozarich, *J. Am. Chem. Soc.* **1990**, 112, 3196–3203; e) L. E. Rabow, G. H. McGall, J. Stubbe, J. W. Kozarich, *J. Am. Chem. Soc.* **1990**, 112, 3203–3208; f) G. H. McGall, L. E. Rabow, G. W. Ashley, S. H. Wu, J. W. Kozarich, J. Stubbe, *J. Am. Chem. Soc.* **1992**, 114, 4958–4967; g) L. Worth, Jr., B. L. Frank, D. F. Christner, M. J. Absalon, J. Stubbe, J. W. Kozarich, *Biochemistry* **1993**, 32, 2601–2609.
- [31] a) H. Sugiyama, R. E. Kikuskie, L.-H. Chang, L.-T. Ma, S. M. Hecht, G. A. van der Marcel, J. H. van Boom, *J. Am. Chem. Soc.* **1986**, 108, 3852–3854; b) H. Sugiyama, C. Xu, N. Murugesan, S. M. Hecht, *Biochemistry* **1988**, 27, 58–67; c) J. R. Barr, R. B. Van Atta, A. Natrajan, S. M. Hecht, *J. Am. Chem. Soc.* **1990**, 112, 4058–4060.
- [32] R. M. Burger, K. Drlica, B. Birdsall, *J. Biol. Chem.* **1994**, 269, 25978–25985.
- [33] a) L. F. Povirk, W. Wubker, W. Kohnlein, F. Hutchinson, *Nucleic Acids Res.* **1977**, 4, 3575–3580; b) L. F. Povirk, C. W. Houlgrave, *Biochemistry* **1988**, 27, 3850–3857; c) L. F. Povirk, Y.-H. Han, R. J. Steighner, *Biochemistry* **1989**, 28, 5808–5814; d) R. J. Steighner, L. F. Povirk, *Proc. Natl. Acad. Sci. USA* **1990**, 87, 8350–8354; e) L. F. Povirk, M. J. F. Austin, *Mutat. Res.* **1991**, 257, 127–143; f) R. A. Bennett, P. S. Swerdlow, L. F. Povirk, *Biochemistry* **1993**, 32, 3188–3195.
- [34] a) R. S. Lloyd, C. W. Haidle, R. R. Hewitt, *Cancer Res.* **1978**, 38, 3191–3196; b) R. S. Lloyd, C. W. Haidle, D. L. Robberson, *Biochemistry* **1978**, 17, 1890–1896.
- [35] M. O. Bradley, K. W. Kohn, *Nucleic Acids Res.* **1979**, 7, 793–804.
- [36] a) C. K. Mirabelli, C.-H. Huang, S. T. Crooke, *Cancer Res.* **1980**, 40, 4173–4177; b) C. K. Mirabelli, C.-H. Huang, R. G. Fenwick, S. T. Crooke, *Antimicrob. Agents Chemother.* **1985**, 27, 460–467.
- [37] T. Lindahl, *Mutat. Res.* **1990**, 238, 305–311.
- [38] B. Demple, L. Harrison, *Annu. Rev. Biochem.* **1994**, 63, 915–948.
- [39] a) M. J. Absalon, J. W. Kozarich, J. Stubbe, *Biochemistry* **1995**, 34, 2065–2075; b) M. J. Absalon, W. Wu, J. W. Kozarich, J. Stubbe, *Biochemistry* **1995**, 34, 2076–2086.
- [40] G. Brazilay, I. D. Hickson, *Bioessays* **1995**, 17, 713–719.
- [41] a) J. A. Tainer, M. M. Thayer, R. P. Cunningham, *Curr. Opin. Struct. Biol.* **1995**, 5, 20–26; b) T. P. Hilbert, R. J. Boorstein, H. C. Kung, P. H. Bolton, D. Xing, R. P. Cunningham, G. Teebor, *Biochemistry* **1996**, 35, 2505–2511.
- [42] a) B. J. Carter, E. de Vroom, E. C. Long, G. A. van der Marcel, J. H. van Boom, S. M. Hecht, *Proc. Natl. Acad. Sci. USA* **1990**, 87, 9373–9377; b) C. E. Holmes, B. J. Carter, S. M. Hecht, *Biochemistry* **1993**, 32, 4293–4307; c) C. E. Holmes, B. J. Carter, S. M. Hecht, *Biochemistry* **1993**, 32, 4293–4307; d) S. M. Hecht, *Bioconjug. Chem.* **1994**, 5, 513–526; e) C. H. Holmes, A. T. Abraham, S. M. Hecht, C. Florentz, R. Giege, *Nucleic Acids Res.* **1996**, 24, 3399–3406.
- [43] R. S. Magliozzo, J. Peisach, M. R. Ciolo, *Mol. Pharmacol.* **1989**, 35, 428–432.
- [44] a) M. J. Absalon, C. R. Krishnamoorthy, G. McGall, J. W. Kozarich, J. Stubbe, *Nucleic Acids Res.* **1992**, 20, 4179–4185; b) M. Bansal, J. S. Lee, J. Stubbe, J. W. Kozarich, *Nucleic Acids Res.* **1997**, 25, 1836–1845; c) M. Bansal, J. Stubbe, J. W. Kozarich, *Nucleic Acids Res.* **1997**, 25, 1846–1853.
- [45] Deglycobleomycin A₂: a) N. J. Oppenheimer, C. Chang, L.-H. Chang, G. Ehrenfeld, L. O. Rodriguez, S. M. Hecht, *J. Biol. Chem.* **1982**, 257, 1606–1609; b) Y. Sugiura, T. Suzuki, M. Otsuka, S. Kobayashi, M. Ohno, T. Takita, H. Umezawa, *J. Biol. Chem.* **1983**, 258, 1328–1336; c) Y. Sugiura, J. Kuwahara, T. Suzuki, *FEBS Lett.* **1985**, 182, 39–42. d) A. Kenani, G. Lamblin, J.-P. Henichart, *Carbohydr. Res.* **1988**, 177, 81–89; e) D. L. Boger, R. F. Menezes, W. Yang, *Bioorg. Med. Chem. Lett.* **1992**, 2, 959–962.
- [46] iso-Bleomycin A₂: Y. Nakayama, M. Kunishima, S. Omoto, T. Takita, H. Umezawa, *J. Antibiot.* **1973**, 26, 400–402.
- [47] epi-Bleomycin A₂: Y. Muraoka, H. Kobayashi, A. Fujii, M. Kunishima, T. Fujii, Y. Nakayama, T. Takita, H. Umezawa, *J. Antibiot.* **1976**, 29, 853–856.
- [48] Deamidobleomycin A₂: H. Umezawa, S. Hori, T. Sawa, T. Yoshioka, T. Takeuchi, *J. Antibiot.* **1974**, 27, 419–424.
- [49] Deamidobleomycin A₂ and depyruvamidebleomycin A₂: Y. Sugiura, *J. Am. Chem. Soc.* **1980**, 102, 5208–5215.
- [50] Decarbamoylbleomycin A₂: H. Sugiyama, G. M. Ehrenfeld, J. B. Shipley, R. E. Kikuskie, L.-H. Chang, S. M. Hecht, *J. Nat. Prod.* **1985**, 48, 869–877.
- [51] PEMH and iso-bithiazole bleomycin A₂: a) T. Morii, T. Matsuura, I. Saito, T. Suzuki, J. Kuwahara, Y. Sugiura, *J. Am. Chem. Soc.* **1986**, 108, 7089–7094; b) T. Morii, I. Saito, T. Matsuura, J. Kuwahara, Y. Sugiura, *J. Am. Chem. Soc.* **1987**, 109, 938–939.
- [52] a) W. Wu, D. E. Vanderwall, S. M. Lui, X.-J. Tang, C. J. Turner, J. W. Kozarich, J. Stubbe, *J. Am. Chem. Soc.* **1996**, 118, 1268–1280; b) W. Wu, D. E. Vanderwall, C. J. Turner, J. W. Kozarich, J. Stubbe, *J. Am. Chem. Soc.* **1996**, 118, 1281–1294; c) W. Wu, D. E. Vanderwall, J. Stubbe, J. W. Kozarich, C. J. Turner, *J. Am. Chem. Soc.* **1994**, 116, 10843–10844; d) D. E. Vanderwall, S. M. Lui, W. Wu, C. J. Turner, J. W. Kozarich, J. Stubbe, *Chem. Biol.* **1997**, 4, 373–387; e) S. M. Lui, D. E. Vanderwall, W. Wu, X.-J. Tang, C. J. Turner, J. W. Kozarich, J. Stubbe, *J. Am. Chem. Soc.* **1997**, 119, 9603–9613; f) W. Wu, D. E. Vanderwall, S. Teramoto, S. M. Lui, S. Hoehn, X.-J. Tang, C. J. Turner, D. L. Boger, J. W. Kozarich, J. Stubbe, *J. Am. Chem. Soc.* **1998**, 120, 2239–2250.

- [53] a) R. A. Manderville, J. F. Ellena, S. M. Hecht, *J. Am. Chem. Soc.* **1994**, *116*, 10851–10852; b) R. A. Manderville, J. F. Ellena, S. M. Hecht, *J. Am. Chem. Soc.* **1995**, *117*, 7891–7903.
- [54] a) R. X. Xu, W. E. Antholine, D. H. Petering, *J. Biol. Chem.* **1992**, *267*, 944–949; b) Q. Mao, P. Fulmer, W. Li, E. F. DeRose, D. H. Petering, *J. Biol. Chem.* **1996**, *271*, 6185–6191; c) J. D. Otvos, W. E. Antholine, S. Wehrli, D. H. Petering, *Biochemistry* **1996**, *35*, 1458–1465; d) P. Fulmer, C. Zhao, W. Li, E. DeRose, W. E. Antholine, D. H. Petering, *Biochemistry* **1997**, *36*, 4367–4374; e) R. X. Xu, D. Nettekheim, J. D. Otvos, D. H. Petering, *Biochemistry* **1994**, *33*, 907–916.
- [55] A. M. Calafat, H. Won, L. G. Marzilli, *J. Am. Chem. Soc.* **1997**, *119*, 3656–3664.
- [56] T. E. Lehmann, L.-J. Ming, M. E. Rosen, L. Que, Jr., *Biochemistry* **1997**, *36*, 2807–2816.
- [57] a) J. Caceres-Cortes, H. Sugiyama, K. Ikudome, I. Saito, A. H.-J. Wang, *Eur. J. Biochem.* **1997**, *244*, 818–828; b) J. Caceres-Cortes, H. Sugiyama, K. Ikudome, I. Saito, A. H.-J. Wang, *Biochemistry* **1997**, *36*, 9995–10005.
- [58] Y. Yang, L. Huang, R. T. Pon, S.-F. Cheng, D.-K. Chang, J. W. Lown, *Bioconjug. Chem.* **1996**, *7*, 670–679.
- [59] a) J. D. Glickson, R. P. Pillai, T. T. Sakai, *Proc. Natl. Acad. Sci. USA* **1981**, *78*, 2967–2971; b) M. P. Gamcsik, J. D. Glickson, G. Zon, *J. Biomol. Struct. Dyn.* **1990**, *7*, 1117–1133.
- [60] a) M. A. J. Akkerman, C. A. G. Haansnoot, C. W. Hilbers, *Eur. J. Biochem.* **1988**, *173*, 211–225; b) M. A. J. Akkerman, E. W. J. F. Neijman, S. S. Wijmenga, C. W. Hilbers, W. Bermel, *J. Am. Chem. Soc.* **1990**, *112*, 7462–7474.
- [61] a) N. J. Oppenheimer, L. O. Rodriguez, S. M. Hecht, *Biochemistry* **1979**, *18*, 3439–3445; b) N. J. Oppenheimer, L. O. Rodriguez, S. M. Hecht, *Proc. Natl. Acad. Sci. USA* **1979**, *76*, 5616–5620; c) G. M. Ehrenfeld, L. O. Rodriguez, S. M. Hecht, C. Chang, V. J. Basus, N. J. Oppenheimer, *Biochemistry* **1985**, *24*, 81–92.
- [62] D. M. Chen, T. T. Sakai, J. D. Glickson, D. J. Patel, *Biochem. Biophys. Res. Commun.* **1980**, *92*, 197–205.
- [63] H. Kurosaki, K. Hayashi, Y. Ishikawa, M. Goto, *Chem. Lett.* **1995**, 691–692.
- [64] H. Urata, Y. Ueda, Y. Usami, M. Akagi, *J. Am. Chem. Soc.* **1993**, *115*, 7135–7138.
- [65] H. Hiroaki, T. Nakayama, M. Ikehara, S. Uesugi, *Chem. Pharm. Bull.* **1991**, *39*, 2780–2786.
- [66] M. Chien, A. P. Grollman, S. B. Horwitz, *Biochemistry* **1977**, *16*, 3641–3647.
- [67] a) N. J. Oppenheimer, L. O. Rodriguez, S. M. Hecht, *Biochemistry* **1980**, *19*, 4096–4103; b) N. J. Oppenheimer, C. Chang, L. O. Rodriguez, S. M. Hecht, *J. Biol. Chem.* **1981**, *256*, 1514–1517; c) J. Kross, W. D. Henner, W. A. Haseltine, L. Rodriguez, M. D. Levin, S. M. Hecht, *Biochemistry* **1982**, *21*, 3711–3721.
- [68] a) S. J. Brown, S. E. Hudson, P. K. Mascharak, M. M. Olmstead, *J. Am. Chem. Soc.* **1989**, *111*, 6446–6448; b) S. J. Brown, M. M. Olmstead, P. K. Mascharak, *Inorg. Chem.* **1990**, *29*, 3229–3234; c) J. D. Tan, S. E. Hudson, S. J. Brown, M. M. Olmstead, P. K. Mascharak, *J. Am. Chem. Soc.* **1992**, *114*, 3841–3853; d) E. Farinas, J. D. Tan, N. Baidya, P. K. Mascharak, *J. Am. Chem. Soc.* **1993**, *115*, 2996–2997; e) R. J. Guajardo, S. E. Hudson, S. J. Brown, P. K. Mascharak, *J. Am. Chem. Soc.* **1993**, *115*, 7971–7977; f) R. J. Guajardo, J. D. Tan, P. K. Mascharak, *Inorg. Chem.* **1994**, *33*, 2838–2840; g) R. J. Guajardo, F. Chavez, E. T. Farinas, P. K. Mascharak, *J. Am. Chem. Soc.* **1995**, *117*, 3883–3884; h) K. E. Loeb, J. M. Zaleski, T. W. Westre, R. J. Guajardo, P. K. Mascharak, B. Hedman, K. O. Hodgson, E. I. Solomon, *J. Am. Chem. Soc.* **1995**, *117*, 4545–4561; i) E. T. Farinas, J. D. Tan, P. K. Mascharak, *Inorg. Chem.* **1996**, *35*, 2637–2643.
- [69] a) R. X. Xu, W. E. Antholine, D. H. Petering, *J. Biol. Chem.* **1992**, *267*, 950–955; b) W. E. Antholine, J. S. Hyde, R. C. Sealy, D. H. Petering, *J. Biol. Chem.* **1984**, *259*, 4437–4440; c) J. C. Dabrowiak, M. Tsukayama, *J. Am. Chem. Soc.* **1981**, *103*, 7543–7550.
- [70] S. Takahashi, J. W. Sam, J. Peisach, D. L. Rousseau, *J. Am. Chem. Soc.* **1994**, *116*, 4408–4413.
- [71] A. Veselov, H. Sun, A. Sienkiewicz, H. Taylor, R. M. Burger, C. P. Scholes, *J. Am. Chem. Soc.* **1995**, *117*, 7508–7512.
- [72] a) B. C. Carter, V. S. Murty, K. S. Reddy, S.-N. Wang, S. M. Hecht, *J. Biol. Chem.* **1990**, *265*, 4193–4196; b) N. Hamamichi, A. Natrajan, S. M. Hecht, *J. Am. Chem. Soc.* **1992**, *114*, 6278–6291; c) S. Kane, A. Natrajan, S. M. Hecht, *J. Biol. Chem.* **1994**, *269*, 10899–10904.
- [73] a) A. Kittaka, Y. Sugano, M. Otsuka, M. Ohno, *Tetrahedron* **1988**, *44*, 2811–2820; b) M. Otsuka, T. Masuda, A. Haupt, M. Ohno, T. Shiraki, Y. Sugiura, K. Maeda, *J. Am. Chem. Soc.* **1990**, *112*, 838–845; c) T. Owa, T. Sugiyama, M. Otsuka, M. Ohno, *Tetrahedron Lett.* **1990**, *31*, 6063–6066; d) T. Owa, A. Haupt, M. Otsuka, S. Kobayashi, N. Tomioka, A. Itai, M. Ohno, T. Shiraki, M. Uesugi, Y. Sugiura, *Tetrahedron* **1992**, *48*, 1193–1208; e) T. Sugiyama, M. Ohno, M. Shibasaki, M. Otsuka, Y. Sugiura, S. Kobayashi, K. Maeda, *Heterocycles* **1994**, *37*, 275–282; f) A. Kittaka, Y. Sugano, M. Otsuka, M. Ohno, *Tetrahedron* **1988**, *44*, 2821–2833.
- [74] a) K. Shinozuka, H. Morishita, T. Yamazaki, Y. Sugiura, H. Sawai, *Tetrahedron Lett.* **1991**, *32*, 6869–6872; b) J. Kohda, K. Shinozuka, H. Sawai, *Tetrahedron Lett.* **1995**, *36*, 5575–5578; c) T. Arai, K. Shinozuka, H. Sawai, *Bioorg. Med. Chem. Lett.* **1997**, *7*, 15–18.
- [75] a) L. Huang, J. C. Quada, Jr., J. W. Lown, *Tetrahedron Lett.* **1994**, *35*, 5323–5326; b) L. Huang, J. W. Lown, *Heterocycles* **1995**, *41*, 1181–1185.
- [76] a) M. J. McLean, A. Dar, M. J. Waring, *J. Mol. Recognit.* **1989**, *1*, 184–192; b) K. Toshima, K. Ohta, A. Ohashi, T. Nakamura, M. Nakata, K. Tatsuta, S. Matsumura, *J. Am. Chem. Soc.* **1995**, *117*, 4822–4831; c) C. Bailly, M. J. Waring, *J. Am. Chem. Soc.* **1995**, *117*, 7311–7316; d) C. Bailly, A. Kenani, M. J. Waring, *FEBS Lett.* **1995**, *372*, 144–147; e) S. Jennewein, M. J. Waring, *Nucleic Acids Res.* **1997**, *25*, 1502–1509; f) C. Bailly, A. Kenani, M. J. Waring, *Nucleic Acids Res.* **1997**, *25*, 1516–1522.
- [77] a) L. F. Povirk, M. Hogan, N. Dattagupta, *Biochemistry* **1979**, *18*, 96–101; b) L. F. Povirk, M. Hogan, N. Dattagupta, M. Buechner, *Biochemistry* **1981**, *20*, 655–671; c) T. Suzuki, J. Kuwahara, M. Goto, Y. Sugiura, *Biochim. Biophys. Acta* **1985**, *824*, 330–335; d) D. Suh, L. F. Povirk, *Biochemistry* **1997**, *36*, 4248–4257.
- [78] a) A. Kenani, C. Bailly, N. Helbecque, J.-P. Catteau, R. Houssin, J.-L. Bernier, J.-P. Henichart, *Biochem. J.* **1988**, *253*, 497–504; b) A. Kenani, C. Bailly, R. Houssin, J. P. Henichart, *Anticancer Drugs* **1994**, *5*, 199–201.
- [79] M. Ohno, M. Otsuka, A. Kittaka, Y. Sugano, Y. Sugiura, T. Suzuki, J. Kuwahara, K. Umezawa, H. Umezawa, *Int. J. Exp. Clin. Chemother.* **1988**, *1*, 12.
- [80] a) R. E. Dickerson in *Mechanisms of DNA Damage and Repair: Implications for Carcinogenesis and Risk Assessment in Basic Life Sciences* (Eds.: M. G. Sini, L. Grossman), Plenum, New York, **1986**, pp. 245–255; b) R. Kuroda, H. Satoh, M. Shinomiya, T. Watanabe, M. Otsuka, *Nucleic Acids Res.* **1995**, *23*, 1524–1530.
- [81] J.-P. Henichart, J.-L. Bernier, N. Helbecque, R. Houssin, *Nucleic Acids Res.* **1985**, *13*, 6703–6717.
- [82] a) T. Takita, Y. Umezawa, S. Saito, H. Morishima, H. Naganawa, H. Umezawa, T. Tsushiya, T. Miyake, S. Kageyama, S. Umezawa, Y. Muraoka, M. Suzuki, M. Otsuka, M. Narita, S. Kobayashi, M. Ohno, *Tetrahedron Lett.* **1982**, *23*, 521–524; b) T. Takita, Y. Umezawa, S. Saito, H. Morishima, H. Umezawa, Y. Muraoka, Y. Suzuki, M. Otsuka, S. Kobayashi, M. Ohno, *Tetrahedron Lett.* **1981**, *22*, 671–674; c) S. Saito, Y. Umezawa, H. Morishima, T. Takita, H. Umezawa, M. Narita, M. Otsuka, S. Kobayashi, M. Ohno, *Tetrahedron Lett.* **1982**, *23*, 529–532; d) T. Tsuchiya, T. Miyake, S. Kageyama, S. Umezawa, H. Umezawa, T. Takita, *Tetrahedron Lett.* **1981**, *22*, 1413–1416; e) S. Saito, Y. Umezawa, T. Yoshioka, Y. Muraoka, T. Takita, H. Umezawa, *Pept. Chem.* **1983**, *20*, 133–138; f) S. Saito, Y. Umezawa, T. Yoshioka, T. Takita, H. Umezawa, Y. Muraoka, *J. Antibiot.* **1983**, *36*, 92–95; g) M. Otsuka, M. Narita, M. Yoshida, S. Kobayashi, M. Ohno, Y. Umezawa, H. Morishima, S. Saito, T. Takita, H. Umezawa, *Chem. Pharm. Bull.* **1985**, *33*, 520–526; h) T. Miyake, T. Tsuchiya, S. Umezawa, S. Saito, H. Umezawa, *Bull. Chem. Soc. Jpn.* **1986**, *59*, 1387–1395.
- [83] a) Y. Aoyagi, K. Katano, H. Suguna, J. Primeau, L.-H. Chang, S. M. Hecht, *J. Am. Chem. Soc.* **1982**, *104*, 5537–5538; b) Y. Aoyagi, H. Suguna, N. Murugesan, G. M. Ehrenfeld, L.-H. Chang, T. Ohgi, M. S. Shekhani, M. P. Kirkup, S. M. Hecht, *J. Am. Chem. Soc.* **1982**, *104*, 5237–5239; c) V. Pozsgay, T. Ohgi, S. M. Hecht, *J. Org. Chem.* **1981**, *46*, 3761–3763; d) K. Katano, P.-I. Chang, A. Millar, V. Pozsgay,

- D. K. Minster, T. Ohgi, S. M. Hecht, *J. Org. Chem.* **1985**, *50*, 5807–5815.
- [84] a) D. L. Boger, Q. Dang, *J. Org. Chem.* **1992**, *57*, 1631–1633; b) D. L. Boger, W. Yang, *Bioorg. Med. Chem. Lett.* **1992**, *2*, 1649–1654.
- [85] a) Y. Iitaka, H. Nakamura, T. Nakatani, Y. Muraoka, A. Fujii, T. Takita, H. Umezawa, *J. Antibiot.* **1978**, *31*, 1070–1072; b) T. Takita, Y. Muraoka, T. Nakatani, A. Fujii, Y. Iitaka, H. Umezawa, *J. Antibiot.* **1978**, *31*, 1073–1077.
- [86] a) *Hetero Diels–Alder Methodology in Organic Synthesis* (Eds.: D. L. Boger, S. M. Weinreb), Academic Press, San Diego, **1987**; b) D. L. Boger, *Tetrahedron* **1983**, *39*, 2869–2939; c) D. L. Boger, *Chem. Rev.* **1986**, *86*, 781–793; d) D. L. Boger, M. Patel, *Prog. Heterocycl. Chem.* **1989**, *1*, 30–64; e) D. L. Boger, *Bull. Soc. Chim. Belg.* **1990**, *99*, 599–615; f) D. L. Boger, *Chemtracts: Org. Chem.* **1996**, *9*, 149–189.
- [87] a) D. L. Boger, Q. Dang *Tetrahedron* **1988**, *44*, 3379; b) D. L. Boger, M. J. Kochanny, *J. Org. Chem.* **1994**, *59*, 4950–4955.
- [88] D. L. Boger, T. Honda, *Tetrahedron Lett.* **1993**, *34*, 1567–1570.
- [89] D. L. Boger, R. F. Menezes, *J. Org. Chem.* **1992**, *57*, 4331–4333.
- [90] T. Owa, M. Otsuka, M. Ohno, *Chem. Lett.* **1988**, 1873–1874.
- [91] D. A. Evans, A. E. Weber, *J. Am. Chem. Soc.* **1986**, *108*, 6757–6761.
- [92] T. T. Sakai, J. M. Riordan, T. E. Booth, J. D. Glickson, *J. Med. Chem.* **1981**, *24*, 279–285.
- [93] H. Kasai, H. Naganawa, T. Takita, H. Umezawa, *J. Antibiot.* **1978**, *31*, 1316–1320.
- [94] S. N. Roy, G. A. Orr, F. Brewer, S. B. Horwitz, *Cancer. Res.* **1981**, *41*, 4471–4477.
- [95] P. Sieber, B. Riniker, *Tetrahedron Lett.* **1987**, *28*, 6031–6034.
- [96] J. B. Shipley, S. M. Hecht, *Chem. Res. Toxicol.* **1988**, *1*, 25–27.
- [97] D. L. Boger, S. Teramoto, J. Zhou, *J. Am. Chem. Soc.* **1995**, *117*, 7344–7356.
- [98] D. L. Boger, S. Teramoto, H. Cai, *Bioorg. Med. Chem.* **1996**, *4*, 179–193.
- [99] In retrospect, the latter observations of Mascharak are especially interesting, but on the surface curious. They do not incorporate the key C4 amino group that is implicated in the structural studies of Stubbe et al. and discussed in detail in Section 3.2.8. They do, however, maintain the bleomycin pyrimidine N3, which acts as a H-bond acceptor from the guanine C2-amine cleavage site. It is conceivable that a reduced guanine cleavage selectivity is derived from a single versus double H-bonding interaction.
- [100] D. L. Boger, S. Teramoto, T. Honda, J. Zhou, *J. Am. Chem. Soc.* **1995**, *117*, 7338–7343.
- [101] D. L. Boger, T. M. Ramsey, H. Cai, *Bioorg. Med. Chem.* **1996**, *4*, 195–207.
- [102] D. L. Boger, R. F. Menezes, Q. Dang, *J. Org. Chem.* **1992**, *57*, 4333–4336.
- [103] a) C. Nishimura, N. Tanaka, H. Suzuki, N. Tanaka, *Biochemistry* **1987**, *26*, 1547; b) C. Nishimura, H. Suzuki, N. Tanaka, H. Yamaguchi, *Biochem. Biophys. Res. Commun.* **1989**, *163*, 788–796.
- [104] a) S. M. Sebt, J. C. Deleon, J. S. Lazo, *Biochemistry* **1987**, *26*, 4213–4219; b) S. M. Sebt, J. E. Mignano, J. P. Jani, S. Srmatkandada, J. S. Lazo, *Biochemistry* **1989**, *28*, 6544–6548.
- [105] D. L. Boger, T. M. Ramsey, H. Cai, S. T. Hoehn, J. W. Kozarich, J. Stubbe, *J. Am. Chem. Soc.* **1998**, *120*, 53–65.
- [106] K. P. Nightingale, K. R. Fox, *Nucleic Acids Res.* **1993**, *21*, 2549–2555.
- [107] a) R. E. Kilkuskie, H. Suguna, B. Yellin, N. Murugesan, S. M. Hecht, *J. Am. Chem. Soc.* **1985**, *107*, 260–261; b) D. C. Heimbrook, R. L. Mulholland, Jr., S. M. Hecht, *J. Am. Chem. Soc.* **1986**, *108*, 7839–7840.
- [108] D. L. Boger, R. F. Menezes, Q. Dang, W. Yang, *Bioorg. Med. Chem. Lett.* **1992**, *2*, 261–266.
- [109] a) D. L. Boger, T. M. Ramsey, H. Cai, S. T. Hoehn, J. Stubbe, *J. Am. Chem. Soc.* **1998**, *120*, 9149–9158; b) D. L. Boger, S. L. Colletti, S. Teramoto, T. M. Ramsey, J. Zhou, *Bioorg. Med. Chem.* **1995**, *3*, 1281–1295.
- [110] D. L. Boger, T. M. Ramsey, H. Cai, S. T. Hoehn, J. Stubbe, *J. Am. Chem. Soc.* **1998**, *120*, 9139–9148.
- [111] a) M. Vasquez, G. Nemethy, H. Scheraga, *Macromolecules* **1983**, *16*, 1043–1049; b) S. S. Zimmerman, M. S. Pottle, G. Nemethy, H. Scheraga, *Macromolecules* **1977**, *10*, 1–9.
- [112] D. L. Boger, S. Teramoto, H. Cai, *Bioorg. Med. Chem.* **1997**, *5*, 1577–1589.

New Insight into the Source of Biomolecular Homochirality: An Extraterrestrial Origin for Molecules of Life?

Joachim Podlech*

Crucial organic molecules associated with life (for example, amino acids, nucleic acids, sugars) are chiral and usually occur in nature in only one of the two enantiomeric forms. The reason for this homochirality, which seems to be essential for the existence of life, is still a puzzle and several controversial theories have been presented.^[1–3] Since all mechanisms discussed can justify only small amounts of enantiomeric excess, several amplification theories have been proposed.^[1, 4] Extraterrestrial processes have been considered as well. Nevertheless, the parity-violating aspect of the electroweak interaction, which might be suspected to be responsible for homochirality, seems to be too weak. Amplification by factors of about 10^{17} would be required to account for homochirality.^[5] Evidence is hard to obtain in this field and, understandably, proofs are less conclusive. Support for an extraterrestrial origin has come from recent findings.

Carbonaceous, chondritic meteorites, especially the Murchison meteorite (which fell in Australia in 1969), have been examined intensively. A plethora of amino (α -, β -, γ -, δ -),^[6] hydroxy,^[7] phosphonic, and sulfonic acids,^[8] as well as other organic compounds^[9] have been found in these meteorites (Figure 1).

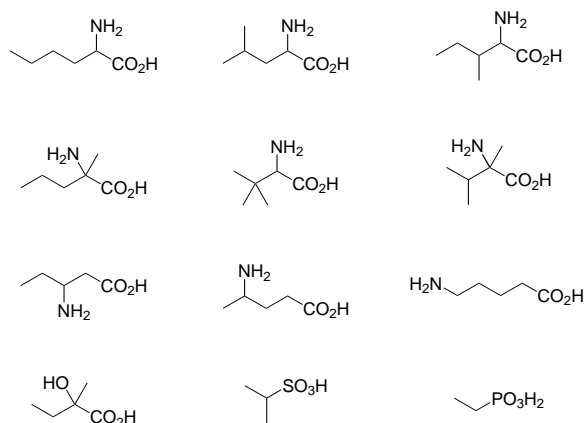


Figure 1. A selection of amino, hydroxy, sulfonic, and phosphonic acids isolated from the Murchison meteorite.

[*] Dr. J. Podlech
Institut für Organische Chemie der Universität
Pfaffenwaldring 55, D-70569 Stuttgart (Germany)
Fax: (+49) 711-685-4269
E-mail: joachim.podlech@po.uni-stuttgart.de

In particular the amino acids, which are essential for life, have attracted considerable interest. In this context a report by Cronin et al. on the enantiomeric excesses in several meteoritic amino acids was quite surprising.^[10] To avoid enantiomeric enrichment by the analytic methods and to exclude terrestrial contamination the authors focused on α -ramified amino acids, which have never been reported in the geosphere (Figure 2).^[11] Additionally, the amino acid **1** bears

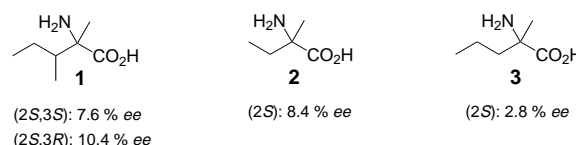


Figure 2. Nonracemic amino acids from the Murchison meteorite and their corresponding enantiomeric excesses.

two centres of chirality; therefore an enantiomeric enrichment as an analytical artefact (for example, by the aqueous processing) seems to be highly unlikely. The analyses were carefully carried out and gave enantiomeric excesses up to 10 % for amino acids **1–3**. α -Aminobutyric acid and norvaline gave no significant *ee* values.

With this result, the origin of these findings was still elusive! A recent contribution of Bailey and co-workers brought new insight in this topic. They reported on the observation of circularly polarized infrared light, whose source is a cloud of dust in the Orion constellation.^[5] This cloud is a region of high-mass star formation that contains many organic molecules. The authors suspect that this polarization might be caused by light scattering on nonspherical grains, which are aligned by a magnetic field, but other mechanisms are possible as well. Calculations show that the presence of circularly polarized IR light implies the existence of the corresponding polarized UV radiation. Unfortunately, the dust cloud responsible for the polarization obscures UV radiation and prevents it from being observed directly. It has been known since the 1970s that amino acids and other chiral compounds can be enantiomerically enriched by circularly polarized UV light. One of the enantiomers is photodegraded predominantly depending on the sign of polarization.^[12] The *ee* values obtained are about the same as have been found in the Murchison meteorite.

A simple calculation shows that during the history of the earth about 6×10^7 million tons of amino acids (present in a

concentration of 60 ppm in the carbonaceous chondrites, which are 3 % of all meteorites) have reached the earth, with 6×10^5 million tons arriving during a period when the earth was cold enough for the persistence of the amino acids.^[2] Therefore, it seems possible that during development of life the earth was covered with matter (dust, meteorites, or comets) that stemmed from a region that was exposed to circularly polarized irradiation. The thus resulting enantiomeric excess of the amino acids might have tipped the scales towards the development of life. The global enantiomeric excess on earth—from racemization and dilution—was certainly less than in the meteorites. Bailey et al. guess that it might have been in the range of 5×10^{-3} to 10^{-7} % ee, and eventually higher in the vicinity of meteorite impacts.^[5] These enantiomeric excesses are larger by orders of magnitudes than those explainable by the parity violation (10^{-17} %) or by stochastic effects.^[1, 5] From this mechanism one might find molecules with opposite homochirality in other regions of the universe, depending on the polarization of the radiation.

Undoubtedly many questions on this topic are still unanswered and arguments are far from closed. Nevertheless, the herein presented perceptions possibly give new ideas as to where life might have originated.

German version: *Angew. Chem.* **1999**, *111*, 501–502

Keywords: amino acids • chirality • extraterrestrial chemistry • prebiotic chemistry

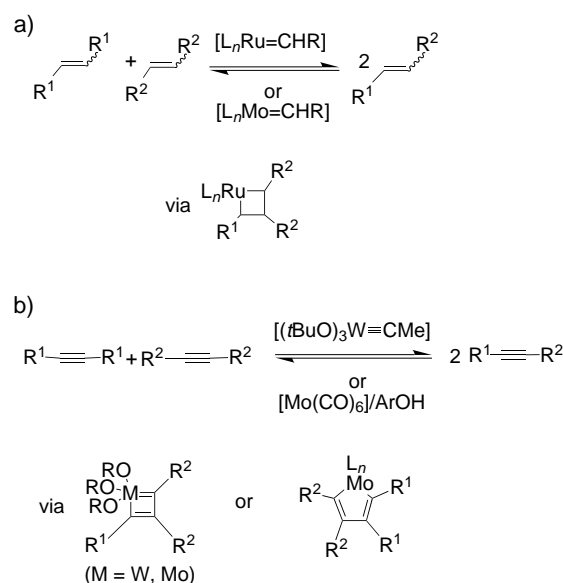
- [1] W. A. Bonner, *Origins Life Evol. Biosphere* **1991**, *21*, 59–111.
- [2] *Comets and the Origin and Evolution of Life* (Eds.: P. J. Thomas, C. F. Chyba, C. P. McKay), Springer, New York, **1997**.
- [3] a) J. S. Siegel, *Chirality* **1998**, *10*, 24–27; b) M. Quack, *Angew. Chem.* **1989**, *101*, 588–604; *Angew. Chem. Int. Ed. Engl.* **1989**, *28*, 571–586; c) M. Quack, *Chem. Phys. Lett.* **1994**, *231*, 421–428.
- [4] a) M. Bolli, R. Micura, A. Eschenmoser, *Chem. Biol.* **1997**, *4*, 309–320; b) a particularly high chiral amplification was obtained through polymerization. see M. M. Green, J. V. Selinger, *Science* **1998**, *282*, 880–881.
- [5] J. Bailey, A. Chrysostomou, J. H. Hough, T. M. Gledhill, A. McCall, S. Clark, F. Ménard, M. Tamura, *Science* **1998**, *281*, 672–674.
- [6] J. R. Cronin, S. Pizzarello, *Geochim. Cosmochim. Acta* **1986**, *50*, 2419–2427.
- [7] J. R. Cronin, S. Pizzarello, S. Epstein, R. V. Krishnamurthy, *Geochim. Cosmochim. Acta* **1993**, *57*, 4745–4752.
- [8] G. W. Cooper, W. M. Onwo, J. R. Cronin, *Geochim. Cosmochim. Acta* **1992**, *56*, 4109–4115.
- [9] J. R. Cronin, S. Chang in *The Chemistry of Life's Origins* (Eds.: J. M. Greenberg, C. X. Mendoza-Gomez, V. Pirronello), Kluwer, Dordrecht, **1993**, pp. 209–258.
- [10] J. R. Cronin, S. Pizzarello, *Science* **1997**, *275*, 951–955.
- [11] Reports in the 1980s on the enantiomeric excesses of biogenic amino acids have been doubted since contaminations could not be excluded. See citations in ref. [10].
- [12] a) J. J. Flores, W. A. Bonner, G. A. Massey, *J. Am. Chem. Soc.* **1977**, *99*, 3622–3625; b) recently it was shown that leucine or valine (enantiomerically enriched to about 2 % ee by, for example, circularly polarized light) can act as a chiral initiator of an autocatalytic asymmetric dialkylzinc addition to aldehydes. The product was obtained with ee values up to 50%: T. Shibata, J. Yamamoto, N. Matsumoto, S. Yonekubo, S. Osanai, K. Soai, *J. Am. Chem. Soc.* **1998**, *120*, 12157–12158.

Alkyne Metathesis as a New Synthetic Tool: Ring-Closing, Ring-Opening, and Acyclic

Uwe H. F. Bunz* and Lioba Kloppenburg

In recent years alkene metathesis (Scheme 1a) has firmly established itself in the “tool box” of the organic chemist, and it is increasingly replacing other methods of C=C bond formation such as the Wittig reaction or the McMurry coupling. Schrock^[1] and Grubbs^[2] have developed active and efficient catalysts for metathesis which are commercially available and thus have made a major contribution to the spectacular success of this method in the preparation of complex natural products and novel materials. Recent reviews by Blechert^[3a] and Fürstner^[3b] summarize current developments in this area. An additional and important commercial aspect of the continuing interest in homogeneously catalyzed alkene metathesis is its potential for the synthesis of highly cross-linked polymers.^[4]

[*] Prof. Dr. U. H. F. Bunz, Dr. L. Kloppenburg
Department of Chemistry and Biochemistry
University of South Carolina
Columbia, SC 29208 (USA)
Fax: (+1) 803-929-0267
E-mail: bunz@psc.sc.edu



Scheme 1. a) Alkene metathesis; b) alkyne metathesis.

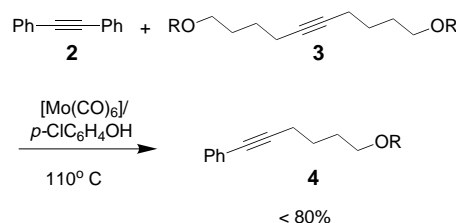
Basic Concepts

Until now, *alkyne* metathesis (Scheme 1 b) has remained in the shadow of alkene metathesis. The first example of a homogeneously catalyzed metathesis reaction of a C–C triple bond, described by Mortreux et al., was the statistical disproportionation of 4-methyltolan to tolan and 4,4'-dimethyltolan with a $[\text{Mo}(\text{CO})_6]/\text{resorcinol}$ catalyst formed in situ.^[5] Attempts to convert terminal alkynes by metathesis were unsuccessful with this catalyst system. Instead, cyclotrimers and polymers of unknown constitution were isolated. However, the defined Schrock carbyne complex $[(t\text{BuO})_3\text{W}\equiv\text{CtBu}]$ (**1**; see below) exhibits a certain activity in the metathesis of readily available terminal alkynes, where metathesis is accompanied by the evolution of gaseous acetylene during the first minute of the reaction. It has, however, not yet been possible to suppress the main reaction, which leads to the polymerization of the alkyne with the formation of polyacetylenes. If diethyl ether is used as solvent, the yield of metathesis product is about 90 %, although conversion is low (ca. 15 %, 1-heptyne \rightarrow 6-dodecyne + $\text{C}_2\text{H}_2 \uparrow$). This otherwise attractive variant (readily accessible substrate) suffers from the restriction of low conversion, and requires further development.^[6]

The metathesis of dialkylalkynes can be carried out photochemically at room temperature with catalyst systems that are generated in situ if both *meta*-chlorophenol and $[\text{Mo}(\text{CO})_6]$ are present in the reaction solution.^[7] The catalytically active species in all these (thermally and photochemically activated) systems is unknown. However, experiments by Schrock, who prepared defined molybdenum-alkylidyne in 1984, suggest that the Mortreux catalysts may have a similar structure.^[8] Analogously, the tungsten–carbyne complex **1**, obtained by Schrock in a multistep synthesis, is thermally stable, highly sensitive to water and atmospheric oxygen and is likewise superbly active in the metathesis of disubstituted alkynes.

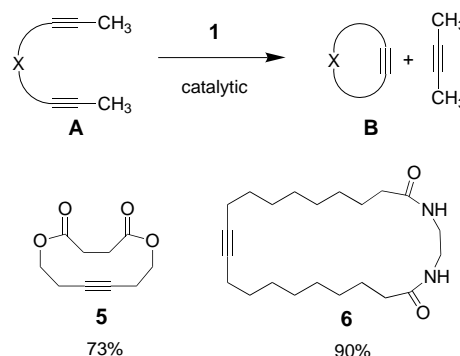
Applications to Organic Synthesis

In 1995 Mori investigated the cross-metathesis of **3** with an excess of tolan (**2**, 11 equiv) in the presence of a Mortreux-type catalyst $[\text{Mo}(\text{CO})_6]/\textit{para}$ -chlorophenol. She found that the corresponding mixed alkynes **4** are formed in yields of 50–80 %. The great advantage of catalysts that are prepared in situ is this simple experimental set up, which unfortunately did not always proceed in good yields.^[10]



In a spectacular report, Fürstner^[11] showed recently that functionalized diynes of type **A** could be converted in good yields into the corresponding macrocycles **B** (12- to 28-membered rings) with the concomitant expulsion of butyne (ring-closing *alkyne* metathesis, RCAM). Typically, however,

high dilution conditions had to be employed to guarantee an efficient ring closure of **A**. The substrates used in this work carried either one or two ester groups (for example, the formation of **5**), but it was also possible to cyclize a bisamide

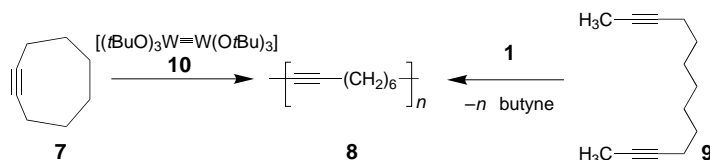


to the macrocyclic lactam **6** in 90 % yield. This is a) the first published case of a ring-closing alkyne metathesis (for the identification of *meta*-coupled cyclophenylene-ethynylenes see reference [12]), and also b) an example of the unexpected compatibility of the tungsten–carbyne complex **1** with both polar ester groups and the amide functionalities in the lactam **6** and its precursors. Similar behavior, which underscores the excellent compatibility of Schrock carbyne complexes with ester groups, had been demonstrated previously by Weiss with the synthesis of the carbyne complex $[\text{EtO}_2\text{CC}_6\text{H}_4\text{C}\equiv\text{W}(\text{OtBu})_3]$.^[12]

According to Fürstner and Seidel, the RCAM method is valuable for the synthesis of cyclic alkenes, since the alkyne units can be converted stereoselectively into the corresponding *Z*- or *E*-alkenes by hydroboration and subsequent protonation, as well as by other methods.

Polymers

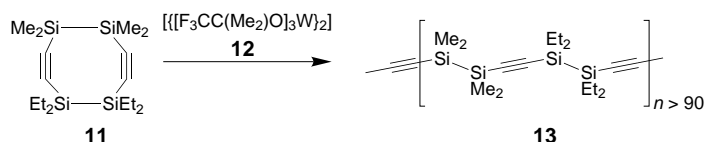
Ring closing and ring opening are two sides of the same coin, so it is not surprising that ring opening of cycloalkynes by alkyne metathesis has been investigated. Schrock and Krouse^[13] polymerized the strained cycle **7** by ring opening utilizing the catalyst precursor **10**, and obtained the almost insoluble elastomer **8**. The wide molecular weight distribution $M_w/M_n > 4$ suggests that this polymerization cannot be



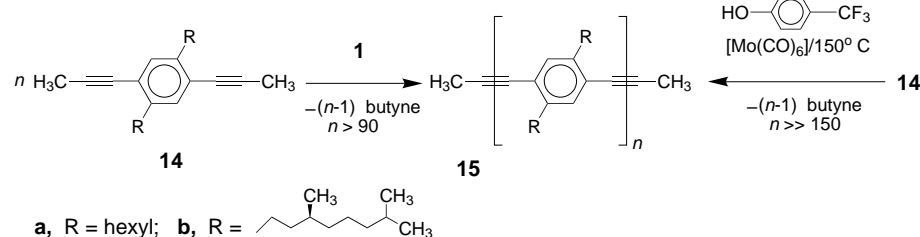
regarded as “living”; that is, initiation occurs only sluggishly, or, as is often observed in polymerizations by ring opening, the polymer already formed is partially degraded catalytically to form cyclooligomers. Schrock was able to demonstrate that the reaction of **7** with stoichiometric amounts of the dimer **10** takes place with the formation of well-defined carbyne complexes that can be detected by NMR spectroscopy. The corresponding polyoctynamer **8** can be obtained by ring-opening metathesis polymerization (ROMP) of **7** as well as by

facile *acyclic diyne metathesis* (ADIMET) of 2,10-dodecadiyne catalyzed by **1** under concomitant loss of 2-butyne.^[14]

A further application of ring-opening alkyne metathesis has since been reported by Bazan,^[15] who polymerized the somewhat exotic but stable cyclodiyne **11** stereospecifically to the head-to-tail coupled product **13** by employing catalyst precursor **12**. According to the authors, replacement of a methyl group in **10** by a trifluoromethyl group (**12**) is necessary to obtain a catalyst with increased activity. The silane polymer **13** becomes conducting when it is treated with SbF₅, and this semiconductor is also claimed to exhibit attractive optical properties.



In general, it should be possible to prepare completely conjugated organic polymers of the poly(*p*-phenyleneethynylene) (PPE) type **15** with the ADIMET reaction.^[14] It has been shown that the ADIMET reaction of **14** to **15** is catalyzed by **1**, and the polymer **15a** (R = hexyl) is obtained in 68% yield and with a degree of polymerization *n* of greater than 90 and a *M_w/M_n* (polydispersity) value of 2.^[14] This molecular weight distribution suggests that the reaction is a classical polycondensation. Only propynyl groups are present as end groups in



15a when it is prepared by metathesis, which was demonstrated by model experiments and NMR studies. The ADIMET reactions are superior to classical Pd-catalyzed couplings in amine solvents^[16] since not only is a higher degree of polymerization obtained, but the typical problems that are associated with the removal of Pd and phosphane-containing catalyst residues and the occurrence of butadiyne defect structures are elegantly avoided.^[17] Owing to their extremely high fluorescence quantum yields, their thermal stability at temperatures of up to 200 °C, and, with suitable substitution, their excellent solubility in organic solvents, PPEs are attractive potential emitter layers in light-emitting devices (LEDs)^[18] for electroluminescent applications as organic “plastic” lasers,^[17] and polarizers in liquid crystal display screens.^[19] To circumvent the tedious synthesis of the carbyne complex **1** in the ADIMET reaction of **14**, and to develop a simple route to **15**, we treated monomer **14** with a modified Mortreux catalyst system prepared from *para*-trifluorocresol and [Mo(CO)₆] at 150 °C.^[20] The butyne formed during the reaction was removed from the reaction solution with a stream of nitrogen. The alkyl-substituted PPEs **15** were

usually formed in quantitative yield. In a particularly good example we were able to show that chiral **14b**, doubly substituted by 3,7-dimethyloctyl groups, gave a highly soluble, optically active PPE (**15b**) with a degree of polymerization *n* of 150 or more. The big advantage of these catalyses lies in the application of commercially available catalyst precursors in solvents used without further purification or drying.

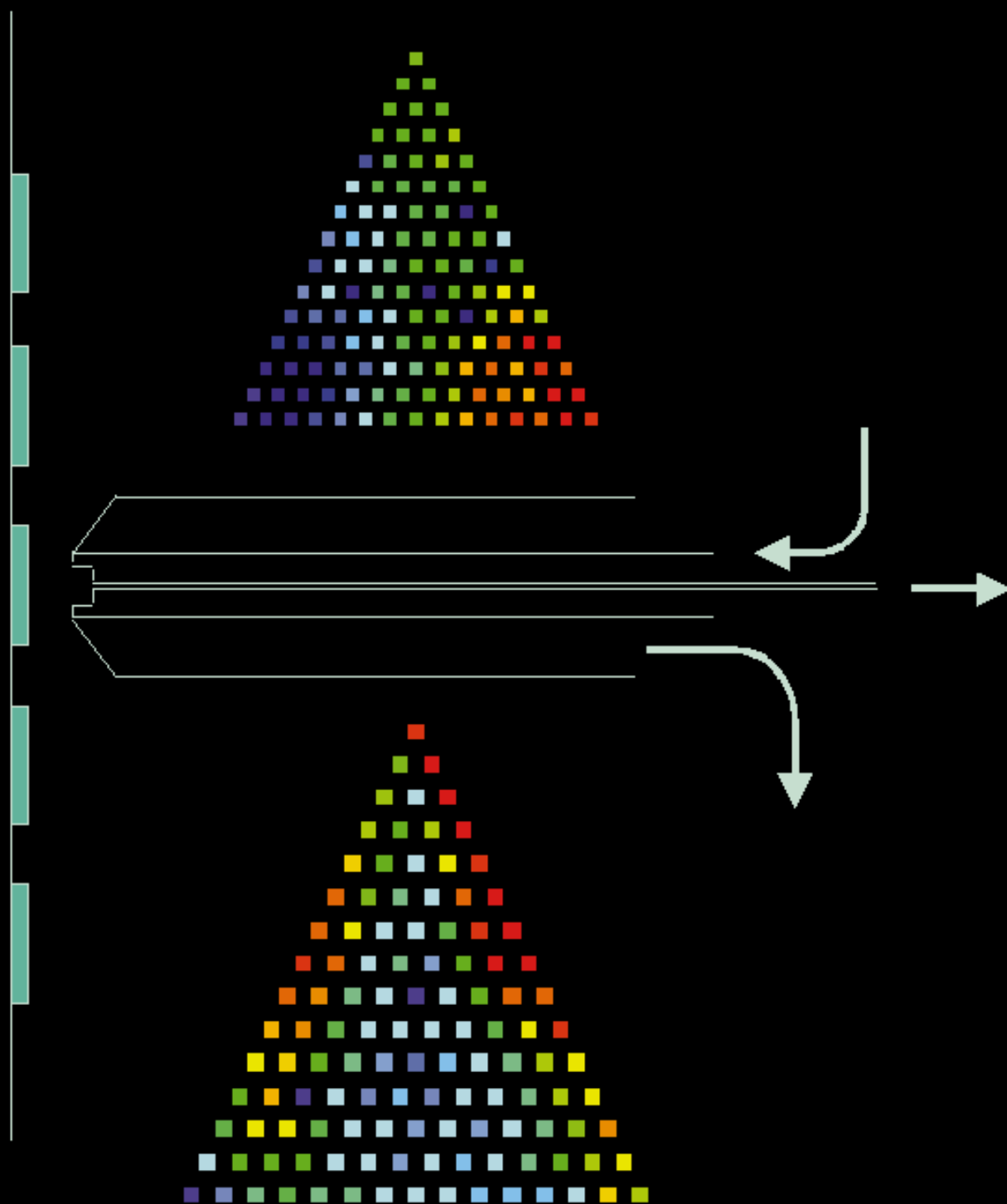
The highly promising developments described in this article should ensure that alkyne metathesis will emerge in the near future as an efficient method in both the arsenal of the organic chemist and in polymer synthesis. Alkyne metathesis will prove to be a useful complement and augmentation of the popular Cu- and Pd-catalyzed coupling reactions in alkyne chemistry. The efficient metathesis of terminal alkynes,^[6] the reversibility of alkyne metathesis, which could lead to the degradation of polymers with integrated triple bonds, and the question of whether alkyne metathesis can be carried out efficiently in water as an environmentally friendly solvent, are important but poorly (if at all) investigated aspects of this fascinating reaction.

German version: *Angew. Chem. Int. Ed.* **1999**, 38, 503–505

Keywords: alkynes • carbyne complexes • metathesis • ring-opening polymerization

- [1] R. R. Schrock, *Polyhedron* **1995**, 14, 3177.
- [2] R. H. Grubbs, S. Chang, *Tetrahedron* **1998**, 54, 4413, and references therein.
- [3] a) M. Schuster, S. Blechert, *Angew. Chem.* **1997**, 109, 2124; *Angew. Chem. Int. Ed. Engl.* **1997**, 36, 2036; b) A. Fürstner, *Top. Catal.* **1997**, 4, 285.
- [4] B. R. Maughon, R. H. Grubbs, *Macromolecules* **1996**, 29, 5765.
- [5] a) A. Mortreux, M. Blanchard, *J. Chem. Soc. Chem. Commun.* **1974**, 786; for highly active catalyst systems, see A. Bencheik, M. Petit, A. Mortreux, F. Petit, *J. Mol. Catal.* **1982**, 15, 93; D. Villemin, P. Cadiot, *Tetrahedron Lett.* **1982**, 5139; b) T. J. Katz, J. McGinnis, *J. Am. Chem. Soc.* **1975**, 97, 1592.
- [6] A. Mortreux, F. Petit, M. Petit, T. Szymanska-Buzar, *J. Mol. Catal. A* **1995**, 96, 95; A. Bray, A. Mortreux, F. Petit, M. Petit, T. Szymanska-Buzar, *J. Chem. Soc. Chem. Commun.* **1993**, 197.
- [7] A. Mortreux, J. C. Delgrange, M. Blanchard, B. Lubochinsky, *J. Mol. Catal.* **1977**, 2, 73.
- [8] L. G. McCulloch, R. R. Schrock, *J. Am. Chem. Soc.* **1984**, 106, 4067.
- [9] R. R. Schrock, D. N. Clark, J. Sancho, J. H. Wengrovius, S. M. Rocklage, S. F. Pedersen, *Organometallics* **1982**, 1, 1645.
- [10] N. Kaneta, T. Hirai, M. Mori, *Chem. Lett.* **1995**, 627; N. Kaneta, K. Hikichi, S. Asaka, M. Uemura, M. Mori, *Chem. Lett.* 1055.
- [11] A. Fürstner, G. Seidel, *Angew. Chem.* **1998**, 110, 1758; *Angew. Chem. Int. Ed.* **1998**, 37, 1734.
- [12] K. Weiss, unpublished results; U. H. F. Bunz, P. H. Ge, unpublished results; see also A. Michel, Dissertation, Bayreuth, **1997**.
- [13] S. A. Krouse, R. R. Schrock, *Macromolecules* **1989**, 22, 2569; *Macromolecules* **1987**, 20, 903; stoichiometric alkyne metathesis: J. Sancho, R. R. Schrock, *J. Mol. Catal.* **1982**, 15, 75.
- [14] K. Weiss, A. Michel, E.-M. Auth, U. H. F. Bunz, T. Mangel, K. Müllen, *Angew. Chem.* **1997**, 109, 522; *Angew. Chem. Int. Ed. Engl.* **1997**, 36, 506.
- [15] X.-P. Zhang, G. C. Bazan, *Macromolecules* **1994**, 27, 4627.
- [16] T. Mangel, A. Eberhardt, U. Scherf, U. H. F. Bunz, K. Müllen, *Macromol. Rapid Commun.* **1995**, 16, 571; Q. Zhou, T. J. Swager, *J. Am. Chem. Soc.* **1995**, 117, 12593; H. Li, D. R. Powell, R. K. Hayashi,

- R. West, *Macromolecules* **1998**, *31*, 52; C. Weder, M. S. Wrighton, *Macromolecules* **1996**, *29*, 5157.
- [17] F. E. Goodson, T. I. Wallow, B. M. Novak, *J. Am. Chem. Soc.* **1997**, *119*, 12441.
- [18] D. D. C. Bradley, *Synthet. Met.* **1993**, *54*, 401; P.-W. Wang, Y.-J. Liu, J. S. Moore, *Adv. Mater.* **1996**, *8*, 237; F. Hide, M. A. Diaz-Garcia, B. J. Schwartz, A. J. Heeger, *Acc. Chem. Res.* **1997**, *30*, 430.
- [19] C. Weder, C. Sarwa, A. Montali, C. Bastiaansen, P. Smith, *Science* **1998**, *279*, 835.
- [20] L. Kloppenburg, D. Song, U. H. F. Bunz, *J. Am. Chem. Soc.* **1998**, *120*, 7973.
-



A new high-throughput screening instrument for libraries of combinatorial heterogeneous catalysts is presented on the following pages. This instrument can measure the activity *and* selectivity of a single catalyst within one minute.

High-Throughput Synthesis and Screening of Combinatorial Heterogeneous Catalyst Libraries

Peijun Cong, Robert D. Doolen, Qun Fan, Daniel M. Giaquinta, Shenheng Guan, Eric W. McFarland, Damodara M. Poojary, Kyle Self, Howard W. Turner, and W. Henry Weinberg*

Combinatorial chemistry has had an enormous impact on drug discovery research in the pharmaceutical and biotechnology industries in recent years. It is now being extended to the discovery of new solid-state materials.^[1–6] Heterogeneous catalysts is one class of solid-state inorganic materials that is an obvious and attractive area for combinatorial exploration. Heterogeneous catalysts are at the core of modern chemical and petroleum industries, and they are discovered and optimized through lengthy and largely trial-and-error procedures. Combinatorial synthetic techniques offer the means to synthesize rapidly a large number of chemically distinct entities. The discovery process for new heterogeneous catalysts can be shortened dramatically if their catalytic properties can be measured in a similarly high throughput fashion. There have been some reports pertaining to the issue of high-throughput screening of heterogeneous catalyst libraries.^[7–9] The techniques are based either on infrared thermography^[7, 9] or resonance-enhanced multiphoton ionization.^[8] Although infrared thermography can identify exothermic reactions, there is no chemically specific information, which renders the technique of limited general value. Senkan^[8] recently applied resonance-enhanced multiphoton ionization detection to the screening of an eight-member catalyst library for the dehydrogenation of cyclohexane to benzene. Since only the benzene product was measured, however, no selectivity information was available.

A systematic and integrated approach is necessary to realize fully the promise of combinatorial chemistry in heterogeneous catalysis. We report here preliminary results in developing such an approach through the catalytic oxidation of CO and the reduction of NO by metal alloy catalysts that consist of Rh, Pd, Pt, and Cu as an example. The oxidation of CO by either O₂ or NO is one of most thoroughly studied heterogeneous catalytic reactions^[10–12] and is thus an ideal system to test and validate the combinatorial synthesis and screening techniques.

A 15 × 15 × 15 triangular library that contained 120 different catalysts was prepared by depositing three metals (for example, Rh, Pd, and Pt) by radiofrequency (RF) sputtering through masks onto a quartz wafer (75 mm diameter, 1.5 mm thick); each catalyst has a diameter of 1.5 mm and a thickness of approximately 100 nm. Each site at the apex of the triangle contains the pure metal, with its concentration decreasing linearly when going away from the apex and reaching zero at

the adjacent side of the triangle; the adjacent side is composed of binary mixtures of the other two metals. A row of 16 blank elements was added to one side of the triangle as a control to provide a measure of the background of the system. The deposition was accomplished by ten repeated steps. A total of 10 nm of material per catalyst site, with the desired concentration of each metal, was deposited in each step. The total deposition time for such a library is about one hour. The superlattice structure of the films is important for the mixing of the three metals. Powder X-ray data^[13] taken after the library was annealed at 773 K in a stream of 5 % H₂ and 95 % Ar for two hours show no diffraction signals that originate from the pure metals in the mixtures, which indicates good intermetal mixing in the various alloy catalysts. Given the density of the noble metals (10–20 g cm^{−3}) and the diameter (1.5 mm) and thickness (100 nm) of the catalyst, the loading per site is approximately 2–4 μg. The Rh-Pt-Cu and Rh-Pd-Cu libraries were prepared in a similar manner. An additional Rh-Pd-Pt library was made by sol–gel based techniques by using automated liquid deposition robotics. The results are identical to those obtained from RF-sputtered libraries.

A schematic representation of the experimental apparatus for screening catalytic activity is shown in Figure 1. The substrate containing the catalyst library is loaded onto a two-dimensional screening stage underneath a probe with concentric tubings for gas delivery/removal and sampling.^[14] Only

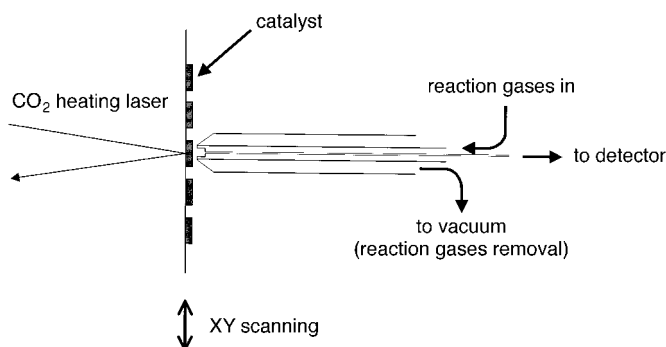


Figure 1. Schematic representation of the experimental apparatus used for screening catalytic activity. For more details see the text and ref. [14].

the catalyst that is being tested is exposed to the reactant stream, and the excess reactants are removed from the system by a vacuum line. The catalyst is heated by a CO₂ laser to the desired temperature before the measurement commences. No other catalyst experiences heat or the reactant stream since the heating is localized and the reactants are delivered locally, which allows a measurement of the initial activity (and selectivity) of each catalyst. The measurement of product as well as reactant concentrations is achieved by sampling the gas mixture directly above the catalyst and transporting it into a mass spectrometer or an optical detector through a capillary transfer line. Each measurement takes about one minute to complete, and only slightly more than two hours are needed to complete the 136 element library. To accomplish a similar goal with individually loaded micro-reactors would take hundreds, if not thousands, of hours.

[*] W. H. Weinberg, P. Cong, R. D. Doolen, Q. Fan, D. M. Giaquinta, S. Guan, E. W. McFarland, D. M. Poojary, K. Self, H. W. Turner
Symyx Technologies
3100 Central Expressway, Santa Clara, CA 95051 (USA)
Fax: (+1) 408-748-0175
E-mail: hweinberg@symyx.com

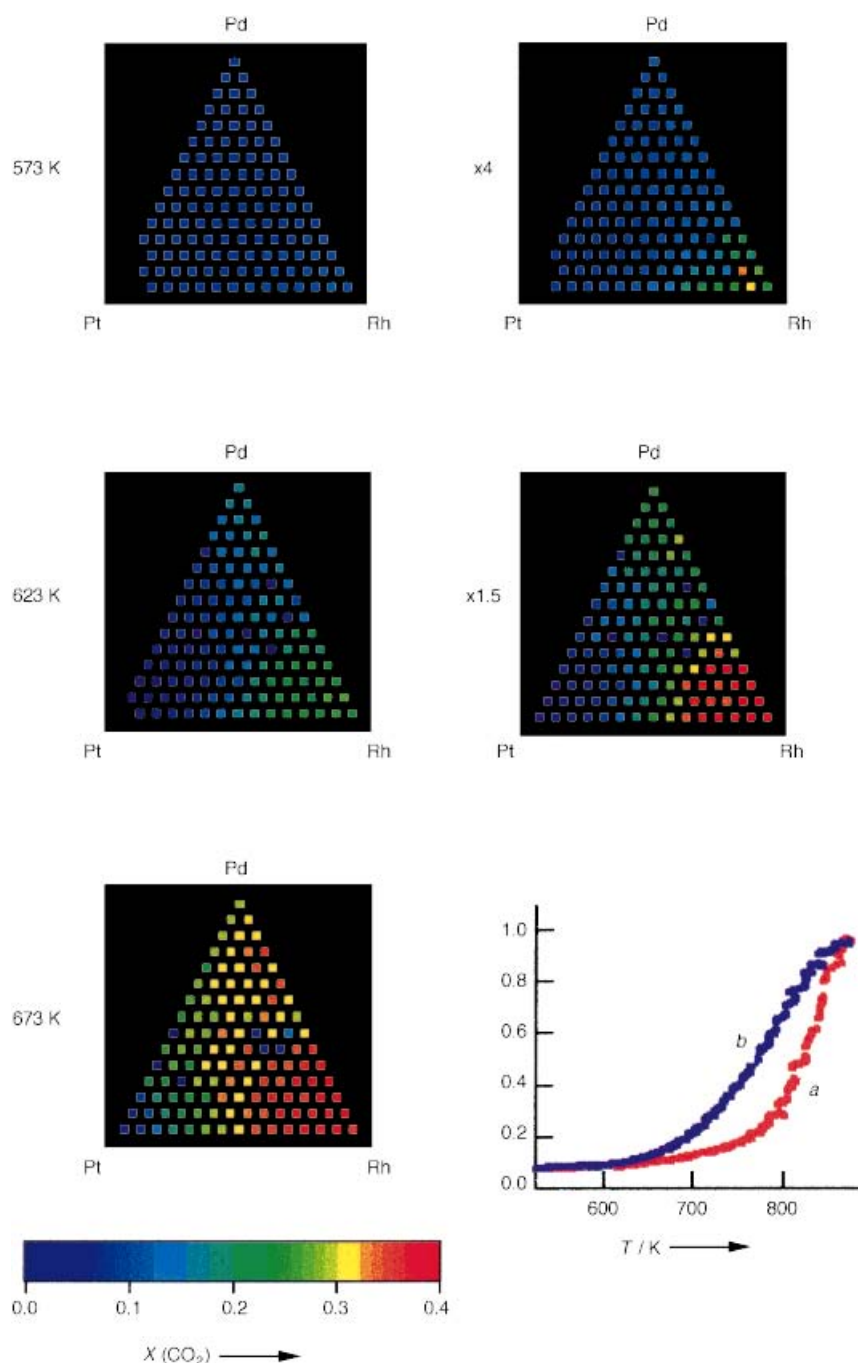


Figure 2. CO_2 production from a Rh-Pd-Pt ternary library. The displayed ion current (in 10^{-10} A) was corrected for filament emission current drift in the ion source. For clarity the data at 573 K and 623 K were rescaled and replotted in the right panel. See the text for details. The hysteresis loop of one of the elements in the library, pure Pt, is displayed in the lower right corner. The ordinate shows the ion current of CO_2 produced, in units of 10^{-10} A. The heating (a) and cooling (b) rates are both 1 K s^{-1} .

Figure 2 shows the CO_2 production from the Rh-Pd-Pt library at three different temperatures. The reaction was carried out with a mixture of CO, O_2 , and Ar in a ratio of approximately 2:1:4 and a pressure of about one atmosphere. Clearly, the order of activity for producing CO_2 at all three temperatures is $\text{Rh} > \text{Pd} > \text{Pt}$. This is in good agreement with results from experiments with single-crystalline surfaces as well as supported catalysts.^[11, 12, 15] The oxidation of CO proceeds in two distinct regimes on the platinum group

metals. At temperatures below the ignition point the reaction is relatively slow and is limited by the desorption of CO. When the surfaces reach the ignition temperature a kinetic phase transition that involves CO desorption occurs. Above this temperature the reaction proceeds much faster. These two regimes have different apparent activation energies and kinetic orders in CO and O_2 . There may also be hysteresis behavior, that is, the reaction rate may have two values at the same temperature depending on whether the catalyst is being heated or cooled. The hysteresis curve for pure Pt is shown in the lower right corner of Figure 2.

Some of the discontinuities in catalyst activity seen in Figure 2 (namely, low activity elements surrounded by much more active elements) may be caused by these kinetic instabilities. They are not likely to be caused by thermal damage, since different catalysts show low activities in different runs. In spite of these discontinuities, the global trend across the ternary system is obvious and reproducible. The more active elements are localized in the Rh-rich region, and the most active element below 623 K has the composition of 86 % Rh, 7 % Pd, and 7 % Pt. At 673 K the peak of activity shifted one to two gradient steps further away from the Rh corner and contains 79–71 % Rh. The reaction rate is not a sensitive function of the remaining Pt to Pd ratio. The enhancement of the most active catalyst relative to pure Rh is between 10 and 30 %, depending on the reaction temperature.

While it is interesting to observe the small, yet significant, enhancement of catalytic activity that arises from metal alloying, it does not constitute a major breakthrough in finding a superior oxidation catalyst for CO. On the other hand, if one of

the expensive noble metals could be replaced by a much less expensive metal and the resulting catalyst still maintain significant oxidation activity the situation might be different. To explore such a possibility Cu was introduced as a replacement for one of the noble metals. Figure 3 shows the results from a Rh-Pd-Cu library. This library was made in the same way as the Rh-Pd-Pt one, except that the total thickness of the film was 800 \AA rather than 1000 \AA (eight deposition steps instead of ten).

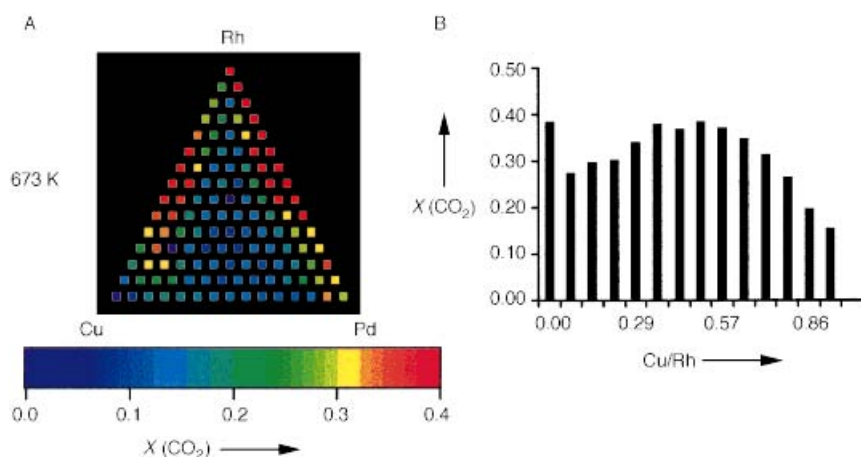


Figure 3. A) CO_2 production as measured by ion current (in units of 10^{-10} A) from a Rh-Pd-Cu ternary library at 673 K. B) The same data along the Rh-Cu binary axis replotted. The abscissa shows the mole fraction of Cu.

The performance of Rh-Cu binary mixtures is worth particular attention (see Figure 3). The 1:1 Cu:Rh catalyst is as active as the pure Rh catalyst at 673 K. While the activity of pure Cu is at least two orders of magnitude lower than that of Rh, a mixture of 93 % Cu and 7 % Rh maintains 40 % of the activity of pure Rh, and this trend is also observed at lower temperatures. Furthermore, Pt-Cu and Pd-Cu binaries show similar enhancements over the respective pure metals, and the enhancement is stronger at low temperatures than at high temperatures. The maxima are located on the Cu-rich side of the binaries at an approximately 60:40 ratio of Cu:Pt(Pd). These findings are in general agreement with recent literature on Cu modified (through evaporative coating) single-crystalline surfaces of Rh,^[16] Pt,^[17] and Pd.^[18] A preliminary aging test was performed on the 1:1 Rh:Cu alloy by observing the activity for more than 60 minutes at one atmosphere and 673 K. A 30 % reduction in activity was observed, which is less than that reported by Szanyi and Goodman^[16] for a Rh(100) surface with Cu overlayers.

The oxidation of CO by NO ($\text{CO} + \text{NO} \rightarrow \text{CO}_2 + \frac{1}{2}\text{N}_2$) is a more complex and challenging reaction relative to the oxidation of CO by O_2 . The reaction probabilities are much smaller,^[15] and incomplete reduction of NO to N_2O is possible. To distinguish the N_2 that is produced from unreacted CO and to distinguish N_2O from CO_2 in the mass spectrometer, ^{15}NO was employed. The same Rh-Pd-Pt library used for the oxidation of CO by O_2 reaction was used also for the oxidation with NO after regeneration in 5 % H_2 in Ar at 500 °C for two hours. The results are summarized in Figure 4. The reactions were carried out at 673, 773, and 873 K because of the lower reaction probabilities. The reactant mixture of CO, NO, and Ar was delivered with a 1:1:6 ratio at approximately one atmosphere. The order of activity for N_2 and CO_2 (not shown) production is once again Rh > Pd > Pt. This trend is also well documented in the literature^[15, 19, 20]. In general, the Rh-Pt binaries are more active than Rh-Pd alloys. The N_2O production, however, exhibits a quite interesting trend. At 673 K Rh and Rh-Pt alloys produced the most N_2O ; at 773 K this maximum shifted to Rh-Pd alloys; and at 873 K this reaction became less competitive

relative to the complete reduction of NO to N_2 , and the maximum activity shifted to the Pd-rich region along the Pd-Rh binary axis. The following trends are observed when the selectivity of the individual catalysts at fixed temperatures is considered. The ratio of N_2 to N_2O for Rh at 673 K is 1.2:1, after the ion currents are corrected for ionization efficiencies; this ratio is 22:1 at 873 K. The same ratio changed from 2.5:1 to 1.5:1 for Pd. Clearly, the N_2 production channel is favored at high temperatures for Rh and Rh-rich catalysts. On the other hand, the N_2O channel becomes relatively more important at high temperatures for Pd and Pd-rich catalysts. This finding correlates well with the branching ratios of

the same reaction on single-crystalline Pd surfaces reported by Vesecky et al.^[21]

Rapid catalyst deactivation was observed when libraries of Cu were screened for the oxidation of CO by NO. The Rh-Cu binaries showed significant enhancement in catalytic activity over pure Rh for both N_2 and N_2O production immediately after they had been annealed under a reducing atmosphere. However, this enhancement decays to less than that of Rh within a few minutes of exposure to the reactants at 673 K or higher. After this short “aging” time, the catalytic activity along the Rh-Cu axis can be described as an approximately linear decay from Rh to Cu, with Cu being no different from a blank element.

In summary, integrated combinatorial synthesis and screening methodologies have been developed for heterogeneous catalysis. This approach was demonstrated with the $\text{CO} + \text{O}_2$ and $\text{CO} + \text{NO}$ reactions with noble metal as well as Cu substituted noble metal libraries. The trends observed for the noble metal libraries are in complete agreement with the more limited data set reported previously in the literature. For the Cu-containing libraries, the Rh-Cu binary mixtures showed promising oxidation activity.

Received: October 19, 1998 [Z12542IE]
German version: *Angew. Chem.* **1999**, *111*, 508–512

Keywords: combinatorial chemistry • heterogeneous catalysis • mass spectrometry • screening methods

- [1] X.-D. Xiang, X. Sun, G. Briceno, Y. Lou, K.-A. Wang, H. Chang, W. G. Wallace-Freedman, S.-W. Chen, P. G. Schultz, *Science* **1995**, *268*, 1738–1740.
- [2] G. Briceno, H. Chang, X.-D. Sun, P. G. Schultz, X.-D. Xiang, *Science* **1995**, *270*, 273–275.
- [3] X.-D. Sun, K.-A. Wang, Y. Yoo, W. G. Wallace-Freedman, C. Gao, X.-D. Xiang, P. G. Schultz, *Adv. Mater.* **1997**, *9*, 1046–1049.
- [4] J. Wang, Y. Young, C. Gao, I. Takeuchi, X. Sun, H. Chang, X.-D. Xiang, P. G. Schultz, *Science* **1998**, *279*, 1712–1714.
- [5] E. Danielson, J. H. Golden, E. W. McFarland, C. M. Reaves, W. H. Weinberg, X. D. Wu, *Nature* **1997**, *389*, 944–948.

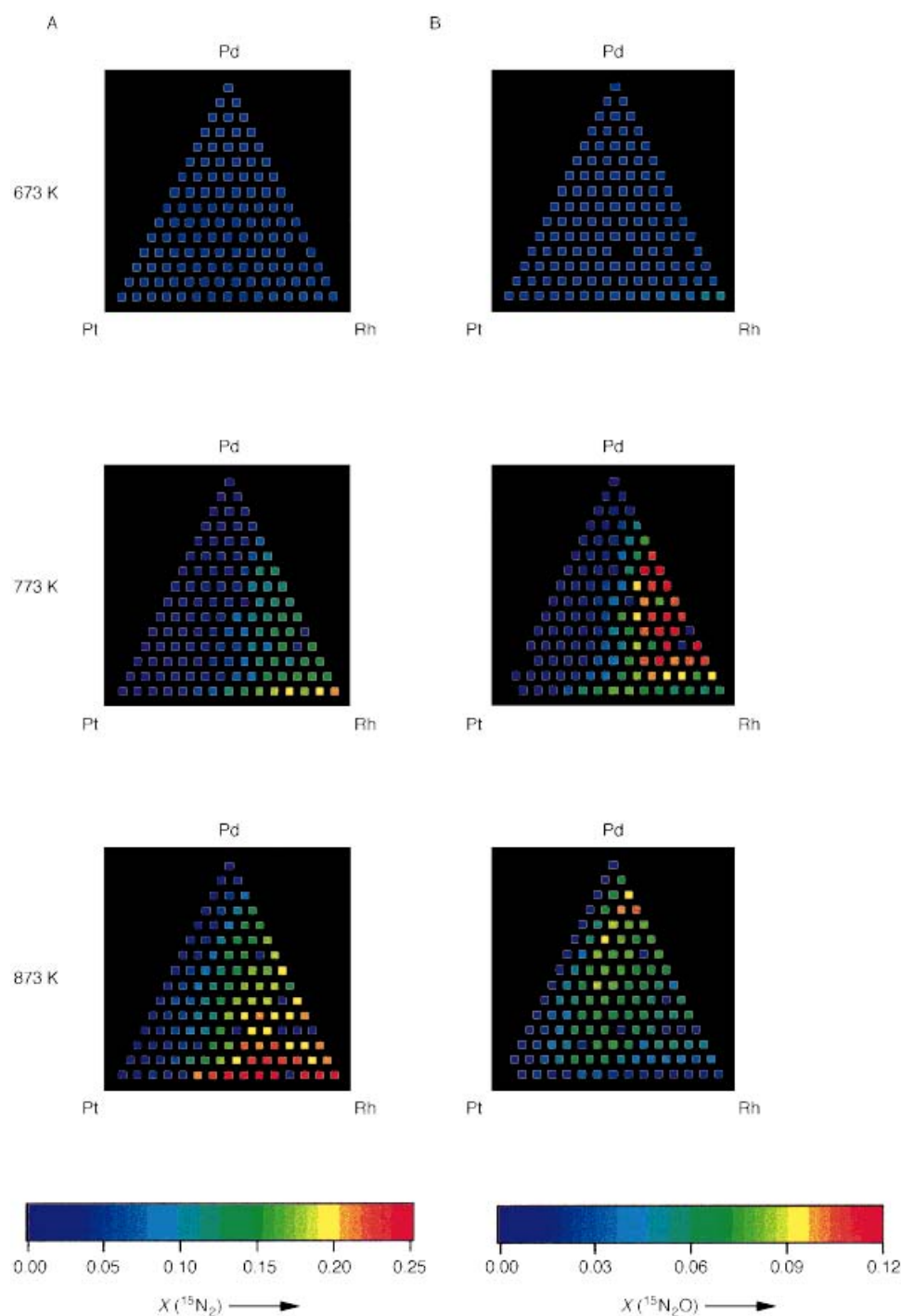


Figure 4. A) $^{15}\text{N}_2$ production (in units of 10^{-10} A ion current) from the same Rh-Pd-Pt library of Figure 2 at 673, 773, and 873 K. B) The corresponding $^{15}\text{N}_2\text{O}$ production from the same library. Note the different scales in the two cases.

- [6] E. Danielson, M. Devenney, D. M. Giaquinta, J. H. Golden, R. C. Haushalter, E. W. McFarland, D. M. Poojary, C. M. Reaves, W. H. Weinberg, X. D. Wu, *Science* **1998**, 279, 837–839.
- [7] F. C. Moates, M. Somani, J. Annamalai, J. T. Richardson, D. Luss, R. C. Wilson, *Ind. Eng. Chem. Res.* **1996**, 35, 4801–4803. A related patent application (PCT US 97/02756) is broader in scope, but of less interest since no experiments were run.
- [8] S. M. Senkan, *Nature* **1998**, 394, 350–352.
- [9] A. Holzwarth, H.-W. Schmidt, W. F. Maier, *Angew. Chem.* **1998**, 110, 2788–2792; *Angew. Chem. Int. Ed.* **1998**, 37, 2644–2647.
- [10] T. Engel, G. Ertl, *Adv. Catal.* **1979**, 28, 1–78.
- [11] K. C. Taylor, *Ind. Eng. Chem. Prod. Res. Dev.* **1976**, 15, 264–268.
- [12] R. M. Heck, R. J. Farrauto, *Catalytic Air Pollution Control: Commercial Technology*, Van Nostrand Reinhold, New York, **1995**.
- [13] The catalysts in the library were characterized by X-ray powder diffraction with a scanning microdiffractometer, GADDS from Bruker AXS. Data were measured with $\text{CuK}\alpha$ radiation (2-kW generator, $\lambda = 1.5418 \text{ \AA}$) in the range $10 < 2\theta < 72^\circ$ with an exposure time of 10 min per catalyst. The primary beam was focussed to a spot of 700 μm in diameter by means of bent Göbel mirrors and a collimator. The library was mounted on the XYZ stage of the diffractometer and initial alignments were carried out with a laser and video microscope assembly.
- [14] W. H. Weinberg, E. W. McFarland, P. Cong, S. Guan (Symyx Technologies), WO-A 98/15969 A2, **1998**.
- [15] J. A. Rodriguez, D. W. Goodman, *Surf. Sci. Rep.* **1991**, 14, 1–107.
- [16] J. Szanyi, D. W. Goodman, *J. Catal.* **1994**, 145, 508–515.

- [17] R. E. R. Colen, M. Kolodziejczyk, B. Delmon, J. H. Block, *Surf. Sci.* **1998**, 412, 447–457.
 [18] R. W. Vook, B. Oral, *Appl. Surf. Sci.* **1992**, 60, 681–687.
 [19] W. F. Egelhoff, Jr. in *The Chemical Physics of Solid Surfaces and Heterogeneous Catalysis*, Vol. 4 (Eds.: D. A. King, D. P. Woodruff), Elsevier, Amsterdam, **1982**, pp. 397–426.
 [20] K. C. Taylor, *Stud. Surf. Sci. Catal.* **1987**, 30, 97–116.
 [21] S. M. Vesecky, P. Chen, X. Xu, D. W. Goodman, *J. Vac. Sci. Technol. A* **1995**, 13, 1539–1543.

The Hume–Rothery Compound $\text{Mn}_8\text{Ga}_{27.4}\text{Zn}_{13.6}$: Separated Zn_{13} -Clusters Interspersed in a Primitive Cubic Host Lattice**

Ulrich Häussermann,* Per Viklund, Christer Svensson,
 Sten Eriksson, Pedro Berastegui, and Sven Lidin

The interpretation of structural stability and chemical bonding in intermetallic compounds is a continuous challenge in chemistry because metallic systems evade the simple and powerful rules developed by chemists which allow the linking of electron counts to particular geometrical arrangements of atoms.^[1, 2] However, there exists a number of intermetallic compounds where the valence electron concentration (VEC, average number of valence electrons per atom) plays a decisive role for structural stability, and these compounds are usually classified as electron compounds^[3] or Hume–Rothery compounds.^[4] One group of such Hume–Rothery compounds comprises E-rich systems T_mE_n ($n/m \geq 3$) where T is a transition metal from the V–Co groups and E is preferably Al or Ga. In these compounds the transition metal atoms appear uniformly distributed in a matrix of E atoms, and the resulting structures (e.g., VAl_{10} , WAl_{12} , MnAl_6 , Co_2Al_9 , MnGa_4 , V_8Ga_{41} , V_7Al_{45}) are very often large and complex. Remarkably the T atoms are separated by the largest distance possible and, thus, are only coordinated by E atoms in the first coordination sphere. The resulting TE_p coordination polyhedra are rather regular ($p = 8–12$) and appear as discrete

entities (VAl_{10} , WAl_{12}), as vertex-linked (Co_2Al_9 , MnGa_4 , V_8Ga_{41}), or as edge-linked (MnAl_6) networks. Many of these T_mE_n Hume–Rothery compounds were prepared and characterized 20 years ago, but have experienced a renaissance recently with the discovery of further examples such as MoAl_6 , WAl_6 , $\text{Mo}_5\text{Al}_{22}$, and the ternary $\text{Mo}_7\text{Sn}_{12}\text{Zn}_{40}$ by Hillebrecht et al.^[5]

The origin of the important role of VEC for the stability of this group of Hume–Rothery compounds lies in the occurrence of a pronounced pseudo gap in the density of states (DOS) which is a result of strong bonding between T and E atoms.^[6] We want to exemplify the characteristic features of the electronic structure of these compounds with the DOS of V_8Ga_{41} ^[7] shown in Figure 1 a: At low energy the density of

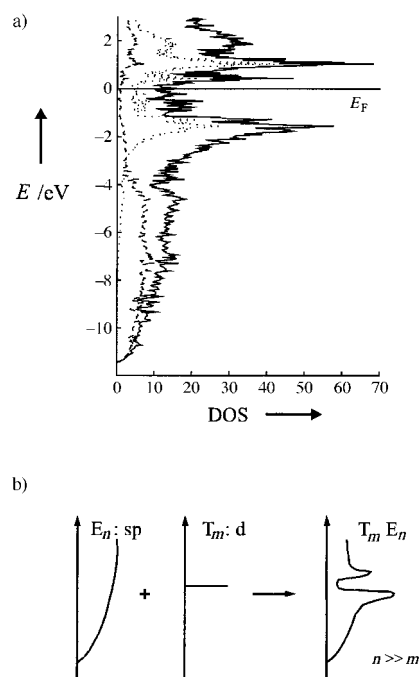


Figure 1. a) Total density of states (DOS (states/eV cell)) together with the d orbital contribution from V (dotted lines) and the s orbital contribution from Ga (dashed lines) of the compound V_8Ga_{41} as obtained from LMTO–ASA calculations. b) Schematic construction of the DOS of the T_mE_n Hume–Rothery compounds as a perturbation of free-electron like states of the E atom matrix by T atom d states.

states is dominated by approximately parabolically distributed (free-electron like) states stemming from the sp bands of the E atom matrix, which at higher energy are perturbed by the T atom d states. The strong d–sp interaction in these compounds opens up a pseudo gap (or sometimes even a narrow band gap) at or close to the Fermi level (E_F) which separates d–sp bonding and antibonding states. Figure 1 b summarizes in a simplified manner how the DOS of the T_mE_n Hume–Rothery compounds is built up by this perturbation process. As a consequence the TE_p coordination polyhedra represent strongly bonded entities, and the position of the pseudo gap determines the optimum VEC, or in the case of broad pseudo gaps a range of optimum VECs, for a particular Hume–Rothery compound. In V_8Ga_{41} ^[8] only one kind of TE_p polyhedron—corresponding to a VGa_{10} unit—occurs. This

[*] Dr. U. Häussermann, Prof. S. Lidin
 Department of Inorganic Chemistry, Stockholm University
 10691 Stockholm (Sweden)
 Fax: (+46)8-152187
 E-mail: ulrich@inorg.su.se
 Dr. P. Viklund, Dr. C. Svensson
 Department of Inorganic Chemistry 2
 Lund University (Sweden)
 S. Eriksson
 Studsvik Neutron Research Laboratory
 Uppsala University (Sweden)
 Dr. P. Berastegui
 ISIS Facility, Rutherford Appleton Laboratory
 Chilton, Didcot, Oxon (UK)

[**] This work was supported by the Swedish National Science Research Council (NFR) and the Göran Gustafsson Foundation.

VGa_{10} coordination polyhedron represents a hybrid composed of one half of a cube ($\text{VGa}_{8/2}$) and one half of an icosahedron ($\text{VGa}_{12/2}$)^[9] and is depicted in Figure 2a. In the V_8Ga_{41} structure these polyhedra exclusively share corners (Figure 2b) and are arranged in such a way that one triangular

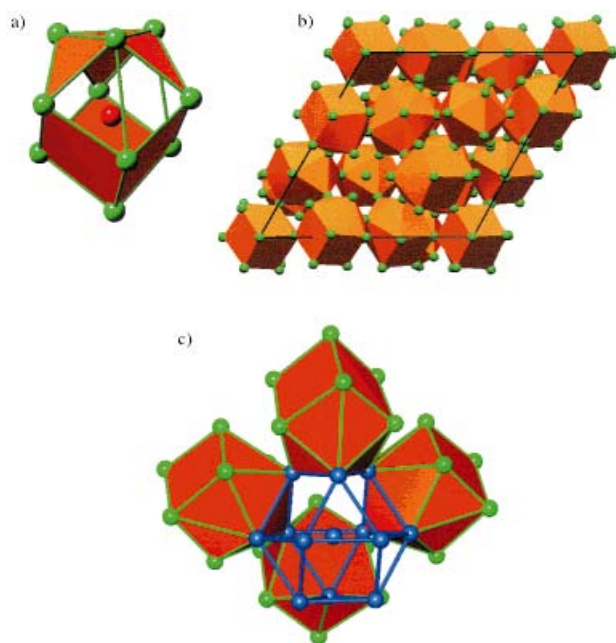


Figure 2. a) The hybrid coordination polyhedron of the V atoms in V_8Ga_{41} consisting of one half of a cube (lower part) and one half on an icosahedron (upper part). b) The structure of V_8Ga_{41} along [001] build up by corner-sharing VGa_{10} polyhedra (red). c) The cuboctahedron in V_8Ga_{41} defined by eight VGa_{10} hybrid polyhedra (only four of them are shown for clarity).^[17]

face of each polyhedron is at the same time part of a cuboctahedron which is centered by an additional Ga atom. Thus such a cuboctahedron is defined by eight VGa_{10} polyhedra (Figure 2c) which yields the stoichiometry $\text{Ga}(\text{VGa}_{10/2})_8 = \text{V}_8\text{Ga}_{41}$ for this compound.

In the course of our investigation of the stability ranges of Hume–Rothery compounds we obtained the new phase $\text{Mn}_8\text{Ga}_{41-x}\text{Zn}_x$ from Zn/Ga melts^[10] with a rather narrow homogeneity range^[11] which can be regarded as a $\text{T}_m\text{E}_{n-x}\text{E}'_x$ Hume–Rothery compound. The X-ray structure determination^[12] of a single crystal from a sample with the nominal composition $\text{Mn}_4\text{Zn}_{32}\text{Ga}_{64}$ exhibited a rhombohedral structure for a compound $\text{Mn}_8\text{Ga}_{\approx 27}\text{Zn}_{\approx 14}$ which at first sight appeared as a simple ternary variant of the V_8Ga_{41} structure where Ga atoms in the E atom matrix have partly been replaced by Zn atoms. When counting Zn as an E atom that only contributes to bonding with its 4s electrons one might consider a random replacement of Ga with the neighboring element Zn as a means to balance the increase of VEC due to the electron richer T component in $\text{Mn}_8\text{Ga}_{41-x}\text{Zn}_x$. Then VEC yields a value of 3.367 in $\text{Mn}_8\text{Ga}_{27}\text{Zn}_{14}$, which is slightly higher than that in V_8Ga_{41} but the Fermi level would still be within the pseudo gap of V_8Ga_{41} when assuming a rigid-band behavior of the band structure (Figure 1). In order to be able to discriminate reliably between Ga and Zn atoms and to investigate their distribution in the E atom matrix we

performed a neutron powder diffraction study.^[13] The Rietveld refinement (Figure 3) revealed an average composition $\text{Mn}_8\text{Ga}_{27.4(1)}\text{Zn}_{13.6(1)}$ of the crystals from the sample $\text{Mn}_4\text{Zn}_{32}\text{Ga}_{64}$ and an intriguing segregation of the Zn and Ga atoms in the E atom substructure of $\text{Mn}_8\text{Ga}_{27.4}\text{Zn}_{13.6}$.^[14] This, together with some small but decisive geometric

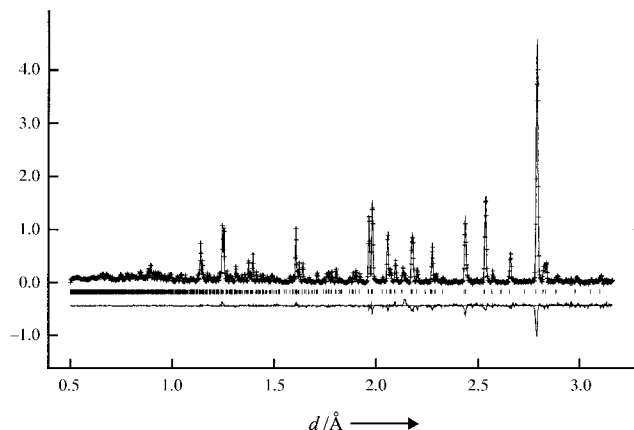
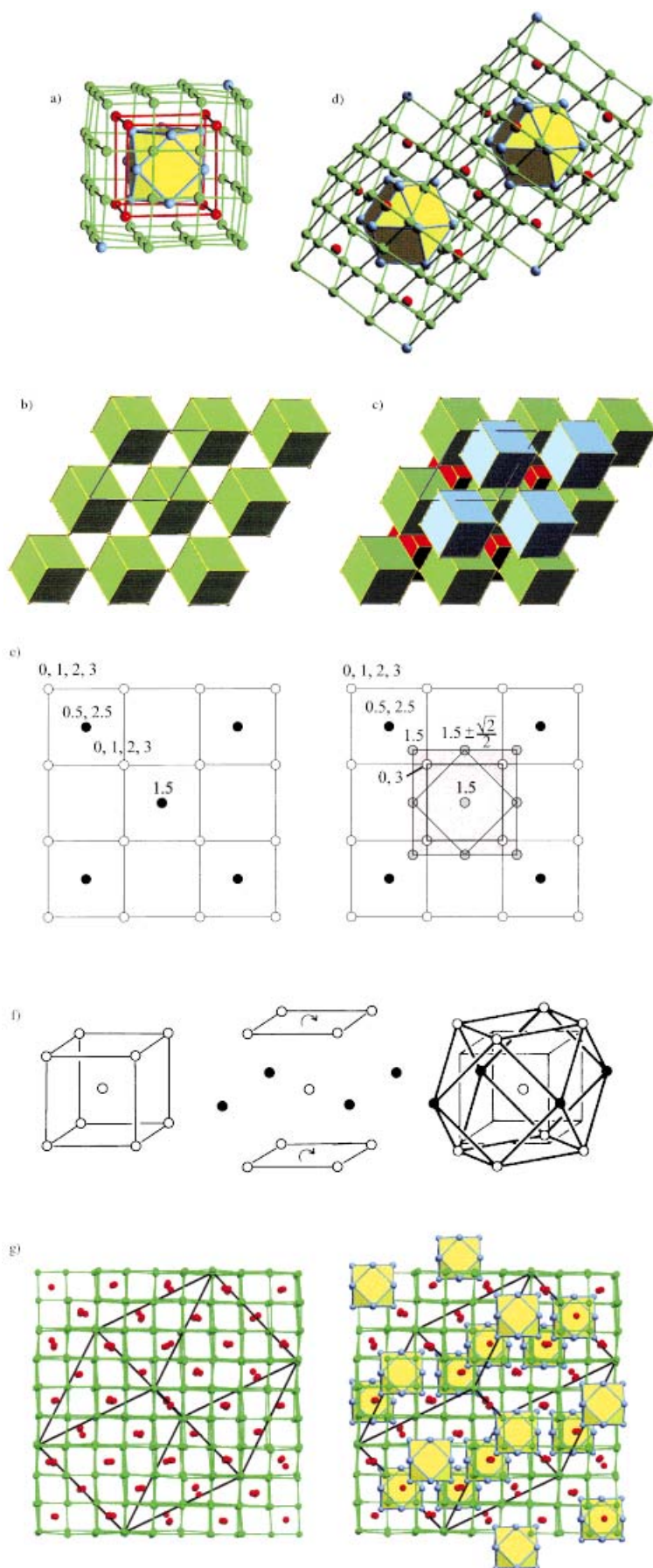


Figure 3. The Rietveld-fitted profile and difference plot (time-of-flight neutron powder diffraction data) for $\text{Mn}_8\text{Ga}_{27.4}\text{Zn}_{13.6}$. The vertical axis shows counts per μs .

deviations from the parent V_8Ga_{41} type turns the ternary $\text{Mn}_8\text{Ga}_{27.4}\text{Zn}_{13.6}$ into a very remarkable structure. The most remarkable feature of $\text{Mn}_8\text{Ga}_{27.4}\text{Zn}_{13.6}$ is the occurrence of separated Zn_{12}E cluster entities; that is, the two atomic positions defining the cuboctahedron are exclusively occupied by Zn atoms (positions Zn1 and Zn2), and the center of these clusters represents the only significantly detected random occupied atomic position in this structure (position E: 61(9) % Zn and 39(9) % Ga). Moreover, the distances between neighboring atoms in the Zn_{12}E clusters are in the very narrow range between 2.754 and 2.814 \AA ($d(\text{E}-\text{Zn1})$ 2.790 ($6\times$), $d(\text{E}-\text{Zn2})$ 2.779 ($6\times$), $d(\text{Zn1}-\text{Zn1})$ 2.790 ($6\times$), $d(\text{Zn1}-\text{Zn2})$ 2.780 ($6\times$), 2.814 ($6\times$), $d(\text{Zn2}-\text{Zn2})$ 2.754 \AA ($6\times$)) compared to the range of 2.885 to 3.034 \AA between the corresponding pairs of Ga atoms in V_8Ga_{41} .^[8] As a consequence of this idealization of the cuboctahedral units in $\text{Mn}_8\text{Ga}_{27.4}\text{Zn}_{13.6}$ the distances between Mn and the Zn atoms of the cuboctahedra are enlarged and the MnE_{10} polyhedra appear as more distorted than their VGa_{10} counterparts in V_8Ga_{41} . Thus the Zn_{12}E clusters in $\text{Mn}_8\text{Ga}_{27.4}\text{Zn}_{13.6}$ can be regarded as small volumes of face-centered cubic metal which are separated by at least 3.929 \AA as the shortest distance between Zn atoms belonging to neighboring cuboctahedra; the distance between the centers of the clusters is 9.240 \AA . The mean distance between neighboring atoms in the centered cuboctahedra is 2.785 \AA , which compares very well with the mean interatomic distance of 2.789 \AA between nearest neighbors in the elemental structure of Zn. Thus, $\text{Mn}_8\text{Ga}_{27.4}\text{Zn}_{13.6}$ appears not only as an ordinary variant of the binary Hume–Rothery compound V_8Ga_{41} where the exchange of Ga by Zn supplies an optimum value of VEC, but exhibits a subtle ordering tendency of Ga and Zn in the flexible E atom substructure which accounts for the different



bonding behavior of these elements: the tendency of Ga to form homonuclear E–E and heteronuclear T–E bonds and the tendency of Zn to segregate into more metallic bonded entities. In contrast to the V_8Ga_{41} structure in which strong-bonded VGa_{10} polyhedra are the essential building units, for $Mn_8Ga_{27.4}Zn_{13.6}$ we assign this role to the centered cuboctahedra $Zn_{12}E$. When focussing on these cluster entities as the central structural units it is possible to define a large three-shell building block consisting of 77 atoms. The interior of such a building block (Figure 4a) is formed by a $Zn_{12}E$ cluster, and eight Mn atoms which coordinate the triangular faces of the cuboctahedron constitute its second shell. Thus the Mn atoms are arranged as a cube, which is slightly distorted, and the average distance between two Mn atoms is 5.21 Å. The outer shell or surface of the large building block consists of 56 E atoms (54 Ga atoms and two Zn atoms (position Zn3)) and has also the shape of a (slightly distorted) cube, exhibiting the same orientation as the inner cube formed by the Mn atoms.

This large “supercube” is equivalent in volume and shape to the primitive rhombohedral unit cell of $Mn_8Ga_{27.4}Zn_{13.6}$ with $a = 9.240$ Å and $\alpha = 95.80^\circ$, but with a different orientation (cf. Figure 4b). On each face of a supercube 16 E atoms are located which divide the area into 3×3 smaller arrays. The two Zn3 atoms sit on opposite corners ((0,0,0) and (1,1,1)) along a body diagonal (cf. Figure 4a) and the distance between these atoms and the closest Zn atoms of the $Zn_{12}E$ cluster in the center of the building block is 5.269 Å. The total composition of the stuffed supercube is T_8E_{69} and such building blocks composed of three shells might even occur in the formation process of the compound in the Zn/Ga (E atom) melt, starting off the centered cuboctahedra $Zn_{12}E$ as nucleation centers. In the hexagonal setting of the $Mn_8Ga_{27.4}Zn_{13.6}$ structure the stuffed supercubes are oriented along the body diagonal defined by the two Zn3 atoms. This orientation corresponds to the c axis, and the

Figure 4. a) The stuffed “supercube” building block in $Mn_8Ga_{27.4}Zn_{13.6}$. The inner shell represents a centered $Zn_{12}E$ cuboctahedron (yellow), the second shell corresponds to a cube of eight Mn atoms (red circles), and the outer shell to a cube with 56 E atoms (54 Ga (green circles) and two Zn atoms (blue circles)) on its surface. b) Layer of hexagonally arranged stuffed supercubes, oriented along a body diagonal (c direction) and not connected, in $Mn_8Ga_{27.4}Zn_{13.6}$. c) ABC stacking of layers of stuffed supercubes yield the total structure of $Mn_8Ga_{27.4}Zn_{13.6}$. d) Two condensed stuffed supercubes in two consecutive layers AB of $Mn_8Ga_{27.4}Zn_{13.6}$. e) From the $PtHg_4$ structure ($MnGa_4$) to the stuffed “supercube” building block in $Mn_8Ga_{27.4}Zn_{13.6}$. Black circles represent Mn atoms, lighter circles E atoms. The heights of the atoms are indicated. f) Generation of a cuboctahedron from a cube after Hyde and Andersson.^[15] g) Left: part of the structure of $Mn_8Ga_{27.4}Zn_{13.6}$ which corresponds to the $PtHg_4$ type (red circles: Mn atoms (Pt), green circles: E atoms (Hg)); right: $Mn_8Ga_{27.4}Zn_{13.6}$ -interspersed $Zn_{12}E$ clusters (yellow) in a primitive cubic host lattice.

distance between the two Zn3 atoms is the repeating unit in this direction. The supercubes are arranged in hexagonally packed layers as indicated in Figure 4b, but are not connected within such a layer. The complete structure of $\text{Mn}_8\text{Ga}_{27.4}\text{Zn}_{13.6}$ results from an ABC stacking of such layers in the c direction (Figure 4c). Within the sequence ABC, supercubes are condensed in the ab plane by sharing 9 of the 16 E atoms located on each face, equivalent to 4/9 of the area of the face (Figure 4d). Thus each building unit is surrounded octahedrally by six neighbors in such a partly face-sharing way. The shared atoms are always Ga atoms, whereas the remaining (Zn3) atoms situated at opposite corners at the heights $z = 0$, $\frac{2}{3}$, $\frac{2}{3}$ are used to connect supercubes in the c direction.

The structural description of $\text{Mn}_8\text{Ga}_{27.4}\text{Zn}_{13.6}$ in terms of stuffed supercubes reveals the close connection of this structure with the PtHg_4 type in which also the compound MnGa_4 crystallizes. The cubic PtHg_4 type can be regarded as a defect CsCl structure where $\frac{3}{4}$ of the Cs atoms have been removed in such a way that an array of corner-connected cubes $[\text{PtHg}_8]$ ($[\text{MnGa}_8]$) is formed (Figure 4e). The stuffed supercube in $\text{Mn}_8\text{Ga}_{27.4}\text{Zn}_{13.6}$ corresponds to a volume 1.5³ times that of the body-centered unit cell of MnGa_4 of which the atoms defining the central cube $[\text{MnGa}_8]$ has been replaced by the Zn_{12}E cluster. The transformation process from a cube to a cuboctahedron is simple and was described by Hyde and Andersson^[15] (Figure 4f): First a square of four more (Zn) atoms is added at the height of the center of the cube. Then the cube is elongated in the direction perpendicular to the plane defined by the additional atoms and its remaining two square faces are rotated by 45° to yield a cuboctahedron. The generation of a cuboctahedron from a cube raises the coordination number of the surrounding Mn atoms from 8 to 10, which results in the hybrid coordination polyhedron shown in Figure 1a. Beyond this the PtHg_4 type host structure of MnGa_4 is unaffected and the Zn_{12}E cluster in $\text{Mn}_8\text{Ga}_{27.4}\text{Zn}_{13.6}$ appear as separated, interspersed entities in a primitive cubic array in which the Ga atoms are segregated (Figure 4g).

The cubic primitive lattice is a perfect host for cuboctahedral units where square antiprims of flexible size serve as an interface and thus also allow some flexibility in the size of the cuboctahedra (cf. Figure 4e). For $\text{Mn}_8\text{Ga}_{27.4}\text{Zn}_{13.6}$, the distribution of the centered cuboctahedra formed by Zn atoms in the MnGa_4 host structure ensures for all Mn atoms the same coordination, but one could also think of a structural series T_nE_{4n} (PtHg_4 type host) $\rightarrow \text{T}_{n-1}\text{E}_{1,4n-8}\text{E}_{2,13}$ where T atoms occupy E_{10} hybrid polyhedra as well as cubes and E1 atoms participate in the cubic primitive lattice into which centered cuboctahedra (small volumes of face-centered cubic metal) formed by the E2 atoms are distributed. $\text{Mn}_8\text{Ga}_{27.4}\text{Zn}_{13.6}$ ($\text{Mn}_8[\text{Ga}_{27}\text{Zn}]\text{Zn}_{12}\text{E}$) would be the first member with $n = 9$. Such a homologous series with the same structural principle based on the fluorite type as host structure is, for example, known for the ionically bonded system CaF_2/YF_3 , including the mineral tveitite $\text{Ca}_{14}\text{Y}_5\text{F}_{43}$, where “excess” fluoride ions form the centered cuboctahedra.^[16]

Received: July 31, 1998 [Z.122331E]

German version: *Angew. Chem.* **1999**, *111*, 580–584

Keywords: bond theory • clusters • intermetallic phases • structure elucidation • zinc

- [1] R. Nesper, *Angew. Chem.* **1991**, *103*, 805; *Angew. Chem. Int. Ed. Engl.* **1991**, *30*, 789, and references therein.
- [2] G. J. Miller in *Chemistry, Structure and Bonding of Zintl Phases and Ions* (Ed.: S. M. Kauzlarich), VCH, New York, **1996**, pp. 1–59, and references therein.
- [3] R. Ferro, A. Saccone in *Materials Science and Technology, Vol. 1 (The Structure of Solids)* (Eds.: R. W. Cahn, P. Haasen, E. J. Kramer), VCH, Weinheim, **1993**, pp. 123–215.
- [4] The expression Hume–Rothery compound or Hume–Rothery phase for electron compound is frequently used by the physical community. It is not only restricted to the representatives of the specific structural series face-centered cubic \rightarrow body-centered cubic \rightarrow γ -brass \rightarrow hexagonally close-packed, which is the classic example of VEC-controlled stability ranges in intermetallic systems.
- [5] H. Hillebrecht, *Z. Kristallogr. Suppl.* **1994**, *8*, 340; M. Ade, H. Hillebrecht, *Z. Kristallogr. Suppl.* **1995**, *10*, 101; H. Hillebrecht, V. Kuntze, K. Gebhardt, *Z. Kristallogr.* **1997**, *212*, 840.
- [6] G. Trambly de Laissardière, D. Nguyen Manh, L. Magaud, J. P. Julien, F. Cyrot-Lackmann, D. Mayou, *Phys. Rev. B* **1995**, *52*, 7920.
- [7] The density of states of V_8Ga_{41} was calculated self-consistently using the local density-functional approximation and the scalar relativistic linear muffin-tin orbital (LMTO) method in the atomic sphere approximation (ASA) (M. van Schilfgarde, T. A. Paxton, O. Jepsen, G. Krier, A. Burkhard, O. K. Andersen, *Program TB-LMTO 4.6*; Max-Planck Institut Stuttgart, Stuttgart, **1994**). The exchange-correlation potential was parametrized according to von Barth and Hedin (U. von Barth, L. Hedin, *J. Phys. C* **1972**, *5*, 1629). The reciprocal space integrations were performed with the tetrahedron method (O. Jepsen, O. K. Andersen, *Solid State Commun.* **1971**, *9*, 1763) using 40 irreducible k -points.
- [8] K. Giris, W. Peter, G. Pupp, *Acta Crystallogr. Sect. B* **1975**, *31*, 113.
- [9] K. Yvon, *Acta Crystallogr. Sect. B* **1975**, *31*, 117.
- [10] The phase $\text{Mn}_8\text{Ga}_{41-x}\text{Zn}_x$ ($\approx 14 < x < \approx 16$) was prepared from mixtures of the pure elements containing 1 mmol Mn and a total amount of 20 mmol E component with various ratios Zn/Ga. The reactants were pressed into pellets and loaded into quartz ampoules, which were sealed under vacuum. The samples were heated to 600 °C for 60 h and then slowly cooled to room temperature at an approximate rate of 10 °C h⁻¹. Excess E metal was dissolved with 4 M HCl. The homogeneity of the crystalline product was confirmed by powder X-ray diffraction. Mixtures with a Ga/Zn ratio larger than 3 yielded the compound MnGa_4 and virtually no $\text{Mn}_8\text{Ga}_{41-x}\text{Zn}_x$.
- [11] The homogeneity range of $\text{Mn}_8\text{Ga}_{41-x}\text{Zn}_x$ was estimated to be $\approx 14 < x < \approx 16$ by means of semiquantitative elemental analyses of crystals from samples with different Zn/Ga ratios with the energy dispersive X-Ray (EDX) method in a JEOL scanning microscope.
- [12] Crystal structure determination of $\text{Mn}_8\text{Ga}_{27}\text{Zn}_{14}$ from a sample $\text{Mn}_4\text{Zn}_{32}\text{Ga}_{64}$, silvery cube-shaped or tabular crystals, crystal size: $0.1 \times 0.06 \times 0.06 \text{ mm}^3$, $a = 13.6033(6)$, $c = 14.6058(16) \text{ Å}$ (based on least squares from 30 measured and indexed lines of a Guinier powder diagram ($\text{Cu}_{K\alpha}$, Si (NIST) standard)), $\rho_{\text{calc}} = 6.889 \text{ g cm}^{-3}$, rhombohedral, space group $R\bar{3}$ (No. 148), $Z = 3$, Siemens SMART CCD diffractometer (Siemens Analytical X-ray Instruments Inc. *SMART Reference Manual*, Madison, Wisconsin, USA, **1996**), $\text{Mo}_{K\alpha}$ radiation, $\mu = 36.45 \text{ mm}^{-1}$, data reduction with SAINT (Siemens Analytical X-ray Instruments Inc. ASTRO and SAINT: Data Collection and Processing Software for the SMART System, Madison, Wisconsin, USA, **1995**), absorption correction with SADABS (G. M. Sheldrick, *SADABS User Guide*, Universität Göttingen, **1996**), 31809 measured reflections ($2^\circ < 2\theta < 110.63^\circ$), 6678 unique reflections ($R_{\text{int}} = 0.062$), structure determination with direct methods (G. M. Sheldrick, SHELXL-86 Program for the Solution of Crystal Structures, Universität Göttingen, **1990**), structure refinement against F^2 (G. M. Sheldrick, SHELXL-93 Program for the Refinement of Crystal Structures, Universität Göttingen, **1993**), 79 parameters, $w = [\sigma^2(|F_o|)^2 + (0.0423 P)^2 + 3.03 P]^{-1}$, R for 4737 $F_o > 4\sigma(F_o) = 0.0383$, $R_w(F^2)$ for all

6678 data = 0.094, GOF = 1.019, largest hole and peak = -2.72 and 2.38 e Å⁻³. The refinement of the occupancies for the Ga and Zn positions gave the tentative composition Mn₈Ga₂₇Zn₁₄ which coincides with the Ga/Zn ratio of the reaction mixture. Further details of the crystal structure investigation can be obtained from the Fachinformationszentrum Karlsruhe, D-76344 Eggenstein-Leopoldshafen, Germany (fax: (+49) 7247-808-666; e-mail: crysdata@fiz-karlsruhe.de), on quoting the depository number CSD-410318.

- [13] The neutron scattering lengths of Ga and Zn differ by about 20%. Time-of-flight neutron powder diffraction data was collected at room temperature using the POLARIS diffractometer at the ISIS Facility, UK. The backscattering detector bank which covers the scattering angles 130° < 2θ < 160° was used, providing data over the *d*-spacing range 0.2 < *d* < 3.2 Å with a resolution of Δ*dd*⁻¹ = 5 × 10⁻³. The normalized diffraction data was corrected for absorption.
- [14] Rietveld analysis was carried out using the program GSAS (A. C. Larson, R. B. von Dreele, M. Lujan, *GSAS: The General Structure Analysis System*, Los Alamos National Laboratory, Los Alamos, NM, 1994). The refined parameters included an extinction correction. Due to a strong correlation between temperature factors and occupancies, only two temperature factors, for the Mn and Ga atoms and for Zn atoms, respectively, were refined (3687 data points, *R*_p = 0.0452, *R*_{wp} = 0.0216, χ² = 1.982 (for 38 variables), *R*_p = Σ|*y*_{oi} - *y*_{ci}|/Σ|*y*_{oi}|, *R*_{wp} = (Σ*w*|*y*_{oi} - *y*_{ci}|²/Σ*w*|*y*_{oi}|²)^{0.5}.
- [15] B. G. Hyde, S. Andersson, *Inorganic Crystal Structures*, Wiley, New York, 1989, p. 196.
- [16] D. J. Bevan, O. Greis, J. Strähle, *Acta Crystallogr. Sect. A* 1980, 36, 889.
- [17] P. Hofmann, R. Nesper, COLTURE: program for interactive visualisation of crystal structures, ETH Zürich, Zürich, 1995.

Helical Coordination Polymers with Large Chiral Cavities**

Kumar Biradha, Corey Seward, and Michael J. Zaworotko*

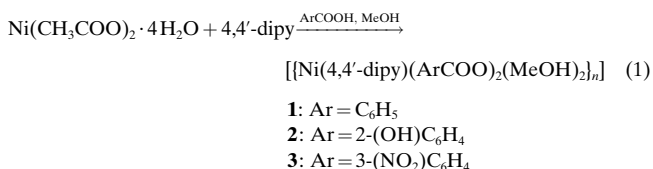
The concept of crystal engineering^[1, 2] owes much to recent advancements in supramolecular chemistry and recognition, understanding, and exploitation of supramolecular syntheses.^[3] Crystal engineering offers the intriguing promise of facile development of a new generation of functional solids that have been designed from first principles. Therefore, a degree of control over substrates, structure and, ultimately, bulk properties that is not inherently present in naturally occurring compounds is potentially offered. Furthermore, it is already clear that the construction of architectures that are unprecedented in naturally occurring solids becomes feasible.

[*] Prof. Dr. M. J. Zaworotko, Dr. K. Biradha, C. Seward
Department of Chemistry, The University of Winnipeg
515 Portage Avenue, Winnipeg, Manitoba, R3B 2E9 (Canada)
Fax: (+1) 204-783-7981
E-mail: mike.zaworotko@uwinnipeg.ca

[**] We thank the Environmental Science and Technology Alliance Canada (ESTAC) and the Natural Sciences and Engineering Research Council of Canada (NSERC) for providing financial support for this work.

In the context of metal-organic solids, infinite molecular brick walls,^[4] ladders,^[5] bilayers,^[6] and helices^[7, 8] represent just four examples of this new generation of solids. Of particular current interest are these and other examples of open framework metal-organic^[9, 10] and organic^[11, 12] zeolite mimics which incorporate organic guests and "organic clay mimics" which are able to exchange metal cations.^[13] Herein we report on a new class of host compound, helical coordination polymers that spontaneously resolve to generate chiral cavities that are large enough to contain supramolecular complexes of organic guest molecules. Significantly, these chiral architectures are generated from simple and inexpensive achiral building blocks.

A weak but commonly encountered supramolecular synthon is the T-shape or edge-to-face stacking interaction.^[14] This type of C-H...π interaction^[15] occurs, for example, in the crystal structure of benzene and appears to be the key driving force for the architecture that is exhibited by the simple and facile to synthesize compound **1**. Crystals of **1** were grown by dissolving [Ni(acetate)₂] and benzoic acid in MeOH and layering with a solution of 4,4'-dipy in MeOH [Eq. (1); 4,4'-dipy = 4,4'-bipyridine].



An X-ray structure analysis^[16] reveals that **1** acts as a host compound if crystals are grown in the presence of the guest molecules nitrobenzene, benzene, veratrole, phenol, chloroform, and dioxane to generate the inclusion compounds **1a–f**, respectively. These exhibit isostructural helical architectures with large chiral cavities. The helices are generated around crystallographic 4₁ or 4₃ screw axes and each coil of the helix therefore contains four residues (Figure 1). The distance between coils corresponds to the unit cell length, which ranges from 27.02 to 27.91 Å. As revealed by Scheme 1, this architecture is one of at least three possible architectures that might reasonably exist for **1**. Square boxes based upon 4,4'-dipy have attracted considerable recent attention,^[17] but we are un-

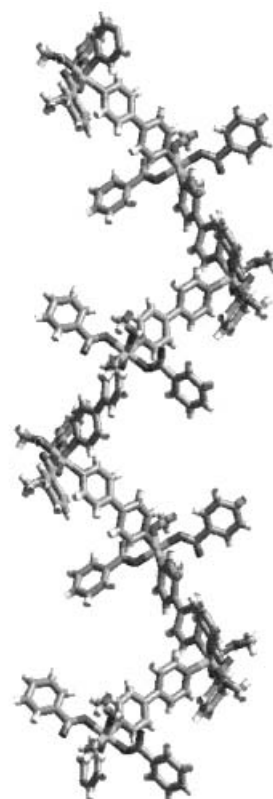
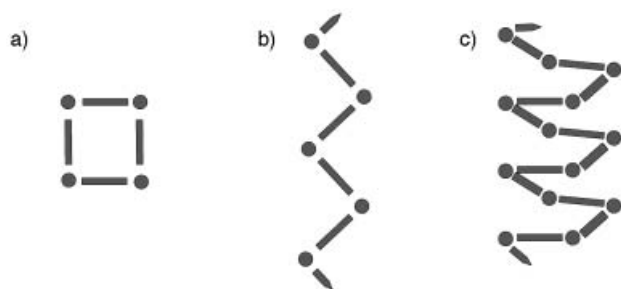


Figure 1. A portion of the helical structure exhibited by compounds **1a–f**.



Scheme 1. Possible supramolecular isomers for compounds constituted from a *cis*-octahedral or square-planar coordinated metal ion and a linear "spacer" ligand. a) square box, b) zigzag, c) helix. Circle: metal ion, rod: ligand.

aware of any other examples of helical structures sustained by 4,4'-dipy.

Examination of the crystal packing in **1a–f** reveals the existence of T-shape stacking interactions between benzoate ligands of each helix and the 4,4'-dipy ligands on adjacent helices. The stacking is inherently directional and appears to manifest itself in two salient ways. First, the 3D nature of the crystal packing induces spontaneous resolution of the helices, that is they align in the same direction. Second, adjacent helices are staggered by half the length of the unit cell. Consequently, large chiral cavities that are suitable for incorporation of organic guest molecules exist in between the helices (Figure 2).

The cavities that exist in **1a–f** deserve special attention. They are large in both absolute and relative terms (about 400–500 Å³ in volume and 24–28% of unit cell volume, respectively) and they are inherently disymmetric. Indeed, the cavity is large enough to enclose aromatic dimers and few examples of cavities greater than this size have been reported in existing crystalline solids.^[18] Furthermore, there is very little difference in the crystal packing amongst **1a–f**. Indeed, the six compounds are in effect isostructural and exhibit almost identical cell parameters.^[16] Predictably, given the coil nature of a helix, the only significant variation is the about 1 Å range observed in the length of the helical axis. Within a particular batch of crystals the collection of datasets on several suitable crystals revealed that individual crystals are randomly left-handed or right-handed. The inherent chirality of the cavity appears to induce chirality into the supramolecular adducts that are formed by the achiral guest molecules. Figure 3 illustrates the disymmetric C₂ dimer of nitrobenzene molecules that occurs in **1a** and its environment. The primary interaction between the nitrobenzene guest molecules and the walls of the cavities results from C–H⋯O hydrogen bonding between benzoate ligands and nitro groups. These molecular recognition features mean that the cavity has a profound effect upon the structure of the face-to-face dimer, and it would be reasonable to call this cavity a primitive analogue of the type of cavity that can be observed in enzymes. Interestingly, loss of guest molecules is slow under ambient conditions and does not appear to result in loss of crystallinity.

That C–H⋯π stacking is an important factor in determining and sustaining the crystalline architecture is supported by our observations in two related compounds in which the

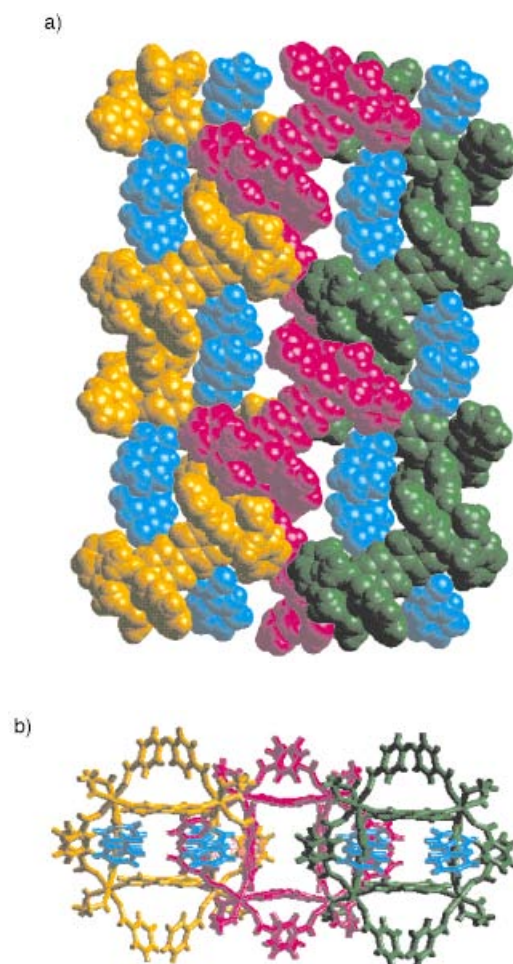


Figure 2. Illustrations of the crystal packing in compound **1a**: a) A space-filling view of the crystallographic *ac* plane in **1a**. Crystals of **1a** are randomly left-handed or right-handed. The right-handed helices presented in the illustration are staggered but orient parallel to one another. Nitrobenzene guest molecules are colored turquoise and form face-to-face dimers. b) A view of the crystallographic *ab* plane in **1a**.

benzoate ligands are functionalized. First, replacement of the key benzoate C–H functionality by a nitro group, thereby sterically and chemically precluding edge-to-face aromatic stacking, results in another interesting but dramatically different supramolecular isomer of **1**. The crystal structure of **2** consists of linear chains which stack to generate a trigonal architecture (space group *P*3₁, *a* = 11.2989(5), *c* = 17.5432(10) Å, *V* = 1936.6(2) Å³). Second, replacement of a less critical C–H moiety affords the same architecture as **1a–f**. Specifically, **3** exhibits C–H⋯π interactions and crystallizes with an almost identical structure, including cavities, to that of **1a–f** (space group *I*4₁22, *a* = 14.8633(10), *c* = 27.494(3) Å, *V* = 6074.0(8) Å³).

There are several observations and conclusions that we consider of particular relevance concerning the results reported herein:

- It is becoming abundantly clear that *chiral* crystalline architectures and cavities or channels^[19, 20] can be achieved by using the most simple of *achiral* molecular components. Furthermore, the nature of the cavities means that achiral guests are induced to form chiral adducts.

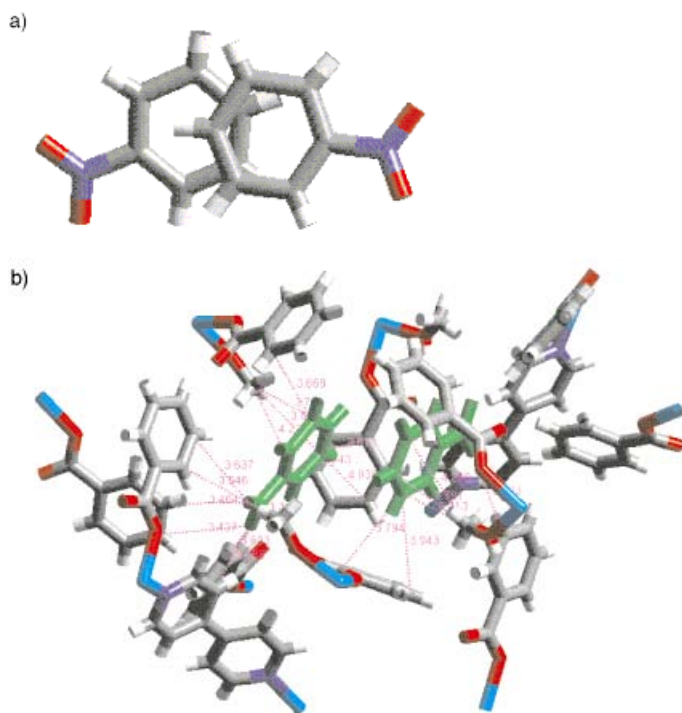


Figure 3. a) A perspective view of the disymmetric (nitrobenzene)₂ adduct that occurs in **1a**. b) A view of this adduct and its environment in the chiral cavity. Note the presence of pairs of C–H···O hydrogen bonds between benzoate ligands and nitro groups.

- Chiral and/or chiral porous materials clearly have implications for the developing fields of stereospecific synthesis^[21] and enantioselective separations. Furthermore, the bulk properties of helical urea inclusion compounds have already drawn attention.^[20]
- We confirm^[3] that even the weakest of intermolecular attractive forces, C–H··· π interactions, can profoundly and, more importantly, rationally influence crystalline architecture (parallel, staggered alignment of helices and the generation of large cavities) and sustain robust and reproducible networks.
- It appears likely that the compounds reported herein are prototypal for a plethora of similar compounds based upon helices generated from a range of *cis*-metal moieties, counterions, and linear spacer ligands. We consider it important to note that the synthetic procedures described herein involve a “one-pot synthesis”, utilize simple and inexpensive substrates, and are relatively trivial.

In summary, the compounds reported herein represent prototypes of a new class of compounds: helical coordination polymers with large chiral cavities that are suitable for the incorporation of several organic guest molecules. They therefore effectively combine the presence of polarity and porosity in the solid state, both of which are of significant relevance to applications in chemistry and materials science.

Received: August 10, 1998 [Z12271 IE]
German version: *Angew. Chem.* **1999**, *111*, 584–587

Keywords: chirality • coordination polymers • crystal engineering • helical structures • supramolecular chemistry

- [1] G. M. J. Schmidt, *Pure. Appl. Chem.* **1971**, *27*, 647–678.
- [2] M. W. Hosseini, A. De Cian, *Chem. Commun.* **1998**, 727.
- [3] G. R. Desiraju, *Angew. Chem.* **1995**, *107*, 2541–2558; *Angew. Chem. Int. Ed. Engl.* **1995**, *34*, 2311–2327.
- [4] M. Fujita, Y. J. Kwon, S. Washizu, K. Ogura, *J. Am. Chem. Soc.* **1994**, *116*, 1151.
- [5] P. Losier, M. J. Zaworotko, *Angew. Chem.* **1996**, *108*, 2957–2960; *Angew. Chem. Int. Ed. Engl.* **1996**, *35*, 2779–2782.
- [6] a) T. L. Hennigar, P. Losier, D. C. MacQuarrie, M. J. Zaworotko, R. D. Rogers, *Angew. Chem.* **1997**, *109*, 1044–1046; *Angew. Chem. Int. Ed. Engl.* **1997**, *36*, 972–973; b) M. Kondo, T. Yoshitomi, K. Seki, H. Matsuzaka, S. Kitagawa, *Angew. Chem.* **1997**, *109*, 1844–1846; *Angew. Chem. Int. Ed. Engl.* **1997**, *36*, 1725–1727.
- [7] a) J. D. Radford, J. J. Vittal, D. Wu, *Angew. Chem.* **1998**, *110*, 1159–1162; *Angew. Chem. Int. Ed.* **1998**, *37*, 1114–1116; b) V. Soghomonian, Q. Chen, R. C. Haushalter, J. Zubieta, C. J. O'Connor, *Science* **1993**, *259*, 1596–1599; c) O. J. Gelling, F. van Bolhuis, B. L. Feringa, *Chem. Commun.* **1991**, 917–919; d) Y. Dai, T. J. Katz, D. A. Nichols, *Angew. Chem.* **1996**, *108*, 2230–2232; *Angew. Chem. Int. Ed. Engl.* **1996**, *35*, 2109–2111; e) B. Wu, W.-J. Zhang, S.-Y. Yu, X.-T. Wu, *Chem. Commun.* **1997**, 1795–1796; f) C. Kaes, M. W. Hosseini, C. E. F. Rickard, B. W. Skelton, A. H. White, *Angew. Chem.* **1998**, *110*, 970–973; *Angew. Chem. Int. Ed.* **1998**, *37*, 920–922; g) J. S. Fleming, K. L. V. Mann, S. M. Couchman, J. C. Jeffrey, J. A. McLverty, M. D. Ward, *J. Chem. Soc. Dalton Trans.* **1998**, 2047; h) S. R. Batten, B. F. Hoskins, R. Robson, *Angew. Chem.* **1997**, *109*, 652–653; *Angew. Chem. Int. Ed. Engl.* **1997**, *36*, 636–637.
- [8] A related class of compound is exemplified by [Ag{3,6-di(4-pyridyl)-1,2,4,5-tetrazine}(NO₃)], which exists as linear chains that pack in a manner that lead to a helical array: M. A. Withersby, A. J. Blake, N. R. Champness, P. Hubberstey, W.-S. Li, M. Schorder, *Angew. Chem.* **1997**, *109*, 2421–2423; *Angew. Chem. Int. Ed. Engl.* **1997**, *36*, 2327–2329. The helicity in these compounds is not inherently present in the polymer itself.
- [9] O. M. Yaghi, G. Li, H. Li, *Nature* **1995**, *378*, 703–706.
- [10] D. Venkataraman, G. B. Gardner, S. Lee, J. S. Moore, *J. Am. Chem. Soc.* **1995**, *117*, 11600–11601.
- [11] P. Brunet, M. Simard, J. D. Wuest, *J. Am. Chem. Soc.* **1997**, *119*, 2737–2738.
- [12] K. Endo, T. Sawaki, M. Koyanagi, K. Kobayashi, H. Masuda, Y. Aoyama, *J. Am. Chem. Soc.* **1995**, *117*, 8341–8352.
- [13] A. W. Coleman, S. G. Bott, S. D. Morley, C. M. Means, K. D. Robinson, H. Zhang, J. L. Atwood, *Angew. Chem.* **1988**, *100*, 1412; *Angew. Chem. Int. Ed. Engl.* **1988**, *27*, 1361–1362.
- [14] W. L. Jorgensen, D. L. Severance, *J. Am. Chem. Soc.* **1990**, *112*, 4768–4774.
- [15] Recent References on C–H··· π interactions: a) T. Steiner, M. Tamm, B. Lutz, J. van der Mass, *Chem. Commun.* **1996**, 1127; b) M. Asakawa, P. R. Ashton, S. E. Boyd, C. L. Brown, S. Menzer, D. Pasini, J. F. Stoddart, M. S. Tolley, A. J. P. White, D. J. Williams, P. G. Wyatt, *Chem. Eur. J.* **1997**, *3*, 463; c) N. N. L. Madhavi, A. K. Katz, H. L. Carrell, A. Nangia, G. R. Desiraju, *Chem. Commun.* **1997**, 1953; d) H.-C. Weiss, D. Bläser, R. Boese, B. M. Doughan, M. M. Haley, *Chem. Commun.* **1997**, 1703.
- [16] Crystal structure analysis of **1a** (1·nitrobenzene), tetragonal, space group *P*₄₃₂₁₂ or *P*₄₁₂₁₂ (full structural characterization of several crystals revealed that they are randomly left-handed or right-handed), *a* = 14.9890(8), *c* = 27.913(2) Å, *V* = 6271.1(6) Å³, *Z* = 8, ρ = 1.365 Mg m^{−3}, *R*₁ = 0.0522, *wR*₂ = 0.1178 for 5488 out of 5533 reflections with *I* > 2 σ (*I*). In a typical example, the enantiomorph was confirmed by refinement of the Flack parameter to 0.07(2) and comparison with the other enantiomorph (*R*₁ = 0.0626, Flack parameter = 0.93(2)). Data were collected on a Siemens SMART/CCD diffractometer at 178 K and the structure was solved and refined using SHELX/TL. Compounds **1b–f** are isostructural with **1a** and crystallize with the following cell parameters [Å]: **1b**: *a* = 15.0406(9), *c* = 27.442(2); **1c**: *a* = 15.0789(6), *c* = 27.167(2); **1d**: *a* = 15.0211(8), *c* = 27.0920(14); **1e**: *a* = 14.9608(9), *c* = 27.180(2); **1f**: *a* = 15.0643(6), *c* = 27.0204(14). Solvent or guest was observed to be disordered inside the chiral cavity in all compounds except for **1a** and **1e**, for which dimers of nitrobenzene and chloroform, respectively, were resolved. IR spectroscopy confirmed the presence of guest in **1b–d** and **1f**.

Crystallographic Data Centre as supplementary publication nos. CCDC-102586 and CCDC-102587 (**1a** and **1e**, respectively). Copies of the data can be obtained free of charge on application to CCDC, 12 Union Road, Cambridge, CB2 1EZ, UK (Fax: (+44)1223-336-033; E-mail: deposit@ccdc.cam.ac.uk).

- [17] a) M. Fujita, O. Sasaki, T. Mitsuhashi, T. Fujita, J. Yazaki, K. Yamaguchi, K. Ogura, *Chem. Commun.* **1996**, 1535; b) P. J. Stang, D. H. Cao, S. Saito, A. M. Arif, *J. Am. Chem. Soc.* **1995**, *117*, 6273; c) R. V. Slone, D. I. Yoon, R. M. Calhoun, J. T. Hupp, *J. Am. Chem. Soc.* **1995**, *117*, 11813.
[18] L. R. MacGillivray, J. L. Atwood, *Nature* **1997**, *389*, 469–472.
[19] R. Hoss, O. Konig, V. Kramer-Ross, U. Berger, P. Rogin, J. Hulliger, *Angew. Chem.* **1996**, *108*, 1774; *Angew. Chem. Int. Ed. Engl.* **1996**, *35*, 1664.
[20] M. E. Brown, M. D. Hollingsworth, *Nature* **1995**, *376*, 323–326.
[21] M. Sakamoto, *Chem. Eur. J.* **1997**, *3*, 684–689.

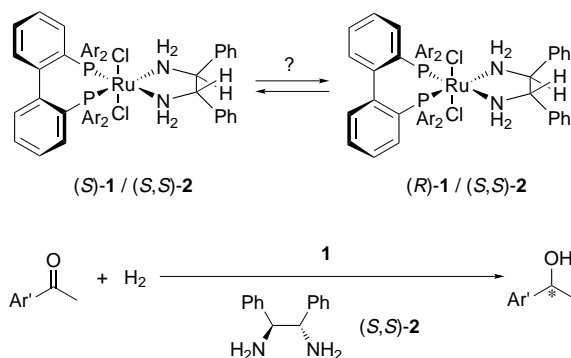
Conformationally Flexible Biphenylphosphane Ligands for Ru-Catalyzed Enantioselective Hydrogenation**

Koichi Mikami,* Toshinobu Korenaga, Masahiro Terada, Takeshi Ohkuma, Trang Pham, and Ryoji Noyori*

In asymmetric catalytic reactions,^[1] racemic catalysts inherently give only racemic products, whereas nonracemic catalysts generate nonracemic products with or without a nonlinear relationship.^[2] Conversely, we reported a conceptually new strategy for asymmetric catalysis using racemic catalysts wherein a chiral additive selectively activates,^[3] rather than deactivates,^[4] one enantiomer of the racemic catalyst. We here describe an advanced strategy that uses conformationally flexible bis(phosphanyl)biphenyl ligands (BIPHEP)^[5] for a Ru catalyst which, following activation by a chiral diamine,^[3d, 6] achieves high enantioselectivity in the hydrogenation of carbonyl compounds (see Scheme 1). Combination of a racemic BINAP/RuCl₂ species (BINAP = 2,2'-bis(diphenylphosphanyl)-1,1'-binaphthyl) with an equimolar amount of an enantiomerically pure diamine gives a 1:1 mixture of two diastereomeric diphosphane/diamine complexes.^[3d] When the BINAP ligand is replaced by the flexible and proatropisomeric BIPHEP, diastereomeric complexes are

formed, in principle, in unequal amounts. Here, if the major diastereomer shows higher chiral efficiency than does the minor isomer, this strategy becomes more beneficial than the use of structurally similar BINAP analogues.

The hydrogenation of a carbonyl compound by the complex formed from [RuCl₂(dm-biphep)(dmf)_n] (**1**; DM-BIPHEP = 2,2'-[(3,5-dimethylphenyl)phosphanyl]biphenyl) and enantiopure (*S,S*)-1,2-diphenylethylenediamine (*(S,S)*-DPEN; (*S,S*)-**2**)^[7] is shown in Scheme 1. Conformational flexibility of the



Scheme 1. Enantioselective hydrogenation of carbonyl compounds to optically active alcohols catalyzed by Ru complexes containing conformationally flexible BIPHEP ligands. In each case, (*S*)-**1** and (*R*)-**1** (Ar = 3,5-dimethylphenyl) is fixed in the respective configuration. The chiral amine (*S,S*)-**2** is added as activator to complex **1** prior to the hydrogenation.

BIPHEP/RuCl₂/diamine complexes was proven by ¹H NMR spectroscopic analysis. A mixture of **1** and **2** in CDCl₃ at room temperature showed a ¹H NMR spectrum that is quite similar to that of the racemic DM-BINAP/RuCl₂/*(S,S)*-DPEN complex.^[8, 9] This indicated the initial formation of an equimolar mixture of *S*- and *R*-fixed DM-BIPHEP/RuCl₂/*(S,S)*-DPEN diastereomers in this solvent (¹H NMR (CDCl₃): (*S*)-DM-BIPHEP/RuCl₂/*(S,S)*-DPEN: δ = 3.42, 3.43, 4.33; (*R*)-DM-BIPHEP/RuCl₂/*(S,S)*-DPEN: δ = 3.28, 4.06, 4.59). However, when this mixture was diluted with [D₈]2-propanol (CDCl₃/(CD₃)₂CDOD 1/2) and allowed to stand at room temperature for 3 h or at 80 °C for 30 min, a 3:1 mixture of the *S/S,S* and *R/S,S* diastereomers was formed (Figure 1, Scheme 2; ¹H NMR

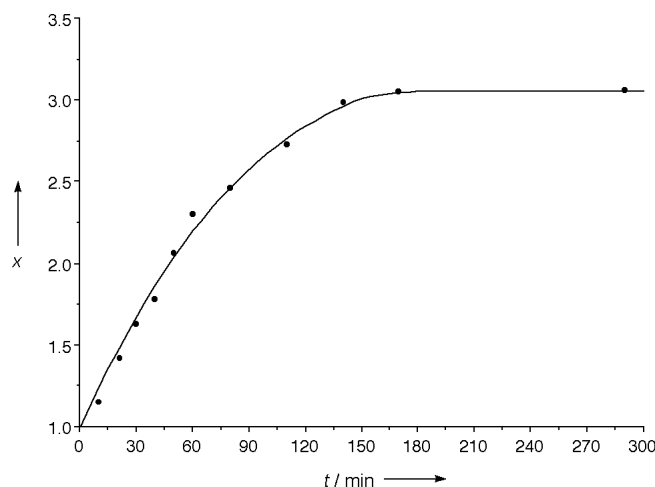


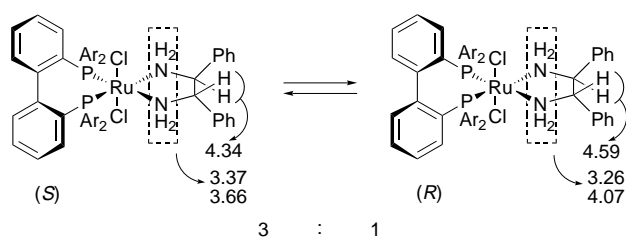
Figure 1. Stereomutation of DM-BIPHEP/RuCl₂/*(S,S)*-DPEN diastereomers in CDCl₃/(CD₃)₂CDOD (1/2) at 25 °C. x = ratio of (*S*)-DM-BIPHEP/RuCl₂/DPEN to (*R*)-DM-BIPHEP/RuCl₂/DPEN.

[*] Prof. Dr. K. Mikami, T. Korenaga, Dr. M. Terada
Department of Chemical Technology
Tokyo Institute of Technology
Ookayama, Meguro-ku, Tokyo 152–8552 (Japan)
Fax: (+81)3-5734-2776
E-mail: kmikami@o.cc.titech.ac.jp

Prof. Dr. R. Noyori, Prof. Dr. T. Ohkuma, Dr. T. Pham
Department of Chemistry and Molecular Chirality
Research Unit, Nagoya University
Chikusa, Nagoya 464–8602 (Japan)
Fax: (+81)52-783-4177
E-mail: noyori@chem3.chem.nagoya-u.ac.jp

[**] We are grateful to Dr. H. Kumobayashi and Dr. N. Sayo of Takasago International Corp. for providing BINAP ligands. This work was financially supported by the Ministry of Education, Science, Sports and Culture of Japan (nos. 07CE2004, 09238209, and 10208204).

(CDCl₃/(CD₃)₂CDOD 1/2): (*S*)-DM-BIPHEP/RuCl₂/(*S,S*)-DPEN: δ = 3.37, 3.66, 4.34; (*R*)-DM-BIPHEP/RuCl₂/(*S,S*)-DPEN: δ = 3.26, 4.07, 4.59). Stereomutation of the DM-BIPHEP/RuCl₂/DPEN complex could occur through rupture of a Ru–P bond, rotation about the Cl–Cl' bond to invert the



Scheme 2. Assignment of ¹H NMR signals for DM-BIPHEP/RuCl₂/(*S,S*)-DPEN diastereomers in CDCl₃/(CD₃)₂CDOD (1/2). In each case, the *R* and *S* configuration is fixed. Ar = 3,5-dimethylphenyl.

configuration of the diphosphane,^[5a] and recoordination of P to Ru.^[10] Alternatively, the configuration of the diphosphane-chelated seven-membered ring might be directly inverted. The dichloro complexes may further be converted into active mono- or dihydrido Ru species under hydrogenation conditions.^[11]

The enantioselective hydrogenation was performed after addition of KOH and a ketone (e.g. **3**) to a mixture of **1** and **2** with or without preheating at 80 °C for 30 min [Eq. (1), Table 1]. The advantage of the conformationally flexible

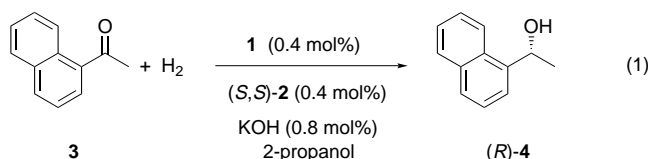


Table 1. Results of the enantioselective hydrogenation of ketone **3** to alcohol **4**. Equation (1) shows the reaction catalyzed by the complex formed from [RuCl₂(dm-biphep)(dmf)_n] (**1**) and (*S,S*)-1,2-diphenylethylenediamine ((*S,S*)-**2**).^[a]

Run	Phosphane	<i>S/S,S</i> : <i>R/S,S</i> ^[b]	<i>p</i> (H ₂) [atm]	<i>T</i> [°C]	<i>t</i> [h]	<i>ee</i> [%]	Yield [%]
1	DM-BIPHEP	1:1	8	28	4	63	> 99
2	DM-BIPHEP	2:1	8	28	4	73	> 99
3 ^[c]	DM-BIPHEP	3:1	8	28	4	84	> 99
4	(±)-DM-BINAP		8	28	4	80	> 99
5 ^[c]	DM-BIPHEP	3:1	40	– 35	12	92	> 99
6	(±)-DM-BINAP		40	– 35	7	89	> 99

[a] Hydrogenation performed as described in the text without preheating, unless otherwise noted. [b] The ratio of (*S*)-**1**/(*S,S*)-**2** to (*R*)-**1**/(*S,S*)-**2** was determined by ¹H NMR spectroscopy. [c] **1**/(*S,S*)-**2** in 2-propanol was preheated at 80 °C for 30 min.

BIPHEP/RuCl₂/diamine complexes is clear in the ratio-dependent enantioselectivity of hydrogenation of 1'-acetonaphthone (**3**) in comparison with the enantioselectivity obtained using the (±)-DM-BINAP/RuCl₂/(*S,S*)-diamine pair (Table 1, runs 1–3 versus run 4). The lower enantioselectivity of the 1:1 BIPHEP chelate complex pair compared with the 1:1 BINAP chelate pair (runs 1 versus 4) indicates the differences in steric demand of the two types of ligands. Even

so, a higher enantioselectivity with a 3:1 BIPHEP-chelate equilibrium (run 3) clearly indicated the advantage of conformationally flexible BIPHEP compared with that of a 1:1 BINAP pair (run 4).

Further increase in enantioselectivity was attained at a lower reaction temperature (– 35 °C, run 5). The enantioselectivity by **1**/(*S,S*)-**2** was higher than that by the (±)-DM-BINAP/RuCl₂/(*S,S*)-diamine complex at the same low temperature and high pressure (run 6). Thus, (*R*)-1-(1-naphthyl)ethanol (**4**)^[12] was obtained with 92 % *ee* in quantitative yield. DM-BIPHEP/RuCl₂/DPEN was also employable in the reduction of *o*-methylacetophenone with H₂ (8 atm). The reaction was carried out with KOH and 2-propanol at 0 °C for 4 h to provide 1-*o*-methylphenylethanol quantitatively and with 88 % *ee* (for comparison, the analogous reaction with (±)-DM-BINAP/RuCl₂/(*S,S*)-DPEN proceeds with 86 % *ee*).

In summary, we have presented an enantioselective hydrogenation by a conformationally flexible BIPHEP-Ru catalyst containing a chiral diamine ligand. The asymmetric activation will provide a general strategy for the use of not only racemic but also conformationally flexible ligands.

Experimental Section

4: A 100-mL autoclave was charged with solid **1** (11.4 mg, 0.012 mmol) and **2** (2.6 mg, 0.012 mmol). 2-Propanol (3.3 mL) was added to the autoclave under a stream of argon. The solution was preheated at 80 °C for 30 min, and KOH/2-propanol (0.5 M, 48 μL, 0.024 mmol) was added with stirring at room temperature over 30 min. 1'-Acetonaphthone (**3**; 0.46 mL, 3.00 mmol) was added to the autoclave at room temperature under a stream of argon, and then hydrogen (40 atm) was introduced. After the mixture was vigorously stirred for 12 h at – 35 °C, the solution was concentrated under reduced pressure. The resulting residue was filtered through a short column of silica gel. The chemical yield and enantiomeric ratio of **4** were calculated by chiral GC (> 99 %, (*R*)-**4**:(*S*)-**4** = 96.0:4.0). Product **4** can also be isolated (510 mg, 99 %) by column chromatography on silica gel (eluent: hexane/EtOAc 5/1). [α]_D²⁵ = + 69.0 (*c* = 1.0, CHCl₃; lit. value:^[12] [α]_D²⁵ = + 78.9 (*c* = 1, CHCl₃, *R* isomer); GC (column: CP-Cyclodextrin- β -2,3,6-M-19, inner diameter: 0.25 mm \times 25 m, CHROM-PACK, carrier gas: nitrogen (75 kPa), column temperature: 160 °C, injection temperature: 190 °C, split ratio: 100:1, retention time *t*_R = 32.7 min ((*R*)-**4**, 96.0 %), 31.6 min ((*S*)-**4**, 4.0 %), 21.3 min (**3**, 0 %).

Received: July 8, 1998

Revised version: November 3, 1998 [Z12118IE]

German version: *Angew. Chem.* **1999**, *111*, 517–519

Keywords: activation • asymmetric catalysis • atropisomerism • P ligands • ruthenium

- a) R. Noyori, *Asymmetric Catalysis in Organic Synthesis*, Wiley, New York, **1994**; b) H. Brunner, W. Zettlmeier, *Handbook of Enantioselective Catalysis*, VCH, Weinheim, **1993**; c) *Catalytic Asymmetric Synthesis* (Ed.: I. Ojima), VCH, New York, **1993**; d) H. B. Kagan, *Comprehensive Organic Chemistry*, Vol. 8, Pergamon, Oxford, **1992**.
- Reviews: R. Noyori, M. Kitamura, *Angew. Chem.* **1991**, *103*, 34–55; *Angew. Chem. Int. Ed. Engl.* **1991**, *30*, 49–69; H. B. Kagan, D. Guillauneux, D. Rainford, O. Samuel, S.-H. Zhao, *Acta Chem. Scand.* **1996**, *50*, 345–352; M. Avalos, R. Babiano, P. Cintas, J. L. Jiménez, J. C. Palacios, *Tetrahedron Asymmetry* **1997**, *8*, 2997–3017; C. Girard, H. B. Kagan, *Angew. Chem.* **1998**, *110*, 3088–3127; *Angew. Chem. Int. Ed.* **1998**, *37*, 2922–2959; examples: a) D. Guillauneux, S.-H. Zhao, O. Samuel, D. Rainford, H. B. Kagan, *J. Am. Chem. Soc.* **1994**, *116*, 9430–9439; C. Puchot, O. Samuel, E. Dunach, S. Zhao, C. Agami, H. B. Kagan, *J. Am. Chem. Soc.* **1986**, *108*, 2353–2357; b) M.

Super High Throughput Screening (SHTS) of Chiral Ligands and Activators: Asymmetric Activation of Chiral Diol–Zinc Catalysts by Chiral Nitrogen Activators for the Enantioselective Addition of Diethylzinc to Aldehydes**

Kuiling Ding, Akihiro Ishii, and Koichi Mikami*

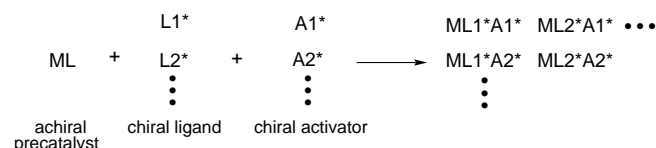
- Kitamura, S. Suga, M. Niwa, R. Noyori, *J. Am. Chem. Soc.* **1995**, *117*, 4832–4842; c) N. Oguni, Y. Matsuda, T. Kaneko, *J. Am. Chem. Soc.* **1988**, *110*, 7877–7877; d) K. Mikami, Y. Motoyama, M. Terada, *J. Am. Chem. Soc.* **1994**, *116*, 2812–2820; K. Mikami, M. Terada, *Tetrahedron* **1992**, *48*, 5671–5680; M. Terada, K. Mikami, T. Nakai, *J. Chem. Soc. Chem. Commun.* **1990**, 1623–1624.
- [3] a) K. Mikami, S. Matsukawa, *Nature* **1997**, *385*, 613–615; b) S. Matsukawa, K. Mikami, *Tetrahedron Asymm.* **1997**, *8*, 815–816; c) *Enantiomer* **1996**, *1*, 69–73; d) T. Ohkuma, H. Doucet, T. Pham, K. Mikami, T. Korenaga, M. Terada, R. Noyori, *J. Am. Chem. Soc.* **1998**, *120*, 1086–1087.
- [4] For an opposite strategy of deactivation, see N. W. Alcock, J. M. Brown, P. J. Maddox, *J. Chem. Soc. Chem. Commun.* **1986**, 1532–1534; J. M. Brown, P. J. Maddox, *Chirality* **1991**, *3*, 345–354; K. Maruoka, H. Yamamoto, *J. Am. Chem. Soc.* **1989**, *111*, 789–790; J. W. Faller, J. Parr, *J. Am. Chem. Soc.* **1993**, *115*, 804–805.
- [5] a) The activation barrier to axial torsion in selectively deuterated BIPHEP is measured to be only (22 ± 1) kcal, which suggests that axial rotation takes place at room temperature or above: O. Desponds, M. Schlosser, *Tetrahedron Lett.* **1996**, *37*, 47–48, and references therein; b) see also 6,6'-substituted analogues: G. Trabesinger, A. Albinati, N. Feiken, R. W. Kunz, P. S. Pregosin, M. Tschöerner, *J. Am. Chem. Soc.* **1997**, *119*, 6315–6323, and references therein.
- [6] a) T. Ohkuma, H. Ooka, S. Hashiguchi, T. Ikariya, R. Noyori, *J. Am. Chem. Soc.* **1995**, *117*, 2675–2676; b) T. Ohkuma, H. Ooka, T. Ikariya, R. Noyori, *J. Am. Chem. Soc.* **1995**, *117*, 10417–10418; c) H. Doucet, T. Ohkuma, K. Murata, T. Yokozawa, M. Kozawa, E. Katayama, A. F. England, T. Ikariya, R. Noyori, *Angew. Chem.* **1998**, *110*, 1792–1796; *Angew. Chem. Int. Ed.* **1998**, *37*, 1703–1707.
- [7] a) P. Mangeney, T. Tejero, A. Alexakis, F. Grosjean, J. Normant, *Synthesis* **1988**, 255–257; b) S. Pikul, E. J. Corey, *Org. Synth.* **1993**, *71*, 22–29.
- [8] 3,5-Dimethylphenyl-BINAP: K. Mashima, Y. Matsumura, K. Kusano, H. Kumabayashi, N. Sayo, Y. Hori, T. Ishizaki, S. Akutagawa, H. Takaya, *J. Chem. Soc. Chem. Commun.* **1991**, 609–610.
- [9] ¹H NMR (CDCl₃): (S)-DM-BINAP/RuCl₂/(S,S)-DPEN: δ = 3.02, 3.16, 4.19; (R)-DM-BINAP/RuCl₂/(S,S)-DPEN: δ = 2.62, 3.86, 4.43. ¹H NMR (CDCl₃/(CD₃)₂CDOD 1/2): (S)-DM-BINAP/RuCl₂/(S,S)-DPEN: δ = 2.98, 3.36, 4.21; (R)-DM-BINAP/RuCl₂/(S,S)-DPEN: δ = 2.60, 3.87, 4.42.
- [10] Although the DM-BIPHEP/RuCl₂/DPEN complex was treated with DM-BINAP in 2-propanol, it was not observed by ¹H NMR spectroscopy.
- [11] R. L. Chowdhury, J.-E. Bäckvall, *J. Chem. Soc. Chem. Commun.* **1991**, 1063–1064; K.-J. Haack, S. Hashiguchi, A. Fujii, T. Ikariya, R. Noyori, *Angew. Chem.* **1997**, *109*, 297–300; *Angew. Chem. Int. Ed. Engl.* **1997**, *36*, 285–288; R. Noyori, S. Hashiguchi, *Acc. Chem. Res.* **1997**, *30*, 97–102.
- [12] P. D. Theisen, C. H. Heathcock, *J. Org. Chem.* **1988**, *53*, 2374–2378; W. H. Pirkle, S. D. Beare, *J. Am. Chem. Soc.* **1967**, *89*, 5485–5487.

Combinatorial chemistry has been well recognized as a useful strategy for the discovery and optimization of bioactive drugs, coordination complexes, and solid-state materials.^[1] Of the split-and-mix and parallel-matrix strategies, the latter is more employable for lead optimization, and high-throughput screening (HTS) is essential for tuning a variety of modifications.^[2] However, only a limited number of investigations has so far been reported on the optimization of chiral ligands for metal complexes.^[3] With HPLC or gas chromatography (GC) on chiral columns, it takes a tediously long time to separate enantiomeric products and then to determine the enantioselectivity of the reactions. The application of a detection system based on circular dichroism (CD) to HPLC on nonchiral stationary phases allows the simultaneous monitoring of the CD signal $\Delta\epsilon$, the absorption ϵ , and their ratio $g = \Delta\epsilon/\epsilon$. The dissymmetry factor g is independent of concentration and is linearly related to the enantiomeric excess.^[4] With this technique, the enantiomeric excess of the product could be determined within minutes without separation of the enantiomeric products. Therefore, combined application of the combinatorial chemistry (CC) factory (Dainippon Seiki, DNC) for reactions and HPLC-CD provide a highly efficient screening system, which we refer to as the super high throughput screening (SHTS) system, for finding the most effective catalyst through asymmetric activation.

Asymmetric activation of a chiral catalyst with a chiral additive may enhance the levels of catalyst efficiency and enantioselectivity.^[5] The advantage of this approach over the deactivation strategy^[6] is that the activated catalyst can produce a greater enantiomeric excess in the products than can the enantiomerically pure catalyst on its own. Sharpless et al. emphasized the importance of “chiral ligand acceleration” through the construction of an asymmetric catalyst from an achiral precatalyst by ligand exchange with a chiral ligand.^[7] Chiral catalysts thus obtained with chiral ligands (L1*, L2*,...) may be further evolved with chiral activators (A1*, A2*,...) into the most catalytically active and enantioselective chiral catalysts (Scheme 1).

[*] Prof. Dr. K. Mikami, Prof. Dr. K. Ding, A. Ishii
Department of Chemical Technology, Faculty of Engineering
Tokyo Institute of Technology
2-12-1 Ookayama, Meguro-ku, Tokyo 152 (Japan)
Fax: (+81)3-5734-2776
E-mail: kmikami@o.cc.titech.ac.jp

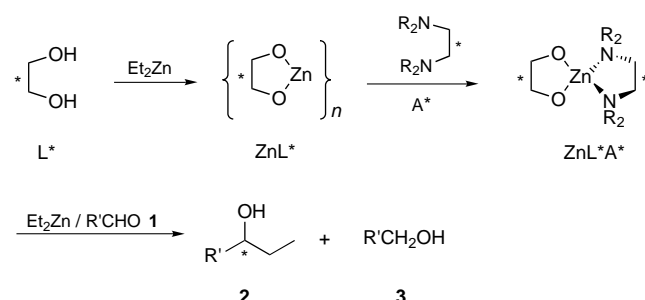
[**] This work was aided by the Ministry of Education, Science, Sports and Culture of Japan (nos. 09238209 and 10208204). A UNESCO research fellowship for K. D. is gratefully acknowledged. We are grateful to Mr. Naotaka Sawada of Dainippon Seiki Co., Ltd., Dr. Akito Tanaka of Fujisawa Pharmaceutical Co., Ltd., and Mr. Kenichi Kudo of JASCO Corp. for their technical assistance.



Scheme 1. General principle for the creation of a catalyst system by asymmetric activation.

We now report the SHTS of parallel solution libraries of chiral ligands and activators for diol–zinc catalysts in the addition of diethylzinc to aldehydes by using the CC factory and HPLC-CD. For C–C bond forming reactions, enantioselective addition of diorganozinc reagents to aldehydes constitutes one of the most important and fundamental asymmetric reactions.^[8] Since the initial report by Oguni and Omi,^[9] various chiral ligands, including β -amino alcohols, have been used for this type of reaction.^[10–12] However, less attention has been paid to C_2 -symmetric chiral diols, probably due to their lower catalytic activity and enantioselectivity for the reaction.^[13] Only very recently, some derivatives of 2,2'-dihydroxy-1,1'-binaphthyl (BINOL) were found to be effective,^[14] but the simple BINOL itself is very inert to the reaction.

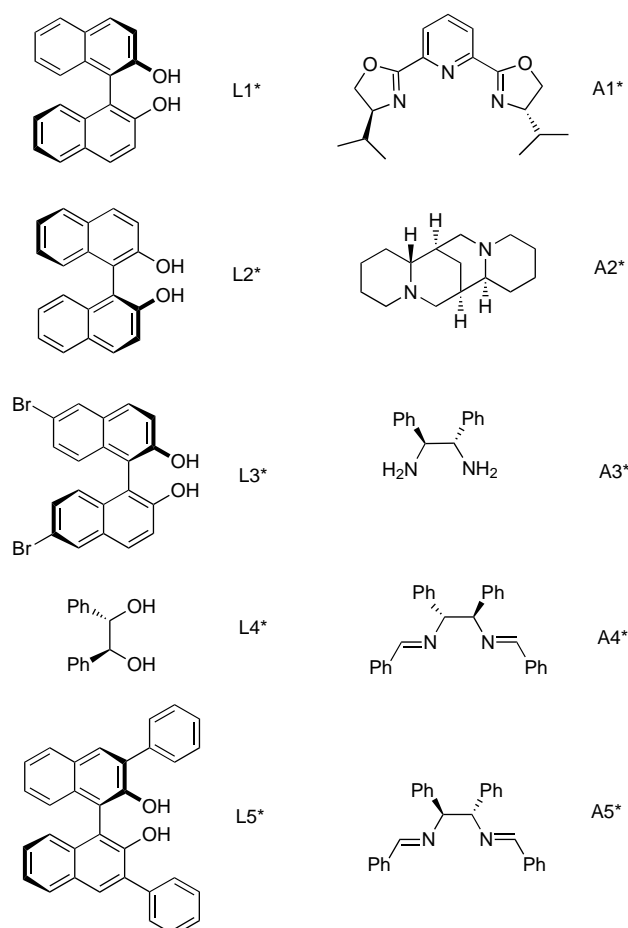
It is reasonable to assume that the active catalyst in the addition of diethylzinc to aldehydes is a monomeric zinc alkoxide; the cleavage of the higher aggregates could result in an activation of overall catalyst system.^[15] As shown in Scheme 2, for activation of the diol–zinc catalyst system,



Scheme 2. Asymmetric activation of diol–zinc catalysts by nitrogen ligands.

addition of a chiral nitrogen ligand is most efficient because of its ability to coordinate so strongly to the zinc cation. As a result, a monomeric zinc complex is expected to be formed in a manner similar to that of a chiral salen–zinc complex (salen = *N,N'*-bis(salicylidene)ethylenediamine dianion).^[16] Furthermore, bimolecular combination of chiral activators with the diol–zinc complexes should be more convenient than the unimolecular combination. Thus, we initially examined the primary combinatorial library of chiral ligands ($L1^*$ – $L5^*$) and chiral activators ($A1^*$ – $A5^*$), from which the lead compound could be further optimized for the next generation of the chiral ligands and activators.

The reactions were carried out as described in the Experimental Section. As shown in Figure 1, under the experimental conditions we observed an effect of the activation in terms of catalyst efficiency (Figures 1a and b).



Enantioselectivity of the reaction is also increased by matched combination of diol ligands and nitrogen activators (Figure 1c). For example, $L1^*$ and $A4^*$ promote the reaction to give (*S*)-1-phenylpropanol with 8.2% *ee* (54% yield) and 1.1% *ee* (64% yield), respectively. However, the combined use of $L1^*$ and $A4^*$ quantitatively provides the product with 37.4% *ee* (*S*). The substitution of the 3- and 3'-positions with bulky phenyl groups further prevents the aggregation of BINOL/Zn and increases the enantioselectivity, the best combinations were found to be $L5^*/A4^*$ and $L5^*/A5^*$ to provide (*S*)-1-phenylpropanol with up to 65% *ee* and in quantitative yields.

On the basis of the results derived from primary combinatorial libraries, we then created a new library of diimines (activators; $A4^*$ – $A15^*$) with 12 members by simple condensation of enantiopure 1,2-diphenylethylenediamine or 1,2-diaminocyclohexane with two equivalents of aromatic aldehydes respectively. As shown in Figure 2, all library members significantly activate the $Zn(L5^*)$ complex and produce 1-phenylpropanol in higher yields and with higher enantioselectivities than those complexes obtained by only using the ligands themselves. The reaction could be completed within minutes in the case of $L5^*/A9^*$. The chirality of the nitrogen activators has little effect on the configuration of the product, but may influence the enantioselectivity, particularly in the cases of $L5^*$ with $A8^*$, $A9^*$, $A12^*$, or $A13^*$. Therefore, the absolute configuration of product is determined primarily by that of the diol, which is consistent with the empirical rule

Table 1. Asymmetric addition of Et₂Zn to aldehydes in the presence of L5*/A9* to provide alcohol **2**.

Entry	R	Yield [%] of 2 ^[a]	ee [%] of 2 ^[b]	Config. ^[c]
1	phenyl	100	99.0	S
2	phenyl ^[d]	100	97.0	S
3	<i>p</i> -methoxyphenyl	100	98.5	n.d.
4	<i>m</i> -methoxyphenyl ^[e]	100	96.4	n.d.
5	<i>p</i> -chlorophenyl	99	98.5	S
6	<i>p</i> - <i>tert</i> -butylphenyl	100	99.0	n.d.
7	β -naphthyl	100	93.8	S
8	α -naphthyl	93	91.5	S

[a] Yield of isolated **2** based on the consumed aldehydes. [b] Determined by HPLC on a Daicel OD-H column unless otherwise noted. [c] Assigned by comparison of chiroptical values with those in the literature. n.d. = not determined. [d] 2 mol % of L5*/A9* was used. [e] Determined by HPLC on a Chiracel OB-H column.

In summary, we have successfully developed a new strategy for super high throughput screening of chiral ligands and activators by employment of the CC factory and HPLC-CD. This SHTS technique combined with our concept of asymmetric activation will provide a very powerful methodology for finding the best activated catalyst.^[17]

Experimental Section

General procedure for SHTS: All reactions were performed under nitrogen. Weighed amounts of chiral ligands L* (0.01 mmol) or chiral activators A* (0.01 mmol) or both (0.01 mmol each) were introduced into 1-mL polypropylene microtubes. CH₂Cl₂ (100 μ L) and Et₂Zn (200 μ L, 1M in hexane) were added with micropipettes. The microtubes were then set up in the CC factory to maintain the temperature at 0 °C for 30 min, and finally benzaldehyde (11 μ L, 0.1 mmol) was introduced. After agitation for 20 h at 0 °C, the tubes were opened. The programed quench with water and extraction with ethyl acetate were performed by the CC factory. The product mixtures were then submitted to a JASCO CD-995 instrument with an autosampler on a CrestPak C18S column (4.6 \times 150 mm) with CH₃CN/H₂O (1/1) as eluent. The retention time for 1-phenylpropanol is 3.0 min. Based on the dissymmetry factor *g* measured for 1-phenylpropanol with known enantiomeric excesses at 275 nm, the enantiomeric excesses of the products could be calculated conveniently.

Optimized procedure: Under argon to a predried flask were added L5* (44 mg, 0.1 mmol), A9* (47 mg, 0.1 mmol), CH₂Cl₂ (1 mL), and diethylzinc (2 mL of 1M solution in hexane, 2 mmol) at room temperature. The flask was cooled to –78 °C, and then benzaldehyde (106 mg, 1 mmol) was introduced dropwise by a microsyringe. After the reaction mixture was stirred at –78 °C for 4 h and then at –20 °C for 1 h, water (2 mL) was added to quench the reaction. The aqueous layer was extracted with diethyl ether, and the combined organic phase was washed with brine and then dried over anhydrous MgSO₄. After removal of the solvent, the residue was analyzed by ¹H NMR spectroscopy to determine the benzaldehyde conversion and product ratio. The crude product was purified by column chromatography on silica gel with EtOAc/hexane (1/5) as eluent to give pure 1-phenylpropanol as a colorless liquid in quantitative yield and with 99 % ee; HPLC on Daicel OD-H column: eluent hexane/2-propanol (99/1); flow rate 0.8 mL min^{–1}; UV detection at λ = 254 nm; retention time = 22.9 min (*R* enantiomer), 26.0 min (*S* enantiomer).

Received: August 25, 1998 [Z12329IE]
German version: *Angew. Chem.* **1999**, *111*, 519–523

Keywords: asymmetric activation • asymmetric catalysis • binaphthol • combinatorial chemistry • zinc

- [1] Special issues on combinatorial chemistry: a) *Acc. Chem. Res.* **1996**, *29*(3); b) *Chem. Eng. News* **1996**, *74*(4); reviews: c) F. Balkenhohl,

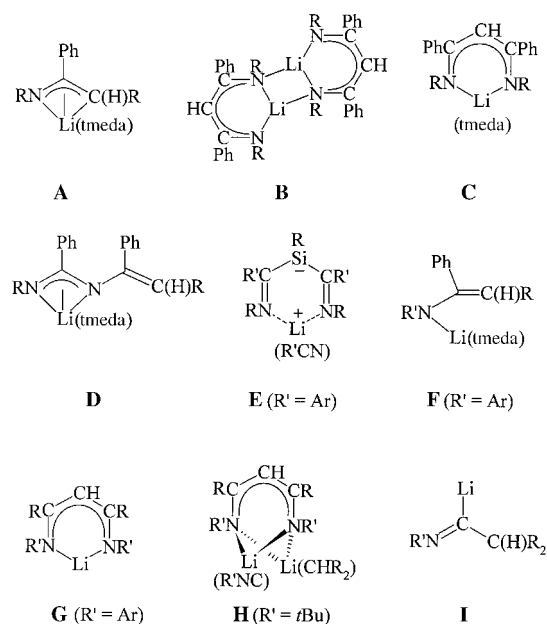
- C. B. Hunnefeld, A. Lansky, C. Zechel, *Angew. Chem.* **1996**, *108*, 2437–2476; *Angew. Chem. Int. Ed. Engl.* **1996**, *35*, 2288–2337; d) C. Gennari, H. P. Nestler, U. Piarulli, B. Salom, *Liebigs Ann.* **1997**, 637–647; e) *Combinatorial Chemistry: Synthesis and Application* (Eds.: S. R. Wilson, A. W. Czarink), Wiley, New York, **1997**.
- [2] *High Throughput Screening* (Ed.: J. P. Devlin), Marcel Dekker, New York, **1997**.
- [3] For examples, see a) M. S. Sigman, E. N. Jacobsen, *J. Am. Chem. Soc.* **1998**, *120*, 4901–4902; b) K. Burgess, H.-J. Lim, A. M. Porte, G. A. Sulikowski, *Angew. Chem.* **1996**, *108*, 192–194; *Angew. Chem. Int. Ed. Engl.* **1996**, *35*, 220–222; c) B. M. Cole, K. D. Shimizu, C. A. Krueger, J. P. A. Harrity, M. L. Snapper, A. H. Hoveyda, *Angew. Chem.* **1996**, *108*, 1776–1779; *Angew. Chem. Int. Ed. Engl.* **1996**, *35*, 1667–1671; d) G. Liu, J. A. Ellman, *J. Org. Chem.* **1995**, *60*, 7712–7713.
- [4] For the application of a CD detection system to measure optical purity by HPLC on nonchiral stationary phases, see a) C. Bertucci, P. Salvadori, L. F. L. Guimaraes, *J. Chromatogr. A* **1994**, *666*, 535–539; b) P. Salvadori, C. Bertucci, C. Rosini, *Chirality* **1991**, *3*, 376–385; c) A. F. Drake, J. M. Gould, S. F. Mason, *J. Chromatogr.* **1980**, *202*, 239–245.
- [5] a) K. Mikami, S. Matsukawa, *Nature* **1997**, *385*, 613–615; b) S. Matsukawa, K. Mikami, *Tetrahedron: Asymmetry* **1995**, *6*, 2571–2574; c) S. Matsukawa, K. Mikami, *Tetrahedron: Asymmetry* **1997**, *8*, 815–816; d) S. Matsukawa, K. Mikami, *Enantiomer* **1996**, *1*, 69–73; e) T. Ohkuma, H. Doucet, T. Pham, K. Mikami, T. Korenaga, M. Terada, R. Noyori, *J. Am. Chem. Soc.* **1998**, *120*, 1086–1087; f) S. Casolari, P. G. Cozzi, P. Orioli, E. Tagliavini, A. Umani-Ronchi, *Chem. Commun.* **1997**, 2123–2123; g) C. M. Yu, H. S. Choi, W. H. Jung, H. J. Kim, J. Shin, *Chem. Commun.* **1997**, 761–762; h) C. M. Yu, S. K. Yoon, W. H. Joon, H. S. Choi, K. Baek, *Chem. Commun.* **1997**, 763–764.
- [6] a) K. Maruoka, Y. Yamamoto, *J. Am. Chem. Soc.* **1989**, *111*, 789–790; b) J. W. Faller, D. W. Sams, X. Liu, *J. Am. Chem. Soc.* **1993**, *115*, 804–805; c) J. W. Faller, D. W. Sams, X. Liu, *J. Am. Chem. Soc.* **1996**, *118*, 1217–1218; d) J. W. Faller, M. Tokunaga, *Tetrahedron Lett.* **1993**, *34*, 7359–7362; e) R. Sablong, J. A. Osborn, J. W. Faller, *J. Organomet. Chem.* **1997**, *527*, 65–70; f) N. W. Alcock, J. M. Brown, P. J. Maddox, *J. Chem. Soc. Chem. Commun.* **1986**, 1532–1534; g) J. M. Brown, P. J. Maddox, *Chirality* **1991**, *3*, 345–354; h) J. W. Faller, M. R. Mazzieri, J. T. Nguyen, J. Parr, M. Tokunaga, *Pure Appl. Chem.* **1994**, *66*, 1463–1469.
- [7] D. J. Berrisford, C. Bolm, K. B. Sharpless, *Angew. Chem.* **1995**, *107*, 1159–1171; *Angew. Chem. Int. Ed. Engl.* **1995**, *34*, 1059–1070.
- [8] For a general discussion, see a) R. Noyori, *Asymmetric Catalysis in Organic Synthesis*, Wiley, New York, **1994**; b) *Catalytic Asymmetric Synthesis* (Ed.: I. Ojima), VCH, New York, **1993**; c) *Advances in Catalytic Processes, Vol. 1* (Ed.: M. P. Doyle), JAI Press, Greenwich, USA, **1995**; d) H. B. Kagan, *Comprehensive Organic Chemistry*, Vol. 8, Pergamon, Oxford, **1992**; e) *Handbook of Enantioselective Catalysis* (Eds.: H. Brunner, W. Zettlmeier), VCH, New York, **1993**; reviews: f) R. Noyori, M. Kitamura, *Angew. Chem.* **1991**, *103*, 34–55; *Angew. Chem. Int. Ed. Engl.* **1991**, *30*, 49–69; g) K. Soai, S. Niwa, *Chem. Rev.* **1992**, *92*, 833–885; h) “Stereoselective Synthesis”: R. M. Devant, H. E. Radunz, *Methoden Org. Chem. (Houben-Weyl) 4th ed.* **1995**, Vol. E21b, **1996**, pp. 1314–1334.
- [9] N. Oguni, T. Omi, *Tetrahedron Lett.* **1984**, *25*, 2823–2824.
- [10] For examples of titanium complexes as catalysts, see a) D. Seebach, A. K. Beck, B. Schmidt, Y. M. Wang, *Tetrahedron* **1994**, *50*, 4363–4384; b) D. Seebach, L. Behrendt, D. Felix, *Angew. Chem.* **1991**, *103*, 100–101; *Angew. Chem. Int. Ed. Engl.* **1991**, *30*, 99–101; c) J. Qiu, C. Guo, X. Zhang, *J. Org. Chem.* **1997**, *62*, 2665–2668; d) F. Y. Zhang, C. W. Yip, R. Cao, A. S. C. Chan, *Tetrahedron: Asymmetry* **1997**, *8*, 585–589; e) F. Y. Zhang, A. S. C. Chan, *Tetrahedron: Asymmetry* **1997**, *8*, 3651–3655; f) T. Takahashi, T. Kawakita, M. Ohno, M. Yoshioka, S. Kobayashi, *Tetrahedron* **1992**, *48*, 5691–5700; g) M. Mori, T. Nakai, *Tetrahedron Lett.* **1997**, *38*, 6233–6236; h) W. Brieden, R. Ostwald, P. Knochel, *Angew. Chem.* **1993**, *105*, 629–631; *Angew. Chem. Int. Ed. Engl.* **1993**, *32*, 582–584; i) S. Pritchett, D. H. Woodmansee, P. Gantzel, P. J. Walsh, *J. Am. Chem. Soc.* **1998**, *120*, 6423–6424.
- [11] For asymmetric autocatalysis, see a) K. Soai, T. Shibata, H. Morioka, K. Choji, *Nature* **1995**, *378*, 767–768; b) T. Shibata, H. Morioka, T. Hayase, K. Choji, K. Soai, *J. Am. Chem. Soc.* **1996**, *118*, 471–742;

- c) S. J. Li, Y. Z. Jiang, A. Q. Mi, G. S. Yang, *J. Chem. Soc. Dalton Trans.* **1993**, 885–886; d) K. Soai, T. Shibata, *J. Synth. Org. Chem. Jpn.* **1997**, 55(11), 72–83.
- [12] For planar chiral heterocycles as ligands, see a) P. I. Dosa, J. C. Ruble, G. C. Fu, *J. Org. Chem.* **1997**, 62, 444–445; for examples of β -amino thiols as ligands, see b) J. Kang, J. W. Lee, J. I. Kim, *J. Chem. Soc. Chem. Commun.* **1994**, 2009–2010; c) Y. Arai, N. Nagata, Y. Masaki, *Chem. Pharm. Bull.* **1995**, 43, 2243–2245; d) E. Rijnberg, N. J. Hovestad, A. W. Kleij, J. T. B. H. Jastrzebski, J. Boersma, M. D. Janssen, A. L. Spek, G. van Koten, *Organometallics* **1997**, 16, 2847–2857; for β -amino thiocarboxylate as ligand, see e) M.-J. Jin, S.-J. Ahn, K.-S. Lee, *Tetrahedron Lett.* **1996**, 37, 8767–8770; for piperazines as chiral ligands, see f) S. Niwa, K. Soai, *J. Chem. Soc. Perkin Trans.1* **1991**, 2717–2722; g) T. Shono, N. Kise, E. Shirakawa, H. Matsumoto, E. Okazaki, *J. Org. Chem.* **1991**, 56, 3063–3067; for oxazaborolidines as ligands, see h) N. N. Joshi, M. Srebnik, H. C. Brown, *Tetrahedron Lett.* **1989**, 30, 5551–5554.
- [13] a) C. Rosini, L. Franzini, D. Pini, P. Salvadori, *Tetrahedron: Asymmetry* **1990**, 1, 587–588; b) K. R. K. Prasad, N. N. Joshi, *Tetrahedron: Asymmetry* **1996**, 7, 1957–1960.
- [14] a) H. Kitajima, K. Ito, Y. Aoki, T. Katsuki, *Bull. Chem. Soc. Jpn.* **1997**, 70, 207–217; b) Q. S. Hu, W. S. Huang, D. Vitharana, X. F. Zhang, L. Pu, *J. Am. Chem. Soc.* **1997**, 119, 12454–12464; c) W. S. Huang, Q. S. Hu, L. Pu, *J. Org. Chem.* **1998**, 63, 1364–1365; d) Q. S. Hu, W. S. Huang, L. Pu, *J. Org. Chem.* **1998**, 63, 2798–2799.
- [15] a) C. Bolm, J. Muller, *Tetrahedron* **1994**, 50, 4355–4362. For example, $[\text{Zn}(\text{acac})_2]$ (acac = acetylacetone) has a trimeric structure, but the tri(3-phenylpyrazol-1-yl)borate complex of zinc is a monomer; b) M. J. Bennett, F. A. Cotton, R. Eiss, R. C. Elder, *Nature* **1967**, 213, 174; c) A. Kremer-Aach, W. Klau, R. Bell, A. Strerath, H. Wunderlich, D. Mootz, *Inorg. Chem.* **1997**, 36, 1552–1563. Very recently, Denmark et al. reported an excellent example of deaggregation of a sulfonamide–zinc complex with nitrogen ligands; d) S. E. Denmark, S. P. O'Connor, S. R. Wilson, *Angew. Chem.* **1998**, 110, 1162–1165; *Angew. Chem. Int. Ed.* **1998**, 37, 1149–1151.
- [16] P. G. Cozzi, A. Papa, A. Umani-Ronchi, *Tetrahedron Lett.* **1996**, 37, 4613–4616.
- [17] Recently, IR thermography was employed for qualitative analysis of catalytic (asymmetric) processes: in homogeneous catalysis: M. T. Reetz, M. H. Becker, K. M. Kuhling, A. Holzwarth, *Angew. Chem.* **1998**, 110, 2792–2795; *Angew. Chem. Int. Ed.* **1998**, 37, 2647–2650 (we thank Prof. Dr. Manfred T. Reetz for kindly sending us a copy of this manuscript prior to publication); in heterogeneous catalysis: G. Georgiadis, V. A. Self, P. A. Sermon, *Angew. Chem.* **1987**, 99, 1050–1052; *Angew. Chem. Int. Ed. Engl.* **1987**, 87, 1042–1043; b) F. C. Moates, M. Somani, J. Annamalai, J. T. Richardson, D. Luss, R. C. Willson, *Ind. Eng. Chem. Res.* **1996**, 35, 4801–4803; c) D. E. Bergbreiter, *Chemtract: Org. Chem.* **1997**, 10, 683–686; d) S. J. Tayler, J. P. Morken, *Science* **1998**, 280, 267–270, and references cited therein. IR thermography may be applied for quantitative analysis of catalytic asymmetric processes in the near future.

A 1-Aza-2-silacyclobut-3-ene and an Alkyne from $[\text{Li}(\text{Si}(\text{SiMe}_3)_3)(\text{thf})_3]$ and the Isocyanide 2,6-Me₂C₆H₃NC

Peter B. Hitchcock, Michael F. Lappert,* and Marcus Layh

The interaction of a trimethylsilylmethylolithium reagent $\text{Li}[\text{CH}_{3-n}(\text{SiMe}_3)_n]$ ($n=1, 2$, or 3) and an α -H-free nitrile $\text{R}'\text{CN}$ can yield a 1-azaallyl-, β -diketiminato-, or 1,3-diazaallyllithium, depending on n , the nature of R' , the stoichiometry, and the absence or presence of a neutral coligand. Examples of such products from LiCHR_2 ($\text{R}=\text{SiMe}_3$) and PhCN are **A**,^[1] **B**,^[2] **C**,^[3] or **D**,^[1] each formed by initial insertion of PhCN into the $\text{Li}-\text{C}$ bond of $\text{Li}(\text{CHR}_2)$ and a 1,3-Me₃Si shift from C to N, followed for **B–D** by insertion of a further PhCN molecule into an $\text{Li}-\text{N}$ or $\text{Li}-\text{C}$ bond of **A** and a final 1,3-Me₃Si $\text{N} \rightarrow \text{N}$ or $\text{C} \rightarrow \text{N}$ shift. This chemistry was extended to the lithium silyl and germyl congeners of LiCR_3 . Thus, $[\text{Li}(\text{SiR}_3)(\text{thf})_3]$ with 2,6-Me₂C₆H₃NC (ArCN) yielded the zwitterionic 3-sila- β -diketiminatolithium complex **E**, a process involving a hitherto unprecedented 1,3-Me₃Si shift from Si to N.^[4] We also previously demonstrated that from LiCHR_2 and an isocyanide $\text{R}'\text{NC}$, a similar diversity of

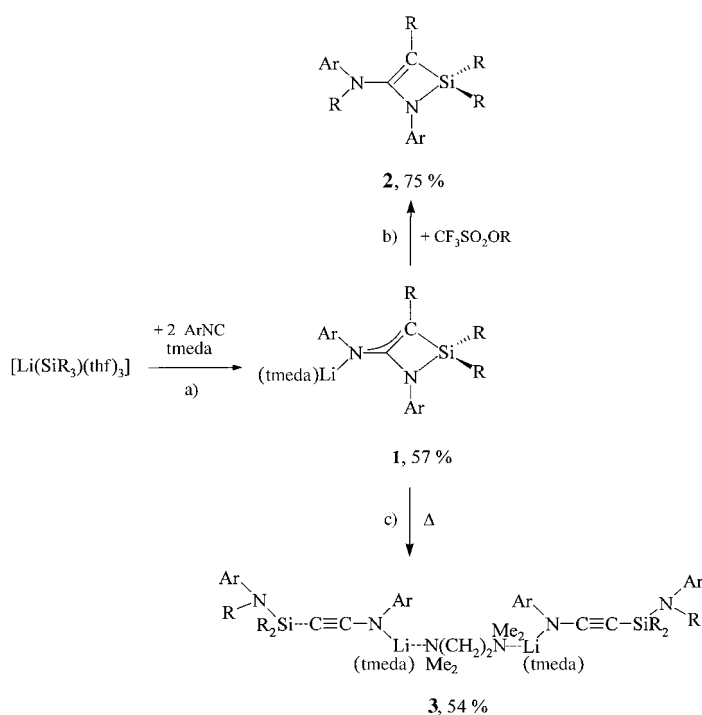


products **F–H** is available, each formed via successively the 1:1 adduct and the lithioaldimine **I**.^[1] Compound **I**, by a 1,2-Me₃Si $\text{C} \rightarrow \text{C}$ shift, is transformed into **F**, which by a similar sequence generates **G** and **H**.

We now report the results presented in Scheme 1: Treatment of $[\text{Li}(\text{SiR}_3)(\text{thf})_3]$ ^[5] with the isocyanide ArNC yields

[*] Prof. M. F. Lappert, Dr. P. B. Hitchcock, Dr. M. Layh
School of Chemistry, Physics and Environmental Science
University of Sussex
Brighton BN1 9QJ (UK)
Fax: (+44) 1273-677196
E-mail: m.f.lappert@sussex.ac.uk

[**] We thank EPSRC for a fellowship for M.L. and other support.



Scheme 1. Synthesis of compounds **1–3**; R = SiMe₃, Ar = 2,6-Me₂C₆H₃, tmeda = *N,N,N',N'*-tetramethylethylenediamine. See text for details.

the novel, crystalline 4-aryl(lithio)amino-1-aza-2-silacyclobut-3-ene derivative **1** (step a), which upon being quenched with trimethylsilyl triflate was converted into **2** (step b). In contrast, heating **1** in refluxing benzene afforded the crystalline alkyne derivative **3** (step c), the C≡C fragment of which remarkably arises from the ArNC units. Moreover, we present X-ray crystallographic data which establish the molecular structures of the crystalline amidolithium compounds **1** and **3**.

The formation of **1** was independent of whether one or two equivalents of ArNC were employed and of solvent (pentane or Et₂O). The conversion of **1** into **3** (Scheme 1, step c) was

monitored by ¹H NMR spectroscopy on a sample of **1** in C₆D₆ in a sealed NMR tube; quantitative conversion was achieved at 80 °C in 14 h if tmeda (0.5 mol) was added. On a preparative scale, optimal results from **1** alone were achieved by heating in benzene at 80 °C for 2 h.

Each of the compounds **1–3** gave satisfactory elemental analyses and multinuclear NMR spectra, and for **1** and **2** acceptable EI mass spectra were also obtained (see Experimental Section). In addition, single-crystal X-ray diffraction data revealed the molecular structures of crystalline **1** and **3** (see Figure 1). The unusual structure of **1** was maintained in solution, as established by a series of NOE difference NMR spectra.

Compound **1** is a monomer, in which the atoms of the four-membered heterocyclic ring and the exocyclic N atom N1 are essentially coplanar and the geometry at N1 and each of the ring atoms N2, C1, and C2 is almost planar (Figure 1, left). Of the endocyclic bond angles, only C2–C1–N1 is obtuse (105.2(5)°), and of the remainder only that at Si1 (76.9(3)°) deviates significantly from 90°. The Li atom is directly bonded only to N1 and the two nitrogen atoms of tmeda, having no close contacts to C1 or C2, although the N1–C1 (1.331(7) Å) and C1–C2 (1.411(8) Å) bond lengths indicate significant delocalization of π-electron density between these three atoms. In this respect, the situation resembles that in [Li{N(R)C(4-BrC₆H₄)=CR₂}(thf)], which has a structure such as that of **1**^[6] and corresponding N–C (1.35(1) Å) and C–C (1.40(2) Å) bond lengths similar to those of **1**; but the azaallyl differs from **1** in having relatively close Li...C contacts of 2.23(2) and 2.32(2) Å.^[6] We conclude that **1** is best described as a resonance hybrid of the enamidolithium structure **1a** and the dipolar **1b**. As far as we are aware, only two SiNCC heterocycles have previously been crystallographically characterized, both being 1-aza-2-silacyclobutanes with C–C single bond lengths of 1.541(5) Å in Si(*t*Bu)₂N(Si(*t*Bu)₂Ph)-C(H(OEt))CH₂^[7] and 1.569(5) Å Si(Ph)₂N(SiMe₂Ph)C(H(Ph))CH₂Pr.^[8] In silacyclobutenes, the C=C bond lengths are unexceptional; ^[9, 10] they lie in the range 1.34–1.37 Å, for

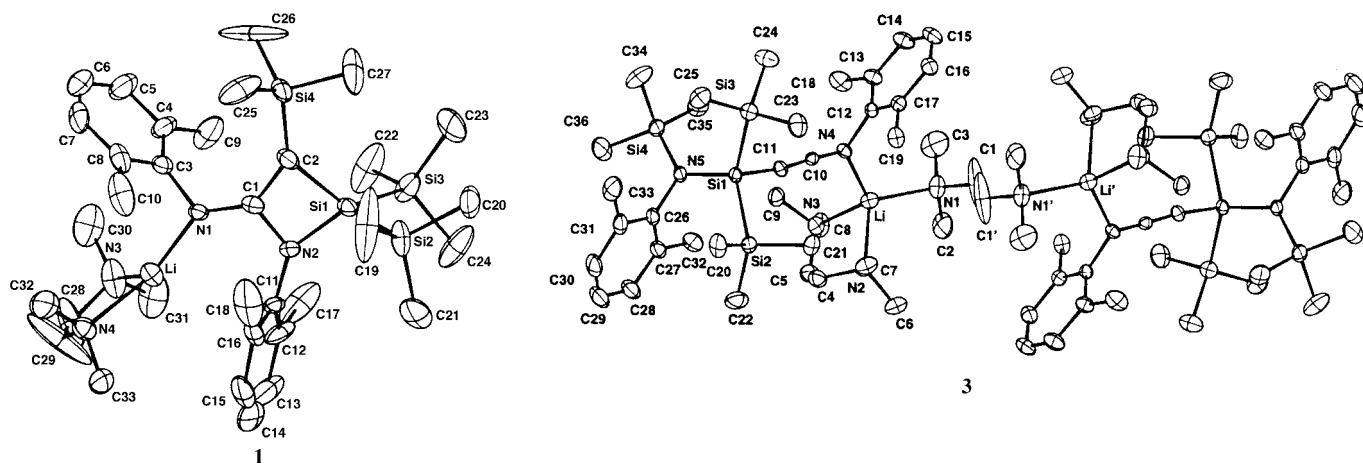
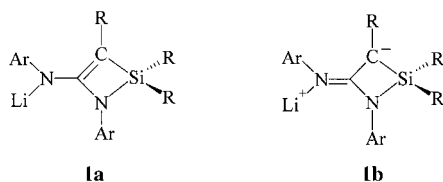


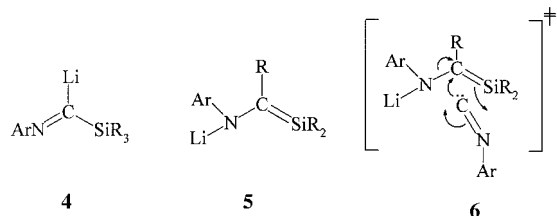
Figure 1. Crystal structures and atomic labeling schemes of **1** and **3**. Selected bond lengths [Å] and angles [°]: **1**: Li–N1 1.958(11), Li–N3 2.119(12), Li–N4 2.162(11), Si1–N2 1.785(5), Si1–C2 1.831(7), Si1–Si3 2.346(3), Si1–Si2 2.353(3), N1–C1 1.331(7), N2–C1 1.421(7), C1–C2 1.411(8); N2–Si1–C2 76.9(3), C1–N2–Si1 89.7(3), C1–C2–Si1 88.1(4), C2–C1–Si1 105.2(5), C1–N1–Li 134.1(5). **3**: Li–N1 2.241(6), Li–N2 2.175(6), Li–N3 2.210(6), Li–N4 2.029(6), N4–C10 1.317(4), C10–C11 1.221(4), Si1–C11 1.796(3), Si1–N5 1.769(3); C11–C10–N4 175.3(3), C10–C11–Si1 171.5(3).



example,^[9] 1.338(4) Å in (2,4,6-*i*-Pr₃C₆H₂)₃Si(Me)C(H)=C(Ph)C–(SiMe₂OSiMe₃)Ad (Ad = adamantyl). The very different electronic environments at C1 and C2 of **1** are also evident from their ¹³C{¹H} NMR chemical shifts in C₆D₆: δ = 168.4 and 48.6, respectively.

The crystalline lithioaminoalkyne **3** is a dimer (Figure 1, right), in which a bridging tmeda molecule links the two mononuclear fragments. (It is somewhat rare for tmeda to behave in this fashion; previous selected examples are given in ref. [11].) Features typical for an alkyne include the short C10–C11 bond of 1.221(4) Å and the near linearity at C10 (175.3(3)°) and C11 (171.5(3)°). The C_{sp}–Si bond length of 1.796(3) Å is slightly shorter than those of trimethylsilylalkynes (1.84 Å^[12]), while the C–N bond length of 1.317(4) Å can be compared with that of 1.344(3) Å in the aminoalkyne C₁₂H₈N–C≡C–NC₁₂H₈.^[13] As expected, the Li–N4 distance of 2.029(6) Å in the four-coordinate lithium compound **3** is longer than that of the three-coordinate complex **1**.

The initial two steps in the reaction pathway from [Li(SiR₃)(thf)₃] and ArNC to **1** probably resemble those in the corresponding Li(CHR₂)/ArNC system. Thus, initial formation of the lithioaldimine **4** (cf. **1**^[4]) is followed by a 1,2-Me₃Si Si→C shift that converts **4** into the isomer **5** (cf. **1**^[4]). An electrocyclic cycloaddition of ArNC to **5** (see **6**)



yields **1**. The transformation of **1** into **3** requires a 1,3-Me₃Si shift from C2 to N2 (facilitated by the partial carbanionic character of C2 (see **1b**) and N2–C1 ring scission).

The head-to-head coupling of two isocyanide molecules to generate an alkyne has a precedent, the transformation of the isocyanide R'NC into the alkyne PhMe₂Si(R')NC≡CN–(R')SiMe₂R'' (**J**) by successive treatment with LiSiMe₂Ph and R''Me₂SiCl (R' = *cyclo*-C₆H₁₁, *s*Bu, or *i*Pr; R'' = Me or Ph).^[14] While the molecular formulas and the presence of the alkyne moiety in **J** were unambiguously established, the present results suggest that an isomeric (aminosilyl)(silylamino)alkyne structure should be considered.

Compounds **1** and **3** have potential as ligand-transfer reagents, and **2** contains a hitherto unknown C=CSiN ring system. The reactions of isocyanides with trimethylsilylmethyl or -silyl compounds are being extended to -germyls and -stannyls and to isoelectronic analogues of the Group 15 elements.

Experimental Section

1: 2,6-Me₂C₆H₃NC (0.40 g, 3.01 mmol) was added at –80 °C to a solution of [Li(SiMe₃)(thf)₃] (0.67 g, 1.53 mmol) in pentane (50 mL) and tmeda (0.23 mL, 1.55 mmol). The reaction mixture was stirred for 1 h, then allowed to warm slowly to room temperature, and stirred for 24 h. All volatile components were removed in vacuo, the residue was extracted with pentane (40 mL) and filtered, and the filtrate was concentrated and cooled. After 1 d colorless crystals of **1** (0.55 g, 57%) were obtained. M.p. 124 °C (decomp.); elemental analysis calcd for C₃₅H₆₁LiN₄Si₄: C 62.6, H 9.71, N 8.84; found: C 62.6, H 9.57, N 8.53; EI-MS: *m/z* (%): 523 (10) [*M*⁺]; ¹H NMR (C₆D₆, 300.1 MHz): δ = 0.15 (s, CSiMe₃), 0.43 (s, SiSiMe₃), 1.09 (s, NCH₂), 1.33 (s, NMe), 2.54 (s, Me (LiNAr)), 2.59 (s, Me (NAr ring)), 6.71 (t, 1H, *J* = 7.4 Hz, Ph), 6.83 (d, 2H, *J* = 7.4 Hz, Ph) (both NAr rings), 6.94 (t, 1H, *J* = 7.5 Hz, Ph), 7.11 (d, 2H, *J* = 7.5 Hz, Ph) (both LiNAr units); ⁷Li NMR (C₆D₆, 116.6 MHz): δ = –0.59; ²⁹Si NMR (C₆D₆, 99.4 MHz): δ = –21.2 (s, CSiMe₃(C)), –20.0 (s, Si(SiMe₃)₂), 8.0 (s, Si(SiMe₃)₂); ¹³C NMR (C₆D₆, 75.5 MHz): δ = 0.5 (s, Si(SiMe₃)₂), 3.9 (s, CSiMe₃), 20.8, 20.9 (s, Me), 45.1 (s, NMe), 48.6 (s, CSiMe₃), 56.5 (s, NCH₂), 121.7, 122.8 (s, *p*-Ph), 128.5, 128.8 (s, *m*-Ph), 134.1, 137.0, 144.2, 150.9 (s, *ipso*-C), 168.4 (s, CN₂).

2: CF₃SO₂SiMe₃ (0.1 mL, 0.87 mmol) in pentane (10 mL) was slowly added to a solution of **1** (0.55 g, 0.87 mmol) in pentane (30 mL) at –40 °C. The mixture was allowed to warm to room temperature and was stirred for 6 h. Removal of the volatile substances in vacuo and extraction of the residue with pentane (20 mL), filtration and concentration of the filtrate gave, upon cooling, colorless crystals of **2** (0.38 g, 75%). M.p. 205 °C (decomp.); elemental analysis calcd for C₃₀H₅₄N₂Si₅: C 61.8, H 9.33, N 4.80; found: C 61.5, H 9.33, N 4.84; EI-MS: *m/z* (%): 582 (57) [*M*⁺], 567 (42) [*M* – Me]⁺, 509 (100) [*M* – SiMe₃]⁺; ¹H NMR (C₆D₆, 300.1 MHz): δ = –0.20, –0.22 (s, 9H, SiMe₃), 0.22 (s, 18H, SiMe₃), 2.39, 2.60 (s, Me), 6.85 (s, 3H, Ph), 6.91 (s, 3H, Ph); ²⁹Si NMR (C₆D₆, 99.4 MHz): δ = –19.2 (s, CSiMe₃), –17.9 (s, Si(SiMe₃)₂), 9.3 (s, Si(SiMe₃)₂), 13.8 (s, NSiMe₃); ¹³C NMR (C₆D₆, 75.5 MHz): δ = 0.5 (s, Si(SiMe₃)₂), 2.7, 2.8 (s, SiMe₃), 20.5, 21.0 (s, Me), 76.7 (s, CSiMe₃), 123.8, 129.6 (s, *p*-Ph), 129.5, 129.8 (s, *m*-Ph), 134.4, 138.5, 143.7, 143.9 (s, *ipso*-C), 162.8 (s, CN₂).

3: **1** (0.64 g, 1.01 mmol) was dissolved in benzene (5–10 mL) and heated for 2.5 h to 80 °C. The volatile substances were removed in vacuo. The residue was extracted with pentane (60 mL), and the extract filtered to remove a small amount of precipitate. The filtrate was concentrated and cooled to give colorless crystals of **3** (0.4 g, 54%). Elemental analysis calcd for C₇₂H₁₃₈Li₂N₁₀Si₈: C 62.6, H 10.06, N 10.13; found: C 62.4, H 9.76, N 9.99; the mass spectrum showed only peaks due to fragmentation of the ligands; IR (Nujol) $\tilde{\nu}$ = 2032 cm^{–1} (C≡C); ¹H NMR (C₆D₆, 300.1 MHz): δ = 0.29 (s, Si(SiMe₃)₂), 0.37 (s, NSiMe₃), 1.60 (s, NCH₂), 1.78 (s, NMe), 2.54, 2.61 (s, Me), 6.88 (m, Ph), 7.01 (d, Ph), 7.13 (d, Ph); ⁷Li NMR (C₆D₆): δ = 0.93; ²⁹Si NMR (C₆D₆, 99.4 MHz): δ = 4.5 (NSiMe₃), –19.1 (Si(SiMe₃)₂), –42.2 (Si(SiMe₃)₂); ¹³C NMR (C₆D₆, 75.5 MHz): δ = 1.5 (s, Si(SiMe₃)₂), 3.5 (s, NSiMe₃), 20.4, 21.7 (s, Me), 44.9 (s, NMe), 47.9 (s, C≡C), 56.1 (s, NCH₂), 119.6, 123.8 (s, *p*-Ph), 128.5, 128.6 (s, *m*-Ph), 130.8, 137.7, 149.6, 150.9 (s, *ipso*-C).

Crystal data for **1**: C₃₅H₆₁LiN₄Si₄, *M*_r = 633.2, monoclinic, space group *P*2₁/*n* (No. 14), *a* = 13.196(1), *b* = 18.965(2), *c* = 17.006(2) Å, β = 110.10(1)°, *V* = 3996.7(7) Å³, *Z* = 4, ρ_{calcd} = 1.05 Mg m^{–3}, *F*(000) = 1384, λ(MoKα) = 0.71073 Å, μ = 0.17 mm^{–1}; for **3**: C₇₂H₁₃₈Li₂N₁₀Si₈(C₅H₁₀), *M*_r = 1454.7, triclinic, space group *P*1̄ (No. 2), *a* = 10.519(2), *b* = 13.944(2), *c* = 18.074(3) Å, α = 108.36(1), β = 90.58(1), γ = 111.69(1)°, *V* = 2313.8(7) Å³, *Z* = 1, ρ_{calcd} = 1.04 Mg m^{–3}, *F*(000) = 800, λ(MoKα) = 0.71073 Å, μ = 0.16 mm^{–1}. Data were collected at 173(2) K on a Enraf-Nonius CAD4 diffractometer in the ω/2θ mode for the range of 2 > θ > 22° (**1**) and 2 > θ > 25° (**3**). The structure was solved by direct methods (SHELXS86) and refined by full-matrix least-squares methods on all *F*² (SHELXL93). All non-hydrogen atoms were anisotropic, and hydrogen atoms were included in the riding mode with *U*_{iso}(H) = 1.2 *U*_{eq}(C) or 1.5 *U*_{eq}. The *o*-methyl groups of the phenyl rings were fixed for **1** at idealized geometry but with refinement of the torsion angle defining the H atom positions. Final residuals for **1** (**3**) for 4876 (8144) independent reflections were *R*₁ = 0.137 (0.097), *wR*₂ = 0.200 (0.164) and for the 3131 (5584) reflections with *I* > 2σ(*I*), *R*₁ = 0.085 (0.059), *wR*₂ = 0.166 (0.139), GOF = 1.021 (1.034); parameters refined 383 (447); largest difference peak 0.55 (0.70) e Å^{–3}. Crystallographic data (excluding structure factors) for the structure

reported in this paper have been deposited with the Cambridge Crystallographic Data Centre as supplementary publications no. CCDC-102645 (**1**) and CCDC-102646 (**3**). Copies of the data can be obtained free of charge on application to CCDC, 12 Union Road, Cambridge CB21EZ, UK (fax: (+44) 1223-336-033; e-mail: deposit@ccdc.cam.ac.uk).

Received: August 6, 1998 [Z12263IE]
German version: *Angew. Chem.* **1999**, *111*, 562–565

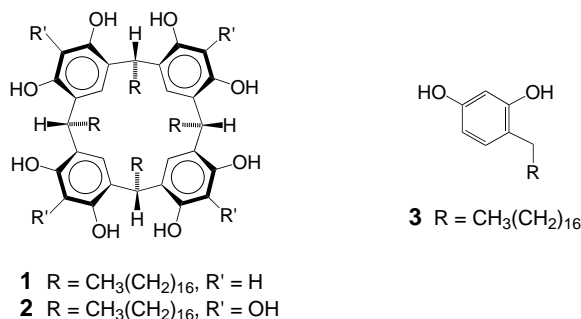
Keywords: heterocycles • insertions • lithium • silicon

- [1] P. B. Hitchcock, M. F. Lappert, M. Layh, *Chem. Commun.* **1998**, 201.
- [2] P. B. Hitchcock, M. F. Lappert, D.-S. Liu, *J. Chem. Soc. Chem. Commun.* **1994**, 1699.
- [3] P. B. Hitchcock, M. F. Lappert, S. Tian, unpublished results.
- [4] P. B. Hitchcock, M. F. Lappert, M. Layh, *Chem. Commun.* **1998**, 2179.
- [5] a) A. Heine, R. Herbst-Irmer, G. M. Sheldrick, D. Stalke, *Inorg. Chem.* **1993**, *32*, 2694; b) H. V. R. Dias, M. M. Olmstead, K. Ruhlandt-Senge, P. P. Power, *J. Organomet. Chem.* **1993**, *462*, 1.
- [6] P. B. Hitchcock, M. F. Lappert, M. Layh, *Tetrahedron Lett.* **1998**, *39*, 4745.
- [7] J. Niesmann, U. Klingebiel, S. Rudolph, R. Herbst-Irmer, M. Noltemeyer, *J. Organomet. Chem.* **1996**, *515*, 43.
- [8] K. Tamao, Y. Nagakawa, Y. Ito, *J. Am. Chem. Soc.* **1992**, *114*, 218.
- [9] P. Lassacher, A. G. Brook, A. J. Lough, *Organometallics* **1995**, *14*, 4359.
- [10] M. Ishikawa, T. Horio, Y. Yuzuriha, A. Kunai, T. Tsukihara, H. Naitou, *Organometallics* **1992**, *11*, 597; M. Ishikawa, S. Matsuzawa, K. Hirotsu, S. Kamitori, T. Higuchi, *Organometallics* **1984**, *3*, 1930; A. G. Brook, A. Baumegger, A. J. Lough, *Organometallics* **1992**, *11*, 3088; M. Ishikawa, H. Sugisawa, H. Akitomo, K. Matsusaki, S. Kamitori, K. Hirotsu, T. Higuchi, *Organometallics* **1986**, *5*, 2447; M. J. Fink, D. B. Puranik, M. P. Johnson, *J. Am. Chem. Soc.* **1988**, *110*, 1315.
- [11] B. Teclé, W. H. Ilsley, J. P. Oliver, *Organometallics* **1982**, *1*, 875; S. Harder, J. Boersma, L. Brandsma, J. A. Kanters, *J. Organomet. Chem.* **1988**, *339*, 7; M. P. Bernstein, F. E. Romesberg, D. J. Fuller, A. T. Harrison, D. B. Collum, Q.-Y. Liu, P. G. Williard, *J. Am. Chem. Soc.* **1992**, *114*, 5100; M. A. Nichols, P. G. Williard, *J. Am. Chem. Soc.* **1993**, *115*, 1568; D. Hoffmann, A. Dorigo, P. von R. Schleyer, H. Reif, D. Stalke, G. M. Sheldrick, E. Weiss, M. Geissler, *Inorg. Chem.* **1995**, *34*, 262; H. Braunschweig, B. Gehrhus, P. B. Hitchcock, M. F. Lappert, *Z. Anorg. Allg. Chem.* **1995**, *621*, 1922.
- [12] See, for example, H. Sakurai, Y. Nakadaira, A. Hosomi, Y. Eriyama, C. Kabuto, *J. Am. Chem. Soc.* **1983**, *105*, 3359; R. Appel, C. Casser, F. Knoch, *Chem. Ber.* **1984**, *117*, 2693.
- [13] J. J. Mayerle, M. A. Flandera, *Acta Crystallogr. Sect. B* **1978**, *34*, 1374.
- [14] Y. Ito, T. Matsuura, S. Nishimura, M. Ishikawa, *Tetrahedron Lett.* **1986**, *27*, 3261.

Selective Vesicle Formation from Calixarenes by Self-Assembly**

Yasutaka Tanaka,* Masami Miyachi, and Yoshiaki Kobuke

All living systems are compartmentalized by vesicles, in which various membrane proteins including channel proteins are incorporated, and thus specific biological functions can be carried out. The characterization of the shape, size, and properties of vesicles formed from various amphiphiles, including some synthetic ones, is crucial not only for the study of the structure and function of model membranes,^[1] but also for the potential application of these membrane system as sensors and in technologies such as drug entrapment and release, and photochemical solar energy conversion.^[2] Previously we reported that a simple polyhydroxy macrocyclic amphiphile, calix[4]resorcarene (**1**), behaves as an artificial potassium ion channel when embedded in planar bilayers of



soybean lecithin.^[3] The cylindrical macrocycle formed by four benzene rings and four extended alkyl chains provides the channel pore for ion passage through the lipid bilayer.^[3] One would expect that amphiphiles such as **1** and calix[4]pyrogallolarene (**2**) would be aggregated in water and yield a specific self-assembled structure. Here we describe the selective formation of vesicles from the polyhydroxy macrocyclic amphiphiles **1** and **2**.^[4]

Injection of a solution of **1** or **2** (6.7 mM) in tetrahydrofuran (0.4–2.0 mL) into a buffer (HEPES–Tris 5 mM, 4 mL, pH 7.0; HEPES = 2-[4-(hydroxyethyl)piperazine-1-yl]ethanesulfonic acid, Tris = tris(hydroxymethyl)aminomethane) at 60 °C immediately gave a dispersion of amphiphiles.^[5] The dispersion was a slightly white suspension and remained in this form for more than a few months. Several characteristics of typical self-assembled structures have been observed for the dispersion obtained.

[*] Prof. Dr. Y. Tanaka

PRESTO Japan Science and Technology Corporation
and Department of Materials Science, Shizuoka University
Hamamatsu, Shizuoka 432-8561 (Japan)
Fax: (+81) 53-478-1199
E-mail: tcytana@ipch.shizuoka.ac.jp
M. Miyachi, Prof. Y. Kobuke
Shizuoka University (Japan)

[**] We are grateful to Dr. K. Nakazato (PRESTO, JST) for the TEM analyses and helpful discussions. We also thank Dr. M. Mehta, Prof. T. Fujinami, W. Tomoda, Prof. S. Kaneko, and Prof. H. Suzuki (Shizuoka University) for helpful discussions.

- 1) Negatively stained (1.5 % phosphotungstic acid, pH 7) and freeze-fracture replica micrographs revealed the formation of spherical and ellipsoidal particles. The diameters of the particles ranged from 50 to 200 nm for both **1** and **2** (Figure 1).^[6]

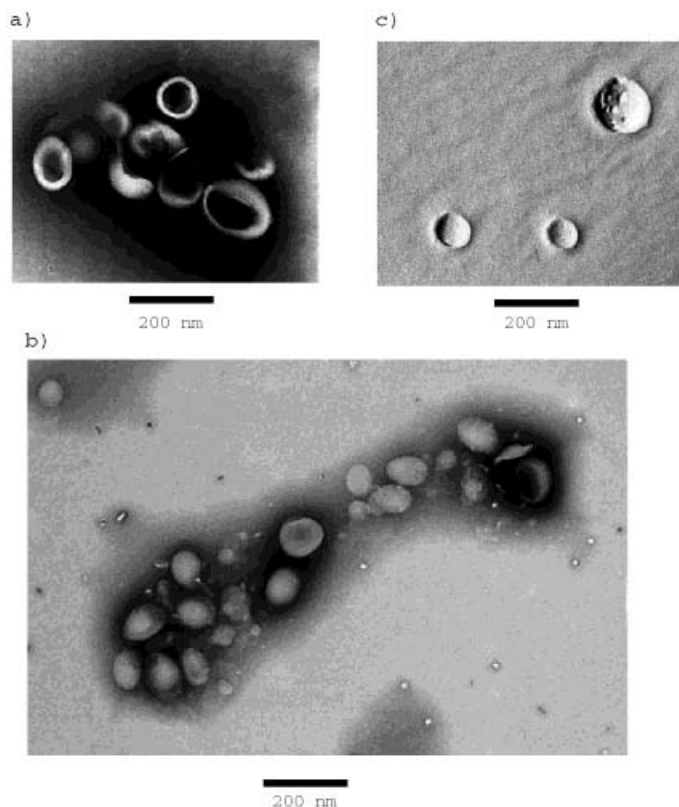


Figure 1. Transmission electron micrographs of vesicles formed from a) **1** and b) **2** (negative staining, magnification 40 000 times, 80 kV), and c) **2** (freeze-fracture replica, magnification 40 000 times, 100 kV).

- 2) Atomic force microscopy (AFM) images of the dispersion spread on a mica plate also indicated the presence of particles with diameters in the range of 40 to 250 nm (Figure 2).^[7, 8]

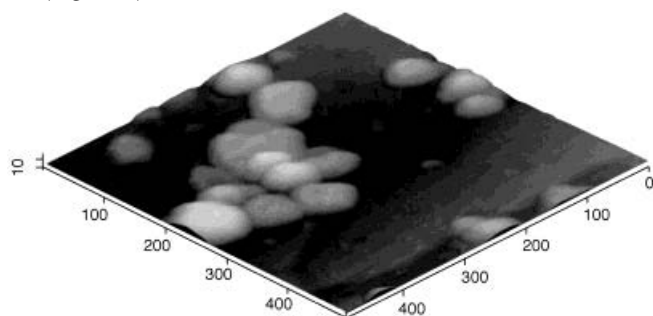


Figure 2. Atomic force micrograph of vesicles of **1** adsorbed on a mica plate. Scale in nm.

- 3) These particle sizes were also confirmed by dynamic light scattering experiments conducted with an Otsuka SELS-800Y instrument.

The size distribution is between 30 and 240 nm (4.0×10^{-4} M), and the maximum population of particles is at about 53 nm. These results indicate that the dispersion consists of

spherical and ellipsoidal vesicles with uniform diameters. Each of the vesicles consist of noncovalent self-assemblies of the macrocyclic amphiphiles. The vesicles obtained were deduced to be closed systems—a typical vesicular property—from dye encapsulation experiments.^[1, 9] Particles with the same size and shape as described above were observed after two weeks by transmission electron microscopy (TEM) and AFM, indicating the stability of vesicles formed in water over this time. In addition, no obvious change of morphology was observed after isolation of these vesicles, dehydration by drying under a high vacuum, and subsequent rehydration of the dried vesicles by addition of water.

Compounds **1** and **2** adopt the configuration in which the four alkyl chains are all-axial and all-*cis*.^[10] The fully extended alkyl chains on the macrocyclic moiety are about 2.6 nm in length, as estimated from space-filling models and by molecular simulation. When the vesicle solution was spread on a mica plate and dried in vacuo, AFM measurements indicated that the vesicle particles had a flattened shape with rounded edges and a slightly convex top surface. The average vertical cross-sectional thickness of more than ten particles formed from either **1** or **2** was about 10 nm. This was consistent with the thickness of two bilayers of **1** or **2** (Figure 3). Similar AFM measurements have been carried out

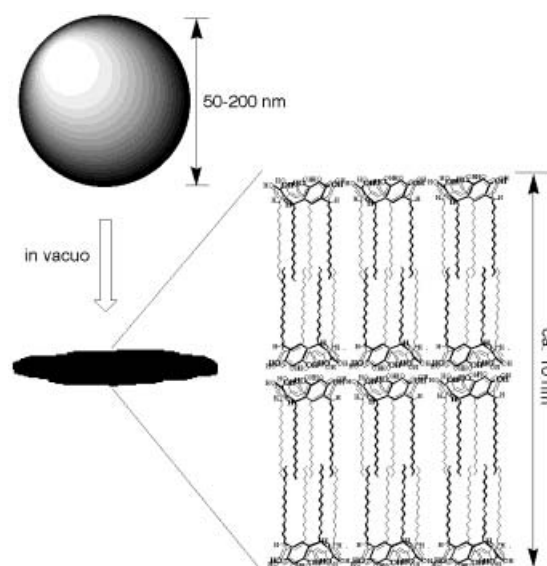


Figure 3. A hypothetical representation of the vesicle formed from **2** and its flattened image.

on unilamellar liposomes from phosphatidylcholine.^[11] The average observed thickness of approximately 9.5 nm for the liposome is in good agreement with that of two phosphatidylcholine bilayers, which has previously been reported.^[12] The bilayer structure was also confirmed by differential scanning calorimetry (DSC) measurements of the vesicle solution prepared from **1**.^[13] The endothermic peak (recorded when the sample temperature was rising) was observed at 65.1 °C, probably due to the gel-to-liquid-crystal phase transition, which is one of the fundamental characteristics of bilayer membranes.^[14] This suggests that the vesicles from **1** and **2** are composed of unilamellar membranes, in which the macrocyclic amphiphiles are aligned with their hydrophilic hydroxyl groups facing the aqueous phase.

Amphiphiles with different chemical structures and arrangement of hydrophilic and hydrophobic groups have been reported, and their structural features determine the morphological and functional properties of those self-assemblies formed in water.^[15] The formation of vesicles from mono-alkylphenol derivatives is in theory unexpected because of the conelike shape of the molecules and the high pK_a value of the OH groups. In fact, alkylresorcinol **3**, which has an alkyl chain as long as that in **1** and **2** but lacks a macrocyclic structure, forms micellelike aggregates under conditions identical to those described here. Aggregates of **3** with diameters less than 16 nm were confirmed by AFM.^[16] In contrast, owing to the macrocyclic structures of **1** and **2** composed of four alkylresorcinol and alkylpyrogallol moieties, respectively, the amphiphiles have a cylindrical shape, and thus vesicles are the preferred morphology of aggregates formed in water.

The FT-IR spectrum of the dehydrated vesicles of **1** shows the stretching band of the hydrogen-bonded OH groups (3500 cm^{-1}).^[17] A pair of hydroxyl groups on adjacent benzene rings form a hydrogen bond due to their proximity, which stabilizes the all-axial and all-*cis* configuration, and probably promotes the dissociation of one OH group in the pair at the experimental pH. This also suggests the existence of intermolecular OH \cdots O hydrogen bonds. This phenomenon along with the shape of the amphiphile and hydrogen bonds in **1** and **2** should help stabilize the vesicle structure. To the best of our knowledge this is the first example in which a phenolic surfactant self-assembles to furnish a vesicle.

We have shown that a macrocycle consisting of four phenolic amphiphiles and having a cylindrical molecular shape self-assembles selectively to form a vesicle. The intra- and intermolecular hydrogen bonds between OH groups on **1** and **2** play an essential role in stabilizing the assembled structure. This work, therefore, may open the way for the study of calixarenes in assembled form, in contrast to previous studies dealing mainly with their unimolecular function.

Received: November 24, 1997

Revised version: October 26, 1998 [Z11191IE]

German version: *Angew. Chem.* **1999**, *111*, 565–567

Keywords: calixarenes • hydrogen bonds • self-assembly • vesicles

- [1] a) J. H. Fendler, *Membrane Mimetic Chemistry*, Wiley, New York, **1982**; b) T. Kunitake, *Angew. Chem.* **1992**, *104*, 692; *Angew. Chem. Int. Ed. Engl.* **1992**, *31*, 709.
- [2] a) *Liposomes as Drug Carriers: Recent Trends and Progress*, (Ed.: G. Gregoriadis), Wiley, Chichester, **1988**; b) A. Kay, M. Grätzel, *J. Phys. Chem.* **1993**, *97*, 6272.
- [3] Y. Tanaka, Y. Kobuke, M. Sokabe, *Angew. Chem.* **1995**, *107*, 717; *Angew. Chem. Int. Ed. Engl.* **1995**, *34*, 693.
- [4] For the formation of vesicles from macrocyclic amphiphiles see: a) S. Arimoto, T. Nagasaki, S. Shinkai, *J. Chem. Soc. Perkin Trans. 2* **1995**, 679; b) P. Ghosh, T. Khan, P. K. Bharadwaj, *Chem. Commun.* **1996**, 189, and references therein. For the self-assembly of calix[4]resorcinarene in an organic solvent see: c) L. R. MacGillivray, J. L. Atwood, *Nature* **1997**, *389*, 469.
- [5] To remove the organic solvent the aqueous buffer was heated at 60°C . The spherical particles were also obtained by sonication of the buffer containing macrocyclic amphiphiles. Compound **2** was obtained as colorless crystals and the spectroscopic data (^1H and ^{13}C NMR, IR, and mass spectra) were consistent with the given structure. The

dodecaacetylated derivative of **2** was used to obtain a correct C,H,O analysis because of the extremely high hygroscopicity of unsubstituted **2**.

- [6] Electron micrographs were recorded on JEOL TEM-2000F and TEM-1010 instruments. The freeze-fracture replicas were fabricated with a JEOL JFD-9010 instrument.
- [7] For AFM measurements of vesicles and the determination of their shape, diameter, and thickness, and estimation of the number of membrane layers, see: S. Singh, D. J. Keller, *Biophys. J.* **1991**, *60*, 1401.
- [8] AFM images were recorded on an SPI-3700 instrument from Seiko Instruments Inc. operating in cyclic contact and noncontact modes using a silicon cantilever with force constants of 20 N m^{-1} and 3 N m^{-1} , respectively, under atmospheric conditions. These two operating modes provided almost the same images for an identical sample.
- [9] The vesicle solution ($2.5 \times 10^{-3}\text{ M}$, 4 mL) containing a fluorescent dye (sodium 8-amino-1,3,6-naphthalenetrisulfonate, 34.2 mg) was separated with Sephadex G-50 ($1\text{ cm} \times 20\text{ cm}$) using the buffer as the eluent. The vesicles were obtained in the 0.36–0.63 mL fraction, whereas the free dye was obtained after elution of 0.9 mL. The vesicle fraction fluoresced at 515 nm when irradiated at 370 nm.
- [10] a) Y. Aoyama, Y. Tanaka, S. Sugahara, *J. Am. Chem. Soc.* **1989**, *111*, 5397; b) Y. Tanaka, Y. Aoyama, *Bull. Chem. Soc. Jpn.* **1990**, *63*, 3343.
- [11] J. Sunamoto, K. Iwamoto, H. Kondo, *Biochem. Biophys. Res. Commun.* **1980**, *94*, 1367.
- [12] J. N. Israelachvili, *Intermolecular and Surface Forces*, 2nd ed., Academic Press, London, **1992**.
- [13] DSC was recorded on a Perkin Elmer Pyris 1 instrument. Measurements were repeated four times for the same sample with a heating cycle of 15 to 90°C . The reproducibility of the peak top temperature (T_c) was $\pm 0.5^\circ\text{C}$. After the sample had been cooled to -50°C it showed a higher T_c of 82.6°C .
- [14] Y. Okahata, R. Ando, T. Kunitake, *Ber. Bunsen-Ges. Phys. Chem.* **1981**, *85*, 789.
- [15] J. N. Israelachvili, D. J. Mitchell, B. W. Ninham, *J. Chem. Soc. Faraday Trans. 1* **1976**, *72*, 1525.
- [16] C. Huang, J. T. Mason, *Proc. Natl. Acad. Sci. USA* **1978**, *75*, 308.
- [17] For IR spectra of the dried vesicles and the contribution of hydrogen bonds towards the stabilization of the vesicle, see: T. Shimizu, M. Kogiso, M. Masuda, *Nature* **1996**, *383*, 487.

Adsorption of Acetone onto MgO: Experimental and Theoretical Evidence for the Presence of a Surface Enolate**

Javier F. Sanz,* Jaime Oviedo, Antonio Márquez, José Antonio Odriozola, and Mario Montes

Basic catalysts are widely used in heterogeneous catalytic processes either as supports or active components. Among these processes, aldol condensation of ketones is of out-

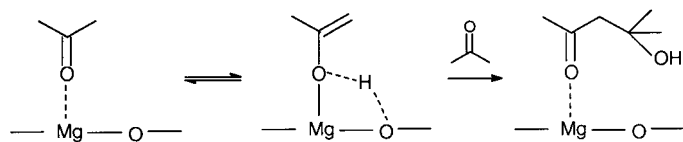
[*] Prof. Dr. J. F. Sanz, Dr. J. Oviedo, Prof. Dr. A. Márquez
Departamento de Química Física, Facultad de Química
Universidad de Sevilla
E-41012, Sevilla (Spain)
Fax: (+349) 954-557-174
E-mail: sanz@cica.es

Prof. Dr. J. A. Odriozola
Departamento de Química Inorgánica e Instituto de Ciencias de los Materiales de Sevilla
Universidad de Sevilla-CSIC (Spain)

Prof. Dr. M. Montes
Departamento de Química Aplicada, Facultad de Química
Universidad del País Vasco, San Sebastián (Spain)

[**] This work was supported by the DGICYT (Spain, project no. PB95-1247) and by the European Commission (contract no. ERBCT1-CT94-0064).

standing industrial interest. For example, aldol addition of acetone gives diacetone alcohol (DAA), which is used as a cellulose solvent and also as an intermediate in the synthesis of methyl isobutyl ketone, an important solvent in the chemical industry. From a mechanistic point of view, aldol additions are base-catalyzed reactions which occur through formation of an enolic species on a basic center of the MgO surface, which then adds to a C=O double bond to yield DAA (Scheme 1).



Scheme 1.

Although the catalytic activity of MgO is lower than other more basic solids, such as heavier alkaline earth oxides^[1] or aluminum phosphorous oxinitrides catalysts,^[2] its well-known structure makes it suitable for mechanistic studies.^[3] In fact, the acetone–MgO system has been the subject of several infrared and temperature-programmed desorption studies,^[4] and ^1H – ^2H exchange experiments have also been reported.^[5] Despite all this work, some aspects of the surface reaction still remain open. In particular, the ^1H – ^2H exchange studies suggested a slow formation of the C–C bond by reaction of the enolate species with acetone. However, no spectroscopic evidence for the presence of an enol species on the MgO surface has been reported. This could, in principle, be due to poor resolution of the earlier IR spectra, and we were prompted to revisit this system using a much more sophisticated tool based on diffuse reflectance Fourier transform techniques (DRIFT). Such a study was found to be of increased interest when a recent theoretical paper was taken into account.^[6] The effect of a MgO surface on the keto–enol equilibrium for acetone was shown to significantly decrease the energy difference between the keto and enol tautomers. Such a stabilization of the enol tautomer necessarily involves an increment of its surface concentration, which would account for the catalytic activity of the surface.

With the aim of investigating the presence of an enolic tautomer on the MgO surface, we undertook a DRIFT spectroscopic study of the acetone–MgO system. The most outstanding result is the appearance of a new band at 1640 cm^{-1} which could be assigned to an adsorbed enolic species. To support this interpretation, theoretical calculations of the vibrational frequencies for acetone and isopropenol chemisorbed on a MgO surface have been performed. These computations were carried out by means of second-order Möller–Plesset *ab initio* Hartree–Fock cluster-embedded calculations.

The DRIFT spectra were recorded with a Nicolet 510P spectrometer equipped with a high-temperature cell with a volume of about 1.5 cm^3 (Spectra-Tech) and ZnSe windows. MgO samples were outgassed *in situ* at 500°C under a flow of nitrogen. The spectrum of such a sample was taken as the reference for the later enhancement of the contribution of

adsorbed species. Nitrogen gas was bubbled through a saturator which contained acetone at 25°C ; this stream was then admitted into the DRIFT cell. In Figure 1 b, the spectrum

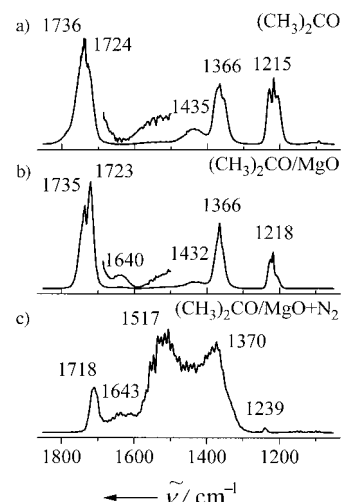


Figure 1. Experimental room-temperature DRIFT spectra. a) Acetone in the gas phase. b) MgO in contact with dry N_2 and acetone vapor. c) After outgassing in a dry N_2 flow. Intensities in arbitrary units.

of the adsorbed phase, recorded in a flow of acetone, is reported in the $800\text{--}2000\text{ cm}^{-1}$ region. For comparative purposes, the spectrum of gas-phase acetone recorded under the same conditions is reported in Figure 1 a. In this case, the intensity of the interferogram was ratioed to the signal which corresponded to an aluminum mirror. When these spectra are compared, they appear quite similar. In the acetone–MgO system, two bands are observed in the CO stretching region (1735 and 1723 cm^{-1}), in agreement with high-resolution spectra of ketones. These two peaks are generally explained by a Fermi resonance between the fundamental CO vibration and an overtone. The shift of these frequencies with respect to the gas-phase IR spectrum (1739 , 1724 cm^{-1}) is negligible and within the resolution of the instrument (4 cm^{-1}), which indicates weak physisorption of an electrostatic nature between the acetone molecule and the surface, in agreement with previous theoretical work.^[6] This band is followed by a small shoulder at 1640 cm^{-1} which is not present in the gas-phase spectrum of acetone and is clearly appreciable in the overlaid spectrum obtained after amplification by a factor of ten. The intense bands in the $1437\text{--}1365\text{ cm}^{-1}$ region correspond to symmetric and asymmetric bending vibrations of methyl groups, while the $1207\text{--}1225\text{ cm}^{-1}$ absorption bands are commonly assigned to C–C stretching vibrations. In summary, both spectra are similar, with the exception of the 1640 cm^{-1} band, whose presence suggests the formation of a new surface species. It should be noted that this band is observed in a relatively wide range of experimental conditions, from room temperature up to 140°C . At higher temperatures, new signals which correspond to addition products are observed.

A further point was to determine whether this band is due to a species directly adsorbed on the surface or if it is due to a species present in a possible multilayer. Therefore, acetone

was flushed out of the cell by a dry N_2 flow. Under these conditions, it is expected that only strongly adsorbed species will remain. As shown in Figure 1c, the spectrum is dominated by the strong absorption bands of carboxylate-like species^[7] which arise from the well-known oxidation reaction of acetone on metal oxide surfaces;^[8–10] the 1640 cm^{-1} band is still present, however. This band cannot be assigned to the water-bending mode since, firstly, the spectra are displayed with MgO under the same conditions as the reference. Secondly, inspection of the OH region of the spectrum shows that the band associated to hydrogen-bridged OH groups has a very low intensity and it is known that the intensity of the water-bending vibration is even less intense. Moreover, this band could be correlated with those observed in the FT-IR spectra of acetone adsorbed on vanadia-titania (1565 cm^{-1}) and Fe_2O_3 (1540 cm^{-1}) surfaces,^[8, 11] and which have been assigned to an enolate species because of their similarity to the band at 1582 cm^{-1} observed in a solution of the sodium salt of malonaldehyde in DMSO.^[12]

To attempt a more reliable assignment of this band, *ab initio* embedded-cluster calculations of the vibrational spectrum for both acetone and isopropanol adsorbed on a MgO (100) surface were undertaken. To model the surface, a $[MgO_5]^{8-}$ cluster embedded in an array of model potentials and point charges was chosen as described in reference [6]. For the Mg^{2+} cation, the basis set proposed by Huzinaga was used,^[13] enlarged with two s primitive functions to represent the 3s orbital; the contraction was (9s4p)/[4s2p]. For surface oxygen atoms, the basis set optimized for O^- was chosen, with the (9s5p)/[4s3p] contraction.^[14] The standard DZP basis set was used for the carbon, oxygen, and hydrogen atoms of the adsorbate. In the calculations, surface ions were fixed at their ideal crystallographic positions ($d(Mg-O) = 2.105\text{ Å}$ ^[15]), while the adsorbed acetone or isopropanol geometries were optimized at the MP2 level of theory.^[16] The equilibrium geometries are reported in Figure 2. As can be seen, acetone

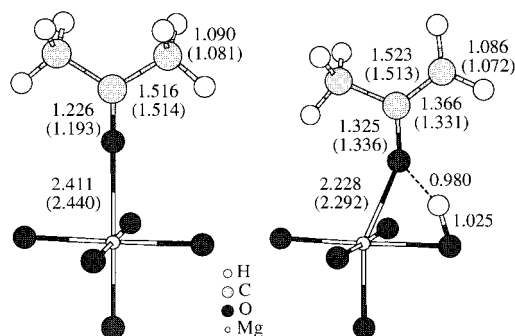


Figure 2. Selected optimized structural parameters for acetone (left) and isopropanol (right) adsorbed on a MgO (100) surface obtained from *ab initio* MP2 embedded-cluster calculations. Values in parentheses are those obtained at the Hartree–Fock level.

adsorbs with the carbonyl group perpendicular to the surface through interaction between a Mg^{2+} cation and the oxygen atom, with local C_{2v} symmetry. Isopropanol dissociates to give the corresponding enolate and a proton bound to a surface oxygen atom. It should be noted that at the HF level (values in parentheses), the preferred form is the enol instead of the

enolate, as previously mentioned,^[6] where the enolate was only found when the surface was allowed to relax.

Vibrational frequencies and intensities of infrared bands were then computed, and the results are summarized in Figure 3. The spectrum for the acetone–MgO system is

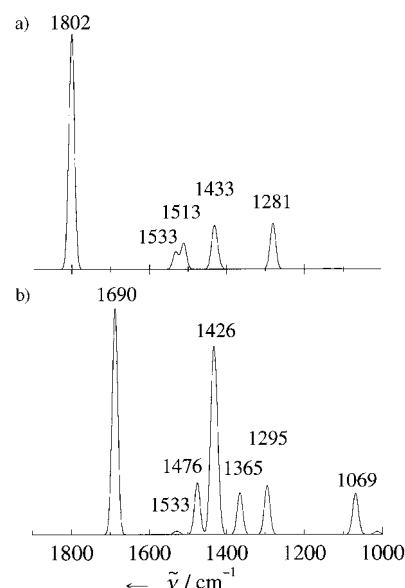


Figure 3. Theoretical IR spectra for a) acetone and b) enolate adsorbed on MgO obtained from *ab initio* MP2 embedded-cluster calculations. Intensities in arbitrary units.

reported in Figure 3a, and excellent agreement is found with the experimental spectrum, both in the shape and position of the bands. The theoretical frequencies appear to be somewhat higher, and the differences ($50\text{--}70\text{ cm}^{-1}$) agree with the shifts known for the harmonic approximation. Figure 3b shows the IR spectrum of the enolate–MgO system. The most outstanding feature of this spectrum is the band computed at 1690 cm^{-1} which, after the analysis of its associated normal coordinate, is unambiguously assigned to the asymmetric stretching vibration of the C–C–O group. The second most intense peak appears at 1426 cm^{-1} and corresponds to the symmetric stretching vibration mixed with some methyl bending, and, although its intensity is considerable, it would be buried by the bands of acetone and acetate present in this region of the experimental spectra. This frequency agrees with those observed at 1380 cm^{-1} in the acetone/vanadia-titania spectrum^[8] and 1374 cm^{-1} in the malonaldehyde sodium salt spectra.^[12]

In summary, the present work shows that acetone adsorption on MgO gives rise to a band at 1640 cm^{-1} in the DRIFT spectrum that, based on a careful theoretical analysis, is assigned to a surface enolate species. This assignment also confirms the proposed origin of the bands observed in the FT-IR spectra of acetone adsorbed on titanium and iron oxides at 1565 and 1540 cm^{-1} . The frequency shift of these bands with respect to the one reported here can be easily understood because, according to our models, the interaction between both acetone and enolate with the surface occurs through coordination of a surface metal center and the oxygen of the

adsorbed molecule. Because of the stronger Lewis character of Ti^{IV} and Fe^{III} centers, a larger adsorbate-surface interaction and, consequently, a weakening of the C–O and C–C–O bonds can be expected.^[17] Finally, the existence of such an enolate species seems to confirm that the acetone surface condensation reaction occurs through a standard aldol mechanism.

Received: July 1, 1998

Revised version: November 16, 1998 [Z12080IE]

German version: *Angew. Chem.* **1999**, *111*, 567–570

Keywords: ab initio calculations • enols • heterogeneous catalysis • IR spectroscopy • surface chemistry

- [1] G. Zhang, H. Hattori, K. Tanabe, *Appl. Catal.* **1988**, *36*, 189.
- [2] a) P. Grange, P. Bastians, R. Conacec, R. Marchand, Y. Laurent, L. Gandia, M. Montes, J. F. Sanz, J. A. Odriozola, *Stud. Surf. Sci. Catal.* **1995**, *91*, 381; b) R. Marchand, R. Conacec, Y. Laurent, P. Bastians, P. Grange, L. Gandia, M. Montes, J. F. Sanz, J. A. Odriozola (Université de Rennes 1, Université Catholique de Louvain, Universidad del Paris Vasco, Universidad de Sevilla, Cernix), FR-B 9401081 **1994**.
- [3] When MgO is used as the catalyst in a fixed-bed reactor at 1 atm and 200 °C, acetone condensation takes place with a conversion of around 4 %, with 85 % selectivity to mesityl oxide (4-methyl-3-penten-2-one) and 15 % to isomesityl oxide.
- [4] a) J. A. Lercher, H. Noller, G. Ritter, *J. Chem. Soc. Faraday Trans. 1* **1981**, *77*, 621; b) H. Miyata, Y. Toda, Y. Kubokawa, *J. Catal.* **1974**, *32*, 155.
- [5] G. Zhang, H. Hattori, K. Tanabe, *Appl. Catal.* **1988**, *36*, 183.
- [6] J. Oviedo, J. F. Sanz, *Surf. Sci.* **1998**, *397*, 23.
- [7] C. Xu, B. E. Koel, *J. Chem. Phys.* **1995**, *102*, 8158.
- [8] V. Sánchez Escribano, G. Busca, V. Lorenzelli, *J. Phys. Chem.* **1990**, *94*, 8939.
- [9] H. Knözinger, H. Kitenbrink, H. D. Müller, W. Schulz, *Proc. 6th ICC* (London, UK) **1976**, 183.
- [10] E. W. Thornton, P. G. Harrison, *J. Chem. Soc. Faraday Trans. 1* **1975**, *71*, 2468.
- [11] G. Busca, V. Lorenzelli, *J. Chem. Soc. Faraday Trans. 1* **1982**, *78*, 2911.
- [12] W. O. George, V. G. Mansell, *Spectrochim. Acta* **1968**, *24*, 145.
- [13] S. Huzinaga, *Gaussian Basis Sets for Molecular Calculations*, Physical Science Data 16, Elsevier, Amsterdam, **1984**.
- [14] J. Q. Broughton, P. S. Bagus, *Phys. Rev. B* **1984**, *30*, 4761; J. Q. Broughton, P. S. Bagus, *Phys. Rev. B* **1987**, *36*, 2813.
- [15] R. W. Wyckoff, *Crystal Structures*, Wiley, New York, **1963**.
- [16] M. Dupuis, S. Chin, A. Márquez in *Relativistic and Electron Correlation Effects in Molecules and Clusters* (Ed.: G. L. Malli), NATO ASI Series, Plenum Press, New York, **1992**.
- [17] J. Oviedo, C. J. Calzado, M. A. San Miguel, A. Márquez, J. F. Sanz, *J. Mol. Struct. (Theochem.)* **1997**, *390*, 177.

Chemo-Enzymatic Synthesis of Fluorescent Rab 7 Proteins: Tools to Study Vesicular Trafficking in Cells**

David J. Owen, Kirill Alexandrov, Elena Rostkova, Axel J. Scheidig, Roger S. Goody,* and Herbert Waldmann*

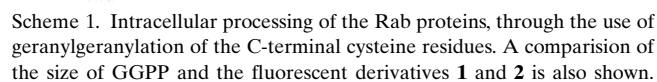
Proteins that are S-farnesylated and S-geranylgeranylated at C-terminal cysteine residues play critical roles in cell processes such as signal transduction and intracellular trafficking.^[1–3] Although our understanding of the biological consequences of protein prenylation has increased significantly over the last few years, there is still relatively little known about the molecular details that govern its functional role, for instance in vesicular trafficking. A particularly relevant example is the role of the Rab proteins in intracellular membrane trafficking. The Rab proteins are a group of small G-proteins that associate with specific membrane components. They are believed to control the events of docking and fusion of intracellular vesicles.^[4] Rab proteins are subjected to geranylgeranylation through a process that involves Rab geranylgeranyltransferase (RabGGTase) and an accessory protein termed a Rab escort protein (REP). Thus, in order to undergo prenylation, a newly synthesized Rab protein must bind and form a stable complex with REP, which only then (in contrast to other known prenyltransferases) is recognized by RabGGTase.^[5, 6] Upon prenylation the Rab protein remains bound to REP and accompanies it to the corresponding membrane.^[7] Subsequent REP-mediated membrane insertion of prenylated Rab proteins is believed to proceed through a putative membrane receptor. The free REP protein is then released and can support another round of Rab prenylation.

Unfortunately, very little is known about the molecular details of this general scenario. Major questions such as whether the lipid groups participate in protein–protein recognition, or the exact mechanism by which the lipidated Rab/REP complex is directed to specific intracellular compartments remain unanswered. Furthermore, despite a number of related reports, the exact affinities of RabGGTase for its lipid substrate are unknown, and the reaction mechanism of the prenylation reaction is also unelucidated. Specific fluorescent probes should enable the dissection of the reaction mechanism through the use of fluorescent spectroscopy. Such probes would allow real-time imaging of the

[*] Prof. Dr. R. S. Goody, Dr. K. Alexandrov, M.Sc. E. Rostkova, Dr. A. S. Scheidig
Abteilung Physikalische Biochemie
Max-Planck-Institut für Molekulare Physiologie
Rheinlanddamm 201, D-44139 Dortmund (Germany)
Prof. Dr. H. Waldmann, Dr. D. J. Owen
Institut für Organische Chemie der Universität
Richard-Willstätter-Allee 2, D-76128 Karlsruhe (Germany)
Fax: (+49) 721-608-4825
E-mail: waldmann@ochhades.chemie.uni-karlsruhe.de

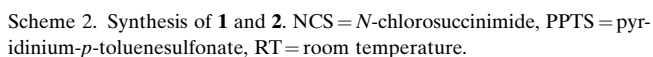
[**] This research was supported by the Deutsche Forschungsgemeinschaft and the Fonds der Chemischen Industrie. D.J.O. gratefully acknowledges financial support from the Alexander von Humboldt Foundation in the form of a postdoctoral fellowship.

Here we describe the synthesis of two *N*-methylantraniloylisoprenoid diphosphate derivatives, compounds **1** and **2** (Scheme 1). These compounds bind to RabGGTase and are

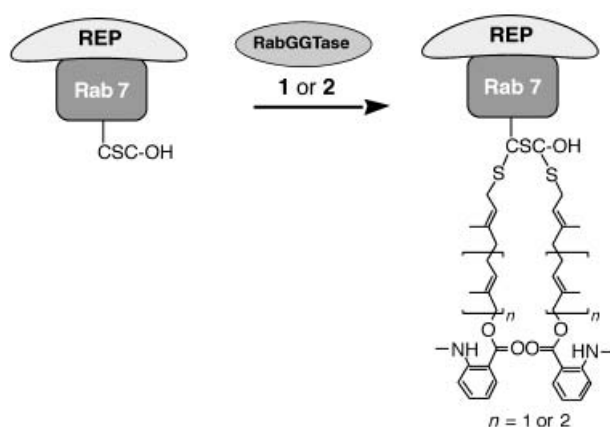


510

© WILEY-VCH Verlag GmbH, D-69451 Weinheim, 1999



Analysis of the excitation/emission spectra of both compounds revealed that, as expected from the type of reporter group used, the fluorescence had the excitation maximum at 340 nm and an emission at 450 nm. Subsequently performed kinetic experiments showed that both diphosphates **1** and **2** bind to RabGGTase, with **2** binding better than **1**.^[17] The affinity difference between both compounds was consistent with the size difference, as compound **2** has essentially the same length as geranylgeranyl diphosphate (GGPP), while **1** is closer in length to farnesyl diphosphate (FPP; Scheme 1). To determine if both derivatives could substitute for GGPP in the enzymatic protein prenylation we investigated if the fluorescent derivatives could be transferred enzymatically to a Rab protein by RabGGTase (Scheme 3).^[18] Rab 7, a protein that controls the biogenesis of late endosomes, was chosen as a substrate.^[19] To rule out the possibility of unspecific



Scheme 3. Enzymatic transfer of **1** and **2** onto Rab 7 by RabGGTase and REP-1.

incorporation of the analogues we performed control reactions without REP-1, as it had previously been demonstrated that REP-1 is essential for catalytic activity of RabGGTase.^[6, 20] As an additional control the reactions were supplemented with GGPP as a competitive substrate. After an incubation period the proteins were precipitated with trichloroacetic acid, washed with acetone to remove the excess of free lipid, and finally separated on a SDS-PAGE gel. Fluorescently labeled proteins could be visualized by excitation of the *N*-methylanthraniloyl group at 340 nm by a fluorescence scanner. As shown on Figure 1 there was an easily detectable

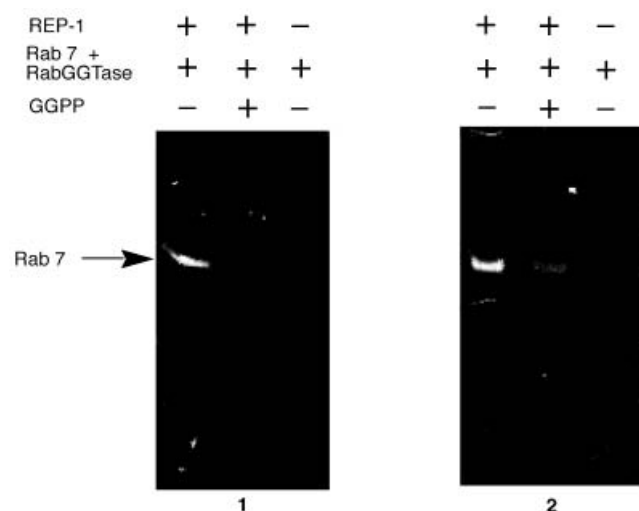


Figure 1. Results of the SDS-PAGE gel of the fluorescently labeled Rab 7 protein after prenylation with the fluorescent lipid derivatives **1** and **2**, plus control reactions.

fluorescent band of about 26 kDa. Coomassie staining of the gel confirmed that fluorescence was localized with the Rab 7 band (data not shown). There was no detectable fluorescence in the samples that lacked REP-1. Finally, fluorescence of the control reactions supplemented with GGPP was suppressed, either by more than 70% in the case of **2**, or to an undetectable level in the case of **1**. The observed inhibition is consistent with the difference in binding affinities of RabGGTase for compounds **1** and **2**. In the absence of the competing GGPP there was, however, no observable differ-

ence in prenylation efficiency with both analogues. This suggests that both compounds were transferred efficiently at the chosen concentrations.

In conclusion, we have synthesized two novel fluorescent derivatives of geranylgeranyl diphosphate. These compounds could be efficiently attached to the vesicular trafficking protein Rab 7 through an enzymatic transfer reaction that requires both RabGGTase and REP-1. It is believed that **1** and **2** should pave the way to the elucidation of the functional mechanism of RabGGTase. Moreover, the fluorescent Rab 7 proteins can now be utilized for in-vivo studies on vesicular trafficking processes. However, the interaction of fluorescent Rab 7 with lipid bilayers remains to be tested to determine if the introduction of a hydrophilic ester has any effect on the overall binding affinity.

Received: July 13, 1998 [Z12129IE]

German version: *Angew. Chem.* **1999**, *111*, 570–573

Keywords: enzyme catalysis • fluorescence spectroscopy • isoprenoids • lipoproteins • signal transduction

- [1] K. Hinterding, D. Alonso-Diaz, H. Waldmann, *Angew. Chem.* **1998**, *110*, 716–780; *Angew. Chem. Int. Ed.* **1998**, *37*, 688.
- [2] F. L. Zhang, P. J. Casey, *Annu. Rev. Biochem.* **1996**, *65*, 241.
- [3] P. J. Casey, *Science* **1995**, *268*, 221.
- [4] P. Novick, M. Zerial, *Curr. Opin. Cell Biol.* **1997**, *9*, 496.
- [5] D. A. Andres, M. C. Seabra, M. S. Brown, S. A. Armstrong, T. E. Smeland, F. P. M. Cremmers, J. L. Goldstein, *Cell* **1993**, *73*, 1091.
- [6] S. Araki, K. Kaibuchi, T. Sasaki, Y. Hata, Y. Takai, *Mol. Cell Biol.* **1991**, *11*, 1438.
- [7] K. Alexandrov, H. Horiuchi, O. Steele-Mortimer, M. C. Seabra, M. Zerial, *EMBO J.* **1994**, *13*, 5262.
- [8] Previous studies of the interaction of prenyltransferases with their lipid substrate have been conducted primarily with radiolabeled phosphoisoprenoids or by using the change in the fluorescence of endogenous tryptophane upon substrate binding. See a) M. C. Seabra, M. S. Brown, C. A. Slaughter, T. C. Sudhof, J. L. Goldstein, *Cell* **1992**, *70*, 1049; b) F. Beranger, K. Cadwallader, E. Porifi, S. Powers, T. Evans, J. de Gunzburg, J. F. Hancock, *J. Biol. Chem.* **1994**, *269*, 13637.
- [9] a) T. C. Turek, I. Gaon, D. Gamache, M. D. Distefano, *Bioorg. Med. Chem. Lett.* **1997**, *7*, 2125–2130; b) I. Gaon, T. C. Turek, V. A. Weller, R. L. Edelstein, S. K. Singh, M. D. Distefano *J. Org. Chem.* **1996**, *61*, 7738.
- [10] M. A. Umbriet, K. B. Sharpless, *J. Am. Chem. Soc.* **1977**, *99*, 5526.
- [11] a) M. C. Venuti, *Synthesis* **1982**, 266; b) for reviews on isatoic anhydrides, see G. M. Coppola *Synthesis* **1980**, 505.
- [12] E. J. Corey, C. V. Kim, M. Taheeda, *Tetrahedron Lett.* **1972**, *28*, 4339.
- [13] V. J. Davisson, A. B. Woodside, T. R. Neal, K. E. Stremler, M. Muehlbacher, C. D. Poulter *J. Org. Chem.* **1986**, *51*, 4768.
- [14] Diphosphate **1** was obtained as a pure white powder, and was stored at -78°C until required: Characteristic data: $R_f=0.8$ (*i*PrOH/25 mM NH_4HCO_3 1:3 on RP18 silica gel); UV (H_2O): λ_{max} (ϵ) 220 (27076), 251 (7971), 355 nm (4817); ^1H NMR (500 MHz, D_2O): $\delta=7.67$ (m, 1H), 7.22 (m, 1H), 6.44–6.57 (m, 2H), 5.26–5.35 (m, 2H), 4.45 (s, 1H), 4.41 (s, 1H), 4.29 (t, $J=6.3$ Hz, 2H), 2.67, 2.63 (2s, 3H), 1.87–2.04 (m, 4H), 1.53, 1.49 (2s, 3H), 1.52 (s, 3H), NH signal was not observed; HR-MS (FAB) calcd for $\text{C}_{18}\text{H}_{28}\text{NO}_9\text{P}_2$ [$M+1$] $^+$: 464.1239; found: 464.1294.
- [15] Diphosphate **2** was obtained as a white powder, and was stored at -78°C until required: Characteristic data: $R_f=0.5$ (*i*PrOH/25 mM NH_4HCO_3 1:3, on RP18 silica gel); UV (H_2O): λ_{max} (ϵ) 194 (32498), 220 (23235), 253 (7340), 353 nm (5236); ^1H NMR (500 MHz, D_2O): $\delta=7.58$ (brd, $J=7.7$ Hz, 1H), 6.96 (m, 1H), 6.19–6.26 (m, 1H), 5.14–5.24 (m, 2H), 4.78 (brs, 1H), 4.25–4.36 (m, 4H), 2.45 (m, 3H), 1.67–1.80 (m, 8H), 1.45 (s, 3H), 1.34 (s, 3H), 1.25 (s, 3H), NH signal was not observed; HR-MS (FAB) calcd for $\text{C}_{23}\text{H}_{36}\text{NO}_9\text{P}_2$ [$M+1$] $^+$: 532.1865; found: 532.1930.

- [16] It is interesting to note that a doubling of the signals in both the ^1H and ^{13}C spectra was observed in the NMR spectra of the diphosphate compounds. This result was found to be concentration and substrate dependent, and is thought to reflect slow rotation about the vinyl-ogous carbamate bonds. The doubling of signals was especially prevalent in the farnesyl derivative **2**, and was observed, although to a less degree (ca. 10–15%), in the intermediates that lead up to the farnesyl diphosphate derivative (**5b** and **6b**). The doubling of the NMR signals however, was not observed for the geranyl intermediates (**5a** and **6a**).
- [17] K. Alexandrov, E. Rostkova, A. J. Scheidig, R. S. Goody, D. Owen, H. Waldmann, unpublished results.
- [18] Standard prenylation assay: 50 μL of the assay contained: 120 pmol Rab 7, 120 pmol REP-1, 120 pmol RabGGTase, and 2.4 nmol of either **1** or **2**. Buffer: 20 mM Hepes pH 7.2, 20 mM NaCl, 5 mM 2-sulfany-ethanol (BME), 1 mM NP-40. The mixture was incubated at 37 °C for 20 minutes and the reaction stopped by diluting the samples with cold H_2O and precipitating the protein with 10% trichloroacetic acid. The protein pellet was washed with cold acetone and re-suspended in SDS-PAGE loading buffer. Proteins were resolved on the 15% SDS-PAGE gel and the prenylated proteins were visualized with a Fluor 100 (BioRad) fluorescence scanner.
- [19] I. Simon, M. Zerial, R. S. Goody, *J. Biol. Chem.* **1996**, *271*, 20470.
- [20] F. Shen, M. C. Seabra, *J. Biol. Chem.* **1996**, *271*, 3692.
- [21] For the expression and purification of REP-1, see K. Alexandrov, I. Simon, A. Iakovenko, B. Holz, R. S. Goody, A. Scheidig *FEBS Lett.* **1998**, *425*, 460. RabGGTase baculoviral expression vectors pVL-RabGGTalpha and pVL-RabGGTbeta were obtained from the American Type Culture Collection (order numbers 87154 and 87155, respectively). Baculoviruses were generated and RabGGTase was expressed and purified as described previously: F. P. Cremers, S. A. Armstrong, M. C. Seabra, M. C. Brown, J. L. Goldstein *J. Biol. Chem.* **1994**, *269*, 2111.

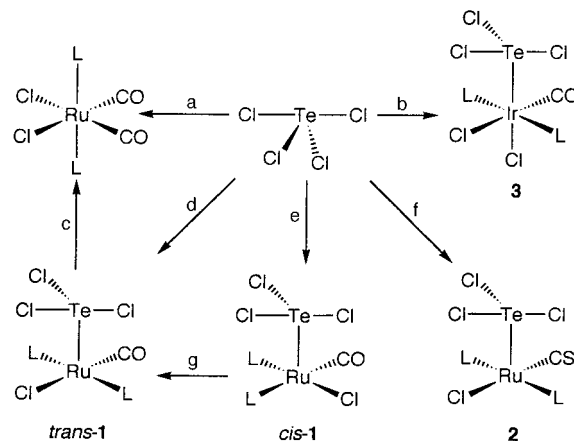
Tetravalent Tellurium Ligands

Paul J. Dyson, Anthony F. Hill,* Alexander G. Hulkes, Andrew J. P. White, and David J. Williams

The comparatively sparse chemistry of tellurium-donor ligands typically involves the chalcogen being formally in the divalent state, that is, telluroethers and tellurolates. In recent times, a substantial group of compounds involving “naked” (i.e., substituent-free) tellurium has emerged,^[1] heralded by the unsurpassed elegance of the complex $[\text{Te}\{\text{Mn}(\text{CO})_2(\eta\text{-C}_5\text{H}_5)\}_3]$ discovered by Herberhold et. al.^[2] Clearly, oxidation states are however of limited use in describing such compounds. Well-defined ligands based on dative tellurium in higher oxidation states are however unknown, although Whitmire and Eveland have recently reported the Zintl cluster $[\text{Fe}_2(\text{CO})_6(\eta^2\text{-}\mu_2\text{-Te}_4)(\mu\text{-TeCl}_2)]$, wherein the “ TeCl_2 ” bridge might be described as based on either di- or tetravalent tellurium.^[3] Tetravalent sulfur ligands are of course well known in the form of sulfoxides, sulfur dioxide,

sulfines, sulfur diimides, and iminoxosulfuranes,^[4] however such compounds based on tellurium are either transient or oligomeric in nature. Complexes of the SF_3 and $\text{Se}(\text{=O})\text{Cl}$ ligands have been previously reported from the oxidative addition of SF_4 or O=SeCl_2 to $[\text{IrCl}(\text{CO})(\text{PET}_3)_2]$ ^[5] or $[\text{IrCl}(\text{CO})(\text{PPh}_3)_2]$,^[6] respectively. A Lewis base adduct of TeCl_4 with the pentacarbonyl manganate anion has also been described very recently.^[5b] Herein we report the first mononuclear transition metal complexes ligated by the tetravalent trichlorotellurium group. These result from the reactions of $[\text{IrCl}(\text{CO})(\text{PPh}_3)_2]$ or $[\text{Ru}(\text{CH=CH}_2)\text{Cl}(\text{CA})(\text{PPh}_3)_2]$ ($\text{A} = \text{O}, \text{S}$) with tellurium tetrachloride.

We encountered the first trichlorotellurium ligand in the product of the reaction of $[\text{Ru}(\text{CH=CH}_2)\text{Cl}(\text{CO})(\text{PPh}_3)_2]$ ^[7] with TeCl_4 . In addition to polyvinylchloride, a bright yellow complex formulated as $[\text{Ru}(\text{TeCl}_3)\text{Cl}(\text{CO})(\text{PPh}_3)_2]$ (**1**) is obtained in 37% yield after recrystallization (Scheme 1). If the preparation is carried out at room temperature a 1:1 mixture of *cis*/*trans*-bis(phosphane) isomers results; however, at 50 °C the *trans*-bis(phosphane) arrangement is formed exclusively. The same reaction with $[\text{Ru}(\text{CH=CH}_2)\text{Cl}(\text{CS})(\text{PPh}_3)_2]$ however provides only the isomer of $[\text{RuCl}(\text{TeCl}_3)(\text{CS})(\text{PPh}_3)_2]$ (**2**) with *trans*-coordinated phosphanes. It is noteworthy that whilst the TeCl_3 ligand in **1** rotates freely at room temperature (singlet ^{31}P resonance), an apparently static structure is adopted for **2** ($^{31}\text{P}_\text{A}$, $^{31}\text{P}_\text{B}$ system, *trans*- $J(\text{AB}) = 335$ Hz). This is consistent with the enhancement of a (presumably weak) π -dative component to the Te–Ru interaction to the more π -acidic but isosteric ruthenium center in **2**. The subsequent chemistry of complexes **1** and **2** has so far proven disappointing in that all attempts to introduce phosphanes, isocyanides, or even CO(!) as a sixth ligand (and thereby coordinative saturation) at ruthenium resulted in deposition of elemental tellurium. Similar deposition of tellurium occurs on treatment with amines or alcohols.



Scheme 1. Reagents and conditions (25 °C unless otherwise indicated, L = PPh_3): a) $[\text{Ru}(\text{CO})_2\text{L}_3]$, C_6H_6 ; b) $[\text{IrCl}(\text{CO})\text{L}_2]$, THF; c) CO, CH_2Cl_2 ; d) $[\text{Ru}(\text{CH=CH}_2)\text{Cl}(\text{CO})(\text{PPh}_3)_2]$, C_6H_6 , 50 °C; e) $[\text{Ru}(\text{CH=CH}_2)\text{Cl}(\text{CO})(\text{PPh}_3)_2]$, C_6H_6 ; f) $[\text{Ru}(\text{CH=CH}_2)\text{Cl}(\text{CS})(\text{PPh}_3)_2]$, C_6H_6 ; g) CDCl_3 , seven days.

This apparent lack of synthetic utility, coupled with our failure to obtain crystallographic grade crystals of **1** or **2**, led us to explore alternative examples of this ligand. As noted above, the complexes $[\text{IrCl}(\text{CO})(\text{PR}_3)_2]$ ($\text{R} = \text{Et}, \text{Ph}$) oxida-

[*] Dr. A. F. Hill, Dr. P. J. Dyson, A. G. Hulkes, Dr. A. J. P. White, Prof. D. J. Williams
Department of Chemistry
Imperial College of Science, Technology and Medicine
South Kensington, London SW7 2AY (UK)
Fax: (+44) 171-5945804
E-mail: a.hill@ic.ac.uk

tively add tetravalent halides of sulfur and selenium. Accordingly the reaction of Vaska's complex with TeCl_4 was investigated: one major product $[\text{IrCl}_2(\text{TeCl}_3)(\text{CO})(\text{PPh}_3)_2]$ (**3**) can be isolated (52%), in addition to small amounts of $[\text{IrCl}_3(\text{CO})(\text{PPh}_3)_2]$ and $[\text{IrHCl}_2(\text{CO})(\text{PPh}_3)_2]$. The formulation of the orange compound follows from spectroscopic data (see Experimental Section) and was confirmed by a crystallographic study (Figure 1).^[8] The geometry at the iridium center

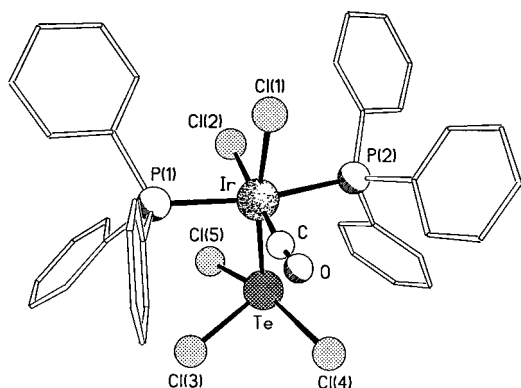


Figure 1. Molecular Structure of **3**. Phenyl groups simplified for clarity.

is essentially octahedral with *cis* interligand angles in the range 82.5(5)–100.70(8)°. The geometry of the “ $\text{IrCl}_2(\text{CO})(\text{PPh}_3)_2$ ” unit is generally unremarkable other than to note that the two *cis* Ir–Cl bond lengths (Ir–Cl(1) 2.414(3), Ir–Cl(2) 2.372(3) Å) reflect a lesser *trans* influence for the carbonyl than the trichlorotelluronium ligand (14σ). The ligand of interest is the “ TeCl_3 ” group and it is reassuring that the geometry at tellurium is entirely as expected based on VSEPR considerations. Thus a virtual trigonal bipyramid is apparent with the two bulkiest substituents (iridium and a lone pair of electrons) occupying equatorial sites; the two “axial” chlorides (Te–Cl(4) 2.609(6), Te–Cl(5) 2.429(6) Å)^[9] are folded away from the iridium center (Cl(4)–Te–Cl(5) 163.1(2)°). The “equatorial” Te–Cl(3) bond length at 2.322(4) Å is substantially shorter than those to the axial chlorides. The plane containing Ir, P(1), P(2), and Te is steeply inclined (73°) to that defined by Ir, Te, Cl(4), and Cl(5). If any substantial π -component contributed to the Ir–Te interaction, a value of 0 or 90° might be expected. The iridium–tellurium bond length of 2.656(1) Å is significantly longer (41σ) than that found in the only other structurally characterized mononuclear complex containing an Ir–Te bond, $[\text{Ir}(\text{Te}-2,4,6\text{-}t\text{Bu}_3\text{C}_6\text{H}_2)(\text{CO})(\text{PPh}_3)_2]$ (2.615(1) Å).^[10]

Although the TeCl_3 ligand is unprecedented in transition metal chemistry, the structural features of **3** are entirely as expected. This begs the question of generality for the synthetic approach. Preliminary studies do not however bode well. In the other low-valent systems so far investigated, TeCl_4 serves ultimately as a mild chlorinating agent rather than simply as an electrophile: $[\text{Fe}(\text{CO})_5]$ and $[\text{Fe}(\text{CO})_3(\text{PPh}_3)_2]$ react with TeCl_4 to cleanly provide (albeit conveniently) $[\text{FeCl}_2(\text{CO})_4]$ and *cis,cis,trans*- $[\text{FeCl}_2(\text{CO})_2(\text{PPh}_3)_2]$. The quantitative reaction of $[\text{Ru}(\text{CO})_2(\text{PPh}_3)_3]$ with TeCl_4 is solvent dependent: in benzene, the product *cis,cis,trans*- $[\text{RuCl}_2$ -

$(\text{CO})_2(\text{PPh}_3)_2]$ is obtained, whilst in THF the all-*trans* isomer is obtained. It seems reasonable that these reactions fail to provide trichlorotelluronium complexes because in each case one or more ligands can be liberated, which, as shown in the case of **1**, are capable of reducing the intermediate tetravalent tellurium species. This problem is clearly obviated in the case of **3**.

Experimental Section

trans-1: $[\text{Ru}(\text{CH}=\text{CH}_2\text{Cl})(\text{CO})(\text{PPh}_3)_2]$ (0.25 g, 0.35 mmol) was added to a solution of TeCl_4 (0.10 g, 0.37 mmol) in benzene (35 mL) which was held at 50°C. The resulting yellow solution was stirred for 15 min, filtered, concentrated to 10 mL, and the crude product isolated by precipitation with diethyl ether (30 mL). The precipitate was recrystallised three times from a mixture of dichloromethane and diethyl ether. Yield 0.12 g (37%). IR (CH_2Cl_2): $\tilde{\nu}$ = 1972 cm^{-1} (CO); (Nujol): $\tilde{\nu}$ = 1972 (CO), 333, 302 cm^{-1} (TeCl/RuCl); ^{31}P NMR (CDCl_3 , 25°C): δ = 27.4; FAB-MS: m/z : 1411 $[\text{Ru}_2\text{Cl}_3(\text{CO})_2(\text{PPh}_3)_4]^+$, 1185 $[\text{M}+\text{PPh}_3]^+$, 717 $[\text{M}-\text{TeCl}_3+\text{CO}]^+$, 689 $[\text{M}-\text{TeCl}_3]^+$; m.p. 174–176°C (decomp); elemental analysis calcd for $\text{C}_{37}\text{H}_{30}\text{Cl}_4\text{OP}_2\text{RuTe}$ (%): C 48.1, H 3.3%; found: C 48.5, H 3.3.

cis-1 (spectroscopically observed when the above procedure was carried out at room temperature) IR Nujol: $\tilde{\nu}$ = 1961 $[\tilde{\nu}(\text{CO})]$ cm^{-1} ; ^{31}P NMR (CDCl_3 , 25°C): δ = 30.4, 45.9 (AB, $J(\text{AB})$ = 19.7 Hz). The *cis* isomer converts to the *trans* isomer slowly on standing in solution.

3: $[\text{IrCl}(\text{CO})(\text{PPh}_3)_2]$ (0.20 g, 0.26 mmol) in THF (15 mL) was treated with TeCl_4 (0.070 g, 0.26 mmol). The resulting orange/yellow solution was stirred for 25 min and then diluted with diethyl ether (20 cm^3). The filtered solution was then further diluted with hexane (10 mL) and then concentrated under reduced pressure to provide yellow crystals of the bis(thf) solvate. Yield 0.16 g (52%). IR (Nujol): $\tilde{\nu}$ = 2090 (CO), 345, 297, 271 cm^{-1} (TeCl/IrCl); ^{31}P NMR (CDCl_3 , 25°C): δ = –20.5; FAB-MS (3-nitrobenzyl alcohol (nba) matrix): m/z : 1246 $[\text{M}+2\text{nba}-3\text{HCl}]^+$, 815 $[\text{M}-\text{TeCl}_3]^+$, 787 $[\text{M}-\text{PPh}_3]^+$, 780 $[\text{M}-\text{TeCl}_3]^+$, 752 $[\text{M}-\text{PPh}_3-\text{HCl}]^+$, 715 $[\text{M}-\text{PPh}_3-2\text{HCl}]^+$; elemental analysis calcd for $\text{C}_{37}\text{H}_{30}\text{Cl}_3\text{IrOP}_2\text{Te} \cdot 2\text{C}_4\text{H}_8\text{O}$ (%): C 45.3, H 3.88; found: C 45.70, H 4.00. The complex was also characterised crystallographically.^[8]

Received: July 22, 1998

Revised version: November 12, 1998 [Z 12194 IE]

German version: *Angew. Chem.* **1999**, *111*, 573–575

Keywords: iridium • oxidative addition • tellurium

- a) K. H. Whitmire, *Adv. Organomet. Chem.* **1998**, *42*, 1; b) P. Mathur, *Adv. Organomet. Chem.* **1997**, *41*, 243; c) W. A. Herrmann, *Angew. Chem.* **1986**, *98*, 57; *Angew. Chem. Int. Ed. Engl.* **1986**, *25*, 56.
- M. Herberhold, D. Reiner, D. Neuge, *Angew. Chem.* **1983**, *95*, 46; *Angew. Chem. Int. Ed. Engl.* **1983**, *22*, 59; *Angew. Chem. Suppl.* **1983**, 10.
- J. R. Eveland, K. H. Whitmire, *Angew. Chem.* **1996**, *95*, 736; *Angew. Chem. Int. Ed. Engl.* **1996**, *35*, 741.
- A. F. Hill, *Adv. Organomet. Chem.* **1994**, *36*, 159.
- a) R. W. Cockman, E. A. V. Ebsworth, J. H. Holloway, *J. Am. Chem. Soc.* **1987**, *109*, 2194. A preliminary report has suggested on the basis of ^{19}F and ^{31}P NMR data that the reaction of $[\text{RhCl}(\text{CO})(\text{PEt}_3)_2]$ with TeF_4 provides $[\text{RhCl}(\text{TeF}_3)(\text{CO})(\text{PEt}_3)_2][\text{TeF}_5]$: E. A. V. Ebsworth, J. H. Holloway, P. G. Watson, *J. Chem. Soc. Chem. Commun.* **1991**, 1443; b) W. F. Liaw, S. J. Chiou, G. H. Lee, S. M. Peng, *Inorg. Chem.* **1998**, *37*, 1131.
- J. Cartwright, A. F. Hill, *Polyhedron* **1995**, *15*, 157.
- J. C. Cannadine, A. F. Hill, A. J. P. White, D. J. Williams, J. D. E. T. Wilton-Ely, *Organometallics* **1996**, *15*, 5409.
- Crystal data for **3**: $\text{C}_{37}\text{H}_{30}\text{Cl}_3\text{IrOP}_2\text{Te} \cdot \text{C}_4\text{H}_8\text{O}$, M_r = 1121.7, triclinic, space group $P\bar{1}$ (no. 2), a = 12.345(1), b = 12.820(1), c = 15.147(2) Å, α = 95.62(1)°, β = 96.18(1)°, γ = 99.76(1)°, V = 2332.1(4) Å³, Z = 2, ρ_{calcd} = 1.60 g cm^{-3} , $\mu(\text{CuK}\alpha)$ = 139 cm^{-1} , $F(000)$ = 1088. A yellow prism

of dimensions $0.28 \times 0.13 \times 0.07$ mm was used. A total of 6403 independent reflections were measured on a Siemens P4/PC diffractometer with graphite-monochromated $\text{Cu}_{K\alpha}$ radiation using ω scans. The structure was solved by the heavy atom (Patterson) method and all the major occupancy non-hydrogen atoms were refined anisotropically with absorption corrected (lamina [100]) data using full-matrix least-squares based on F^2 to give $R_1 = 0.071$, $wR_2 = 0.190$ for 5193 independent observed reflections ($|F_o| > 4\sigma(|F_o|)$, $2\theta \leq 120^\circ$) and 443 parameters. Crystallographic data (excluding structure factors) for the structure reported in this paper have been deposited with the Cambridge Crystallographic Data Centre as supplementary publication no. CCDC-102341. Copies of the data can be obtained free of charge on application to CCDC, 12 Union Road, Cambridge CB2 1EZ, UK (fax: (+44) 1223-336-033; e-mail: deposit@ccdc.cam.ac.uk).

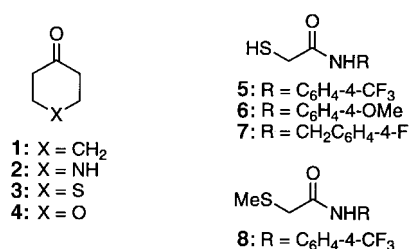
- [9] An examination of contacts does not reveal any obvious reason for this difference in bond lengths. There is however an intermolecular contact between Cl(5) and its symmetry-related counterpart (3.51 Å).
 [10] P. J. Bonasia, J. Arnold, *J. Organomet. Chem.* **1993**, *449*, 147; Ir–Te bond lengths in the range 2.626(1)–2.643(1) Å are observed in the cubane $[\text{Ir}_4(\mu\text{-Te})_4(\eta\text{-C}_5\text{Me}_5)_4]$; S. Schulz, M. Andruh, T. Pape, T. Heinze, H. W. Roesky, L. Häming, A. Kuhn, R. Herbst-Irmer, *Organometallics*, **1994**, *13*, 4004.

Hydrolysis of Amides Catalyzed by 4-Heterocyclohexanones: Small Molecule Mimics of Serine Proteases**

Mousumi Ghosh, Jeffrey L. Conroy, and Christopher T. Seto*

One of the long-standing problems in bioorganic chemistry is the design of catalysts that hydrolyze amide bonds under mild conditions.^[1, 2] Amides are stable species; the half-life for peptide hydrolysis under neutral conditions at 25 °C has been estimated to be seven years.^[3] However, nature has been able to develop four different classes of proteases that are capable of sequence-specific hydrolysis of peptides with tremendous rate accelerations. Therefore, the design of artificial catalysts that begin to approach the activity and specificity of protein-based catalysts is a fascinating and challenging problem. Here we report that the cyclohexanone **1** and the 4-heterocyclohexanones **2–4** are efficient catalysts for the base-promoted hydrolysis of amides.

We have shown previously that 4-heterocyclohexanones can be used to synthesize inhibitors of cysteine proteases.^[4] These compounds inhibit the protease by reaction of the



4-heterocyclohexanone carbonyl group with the active-site cysteine nucleophile of the enzyme with reversible formation of a hemithioacetal adduct.^[5] In our current studies we are interested in developing catalysts of amide hydrolysis, and we reasoned that the amide substrates **5–7** could be anchored reversibly to a 4-heterocyclohexanone catalyst to form similar hemithioacetal adducts. Hydrolysis of the amide could then occur through a series of reactions that mimic the mechanism used by serine proteases to catalyze hydrolysis of peptides, as discussed below. These reactions serve as a model for hydrolysis of peptides specifically on the C-terminal side of cysteine residues.

We have monitored the hydrolysis of **5–7** catalyzed by 4-heterocyclohexanones by ¹H or ¹⁹F NMR spectroscopy, or reverse-phase HPLC.^[6] The reactions were performed under pseudo-first-order conditions, and they showed an exponential decrease in the substrate concentration as a function of time. Table 1 shows the observed rate constants for several

Table 1. Observed rate constants for hydrolysis of amides catalyzed by 4-heterocyclohexanones.^[a]

Entry	Catalyst	Substrate	k_{obs} [s ⁻¹]	k_{rel} ^[b]
1	none	5	1.5×10^{-8}	
2	1	5	2.5×10^{-8}	2
3	2	5	5.9×10^{-8}	4
4	3 ^[c]	5	3.7×10^{-8}	2
5	4	5	2.2×10^{-4}	14700
6	4	6	1.5×10^{-4}	10000
7	none	6	1.5×10^{-8}	
8	4	7	1.2×10^{-4}	3900
9	none	7	3.1×10^{-8}	
10	4 ^[c]	8	1.0×10^{-7}	

[a] All reactions were performed at 25 °C with 20 mM substrate, 200 mM NaOD, and 600 mM catalyst (where present) D₂O/CD₃OD (4/1) unless otherwise specified. [b] Rate constant relative to the background reaction (no catalyst) with the same substrate. [c] Reaction was performed in D₂O/CD₃OD (1/1) because of low solubility of the catalyst or substrate in aqueous solution.

reactions with a variety of substrates and catalysts. The most efficient catalysis that we have measured is shown in entry 5. In this reaction the hydrolysis of **5** is accelerated by more than four orders of magnitude relative to the background reaction when it is carried out in the presence of 600 mM tetrahydropyranone (THP, **4**).

The efficiency of the hydrolysis reaction is highly dependent on the heteroatom in the 4-heterocyclohexanone catalyst (compare entries 2–5, Table 1). The reactivity of the carbonyl group in the catalyst is controlled by a through-space electrostatic repulsion between the dipoles of the ketone and the heteroatom. We have demonstrated previously that the equilibrium constant for addition of a thiol to 4-heterocyclo-

[*] Prof. Dr. C. T. Seto, M. Ghosh, J. L. Conroy
 Department of Chemistry
 Brown University
 324 Brook Street, Box H, Providence, RI 02912 (USA)
 Fax: (+1) 401-863-2594
 E-mail: christopher_seto@brown.edu

[**] This work was supported by the U.S. Army Medical Research and Material Command (DAMD17-96-1-6161, Career Development Award to C.T.S.). J.L.C. was supported by a GAANN Fellowship from the U.S. Department of Education and a University Fellowship from Brown University.

Supporting information for this article is available on the WWW under <http://www.wiley-vch.de/home/angewandte/> or from the author.

hexanones is correlated with the strength of this electrostatic repulsion.^[4] Thus THP, which has the strongest through-space interaction, is the most substrate bound and has the most effective catalyst at nonsaturating concentrations of substrate and catalyst.^[7] In addition to simple binding of the substrate to the catalyst, this type of through-space electrostatic interaction can also exert other effects which significantly influence the rate of the hydrolysis reaction. For example, electrostatic interactions should alter the pK_a of the hemithioacetal hydroxyl group which is involved in catalysis. A combination of these effects causes THP to be a much better catalyst than the corresponding carbon, nitrogen, and sulfur analogues. It is interesting to note that benzaldehyde, acetophenone, and trifluoromethyl ketone derivatives are not effective catalysts for these hydrolysis reactions.

To investigate the mechanism of this reaction we have examined the kinetic order for hydrolysis of **5** catalyzed by THP by varying the NaOD and catalyst concentrations under pseudo-first order conditions (Figure 1). The observed rate

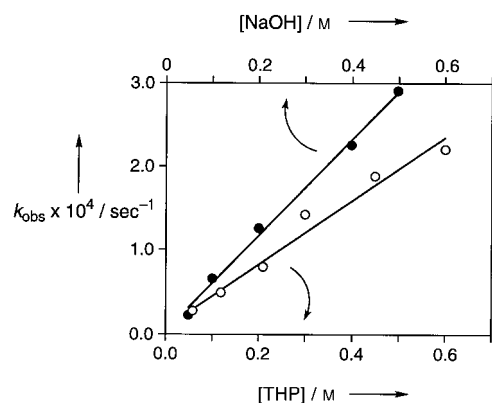


Figure 1. Hydrolysis of **5** catalyzed by tetrahydropyranone (THP, **4**) in D_2O/CD_3OD 4/1. ●: reactions with 20 mM substrate, 300 mM tetrahydropyranone, and NaOD in concentrations from 50 to 500 mM; slope = $5.72 \times 10^{-3} M^{-1} s^{-1}$. ○: reactions with 20 mM substrate, 200 mM NaOD, and THP in concentrations from 60 to 600 mM; slope = $3.77 \times 10^{-3} M^{-1} s^{-1}$.

constant increases linearly with the concentration of NaOD or THP. These results indicate that the rate expression for the hydrolysis reaction is defined by Equation (1).

$$\text{rate} = k_{\text{hydr}}[\text{substrate}][\text{catalyst}][\text{NaOH}] \quad (1)$$

We have used the slopes of the plots shown in Figure 1 to calculate the value of the third-order rate constant k_{hydr} . The experiments in which the catalyst concentration was varied (open circles) give a calculated rate constant of $k_{\text{hydr}} = 1.88 \times 10^{-3} M^{-2} s^{-1}$, while the experiments in which the NaOD concentration was varied (closed circles) give $k_{\text{hydr}} = 1.91 \times 10^{-3} M^{-2} s^{-1}$. The excellent agreement between these values provides further evidence that the rate expression formulated in Equation (1) is correct.

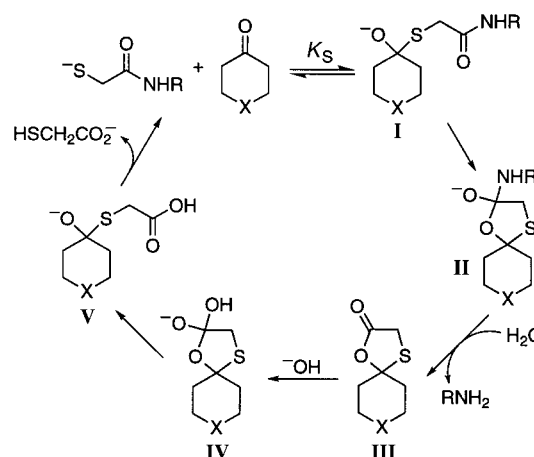
The observed rate constant for these reactions is a linear function of the catalyst concentration over the range of 60–600 mM THP (Figure 1). However, at concentrations at which the substrate is fully bound by catalyst, the rate constant should become independent of catalyst. These observations

indicate that the association constant K_S for the binding of **5** to THP is less than $1.7 M^{-1}$.^[7]

To explore the scope of this reaction, we have measured the hydrolysis rates for the three substrates **5**–**7**. Interestingly, there is less than a twofold difference in the rate constants between **5**, which is an relatively activated substrate, and **7**, which is an example of an unactivated amide. These results indicate that THP can accelerate significantly the rate of hydrolysis of unactivated amides, and suggest that it may serve as a useful catalyst for the cleavage of peptide bonds.

Under strongly basic conditions, the rate of uncatalyzed amide hydrolysis typically shows a small dependence on the nature of the leaving group.^[8] This observation can be rationalized because substituents on the leaving group have opposite effects on the rate of hydroxide addition to the amide carbonyl group and the rate of departure of the leaving group, which must be partially or fully protonated during this step. The small dependence of the rate of the catalyzed reaction on the nature of the leaving group suggests a similarity between the mechanisms of the catalyzed and uncatalyzed reactions.

Scheme 1 shows a plausible mechanism for the hydrolysis of amides catalyzed by 4-heterocyclohexanones. This mechanism mimics the series of reactions that occur during the



Scheme 1. Proposed mechanism for the hydrolysis of amides catalyzed by 4-heterocyclohexanones.

hydrolysis of peptides by serine proteases. Three important features of the enzymatic reaction are replicated in the proposed mechanism: 1) The substrate binds to the catalyst in a reaction that reaches equilibrium faster than amide hydrolysis. In Scheme 1 this entails nucleophilic attack by the substrate thiolate on the carbonyl group of the 4-heterocyclohexanone to yield hemithioacetal **I**. This strategy, which involves formation of a reversible covalent bond, provides a reliable method for anchoring the substrate to the catalyst in a well-defined geometry. 2) The substrate reacts with a catalyst nucleophile to generate an acyl-enzyme intermediate. In the small-molecule system, the anion in hemithioacetal **I** is positioned for nucleophilic attack on the amide carbonyl group through formation of a five-membered ring to give tetrahedral intermediate **II**. Breakdown of this tetrahedral intermediate releases the amine leaving group and

generates acyl-catalyst intermediate **III**. Similar mechanisms have been observed in the neighboring group participation by carbonyl hydrates during the hydrolysis of carboxylate and phosphate esters. However these examples are stoichiometric reactions that are promoted by intramolecular carbonyl groups.^[9–11] 3) Deacylation of the acyl-enzyme intermediate regenerates the catalysts. This process is mimicked by reaction of **III** with hydroxide to give tetrahedral intermediate **IV**, which then breaks down to yield hemithioacetal **V**. Dissociation of **V** releases the carboxylate anion and regenerates the 4-heterocyclohexanone catalyst.

We have performed two additional experiments to probe the validity of this proposed mechanism. First, we have synthesized control compound **8** in which the thiol group is blocked as the methyl thioether in order to determine if a thiol functionality in the substrate is necessary for catalysis. Comparison of entries 1 and 10 in Table 1 shows that the rate of hydrolysis of **8** in the presence of 600 mM catalyst is only sevenfold faster than the rate of hydrolysis of substrate **5** in the absence of catalyst. This comparison shows that a free thiol group in the substrate is required for catalysis. In addition, the results show that the mechanism of the catalyzed reaction cannot involve simple intermolecular nucleophilic attack by the anion of the 4-heterocyclohexanone hydrate on the carbonyl of the amide substrate.

In a second experiment we have independently synthesized the acyl-catalyst intermediate **III** (Scheme 1) in which X = S, and we monitored its rate of hydrolysis under the reaction conditions. We find that this intermediate is hydrolyzed much faster than the amide substrates in any of the catalyzed reactions. These two observations are consistent with the mechanism proposed in Scheme 1, and they suggest that the rate-limiting step for the catalyzed reaction occurs before hydrolysis of intermediate **III**.

In conclusion, we have demonstrated that tetrahydropyranone (**4**) is an effective catalyst for the hydrolysis of amide substrates that contain an adjacent thiol functionality. The reaction displays two features that are most often associated with enzymatic systems. First, the substrate is bound to the catalyst through a preliminary equilibrium in order to decrease the entropic barrier to reaction. The catalysts employ reversible formation of a hemithioacetal to establish this equilibrium. We believe that formation of reversible covalent bonds of this type will prove to be a useful method for mediating the molecular recognition processes that are involved in catalysis and self-assembly. Reversible covalent bonds are complementary to the noncovalent interactions—such as hydrogen bonds, hydrophobic interactions, and electrostatic interactions—that are typically observed in biological recognition processes. A second similarity to enzymatic catalysis is that the reaction is catalyzed through the participation of neighboring groups. We are currently conducting experiments to characterize further the mechanism of the reaction, and also to explore the possibility of using 4-heterocyclohexanones to catalyze the cysteine-specific hydrolysis of peptides.

Received: August 17, 1998

Revised version: October 15, 1998 [Z12293IE]

German version: *Angew. Chem.* **1999**, *111*, 575–578

Keywords: amides • electrostatic interactions • enzyme mimetics • hydrolyses • synthetic proteases

- [1] For amide hydrolysis promoted by metals, see a) J. T. Groves, L. A. Baron, *J. Am. Chem. Soc.* **1989**, *111*, 5442; b) A. W. Czarnik, K. Chen, S. P. Wathen, *Tetrahedron Lett.* **1992**, *33*, 6303; c) R. Breslow, A. Schepartz, *J. Am. Chem. Soc.* **1987**, *109*, 1814; d) N. N. Murthy, M. Mahroof-Tahir, K. D. Karlin, *J. Am. Chem. Soc.* **1993**, *115*, 10404; e) L. M. Sayre, K. V. Reddy, A. R. Jacobson, W. Tang, *Inorg. Chem.* **1992**, *31*, 937; f) T. J. Przystas, T. H. Fife, *J. Chem. Soc. Perkin Trans. 2* **1990**, 393; g) J. Chin, V. Jubian, K. Mrejen, *J. Chem. Soc. Chem. Commun.* **1990**, 1326; for examples of other types of catalysts, see h) J. W. Keillor, A. A. Neverov, R. S. Brown, *J. Am. Chem. Soc.* **1994**, *116*, 4669; i) J. Suh, I. M. Klotz, *J. Am. Chem. Soc.* **1984**, *106*, 2373.
- [2] For catalytic hydrolysis of esters, see a) B. Zhang, R. Breslow, *J. Am. Chem. Soc.* **1997**, *119*, 1676; b) F. Diederich, G. Schurmann, I. Chao, *J. Org. Chem.* **1988**, *53*, 2744; c) F. M. Menger, L. G. Whitesell, *J. Am. Chem. Soc.* **1985**, *107*, 707; for a related transesterification reaction, see d) T. Sammakia, T. B. Hurley, *J. Am. Chem. Soc.* **1996**, *118*, 8967.
- [3] D. H. Kahne, W. C. Still, *J. Am. Chem. Soc.* **1988**, *110*, 7529.
- [4] J. L. Conroy, T. C. Sanders, C. T. Seto, *J. Am. Chem. Soc.* **1997**, *119*, 4285.
- [5] J. L. Conroy, C. T. Seto, *J. Org. Chem.* **1998**, *63*, 2367.
- [6] See the supporting information for representative examples.
- [7] The apparent equilibrium constant for addition of 3-mercaptopyruvic acid to tetrahydropyranone under neutral conditions in 100% D₂O is 1.3 M^{−1}; see reference [4] for details.
- [8] a) M. L. Bender, R. J. Thomas, *J. Am. Chem. Soc.* **1961**, *83*, 4183; b) R. L. Schowen, H. Jayaraman, L. Kershner, *J. Am. Chem. Soc.* **1966**, *88*, 3373; c) L. D. Kershner, R. L. Schowen, *J. Am. Chem. Soc.* **1971**, *93*, 2014.
- [9] See K. Bowden, *Chem. Soc. Rev.* **1995**, *24*, 431, and references therein.
- [10] A similar mechanism has been proposed for the hydrolysis of sulfate esters catalyzed by human arylsulfatase A. This reaction involves participation by an aldehyde hydrate: G. Lukatela, N. Krauss, K. Theis, T. Selmer, V. Gieselmann, K. von Figura, W. Saenger, *Biochemistry* **1998**, *37*, 3654.
- [11] For the hydrolysis of α -aminonitriles assisted by aldehydes and ketones, see M. Paventi, F. L. Chubb, J. T. Edwards, *Can. J. Chem.* **1987**, *65*, 2114, and references therein.

Highly Enantioselective Hydrogenation of Cyclic Enol Acetates Catalyzed by a Rh–PennPhos Complex**

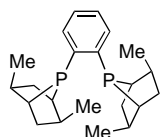
Qiongzhong Jiang, Dengming Xiao, Zhaoguo Zhang, Ping Cao, and Xumu Zhang*

The growing demand for practical and effective chiral ligands and/or catalysts has fueled much recent progress in ligand design. Although benchmark ligands such as 2,2'-

[*] Prof. X. Zhang, Dr. Q. Jiang, D. Xiao, Dr. Z. Zhang, P. Cao
Department of Chemistry
The Pennsylvania State University
University Park, PA 16802 (USA)
Fax: (+1) 814-863-8403
E-mail: xumu@chem.psu.edu

[**] This work was supported by a Camille and Henry Dreyfus New Faculty Award and Teaching Scholar Award, an ONR Young Investigator Award, a DuPont Young Faculty Award, Catalytica Pharmaceuticals, and DuPont Agrochemical Products. We acknowledge a generous loan of precious metals from Johnson Matthey Inc. and a gift of chiral GC columns from Supelco. PennPhos = *P,P'*-1,2-phenylenebis(endo-2,5-dialkyl-7-phosphabicyclo[2.2.1]heptanes).

bis(diphenylphosphanyl)-1,1'-binaphthyl (BINAP) and 1,2-bis(phospholano)benzene (DuPhos) have shown broad utilities for catalytic asymmetric hydrogenation,^[1] changes in the steric and electronic properties of the substrates sometimes lead to unexpected results. In our continuing effort to develop a general asymmetric hydrogenation of ketones, we became interested in exploring a related reaction, the enantioselective hydrogenation of readily accessible enol acetates,^[2] as an attractive alternative to direct hydrogenation of unfunctionalized ketones. An advantage that may accrue for enol acetate substrates is chelation, which can restrict the mobility of metal substrates and could therefore promote high enantioselectivities upon asymmetric hydrogenation.^[3a-f] While good to excellent enantioselectivities have been achieved upon asymmetric hydrogenation of some acyclic enol esters^[3] (e.g., Rh–DuPhos-catalyzed hydrogenation of enol acetates bearing electron-withdrawing carboxylate groups^[3i]), the asymmetric hydrogenation of cyclic enol acetates has not been reported. Recently we have developed a new family of electron-rich and conformationally rigid chiral bisphosphanes, *P,P'*-1,2-phenylenebis(*endo*-2,5-dialkyl-7-phosphabicyclo[2.2.1]heptanes) (PennPhos); an example is (*R,S,R,S*)-Me-PennPhos. A Rh–PennPhos complex was demonstrated to be an effective



(*R,S,R,S*)-Me-PennPhos

enantioselective catalyst for hydrogenation of simple ketones.^[4c] Herein we report the first highly enantioselective hydrogenation of cyclic enol acetates catalyzed by a Rh–PennPhos complex.

We initially chose the hydrogenation of 3,4-dihydronaphth-1-yl acetate for optimization studies in this series (Table 1). The reaction was carried at room temperature under an initial hydrogen pressure of 1.7 bar for 24 h. The catalyst was generated in situ by stirring a solution of [Rh(cod)₂]BF₄ (cod = 1,5-cyclooctadiene) as the Rh precursor and the ligand, and a substrate:[Rh]:ligand ratio of 1:0.01:0.011 was used.

Table 1. Rhodium-catalyzed asymmetric hydrogenation of 3,4-dihydronaphth-1-yl acetate.^[a]

Entry	Ligand	Solvent	Conversion [%]	<i>ee</i> [%] (config.) ^[a]
1	(<i>R,S,R,S</i>)-Me-PennPhos	toluene	64	98.3 (<i>R</i>)
2	(<i>R,S,R,S</i>)-Me-PennPhos	CH ₂ Cl ₂	100	86.8 (<i>R</i>)
3	(<i>R,S,R,S</i>)-Me-PennPhos	THF	100	98.7 (<i>R</i>)
4	(<i>R,S,R,S</i>)-Me-PennPhos	MeOH	100	99.1 (<i>R</i>)
5 ^[c]	(<i>R,S,R,S</i>)-Me-PennPhos	MeOH	99.2	98.3 (<i>R</i>)
6	(<i>R</i>)-BINAP	THF	2.4	18.0 (<i>R</i>)
7	(<i>R</i>)-BINAP	MeOH	1.9	3.1 (<i>R</i>)
8	(<i>R,R</i>)-Me-DuPhos	THF	1.3	12.3 (<i>S</i>)
9	(<i>R,R</i>)-Me-DuPhos	MeOH	— ^[d]	— ^[d]

[a] For details, see text and the Experimental Section. [b] Enantiomeric excesses were determined by gas chromatography using a Supelco Chiral Select 1000 column. The absolute configurations were determined from the optical rotation. [c] [[Rh(cod)Cl]₂] was used as the catalyst precursor. [d] No reaction.

Compared with toluene (Table 1, entry 1) and CH₂Cl₂ (entry 2), THF (entry 3) and MeOH (entry 4) are better solvents for the asymmetric hydrogenation reaction catalyzed by Rh–(*R,S,R,S*)-Me-PennPhos. Up to 99% *ee* was achieved for the hydrogenation of 3,4-dihydronaphth-1-yl acetate in MeOH using [Rh(cod)₂]BF₄ as the catalyst precursor and a PennPhos as the ligand (entry 4), which is the benchmark for this transformation. The neutral Rh precursor [[Rh(cod)Cl]₂] is also effective (entry 5), although the enantiomeric excess is slightly lower than that resulting from reaction with the cationic precursor [Rh(cod)₂]⁺. Interestingly, Rh–BINAP as well as Rh–DuPhos complexes are not effective catalysts for hydrogenation of 3,4-dihydronaphth-1-yl acetate in terms of enantioselectivity and activity (entries 6–8). In contrast to the excellent *ee* values obtained in the Rh–DuPhos-catalyzed hydrogenation of electron-deficient enol acetates with carboxylate groups in the α position,^[3i] poor enantioselectivities were observed with the electron-rich cyclic enol acetate used in the present study (entries 8 and 9).

Under optimized conditions, several cyclic enol acetates as well as acyclic enol acetates were hydrogenated with Rh–diphosphane catalysts (Table 2). The enol acetate derived

Table 2. Rhodium-catalyzed asymmetric hydrogenation of enol acetates.^[a]

Entry	Substrate	Ligand	Solvent	Conversion [%]	<i>ee</i> [%] (config.) ^[b]
1		(<i>R,S,R,S</i>)-Me-PennPhos	MeOH	100	99.1 (<i>R</i>)
2		(<i>R,S,R,S</i>)-Me-PennPhos	MeOH	100	98.2 (<i>R</i>)
3		(<i>R</i>)-BINAP	MeOH	5.0	66.1 (<i>R</i>)
4		(<i>R,R</i>)-Me-DuPhos	MeOH	4.9	69.4 (<i>R</i>)
5		(<i>R,S,R,S</i>)-Me-PennPhos	MeOH	100	> 99 (<i>R</i>)
6		(<i>R,S,R,S</i>)-Me-PennPhos	THF	100	98.5 (<i>R</i>)
7		(<i>R,S,R,S</i>)-Me-PennPhos	THF	100	84.8 (<i>R</i>)
8		(<i>R,S,R,S</i>)-Me-PennPhos	MeOH	100	83.5 (<i>R</i>)
9		(<i>R,S,R,S</i>)-Me-PennPhos	THF	100	80.9 (<i>R</i>)
10		(<i>R,S,R,S</i>)-Me-PennPhos	THF	100	83.9 (<i>R</i>)
11		(<i>R,S,R,S</i>)-Me-PennPhos	THF	100	83.0 (<i>R</i>)
12		(<i>R,S,R,S</i>)-Me-PennPhos	THF	100	80.9 (<i>R</i>)
13		(<i>R,S,R,S</i>)-Me-PennPhos	THF	100	82.0 (<i>R</i>)

[a] For details, see text and the Experimental Section. [b] Enantiomeric excesses were determined by gas chromatography using a Supelco Chiral Select 1000 column. The absolute configurations were determined from the optical rotation.

from 1-indanone was also reduced in high enantioselectivity using the Rh-(*R,S,R,S*)-Me-PennPhos complex (entry 2) while *ee* values achieved with either Rh-BINAP or Rh-Me-DuPhos complexes were significantly lower (entries 3 and 4). Hydrogenation of a substituted 3,4-dihydronaphth-1-yl acetate gave outstanding enantioselectivities with the Rh-(*R,S,R,S*)-Me-PennPhos catalytic system (entries 5 and 6). The highly enantioselective hydrogenation of five- and six-membered ring enol acetates provides a practical route for the syntheses of the corresponding chiral secondary alcohols.

Several acyclic enol acetates were also hydrogenated with the Rh-(*R,S,R,S*)-Me-PennPhos catalyst (entries 7–13). The enantioselectivities were lower than those achieved with cyclic enol acetates. Modifying the steric or electronic properties of these acyclic enol acetates had only small effects on the enantioselectivities (observed ranging from 80 to 85% *ee*). For the enol acetate derived from acetophenone, the enantioselectivity obtained with Rh-(*R,S,R,S*)-Me-PennPhos (entries 7 and 8) was comparable to those obtained with Rh-DuPhos compounds (77% *ee* in THF catalyzed by [Rh(Me-DuPhos)(cod)]BF₄, 89% *ee* in MeOH with [Rh(Me-DuPhos)(cod)]OTf;^[3f] OTf = trifluoromethanesulfonate). Further modification of the Rh-PennPhos structure may lead to practical catalysts for the hydrogenation of electron-rich acyclic enol acetates.

The rationale for the highly enantioselective hydrogenation of cyclic enol acetates is not clear. Phosphabicyclo[2.2.1]heptanes are electron-rich and conformationally rigid ligands with a well-defined deep chiral pocket. Our previous work has shown that this novel motif imparts valuable properties to this catalytic system.^[4] Since enol acetates are likely to be chelating substrates, the constrained geometry of the cyclic enol acetates may enhance recognition toward chiral transition metal complexes compared with acyclic enol acetates.

Experimental Section

All reactions and manipulations were performed in a nitrogen-filled glovebox or using standard Schlenk techniques. Toluene and THF were distilled from sodium benzophenone ketyl under nitrogen. CH₂Cl₂ was distilled from CaH₂. MeOH was distilled from Mg under nitrogen. The chiral PennPhos ligand was prepared as previously described.^[4c] Gas chromatography was carried out on Hewlett-Packard 5890 and 6890 gas chromatographs using the Chiral Select 1000 column (15 m × 0.25 mm (inner diameter), carrier gas: He (1 mL min⁻¹)).

General procedure for the asymmetric hydrogenation: To a solution of [Rh(cod)₂](BF₄) (5.0 mg, 0.012 mmol) in MeOH (10 mL) in a glovebox was added (*R,S,R,S*)-Me-PennPhos (0.15 mL of a 0.1 M solution in MeOH, 0.015 mmol). After the mixture was stirred for 30 min, the enol acetate (1.2 mmol) was added. The hydrogenation was performed at room temperature under 1.7 bar of hydrogen for 24 h. After the hydrogen was released, the reaction mixture was passed through a short silica gel column to remove the catalyst. The enantiomeric excess was measured by capillary GC without any further purification. The absolute configurations of the products were determined by comparing the observed optical rotations with those of chiral acetates made from readily available secondary alcohols.

Received: August 27, 1998 [Z12345IE]
German version: *Angew. Chem.* **1999**, *111*, 578–580

Keywords: alcohols • asymmetric catalysis • enols • hydrogenations • rhodium

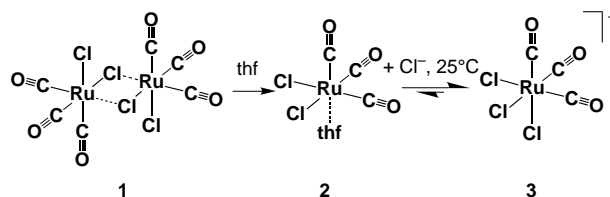
- [1] a) *Catalytic Asymmetric Synthesis* (Ed.: I. Ojima), VCH, New York, **1993**; b) R. A. Sheldon, *Chirotechnology*, Marcel Dekker, New York, **1993**; c) R. Noyori, *Asymmetric Catalysis in Organic Synthesis*, Wiley, New York, **1994**; d) R. Noyori, H. Takaya, *Acc. Chem. Res.* **1990**, *23*, 345; e) M. J. Burk, M. F. Gross, G. P. Harper, C. S. Kalberg, J. R. Lee, J. P. Martinez, *Pure Appl. Chem.* **1996**, *68*, 37.
- [2] For the synthesis of enol esters, see R. C. Larock, *Comprehensive Organic Transformations*, VCH, New York, **1989**, p. 743.
- [3] For selected examples of asymmetric hydrogenations of enol acetates, see a) K. E. Koenig, G. L. Bachman, B. D. Vineyard, *J. Org. Chem.* **1980**, *45*, 2362; b) R. E. Merrill, *ChemTech* **1981**, 118; c) T. Hayashi, K. Kanehira, M. Kumada, *Tetrahedron Lett.* **1981**, *22*, 4417; d) J. M. Brown, B. A. Murrer, *J. Chem. Soc. Perkin Trans. 2* **1982**, 489; e) K. E. Koenig in *Asymmetric Synthesis*, Vol. 5 (Ed.: J. D. Morrison), Academic Press, Orlando, **1985**, p. 71; f) M. J. Burk, *J. Am. Chem. Soc.* **1991**, *113*, 8518; g) T. Ohta, T. Miyake, N. Seido, H. Kumabayashi, S. Akutagawa, H. Takaya, *Tetrahedron Lett.* **1992**, *33*, 635; h) Y. Cramer, R. Schmid, T. Siegfried (Hoffmann-La Roche AG), EP-B 0691325 A1, **1996** [*Chem. Abstr.* **1996**, *124*, 260450x]; i) M. J. Burk, C. S. Kalberg, A. Pizzano, *J. Am. Chem. Soc.* **1998**, *120*, 4345; j) N. W. Boaz, *Tetrahedron Lett.* **1998**, *39*, 5505.
- [4] a) G. Zhu, Z. Chen, Q. Jiang, D. Xiao, P. Cao, X. Zhang, *J. Am. Chem. Soc.* **1997**, *119*, 3836; b) Z. Chen, Q. Jiang, G. Zhu, D. Xiao, P. Cao, C. Guo, X. Zhang, *J. Org. Chem.* **1997**, *62*, 4521; c) Q. Jiang, Y. Jiang, D. Xiao, P. Cao, X. Zhang, *Angew. Chem.* **1998**, *110*, 1203; *Angew. Chem. Int. Ed.* **1998**, *37*, 1100.

Reactions of a Transient Carbonyl(chloro)(hydrido)ruthenium(II) Complex with Ethylene, Alkynes, and CO; Chemistry of the New Anion [Ru₂(CO)₄Cl₅]^{-*}

Matthieu Faure, Luc Maurette, Bruno Donnadieu, and Guy Lavigne*

Dedicated to Professor Helmut Werner
on the occasion of his 65th birthday

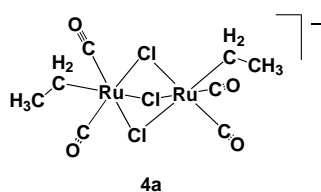
In spite of the high interest in halide salts as promoters for a variety of carbon–carbon bond-forming reactions,^[1–4] little is known about the reactivity of simple carbonyl(halo)ruthenium(II) complexes such as the interconvertible species **1–3** (Scheme 1).^[5]



Scheme 1.

[*] Dr. G. Lavigne, Dipl.-Chem. M. Faure, Dipl.-Chem. L. Maurette, Dr. B. Donnadieu
Laboratoire de Chimie de Coordination du CNRS associé à l'Université Paul Sabatier et à l'Institut National Polytechnique
205 route de Narbonne, F-31077 Toulouse Cedex 4 (France)
Fax: (+33) 561553003
E-mail: lavigne@lcc-toulouse.fr

[**] This work was supported by the CNRS. We thank Prof. Herbert D. Kaesz, Prof. John Bradley, and Dr Noël Lugan for helpful discussions.

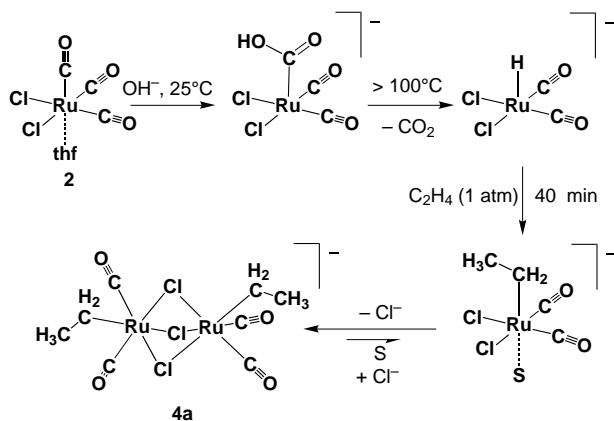


It was previously shown that $[(\text{PPh}_3)_2\text{N}][\text{Ru}(\text{CO})_3\text{Cl}_3]$ ([PPN]-**3**) is a catalyst precursor for the hydroesterification of ethylene with alkyl formates.^[3d,e]

More recently, Fabre et al.^[6] made the intriguing

observation that a novel, and yet very simple alkyl(carbonyl)(chloro)ruthenium(II) complex $[(\text{PPh}_3)_2\text{N}][\text{Ru}_2(\mu\text{-Cl})_3(\text{CO})_4(\text{CH}_2\text{CH}_3)_2]$ ([PPN]-**4a**) is produced in the reactor, and we believe this to be the resting state of the catalyst.

Assuming the anion **4a** results from the insertion of ethylene into an Ru–H bond of a precursor hydrido complex, we were challenged to devise a rational route to such a species in the absence of formate and to examine its aptitude to undergo insertion reactions with representative unsaturated organic substrates. Our approach (Scheme 2) is based in part on the principle of the water gas shift reaction.^[7]

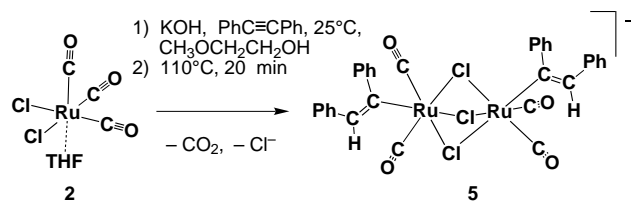


Scheme 2. Strategy for the synthesis of the ethyl complex **4a**. S = solvent.

Treatment of a solution of **2** in 2-methoxyethanol with one equivalent of KOH (1M in methanol) at 25°C led to instantaneous formation of the hydroxycarbonyl adduct $[\text{Ru}(\text{CO})_2\text{Cl}_2[\text{C}(\text{O})\text{OH}]]^-$.^[8] Decarboxylation of the latter at 100–110°C under a stream of ethylene (1 atm) for 40 min gave **4a** in quantitative yield (by spectroscopy).^[9] The reaction is easily monitored by IR spectroscopy by following the disappearance of the characteristic band of the $\text{C}(\text{O})\text{OH}$ group at 1527 cm^{-1} . The elusive intermediate hydrido species “ $[\text{Ru}(\text{CO})_2\text{Cl}_2\text{H}]^-$ ” was not detected in the presence of the olefin, and the mononuclear solvent-stabilized alkyl intermediate was observed only in dimethylformamide. Dimerization with the loss of a halide ligand is a means for the 16-electron organometallic fragment to relieve its unsaturation and to release the excess negative charge. The complex was recrystallized as its PPN salt and recovered in 60–70% yield. This synthetic procedure is milder and faster than the original route with an alkyl formate as hydride source.^[6]

The reaction sequence of Scheme 2 is applicable to a variety of other olefins;^[10] hence, we were interested in its possible extension to alkynes. Thermal decarboxylation of the hydroxycarbonyl adduct at 100–110°C for 20 min in the presence of

one equivalent of diphenylacetylene gave the alkenyl complex **K-5** (Scheme 3). The complex was isolated as the PPN salt in 78% yield. The dimeric anionic unit of [PPN]-**5** (Figure 1)^[11] consists of a face-sharing bi-octahedron (*gauche* isomer).



Scheme 3.

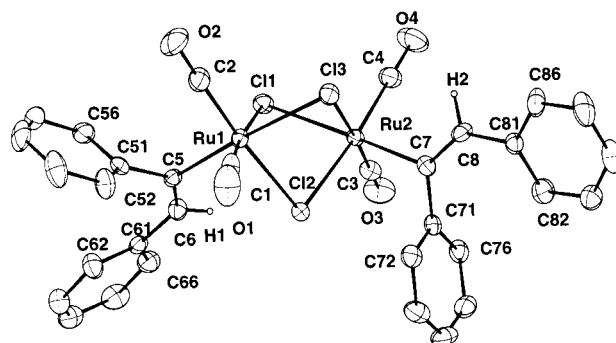
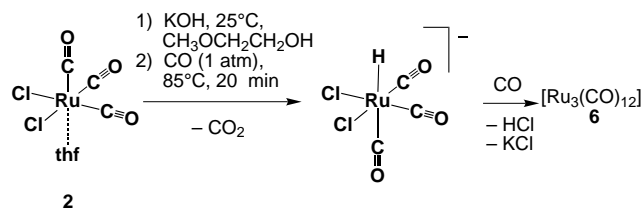


Figure 1. Perspective view of the anionic unit of the alkenyl complex [PPN]-**5**. Selected interatomic distances [Å] and angles [°]: Ru1–Ru2 3.2585(4), Ru1–Cl1 2.445(1), Ru1–Cl2 2.450(1), Ru1–Cl3 1.842(4), Ru1–C5 1.833(4), Ru1–C5 2.086(4), Ru2–Cl1 2.576(1), Ru2–Cl2 2.470(1), Ru2–Cl3 2.450(1), Ru2–C3 1.837(4), Ru2–C4 1.822(4), Ru2–C7 2.096(4), C5–C6 1.338(6), C7–C8 1.336(6); Ru1–C5–C6 119.1(3), Ru2–C7–C8 121.4(3).

In an attempt to trap the elusive hydrido intermediate in the absence of olefinic or acetylenic substrates, we decarboxylated the hydroxycarbonyl adduct at 85°C under a stream of carbon monoxide. This resulted in formation of $[\text{Ru}_3(\text{CO})_{12}]$ (**6**) as orange crystals (97% yield) on the walls of the glassware (Scheme 4). The reduction of Ru^{II} to Ru^0 can be



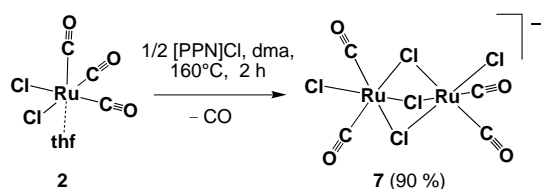
Scheme 4.

explained in terms of the reductive elimination of HCl from an elusive hydrido species “ $\text{K}[\text{Ru}(\text{CO})_3\text{Cl}_2\text{H}]$ ”. The acidity of the latter reflects the fact that halide ligands behave as Brønsted bases when the coordination sphere of ruthenium is saturated, which behavior was originally noted by Caulton et al. in studies on related chloro-phosphine Ru^{II} complexes.^[12] The evolution of HCl gas under our experimental conditions was detected by means of an aqueous solution of AgNO_3 in a bubbler at the gas exit of the reflux condenser.

Due to the insolubility of $[\text{Ru}_3(\text{CO})_{12}]$ in 2-methoxyethanol, the solution is almost colorless at the end of the reaction since it contains only KCl.^[13] Significantly, this synthesis can be

performed directly from commercial $\text{RuCl}_3 \cdot 3\text{H}_2\text{O}$ with almost the same efficiency in a one-pot procedure with two steps: treatment of $\text{RuCl}_3 \cdot 3\text{H}_2\text{O}$ with CO (1 atm) at 125°C for 2 h to generate the carbonylchloro species (characteristic yellow color) and addition of KOH under CO (at 25°C) followed by thermal decarboxylation at 85°C under CO for 20 min. Crystals of $[\text{Ru}_3(\text{CO})_{12}]$ (80–90 % yield) can then be isolated by simple filtration. In contrast, the published procedure with zinc as a halide acceptor^[14] is less efficient (50–60 % yield), takes about 12 h, and requires further workup for separation and recrystallization.

Given the propensity of chloro-ruthenium complexes to adopt face-sharing bioctahedral structures,^[12, 15] we were intrigued by the fact that the hypothetical binary carbonylchloro anion $[\text{Ru}_2(\mu\text{-Cl})_3(\text{CO})_4\text{Cl}_2]^-$ (**7**) has not been reported, whereas the dianionic complex $[\text{Ru}_2(\mu\text{-Cl})_2(\text{CO})_4\text{Cl}_4]^{2-}$ (**8**) is readily available by thermal decarbonylation of **1** or **2** in the presence of one equivalent of halide ion per ruthenium unit.^[16] We have now discovered a route to **7**: it is readily prepared by thermal decarbonylation of **2** in dimethylacetamide (dma) in the presence of [PPN]Cl (Scheme 5).



Scheme 5.

The X-ray structure of **7** is shown in Figure 2.^[17] The complex adopts a face-sharing bioctahedral structure and is again obtained only as the *gauche* isomer, as evidenced by ^{13}C NMR data. Since the known ruthenium carbonyl-chloro

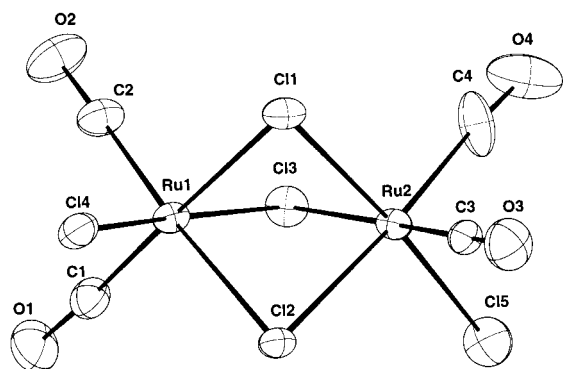
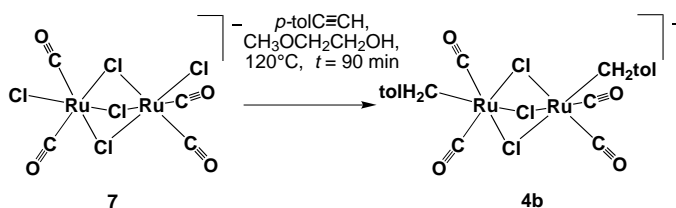


Figure 2. Perspective view of the anionic unit of the carbonyl-chloro complex [PPN]-**7**. Selected interatomic distances [Å]: Ru1–Ru2 3.1757(6), Ru1–Cl1 2.470(1), Ru1–Cl2 2.458(1), Ru1–Cl1 1.834(6), Ru1–C2 1.854(6), Ru1–Cl4 2.361(1), Ru2–Cl1 2.436(1), Ru2–Cl2 2.456(1), Ru2–Cl3 2.464(1), Ru2–Cl5 2.395(2), Ru2–C3 1.876(6), Ru2–C4 1.920(7).

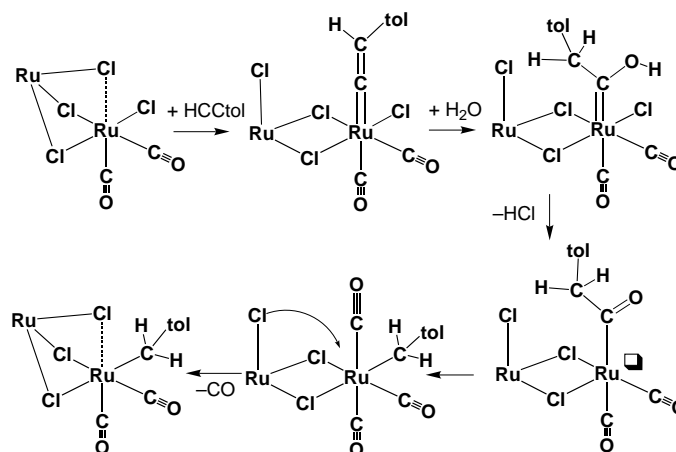
species $[\text{Ru}(\text{CO})_2\text{Cl}_2]^{[5c]}$ exists only as a polymer of undefined structure, **7** represents the simplest association of two neutral $14 e^-$ “ $\text{Ru}(\text{CO})_2\text{Cl}_2$ ” units slightly stabilized by one additional halide ion. With such a simple non-hydridic carbonyl-chloro

Ru^{II} prototype in hand, we expected to observe the activation of terminal alkynes in the form of vinylidenes.^[18] Instead, the reaction of the PPN salt of **7** with *para*-tolylacetylene (*p*-tolC≡C) in 2-methoxyethanol led exclusively to the alkyl derivative, [PPN]-**4b** (Scheme 6), which was formed in



Scheme 6.

quantitative yield according to spectroscopy and recovered as an oil in 58 % yield. The cleavage of the carbon–carbon triple bond of the alkyne can be rationalized by analogy to the reaction of vinylidene complexes with water.^[19] The proposed reaction sequence leading to **4b** is summarized in Scheme 7.



Scheme 7. Proposed reaction pathway leading to the alkyl complex **4b**. tol = *p*-tolyl. □ denotes a vacant coordination site.

The reaction of [PPN]-**7** with trimethylsilylacetylene cleanly gave the methyl derivative $[(\text{PPh}_3)_2\text{N}][\text{Ru}_2(\mu\text{-Cl})_3(\text{CO})_4(\text{CH}_3)_2]$ ([PPN]-**4c**),^[20] obtained for the first time as pure crystals in 65 % yield and fully characterized by spectroscopic methods and X-ray diffraction.^[21] Significantly, the acetylide complexes $[(\text{PPh}_3)_2\text{N}][\text{Ru}_2(\mu\text{-Cl})_3(\text{CO})_4(\text{CCH})_2]$ ([PPN]-**9a**) and $[(\text{PPh}_3)_2\text{N}][\text{Ru}_2(\mu\text{-Cl})_3(\text{CO})_4(\text{CCSiMe}_3)_2]$ ([PPN]-**9b**; traces) were also detected (by mass spectrometry) when the reaction was carried out in the absence of water in a nonprotic solvent such as dioxane. There is a precedent for the formation of a ruthenium acetylide ($[\text{Ru}]\text{-C}\equiv\text{CH}$) on activation of trimethylsilylacetylene by a chloro ruthenium complex with concomitant elimination of SiMe_3Cl .^[22] Here the hydration of **9a** to give **4c** probably involves an α -hydroxyvinyl intermediate $[\text{Ru}]\text{-C}(\text{OH})=\text{CH}_2$, isomerization of which into an acyl complex $[\text{Ru}]\text{-C}(=\text{O})\text{CH}_3$ followed by decarbonylation produces the methyl complex.

Thus, the facile transformations of terminal alkynes observed here can be accounted for by the existence of intermediate vinylidene complexes that are highly reactive

due to the absence of electronic stabilization and steric protection of their α -carbon atom. The next challenge will be to trap such intermediates and to examine their potential applications in organic synthesis.^[23]

Experimental Section

2 (optimization of published procedure):^[5a] A solution of $\text{RuCl}_3 \cdot 3\text{H}_2\text{O}$ (5 g) in 2-methoxyethanol (100 mL) was treated with CO (1 atm) for 3 h at 125 °C and then for 7 h at 25 °C to give a pale yellow solution of **1**. After evaporation of the solvent (50 °C, reduced pressure), the residue was extracted with hot THF (30 mL). Complex **2** crystallized at –30 °C as white needles (4.24 g, 70 % yield). IR: $\tilde{\nu}$ = 2115 (vs), 2035 cm^{-1} (vs). Isolation of a second crop of crystals from the concentrated filtrate gave a total yield of **2** of 89 %. The complex was identified as the *fac* isomer by X-ray diffraction.

Standard solutions of the hydroxycarbonyl adduct $\text{K}[\text{Ru}(\text{CO})_2\text{Cl}_2\cdot\{\text{C}(\text{O})\text{OH}\}]$ (IR: $\tilde{\nu}$ = 2048 (s), 1981 (vs), 1647 (m), 1527 cm^{-1} (ms)) were prepared from **2** (500 mg, 1.52 mmol) in 2-methoxyethanol (25 mL) by adding 1.5 mL of a 1 M methanolic solution of KOH.

[PPN]-**4a**: Ethylene was bubbled into a freshly prepared solution of the hydroxycarbonyl adduct at 100–110 °C. The formation of **K-2** was complete after 40 min (spectroscopy). After addition of [PPN]Cl and evaporation of the solvent, the THF-soluble fraction was recrystallized from acetone/ethanol (1/5) at –30 °C to give [PPN]-**4a**^[6] (490 mg, 65 % yield). IR (CH_2Cl_2): $\tilde{\nu}$ = 2030 (w,sh), 2018(vs), 1943 cm^{-1} (vs).

[PPN]-**5**: Diphenylacetylene (270 mg, 1.5 mmol) was added to a freshly prepared solution of the hydroxycarbonyl adduct, and the reaction mixture heated at 100–110 °C until the IR bands of **K-5** reached maximum intensity (ca. 20 min). Treatment with [PPN]Cl and recrystallization (acetone/ethanol) gave crystals of [PPN]-**5**·(CH_3)₂CO in 78 % yield. IR (CH_2Cl_2): $\tilde{\nu}$ = 2044 (w, sh), 2034 (vs), 1967 cm^{-1} (vs); ¹H NMR (250 MHz, CDCl_3): δ = 6.68–7.62 (m, vinylic and phenyl protons); MS (electrospray): *m/z*: 779.

6 from **2**: A freshly prepared solution of the hydroxycarbonyl adduct was heated at 85 °C under a CO stream for 20 min. After cooling, crystals of **6** were recovered by filtration and washed with ethanol (310 mg, 97 % yield).

6 from $\text{RuCl}_3 \cdot 3\text{H}_2\text{O}$: A solution of $\text{RuCl}_3 \cdot 3\text{H}_2\text{O}$ (1 g, 3.82 mmol) in 2-methoxyethanol (40 mL) was heated at 125 °C under CO until a yellow color was obtained (ca. 2 h). After cooling, a methanolic solution of KOH (1 M, 4.2 mL) was added at 20 °C, and the temperature was raised to 85 °C for 20 min. Compound **6** was recovered by filtration (ca. 700 mg, 86 % yield).

[PPN]-**7**: Compound **2** (1 g, 3 mmol) and [PPN]Cl (874 mg, 1.5 mmol) were dissolved in dimethylacetamide (20 mL). After heating for 2 h at 160 °C, the solvent was evaporated (90 °C, reduced pressure). The solid residue was washed with hexane. Recrystallization from dichloromethane/hexane gave [PPN]-**7** (1390 mg, 90 % yield). IR (CH_2Cl_2): $\tilde{\nu}$ = 2068 (vs), 2008 cm^{-1} (vs, br); ¹³C NMR (250 MHz, CDCl_3): δ = 191.44, 191.88 (CO); MS (electrospray): *m/z*: 492.6.

[PPN]-**4b**: A solution of [PPN]-**7** (1390 mg, 1.35 mmol) in 2-methoxyethanol (30 mL) and *p*-tolylacetylene (340 mg, 2.93 mmol) was heated at 110–120 °C for 90 min. After solvent evaporation (90 °C, reduced pressure), the resulting oil was washed several times with hexane and ethanol to give [PPN]-**4b** (910 mg, 58 % yield). IR (2-methoxyethanol): $\tilde{\nu}$ = 2031 (sh), 2019 (vs), 1948 cm^{-1} (vs, br); ¹³C NMR (250 MHz, CD_2Cl_2): δ = 22.10 (t, $\text{CH}_2\text{C}_6\text{H}_4\text{CH}_3$, J_{CH} = 134 Hz), 20.87 (q, $\text{CH}_2\text{C}_6\text{H}_4\text{CH}_3$, J_{CH} = 126 Hz), 126–135 (m, C_6H_4), 197.82 and 198.23 (s, CO); ¹H NMR (250 MHz, CD_2Cl_2): δ = 3.46 (s, $\text{CH}_2\text{C}_6\text{H}_4\text{CH}_3$), 2.25 (s, $\text{CH}_2\text{C}_6\text{H}_4\text{CH}_3$); MS (electrospray): *m/z*: 633.

[PPN]-**4c**: An analogous procedure starting from [PPN]-**7** (250 mg, 0.243 mmol) and trimethylsilylacetylene (0.067 mL, 0.485 mmol) gave crystalline [PPN]-**4c** (158 mg, 65 % yield). IR (2-methoxyethanol): $\tilde{\nu}$ = 2021 (sh), 2019 (vs), 1946 cm^{-1} (vs, br) ¹³C NMR (250 MHz, CD_2Cl_2): δ = –7.93 (q, CH_3 , J_{CH} = 134 Hz); 126–134 (m, C_6H_5), 197.86 and 198.13 (s, CO); ¹H NMR (250 MHz, CD_2Cl_2): δ = 0.84 (s, CH_3), 7.3–7.7 (m, C_6H_5); MS (electrospray): *m/z*: 453.

Keywords: alkylations • C–C activation • carbonyl complexes • insertions • ruthenium

- [1] Syngas reactions and C_1 chemistry: a) B. D. Dombek, *J. Organomet. Chem.* **1989**, 372, 151–161, and references therein; b) J. Knifton in *Aspects of Homogeneous Catalysis*, Vol. 6 (Ed.: R. Ugo), Reidel, Dordrecht, **1988**, pp. 1–58, and references therein; c) G. Braca, G. Sbrana, G. Valentini, G. Andrich, G. Gregoria, *J. Am. Chem. Soc.* **1978**, 100, 6238–6240; d) K.-I. Tominaga, Y. Sasaki, T. Watanabe, M. Saito, *Bull. Chem. Soc. Jpn.* **1995**, 68, 2837–2842; e) G. Süss-Fink, J.-M. Soulié, G. Rheinwald, H. Stoeckli-Evans, Y. Sasaki, *Organometallics* **1996**, 15, 3416–3422.
- [2] Reduction of aromatic nitro compounds to carbamates: S. Cenini, C. Crotti, M. Pizzotti, F. Porta, *J. Org. Chem.* **1988**, 53, 1243–1250.
- [3] Olefin hydroesterification: a) M. Hiday, Y. Koyasu, K. Chikanari, Y. Uchida, *J. Mol. Catal.* **1987**, 40, 243–254; b) C. Legrand, Y. Castanet, A. Mortreux, F. Petit (Atochem), EP-B 449693A, **1991**; c) C. Legrand, Y. Castanet, A. Mortreux, F. Petit, *J. Chem. Soc. Chem. Commun.* **1994**, 1173–1174; d) G. Lavigne, N. Lugan, P. Kalck, J.-M. Soulié, O. Lerouge, J.-Y. Saillard, J.-F. Halet, *J. Am. Chem. Soc.* **1992**, 114, 10669–10670; e) N. Lugan, G. Lavigne, J.-M. Soulié, P. Kalck, J.-Y. Saillard, J.-F. Halet, *Organometallics* **1995**, 14, 1713–1731.
- [4] For alkyne-based reactions, see: a) N. Chatani, K. Kataoka, S. Murai, N. Furukawa, Y. Seki, *J. Am. Chem. Soc.* **1998**, 120, 9104–9105; b) N. Chatani, T. Morimoto, T. Muto, S. Murai, *J. Am. Chem. Soc.* **1994**, 116, 6049–6050.
- [5] a) M. I. Bruce, F. G. A. Stone, *J. Chem. Soc. A* **1967**, 1238–1241; b) W. Manchot, J. König, *Chem. Ber.* **1924**, 57, 2130; c) J. Chatt, B. L. Shaw, A. E. Field, *J. Chem. Soc.* **1964**, 3466–3475; d) J. Halpern, B. R. James, L. W. Kemp, *J. Am. Chem. Soc.* **1966**, 88, 5142–5147; e) G. Braca, G. Sbrana, P. Pino, E. Benedetti, *Chim. Ind. (Milan)* **1967**, 49, 1381–1383; f) F. Calderazzo, F. L'Eplattenier, *Inorg. Chem.* **1967**, 6, 1220–1225; g) B. F. G. Johnson, R. D. Johnston, J. Lewis, *J. Chem. Soc. A* **1969**, 792–797; h) G. Sbrana, G. Braca, E. Benedetti, *J. Chem. Soc. Dalton Trans.* **1975**, 754–761.
- [6] S. Fabre, P. Kalck, G. Lavigne, *Angew. Chem.* **1997**, 109, 1167–1169; *Angew. Chem. Int. Ed. Engl.* **1997**, 36, 1092–1095.
- [7] P. C. Ford, A. Rokicki, *Adv. Organomet. Chem.* **1988**, 28, 139–217.
- [8] The hydroxycarbonyl adduct can be indifferently generated in situ from any of the precursors **1–3** in solvents such as alcohols, THF, and DMF. In noncoordinating solvents (dichloromethane), it can dimerize by forming hydroxycarbonyl bridges. A related complex with methoxycarbonyl bridges is known.^[1e]
- [9] The reaction can be alternatively conducted with the same efficiency in a closed reactor under ethylene pressure (20 atm), but otherwise identical conditions.
- [10] Related alkyl complexes are formed with methyl acrylate, styrene, and propylene (G. Lavigne, unpublished results).
- [11] a) Crystallographic data for [PPN]-**5**·(CH_3)₂CO: orthorhombic, space group $P2_12_12_1$, a = 10.346(1), b = 22.277(2), c = 27.519(3) Å; V = 6343(2) Å³; R = 0.021, R_w = 0.027. b) Crystallographic data (excluding structure factors) for the structures reported in this paper have been deposited with the Cambridge Crystallographic Data Center as supplementary publication no. CCDC-103293 ([PPN]-**5**), CCDC-103294 ([PPN]-**7**), and CCDC-112413 ([PPN]-**4c**). Copies of the data can be obtained free of charge on application to CCDC, 12 Union Road, Cambridge CB2 1EZ, UK (fax: (+44) 1223-336-033; e-mail: deposit@ccdc.cam.ac.uk).
- [12] D. Huang, K. Folting, K. G. Caulton, *Inorg. Chem.* **1996**, 35, 7035–7040.
- [13] If KOH is used in less than stoichiometric amount, the IR spectrum shows the characteristic bands of $\text{K}[\text{Ru}(\text{CO})_3\text{Cl}_3]$ (**K-3**), which results from the addition of KCl to the neutral fragment “[$\text{Ru}(\text{CO})_3\text{Cl}_2$]”. However, the reaction can be completed by adding further KOH.
- [14] A. Mantovani, S. Cenini, *Inorg. Synth.* **1976**, 16, 46–47.
- [15] See, for example, a) T. Ohta, Y. Tonomura, K. Nozaki, H. Takaya, K. Mashima, *Organometallics*, **1996**, 15, 1521–1523; b) D. R. Fogg, B. R. James, *Inorg. Chem.* **1995**, 34, 2557–2561.
- [16] M. L. Berch, A. Davison, *J. Inorg. Nucl. Chem.* **1973**, 35, 3763–3767.
- [17] Crystal data for [PPN]-**7**: triclinic, space group $P\bar{1}$, a = 10.019(2), b = 14.773(2), c = 14.862(3) Å, α = 78.51(2)°, β = 96.917(6)°, γ = 74.96(2)°; V = 2054(2) Å³; R = 0.031, R_w = 0.036.^[11b]

Received: October 6, 1998 [Z 12499 IE]
German version: *Angew. Chem.* **1999**, 111, 539–542

- [18] a) D. Touchard, S. Guesmi, M. Bouchaib, P. Haquette, A. Daridor, P. H. Dixneuf, *Organometallics* **1996**, *15*, 2579–2581; b) review: M. I. Bruce, *Chem. Rev.* **1991**, *91*, 197–257.
- [19] a) M. I. Bruce, A. G. Swincer, *Aust. J. Chem.* **1980**, *33*, 1471–1483; b) C. Bianchini, J. A. Casares, M. Peruzzini, A. Romerosa, F. Zanobini, *J. Am. Chem. Soc.* **1996**, *118*, 4585–4594, and references therein; c) M. L. Buil, M. A. Esteruelas, A. M. Lopez, E. Onate, *Organometallics* **1997**, *16*, 3169–3177.
- [20] This species was originally detected in an inseparable mixture of complexes resulting from a metal-mediated degradation of methyl formate.^[6]
- [21] Crystal data for [PPN]-**4c**: Monoclinic, space group $P2_1/n$; $a = 29.322(4)$, $b = 15.558(2)$, $c = 9.656(2)$ Å, $\beta = 92.77(2)$, $V = 4400(2)$ Å³; $R = 0.046$, $R_w = 0.050$.^[11b]
- [22] a) R. M. Bullock, *J. Chem. Soc. Chem. Commun.* **1989**, 165–167.
- [23] Carbenoid species derived from simple carbonyl-chloro Ru^{II} complexes have been recently proposed by Murai et al. as intermediates in the construction of polycyclic ring systems from enynes.^[4a]

Reaction of RGeBr₃ (R = *i*Pr₂C₆H₃NSiMe₃) with Ammonia To Give (RGe)₂(NH₂)₄(NH): A Compound Containing Terminal NH₂ Groups**

Karsten Wraage, Lutz Lameyer, Dietmar Stalke, and Herbert W. Roesky*

In memory of Jean Rouxel

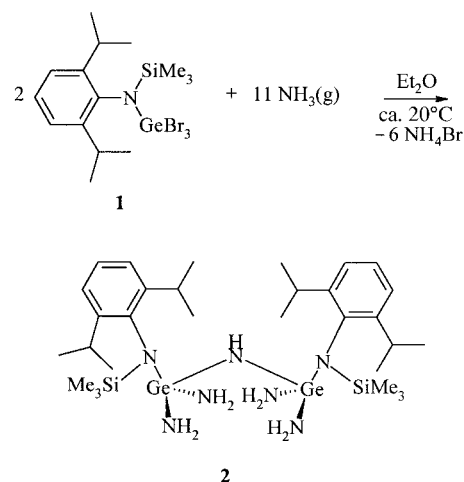
In the past few years Power et al.,^[1] Schnick et al.,^[2] and others^[3, 4] have shown that amino and imino derivatives containing silicon can undergo interesting reactions. In this respect they resemble the oxygen derivatives to some extent, but they can also differ from them quite considerably.^[5] For example, RSi(NH₂)₃ compounds react with AlMe₃ and [Cp*TiMe₃] (Cp* = C₅Me₅) with elimination of methane to form interesting, new, soluble heterocycles. We were interested in finding out whether there is a similar successive chemistry for germanium derivatives. We quickly discovered that the preferred starting compound for the reaction with ammonia—namely, RGeCl₃ (R = *i*Pr₂C₆H₃NSiMe₃)—is not accessible in a pure form. Until now, only one monoamino-germanium compound with the composition Mes₃GeNH₂ (Mes = Me₃C₆H₂) was known which is stable with regard to condensation reactions.^[6] We report here on the preparation and structure of an amino-iminogermanium compound with free amino groups that have not undergone condensation reactions.

[*] Prof. H. W. Roesky, Dipl.-Chem. K. Wraage
Institut für Anorganische Chemie der Universität
Tammannstrasse 4, D-37077 Göttingen (Germany)
Fax: (+49) 551-393-373
E-mail: hroesky@gwdg.de

Dipl.-Chem. L. Lameyer, Prof. D. Stalke
Institut für Anorganische Chemie der Universität Würzburg
(Germany)

[**] This work was supported by the Deutsche Forschungsgemeinschaft.

To obtain a suitable reagent for the synthesis of an amino derivative, we first prepared tribromogermanium compounds of the type RGeBr₃. The compound *i*Pr₂C₆H₃NSiMe₃GeBr₃ (**1**) was obtained by reaction of *i*Pr₂C₆H₃NSiMe₃Li with GeBr₄ in diethyl ether at –78 °C under elimination of LiBr. The reaction of **1** in liquid ammonia, which was performed analogous to the synthesis of RSi(NH₂)₃ derivatives,^[1, 3] proved to be unsuccessful; due to condensation reactions no definitive product could be isolated. If **1** is dissolved at room temperature in diethyl ether and ammonia is passed through the reaction solution, however, (RGe)₂(NH₂)₄(NH) (**2**) is obtained in good yield (Scheme 1).



Scheme 1. Synthesis of **2** from **1**.

Compound **2** was studied by NMR spectroscopy, mass spectrometry, and structure analysis. In the ¹H NMR spectrum the characteristic signals for the NH and NH₂ protons are recognizable as broad singlets ($\delta = 0.65$ for (RGe)₂(NH₂)₄–(NH) and $\delta = 0.75$ for (RGe)₂(NH₂)₄NH). The IR spectrum shows three N–H bands in the bond stretching region (3325–3402 cm^{–1}), and the bands at 1540 and 1578 cm^{–1} have been provisionally assigned to the NH₂ bending vibrations.

Single crystals of **2** are obtained on recrystallization from *n*-hexane. Compound **2** crystallizes in the space group $P\bar{1}$;^[11] two RGe(NH₂)₂ fragments bridged by a NH group are shown in the asymmetric unit in Figure 1a. In spite of their comparatively large spatial requirement, both of the *N*-(2,6-diisopropylphenyl)-*N*-(trimethylsilyl)amino groups are located on one side of the molecule and the four NH₂ groups on the opposite side. This cisoid arrangement is the result of a network of bridging hydrogen bonds (Figure 1b). The centrosymmetric dimer has four weak N···H–N bridges.^[7] The N···H distances are 250.5 pm (H21···N5A, H21A···N5; Figure 1b) and 267.8 pm (H31···N2A, H31A···N2; Figure 1b). All the Ge–N bond lengths to the hydrogen-substituted nitrogen atoms N1, N2, N3, N5, and N6 lie in the range from 181.1(2) to 182.4(2) pm, the bonds to the aryl-substituted nitrogen atoms N4 and N7 (both 184.2(2) pm) are about 3 pm longer.

The Ge–N bond lengths all lie in the expected region. Similar derivatives, such as the NH-bridged compound [Me₂Si(N*t*Bu)₂Ge(*t*Bu)]NH[(C₅H₄N)Ge(N*t*Bu)₂SiMe₂] described by Veith et al. and the cyclotris(dithiolato)germanium imide [(*t*BuS)₂Ge(NH)]₃ described by George et al., have

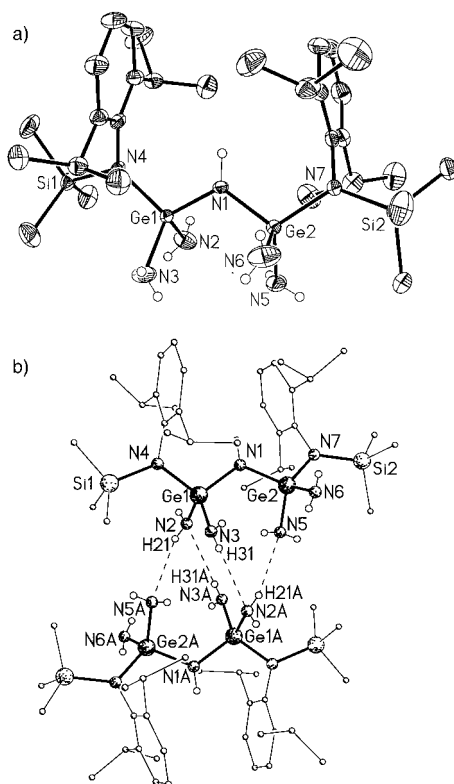


Figure 1. a) Structure of **2** in the crystal. Selected bond lengths [pm] and angles [°]: Ge1–N1 181.8(2), Ge1–N2 181.8(2), Ge1–N3 181.5(2), Ge1–N4 184.2(2), Ge2–N1 181.1(2), Ge2–N5 182.4(2), Ge2–N6 181.4(2), Ge2–N7 184.2(2); Ge1–N1–Ge2 120.89(9), N1–Ge1–N4 108.61(8), N2–Ge1–N3 101.80(10), N1–Ge2–N7 109.55(8), N5–Ge2–N6 104.54(11). b) Bridging hydrogen bonds between two molecules of **2**. Distances [pm] and angles [°] (the hydrogen atom positions were determined by difference Fourier synthesis and freely refined): H21...N5A 250.5, H31...N2A 267.8; N2–H21...N5A 164.28, N3–H31...N2A 174.08.

Ge–N bond lengths similar to those in **2**.^[8,9] In the *Nt*Bu-bridged amide [*t*BuN(CH₂)₂*Nt*Bu](Me)Si[N(*t*Bu)[Ge(N(H)–SiMe₃)(OSiMe₃){OCH₂N(CH₃)₂}], which contains sterically more demanding substituents on the nitrogen atom, the Ge–N bond is 184.2 pm long, and thus lies in the same range as the Ge–NAr(SiMe₃) bond lengths in **2** (Ge1–N4, Ge2–N7).^[10] The dimers exist in the solid as isolated molecules, however, and there are no bridging intermolecular hydrogen bonds.

The synthesis of **2** demonstrates that stable amino-imino-germanium derivatives can be prepared through the ammonolysis of a RGeBr₃ compound. Compound **2** contains reactive hydrogen atoms which should prove predestined for the synthesis of heterocycles containing germanium. The reaction of **2** with trimethylaluminum leads to the formation of a six-membered (GeN)₃ heterocycle and methane. Terminal NH₂ groups are located on each of the germanium atoms in the ring. The high hydrogen content should favor the elimination of the organic groups in **2**, so that new Ge–N phases should become accessible.

Experimental Section

1: GeBr₄ (5.2 g, 16.6 mmol) was dissolved in diethyl ether (100 mL). A solution of *i*Pr₂C₆H₃NSiMe₃Li (3.8 g, 14.9 mmol, 0.9 equiv.) dissolved in

diethyl ether (80 mL) was added slowly to the GeBr₄ solution at –78 °C. After the mixture was warmed slowly and stirred for about 12 h, the solvent was removed under reduced pressure and the residue taken up in *n*-hexane (70 mL). Insoluble components were filtered off, and the product subsequently recrystallized from *n*-hexane (5 mL). Yield: 7.5 g (80%) of **1**. C₁₅H₂₆Br₃GeNSi (*M* = 560.8 g mol^{–1}); sublimation at 150–160 °C; ¹H NMR (200 MHz, C₆D₆, TMS_{ext}): δ = 0.32 (s, 9H; Si(CH₃)₃), 1.15 (d, ³J(H,H) = 6.9 Hz, 6H; CH(CH₃)₂), 1.25 (d, ³J(H,H) = 6.9 Hz, 6H; CH(CH₃)₂), 3.45 (sept, 2H; CH(CH₃)₂), 7.05 (m, 3H; H_{arom}); ²⁹Si NMR (49 MHz, C₆D₆, TMS_{ext}): δ = 13.1 (Si(CH₃)₃); MS (EI, 70 eV): *m/z* (%): 560.9 (100) [*M*⁺], 545.8 (90) [*M*⁺ – CH₃]; correct elemental analysis.

2: *i*Pr₂C₆H₃NSiMe₃GeBr₃ (**1**, 0.56 g, 1 mmol) was dissolved in diethyl ether (10 mL). Ammonia (120 mL min^{–1}) was introduced under continuous stirring at room temperature. After 1 min the originally orange solution had turned colorless and a white precipitate formed. The reaction mixture was stirred for a further 0.5 h, and the precipitate then filtered off and recrystallized from *n*-hexane (5 mL). Yield: 0.3 g (81%) of **2**. C₃₀H₆₁Ge₂N₇Si₂ (*M* = 721.3 g mol^{–1}); m.p. 139 °C; ¹H NMR (250 MHz, CDCl₃, TMS_{ext}): δ = 0.07 (s, 18H; Si(CH₃)₃), 0.65 (s, 1H; (H₂N)₂GeNHGe(NH₂)₂), 0.75 (s, 8H; (H₂N)₂GeNHGe(NH₂)₂), 1.15 (dd, 24H; CH(CH₃)₂), 3.45 (sept, 4H; CH(CH₃)₂), 7.05 (m, 6H; H_{arom}); ²⁹Si NMR (79 MHz, CDCl₃, TMS_{ext}): δ = 4.9 (Si(CH₃)₃); IR (KBr): $\tilde{\nu}$ = 1540, 1578, 3325, 3389, 3402 cm^{–1}; MS (EI, 70 eV): *m/z* (%): 705 (2) [*M*⁺ – CH₃], 473 (100) [*M*⁺ – *i*Pr₂C₆H₃NSiMe₃]; correct elemental analysis.

Received: September 28, 1998 [Z 12457]

German version: *Angew. Chem.* **1999**, *111*, 542–544

Keywords: amides • bromine • germanium • imides

- [1] K. Ruhlandt-Senge, R. A. Bartlett, M. M. Olmstead, P. P. Power, *Angew. Chem.* **1993**, *105*, 459; *Angew. Chem. Int. Ed. Engl.* **1993**, *32*, 425.
- [2] H. Huppertz, W. Schnick, *Angew. Chem.* **1997**, *109*, 2765; *Angew. Chem. Int. Ed. Engl.* **1997**, *36*, 2651.
- [3] K. Wraage, A. Künzel, M. Noltemeyer, H.-G. Schmidt, H. W. Roesky, *Angew. Chem.* **1995**, *107*, 2954; *Angew. Chem. Int. Ed. Engl.* **1995**, *34*, 2645.
- [4] C. Rennekamp, A. Gouzyr, A. Klemp, H. W. Roesky, C. Brönneke, J. Kärcher, R. Herbst-Irmer, *Angew. Chem.* **1997**, *109*, 413; *Angew. Chem. Int. Ed. Engl.* **1997**, *36*, 404.
- [5] R. Murugavel, A. Voigt, M. G. Walawalkar, H. W. Roesky, *Chem. Rev.* **1996**, *96*, 2205.
- [6] M. Rivière-Baudet, A. Morère, *J. Organomet. Chem.* **1992**, *423*, C5.
- [7] a) J. Emsley, *Chem. Soc. Rev.* **1980**, *9*, 91; b) G. R. Desiraju, *Angew. Chem.* **1995**, *107*, 2541; *Angew. Chem. Int. Ed. Engl.* **1995**, *34*, 2328.
- [8] M. Veith, E. Werle, V. Huch, *Z. Anorg. Allg. Chem.* **1993**, *619*, 641.
- [9] C. George, A. P. Purdy, *Acta Crystallogr. Sect. C* **1996**, *52*, 2489.
- [10] M. Veith, A. Rammo, *Z. Anorg. Allg. Chem.* **1997**, *623*, 861.
- [11] Crystal structure analysis of **2**: C₃₀H₆₁Ge₂N₇Si₂, *M_r* = 721.22, triclinic, space group *P* $\bar{1}$, *a* = 1035.0(2), *b* = 1264.3(3), *c* = 1556.7(3) pm, α = 101.59(3), β = 90.86(3), γ = 109.39(3)°, *V* = 1.8749(6) nm³, *Z* = 2, ρ_{calcd} = 1.278 Mg m^{–3}, *F*(000) = 764, λ = 71.073 pm, *T* = 173(2) K, absorption coefficient 1.696 mm^{–1}. Crystal size: 0.40 × 0.30 × 0.30 mm³, measured θ region 2.09–25.99°; of 26875 reflections measured, 6810 were independent (*R*_{int} = 0.1052); 62 restraints, 408 refined parameters, *R* values [*I* > 2σ(*I*)] : *R*1 = 0.0290, *wR*2 = 0.0741, *R* values (for all data): *R*1 = 0.0354, *wR*2 = 0.0764; weighting scheme *w* = 1/[σ²(*F*_o²) + (0.0560 *P*)²] with *P* = (max(*F*_o², 0) + 2 *F*_c²)/3; max./min. residual electron density: 559/–734 e nm^{–3}. All non-hydrogen atoms were refined anisotropically. The hydrogen atoms on N2, N3, N5, and N6 (H21, H22, H31, H32, H51, H52, H61, and H62) were localized by difference Fourier syntheses and freely refined using distance restraints. The ideal geometrical positions of all the other hydrogen atoms were calculated and refined using a riding model. Crystallographic data (excluding structure factors) for the structure reported in this paper have been deposited with the Cambridge Crystallographic Data Centre as supplementary publication no. CCDC-103202. Copies of the data can be obtained free of charge on application to CCDC, 12 Union Road, Cambridge CB2 1EZ, UK (fax: (+44) 1223-336-033; e-mail: deposit@ccdc.cam.ac.uk).

Ag₂Cu₂O₃: The First Silver Copper Oxide**

Pedro Gómez-Romero,* Eva M. Tejada-Rosales, and M. Rosa Palacín

Among cuprate superconductors the highest critical temperatures T_c are shown by mercury-containing derivatives.^[1–3] These complex oxides are superior to thallium-based superconductors, which in turn were an improvement over the family of bismuth superconductors. This heavy metal trend shows an undesired but tenacious presence of toxic metals in superconducting materials,^[4] and continuing efforts to design and prepare more benign high- T_c superconductors have been made.

One of the most promising strategies in this sense was the substitution of silver for mercury. The ions Ag^I and Hg^{II} show similar crystal chemistry, have comparable ionic radii, and tend to occupy linear coordination environments such as that found in the new mercury-based superconductors. Many attempts have been made in laboratories around the world to prepare layered oxides related to those in the mercury family, but containing silver. For this purpose, solid-state reactions under high pressures of oxygen have generally been used owing to the low thermal stability of silver oxides.^[5] This approach has not led to the isolation of a silver copper oxide, although a new series of copper/carbonate superconductors prepared under high pressure was discovered.^[6, 7]

As a first step into the investigation of the crystal chemistry of complex silver copper oxides, we considered the synthesis and study of simple ternary oxides. Several database searches failed to show any precedent of such an oxide, natural nor synthetic.^[8] Consequently we decided to tackle this problem as a basic aspect of fundamental chemical interest as well as of potential application in the chemistry of cuprate superconductors.

As an alternative to methods with high oxygen pressures, we concentrated on the use of low temperatures for the synthesis of the new oxide in order to avoid the anticipated decomposition problems. In addition to the common Ag₂O and CuO, several silver oxides^[9–11] and copper oxides^[12–14] have been obtained by electrochemical deposition from aqueous solutions or molten hydroxides fluxes. The electrochemical potential is a tool for controlling the oxidation state.^[11, 13] We have used basic aqueous media or molten hydroxide fluxes to precipitate the precursor to the new oxide Ag₂Cu₂O₃ (see the Experimental Section); the application of electrochemical potential was not necessary for the isolation of this particular oxide.

Chemical and thermogravimetric analyses (TGA) indicated a formula of Ag₂Cu₂O₃ for the new compound (53.4 % Ag, 33.0 % Cu by atomic absorption; 12.3 % O by TGA; expected values for Ag₂Cu₂O₃: 55.2 % Ag, 32.5 % Cu, 12.3 % O). Furthermore, energy dispersive X-ray analyses (EDX) carried out in the analytical electron microscope (TEM) showed a constant ratio for Ag and Cu in all 20 microcrystals analyzed, which confirmed the isolation of a pure homogeneous phase. The thermal stability of this new oxide is enhanced with respect to that of Ag₂O or even CuO. Thus, TGA shows the decomposition of Ag₂Cu₂O₃ at 260 °C (inflection point of the weight loss), whereas a mixture of Ag₂O and CuO under the same experimental conditions presents the two corresponding decomposition processes at 100 and 225 °C, respectively. The reasons for this can be found in the structural features described below.

X-ray powder diffraction patterns were indexed in the tetragonal system ($a = 5.89$ Å, $c = 10.7$ Å), whereas electron diffraction studies allowed the reconstruction of the reciprocal lattice and the spotting of systematic absences which were unambiguously consistent with space group $I4_1/amd$. The structure of Ag₂Cu₂O₃ was refined by the Rietveld method (Figure 1) with the structure of the mineral paramelaconite

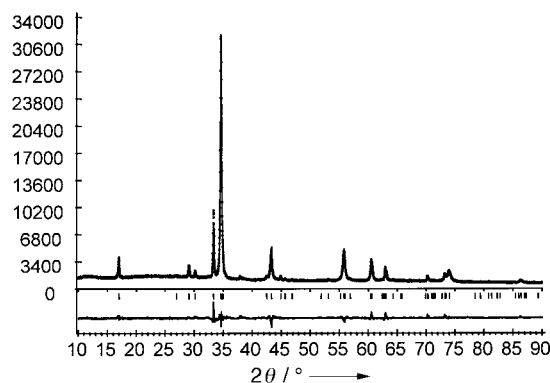


Figure 1. Powder X-ray diffraction pattern and Rietveld analysis for Ag₂Cu₂O₃. The dots correspond to experimental data, the continuous line is the calculated profile, and the bottom line represents the difference between the two. The small vertical lines mark the positions of allowed Bragg reflections.

(Cu₄O₃) as a starting model.^[15] The structure of Ag₂Cu₂O₃ consists of alternating chains of edge-sharing square-planar CuO₄ units and zigzag chains of AgO₂ units with linearly coordinated silver ions. These chains run parallel to a and b consecutively as we move along the c direction (Figure 2). This structure is related to that of PdO, although in Ag₂Cu₂O₃ silver is linearly coordinated and the alternation of Cu and Ag leads to a doubling of the unit cell in all three directions of space. The coordination of the metals is typical of Cu^{II} and Ag^I, but there are several unique features. There are two nonequivalent oxygen atoms (O1, bonded to two Cu and two Ag atoms, and O2, bonded to four Cu atoms). The square-planar coordination of Cu^{II} suffers a concurrent rhombic distortion with a short Cu–O1 bond and a longer Cu–O2 bond. The Ag–O1 bond (2.13(1) Å) is correspondingly longer than those found in silver oxides with analogous linear

[*] Dr. P. Gómez-Romero, E. M. Tejada-Rosales, M. R. Palacín
Institut de Ciència de Materials de Barcelona (CSIC)
Campus de la UAB, E-08193 Bellaterra, Barcelona (Spain)
Fax: (+349) 93-5805729
E-mail: pedro.gomez@icmab.es

[**] This work was supported by CICYT (Spain; MAT96-1057-C02-01 and MAT98-0807-C02-02). We thank the Ministry of Education and Culture (Spain) for a predoctoral fellowship awarded to E.M.T.-R.

Supporting information for this article is available on the WWW under <http://www.wiley-vch.de/home/angewandte/> or from the author.

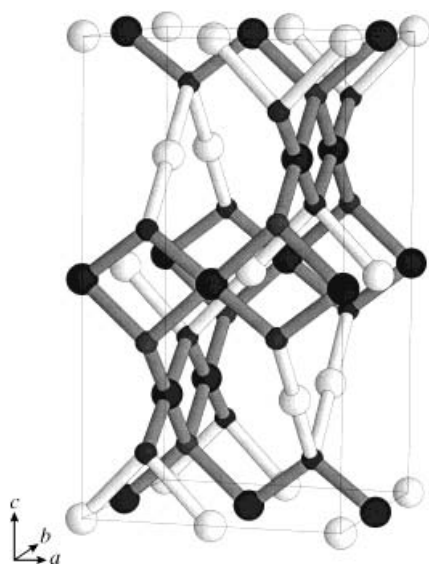


Figure 2. Crystal structure of $\text{Ag}_2\text{Cu}_2\text{O}_3$ (Ag^{I} : white spheres, Cu^{II} : large black spheres, O: small black spheres). Hexagonal tunnels running parallel to a and b are interconnected through tetrahedral vacant oxygen sites at $(0, 3/4, 1/8)$. Bond distances [\AA] and angles [$^\circ$] (O1 is bonded to two Cu and two Ag atoms, and O2 to four Cu atoms): Ag–O1 2.13(1), Cu–O1 1.858(8), Cu–O2 1.9874(1), $\text{M}\cdots\text{M}=\text{M}\cdots\text{M}'$ 2.9429(2), 3.3865(1); O1–Cu–O2 100.1(3), 79.9(6), Ag–O1–Ag 87.5(4), Cu–O1–Cu 104.7(4), Cu–O2–Cu 116.860(8), 95.530(8), Ag–O1–Cu 116.2(4).

coordination (2.02–2.04 \AA). The displacement of O1 towards Cu^{II} and away from Ag^{I} is easy to understand from a simple ionic point of view and explains the thermal stabilization of $\text{Ag}_2\text{Cu}_2\text{O}_3$ mentioned above.

The remarkable structure of $\text{Ag}_2\text{Cu}_2\text{O}_3$ presents a three-dimensional array of tunnels (parallel to a and b) with a minimum dimension corresponding to the $\text{Ag}\cdots\text{Cu}$ separation of 2.9429(2) \AA ($a/2$). As in $\text{YBa}_2\text{Cu}_3\text{O}_6$, these metal-constrained tunnels could be most adequate for the diffusion of oxygen species. The tunnels lead directly to vacant oxygen sites, which could possibly be occupied with concomitant oxidation of Ag^{I} (linear) to Ag^{III} (square planar). Similarly, the structure could easily stand the elimination of one oxygen atom (O2) with the simultaneous reduction of Cu^{II} (square planar) to Cu^{I} (linear). This rich solid-state redox crystal chemistry should lead to a very interesting electroactive phase. Indeed, preliminary cyclic voltammograms of this novel phase confirm this potential.

On the other hand, the efficient low-temperature route to $\text{Ag}_2\text{Cu}_2\text{O}_3$ shows the way for preparing many other silver-containing cuprates of increasing complexity. In combination with the electrochemical control of oxidation states, the low-temperature synthesis and crystallization approach represents a serious alternative to the high-temperature, high-pressure search for silver-based superconductors.

Experimental Section

$\text{Ag}_2\text{Cu}_2\text{O}_3$: $\text{Cu}(\text{NO}_3)_2 \cdot 3\text{H}_2\text{O}$ (0.77 g, 3.2 mmol; Merck, p.a. 99.5%) and AgNO_3 (0.52 g, 3.1 mmol; Panreac, p.a. 99.98%) were dissolved in deionized water (2 mL). An aqueous solution of 3 M NaOH (4 mL) was added with stirring. The very dark green precipitate formed was isolated by filtration under vacuum and washed with water until the pH value of the filtrate was neutral. This solid precursor of unknown structure was heated in air at 90 $^\circ\text{C}$ for 24 hours to yield the black oxide $\text{Ag}_2\text{Cu}_2\text{O}_3$ quantitatively.

Collection of powder X-ray data: $10 < 2\theta < 90^\circ$, step 0.02° , $\text{Cu}_{\text{K}\alpha}$ radiation ($\lambda = 1.5418 \text{ \AA}$). Refined profile parameters: scale factor $1.155(7) \times 10^{-5}$, zero point $-0.185(2)$, $U = 0.87(4)$, $V = -0.20(3)$, $W = 0.037(5)$; η (pseudo-Voigt peak shape parameter) = 0.64(1). Crystal structure analysis of $\text{Ag}_2\text{Cu}_2\text{O}_3$: tetragonal, $a = 5.8857(3)$, $c = 10.6868(7) \text{ \AA}$, space group $I4_1/amd$, origin choice 2, $Z = 4$; atom (site; fractional coordinates; B_{iso} ; occupancy): Ag (8c; 0,0,0; 3.01(7); 2), Cu (8d; 0,0,0.5; 2.7(1); 2), O1 (8e; 0,0.25,0.144(1); 2.2(6); 2), O2 (4b; 0,0.25,0.375; 1.0(8); 1). $R = 0.0391$, $R_{\text{wp}} = 0.0561$, $R_{\text{expected}} = 0.0267$, $\chi^2 = 4.41$.

Received: August 5, 1998 [Z 12258 IE]

German version: *Angew. Chem.* **1999**, *111*, 544–546

Keywords: copper • oxygen • silver • solid-state structures • superconductors

- [1] S. N. Putilin, E. V. Antipov, O. Chmaissem, M. Marezio, *Nature* **1993**, *362*, 226–228.
- [2] A. Schilling, M. Cantoni, J. D. Guo, H. R. Ott, *Nature* **1993**, *363*, 56–58.
- [3] A. Tokiwa-Yamamoto, K. Isawa, M. Itoh, S. Adachi, H. Yamauchi, *Physica C* **1993**, *216*, 250–256.
- [4] R. J. Cava, *Nature* **1993**, *362*, 204–205.
- [5] N. N. Greenwood, A. Earnshaw, *Chemistry of the Elements*, University Press, Cambridge, **1984**, p. 1373.
- [6] M. A. Alario-Franco, *Adv. Mater.* **1995**, *7*, 229–232.
- [7] a) M. A. Alario-Franco, C. Chaillout, J. J. Capponi, J.-L. Tholence, B. Souletie, *Physica C* **1994**, *222*, 52–56; b) M. A. Alario-Franco, P. Bordett, J.-J. Capponi, C. Chaillout, J. Chenavas, T. Fournier, M. Marezio, B. Souletie, A. Sulpice, J.-L. Tholence, C. Colliex, R. Argoud, J. L. Balonardo, M. F. Gorius, M. Perroux, *Physica C* **1994**, *231*, 103–108.
- [8] We could find a few examples of minerals that are Ag–Cu sulfides or halides, but none of oxides.
- [9] B. Standke, M. Jansen, *Angew. Chem.* **1986**, *98*, 78–79; *Angew. Chem. Int. Ed. Engl.* **1986**, *25*, 77–78.
- [10] B. Standke, M. Jansen, *J. Solid State Chem.* **1987**, *67*, 278–284.
- [11] P. Fischer, M. Jansen, *Solid State Ionics* **1990**, *43*, 61–67.
- [12] W. K. Ham, G. F. Holland, A. M. Stacy, *J. Am. Chem. Soc.* **1988**, *110*, 5214–5215.
- [13] T. L. Friedman, A. M. Stacy, *J. Solid State Chem.* **1994**, *109*, 203–204.
- [14] S. W. Keller, V. A. Carlson, D. Sandford, F. Stenzel, A. M. Stacy, G. H. Kwei, M. Alario-Franco, *J. Am. Chem. Soc.* **1994**, *116*, 8070–8076.
- [15] M. O'Keeffe, J.-O. Bovin, *Am. Mineral.* **1978**, *63*, 180–185.

A Self-Assembled Calix[4]arene Dimer Linked through Hydrogen-Bonded 2-Ureidopyrimidin-4(1H)-one Groups**

Juan J. González, Pilar Prados, and Javier de Mendoza*

The self-assembly of simple fragments to form structures with designed cavities and networks mediated by noncovalent, complementary interactions such as hydrogen bonding, hydrophobic interactions, and metal–ligand bonding is a

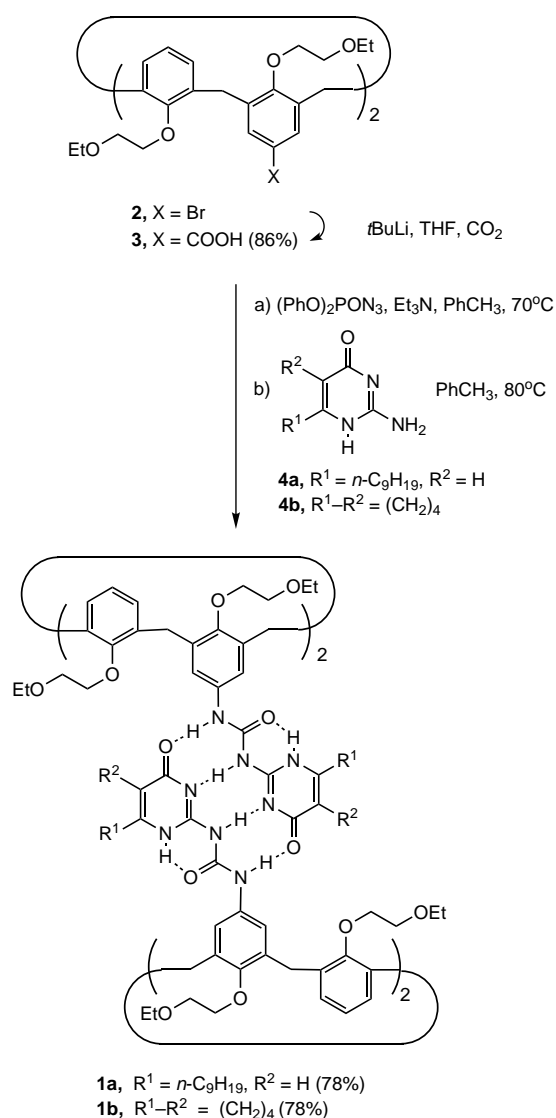
[*] Prof. Dr. J. de Mendoza, Dr. J. J. González, Prof. Dr. P. Prados
Departamento de Química Orgánica
Universidad Autónoma de Madrid
Cantoblanco, E-28049 Madrid (Spain)
Fax: (+349) 1-397-3966
E-mail: javier.demendoza@uam.es

[**] This work was supported by CICYT (project PB93-0283).

Supporting information for this article is available on the WWW under <http://www.wiley-vch.de/home/angewandte/> or from the author.

current major goal in supramolecular chemistry.^[1, 2] A number of calixarene derivatives have been shown to self-assemble through hydrogen bonding in apolar solvents.^[3] The dimerization of calix[4]arenes containing urea substituents at the upper rim has been extensively studied by Rebek et al. and Böhmer et al. independently.^[4] Molecules the size of benzene can be encapsulated in these dimers. However, for larger guests, several molecular platforms linked through a more robust network of hydrogen bonds are required to assure the self-assembly of a stable, multicomponent, cavity-containing host. Recently, Meijer et al. have described the dimerization of 6-substituted 2-ureidopyrimidin-4(1*H*)-ones (R^1 = alkyl or aryl, R^2 = H) mediated by a strong linear array of hydrogen bonds in a DDAA arrangement (D = donor, A = acceptor; $K_{\text{ass}} > 10^6 \text{ M}^{-1}$).^[5] We report here the synthesis of calix[4]arenes dimers **1a** and **1b** in which the calixarenes are in 1,3-*alternate* conformation and linked by eight hydrogen bonds between ureidopyrimidinonyl groups.^[6]

The synthesis of compounds **1a** and **1b** was straightforward (Scheme 1). The 1,3-*alternate* calix[4]arene dibromide **2**^[6b] was first readily transformed into the corresponding dicarboxylic



Scheme 1. Synthesis of **1a** and **1b**.

acid **3** by bromine/lithium exchange. Then, in a single, one-pot reaction **3** underwent a Curtius rearrangement with diphenylphosphoryl azide (DPPA),^[7] and the resulting bis-isocyanate was allowed to react in situ with the appropriate 2-aminopyrimidinone **4** to yield the corresponding ureidopyrimidinonyl calix[4]arenes as dimers **1a** and **1b** in 78% overall yield from **3**.

Dimers **1a** and **1b** are soluble in nonpolar solvents such as benzene and toluene but almost insoluble in DMSO and acetone at 30°C . The ^1H NMR spectrum of **1a** (CDCl_3) shows large downfield shifts for the urea NH protons at $\delta = 12.02$ and 11.95 , consistent with the four DDAA hydrogen bonds present in the dimer. The chelated NH group at position 1 gives rise to a signal at $\delta = 13.37$. None of these signals shift upon dilution (up to 10^{-4} M), a good indication of a strong association ($K_{\text{ass}} > 10^6 \text{ M}^{-1}$). Two independent signals are clearly observed for the protons of the substituted arene rings at $\delta = 6.97$ and 7.80 as a consequence of the hindered rotation about the calixarene-urea C-N bond. A similar phenomenon has been described for calix[4]arene tetraurea dimers.^[4]

Similar results were obtained for **1b** (signals at $\delta = 13.23$, 12.10 , 11.89 , 7.84 , 7.05). In addition, a heterodimer slowly formed when a 1:1 mixture of **1a** and **1b** in CDCl_3 was kept at room temperature; this was supported by a new set of signals in the ^1H NMR spectrum ($\delta = 11.97$, 11.84 , 7.76 , 5.93).^[8]

Dimer **1a** was further studied in mixtures of CDCl_3 and $[\text{D}_6]\text{DMSO}$, a strong hydrogen-bond acceptor. Only at $\chi_{\text{DMSO}} \geq 0.5$ was the monomer observed by ^1H NMR spectroscopy; the NH protons gave rise to broad singlets centered at $\delta = 11.3$, 9.6 , and 9.1 ($\chi_{\text{DMSO}} = 0.88$). The monomer was the only species observed in pure $[\text{D}_6]\text{DMSO}$ at 373 K . The apparent constant of association (Figure 1 a) was determined

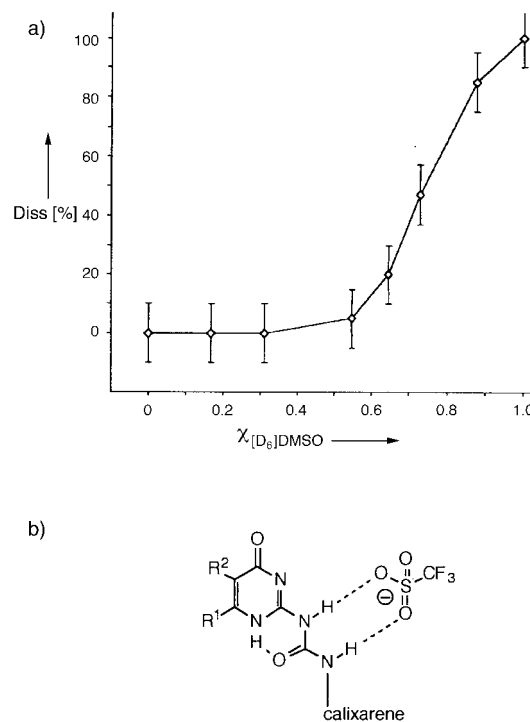


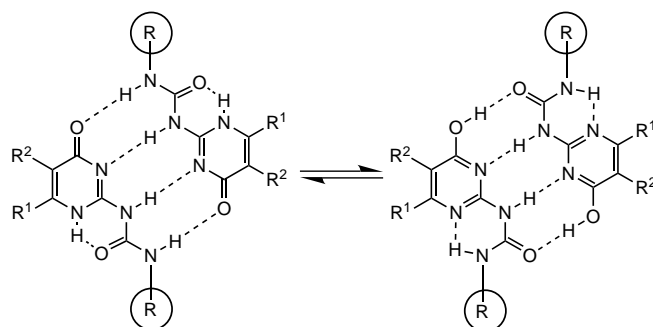
Figure 1. a) Plot of the extent of dissociation versus solvent composition for dimers of **1a** in $\text{CDCl}_3/[\text{D}_6]\text{DMSO}$ mixtures. The line connecting the data points does not reflect a mathematical function but only serves to guide the eye. b) The complex formed by monomer **1a** and a triflate ion.

by integration at $\chi_{\text{DMSO}} = 0.64$ ($K_{\text{ass}}^* = 2500 \pm 20 \text{ M}^{-1}$) and at $\chi_{\text{DMSO}} = 0.73$ ($K_{\text{ass}}^* = 572 \pm 20 \text{ M}^{-1}$).^[9] Another way to break the dimers was the addition of an oxoanion that could act as a strong competitor for the urea hydrogen donors. Thus, in the presence of a trifluoromethanesulfonate (triflate) salt, a less rigid triflate–monomer complex was apparent by NMR spectroscopy (Figure 1b).

Additional evidence for the dimeric structure of **1a** came from mass spectrometry and vapor pressure osmometry (VPO). In addition to a peak at m/z 1270 (100% rel. intensity), ascribable to the monomer (calculated mass = 1269), the positive-ion FAB mass spectrum of **1a** shows a sizeable peak at m/z 2539 (30%). An average molecular mass of 2535 ± 120 was determined by VPO in chloroform (30 °C, benzil as the standard). These values fully agree with the mass calculated for the proposed dimeric structure ($M_w = 2539$).

Similar results were obtained for the cyclohexane-annulated calix[4]arene dimer **1b**. The positive-ion FAB mass spectrum of **1b** shows a monomer peak at m/z 1126 (100%) and another for the dimer at m/z 2250 (6%). So far, only dimers from 2-ureidopyrimidinones without substituents at position 5 ($R^2 = \text{H}$) have been reported.^[5] Our results show that introduction of a substituent in this position (as in **1b**) does not affect the dimerization.

2-Ureidopyrimidin-4(1H)-ones are tautomeric structures in solution.^[5b] Equilibria are limited to the pyrimidin-4(1H)-one and pyrimidin-4-ol forms in the dimers (Scheme 2). The



Scheme 2. 2-Ureidopyrimidin-4(1H)-one tautomers.

pyrimidinone tautomer in which the terminal R residues attached to the ureas are almost perfectly aligned is highly favored over the pyrimidin-4-ol tautomer when R^1 is alkyl.^[5b] For calix[4]arene dimers **1a** and **1b** the pyrimidinone tautomer is also the only one observed by FT-IR spectroscopy (KBr, absence of a 2500 cm^{-1} band) and ROESY NMR experiments.^[10] An additional reason for this preference was found in the relative orientation of the terminal R groups attached to the ureas (see Scheme 2, $R = \text{calixarene}$): the residues are almost perfectly aligned in opposite directions in the pyrimidinone case but slightly shifted in the pyrimidin-4-ol tautomer. In the rigid calix[4]arene framework this would likely cause some torsional strain, as can be surmised by simple inspection of space-filling molecular models.

However, as the result of the two relative orientations of the flat hydrogen-bonded 2-ureidopyrimidinone surfaces, each dimer exists in two *syn*–*anti* isomeric forms. The

^1H NMR spectra in CDCl_3 indicate roughly a 5:1 ratio of isomers for each dimer (integration of peak areas), which slowly exchange at room temperature on the NMR time scale (Figure 2). Simple inspection of space-filling models shows

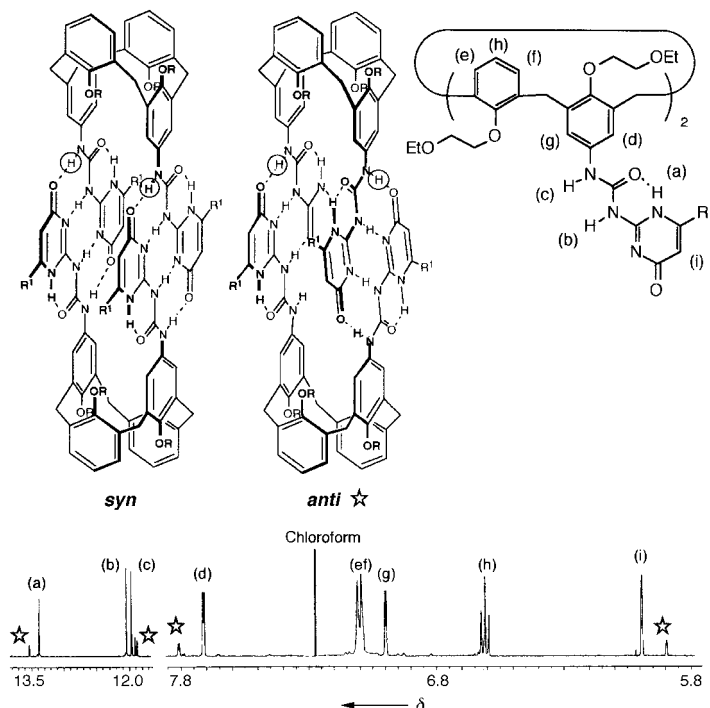


Figure 2. ^1H NMR spectrum (500 MHz, CDCl_3) of **1a** showing signals arising from the two *syn*–*anti* isomers. $R = \text{OCH}_2\text{CH}_2\text{OEt}$; $R^1 = n\text{-C}_9\text{H}_{19}$.

that the *anti* isomers are twisted and more strained than the corresponding *syn* isomers. Thus, a *syn* arrangement for the major component of these mixtures is likely.

We have shown that 2-ureido-4-pyrimidinone groups can be easily introduced on calixarene platforms. Bridging positions 5 and 6 with a cyclohexane unit does not perturb the calixarene dimerization. This opens up interesting perspectives in the design of more sophisticated self-assembled supramolecular structures.

Experimental Section

General procedure for the synthesis of 1a and 1b: To a suspension of **3** (270 mg, 0.34 mmol) and Et_3N (110 μL , 0.74 mmol) in toluene (5 mL) at 40 °C was added DPPA (160 μL , 0.74 mmol). The solution was stirred for 1 h at 40 °C and for 4 h at 80 °C. Then a suspension of **4** (1.35 mmol) in toluene (3 mL) was added, and the reaction mixture was heated for 16 h at 80 °C. The reaction mixture was concentrated to dryness and triturated with methanol to give **1**.

1a: 78% yield; (5:1 mixture of isomers); m.p. 212–214 °C; ^1H NMR (500 MHz, CDCl_3 , 25 °C): major isomer: $\delta = 13.37$ (s, 4H; NH), 12.02 (s, 4H; NH), 11.95 (s, 4H; NH), 7.70 (d, $^4J(\text{H,H}) = 2.4 \text{ Hz}$, 4H; ArH), 7.09 (d, $^3J(\text{H,H}) = 7.6 \text{ Hz}$, 8H; ArH), 6.98 (d, $^4J(\text{H,H}) = 2.4 \text{ Hz}$, 4H; ArH), 6.59 (t, $^3J(\text{H,H}) = 7.6 \text{ Hz}$, 4H; ArH), 5.96 (s, 4H; pyrimidinonyl (pyrim)), 4.31–4.00 (m, 16H; CH_2), 3.90–3.80 (m, 8H; CH_2), 3.74 (t, $^3J(\text{H,H}) = 4.5 \text{ Hz}$, 8H; CH_2), 3.69–3.56 (m, 20H; CH_2 , ArCH_2Ar), 3.56 (d, $^2J(\text{H,H}) = 12.7 \text{ Hz}$, 4H; ArCH_2Ar), 3.52 (d, $^2J(\text{H,H}) = 12.5 \text{ Hz}$, 4H; ArCH_2Ar), 3.41 (d, $^2J(\text{H,H}) = 12.5 \text{ Hz}$, 4H; ArCH_2Ar), 2.28 (m, 8H; CH_2), 1.60 (m, 8H; CH_2), 1.28 (t, $^3J(\text{H,H}) = 7.0 \text{ Hz}$, 12H; CH_3), 1.20 (t, $^3J(\text{H,H}) = 7.0 \text{ Hz}$, 12H; CH_3), 1.24–1.16 (m, 48H; CH_2), 0.87 (t, $^3J(\text{H,H}) = 6.5 \text{ Hz}$, 12H; CH_3); minor isomer (only signals different from those of the major isomer):

$\delta = 13.52$ (s, 4H; NH), 11.88 (s, 4H; NH), 11.86 (s, 4H; NH), 7.80 (d, $^4J(\text{H,H}) = 2.3$ Hz, 4H; ArH), 5.87 (s, 4H; pyrim); ^1H NMR (300 MHz, $[\text{D}_6]\text{DMSO}$, 100 °C): $\delta = 10.70$ – 10.00 (brs, 4H; NH), 9.40 (s, 2H; NH), 7.18 (s, 4H; ArH), 7.04 (d, $^3J(\text{H,H}) = 7.5$ Hz, 4H; ArH), 6.64 (t, $^3J(\text{H,H}) = 7.5$ Hz, 2H; ArH), 5.73 (s, 2H; pyrim), 3.80–3.30 (m, 32H; CH_2), 2.42 (t, $^3J(\text{H,H}) = 7.5$ Hz, 4H; CH_2), 1.63 (m, 4H; CH_2), 1.50–1.20 (m, 24H; CH_2), 1.17 (t, $^3J(\text{H,H}) = 7.0$ Hz, 6H; CH_3), 1.09 (t, $^3J(\text{H,H}) = 7.0$ Hz, 6H; CH_3), 0.85 (t, $^3J(\text{H,H}) = 7.0$ Hz, 6H; CH_3); ^{13}C NMR (75 MHz, CDCl_3 , 25 °C, Heteronuclear Multiple Quantum Correlation (HMQC)): major isomer: $\delta = 172.2$, 156.0 (CO), 155.1, 154.8, 152.1, 151.2, 133.3, 133.2, 133.1, 131.3 (ArC, pyrimC), 129.6, 129.5, 123.5, 122.6, 121.4 (ArCH), 105.2 (pyrimCH), 72.3, 72.1, 70.0, 69.7 ($\text{OCH}_2\text{CH}_2\text{O}$), 66.6, 66.1 (OCH_2CH_3), 34.1, 33.5 (ArCH_2Ar), 32.9, 31.8, 29.5, 29.3, 29.2, 29.1, 27.3, 22.6 (CH_2), 15.6, 15.3 (OCH_2CH_3), 14.1 (CH_3); IR (KBr): $\tilde{\nu} = 3357$, 1701, 1654, 1587, 1465, 1245 cm^{-1} ; positive-ion FAB MS (2-nitrophenyloctyl ether matrix): m/z (%): 2539 (30) $[2\text{M}+\text{H}]^+$, 1270 (100) $[\text{M}+\text{H}]^+$; elemental analysis calcd for $\text{C}_{72}\text{H}_{100}\text{N}_8\text{O}_{12}$ (%): C 68.11, H 7.94, N 8.83; found: C 67.77, H 8.28, N 8.68.

1b: 78% yield; (mixture of isomers in proportion 3:1): m.p. 264–266 °C; ^1H NMR (300 MHz, CDCl_3 , 25 °C): major isomer: $\delta = 13.23$ (s, 4H; NH), 12.10 (s, 4H; NH), 11.89 (s, 4H; NH), 7.84 (d, $^4J(\text{H,H}) = 2.3$ Hz, 4H; ArH), 7.15–7.05 (m, 8H; ArH), 7.05 (d, $^4J(\text{H,H}) = 2.3$ Hz, 4H; ArH), 6.60 (t, $^3J(\text{H,H}) = 7.0$ Hz, 4H; ArH), 4.20–3.40 (m, 64H; CH_2), 2.62–2.30 (m, 16H; CH_2), 1.78 (m, 16H; CH_2), 1.34 (t, $^3J(\text{H,H}) = 7.0$ Hz, 12H; CH_3), 1.19 (t, $^3J(\text{H,H}) = 7.0$ Hz, 12H; CH_3); minor isomer (only signals different from those of the major isomer): $\delta = 13.35$ (s, 4H; NH), 12.00 (s, 4H; NH), 11.96 (s, 4H; NH); ^{13}C NMR (75 MHz, CDCl_3 , 25 °C): major isomer: $\delta = 171.8$, 156.1 (CO), 155.0, 153.6, 152.0, 143.7, 133.7, 133.0 (multiple peaks), 131.9 (ArC, pyrimC), 129.7, 129.5, 123.1, 122.0, 121.3 (ArCH), 114.9 (pyrimCH), 72.2, 71.5, 70.0, 69.6 ($\text{OCH}_2\text{CH}_2\text{O}$), 66.6, 66.3 (OCH_2CH_3), 34.5, 33.9 (ArCH_2Ar), 26.7, 22.3, 21.7 (CH_2), 15.4, 15.3 (CH_3); minor isomer (only signals different from those of the major isomer): $\delta = 154.7$, 153.8, 143.3, 132.2 (ArC, pyrimC), 129.4, 129.2, 121.8, 121.5 (ArCH), 115.4 (pyrimCH), 72.3, 71.8 ($\text{OCH}_2\text{CH}_2\text{O}$), 66.4 (OCH_2CH_3), 34.1 (ArCH_2Ar), 22.0, 21.5 (CH_2), 15.7 (CH_3); IR (KBr): $\tilde{\nu} = 3337$, 1703, 1653, 1584, 1460, 1245 cm^{-1} ; positive-ion FAB-MS (*m*-nitrobenzyl alcohol matrix): m/z (%): 2250 (6) $[2\text{M}+\text{H}]^+$, 1126 (100) $[\text{M}+\text{H}]^+$.

Received: September 7, 1998 [Z12391IE]
German version: *Angew. Chem.* **1999**, *111*, 546–549

Keywords: calixarenes • hydrogen bonds • self-assembly • supramolecular chemistry

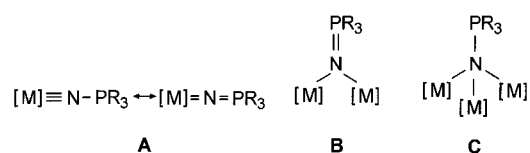
- [1] For review articles, see: a) D. Philp, J. F. Stoddart, *Angew. Chem.* **1996**, *108*, 1242–1286; *Angew. Chem. Int. Ed. Engl.* **1996**, *35*, 1154–1196; b) M. M. Conn, J. Rebek, Jr., *Chem. Rev.* **1997**, *97*, 1647–1668; c) J. de Mendoza, *Chem. Eur. J.* **1998**, *4*, 1373–1377.
- [2] For designs based on metal coordination, see: P. J. Stang, *Chem. Eur. J.* **1998**, *4*, 19–27.
- [3] a) K. Koh, K. Araki, S. Shinkai, *Tetrahedron Lett.* **1994**, *35*, 8255–8258; b) R. H. Vreekamp, W. Verboom, D. N. Reinhoudt, *J. Org. Chem.* **1996**, *61*, 4282–4288; c) A. Arduini, L. Domiano, L. Ogliosi, A. Pochini, A. Secchi, R. Ungaro, *J. Org. Chem.* **1997**, *62*, 7866–7868.
- [4] a) K. D. Shimizu, J. Rebek, Jr., *Proc. Natl. Acad. Sci. USA* **1995**, *92*, 12403–12407; b) B. C. Hamann, K. D. Shimizu, J. Rebek, Jr., *Angew. Chem.* **1996**, *108*, 1425–1427; *Angew. Chem. Int. Ed. Engl.* **1996**, *35*, 1326–1329; c) R. K. Castellano, D. M. Rudkevich, J. Rebek, Jr., *J. Am. Chem. Soc.* **1996**, *118*, 10002–10003; d) O. Mogck, V. Böhmer, W. Vogt, *Tetrahedron* **1996**, *52*, 8489–8496; e) O. Mogck, E. F. Paulus, V. Böhmer, I. Thondorf, W. Vogt, *Chem. Commun.* **1996**, 2533–2534; f) O. Mogck, M. Pons, V. Böhmer, W. Vogt, *J. Am. Chem. Soc.* **1997**, *119*, 5706–5712; g) R. K. Castellano, J. Rebek, Jr., *J. Am. Chem. Soc.* **1998**, *120*, 3657–3663.
- [5] a) R. P. Sijbesma, F. H. Beijer, L. Brunsveld, B. J. B. Folmer, J. H. K. K. Hirschberg, R. F. M. Lange, J. K. L. Lowe, E. W. Meijer, *Science* **1997**, *278*, 1601–1604; b) F. H. Beijer, R. P. Sijbesma, H. Kooijman, A. L. Spek, E. W. Meijer, *J. Am. Chem. Soc.* **1998**, *120*, 6761–6769.
- [6] For covalently linked 1,3-*alternate* calix[4]arene dimers see: a) Z. Asfari, S. Wenger, J. Vicens, *Pure Appl. Chem.* **1995**, *67*, 1037–1043;

- b) J. A. Pérez-Adelmar, H. Abraham, C. Sánchez, K. Rissanen, P. Prados, J. de Mendoza, *Angew. Chem.* **1996**, *108*, 1088–1090; *Angew. Chem. Int. Ed. Engl.* **1996**, *35*, 1009–1011.
- [7] K. Ninomiya, T. Shioiri, S. Yamada, *Tetrahedron* **1974**, *30*, 2151–2157.
- [8] No heterodimers were observed, however, by addition of 6-*n*-nonyl-2-*n*-octylureidopyrimidin-4(1*H*)-one to **1a**.
- [9] The apparent association constant (K_{ass}^*) was determined from the integrals (*I*) of the signals of the pyrimidinyl proton in the monomer ($\delta = 5.6$) and dimer ($\delta = 5.9$) using the formula $K_{\text{ass}}^* = (1 - \alpha_{\text{diss}}) / 4c_0\alpha_{\text{diss}}^2$, where $\alpha_{\text{diss}} = I_{\text{monomer}} / (I_{\text{monomer}} + I_{\text{dimer}})$ and c_0 is the initial concentration of the dimer. Furthermore, the value of K_{ass}^* determined by integration of one signal of the calixarene unit in the monomer ($\delta = 6.6$, t) and dimer ($\delta = 6.5$, t) was on same order of magnitude.
- [10] NH signals were assigned by this experiment.

[Cu₁₂(NPET₃)₈]⁴⁺ and [Ag₁₂(NPET₃)₈]⁴⁺: Cubane Structures**

Ulrike Riese, Naim Faza, Werner Massa, and Kurt Dehnicke*

Phosphoraneiminato complexes of transition metals are known in a large variety of forms.^[1] The phosphoraneiminato ligands NPR_3^- that are isoelectronic with silanولات OSiR_3^- show great flexibility with regard to coordination chemistry aspects. The terminal bonding mode **A** is preferably realized with electron-deficient transition metals, while increasingly electron-rich transition metals form the μ -bridging type **B** or even the μ_3 -type **C**. With divalent transition metals of Mn, Fe, Co, Ni, Zn, and Cd type **C** leads to tetrameric complexes $[\text{XM}(\text{NPR}_3)]_4$ (X = halogen, organic residue) with M_4N_4

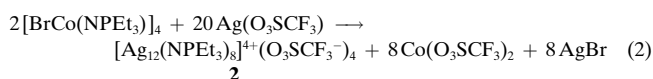
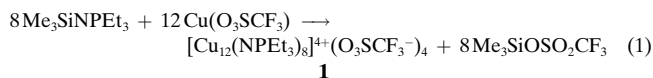


heterocubane structures. With Cu^I, Ag^I, and Au^I such an architecture cannot develop because of their tendency towards sp hybridization. In fact, the build-up of the phosphoraneiminato complexes of Au^I, $[\text{R}_3\text{PN}\{\text{Au}(\text{P}^{\text{R}}_3)\}_3]^{2+}$ (R = Ph, NMe₂), leads to coordination type **C** with linear axes N–Au–P'.^[2]

We have now found that reactions of the silylated phosphoraneimine $\text{Me}_3\text{SiNPET}_3$ with anhydrous copper(I) trifluoromethanesulfonate (triflate) [Eq. (1)] and of the heterocubane $[\text{BrCo}(\text{NPET}_3)]_4$ ^[3] with excess silver triflate [Eq. (2)] provide

[*] Prof. Dr. K. Dehnicke, Dr. U. Riese, Dr. N. Faza, Prof. Dr. W. Massa
Fachbereich Chemie der Universität
Hans-Meerwein-Strasse, D-35032 Marburg (Germany)
Fax: (+49) 6421-28-8917

[**] This work was supported by the Deutsche Forschungsgemeinschaft and by the Fonds der Chemischen Industrie.



access to a new type of phosphoraneiminato complexes with cubane structure. While reaction (2) proceeds in dichloromethane already at 20 °C, the synthesis of **1** according to Equation (1) requires the starting materials to be heated together at 190 °C. An exchange of the reagents $\text{Me}_3\text{SiNPET}_3$ and $[\text{BrCo}(\text{NPET}_3)_4]$ in the reactions (1) and (2) leads to a drastic loss in yield. Compounds **1** and **2** form colorless, light-sensitive crystals, which dissolve readily in dichloromethane and acetonitrile. According to the crystal structure analyses,^[4] the tetracations of **1** (with C_i symmetry) and of **2** (with C_{3i} symmetry) form almost perfect cubane structures of coordination type C, in which the metal atoms occupy the edges of the cube skeletons, while the N atoms of the phosphoraneiminato ligands occupy the corner positions (Figures 1 and 2). Thus, these tetracations of **1** and **2** display

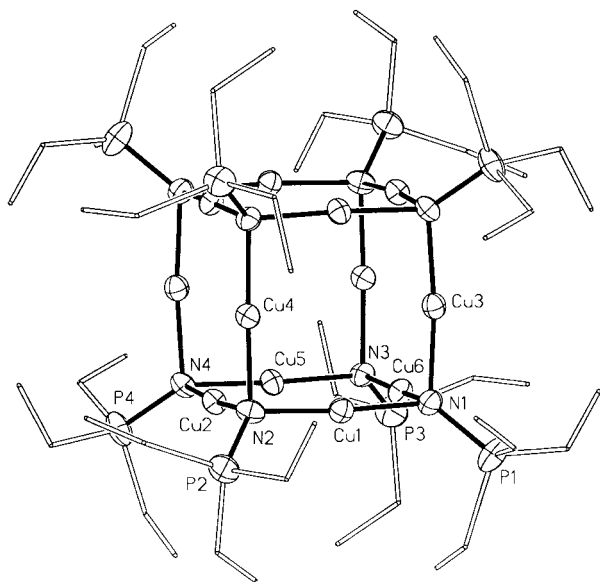


Figure 1. Structure of the cation $[\text{Cu}_{12}(\text{NPET}_3)_8]^{4+}$ of **1** in the crystal. In disordered ethyl groups only the more strongly occupied orientation is shown. Selected average bond lengths [pm] and angles [°] (the standard deviations correspond to those of the single values): Cu–N 188.0(7), Cu···Cu 274.6(1), P–N 161.7(6); N–Cu–N 174.5(3), Cu–N–Cu 94.1(3), Cu–N–P 122.5(4).

an inverted population of corners and edges by anions and cations in comparison with those “organometallic boxes” of the $[(\text{C}_5\text{Me}_4\text{Et})_8\text{Co}_4\text{Rh}_4(\text{CN})_{12}]^{4+}$ type recently described,^[5] in which the eight metal atoms occupy the corners and the twelve cyanide ions occupy the edges of the cube skeletons. Up to now, such an inverted population has been known only with the topologically related tetraanions $[\text{Cu}_{12}\text{S}_8]^{4-}$ ^[6] and $[\text{Au}_{12}\text{S}_8]^{4-}$.^[7]

The Cu_{12}N_8 skeleton of **1** can be considered as a molecular section of the structure of the copper nitride Cu_3N ,^[8] in which the ReO_3 lattice type is realized with an inverted population of corners and edges. The Cu–N distances in Cu_3N (191 pm)

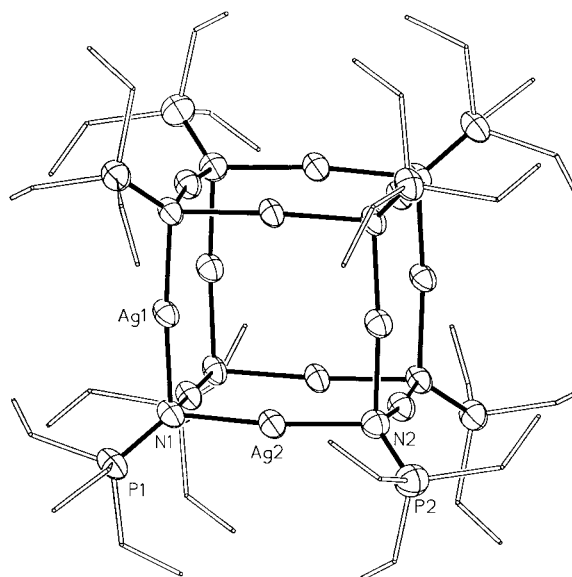


Figure 2. Structure of a cation $[\text{Ag}_{12}(\text{NPET}_3)_8]^{4+}$ of **2** in the crystal. Selected average bond lengths [pm] and angles [°] (the standard deviations correspond to those of the single values): Ag–N 208.8(5), Ag···Ag 306.8(1), P–N 159.1(6); N–Ag–N 173.4(3), Ag–N–Ag 94.7(3), Ag–N–P 122.0(3).

are also comparable to the mean value in **1** (188.0 pm); the shortening of the Cu–N distance is due to the tetrapositive charge of **1**. The metal atoms in **1** and **2** deviate only slightly from linearity, showing mean values of the internal angles of 174.3° for Cu and of 173.4° for Ag. The M–N–M bond angles, on the other hand, (93.4° in **1** and 94.5° in **2**) are greater than 90°, therefore the “boxes” are a bit convexed. In Cu_3N , too, the N–Cu–N axes are not exactly linear, due to a slight tilting of the NCu_6 octahedra; the bond angles are 173° at 21 °C and 176° at –143 °C.^[8] Considering the van der Waals radii, **1** only offers a cavity which is 269 pm in free diameter, **2** one of 266 pm; these are too small to take in guest molecules.

The square faces of the cubanes **1** and **2** represent structural elements akin to those in the tetrameric molecular complexes $[\text{M}(\text{amide})_4]$ of copper(II)^[9a–f] and silver(II)^[10] with a planar M_4N_4 skeleton. Analogous building units are also found in the tetrameric ketimine complexes of copper(II),^[9g] and—with a planar Cu_4O_4 skeleton—in siloxy complexes $[\text{CuOSiR}_3]_4$.^[9h,i] In these compounds the Cu···Cu and the Ag···Ag distances are all somewhat shorter than in **1** (av 274.6 pm) and in **2** (av 306.8 pm) because the metal atoms are deflected towards the M_4N_4 ring center; therefore, bonding metal–metal interactions have been assumed time and again.^[9, 10] But according to results of recent density functional theory calculations, not even $\text{Cu}^I\cdots\text{Cu}^I$ distances of only 238 pm can be assumed to signify Cu–Cu bonds.^[11]

The ^{109}Ag NMR spectrum^[12] of **2** in CD_3CN solution shows only one signal at $\delta = 1106$, consistent with the solid-state structure. Compared with the spectrum of a 3.0 M silver triflate solution in CD_3CN ($\delta = 503$),^[13] this signal is shifted downfield in accord with strong deshielding; this can be explained by the neighborhood of the phosphorus atoms—the positive nature of which is increased—of the NPET_3^- groups. Similarly strong deshielding has recently been observed in the ^{109}Ag NMR spectrum of the imidazolate (im) complex $[\text{Ag}(\text{im})(\text{PPh}_3)_3]$

with $\delta = 1186$.^[14] The phosphonium character of the P atoms in **1** and **2** is also reflected in the downfield position in the ³¹P NMR spectra, in which a singlet occurs at $\delta = 64.0$ for **1** and at $\delta = 66.0$ for **2**, and lies close to the signal positions in the ³¹P NMR spectra of tri(phosphorano)borazinium ions^[17] with extremely deshielded phosphorus nuclei.

Experimental Section

1: A mixture of anhydrous copper(II) trifluoromethanesulfonate^[20] (2.90 g, 13.6 mmol) and trimethylsilyltriethylphosphaneimine^[21] (8.00 mL, 36.2 mmol) was heated slowly to 190 °C and maintained at this temperature for 4 h. During this time, emerging trimethylsilyltriflate was continuously distilled off with a Vigreux column. After cooling the mixture, excess Me₃SiNPEt₃ was rinsed out with dichloromethane (3 × 5 mL), the residue washed with *n*-hexane (2 × 4 mL) and dried in vacuo. Yield 1.69 g (62 %); elemental analysis calcd for C₅₂H₁₂₀Cu₁₂F₁₂N₈O₁₂P₈S₄ (%): C 25.85, H 5.01, N 4.64; found: C 25.61, H 5.04, N 4.64. Single crystals of **1** · 2H₂O were obtained by cooling and leaving a saturated solution of **1** in acetonitrile/dichloromethane (1:3) at 8 °C. ¹H NMR (500 MHz, CD₃CN): $\delta = 1.29$ (dt, ³J(H,H) = 7.7, ³J(H,P) = 18 Hz, 72H; CH₃), 1.87 (dq, ³J(H,H) = 7.7, ²J(H,P) = 11 Hz, 48H; CH₂); ¹³C NMR (126 MHz, CD₃CN): $\delta = 7.0$ (d, ²J(C,P) = 4.3 Hz; CH₃), 23.4 (d, ¹J(C,P) = 62 Hz; CH₂).

2: A solution of [CoBr(NPEt₃)₃]^[3] (2.04 g, 1.88 mmol) in dichloromethane (10 mL) was added dropwise under stirring at 20 °C to a suspension of silver(II) trifluoromethanesulfonate (Merck) (4.95 g, 19.3 mmol) in dichloromethane (15 mL). After having been stirred for 5 d, the charge was filtered, the residue washed with dichloromethane (2 × 5 mL), and the collected filtrates were evaporated in vacuo to 5 mL. Addition of *n*-hexane (5 mL) led to a white precipitate, which was filtered, washed with *n*-hexane, and dried in vacuo. Yield 1.10 g (40 %). Elemental analysis calcd for C₅₂H₁₂₀Ag₁₂F₁₂N₈O₁₂P₈S₄ (%): C 21.19, H 4.10, N 3.80; found: C 21.10, H 4.02, N 4.02. Single crystals of **2** · CH₂Cl₂ · CH₃CN were obtained by leaving an oversaturated solution of **2** in dichloromethane/acetonitrile (30:1) at 20 °C. ¹H NMR (500 MHz, CD₂Cl₂): $\delta = 1.29$ (dt, ³J(H,H) = 7.7, ³J(H,P) = 17 Hz, 72H; CH₃), 1.86 (dq, ³J(H,H) = 7.7, ²J(H,P) = 11 Hz, 48H; CH₂); ¹³C NMR (126 MHz, CD₂Cl₂): $\delta = 6.6$ (d, ²J(C,P) = 4.8 Hz, CH₃), 23.5 (d, ¹J(C,P) = 63 Hz, CH₂).

Received: October 2, 1998 [Z 12481 IE]
German version: *Angew. Chem.* **1999**, *111*, 549–551

Keywords: cage compounds • copper • N ligands • silver

- Reviews: K. Dehnicke, J. Strähle, *Polyhedron* **1989**, *8*, 707; K. Dehnicke, M. Krieger, W. Massa, *Coord. Chem. Rev.* **1998**, in press.
- A. Bauer, F. P. Gabbaï, A. Schier, H. Schmidbaur, *Phil. Trans. R. Soc. Lond.* **1996**, A354, 381; A. Bauer, N. W. Mitzel, A. Schier, D. W. H. Rankin, H. Schmidbaur, *Chem. Ber.* **1997**, *130*, 323.
- U. Riese, K. Harms, B. Neumüller, K. Dehnicke, *Z. Anorg. Allg. Chem.* **1998**, *624*, 1279.
- Crystal structure determination of **1** · 2H₂O: C₅₂H₁₂₄Cu₁₂F₁₂N₈O₁₄P₈S₄, area detector system (IPDS, Stoe) MoK α radiation, graphite monochromator. Space group *P* $\bar{1}$, *a* = 1355.7(2), *b* = 1358.1(2), *c* = 1490.1(3) pm, $\alpha = 106.90(2)$, $\beta = 113.79(1)$, $\gamma = 94.45(2)^\circ$, *V* = 2341.8(7) Å³, *Z* = 1, $\rho_{\text{calcd}} = 1.739$ g cm⁻³, *T* = 243(2) K. Of 21154 reflections collected, 7741 were independent (*R*_{int} = 0.1028) and 5104 with *I* > 2σ(*I*), direct methods, refinement against *F*², semiempirical absorption correction, $\mu(\text{MoK}\alpha) = 29.67$ cm⁻¹, H atoms in calculated positions, 545 parameters, *R* = 0.0663, *wR*₂ (all data) = 0.1906. Calculations performed with: Stoe IPDS software, SHELXS-97, SHELXL-97, SHELXTL. The asymmetric unit of the structure holds half a cation, two triflate anions, and one molecule of water of crystallization. In the cation five of the twelve independent ethyl residues are disordered. They were treated with split atom refinement. One of the triflate ions and the water molecule show high and strongly anisotropic displacement parameters, which point to either disorder or strong motion. Attempts to collect data at lower temperatures

failed because of the reduction of the crystal quality probably caused by a phase transition. Crystal structure determination of **2** · CH₂Cl₂ · CH₃CN: C₅₅H₁₂₅Ag₁₂Cl₂F₁₂N₉O₁₂P₈S₄, Siemens P4 four-circle diffractometer, MoK α radiation, graphite monochromator. Space group *R* $\bar{3}$, *a* = *b* = 1554.9(1), *c* = 4071.1(1) pm, *V* = 8524.1(8) Å³, *Z* = 3, $\rho_{\text{calcd}} = 1.796$ g cm⁻³, *T* = 223(2) K. Of 4079 reflections collected, 3339 were independent (*R*_{int} = 0.0413) and 2232 with *I* > 2σ(*I*), Patterson method, refinement against *F*², numerical absorption correction, $\mu(\text{MoK}\alpha) = 23.73$ cm⁻¹, H atoms in calculated positions. Calculations performed with: SHELXS-96, SHELXL-96, SHELXTL. Here, the asymmetric unit is built-up from the sixth of a cation which is completed to form a cubane by C_{3i} symmetry. Here, too, one of the four independent ethyl groups is disordered. Two triflate anions per cubane unit are located on C₃ axes, two further triflate anions are disordered in general positions along with CH₂Cl₂, additionally, one CH₃CN molecule is situated with a sixfold orientation disorder on a C_{3i} position. *R* values of *wR*₂ = 0.188 and *R* = 0.062 were obtained with appropriate disorder models. Because of the less than satisfactory possibility of describing these complicated conditions of disorder in a split atom model, the influence of the range of the disordered groups (two triflate anions, CH₂Cl₂, CH₃CN) on the structure factors was calculated by way of Back-Fourier transformation^[18, 19] and subtracted from the data set. Thereafter, the core structure was refined with 130 parameters to give *wR*₂ = 0.128 and *R* = 0.0476, and the standard deviations were improved by approximately 1/3. The geometrical parameters discussed here refer to this refinement. Both the results of refinement have been deposited. Crystallographic data (excluding structure factors) for the structures reported in this paper have been deposited with the Cambridge Crystallographic Data Centre as supplementary publications no. CCDC-103252 (**1**) and CCDC-103254 (**2**, Back-Fourier transformation), and CCDC-103253 (disorder model). Copies of the data can be obtained free of charge on application to CCDC, 12 Union Road, Cambridge CB2 1EZ, UK (fax: (+44) 1223-336-033; e-mail: deposit@ccdc.cam.ac.uk).

- K. K. Klausmeyer, T. B. Rauchfuss, S. R. Wilson, *Angew. Chem.* **1998**, *110*, 1808; *Angew. Chem. Int. Ed.* **1998**, *37*, 1694.
- P. Betz, B. Krebs, G. Henkel, *Angew. Chem.* **1984**, *96*, 293; *Angew. Chem. Int. Ed. Engl.* **1984**, *23*, 311.
- G. Marbach, J. Strähle, *Angew. Chem.* **1984**, *96*, 695; *Angew. Chem. Int. Ed. Engl.* **1984**, *23*, 715.
- U. Zachwieja, H. Jacobs, *J. Less-Common Met.* **1990**, *161*, 175.
- a) S. Gambarotta, M. Bracci, C. Floriani, A. Chiesi-Villa, C. Guastini, *J. Chem. Soc. Dalton Trans.* **1987**, 1883; b) P. Miele, J. D. Foulon, N. Hovnanian, J. Durand, L. Cot, *Eur. J. Solid State Inorg. Chem.* **1992**, *29*, 573; c) H. Chen, M. M. Olmstead, S. C. Shoner, P. P. Power, *J. Chem. Soc. Dalton Trans.* **1992**, 451; d) M. Veith, K. L. Woll, *Chem. Ber.* **1993**, *126*, 2383; e) D. Barr, A. J. Edwards, S. Pullen, M. A. Paver, P. R. Raithby, M.-A. Rennie, C. A. Russell, D. S. Wright, *Angew. Chem.* **1994**, *106*, 1960; *Angew. Chem. Int. Ed. Engl.* **1994**, *33*, 1875; f) A. M. James, R. K. Laxman, F. R. Fronczek, A. W. Maverick, *Inorg. Chem.* **1998**, *37*, 3785; g) M. K. Davies, P. R. Raithby, M.-A. Rennie, A. Steiner, D. S. Wright, *J. Chem. Soc. Dalton Trans.* **1995**, 2707; h) M. J. McGeary, R. C. Wedlich, P. S. Coan, K. Folting, K. G. Caulton, *Polyhedron* **1992**, *11*, 2459; i) K. W. Terry, C. G. Lugmair, P. K. Gantzel, T. D. Tilley, *J. Chem. Mater.* **1996**, *8*, 274.
- P. B. Hitchcock, M. F. Lappert, L. J.-M. Pierrssens, *Chem. Commun.* **1996**, 1189; M. A. Beswick, N. L. Cromhout, C. N. Harmer, M. A. Paver, P. R. Raithby, M.-A. Rennie, A. Steiner, D. S. Wright, *Inorg. Chem.* **1997**, *36*, 1740.
- F. A. Cotton, X. Feng, D. J. Timmons, *Inorg. Chem.* **1998**, *37*, 4066.
- A 0.25 M solution in CD₃CN equivalent to a silver ionic concentration of 3.0 mol L⁻¹, 18.6 MHz, 25 °C, external standard saturated solution of AgClO₄ in D₂O.
- Judging the chemical shifts in the NMR spectra of silver salts in acetonitrile and other N-donor molecules, however, one has to consider their dependence on contact-ion pairs of the solvated silver ions such as [Ag(NCCH₃)₂]⁺ with their anions.^[15, 16] Thus, for example, the chemical shift of a 3.0 M AgNO₃ solution in acetonitrile is 380 ppm.^[16]
- K. Nomiya, K. Tsuda, N. C. Kasuga, *J. Chem. Soc. Dalton Trans.* **1998**, 1653.
- K. Jucker, W. Sahm, A. Schwenk, *Z. Naturforsch. A* **1976**, *31*, 1532.

- [16] A. K. Rahimi, A. I. Popov, *Inorg. Nucl. Chem. Lett.* **1976**, 12, 703.
 [17] M. Möhlen, B. Neumüller, K. Harms, H. Krautscheid, D. Fenske, M. Diedenhofen, G. Frenking, K. Dehnicke, *Z. Anorg. Allg. Chem.* **1998**, 624, 1105.
 [18] P. van der Sluis, A. L. Spek, *Acta Crystallogr. Sect. A* **1990**, 46, 194.
 [19] A. L. Spek, PLATON 94, Crystallographic Program System, University of Utrecht **1994**.
 [20] R. G. Solomon, J. K. Kochi, *J. Chem. Soc. Chem. Commun.* **1972**, 599.
 [21] H. Schmidbaur, W. Wolfsberger, *Chem. Ber.* **1967**, 100, 1000.

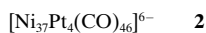
New Ni–Pt Carbonyl Clusters with a Tetrahedron of Platinum Atoms Encapsulated in an Incomplete Tetrahedron of Nickel Atoms: $[\text{Ni}_{36}\text{Pt}_4(\text{CO})_{45}]^{6-}$ and $[\text{Ni}_{37}\text{Pt}_4(\text{CO})_{46}]^{6-}$ **

Francesco Demartin, Cristina Femoni, M. Carmela Iapalucci, Giuliano Longoni,* and Piero Macchi

Only a limited number of structurally characterized carbonyl or carbonyl-substituted metal clusters containing more than 30 metal atoms is known.^[1–3] Metal clusters of high nuclearity provide useful models for experimental^[4] and theoretical^[5] studies of the metallization process. For instance, we have recently ascertained that carbonyl clusters containing highly connected (coordination number 12 and 13) metal atoms behave as electron sinks; thus, $[\text{H}_{6-n}\text{Ni}_{38}\text{C}_6(\text{CO})_{42}]^{n-}$ ($n = 5, 6$)^[3b] and $[\text{Ni}_{32}\text{C}_6(\text{CO})_{36}]^{6-}$ ^[3d] display an unusually rich redox chemistry^[6] that encompasses up to six oxidation states.^[7] Furthermore, the almost constant separation of about 0.3 V between the formal potentials of their electrochemically reversible consecutive redox couples indicates the absence of a well defined HOMO–LUMO gap.^[7] This finding led us to pursue the synthesis of other carbonyl metal clusters with several interstitial metal atoms to gain a better understanding of the metallization process.

Here we report the synthesis and structural characterization of the complex hexaanions **1** and **2**, which are chemically and structurally related to the previously reported clusters $[\text{H}_{6-n}\text{Ni}_{38}\text{Pt}_6(\text{CO})_{48}]^{n-}$ ($n = 4, 5, 6$).^[5a] The latter have a cherry structure in which a Pt_6 octahedron is fully encapsulated in a ν_3 ^[8] Ni_{38} octahedron; the present clusters may be considered

as being derived by encapsulation of a Pt_4 tetrahedron in an incomplete ν_5 tetrahedron of nickel atoms.



The cluster anions **1** and **2** were obtained by reaction of $[\text{NMe}_4]_2[\text{Ni}_6(\text{CO})_{12}]$ with $\text{K}_2[\text{PtCl}_4]$ in the molar ratio 2.5:1 in acetonitrile under nitrogen. The final brown mixture of products was separated by extraction with THF ($[\text{Ni}_9(\text{CO})_{18}]^{2-}$, $[\text{HNi}_9\text{Pt}_3(\text{CO})_{21}]^{3-}$),^[9, 10] acetone ($[\text{H}_2\text{Ni}_{38}\text{Pt}_6(\text{CO})_{48}]^{4-}$), propionitrile ($[\text{Ni}_9\text{Pt}_3(\text{CO})_{21}]^{4-}$, $[\text{HNi}_{38}\text{Pt}_6(\text{CO})_{48}]^{5-}$), and acetonitrile ($[\text{Ni}_{36}\text{Pt}_4(\text{CO})_{45}]^{6-}$, $[\text{Ni}_{37}\text{Pt}_4(\text{CO})_{46}]^{6-}$). The hexaanions **1** and **2** are indistinguishable by IR spectroscopy, and their $[\text{NMe}_4]^+$ salts cocrystallize when a solution in acetonitrile is layered with diisopropyl ether. The tetramethylammonium salts were converted to other quaternary ammonium and phosphonium salts by metathesis with the corresponding halides in DMSO, precipitation with water, and crystallization from acetonitrile/diisopropyl ether. The **1/2** mixture as the $[\text{NMe}_3\text{CH}_2\text{Ph}]^+$ salts shows strong carbonyl absorption bands in acetonitrile at 2003 and 1856 cm^{-1} . The ^1H NMR spectrum ($[\text{D}_3]\text{acetonitrile}$, 25 °C) only shows signals for the trimethylbenzylammonium cation and organic solvents over the range $\delta = -50$ to $+50$.

The asymmetric unit of the cocrystallized mixture of $[\text{NMe}_3\text{CH}_2\text{Ph}]_6\text{-1}$ and $[\text{NMe}_3\text{CH}_2\text{Ph}]_6\text{-2}$ consists of one anion (**1** or **2**) located on a crystallographic C_3 axis with an average occupancy factor of 0.5, two $[\text{NMe}_3\text{CH}_2\text{Ph}]^+$ cations in general positions, and a disordered isopropanol molecule located on a crystallographic C_3 axis.^[11] The idealized metal framework of **1** can be derived from a ν_5 Ni_{36} tetrahedron (Figure 1 top) by

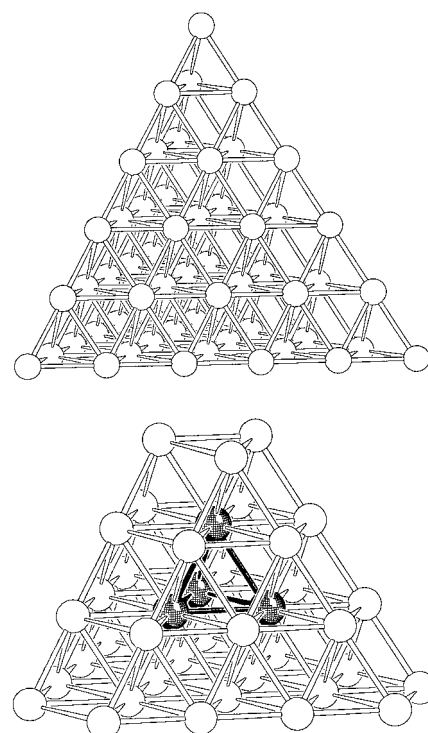


Figure 1. The ν_5 Ni_{36} tetrahedron (top) and the derived idealized $\text{Ni}_{36}\text{Pt}_4$ metal framework of **1** (bottom).

[*] Prof. G. Longoni, Dr. C. Femoni, Dr. M. C. Iapalucci
 Dipartimento di Chimica Fisica ed Inorganica
 viale Risorgimento 4, I-40136 Bologna (Italy)
 Fax: (+390)51-6443690
 E-mail: longoni@ms.fci.unibo.it

Prof. F. Demartin, Dr. P. Macchi
 Dipartimento di Chimica Strutturale e Stereochimica Inorganica
 via G. Venezian 21, I-20133 Milano (Italy)
 Fax: (+390)2-70635288
 E-mail: demartin@csmto.mi.cnr.it

[**] This work was supported by the MURST and the University of Bologna by the project “Sintesi, modelli e caratterizzazione per materiali funzionali”.

replacing the four interstitial nickel atoms by platinum atoms and by removing the 16 nickel atoms that belong to a set of three edges having a common vertex (Figure 1 bottom). The experimentally determined structure of the **1** is shown in Figure 2 top. The departures of the metal framework from the idealized model given in Figure 1 bottom consist of a helicoidal twist around the C_3 axis and enlargement of the bottom face of the outer Ni_{36} polyhedron. These distortions efficiently minimize the energy of the molecule by increasing the number of Ni–Ni interactions (105 Ni–Ni distances within the range given in Figure 2 versus 102 in the idealized structure),

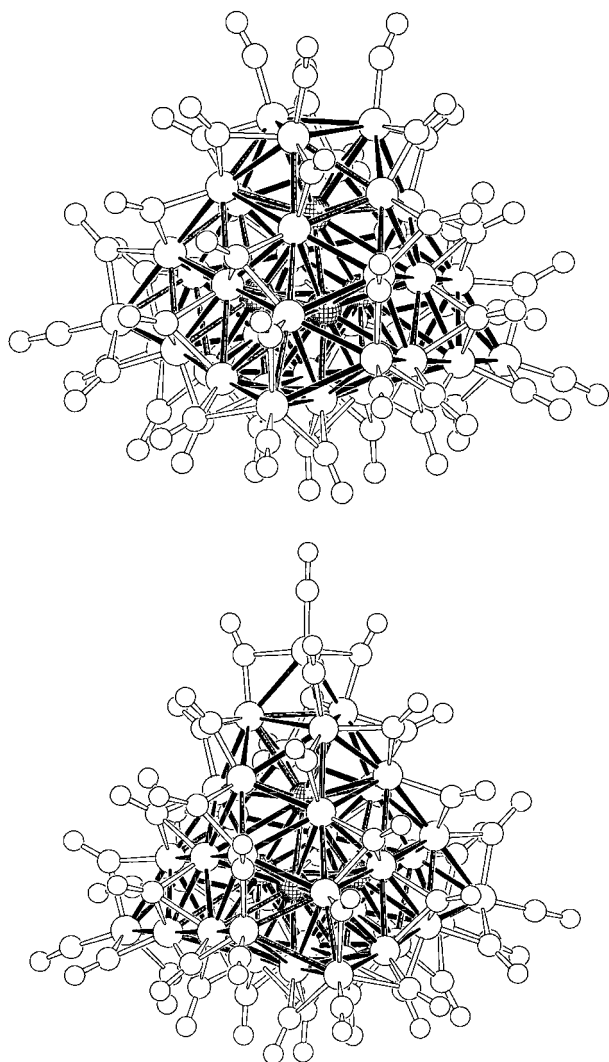


Figure 2. The structure of $[Ni_{36}Pt_4(CO)_9(\mu-CO)_{24}(\mu_3-CO)_{12}]^{6-}$ (top) and $[Ni_{37}Pt_4(CO)_7(\mu-CO)_{27}(\mu_3-CO)_{12}]^{6-}$ (bottom). Metal–metal distances [Å]: Pt–Pt 2.709(1)–2.733(1), Pt–Ni 2.536(2)–2.776(2), Ni–Ni 2.421(2)–2.782(2).

provide better accommodation for the bulkier encapsulated Pt_4 tetrahedron, and minimize nonbonding repulsions between the carbonyl ligands, which comprise nine terminal, 24 edge-bridging, and 12 face-bridging ligands.

Figure 2 bottom shows the structure of $[Ni_{37}Pt_4(CO)_7(\mu-CO)_{27}(\mu_3-CO)_{12}]^{6-}$ (**2**), which is derived by capping the unique triangular face that constitutes the truncated vertex of the polyhedron of Figure 2 top with a $Ni(CO)$ moiety and by

tilting three formerly terminal carbonyl ligands into edge-bridging positions. The addition of $Ni(CO)$ fragments to clusters does not alter the number of skeletal electron pairs, and often subsequent additions (or subtractions) of this moiety can be carried out.^[3b–d, 15] The recently reported cluster $[H_{12}Pd_{28}Pt_{13}(CO)_{27}(PMe_3)(PPh_3)_{12}]^{[3b]}$ has the same nuclearity as **2** and analogously contains a fully interstitial Pd_4 tetrahedron. However, the two are neither isoelectronic nor isostructural.

The mixture of **1** and **2** is readily degraded by carbon monoxide at atmospheric pressure to $[Ni_9Pt_3(CO)_{21}]^{4+}$, whereas oxidation with K_2PtCl_4 yields $[H_{6-n}Ni_{38}Pt_6(CO)_{48}]^{n-}$ derivatives. These reactions are probably the origin of most the side products in the synthesis of **1** and **2**. In contrast, preliminary experiments indicate that the cluster anions of **1** and **2** can remain intact over several reduction steps. Indeed, as shown by IR monitoring, they are reduced by sodium naphthalene in DMF in at least three distinct steps and can be quantitatively reoxidized with tropylium tetrafluoroborate. Electrochemical studies to evaluate the electron-sink behavior and the separation between the one-electron energy levels in the frontier region of **1/2** and $[H_{6-n}Ni_{38}Pt_6(CO)_{48}]^{n-}$ are in progress.

Experimental Section

1/2: K_2PtCl_4 (0.80 g, 1.96 mmol) was added in portions over 6 h to a solution of $[NMe_4]_6[Ni_6(CO)_{12}]$ (4.03 g, 4.82 mmol) in acetonitrile (60 mL) under a continuously renewed nitrogen atmosphere with stirring. The mixture was stirred for 48 h. The resulting dark brown suspension was filtered, and the filtrate evaporated to dryness. The residue was thoroughly washed in sequence with water (40 mL), THF (60 mL), acetone (40 mL), and propionitrile (60 mL). The brown residue was extracted with acetonitrile (40 mL) and precipitated by layering with diisopropyl ether (40 mL) to give black plates of cocrystallized $[NMe_4]_6$ -**1** and $[NMe_4]_6$ -**2** (610 mg, 0.13 mmol, 26.5% based on Pt). The salts are soluble in acetonitrile, dimethylformamide, DMSO, and *N*-methylpyrrolidinone, sparingly soluble in acetone, and insoluble in THF, alcohols, and nonpolar solvents. Elemental analysis for $[NMe_4]_6[Ni_{36}Pt_4(CO)_{45}]$ and $[NMe_4]_6[Ni_{37}Pt_4(CO)_{46}]$: calcd (1:1 mixture) (%): Ni 46.16, Pt 16.81, C 17.97, H 1.55, N 1.81; found: Ni 45.87, Pt 16.52, C 18.08, H 1.63, N 1.70.

The corresponding cocrystallized mixture of $[NMe_3CH_2Ph]_6$ -**1** and $[NMe_3CH_2Ph]_6$ -**2** was obtained by metathesis of the tetramethylammonium salts in DMSO solution with an aqueous solution of trimethylbenzylammonium chloride. The salt was precipitated with water, washed with isopropanol, and crystallized from acetonitrile/diisopropyl ether. IR (CH_3CN): $\bar{\nu}_{CO}$ = 2002 (s) and 1854 cm^{-1} (s); elemental analysis: calcd (1:1 mixture) (%): Ni 42.03, Pt 15.31, C 24.84, H 1.88, N 1.65; found: Ni 41.87, Pt 15.12, C 24.94, H 1.93, N 1.56.

Received: September 18, 1998 [Z12430IE]

German version: *Angew. Chem.* **1999**, *111*, 552–554

Keywords: carbonyl complexes • clusters • nickel • platinum • structure elucidation

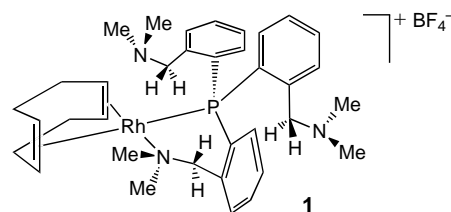
- [1] G. Longoni, M. C. Iapalucci in *Clusters and Colloids: From Theory to Applications* (Ed.: G. Schmid), VCH, Weinheim, **1994**, p. 91.
- [2] A. Ceriotti, R. Della Pergola, L. Garlaschelli in *Physics and Chemistry of Metal Cluster Compounds, Vol. 18* (Ed.: L. J. de Jongh), Kluwer Academic, Dordrecht, **1994**, p. 41.
- [3] a) $[HNi_{38}Pt_6(CO)_{48}]^{5-}$: A. Ceriotti, F. Demartin, G. Longoni, M. Manassero, M. Marchionna, G. Piva, M. Sansoni, *Angew. Chem.* **1985**, *97*, 708; *Angew. Chem. Int. Ed. Engl.* **1985**, *24*, 697; b) $[H_{6-n}Ni_{38}C_6-$

A Chelate with Conformational Memory?*

M. Aránzazu Alonso, Juan A. Casares, Pablo Espinet,* and Katerina Soulantica

Advances in NMR techniques have enabled detailed observation of some dynamic phenomena at the molecular level. One problem that has attracted attention is restricted rotation around single bonds,^[1] particularly in chiral molecules. Because of their movements, some molecular systems have been referred to as molecular motors, brakes, ratchets, etc.^[2–5] The possible selective directionality of these restricted rotations is governed by the principle of microscopic reversibility: Rotations that interconvert degenerate states cannot have a preferred sense.^[3,6] An illustrative case of this and other related basic aspects is presented here.

The complexes $[\text{Rh}(\text{diene})\{\text{P}(\text{bzN})_3\}]\text{BF}_4$ (**1**: diene = 1,5-cyclooctadiene (cod), **2**: diene = tetrafluorobenzobarrelene (tfb); bzN = 2-(dimethylaminomethyl)phenyl) are square planar in solution, and the $\text{P}(\text{bzN})_3$ ligand acts as a P,N chelate



with two pendant amino group arms. The chelate ring has a boat conformation, which makes the complexes chiral (racemic).^[7] Racemization by inversion of the boat is slow on the NMR time scale at room temperature, as can be seen in the ¹H COSY spectrum of **1** (Figure 1). The four olefinic hydrogen atoms are inequivalent, the CH₂ groups give rise to three AB systems, and the methyl groups give four singlets (3:3:6:6); hence, the two methyl groups on the coordinated N center are inequivalent, and those at each pendant N atom are equivalent owing to fast inversion of the amino group, although the two pendant arms are inequivalent.^[8] The coordination plane clearly defines two half-spaces, one concave and one convex,^[9] which contain the two possible positions for nucleophilic attack by an entering ligand (Scheme 1).

[*] Prof. Dr. P. Espinet, M. A. Alonso, Dr. J. A. Casares, Dr. K. Soulantica
Departamento de Química Inorgánica, Facultad de Ciencias
Universidad de Valladolid
E-47005 Valladolid (Spain)
Fax: (+349) 983-423013
E-mail: espinet@qi.uva.es

[**] This work was supported by the Dirección General de Investigación Científica y Técnica (Spain, project PB96-0363), and the Junta de Castilla y León (Spain, project VA40/96). M.A.A. acknowledges a grant from the Dirección General de Enseñanza Superior (Spain). K.S. acknowledges grants by the Dirección General de Investigación Científica y Enseñanza Superior (Spain, SB95-BOZ67791015) and the Commission of the European Communities (Network "Selective Processes and Catalysis Involving Small Molecules" CHR-X-CT93-0147).

- (CO)₄₂]⁹⁻: A. Ceriotti, A. Fait, G. Longoni, G. Piro, F. Demartin, M. Manassero, N. Masciocchi, M. Sansoni, *J. Am. Chem. Soc.* **1986**, *108*, 8091; c) [H₆₋₈Ni₃₄C₄(CO)₃₈]⁹⁻: A. Ceriotti, A. Fait, G. Longoni, G. Piro, L. Resconi, F. Demartin, M. Manassero, N. Masciocchi, M. Sansoni, *J. Am. Chem. Soc.* **1986**, *108*, 5370; d) [Ni₃₂C₆(CO)₃₆]⁶⁻: F. Calderoni, F. Demartin, M. C. Iapalucci, G. Longoni, *Angew. Chem.* **1996**, *108*, 2393; *Angew. Chem. Int. Ed. Engl.* **1996**, *35*, 2225; e) [Pd₃₈(CO)₂₈(PEt₃)₁₂]: E. G. Mednikov, N. K. Eremenko, Yu. L. Slovakhov, Yu. T. Struchkov, *J. Chem. Soc. Chem. Commun.* **1987**, 218; f) [Pd₃₄(CO)₂₄(PEt₃)₁₂]: E. G. Mednikov, N. I. Kanteeva, *Russ. Chem. Bull.* **1995**, *44*, 163; g) [Ni₉Pd₃₃(CO)₄₁(PPh₃)₆]⁴⁻: M. Kawano, J. W. Bacon, C. F. Campana, L. F. Dahl, *J. Am. Chem. Soc.* **1996**, *118*, 7869; h) [H₁₂Pd₂₈Pt₁₃(CO)₂₇(PMe₃)(PPh₃)₁₂]: J. M. Bemis, L. F. Dahl, *J. Am. Chem. Soc.* **1997**, *119*, 4545.
- [4] J. M. van Ruitenbeek, D. A. van Leeuwen, L. J. de Jongh in *Physics and Chemistry of Metal Cluster Compounds*, Vol. 18 (Ed.: L. J. de Jongh), Kluwer Academic, Dordrecht, **1994**, p. 277.
- [5] N. Rösch, G. Pacchioni in *Clusters and Colloids: From Theory to Applications* (Ed.: G. Schmid), VCH, Weinheim, **1994**, p. 5.
- [6] P. Zanello in *Stereochemistry of Organometallic and Inorganic Compounds*, Vol. 5 (Ed.: P. Zanello), Elsevier, Amsterdam, **1994**, p. 163.
- [7] F. Calderoni, F. Demartin, F. Fabrizi De Biani, C. Femoni, M. C. Iapalucci, G. Longoni, P. Zanello, *Inorg. Chem.*, submitted.
- [8] D. A. Nagaki, L. D. Lower, G. Longoni, P. Chini, L. F. Dahl, *Organometallics* **1986**, *5*, 1764.
- [9] A. Ceriotti, F. Demartin, G. Longoni, M. Manassero, G. Piva, G. Piro, M. Sansoni, B. T. Heaton, *J. Organomet. Chem.* **1986**, *301*, C5.
- [10] B. K. Teo, H. Zhang, *J. Cluster Sci.* **1990**, *1*, 155.
- [11] Crystal data for 0.5[NMe₃CH₂Ph]₆[Ni₃₆Pt₄(CO)₄₅]/0.5[NMe₃CH₂Ph]₆[Ni₃₇Pt₄(CO)₄₆]·C₃H₈O: hexagonal, space group P6₃ (no. 173), *a* = 17.853(9), *c* = 27.127(13) Å, *V* = 7488(6) Å³, *Z* = 2, ρ_{calcd} = 2.29 g cm⁻³, graphite-monochromatized MoK_α radiation (λ = 0.71073 Å), μ(MoK_α) = 82.5 cm⁻¹. A total of 86976 reflections with 3 < θ < 29° were measured on a Siemens CCD area-detector SMART diffractometer at 210 K on a crystal of approximate dimensions 0.10 × 0.15 × 0.08 mm, mounted in air but protected by the cooling N₂ stream during data collection. Data were corrected for Lorentzian polarization and absorption effects (empirical absorption correction with SADABS;^[12] transmission factors in the range 0.61–1.00). The structure was solved by direct methods (SIR97^[13]) and refined with full-matrix least-squares (SHELX93^[14]) on 9209 independent reflections with *I* > 3σ(*I*). Anisotropic displacement parameters were assigned to all atoms of the anions. The final *R* value was 0.057 (*R*_w = 0.128). Maximum Δρ = 2.2 e Å⁻³ close to the Pt atoms. Crystallographic data (excluding structure factors) for the structure reported in this paper have been deposited with the Cambridge Crystallographic Data Centre as supplementary publication no. CCDC-102917. Copies of the data can be obtained free of charge on application to CCDC, 12 Union Road, Cambridge CB21EZ, UK (fax: (+44) 1223-336-033; e-mail: deposit@ccdc.cam.ac.uk).
- [12] G. M. Sheldrick, SADABS, Universität Göttingen, Germany, unpublished results.
- [13] A. Altomare, G. Cascarano, C. Giacovazzo, A. Guagliardi, M. C. Burla, G. Polidori, M. Camalli, *J. Appl. Crystallogr.* **1994**, *24*, 435.
- [14] G. M. Sheldrick, SHELX93, program for the refinement of crystal structures, Universität Göttingen, Germany, **1993**.
- [15] a) A. Ceriotti, G. Longoni, M. Manassero, M. Perego, M. Sansoni, *Inorg. Chem.* **1985**, *24*, 117; b) A. Ceriotti, G. Longoni, M. Manassero, L. Resconi, M. Sansoni *J. Chem. Soc. Chem. Commun.* **1985**, 181; c) A. Ceriotti, G. Longoni, M. Manassero, N. Masciocchi, G. Piro, L. Resconi, M. Sansoni *J. Chem. Soc. Chem. Commun.* **1985**, 1402; d) A. Ceriotti, G. Longoni, G. Piro, M. Manassero, N. Masciocchi, M. Sansoni, *New J. Chem.* **1988**, *12*, 501.

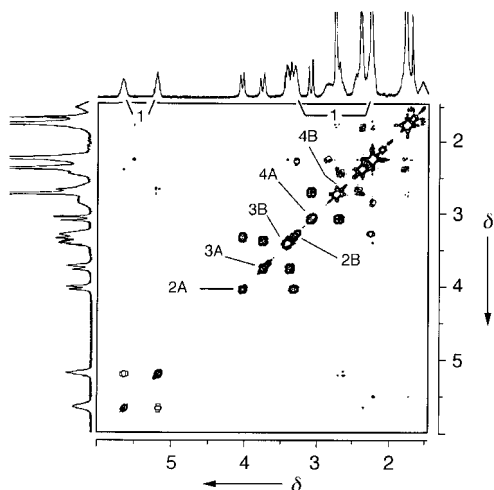
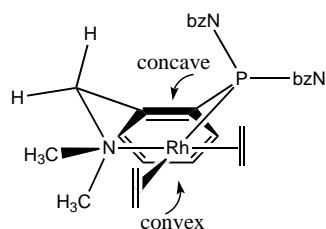


Figure 1. ^1H COSY spectrum (300 MHz, CDCl_3 , 20°C) of **1**. 2A/2B, 3A/3B, and 4A/4B are the three methylene groups, each of which constitutes an AB spin system. Label 1 denotes the olefinic protons: *cis* to the coordinated N atom to the left, and *cis* to the coordinated P atom to the right; note the pronounced upfield shift of the olefinic proton at $\delta \approx 2.1$, probably due to anisotropic shielding by the aromatic rings of the pendant arms.



Scheme 1. Two possible positions for nucleophilic attack by an entering nucleophile.

The striking behavior of **1** and **2** is that they undergo exchange between the coordinated and pendant amino groups with complete retention of the conformation of the ring. It can be said that the molecule remembers the conformation of the ring during the exchange process. This is clearly seen in the ^1H EXSY spectrum of **1** at room temperature (Figure 2):^[10] 1) All

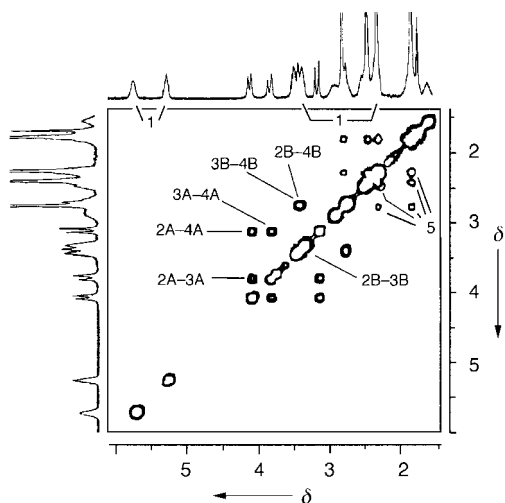
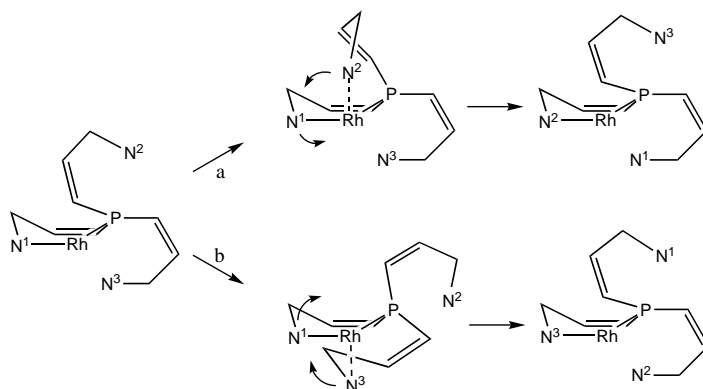


Figure 2. ^1H EXSY spectrum (300 MHz, CDCl_3 , 20°C) of **1**. Label 5 indicates cross-peaks of the methyl groups, and the others are cross-peaks of the methylene protons, numbered as in the COSY spectrum of Figure 1.

the methyl groups exchange with each other; 2) the olefinic protons do not exchange; and 3) all the methylene groups undergo selective exchange, in which the inequivalence of their two protons is conserved. This is consistent only with an associative substitution mechanism, in which the incoming ligand adopts the same configuration as the leaving group. A dissociative mechanism or a fast inversion of the boat can be discounted, as both should lead to exchange of the olefinic protons on the same double bond and of all methylene protons; that is, racemization would occur simultaneously with exchange of the N centers. (A three-coordinate intermediate would have a symmetry plane, and fast inversion of the boat would generate a time-averaged plane of symmetry in the square-planar complex or in the trigonal bipyramidal pentacoordinate intermediate.) These observations are further supported by magnetization transfer experiments,^[11] which clearly show that the selective inversion of a given methylene proton leads to magnetization transfer to only two other methylene protons, each on a different methylene group; moreover, the magnitude of the magnetization transfer to these is, within the experimental error, the same. Hence, the two pendant arms exchange at the same rate with a coordinated arm, that is, attack at the concave and the convex positions occurs at the same rate, and both produce the conformation of the ring that is already present in the molecule.

The two processes were investigated independently for **2**. The rate of ligand exchange was measured by line-shape analysis of the singlets of the methyl groups,^[12] which afforded $\Delta G^\ddagger_{298} = 55.7 \text{ kJ mol}^{-1}$ ($\Delta H^\ddagger = 51.5 \pm 2.7 \text{ kJ mol}^{-1}$, $\Delta S^\ddagger = -14 \pm 10 \text{ J K}^{-1} \text{ mol}^{-1}$). The inversion of the boat conformation was studied by magnetization transfer on the F atoms of the tfb ligand, which gave $\Delta G^\ddagger_{298} = 66.9 \text{ kJ mol}^{-1}$ ($\Delta H^\ddagger = 49.6 \pm 2.7 \text{ kJ mol}^{-1}$; $\Delta S^\ddagger = -58 \pm 10 \text{ J K}^{-1} \text{ mol}^{-1}$). At 298 K the rate of exchange of pendant and coordinated amino groups in **2** is about 100 times faster than the inversion of the boat.

The associative substitution mechanism is shown in Scheme 2, starting from one of the two enantiomers. It deserves several comments on the concept of chirality:



Scheme 2. a) Nucleophilic attack at the concave site. b) Nucleophilic attack at the convex site. For clarity the aromatic ring is represented by a double bond, and the olefin bound to Rh has been omitted.

1) The two pendant arms are disposed in such a way that N^2 can attack the concave position, and N^3 the convex position.

Although steric hindrance at the two sites appears to be very different, attack occurs at the same rate at both. Otherwise there would be a preferred sense for rotation, but this cannot occur if both rotations give rise to identical molecules, that is, the motion interconverts degenerate states. This problem was discussed in detail for the rotation of triptycenes^[4] and an aryl ring.^[3] Although the approach to one of the two sites is initially less hindered, the rate of substitution is controlled only by the energy of the transition state, which is the same regardless of the initial position of attack.

2) The pendant arms are not chiral, but they are “prochiral” in the sense that chirality is produced upon coordination and adoption of a particular conformation. Thus, in the substitution reaction chirality is efficiently induced in the “prochiral” entering arm by the chiral leaving arm. It can be said that the system exhibits “strong chirality towards the entering arm,”^[13] the origin of which is clearly geometric: The pentacoordinate intermediate has severe steric constraints which can be minimized only if the two nonplanar rings are stacked concave/concave (or convex/convex), but not concave/convex. The incoming ligand adopts the conformation with the best “steric complementarity” to the coordinated ligand.^[14]

3) The system is an example of the principle of self-regeneration of stereocenters.^[15] Here the “stereocenter” is the conformation of the chelating ring, which, for a given arm, is lost and regenerated during the exchange process.

4) Racemization of the complex requires inversion of the boat conformation, which takes place ($k_{298} = 11.7 \text{ s}^{-1}$) without any bond scission. Thus the system possesses what has been called “dynamic chirality”, and consequently the exchange process is an example of a reaction with “memory of chirality”.^[16] Clearly, its “good memory” is also associated with the large difference in rate between the exchange and the racemization processes: On the time scale of the exchange process ($k_{298} = 1054.7 \text{ s}^{-1}$) the conformation of the boat is static.

In summary, there is no need for coining a new term, as the “conformational memory” of these molecules can be analyzed on the basis of well-known concepts: The induction of chirality, the effect of differences in the rates of “simultaneous” processes, and the principle of microscopic reversibility.

Experimental Section

Compounds **1** and **2** were prepared from their corresponding precursors^[17] as follows: A solution of $[\text{Rh}(\text{diene})(\mu\text{-Cl})_2]$ and $\text{P}(\text{bzN})_3$ in acetone was treated with AgBF_4 (for **1**) or TlBF_4 (for **2**). After 1 h insoluble MCl ($\text{M} = \text{Ag}, \text{Tl}$) was filtered off, and the complex was crystallized by concentration to a small volume, addition of ethanol, and cooling to -20°C . **1**: Yield: 78%; elemental analysis calcd for $\text{C}_{35}\text{H}_{48}\text{BF}_4\text{N}_3\text{PRh}$: C 57.47, N 5.75, H 6.61; found: C 57.19, N 5.88, H 6.31; ^1H NMR (CDCl_3 , 300 MHz, 20°C): $\delta = 10.08$ (m, 1H), 8.06 (m, 1H), 7.93 (m, 1H), 7.85 (m, 3H), 7.63 (m, 2H), 7.50 (m, 1H), 7.40–7.10 (m, 3H), 5.60 (m, 1H), 5.25 (m, 1H), 4.08 (d, 1H), 3.81 (d, 1H), 3.45 (d, 1H), 3.39 (m, 2H), 3.12 (d, 1H), 2.88 (m, 1H), 2.80 (s, 3H), 2.72 (m, 2H), 2.50 (m, 2H), 2.43 (s, 3H), 2.31 (m, 8H), 1.82 (s, 6H), 1.78 (m, 2H), 1.57 (m, 1H); ^{31}P NMR (CDCl_3 , 121.4 MHz, 20°C): $\delta = 21.4$ (d, $J_{\text{Rh,P}} = 153 \text{ Hz}$). **2**: Yield: 71%; elemental analysis calcd for $\text{C}_{39}\text{H}_{42}\text{BF}_4\text{N}_3\text{PRh}$: C 55.14, N 4.94, H 4.98; found: C 54.59, N 4.53, H 5.10; ^1H NMR (CDCl_3 , 300 MHz, 213 K): $\delta = 10.25$ (m, 1H), 7.93 (m, 2H), 7.79 (m, 1H), 7.70 (m, 1H), 7.55 (m, 2H), 7.45 (m, 1H), 7.35 (m, 2H), 7.17

(m, 1H), 6.97 (m, 1H), 6.03 (m, 1H), 5.88 (m, 1H), 5.45 (m, 1H), 5.33 (m, 1H), 4.01 (m, 1H), 3.82 (m, 1H), 3.38 (m, 2H), 3.21 (m, 1H), 3.16 (m, 1H), 2.89 (m, 1H), 2.79 (s, 3H), 2.43 (s, 6H), 2.39 (s, 3H), 2.15 (m, 1H), 1.84 (s, 6H); ^{31}P NMR (NMR, 121.4 MHz, CDCl_3 , 213 K): $\delta = 26.3$ (d, $J_{\text{Rh,P}} = 172 \text{ Hz}$). ^{19}F NMR (CDCl_3 , 20°C): $\delta = -145.6$ (m, 1F), -146.7 (m, 1F), -152.07 (s, 4F, BF_4^-), -158.7 (m, 2F).

Received: August 20, 1998 [Z12307IE]

German version: *Angew. Chem.* **1999**, *111*, 554–557

Keywords: asymmetric synthesis • chirality • N ligands • P ligands • rhodium

- [1] See, for instance, M. Oki, *The Chemistry of Rotational Isomers*, Springer, Heidelberg, **1993**.
- [2] T. R. Kelly, I. Tellitu, J. Pérez-Sestelo, *Angew. Chem.* **1997**, *109*, 1966; *Angew. Chem. Int. Ed. Engl.* **1997**, *36*, 1866.
- [3] J. A. Casares, S. Coco, P. Espinet, Y.-S. Lin, *Organometallics* **1995**, *14*, 3058.
- [4] T. R. Kelly, M. C. Bowyer, K. V. Bhasakar, D. Bebbington, A. García, F. Lang, M. H. Kim, M. P. Jette, *J. Am. Chem. Soc.* **1994**, *116*, 3657.
- [5] F. P. Fanizzi, M. Lanfranchi, G. Natile, A. Tiripicchio, *Inorg. Chem.* **1994**, *33*, 3331.
- [6] A. P. Davis, *Angew. Chem.* **1998**, *110*, 953; *Angew. Chem. Int. Ed.* **1998**, *37*, 909, and references therein.
- [7] This boat conformation has been found for Pd and Pt complexes with the same chelate ring: a) W. de Graaf, S. Harder, J. Boersma, G. van Koten, J. A. Kanter, *J. Organomet. Chem.* **1988**, *358*, 545; b) N. C. Payne, G. R. Tobin, *Acta Crystallogr. Sect. C* **1992**, *48*, 45; c) G. M. Kapteijn, M. P. R. Spee, D. M. Grove, H. Kooijman, A. L. Spek, G. van Koten, *Organometallics* **1996**, *15*, 1405.
- [8] Related complexes with the less sterically hindered ligand $\text{P}(\text{bzN})\text{Ph}_2$ show a somewhat faster inversion of the boat, with $\Delta G^\ddagger = 36.6 \text{ kJ mol}^{-1}$ for Rh^I (T. B. Rauchfuss, F. T. Patino, D. M. Roudhill, *Inorg. Chem.* **1975**, *14*, 652) and 46 kJ mol^{-1} for Pd^{II} complexes.^[7c]
- [9] G. Helmchen, R. Schmierer, *Angew. Chem.* **1981**, *93*, 208; *Angew. Chem. Int. Ed. Engl.* **1981**, *20*, 205, and references therein.
- [10] The EXSY experiments were carried out with a standard NOESY program in phase-sensitive mode with a 5% random variation of the evolution time to avoid COSY cross-peaks and a mixing time of 0.6 s.
- [11] The magnetization transfer experiments were carried out by using a 180° Gaussian shaped soft pulse for the selective excitation of the desired signal, followed by a variable delay (ten values were used: 10^{-4} , 0.005, 0.01, 0.015, 0.02, 0.03, 0.04, 0.06, 0.08, and 0.10 s) and a 90° nonselective pulse. The data were analyzed as described in M. L. H. Green, A. Sella, L.-L. Wong, *Organometallics* **1992**, *11*, 2650.
- [12] Line-shape analysis was carried out using the standard DNMR6 program: DNMR6, Quantum Chemical Program Exchange (QCPE 633), Indiana University, Bloomington, IN, **1995**.
- [13] For a discussion on the quantification of chirality, see A. B. Buda, T. Auf der Heyde, K. Mislow, *Angew. Chem.* **1992**, *104*, 1012; *Angew. Chem. Int. Ed. Engl.* **1992**, *31*, 989.
- [14] J.-M. Lehn *Supramolecular Chemistry*, VCH, Weinheim, **1995**.
- [15] D. Seebach, A. R. Sting, M. Hoffmann, *Angew. Chem.* **1996**, *108*, 2880; *Angew. Chem. Int. Ed. Engl.* **1996**, *35*, 2708.
- [16] K. Fuji, T. Kawabata, *Chem. Eur. J.* **1998**, *4*, 373.
- [17] a) $[\text{Rh}_2(\mu\text{-Cl})_2(1,5\text{-cod})_2]$: G. Giordano, R. H. Crabtree, *Inorg. Synth.* **1990**, *28*, 84; b) $[\text{Rh}_2(\mu\text{-Cl})_2(\text{tfb})_2]$: R. Usón, L. A. Oro, M. Valderrama, C. Claver, *Synth. React. Inorg. Met. Org. Chem.* **1979**, *9*, 577; c) $\text{P}(\text{bzN})_3$: C. Chuit, R. J. P. Corriu, P. Monforte, C. Reyé, J.-P. Declercq, A. Dubourg, *Angew. Chem.* **1993**, *105*, 1529; *Angew. Chem. Int. Ed. Engl.* **1993**, *32*, 1430.

Crystal Engineering of Acentric Diamondoid Metal–Organic Coordination Networks**

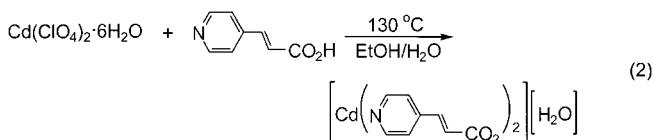
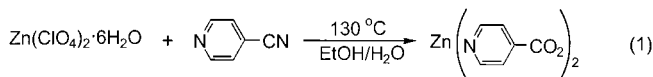
Owen R. Evans, Ren-Gen Xiong, Zhiyong Wang, George K. Wong, and Wenbin Lin*

Many bulk properties of solid materials including second-order nonlinear optical (NLO) effects require the absence of a center of symmetry.^[1] The rational synthesis of such acentric solids presents a formidable challenge to synthetic chemists.^[2] Diamondoid networks have been recognized as potential structural motifs for the construction of acentric solids since the pioneering work of Ermer et al. on hydrogen-bonded networks of adamantane-1,3,5,7-tetracarboxylic acid and methanetetraacetic acid.^[3] Diamondoid networks are not predisposed to pack in centric space groups owing to the lack of inversion centers on each tetrahedral connecting point. Moreover, diamondoid networks are generally robust.^[4] Over the past decade, many metal–organic diamondoid networks have been synthesized.^[5] To date, however, a low-temperature polymorph of potassium dideuterophosphate (KDP) remains as the only NLO-active diamondoid network.^[6] Herein we report the first rational crystal engineering of acentric, NLO-active metal–organic coordination networks based on diamondoid structures.

Our strategy for the construction of acentric diamondoid metal–organic coordination networks lies in the recognition that an acentric diamond net will arise if unsymmetrical bridging ligands are used to link tetrahedrally connected metal centers. The use of unsymmetrical, bifunctional bridging ligands (e.g., pyridinecarboxylates) also introduces the electronic asymmetry (push–pull effects) that is essential for second-order optical nonlinearity. On the other hand, it is well established that diamondoid networks tend to interpenetrate to fill the voids generated within a single diamond net.^[5a, 7] Such interpenetration could potentially introduce an inversion center, which will complicate the crystal engineering of acentric solids based on diamondoid networks. We demonstrate in this communication that, by using unsymmetrical bridging ligands of suitable length, diamondoid networks with an *odd* number of interpenetrating nets can be constructed, thereby avoiding the potential undesirable introduction of inversion centers through interpenetration. We describe here the synthesis, X-ray single-crystal structures, preliminary

NLO properties, and high thermal stabilities of the acentric diamondoid networks bis(isonicotinato)zinc (**1**) and bis(4-pyridylacrylate)cadmium·H₂O (**2**).

Compound **1** was synthesized hydro(solvo)thermally by treating Zn(ClO₄)₂·6H₂O and 4-cyanopyridine at 130 °C [Eq. (1)], while compound **2** was obtained by treating Cd(ClO₄)₂·6H₂O and *trans*-4-pyridylacrylic acid at 130 °C [Eq. (2)]. The isonicotinate group in **1** evidently results from



the hydrolysis of 4-cyanopyridine under the reaction conditions.^[8] The large difference between the antisymmetric and symmetric C=O stretching frequencies (1560 and 1365 cm^{−1}, respectively) for **1** suggests monodentate coordination of the carboxylate group, while the antisymmetric and symmetric C=O stretches at 1545 and 1400 cm^{−1} in **2** are consistent with chelation of the carboxylate group.^[9] The formulations of **1** and **2** are supported by elemental analysis and thermogravimetric analysis results.

An X-ray single-crystal structure determination reveals that Zn^{II} centers are four-coordinate in **1** (Figure 1a).^[10] Each Zn^{II} center coordinates to two pyridine atoms of two isonicotinate groups, and to two carboxylate groups of two other isonicotinate groups in a monodentate fashion. The Zn^{II} centers thus have a tetrahedral geometry and extend three-dimensionally to form a diamondoid network (Figure 1a). With Zn–Zn separations of 8.74 and 8.81 Å, a large void is generated within a single diamondoid cage. The void space in **1** is filled by the formation of a threefold diamondoid structure, in which three independent diamond nets mutually interpenetrate (Figure 2a).^[11] As a result of the unsymmetrical nature of isonicotinate groups and the threefold interpenetration, **1** crystallizes in the chiral space group *P*2₁2₁2₁. In contrast to the tetrahedral coordination of Zn^{II} centers in **1**, the Cd^{II} centers in **2** adopt a distorted octahedral geometry by coordinating to two pyridyl nitrogen atoms and chelating to two carboxylate groups of *trans*-(4-pyridyl)acrylate groups (Figure 1b). If the chelating carboxylates are treated as one connecting point, the Cd^{II} centers in **2** have a pseudo-tetrahedral geometry. Each Cd^{II} center in **2** is thus connected to four other Cd^{II} centers to result in a diamondoid network (Figure 1b). Owing to the larger length of the *trans*-(4-pyridyl)acrylate group versus the isonicotinate group (the Cd–Cd separations are 11.52 and 11.53 Å), **2** adopts a fivefold diamondoid structure and crystallizes in the acentric space group *Cc* (Figure 2b). Interestingly, **2** also includes a water guest molecule, evidently to occupy the extra space within the interpenetrated diamondoid network. We have thus demonstrated that acentric polymeric networks based on diamondoid structures can be readily constructed with judicious choice of unsymmetrical bridging ligands.

[*] Dr. W. Lin, O. R. Evans, Dr. R.-G. Xiong, Dr. Z. Wang

Department of Chemistry
Brandeis University
Waltham, MA 02454 (USA)
Fax: (+1) 781-736-2516
E-mail: wlin@brandeis.edu

Dr. G. K. Wong

Department of Physics, The Hong Kong University of Science and Technology, Clear Water Bay, Kowloon, Hong Kong (China)

[**] The authors are indebted to Dr. Scott R. Wilson and the Materials Chemistry Laboratory at University of Illinois at Urbana-Champaign for X-ray data collection, and to Dr. Bruce M. Foxman for helpful discussions. We acknowledge NSF (CHE-9727900) and ACS-PRF for financial support.



Supporting information for this article is available on the WWW under <http://www.wiley-vch.de/home/angewandte/> or from the author.

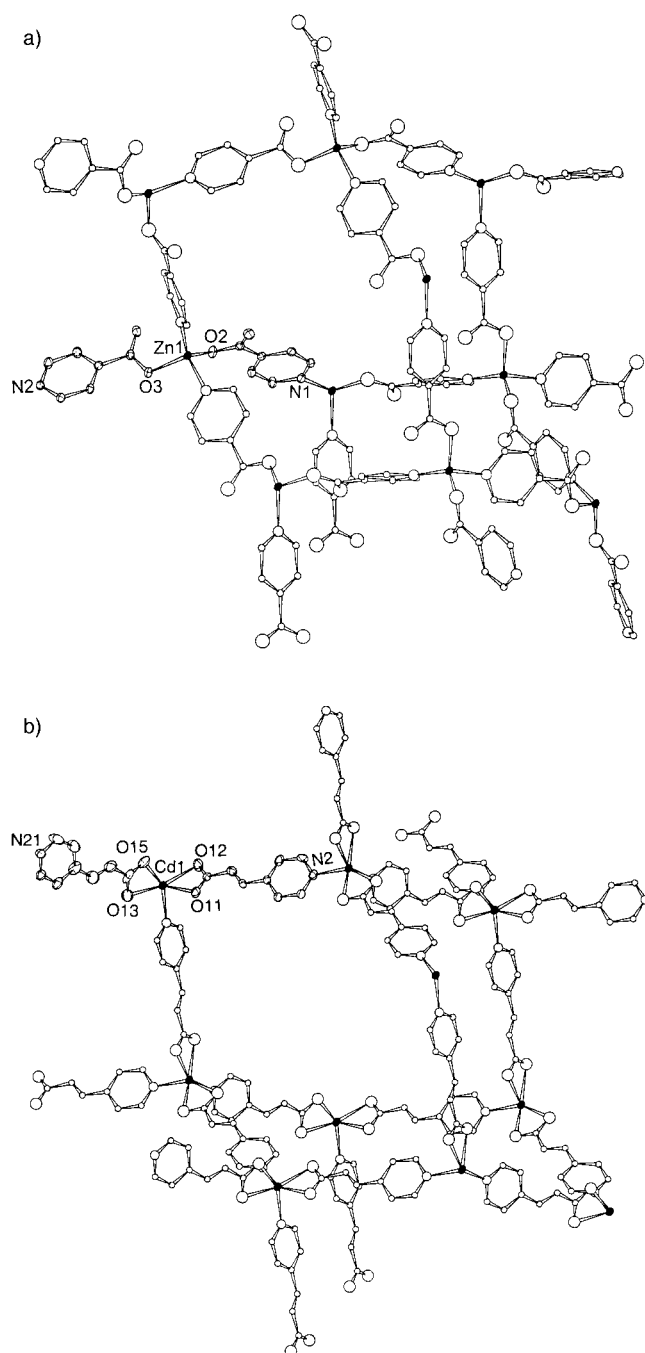


Figure 1. Diagrams showing the diamondoid cages in a) **1** and b) **2**. The solid ellipsoids represent metal centers, while open circles with increasing sizes represent C, N, and O, respectively. The asymmetric units are shown in ellipsoids at 50% and 40% probability for **1** and **2**, respectively. The guest water molecules have been omitted in **2**. Selected bond lengths [Å]: **1**: Zn1–O2 1.928(1), Zn1–O3 1.944(2), Zn1–N1 2.046(2), Zn1–N2 2.018(2); **2**: Cd1–N2 2.276(6), Cd1–N21 2.282(6), Cd1–O11 2.340(5), Cd1–O12 2.348(5) Å, Cd1–O13 2.433(6), Cd1–O15 2.348 (5).

Preliminary second harmonic generation measurements show that **1** possesses an effective d coefficient of $1.2 \pm 0.6 \text{ pm V}^{-1}$, a value about three times that of KDP. A Kurtz powder test indicates that **2** exhibits a second-order coefficient equivalent to that of KDP. The nonlinear optical activities of **1** and **2** are consistent with their acentric structures. Compounds **1** and **2** also exhibit remarkable thermal stability. Thermogravimetric analyses reveal that **1**

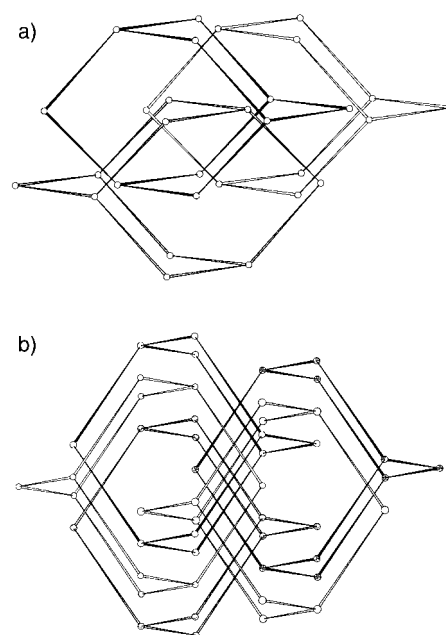


Figure 2. Diagrams showing a) threefold interpenetrating diamondoid network in **1** and b) fivefold interpenetrating diamondoid network in **2**. The bridging ligands are omitted for clarity, and the guest water molecules have been omitted in **2**.

has an onset temperature for decomposition of 420°C . Compound **2** loses the guest water molecule by 70°C , but maintains its diamondoid network structure up to 400°C .^[12] Additionally, both **1** and **2** are insoluble in common solvents because of their neutral three-dimensional polymeric structures. The above attributes make **1** and **2** excellent candidates for practical NLO applications. This work represents a significant advance in the field of supramolecular engineering of functional solids. We are currently further evaluating the optical properties of these new materials as well as extending this novel approach to the synthesis of other acentric polymeric networks.

Experimental Section

1: A heavy-walled Pyrex tube containing a mixture of $\text{Zn}(\text{ClO}_4)_2 \cdot 6\text{H}_2\text{O}$ (0.186 g, 0.5 mmol) and 4-cyanopyridine (0.104 g, 1 mmol) in ethanol (0.4 mL) and water (0.1 mL) was frozen and sealed under vacuum, and placed inside an oven at 130°C . Colorless prismatic crystals were obtained after 48 h of heating. Yield: (0.136 g, 88%); elemental analysis calcd (found) for $\text{ZnC}_{12}\text{H}_8\text{O}_4\text{N}_2$ (%): C 46.2 (46.5), H 2.61 (2.59), N 9.01 (9.05).

2: The reaction was carried out exactly in the same fashion as for **1** except that $\text{Cd}(\text{ClO}_4)_2 \cdot 6\text{H}_2\text{O}$ (0.22 g, 0.5 mmol) and *trans*-4-pyridylacrylic acid (0.15 g, 1 mmol) in ethanol (0.4 mL) were used. Yield: (0.11 g, 53%); elemental analysis calcd (found) for $\text{CdC}_{16}\text{H}_{14}\text{O}_5\text{N}_2$ (%): C 45.0 (44.6), H 2.83 (3.16), N 6.56 (6.49).

Second harmonic generation was performed on a single crystal of **1** with dimensions of $\sim 1 \times 1 \times 0.4 \text{ mm}$ using Maker fringe technique. The fundamental wavelength of 1064 nm from a Nd:YAG laser was used. The second harmonic signal was compared to that of α -quartz, and a d_{eff} of $1.2 \pm 0.6 \text{ pm V}^{-1}$ was estimated. A Kurtz powder test was performed on **2** with a particle size of $76 \pm 13 \mu\text{m}$. A relative second harmonic intensity of 0.1 versus urea was obtained. This powder test can severely underestimate the second-order optical nonlinearity of **2** owing to the potentially smaller coherence length of **2**.

Received: August 18, 1998 [Z12302IE]

German version: *Angew. Chem.* **1999**, *111*, 557–559

Keywords: coordination polymers • crystal engineering • network structures • nonlinear optics • solid-state structures

Highly Efficient Ruthenium-Based Catalytic Systems for the Controlled Free-Radical Polymerization of Vinyl Monomers**

François Simal, Albert Demonceau,* and Alfred F. Noels

The ability to control molecular architecture constitutes a major challenge for synthetic polymer chemists.^[1] Controlled free-radical polymerization (also referred to as “living” or “pseudoliving”) has in recent years revitalized the rather mature field of radical olefin polymerization in an unprecedented way, and has provided access to well-defined polymers and copolymers. Stable free radicals, such as nitroxides, have been introduced for control of radical polymerization.^[1] Recently, the groups of Matyjaszewski, Sawamoto, Jérôme, and others have replaced the stable nitroxide free radical with transition metal species to obtain inter alia a variety of copper-,^[2] iron-,^[3] nickel-,^[4] palladium-,^[5] or rhodium-mediated^[6] controlled free-radical polymerization systems, a methodology which goes by the name of atom transfer radical polymerization (ATRP).

Ruthenium was introduced by Sawamoto et al. for the polymerization reaction,^[7] but $[\text{RuCl}_2(\text{PPh}_3)_3]$ (the most widely used ruthenium complex) requires the presence of a Lewis acid activator. We now report on the exceptional efficacy of new catalytic systems based on well-defined and fully characterized $[\text{RuCl}_2(p\text{-cymene})(\text{PR}_3)]$ complexes ($p\text{-cymene}$ = 4-isopropyltoluene) for promotion of the controlled free-radical polymerization of vinyl monomers *without* cocatalyst activation. These readily prepared and air-stable catalysts compare favorably with the most active ATRP catalysts reported to date.

Methyl methacrylate (MMA) was chosen as a model substrate, and polymerization was initiated by ethyl 2-bromo-2-methylpropionate in the presence of various $[\text{RuCl}_2(p\text{-cymene})(\text{PR}_3)]$ complexes at 85 °C. From the results summarized in Table 1, it appears that only phosphanes which are both strongly basic (the $\text{p}K_a$ being taken as a reasonable measure of the σ -donating ability of the ligand) and which possess a well-defined steric bulk ($160^\circ < \theta < 170^\circ$, θ = cone angle of the phosphane) present both high catalytic activity and high control of the polymerization process (high initiation efficiency f , and molecular weight distribution $M_w/M_n = 1.1$). A polydispersity as narrow as $M_w/M_n = 1.07$ is observed when the catalyst is prepared in situ from the ruthenium dimer $[\{\text{RuCl}_2(p\text{-cymene})\}_2]$ and tricyclohexylphosphane in the ratio $\text{Ru}:\text{PCy}_3 = 2:1$.

Under these experimental conditions, all the criteria of living polymerization are fulfilled. Indeed, the plots of

- [1] a) J. Zyss, *Molecular Nonlinear Optics: Materials, Physics, and Devices*, Academic Press, New York, **1993**; b) F. Agulló-López, J. M. Cabrera, F. Agulló-Rueda, *Electrooptics: Phenomena, Materials and Applications*, Academic Press, New York, **1994**; c) R. E. Newnham, *Structure-Property Relations*, Springer, New York, **1975**.
- [2] a) G. R. Desiraju, *Crystal Engineering: The Design of Organic Solids*, Elsevier, New York, **1989**; b) J.-M. Lehn, *Supramolecular Chemistry: Concepts and Perspectives*, VCH Publishers, New York, **1995**.
- [3] a) O. Ermer, A. Eling, *Angew. Chem.* **1988**, *100*, 856–860; *Angew. Chem. Int. Ed. Engl.* **1988**, *27*, 829–833; b) O. Ermer, *J. Am. Chem. Soc.* **1988**, *110*, 3747–3754.
- [4] D. M. Proserpio, R. Hoffmann, P. Preuss, *J. Am. Chem. Soc.* **1994**, *116*, 9634–9637.
- [5] a) S. R. Batten, R. Robson, *Angew. Chem.* **1998**, *110*, 1558–1595; *Angew. Chem. Int. Ed.* **1998**, *37*, 1460–1494; b) M. J. Zaworotko, *Chem. Soc. Rev.* **1994**, 283–288; c) L. R. MacGillivray, S. Subramanian, M. J. Zaworotko, *J. Chem. Soc. Chem. Commun.* **1994**, 1325–1326; d) S. Lopez, M. Kahraman, M. Harmata, S. W. Keller *Inorg. Chem.* **1997**, *36*, 6138–6140; e) K. A. Hirsch, D. Venkataraman, S. R. Wilson, J. S. Moore, S. Lee, *J. Chem. Soc. Chem. Commun.* **1995**, 2199–2200; f) K.-W. Kim, M. G. Kanatzidis, *J. Am. Chem. Soc.* **1992**, *114*, 4878–4883; g) M. Munakata, L. P. Wu, M. Yamamoto, T. Kuroda-Sowa, M. Maekawa, *J. Am. Chem. Soc.* **1996**, *118*, 3117–3124; h) A. Michaelides, V. Kiritis, S. Skoulis, A. Aubry, *Angew. Chem.* **1993**, *105*, 1525–1526; *Angew. Chem. Int. Ed. Engl.* **1993**, *32*, 1495–1497; i) K. Sinzger, S. Hünig, M. Jopp, D. Bauer, W. Bietsch, J. U. von Schütz, H. C. Wolf, R. K. Kremer, T. Metzenthin, R. Bau, S. I. Khan, A. Lindbaum, C. L. Langauer, E. Tillmanns, *J. Am. Chem. Soc.* **1993**, *115*, 7696–7705; j) “Supramolecular Architectures”: R. Robson, B. F. Abrahams, S. R. Batten, R. W. Gable, B. Hoskins, J. Liu, *ACS Symp. Ser.* **1992**, *499*, 257–273.
- [6] a) S. Endo, T. Chino, S. Tsuboi, K. Koto, *Nature* **1989**, *340*, 452–455; b) B. C. Frazer, R. Pepinsky, *Acta Crystallgr.* **1953**, *6*, 273–285.
- [7] a) A. J. Blake, N. R. Champness, S. S. M. Chung, W.-S. Li, M. Schröder, *Chem. Commun.* **1997**, 1005–1006; b) K. A. Hirsch, S. R. Wilson, J. S. Moore, *Chem. Eur. J.* **1997**, *3*, 765–771.
- [8] J. D. Martin, R. F. Hess, *Chem. Commun.* **1996**, 2419–2420.
- [9] R. C. Mehrotra, R. Bohra, *Metal Carboxylates*, Academic Press, New York, **1983**.
- [10] X-ray single crystal diffraction data for both **1** and **2** were collected on a Siemens SMART CCD diffractometer. Crystal data for **1**: crystal size $0.16 \times 0.22 \times 0.34$ mm, orthorhombic, space group $P2_12_12_1$, $a = 8.2149(1)$, $b = 11.6635(2)$, $c = 12.7420(1)$ Å, $U = 1220.9(1)$, $Z = 4$, $\rho_{\text{calcd}} = 1.68 \text{ g cm}^{-3}$, $\rho_{\text{obs}} = 1.65(1) \text{ g cm}^{-3}$, $T = 123$ K, $\text{MoK}\alpha$ radiation ($\lambda = 0.71073$ Å). Least-squares refinement based on 2755 reflections with $I > 3\sigma(I)$ and 173 parameters led to convergence, with a final value of $R = 0.026$ and $R_w = 0.031$. Crystal data for **2**: crystal size $0.14 \times 0.40 \times 0.40$ mm, monoclinic, space group Cc , $a = 12.0137(2)$, $b = 22.3435(4)$, $c = 7.7738(1)$ Å, $\beta = 123.509(1)^\circ$, $U = 1739.9(1) \text{ Å}^3$, $Z = 4$, $\rho_{\text{calcd}} = 1.63 \text{ g cm}^{-3}$, $\rho_{\text{obs}} = 1.63(1) \text{ g cm}^{-3}$, $T = 198$ K, $\text{MoK}\alpha$ radiation ($\lambda = 0.71073$ Å). Least-squares refinement based on 2034 reflections with $I > 3\sigma(I)$ and 226 parameters led to convergence, with a final value of $R = 0.039$ and $R_w = 0.043$. – Further details of the crystal structure investigation(s) can be obtained from the Fachinformationszentrum Karlsruhe, D-76344 Eggenstein-Leopoldshafen, Germany (fax: (+49) 7247-808-666; e-mail: crysdata@fiz-karlsruhe.de), on quoting the depository numbers CSD-391070 and CSD-391071.
- [11] Interestingly, when attempts were made to synthesize the Cd^{II} analogue of **1**, a twofold diamondoid structure with a formula $[\text{Cd}(\text{isonicotinate})_2(\text{EtOH})][\text{EtOH}]$ was obtained. The formation of twofold (but not threefold) diamondoid structure is presumably a consequence of the larger size of Cd^{II} versus Zn^{II} . $[\text{Cd}(\text{isonicotinate})_2(\text{EtOH})][\text{EtOH}]$ adopts a centrosymmetric structure (space group $Pbca$, SHG-inactive) due to the twofold interpenetration: W. Lin, R. Xiong, O. Evans, Z. Wang, unpublished results.
- [12] The Fdntal X-ray powder diffraction patterns were obtained for samples of **2** before and after the removal of water guest molecules.

[*] Prof. Dr. A. Demonceau, F. Simal, Prof. Dr. A. F. Noels
Laboratory of Macromolecular Chemistry and
Organic Catalysis, C.E.R.M.
University of Liège
Sart-Tilman (B.6a), B-4000 Liège (Belgium)
Fax: (+32) 4-366-34-97
E-mail: a.demonceau@ulg.ac.be

[**] We thank the Fonds National de la Recherche Scientifique (F.N.R.S.), Belgium, for the purchase of major instrumentation.

Table 1. Ruthenium-catalyzed controlled atom transfer radical polymerization of methyl methacrylate.^[a]

Catalyst	θ [°]	pK_a	T_D [°C] ^[b]	Yield [%]	M_n ^[c]	M_w/M_n	f ^[d]
[RuCl ₂ (<i>p</i> -cymene)(PR ₃)]							
PR ₃ = P(OPh) ₃	128	−2.0	195	0	—	—	—
PR ₃ = PMe ₃	118	8.65	216	26	157 000	1.75	0.07
PR ₃ = P(<i>n</i> Bu) ₃	132	8.43	198	44	36 000	1.6	0.5
PR ₃ = PBn ₃	165	6.0	223	30	21 000	1.6	0.55
PR ₃ = PPh ₃	145	2.73	213	20	25 000	1.6	0.3
PR ₃ = PPPh ₂ Cy	153	5.05	211	58	41 000	1.25	0.55
PR ₃ = PPhCy ₂	161	7.38	189	90	60 500	1.10	0.6
PR ₃ = PCy ₃	170	9.7	163	100	41 500	1.12	0.95
PR ₃ = P <i>i</i> Pr ₃	160	9.0	172	80	40 500	1.10	0.8
[(RuCl ₂ (<i>p</i> -cymene)) ₂] + PCy ₃ (1:1)	—	—	—	98	51 500	1.07	0.75
[RuCl ₂ (=CHPh)(PCy ₃) ₂]	—	—	—	95	66 000	1.28	0.6

[a] [MMA]₀: [initiator]₀: [Ru]₀ = 800:2:1 (for details, see the Experimental Section).
 [b] Temperature at which the arene ligand is liberated as determined by TGA.
 [c] Determined by size-exclusion chromatography (SEC) with PMMA calibration.
 [d] Initiation efficiency $f = M_{n,theor}/M_{n,exp}$ with $M_{n,theor} = ([MMA]_0/[initiator]_0) \times M_w(MMA) \times \text{conversion}$. θ is the cone angle of the phosphane ligand;^[16] TGA = thermogravimetric analysis, *p*-cymene = 4-isopropyltoluene, Bn = benzyl, Cy = cyclohexyl.

$\ln([M]_0/[M])$ versus time (Figure 1) and of M_n versus monomer conversion (Figure 2) are linear. The linear time dependence of $\ln([M]_0/[M])$ indicates that the concentration of the

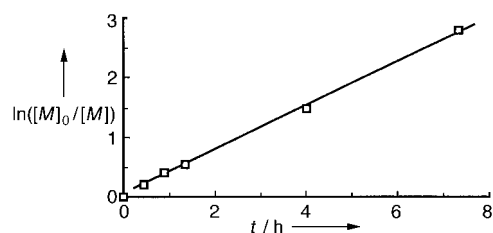


Figure 1. Time dependence of $\ln([M]_0/[M])$ at 85 °C where $[M]_0$ and $[M]$ are the MMA concentration at times 0 and t ($y = 3.60 \times 10^{-2} + 0.375x$; $r^2 = 0.999$). Reaction conditions are the same as in Table 1 (catalyst = [RuCl₂(*p*-cymene)(PCy₃)]).

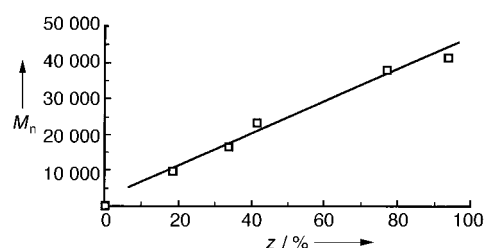


Figure 2. Dependence of the PMMA molecular weight M_n on monomer conversion z ($y = 1655 + 449.5x$; $r^2 = 0.985$). Reaction conditions are the same as in Table 1 (catalyst = [RuCl₂(*p*-cymene)(PCy₃)]).

active species remains constant during polymerization. The lack of transfer reactions is supported by the linearity of the plot of M_n versus conversion. Furthermore, control of MMA polymerization was confirmed by the addition of a second equivalent of MMA feed to the completely polymerized system. This second polymerization reaction is also quantitative, and only a slight increase in polydispersity is observed (Figure 3). Under similar reaction conditions (MMA, neat or

in toluene), high molecular weight PMMA is obtained ($M_n = 150\,000$) with polydispersities that remain relatively low ($M_w/M_n = 1.35 - 1.45$).

A further advantage of this new catalytic system is that it is highly soluble in neat MMA. [RuCl₂(*p*-cymene)-(PR₃)] complexes are also quite soluble in common organic solvents including heptane, which is the solvent used for precipitation of the polymer. This yields white PMMA as opposed to pale green or light brown PMMA precipitated from reaction mixtures of nickel-^[3] or iron-mediated^[8] polymerization reactions.

The polymerization mechanism is likely to be radical since the PMMA tacticity (typically $rr:rm:mm = 57.8:36.8:5.4$, $\rho = 0.99$) fits the tacticity known for a radical polymerization reaction. Furthermore, galvinoxyl (5 equiv relative to the initiator), a well-known radical inhibitor, inhibits the MMA polymerization, and reaction mixtures in air also fail to polymerize. Surprisingly, the best catalyst systems for ATRP of MMA have been shown to be also the most active ones for the ring-opening metathesis polymerization (ROMP) of strained and low-strain cycloolefins.^[9] In both reactions, the same stereoelectronic requirements for the phosphane ligand of the ruthenium complex (sterically demanding phosphanes, typically tricyclohexylphosphane PCy₃) have been demonstrated. Furthermore, the ease with which the arene ligand is disengaged from the different [RuCl₂(*p*-cymene)(PR₃)] complexes reported in Table 1 (as quantified by standardized thermogravimetric measurements^[10] and ¹H NMR spectroscopy at 85 °C) indicates a direct relationship between arene ligand lability and catalyst activity in both reactions. This suggests that the *p*-cymene ligand is released in the process and the question arises about the possible coordination of the monomer during the ATRP reaction. Hence, [RuCl₂(=CHPh)(PCy₃)₂], the Grubbs ruthenium–carbene complex commonly used for polymerization of MMA (Table 1). This catalyst was found to be even more active ($k_{app} = 1.95 \times 10^{-4} \text{ s}^{-1}$) than [RuCl₂(*p*-cymene)-(PCy₃)] ($k_{app} = 1.05 \times 10^{-4} \text{ s}^{-1}$), [RuCl₂(*p*-cymene)(P*i*Pr₃)] ($k_{app} = 5.65 \times 10^{-5} \text{ s}^{-1}$), or [RuCl₂(*p*-cymene)(PPhCy₂)] ($k_{app} = 5.2 \times 10^{-5} \text{ s}^{-1}$), but to the detriment of polymer control ($M_w/M_n = 1.28$; $f = 0.60$). The synthesis of potential ATRP catalysts based on ruthenium–carbene complexes is presently in progress.^[12]

Other vinyl monomers such as methacrylates, *n*-butyl acrylate, and 4-substituted styrenes have also been success-

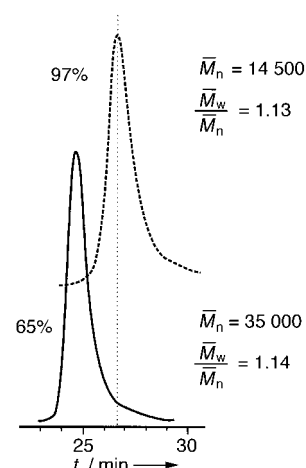


Figure 3. Size-exclusion chromatograms of the PMMA after a first feed of MMA (solid line; [MMA]₀₍₁₎: [initiator]₀: [RuCl₂(*p*-cymene)(PCy₃)]₀ = 200:2:1; conversion = 97 %), and after a second feed of MMA (dashed line; [MMA]₀₍₂₎: [initiator]₀: [RuCl₂(*p*-cymene)(PCy₃)]₀ = 400:2:1; conversion = 65 % (230 % when expressed according to Sawamoto et al.^[15])).

fully polymerized (see Table 2), although with a somewhat lesser control (the reactions were not optimized). Vinyl acetate, a substrate known to be reluctant to undergo ATRP, is not polymerized under the same reaction conditions.

Table 2. [RuCl₂(*p*-cymene)(PCy₃)₂]-catalyzed polymerization of various vinyl monomers.^[a]

Monomer	Yield [%]	<i>M</i> _n ^[b]	<i>M</i> _w / <i>M</i> _n	<i>f</i> ^[c]
methyl methacrylate	100	41 500	1.12	0.95
<i>tert</i> -butyl methacrylate	80	33 500	1.2	0.95
isobornyl methacrylate	70	25 000	1.2	1.1 ^[d]
<i>n</i> -butyl acrylate	80	37 500	1.95	0.85
styrene	64	28 500	1.3	0.9
vinyl acetate	0	–	–	–

[a] Reaction conditions same as in Table 1, except for styrene (initiator, (1-bromoethyl)benzene; temperature, 110 °C). [b] Apparent *M*_n for poly(*tert*-butyl methacrylate), poly(isobornyl methacrylate), and poly(*n*-butyl acrylate) determined with PMMA calibration. For poly(methyl methacrylate) and polystyrene, PMMA and PS calibrations were used, respectively. [c] Initiation efficiency $f = M_{n,theor}/M_{n,exp}$, with $M_{n,theor} = ([MMA]_0/[initiator]_0) \times M_w(MMA) \times \text{conversion}$. [d] An initiation efficiency higher than 1 could mean that the PMMA calibration is not suitable for poly(isobornyl methacrylate).

However, similar reactions with methacrylic acid (MA) and 2-hydroxyethyl methacrylate (HEMA) are successful, as well as controlled copolymerizations (95 % MMA/5 % MA and 90 % MMA/10 % HEMA) (*M*_w/*M*_n = 1.24 and 1.17). Since ATRP requires a suitable adjustment between the structure of the monomer, initiator, and atom (or group of atoms) to provide reversible termination, the catalyst has to be fine-tuned to each monomer. This has been exemplified for *n*-butyl acrylate. For this monomer, the molecular weight distribution dropped from 1.9 to 1.4 simply by the use of PiPr₃ as the phosphane (instead of PCy₃), which demonstrates the versatility of the catalyst system.

Experimental Section

All reagents and solvents were dried, distilled, and stored under nitrogen at –20 °C with conventional methods. Ruthenium complexes were synthesized and purified according to the literature.^[9, 13, 14] Grubbs catalyst, [RuCl₂(=CHPh)(PCy₃)₂], was used as received (Strem).

Polymerization of MMA: Ruthenium complex (0.0116 mmol) was placed in a glass tube containing a bar magnet and capped by a three-way stopcock. The reactor was purged of air (three vacuum–nitrogen cycles) before methyl methacrylate (1 mL, 9.35 mmol), and the initiator (ethyl 2-bromo-2-methylpropionate 0.1 M in toluene, 0.232 mL) were added. All liquids were handled with dried syringes under nitrogen. The mixture was heated in a thermostated oil bath for 16 h at 85 °C and, after cooling, dissolved in THF and the product precipitated in heptane. The polymer was filtered off and dried overnight at 80 °C under vacuum.

Received: July 20, 1998 [Z121671E]

German version: *Angew. Chem.* **1999**, *111*, 559–562

Keywords: P ligands • polymerizations • radical reactions • ruthenium

- [1] C. J. Hawker, *Acc. Chem. Res.* **1997**, *30*, 373–382, and references therein.
 [2] a) J. Xia, K. Matyjaszewski, *Macromolecules* **1997**, *30*, 7697–7700;
 b) K. Matyjaszewski, J.-L. Wang, T. Grimaud, D. A. Shipp, *Macro-*

- molecules* **1998**, *31*, 1527–1534; c) K. Matyjaszewski, Y. Nakagawa, C. B. Jasieczek, *Macromolecules* **1998**, *31*, 1535–1541; d) V. Percec, B. Barboiu, H.-J. Kim, *J. Am. Chem. Soc.* **1998**, *120*, 305–316; e) D. M. Haddleton, A. M. Heming, D. Kukulj, D. J. Duncalf, A. J. Shooter, *Macromolecules* **1998**, *31*, 2016–2018, and references therein.
 [3] a) T. Ando, M. Kamigaito, M. Sawamoto, *Macromolecules* **1997**, *30*, 4507–4510; b) K. Matyjaszewski, M. Wei, J. Xia, N. E. McDermott, *Macromolecules* **1997**, *30*, 8161–8164.
 [4] a) C. Granel, P. Dubois, R. Jérôme, P. Teyssié, *Macromolecules* **1996**, *29*, 8576–8582; b) H. Uegaki, Y. Kotani, M. Kamigaito, M. Sawamoto, *Macromolecules* **1997**, *30*, 2249–2253.
 [5] P. Lecomte, I. Drapier, P. Dubois, P. Teyssié, R. Jérôme, *Macromolecules* **1997**, *30*, 7631–7633.
 [6] G. Moineau, C. Granel, P. Dubois, R. Jérôme, P. Teyssié, *Macromolecules* **1998**, *31*, 542–544.
 [7] a) T. Ando, M. Kamigaito, M. Sawamoto, *Tetrahedron* **1997**, *53*, 15445–15457; b) J. Ueda, M. Matsuyama, M. Kamigaito, M. Sawamoto, *Macromolecules* **1998**, *31*, 557–562.
 [8] G. Moineau, P. Dubois, R. Jérôme, T. Senninger, P. Teyssié, *Macromolecules* **1998**, *31*, 545–547.
 [9] A. Demonceau, A. W. Stumpf, E. Saive, A. F. Noels, *Macromolecules* **1997**, *30*, 3127–3136.
 [10] A. Hafner, A. Mühlebach, P. A. van der Schaaf, *Angew. Chem.* **1997**, *109*, 2213–2216; *Angew. Chem. Int. Ed. Engl.* **1997**, *36*, 2121–2124.
 [11] a) R. H. Grubbs, S. J. Miller, G. C. Fu, *Acc. Chem. Res.* **1995**, *28*, 446–452; b) M. Schuster, S. Blechert, *Angew. Chem.* **1997**, *109*, 2124–2145; *Angew. Chem. Int. Ed. Engl.* **1997**, *36*, 2036–2056; c) S. K. Armstrong, *J. Chem. Soc. Perkin Trans. 1* **1998**, 371–388; d) R. H. Grubbs, S. Chang, *Tetrahedron* **1998**, *54*, 4413–4450, and references therein.
 [12] a) W. A. Herrmann, M. Elison, J. Fischer, C. Köcher, G. R. J. Artus, *Chem. Eur. J.* **1996**, *2*, 772–780; b) W. A. Herrmann, C. Köcher, L. J. Gooßen, G. R. J. Artus, *Chem. Eur. J.* **1996**, *2*, 1627–1636.
 [13] R. A. Zelinka, M. C. Baird, *Can. J. Chem.* **1972**, *50*, 3063–3072.
 [14] M. A. Bennett, A. K. Smith, *J. Chem. Soc. Dalton Trans.* **1974**, 233–241.
 [15] Y. Kotani, M. Kato, M. Kamigaito, M. Sawamoto, *Macromolecules* **1996**, *29*, 6979–6982.
 [16] C. A. Tolman, *Chem. Rev.* **1977**, *77*, 313–348.

Modeling the Selectivity of Potassium Channels with Synthetic, Ligand-Assembled π Slides**

Maureen M. Tedesco, Bereket Ghebremariam, Naomi Sakai, and Stefan Matile*

Since Hodgkin and Huxley's demonstration almost fifty years ago that nerve signals originate from selective flux of Na⁺ and K⁺ ions across cell membranes, the mechanism of ion selectivity, particularly that of K⁺ channels, has remained a fascinating and central question in life sciences.^[1–3] The classical view of amide oxygen atoms serving as selective K⁺ binding sites has received substantial support from site-

[*] Prof. S. Matile, M. M. Tedesco, B. Ghebremariam, N. Sakai
 Department of Chemistry
 Georgetown University
 Washington, DC 20057-1227 (USA)
 Fax: (+1) 202-687-6209
 E-mail: matiles@gusun.georgetown.edu

[**] This work was supported by NIH (GM56147), the donors of the Petroleum Research Fund (administered by the American Chemical Society), Research Corporation (Research Innovation Award), Sun-
 tory Institute for Bioorganic Research (SUNBOR Grant), and Georgetown University. B.G. is a Fulbright Fellow.

specific mutagenesis and X-ray analysis of K^+ channel proteins.^[1] However, the conflicting recent model which also considers the interaction of cations with π electrons of the multiple aromatic amino acid residues in the pore region of K^+ channels continues to attract a great deal of attention as well.^[2] Computational studies of benzene-cation-benzene complexes in water with fixed and, more convincingly, with flexible benzene–benzene distances have provided persuasive support for the latter model.^[4] Subsequent experimental results with cleverly devised synthetic models^[5–7] reaffirmed the anticipated^[4] limitations of fixed arene–arene distances, and thus provided additional incentive to explore the potential significance of flexible cyclic arene arrays for K^+ selectivity. Here we report the first synthetic, ligand-gated^[8] K^+ channel model with flexible arene–arene distances.

The cell-surface receptor model **1** consists of a ligand binding site, a spacer, and a membrane-spanning, rigid, rod-shaped “ π slide” (Figure 1).^[9] The iminodiacetate (IDA) group was selected as the external ligand binding site because multivalent binding of IDA to polyhistidine (pHis) through Cu^{2+} has been shown to induce aggregation of IDA–lipid conjugates in lipid bilayers.^[10] The IDA group was linked through a hydrophilic spacer to one terminus of a septi(*p*-phenylene). This rigid-rod molecule may serve as a consecutive cation binding site or π slide for cations.^[11–13]

Binding and organization of rigid-rod fluorophore **1** in lipid bilayers were investigated using spin-labeled lipids as previously reported for other oligo(*p*-phenylene)s.^[11, 13] Compared to the emission intensity of **1** at 380 nm in unlabeled EYPC-SUVs, the fluorescence of heptamer **1** (5 μ M) was quenched about 35 % by both 5- and 12-DOXYL-PC-labeled vesicles.^[14] Almost identical quenching efficiencies with differently located spin labels prove transmembrane orientation of the receptor model, as shown in Figure 1.

In the circular dichroism (CD) spectra, the membrane-bound receptor model **1** exhibits a negative Cotton effect (CE) at 305 nm and a broad positive CE at about 260 nm centered around the red-shifted absorption maximum at 285 nm (Figure 2, curves a and g). The dependence of the CD absorption ($\Delta\epsilon$) on the oligophenylene concentration implies that the observed induced CD originates from intermolecular exciton coupling within a ligand-free self-assembly **2**.^[15] The additional presence of membrane-bound receptor models **3** cannot, however, be excluded.

The addition of increasing concentrations of the multivalent ligand pHis caused a hypsochromic shift of the absorption maximum and a strong increase of the bathochromic CE; changes of the broad positive CE below 275 nm were obscured by contributions of pHis and light scattering from the vesicles (Figure 2). Consistent with ligand-induced formation of transmembrane, well-ordered “H” aggregates (or perhaps even of single, chiral “pinwheel” units),^[16] these spectroscopic changes were dependent on the concentration of the receptor as well as the ligand/receptor ratio, and were observed neither with the univalent imidazole ligand nor in the absence of $CuCl_2$.

The ion transport activity of the ligand–receptor complex **4** was assessed using EYPC-SUVs with entrapped pH-sensitive fluorophore 8-hydroxypyrene-1,3,6-trisulfonic acid (HPTS) as

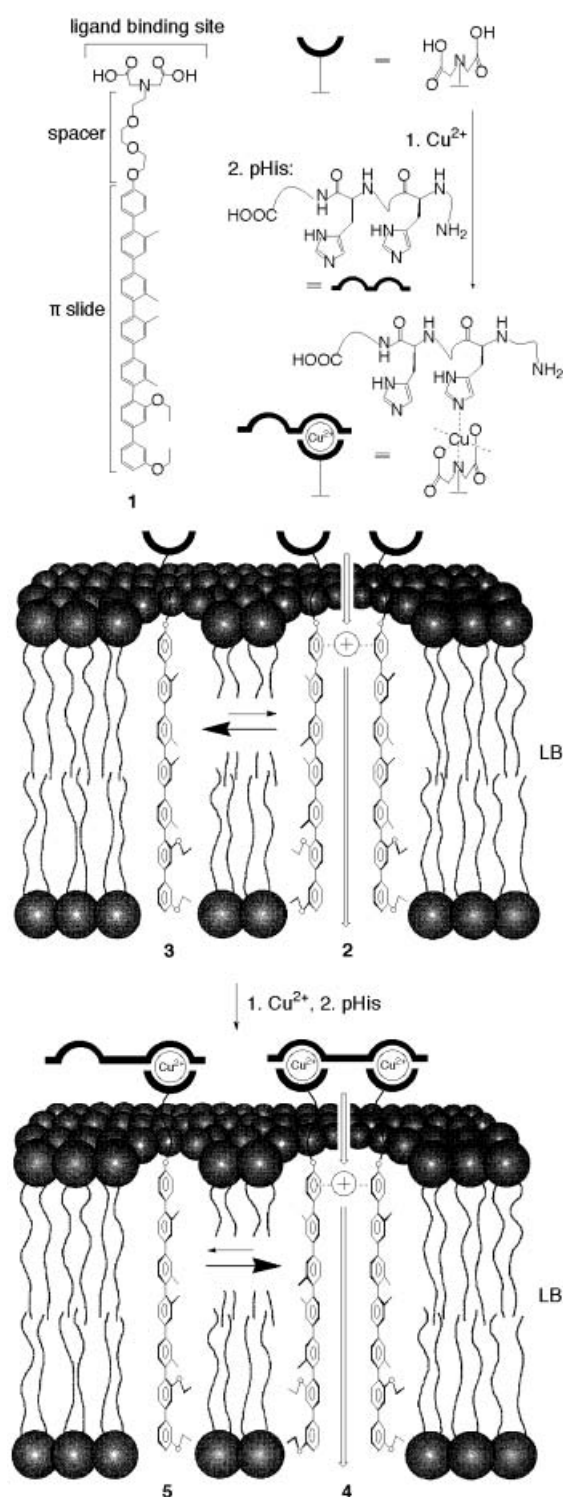


Figure 1. Structure and active suprastructures of receptor model **1**. In all cases, only two oligophenylenes out of an aggregate are shown; \oplus indicates cations bound to multiple arenes, and \rightarrow the direction of cation flux during cation/proton exchange (see Figure 3). The structure of pHis (average His/polymer ratio = 104) is simplified. LB = lipid bilayer.

well as high external K^+ and high internal H^+ and Na^+ concentrations (Figure 3B). Under these conditions, the transport activity of complex **4** (i.e., the rate of intravesicular pH change) was comparable to that of the K^+ channel forming antifungal polyene amphotericin B (AmB; Figure 3A,

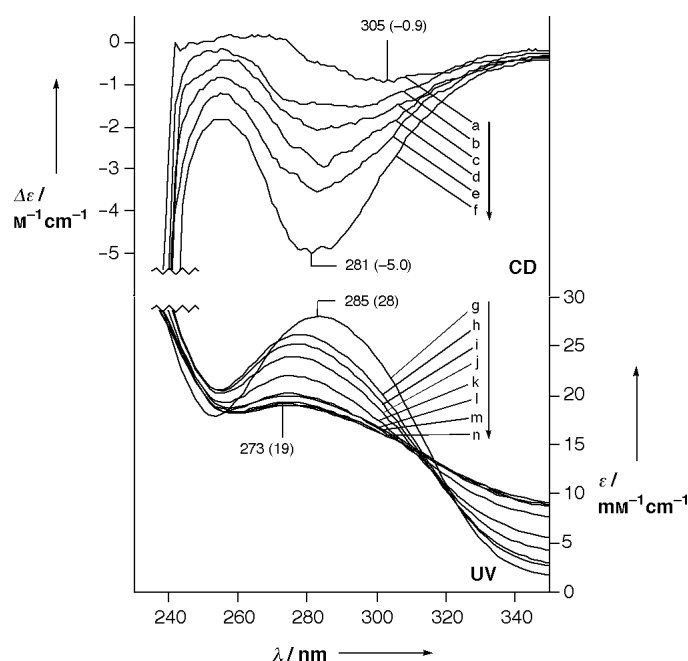


Figure 2. Representative circular dichroism and absorption spectra for receptor model **1** (40 μM) and CuCl_2 (60 μM) in the presence of EYPC-SUVs and the following concentrations of pHis [nM]: a) 0, b) 80, c) 100, d) 120, e) 140, f) 160, g) 0, h) 80, i) 100, j) 120, k) 140, l) 160, m) 180, n) 200, 220, and 240.

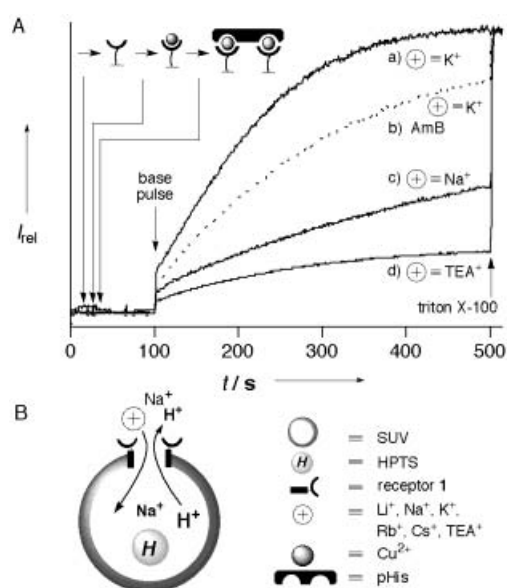


Figure 3. A) Representative cation/proton exchange curves with ligand-receptor complex **4** (2.5 μM **1**, 10 μM CuCl_2 , $\approx 0.2 \mu\text{M}$ pHis) and various extravesicular salts MCl: a) $\text{M} = \text{K}^+$, b) AmB (2.5 μM) with extravesicular K^+ without Cu-pHis , c) $\text{M} = \text{Na}^+$, d) $\text{M} = \text{TEA}^+$. Intravesicular pH was monitored ratiometrically [$I_t = I_a(\lambda_{\text{cm}} = 510 \text{ nm}, \lambda_{\text{ex}} = 460 \text{ nm}) / I_b(\lambda_{\text{cm}} = 510 \text{ nm}, \lambda_{\text{ex}} = 405 \text{ nm})$] and normalized [$(I_t - I_0) / (I_{\infty} - I_0)$]. B) Schematic representation of the transport experiments.

curves a and b).^[17] Replacement of the external K^+ with identical concentrations of Rb^+ , Cs^+ , Li^+ , and Na^+ gave up to 3.1-times reduced rates (Figure 3A, curves a and c). This increased transport selectivity for K^+ with respect to Na^+ is among the highest observed so far with synthetic models.^[5, 18]

The selectivity topology of transmembrane ion transport mediated by supramolecule **4**, an Eisenman sequence IV with a “lithium anomaly”, is similar to that of the permeability ratios of K^+ channel proteins (Figure 4, ■, □, ●).^[19] The

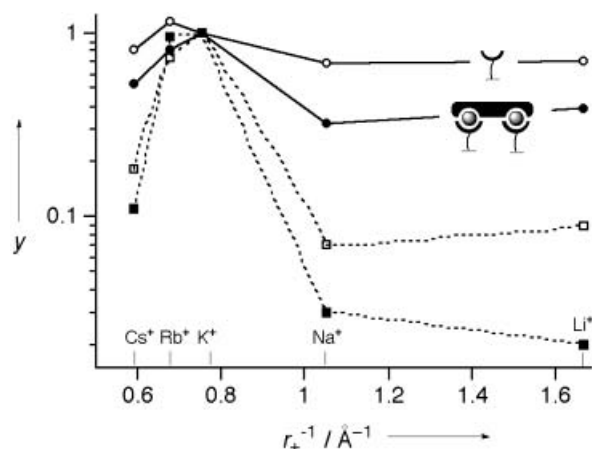


Figure 4. The selectivity topology y of two K^+ channels and model compound **1**. The logarithm of permeability ratios (for K^+ channels),^[19] or the logarithm of transport efficiency ratios (for models), is plotted against the reciprocal cation radius; (□) delayed K^+ current, helix neurons; (■) delayed K^+ current, skeletal muscle; (●) membrane-bound ligand-receptor complex **4**; (○) membrane-bound ligand-free receptor **2**.

selectivity for the ligand-free supramolecule **2** is lower than that of **4**, and its topology is an Eisenman sequence III, indicating weaker interactions between ion and binding site (Figure 4, ○). The higher field strength of supramolecule **4** compared to that of ligand-free receptor **2** strongly implies ligand-induced organization of the π slides to form consecutive cyclic cation binding sites, which is in good agreement with the spectroscopic results (Figure 2).

In the presence of external tetraethylammonium cation (TEA^+), transmembrane ion transport mediated by **4** was practically inhibited (Figure 3A, curve d). TEA^+ is a potent K^+ channel blocker that is thought to act by binding to a cyclic arene tetrad in the ion-conducting pore.^[1] Thus, TEA^+ blockage of **4** further supports that the observed ion selectivity originates with all likelihood from ligand-assembled, consecutive arene arrays.

In conclusion, we have demonstrated that transmembrane ion transport by ligand-assembled π slides occurs with a selectivity topology comparable to that of K^+ channels, and can be inhibited by a common K^+ channel blocker. These results imply that flexible, “dynamic” arene arrays may indeed contribute to the selectivity of K^+ channels.

Experimental Section

EYPC-SUVs were prepared as previously reported,^[11] but with phosphate buffer (10 mM $\text{Na}_2\text{HPO}_4/\text{NaH}_2\text{PO}_4$, pH 6.4, 100 mM NaCl (negative controls: 100 mM LiCl), 0.1 mM HPTS). For a transport experiment, an MCl buffer (1750 μL ; 10 mM $\text{Na}_2\text{HPO}_4/\text{NaH}_2\text{PO}_4$, pH 6.4, 100 mM MCl, $\text{M} = \text{Cs}$, Rb , K , Na , Li , or TEA) was placed in a thermostated fluorescence cell, and an aliquot (50 μL) of EYPC-SUVs stock solution (10 mM) was added. To the stirred suspension, 250 μM **1** in DMSO/THF (20 μL , positive control: 250 μM AmB, negative control: DMSO/THF), 1 mM CuCl_2 (20 μL ; for AmB/2: MCl buffer), MCl buffer (200 μL) with ca. 2 μM pHis (Sigma, for

AmB/2: MCl buffer), and 0.5 M NaOH (20 μ L) were subsequently added. Usually 400 sec after the base pulse, 10% triton X-100 (50 μ L) was added to determine complete collapse of the pH gradient (final pH 7.4). Relative transport efficiencies were calculated from the initial rate constants in comparison to that with external K^+ ($k = 1.6 \times 10^{-2} \text{ s}^{-1}$), and are given in Figure 4. The CD, UV/Vis, and fluorescence quenching experiments were performed as reported before.^[11]

Received: May 29, 1998

Revised version: September 25, 1998 [Z11921IE]

German version: *Angew. Chem.* **1999**, *111*, 523–526

Keywords: ion channels • ligand effects • membranes • protein mimetics • supramolecular chemistry

Easy Access to Soluble Polyanions—Stabilization of the One-Dimensional Chain $^1_\infty[\text{K}_4\text{Sn}_9]$ by [18]Crown-6 in $[\text{K}_4\text{Sn}_9(\text{[18]crown-6})_3] \cdot \text{ethylenediamine}^{**}$

Thomas F. Fässler* and Rudolf Hoffmann

Dedicated to Professor Ernst Otto Fischer on the occasion of his 80th birthday

The reduction of metal salts provides an important way for the synthesis of element nanoparticles. Though routes for the generation of large transition metal clusters are well elaborated,^[1] comparably little is known about analogous accesses to main group element clusters.^[2] A general problem of the synthesis of nanoparticles is the broad distribution of particle size.^[3] In contrast, a directed synthesis of small, charged main group element clusters of uniform size exists, and recently the chemistry of homoatomic clusters of Group 14 elements received new impulses through the synthesis and structure determination of the phases $\text{Rb}_{12}\text{Si}_{17}$,^[4] A_4Ge_9 ($\text{A} = \text{K}, \text{Cs}$),^[5, 6] $\text{K}_{12}\text{Ge}_{17}$,^[5] and K_4Pb_9 .^[7] The crystalline compounds, which are synthesized from the elements at several hundred degrees, are Zintl phases with discrete nine-atom E_9^{4-} clusters. In the case of the 12:17 phases additional tetrahedral E_4^{4-} units are present. The crystal structure of the corresponding phase A_4Sn_9 or $\text{A}_{12}\text{Sn}_{17}$ ($\text{A} = \text{alkali metal}$) could not be elucidated due to poor crystal quality.^[6] Though nine-atom clusters were observed in solution over 100 years ago^[8] and the first structural characterization was carried out already in 1976,^[9] only small amounts of well-defined products could be isolated from solution. In the course of our studies of soluble, homoatomic Zintl ions,^[10] we report here a novel, very simple and efficient access to homoatomic polyanions from the elements at low temperatures.

We found that the alkali metals K, Rb, and Cs are soluble in the crown ether [18]crown-6, which is liquid at 40 °C.^[11] The deep blue color of the melt indicates the formation of an alkali or electride. The blue color vanishes after addition of an element of Group 14 to 16, indicating a reaction. To obtain crystalline products small amounts of solvent are added to the mixture. So far we were able to apply this procedure to the elements C (as C_{60}), Sn, Pb, As, Sb, Bi, and Te. Single-crystal structure analyses reveal the presence of the anions C_{60}^{3-} ,^[12a] Sn_9^{4-} , Pb_9^{4-} , As_7^{3-} , Sb_7^{3-} , and Te_4^{2-} .^[12b] For As, Sb,^[13] and Te,^[14] the formation of larger homoatomic polyanions in solution from the elements and their isolation in crystalline form was already known. However, in the case of Sn and Pb crystalline products were only obtained by extraction of binary or ternary phases.^[15] With the exception of $[\text{Na}_4(\text{en})_7]\text{Sn}_9$, which was characterized by Kummer and Strähle and which contains disordered en molecules ($\text{en} = \text{ethylenediamine}$),^[16] the struc-

- [1] D. A. Doyle, J. M. Cabral, R. A. Pfuetzner, A. Kuo, J. M. Gulbis, S. L. Cohen, B. T. Chait, R. MacKinnon, *Science* **1998**, *280*, 69.
- [2] D. A. Dougherty, *Science* **1996**, *271*, 163.
- [3] C. Miller, *Science* **1991**, *252*, 1092.
- [4] R. A. Kumpf, D. A. Dougherty, *Science* **1993**, *261*, 1708.
- [5] Y. Tanaka, Y. Kobuke, M. Sokabe, *Angew. Chem.* **1995**, *107*, 717; *Angew. Chem. Int. Ed. Engl.* **1995**, *34*, 693.
- [6] P. Schmitt, P. D. Beer, M. G. B. Drew, P. D. Sheen, *Angew. Chem.* **1997**, *109*, 1926; *Angew. Chem. Int. Ed. Engl.* **1997**, *36*, 1840.
- [7] N. Kimizuka, T. Wakiyama, A. Yanagi, S. Shinkai, T. Kunitake, *Bull. Chem. Soc. Jpn.* **1996**, *69*, 3681.
- [8] T. M. Fyles, B. Zeng, *Chem. Commun.* **1996**, 2295.
- [9] The synthesis of **1** is described in: B. Ghebremariam, S. Matile, *Tetrahedron Lett.* **1998**, *39*, 5335.
- [10] K. M. Maloney, D. R. Shnek, D. Y. Sasaki, F. H. Arnold, *Chem. Biol.* **1996**, *3*, 185, and references therein.
- [11] L. A. Weiss, N. Sakai, B. Ghebremariam, C. Ni, S. Matile, *J. Am. Chem. Soc.* **1997**, *119*, 12142.
- [12] N. Sakai, K. C. Brennan, L. A. Weiss, S. Matile, *J. Am. Chem. Soc.* **1997**, *119*, 8726.
- [13] C. Ni, S. Matile, *Chem. Commun.* **1998**, 755.
- [14] DOXYL = 2,2-disubstituted-4,4-dimethyl-3-oxazolidinyloxy, free radical, EYPC-SUVs: small unilamellar vesicles composed of egg yolk phosphatidylcholine; 5-DOXYL-PC: 1-palmitoyl-2-stearoyl(5-DOXYL)-sn-glycero-3-phosphocholine; 12-DOXYL-PC: 1-palmitoyl-2-stearoyl(12-DOXYL)-sn-glycero-3-phosphocholine.
- [15] K. Nakanishi, N. Berova in *Circular dichroism—principles and applications* (Eds.: K. Nakanishi, N. Berova, R. W. Woody), VCH, New York, **1994**, p. 361.
- [16] a) X. Song, J. Perlstein, D. G. Whitten, *J. Am. Chem. Soc.* **1997**, *119*, 9144; b) X. Song, C. Geiger, U. Leinhos, J. Perlstein, D. G. Whitten, *J. Am. Chem. Soc.* **1994**, *116*, 10340; c) D. G. Whitten, *Acc. Chem. Res.* **1993**, *26*, 502.
- [17] a) S. C. Hartsel, S. K. Benz, R. P. Peterson, B. S. Whyte, *Biochemistry* **1991**, *30*, 77; b) J. Bolard, P. Legrand, F. Heitz, B. Cybulska, *Biochemistry* **1991**, *30*, 5707.
- [18] G. W. Gokel, O. Murillo, *Acc. Chem. Res.* **1996**, *29*, 425.
- [19] G. Eisenman, R. Horn, *J. Membrane Biol.* **1983**, *76*, 197.

[*] Priv.-Doz. Dr. T. F. Fässler, R. Hoffmann
Laboratorium für Anorganische Chemie
der Eidgenössischen Technischen Hochschule
Universitätstrasse 6, CH-8092 Zürich (Switzerland)
Fax: (+41)1-632-1149
E-mail: faessler@inorg.chem.ethz.ch

[**] This work has been supported by the ETH Zürich and the Swiss National Science Foundation.

tural characterization of nine-atom clusters was only accomplished on single crystals containing $[A([2.2.2]\text{crypt})]^+$ ($A = \text{Na}, \text{K}$) as counter ions.^[17, 18] Attempts to use other cations did not result in crystalline products.^[19]

Following the experimental procedure introduced here, we obtained from the reaction of K and Sn in liquid [18]crown-6 different crystal types depending on the workup process. X-ray single-crystal structure determinations^[20] confirm that both crystal types contain four potassium ions for each Sn_9 polyhedron and that they differ in the ratio of K to [18]crown-6. The composition of four K atoms per cluster is in agreement with a fourfold negative charge for each polyanion. Whereas in $[\text{K}([18]\text{crown-6})]_4\text{Sn}_9$ (**2**) only two of the four K atoms are in contact with the cluster (Figure 1), $[\text{K}([18]\text{crown-6})]_3\text{KSn}_9 \cdot \text{en}$ (**1**) has a remarkable one-dimensional substructure of the composition K_4Sn_9 (Figure 2). A Zintl phase of such a composition has not yet been structurally described. In the title compound **1** the nine-atom tin clusters have contacts to all K atoms (Figure 1). Three K atoms are additionally

coordinated to crown ether units in such way that in **1** the "saltlike intermetallic"^[8b] chains ${}^1[\text{K}_4\text{Sn}_9]$ are separated by organic molecules. Linear chains which exhibit alternating nine-atom clusters and noncomplexed K atoms are already known. However, in $[\text{K}([2.2.2]\text{crypt})]_3\text{KSn}_9$ three K atoms have no contact with the anions due to full inclusion in the cryptand molecules.^[21] In the present structure an uncharged unit K_4Sn_9 is formed. The compound is an intermediate between typical molecular (ionic) representatives and binary intermetallic phases (Zintl phases). The pronounced anisotropy of this structure should be reflected in the properties—semiconducting along the *a* axis and isolating in the perpendicular directions.

In **2** only two K atoms are directly bound to the polyanions (Figure 1). The K atoms of the two other $[\text{K}([18]\text{crown-6})]$ units possess significantly larger distances to nearest atoms of the polyanions ($>6.98 \text{ \AA}$). The K–Sn distances of the $[\text{K}([18]\text{crown-6})]$ units in **1** and **2** are in the range of 3.535 to 4.154 \AA (Figure 1) and vary around the values observed in the Zintl phase KSn .^[22] Taking into account two slightly longer contacts in **1** (K1–Sn2 4.438(2) and K2–Sn2 4.353(2) \AA) the polyanions set up η^3 coordination to the K atoms. The K4 atom, which is not coordinated to [18]crown-6, possesses a slightly distorted and elongated trigonal-prismatic coordination polyhedron of six Sn atoms with K–Sn distances of 3.603(3)–4.048(4) \AA . The $[\text{K}([18]\text{crown-6})]$ entity proves to be an advantageous connecting device between intermetallic and organic networks. In addition to contacts of the K atoms, weak intermolecular interactions between the H atoms of the crown ethers and the atoms Sn1, Sn5, and Sn7 ($d(\text{Sn} \cdots \text{H}) = 3.13\text{--}3.17 \text{ \AA}$)^[23] enable the construction of the aggregate in **1** (Figure 2). The structure of **1** can therefore be regarded as a supramolecular arrangement of a "saltlike intermetallic" part of the composition K_4Sn_9 and an organic component.

The structures of the anions in **1** and **2** differ significantly from those of known Sn_9^{4-} anions (Table 1). The classification of their structures to the polyhedra **A** and **B** can be accomplished according to the criteria in Scheme 1 and Table 1: An ideal threefold capped trigonal prism **A** with equal prism heights *h* and edge lengths *e* has an *h/e* ratio of 1.0 as well as three equal dihedral angles α , whereas in an ideal monocapped square antiprism one angle α equals zero. The noncapped face in **B** possesses two diagonals of same length *d*. As predicted from Wade's rules^[24] all previously structurally well characterized Sn_9^{4-} anions exhibit nearly undistorted clusters of type **B**.^[21, 25] More electron

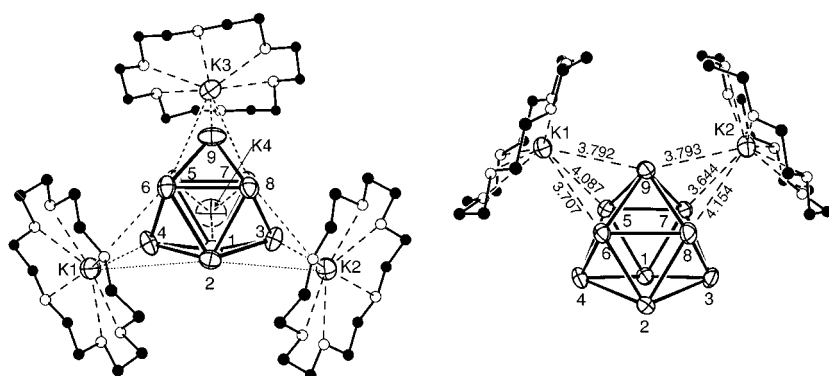


Figure 1. Details of the crystal structures of **1** (left) and **2** (right). The displacement parameters of the Sn and K atoms are shown with 50% probability ellipsoids. For reasons of clarity crown ether molecules are shown as stick-and-ball models. Distances in \AA (standard deviation 0.005 \AA). For further distances, see text and reference [30].

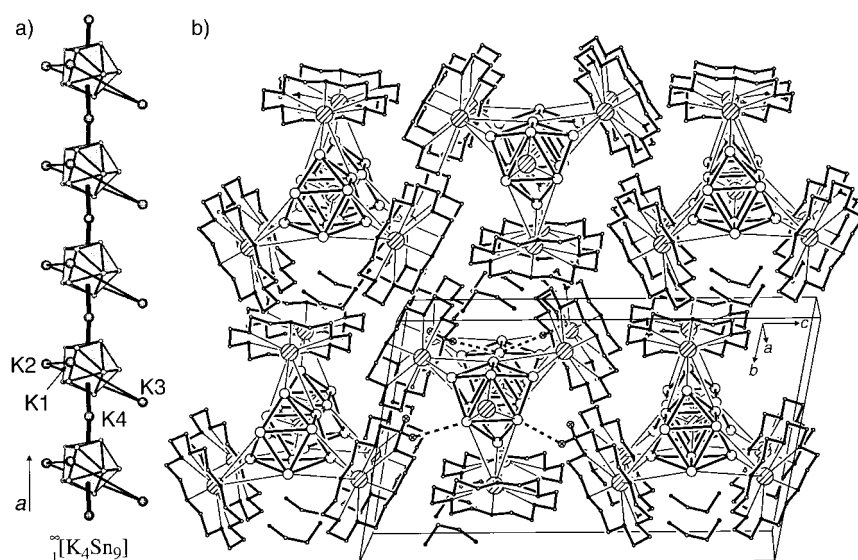
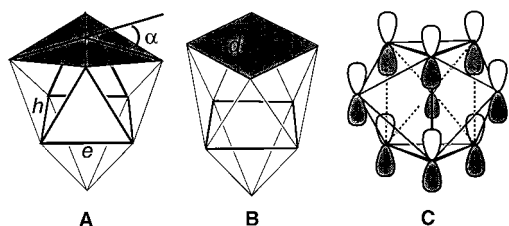


Figure 2. Larger sections of the structure of **1**. a) A one-dimensional moiety of the composition K_4Sn_9 aligns parallel to the *a* axis. b) Relative arrangement of ions and molecules as viewed down the *a* axis. Atom symbols: hatched circles: K, large and small open circles: Sn and C, respectively, filled circles: O and N. The shortest $\text{Sn} \cdots \text{H}$ contacts of geometrically determined H positions (circles marked with crosses) are shown as dashed lines. The remaining H atoms are omitted.

Table 1. Structural parameters of nine-atom tin clusters (see Scheme 1).

Compound ^[a]	h_1, h_2, h_3 ^[b]	h/e ^[c]	α [°] ^[d]	d [Å] ^[e]
[K([2.2.2]crypt)] ₆ Sn ₉ Sn ₉ ^[10a]	1.10, 1.02, 1	1.08	13, 19, 23	3.315, 4.813
[K([2.2.2]crypt)] ₅ Sn ₉ ^[25]	1.04, 1.04, 1.02	1.08	17, 18, 18	3.501, 4.680
[K([2.2.2]crypt)] ₃ KSn ₉ ^[21]	1.29, 1.03, 1.00	1.19 ^[f]	2, 28, 29	4.129, 4.229
[Na([2.2.2]crypt)] ₄ Sn ₉ ^[24]	1.32, 1.04, 1.01	1.19 ^[f]	3, 29, 30	4.163, 4.205
[K([18]krone-6)] ₃ KSn ₉ 1	1.17, 1.06, 1.05	1.15	13, 22, 24	3.722, 4.506
[K([18]krone-6)] ₄ Sn ₉ 2	1.11, 1.08, 1.04	1.14	15, 17, 22	3.531, 4.673

[a] Formulae without solvent molecules. [b] Normalized heights of the trigonal prism **A** (reference value is the shortest height (3.194 Å) of the nondisordered anion in [K-([2.2.2]crypt)]₆Sn₉Sn₉). Heights h_1 – h_3 correspond to the distances Sn7–Sn8, Sn5–Sn6, and Sn1–Sn2, respectively. [c] h and e are the mean values of the prism heights and the triangular edges, respectively. [d] Dihedral angles Sn3–Sn7–Sn8–Sn9, Sn4–Sn5–Sn6–Sn9, Sn3–Sn1–Sn2–Sn4. [e] Distances Sn7–Sn8 and Sn4–Sn9. [f] For the calculation, the shorter diagonal of the open square face in **B** is regarded as third prism height in **A**.



Scheme 1. Structures of nine-atom clusters as expected from Wade's rules: *closo*-type **A**, threefold capped trigonal prism (D_{3h}); *nido*-type **B**, singly capped square antiprism (C_{4v}). The parameters prism height h , dihedral angle α (angle which is defined by one prism height h and the corresponding capping atoms), edge length e of the triangles of the prism in **A** as well as the diagonal lengths d in **B** characterize the two boundary structures. The energetically lowest unoccupied orbital (LUMO) **C** of a cluster with structure **A** and 20 skeletal electrons is antibonding along the prism heights.

deficient, paramagnetic Sn_9^{3-} ions have structures which lie between the two boundary structures **A** and **B**.^[10a, 26] The structure of these polyhedra are described as distorted variants derived from type **A**, that is, elongated prism with larger h/e ratios than the ideal polyhedron **A** (Table 1). The origin of this distortion is the occupation of the LUMO **C** of a hypothetical *closo* cluster Sn_9^{3-} with one electron (Scheme 1). The orbital interaction in **C** is antibonding along the prism heights. The Sn_9^{4-} ions described here do not possess C_{4v} point group symmetry. The deviation from a C_{4v} -symmetrical **B** is significant, as the parameter α and the different diagonal lengths d demonstrate. Deduced from type **A**, they have even larger h/e ratios than Sn_9^{3-} anions, a fact expected from the occupation of orbital **C** with two electrons.^[27] The anions display approximately C_{2v} point group symmetry and can be described as threefold capped trigonal prisms, with one prism height about 10% longer than the other two.^[18, 28] In comparison to other known anion structures the findings here demonstrate that a correlation of electron number and structure with respect to Wade's rules does not hold for naked main group element clusters.^[31]

The reaction procedure reported here using crown ether as reaction medium offers the advantage of a "one-pot synthesis" that starts from the elements and which can be carried out at 40 °C in Schlenk tubes. The resulting reaction products are crystalline and soluble not only in amines but also in DMF and acetonitrile. This method should also be applicable using main group element and transition metal halides as reactants.

The possible usage of polyethyleneoxides instead of cyclic crown ethers is currently under investigation.

Experimental Section

1: [18]Crown-6 (800 mg, 3.0 mmol), K (98 mg, 2.5 mmol), and Sn (200 mg, 1.7 mmol) are mixed in a Schlenk tube (20 mL). The mixture is heated to 40–50 °C, just allowing the crown ether to melt, and stirred at this temperature for 1 h. Alternatively K and [18]crown-6 can be stirred at 40 °C, and Sn added in a second step to the deep blue melt. The color of the originally blue melt changes during the reaction from light gray to dark gray. Ethylenediamine (2 mL) is added to the cooled melt, and the mixture is sonicated for 15 min. Thereafter the solution is layered with toluene (4.5 mL). After one week **1** is obtained in the form of dark red, nearly black needles (yield: 120 mg, 31 % based on employed Sn and 40 % based on Sn undergoing reaction).

2: Analogously to the preparation of **1** [18]crown-6 (800 mg, 3.0 mmol), K (98 mg, 2.5 mmol), and Sn (475 mg, 4.75 mmol) are allowed to react. The dark red solution is filtered. After four weeks **2** is obtained in the form of brown plates (yield: 105 mg, 11 % based on employed Sn).

Elemental analysis of the vacuum-dried products: **1** ($\text{C}_{36}\text{H}_{72}\text{K}_4\text{O}_{18}\text{Sn}_9$, 2017.56 g mol⁻¹): calcd (found) [%]: C 21.43 (20.58), H 3.60 (3.67), K, 7.75 (7.94), Sn 52.95 (51.05); **2** ($\text{C}_{48}\text{H}_{96}\text{K}_4\text{O}_{24}\text{Sn}_9$, 2282.06 g mol⁻¹): calcd (found) [%]: C 25.26 (25.00), H 4.24 (4.24), K 6.85 (7.20), Sn 46.82 (46.60).

Received: August 21, 1998

Revised version: November 2, 1998 [Z 12310 IE]

German version: *Angew. Chem.* **1999**, *111*, 526–529

Keywords: clusters • crown compounds • potassium • tin • Zintl anions

- [1] M. J. Wagner, J. L. Dye in *Comprehensive Supramolecular Chemistry*, Vol. 1 (Eds.: J. L. Atwood, J. E. D. Davies, D. D. MacNicol, F. Vögtle, J.-M. Lehn), Pergamon, Oxford, **1996**; M. T. Reetz, S. A. Quaiser, *Angew. Chem.* **1995**, *107*, 246; *Angew. Chem. Int. Ed. Engl.* **1995**, *34*, 2240.
- [2] J. R. Heath, *Science* **1992**, *258*, 1131; L. Brus, *Adv. Mater.* **1993**, *5*, 286; R. A. Bley, S. M. Kauzlarich, *J. Am. Chem. Soc.* **1996**, *118*, 12461.
- [3] G. Schmid, *Clusters and Colloids*, VCH, Weinheim, **1994**.
- [4] V. Quéneau, E. Todorov, S. C. Sevov, *J. Am. Chem. Soc.* **1998**, *120*, 3263.
- [5] V. Quéneau, S. C. Sevov, *Angew. Chem.* **1997**, *109*, 1818; *Angew. Chem. Int. Ed. Engl.* **1997**, *36*, 1754.
- [6] H. G. von Schnering, M. Baitinger, U. Bolle, W. Carrillo-Cabrera, J. Curda, Y. Grin, F. Heinemann, J. Llanos, K. Peters, A. Schmeding, M. Somer, *Z. Anorg. Allg. Chem.* **1997**, *623*, 1037.
- [7] V. Quéneau, S. C. Sevov, *Inorg. Chem.* **1998**, *37*, 1358.
- [8] a) A. Joannis, *C.R. Hebd. Seances Acad. Sci.* **1891**, *113*, 795; C. A. Kraus, *Trans. Am. Electrochem. Soc.* **1924**, *45*, 175; b) E. Zintl, J. Goubenau, W. Dullenkopf, *Z. Physikal. Chem. A* **1931**, *154*, 1; E. Zintl, A. Harder, *Z. Physikal. Chem. A* **1931**, *154*, 47.
- [9] The structure of an Sn_9^{4-} anion was determined for the first time in $[\text{Na}_4(\text{en})_7]\text{Sn}_9$.^[16] The anion strongly deviates from the ideal structures **A** and **B** in Scheme 1. In spite of severe disorder of solvent molecules, the Sn_9^{4-} anion was unambiguously identified. A more precise structural investigation of a C_{4v} -symmetrical anion was carried out later with $[\text{Na}([2.2.2]\text{crypt})]_4\text{Sn}_9$.^[25]
- [10] a) T. F. Fässler, M. Hunziker, *Z. Anorg. Allg. Chem.* **1996**, *622*, 837; b) T. F. Fässler, H.-J. Muhr, M. Hunziker, *Eur. J. Inorg. Chem.* **1998**, *1433*; T. F. Fässler, M. Hunziker, *Inorg. Chem.* **1994**, *33*, 5380; T. F. Fässler, Habilitationsschrift, ETH Zürich, **1997**.
- [11] [18]Crown-6 = 1,7,10,13,16-hexaoxacyclooctadecane.
- [12] a) T. F. Fässler, R. Hoffmann, unpublished results; b) T. F. Fässler, R. Hoffmann, *Chimia* **1998**, *52*, 158.
- [13] N. Korber, F. Richter, *Angew. Chem.* **1997**, *109*, 1575; *Angew. Chem. Int. Ed. Engl.* **1997**, *36*, 1512.
- [14] R. Zagler, B. Eisenmann, H. Schäfer, *Z. Naturforsch. B* **1987**, *42*, 151.

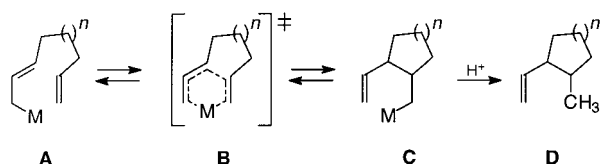
- [15] D. Kummer, L. Diehl, *Angew. Chem.* **1970**, 82, 881; *Angew. Chem. Int. Ed. Engl.* **1970**, 9, 895; J. D. Corbett, *Chem. Rev.* **1985**, 85, 383.
- [16] L. Diehl, K. Khodadadeh, D. Kummer, J. Strähle, *Chem. Ber.* **1976**, 109, 3404.
- [17] [2.2.2]Crypt = 4,7,13,16,21,24-hexaoxa-1,10-diazabicyclo[8.8.8]hexacosane.
- [18] J. D. Corbett, *Structure and Bonding* **1997**, 87, 157.
- [19] R. G. Teller, L. J. Krause, R. C. Haushalter, *Inorg. Chem.* **1983**, 22, 1809.
- [20] Crystal structure determination: Crystals were mounted in glass capillaries. Structure solution (SHELXS-97) and refinement (SHELXL-97) was carried out with direct and full-matrix least-square methods based on F^2 for all atoms with anisotropic displacement parameters. **1**: crystal dimensions $0.12 \times 0.45 \times 0.50$ mm³, lattice constants at 243 K: $a = 10.220(2)$, $b = 14.957(3)$, $c = 23.690(5)$ Å, $\alpha = 99.86(3)^\circ$, $\beta = 91.43(3)^\circ$, $\gamma = 103.79(3)^\circ$, $V = 3456(1)$ Å³; space group $P\bar{1}$ (no 2), $Z = 2$, $\rho_{\text{calc}} = 1.996$ g cm⁻³, $\mu = 3.489$ mm⁻¹; Data collection: STOE IPDS, Mo_K α radiation, $2\theta_{\text{max}} = 48.18^\circ$ (imaging plate distance 80 mm); of 20081 total reflections, 10171 were independent ($R_{\text{int}} = 0.052$); $R_1 = 0.046$ and $wR = 0.123$ for 620 parameters and 10168 reflections with $I > 2\sigma(I)$; max./min. residual electron density 1.57/−1.32 e Å⁻³. **2**: crystal dimensions $0.24 \times 0.34 \times 0.46$ mm³, lattice constants at 193 K: $a = 14.839(3)$, $b = 22.012(4)$, $c = 14.910(3)$ Å, $\beta = 108.97(3)^\circ$, $V = 4605(2)$ Å³; space group $P2_1$ (no. 4), $Z = 2$, $\rho_{\text{calc}} = 1.645$ g cm⁻³, $\mu = 2.631$ mm⁻¹; data collection: STOE IPDS, Mo_K α radiation, $2\theta_{\text{max}} = 48.18^\circ$ (imaging plate distance 80 mm); of 26456 total reflections, 13778 were independent ($R_{\text{int}} = 0.051$); $R_1 = 0.078$ and $wR = 0.209$ for 766 parameters and 13321 reflections with $I > 2\sigma(I)$; max./min. residual electron density 1.86/−1.05 e Å⁻³. Crystallographic data (excluding structure factors) for the structures reported in this paper have been deposited with the Cambridge Crystallographic Data Centre as supplementary publication no. CCDC-102741 (**1**) and CCDC-102742 (**2**). Copies of the data can be obtained free of charge on application to CCDC, 12 Union Road, Cambridge CB21EZ, UK (fax: (+44)1223-336-033; e-mail: deposit@ccdc.cam.ac.uk).
- [21] R. Burns, J. D. Corbett, *Inorg. Chem.* **1985**, 24, 1489.
- [22] KSn contains discrete, tetrahedral Sn₄⁴⁺ units: I. F. Hewaidy, E. Busmann, W. Klemm, *Z. Anorg. Allg. Chem.* **1964**, 328, 283.
- [23] The sum of van der Waals radii is 3.30 Å: A. Bondi, *J. Phys. Chem.* **1964**, 68, 441.
- [24] K. Wade, *Adv. Inorg. Chem. Radiochem.* **1976**, 18, 1.
- [25] J. D. Corbett, P. A. Edwards, *J. Am. Chem. Soc.* **1977**, 99, 3313.
- [26] S. C. Critchlow, J. D. Corbett, *J. Am. Chem. Soc.* **1983**, 105, 5715.
- [27] M. E. O'Neill, K. Wade, *Polyhedron* **1983**, 2, 963; T. F. Fässler in *Metal Clusters in Chemistry* (Eds.: P. Braunstein, L. A. Oro, P. R. Raithby), WILEY-VCH, submitted.
- [28] A cluster with a similar structure is also observed in [Na₄(en)₇]Sn₆^[16] and for the isoelectronic cation Bi₆³⁺.^[29]
- [29] A. Hershaft, J. D. Corbett, *Inorg. Chem.* **1963**, 2, 979; R. M. Friedman, J. D. Corbett, *Inorg. Chem.* **1973**, 12, 1134.
- [30] Distances [Å] in **1**: Sn1–Sn2 3.355(2), Sn5–Sn6 3.412(2), Sn7–Sn8 3.722(2), Sn1–Sn5 3.116(1), Sn1–Sn7 3.014(1), Sn5–Sn7 2.951(1), Sn2–Sn6 3.081(1), Sn2–Sn8 2.993(1), Sn6–Sn8 3.019(1), Sn1–Sn3 2.915(1), Sn2–Sn3 2.985(1), Sn7–Sn3 2.939(1), Sn8–Sn3 2.944(1), Sn1–Sn4 2.925(1), Sn2–Sn4 2.975(1), Sn5–Sn4 2.932(2), Sn6–Sn4 2.940(1), Sn5–Sn9 2.952(1), Sn6–Sn9 2.938(2), Sn7–Sn9 2.942(1), Sn8–Sn9 2.906(1); K1–Sn2,Sn4,Sn6 4.438(2), 3.544(2), 4.074(3); K2–Sn2,Sn3,Sn8 4.353(2), 3.535(2), 4.072(2); K3–Sn5,Sn7,Sn9 4.039(3), 4.021(2), 3.542(3). Sn–Sn distances [Å] in **2** (same order as for **1**): 3.335(2), 3.450(2), 3.531(2), 3.045(2), 3.010(2), 2.990(2), 3.038(2), 3.030(2), 2.987(2), 2.974(2), 2.959(2), 2.930(2), 2.923(2), 2.958(2), 2.980(2), 2.930(2), 2.928(2), 2.942(2), 2.984(2), 2.982(2), 2.941(2).
- [31] For the controversial discussion on the charge allocation to the nonequivalent anions in [K([2.2.2]crypt)]₆Ge₆, see C. H. E. Belin, J. D. Corbett, A. Cisar, *J. Am. Chem. Soc.* **1977**, 99, 7163; T. F. Fässler, U. Schütz, *Inorg. Chem.*, in press; and references [10, 18].

Chiral Induction by Elimination-Coupled Lithium–Ene Reaction: Synthesis of (+)-(3*R*,4*R*)-1,2-Dihydromultifidene**

Alexander Deiters and Dieter Hoppe*

Dedicated to Professor Bernt Krebs
on the occasion of his 60th birthday

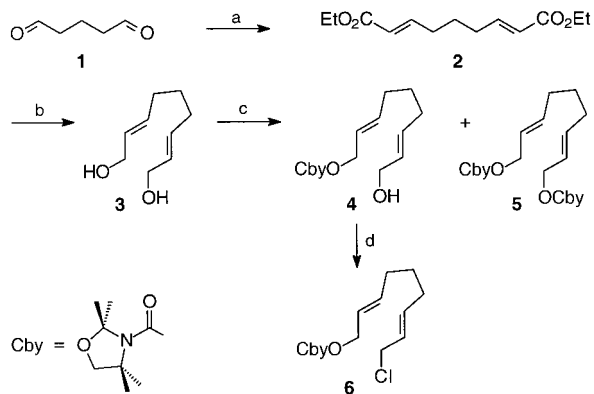
Intramolecular metallo–ene reactions are efficient methods for the construction of substituted ring systems.^[1] As the Type 1 metallo–ene reaction illustrates, 2, ($\omega - 1$)-alkadienyl-metal compounds **A** cyclize via the cyclic conjugated transition state **B** to form a (2-vinylcycloalkyl)methylmetal intermediate **C**, which is then protonated to give cycloalkanes **D** (Scheme 1). One problem is the poorly developed equilibrium state. Moreover, the previously described metallo–ene



Scheme 1. Metallo–ene reaction of Type 1 ($n = 1, 2$; M = Li, MgHal).

reaction where M = Li^[2] and M = MgHal^[3] give racemic products.^[1, 4]

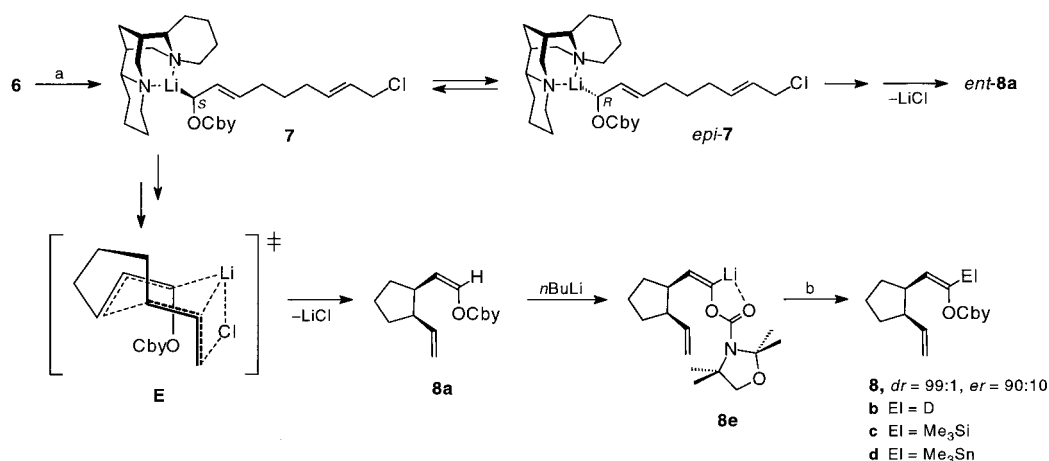
We report here the first asymmetric lithium–ene reaction, the basis of which is the enantioselective (–)-sparteine-induced deprotonation of 2-alkenyl carbamates.^[5, 6] We selected (2*E*,7*E*)-9-chloronona-2,7-dienyl carbamate (**6**)^[7] as substrate in order to compensate for the unfavorable equilibrium state of the cyclization with an irreversible elimination step.^[8] Compound **6** was obtained from pentanedial (**1**) by standard methods (Scheme 2). Treatment of **6** ($E:Z = 98:2$)



Scheme 2. Synthesis of **6**. a) EtO₂CCH₂PO(OEt)₂ (2.2 equiv), K₂CO₃ (5.0 equiv), H₂O, 35% aq. NaOH, 92%; b) DIBAL-H (5.0 equiv), PhCH₃, 92%; c) NaH (1.1 equiv), CbyCl (1.0 equiv), THF, 19% **3**, 39% **4**, and 22% **5**; d) LiCl (5.0 equiv), *n*BuLi (1.0 equiv), CH₃SO₂Cl (1.1 equiv), THF, 90% **6**.^[26] DIBAL-H = diisobutylaluminum hydride.

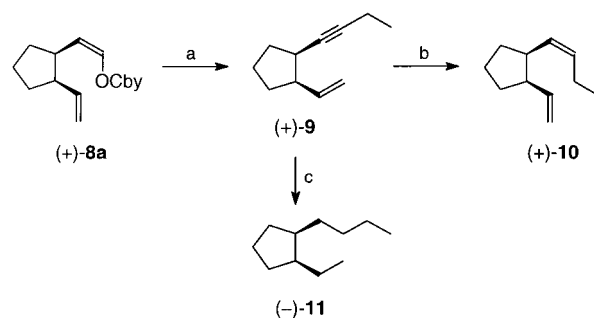
* Prof. Dr. D. Hoppe, Dipl.-Chem. A. Deiters
Organisch-chemisches Institut der Universität
Corrensstrasse 40, D-48149 Münster (Germany)
Fax: (+49)251-8339772

** This work was supported by the Fonds der Chemischen Industrie and the Studienstiftung des deutschen Volkes. We thank Prof. Dr. E.-U. Würthwein and Dr. C. Mück-Lichtenfeld for the semi-empirical calculations on the reaction pathway.



Scheme 3. Enantioselective lithium-ene reaction. a) $n\text{BuLi}/(-)\text{-sparteine}$ (2.2 equiv), PhCH_3 , -90°C ; b) EIX (5 equiv); 8a: MeOH , 90%, $dr = 99:1$, $er = 90:10$ (80% ee); 8b: MeOD , 90%; 8c: Me_3SiCl , 84%; 8d: Me_3SnCl , 75%.^[26]

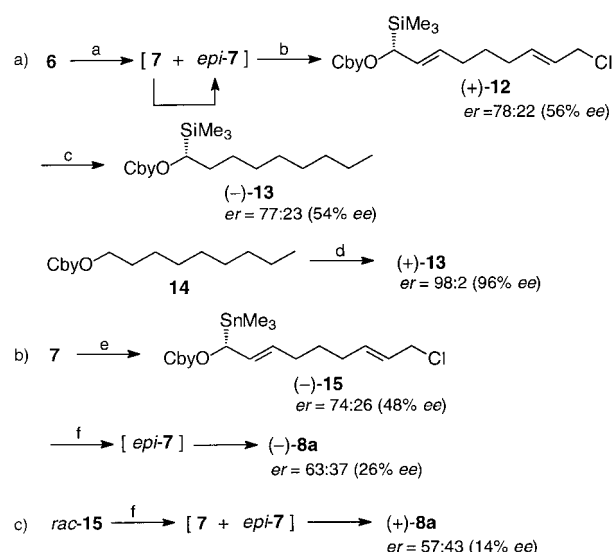
with 2.2 equivalents of n -butyllithium/ $(-)$ -sparteine in toluene at -90°C and subsequent hydrolysis of the reaction mixture gave the cyclopentane (+)-8a in 90% yield with a diastereomeric ratio (dr) *cis:trans* of over 99:1 and an enantiomeric ratio (er) of 90:10 (80% ee ; Scheme 3). At -78°C (+)-8a was again obtained in 90%, but with only 66% ee ($er = 83:17$).^[10-12] Reaction product 8a is once more deprotonated under the reaction conditions,^[13] and the intermediate vinyl lithium compound 8e can be captured by protons or other electrophiles with retention of the double bond geometry to yield 8b-d. The absolute configuration (1*R*,2*R*) of (+)-8a was confirmed by conversion into the known (+)-(3*R*,4*R*)-1,2-dihydromultifidene (+)-10 and the perhydro product (-)-11 (Scheme 4).^[14, 15] The key step is a Fritsch-Buttenberg-Wiechell rearrangement of the lithiated vinyl carbamate by the Kocienski method.^[13]



Scheme 4. Stereochemical correlation of (+)-8a. a) 1. $n\text{BuLi}/\text{TMEDA}$ (3.0 equiv), THF , -78°C , 1.5 h; 2. 20°C , 2 h; 3. 0°C , EtI (4.0 equiv); 4. 40°C , 12 h, 65%; b) H_2 , 30 wt % Lindlar catalyst, quinoline, C_5H_{12} , 76%; c) H_2 , 50 wt % Pt/C , C_5H_{12} , 82%.^[26] TMEDA = N,N,N',N' -tetramethylethylenediamine.

The details of the mechanism and the topology of the transition state which leads to (+)-8 were elicited by further experiments (Scheme 5):

- Deprotonation of 6 with n -butyllithium/ $(-)$ -sparteine in the presence of Me_3SiCl gave the silane (+)-(*R*)-12^[16] with $er = 78:22$ (56% ee). The *R* configuration was confirmed by correlation with (+)-(*S*)-13, which was obtained by the $(-)$ -sparteine method from the saturated alkyl carbamate 14.^[17] Since silylation and stannylation of lithiated allyl carbamates generally take place with inversion of config-



Scheme 5. Studies on the mechanism of the lithium-ene reaction. a) $n\text{BuLi}/(-)\text{-sparteine}$ (1.5 equiv), PhCH_3 , -78°C ; b) Me_3SiCl (1.5 equiv, present in (a)), 70%; c) H_2 , 200 wt % Pd/C , NaOAc (10.0 equiv), MeOH , 90%; d) $s\text{BuLi}/(-)\text{-sparteine}$ (1.5 equiv), Me_3SiCl (3.0 equiv), Et_2O , -78°C , 80%; e) Me_3SnCl (2.5 equiv), 16% 15, 7% 8d, 53% 8a, and 18% 6; f) $n\text{BuLi}/(-)\text{-sparteine}$ (2.0 equiv), PhCH_3 , -78°C , 100%.^[26]

uration,^[18] the predominant lithium compound 7 was assigned the 1*S* configuration.

- The configuration of 7 was inverted to *epi*-7 by trimethylstannylation to the tin compound (-)-(*R*)-15 (49% ee)^[18] and lithiodestannylation with n -butyllithium/ $(-)$ -sparteine.^[19] In this way, (-)-(*1S,2S*)-8a ($er = 63:37$, 26% ee) was prepared in quantitative yield.
- Starting from *rac*-15, (+)-8a ($er = 57:43$, 14% ee) was obtained in quantitative yield.

According to the stereochemical information that is "conserved" in the product (1*R*,2*R*; *cis* arrangement of the side chains, *Z* configuration of the vinyl carbamate unit),^[20] the transition state which leads to the main product (+)-8 is assigned the structure **E** (see Scheme 3).^[21] It is probable that no discrete lithium intermediate is formed; instead β -elimination of lithium chloride occurs concurrently with its formation.^[23] Experiments (b) and (c), illustrated in Scheme 5, suggest a comparably slow epimerization of 7 into *epi*-7, when the $(-)$ -sparteine complex 7 cyclizes somewhat more rapidly

than *epi*-**7**.^[24] Overall, chiral induction by an elimination-coupled lithium–ene reaction offers a new and potentially useful route to enantiomerically enriched carbocycles.^[25]

Experimental Section

Compound **6** (100 mg, 0.30 mmol) and (–)-sparteine (155 mg, 0.66 mmol) were dissolved in toluene (4 mL) under argon. After the solution had been cooled to –90 °C, a 1.6 M hexane solution of *n*-butyllithium (0.41 mL, 0.66 mmol) was added slowly, and the solution was stirred at this temperature for 2 h. Methanol (1 mL) and saturated NH₄Cl solution (1 mL) were then added, and the reaction mixture was warmed to room temperature. The crude product was isolated by usual procedures and purified by column chromatography with Et₂O/pentane (1/5) to yield **8a** as a colorless oil (79 mg, 90%, 80% ee).^[11, 26]

Received July 8, 1998 [Z 12112]

German version: *Angew. Chem.* **1999**, *111*, 529–532

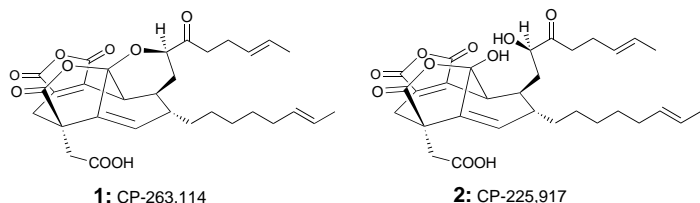
Keywords: asymmetric synthesis • carbocycles • ene reactions • metalations

- [1] Review: W. Oppolzer, *Angew. Chem.* **1989**, *101*, 39–53; *Angew. Chem. Int. Ed. Engl.* **1989**, *28*, 38–52.
- [2] A. D. Josey, *J. Org. Chem.* **1974**, *39*, 139–145.
- [3] H. Felkin, J. D. Umpleby, E. Hagaman, E. Wenkert, *Tetrahedron Lett.* **1972**, 2285–2288.
- [4] A single example of a Pd–ene reaction induced by a chiral ligand has been described (47% ee, *cis:trans* = 87:13): W. Oppolzer, D. L. Kuo, M. W. Hutzinger, R. Léger, J.-O. Durand, C. Leslie, *Tetrahedron Lett.* **1997**, *38*, 6213–6216.
- [5] a) O. Zschage, D. Hoppe, *Angew. Chem.* **1989**, *101*, 67–69; *Angew. Chem. Int. Ed. Engl.* **1989**, *28*, 67–69; b) O. Zschage, D. Hoppe, *Tetrahedron* **1992**, *48*, 8389–8392; c) H. Paulsen, C. Graeve, D. Hoppe, *Synthesis* **1996**, 141–144.
- [6] Reviews: a) D. Hoppe, T. Hense, *Angew. Chem.* **1997**, *109*, 2376–2410; *Angew. Chem. Int. Ed. Engl.* **1997**, *36*, 2282–2316; b) P. Beak, A. Basu, D. J. Gallagher, Y. S. Park, S. Thayumanavan, *Acc. Chem. Res.* **1996**, *29*, 552–560.
- [7] The *E* geometry of the double bonds of the diester **2** and the dicarbamate **5** were confirmed by the ¹H NMR coupling constants of the alkene protons (15.7 and 15.2 Hz)
- [8] Previous attempts to cyclize simple 2,7-alkadienyl carbamates (**6**, H or C₆H₅ for CH₂Cl) by lithiation with *n*BuLi/TMEDA were unsuccessful. Only the dicarbamate **5** gave *rac*-**8a** in 10% yield.^[10]
- [9] a) J. Villieras, M. Raumbaud, M. Graff, *Synth. Commun.* **1986**, *16*, 149–156; b) F. Hintze, D. Hoppe, *Synthesis* **1992**, 1216–1218.
- [10] A. Deiters, Diplomarbeit, Universität Münster, **1998**.
- [11] **8a**: [α]_D²⁰ = +50.7 (*c* = 0.34 in CHCl₃) for *er* = 90:10 (80% ee); ¹H NMR (300 MHz, CDCl₃): δ = 1.21–1.65 (m, 14H; CH₂, CH₃(Cby)), 1.76–1.85 (m, 4H; CH₂), 2.52–2.68 (m, 1H; CH), 2.97–3.15 (m, 1H; CH), 3.77 (s, 2H; CH₂(Cby)), 4.70 (dd, ³*J* = 6.5, 9.6 Hz, 1H; CH=CH–O), 4.95–5.03 (m, 2H; CH=CH₂), 5.72–5.84 (m, 1H; CH=CH₂), 6.96 (d, 1H; CH=CH–O). The *cis* arrangement of the alkyl groups in **8a**, **9**, and **10** was confirmed by NOE experiments. The *Z* geometry of the enol carbamate group in **8a** is derived from ¹H NMR coupling constants of the alkene protons at 6.5 Hz. The enantiomeric ratio was determined by gas chromatography on a chiral stationary phase (Beta-Dex 120, Supelco, USA).
- [12] Compound *rac*-**8a** is also obtained in 90% yield with *n*BuLi/TMEDA. At least two equivalents of base are required because **8a** is deprotonated to **8e** under the reaction conditions: B. Peschke, Dissertation, Kiel University, **1991**; S. Sengupta, V. Snieckus, *J. Org. Chem.* **1990**, *55*, 5680–5683; H. Paulsen, D. Hoppe, *Tetrahedron* **1992**, *48*, 5667–5670 and reference [13].
- [13] P. Kocienski, N. J. Dixon, *Synlett* **1989**, 52–54; P. Kocienski, C. Barber, *Pure Appl. Chem.* **1990**, *62*, 1933–1940.
- [14] W. Boland, K. Mertes, L. Jaenicke, D. G. Müller, E. Fölster, *Helv. Chim. Acta* **1983**, *66*, 1905–1913.
- [15] The optical rotations corrected to 100% ee [(+)-**10**: [α]_D²⁰ = +52.0 (*c* = 0.39 in pentane); (–)-**11**: [α]_D²⁰ = –3.5 (*c* = 2.84 in pentane)] agree well with the literature values [(+)-**10**: [α]_D²⁰ = +55.8 (*c* = 2.56 in pentane); (–)-**11**: [α]_D²⁰ = –7.1 (*c* = 0.64 in pentane)].^[14]
- [16] The enantiomeric excesses of the silanes and stannanes (**12**, **13** and **15**) were determined by ¹H NMR shift experiments with [Eu(hfc)₃] (hfc = 3-(heptafluoropropylhydroxymethylene)-D-camphorate)). The rotations were: (+)-**12**: [α]_D²⁰ = +11.7 (*c* = 0.73 in CHCl₃); (+)-**13**: [α]_D²⁰ = +7.1 (*c* = 2.08 in CHCl₃); (–)-**13**: [α]_D²⁰ = –3.9 (*c* = 2.55 in CHCl₃); (–)-**15**: [α]_D²⁰ = –9.5 (*c* = 0.40 in CHCl₃).
- [17] D. Hoppe, M. Paetow, F. Hintze, *Angew. Chem.* **1993**, *105*, 430–432; *Angew. Chem. Int. Ed. Engl.* **1993**, *32*, 394–396.
- [18] For precedences on inversion of configuration during silylation and stannylation reactions with allyllithium–(–)-sparteine complexes, see K. Behrens, Dissertation, Münster University **1997** and reference [5c].
- [19] For inversion of configuration of chiral benzyl lithium compounds during stannylation (inversion) and lithium destannylation (retention), see A. Carstens, D. Hoppe, *Tetrahedron* **1994**, *50*, 6097–6108; G. A. Weisenburger, P. Beak, *J. Am. Chem. Soc.* **1996**, *118*, 12218–12219 and reference [18].
- [20] The carbamoyloxy group in γ -monosubstituted lithiated allyl carbamates (e.g., **7**) preferentially adopts the *endo* configuration, which leads to a 1Z double bond in the products (e.g., **8a**): D. Hoppe, R. Hanko, A. Brönneke, F. Lichtenberg, E. von Hülsen, *Chem. Ber.* **1985**, *118*, 2822–2851.
- [21] A previously unexplained discrepancy exists here: The transition state **E** requires (1*R*)-**7** as substrate, whereas the capture experiments suggest an excess of (1*S*)-**7**.^[22] We tentatively speculate that the cyclization step is preceded by a lithium–lithium exchange with inversion of configuration, in which the Li⁺/(–)-sparteine is replaced by a less sterically congested lithium cation, which in turn leads to a higher rate of reaction. Control experiments with the addition of lithium chloride or lithium butoxide lead to an enantiomeric enrichment factor of up to 1.2; these results agree with the proposed reaction pathway.
- [22] We thank one of the referees for stimulating suggestions.
- [23] The results of PM3 calculations suggest a reaction pathway with a lowest energy barrier in which the lithium atom comes into contact with C-8 and the chlorine atom. Accordingly, the reaction commences as a lithium–ene reaction which then merges into the reaction path of a *syn*-S_N' reaction: E.-U. Würthwein, C. Mück-Lichtenfeld, unpublished results.
- [24] Experiments (b) and (c) in Scheme 5 gave the cyclopentanes (+)-**8a** and (–)-**8a** in quantitative yields. If the lithium intermediates **7** and *epi*-**7** were of unrestricted configurational stability, and if both complexes were to cyclize at the same rate, the same enantiomeric ratio would be expected in the product **8a** as in respective educts **15** (74:26 and 50:50, respectively). In both cases a shift in favor of the product (+)-**8a** would be recorded; that is, **7** is involved to a greater extent in product formation than *epi*-**7**.
- [25] For the synthesis of enantiomer-enriched cyclopentanol by (–)-Sparteine-induced intramolecular carbolithiation, see M. J. Woltering, R. Fröhlich, D. Hoppe, *Angew. Chem.* **1997**, *109*, 1804–1805; *Angew. Chem. Int. Ed. Engl.* **1997**, *36*, 1764–1765; M. Oestreich, R. Fröhlich, D. Hoppe, *Tetrahedron Lett.* **1998**, *39*, 1745–1748.
- [26] All new compounds gave satisfactory elemental analyses (C, H, N; \pm 0.4).

A Novel Route to the Fused Maleic Anhydride Moiety of CP Molecules**

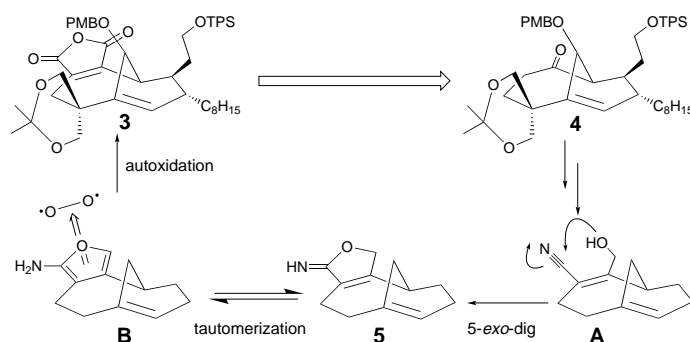
K. C. Nicolaou,* Phil S. Baran, Rolf Jautelat, Yun He, Kin Chiu Fong, Ha-Soon Choi, Won Hyung Yoon, and Yong-Li Zhong

The structures of the CP molecules (CP-263,114, **1** and CP-225,917, **2**) represent some of the most striking molecular architectures to be derived from nature (unidentified fungus) in recent years.^[1] Challenged by these unusual molecules and tempted by the high probability of new discoveries and



inventions, synthetic chemists are paying attention to them as opportunistic targets.^[2] Herein we describe a number of our explorations and discoveries en route to these target molecules. Specifically, we report a novel construction of the fused maleic anhydride moiety within the confined structural framework of the CP molecules.

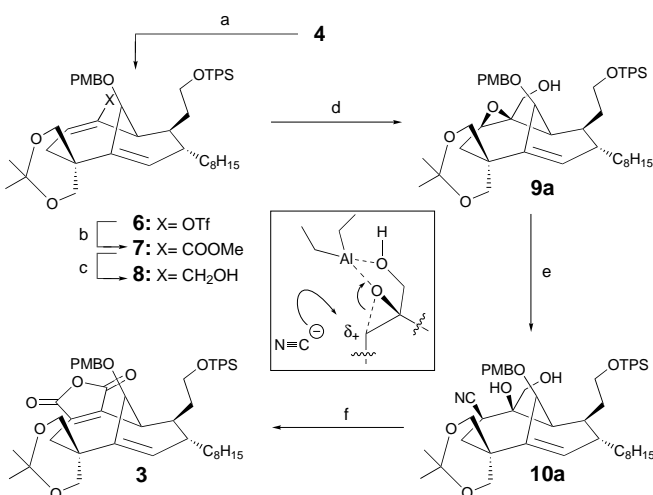
In order to explore a possible pathway to the maleic anhydride functionality of the CP molecules, advanced intermediate **4** (Scheme 1) was employed as a model system.^[3] The main objective was to develop an efficient strategy for the conversion of ketone **4** to anhydride **3** were unsuccessful.^[4] Thus, we designed an approach which exploited the unique steric and electronic facets of ketone **4**. We reasoned that a 2-aminofuran (**B**) (Scheme 1) may serve as an unprecedented chemical cloak of the maleic anhydride functionality due to its propensity for oxidation.^[5] This transient and unstable furan was envisaged to be accessible from its corresponding tautomeric imino butenolide form, **5**.^[6] To the best of our knowledge there is no precedent for the use of this type of



Scheme 1. Strategy for the conversion of ketone **4** to anhydride **3**. Appendages in **A**, **B**, and **5** have been deleted for clarity. PMB = *p*-methoxybenzyl; TPS = *tert*-butylphenylsilyl.

imino butenolide in synthesis, and this type of compound has so far evaded isolation. The highly favored 5-*exo*-dig attack of a pendant alcohol upon a proximal cyanide residue as in **A** (Scheme 1) was expected to furnish the recalcitrant imino butenolide **5**. Consequently, our synthetic venture was initially targeted at cyanide **A**.

We inaugurated our drive to the maleic anhydride **3** with conversion of ketone **4** to the corresponding enol triflate **6** (Scheme 2). Palladium-catalyzed carboxymethylation of **6**



Scheme 2. Construction of maleic anhydride **3** from ketone **4**. a) KHMDS (1.5 equiv), 0 °C, then PhNTf₂ (2.0 equiv), THF, 10 min, 95 %; b) Pd(OAc)₂ (0.06 equiv), PPh₃ (0.12 equiv), MeOH (40 equiv), Et₃N (2.0 equiv), DMF, CO, 25 °C, 10 min, then **6**, 50 °C, 20 min, 76 %; c) DIBAL (3.0 equiv), toluene, –78 °C, 95 %; d) [V(O)(acac)₂] (0.2 equiv), *t*BuOOH (1.4 equiv), benzene, 25 °C, 0.5 h, 85 %, 3.7:1 (**9a**:**9b**); e) Et₂AlCN (5.0 equiv), toluene, 0 °C, 15 min, then 25 °C, 2.5 h, 68 %; f) 1. MsCl (3.0 equiv), Et₃N (10 equiv), THF, 0 °C, 5 min; 2. K₂CO₃ (20 equiv), MeOH, 30 min; 3. Et₂O, 10 % oxalic acid (5 % v/v), air, 0.5 h, 60 %.

provided the α,β -unsaturated ester **7** in 76 % yield. DIBAL reduction of **7** followed by directed epoxidation of the resulting allylic alcohol **8** (85 % yield, 3.7:1 in favor of epoxide **9a**)^[7] furnished epoxide **9a**. Diethylaluminum cyanide mediated epoxide rupture resulted in the formation of the cyano diol **10a** (see inset, Scheme 2), wherein the correct geometrical arrangement for the ensuing reactions was secured (*vide infra*).^[8] In essentially one operation, diol **10a** was transformed to maleic anhydride **3** in 60 % yield. Thus, **10a**

[*] Prof. Dr. K. C. Nicolaou, P. S. Baran, Dr. R. Jautelat, Y. He, Dr. K. C. Fong, Dr. H.-S. Choi, W. H. Yoon, Dr. Y.-L. Zhong
Department of Chemistry and
The Skaggs Institute for Chemical Biology
The Scripps Research Institute
10550 North Torrey Pines Road, La Jolla, CA 92037 (USA)
Fax: (+1) 619-784-2469
E-mail: kcn@scripps.edu

and Department of Chemistry and Biochemistry
University of California, San Diego
9500 Gilman Drive, La Jolla, CA 92093 (USA)

[**] We thank Dr. D. H. Huang and Dr. G. Siuzdak for NMR spectroscopic and mass spectrometric assistance, respectively. This work was financially supported by the National Institutes of Health (USA), The Skaggs Institute for Chemical Biology, postdoctoral fellowships from the Humboldt Foundation (Feodor Lynen Fellowship to R. J.) and the Korea Science and Engineering Foundation (to H.-S. C.), doctoral fellowships from the National Science Foundation (to P. S. B.) and Boehringer Ingelheim (to Y. H.), and grants from Pfizer, Schering Plough, Hoffmann La Roche, Merck, and Dupont.

was submitted to mesylation followed by treatment of the crude mesylate **15** with potassium carbonate in methanol; evaporation of the solvent, dissolution in diethyl ether, and addition of a 10 % aqueous solution of oxalic acid resulted in the generation of maleic anhydride **3** (Table 1). This tandem seven-step sequence for the conversion of **10a** to **3** achieved: a) selective mesylation; b) epoxide formation; c) epoxide lysis (by β -elimination); d) 5-*exo*-dig cyclization; e) reiterative oxidation, and f) nitrogen–oxygen exchange (>93 % yield per step).

Under suitable conditions (see footnote in Table 1), we were able to isolate and unambiguously prove the existence of the acid- and air-sensitive imino butenolide compound **5** as the intermediate resulting from basic treatment of mesylate **15**.^[9] The protocol used for the conversion of imino butenolide **5** to the anhydride **3** involved treatment of an ethereal solution of **5** with a 10 % oxalic acid solution under atmospheric conditions. After 30–40 min, the reaction was

Table 1. Selected spectroscopic data of **3**, **5**, and **11a**.

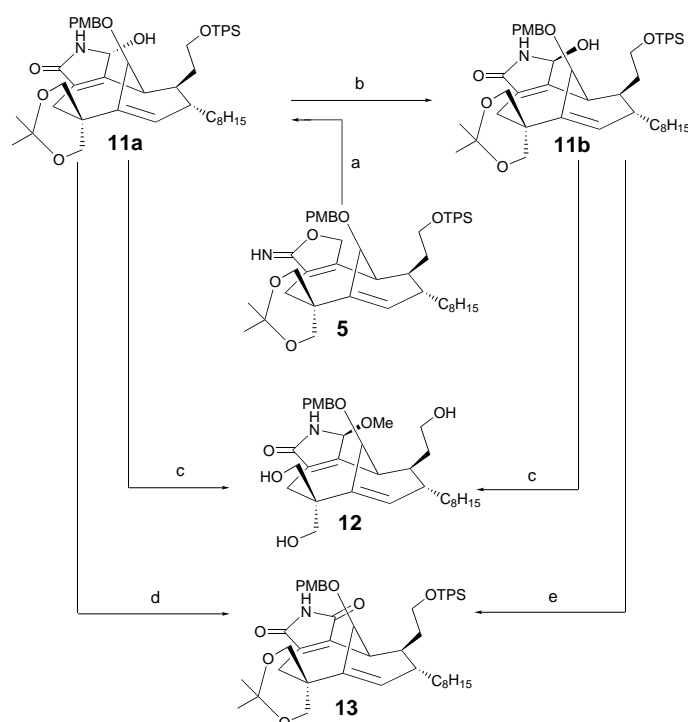
3: R_f = 0.47 (silica gel, ethyl acetate:hexane 1/5); IR (film): $\tilde{\nu}$ = 2928, 2855, 1765, 1611, 1512, 1465, 1427, 1382, 1250, 1197, 1092, 1035, 916, 823, 702 cm^{-1} ; ^1H NMR (400 MHz, CDCl_3): δ = 7.74–7.65 (m, 4H), 7.40–7.36 (m, 6H), 7.10 (d, J = 8.5 Hz, 2H), 6.82 (d, J = 8.5 Hz, 2H), 5.42–5.39 (m, 2H), 5.28 (s, 1H), 4.38 (d, J = 11.2 Hz, 1H), 4.25 (d, J = 11.0 Hz, 1H), 4.22 (d, J = 11.2 Hz, 1H), 4.13 (s, 1H), 4.00–3.85 (m, 2H), 3.99 (d, J = 14.5 Hz, 1H), 3.92 (d, J = 14.5 Hz, 1H), 3.78 (s, 3H), 3.31 (d, J = 11.1 Hz, 1H), 3.22 (d, J = 16.6 Hz, 1H), 3.02 (s, 1H), 2.88 (d, J = 16.6 Hz, 1H), 1.95 (m, 2H), 1.83 (m, 1H), 1.71–1.11 (m, 11H), 1.64 (d, J = 3.5 Hz, 3H), 1.44 (s, 3H), 1.41 (s, 3H), 1.07 (s, 9H); ^{13}C NMR (150 MHz, CDCl_3): δ = 166.2, 165.6, 159.5, 146.1, 142.4, 141.8, 135.7, 135.6, 134.8, 133.9, 133.8, 131.4, 129.7, 129.4, 129.1, 129.0, 127.7, 124.8, 114.0, 97.9, 71.2, 68.1, 66.1, 62.2, 55.3, 46.1, 43.1, 42.4, 40.8, 37.6, 33.4, 32.5, 29.7, 29.5, 29.4, 29.2, 27.9, 26.9, 26.6, 26.1, 21.2, 19.2, 17.9; HR MS (FAB): calcd for $\text{C}_{51}\text{H}_{64}\text{O}_8\text{SiC}$ [$M+\text{Cs}^+$]: 965.3425; found: 965.3397

5 (unstable to air and silica gel):^[a] IR (film): $\tilde{\nu}$ = 2929, 2857, 1666, 1613, 1513, 1463, 1427, 1369, 1250, 1112, 1034, 965, 823, 702 cm^{-1} ; ^1H NMR (600 MHz, $[\text{D}_8]\text{THF}$): δ = 7.65–7.55 (m, 4H), 7.35–7.22 (m, 5H), 7.08 (d, J = 7.5 Hz, 2H), 6.73 (s, 1H), 6.72 (d, J = 7.5 Hz, 2H), 5.32 (s, 1H), 5.30–5.28 (m, 2H), 4.49 (d, J = 15.2 Hz, 1H), 4.41 (d, J = 11.3 Hz, 1H), 4.29 (d, J = 11.3 Hz, 1H), 4.14 (d, J = 15.0 Hz, 1H), 4.12 (s, 1H), 3.96 (d, J = 11.0 Hz, 1H), 3.92 (d, J = 11.0 Hz, 1H), 3.82–3.73 (m, 2H), 3.75 (d, J = 11.4 Hz, 1H), 3.61 (s, 3H), 3.27 (d, J = 11.4 Hz, 1H), 2.91 (d, J = 15.5 Hz, 1H), 2.66 (s, 1H), 2.53 (d, J = 15.5 Hz, 1H), 1.90–1.82 (m, 2H), 1.64–1.00 (m, 12H), 1.50 (br.s, 3H), 1.24 (s, 3H), 1.19 (s, 3H), 0.95 (s, 9H); ^{13}C NMR (150 MHz, $[\text{D}_8]\text{THF}$): δ = 172.8, 160.3, 153.4, 145.3, 136.3, 136.2, 134.4, 134.3, 132.2, 132.1, 131.1, 130.5, 129.8, 128.5, 128.4, 127.9, 126.1, 125.2, 114.3, 97.9, 79.4, 73.6, 71.7, 68.5, 62.7, 55.2, 49.7, 47.2, 43.2, 43.0; MS (ESI): m/e 818 [$M+\text{H}^+$], 856 [$M+\text{K}^+$]

11a: R_f = 0.25 (silica gel, ethyl acetate/hexane 1/2); IR (film): $\tilde{\nu}$ = 3315, 2929, 2856, 1694, 1611, 1513, 1463, 1427, 1370, 1250, 1197, 1112, 1036, 966, 910, 823, 735, 702 cm^{-1} ; ^1H NMR (500 MHz, CDCl_3): δ = 7.68–7.66 (m, 4H), 7.45–7.37 (m, 6H), 7.14 (d, J = 8.5 Hz, 2H), 6.81 (d, J = 8.5 Hz, 2H), 4.43 (s, 2H), 4.18 (s, 1H), 4.14 (d, J = 11.5 Hz, 1H), 4.07 (d, J = 11.5 Hz, 1H), 3.91–3.86 (m, 2H), 3.87 (d, J = 11.5 Hz, 1H), 3.75 (s, 3H), 3.46 (d, J = 11.5 Hz, 1H), 2.95 (s, 1H), 2.75 (d, J = 15.5 Hz, 1H), 2.67 (d, J = 15.5 Hz, 1H), 2.42 (d, J = 6.0 Hz, 1H), 1.97 (m, 2H), 1.64 (d, J = 2.5 Hz, 3H), 1.72–1.11 (m, 12H), 1.44 (s, 3H), 1.39 (s, 3H), 1.06 (s, 9H); ^{13}C NMR (150 MHz, CDCl_3): δ = 173.8, 159.2, 157.7, 143.8, 135.6, 133.7, 131.5, 130.2, 129.9, 129.3, 128.7, 128.6, 128.1, 127.8, 127.7, 124.7, 113.9, 97.8, 78.3, 78.2, 70.9, 67.9, 66.9, 61.6, 55.2, 45.2, 42.3, 42.1, 41.7, 40.6, 36.9, 33.6, 32.6, 29.6, 29.4, 29.3, 28.0, 27.9, 27.0, 23.8, 19.2; HR-MS (FAB): calcd for $\text{C}_{51}\text{H}_{67}\text{NO}_7\text{SiNa}$ [$M+\text{Na}^+$]: 856.4585; found: 856.4615

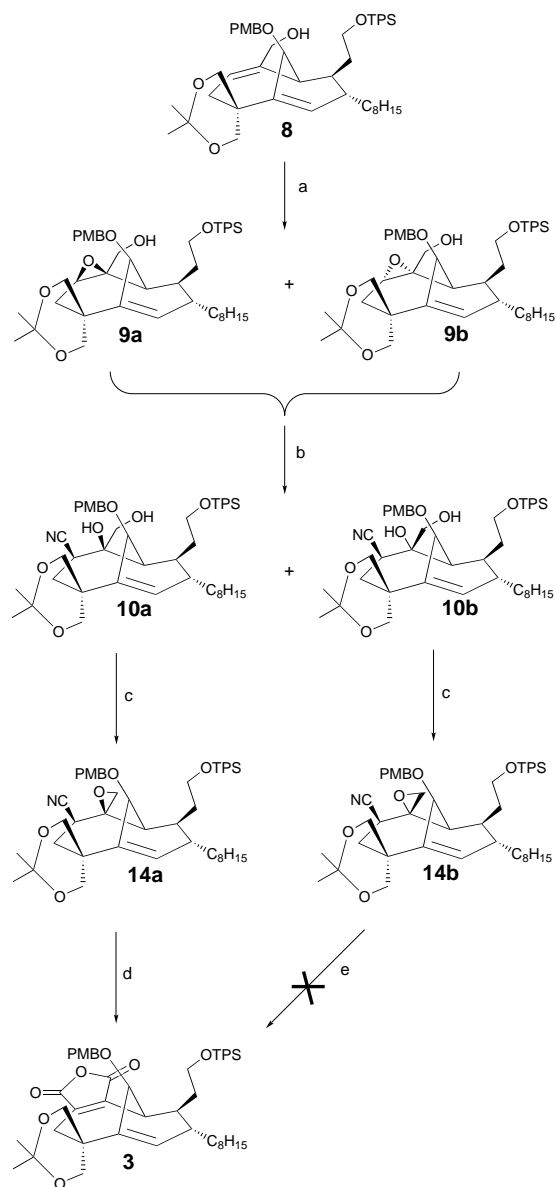
[a] The elusive imino butenolide **5** was isolated after removal of methanol, quick dissolution in $[\text{D}_8]\text{THF}$, and filtration through a cotton plug to remove inorganic material.

complete and **3** was isolated in 60 % yield along with traces of maleimide **13** and hydroxy amide **11a** (vide infra). Interestingly, we found that the ratio of hydroxy amide **11a** to anhydride **3** formed from the imino butenolide **5** differed as a function of the workup protocol. Adjusting the pH of the media granted complete control in the formation of either anhydride **3** or hydroxy amide **11a** (Scheme 3). Attempts to acetylate **11a** led to its epimer **11b**, both of which could be converted to methoxy amide **12** under standard reaction conditions.^[10] Furthermore, oxidation of both epimers led to maleimide **13** (Scheme 3).^[11]



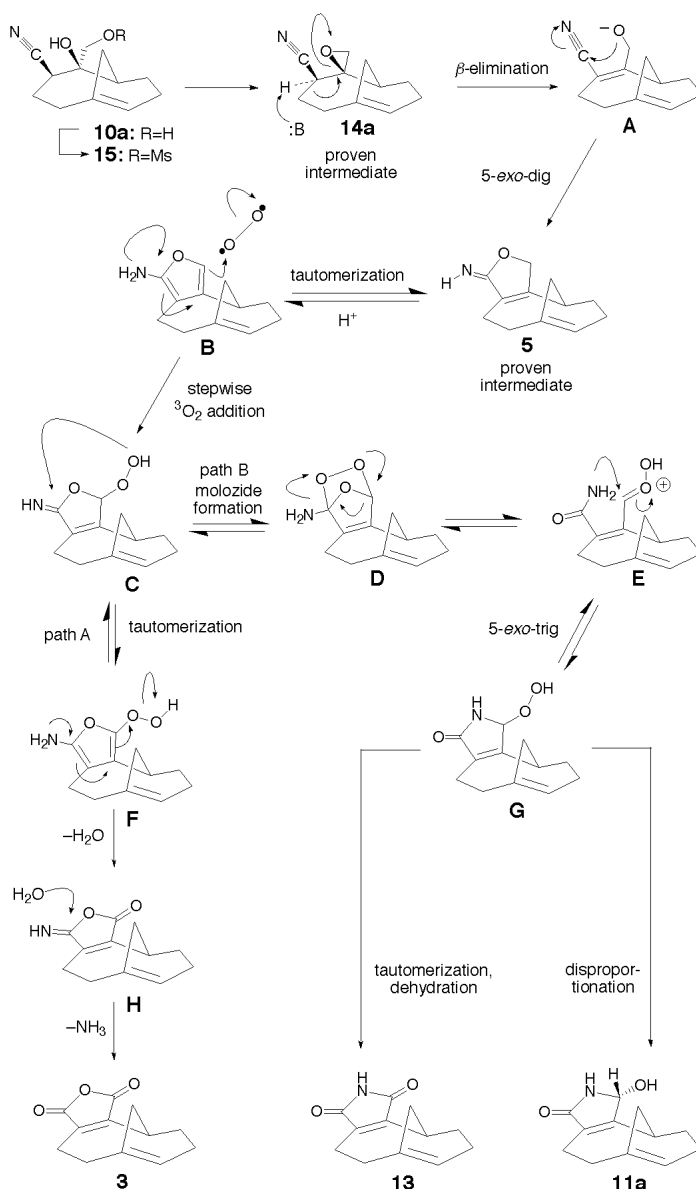
Scheme 3. Conversion of imino butenolide **5** to hydroxy amide **11a** under neutral/weakly acidic conditions and exploratory studies on hydroxy amide **11a**. a) Silica gel, air, 10 min, 80 %; b) Ac_2O (10 equiv), Et_3N (20 equiv), CH_2Cl_2 , 3 h, 85 %; c) HCl (5.0 equiv), MeOH , 12 h, 75 %; d) PDC (4 equiv), CH_2Cl_2 , 10 min, 90 %; e) PDC (10 equiv), CH_2Cl_2 , 48 h, 15 %. PDC = pyridinium dichromate.

In order to resolve whether an antiperiplanar geometry is necessary for this novel cascade, epoxide **14b**, which has the opposite configuration at C11,^[1] was synthesized (Scheme 4). Indeed, treatment of **14a** with potassium hydride in wet DME smoothly proceeded to furnish anhydride **3** via the intermediacy of imino butenolide **5**, while only starting material was recovered in the reaction of **14b**. Based on these results, we propose the following mechanism to account for the formation of anhydride **3**, imino butenolide **5**, hydroxy amide **11a**, and maleimide **13** from cyano alcohol **10a** (Scheme 5). Thus, treatment of mesylate **15** with base leads to tandem epoxide formation, β -elimination (to afford intermediate **A**) and spontaneous attack by the pendant alkoxide at the electrophilic locus of the cyanide residue (5-*exo*-dig) to afford the labile imino butenolide **5**. Slightly acidic conditions promote the energetically favored tautomerization^[6] of **5** to the fleeting



Scheme 4. Synthesis of the geometrically incorrect epoxide **14b** and its inability to be converted into anhydride **3**. a) $[\text{V}(\text{O})(\text{acac})_2]$ (0.2 equiv), $t\text{BuOOH}$ (1.4 equiv), benzene, 25°C , 0.5 h, 85 %, 3.7:1 (**9a**:**9b**); b) Et_2AlCN (5 equiv), toluene, 0°C , 15 min then 25°C , 2.5 h, 62 % **10a**, 30 % **10b**; c) KH (10 equiv), toluene, 1 h, 90 %; d) 1. KH (40 equiv), DME/0.1 % H_2O , 30 s; 2. H_2O /acetone, PPTS (1.0 equiv), 38–45 %; e) conditions as in d), 4 h, ca. 90 % recovered **14b**.

2-aminofuran **B**, which combines with triplet oxygen quite rapidly to afford hydroperoxide **C**.^[5] Two pH-controlled divergent pathways may originate from intermediate **C**. Under acidic conditions (path A), rapid tautomerization of **C** followed by loss of water furnishes anhydride surrogate **H** via intermediate **F** which rapidly expels ammonia to generate **3**. Under weakly acidic conditions (decreased propensity for tautomerization), path B predominates with the formation of molozonide **D**, followed by fragmentation to compound **E**, a cascade which is reminiscent of the venerable ozonolysis reaction.^[12] Rapid 5-*exo*-trig collapse of the amide upon the nearby electron sink furnishes intermediate **G**, which is simply an isomer of intermediate **C** but reacts quite different at this point. Due to the increase in pH-value (general conditions for



Scheme 5. Proposed mechanistic underpinnings in the conversion of cyano alcohol **10a** into **3**, **5**, **11a**, and **13**. Appendages have been deleted from the structures for clarity. DME = dimethoxyethane.

path B) and the all over diminished tendency of intermediate **G** to tautomerize,^[6] it mainly gives rise to hydroxy amide **11a** by the well known disproportionation of its hydroperoxide moiety^[5, 13] and affords maleimide **13** by the tautomerizational dehydration pathway (see above) only in trace amounts.

The combination of a lack of electronic stabilization yet structural rigidity granted by the CP skeleton presumably stands as a paramount driving force for these unique merging processes. The mild conditions used to initiate the cascade transformation from cyano diol **10a** to anhydride **3** via the unprecedented imino butenolide compound **5** are easily reproducible, and remarkably reliable. The implementation of this new synthetic technology to the total synthesis of the CP molecules and analogues thereof will be reported in due course.

Received: August 25, 1998 [Z12333IE]
German version: *Angew. Chem.* **1999**, *111*, 532–535

Keywords: antibiotics • autoxidation • cyclizations • Domino reactions • intermediates

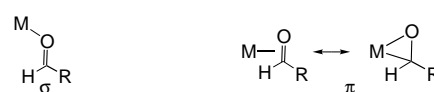
- [1] T. T. Dabrah, T. Kaneko, W. Massefski, Jr., E. B. Whipple, *J. Am. Chem. Soc.* **1997**, *119*, 1594–1598; T. T. Dabrah, H. J. Harwood, Jr., L. H. Huang, N. D. Jankovich, T. Kaneko, J.-C. Li, S. Lindsey, P. M. Moshier, T. A. Subashi, M. Therrien, P. C. Watts, *J. Antibiot.* **1997**, *50*, 1–7.
- [2] a) K. C. Nicolaou, M. W. Härter, L. Boulton, B. Jandeleit, *Angew. Chem.* **1997**, *109*, 1243–1245; *Angew. Chem. Int. Ed. Engl.* **1997**, *36*, 1194–1196; b) K. C. Nicolaou, M. H. D. Postema, N. D. Miller, G. Yang, *Angew. Chem.* **1997**, *109*, 2922–2925; *Angew. Chem. Int. Ed. Engl.* **1997**, *36*, 2821–2823; c) H. M. L. Davies, R. Calvo, G. Ahmed, *Tetrahedron Lett.* **1997**, *38*, 1737–1740; d) P. W. M. Sgarbi, D. L. J. Clive, *Chem. Commun.* **1997**, 2157–2158; e) A. Armstrong, T. J. Critchley, A. A. Mortlock, *Synlett* **1998**, 552–553; f) O. Kwon, D.-S. Su, D. Meng, W. Deng, D. C. D'Amico, S. J. Danishefsky, *Angew. Chem.* **1998**, *110*, 1978–1981; *Angew. Chem. Int. Ed.* **1998**, *37*, 1877–1880; g) O. Kwon, D.-S. Su, D. Meng, W. Deng, D. C. D'Amico, S. J. Danishefsky, *Angew. Chem.* **1998**, *110*, 1981–1983; *Angew. Chem. Int. Ed.* **1998**, *37*, 1880–1882; h) N. Waizumi, T. Itoh, T. Fukuyama, *Tetrahedron Lett.* **1998**, *39*, 6015–6018.
- [3] The synthesis of **4** by a route superior to that presented in ref. [2a] will be reported in due course.
- [4] Strategies involving alkylation α to the ketone in **4** followed by several attempts to append various substituents onto the ketone failed presumably due to excessive steric screening; details will be provided in a full account of this work.
- [5] K. Ito, K. Yakushijin, *Heterocycles* **1978**, *9*, 1603–1606; K. Yakushijin, M. Kozuka, H. Furukawa *Chem. Pharm. Bull.* **1980**, *28*, 2178–2184; D. J. Lythgoe, I. McCleanaghan, C. A. Ramsden, *J. Heterocycl. Chem.* **1993**, *30*, 113–117.
- [6] N. Bodor, M. J. S. Dewar, A. J. Harget, *J. Am. Chem. Soc.* **1970**, *92*, 2929–2936.
- [7] K. B. Sharpless, R. C. Michaelson, *J. Am. Chem. Soc.* **1973**, *95*, 6136–6137.
- [8] a) W. Nagata, M. Yoshioka, T. Okumura, *Tetrahedron Lett.* **1966**, 847–852; b) G. Liu, T. C. Smith, H. Pfander, *ibid.* **1995**, *36*, 4979–4982. The configuration was confirmed by ROESY and COSY spectra.
- [9] HMQC and COSY spectra were also in accordance with the proposed structure **5**.
- [10] F. Farina, M. V. Martin, M. C. Paredes, *Synthesis* **1973**, 167–168.
- [11] The configuration and connectivities of compounds **11a**, **11b**, and **12** were determined using ROESY, COSY and HMQC NMR spectroscopy.
- [12] C. Geletneky, S. Berger, *Eur. J. Org. Chem.* **1998**, 1625–1627.
- [13] R. A. Jones in *Comprehensive Heterocyclic Chemistry*, Vol. 4 (Eds.: A. R. Katritzky, C. W. Rees) Pergamon Press, Oxford, **1984**, pp. 57–255.

Structure and Reactivity of a Cobalt(II) Phthalaldehyde Complex with Both σ - and π -Bonded Aldehyde Groups**

Christian P. Lenges, Maurice Brookhart,* and Peter S. White

Dedicated to Professor Helmut Werner on the occasion of his 65th birthday

The coordination of the carbonyl group of a ketone or aldehyde to a transition metal is of importance in metal-mediated catalysis and has been investigated in some detail. Aldehydes coordinate in a σ or π fashion, depending on the metal center, the oxidation state, the formal charge of the complex, and the steric requirements of the substrate or ancillary ligands (Scheme 1). In some cases an equilibrium



Scheme 1. Coordination modes of dialdehydes to transition metal complexes.

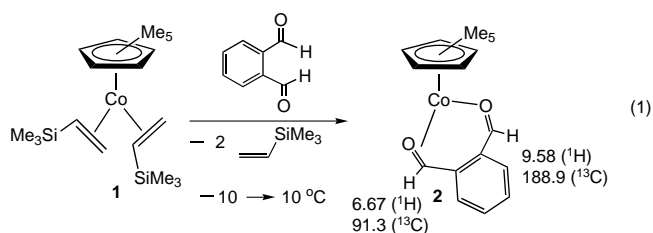
between the coordination modes is established.^[1–16] Here we describe the unique structure and reactivity of a Co^I phthalaldehyde complex in which both coordination modes are realized.

Cobalt aldehyde^[17, 18] complexes are quite rare, and transition metal complexes of dialdehydes such as phthalaldehyde are also uncommon.^[19, 20] Bosnich et al. reported^[19] the spectroscopic characterization of the cationic Rh^I phthalaldehyde complex $[\text{Rh}(\text{dcpe})\{\eta^1, \eta^2\text{-(C(O)H)}_2\text{C}_6\text{H}_4\}]^+$.^[21] This rhodium complex is stable only at low temperatures and undergoes catalytic formation of a five-membered lactone. The resting state of the catalyst in this process is unknown. The cobalt complex reported here is to our knowledge the first structurally characterized transition metal complex in which a dialdehyde exhibits both coordination modes in the same molecule. The complex is also the resting state in a catalytic intramolecular aldehyde condensation reaction (Tishchenko reaction)^[22–31] that generates a five-membered lactone.

Treatment of the labile Co^I bis-olefin complex **1**^[32] with phthalaldehyde according to equation (1) ($[\text{D}_6]$ acetone, -10°C , 10 equiv) resulted in a rapid color change from orange to dark green; NMR analysis showed complete substitution of coordinated olefin to generate a single new Co species after 10 min. One new C_5Me_5 signal was observed at $\delta = 1.70$ (s, 15 H) along with four resonances in the aromatic

[*] Prof. M. Brookhart, Dipl.-Chem. C. P. Lenges, Dr. P. S. White
Department of Chemistry
University of North Carolina at Chapel Hill
Chapel Hill, NC 27599-3290 (USA)
Fax: (+1) 919-962-2476
E-mail: brook@net.chem.unc.edu

[**] We thank the National Institutes of Health (Grant GM 28938) for financial support. C.P.L. thanks the Fonds der Chemischen Industrie, Germany, for a Kekulé fellowship.



region for an unsymmetrically bound phthalaldehyde molecule at $\delta = 7.29, 7.62, 7.66$, and 8.09 . Most significant are two singlets for the aldehyde protons at $\delta = 6.67$ and 9.58 . The ^{13}C NMR spectrum (-10°C , $[\text{D}_6]\text{acetone}$) showed signals at $\delta = 91.3$ (d, $J_{\text{C,H}} = 173$ Hz) and 188.9 (d, $J_{\text{C,H}} = 188$ Hz) for the two differently coordinated carbonyl groups. Free phthalaldehyde has NMR signals for the equivalent aldehyde groups at $\delta = 10.52$ (^1H) and 192 (^{13}C) in $[\text{D}_6]\text{acetone}$. On the basis of this NMR evidence, **2** was formulated as a Co phthalaldehyde complex in which one aldehyde group is coordinated in a σ fashion and the other in a π fashion.

Attempts to isolate **2** by chromatography were unsuccessful, but **2** could be crystallized from acetone at -78°C after 3 d in moderate yield (32%). Black-green crystals were obtained which are air sensitive and decompose under ambient conditions in an inert atmosphere.

Complex **2** was characterized by single-crystal X-ray structure determination (Figure 1), which confirmed the proposed structure. The two aldehyde groups of a phthalaldehyde molecule are coordinated to the $(\text{C}_5\text{Me}_5)\text{Co}^{\text{I}}$ moiety to generate an

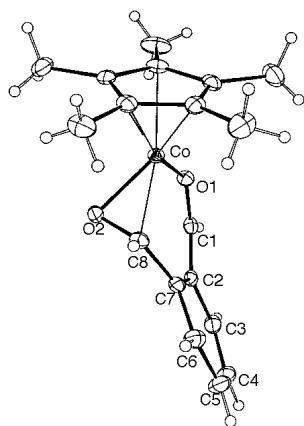


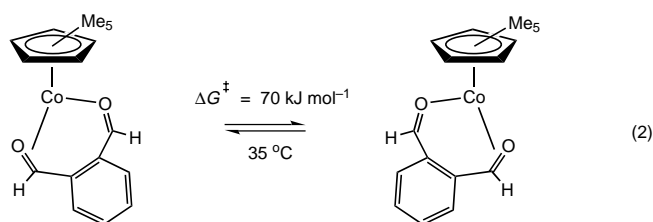
Figure 1. Crystal structure of **2** (ORTEP plot, 50% probability ellipsoids). Selected bond lengths [\AA] and angles [$^\circ$]: Co–O1 1.8900(1), Co–O2 1.8932(10), Co–C8 2.0036(15), O1–C1 1.2590(19), O2–C8 1.3306(20), C1–C2 1.4305(22), C7–C8 1.4523(22), C2–C7 1.4192(22), C2–C3 1.4161(22), C3–C4 1.371(3), C4–C5 1.385(3), C5–C6 1.377(3), C6–C7 1.4034(23); O1–Co–O2 90.92(4), Co–O1–C1 128.66(10), O1–Co–C8 93.82(6), Co–O2–C8 39.80(6), O2–Co–C8 39.80(6), Co–C8–O2 65.62(8), O2–Co–O1–C1 39.64(14), C8–Co–O1–C1 0.10(14), C1–C2–C7–C8 23.61(16), O1–Co–C8–O2 86.85(17), C2–C3–C4–C5 1.39(17), C5–C6–C7–C2 6.64(18).

asymmetric, 18-electron cobalt(I) bis-aldehyde complex (only two oxygen atoms and one carbon atom of the aldehyde are within bonding distance to cobalt). The C=O bond lengths differ considerably: 1.26 \AA for the σ -coordinated aldehyde (C1–O1) and 1.33 \AA for the π -coordinated aldehyde (C8–O2) group. The elongated C=O bond of the π -coordinated aldehyde indicates considerable backbonding from a filled d orbital

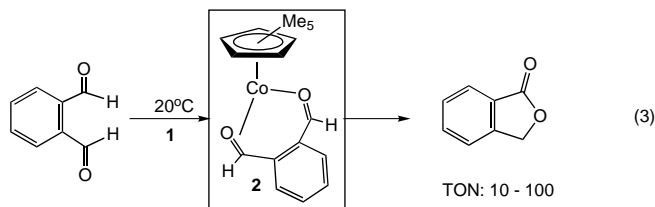
of the cobalt(I) center, thus reducing the C–O bond order. The structurally characterized nickel(0) benzaldehyde complex $[\text{Ni}(\text{PCy}_3)_2(\eta^2\text{-C}_6\text{H}_5\text{CH=O})]$ ^[33–35] has a C=O bond length of $1.325(7)$ \AA (^1H NMR: $\delta = 5.58$), which is similar to that of the π -coordinated aldehyde in **2**. The shorter C=O distance of the other aldehyde group is indicative of the greater double-bond character typical of a σ -bound aldehyde group. This bond length lies in the range reported for cationic and neutral Lewis acidic transition metal aldehyde adducts which bind aldehydes in a σ fashion.^[1–3, 6, 36–38] The two Co–O distances are quite similar (Co–O1 1.8900(1), Co–O2 1.8932(10) \AA). The Co–C1 distance is well outside bonding range (2.85 \AA), and the long Co–C8 bond (2.00 \AA) suggests that a change in coordination mode, which may be required for further reactions of this complex, might be initiated along this trajectory.

Coordination of phthalaldehyde to the Co center also clearly influences the bond lengths in the aromatic ring, which range from 1.42 \AA (C2–C7) to 1.37 \AA (C3–C4, C5–C6). The most significant influence of the transition metal on the conformation of phthalaldehyde is the C1–C2–C7–C8 torsion angle of 23° , which reflects the deviation from planarity of the aldehyde units upon coordination to the $(\text{C}_5\text{Me}_5)\text{Co}$ moiety. This leads to a C5–C6–C7–C2 torsion angle of 6.6° in the aromatic ring. The bond angles of the carbonyl groups to the aromatic ring are within the expected range (ca. 120°); however, the O1–Co–O2 angle is only 91° , which seems required to generate a favorable bonding interaction with both aldehyde groups. The O1–Co–C8–O2 torsion angle of 86° indicates that the σ -coordinated aldehyde group (C1–O1) is nearly parallel to the Co–C8 axis, and the angle between the coordination axes of the π - and σ -coordinated aldehyde groups is nearly 90° . This arrangement facilitates backbonding between d orbitals of cobalt and the σ -coordinated aldehyde group.

At -20°C the two aldehyde ^1H NMR signals are sharp singlets ($\nu_{1/2} = 1.5$ Hz). Warming the acetone solution results in line broadening of both peaks; this indicates a dynamic process which exchanges the sites of the π - and σ -coordinated aldehyde groups. Line-shape analysis of spectra obtained at different temperatures gave activation energies for this process of $\Delta G^\ddagger = 69$ kJ mol^{-1} ($k = 45$ s^{-1}) at 51°C , 70 kJ mol^{-1} (11 s^{-1}) at 35°C , and 68 kJ mol^{-1} (4.2 s^{-1}) at 21°C . Since the presence of excess phthalaldehyde had no influence on the line broadening, the process does not involve intermolecular exchange via free phthalaldehyde. Hence, this site exchange on the NMR time scale is attributed to a reversible interchange of σ and π coordination modes of the aldehyde groups. As indicated above, the long distance Co–C8 suggests the release of the π -coordinated aldehyde group and rotation of the $(\text{C}_5\text{Me}_5)\text{Co}$ moiety to generate a σ -bound aldehyde group and vice versa [Eq. (2)].



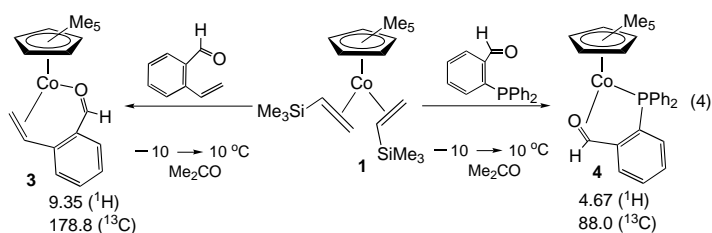
In the presence of excess phthalaldehyde, catalytic formation of the five-membered lactone occurs at 5 °C and above. Turnover numbers (TON) on the order of 100 were observed in the reaction of 1 mol % of **1** with phthalaldehyde. To obtain more detailed information, the reaction of 20 equivalents of phthalaldehyde with **1** at 20 °C was monitored by NMR spectroscopy. Complex **2** is generated rapidly in the initial phase of catalysis. After 9 h 50 % conversion to the lactone is observed in toluene, and after 24 h conversion of the aldehyde is complete [Eq. (3)]. In the initial stages of catalysis, **2** is the



only cobalt-containing species present; after 3 h other organometallic cobalt complexes had been formed, and after complete conversion a variety of unidentified cobalt complexes were observed, which primarily arise from decarbonylation reactions.^[39] This suggests that the rate of lactonization is independent of aldehyde concentration and that the intramolecular cyclization is the slow step in this process.

With simple aldehydes **1** undergoes oxidative addition reactions to generate cobalt(III) acyl hydride complexes, which are intermediates in catalytic hydroacylation.^[40] In the presence of an excess of various alkyl aldehydes, catalytic dimerization to give the Tishchenko esters was observed. This suggests that the intramolecular Tishchenko reaction also follows a pathway that is initiated by oxidative addition of the aldehyde. This mechanistic scenario was also proposed by Bosnich et al. for cationic rhodium bis-phosphane complexes as catalysts.^[19]

It is informative to compare compound **2** with other Co^I aldehyde complexes. We previously reported the synthesis of the chelated aldehyde olefin complex **3**^[32] [Eq. (4)] by



reaction of **1** with *o*-formylstyrene. The NMR data for the aldehyde group of **3** suggest σ coordination. However in complex **4**, which was prepared quantitatively in an analogous fashion by adding a stoichiometric amount of *o*-diphenylphosphanylbenzaldehyde to a solution of **1** in acetone, the aldehyde coordinates in a π fashion to the cobalt center, as suggested by the ¹H NMR signal [Eq. (4)]. In these cases the ambivalent nature of the carbonyl group allows σ or π coordination, depending on the bonding mode of the other ligated group of the bidentate ligand. In **3** the olefin can only bind in a π -fashion; its significant π acidity removes electron

density from the Co^I center and thus favors σ binding of the aldehyde by interaction with the lone pair of electrons of the carbonyl group. In complex **4**, the PPh₂ group binds predominantly by a σ -donor interaction, and the higher electron density at the Co^I center favors binding of the aldehyde in a π fashion with significant backbonding from cobalt to the π^* orbital of the carbonyl group. On the basis of the behavior of complexes **3** and **4**, it is easy to rationalize why the dialdehyde complex **2** prefers to bind through one σ and one π interaction.

Experimental Section

All operations were carried out under an argon atmosphere. All solvents were degassed and purified by standard methods.

2: Five equivalents of phthalaldehyde were added to a solution of **1** (0.15 g, 0.38 mmol) in acetone (5 mL) at 0 °C. The mixture was stirred for 1 h at this temperature during which time the color changed to dark green. Cooling to -78 °C resulted in the deposition of black-green crystals, which were isolated by filtration and stored at -20 °C in a dry-box freezer (yield: 0.04 g, 0.12 mmol, 32 %). The material obtained in this way was suitable for X-ray structure analysis. ¹H NMR (300 MHz, [D₆]acetone, -10 °C): δ = 1.70 (s, 15H; C₅Me₅), 6.67 (s, 1H; π -C(O)H), 7.29, 7.62–7.66, 8.09 (m, 4H; ArH), 9.58 (s, 1H; σ -C(O)H); ¹³C{¹H} NMR: δ = 8.6 (C₅Me₅), 88.6 (C₅Me₅), 91.3 (d, J = 173 Hz; π -C(O)H), 188.9 (d, J = 188.2 Hz; σ -C(O)H), 123.4, 125.6, 126.7, 131.2, 133.5, 143.6 (Ar).

Crystal structure data for **2**: C₁₈H₂₁O₂Co, M_r = 328.29, monoclinic, space group $P2_1/n$, Z = 4, a = 10.1111(5), b = 8.7370(4), c = 17.4463(8) Å, β = 96.1400(10)°, V = 1532.38(12) Å³, ρ_{calc} = 1.423 g cm⁻³, T = -110 °C, $2\theta_{\text{max}}$ = 60°, MoK α radiation (λ = 0.71073 Å); 20178 reflections were measured, 4435 unique reflections were obtained, and 3914 of these with $I > 2.5\sigma(I)$ were used in the refinement; data were collected on a Siemens SMART diffractometer by the omega scan method. For significant reflections $R(\text{merge})$ = 0.022; residuals: R_F = 0.032, R_w = 0.037 (significant reflections), GOF = 3.11.^[41]

4: To a stirred solution of **1** (0.15 g, 0.38 mmol) in acetone was added one equivalent of *o*-diphenylphosphanylbenzaldehyde at 20 °C. An immediate color change from red to brown was observed, and stirring was continued for 30 min. Removal of all volatile materials left **4** as a brown oil (0.18 g, 0.38 mmol). ¹H NMR (300 MHz, [D₆]acetone, -10 °C): δ = 1.49 (s, 15H; C₅Me₅), 4.67 (s, 1H; C(O)H), 7.05–7.19 (m, 3H; ArH), 7.36–7.45 (m, 6H; ArH), 7.52 (m, 4H; ArH), 8.33 (m, 1H; ArH); ¹³C{¹H} NMR: δ = 9.61 (C₅Me₅), 88.01 (d, 168.6 Hz, C(O)H), 90.80 (C₅Me₅), 124.1, 126.6, 128.8, 129.9, 130.1, 133.3, 135.0, 133.2, 137.2, 159.5 (Ar); ³¹P{¹H} NMR: δ = 58.1 (br).

Received: October 12, 1998 [Z12520IE]
German version: *Angew. Chem.* **1999**, *111*, 535–538

Keywords: aldehydes • C–H activation • cobalt • coordination modes • structure elucidation

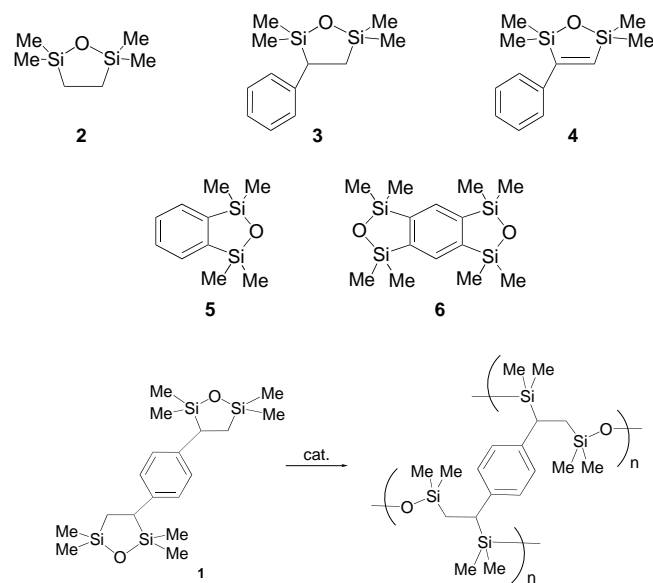
- [1] Y. H. Huang, J. A. Gladysz, *J. Chem. Educ.* **1988**, *65*, 298, and references therein.
- [2] B. J. Boone, D. P. Klein, J. W. Seyler, N. Q. Mendez, A. M. Arif, J. A. Gladysz, *J. Am. Chem. Soc.* **1996**, *118*, 2411–2421.
- [3] R. L. Cicero, J. D. Protasiewicz, *Organometallics* **1995**, *14*, 4792–4798; the C=O distance of 1.221 Å in [CpFe(CO)₂(σ -p-O=C(H)C₆H₄Cl)] is typical.
- [4] C. M. Garner, N. Q. Mendez, J. J. Kowalczyk, J. M. Fernandez, K. Emerson, R. D. Larson, J. A. Gladysz, *J. Am. Chem. Soc.* **1990**, *112*, 5146.
- [5] N. Q. Mendez, J. W. Seyler, A. M. Arif, J. A. Gladysz, *J. Am. Chem. Soc.* **1993**, *115*, 2323–2334.
- [6] D. M. Schuster, P. S. White, J. L. Templeton, *Organometallics* **1996**, *15*, 5467–5469.

- [7] D. M. Schuster, J. L. Templeton, *Organometallics* **1998**, *17*, 2702–2715.
- [8] K. L. Brown, G. R. Clark, C. E. L. Headford, K. Marsden, W. R. Roper, *J. Am. Chem. Soc.* **1979**, *101*, 503.
- [9] B. N. Chaudret, D. J. Cole-Hamilton, R. S. Nohr, G. Wilkinson, *J. Chem. Soc. Dalton Trans.* **1977**, 1546.
- [10] H. Brunner, J. Wachter, I. Bernal, M. Creswick, *Angew. Chem.* **1979**, *91*, 920; *Angew. Chem. Int. Ed. Engl.* **1979**, *18*, 861.
- [11] D. Rabinovich, G. Parkin, *J. Am. Chem. Soc.* **1991**, *113*, 5904–5905.
- [12] B. M. Foxman, P. T. Klemarczyk, R. E. Liptrot, M. Rosenblum, *J. Organomet. Chem.* **1980**, *187*, 253.
- [13] W. Beck, W. Sacher, M. Appel, *J. Organomet. Chem.* **1987**, *322*, 351–356.
- [14] F. R. Askham, K. M. Carroll, S. J. Alexander, A. L. Rheingold, B. S. Haggerty, *Organometallics* **1993**, *12*, 4810.
- [15] G. Erker, U. Hoffmann, R. Zwettler, P. Betz, C. Krüger, *Angew. Chem.* **1989**, *101*, 644; *Angew. Chem. Int. Ed. Engl.* **1989**, *28*, 630.
- [16] K. R. Pörschke, W. Schröder, Y.-H. Tsay, C. Krüger, *Angew. Chem.* **1987**, *99*, 953; *Angew. Chem. Int. Ed. Engl.* **1987**, *26*, 919.
- [17] D. P. Graddon, G. M. Mockler, *Aust. J. Chem.* **1968**, *21*, 1487–1495.
- [18] I. Karadjova, S. Arpadjan, L. Shishkova, *Polyhedron* **1992**, *11*, 2525–2529.
- [19] S. H. Bergens, D. P. Fairlie, B. Bosnich, *Organometallics* **1990**, *9*, 566–571; at -60°C the coordinated aldehyde has signals at $\delta = 10.03$ and 6.94 in the ^1H NMR spectrum, and at $\delta = 200.5$ and 62.8 in the ^{13}C NMR spectrum.
- [20] P. Leoni, M. Pasquali, E. Grilli, M. Tomassini, *J. Chem. Soc. Dalton Trans.* **1986**, 879–881.
- [21] dcpe = bis(dicyclohexylphosphanyl)ethane.
- [22] R. Grigg, T. R. B. Mitchell, S. Sutthivaiyakit, *Tetrahedron* **1981**, *37*, 4313–4319.
- [23] M. Massoui, D. Beaupere, L. Ndjo, R. Uzan, *J. Organomet. Chem.* **1983**, *259*, 345–353.
- [24] P. W. Roesky, H. Berberich, *Angew. Chem.* **1998**, *110*, 1618–1620; *Angew. Chem. Int. Ed.* **1998**, *37*, 1560–1562.
- [25] L. Claisen, *Ber. Dtsch. Chem. Ges.* **1887**, *20*, 646–650.
- [26] W. Tischtschenko, *Chem. Zentralbl.* **1906**, *77*, 1309.
- [27] L. Lin, A. R. Day, *J. Am. Chem. Soc.* **1952**, *74*, 5133.
- [28] P. R. Stapp, *J. Org. Chem.* **1973**, *38*, 1433.
- [29] S. Onozawa, T. Sakakura, M. Tanaka, M. Shiro, *Tetrahedron* **1996**, *52*, 4291.
- [30] K.-I. Morita, Y. Nishiyama, Y. Ishii, *Organometallics* **1993**, *12*, 3748.
- [31] T. Ito, H. Horino, Y. Koshiro, A. Yamamoto, *Bull. Chem. Soc. Jpn.* **1982**, *55*, 504.
- [32] C. P. Lenges, M. Brookhart, *J. Am. Chem. Soc.* **1997**, *119*, 3165.
- [33] D. Walther, *J. Organomet. Chem.* **1980**, *190*, 393–401.
- [34] J. Kaiser, J. Sieler, D. Walther, E. Dinjus, L. Golic, *Acta Crystallogr. Sect. B* **1982**, *38*, 1584–1586.
- [35] A structurally characterized Ni^0 ethylene formaldehyde complex has a C=O bond length of 1.311 \AA .^[16]
- [36] P. Courtot, R. Pichon, J. Y. Salaun, *J. Organomet. Chem.* **1985**, *286*, C17.
- [37] J. Auffret, P. Courtot, R. Pichon, J. Y. Salaun, *J. Chem. Soc. Dalton Trans.* **1987**, 1687.
- [38] The C=O bond length of $[\text{TpMo}(\text{MeC}_2\text{Me})(\text{CO})(\eta^1\text{-p-O=CHC}_6\text{H}_4\text{OMe})]^+$ is 1.237 \AA .^[6]
- [39] This assignment is supported by the formation of benzene and additional aldehyde, presumably benzaldehyde, in the deactivation process. NMR signals in the C_5Me_5 region also indicate the formation of species such as $[(\text{C}_5\text{Me}_5)\text{Co}(\text{CO})]_2$.
- [40] M. Brookhart, C. P. Lenges, P. S. White, *J. Am. Chem. Soc.* **1998**, *120*, 6965–6979.
- [41] Crystallographic data (excluding structure factors) for the structure reported in this paper have been deposited with the Cambridge Crystallographic Data Centre as supplementary publication no. CCDC-113115. Copies of the data can be obtained free of charge on application to CCDC, 12 Union Road, Cambridge CB2 1EZ, UK (fax: (+44) 1223-336-033; e-mail: deposit@ccdc.cam.ac.uk).

Phenylene-Bridged Cyclic Siloxanes as Precursors to Nonshrinking Sol–Gel Systems and Their Use as Encapsulants

Douglas A. Loy,* Kamyar Rahimian, and Michael Samara

Sol–gel polymerization has been the focus of much attention in the design and preparation of highly cross-linked polysiloxane gels.^[1, 2] However, application of sol–gel systems has been limited by the shrinkage associated with the evaporation of the solvent needed for monomer/water miscibility and the resulting condensation products formed during polymerization. An attractive strategy for reducing shrinkage is to eliminate solvent^[3] and condensation by-products entirely by replacing the step-growth polymerization used in the sol–gel processing of alkoxyisilanes with a chain-growth polymerization, such as ring-opening polymerization (ROP). ROP is a chain-growth process that has proven to be an effective means for reducing or, as with the polymerization of spiroorthocarbonates, completely eliminating shrinkage in linear, hydrocarbon polymers.^[4] In this study, we have prepared a new class of sol–gel processed, hybrid organic–inorganic materials based on the ROP of monomers **1–3** bearing one or more 2,2,5,5-tetramethyl-2,5-disilaoxacyclopentane groups (Scheme 1).



Scheme 1. Ring-opening polymerization of **1** to the corresponding polymer.

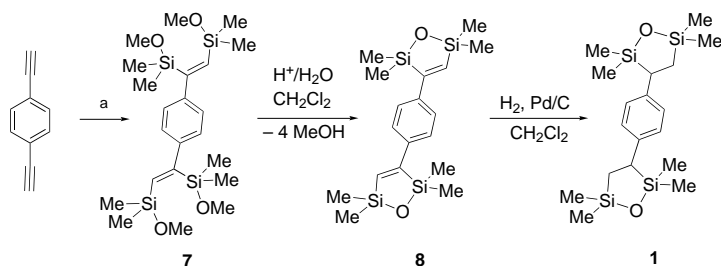
Unlike the sol–gel chemistry of alkoxyisilanes, which requires stoichiometric quantities of water, ROP of disila-oxacyclopentane groups only requires catalytic quantities of an anionic base, such as tetrabutylammonium hydroxide

[*] Dr. D. A. Loy, K. Rahimian, M. Samara
Sandia National Laboratories, Encapsulants and Foams Department
P.O. Box 5800, MS 1407, Albuquerque, NM 87185 (USA)
Fax: (+) 505-844-9624
E-mail: daloy@sandia.gov

Supporting information for this article is available on the WWW under <http://www.wiley-vch.de/home/angewandte/> or from the author.

(TBAH). We showed previously that ROP of neat monomer **2** is accompanied by a shrinkage of less than 5%.^[5] Likewise, ROP of **3** results in a similar loss of volume during the ROP reaction. Despite the structural similarity of **3** and **4**, disilaoxacyclopentene **4**, and the disilaindoles **5** and **6**,^[6] do not undergo ROP with a variety of anionic catalysts and reaction conditions.

A monomer with two or more of the disilaoxacyclopentane groups is required to generate the cross-linked network necessary for forming sol–gels. Monomer **1**, readily prepared in three steps from diethynylbenzene (Scheme 2), possesses



Scheme 2. Synthesis of **1**. a) $\text{Me}_4\text{Si}_2(\text{OMe})_2$, $[\text{Pd}(\text{PPh}_3)_4]$, 110 °C.

two of the strained rings bridged by a phenylene group. Fortuitously, the lower reactivity of the disilaoxacyclopentenes (see above) facilitated the preparation of **1** by allowing ring closure to provide the precursor **8** with two unsaturated five-membered rings without threat of polymerization. Palladium-catalyzed hydrogenation of **8** afforded **1** in quantitative yield.

Monomer **1** can readily be polymerized either in THF or when dissolved in monomer **2** (used as a solvent/comonomer) to give transparent, yellow-tinted gels that showed no visible shrinkage during polymerization. The gels of both the homopolymer and copolymer with **2** were insoluble materials. The opening of the disilaoxacyclopentane rings was confirmed by an upfield shift in the ^{29}Si NMR spectrum (Figure 1), which is consistent with the release of ring strain in the five membered ring with ROP.^[7]

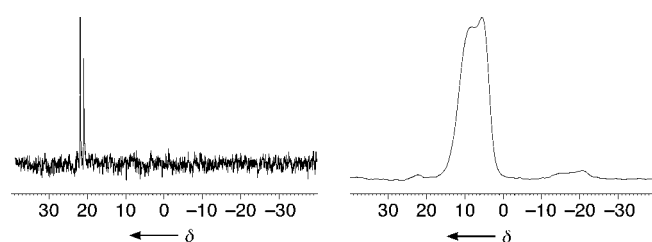


Figure 1. ^{29}Si NMR spectra of monomer **1** (left, $\delta = 21.9$ and 20.9) and its homopolymer (right, $\delta = 9.8$ and 5.5).

By using **2** as both a solvent and a comonomer in the polymerization the solvent is converted into part of the network polymer and shrinkage can be further reduced. The exothermic polymerization of a mixture of **2** and **1** (80:20 by weight) with TBAH (0.2 mol% based on **2**) gave rise to a transparent, crack-free gel within seconds of mixing. A higher concentration of the catalyst (1 mol% based on **2**) led to the generation of more heat during polymerization, which caused

bubbles to form (presumably a result of volatilization of monomer **2**) and become entrapped within the gel. Solid state ^{13}C and ^{29}Si NMR spectroscopy revealed a polymer composition representative of the starting comonomer ratio (80:20) and with no detectable unreacted monomer in the final gel.

Thermal gravimetric analysis (TGA) of the polymers (Figure 2) revealed the homopolymer of **1** and its copolymer with **2** were relatively robust materials relative to the homopolymer of **2**, which begins to degrade at 250 °C and is completely depolymerized before 500 °C. In contrast, the homopolymer of **1** begins to decompose at 375 °C and leaves a

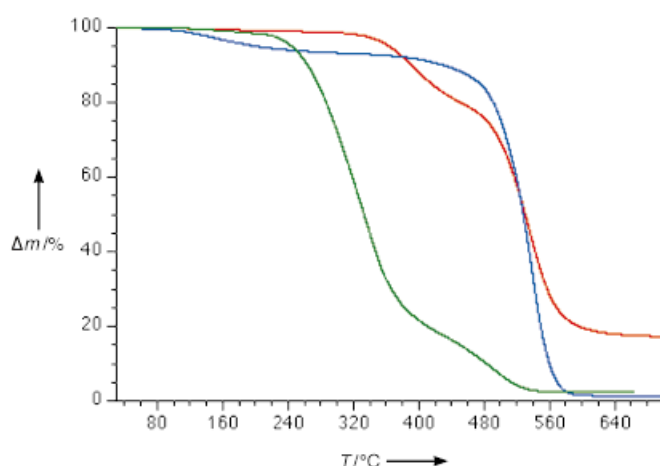


Figure 2. TGA data of the homopolymer of **1** (red), its copolymer with **2** (blue), and the homopolymer of **2** (green).

ceramic residue (17.1%). The copolymer shows an initial weight loss of about 4% followed by complete degradation, which starts at 500 °C. The addition of the phenylene-bridged cross-linker to the polymer of **2** increases the thermal stability by over 150 °C. Nitrogen sorption porosimetry and scanning electron microscopy of the homopolymer of **1**, prepared in THF, and the copolymer of **1** and **2** revealed no significant micro- and mesoporosity. This lack of porosity suggests that the gels are composed of network polymers that are compliant enough to permit collapse of the pores.^[8]

Encouraged by these results and by the lack of significant shrinkage in the copolymer of **1** and **2**, a microelectronic test chip was successfully encapsulated with the ROP of the 80:20 mixture of **2** and **1**. The copolymer formed quickly around the test chip as a transparent, slightly yellow resin with only a few bubbles formed because of the heat of polymerization (Figure 3). No visible cracks or shrinkage of the encapsulant were observed.

In summary, we have demonstrated that highly cross-linked sol–gel systems of siloxane gels can be prepared by a ring-opening polymerization process. The polymerization does not require water or solvent and does not generate condensation by-products. This discovery opens the



Figure 3. Encapsulated test microchip from a 80:20 copolymer mixture of **2** and **1**.

way for application of sol–gel processing to encapsulation, coatings, or net-shape casting. Current efforts are being directed at expanding this family of ROP monomers and determination of the mechanical properties of the gels.

Received: August 24, 1998 [Z 12319 IE]
German version: *Angew. Chem.* **1999**, *111*, 515–516

Keywords: ring-opening polymerization • sol–gel processes
• siloxanes

- [1] C. J. Brinker, G. W. Scherer, *Sol–Gel Science: The Physics and Chemistry of Sol–Gel Processing*, Academic Press, San Diego, **1996**.
[2] D. A. Loy, K. J. Shea, *Chem. Rev.* **1995**, *95*, 1431.
[3] M. W. Ellsworth, B. M. Novak, *Chem. Mater.* **1993**, *5*, 839.
[4] R. K. Sathir, R. M. Luck, *Expanding Monomers: Synthesis, Characterization, and Applications*, CRC Press, USA, **1992**.
[5] a) B. Suryanarayanan, B. W. Peace, K. G. Mayhan, *J. Polym. Sci.* **1974**, *12*, 1089; b) M. Samara, D. A. Loy, *Polym. Prepr.* **1995**, *39*, 599.
[6] W. Fink, *Helv. Chim. Acta* **1974**, *57*, 1010.
[7] D. Seyferth, J. Robison, *Macromolecules* **1993**, *26*, 407.
[8] J. H. Small, K. J. Shea, D. A. Loy, *J. Non-cryst. Solids* **1993**, *1*.

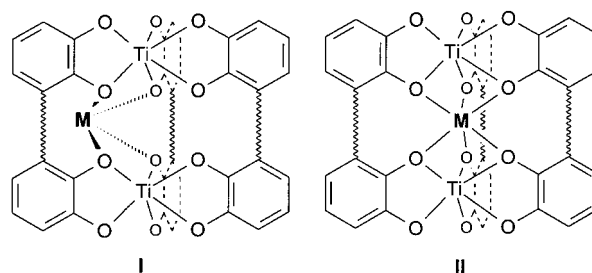
Template-Directed Self-Recognition of Alkyl-Bridged Bis(catechol) Ligands in the Formation of Helicate-Type Complexes**

Markus Albrecht,* Matthias Schneider, and Herbert Röttele

(Metallo-)supramolecular aggregates are formed in spontaneous self-assembly processes. Hereby the steric and electronic information that is embedded in each single molecular component often forces the system to follow a program which affords only one defined supramolecular species.^[1–3] Self-recognition of linear ligand strands during the formation of double- or triple-stranded helicates from mixtures of different ligands leads to the self-assembly of structurally well-defined coordination compounds out of a number of different possibilities. Mixtures of complexes are formed that contain only one type of ligand per complex.^[4–6] “Hetero”-recognition, on the other hand, leads to compounds that are composed of different ligands.^[7, 8]

Lehn et al. described examples in which the self-recognition of ligands in the formation of helicates is influenced by 1) the number of binding sites of the ligands or 2) the preferred coordination geometry of the metal ions in combination with an appropriate structure of the ligands.^[4] On the other hand, Raymond et al. performed a study in which the self-recog-

nition during the self-assembly of triple-stranded homoleptic helicates from a mixture of ligands is based on the length of different rigid spacers which bridge two catecholamide moieties.^[5] Self-recognition also can be controlled by the chirality of the organic ligands.^[6, 7] Herein we describe investigations on the self-recognition of alkyl-bridged bis-(catechol) ligands **1-H₄** and **2-H₄** on the formation of a mixture of dinuclear titanium(IV) complexes. During this process binding of the counteranions to the tetraanionic complexes plays a crucial role in the selective formation of specific coordination compounds (Scheme 1).



Scheme 1. Possible binding modes of alkali metal cations **M** by which dinuclear helicate-type complexes are stabilized: “Outside” coordination (**I**)^[9] or “inside” coordination (**II**).^[10]

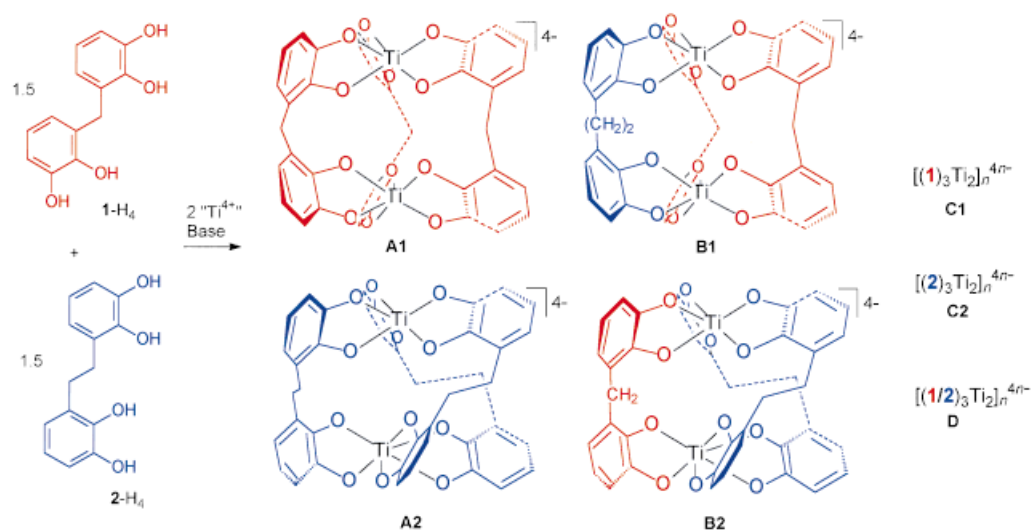
In principle, reaction of a 1:1 mixture of **1-H₄** and **2-H₄** (1.5 equiv of each) with two equivalents titanium(IV) ions (Ti(OMe)₄ or (acac)₂TiO) in the presence of alkali metal carbonate (2 equiv) as base could lead to the homoleptic dinuclear complexes **A1** and **A2**, the heteroleptic dinuclear complexes **B1** and **B2**, the homoleptic oligomeric complexes **C1** and **C2**, and/or the heteroleptic oligomeric complexes **D** (Scheme 2). In earlier investigations we already isolated and characterized the lithium and sodium salts of the *meso*-helicate **A1**. With potassium cations only the oligomeric (but still soluble!) complex **C1** was obtained.^[9] The dinuclear helicate **A2** was formed in the presence of lithium, sodium, potassium as well as many other counteranions.^[10]

For entropic reasons the formation of the dinuclear complexes **A** and **B** should be favored over the oligonuclear species **C** and **D**.^[5] However, the binding of the counteranions to the anionic coordination compounds either stabilizes the dinuclear complexes or destabilizes them leading to the formation of the oligomers **C** or **D**.^[9, 11]

A red soluble solid is obtained when a 1:1 mixture of **1-H₄** and **2-H₄** with Ti(OMe)₄ (methanol, reflux or (acac)₂TiO, methanol, room temperature) is treated with potassium carbonate as base and the solvent is removed. The ¹H and ¹³C NMR spectra (in [D₄]methanol) of this red solid show only signals of the homoleptic helicate **A2** (positive-ion FAB MS (3-nitrobenzyl alcohol (3-NBA) matrix): *m/z*: 940 {K₃H-[(2)₃Ti₂]}⁺). Signals of a titanium complex of ligand **1** are not observed. This is attributed to the formation of the oligomeric species **C1**, which leads to very broad signals in the NMR spectrum, as described previously.^[9] However, the presence of titanium complexes of **1** was shown by acidic hydrolysis (2N HCl) of the red solid obtained. After extraction of the aqueous phase with diethyl ether, the

[*] Priv.-Doz. Dr. M. Albrecht, M. Schneider, Dr. H. Röttele
Institut für Organische Chemie der Universität
Richard-Willstätter-Allee, D-76131 Karlsruhe (Germany)
Fax: (+49) 721-698529
E-mail: albrecht@ochhades.chemie.uni-karlsruhe.de

[**] This work was supported by the Fonds der Chemischen Industrie and the Deutsche Forschungsgemeinschaft.



Scheme 2. Possible homoleptic (**A1**, **A2**) and heteroleptic (**B1**, **B2**) dinuclear and oligomeric (**C1**, **C2**, **D**) complexes obtained from a 1:1 mixture of the ligands **1-H₄** (1.5 equiv) and **2-H₄** (1.5 equiv) by reaction with titanium(IV) ions (2 equiv) in the presence of alkali metal carbonates (2 equiv) as base.

organic phase contained a 1:1 mixture (by ^1H NMR spectroscopy) of the free ligands **1-H₄** and **2-H₄**. This indicates that a sorting of the ligands takes place during the formation of the titanium complexes leading in a self-recognition process to a mixture of the two thermodynamically most favored species **A2** and **C1** which both contain only one kind of ligand. The formation of the oligomer **C1** is favored over the formation of **A1** because potassium ions bind to internal oxygen atoms of ligand **1** and thus destabilize the dinuclear titanium complex.

When sodium carbonate is used instead of potassium carbonate, a different result is obtained. In this case a mixture of the two homoleptic dinuclear complexes **A1** (positive-ion FAB MS (3-NBA matrix): m/z : 873 $\{Na_4H[(1)_3Ti_2]\}^+$) and **A2** (positive-ion FAB MS (3-NBA matrix): m/z : 892 $\{Na_3H[(2)_3Ti_2]\}^+$) is formed. In contrast to the potassium ion, the sodium ion is able to stabilize the dinuclear complex **A1**^[9] and no oligomer **C1** is formed. Thus, in the presence of Na^+ the template-directed self-recognition process affords a mixture of the homoleptic *meso*-helicate **A1** as well as the helicate **A2**.

With lithium carbonate as base, again a red soluble solid is obtained quantitatively. The NMR spectra at room temperature show the signals of the two homoleptic coordination compounds **A1** and **A2**, as well as additional signals of a metal complex (Figure 1). The compound displays resonances of diastereotopic methylene protons of coordinated ligand **1** as doublets at $\delta = 2.91$, 3.11, 4.09, and 4.62 (ratio 1:1:1:1). The appearance of four signals for alkyl protons indicates that in addition to the homoleptic dinuclear complexes **A** the heteroleptic coordination compound **B1** is formed. However, no defined signals are observed for the ligand **2** of **B1** at room temperature. ^1H NMR spectroscopy at 333 K reveals defined signals for the protons of the alkyl bridges. Besides the signals of **A1** ($\delta = 4.15$, 3.04, 2 d) and **A2** ($\delta = 2.75$, s) the resonances of **B1** are observed at $\delta = 4.64$, 4.07, 3.10, 3.02, 2.91, and 2.54 (6d, intensity ratio: 1:1:1:2:1:2). The doublets at $\delta = 3.02$ and 2.54 ($J = 8.5$ Hz) correspond to the spacer protons of the ligand strand **2**. Due to a fast inversion of **2** (Scheme 3) only two signals can be observed for this ligand. The two ligands **1**

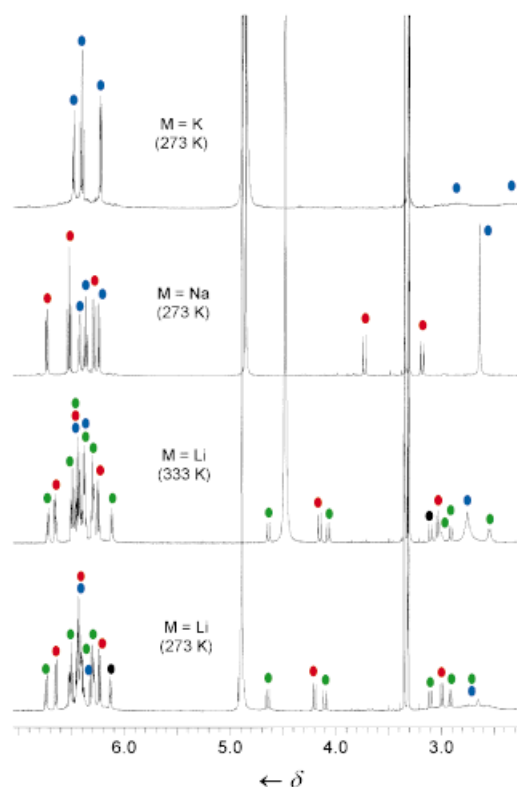
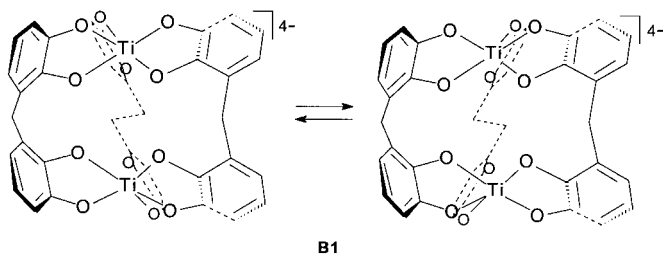


Figure 1. ^1H NMR spectra ($[D_4]$ methanol, 500 MHz) of the complexes obtained from a 1:1 mixture of **1-H₄** and **2-H₄** and titanium(IV) ions in the presence of M_2CO_3 ($M = K, Na, Li$). Blue: signals of **A2**; red: signals of **A1**; green: signals of **B1**. Different NMR shifts and line width are observed for similar dinuclear titanium complexes due to the different counteranions which bind to the anions. The signals of the lithium salts were assigned on the basis of NOESY and COSY NMR spectroscopy.

are rigid and the shifts of the spacer protons are not influenced by the temperature.

The positive-ion FAB-MS (3-NBA matrix) shows in addition to signals of the **A** type complex salts at m/z 851 ($\{Li_4H[(2)_3Ti_2]\}^+$) and 815 ($\{Li_5(1)_3Ti_2\}^+$) a peak at m/z 823 which is assigned to the heteroleptic complex $\{Li_4H-$



B1

Scheme 3. Dynamic behavior of **B1**: The flexible ligand **2** can switch between two different orientations, while the two rigid ligands **1** are fixed in one position.

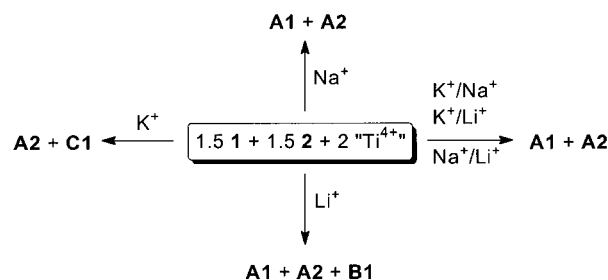
$[(1)_2(2)Ti_2]^+ (B1 + 4Li + H)$. **B1** also is formed if the two complex salts $Li_4[(1)_3Ti_2]$ and $Li_4[(2)_3Ti_2]$ (1:1) are dissolved in $[D_4]$ methanol and heated for several days. However, the ratio of the coordination compounds is different to that observed in the case of complexation of the ligand mixture.

The formation of the dinuclear titanium complex **B1**, which contains two ligands **1** and one ligand **2**, might be due to the ability of lithium ions to bind to the "square" of the four internal oxygen atoms of ligand **1** that is formed upon coordination to titanium(IV) ions.^[9] By this binding the cation stabilizes the dinuclear complex. In case of **B2** such a binding site for Li^+ is not present.

Besides the experiments with pure alkali metal carbonates as base, reactions were performed with 1:1 mixtures of two different carbonates. Thus the reaction of a mixture of sodium carbonate and potassium carbonate with **1-H**₄ and **2-H**₄ and titanium(IV) ions produced a red material which contains the complexes **A1** and **A2**. The ¹H NMR spectroscopic shifts of the methylene protons of **A1** are similar to those observed for the pure salt $Na_4[(1)_3Ti_2]$. This indicates that the *meso*-helicite structure here is stabilized by binding of sodium ions to the tetraanion. The hydrogen resonances observed for **A2** are similar to those observed for $K_4[(2)_3Ti_2]$ in the presence of sodium salts.^[10]

Similarly, if a mixture of lithium carbonate and potassium carbonate is used for the deprotonation of the ligands, only signals of the dinuclear complexes **A1** and **A2** are detected by ¹H and ¹³C NMR spectroscopy. In contrast to the complex formation in the presence of pure potassium carbonate as base (resulting in **A2** and **C1**), in the latter cases besides K^+ , templates are present (Li^+ or Na^+) that can stabilize **A1** and thus favor its assembly. No indication for the formation of oligomeric material **C1** is found. To obtain a complete picture, the complexation of the ligand mixture was also performed in the presence of a mixture of lithium carbonate and sodium carbonate. Again only the two titanium complexes **A1** and **A2** were observed.

In conclusion, the self-assembly of dinuclear helicates and *meso*-helicates from ligands **1-H**₄ and **2-H**₄ and titanium(IV) ions proceeds with self-recognition of the ligands. Hereby the formation of homoleptic dinuclear complexes (**A**) strongly depends on the counteranions, which act as templates (Scheme 4). With sodium ions or with mixtures of cations (Na/K , Na/Li , Li/K) only the dinuclear homoleptic complexes **A1** and **A2** are obtained. With Li^+ ions the heteroleptic complex **B1** is formed in addition to the homoleptic com-



Scheme 4. Overview of the dinuclear and oligomeric complexes obtained with different cations and mixtures of cations.

plexes **A**. In the presence of potassium ions self-recognition takes place but leads to the dinuclear complex **A2** and the oligomer **C1**. The results presented represent an unprecedented example for a new control mechanism in self-recognition of linear ligands upon formation of helicate-type complexes. In the future, mechanisms like the one discussed might allow the construction of complex supramolecular aggregates starting from simple building blocks but using different directing forces to control and influence the supramolecular construction plan.

Received: September 23, 1998 [Z12445IE]

German version: *Angew. Chem.* **1999**, *111*, 512–515

Keywords: alkali metals • helical structures • supramolecular chemistry • titanium

- [1] J.-M. Lehn, *Supramolecular Chemistry*, VCH, Weinheim, **1995**.
- [2] C. Piguet, G. Bernardinelli, G. Hopfgartner, *Chem. Rev.* **1997**, *97*, 2005.
- [3] M. Albrecht, *Chem. Soc. Rev.* **1998**, *27*, 281, and references therein.
- [4] a) R. Krämer, J.-M. Lehn, A. Marquis-Rigault, *Proc. Natl. Acad. Sci. USA* **1993**, *90*, 5394; b) R. Stiller, J.-M. Lehn, *Eur. J. Inorg. Chem.* **1998**, 977.
- [5] D. L. Caulder, K. N. Raymond, *Angew. Chem.* **1997**, *109*, 1508; *Angew. Chem. Int. Ed. Engl.* **1997**, *36*, 1440.
- [6] M. A. Masood, E. J. Enemark, T. D. P. Stack, *Angew. Chem.* **1998**, *110*, 973; *Angew. Chem. Int. Ed.* **1998**, *37*, 928.
- [7] R. Noyori, M. Kitamura, *Angew. Chem.* **1991**, *103*, 34; *Angew. Chem. Int. Ed.* **1991**, *30*, 49.
- [8] B. Hasenknopf, J.-M. Lehn, G. Baum, D. Fenske, *Proc. Natl. Acad. Sci. USA* **1996**, *93*, 1397.
- [9] a) M. Albrecht, S. Kotila, *Chem. Commun.* **1996**, 2309; b) M. Albrecht, *Chem. Eur. J.* **1997**, *3*, 1466.
- [10] a) M. Albrecht, S. Kotila, *Angew. Chem.* **1996**, *108*, 1299; *Angew. Chem. Int. Ed. Engl.* **1996**, *35*, 1208; b) M. Albrecht, M. Schneider, H. Röttele, *Chem. Ber.* **1997**, *130*, 615.
- [11] For the influence of cations on helicate formation see: a) M. Albrecht, O. Blau, *Chem. Commun.* **1997**, 345; b) M. Albrecht, O. Blau, R. Fröhlich, *Chem. Eur. J.* **1999**, *5*, 48.

Selective RGD-Mediated Adhesion of Osteoblasts at Surfaces of Implants**

Martin Kantlehner, Dirk Finsinger, Jörg Meyer, Patricia Schaffner, Alfred Jonczyk, Beate Diefenbach, Berthold Nies, and Horst Kessler*

The nonphysiological character of synthetic materials often leads to poor integration after implantation into human or animal tissues. Graft rejection, low mechanic stability of the biomaterial–tissue interface, infections, and inflammations are undesired side effects of insufficiently active interactions between implant and surrounding tissue. They often make a revision of the graft necessary. The boundary between implant and tissue can be strengthened by coating of such implants with integrin-specific and cell-selective molecules to bind and activate the integrin-expressing cells, the osteoblasts. These processes of tissue remodeling require a tuned interaction of bone-forming osteoblasts with bone-resorbing osteoclasts whose activities are in a natural equilibrium.^[1] Natural full-length adhesion proteins of the extracellular matrix (fibronectin, vitronectin, collagen)^[2] as well as short peptide sequences which contain the adhesion-mediating sequence (e.g. the RGD sequence) can be used for this purpose.^[3–9] Here we report a new optimized method for the coating of implants using integrin-specific peptide ligands and the direct covalent anchoring of these peptides to the common graft material poly(methyl methacrylate) (PMMA). We demonstrate that these surfaces bind osteoblasts, stimulate their proliferation, and therefore trigger biological tissue regeneration (Figure 1).

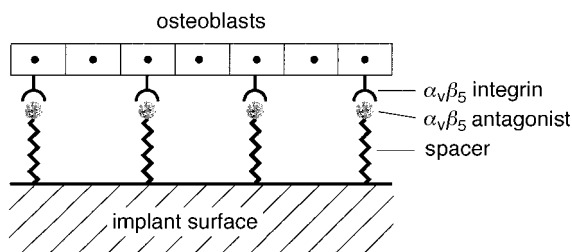


Figure 1. Adhesion of osteoblasts on PMMA surfaces mediated by $\alpha_v\beta_5$ integrin.

We used the cyclic pentapeptide c(-RGDfX-) ($f = \text{D-phenylalanine}$),^[10–15] which is selective for the $\alpha_v\beta_3$ and the $\alpha_v\beta_5$ integrin receptors. The residue X is a lysine residue, which

allows us to link the peptide over a length-optimized spacer through an acrylic acid functional group to the PMMA graft used as bone implant. For clinical application it is essential that the pentapeptide with a D-phenylalanine residue following the binding sequence RGD exhibits high activity as well as higher α_v selectivity compared to the platelet receptor $\alpha_{IIb}\beta_3$ to induce the preferred adhesion of osteoblasts rather than of platelets. We could show that RGD peptides which do not fulfill these criteria, such as linear peptides or cyclic peptides containing the D-amino acid in another position, do not possess α_v selectivity and often have lower activities as well.^[11, 14]

In a pilot study we bound c(-RGDfK-) through a *N*-succinylcysteamide linker (\rightarrow thiol peptide **A**)^[16] or through a 3-sulfanypropionic (3-mercaptopropionic) acid linker (\rightarrow thiol peptide **B**)^[16] and maleimide to surfaces coated with bovine serum albumine (BSA) and studied the adhesion of different osteoblast cultures (primary human osteoblasts, primary human osteoprogenitor cells, primary rat osteoblasts, and mouse MC3T3H1 osteoblasts).^[17] Using immuno fluorescence with integrin-specific antibodies, we could prove that all investigated osteoblast cultures express $\alpha_v\beta_5$ and even $\alpha_v\beta_3$ integrin to only a limited extent. It turned out that all osteoblast cultures bind to the c(-RGDfK-)-coated surfaces, while the control cell line M21L, which does not express $\alpha_v\beta_3$ or $\alpha_v\beta_5$ integrins, does not bind (Figure 2).

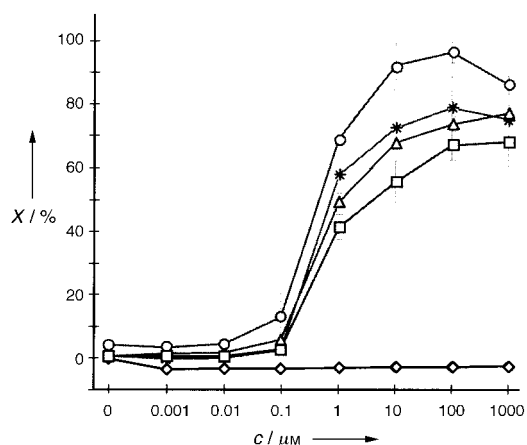


Figure 2. Dependence of the cell plating efficiency *X* of different osteoblast cultures on the concentration *c* of thiol peptide **A** used for the coating protocol. M21L cells which do not express $\alpha_v\beta_3$ or $\alpha_v\beta_5$ integrin receptors do not bind to the surface. Δ : primary human osteoblasts, *: primary human osteoprogenitor cells, \square : primary rat osteoblasts, \circ : MC3T3H1 mouse osteoblasts, \diamond : human melanoma cells (M21L).

Binding of cells occurs through the $\alpha_v\beta_5$ integrin and through $\alpha_v\beta_3$. Cyclopeptide c(-RGDfK-) binds to both receptors.^[11, 12] Adherent cells can be removed from the surface by addition of dissolved c(-RGDfK-). The negative control peptide c(-RbADfK-) (control thiol peptide), for which the insertion of only a single methylene group at the glycine residue (β -alanine) prevents integrin binding completely, does not stimulate any adhesion of osteoblasts (Figure 3). This is additional proof for integrin-RGD-peptide interaction to be the cause for the observed cell adhesion. A

[*] Prof. Dr. H. Kessler, M. Kantlehner, Dr. D. Finsinger
Institut für Organische Chemie und Biochemie der Technischen Universität München
Lichtenbergstrasse 4, D-85747 Garching (Germany)
Fax: (+49) 89-2891-3210
E-mail: kessler@ch.tum.de

Dr. J. Meyer, P. Schaffner, Dr. B. Nies
Merck Biomaterial GmbH, Forschung, Darmstadt (Germany)
Dr. A. Jonczyk, Dr. B. Diefenbach
Merck KGaA, Präklinische Forschung, Darmstadt (Germany)

[**] The authors acknowledge technical assistance from B. Blessing, G. Fleissner, H.-G. Kreysch, and Mona Wolff. Financial support was provided by the Fonds der Chemischen Industrie.

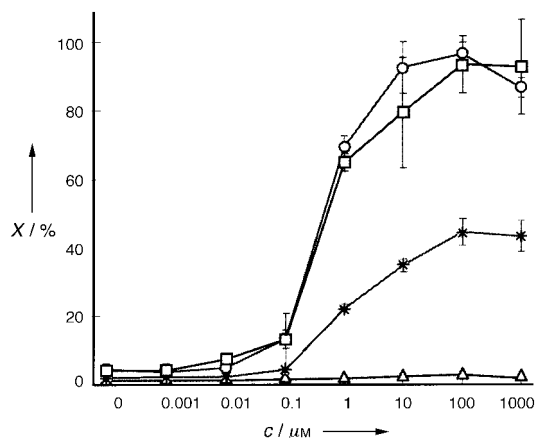
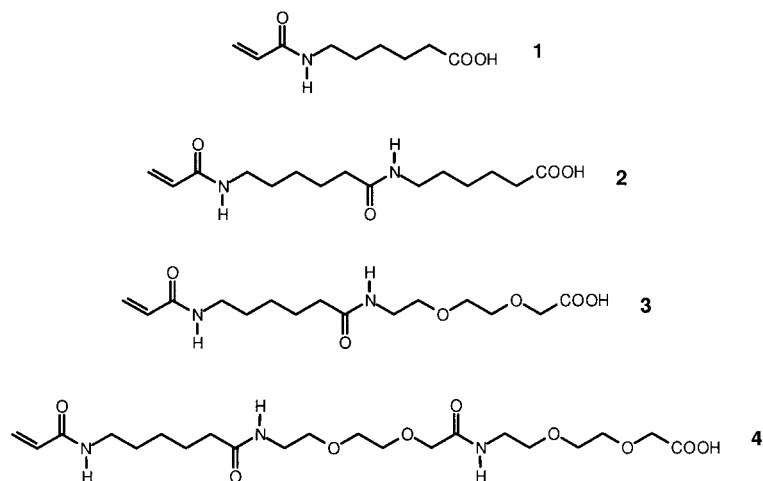


Figure 3. Dependence of the cell plating efficiency X of MC3T3H1 mouse osteoblasts on the concentration c of peptide in the coating solution. The effect of peptide sequence and linker length was studied with thiol peptides **A** (\circ), **B** (\square), **C** (*), and the control thiol peptide (\triangle). The thiol peptides **A** and **B** contain c(-RGDfK-) as highly active and selective integrin antagonist, whereas thiol peptide **C** has c(-RGDEv-) as a ligand. The control thiol peptide contains β -alanine instead of glycine (c(R β ADfK)) and is inactive.

comparison the ligand c(-RGDfK-) containing linkers **A** or **B** with the peptide c(-RGDEv-) synthesized by Delforge et al.^[7] (thiol peptide **C**) clearly indicate an improvement in cell adhesion with c(-RGDfK-) as ligand (Figure 3).

To coat the PMMA surface with c(-RGDfK-) the peptide was linked through a spacer to acrylic acid and then radically polymerized onto the PMMA graft.^[18] Apparently, free double bonds of the polymer are sufficient for this cross-linking.

Initially linker **1**^[19] was used for the RGD peptide. However, the resulting surfaces did not bind osteoblasts (Figure 4). Therefore, we synthesized RGD peptides with longer linkers



2, **3**, and **4**, which also differ in their hydrophilicity/hydrophobicity profile. All three acryl peptides^[21] stimulate adhesion of osteoblasts, and there are no significant differences between them (Figure 4). We therefore conclude that for effective integrin-mediated cell adhesion on surfaces a minimum distance of about 3.5 nm between the ligand and the surface is required. As expected the cell adhesion rate

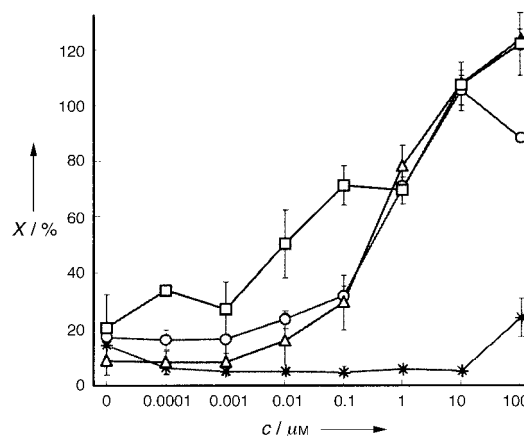


Figure 4. Dependence of the cell plating efficiency X of MC3T3H1 mouse osteoblasts on the concentration c of peptide in the coating solution. Different acrylate peptides were tested which differ only in the nature of the spacer **1–4**. *: acrylate peptide 1, \circ : acrylate peptide 2, \square : acrylate peptide 3, \triangle : acrylate peptide 4. Spacer **1** is too short for effective adhesion of osteoblasts.

(expressed as a percentage; ratio of the number of adherent cells to the number of seeded cells $\times 100$) rises with increasing ligand density at the surface. Even with the relative high numbers of suspended cells (50 000 per cm^2 of surface) used in these experiments, all cells bind to the surface: Cell adhesion rates of up to 100% are obtained (Figure 5). Adhesive cells are tightly bound and cannot be removed from the surface by washing or mechanical shaking.

In a study over 22 days the adherent osteoblasts bound through the RGD peptide to PMMA surfaces were stimulated to proliferate at different ligand densities at the surface. The number of proliferated cells increased over this time span by a factor of 10 in comparison to the untreated PMMA surface

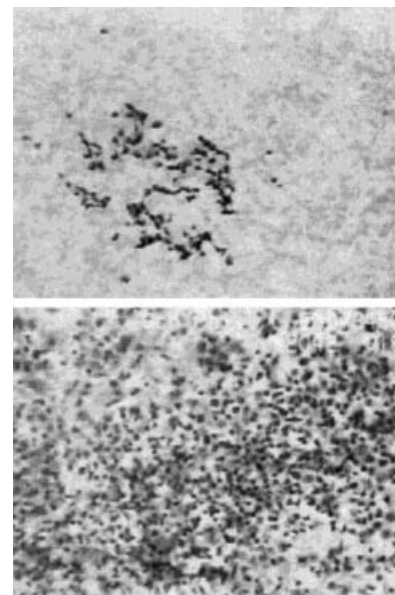


Figure 5. Optical microscopy image of attached MC3T3H1 mouse osteoblasts (dark) on uncoated PMMA surfaces (top) and on PMMA bone cement treated with acrylate peptide 3 (spacer **3**). The peptide concentration in the coating solution was 100 μM . While the top image is representative for the coated surface, the bottom image shows the only area of the untreated surface where cell adhesion was observed at all.

(Figure 6).^[22] This indicates the potential to cover the surface completely and to obtain a natural bonding from implant to the biological tissue.

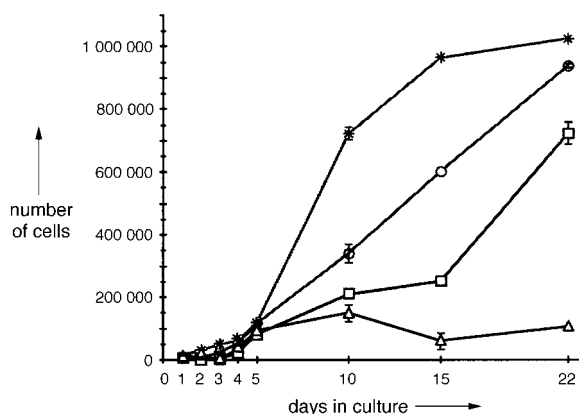


Figure 6. Stimulated proliferation of PMMA-attached MC3T3H1 mouse osteoblasts over a time span of 22 days as a function of ligand density (acrylate peptide 3): *, 100 μM; ○, 1 μM; □, 0.01 μM acrylate peptide 3. An untreated surface served as a control (△).

The results presented here demonstrate an attractive strategy for the development of cell-free and bioactive implants that carry the biological information for the selective activation of those target cells which are needed for selective tissue regeneration.

Received: August 3, 1998 [Z12237IE]

German version: *Angew. Chem.* **1999**, *111*, 587–590

Keywords: bioorganic chemistry • integrins • materials science • peptides • surface chemistry

[1] M. Amling, 7th Annual Meeting of the Surgical Work Group Biomaterials (CAB) of the Deutschen Gesellschaft für Chirurgie, Hamburg, **1998**.
 [2] J. Lahann, D. Klee, H. Klint, A. Ince, H. Höcker, J. Reul, *Proceedings of the 24th Annual Meeting of the Society for Biomaterials*, San Diego, **1998**, 136.
 [3] D. L. Hern, J. A. Hubbell, *J. Biomed. Mater. Res.* **1998**, *39*, 266–276.
 [4] A. Rezanian, C. H. Thomas, A. B. Branger, C. M. Waters, K. E. Healy, *J. Biomed. Mater. Res.* **1997**, *37*, 9–19.
 [5] R. F. Valentini, D. Ferris, C. Di Giovanni, P. Dimond, M. Sherling, G. Moodie, T. Crisco, D. Labrador, M. Ehrlich, *Proceedings of the 23th Annual Meeting of the Society for Biomaterials*, New Orleans, **1997**, 55.
 [6] J. R. Glass, W. S. Craig, K. Dickerson, M. D. Pierschbacher, *Mater. Res. Soc. Symp. Proc.* **1992**, *252*, 331–337.
 [7] D. Delforge, M. Art, B. Gillon, M. Dieu, E. Delaive, M. Raes, J. Remacle, *Anal. Biochem.* **1996**, *242*, 180–186.
 [8] D. Delforge, B. Gillon, M. Art, J. Dewelle, M. Raes, J. Remacle, *Lett. Pept. Sci.* **1998**, *5*, 87–91.
 [9] C. Roberts, C. S. Chen, M. Mrksich, V. Martichonok, D. E. Ingber, G. M. Whitesides, *J. Am. Chem. Soc.* **1998**, *120*, 6548–6555.
 [10] M. Aumailley, M. Gurrath, G. Müller, J. Calvete, R. Timpl, H. Kessler, *FEBS Lett.* **1991**, *291*, 50–54.
 [11] R. Haubner, R. Gratias, B. Diefenbach, S. L. Goodman, A. Jonczyk, H. Kessler, *J. Am. Chem. Soc.* **1996**, *118*, 7461–7472.
 [12] M. Friedlander, P. C. Brooks, R. W. Shaffer, C. M. Kincaid, J. A. Varner, D. A. Cheresh, *Science* **1995**, *270*, 1500–1502.
 [13] M. Pfaff, K. Tangemann, B. Müller, M. Gurrath, G. Müller, H. Kessler, R. Timpl, J. Engel, *J. Biol. Chem.* **1994**, *269*, 20233–20238.
 [14] R. Haubner, D. Finsinger, H. Kessler, *Angew. Chem.* **1997**, *109*, 1440–1456; *Angew. Chem. Int. Ed. Engl.* **1997**, *36*, 1374–1389.

[15] The cyclic peptides are synthesized by classical methods of peptide synthesis.
 [16] Thiol peptide **A** with the *N*-succinylcysteamide anchor is synthesized by reaction of the peptide with succinic anhydride and coupling of *S*-tritylcysteamine: D. Finsinger, Dissertation, Technische Universität München, Germany, **1997**. The synthesis of the thiol peptide **B** with the 3-sulfanylpropionic amide anchor is described in the patent of A. Jonczyk, S. Goodman, B. Diefenbach, A. Sutter, H. Kessler (Merck), WO-A 97/14716, **1997** [*Chem. Abstr.* **1997**, *127*(2), 17965].
 [17] The investigation of cell adhesion was performed according to the procedure of U. Landegren, *J. Immunol. Methods* **1984**, *67*, 379–388.
 [18] The PMMA surfaces are coated by dissolution of the acrylated peptide in small amounts of DMSO, successive dilution with isopropanol, and radical polymerization with campher quinone. The surfaces thus obtained were washed several times and sterilized by γ irradiation.
 [19] D. D. Pless, Y. C. Lee, S. Roseman, R. L. Schnaar, *J. Biol. Chem.* **1983**, *258*, 2348–2349.
 [20] The linkers **1** and **2** were synthesized according to ref. [19], linkers **3** and **4** were synthesized by solid-phase synthesis from Fmoc-[2-(2-aminoethoxy)ethoxy] acetic acid (Fmoc = 9-fluorenylmethoxycarbonyl) and acrylamino hexanoic acid (anchor **1**). The ^1H NMR data of linker **1** agree with the literature data.^[19] ^1H NMR data of the linkers **2–4**: **2** (250 MHz, $[\text{D}_6]\text{DMSO}$, 27 °C): δ = 8.03 (m, 1H; NH), 7.70 (m, 1H; NH), 6.16 (dd, $^3J(\text{H,H})$ = 17, 10 Hz, 1H; =CH), 6.03 (dd, $^3J(\text{H,H})$ = 17, $^2J(\text{H,H})$ = 2.5 Hz, 1H; CH₂=), 5.53 (dd, $^3J(\text{H,H})$ = 10, $^2J(\text{H,H})$ = 2.5 Hz, 1H; CH₂=), 3.15–2.95 (m, 4H; N-CH₂), 2.17 (t, $^3J(\text{H,H})$ = 7 Hz, 2H; CH₂-COO), 2.02 (t, $^3J(\text{H,H})$ = 7 Hz, 2H; CH₂-CON), 1.55–1.15 (m, 12H; (CH₂)₃). **3** (250 MHz, CDCl₃, 27 °C): δ = 6.87 (m, 1H; NH), 6.43 (m, 1H; NH), 6.25 (dd, $^3J(\text{H,H})$ = 17, $^2J(\text{H,H})$ = 2 Hz, 1H; CH₂=), 6.11 (dd, $^3J(\text{H,H})$ = 17, 10 Hz, 1H; -CH=), 5.62 (dd, $^3J(\text{H,H})$ = 10, $^2J(\text{H,H})$ = 2 Hz, 1H; CH₂=), 4.12 (s, 2H; O-CH₂-COO), 3.73–3.23 (m, 10H; CH₂-CH₂-O, N-CH₂), 2.22 (t, $^3J(\text{H,H})$ = 7 Hz, 2H; CH₂-CON), 1.70–1.27 (m, 6H; (CH₂)₃). **4** (250 MHz, CDCl₃, 27 °C): δ = 7.30 (m, 2H; NH), 6.67 (m, 1H; NH), 6.25 (dd, $^3J(\text{H,H})$ = 17, $^2J(\text{H,H})$ = 2 Hz, 1H; CH₂=), 6.11 (dd, $^3J(\text{H,H})$ = 17, 10 Hz, 1H; CH=), 5.62 (dd, $^3J(\text{H,H})$ = 10, $^2J(\text{H,H})$ = 2 Hz, 1H; CH₂=), 4.13 (s, 2H; O-CH₂-COO), 3.99 (s, 2H; O-CH₂-CON), 3.80–3.25 (m, 18H; CH₂-CH₂-O, N-CH₂), 2.20 (t, $^3J(\text{H,H})$ = 7 Hz, 2H; CH₂-CON), 1.75–1.27 (m, 6H; (CH₂)₃).
 [21] The linkers **1–4** were coupled to the peptide with 1-(3-dimethylaminopropyl)3-ethylcarbodiimide hydro chloride (EDCI·HCl) in DMF, the permanent Arg and Asp protecting groups were cleaved with 95% TFA/H₂O, and the acryl peptides were purified by HPLC. The compounds were characterized by ^1H NMR spectroscopy (250 MHz) as well as HPLC-MS. The expected spectra were obtained.
 [22] The cell proliferation of the cells was determined by the WST-1 procedure: J. A. Cook, J. B. Mitchell, *J. Immunol. Methods* **1983**, *65*, 55–63.

A Fully Synthetic Globo H Carbohydrate Vaccine Induces a Focused Humoral Response in Prostate Cancer Patients: A Proof of Principle**

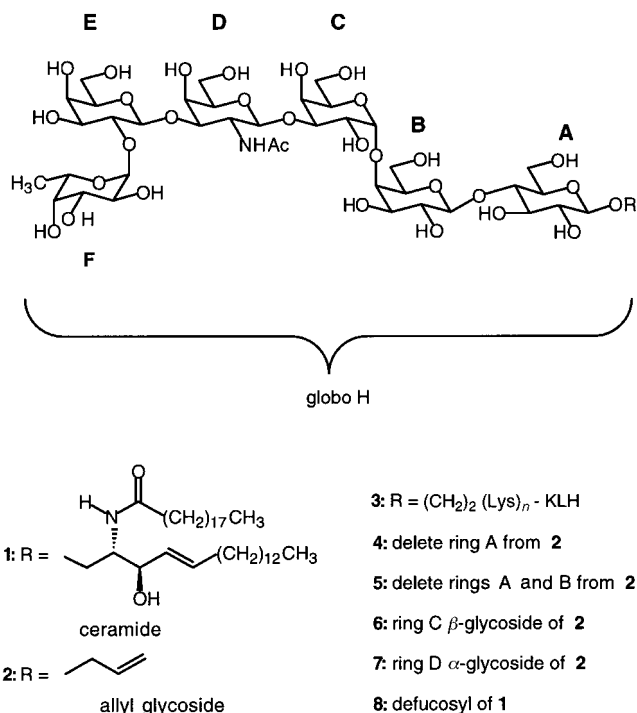
Govindaswami Ragupathi, Susan F. Slovin, Sucharita Adluri, Dalibor Sames, In Jong Kim, Hyunjin M. Kim, Maria Spassova, William G. Bornmann, Kenneth O. Lloyd, Howard I. Scher, Philip O. Livingston, and Samuel J. Danishefsky*

The enlistment of the formidable resources of the human immune system against cancerous lesions has been a long-standing vision in medicine.^[1, 2] Ideally, a vaccine containing a particular tumor-associated antigen or a range of cell-surface antigens, presented in an effective immunostimulatory context, would trigger active immunity against cancer cells expressing counterpart structures on their surfaces.^[3] The focus of our investigation is the development of a vaccine strategy that would be active in an adjuvant or minimum disease setting, providing enhanced protection against micro-metastasis in a context where the primary tumor has been eliminated through surgery, radiation, or chemotherapy. The primary targets of our studies have been carbohydrate-based antigens such as glycolipids, or glycoproteins (including mucins), expressed on the accessible surfaces of tumor cells.^[4, 5]

In this particular study, we have concentrated on the globo H tumor antigen. This antigen was first identified chemically from breast tumor extracts by Hakomori et al.^[6] It was immun characterized by Colnaghi et al. (mAb MBr1),^[7] and more recently by Lloyd et al. (mAb VK-9)^[8] (mAb =

monoclonal antibody). By the criteria of immunohistology, globo H was identified on a number of human cancers (including prostate and breast cancer) and in a restricted number of normal epithelial tissues.^[9]

To proceed in a productive fashion, it was first necessary for us to accomplish a total synthesis of the globo H antigen (**1**) and properly conjugated immunogenic variants thereof, in adequate quantities for preclinical studies. These goals were



[*] Prof. Dr. S. J. Danishefsky,^[+] Dr. D. Sames,^[+] Dr. I. J. Kim, H. M. Kim^[+]

Laboratory for Bioorganic Chemistry
 Sloan-Kettering Institute for Cancer Research
 1275 York Avenue, New York, NY 10021 (USA)
 Fax: (+1) 212-772-8691
 E-mail: c-kandell@ski.mskcc.org

Dr. G. Ragupathi, Dr. S. Adluri, Dr. P. O. Livingston
 Laboratory for Tumor Vaccinology
 Sloan-Kettering Institute for Cancer Research

Dr. S. F. Slovin, Dr. H. I. Scher
 Division of Genitourinary Solid Tumor Oncology
 Sloan-Kettering Institute for Cancer Research

Dr. M. Spassova, Dr. W. G. Bornmann
 Preparative Synthesis Core Facility
 Sloan-Kettering Institute for Cancer Research

Dr. K. O. Lloyd
 Laboratory for Tumor Antigen Immunochemistry
 Sloan-Kettering Institute for Cancer Research

[+] Additional address:

Department of Chemistry, Columbia University
 Havemeyer Hall, New York, NY 10027 (USA)

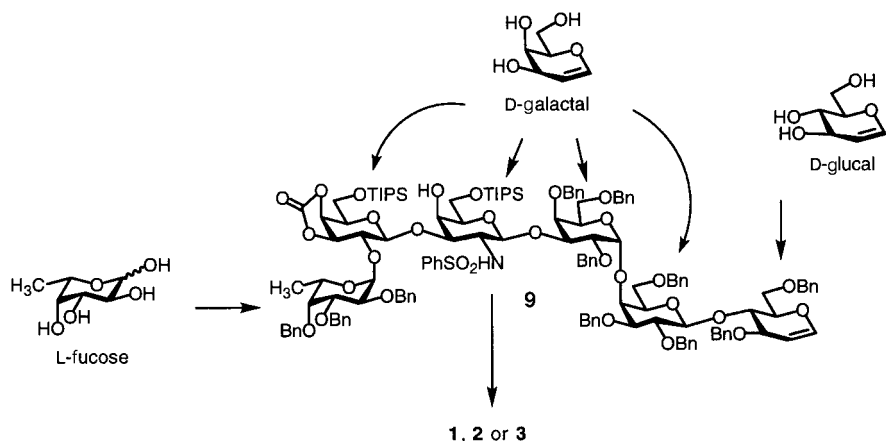
[**] This work was supported by the National Institutes of Health (S.J.D., AI-16943, CA-28824; K.O.L., CA-71506; P.O.L., CA-61422), Sloan Kettering Institute Core Grant (CA-08748), Pepsico, CapCure, the Milstein Family Foundation, and Swim Across America (S.F.S.) Postdoctoral Fellowship support is gratefully acknowledged by D.S. (the Irvington Institute). H.M.K. gratefully acknowledges a graduate fellowship from the US Army (Breast Cancer Grant No. DAMD 17-97-1-7119).

achieved by drawing heavily on the principles of glycal assembly (Scheme 1).^[10, 11] The allyl group in the fully synthetic glycoside (**2**) was used as a spacer element, and as a point of chemical access for conjugating the hexasaccharide antigen of globo H to the carrier protein keyhole limpet hemocyanin (KLH; see structure **3**).

Following favorable serological and cell-surface reactivity in the vaccination of mice with construct **3**,^[12] and after successful scale-ups in the total synthesis, a clinical trial using fully synthetic globo H vaccines in prostate cancer patients was launched. The vaccine construct **3**, in conjunction with the QS-21 adjuvant, had proven to be particularly immunogenic in the murine setting for eliciting globo H-specific responses.^[12]

It should be emphasized that in progressing from a murine to a human setting for the vaccination, two potential risks had to be faced. Human sera and cell-surface glycoproteins present related structures (such as Lewis blood group determinants and, indeed, low levels of globosides). Hence, in the human clinical setting, there were potential issues of immunotolerance or possibly autoimmune responses to be addressed which were not pertinent to the earlier experiments with mice.

Here we report on encouraging early results from our clinical investigation using conjugate system **3** in tandem with QS-21. Five patients with progressive and recurrent prostate cancer received the conjugate vaccine, containing 30 µg of



Scheme 1. The total synthesis of globo H hexasaccharide showing the logic of glycal assembly. Bn = benzyl, TIPS = triisopropylsilyl.

globo H plus QS-21, according to defined clinical protocols. Their sera were submitted for detailed analyses and evaluation. By ELISA (enzyme-linked immunosorbent assay), no detectable IgM or IgG antibodies against synthetic globo H were present prior to vaccination (Figure 1). The pre- and

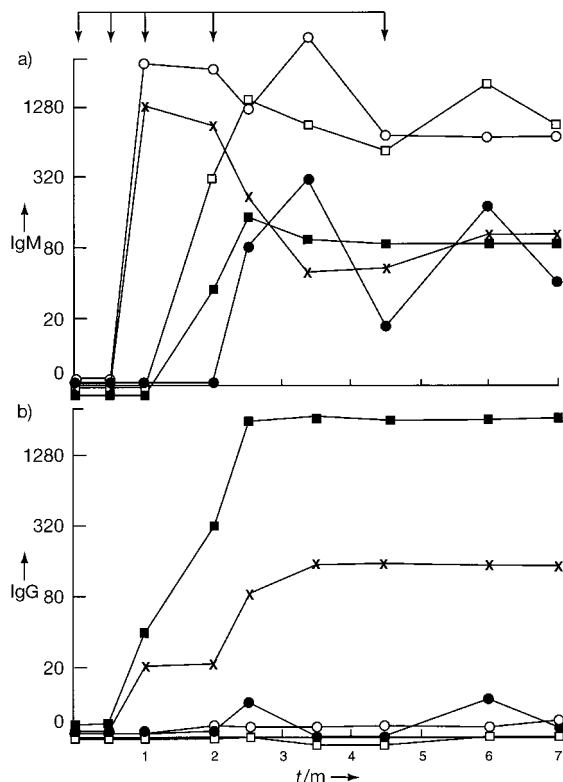


Figure 1. Time course of the induction of antibodies in five patients immunized with globo H-KLH conjugate and QS-21: a) IgM titer, b) IgG titer. ●: patient 1; ×: patient 2; ○: patient 3; □: patient 4; ■: patient 5. The y axis shows the reciprocal titer against globo H by ELISA, and the x axis the time *t* in months. The arrows pointing down indicate vaccinations with globo H-KLH (30 µg) plus QS-21.

post-vaccination IgM and IgG ELISA titers against globo H-ceramide in sera from all five patients are shown in Figure 1. Subsequent to vaccination, all five patients produced a strong

IgM response, while two concurrently generated a high IgG response. The specificity of these antibodies for globo H (derived from synthesis) or for globo H in prostate cancer cell extract from tumor or biopsy, as well as breast cancer biopsy specimens, was analyzed by immune thin layer chromatography (ITLC, Figure 2; results of all five patients are summarized in Table 1). Though the vaccines were based on a synthetic globo H-protein conjugate, the postvaccination sera recognized both synthetic and tumor-derived globo H-ceramide. A similar finding has been described for the VK-9 anti-

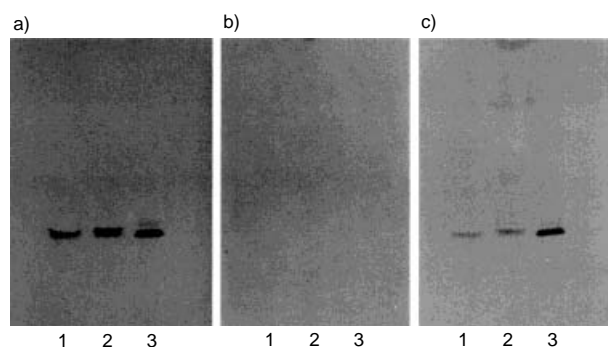


Figure 2. Immune thin-layer chromatography (ITLC) with synthetic and natural antigens and sera from patient 2 vaccinated with globo H-KLH conjugate. In each case, antigen from prostate cancer extract, antigen from breast cancer extract, and synthetic globo H antigen, is applied in lanes 1, 2, and 3, respectively. Detection was achieved a) with a solution of the antibody mAbMBR1, b) with prevaccination sera, and c) with postvaccination sera.

body.^[8,10] By contrast, the sera failed to react with melanoma biopsy specimen extracts, which contain various glycolipids but are globo H negative.

Two different types of ELISA inhibition assays were carried out to determine the specificity of the anti-globo H antibodies in the immunized patients: 1) inhibition of reactivity against globo H-ceramide with structurally related antigens previously obtained by total synthesis in our laboratory^[10,12] as well as structurally unrelated antigens as controls; and 2) inhibition (absorption) by globo H-positive and -negative cell lines. The results of these studies (shown in Figure 3 a, b) demonstrate that globo H-ceramide inhibits anti-globo H reactivity more efficiently than any of the other structurally related congeners obtained through synthesis. For instance, globo H allyl glycoside **2** at a concentration of 500 µM inhibited 40% of the anti-globo H antibody activity while globo H-ceramide **1** at the same concentration inhibited 90% of the reactivity. This finding is particularly interesting in that the immunizing antigen (globo H-KLH) lacked the ceramide moiety. All truncated oligosaccharide isomers of globo H previously prepared by synthesis^[13] were also recognized, though less so than **1**. For example, SSEA-3 (**8**; SSEA = stage-specific embryonic antigen), which lacks the fucose residue, also

Table 1. Summary of immune thin layer chromatography with synthetic and natural antigens and sera from five patients vaccinated with globo H–KLH conjugate.^[a]

Patient	globo H–ceramide		Prostate CA extract		Breast CA extract		Melanoma extract	
	pre	post	pre	post	pre	post	pre	post
1	–	+++	–	+	–	+	–	–
2	–	+++	–	++	–	++	–	–
3	–	++	–	++	–	++	–	–
4	–	++	–	++	–	++	–	–
5	–	+++	–	++	–	++	–	–
mAb Mbr1 ^[b]	++++		+++		+++		–	

[a] CA = carcinoma; pre = before vaccination, post = after vaccination. [b] Reference antibody (positive control).

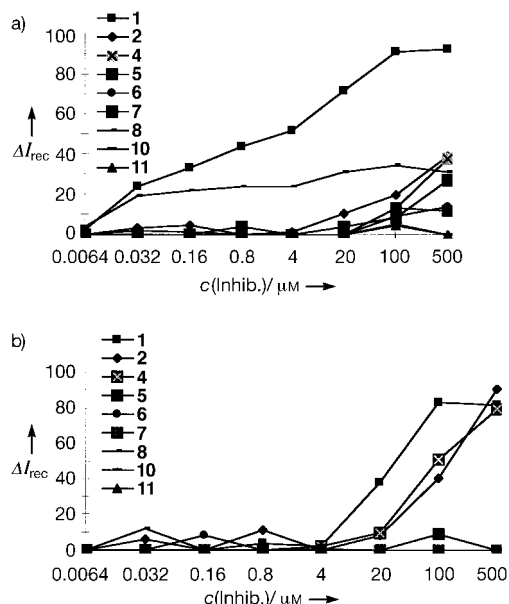
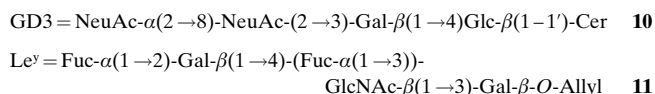


Figure 3. Analysis of the specificity of anti-globo H antiserum by inhibition assays. ELISA reactivity of serum with globo H–ceramide inhibited with compounds **1**, **2**, **4–8**, **10**, **11**: a) IgM antibody response, b) IgG antibody response. ΔI_{rec} = inhibition (%), $c(\text{Inhib.})$ = concentration of the inhibitor.

inhibited 30 % of the antibody reactivity (Figure 3a). As a control, the unrelated glycolipid GD3 **10** containing the ceramide chain, but otherwise lacking any resemblance to the carbohydrate sector of the globo H and synthetic Le^y–allyl glycoside **11**, showed no inhibition.



The IgG response, however, was found to be quite different. In the two antisera demonstrating IgG ELISA reactivity, synthetic hexasaccharides **1** and **2**, as well as a pentasaccharide analogue (see compound **4**) derived from the nonreducing end of the molecule effectively inhibited binding in this assay (Figure 3b). No inhibition was seen with SSEA–3 **8**, which lacks the fucose residue or the tetrasaccharide **5**, which lacks the lactose moiety. Thus, IgG antibodies from both antisera appear to mainly recognize an epitope area encompassing five non-reducing terminal carbohydrate units (see segments B–F).

The lack of recognition of Lewis^y antigen **11** is particularly noteworthy since many of the constituent building blocks in **1**

are also present in **11**. Clearly, the specificity for **1** arises from the difference in the structural and stereochemical connectivity of the antigenic subunits. The general message which comes through from the inhibitory characteristics of our fully synthetic various terminal probe structures is that of a polyclonal, but focused, response against various portions of globo H. The results show that a fucosylated tetra- or pentasaccharide structure is required for an optimal anti-globo H response.

Encouraged by these results, we evaluated whether antibodies elicited by synthetic vaccine **3** recognize the globo H antigen in its natural context, that is, the cell surface. This type of challenge is a crucial milestone in the progression of antitumor vaccines. Two assays were developed to measure the cell surface binding. In the first assay, sera were mixed with globo H-positive (MCF-7) and globo H-negative cell lines (SK-MEL-28). More than 50 % of the ELISA reactivity against globo H–ceramide was lost following incubation with MCF-7 cells in all patients. No decrease in binding activity was observed following incubation with globo H-negative SK-MEL-28 melanoma cells. Comparable results were obtained in control experiments with mAb VK-9.

Furthermore, the cell-surface reactivity of anti-globo H antibodies was tested by flow cytometry (Figure 4). As judged by this assay, sera before vaccination showed very low

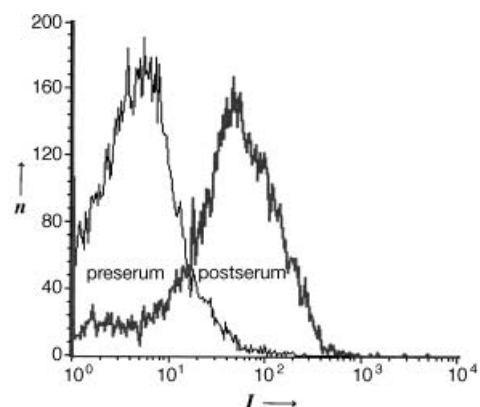


Figure 4. Reactivity of representative pre- and postvaccination sera with MCF-7 cells by flow cytometry. n = relative MCF-7 cell number (counts). I = fluorescence intensity.

reactivities with cell surfaces. However, sera drawn after the fourth vaccination showed an increase of IgM reactivity with MCF-7 breast cancer cells ranging from 11 to 97 %. In a

similar vein, the increase of the IgG antibody cell surface reactivities ranged from 15 to 35 %.

As the last element of the serologic evaluation following vaccination, we also tested the anti-globo H sera for their ability to mediate complement-dependent cytotoxicity (CDC). Three of the five postvaccination sera showed strong CDC to MCF-7 cells. In control experiments, we found that 1) the same sera in the absence of complement, 2) complement without sera, and 3) prevaccination sera with complement failed to exhibit CDC under the same conditions.

In summary, our globo H glycoconjugate based vaccine (3) induces strong and well targeted humoral immune responses in patients. The resultant antibodies not only recognize the synthetic antigens (1 and 2) but also globo H-positive tumor biopsy extracts and tumor tissues. The antisera following vaccination successfully mediated complement-induced lysis of relevant cancer cells.

We note that, in a recent study in melanoma, antibodies induced in the setting of microscopic disease seem to be associated with decreased tumor outgrowth and appear to favor longer patient survival times.^[14] In this context, the serological findings described here through vaccination of prostate cancer patients with the globo H vaccine portend a clinical advantage.

A formal full clinical report on this trial and a related globo H-directed breast cancer trial, conducted in larger patient populations, will be presented separately. Following the important "proof of principle" findings described herein, and other clinical indications associated with tumor-related complex carbohydrate antigens to be described soon, new trials in prostate and breast cancer patients using totally synthetic carbohydrate vaccines are in various stages of development.

Experimental Section

Vaccine preparation and clinical protocol:

The globo H – KLH conjugate was prepared in a manner similar to sialyl Tn cluster – KLH conjugate, as previously described.^[15] Patients with progressive prostate cancer that had a minimum of three rising prostate-specific antigen (PSA) values were vaccinated with globo H-KLH vaccine containing 30 µg of globo H and 100 µg of QS-21. Three vaccinations were administered subcutaneously at one week intervals. Two additional vaccinations were administered at week 7 and 19. Peripheral blood (20–30 mL) was drawn immediately before each vaccination, and two weeks after the fourth and fifth vaccinations. The sera obtained from prevaccination and two weeks after the third, fourth, and fifth vaccinations of all patients were tested for antibodies against globo H – ceramide, truncated globo H analogues, tumor extracts, and the globo H-positive MCF-7 cell-line.

Serological analysis:

ELISA: ELISAs were performed as described previously.^[8, 16] ELISA plates were coated with globo H – ceramide at 0.1 µg per well. Serially diluted patient serum was added to wells of the coated plates, and antibody titer was defined as the highest serum dilution showing an absorbance 0.1 or greater over that of normal patient sera.

Immune thin layer chromatography (ITLC): Immune staining of synthetic globo H – ceramide, and the neutral glycolipid extract obtained from breast and prostate cancers with patient sera or mAb MBr1, was performed after separation on HPTLC silica gel glass plates as previously described.^[8, 16] Patient sera diluted appropriately in phosphate-buffered saline (PBS), and anti-human IgG or IgM antibodies conjugated with horseradish peroxidase (Biosource International, Camarillo, CA) at 1:200 dilution were used.

Inhibition assay: Antisera at appropriate dilution or mAb VK-9 at 0.1 µg mL⁻¹ were mixed with various concentrations of structurally related

and unrelated carbohydrate antigens. The mixture was incubated overnight at 4 °C, and used in ELISA assays as described above. Percentage inhibition was calculated as the difference in absorbance between the uninhibited and inhibited serum.

ELISAs were also performed with sera that had been inhibited (absorbed) by incubation with MCF-7 or SK-MEL-28 cells. For this assay 17 × 10⁶ cells were incubated with sera for 1 h, and the cells removed by centrifugation. ELISA was performed as described above.

Fluorescence-activated cell sorter (FACS) assay: FACS analyses were performed as previously described^[8, 16] using FACS Scan (Becton-Dickinson, CA). Cells from the globo H-positive breast cancer cell line MCF-7 or the globo H-negative melanoma cell line SK-Mel-28 served as targets. An aliquot of 20 µL of diluted (1:20) antisera or mAb MBr1 and 20 µL of 1:30 goat anti-human IgM or IgG-labeled with fluorescein-isothiocyanate (FITC) (Southern Biotechnology Associates, Inc., Birmingham, AL) was used per 2 × 10⁵ cells.

Complement-dependent cytotoxicity (CDC): Complement-dependent cytotoxicity was assayed at a serum dilution of 1:10 with MCF-7 cells and human complement by chromium-release assay as previously described.^[16] All assays were performed in triplicates. Controls included cells incubated only with culture medium, complement, antisera, or mAb MBr1. Spontaneous release was the chromium released by target cells incubated with complement alone. The maximum release was the amount of ⁵¹Cr released from target cells lysed with 1 % Triton-100. Percent cytotoxicity was calculated according to the formula: specific release (%) = (experimental release – spontaneous release)/(maximum release – spontaneous release) × 100.

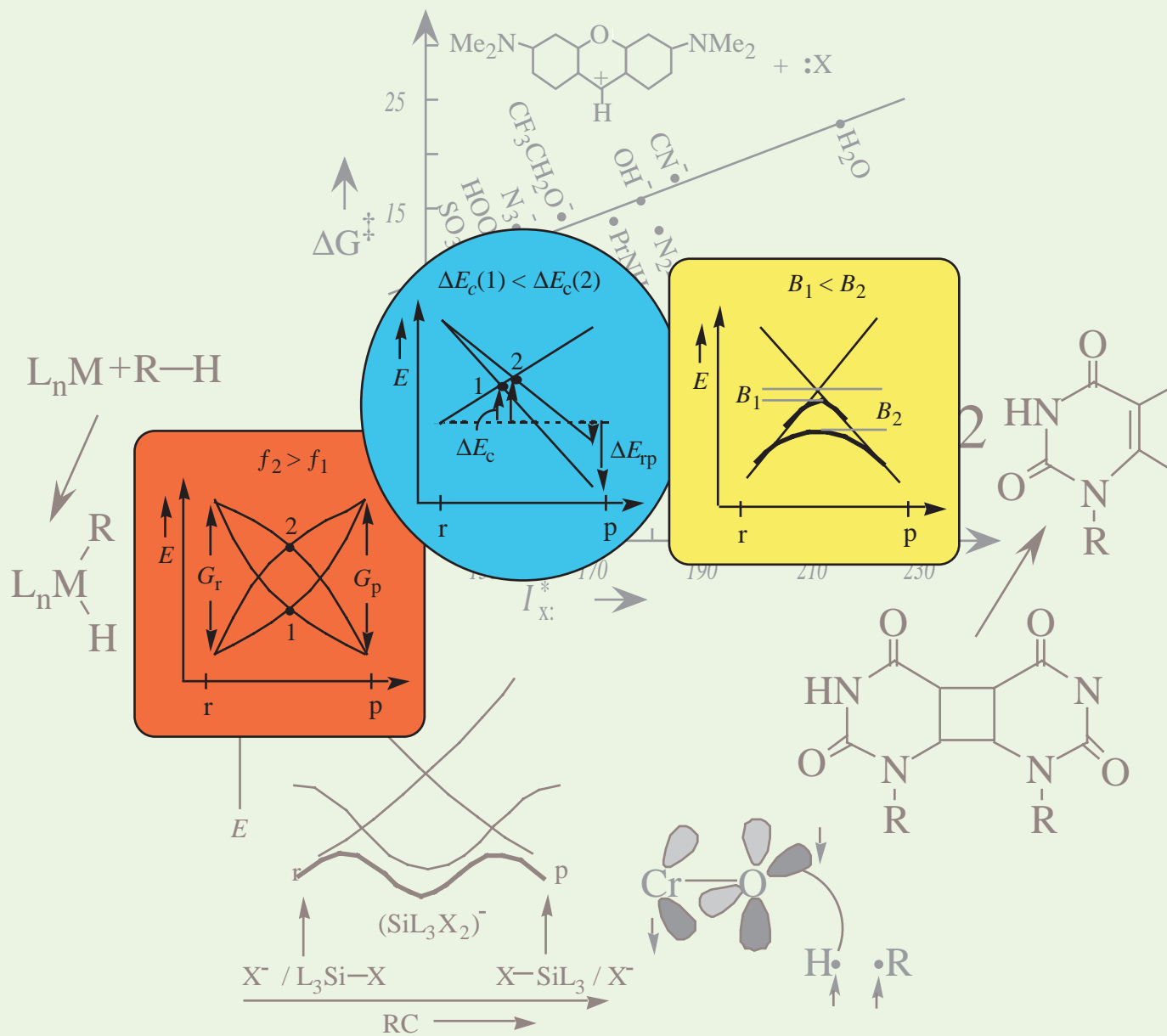
Received: October 19, 1998 [Z12539IE]

German version: *Angew. Chem.* **1999**, *111*, 590–594

Keywords: antitumor agents • carbohydrates • drug research • globo H • glycoconjugates • vaccines

- [1] A. Lanzavecchia, *Science* **1993**, *260*, 937–944.
- [2] D. M. Pardoll, *Curr. Opin. Immunol.* **1993**, *5*, 719–725.
- [3] N. R. Rabinovich, P. McInnes, D. L. Klein, B. F. Hall, *Science* **1994**, *265*, 1401–1404.
- [4] P. O. Livingston, *Immunol. Rev.* **1995**, *145*, 147–166.
- [5] R. R. Koganty, M. A. Reddish, B. M. Longenecker in *Glycopeptides and Related Compounds. Synthesis, Analysis and Applications* (Eds.: D. G. Large, C. D. Warren), Marcel Dekker, New York, **1997**, pp. 707–743.
- [6] E. G. Bremer, S. B. Levery, S. Sonnino, R. Ghidoni, S. Canevari, R. Kannagi, S. Hakomori, *J. Biol. Chem.* **1984**, *259*, 14773–14777.
- [7] S. Menard, E. Tagliabue, S. Canevari, G. Fossati, M. I. Colnaghi, *Cancer Res.* **1983**, *43*, 1295–1300.
- [8] V. Kudryashov, G. Ragupathi, I. J. Kim, M. E. Breimer, S. J. Danishefsky, P. O. Livingston, K. O. Lloyd, *Glycoconjugate J.* **1998**, *15*, 243–249.
- [9] S. Zhang, C. Cordon-Cardo, H. S. Zhang, V. E. Reuter, S. Adluri, W. B. Hamilton, K. O. Lloyd, P. O. Livingston, *Int. J. Cancer* **1997**, *73*, 42–49.
- [10] T. K. Park, I. J. Kim, S. Hu, M. T. Bilodeau, J. T. Randolph, O. Kwon, S. J. Danishefsky, *J. Am. Chem. Soc.* **1996**, *118*, 11488–11500.
- [11] S. J. Danishefsky, M. T. Bilodeau, *Angew. Chem.* **1996**, *108*, 1482–1522; *Angew. Chem. Int. Ed. Engl.* **1996**, *35*, 1380–1419.
- [12] G. Ragupathi, T. K. Park, S. Zhang, I. J. Kim, L. Graber, S. Adluri, K. O. Lloyd, S. J. Danishefsky, P. O. Livingston *Angew. Chem.* **1997**, *109*, 166–169; *Angew. Chem. Int. Ed. Engl.* **1997**, *36*, 125–128.
- [13] I. J. Kim, T. K. Park, S. Hu, S. J. Danishefsky, P. O. Livingston, S. Zhang, *J. Org. Chem.* **1995**, *60*, 7716–7717.
- [14] P. O. Livingston, G. Y. C. Wong, S. Adluri, Y. Tao, M. Padavan, R. Parente, C. Hanlon, F. Helling, G. Ritter, H. F. Oettgen, L. J. Old, *J. Clin. Oncol.* **1994**, *12*, 1036–1044.
- [15] G. Ragupathi, R. R. Koganty, D. X. Qui, K. O. Lloyd, P. O. Livingston, *Glycoconjugate J.* **1998**, *15*, 217–221.
- [16] F. Helling, A. Zhang, A. Shang, S. Adluri, M. Calves, R. R. Koganty, B. M. Longenecker, H. F. Oettgen, P. O. Livingston, *Cancer Res.* **1995**, *55*, 2783–2788.

VB diagrams and chemical reactivity



$$\Delta E^\ddagger = f_{\text{av}} G_{\text{r}} + F(\Delta E_{\text{rp}}) - B$$

Valence Bond Diagrams and Chemical Reactivity

Sason Shaik* and Avital Shurki

Dedicated to Roald Hoffmann on the occasion of his 60th birthday

Eighteen years after the first publication, valence bond (VB) diagrams have developed into a unified system of thought on fundamentals of chemical reactivity: barriers and reaction mechanisms. In this review the reader is led into the model, in a manner which enables to build know-how, through a gamut of applications from the elementary problem of bond breaking to more complex mechanisms where barriers and intermediates are involved in stepwise processes. How does a bond undergo heterolysis, and what is electrostatic catalysis by metal ions? What is the rate-enhancing factor in the *in situ* DNA repair mechanism? When do

“forbidden” reactions become facile, and why do some “allowed” and highly exothermic reactions possess very large barriers? What is the mechanism of C–H activation by CrO_2Cl_2 ? How do lanthanide cations and other metal cations activate C–F bonds? How can we derive stereoselection rules for reaction mechanism and transition state stereochemistry, or stereoselection and mechanistic selection rules for the reactivity of ion radicals and for radical reactions? What are the electronic mechanisms by which complex molecules find low-energy pathways for otherwise high-barrier transformations? What is the difference between

nucleophilic substitutions on silicon and carbon, or between concerted, nucleophilic and electron transfer pathways in polar cycloaddition? What are the origins of the novel $\text{S}_{\text{RN}}2$ and $\text{S}_{\text{RN}}2^{\text{c}}$ reaction mechanisms? What are the origins of reactivity reversals and reactivity zigzags? And what are entangled mechanisms? These are part of the problems which are addressed by use of VB diagrams.

Keywords: avoided crossing • reaction mechanisms • selection rules • transition states • valence bond diagrams

1. Introduction

What are the origins of the barrier to a reaction and the factors which control reaction mechanisms? These are fundamental questions in chemical reactivity. At the threshold of the 21st century such questions are expected to be tackled by applying quantum-chemical approaches which overcome the mathematical complexity of the problem and produce effective and chemically lucid models. Once a quantum-chemical mechanism of barrier formation is formulated, understanding of reactivity patterns is likely to follow, and conceptual means will become available for the generation and solution of new chemical problems.

“What Happens to Molecules as They React? A Valence Bond Approach to Reactivity” was a title of a 1981 paper^[1]

[*] Prof. Dr. S. Shaik, A. Shurki
Department of Organic Chemistry
and
The Lise Meitner-Minerva Center For
Computational Quantum Chemistry
The Hebrew University
91904 Jerusalem (Israel)
Fax: (+972) 26585345
E-mail: sason@yfaat.ch.huji.ac.il

which utilized the connection between molecular orbital (MO) and valence bond (VB) wave functions to derive a general mechanism for barrier formation which could serve as a unified paradigm for chemical reactivity. This was a timely paradigm in some respects. Because on the one hand MO theory, which was the main conceptual matrix, could not offer a mechanism of barrier formation (with the exception of “forbidden” reactions where the principle of orbital-symmetry conservation led to a lucid explanation of the origins of the barrier)^[2] and on the other hand VB theory, which was able to arrive at such a mechanism,^[3] was considered *passé* and its knowledge restricted to a handful of experts who were more inclined at the time to develop the computational know-how of the theory. Thus, the MO–VB relationship was essential to create bridges, and at the same time to generate a reactivity paradigm which enjoyed the qualitative insights of both theories; these are the locality of the bond reorganization—best described by VB structures—and the orbital symmetry and nodal features—best described by MO theory.

It took time for the ideas to ripen through applications to a variety of reactions^[4] and through *ab initio* VB computations of diagrams,^[5] which showed that the qualitative formulations have rigorous computational analogues. The centerpiece of

the model is the VB correlation diagram, which traces the energy of VB states or configurations along the reaction coordinate and, by mixing of the configurations, projects the root cause of the barrier, the nature of the transition state, and the origins and make-up of reaction intermediates. This gamut of reactivity phenomena requires merely two generic diagrams, which are depicted schematically in Figure 1 and which

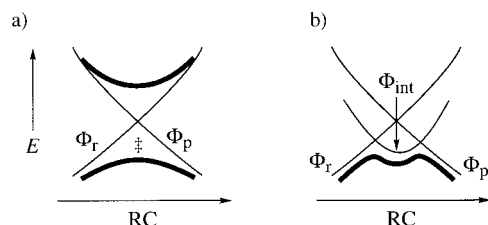


Figure 1. Generic VB diagrams: a) VBSCD, b) VBCMD. Curves of states after VB mixing are shown in the bold. RC = reaction coordinate, Φ_r = wave function of the reactant, Φ_p = wave function of the product, Φ_{int} = wave function of the intermediate state.

enable a unified systematic view of chemical reactivity. The first is a diagram of two interacting states, called a VB state correlation diagram (VBSCD), which describes the formation of a barrier in a single chemical step due to avoided crossing or resonance mixing of the VB states. The second is a three-curve diagram, called a VB configuration mixing diagram (VBCMD), which describes a stepwise mechanism in agreement with the avoided crossing and VB mixing of the three curves.

A review of these VB diagrams in chemical reactivity is deemed timely in view of the surge of interest in these VB concepts by experimentalists, and in the face of the renaissance which VB theory seems to enjoy in recent years.^[6] Thus, a

natural need emerges to create elements of know-how which can serve experimental chemists to apply VB ideas to reactivity.

There is a vast literature on the topic of avoided crossing,^[1–3] and there have been a great many applications to chemical reactions. Even though a few of these applications are mentioned here (e.g., references [3b, 16, 24, 33, 117]), basically the review focuses on VBSCDs and VBCMDs, which as stated above incorporate insights from both VB and MO theories.^[4, 7] Earlier reviews by Shaik,^[4a–c, 7] Pross,^[4e–i] and Hiberty^[4d, 5a–c, 7c] have discussed theoretical aspects of the VB diagrams, and their applications to model reactions as well as to classical physical-organic mechanisms. With an eye toward synthesis of a uniform picture of chemical reactivity, the present review focuses on merging new developments with more classical applications of the model. Thus, we present here a selection of these new applications—such as to bond activation by inorganic and organometallic species,^[8] new mechanisms like $S_{RN}2$ and $S_{RN}2^c$,^[9] ion radical chemistry, the in situ DNA repair mechanism, reactions induced by metal ions (e.g. C–H and C–F activation), electrostatic catalysis, stereo-selection rules, and Zipper reactions—blended into classical problems such as S_N2 and cycloaddition.

Since the review aims at a wide audience of experimentalists working in areas of chemical reactivity, its central role is to develop a didactic and yet effective scheme which will enable application by nonexperts. As such, while the article deviates from the formal structure of a review, it covers many applications of VB theory which are integrated in a problem-solving routine intended to build-up and gradually strengthen the know-how.

The review starts with key elements, the VB configurations which describe a two-electron bond, and shows how to think about various mixing patterns of these configurations and

Sason Shaik started his chemistry studies in Bar-Ilan University, where he obtained his M.Sc. under the supervision of M. Albeck. His M.Sc. studies involved experimental investigations of electrophilic mechanisms of organotellurium reagents. In 1974 he went to the U.S., where he completed his Ph.D. in quantum chemistry under the supervision of Professor N. D. Epiotis. In 1978 Shaik started his postdoctoral studies with Professor R. Hoffmann at Cornell University. In 1980 he began his first academic position as a Lecturer at Ben-Gurion University, where he became Professor in 1988. In 1992 he moved to the Hebrew University, where he teaches and does research now. He has held visiting appointments in Orsay, Kingston, Basel, Lund, Fribourg, Goteborg, Huntsville, Rochester, and the Technische Universität Berlin. He was a Fulbright scholar in the U.S. from 1974 to 1979, and has been awarded the Isreal Chemistry Society Prize for the Young Chemist in 1987, the Bergman Prize in 1996, and the Lise Meitner–Alexander von Humboldt Senior Award in 1995. His research interests are in the use of quantum chemistry to develop paradigms which can lead to the generation and solution of new chemical problems.

Avital Shurki began studying chemistry in 1990 at the Hebrew University, where she finished summa cum laude and was on the Dean's and Rector's Lists. In 1995 she received the Sara Wolf Prize for graduate students. In 1994 she joined the group of S. Shaik and is currently doing her Ph.D. in quantum chemistry. Her research involves applications of VB ideas and calculations to chemical reactivity and bonding.



S. Shaik



A. Shurki

their relationships to reactivity. Then the discussion turns to more complex situations of VB configurations and construction of VBSCDs and VBCMDs, which allow some generalizations and a variety of applications to chemical reactions.

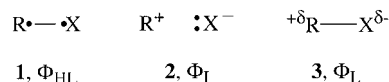
2. Behavior of Valence Bond Configurations in Chemical Reactions

It is worthwhile to review some elementary features of VB configurations in the context of chemical reactivity. The description of VB configurations will rely on cartoon representations, from which we shall try to extract essential characteristics without resort to explicit expressions of wave functions and energetics. Readers who are interested in technical details of VB theory may consult a review^[7a] which teaches an approximate VB theory (see also the appendix of reference [10]) and a monograph which includes a systematic treatise of VB theory.^[11]

2.1. One-Bond Reactions

2.1.1. Valence Bond Configurations of Polar Covalent Bonds

Let us consider the VB configurations in Scheme 1, which mix to form a typical polar C–X bond in a R–X molecule, where R is an alkyl group and X is an electronegative atom or



Scheme 1. VB configurations (1, 2) which mix to form a polar covalent bond (3).

group. Structure **1** is the covalent VB configuration in which the two electrons, occupying the hybrid orbitals on R and X, are paired into a singlet. The pairing is denoted by the line connecting the two dots, which in turn symbolize electrons. For historical reason this structure is called the HL structure (Φ_{HL}) after Heitler and London,^[12] who first used this kind of wave function for the H_2 molecule. The second structure, **2**, is ionic (Φ_{I}), which by mixing with the covalent structure gives the bond its polarity. A third structure of inverse ionicity exists, but for most qualitative purposes its contribution may be neglected due to its high energy. The bond wave function following the VB mixing results in the Lewis structure **3** (Φ_{L}).

The HL and ionic structures have some general features which typify most bonds, albeit important exceptions are well recognized.^[13] The HL structure is generally characterized by a covalent bonding energy which is associated with the spin pairing illustrated in Figure 2a. Thus, to create a singlet-paired HL structure we mix one form which has a spin up–spin down pattern with the one having the opposite pattern (see rule 8 in Section 8.1.4). This mixing contributes the covalent binding energy, which is a resonance energy stabi-

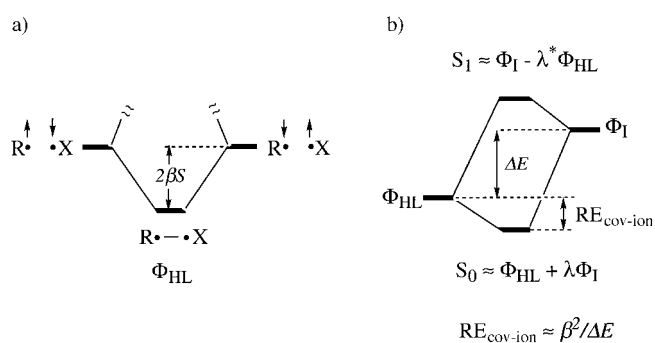


Figure 2. a) The covalent energy stabilization ($2\beta S$) of the HL configuration due to mixing of the spin up–spin down and spin down–spin up forms. b) VB interaction diagram of the mixing of the ionic (Φ_{I}) and covalent structures (Φ_{HL}).

lization and proportional to the product of the resonance integral β and overlap integral S of the bond hybrid orbitals.^[7a]

The ionic structure enjoys electrostatic stabilization, which for alkyl groups is in the range of 90–130 kcal mol^{−1}.^[14] The mixing between the covalent and ionic structures can be represented by the VB interaction diagram^[7a] in Figure 2b, which follows the usual rules of perturbation theory; that is, the mixing results in resonance energy stabilization which is proportional to the resonance integral and inversely proportional to the energy gap between the configurations. This resonance energy due to the mixing of the covalent and ionic structures is significant for R–X bonds; for example, it is of the order of 40 kcal mol^{−1} for $\text{H}_3\text{C}-\text{Cl}$.^[14a] Even though the ionic–covalent resonance energy is large, the principal VB structure of polar covalent bonds is still the HL structure, while the ionic structure remains secondary.

This compact picture contains the essence of bonding, as might be deduced from recent VB ab initio studies.^[13, 14] Figure 3 shows the ab initio VB curves for the isolated CH_3Cl

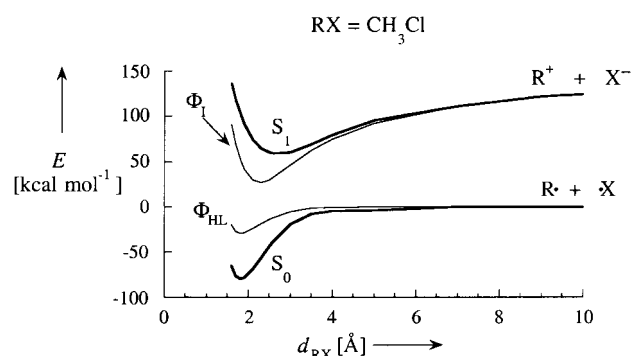


Figure 3. VB correlation diagram for cleavage of the C–Cl bond. Here and in all subsequent figures, VB configurations (here Φ_{HL} and Φ_{I}) are traced in regular lines, while states (here S_0 and S_1) after VB mixing are the bold curves.

molecule along the C–Cl bond stretching coordinate. The HL structure is the lowest and exhibits a minimum at short distances, while the ionic curve lies higher and exhibits a minimum at longer distance. The mixing between the two structures follows the VB interaction diagram of Figure 2b at each point along the “reaction coordinate” (i.e., for every

R–X distance), and leads to bonding and antibonding state curves for the ground (S_0) and excited states (S_1) of the C–Cl bond. In accord with rules of mixing, the ground state is described mainly by the HL structure, while the excited state mainly by the ionic structure. The covalent-ionic resonance energy, which is proportional to β and hence to the overlap between the bond hybrid orbitals, diminishes gradually and becomes zero at infinite R–X distance; at this point, the ground state becomes a purely covalent radical pair, while the excited state purely ionic. Figure 3, which is typical for polar covalent bonds, shows that in the gas phase the profile for bond cleavage is homolytic and proceeds without a transition state separating the R–X “reactants” and the $R^\bullet + \bullet X$ “products”.

2.1.2. Valence Bond Configurations of Ionic Bonds

An ionic bond like in NaCl can be described by the same two structures Φ_{HL} and Φ_I . However, the low ionization energy of Na generates a weak covalent bonding interaction in Φ_{HL} , and, at the same time, this lowers significantly the energy of the ionic structure. The consequences are seen in Figure 4, which exhibits an ionic–covalent curve crossing

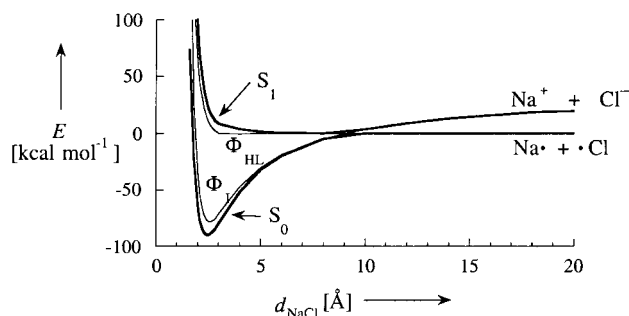


Figure 4. VB diagram for a cleavage of the Na^+Cl^- bond. The curve crossing is avoided by resonance mixing (avoided crossing) of the ionic and covalent configurations.

along the bond stretching coordinate. Now the ground state is primarily ionic, and the excited state is primarily covalent. At the crossing point, the VB mixing generates a pair of bonding and antibonding states, which leads to avoidance of the crossing. It is seen that avoided crossing results from resonance interaction of the VB structures at their point of crossing. Thus, unlike the situation in a covalent bond, here there is a resonating ionic–covalent state en route from the molecule Na^+Cl^- toward the product $Na^\bullet + \bullet Cl$ radical pair. Since at infinite distance the energy gap between the curves is small, the crossing occurs at a long distance between Na and Cl, and the resonance interaction is very tiny. Consequently, the resonating state feature becomes a bottle-neck responsible for the slow dynamics of Na^+Cl^- formation from its atomic constituents.^[15]

2.1.3. Heterolysis of Polar Covalent Bonds in Solution

Let us turn now to an R–X bond cleavage in solution by appeal to Figure 5a. For large alkyl groups like *tert*-butyl, or for R groups with sufficiently low ionization energy (≤ 7 eV), the gap between the ionic and covalent curves is less than

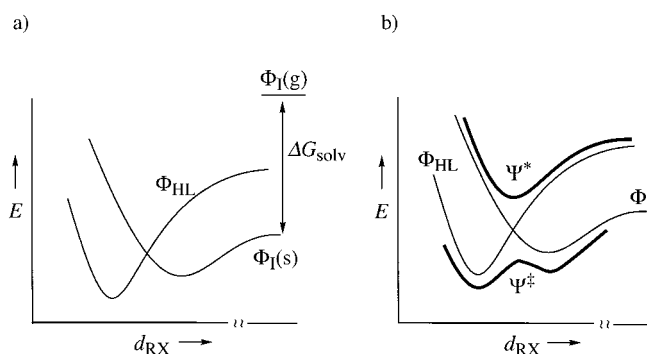


Figure 5. Heterolysis of an R–X bond in solution. ΔG_{solv} = free energy of solvation. a) Solvent-assisted VB curve crossing ((g) and (s) indicate gas phase and solution phase, respectively). b) Resonance mixing and generation of the transition state Ψ^\ddagger and its twin excited state Ψ^* .

about $100 \text{ kcal mol}^{-1}$, while the solvation energy of the two ions exceeds $100 \text{ kcal mol}^{-1}$. Consequently the ionic structure will be much more stable than the covalent structure at long R–X distances.^[3b, 4e, f, 16–18] At shorter distances the solvation decreases, and the ionic curve returns to its position above the HL structure. Consequently, in solution there is a solvent-assisted crossing of the ionic and covalent VB curves along the C–X bond stretching coordinate.

Much the same as in the ionic bond, here too the crossing will be avoided by resonance mixing of the two configurations (Figure 5b). The major difference is that the crossing occurs at a relatively short distance between R and X (ca. $2.2\text{--}2.5 \text{ \AA}$), where overlap is significant and the resonance interaction is therefore large (ca. $\geq 10 \text{ kcal mol}^{-1}$). The resonance mixing will generate two twin states which are the bonding and antibonding combinations of the covalent and ionic structures [Eqs. (1a) and (1b)].^[17] It is seen in Figure 5b that the

$$\Psi^\ddagger = (2)^{-1/2} [(R \cdots X) + (R^+ \cdots X^-)] \quad (1a)$$

$$\Psi^* = (2)^{-1/2} [(R \cdots X) - (R^+ \cdots X^-)] \quad (1b)$$

bonding combination occupies the top of the barrier on the ground-state profile, and may be associated with the transition state which separates the R–X molecule and the solvated R^+ and X^- ions. This general picture has been recently treated qualitatively by Pross and Shaik,^[4e, 17] and quantitatively by Warshel and Weiss^[3b] and by Kim and Hynes,^[18] who used empirical VB calculations including solvation models.

The utility of the avoided-crossing mechanism for conceptualizing reactivity patterns may be illustrated by considering the barrier for ion recombination (Figure 6).^[17]

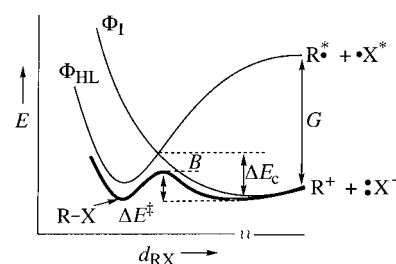


Figure 6. VB diagram showing the origins of the barrier for the ion-recombination process, and the key quantities which control its height.

The barrier is seen to be the balance between the height of the crossing point (ΔE_c) and the resonance energy stabilization B as expressed in Equation (2). The height of the crossing point

$$\Delta E^* = \Delta E_c - B \quad (2)$$

is the destabilization energy of the ions, which is required in order to bring them into resonance with the radicals at the crossing point; resonance mixing establishes a transition state for the reaction.

To apply Equation (2), one may use some typical mathematical curves to obtain a quantitative expression for ΔE_c . However, a much simpler approach is to relate this quantity to the energy gap G separating the two curves at their onset (that is, at infinite R–X distance). This is a vertical gap where both states have a common geometry and solvent orientations, specified by the ground-state ions. A rigorous expression, albeit obvious, is Equation (3a), which shows that the quantity ΔE_c is a fraction f of the gap G . In turn, G is the vertical charge transfer energy, given by Equation (3b) as the difference between the vertical ionization energy ($I_{X^-}^*$) of X^- and the electron attachment energy ($A_{R^+}^*$) of the carbocation. This leads to the final expression for the barrier in Equation (3c).

$$\Delta E_c = fG \quad (3a)$$

$$G = I_{X^-}^* - A_{R^+}^* \quad (3b)$$

$$\Delta E^* = f(I_{X^-}^* - A_{R^+}^*) - B \quad (3c)$$

In solution, the vertical charge transfer energy refers to the process in which the radicals retain the same solvation shells and internal geometries as the ions.^[17] These vertical states of the radicals are denoted in turn by the asterisks [Eqs. (4a) and (4b)], and the associated vertical ionization and attachment

$$X^- \rightarrow X^{\bullet*} + e^- \quad \Delta E = I_{X^-}^* \quad (4a)$$

$$R^+ + e^- \rightarrow R^{\bullet*} \quad \Delta E = -A_{R^+}^* \quad (4b)$$

energies are nonequilibrium quantities, which include also the role of solvent reorganization. These quantities are either available from photoelectron emission spectra and studies of charge transfer to solvent,^[19] or can be readily estimated.^[4a, b, 17, 20] In cases when the ion pair is sufficiently stable, the vertical charge transfer transition energy may be obtained from spectroscopy of the ion pair. To illustrate the use of the covalent-ionic resonance mixing model, consider the ion-recombination reaction described in Equation (5), where the



carbocation Y-pyronein ($Y-P^+$) reacts with a series of nucleophiles in aqueous solution, as studied by Ritchie.^[21]

Since the carbocation does not vary in the series, the charge transfer energy gap G is given by the vertical ionization energy of the nucleophile X^- minus a constant quantity, which is the vertical attachment energy of the Y-pyronein cation. As can be seen from Figure 7, the free energy barriers for all the nucleophiles correlate linearly with the vertical ionization energy of the nucleophile. While the correlation

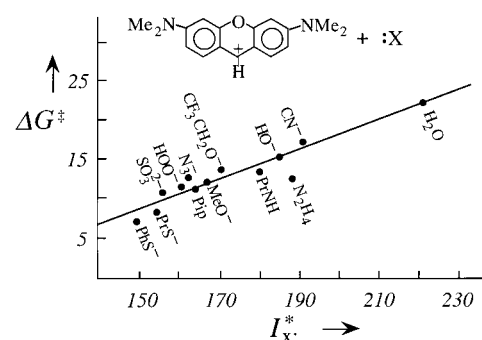


Figure 7. Free energy barriers^[21] for recombination of the pyronin cation with nucleophiles in aqueous solution, plotted against the vertical ionization energy of the nucleophile (adapted from ref. [17]). Energies in kcal mol^{−1}.

coefficient is far from being excellent ($r=0.94-0.96$), it is nevertheless impressive for such a variety of nucleophiles. It shows that nucleophilicity can oftentimes be related to a single fundamental property of the nucleophile. This correlation highlights the role of the vertical charge transfer energy gap G as an organizing quantity of the reactivity in the series, and lends support to the mechanism of activation associated with the covalent-ionic resonance in Figure 6. Furthermore, as discussed before,^[17] the correlation provides a basis for the N^+ nucleophilicity scale of Ritchie, but shows also its inherent limitations noted recently by Mayr and Patz.^[22]

2.1.4. Heterolysis of Polar Covalent Bonds Catalyzed by Metal Ions or External Charges

Bond cleavage can occur also in the presence of an “external” positively charged metal ion or charge $z+$. Let us consider this process with focus on the electrostatic effects exerted on the principal configurations. The electrostatic energy of mono-charged ions like K^+ and Cl^- at their equilibrium distance, given by the sum of ionic radii, is of the order of 130 kcal mol^{−1}, while for a di-positive ion like Zn^{2+} , Ca^{2+} , and Mg^{2+} with Cl^- or F^- , this interaction energy exceeds 260 kcal mol^{−1}. It is apparent therefore that the ionic VB structures of a polar bond will be highly affected by interaction with a positively charged metal ion or external charge. Figure 8 shows the energy levels of the VB configurations for the isolated molecular species, and in the

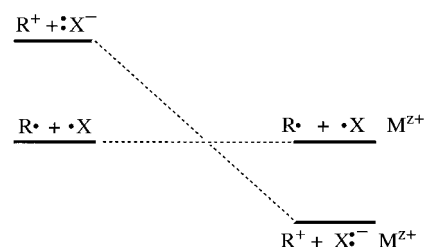


Figure 8. Energy ordering of the ionic and HL configurations at the dissociation limit in the gas phase (left) and in the presence of a metal cation or an external charge (right).

presence of the external charge. It is seen that, while for the isolated molecule the HL configuration is the lowest in energy, in the presence of M^{z+} it is the ionic structure which is

more stable. Thus, a positively charged metal ion promotes a covalent-ionic curve crossing along the bond stretching coordinate, and will heterolyze the bond much like a solvent.

Actually, because electrostatic energies in the case of localized charges exceed solvation energies, it is expected that such metal ions will catalyze bond heterolysis more efficiently. A schematic representation of the effect is illustrated in Figure 9, which shows that the stabilization of the ionic VB

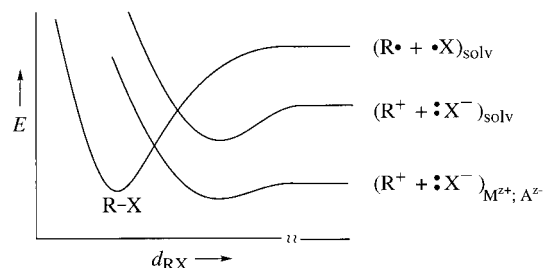


Figure 9. Covalent and ionic VB curves for a polar bond R–X in a solvent and in the field of two immobilized ions.

structure by a pair of external ions (charges) pulls down the ionic curve and lowers the height of the crossing point and hence of the respective barrier. This can be termed “electrostatic catalysis”.

An ideal setup for electrostatic catalysis would be a bond heterolysis that is effected between two external ions M^{z+} and A^{z-} , which are immobilized in a cavity so that their own interaction is constant throughout the bond heterolysis. In such a case, the stabilization of the ionic structure $R^+ :X^-$ will be very large, and the electrostatic catalysis will result in a small heterolysis barrier, if any. The catalytic tetrads of metalloenzymes (e.g., Zn^{2+} proteinases^[23]) have charge setups which may introduce electrostatic catalysis into their native processes. Warshel^[3b, 24] has treated heterolysis of the glycosidic bond of disaccharides in enzymes like lysozyme, and has shown that the electrostatic interactions between the ionized groups in the enzyme’s active site and the ionic fragments of the glycosidic bond can account for the rate enhancement of bond heterolysis relative to the same reaction in a solvent.

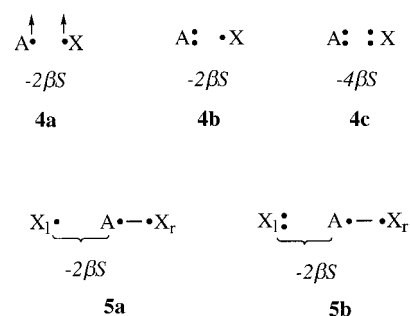
Other effects associated with the stabilization of the ionic VB component of a bond, and which enable thereby bond heterolysis, may be analyzed in a similar manner. Examples are effects of protonation or interaction with a Lewis acid.

2.2. Valence Bond Structures for Two- and Multi-Bond Reactions

To remain consistent in our approach, we shall focus on the principal configurations of the bonds which participate in the process, and only subsequently will we worry about the secondary structures. In so doing there will emerge a general VB correlation diagram based on the principal VB structures (Section 3).

2.2.1. Is There Wisdom in Valence Bond Cartoons? Valence Bond Structures of Many-Center Species

Let us consider first a few features of VB structures which will serve us in subsequent discussions. Structures **4a–c** in



Scheme 2. Archetypal repulsive VB interactions (top) and their use in describing the VB structures of bond exchange reactions in a simple way (bottom).

Scheme 2 depict the archetypal repulsive VB interactions which arise from the combination of the overlap between the bond hybrid orbitals and the Pauli exclusion principle; hence overlap repulsions or Pauli repulsions. Structure **4a** describes the basic quantity of overlap repulsion due to a triplet pair of electrons in two overlapping orbitals. This quantity is proportional to the product of the resonance and overlap integrals between the two orbitals ($\beta < 0$, and hence $-2\beta S > 0$). In **4b** two of the electrons must possess the same spin, and therefore the overlap repulsion equals the basic quantity $-2\beta S$. Similarly, in **4c** there exist two pairs of electrons with identical spins, and the overlap repulsion is twice the basic quantity.

Based on these archetypal interactions, we shall use the cartoon representation of VB structures as a source of information on the wave function. This is illustrated for **5a** and **5b**, which are key structures in bond-exchange reactions. Both structures are seen to involve a HL bond pair and nonbonding electrons which maintain some interaction with the bonding electrons. In VB theory, nonbonding interactions which arise from overlap are repulsive;^[7a] for example, in **5a** the unpaired electron maintains principally a triplet relationship with each one of the bond-pair electrons. It follows that as X_l approaches A, the triplet relationship will develop into a triplet state of the X_l –A linkage, and the energy of the VB structure will duly rise. Similarly, in **5b** the three-electron interaction between the electron pair on X_l and each of the bond-pair electrons will develop into overlap repulsion as the X_l –A distance decreases. Consequently, the VB structure will rise in energy and become a charge transfer excited structure (for the VB ground state in which X_l and A are bonded and X_r is the seat of the electron pair).

The triplet and charge transfer states are the two fundamental states which will appear time and again as excited states in VB correlation diagrams. The reasoning presented in Scheme 2 will be helpful in identifying these excited situations and constructing thereby VB correlation diagrams.

3. Valence Bond Correlation Diagrams for Two-Bond Processes of Covalent Bonds

The essential features of VB diagrams for the exchange of covalent bonds derive from the behavior of the HL structures, which are the principal configurations of covalent bonds. The following sections describe VB correlations for generic processes.

3.1. Radical Exchange Reactions

Figure 10 describes the VB correlation diagram for an identity process which involves bond cleavage by a radical. The two HL structures **6** and **7** evolve along the reaction

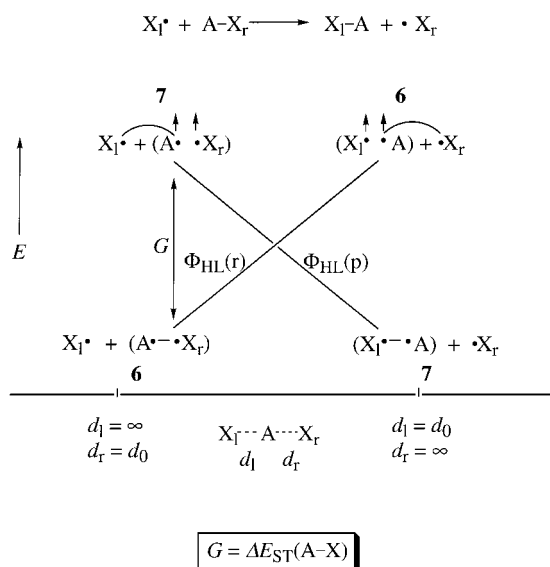


Figure 10. VB correlation diagram of the HL structures of reactants, $\Phi_{\text{HL}}(\text{r})$, and products, $\Phi_{\text{HL}}(\text{p})$, for a radical exchange process. G = promotion energy, $\Delta E_{\text{ST}}(\text{A}-\text{X})$ = singlet–triplet excitation of the A–X bond. The pairing mode of each structure (**6** or **7**) is conserved throughout the respective curve.

coordinate into two intersecting VB curves. Initially, when the left hand side distance (d_l) is infinite and the right hand one (d_r) is short, the ground state is **6**. The structure rises in energy along the reaction coordinate, because the HL bond A–X_r is homolyzed and the X_l–A interaction develops into a triplet pair. At the extreme of the reaction coordinate, where the d_l linkage is short and d_r infinite, **6** becomes an excited state. The ground state at this geometry is **7**, which in turn becomes an excited state along the reverse direction of the reaction coordinate. The energy gap between the two curves at the reactant and product extremes is given approximately by the singlet–triplet excitation energy of the A–X bond which is exchanged during the reactions. A useful way of understanding this gap is as a promotion energy, required in order to enable the A–X_r bond to be broken and be replaced by another bond, X_l–A.

3.2. Nucleophilic Exchange Reactions

Figure 11 illustrates the formation of the VB correlation diagram from the HL structures **8** and **9**, corresponding to a reaction between a nucleophile and a molecule. The ground state at the reactant geometry is **8**, which gets gradually destabilized as the A–X_r bond is homolyzed and the three-electron overlap repulsion builds up across the X_l–A linkage. Structure **9** behaves in the same manner along the reverse of the reaction coordinate. The result is that the two HL structures interchange along the reaction coordinate, and define two ground and two excited states for the VB diagram.

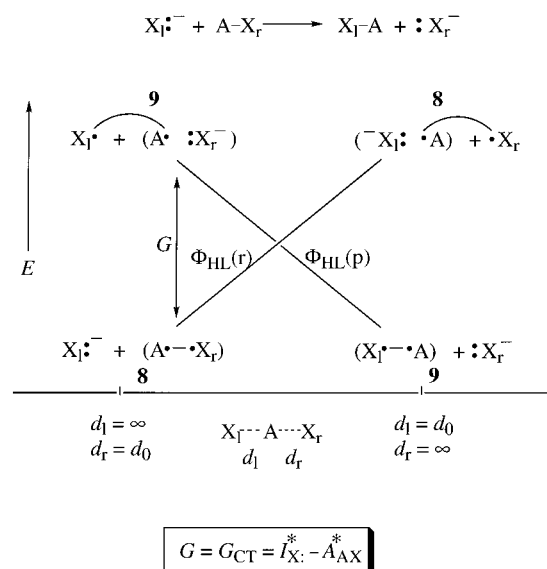


Figure 11. VB correlation diagram of the HL structures of reactants and products for a nucleophilic exchange process. G_{CT} = vertical charge transfer promotion energy. I^* = vertical ionization energy, A^* = vertical attachment energy (electron affinity).

It is seen that in each extreme of the diagram, the excited state is obtained from the ground state by one-electron transfer from the anion X_r^{•−} to the molecule A–X. Thus, the excited states in the diagram will correspond to charge transfer states, and the promotion energy of the reaction will be given by the vertical charge transfer energy.

3.3. Electrophilic Exchange Reactions

Figure 12 shows the behavior of the HL structures **10** and **11** along the same reaction coordinate as in preceding Figures. It is seen that the HL curves interchange along the reaction coordinate, and define two ground and two excited states for

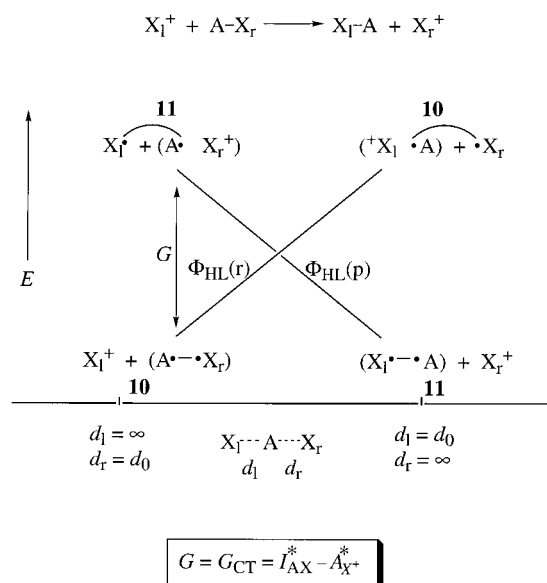


Figure 12. VB correlation diagram of the HL structures of reactants and products for an electrophilic exchange process.

the VB diagram. The excited states are related to the ground states by transfer of an electron from the bond into the empty orbital of the electrophile. As such, the promotion gap in the diagram is the vertical charge transfer energy.

3.4. Examples for Radical, Nucleophilic, and Electrophilic Attacks on Polar Covalent Bonds

To illustrate the relationship between the generic VB diagrams and to exercise their application, we show in Figure 13 three types of processes using an olefin as a common substrate. The three processes correspond to fundamental mechanisms of additions to a double bond by radicals,^[25] nucleophiles,^[26] and carbocations.^[22] Following our discussions above, it is concluded that a common feature for all the mechanisms is the intersection of the HL structures along the reaction coordinate. The resulting VB correlation diagram is anchored in two ground states and two excited states. The two ground states possess the HL bonds for the reactants and products, while the two excited states are obtained from the ground states by electronic promotions which prepare the reacting moieties for the bond and electron reorganization. The promotion energies involve triplet excitation of the π bond in the radical process, and vertical charge transfer energies for the nucleophilic and electrophilic processes.

4. Valence Bond Correlation Diagrams for Two-Bond Processes of Ionic Bonds

Whenever ionic bonds are involved in the exchange process, the respective ionic configurations will dominate the VB diagram. Since the HL structure of an ionic bond possesses a weak covalent bonding energy, the respective HL structure will be secondary and serve to dress the VB diagram, but will not change its essence. To illustrate these VB correlation diagrams we use two specific processes of bond activation by a metallic species. These two processes are then

contrasted with one in which the bond interchange can be described by a single ionic structure.

4.1. Bond Cleavage by Metallic Species

The bond activation which may initiate the Wurtz coupling is described by the VB correlation diagram in Figure 14. A quantitative VB correlation diagram was computed by Sevin

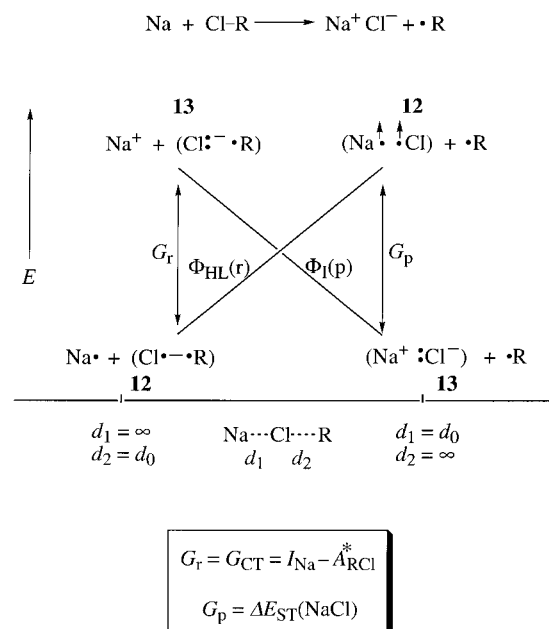


Figure 14. VB correlation diagram consisting of one HL (**12**) and one ionic VB structure (**13**) for C–Cl activation by Na.

et al.^[27] for an analogous process. The R–Cl bond is covalent (**12**), while NaCl is ionic (**13**). The VB curves for **12** and **13** cross along the reaction coordinate. The promotion gaps in the two extremes of the diagram involve the vertical charge transfer energy at the product side, and the singlet–triplet excitation of the NaCl bond at the product side.

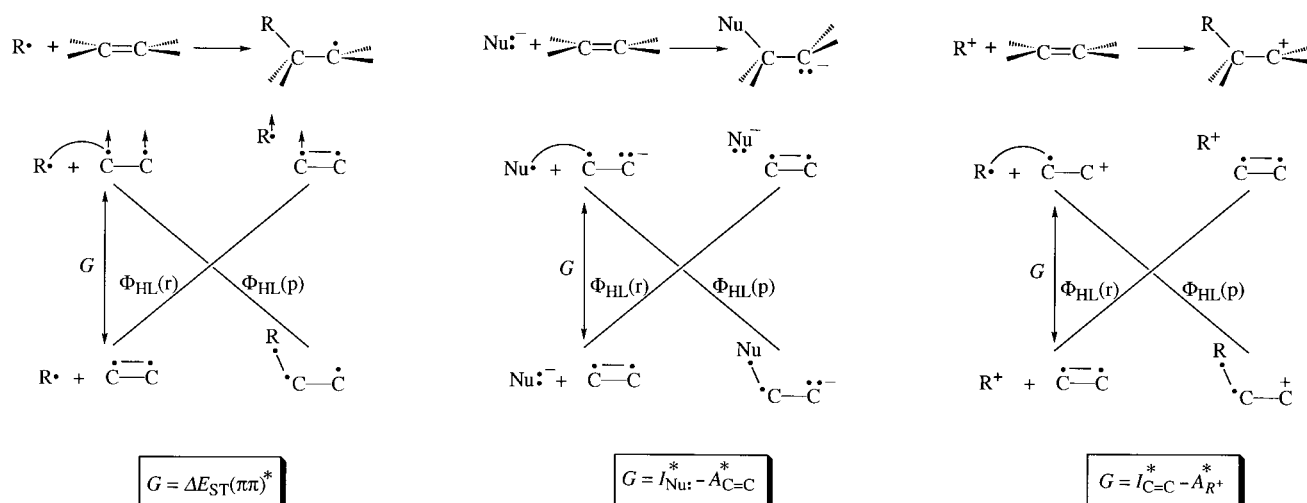
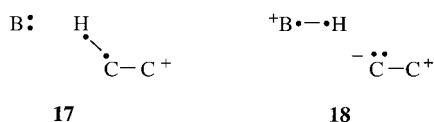


Figure 13. VB correlation diagrams for three elementary addition processes to an olefin. The corresponding promotion energies are specified in the boxes below the diagrams.



Scheme 4. VB structures of reactants (17) and hypothetical products (18) of the deprotonation reaction. For the correct VB description of the products, see Figure 16.

state.^[7a] Thus, the deprotonation of a carbocation is not a simple bond exchange reaction, and this is revealed in Figure 16 by the intersection of the curves for the HL structures along the reaction coordinate. It is seen that the electronic promotion at the reactant side involves triplet unpairing of the C–H bond along with a single electron shift from the base to the carbocationic center. Note, however, that upon renewed pairing of the electrons in the excited state, two of the electrons are paired into a π bond in the C–C moiety, and therefore part of the excitation energy is paid back, as shown in the expression for G in Figure 16.

Figure 17 shows the VB correlation diagram for the Diels–Alder reaction. The excited states in the diagram are seen to involve triplet excitations of all the bonds that are broken

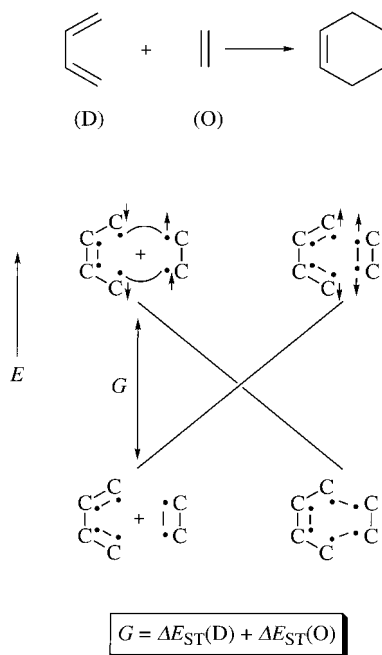


Figure 17. VB correlation diagram of the HL structures for a Diels–Alder reaction.

during the reaction, while pairing of the electrons anew takes place across the new linkages. Thus, the excited state on the reactant side involves a triplet diene that possesses a double bond in the central C–C linkage, and its two unpaired electrons on the termini are coupled into two singlet pairs with the triplet ethylene moiety.

To emphasize the unity of the VB correlation diagram we show in Figure 18 the VB correlation diagram for a cycloaddition of two olefins. Much the same as in the Diels–Alder reaction, here too the curves of the HL structures cross along the reaction coordinate and define two ground states and two excited states. It is seen that, in accord with the bond count in

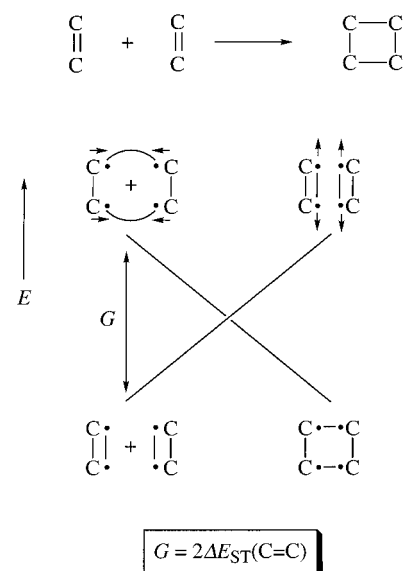


Figure 18. VB correlation diagram of the HL structures for a cycloaddition of two olefins.

the reaction, the promotion energy involves the sum of triplet excitations of the reacting π bonds. Note that unlike the VB crossing in Figure 18, which has a molecular orbital (MO) analogue,^[2] the VB crossing in Figure 17 is masked in the MO approach. Much the same holds true for the other processes discussed so far. Thus, with the exception of “forbidden” reactions, where orbital crossing is apparent, in all other cases the origins of the barrier in MO theory are masked, whereas VB theory provides a lucid and unified mechanism for the barrier formation in terms of the crossing of the curves of the principal VB structures associated with the active bonds and electron pairs which participate in the reaction.

Figure 19 shows an application of the VB diagram to an oxidative addition of an organometallic species L_nM into an R–H bond. The organometallic species which are considered

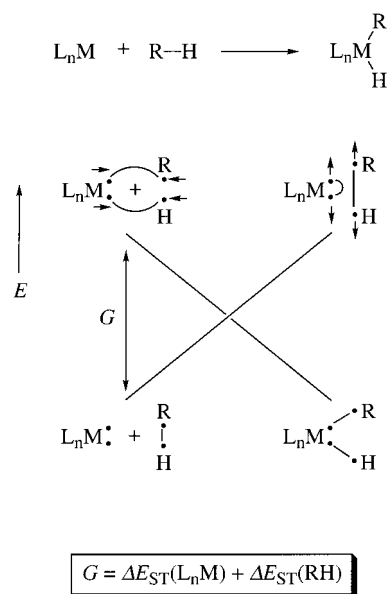


Figure 19. VB correlation diagram of the HL structures for an oxidative addition of a coordinatively unsaturated L_nM fragment across an R–H bond.

possess a filled orbital and a low-lying empty orbital, and are as such isolobal^[29] with singlet carbene. Examples are [Pt(PR₃)₂], which is a d¹⁰ L₂M species, or [Ru(CO)₄] or [Os(CO)₄], which are typical d⁸ L₄M species. Once again, the HL structures form a VB correlation diagram in which the promoted states involve excitation of the two moieties into triplet situations while pairing anew of the unpaired electrons across the intermolecular linkages takes place. Of course, insertion of singlet carbene itself and other main group element analogues into a covalent bond will exhibit precisely the same VB correlation diagram.

Before proceeding to generalize, we draw attention to an important aspect which emerges from Figures 16–19, but which is common to all other VB correlation diagrams. The VB correlations themselves are reflections of the electronic properties of the reactants and products. As such, the VB crossing is independent of either the trajectory of the reaction, or of the assignment of the reaction as either formally “allowed” or “forbidden” (e.g., in Figures 17 and 18). Thus, the pairing of the two new bonds in the promoted state in both Figures 17 and 18 can proceed either in a synchronous manner, as implied in the Figures, or one bond at a time along a stepwise trajectory. The difference in the barriers of the competing synchronous and stepwise processes will depend on other factors, such as the resonance energy for the transition state, as discussed later in the article.

6. Rules for Constructing Valence Bond Correlation Diagrams

The preceding applications project a general form of the VB correlation diagram, which may be summarized in rule 1.

Rule 1: *In any reaction (with restriction of the exchange of ionic bonds unaccompanied by formal redox, as discussed in Section 4.2), the curves of the principal VB configurations intersect along the reaction coordinate. If the bonds which interchange during the reaction are covalent, the intersecting curves are made from the HL structures, whereas when the bonds are primarily ionic the curves will be made from the respective ionic structures.*

An important quantity of the VB correlation diagram is the promotion energy gap at the diagram extremes. The concept of promotion energy emerges naturally from the VB treatment, and inspection of Figures 10–19 shows that the promotion is the mechanism whereby the molecules can break old bonds or electron pairs and replace them by new ones. Since the promoted states are initially vertical states, the mechanism of bond reorganization takes place by VB crossing that interchanges the ground with its promoted state along the reaction coordinate. Eventually part of the promotion energy will enter the barrier of the reaction by the resonance mixing of the VB structures.

As demonstrated in Figures 10–19, the promotion gap is based on two elementary excitations: that of the vertical charge transfer and the singlet–triplet varieties. A simple way to deduce the promotion energy for a given reaction is by “electron bookkeeping” using the formal oxidation states of

the reaction centers (groups or atoms) in the two principal VB structures. To illustrate the procedure, let us turn back to Figures 10 and 11. In Figure 10 the principal structures conserve the oxidation state of the reaction centers, and the only change is the interchange in the spin pairing between the two exchanging bonds. In this case, the promotion energy is the singlet–triplet excitation of the bond that interchanges during the reaction. In Figure 11, however, the principal structures involve a change in the formal oxidation state of the reaction centers, so that a single electron shifts from the anion X[–] to the radical ·X. In this case, the promotion involves a vertical charge transfer from the donor moiety to the acceptor moiety. The nature of the promotion energy can be summarized in rule 2 based on the elementary excitations which are involved in the principal VB configurations.

Rule 2: *An interchange of spin pairing in the two principal configurations requires singlet–triplet excitation, while a change in the formal oxidation state requires charge transfer excitation. For reactions which involve no formal redox process at the reaction centers, the promoted states involve only singlet–triplet excitations, one for each bond which has to be broken in the transformation. For reactions which involve a formal redox process at the reaction centers in addition to bond exchanges, the promoted states involve one charge transfer excitation for each pair of centers which undergo formal redox reactions. The rest of the excitations will be of the singlet–triplet variety. In each case, the unpaired electrons are paired anew across the new linkages.*

7. State Correlation Diagrams—Origins of the Barrier and Reactivity Patterns in Chemical Reactions

As noted at the beginning of Section 2.2, in addition to the principal VB structures there exist secondary ones which mix with the principal structures. As such, there are two alternative approaches to conceptualize reactivity patterns: VB configuration mixing diagrams and state correlation diagrams (the past abbreviations^[1, 4, 7] VBCM and SCD are changed here into VBCMD and VBSCD, respectively, for the sake of consistency). The VBCMD alternative, which is described later in this article, includes explicitly the additional VB structures in the diagram. This way has quite a few advantages (e.g., explicit account of bond ionicity in bond exchange reactions), but the simplicity of the two-curve diagram is lost. The VBSCD alternative, which we shall discuss now, conserves the two-curve format of the VB correlation diagram, by mixing the secondary structures into the principal curves and generating thereby two semi-delocalized state curves which are anchored in spectroscopic-like states, hence the name a state correlation diagram (VBSCD).^[1, 4a, b, 7] An appealing feature of the VBSCD is the retention of simplicity of the two-curve VB correlation diagram, and the advent of a unified mechanism for the origins of the barrier.

To illustrate the relationship of the VBSCD to its VB correlation diagram precursor, we show the nucleophilic exchange process in Figure 20. Figure 20a recalls the VB

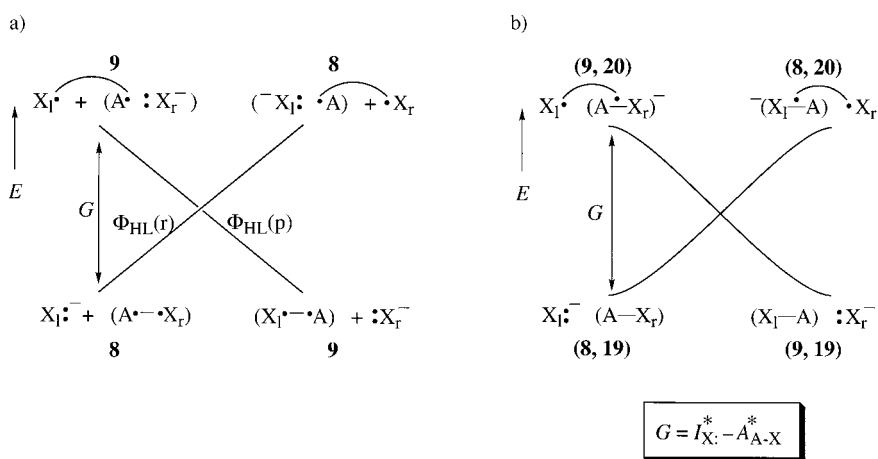
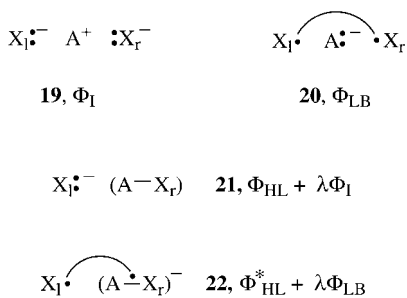


Figure 20. a) VB correlation diagram of the HL structures for a nucleophilic exchange process, b) corresponding VBSCD. See text for details. The contributing VB configurations to the ground and excited anchor states in the VBSCD are shown in parentheses (see also Scheme 5).

correlation diagram based on the HL structures (see Figure 11), while Figure 20b shows the VB state curves; the ground states are the Lewis structures of reactants and products, and the excited states are the corresponding charge transfer states. Scheme 5 shows the two secondary structures



Scheme 5. Secondary VB structures and concrete examples for VB states that play a role in the attack of a nucleophile.

19 and **20**, which by mixing with the HL configurations transform the latter into VB states; a pair of ground and promoted states is depicted explicitly with **21** and **22**. Accordingly, **19** is an ionic structure, which by mixing with the reactant's HL structure (**8**) generates the Lewis ground state structure of the reactants, **21** (λ is the mixing coefficient). The product's Lewis structure is obtained by the mixing of **19** with the product's HL structure **9**. Similarly, **20** is a long-bond structure which possesses three electrons in both A–X linkages. By mixing with the excited HL structure **9**, **20** generates the charge transfer state **22**, where the radical anion moiety has three electrons delocalized over the A and X groups through the VB mixing. The other charge transfer state arises by mixing of **20** with the excited HL structure **8**. These mixing patterns account for the generation of the VB states in Figure 20b.

By comparison of Figure 20a and 20b, it becomes apparent that the VBSCD is anchored at the states which are obtained from the principal VB structures. This enables drawing of the VBSCD in a general form, as shown in Figure 21a, with two ground states and two promoted excited states which can be deduced from the principal VB structures (review rules 1 and 2

in Section 6) for any desired reaction. The promoted states are indicated with two subscripts, the first specifies the geometry and the second the electron-pairing pattern. For example, Ψ_{rp}^* is a vertical excited state at the geometry of the reactants (r) with the electron-pairing pattern of the products (p).

In a subsequent step, the two VBSCD curves are allowed to mix with each other, as shown in Figure 21b. As a result, the crossing of the two curves is avoided by their resonance mixing, which leads to a resonating transition state on the lower energy profile. The barrier for the forward reaction can be expressed as a balance between the destabilization

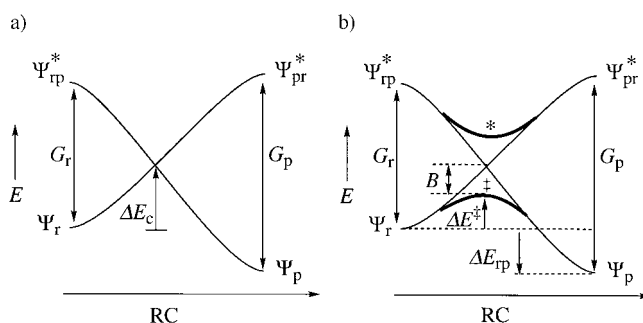


Figure 21. a) Generic VBSCD with two ground states and two promoted excited states, and b) the resulting states due to resonance mixing (avoided crossing). G = promotion energies, ΔE_c = energy of the crossing point relative to the reactant state, ΔE_{rp} = thermodynamic driving force of the reaction, ΔE^* = barrier, B = resonance energy of the transition state, Ψ_r = reactant state, Ψ_p = product state, Ψ_{rp}^* and Ψ_{pr}^* = promoted excited states.

energy ΔE_c needed to reach the crossing point and the resonance interaction energy B . The destabilization energy ΔE_c is a fraction f of the promotion gap G_r that enters under the crossing point. Consequently, the barrier will have the form of Equation (6), which describes a simple activation

$$\Delta E^* = fG_r - B \quad (6)$$

mechanism which is in tune with the electronic reorganization required in order to break old bonds or electron pairs and replace them by new ones during the reaction.

The transition state is the situation where the ground state and the corresponding promoted state are in resonance. Since the two states are initially separated by the promotion energy, structural changes are required to destabilize the ground state (e.g., by means of bond deformations and nonbonding repulsions) and to simultaneously stabilize the promoted state (by bond formation and release of nonbonding repulsions). At some point along the reaction coordinate the promotion gap separating the states is closed and a resonating transition situation is achieved, enabling the bonding pattern to change from reactantlike to productlike.

7.1. Structure–Reactivity Relationships Dominated by the Reaction's Promotion Energy

While both Figure 21b and Equation (6) implicitly show that trends in the barrier will be determined by an interplay of factors, it is apparent that the factor that originates and gauges the barrier is the promotion energy gap which has to be overcome during the reaction. We might therefore anticipate that quite a few reactivity patterns will be dominated by the promotion gap. This restrictive outlook is didactically necessary in order to appreciate the impact of the promotion energy on reactivity. With this in mind we turn to discuss reactivity puzzles and their origins in the variation of the promotion gap. Relying on Figure 21, rule 2 (strictly correct for state curves), and Equation (6), most of the cases are discussed by showing the ground state and promoted state (Ψ_{rp}^*) without constructing the entire VBSCD.

7.1.1. Barriers of Identity Reactions in Hydrogen Abstraction from Alkanes

Identity reactions proceed without a thermodynamic driving force, and project therefore the role of promotion energy as the origins of the barrier. Let us consider the identity process of hydrogen abstraction by an alkyl radical shown in Equation (7). The barriers for a series of radicals have been



computed by Yamataka and Nagase,^[30] and were found to increase as the R–H bond energy D increases. Thus, for example, the relative barriers for $\text{R} = \text{CH}_3$ and $\text{R} = \text{C}(\text{CH}_3)_3$ (22.4 and 15.3 kcal mol^{−1}, respectively) were found to be in accord with the relative bond strengths in the two alkanes (104 and 94 kcal mol^{−1}, respectively). Since the effect of bond breaking and bond making is balanced in the symmetric transition state, one might wonder why should the barrier reflect only the strength of the bond which is broken during the reaction.

This trend has been interpreted by Pross et al.^[31a] using the VBSCD model. Figure 22 depicts the ground states and the promoted state in the respective VBSCD (which follows from

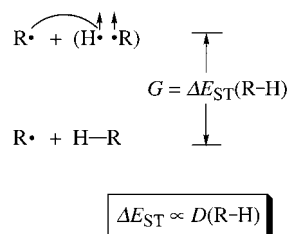


Figure 22. Ground state, promoted excited state, and promotion energy gap for an identity hydrogen atom transfer.

Figure 10 and rule 2). The promotion gap which originates the barrier involves singlet–triplet excitation of the R–H bond. With VB theory^[7a] it is possible to show that the singlet–triplet excitation of a bond is proportional to the respective

bond energy. Therefore, the correlation of the barrier with the bond strength is in fact a correlation with the promotion energy, and reflects the electronic reorganization which is required during the reaction.

A spectacular relationship between excitation energy and the barrier to reaction has been observed for X_3 clusters, which occur en-route for the radical exchange process shown in Figure 23. Here, a very large triplet promotion energy for

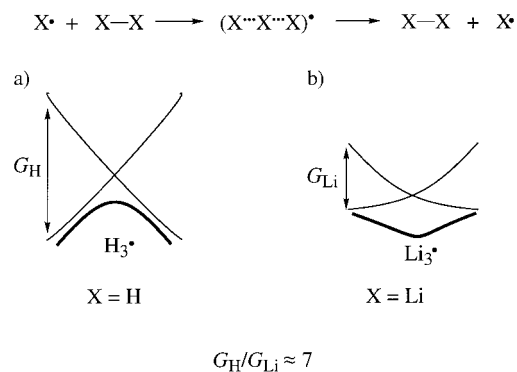


Figure 23. Schematic representations of VBSCDs computed^[5a] with the ab initio VB method for a) H-atom transfer where the avoided crossing leads to a barrier, and b) Li-atom transfer where the avoided crossing leads to an intermediate cluster.

$\text{X} = \text{H}$ (250 kcal mol^{−1}) results in an H_3^\bullet transition state, while the small promotion energy for $\text{X} = \text{Li}$ (32 kcal mol^{−1}) results in a stable Li_3^\bullet cluster. The VB computations by Maitre et al.^[5a] show that, as the promotion gap drops drastically, the avoided crossing leads to a stable cluster as in the case of Li_3^\bullet in Figure 23b.

Of course, effects of bond ionicity exist in general in radical reactions and can be discussed by considering the consequences of mixing the ionic structures on the state curves and on the resonating transition state.^[31b]

7.1.2. One Electron Less, One Electron More: Why Are Cycloaddition Reactions of Ion Radicals So Fast?

It is well known that the cyclodimerization of olefins is a sluggish process which proceeds with a barrier greater than 40 kcal mol^{−1}. In contrast, as shown by the seminal work of Bauld et al.,^[32] the corresponding reaction between an olefin and its cation radical is a very facile process. Figure 24 shows the promotion energies for the two processes along with barriers calculated by Bernardi et al.^[33] and Jungwirth and Bally.^[34] Based on Figure 18 and rule 2, the cyclodimerization of ethylene, which requires unpairing of the electrons of two bonds, has a promotion energy which is twice the singlet–triplet excitation of the π bonds. In contrast, in the attack of a radical cation on a neutral olefin the promotion energy is halved, because now only the neutral olefin needs to be unpaired.^[35] While other factors certainly help (e.g., the reaction driving force and electrostatic interactions), the significant drop in the promotion energy (by about 100 kcal mol^{−1}) accelerates the reaction and accounts for a significant drop in its barrier.

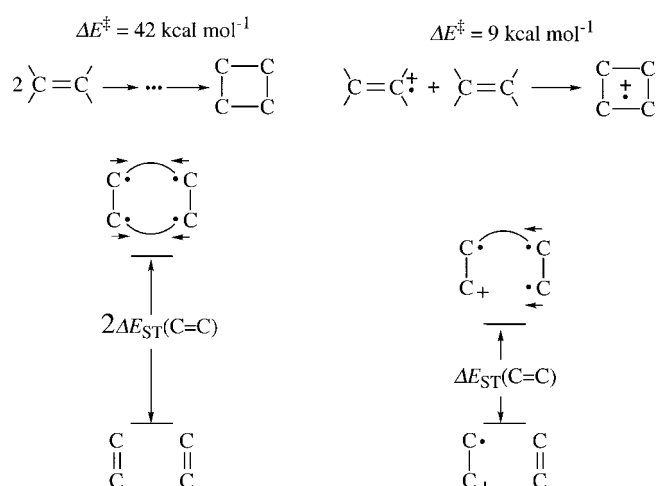


Figure 24. Ground states, promoted excited states, barriers, and promotion energy gaps for a cycloaddition of two neutral ethylene molecules, and for a combination of an ethylene cation radical with a neutral ethylene molecule.

A related catalytic effect is found in the DNA repair mechanism.^[36] One of the DNA damages initiated by sunlight is the dimerization of DNA bases to form cyclobutane photodimers such as the thymine photodimer in the top left of Figure 25. The in situ repair mechanism involves a photo-induced electron transfer from a reduced flavin and folate,

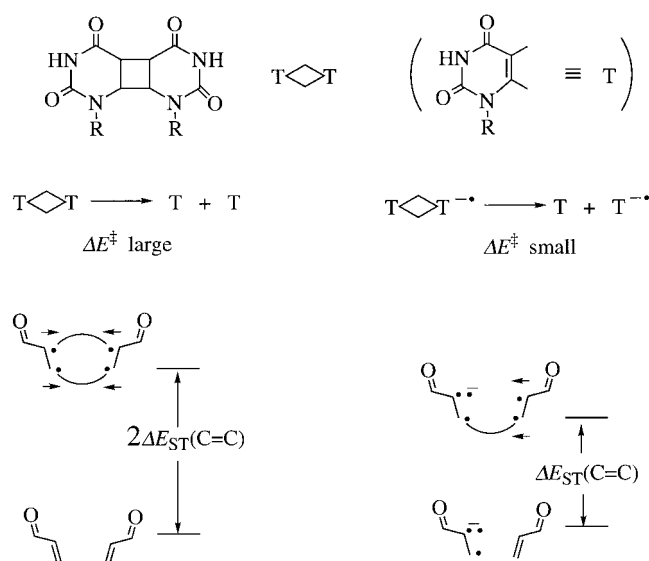


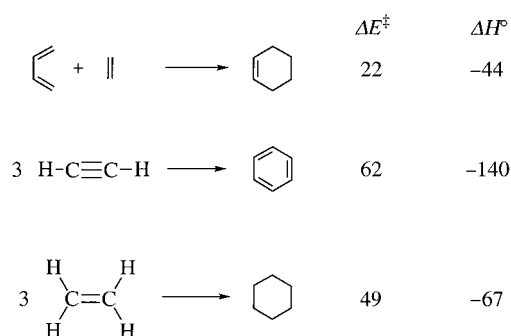
Figure 25. Comparison of the cleavage of the thymine photodimer (left) and the corresponding anion radical, which is responsible for the in situ repair mechanism of DNA (right). Ground states, promoted excited states, and promotion energy gaps are shown for the reverse processes using the enone moieties of thymine.

which are cofactors of the photolyase enzyme. The electron transfer process generates in turn the radical anion of the dimer, which undergoes facile cleavage to its constituents (Figure 25, middle right). This is contrasted with the neutral photodimer, which resists decomposition^[36a] (Figure 25, middle left) even at temperatures above 200 °C and despite the fact that the reaction is exothermic (−27 kcal mol^{−1}).^[36a] To appreciate the effect we show at the bottom of Figure 25 the

VB states for the reverse process, where it is seen that dimerization of the neutral bases will require singlet–triplet excitation of the two reacting π bonds, in comparison with only half of this quantity for the cycloaddition of the anion radical and the neutral molecule. Thus, the DNA repair is catalyzed by the reduction in promotion energy for the reaction.

7.1.3. Why Do Some “Allowed” and Very Exothermic Reactions Possess High Barriers?

Scheme 6 depicts three cycloaddition processes taken from a recent study by Ioffe and Shaik.^[37] All the reactions are formally allowed, but nevertheless the latter two have very



Scheme 6. “Allowed” cycloadditions with very different barriers. The energies are given in kcal mol^{−1}.

high barriers. Moreover, the reactions with the high barriers are extremely exothermic, while the least exothermic Diels–Alder reaction has the lowest barrier. Figure 26 compares the

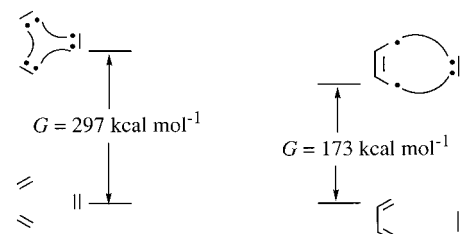


Figure 26. Ground states, promoted excited states, and promotion energy gaps for the trimerization of ethylene (left) in comparison with the Diels–Alder reaction (right).

promotion gaps of the Diels–Alder reaction (right) and the trimerization of ethylene (left), based on the discussion of Figure 18 and rule 2. In the trimerization reaction, the promoted state involves unpairing of the three π bonds into triplets, while pairing anew of the electrons across the infinitely long intermolecular linkages is of no energetic significance. The resulting promotion energy is high (297 kcal mol^{−1}), much larger than the corresponding quantity for the Diels–Alder process (173 kcal mol^{−1}).

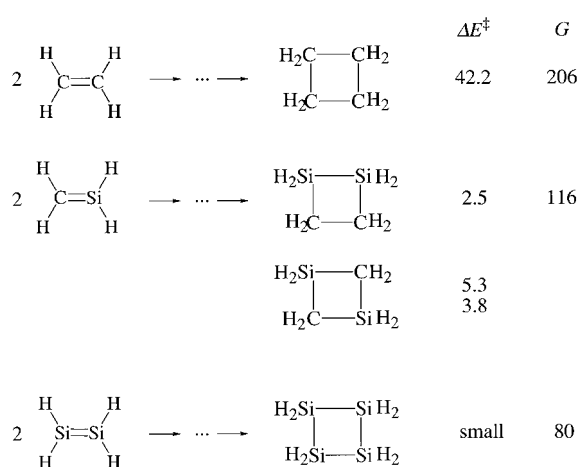
The small promotion energy of the Diels–Alder process originates in the diene, for which the excitation energy is less than half of the corresponding energy for the promotion of two isolated π bonds. Thus, unpairing the double bonds of the ground-state diene to two triplets and pairing anew the four electrons creates a π bond in the central C–C linkage and

localizes two triplet electrons on the termini, thereby minimizing the triplet repulsion energy. These two effects together reduce the promotion energy of the diene to 79 kcal mol^{-1} , in comparison with almost $200 \text{ kcal mol}^{-1}$ for two isolated double bonds. Thus, using a conjugated diene creates a huge intramolecular advantage in the promotion energy over the intermolecular situation and lowers the barrier significantly.

The very high barrier for the trimerization of acetylene (Scheme 6) can now be understood easily by simply considering the promotion gap (ca. $375 \text{ kcal mol}^{-1}$) corresponding to the triplet excitation of three acetylene molecules.

7.1.4. When Do “Forbidden” Reactions Become Facile?

Scheme 7 shows that the computed barrier for ethylene dimerization^[33] is very large, as anticipated. However, the corresponding silaethylene and disilene dimerizations are



Scheme 7. Comparison of the barriers and excitation energies (in kcal mol^{-1}) for several “forbidden” cycloadditions.

seen to have negligible barriers, despite their formal “forbiddenness”. While the computational studies differ in their mechanistic conclusions, regarding the question of whether or not the head-to-tail dimerization of silaethylene proceeds in a concerted fashion,^[38] all calculations agree that the barriers are tiny irrespective of the precise mechanistic details.^[33, 38] These computational trends model faithfully the experimental findings.^[39]

It is true that the dimerizations of the silicon compounds are more exothermic than that of ethylene. However, as noted for the examples in Scheme 6, even extreme exothermicity is insufficient to produce a small barrier when the promotion energy is large. The promotion energy, which is the sum of singlet–triplet energies of the two reactants calculated by us^[40] at the CASSCF/6-311G**//CASSCF/6-311G** level, is displayed in Scheme 7. It is seen that a substitution of carbon by one or two silicon atoms reduces the excitation by a sizeable amount of $100 \text{ kcal mol}^{-1}$ and more, which accounts for a significant lowering of the barriers.

The reduction in the promotion energy in Scheme 7 is in accord with the trends of excitation energies in the periodic table. Thus, small triplet excitation energies generally occur among main group elements which are located in the lower

rows and in the metallic block, and this is where formally forbidden reactions will possess low barriers. In fact, four-center clusters of alkali metals are more stable than their separated diatomic molecules.^[41]

7.1.5. Zipper Reactions: When Are They Facile?

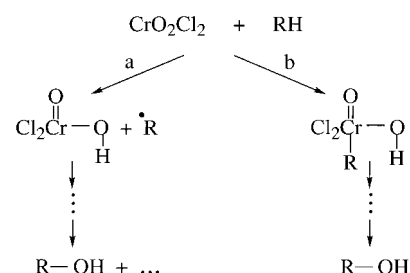
The impact of the promotion energy on reactivity may be appreciated by analyzing the feasibility of zipper reactions, in which many bonds would participate synchronously in an exchange or a cycloaddition process. A similar question was posed by Dewar quite a few years ago.^[42] The answer to this question depends on whether the bonds which participate in the reaction are covalent or ionic.

In the case of covalent or polar covalent bonds the isomerization and structural reorganization require a promotion energy which increases with the number of participating bonds. As such, reactivity tends to be localized in a small number of bonds, and collective zipper reactivity is usually prohibitive. Exceptions may be encountered when the molecules involve either conjugated bonds, or when the bonds are fixed in proximity; in both these situations the reaction will benefit from lowering of the promotion energy by the “intramolecular advantage”,^[37] in analogy to the situation in Figure 26. This reduction of the promotion energy, by the intramolecular or proximity effects, will generally lower the barrier, and may thereby enable zipper reactivity of covalent bonds.

In the case of ionic bonds, such as Na^+Cl^- , isomerization and structural reorganization require no promotion energies, since the entire energy hypersurface of such a reaction will be described by a single VB configuration, that is, the ionic VB structure (**16c** in Scheme 3). Consequently, zipper reactions of ionic bonds are expected to be facile. Ionic exchange reactions have been considered by King and Herschbach,^[43] who dubbed these processes as “no-electron reactions” to emphasize their exclusive ionic nature across the reaction path.

7.1.6. Why Does C–H Activation by CrO_2Cl_2 Exhibit a Radical-Like Selectivity Even Though the Reagent Is Diamagnetic?

The mode of spin pairing in the promoted states of a reaction may serve also as an indicator of mechanistic possibilities. Let us illustrate this feature by considering the intriguing mechanism suggested recently by Mayer and Cook^[44] for C–H activation by CrO_2Cl_2 (Scheme 8a). The



Scheme 8. Mechanistic alternatives of C–H activation by CrO_2Cl_2 .

initial step is a hydrogen abstraction followed by trapping of the alkyl radical to form alcohol, among other products. As was pointed out by Cook and Mayer repeatedly,^[44] CrO_2Cl_2 is a diamagnetic species and nevertheless the process transpires by a stepwise radical mechanism, and its structure–reactivity patterns exhibit a radical-like selectivity. To balance this view, Scheme 8b shows the mechanism discussed by Rappé and Goddard^[45] based on their GVB calculations. Thus, in addition to a radical mechanism of the type found by Mayer and Cook, the calculations suggest that a concerted addition of the C–H bond to the Cr=O bond should also be considered. This last mechanism appears to be the main mechanism of C–H activation by metal oxide cations in the gas phase.^[8, 46]

The electronic structure of the Cr=O bond was investigated by Rappé and Goddard,^[45] and the main features are depicted in Figure 27a. Thus, in analogy with the C=O bond in ketones

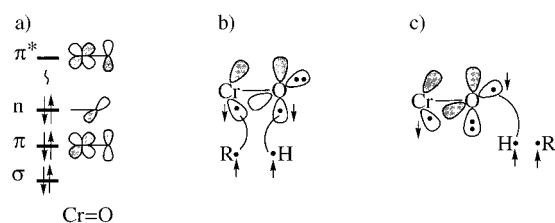


Figure 27. a) Schematic orbital diagram for the Cr=O bond in CrO_2Cl_2 . b, c) Alternative promoted excited states for the reaction of CrO_2Cl_2 with R–H.

or aldehydes, the Cr=O moiety possesses a double bond and a lone pair on the oxygen, whose orbital is perpendicular to the plane of the π bond. By the same analogy to the carbonyl group, two promoted states of the Cr=O bond might be considered to affect the nature of the bond-activation step. The first state (Figure 27b) involves a $\pi\pi^*$ triplet Cr=O coupled to a singlet with the promoted C–H bond moiety. This coupling mode may be associated with the concerted addition mechanism (Scheme 8b) which occur so often in metal oxide cations. The second promoted state (Figure 27c) involves an $n\pi^*$ -promoted coupling of Cr=O to the promoted C–H moiety. This latter situation correlates nicely with the product state of the hydrogen abstraction (Scheme 8a). Based on spectroscopic and computational data,^[47] these two promoted states are expected to be close in energy, and to originate thereby the two possible competing mechanisms. Thus, the modes of electron pairing in the promoted states have mechanistic significance.

7.1.7. What Is the Role of Charge Transfer Promotion in Reactions between Electrophiles and Nucleophiles?

Figure 28 shows a structure–reactivity correlation for the nucleophilic cleavage of an ester, based on the VBSCD analysis of the reaction by Buncel et al.^[48] It is seen that the free energies of activation correlate with the vertical ionization energy of the nucleophiles in the reaction solvent. Furthermore, localized and delocalized nucleophiles appear to generate correlation lines of different slopes. Similar correlations were found for three other esters.^[48] The rate-determining step of the mechanism had been shown by

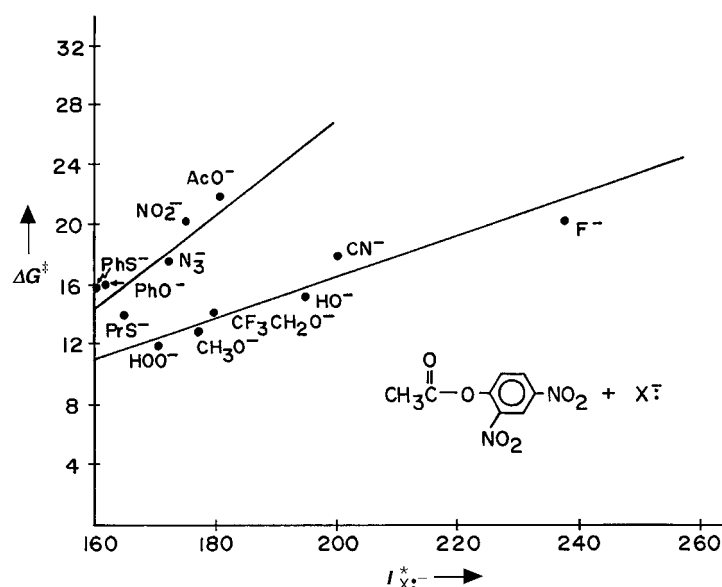


Figure 28. Correlation of free energy barriers with vertical ionization energy of nucleophiles for nucleophilic cleavage of an ester (adapted from ref. [48]). Energies in kcal mol^{-1} .

Schowen et al.^[49] and Gold et al.^[50] to involve the formation of the tetrahedral intermediate, as depicted in Figure 29.

Following the general VBSCD in Figure 21b and rule 2, we show in Figure 29 that the promoted state in the VBSCD for the formation of the tetrahedral intermediate is the vertical charge transfer state. The promotion energy is, accordingly,

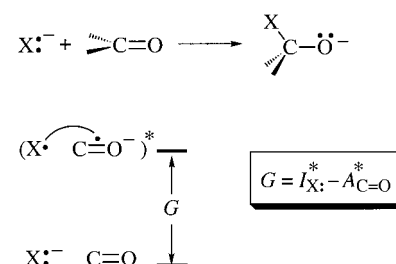


Figure 29. Ground state, promoted excited state, and promotion energy gap for the nucleophilic addition to a carbonyl group to form a tetrahedral intermediate.

the difference between the vertical ionization potential of the nucleophile and the electron attachment energy of the carbonyl group. The latter quantity is a constant for a given ester, and therefore the correlation of barriers with the promotion energy becomes a correlation with the vertical ionization energy of the nucleophiles.

The two correlation lines obtained for the experimental data in Figure 28 are readily understood based on Equation (6) as corresponding to different f values, where the localized nucleophiles possess the smaller f value and hence the smaller structure–reactivity slope in comparison with the delocalized nucleophiles. Thus, when the nucleophiles are delocalized a larger fraction f of the promotion gap enters under the crossing point, reflecting thereby the need to localize the transferred electron in order to form the X–C bond, and effects the correlation of the charge transfer state down to the tetrahedral intermediate product. This

emphasizes that the correlation of reactivity with the vertical charge transfer energy is a manifestation of the mechanism of activation, which consists of bringing the two states in Figure 29 into resonance mixing. It follows therefore that significant lowering of the charge transfer promotion energy will be expected to facilitate the process. The reduction of the charge transfer promotion gap may account in part for the catalysis of ester hydrolysis by proteolytic Zn^{2+} metallo-enzymes (e.g., carboxypeptidase A^[23a]), where the coordination of the metal ion to the carbonyl group increases the electron attachment energy of the ester moiety.

Correlations of free energy barriers with the vertical charge transfer energies have been amply observed for classical “polar” reactions between electrophiles and nucleophiles by Kochi and co-workers in their seminal work on “charge transfer activation”.^[51] A variety of reactions between electrophiles such as bromine, chlorine, and mercury diacetate with π nucleophiles such as olefins and arenes have been found to follow the same charge transfer correlations. The studies were extended by Fukuzumi et al.^[52] to other processes, including hydride transfers. The interpretation of this correlation type has been shrouded with controversy. For example, the recent *mise au point* by Baciocchi and Mandolini^[53] confronts the applicability of this concept to electrophilic aromatic substitution, and concludes that it is “unsound” because the experimental data does not indicate that an electron transfer component plays a role in the reaction.

In our view, much of the controversy originates in a misconception that the correlation necessarily indicates some type of an electron transfer mechanism.^[51] Because of the ubiquity of the correlation, it is important to outline the relationship between a polar and an electron transfer (ET) reaction which can transpire between a pair of closed-shell^[4c, 54] nucleophiles and electrophiles. Figure 30 shows the VBSCDs of the two processes which are initiated from the same pair of states in the center of the diagram, and then

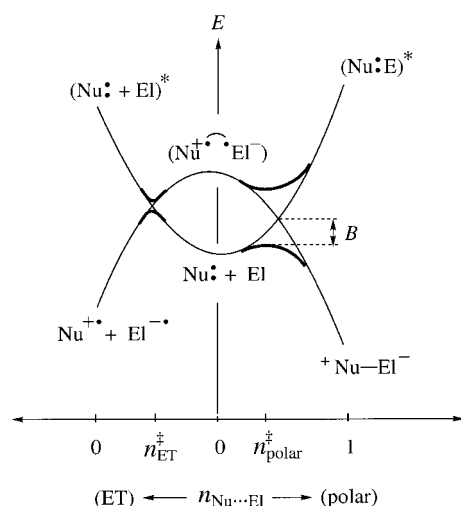


Figure 30. VBSCDs for competing polar and ET pathways available to a pair of closed-shell nucleophile and electrophile ($\text{Nu}\cdot + \text{EI}$). The ground state and promoted excited state of the reactants are common to the two mechanisms, and avoided crossing occurs along different reaction coordinates specified in terms of the bond order n between the two reactants.

proceed along two different reaction coordinates indicated by the bond order n between the reactants. In the polar process, the crossing between the ground and charge transfer states occurs along a reaction coordinate which exhibits a progressive increase of the $\text{Nu}\cdots\text{EI}$ bond order. In this case, the resonance mixing between the two VB configurations is large, and the resonating transition state is typified by strong bonding, that is, a large resonance energy B . To the left, the same two states cross either along a coordinate which keeps a zero bond order throughout—that is, a weakly bonded outersphere ET mechanism—or along a path where the reactants initially approach one another to achieve significant bonding and then recoil to give the separated radicals—that is, a bonded ET mechanism.^[54]

Thus, the polar and ET mechanisms are related in the origins of their barriers by the avoided crossing of the same two states, and hence may exhibit similar free energy correlations with the vertical charge transfer energies. However, in all other aspects these are different mechanisms. This is the reason why we have suggested to call polar reactions “single electron shift processes” to link them to, and at the same time distinguish them from, single electron transfer mechanisms.^[4a, e]

Aspects of this mechanistic dichotomy can be found in the various reviews and monographs.^[4, 55] Recently, Verhoeven et al.^[56a] have used the VBSCD model to explain the correlations found between the hydride transfer process and electron transfer energies. A similar treatment of hydride transfer between carbocations and silanes was later published by Apeloig et al.^[56b] In any event, a simple test can be used to show that a polar reaction is not an ET reaction, as has been reported by Ebersson,^[55] Verhoeven et al.,^[56a] and Mayr, Fukuzumi et al.^[57] Thus, the controversy can be avoided and replaced by efforts to extract useful information about the origins of the barrier and the structure of the transition state from correlations^[48] as those in Figure 28 and in Kochi’s work.^[51]

7.1.8. Origins of the Correlation between C–F Bond Activation Ability of Metal Cations and Their Ionization Energy

Recent studies by Cornehl et al.^[28a] showed that lanthanide cations (Ln^+) are capable of activating C–F bonds quite selectively from aryl and alkyl fluorides, even though there exist weaker C–C and C–H bonds in the substrates. Furthermore, the reactivity patterns of the Ln^+ species did not follow the trends in the C–H/C–C bond activation mechanism,^[58] which involves an initial insertion into the bond. Whereas the insertion efficiency into C–H/C–C bonds was found to correlate with the promotion energy of Ln^+ to a state which contains two non-f electrons capable of covalent bond formation, the C–F activation efficiency did not follow that trend. Instead, the efficiency of C–F activation was found to depend on the ionization energy of the Ln^+ (Figure 31). Similar trends have been noted by Harvey et al.^[28b] for transition metal cations ($\text{M}^+ = \text{Y}^+, \text{Sc}^+, \text{Ti}^+, \text{V}^+$).

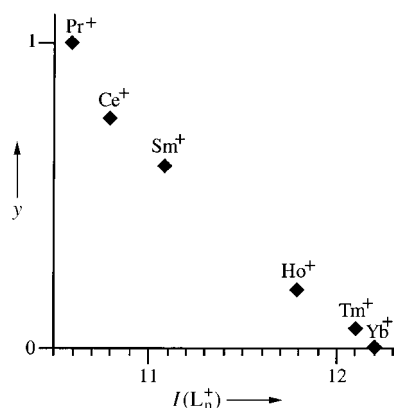
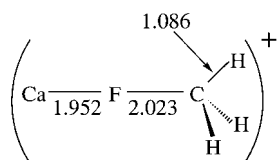


Figure 31. Correlation of relative efficiency y of C–F bond activation by lanthanide cations (Ln^+) with the ionization energy of Ln^+ (adapted from ref. [28a]).

While these trends are suggestive of an electron transfer or a “harpoon” mechanism, it is very clear that a long-distance electron transfer cannot occur due to unfavorable thermodynamics. Moreover, there are clear indications that the C–F activation mechanism involves bonding between the reaction partners and is not a simple electron transfer process. First,



Scheme 9. Calculated transition state of C–F activation by Ca^+ .

the transition state for the C–F bond activation by Ca^+ was computed by Harvey et al.,^[28b] who found it to be structured, as depicted in Scheme 9. Second, for the same M^+ ionization energy, the activation capability was found to be largest for a transition metal ion, intermediate for Ca^+ , and lowest

for a Ln^+ ion, and thus reflecting the respective relative covalency of the essentially ionic $\text{M}^{2+}\text{--F}^-$ bonds. These trends indicate that the correlation in Figure 31 exists for related ions, but its slope will differ for different families of ions, and will reflect thereby the relative covalent bonding in the transition states.

Figure 32 shows a schematic VBSCD for the C–F activation by metal ions. It is seen that the reaction involves an avoided crossing of ground with charge transfer states. The corresponding transition state arises by resonance mixing of the VB state curves, and will possess thereby considerable bonding. The promotion energy for the C–F bond activation is seen to

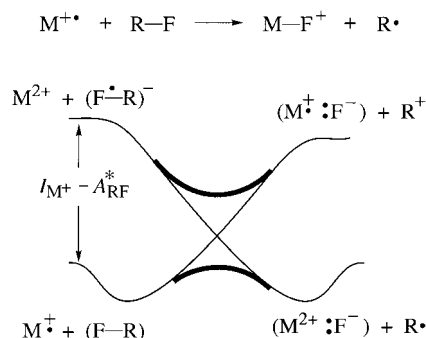


Figure 32. VBSCD for the C–F bond activation by a positive metal ion M^+ (based on the VB correlation in Figure 15).

depend on the ionization energy of the metal ion, and therefore in a family of related ions like Ln^+ one might anticipate that the promotion energy will dominate the reactivity trends. Thus, the experimental correlation in Figure 31 does not indicate an electron transfer mechanism, but is a reflection of the nature of the activation process which overcomes the charge transfer promotion energy and generates a resonating transition state. A similar conclusion was reached for electrophile/nucleophile reactivity (Section 7.1.7).

7.1.9. Other Reactivity Trends Which Respond to the Promotion Energy Gap

There are plenty of other applications of the VBSCD which project the role of the promotion energy. Su^[59] has discussed the reactivity of carbenes and their isolobal organometallic analogues in bond insertion reactions. A related work by Pross and Moss^[60] has shown the role of promotion energies in carbene addition to olefins. Our own treatments of $\text{S}_{\text{N}}2$ reactivity,^[4a-c] β -elimination of organometallic complexes,^[61] nucleophilic cleavages of σ -cation radicals,^[62] nucleophilic vinylic substitution reactions,^[63] stability of clusters with $4n/(4n+2)$ electrons,^[64] hyper coordinated radicals,^[65] and so on^[4, 7] all reflect the impact of promotion energies.

8. General Structure–Reactivity Patterns Based on the VBSCD Model

While the role of the promotion energy as the origin of the barrier is evident by now, the VBSCD model in Figure 21b contains other factors which scale the barrier for a given promotion energy. It is apparent that the height of the crossing point is a fraction f of the promotion gap, as expressed in Equation (6), but there are several ways to express this fundamental relationship explicitly by approximation of the VBSCD curve. Equation (8) is a barrier expression derived^[66] from the VBSCD, and shows the explicit dependence on the two promotion gaps, on the thermodynamic driving force of the reaction, on the resonance energy of the transition state, and on the two f factors of the individual curves. These f factors determine the fraction of the promotion gap which enters under the crossing point in a reference thermoneutral situation. By simplification,^[62, 67] we obtain a more lucid expression in Equation (9), which can be related to Equation (6) through Equation (10). Here it becomes apparent

$$\Delta E^* = [(f_r + f_p)G_r + (1 - f_r - f_p)\Delta E_{\text{rp}}] \frac{(G_p + \Delta E_{\text{rp}})}{(G_r + G_p)} - B \quad (8)$$

$$\Delta E^* = f_{\text{av}}G_r + (0.5 - f_{\text{av}})\Delta E_{\text{rp}} - B; f_{\text{av}} = 0.5(f_r + f_p) \quad (9)$$

$$f = f_{\text{av}} + \frac{\Delta E_{\text{rp}}}{G_r}(0.5 - f_{\text{av}}) \quad (10)$$

that the f used in Equation (6) is an effective parameter that sums up the various effects which determine the fraction of the promotion energy that enters under the crossing point of the VBSCD in Figure 21b.

Equations (8) and (9) have been tested and found to provide reasonable quantitative estimates of barriers.^[4a, 62, 67, 68] The detailed comparison of these and other possible barrier

expressions will be waived since all the VBSCD expressions hold the same qualitative structure – reactivity patterns which are summarized in Figure 33.

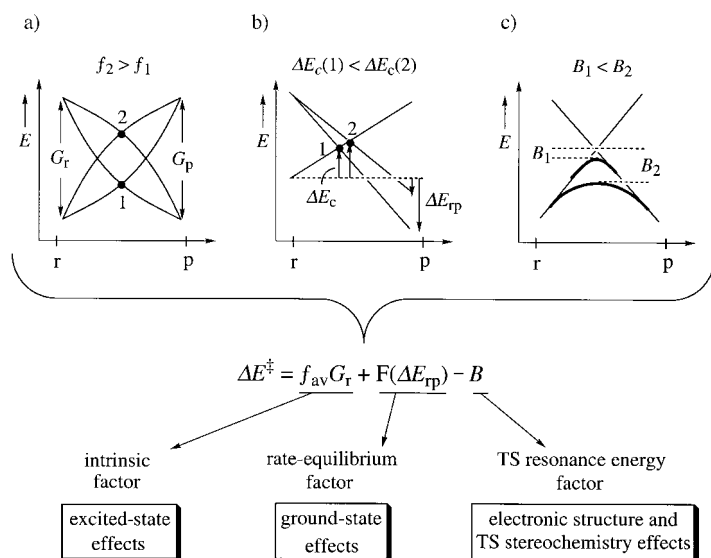


Figure 33. General reactivity patterns predicted by the VBSCD model. a) The effect of f on the height of the crossing point. The fG term brings in excited-state effects on reactivity; f is an intrinsic selectivity factor. b) The effect of the reaction energy driving force (ΔE_{rp}) on the height of the crossing point. $F(\Delta E_{\text{rp}})$ signifies some function of the ΔE_{rp} variable. The ΔE_{rp} term is responsible for rate – equilibrium relationships. c) The effect of the resonance energy B of the transition state; B is the electronic and structural code of the transition state.

The first barrier factor is an intrinsic quantity which reflects the electronic reorganization required in order to break old bonds and make new ones by the resonance mixing mechanism (avoided crossing) in the VBSCD. This term is determined by the promotion energy scaled by the average index f_{av} . Figure 33a shows that the effect of f_{av} is manifested by varying the height of the crossing point through the curvature of the intersecting curves (compare 1 with 2). Thus, f_{av} is a response and a selectivity factor which determines the dependence of the barrier on the promotion energy. In turn, variations of f_{av} size the height of the crossing points, and thereby the extent of bond deformations in the transition states of the series.

The second barrier factor brings in the effect of the thermodynamic driving force. As shown in Figure 33b, changes in the driving force factor modulate the height of the crossing point (compare 1 with 2), and thereby scale the barrier up or down. This dependence is the origin of the widespread rate – equilibrium relationships

Finally, the resonance energy of the transition state B lowers the energy of the transition state below the crossing point to an extent that reflects the electronic structure of the transition state itself and its stereochemical characteristics (Figure 33c). It is here in this factor that orbital symmetry and nodal properties are encoded.^[7]

Thus, the VBSCD incorporates the role of traditional physical-organic factors with novel ones associated with the promotion energy and effects of excited states. The model predicts that reactivity patterns will form a collage which

reflects an interplay of the effects in Figure 33. The straightforward patterns will correlate with a single organizing quantity, which is often the promotion energy and occasionally the reaction thermodynamic driving force. These uniparameter correlations may arise either because the other factors vary in the same direction as the organizing quantity, or are “quasi-constants”. Complex patterns will arise whenever a few reactivity factors vary in an opposing manner, which will generate interesting patterns such as reactivity zigzags.^[4a, 69]

8.1. Qualitative Applications of the Barrier Factors in the VBSCD Model

We proceed now with a few applications of the barrier factors in order to project qualitative insight and provide guidelines. Since the effect of the reaction driving force is well known, in the following we will deal mainly with the factors f and B , and their interplay with other factors (G and ΔE_{rp}). More detailed applications of the barrier equations can be found elsewhere.^[4a, b, 62]

8.1.1. The Intrinsic Selectivity Factor: Chemical Aspects of f

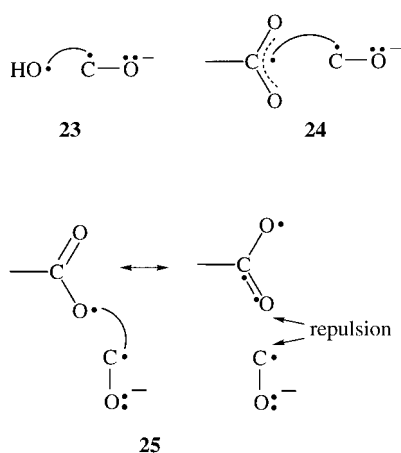
To avoid excessive notations we simply use f for the average and individual indexes. As already pointed out, f determines the response of the barrier to changes in the promotion energy, and as such f is an intrinsic selectivity measure of a reaction series.^[70] We may therefore start with the mechanistic significance of f in rule 3.

Rule 3: The f factor is an intrinsic selectivity measure of a reaction series: the larger the value of f , the more selective the reaction.

According to Figure 33a, f is determined by the descent of the promoted states as well as by the ascent of the ground states toward the crossing point; shallow descent and steep ascent increase the f value. It is clear therefore that f is a collective index of many interactions along the reaction coordinate, for example, interactions due to bond ionicity and delocalization – localization of active electrons. These effects will be manifested in the structure of the transition state as deformations (relative to the reactants) which increase as f increases at a constant value of the promotion energy.

8.1.1.1. Relationship of f to the Electronic Structure of the Promoted States

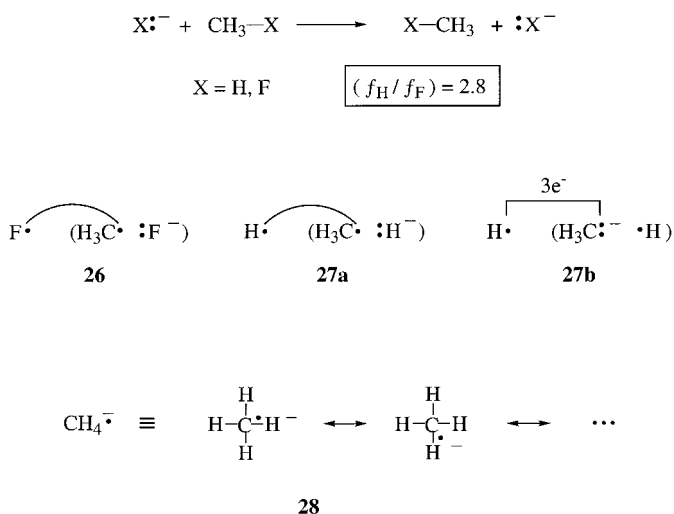
A key factor which determines the ascent of the promoted states is the delocalization of the electrons which must be paired to form the new bonds. Turning back to Figure 28, which shows correlations between barrier and ionization energy for nucleophilic reactivity toward esters, one sees that the nucleophiles fall into two groups, localized ones like hydroxide and delocalized ones like acetate. The promoted states are the charge transfer states, and are depicted in Scheme 10 for the two types of nucleophiles using hydroxide (**23**) and acetate ions (**24**) as specific cases. It is apparent that in the case of hydroxide, the unpaired electron is localized on



Scheme 10. VB structures to explain the different structure–reactivity slopes in the correlations in Figure 28.

the oxygen center and the coupling with the carbonyl radical anion can develop into a new O–C bond without additional electron reorganization. In contrast, in the case of the acetate radical, the unpaired electron is delocalized over the two oxygen centers. Thus, as shown in **25** for the left-hand resonance structure, the O–C bond making will be weakened by the delocalization, and will be further counteracted by exchange repulsion due to the nonbonding interaction in the right-hand resonance structure. These adverse interactions will impair the descent of the charge transfer state for acetate and will lead to a higher f value. It follows, therefore, that the different line slopes in Figure 28 derive from the delocalization properties of the charge transfer species,^[48] such that a delocalized nucleophile produces a more deformed transition state structure in comparison with a localized nucleophile having the same vertical ionization energy.

To illustrate this effect further, the ratio of f values computed by the VB method for two S_N2 reactions^[5b, c] is shown in Scheme 11. The charge transfer promoted state for the F^- exchange which is depicted in **26** has a charge that is virtually localized and is therefore prepared for the new bond making; this situation leads to a small f value. In contrast, for



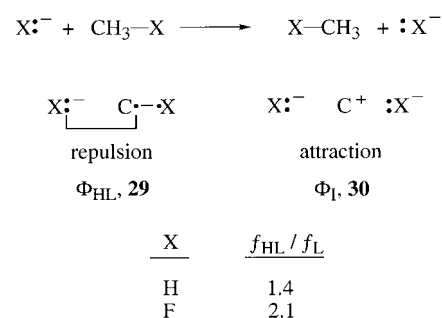
Scheme 11. Influence of the electronic structure of the excited state on f for the example of nucleophilic substitution.

the H^- exchange, the charge in the promoted state is delocalized in two manners, depicted in **27** and **28**. In **27a** and **27b** we show the electron of the radical anion in a single C–H linkage. Since H and C have very similar electronegativities, the electron of the radical anion is delocalized over the two centers, and two VB forms are required to describe the system; **27a** is the form that couples the new H–C bond, while **27b** is typified by three-electron overlap repulsion that counteracts the bond coupling. In addition, **28** shows that since CH_4 has four identical linkages, the electron of the radical anion is delocalized over all of them. This extensive delocalization is expected to lead to a large f value. The impact of delocalization is stated as rule 4.

Rule 4: *Electronic delocalization in the promoted states of the VBSCD will be associated with larger f values and a higher intrinsic selectivity.*

8.1.1.2. Relationship of f to the Electronic Structure of the Ground States

An important electronic factor that affects the ascent of the VBSCD curves is the bond ionicity. Scheme 12 uses the S_N2 reaction to illustrate the effect. Here the C–X bond of the



Scheme 12. Influence of the electronic structure of the ground state on f for the example of nucleophilic substitution.

ground state is a mixture of the HL structure **29** and the ionic structure **30**. It is apparent that the HL structure suffers from a repulsive interaction between the nonbonding $X\cdot^-$ and the HL bond, while the ionic structure maintains an attractive electrostatic interaction. Accordingly increased bond ionicity should lower the f value. This was examined by Sini et al.^[5b, c, 71] using ab initio VB computations of the HL and Lewis (L) curves for several systems. The result for the reactions with $X = H$ and $X = F$ is shown in Scheme 12. The HL curves have larger f values, and the ratio f_{HL}/f_L increases with the electronegativity of X. This trend can be summarized in rule 5.

Rule 5: *Increased bond ionicity in the ground states of the VBSCD will be associated with smaller f values and lower intrinsic selectivity.*

8.1.1.3. Variation of f in the Main Group Element Block

The third important factor of f is manifested as the positions of the atoms in the periodic table change either down a column of the main group elements, or from a nonmetal to a metal. Thus, (for a given bond ionicity) the ascent of the ground state depends on the overlap repulsion of the non-

bonding electrons on the reacting atoms. In turn, the strength of bond coupling of the unpaired electrons in the promoted states affects the descent of these states toward the crossing point. As such, the atom contribution to the f factor will be determined by the ratio of the triplet repulsion to the singlet pairing energy. This ratio is large for strong binders and small for weak binders but especially so for metallic atoms. These trends in f are summarized in rule 6.

Rule 6: Changing the reacting atoms to higher homologues down a column in the periodic table or to metals will be associated with smaller f values and smaller intrinsic selectivity.

Experience with VB computations of the VBSCDs vindicates this rule. For example, exchange reactions of a monovalent atom with the diatomic molecule, studied by Maitre et al.,^[5a] show a threefold decrease in the f values upon changing the atom from H to Li.

8.1.2. Interplay of f and G : Effects on the Barrier Height and Reactivity Reversals

When both the promotion energy and f vary in opposition in a reaction series, relative reactivity may be condensed or exhibit zigzag behavior.^[69] A few examples illustrate these patterns.

8.1.2.1. Why Are Some Gas-Phase S_N2 Barriers Constants?

Recently, Wladkowski et al.^[72] have studied the gas-phase reactivity of identity S_N2 reactions in Equation (11)— $R = CH_3, NCCH_2, ArCH_2$ —and found an approximately constant



central barrier of 12–14 kcal mol⁻¹, irrespective of the substituents on the central carbon atom. This was further supported by AM1 calculations^[72a] which revealed the invariance of the central barrier for a variety of Ar substituents.

This experimental trend had been anticipated in 1983^[69b] by considering the VBSCD in Figure 34. The carbon substituents in Equation (11) are all good electron acceptors relative to H.

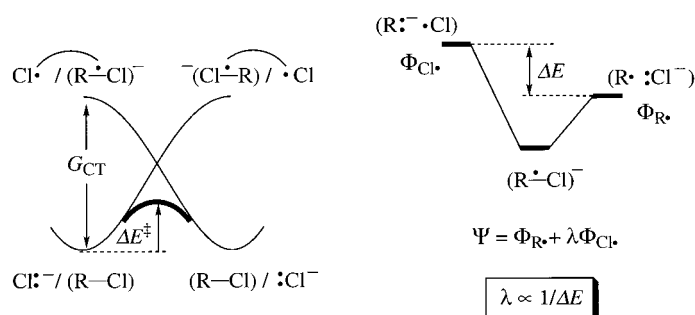


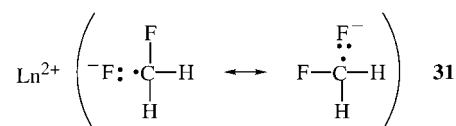
Figure 34. Left: VBSCD (based on Figure 20b) for gas-phase S_N2 reactions of the chloride ion with substituted alkyl chlorides. Right: VB interaction diagram for the formation of the radical ion promoted state from its VB constituents, and the dependence of its extent of delocalization (sized by the mixing coefficient λ) on the substituent on the central carbon atom. The f factor will increase as the radical anion becomes more delocalized (λ increases).

Therefore, they will render their corresponding $R-Cl$ substrates better electron acceptors. As such, the charge transfer promotion energy will be lowered upon substitution of the methyl group with Ar or CN groups. At the same time, as shown in the VB interaction diagram on the right hand side of Figure 34, the substituent affects also the extent of delocalization of the radical anion in the charge transfer state. Thus, the radical anion species is a VB mixture of a form which places the unpaired electron on the R group ($\Phi_{R\cdot}$) and a form which places the electron on the Cl atom ($\Phi_{Cl\cdot}$). The extent of mixing of the latter form increases as the R group becomes a better electron acceptor, and this will increase electronic delocalization and, in turn, raise the value of the f factor according to rule 4. Clearly then, the electron-withdrawing carbon substituents in Equation (11) will, on the one hand, lower the promotion energy but, on the other hand, increase the f factor. Based on Equations (6) or (9), this opposition of the reactivity factors will narrow the range of barrier variation. The observation of this effect by Wladkowski and Brauman^[72] along with similar experimental trends^[4a, 69] indicate the predictive power of the VBSCD model.

8.1.2.2. Polyhalogenated Alkanes: Why Do They Undergo Sluggish S_N2 and Halide-Abstraction Reactions?

A long time ago, Hine et al.^[73] demonstrated that polyhalogenated alkanes undergo very sluggish S_N2 reactions, so much so that reactions of, for example, simple alkyl halides can be carried out in dichloromethane. To understand this trend, consider S_N2 reactivity in the series $Cl^-/CH_3Cl, Cl^-/CH_2Cl_2, Cl^-/CHCl_3, Cl^-/CCl_4$. Here, successive chlorination of the substrate is known to improve modestly its acceptor ability.^[69b] However, this improvement is attended by delocalization of the radical anion state over an increasing number of linkages according to the effect illustrated above for the hydride exchange reaction in **28** (Scheme 11). Evidently, the increase of the f factor overrides the modest reduction of the promotion energy and leads to an increase of the barrier.^[4a, 69]

A related trend has been observed by Cornhel et al.^[28a] and Harvey et al.^[28b] in the C–F activation by metal ions, where polyfluorinated substrates undergo sluggish bond activation, in comparison with CH_3F , even when the reactions are very exothermic as with the early lanthanide cations.^[28b] Scheme 13



Scheme 13. Explanation of the sluggish C–F activation of polyfluorinated substrates by metal ions exemplified by the excited CT states **31** for difluoromethane.

exemplifies the effect using the promoted charge transfer state for difluoromethane in **31**. Here, the delocalization of the negative charge away from the F species that undergoes abstraction reduces the ionic stabilization due to the interaction with the M^{2+} ion. The expected increase of f will raise the barrier, and will contribute to the sluggish reactivity of polyfluorinated substrates.^[28b]

8.1.2.3. What Is the Origin of Reactivity Crossovers in Reactions between Electrophiles and Nucleophiles?

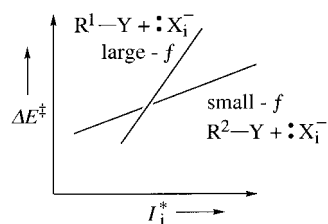


Figure 35. The phenomenon of reactivity reversal due to the opposite trends of f and G factors in the two series. The reversal is illustrated for two S_N2 series formed by substrates with different intrinsic selectivities (f factors).

Reactivity crossovers and zigzags are predicted as manifestations of the f - G opposition.^[4a, 69] Figure 35 is a schematic illustration of the situation for nucleophilic substitution series formed by two substrates with the same group of nucleophiles $:X_i^-$. The first substrate R^1-Y is a better electron acceptor than R^2-Y , but the radical ions formed from it are also more delocalized.

Consequently, the first reaction series will be typified by smaller G values and larger f factors in comparison with the second series. Following rule 3, f is a selectivity factor which measures the slope of $\Delta E^\ddagger - G$ correlation, and hence the substrate with the larger f will be more selective. Consequently the relative reactivity of the two substrates may undergo reversal, as the vertical ionization energy of the nucleophile changes along the series. A situation like that in Figure 35 can be drawn for other reactions between electrophiles and nucleophiles because generally electronic delocalization in the electrophile or nucleophile will enhance their intrinsic selectivity, and may bring thereby reactivity crossover in two reaction series.

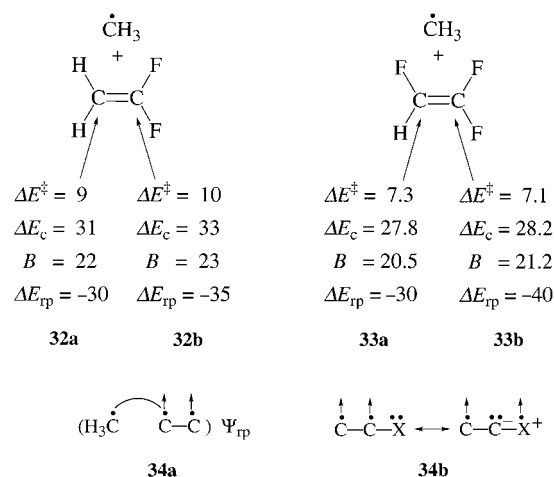
Reactivity crossovers which appear to follow the dictum of f - G opposition have been reported for $\text{NO}_2\text{C}_6\text{H}_4\text{CH}_2\text{Br}/\text{C}_6\text{H}_5\text{CH}_2\text{Br}$,^[74a] $\text{PhCOCH}_2\text{Br}/\text{CH}_3\text{I}$,^[74b] and $\text{Me}_3\text{SiCH}_2\text{Cl}/\text{CH}_3\text{CH}_2\text{CH}_2\text{Cl}$ ^[74c] in S_N2 reactions with a series of nucleophiles.^[4a] Mayr et al.^[22, 75] have observed reactivity reversals in the reactions of carbocations with olefins. Thus, olefins which are better electron donors and form more delocalized radical cation states seem to show higher selectivity toward carbocation addition, in comparison with olefins which are poorer donors but form more localized radical cation states. This situation fits the dictum of f - G opposition, and the observed reversals may well reflect the predictions of the VBSCD.

The situation of f - G opposition may be ubiquitous and occur in a variety of reactions. The foregoing discussion should provide a basis for anticipations of reactivity reversals, and trends in reactivity-selectivity relationships.

8.1.2.4. Regioselectivity Zigzags in Radical Addition to Olefins

The interplay of f with other reactivity factors may lead also to reactivity zigzags, as manifested in radical attacks on substituted olefins. The reaction normally proceeds with preference on the less substituted site, even though this is not necessarily the thermodynamically favorable path.^[25] Certain substitution modes of the olefin disrupt the normal pattern, leading to preferred attack on the more substituted sites. Variation of the radical restores the normal regioselectivity, and the overall picture is one of regioselectivity zigzags.^[76, 77]

This problem has been treated by Shaik and Canadell,^[76] who employed a Morokuma analysis to obtain the VBSCD quantities. Scheme 14 shows in **32a** and **32b** the VBSCD



Scheme 14. Explanation for the zigzag behavior of regioselectivity in radical additions to alkenes.

quantities (in kcal mol^{-1}) for the two possible reactions of 1,1-difluoroethylene with methyl radical. The attack on the more substituted site is typified by a higher crossing point (ΔE_c), which dominates the trends in the barrier and overcomes the opposite preference of the thermodynamic driving force. Since the promotion energy is common for both regiochemical pathways, it follows that the attack on the substituted site (**32b**) must possess a larger f factor. The reason for this is projected in **34b**, which depicts the triplet olefin moiety in the promoted state, itself shown in **34a**. It is seen that the substituent X induces electronic delocalization in the triplet olefin, and depletes thereby the density of the unpaired electron on the substituted site. Consequently the bond coupling of the substituted site with the radical (in **34a**) will be weaker and will possess a larger f factor.

In the case of 1,1-difluoroethylene, the f factor overcomes the opposite directive preference of the thermodynamic driving force. However, in the case of trifluoroethylene, **33**, where the two sites are substituted, the directive preference of the reaction driving force gets larger while the f directivity decreases. Consequently, the regioselectivity shifts in favor of the more substituted site, but will reverse upon use of other radicals such as H and CF_3 , for which the thermodynamic driving force becomes more balanced.^[76] Thus, the regioselectivity zigzag may be understood as a manifestation of the opposition between the intrinsic selectivity factor f and the thermodynamic driving force.

8.1.3. The Resonance Energy of the Transition State: Chemical Aspects of B

Having elaborated the impact of the factors f , G , and ΔE_{tp} and their interplay, we turn to the remaining VBSCD quantity B . The crossing point in the VBSCD (Figure 21a) is the location where the two bonding motifs of reactants and products have equal energy, while B is the resonance energy due to their VB mixing (Figure 21b).^[10] The VB mixing

generates the transition state and its twin-excited state as depicted again in Figure 36, which shows the relationship of the resonance energy and the excitation energy between the two states.^[7a, c, 10, 78] The simplest approximation for this excitation energy is the orbital excitation energy of the

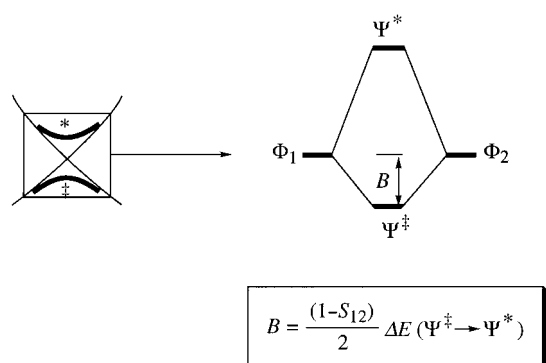
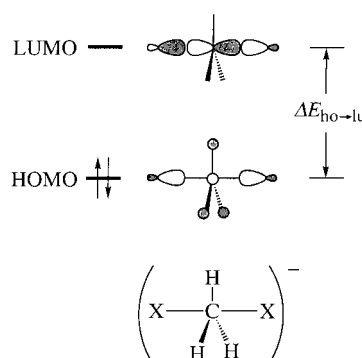


Figure 36. Left: Schematic VBSCD. Right: The resonance mixing which generates the transition state and its twin excited state magnified using the VB interaction diagram which shows the relationship of the transition state's resonance energy to the gap between the states and to the overlap between the VB configurations at the crossing point.

transition state. In many cases these would be the HOMO (ho) and LUMO (lu) of the transition state, as expressed in Equation (12), where S_{12} is the overlap between the VB configurations at the crossing point.

$$B = [0.5(1 - S_{12})] \Delta E_{ho \rightarrow lu} \quad (12)$$

The dependence on the orbital excitation energy projects that the quantity B is a code of the structure and stereochemical preference of the transition state. A lucid example for this aspect is given in Scheme 15, which shows the two



Scheme 15. HOMO and LUMO of the transition state of an identity S_N2 reaction.

orbitals for an identity S_N2 transition state. Since the orbital gap is maximum when the XCX axis is linear, the S_N2 transition state will prefer a trigonal-bipyramidal structure which maximizes the resonance energy. As soon as the angle of the XCX axis deviates from 180° , the LUMO energy decreases sharply, the orbital gap is minimized, and the resonance energy decreases.^[10] At a certain limiting angle of bending, the two orbitals will collapse and the resonance energy of the transition state will drop to zero.

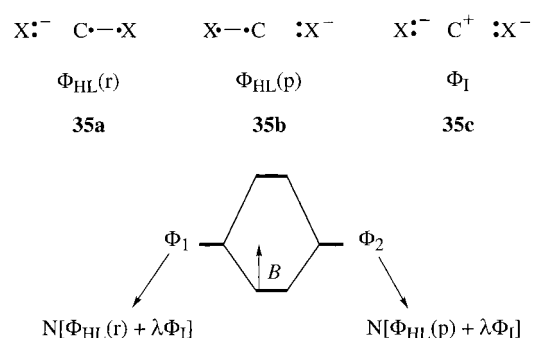
The other important term in Equation (12) is the overlap integral S_{12} . Neglecting all overlap terms between different VB structures, the S_{12} quantity is nonzero only if the bonding motifs at the crossing point contain some common VB structures. We note that electron delocalization and resonance stabilization only occur by mixing of different VB structures, while common structures make no such contribution. Thus, whenever the bonding motifs contain common structures, the resonance energy will be reduced in proportion to the contribution of the common structures, sized by the overlap integral S_{12} . At the limit of $S_{12} = 1$, the transition state is described by a single VB structure and hence will be devoid of resonance energy.

Let us follow therefore with a few illustrative applications which show that B holds the symmetry code and electronic structure characteristics of the transition state.

8.1.3.1. Estimates of Transition State Resonance Energies

Valence bond arguments^[7a, c, 10, 78] show that B is related to the bond strengths or the singlet–triplet excitation energies of the active bonds in the transition state, for example“ the C–X bonds in the S_N2 transition state in Scheme 15. Using this relationship to calibrate an extended Hückel orbital scheme renders Equation (12) very useful.

A good example is the transition state of the identity S_N2 reaction, which can be constructed from two Lewis structures, each of which corresponds to a mixture of one of two HL structures (**35a, b**) and the ionic structure (**35c**) in Scheme 16. The



Scheme 16. Lewis structures, VB structures, and resonance energy for the transition state of an identity S_N2 reaction.

overlap between the bonding motifs of reactants and products is then proportional to the mixing coefficient λ of the ionic structure, which in turn determines the positive charge Q_R on the central alkyl group. With this relationship, and appropriate simplifications, Equation (12) becomes Equation (13),

$$B(S_N2) \approx [(1 - Q_R)/(2 - Q_R)] \Delta E_{ho \rightarrow lu} \quad (13)$$

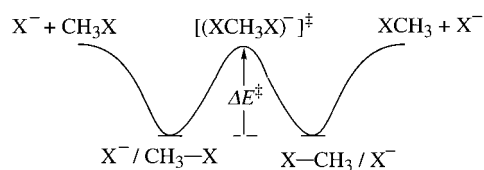
which relates the resonance energy of the transition state to its HOMO–LUMO splitting and its charge distribution. Thus, an increase of the charge in the transition state will lower the resonance energy, which will drop to zero at a charge of unity, where a limiting transition state wavefunction would be described completely by the ionic structure. Equation (13) links the entire gamut of electronic structure, from purely covalent S_N2 transition states to completely ionic ones.

Using Equation (13) enables an approximation of B for a variety of transition states. With reasonable charges for the halide-exchange transition states ($X = \text{F}, \text{Cl}, \text{Br}, \text{I}$ in Scheme 16), the corresponding B values are found to be proportional to the C-X bond energies D_{CX} of the parent molecules.^[78] The range of B values is expressed in Equation (14a). Using them and charge transfer promotion ener-

$$B(\text{XCH}_3\text{X}^-) = m D_{\text{CX}}; m = 0.25, 0.30; X = \text{halogen} \quad (14a)$$

$$\Delta E^\ddagger = f(I_{\text{X}^-}^* - A_{\text{RX}}^*) - B \quad (14b)$$

gies from the literature,^[4a, b] we estimated central barriers for the halide-exchange reaction based on Equation (14b). These barriers are displayed in Scheme 17 and compare quite well



X	ΔE^\ddagger [kcal mol ⁻¹]		ΔE^\ddagger [kcal mol ⁻¹] (ab initio)
	($m=0.25$)	($m=0.30$)	
F	12.4	12.4	12.4
Cl	12.0	12.6	12.8
Br	11.1	10.9	10.8
I	9.6	10.4	9.8

Scheme 17. Barriers of halide exchange reactions from Equations (14a) and (14b) and according to Glukhovtsev et al.^[79]

with the recent ab initio results of Glukhovtsev et al.^[79] obtained at the sophisticated G2 level.

Similar application of Equation (12) to the transition state for hydride exchange between alkyl or silyl groups ($\text{R} \cdots \text{H} \cdots \text{R}^+$) led to B values which range between 20–30 kcal mol⁻¹.^[56b] This study shows that the resonance energy increases as the R-H-R angle deviates from linearity, due to widening of the HOMO–LUMO gap. In addition, as the contribution of the hydrido configuration $[\text{R}^+\text{H}^-\text{R}^+]$ to the transition state increases, the B value decreases. The hydrido configuration is common to the two bonding motifs, and its contribution is expected to reduce resonance energy through the S_{12} term.

The value of B for three-electron species varies in proportion to the bond strength. Thus, B values range from 6 kcal mol⁻¹ for $\text{Li} \cdots \text{Li} \cdots \text{Li}$ to 40–43 kcal mol⁻¹ for $\text{H} \cdots \text{H} \cdots \text{H}$ and $\text{F} \cdots \text{H} \cdots \text{F}$.^[5a, f, 10] Unlike the cases in the preceding paragraph, for three-electron transition states the bonding motifs do not share common structures. Therefore, ionicity of the three-electron transition state will lead to resonating VB structures and an increase in the resonance energy.^[7c] This emphasizes the impact of bond ionicity in atom abstraction reactions.

Resonance energies were quantified also for a variety of six-electron/six-center and four-electron/four-center transition states.^[41, 64, 80] In the six-electron case the resonance energies are significantly larger, as may be understood by invoking Equation (12). Thus, in the “forbidden” geometry of the four-electron cases, the HOMO and LUMO of the transition state are degenerate, and the resonance energy is

15–25 kcal mol⁻¹ due to electron correlation which reduces electron repulsion.^[81] On the other hand, in the “allowed” geometry of the six-electron cases, the HOMO–LUMO gap is very large and therefore the resonance energy is also large (40–60 kcal mol⁻¹). Thus, it is generally expected that “allowed” transition states will possess larger resonance energies in comparison with their “forbidden” analogues. This trend was discovered decades ago by Evans et al.^[82] based on empirical VB calculations. Recent sophisticated computations by Bernardi, Robb et al.^[83] arrived at the same conclusion.

It is apparent, therefore, that orbital-symmetry classification of pericyclic reactivity is based solely on the resonance energy of the transition state.^[7a, c] This means that orbital-symmetry predictions of reaction rates will fail whenever other barrier factors vary in an adverse manner. This conclusion is a lead to the following section.

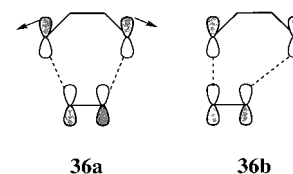
8.1.3.2. Why Do Some “Allowed” Reactions Have High Barriers, while Some “Forbidden” Reactions Have Small Barriers?

This comparison has been implicit in the discussion of the barrier data in Schemes 6 and 7, which show huge barriers for some “allowed” reactions and tiny barriers for some “forbidden” reactions. Since the resonance energy of the transition state is one of the barrier factors, a formally allowed reaction like the trimerization of ethylene can have a high barrier due to the large promotion gap.^[37] In the same logic, a formally forbidden reaction like the dimerization of dislyene can have a tiny barrier, even when the resonance energy is small, because the promotion gap is very small. It is the interplay of the promotion energy and the resonance energy that must be considered for understanding the broader trends of reactivity in these families.

8.1.3.3. Allowed Reactions and Synchronicity of Bond Rearrangement

A related aspect of orbital-symmetry effects is the concertedness or nonsynchronous nature of “allowed” reactions. This has been a hot issue^[84] that was flared recently by the femtosecond dynamics study of Zewail et al., who showed that the retro-Diels–Alder reaction of norbornene proceeds by competing concerted and stepwise pathways.^[85] Their study showed that stereochemistry would be conserved even in the stepwise process, because the diradical intermediate lives on the timescale of bond stretching but not long enough for internal rotation to occur.

The competition between the mechanisms can be discussed by considering the factors which affect transition state’s resonance energy. Equation (12) shows that a wide orbital gap in the transition state would lead to a large resonance energy. The transition state’s orbitals gap is determined, in turn, by the orbital mixing of the separate reactants. As shown with **36a** in Scheme 18, the distance



Scheme 18. Transition state for the concerted symmetric and nonsynchronous [4+2] cycloaddition.

between the diene terminals is significantly longer than the dienophile's C=C bond length, and hence the orbitals are not aligned for a good atomic orbital overlap. Thus, while the synchronous transition state enjoys an orbital-symmetry match, the overlap of the atomic orbitals is impaired by the "loose bite" of the diene. An improvement of the AO overlap may be achieved by rotation of the diene terminals or by decrease of its C-C-C angles, but the extent of these structural changes is limited since they would have to occur with an increase in distortion energy. An alternative nonsynchronous transition state which lines up one pair of orbitals, as shown in **36b**, will compromise the orbital symmetry match-up but will possess a perfect AO alignment in one of the linkages. The net effect of this balance between the symmetry and AO overlap requirements may render the synchronous transition state very susceptible to a distortion to a nonsynchronous structure. This in turn implies that a transition state for the stepwise process may not be too much higher than the synchronous transition state. Computations show that the barrier for the stepwise process is indeed higher by only about 7–12 kcal mol⁻¹ than that for the concerted mechanism.^[84] Thus, given sufficient excess energy, as in the Zewail experiment, the diradical intermediate may become accessible thermally. It is emphasized though that, since the VB state correlation is determined by the nature of reactants and products, both the synchronous as well as the stepwise processes will involve the same type of avoided crossing in the VBSCD (see Figure 44), albeit along different reaction coordinates distinguished by the timing of the two bond formation steps.

8.1.4. Orbital Selection Rules for Reactivity

Trends in the resonance energy of the transition state can be deduced also by direct consideration of the VB mixing between the ground and the promoted states at the crossing point of the VBSCD. In this manner, it becomes possible to derive orbital selection rules^[4a, 7] and make a priori predictions of the preferred stereochemical pathway and transition state structure for a reaction. The stereoselection rules specify the bonding requirements of the transition state in terms of the overlap conditions which must be met to produce an optimal resonance energy.

The principles of VB configuration mixing have been analyzed in detail elsewhere.^[7a, c] The salient features of strong overlap mixing are condensed into rules 7 and 8, which are schematized in Figure 37 for generic situations.

Rule 7: Two VB configurations which differ in a single electron shift between two orbitals will mix in proportion to the overlap of the two orbitals.

Rule 8: Two configurations which differ in a shift of two electrons will mix in proportion to the product of overlaps of the orbitals which partake in the electron shifting.

To employ the rules correctly, electrons must be shifted without changing their spins. Figure 37a shows a case which subscribes to rule 7, where the resonance energy is proportional to the overlap of ϕ_1 and ϕ_2 which partake in the single electron shift. This situation is most common for reactions between electrophiles and nucleophiles or acceptors and

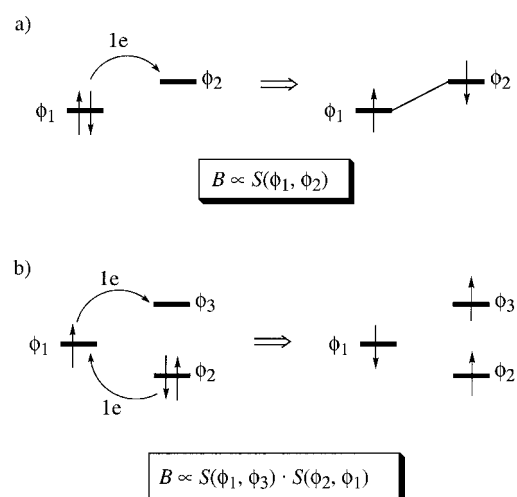


Figure 37. Pictorial representations of the VB mixing rules 7 (a) and 8 (b). Note that electrons are shifted with conservation of their individual spins. The rule is indicated as dependence of the resonance energy B on the specific orbital overlap S .

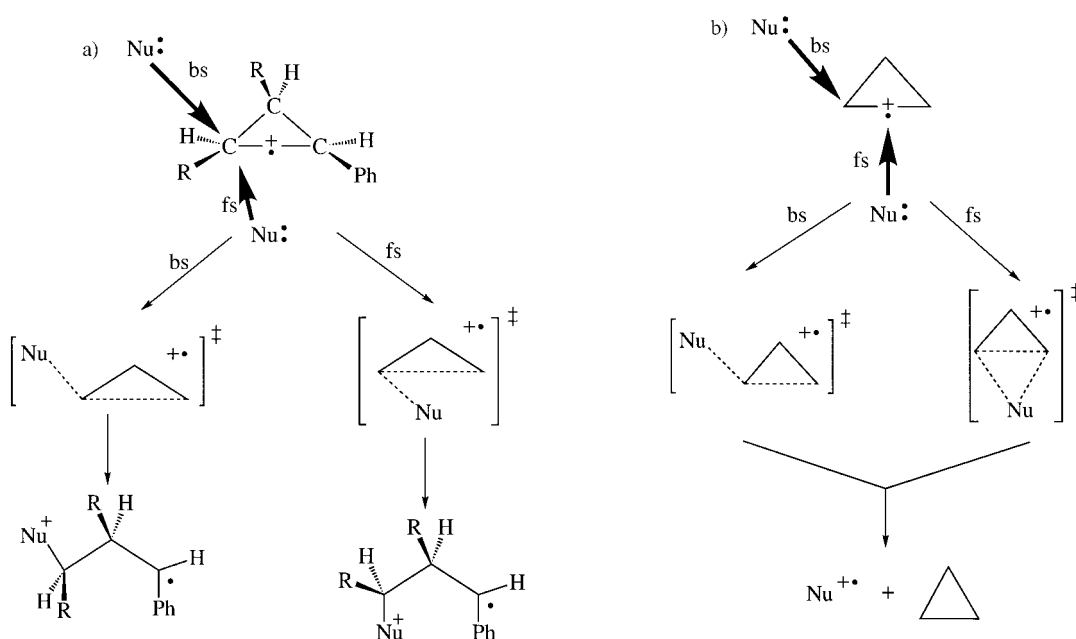
donors, where the promoted state is a charge transfer state generated from the ground state by a single electron shift. Figure 37b describes two single electron shifts from ϕ_1 to ϕ_3 , and from ϕ_2 to ϕ_1 . Following rule 8, the resultant resonance energy is proportional to the product of the overlaps $\phi_1-\phi_3$ and $\phi_1-\phi_2$. This resonance energy will be typical in radical-exchange reactions where the promoted state involves a triplet unpairing of the bond undergoing cleavage during the reaction.

A straightforward way of analyzing the resonance interactions uses fragment orbitals in the VB configurations. These types of configurations have been used by Mulliken^[86] in his theory of charge transfer complexes, and latter by Epiotis^[87] and Shaik.^[1, 4a, 7] Since the fragment orbitals possess information on local symmetry, the resulting orbital selection rules lead to lucid stereochemical predictions. A few derivations of selection rules follow for reactions which involve an odd number of electrons, where the usual MO arguments cannot be applied in a clear manner.

8.1.4.1. Stereoselection Rules for Nucleophilic Cleavage of σ -Radical Cations and for the Competing Electron Transfer Pathway

Shaik and Dinnocenzo^[88] investigated the system of a nucleophile and a cyclopropane radical cation which can participate in a substitution reaction (SUB) and in an electron transfer (ET) reaction (Scheme 19). In both mechanisms, the nucleophile can approach the radical cation from the backside (bs) or frontside (fs) of the one-electron bond. In the case of substitution, the stereochemistry of the transition state is encoded into the products, while in the ET mechanisms the stereochemistry may be probed by kinetic isotope effect measurements.^[62] As shall be seen, the VBSCD model leads to distinct orbital selection rules for the two mechanisms.

The ground state for the reactant and promoted states for the two mechanisms are shown in Figure 38, and the orbital selection rules are specified on the arrows leading from the reactant to the promoted states. In both cases the promoted



Scheme 19. Pathways for nucleophilic cleavage of a σ -radical cation (a) and for the competing ET path (b).

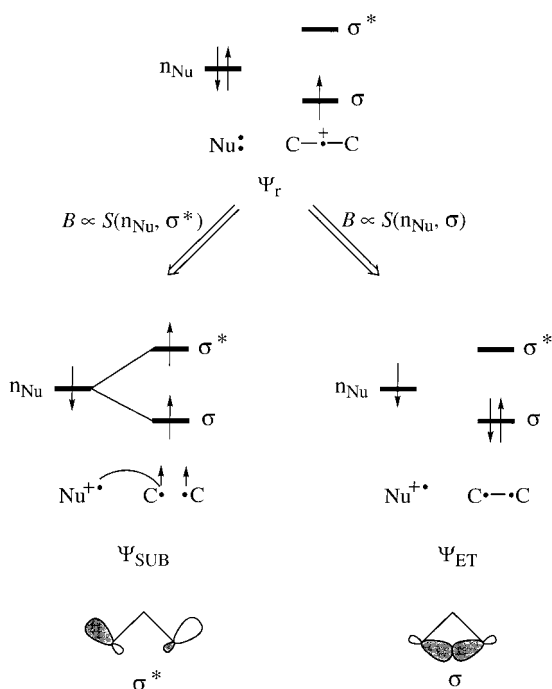


Figure 38. Orbital selection rules for nucleophilic cleavage and ET reactions between a cyclopropane σ -cation radical and a nucleophile. See text for further details.

states are generated by single electron shifts from the reactant state; in the substitution reaction the single electron shifts into the σ^* orbital, while in the competing ET mechanism into the σ orbital.^[62, 88] It is predicted, therefore, that the stereochemical course of the nucleophilic cleavage will be determined by the σ^* orbital of the radical cation moiety, while the course of the ET reaction will be decided by the σ orbital. These orbitals, which are depicted underneath the configurations in Figure 38, illustrate vividly that the substitution reaction will involve a backside attack and lead to stereo-

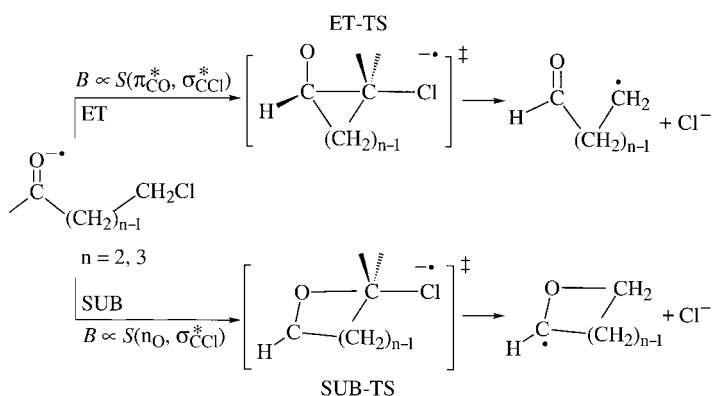
inversion, whereas the ET process will partake in a frontside approach. Recent regiochemical studies by Eberson et al.^[67, 89] provide further support for the orbital selection rules.

Experimental studies by Dinnocenzo et al.^[90] have shown that the substitution reaction proceeds with virtually 100% stereoinversion. These results were followed by an extensive computational study by Shaik et al.^[62] which has demonstrated that the transition state for substitution by a backside attack by the nucleophile is 10–20 kcal mol $^{-1}$ more stable than the transition state for frontside attack, which leads to stereoretention.

There are no matching results for the prediction about the ET mechanisms. Preliminary computational study of an ET reaction between NH_3 and cyclopropane cation radical shows that the transition state should be of the frontside variety.^[91] This stereochemical dichotomy of the two mechanisms is worthy of pursuit.

8.1.4.2. Stereoselection Rules for Nucleophilic and Electron Transfer Reactivity of Ketyl Anion Radicals Toward Alkyl Halides

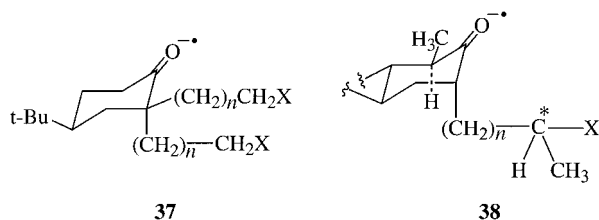
Eberson and Shaik^[54] have derived orbital selection rules for reactions of radical anions with alkyl halides, based on rule 7. Sastry and Shaik^[92] have used these rules to analyze the competing SUB and ET mechanisms in reactions of ketyl radical anions with alkyl halides. Scheme 20 summarizes the computational assignments obtained for the 1-formyl- ω -chloroalkane anion radicals,^[92b] which are simple analogues of the 1-benzoyl- ω -haloalkane systems studied experimentally by Kimura et al.^[93] Thus, the ET reaction, which is predicted^[92b] to optimize the $\pi_{\text{CO}}^* - \sigma_{\text{CCl}}^*$ overlap, proceeds via a transition state which involves a C-C-Cl bonding in the plane perpendicular to that of the formyl group. In contrast, the SUB mechanism, which is predicted by the selection rule to optimize the overlap of the oxygen's lone pair orbital (n_{O}) with σ_{CCl}^* , proceeds via a transition state which involves O-C-



Scheme 20. Stereoselectivity in the reaction of ketyl radical anions with alkyl halides.

Cl bonding in the plane of the formyl group. The computational studies show that these rules are obeyed even when adverse stereochemical constraints exist, such as for $n=3$, where the ET transition state has a strained four-membered ring structure. Thus, the negative charge of the ketyl anion radical is localized mostly on the carbonyl's oxygen atom, and the electron transfer could have occurred via an alternative O-C-Cl structure in a strain-free five-membered ring transition state. Nonetheless the ET reaction proceeds via the strained transition state structure which maintains the C-C-Cl bonding. It follows therefore that the orbital selection rules specify the bonding mode which a transition state of a given reaction must assume.

Scheme 21 shows two systems which may be appropriate probes for testing the selection rules. In **37** the axial chain is



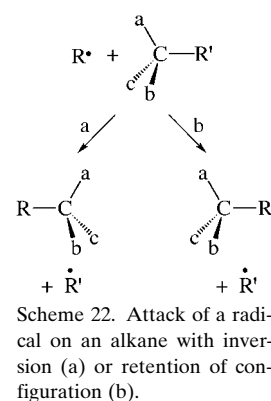
Scheme 21. Two compounds with which the validity of the prediction of stereoselectivity for the reaction of ketyl radical anions with alkyl halides can be tested.

constrained to optimize the $\pi_{CO}^* - \sigma_{CX}^*$ overlap in a C-C-X-type transition state and will undergo therefore only ET, while the equatorial chain is prone to optimize the $n_O - \sigma_{CX}^*$ overlap in a O-C-X-type transition state and will react by the substitution (O-alkylation) mechanism.^[94] System **38** is prone to react via the C-C-X transition structure and will give rise to ET reactivity. Since now the carbon atom of the C-X moiety is chiral, the ET transition state will have two diastereomers, one of which will be lower in energy and will lead to a faster depletion of one of the diastereomers of **38**.^[95] These predictions await their test.

8.1.4.3. Stereoselection Rules for Radical Cleavage of σ Bonds

Consider the reaction of a radical with an alkane, as in Scheme 22. Would this reaction proceed by stereoinversion (a) or stereoretention (b)? Or perhaps the two pathways

should compete and lead to stereorandomization? The configurations which participate in VB mixing to generate the transition state are shown in Figure 39, and it is apparent that they subscribe to the situation depicted in Figure 37b and stated in rule 8. It follows that the resonance energy of the transition state will depend on the overlap product $(\phi_R - \sigma_{CC})(\phi_R - \sigma_{CC}^*)$. Since the σ^* orbital has a node, the overlap product vanishes (becomes zero) in a frontside attack and the transition state formed by backside attack leading to stereoinversion will be preferred. The existing experimental data is



Scheme 22. Attack of a radical on an alkane with inversion (a) or retention of configuration (b).

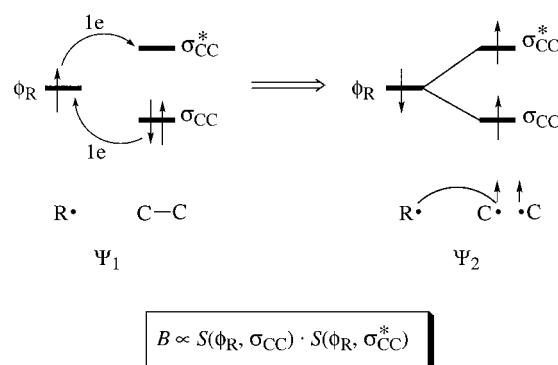


Figure 39. Orbital selection rules for σ -bond cleavage by a radical R^\bullet . The selection rule is indicated as the dependence of the resonance energy B on specific orbital overlaps.

in accord with this prediction.^[96] To the best of our knowledge, no other qualitative approach is capable of deriving stereoselection rules for radical cleavage in an unequivocal manner as the VBSCD model.^[97a]

There are a number of other predictions which can be made by application of rules 7 and 8. An example is the expected lack of synchronicity of bond making in transition states of cycloadditions involving cation radicals.^[97b]

8.2. The Collage of Reactivity Patterns: Summary and Mini-Guide for Using the VBSCD Model

The foregoing sections outline a scheme for the applicability of the VBSCD. The model views reactivity as a collage of trends set by a small number of reactivity factors underlying the VB diagram of two interacting states in Figures 21b and 33. An effective way to apply the model to a new reaction begins with construction of the VBSCD, based on the principal configurations of reactants and products and following rules 1 and 2. Once the VBSCD is constructed and the promotion energy of the reaction is characterized, there already exist means to define the origins of the barrier and assess its gross variation in a reaction series. What follows depends ultimately on the type of questions one wishes to tackle.

Stereoselection questions are the least complex because they allow one to focus on the resonance energy B of the transition state. For polar covalent bonds the VB mixing rules (rules 7 and 8) provide means to predict stereoselectivity. Regioselection questions come next in the hierarchy of complexity because often an interplay of two reactivity factors will determine the regioselectivity.^[67, 76] These may be ΔE_{TP} and f , as discussed in Section 8.1.2.2 for radical additions to olefins,^[76] or B and f , as shown recently^[67] for nucleophilic addition to odd-nonalternant-hydrocarbon cation radicals. Rules 3–6 outline the dependence of f values on fundamental properties of the ground states and the promoted states as well as on their atomic constitution. These rules along with the examples analyzed in Section 8.1 should constitute a reasonable basis for further application.

For situations of high ionicity, as described in Section 7.1.8, both stereo- and regioselectivities will be dominated by the electrostatic interactions, while the resonance energy of the transition state (albeit no longer as a selection rule) will still be determined by the VB mixing of the secondary covalent structures,^[28b] and may be deduced from rules 7 and 8.

Questions of relative reactivity in a reaction series are inherently the most complex, because all the reactivity factors may in principle change simultaneously. A logical hierarchy of application begins with the search for a general correlation of the barriers with the characteristic promotion energy of the reaction, followed by an upgraded complexity of factor consideration. Deviations from the promotion energy trend will be encountered when one or more of the other factors change in a dominant fashion in the series (e.g., changes in f due to bond ionicity effects). A useful way to follow in such an event is to seek reactivity patterns which are set by the interplay of two factors (see Section 8.1.2). More complex situations, due to changes of all reactivity factors, will generally require a quantitative consideration.^[4a, b, 10, 20, 37, 62] There exist by now quantum chemical ways to obtain G and B as well as the height of the crossing point.^[5, 7a, c, 10, 37, 56b, 76, 98]

Yet another compact approach to pattern a set of kinetic data makes use of the various barrier expressions [Eqs. (6), (8), and (9)] as means for assessing the mechanism of activation.^[4a, 7a, 10, 17, 48] For example, a plot of ΔE^\ddagger versus G according to Equation (6) will generate a fingerprint pattern found in reaction series (e.g., Figure 28) with correlation lines possessing different slopes, as illustrated generally in Figure 40. Whenever these plots are physically meaningful, then each line would correspond to a reaction “family” with member transition states which share common f and B values.^[10] For these families, the slope of the line will correspond to f and its intercept to B . Since B is the difference between the heights of the crossing point and the barrier at a definitive structure of the transition state, it can be uniquely defined,^[7c, 78] and the quantities

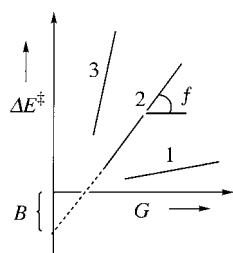


Figure 40. Finger-print reactivity patterns showing three “reaction families” (1–3), predicted by application of Equation (6). A reaction family is typified by a line with a slope equal to f and an intercept equal to B .

extracted from experiment may serve as useful means to deduce the structure of the transition state in the reaction “family”.^[10]

9. Valence Bond Configuration Mixing Diagrams (VBCMDs): Intermediate States and Their Role in Reactivity

The VBCMD is an alternative and a complementary diagram to the VBSCD,^[4a, b, d, e–g, 7] typified by more than two curves which may either be individual VB structures or state curves. Any two-state VBSCD can be transformed into a VBCMD, where the HL and ionic VB structures are plotted explicitly as independent curves instead of being combined into state curves.^[4d, 7, 5b, d, 62] Another type of VBCMD will be obtained whenever the description of a reaction mechanism requires, in addition to the two principal state curves which describe the net transformation from reactants to products, a third state curve which accounts for an intermediate situation. The following sections discuss the generation of VBCMDs and application to chemical problems.

9.1. Features of the VBCMD

Figure 41 shows the generic VBCMD, which features two fundamental curves Φ_r and Φ_p and an intermediate curve Φ_{int} . Figure 41a corresponds to a situation where the intermediate

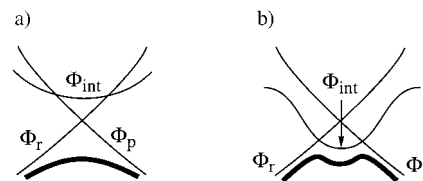
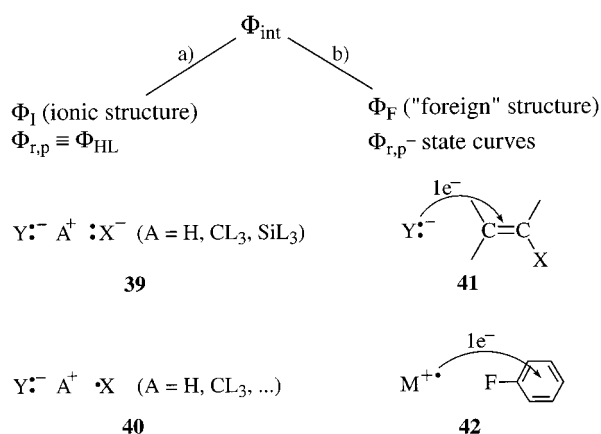


Figure 41. Generic VBCMDs with two fundamental curves of reactants and products (Φ_r and Φ_p) crossed horizontally by an intermediate curve (Φ_{int}). Case (a) is prone to generate a single step reaction, while case (b) a stepwise reaction.

curve lies higher than the crossing point of the fundamental curves, a situation prone to generate a single transition state that has a mixed character of the fundamental and intermediate VB structures. Figure 41b describes a situation where the intermediate curve is more stable than the crossing point of the fundamentals, which is prone, though not always,^[5b] to generate an intermediate state in a stepwise mechanism. Thus, the intermediate structure provides a low-energy pathway that mediates the process, which itself is defined by the fundamental states transformation $\Phi_r \rightarrow \Phi_p$.

Scheme 23 classifies intermediate VB situations which are common in VBCMDs. In case (a) the fundamental curves are the principal HL structures of the active bonds which interchange along the reaction coordinate. The corresponding intermediate curve will then generally correlate to the ionic structure. Examples are **39**, which is a triple-ionic structure in, for example, a proton transfer process, or **40**, which is the corresponding ionic structure in an atom-abstraction reaction.^[31, 99] As a rule, for polar covalent bonds the ionic



Scheme 23. Classification of typical VB intermediate situations; ionic VB structures in (a), foreign states in (b).

structures are higher in energy than the HL structures at the reactant and product geometries. Thus, while the HL curves will interchange along the reaction coordinate, the curve of the ionic VB structure will correlate horizontally and cross thereby those of the two HL structures either above or below their crossing point, as depicted schematically in Figures 41 a and 41 b. In case (b) of Scheme 23, the fundamental curves are the state curves which describe the rearrangements of the active bonds. As such, the intermediate curve is a "foreign" state which involves excitation of bonds and orbitals not associated with the net chemical reaction. For example, **41** is the π -charge transfer state shown^[63] to be the origin of the carbanion intermediate in the $\text{S}_{\text{N}}\text{V}$ mechanism which involves net nucleophilic exchange of the C–X bond by a Y–C bond. Similarly, **42** is a π -charge transfer state in the activation of the F–C σ bond by a metal cation.^[28b] This state has recently been invoked^[28b] to account for the very efficient reaction of aryl fluorides with lanthanide cations and Ca^{2+} , as opposed to the sluggish reactivity of simple alkyl fluorides.^[28]

If we allow to stretch the definition of a "foreign" state we may include in case (b) situations where the intermediate curve constitutes a different spin situation in comparison with the fundamental curves. Such a mechanism has been described recently as two-state reactivity for the C–H bond activation by metal oxide cations like FeO^+ , as well as by the active form of the P-450 enzyme.^[46, 100]

Here, the fundamental curves (see Figure 41 b) correspond to the high-spin situation while the intermediate curve to a low-spin situation which crosses the fundamental curves and provides a low-energy path for the bond activation. Without the intermediate curve the C–H bond activation would not be possible.^[100]

Owing to the ubiquitous significance of intermediate VB structures in most, if not all, chemical reactions, any VBCMD treatment is bound to barely scratch the tip of the iceberg. Therefore, we have limited ourselves to a carefully selected choice of problems,

with the intention to project some novel applications related to the role of intermediate VB structures on reaction rates and reaction mechanisms.

9.2. VBCMDs with Ionic Intermediate Curves

Ionic structures which are the secondary VB configurations of polar covalent bonds can become the dominant configurations in hypercoordinated geometries due to accumulated electrostatic interactions. Alternatively these VB structures can descend in energy below the covalent structures by means of solvent-assisted crossing as well as by metal-ion catalysis (Sections 2.1.3 and 2.1.4). The following examples serve to illustrate the impact of ionic VB structures on the reactivity of covalent bonds.

9.2.1. Proton Transfer Processes and the Intermediary of Low-Barrier Hydrogen Bonds

Since H^+ has no electrons, its ionic radius is small and is determined only by nuclear repulsion with the counterion. This enables very tight ion-pair geometries with large electrostatic energies. Consequently, the triple ionic structure $\text{X:}^- \text{H}^+ \text{:X}^-$ in a proton transfer process will usually possess a deep energy minimum and in some instances may become the dominant VB structure of the reaction and give rise to "low-barrier hydrogen bonds". Since this topic has recently been flared by debates on the role, or lack thereof, of low-barrier hydrogen bonding in enzyme catalysis,^[101] we would like to analyze the case of the $(\text{FHF})^-$ anion, which has a stable symmetric hydrogen bond, and elucidate its bonding features, especially its ionic–covalent resonance energy. It should be emphasized that most other hydrogen-bonded $(\text{XHX})^-$ anions ($\text{X} = \text{Cl}, \text{Br}, \text{I}$) are nearly symmetric and feature double-well minima separated by a tiny barrier for the proton transfer.^[102] An added dimension of the problem is the behavior of the corresponding neutral species, for example $(\text{FHF})^\bullet$, which are all quite high energy transition states for the hydrogen-abstraction reaction.^[5f]

Figure 42a depicts the HL and ionic structures for a proton transfer process between bases X:^- which have moderate or low stability as anions (e.g., carbanions with significant $\text{p}K_{\text{a}}$).

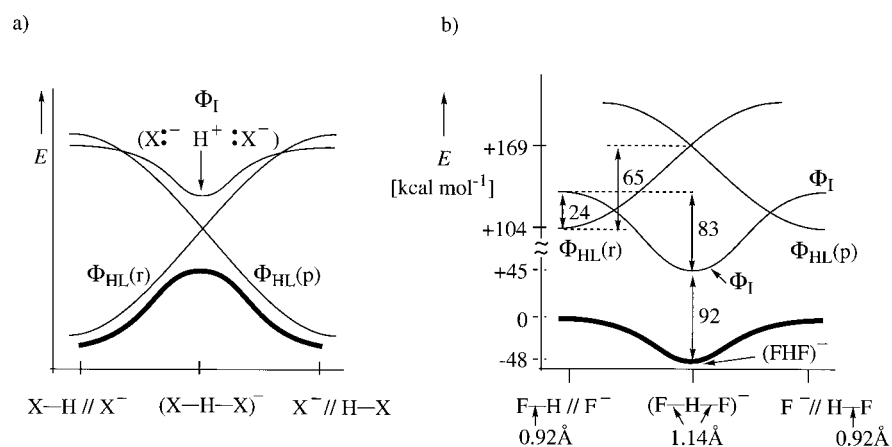


Figure 42. VBCMDs for proton transfer to and from X^- bases. a) The base has a moderate to low stability. b) The VB-computed situation for $\text{X}^- = \text{F}^-$, a stable base.

In such a case, the ionic structure lies above the HL structures in energy, and the avoided crossing leads to a single transition state separating the hydrogen-bonded clusters. Nevertheless, the ionic structure is seen to have a deep minimum near the crossing point of the HL curves, and as such the transition state will be expected to possess a significant triple-ion character.

As the anion X^- gets increasingly more stable, the ionic structure will descend more and more in energy and may dominate the region near the transition state. This is seen in Figure 42b, which depicts the calculated^[71, 103] VB configurations for the F^- exchange along the reaction coordinate. On the side of the reactants, the ionic structure lies above the HL structure by a moderate energy gap of only about 24 kcal mol^{-1} . However, at the symmetric geometry, the lowest VB curve is the ionic structure which undergoes 83 kcal mol^{-1} of stabilization relative to its onset at the reactant geometry. The origins of this remarkable stability of the ionic structure is, as already noted, the small size of H^+ , which leads to short F^-H^+ distances at the cluster geometry of $(FHF)^-$ and thereby to very large electrostatic stabilization. This electrostatic stability along with its energetically low onset make the ionic structure the dominant configuration at the cluster geometry.

The short $H-F$ distance is associated also with the inception of a very large resonance energy due to the mixing of the resonating HL state (which by itself is stabilized by resonance) with the ionic structure. This ionic-covalent resonance energy is seen in Figure 42b to be about 90 kcal mol^{-1} , which makes a significant contribution to the bonding in $(FHF)^-$. Thus, the symmetric hydrogen-bonded species is neither fully ionic nor fully covalent; it is virtually a resonating mixture of the two structures.^[104]

The question of whether or not the symmetric $(FHF)^-$ species will be a minimum on the adiabatic (bold) curve is a question of balance between the difference in electrostatic stabilization and ionic-covalent resonance energies at the cluster geometry relative to the reactant and product geometries. It is seen from Figure 42b that the ionic-covalent resonance energy is largest at the reactant and product geometries. It follows, therefore, that the crucial factor responsible for the stability of the symmetric $(FHF)^-$ species is the electrostatic stabilization, which lowers the curve of the ionic structure well below onset of the curves of the HL structures. It is this difference that causes the final state profile (Figure 42b, in bold) to retain the shape of the ionic curve, and to exhibit a minimum. The relatively small size of the F^- anion is also important for the electrostatic stabilization, and we may expect that, as the anion increases in size (e.g., I^-) or becomes delocalized (e.g., benzoate), the intrinsic stabilization of the ionic structure at the cluster geometry will decrease, and the symmetric geometry may cease to be a minimum of the energy profile.^[102]

Finally, the impact of the ionic structure is vividly appreciated by comparison of $(FHF)^-$ with the radical $(FHF)^\bullet$. Thus, with one electron less in $(FHF)^\bullet$, the triple-ionic structure disappears and is replaced by the $F^-H^+ \cdot F$ structures, which lose half of the electrostatic stabilization, and therefore their curve will remain above the HL curves. This loss has

a tremendous impact on the reaction profile, and the greater than 40 kcal mol^{-1} deep energy well of $(FHF)^-$ becomes an $(FHF)^\bullet$ transition state that is about 18 kcal mol^{-1} above the reactants.^[5f] For the same reason, it is expected therefore that any $(XHX)^\bullet$ species will generally be a transition state^[30, 31] for the hydrogen-abstraction process, with a barrier significantly larger than for the corresponding proton transfer process via the $(XHX)^-$ species.

9.2.2. Nucleophilic Substitution on Silicon—Stable Hypercoordinated Species Exist because Silicenium Ions Are Analogues of H^+

Another demonstration of the role of ionic structure is the nucleophilic substitution on Si which proceeds via pentacoordinated intermediates,^[39b, 105] in contrast to the situation in carbon where the pentacoordinated species is a transition state. Recently, Lauvergnat et al.^[14a] and Sini et al.^[14b] performed VB calculations for $C-X$ and $Si-X$ bonds ($X = H, F, Cl$) and made the interesting observation that the minimum of the ionic curve for Si^+X^- is significantly shorter than the corresponding minimum for C^+X^- . In contrast, the minima of the HL curves for $Si-X$ were found to be at longer distances than for $C-X$. Since X is common for the two bonds, these differences mean that while the covalent radius of Si is longer than that of C; the opposite is true for the ionic radii. Thus, the ionic radii of CH_3^+ was determined as 0.64 \AA , in comparison with only 0.35 \AA for SiH_3^+ .^[14a] It was concluded that the origins of these effective ionic sizes is the charge distribution of the corresponding ions. In CH_3^+ and generally in CL_3^+ ($L = \text{ligand}$) the charge is distributed over the ligands, and the central carbon possesses therefore a relatively small positive charge. Consequently, the minimum distance of approach of an anion X^- toward CL_3^+ will be relatively long, and the electrostatic energy will be small. In contrast, in SiL_3^+ the charge is localized on Si, and consequently the minimum distance of approach of an X^- anion will be relatively short, and the electrostatic stabilization large. Indeed, the depth of the ionic curve $H_3Si^+X^-$ was found to exceed the depth of $H_3C^+X^-$ by more than 50 kcal mol^{-1} . In conclusion, therefore, the silenium ion SiL_3^+ is expected to behave more like the small proton, while the corresponding carbocation CL_3^+ will be bulky.

Based on these differences, it is possible to represent the VBCMDs for typical nucleophilic substitution reactions on Si versus C as shown in Figure 43. The ionic curve for Si (Figure 43a) is seen to be very stable in the pentacoordinated geometry due to the electrostatic energy of the triple ion, much like the case of the $(FHF)^-$ species discussed before. Consequently, the pentacoordinated species will become an intermediate for the reaction. By the same analogy, to the $(FHF)^-$ species, the pentacoordinated silicon intermediate will be neither ionic nor covalent, but rather a resonating mixture of the two structures with bonding augmented by the ionic-covalent resonance.

Figure 43b shows the typical situation for the carbon analogue where the ionic structure is of relatively high energy and the VB mixing leads to a single-step reaction with a pentacoordinated transition state. Intermediate pentacoordinated carbon may be envisioned if the reaction is conducted in

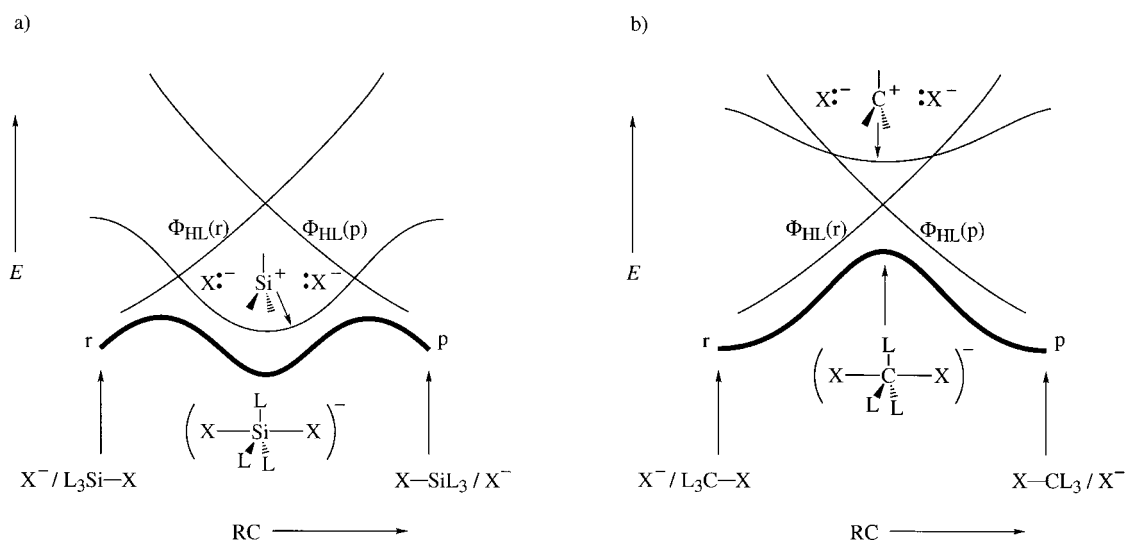


Figure 43. VBCMDs for nucleophilic displacements on a) silicon and b) carbon. Shown are the HL curves of reactants and products as well as the ionic curve.

the presence of external positive ions or immobilized charge centers (see Section 2.1.4) which will stabilize the ionic structure ($X^-CL_3^+X^-$) well below the crossing point of the HL curves. However, even in such an event the pentacoordinated species of carbon will be different than the corresponding silicon species. Thus, due to the small size of SiL_3^+ the covalent–ionic resonance energy will always make an important contribution to the bonding of the species. In contrast, the large size of the CL_3^+ species enables a smaller ionic–covalent resonance energy,^[14a] which will further decrease in the presence of external charges due to the widening energy gap between the ionic ($X^-CL_3^+X^-$) and the HL structures. Consequently, should a pentacoordinated intermediate of carbon become stable, it will generally be highly ionic. A recent study of ion-pair S_N2 reactions by Harder et al.^[106] shows that the presence of a single Li^+ cation or of an XLi_2^+ moiety makes the transition states virtually ionic. One

wonders if more accurate calculations or modification of the external ions will not result in a stable pentacoordinated carbon possessing high ionicity.

9.2.3. Concerted, Nucleophilic, and Electron Transfer Pathways in Polar Cycloadditions

Ionic VB structures play a cardinal role in polar cycloaddition, which has been a subject of intense research by the groups of Huisgen and Sauer,^[107] who were concerned with the orbital symmetry rules and their apparent violations. Let us consider for example, the Diels–Alder reactions of diene–dienophile pairs with varying donor–acceptor properties, a system investigated by Sustmann et al.^[108] Figure 44a shows the VBCMD, based on Figure 17, with the addition of the charge transfer (CT) state Φ_{CT} . For a pair of diene and dienophile with weak to moderate donor–acceptor capabil-

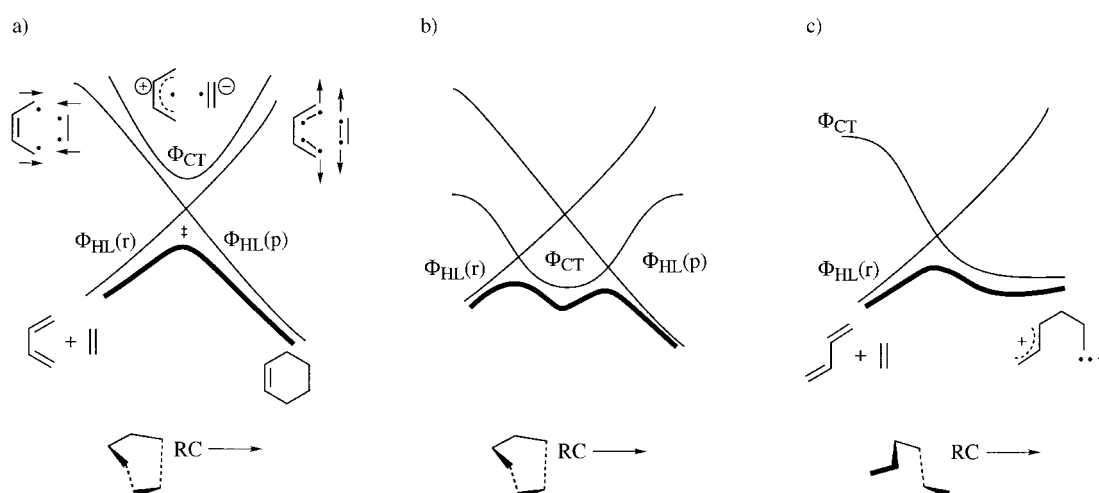
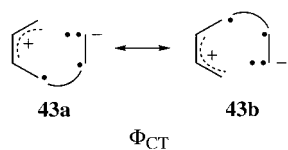


Figure 44. VBCMDs for Diels–Alder reactions. a) A nonpolar situation with a high-lying charge transfer state Φ_{CT} . b) A polar case, where solvent-assisted crossing brings the Φ_{CT} configuration below the crossing point of the HL curves. The cycloaddition proceeds in a synchronous fashion via a pericyclic polar intermediate. c) Nucleophilic attack of the diene on the dienophile along a one-bond coordinate. The Φ_r – Φ_{CT} avoided crossing leads initially to the open form of the zwitterion intermediate. In the case of (a) and (b), the reaction coordinate RC describes the changes in two bonds, and in the case of (c) that of only one bond.

ities, the CT state is significantly higher than the HL curves. Since the mixing of the CT state with the resonating HL state is allowed (see rule 7), this occurs and a polar transition state is formed. The electronic VB structure of the CT state is depicted in the resonance mixture of **43a** and **43b** in Scheme 24, which illustrates that the ion pair possesses pericyclic bonding as long as the structure retains synchronous bonding or approximately so.



Scheme 24. VB structures whose resonance mixing provides the pericyclic charge transfer state of a cycloaddition of the type shown in Figures 44a and 44b.

Figure 44b shows the situation when the diene is a very good donor and the dienophile is a very good acceptor. In this case, the CT state is low in energy at the onset of the VBCMD, and solvation will cause it to descend further, below the HL structures. The CT configuration forms a pericyclic intermediate state which facilitates the cycloaddition by providing a low-energy path in comparison with the less polar cycloaddition in Figure 44a.

Once the CT state is lowered, the intermediate can take up different structures and lead thereby to different mechanisms. Figure 44c shows the VBCMD along a reaction coordinate which involves a one-bond attack of the diene on the dienophile. Since the CT state is lower than the promoted state for the synchronous reaction, the initial step will involve only avoided crossing of the reactant's HL configuration with the charge transfer state, much like a nucleophilic attack of the diene on the dienophile. This avoided crossing will lead to the zwitterion intermediate, which may subsequently close the second bond by an additional avoided crossing, involving Φ_{CT} with the HL configuration of the products. Alternatively, the intermediate may be trapped by the solvent or undergo side reactions (such as oligomerizations) typical of the dipolar nature. By analogy to nucleophile–electrophile reactivity (see Figure 30), here too the formation of the dipolar intermediate will compete with the corresponding electron transfer process^[108c, e] if the avoided crossing in Figure 44c takes place along a coordinate which is either outer sphere or a recoil inner sphere in character, as in Figure 30. Clearly, the accessibility of the ionic structure endows polar cycloadditions with a rich mechanistic scheme of competing concerted and nonconcerted pathways, which is very different from the classical Diels–Alder reaction.^[108]

9.3. VBCMD with “Foreign” States as Intermediate Curves

Every reaction system possesses, in addition to the promoted states which are localized in the active bonds, numerous “foreign” excited states which involve electronic excitations in orbitals and bonds which do not belong to the active bonds. Some of these foreign states are high in energy, while some which are of low energy can become accessible along the reaction coordinate. As already stated, mixing of foreign states is the means by which complex molecules find low-energy pathways for otherwise difficult transformations.

To elucidate this mechanistic feature of the foreign states, we have chosen three mechanisms in which the foreign state plays a cardinal role.

9.3.1. Nucleophilic Cleavage of Esters

Figure 45 shows the reaction in which a nucleophile X^- cleaves the C–OR bond of an ester via a tetrahedral intermediate^[48–50] (see Section 7.1.7). Structures **44** and **45**

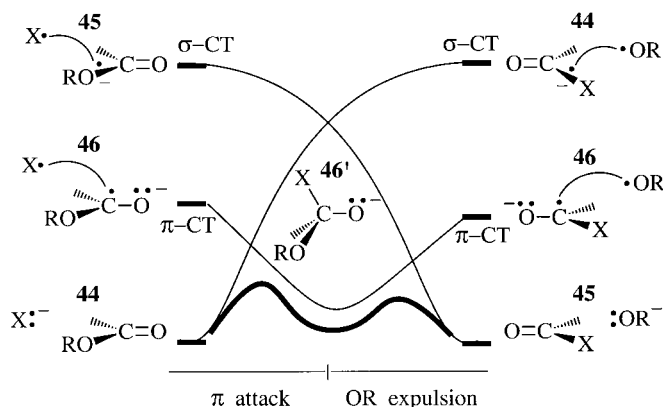


Figure 45. VBCMD showing the cleavage mechanism of an ester by a nucleophile X^- via the tetrahedral intermediate **46'**. See text for details.

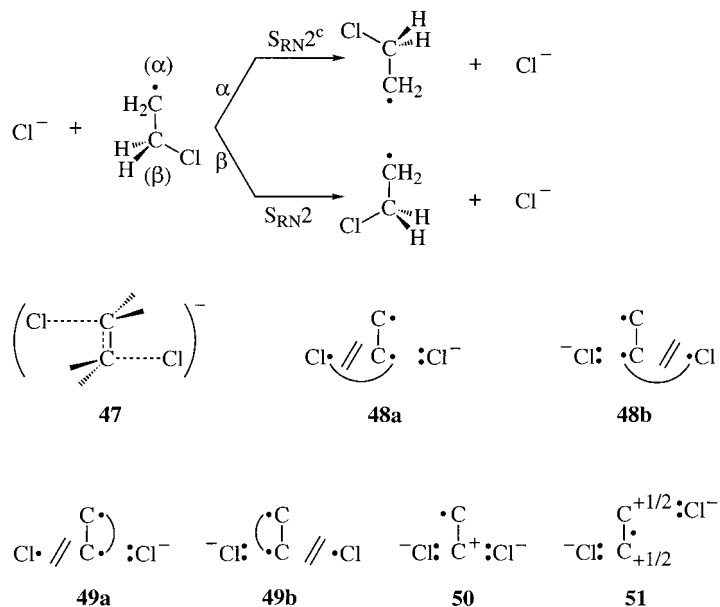
depict the ground state and σ -CT state which form the fundamental curves that describe the net reaction, while **46** is the π -CT state which correlates to the tetrahedral intermediate. It is seen that the ground and σ -CT states generate a high-energy crossing point, due to the large promotion gap. In contrast, the low lying π -CT state can cross the ground state at a lower energy to define a transition state for the formation of the tetrahedral intermediate. The latter then undergoes conformational changes and expels in a subsequent step the RO^- leaving group. Thus, the π -CT state facilitates the exchange of the σ bonds by providing a low-energy path.

Clearly, a single-step reaction which involves a direct backside attack on the C–OR bond will have a significantly higher barrier, due inter alia to the loss of the electronic advantage of mixing of the π -CT state. One may anticipate that in the case of acyl halides (e.g., Br and I), where the σ -CT state is not so high, the π -CT and σ -CT states will be close in energy, so that the avoided crossing will generate a single transition state and the process will become synchronous.^[63] In such an event, a competition between π attack and a backside σ attack similar to that in a S_N2 reaction may ensue. Similar conclusions have been derived for the S_NV mechanism.^[63, 109a]

A dominant backside σ attack on the ester or acyl halide will become likely when the π -CT state rises well above the corresponding σ -CT state. This will require, however, at least an acyl iodide or the use of a catalyst which can activate specifically the bond to the leaving group without affecting the π -CT state of the carbonyl group much. Reagents which form hypercoordinated iodide may serve as such catalysts. A case of this sort has been recently observed experimentally in an S_NV reaction of styryl iodonium salts.^[109b]

9.3.2. The $S_{RN}2$ and $S_{RN}2^c$ Mechanisms

Intermediate states are also capable of changing a reaction mechanism. A case in point is the recent proposition of new nucleophilic substitution mechanisms, termed $S_{RN}2$ and $S_{RN}2^c$, by Zipse as part of his “methylenology” strategy to speed up rates of classical reactions by the presence of a radical center adjacent to the reaction centers.^[9] Scheme 25 shows these



Scheme 25. The identity reaction between Cl^- and the β -chloroethyl radical as well as structures important for an understanding of the mechanisms.

mechanisms for the identity reactions of the β -chloroethyl radical, where Cl^- exchange can occur by attack on the β or α position. It was found by Zipse^[9] that the $S_{RN}2$ mechanism is a single-step reaction with a transition state which is very similar to that of the corresponding S_N2 reaction between Cl^- and ethyl chloride. At the same time, the $S_{RN}2$ barrier was shown to be about 11 kcal mol^{-1} lower than the S_N2 barrier.

Even more intriguing are the most recent findings by Zipse,^[110] triggered by application of the VBCMD model, revealing that the $S_{RN}2^c$ mechanism proceeds in a stepwise manner via a C_{2h} -symmetric intermediate **47**, which is lower by about 3 kcal mol^{-1} relative to the transition state of the $S_{RN}2$ mechanism. Thus, the adjacent radical center on the one hand lowers considerably the barriers for the Cl^- exchange, and on the other hand leads to a novel intermediate species.

The effect of the radical center can be appreciated by inspecting the VB structures **48** and **49**, which correspond to promoted states for the process. Thus, **48a** and **48b** are the standard charge transfer states which arise by electron transfer from the attacking Cl^- into the C–Cl linkage, while pairing the spins across the $\text{Cl}\cdots\text{C}$ intermolecular linkage. There is, however, an alternative way of coupling the spins and generating thereby states with a much lower promotion energy. This alternative is shown in **49a** and **49b**, where the spins are paired across the intramolecular $C_\alpha\text{--}C_\beta$ linkage. The resulting states are lower in energy relative to the standard promoted state in **48**. As such, the resonating combination of **49a** and **49b** will give rise to a low-lying intermediate curve cutting across the fundamental curves.

Figure 46 shows the VBCMD for the two mechanisms. Thus, in both cases there exist two fundamental curves identical to those of the classical S_N2 reaction, and a low-lying intermediate curve. According to the calculations of Zipse^[110] the vertical gap to the intermediate curve is less than half of the promotion energy of the fundamental curve. It is the mixing of this intermediate structure into the fundamental curves that accounts for the much lower energetics of the $S_{RN}2$, and $S_{RN}2^c$ mechanisms in comparison with S_N2 .

The difference between the $S_{RN}2$ and $S_{RN}2^c$ mechanisms is seen to be the relationship between the intermediate structure and the fundamental curves. Our placement of the intermediate curve in Figure 46 is based on the spin and charge-density analysis of Zipse.^[9, 110] The crossing point of the fundamental curves is lower for the $S_{RN}2$ mechanism, because the triple-ion structure shown as **50** in Scheme 25 can optimize better the electrostatic interactions in comparison with the

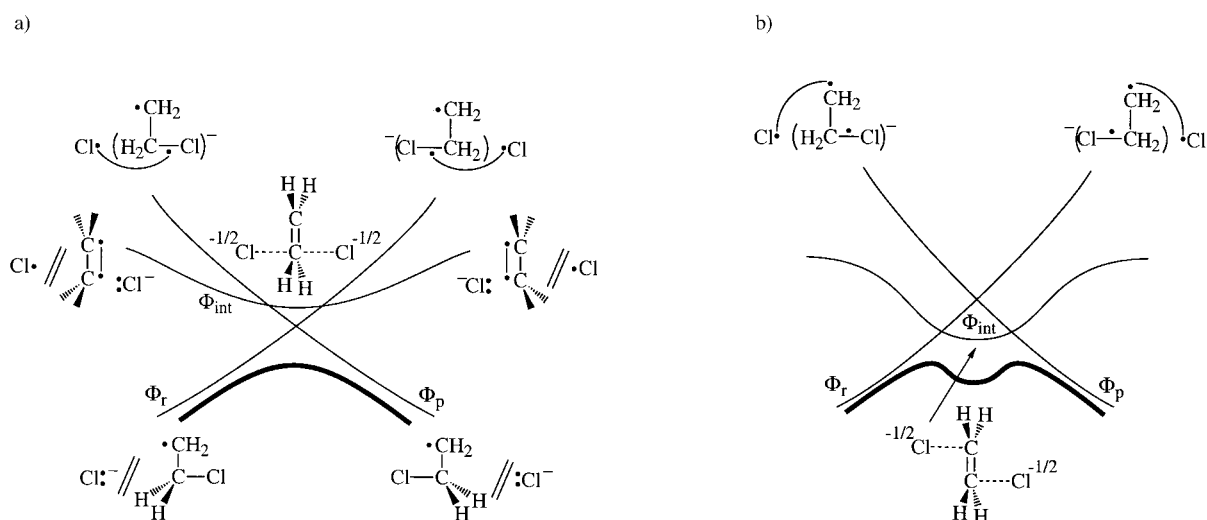


Figure 46. VBCMDs for $S_{RN}2$ (a) and $S_{RN}2^c$ mechanisms (b) for reaction of the chloride ion with the chloroethyl radical. Φ_r , Φ_p = curves of reactant and product, Φ_{int} = intermediate curve.

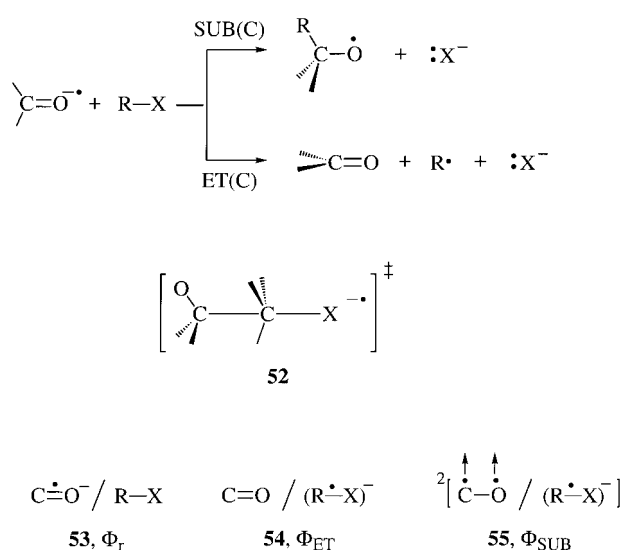
corresponding structure **51** of the $S_{RN}2^c$ mechanism. This effect would be enhanced by the somewhat preferred intrinsic stability of the intermediate structure in the $S_{RN}2^c$ case. Consequently, the crossing point of the fundamental curves for the $S_{RN}2$ mechanism may well be lower than the intermediate curve, as shown in Figure 46a, while the opposite would be true for the $S_{RN}2^c$ mechanism, as shown in Figure 46b. Indeed, the computed^[110] $C_\alpha-C_\beta$ distances, charge development on the C_2H_4 moiety, and the spin density on the chlorine moieties demonstrate that the intermediate state character is more dominant in the $S_{RN}2^c$ mechanism. Thus, $S_{RN}2^c$ is a stepwise mechanism mediated by a low-energy state due to strong electronic coupling with the adjacent radical center.

Clearly, the intermediate VB state **49** (Scheme 25) emerges as the key feature which affects the intrinsic barriers for Cl^- exchange in the $S_{RN}2$ and $S_{RN}2^c$ mechanisms. A radical center adjacent to the reaction center is a novel strategy to generate low-energy pathways via intermediate states.^[9, 111] Furthermore, different substitution patterns may create a whole mechanistic manifold, including intermediates of cation radical states, for example via **50** and **51** (Scheme 25), which feature in Giese's mechanism for radical-induced DNA strand cleavage.^[112]

9.3.3. Mechanistic Crossovers and Entangled Mechanisms

An interesting effect of intermediate configurations can be observed when two mechanisms share a common set of VB structures which mix along the trajectories that lead to the two mechanisms. The competing mechanisms will be entangled, and a series of reactants, with appropriate substituents, will exhibit a mechanistic crossover while the corresponding transition state is undergoing a smooth geometric variation.

This phenomenon has been discovered recently^[92c, 113] for the reactivity of ketyl radical anions and alkyl halides. As shown in Scheme 26, the reactants may undergo both C-alkylation (SUB(C)) as well as dissociative electron trans



Scheme 26. Two mechanistic alternatives occurring via isostructural transition states for the reaction of ketyl radical anions with alkyl halides and important VB structures.

fer (ET(C)) via isostructural transition states (**52**). The key VB structures are **53–55**, the reactant Φ_r , the ET(C) Φ_{ET} , and SUB(C) Φ_{SUB} configurations. The mixing of Φ_r and Φ_{ET} is determined by the $\pi_{CO}^*-\sigma_{CX}^*$ overlap (see Scheme 20), which is optimal in a C-C-X structure. However, in this structure the Φ_{SUB} configuration mixes both with Φ_r and Φ_{ET} . As such, the three configurations blend along the C-C-X trajectory. The resulting species will possess in principle a gamut of electronic structures, with two extremes and probably a grey area in between.

The extremes are shown in Figure 47 and arise from the pairwise avoided crossing of Φ_r with either Φ_{ET} or Φ_{SUB} . Figure 47a shows the $\Phi_r-\Phi_{ET}$ avoided crossing, which leads to

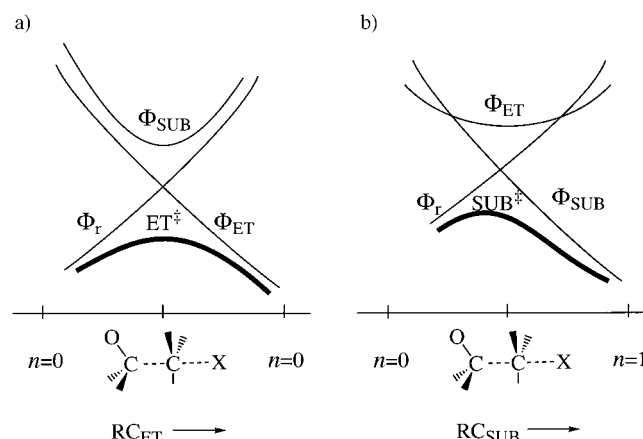


Figure 47. The distinct mechanisms for a reaction between ketyl anion radicals with methyl halides. a) An ET mechanism due to $\Phi_r-\Phi_{ET}$ avoided crossing. b) A C-alkylation mechanism, SUB(C), by $\Phi_r-\Phi_{SUB}$ avoided crossing. In each case, the third configuration mixes into the transition state and creates entangled mechanisms. $n = \text{C-C bond order}$.

the ET transition state having the C-C-X structure (required by the $\pi_{CO}^*-\sigma_{CX}^*$ selection rule in Scheme 20). The Φ_{SUB} configuration serves as an intermediate state which mixes into the ET transition state (ET^+) and endows it with some substitution character. Past the transition state, the C-C bond recoils, leading to dissociated ET products. In the other extreme (Figure 47b) there is a $\Phi_r-\Phi_{SUB}$ pairwise avoided crossing which leads to a SUB(C) transition state (SUB^+). Now, Φ_{ET} is the intermediate curve that mixes into the SUB(C) transition state and endows it with an ET character. Thus, the constituent VB configurations of the two extreme mechanisms are mixed in the C-C-X structure, and the mechanisms are therefore entangled borrowing characters from each other.

The consequences of this entangled nature are vividly represented in Figure 48, taken from a recent computational study by Sastry et al.,^[113a] as a mechanistic crossover with a sharp boundary zone. In the figure the C-C distance in the C-C-X transition state is shown as a function of the parameter α defined by Equation (15) in terms of the ET promotion gap

$$\alpha = \frac{G_{ET}}{2(G_{ET} - \Delta E_{ET})} \quad (15)$$

and reaction energy driving force. Thus, for good donor-acceptor pairs which lead to very exothermic ET, the Φ_{ET} configuration lies well below Φ_{SUB} curve, and the

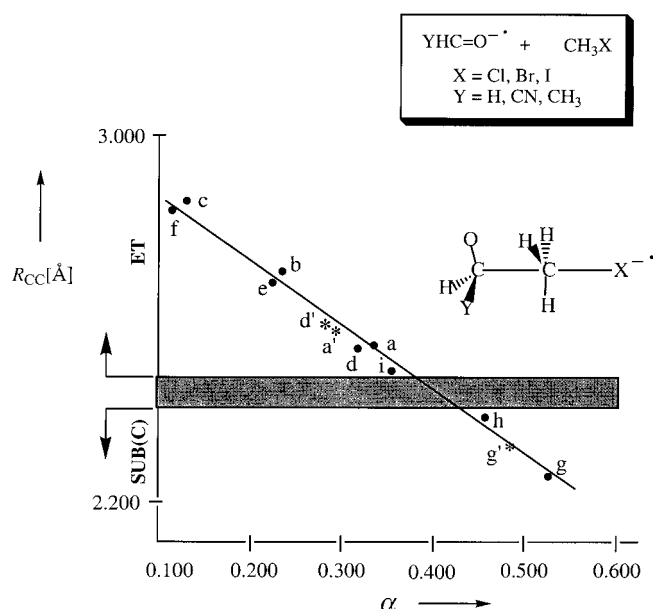


Figure 48. Plot of the C–C distance against the “earliness” parameter α [Eq. (15)] for transition states of the C–C–X type, obtained from the ketyl radical anions and alkyl halides shown in the box (adapted from ref. [113a]). A mechanistic crossover is indicated by the shaded zone. Transition states in the vicinity of the crossover zone may give mixtures of ET and SUB(C) products by surface bifurcation.

$\Phi_r - \Phi_{ET}$ avoided crossing occurs at a longish C–C distance (small α), leading to an ET transition state. As the donor–acceptor relationship becomes poorer, and the ET process less exothermic, the Φ_{SUB} configuration takes over and crosses Φ_r at a shorter C–C distance (larger α) and the corresponding avoided crossing results in a SUB(C) transition state. It is seen that the C–C distance at the C–C–X transition state decreases smoothly, while the mechanism changes abruptly from the ET to the SUB(C) variety within a narrow changeover zone.

The region around the changeover zone is likely to exhibit a borderline in which the three VB configurations are strongly mixed and lead to entangled behavior. Our more recent study of the reaction of H_2CO^- with CH_3Cl (point a in Figure 48)^[113b] shows that the ET transition state is separated from the SUB(C) valley by a shallow energy ridge which will be crossed whenever sufficient kinetic energy becomes available to the system. In this case, the ET transition state will most likely have a leakage channel to the SUB(C) pathway. We expect that ultimately at some limiting situation, the entangled nature of the mechanisms will be strong enough, the ridge which separates the mechanisms will altogether disappear, and a surface bifurcation^[114] will result. In such a limiting situation, the transition state structure will serve as a common species which leads to generation of C-alkylated as well as dissociated ET products. Such behavior must be found near the changeover zone of Figure 48, for example, for the reaction of the cyanoformaldehyde radical anion with CH_3I ^[113a] or with a secondary alkyl chloride.^[113c] Stereochemical studies near the changeover zone may contribute to a better articulation of the entangled-mechanism paradigm. We are looking forward to a molecular dynamics study which will test the notion that a single transition state can serve two different mechanisms.

9.4. The VBCMD: A Primary Model for Chemical Reactivity

The notion that an intermediate VB state or configuration can mediate a transformation by a low-energy path is quite evident by now, and its importance can hardly be over-emphasized. This is very likely the situation in many chemical reactions of large molecules, where many intermediate states are sufficiently low in energy to affect almost any transformation. Applications to organometallic reactivity is an obvious direction because organometallic molecules have plenty of low lying excited states which can mediate low-energy processes.^[100] Creative approaches such as Zipse’s^[9, 110, 111] “methylenology” strategy can be exploited to effectuate other reactions and to generate for them novel intermediates.

From another general viewpoint, not elaborated in this review, the VBCMD model leads to a systematic conceptualization of reaction mechanisms in terms of the constituent building block VB configurations. The elementary processes for a given reactant pair are defined by the pairwise avoided crossings within the VB set, which constitute the mechanistic manifold available for the reactants.^[115] The remaining VB configurations for each pairwise avoided crossing will serve as intermediate curves which can mix in and endow the particular transition states with their characters. In certain cases where the reaction manifold share similar trajectories, there will result “entangled” mechanisms as discussed above, which may exhibit surface bifurcations where a single transition state structure becomes a common critical species for two mechanisms. In other cases, where the trajectories are very distinct, the mechanisms will simply borrow electronic characters from each other through the mixing of the intermediate VB structure, as has recently been shown for nucleophilic cleavages, proton transfers, and electron transfers of cation radicals.^[62, 115]

Thus, as sufficient proficiency in VB theory builds up, it is our feeling that ultimately VBCMD could become a central paradigm for mechanistic chemical reactivity.

10. Summary and Outlook

At this point, the fundamental principles of VB diagrams have been illustrated and applied to a wide range of chemical reactivity problems. The central idea that the curves of VB configurations, which describe the electronic reorganization inherent in the process, cross along the reaction coordinate, generating by resonance mixing barriers and intermediate states, is both chemically lucid as well as resting on solid quantum-chemical principles.^[5] Two generic diagrams, the VBSCD in Figure 21 and the VBCMD in Figure 41, provide a consistent frame of thought for making predictions on barrier heights, transition state structures, selection of reaction mechanisms, the nature of reaction intermediates, and the low-energy pathways available to a chemical process.^[4, 7] The formulation of eight rules along with a presentation of a variety of applications and a few new predictions should provide the reader with a basis and hopefully a drive to extend

the ideas to new chemical problems which certainly overstep the knowledge and imagination of the authors.

There are also limitations in the model as well as challenges which need to be met in the future. A thorny problem of the VB diagram approach is its implicit quantitative aspect. Thus, while quantitative expressions for the barrier [e.g., Eqs. (8)–(10)] exist and have been applied successfully to estimate barrier heights, such as in S_N2 reactivity,^[4a–c] it is not a straightforward matter to quantify the f and B factors routinely for other reactions. It would have been desirable to formulate the barrier equations with explicit expression of the reactivity factors in a manner that enables a routine estimate of the barrier. While this is certainly a worthy challenge, it may not be met easily, if at all, on a general basis.

A major challenge of any reactivity model is its “dialogue” with experiment in a manner which may generate some meaningful physical information from the data, beyond just correlations. A simple idea which is being explored rests on the concept of reaction “family”, discussed above in reference to Figure 40 (Section 8.2), where a family is a series of closely related reactions for which the quantities f and B are constants. Once these parameters are derived from the experimental data, they may be used to model the transition states of the family and lead thereby to a crude resolution of transition state structure under real conditions. Criteria for identifying true reaction families are still being sought (perhaps Hammett series), and while the means for modeling are in principle known,^[10] the task is still difficult.

The role of intermediate states as the means of providing low-energy pathways for difficult reactions has been focused on in the context of organic reactivity. But it is clear that the vast potential for this rests in organometallic reactivity.^[8, 46, 100] This is where future efforts might be fruitful.

The notion of entangled mechanisms (Section 9.3.3) with mechanistic crossovers (see Figure 48) and a borderline transition state which serves several mechanisms has novel aspects which are largely unexplored. We expect that quite a few mechanistic manifolds will exhibit this behavior, for example, substitution and ET mechanisms of ion radicals (Figure 48) or $S_{RN}2/S_{RN}2^c$ reactions^[9, 110] and their isoelectronic mechanistic manifold^[112] with radical-cation intermediate states. In all of these cases a single transition state may serve a few mechanisms (by surface bifurcation). Microscopic reversibility will certainly have to be questioned then as a necessary rule of nature.

Photochemistry is an important field of potential application. Use of VB notions highlights^[116] the role of conical intersections as decay channels^[117] in the chemistry of organic molecules in excited states. A recent application^[78] of VB diagrams to the photochemistry of S_N2 systems^[118a] illustrates a simple mechanism for formation of conical intersections. This mechanism is based on the notion that the twin states Ψ^+ and Ψ^* in the avoided-crossing region of the VBSCD (Figure 36) are related by resonance mixing of degenerate VB configurations. Therefore, there should exist a specific distortion mode which would convert the avoided crossing region into a conical intersection where the twin states Ψ^+ and Ψ^* become degenerate, thereby enabling the excited reaction complex to decay into the ground-state surface. The photo-

products would therefore be characteristic of the distortion mode which is required to convert the avoided crossing region into a conical intersection. This concept works successfully^[78] for the charge transfer photochemistry of S_N2 systems,^[118a] but its potential is extendable to other reactions and may be far reaching. We are currently investigating the photosolvolytic mechanism^[118b] in an attempt to explore the correlation between product distribution and the nature of the distortion modes which convert the avoided crossing states in Figure 5b into a conical intersection.

The notion of twin states has some exciting implications on the characterization of transition states. Thus, since the twin states Ψ^+ and Ψ^* are related electronically, they may also be geometrically coincident or nearly so. Since the excited state Ψ^* is in principle bound, it can be accessed by experimental means and serve thereby as a source of spectral information on the transition state Ψ^+ of the thermal process. Candidates where the geometric coincidence of the states can be manifested are rigid systems. The semibullvalene system in a recent study of Quast et al.^[118c] appears to be a good choice for such explorations.

With all the foregoing features taken together, the VB diagram approach is an art of piecing together reaction profiles from their building blocks, and as such the method has a potential to become a central paradigm for the science of chemical reactivity.

Enduring collaborations with A. Pross and P. C. Hiberty and instructive seminal discussions with H. Köppel and L. S. Cederbaum on avoided crossing are acknowledged. The work has been supported in part by a grant from the Israel Science Foundation (ISF), The Lise Meitner-Minerva Center, and the Volkswagenstiftung. Allocation of computer time by the IUCC is acknowledged. The authors are indebted to H. Zipse for taking on the colossal work of translating this review into German, and for very helpful suggestions throughout the work. The idea of writing this review was conceived during the visit of S. Shaik to the Technische Universität Berlin as an Alexander von Humboldt Awardee. The hospitality and support of H. Schwarz is acknowledged.

Received: July 28, 1997 [Z A247 IE]

German version: *Angew. Chem.* **1999**, *111*, 616–657

- [1] S. S. Shaik, *J. Am. Chem. Soc.* **1981**, *103*, 3692.
- [2] R. B. Woodward, R. Hoffmann, *Angew. Chem.* **1969**, *81*, 797; *Angew. Chem. Int. Ed. Engl.* **1969**, *8*, 781.
- [3] For example, a) M. G. Evans, M. Polanyi, *Trans. Faraday Soc.* **1938**, *34*, 11; b) A. Warshel, R. M. Weiss, *J. Am. Chem. Soc.* **1980**, *102*, 6218; c) W. T. A. M. van der Lugt, L. J. Osterhoff, *J. Am. Chem. Soc.* **1969**, *91*, 6042; d) J. Michl, *Top. Curr. Chem.* **1974**, *46*, 1; e) “Unified Valence Bond Theory of Electronic Structure. Applications”: N. D. Epiotis, *Lect. Notes Chem.* **1983**, *34*, 1; f) L. Salem, *Science* **1976**, *191*, 822.
- [4] a) S. S. Shaik, *Prog. Phys. Org. Chem.* **1985**, *15*, 197; b) S. S. Shaik, H. B. Schlegel, S. Wolfe, *Theoretical Aspects of Physical Organic Chemistry*, Wiley-Interscience, New York, **1992**; c) S. S. Shaik, *Acta Chem. Scand.* **1990**, *44*, 205; d) S. S. Shaik, P. C. Hiberty in *Theoretical Models for Chemical Bonding*, Vol. 4 (Ed.: Z. B. Maksic), Springer, Heidelberg, **1991**, p. 269; e) A. Pross, S. S. Shaik, *Acc. Chem. Res.* **1983**, *16*, 363; f) A. Pross, *Adv. Phys. Org. Chem.* **1985**, *21*, 99; g) A. Pross, *Theoretical and Physical Principles of Organic Reactivity*, Wiley-

- Interscience, New York, **1995**; h) A. Pross, *Acc. Chem. Res.* **1985**, *18*, 212; i) A. Pross, D. M. Chipman, *Free Radicals Biol. Med.* **1987**, *3*, 55.
- [5] a) P. Maitre, P. C. Hiberty, G. Ohanessian, S. S. Shaik, *J. Phys. Chem.* **1990**, *94*, 4089; b) G. Sini, S. Shaik, P. C. Hiberty, *J. Chem. Soc. Perkin Trans. 2* **1992**, 1019; c) G. Sini, S. S. Shaik, J.-M. Lefour, G. Ohanessian, P. C. Hiberty, *J. Phys. Chem.* **1989**, *93*, 5661; d) G. Sini, G. Ohanessian, P. C. Hiberty, S. S. Shaik, *J. Am. Chem. Soc.* **1990**, *112*, 1407; G. Sini, P. C. Hiberty, S. S. Shaik, *J. Chem. Soc. Chem. Commun.* **1989**, 772; e) P. Maitre, F. Volatron, P. C. Hiberty, S. S. Shaik, *Inorg. Chem.* **1990**, *29*, 3047; f) P. R. Benneyworth, G. G. Balint-Kurti, M. J. Davis, I. H. Williams, *J. Phys. Chem.* **1992**, *96*, 4346.
- [6] For recent methods of good accuracy, see for example a) P. C. Hiberty, J. P. Flament, E. Noizet, *Chem. Phys. Lett.* **1992**, *189*, 259; P. C. Hiberty, S. Humbel, C. P. Byrman, J. H. van Lenthe, *J. Chem. Phys.* **1994**, *101*, 5969; b) W. A. Goddard III, L. B. Harding, *Annu. Rev. Phys. Chem.* **1978**, *29*, 363; A. F. Voter, W. A. Goddard III, *J. Chem. Phys.* **1981**, *75*, 3638; c) J. Verbeek, J. H. Langenberg, C. P. Byrman, J. H. van Lenthe, *TURTLE—an Ab Initio VB/VBSCF/VBCI Program*, Theoretical Chemistry Group, Debye Institute, University of Utrecht, **1993**; J. Verbeek, J. H. van Lenthe, *Int. J. Quantum Chem.* **1991**, *XL*, 201; d) D. L. Cooper, J. Gerratt, M. Raimondi, *Adv. Chem. Phys.* **1987**, *69*, 319; D. L. Cooper, J. Gerratt, M. Raimondi, *Chem. Rev.* **1991**, *91*, 929; e) Y. Mo, Q. Zhang, *J. Phys. Chem.* **1995**, *99*, 8535; Y. Mo, Z. Lin, W. Wu, Q. Zhang, *J. Phys. Chem.* **1996**, *100*, 6469; f) W. Wu, R. McWeeny, *J. Chem. Phys.* **1994**, *101*, 4826.
- [7] a) S. S. Shaik in *New Theoretical Concepts for Understanding Organic Reactions*, Vol. C267 (Eds.: J. Bertrán, I. G. Csizmadia), Kluwer, Dordrecht, **1989**, p. 165; b) S. Shaik, *J. Mol. Liq.* **1994**, *61*, 49; c) S. Shaik, P. C. Hiberty, *Adv. Quantum Chem.* **1995**, *26*, 99.
- [8] D. Schröder, H. Schwarz, *Angew. Chem.* **1995**, *107*, 2126; *Angew. Chem. Int. Ed. Engl.* **1995**, *34*, 1973.
- [9] H. Zipse, *Angew. Chem.* **1994**, *106*, 2019; *Angew. Chem. Int. Ed. Engl.* **1994**, *33*, 1985; b) H. Zipse, *J. Am. Chem. Soc.* **1994**, *116*, 10773.
- [10] S. S. Shaik, E. Duzy, A. Bartuv, *J. Phys. Chem.* **1990**, *94*, 6574.
- [11] R. McWeeny, *Methods of Molecular Quantum Mechanics*, 2nd ed., Academic Press, London, **1992**, chapters 4 and 7.
- [12] W. Heitler, F. London, *Z. Phys.* **1927**, *44*, 455.
- [13] S. Shaik, P. Maitre, G. Sini, P. C. Hiberty, *J. Am. Chem. Soc.* **1992**, *114*, 7861.
- [14] a) D. Lauvergnat, P. C. Hiberty, D. Danovich, S. Shaik, *J. Phys. Chem.* **1996**, *100*, 5715; b) G. Sini, P. Maitre, P. C. Hiberty, S. S. Shaik, *J. Mol. Struct. (THEOCHEM)* **1991**, *229*, 163; c) H. Basch, P. Aped, S. Hoz, *Mol. Phys.* **1996**, *89*, 331.
- [15] T. F. O'Malley, *Adv. Atom. Mol. Phys.* **1971**, *7*, 223.
- [16] R. A. Ogg, Jr., M. Polanyi, *Trans. Faraday Soc.* **1935**, *31*, 604.
- [17] S. S. Shaik, *J. Org. Chem.* **1987**, *52*, 1563.
- [18] H. J. Kim, J. T. Hynes, *J. Am. Chem. Soc.* **1992**, *114*, 10508, 10528.
- [19] a) P. Delahay, *Acc. Chem. Res.* **1982**, *15*, 40; b) M. J. Blandamer, M. F. Fox, *Chem. Rev.* **1970**, *70*, 59.
- [20] S. S. Shaik, *J. Am. Chem. Soc.* **1984**, *106*, 1227.
- [21] C. D. Ritchie, *J. Am. Chem. Soc.* **1983**, *105*, 7313.
- [22] H. Mayr, M. Patz, *Angew. Chem.* **1994**, *106*, 990; *Angew. Chem. Int. Ed. Engl.* **1994**, *33*, 938.
- [23] a) H. Feinberg, H. M. Greenblatt, G. Shoham, *J. Chem. Inf. Comput. Sci.* **1993**, *33*, 501; b) H. Feinberg, H. M. Greenblatt, V. Behar, C. Gilon, S. Cohen, A. Bino, G. Shoham, *Acta Crystallogr. Sect. D* **1995**, *51*, 428.
- [24] a) A. Warshel, *Acc. Chem. Res.* **1981**, *14*, 284; b) A. Warshel, *Proc. Natl. Acad. Sci. USA* **1978**, *75*, 5250.
- [25] a) J. M. Tedder, J. C. Walton, *Adv. Phys. Org. Chem.* **1978**, *16*, 51; b) B. Giese, X. Beyrich-Graf, J. Burger, C. Kesselheim, M. Senn, T. Schäfer, *Angew. Chem.* **1993**, *105*, 1850; *Angew. Chem. Int. Ed. Engl.* **1993**, *32*, 1742.
- [26] Z. Rappoport, *Acc. Chem. Res.* **1981**, *14*, 7.
- [27] A. Sevin, P. C. Hiberty, J.-M. Lefour, *J. Am. Chem. Soc.* **1987**, *109*, 1845.
- [28] a) H. H. Cornehl, G. Hornung, H. Schwarz, *J. Am. Chem. Soc.* **1996**, *118*, 9960; b) J. N. Harvey, D. Schröder, W. Koch, D. Danovich, S. Shaik, H. Schwarz, *Chem. Phys. Lett.* **1997**, *278*, 391.
- [29] R. Hoffmann, *Angew. Chem.* **1982**, *94*, 725; *Angew. Chem. Int. Ed. Engl.* **1982**, *21*, 711.
- [30] H. Yamataka, S. Nagase, *J. Org. Chem.* **1988**, *53*, 3232.
- [31] a) A. Pross, H. Yamataka, S. Nagase, *J. Phys. Org. Chem.* **1991**, *4*, 135; b) M. W. Wong, A. Pross, L. Radom, *Isr. J. Chem.* **1993**, *33*, 415.
- [32] D. J. Bellville, D. D. Wirth, N. L. Bauld, *J. Am. Chem. Soc.* **1981**, *103*, 718; D. J. Bellville, N. L. Bauld, *J. Am. Chem. Soc.* **1982**, *104*, 2665; R. A. Pabon, D. J. Bellville, N. L. Bauld, *J. Am. Chem. Soc.* **1983**, *105*, 5158.
- [33] F. Bernardi, A. Bottoni, M. Olivucci, A. Venturini, M. A. Robb, *J. Chem. Soc. Faraday Trans.* **1994**, *90*, 1617.
- [34] P. Jungwirth, T. Bally, *J. Am. Chem. Soc.* **1993**, *115*, 5783.
- [35] The fairly small localization energy of the cation is neglected for simplicity; see also F. M. Bickelhaupt, R. Hoffmann, R. D. Levine, *J. Phys. Chem. A* **1997**, *101*, 8255.
- [36] a) T. P. Begley, *Acc. Chem. Res.* **1994**, *27*, 394; b) H.-W. Park, S.-T. Kim, A. Sancar, J. Deisenhofer, *Science* **1995**, *268*, 1866.
- [37] A. Ioffe, S. Shaik, *J. Chem. Soc. Perkin Trans. 2* **1992**, 2101.
- [38] a) E. T. Seidl, R. S. Grev, H. F. Schaefer III, *J. Am. Chem. Soc.* **1992**, *114*, 3643; b) F. Bernardi, A. Bottoni, M. Olivucci, M. A. Robb, A. Venturini, *J. Am. Chem. Soc.* **1993**, *115*, 3322.
- [39] a) R. West, *Angew. Chem.* **1987**, *99*, 1231; *Angew. Chem. Int. Ed. Engl.* **1987**, *26*, 1201; b) Y. Apeloig in *The Chemistry of Organic Silicon Compounds* (Eds.: S. Patai, Z. Rappoport), Wiley, Chichester, **1989**, chapter 2.
- [40] S. Shaik, A. Ioffe, unpublished results.
- [41] S. S. Shaik, P. C. Hiberty, G. Ohanessian, J.-M. Lefour, *J. Phys. Chem.* **1988**, *92*, 5086.
- [42] M. J. S. Dewar, *J. Am. Chem. Soc.* **1984**, *106*, 209.
- [43] D. L. King, D. R. Herschbach, *Faraday Discuss. Chem. Soc.* **1973**, *55*, 331.
- [44] a) G. K. Cook, J. M. Mayer, *J. Am. Chem. Soc.* **1994**, *116*, 1855; b) G. K. Cook, J. M. Mayer, *J. Am. Chem. Soc.* **1995**, *117*, 7139; c) K. A. Gardner, J. M. Mayer, *Science* **1995**, *269*, 1849.
- [45] A. K. Rappé, W. A. Goddard III, *J. Am. Chem. Soc.* **1982**, *104*, 3287.
- [46] a) A. Fiedler, D. Schröder, S. Shaik, H. Schwarz, *J. Am. Chem. Soc.* **1994**, *116*, 10734; b) M. F. Ryan, A. Fiedler, D. Schröder, H. Schwarz, *J. Am. Chem. Soc.* **1995**, *117*, 2033; c) Y.-M. Chen, D. E. Clemmer, P. B. Armentrout, *J. Am. Chem. Soc.* **1994**, *116*, 7815; d) D. E. Clemmer, Y.-M. Chen, F. A. Khan, P. B. Armentrout, *J. Phys. Chem.* **1994**, *98*, 6522; e) S. Shaik, D. Danovich, A. Fiedler, D. Schröder, H. Schwarz, *Helv. Chim. Acta* **1995**, *78*, 1393; f) S. Shaik, M. Filatov, *J. Phys. Chem. A* **1998**, *102*, 3835.
- [47] a) C. L. Lasko, R. M. Miller, D. S. Tinti, *Chem. Phys. Lett.* **1986**, *130*, 359; b) R. M. Miller, D. S. Tinti, D. A. Case, *Inorg. Chem.* **1989**, *28*, 2738.
- [48] E. Buncel, S. S. Shaik, I.-H. Um, S. Wolfe, *J. Am. Chem. Soc.* **1988**, *110*, 1275.
- [49] I. M. Kovach, J. P. Elrod, R. L. Schowen, *J. Am. Chem. Soc.* **1980**, *102*, 7530.
- [50] D. G. Oakenfull, T. Riley, V. Gold, *J. Chem. Soc. Chem. Commun.* **1966**, 385; V. Gold, D. G. Oakenfull, T. Riley, *J. Chem. Soc. B* **1968**, 515.
- [51] J. K. Kochi, *Angew. Chem.* **1988**, *100*, 1331; *Angew. Chem. Int. Ed. Engl.* **1988**, *27*, 1227.
- [52] S. Fukuzumi, S. Koumitsu, K. Hironaka, T. Tanaka, *J. Am. Chem. Soc.* **1987**, *109*, 305; M. Ishikawa, S. Fukuzumi, *J. Chem. Soc. Faraday Trans.* **1990**, *86*, 3531.
- [53] E. Baciocchi, L. Mandolini, *Tetrahedron* **1987**, *43*, 4035.
- [54] For a discussion of ET mechanisms of ion radicals, see: L. Ebersson, S. S. Shaik, *J. Am. Chem. Soc.* **1990**, *112*, 4484. Note the different VB situation in comparison with ET between closed-shell reactants as depicted in Figure 30
- [55] L. Ebersson, *Electron Transfer Reactions in Organic Chemistry*, Springer, Berlin, **1987**.
- [56] a) J. W. Verhoeven, W. van Gerresheim, F. M. Martens, S. M. van der Kerk, *Tetrahedron* **1986**, *42*, 975; b) Y. Apeloig, O. Merin-Aharoni, D. Danovich, A. Ioffe, S. Shaik, *Isr. J. Chem.* **1993**, *33*, 387.
- [57] M. Patz, H. Mayr, J. Maruta, S. Fukuzumi, *Angew. Chem.* **1995**, *107*, 1351; *Angew. Chem. Int. Ed. Engl.* **1995**, *34*, 1225.
- [58] H. H. Cornehl, C. Heinemann, D. Schröder, H. Schwarz, *Organometallics* **1995**, *14*, 992.
- [59] M.-D. Su, *Inorg. Chem.* **1995**, *34*, 3829.
- [60] A. Pross, R. A. Moss, *Tetrahedron Lett.* **1990**, *31*, 4553.

- [61] S. Goldstein, G. Czapski, H. Cohen, D. Meyerstein, S. Shaik, *J. Chem. Soc. Faraday Trans.* **1993**, *89*, 4045.
- [62] S. Shaik, A. C. Reddy, A. Ioffe, J. P. Dinnocenzo, D. Danovich, J. K. Cho, *J. Am. Chem. Soc.* **1995**, *117*, 3205.
- [63] D. Cohen, R. Bar, S. S. Shaik, *J. Am. Chem. Soc.* **1986**, *108*, 231.
- [64] S. S. Shaik, P. C. Hiberty, J.-M. Lefour, G. Ohanessian, *J. Am. Chem. Soc.* **1987**, *109*, 363.
- [65] A. Demolliens, O. Eisenstein, P. C. Hiberty, J. M. Lefour, G. Ohanessian, S. S. Shaik, F. Volatron, *J. Am. Chem. Soc.* **1989**, *111*, 5623.
- [66] See the appendix to chapter 3 in ref. [4b], pp. 128–131.
- [67] L. Eberson, R. González-Luque, M. Merchán, F. Radner, B. O. Roos, S. Shaik, *J. Chem. Soc. Perkin Trans. 2* **1997**, 463.
- [68] An expression which conserves microscopic reversibility and can be derived from Equation (8), but is quite complex itself, is the following:
- $$\Delta E^{\ddagger} = \frac{(f_r + f_p)G_r G_p}{(G_r + G_p)} + 0.5 \Delta E_{\text{TP}} + x \Delta E_{\text{TP}}^2 - B$$
- $$x = \frac{(1 - f_r - f_p)}{(G_r + G_p)}$$
- Using mean values for both f and G , one obtains:
- $$\Delta E^{\ddagger} = f_{\text{av}} G_{\text{av}} + 0.5 \Delta E_{\text{TP}} + (0.5 - f_{\text{av}}) \frac{\Delta E_{\text{TP}}^2}{G_{\text{av}}} - B$$
- [69] a) S. S. Shaik, *Nouv. J. Chim.* **1983**, *7*, 201; b) S. S. Shaik, *J. Am. Chem. Soc.* **1983**, *105*, 4359.
- [70] a) S. S. Shaik, *Can. J. Chem.* **1986**, *64*, 96; b) S. S. Shaik, *Isr. J. Chem.* **1985**, *26*, 367.
- [71] G. Sini, Dissertation, Université de Paris-Sud, Orsay, France, **1991**.
- [72] a) B. D. Wladkowski, J. L. Wilbur, J. I. Brauman, *J. Am. Chem. Soc.* **1994**, *116*, 2471; b) B. D. Wladkowski, K. F. Lim, W. D. Allen, J. I. Brauman, *J. Am. Chem. Soc.* **1992**, *114*, 9136.
- [73] a) J. Hine, *J. Am. Chem. Soc.* **1950**, *72*, 2438; b) J. Hine, A. M. Dowell, Jr., *J. Am. Chem. Soc.* **1954**, *76*, 2688; c) J. Hine, C. H. Thomas, S. J. Ehrenson, *J. Am. Chem. Soc.* **1955**, *77*, 3886; d) J. Hine, S. J. Ehrenson, W. H. Brader, Jr., *J. Am. Chem. Soc.* **1956**, *78*, 2282.
- [74] a) R. F. Hudson, G. Klopman, *J. Chem. Soc.* **1962**, 1062; V. P. Vitullo, J. Grabowski, S. Sridharan, *J. Am. Chem. Soc.* **1980**, *102*, 6463; F. P. Ballistreri, E. Maccaroni, A. Mamo, *J. Org. Chem.* **1976**, *41*, 3364; b) S. D. Ross, M. Finkelstein, R. C. Petersen, *J. Am. Chem. Soc.* **1968**, *90*, 6411; A. Halvorsen, J. Songstad, *J. Chem. Soc. Chem. Commun.* **1978**, 327; c) C. Eaborn, J. C. Jeffery, *J. Chem. Soc.* **1954**, 4266; M. A. Cook, C. Eaborn, D. R. M. Walton, *J. Organomet. Chem.* **1971**, *29*, 389.
- [75] H. Mayr in *Cationic Polymerizations* (Ed.: K. Matyjaszewski), Marcel Dekker, New York, **1996**, chapter 2, p. 51.
- [76] S. S. Shaik, E. Canadell, *J. Am. Chem. Soc.* **1990**, *112*, 1446.
- [77] E. Canadell, O. Eisenstein, G. Ohanessian, J. M. Poblet, *J. Phys. Chem.* **1985**, *89*, 4856.
- [78] S. Shaik, A. C. Reddy, *J. Chem. Soc. Faraday Trans.* **1994**, *90*, 1631.
- [79] M. N. Glukhovtsev, A. Pross, L. Radom, *J. Am. Chem. Soc.* **1995**, *117*, 2024. The barrier datum for $X = \text{F}$ is used to obtain the f value, which is carried over to all other reactions.
- [80] G. Ohanessian, P. C. Hiberty, J.-M. Lefour, J.-P. Flament, S. S. Shaik, *Inorg. Chem.* **1988**, *27*, 2219.
- [81] Here $B = K_{\text{ab}}$ of the degenerate orbitals $\langle a |$ and $| b \rangle$, and the quantity $\Delta E(\Psi^* \rightarrow \Psi^*)$ in Figure 36 would be $2K_{\text{ab}}$.
- [82] M. G. Evans, E. Warhurst, *Trans. Faraday Soc.* **1938**, *34*, 614; M. G. Evans, *Trans. Faraday Soc.* **1939**, *35*, 824.
- [83] M. A. Robb, F. Bernardi in *New Theoretical Concepts for Understanding Organic Reactions*, Vol. C267 (Eds.: J. Bertrán, I. G. Csizmadia), Kluwer, Dordrecht, **1989**, pp. 101; F. Bernardi, M. Olivucci, M. A. Robb in *New Theoretical Concepts for Understanding Organic Reactions*, Vol. C267 (Eds.: J. Bertrán, I. G. Csizmadia), Kluwer, Dordrecht, **1989**, p. 147.
- [84] a) K. N. Houk, Y. Li, J. D. Evanseck, *Angew. Chem.* **1992**, *104*, 711; *Angew. Chem. Int. Ed. Engl.* **1992**, *31*, 682; b) K. N. Houk, J. González, Y. Li, *Acc. Chem. Res.* **1995**, *28*, 81; c) B. R. Beno, S. Wisley, K. N. Houk, *J. Am. Chem. Soc.*, in press. Note that the diradical in the Zewail experiment may originate in the excited state (K. N. Houk, private communication).
- [85] B. A. Horn, J. L. Herek, A. H. Zewail, *J. Am. Chem. Soc.* **1996**, *118*, 8755.
- [86] R. S. Mulliken, *J. Am. Chem. Soc.* **1952**, *74*, 811; R. S. Mulliken, *J. Phys. Chem.* **1952**, *56*, 801.
- [87] N. D. Epiotis, *Angew. Chem.* **1974**, *86*, 825; *Angew. Chem. Int. Ed. Engl.* **1974**, *13*, 751; N. D. Epiotis, *Theory of Organic Reactions*, Springer, Berlin, **1978**.
- [88] S. S. Shaik, J. P. Dinnocenzo, *J. Org. Chem.* **1990**, *55*, 3434.
- [89] L. Eberson, M. P. Hartshorn, F. Radner, M. Merchán, B. O. Roos, *Acta Chem. Scand.* **1993**, *47*, 176; L. Eberson, F. Radner, *Acta Chem. Scand.* **1992**, *46*, 312, 802.
- [90] J. P. Dinnocenzo, W. P. Todd, T. R. Simpson, I. R. Gould, *J. Am. Chem. Soc.* **1990**, *112*, 2462.
- [91] S. Shaik, A. C. Reddy, unpublished results.
- [92] a) G. N. Sastry, S. Shaik, *J. Am. Chem. Soc.* **1995**, *117*, 3290; b) G. N. Sastry, A. C. Reddy, S. Shaik, *Angew. Chem.* **1995**, *107*, 1619; *Angew. Chem. Int. Ed. Engl.* **1995**, *34*, 1495; c) G. N. Sastry, S. Shaik, *J. Phys. Chem.* **1996**, *100*, 12241.
- [93] N. Kimura, S. Takamuku, *J. Am. Chem. Soc.* **1994**, *116*, 4087; N. Kimura, S. Takamuku, *Bull. Chem. Soc. Jpn.* **1991**, *64*, 2433.
- [94] This system (see ref. [92c]) was suggested by J. P. Dinnocenzo during the sojourn of one of the authors (S.S.) on a sabbatical leave in the university of Rochester.
- [95] This system was suggested by M. Schmittel to one of the authors (S.S.) after his talk at the International Symposium of the Volkswagenstiftung on Intra- and Intermolecular Electron Transfer in Berlin, **1996**.
- [96] a) J. H. Incremona, C. J. Upton, *J. Am. Chem. Soc.* **1972**, *94*, 301; C. J. Upton, J. H. Incremona, *J. Org. Chem.* **1976**, *41*, 523; b) B. B. Jarvis, *J. Org. Chem.* **1970**, *35*, 924; c) G. G. Maynes, D. E. Applequist, *J. Am. Chem. Soc.* **1973**, *95*, 856; d) K. J. Shea, P. S. Skell, *J. Am. Chem. Soc.* **1973**, *95*, 6728; e) M. L. Poutsma, *J. Am. Chem. Soc.* **1965**, *87*, 4293.
- [97] a) The VBSCD selection rule is a product of the two interactions ($\phi_{\text{R}} - \sigma_{\text{CC}}$) and ($\phi_{\text{R}} - \sigma_{\text{CC}}^*$), and hence makes an unequivocal prediction. Frontier MO theory predicts that the sum of these interactions determines the regioselectivity. The sum behaves undecidedly for qualitative reasoning. If one of the interactions is more important than the other, it is not easy to decide which one would that be (see ref. [90]). b) M. Schmittel, C. Wöhrle, I. Bonn, *Chem. Eur. J.* **1996**, *2*, 1031.
- [98] S. Shaik in *Encyclopedia of Computational Chemistry*, Vol. 5 (Eds.: P. von R. Schleyer, N. L. Allinger, T. Clark, J. Gasteiger, P. A. Kollman, H. F. Schaefer III), Wiley, Chichester, pp. 3143–3159.
- [99] G. L. Fox, H. B. Schlegel, *J. Phys. Chem.* **1992**, *96*, 298.
- [100] a) D. Danovich, S. Shaik, *J. Am. Chem. Soc.* **1997**, *119*, 1773; b) S. Shaik, M. Filatov, D. Schröder, H. Schwarz, *Chem. Eur. J.* **1998**, *4*, 193.
- [101] A. Warshel, A. Papazyan, P. A. Kollman, *Science* **1995**, *269*, 102; W. W. Cleland, M. M. Kreevoy, *Science* **1995**, *269*, 104; P. A. Frey, *Science* **1995**, *269*, 104.
- [102] B. S. Ault, *Acc. Chem. Res.* **1992**, *15*, 103. The matrix-isolated hydrogen dihalide anions XHX^- ($\text{X} = \text{Cl}, \text{Br}, \text{I}$) are centrosymmetric or nearly so. The effect of the counterion is not clear though. Our computational results (QCISD/6-311++G(3p,3d)) for ClHCl^- suggest a very small barrier.
- [103] Essentially similar results have been recalculated by us using the BOVB theory described in references [6a,b].
- [104] This resonance energy is different than the B value for the corresponding VBSCD, which is evaluated as 32 kcal mol $^{-1}$ with respect to a Lewis reference structure.^[71, 78]
- [105] a) R. J. P. Corriu, M. Henner, *J. Organomet. Chem.* **1974**, *74*, 1; b) A. E. Reed, P. von R. Schleyer, *J. Am. Chem. Soc.* **1990**, *112*, 1434.
- [106] S. Harder, A. Streitwieser, J. T. Petty, P. von R. Schleyer, *J. Am. Chem. Soc.* **1995**, *117*, 3253.
- [107] a) R. Huisgen, *Acc. Chem. Res.* **1977**, *10*, 117, 199; b) J. Sauer, R. Sustmann, *Angew. Chem.* **1980**, *92*, 773; *Angew. Chem. Int. Ed. Engl.* **1980**, *19*, 779.
- [108] a) R. Sustmann, M. Rogge, U. Nüchter, H. Bandmann, *Chem. Ber.* **1992**, *125*, 1647; b) R. Sustmann, M. Rogge, U. Nüchter, J. Harvey, *Chem. Ber.* **1992**, *125*, 1665; c) M. Rese, M. Dern, K. Lücking, R. Sustmann, *Liebigs Ann.* **1995**, 1139; d) R. Sustmann, M. Rogge, U. Nüchter, H. Bandmann, *Chem. Ber.* **1992**, *125*, 1657; e) K. Lücking, M. Rese, R. Sustmann, *Liebigs Ann.* **1995**, 1129.
- [109] a) M. N. Glukhovtsev, A. Pross, L. Radom, *J. Am. Chem. Soc.* **1994**, *116*, 5961. Note that the large barrier for π attack at the substituted

- carbon atom was analyzed in ref. [63]. This larger π barrier tips the balance in favor of the S_N2 -type attack; b) T. Okuyama, M. Ochiai, *J. Am. Chem. Soc.* **1997**, 119, 4785.
- [110] H. Zipse, *J. Chem. Soc. Perkin Trans. 2* **1997**, 2691.
- [111] H. Zipse, *J. Am. Chem. Soc.* **1997**, 119, 1087, 2889; H. Zipse, *J. Chem. Soc. Perkin Trans. 2* **1996**, 1797.
- [112] B. Giese, X. Beyrich-Graf, J. Burger, C. Kesselheim, M. Senn, T. Schäfer, *Angew. Chem.* **1993**, 105, 1850; *Angew. Chem. Int. Ed. Engl.* **1993**, 32, 1742.
- [113] a) G. N. Sastry, D. Danovich, S. Shaik, *Angew. Chem.* **1996**, 108, 1208; *Angew. Chem. Int. Ed. Engl.* **1996**, 35, 1098; b) S. Shaik, D. Danovich, G. N. Sastry, P. Y. Ayala, H. B. Schlegel, *J. Am. Chem. Soc.* **1997**, 119, 9237; c) G. N. Sastry, S. Shaik, *J. Am. Chem. Soc.* **1998**, 120, 2131.
- [114] H. B. Schlegel, *J. Chem. Soc. Faraday Trans.* **1994**, 90, 1569; P. Valtazanos, K. Ruedenberg, *Theor. Chim. Acta* **1986**, 69, 281.
- [115] A. C. Reddy, D. Danovich, A. Ioffe, S. Shaik, *J. Chem. Soc. Perkin Trans. 2* **1995**, 1525.
- [116] F. Bernardi, M. Olivucci, M. Robb, *Isr. J. Chem.* **1993**, 33, 265.
- [117] U. Manthe, H. Köppel, *J. Chem. Phys.* **1990**, 93, 1669.
- [118] a) D. M. Cyr, G. A. Bishea, M. G. Scranton, M. A. Johnson, *J. Chem. Phys.* **1992**, 97, 5911; b) M. Lipson, A. A. Deniz, K. S. Peters, *J. Am. Chem. Soc.* **1996**, 118, 2992; c) H. Quast, K. Knoll, E.-M. Peters, K. Peters, H. G. von Schnering, *Chem. Ber.* **1993**, 126, 1047.

Deposition of Data from X-Ray Structure Analyses

In order to make life easier for authors and referees the Cambridge Crystallographic Data Centre (CCDC) and the Fachinformationszentrum Karlsruhe (FIZ) have unified their procedures for the deposition of data from single-crystal X-ray structure analyses.

Prior to submitting a manuscript please deposit the data for your compound(s) **electronically** at the appropriate data base, that is, at the CCDC for organic and organometallic compounds and at the FIZ for inorganic compounds. Both data bases will be pleased to provide help (see our *Notice to Authors* in the first issue of this year). In general, you will receive a depository number from the data base within two working days after electronic deposition; please include this number with the appropriate standard text (see our Notice to Authors) in your manuscript. This will enable the referees to retrieve the structure data quickly and efficiently if they need this information to reach their decision.

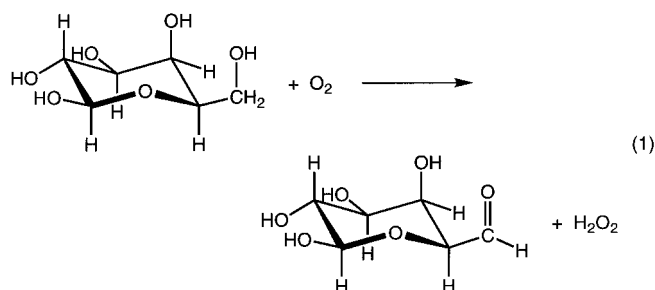
This is now the uniform procedure for manuscripts submitted to the journals *Advanced Materials*, *Angewandte Chemie*, *Chemistry—A European Journal*, *the European Journal of Inorganic Chemistry*, and *the European Journal of Organic Chemistry*.

What Can We Learn from Nature about the Reactivity of Coordinated Phenoxyl Radicals?—A Bioinorganic Success Story

Hans-Jörg Krüger*

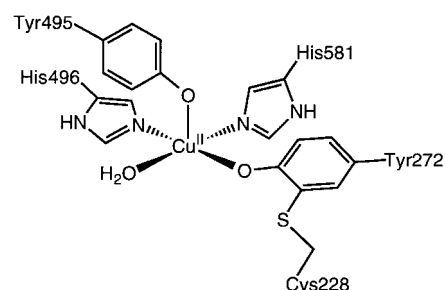
How does nature work on the molecular level? With respect to the function of metal ions in biology, the answer to this important question is intensively pursued by those researchers engaged in the highly interdisciplinary field of bioinorganic chemistry. Inorganic chemists can contribute considerably to the understanding of the structural, electronic, and mechanistic aspects of metal sites in metalloproteins by producing small coordination compounds which mimic the specific properties of those metal sites. Most model complexes concentrate on reproducing specific structural or electronic features; only a few models succeed in displaying stoichiometric or even catalytic reactivity similar to that of the enzymes. But very rarely are both structural *and* functional modeling characters found in a single complex. The latest success story in the development of biomimetic model complexes that mimic structural as well as catalytic aspects of the active sites in metalloproteins was written by Stack et al. with a model for the copper site in the enzyme galactose oxidase.^[1] Independently, a different catalytically functioning system was devised by the group of Wieghardt and Chaudhuri, based on the mechanistic principles of the same enzymatic reaction.^[2]

Galactose oxidase (GO)^[3] is a fungal enzyme that catalyzes the oxidation of galactose and a number of other primary alcohols to the corresponding aldehyde; a reaction in which dioxygen is reduced to hydrogen peroxide [Eq. (1)]. The



[*] Priv.-Doz. Dr. H.-J. Krüger
Institut für Anorganische und Angewandte Chemie der Universität
Martin-Luther-King-Platz 6, D-20146 Hamburg (Germany)
Fax: (+49) 40-41232893
E-mail: krueger@xray.chemie.uni-hamburg.de

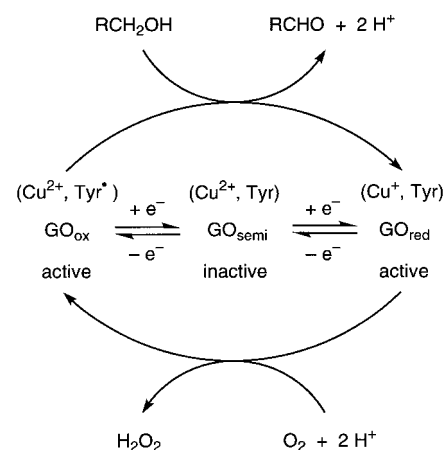
active site consists of a mononuclear copper ion in a square-pyramidal coordination geometry (Scheme 1).^[4] At a pH of 7.0, the copper ion is coordinated to two histidine residues (His496, His581), a tyrosinate residue (Tyr272), and a water



Scheme 1. Schematic view of the active site of galactose oxidase in the inactive state at pH 7.0.^[4]

molecule in the equatorial plane and to a further tyrosinate residue (Tyr495) in the apical position. A unique feature of this active site embodies the modification of the tyrosinate residue located in the equatorial plane by a covalent linkage to the sulfur atom of a nearby cysteine residue.

The mononuclear copper site can be present in three redox forms (Scheme 2); among those, only the fully oxidized and fully reduced redox states, GO_{ox} and GO_{red}, were identified as



Scheme 2. Redox states of galactose oxidase.

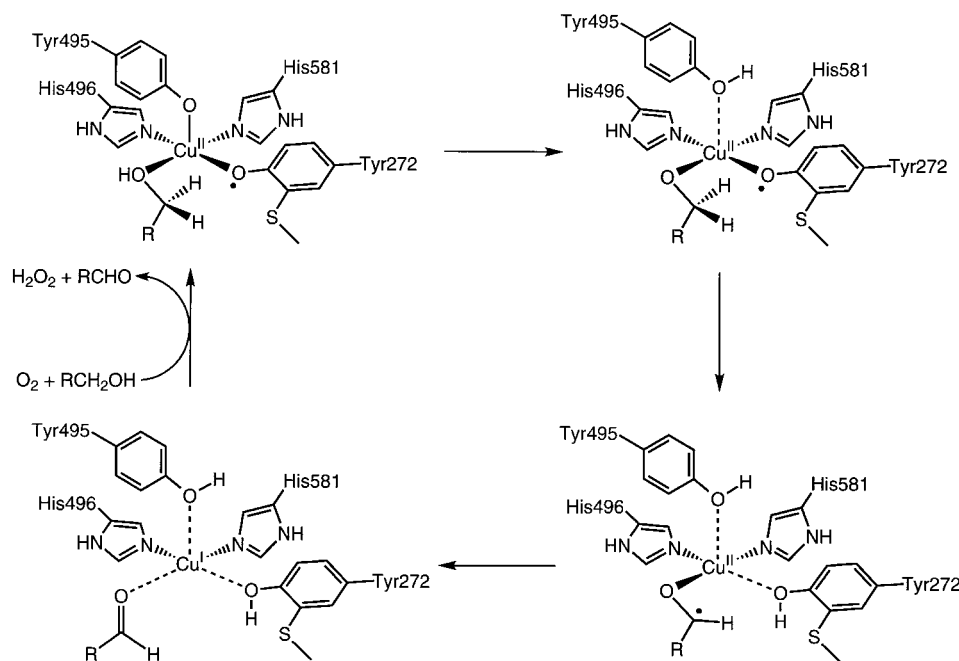
the catalytically active ones. For many years, these redox states were attributed to Cu^{I} , Cu^{II} , and Cu^{III} species, respectively. However, extensive spectroscopic studies of the diamagnetic, fully oxidized enzyme^[5] and the oxidation product of the metal-free apo-enzyme unambiguously established^[6] that the fully oxidized active site consists of a copper(II) ion antiferromagnetically coupled to a tyrosyl radical instead of the originally proposed copper(III) ion. The tyrosyl radical was determined to be derived from the equatorially bound, covalently modified Tyr272 residue.^[7] The covalent modification of the tyrosine residue is thought to ease the oxidation of the coordinated tyrosinate ligand. Also taking the large kinetic isotope effect $k_{\text{H}}/k_{\text{D}}$ ^[8] and the results from inhibitor studies into account,^[9] a radical-based mechanism was proposed for the oxidation of the primary alcohols.^[3a] Thus, the catalytic cycle (Scheme 3) starts with the binding of the galactose molecule to an equatorial coordination site of the copper(II) tyrosyl radical species and subsequent deprotonation of the alcohol, whereby the axial Tyr495 residue acts as the base.^[10] Then, in a rate-determining step, a hydrogen atom is abstracted from the C-6 methylene carbon atom of the galactose substrate by the tyrosyl radical. The resulting ketyl radical is oxidized to the aldehyde by an intramolecular electron transfer to the copper(II) ion. The original copper(II) tyrosyl radical species is restored by the oxidation of the copper(I) ion and the tyrosine residue with dioxygen, whereby hydrogen peroxide is formed. Interestingly, the reactivity of galactose oxidase serves as an excellent example of the involvement of protein radicals in enzyme catalysis—an emerging theme in the research of enzyme mechanisms which has gained considerable importance in recent years.^[3d]

At the time the coordination of a phenoxyl radical to a copper(II) ion was discovered in galactose oxidase, O-bound phenoxyl radical complexes were virtually unknown and

represented quite a synthetic challenge to inorganic chemists. Through the study of the redox chemistry of metal phenolate complexes,^[11, 12] criteria for the ligand were discerned that facilitate the preparation of such phenoxyl radical complexes. Thus, the phenoxyl radical moiety should be part of a multidentate ligand and should exhibit suitable bulky and oxidation-resistant substituents (e.g. *tert*-butyl or methoxy groups) in *ortho* and *para* position to the phenoxyl oxygen atom. Since the O-bound phenoxyl radical complexes are generally generated from the respective metal phenolate complexes by electrochemical or chemical oxidation, diagnostic tools for identifying the oxidation product as a coordinated phenoxyl radical complex needed to be developed. In addition to UV/Vis and ESR spectroscopy,^[11, 12] Resonance Raman^[13] and XANES spectroscopy^[1] have been proven to be very useful in this process. The study of the phenoxyl radical complexes provides new insights into the structural, electronic, and spectroscopic aspects of the coordination chemistry of phenoxyl radicals. For example, with the help of such structural model complexes for the active site in galactose oxidase, Wieghardt et al. were recently able to provide a plausible explanation for the occurrence of a strong intramolecular antiferromagnetic coupling between electron spins of the coordinated tyrosyl radical and the copper(II) ion in the enzyme.^[14] Despite the considerable progress made in synthesizing and characterizing structural model complexes for galactose oxidase, reactivity studies of phenoxyl radicals coordinated to copper(II) ions were scarcely reported presumably due to the instability of the copper(II) phenoxyl radical complexes at room temperature. This lack was recently alleviated by two remarkable studies which established high catalytic activities for the coordinated phenoxyl radicals of mono- and dinuclear copper(II) complexes.

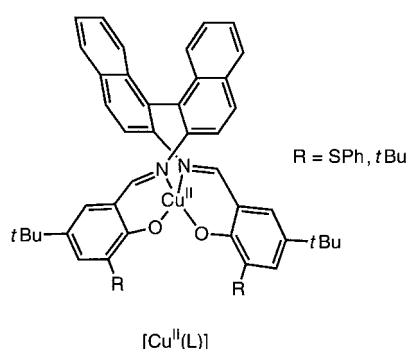
The strategy followed in the first study^[1, 15] to achieve an enzyme-like reactivity with small synthetic analogue-com-

plexes consists in reproducing the structural and electronic features of the active site of the enzyme as closely as possible; by this means, catalytic reactivity similar to that of the enzyme should be feasible if the protein matrix itself is not involved in crucial reaction steps of the enzymatic catalysis and/or if the ligand employed in the model study can imitate certain electronic or structural effects of the protein matrix onto the metal site pertinent to the reactivity. Using this approach Stack et al. prepared copper complexes with various diimine-diphenolate ligands. With respect to the type and the electronic properties of the ligand donor atom set, the two imine and the two phenolate donor groups resemble the first coordination shell of the copper site in the enzyme. Based on an



Scheme 3. Postulated reaction mechanism for galactose oxidase (adapted from Whittaker).^[3a]

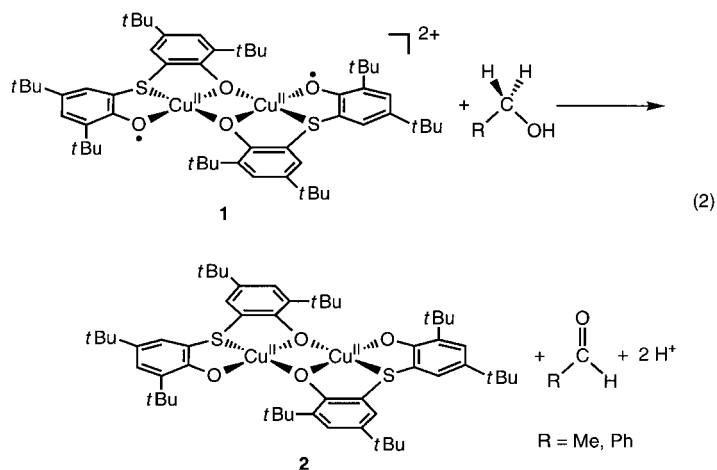
initial study by Kitajima et al.,^[16] Stack et al. realized that, for the catalytic reactivity to occur, a nonplanar coordination environment is needed at the copper ion. Thus, they chose to incorporate a binaphthyl unit in the backbone of the ligand to enforce distortion of the square-planar coordination geometry (which is preferred by copper(II) ions) towards a tetrahedral geometry. This distortion is regarded as a way to increase the stability of the corresponding copper(I) species and to facilitate the coordination of a fifth ligand (i.e. the alcoholate substrate) to the copper(II) ion; both effects are considered to be critical in a catalytic mechanism. Further, in accordance with the results previously obtained from the investigation of structural model complexes, appropriate *ortho* and *para* substituents at the phenolate rings are implanted in order to stabilize the copper(II)-phenoxyl radical species. And indeed, with this type of ligands, Stack et al. were able to synthesize nonplanar copper(II) complexes [Cu(L)] from which they could obtain the corresponding copper(I) complexes [Cu(L)]⁻ and relatively stable phenoxyl-radical copper(II) complexes [Cu(L•)]⁺ by reduction and oxidation, respectively. The three



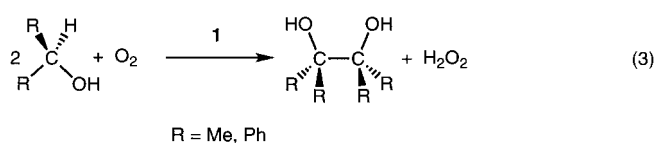
complexes can act as a catalyst or as a precursor for a catalyst in the reaction of benzylic and allylic alcohols with molecular oxygen at room temperature, yielding the respective aldehyde and hydrogen peroxide. Turnover numbers as high as 1300 are reported for the catalytic cycles. Most noteworthy, the catalytic oxidation seems to proceed by the same mechanism as the enzyme-catalyzed reaction. For example, as in the enzyme, the copper(II) phenolate complex [Cu(L)] is not judged to be involved in the catalytic mechanism because an induction period is observed in which this precursor complex is converted to the catalytically active copper(II) phenoxyl-radical species, while no induction periods occur in the catalytic reactions with the other two copper complexes. A comparison of the catalytic performance of the copper complexes with the various ligands demonstrates that the introduction of a thioether function in *ortho* position to the hydroxy function on the phenol units of the ligand L is not essential for the catalytic reactivity, but does improve the number of achieved catalytic turnovers. In contrast to the enzymatic reaction, simple aliphatic primary alcohols are found to be unreactive under these conditions. This lack of reactivity, however, makes it possible to generate a five-coordinate methoxide adduct from the copper(II) phenoxyl radical complex, thereby providing evidence for the participation of an analogous five-coordinate copper benzylalcoholate species as an intermediate in the catalytic cycle. In

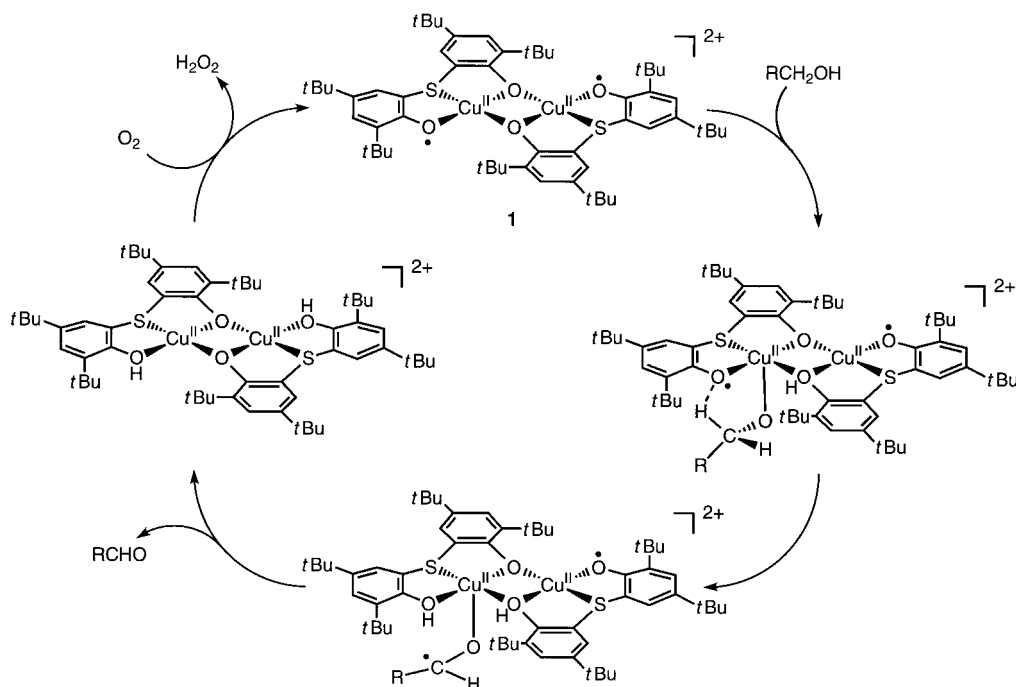
summary, the work by Stack et al. has demonstrated in a very impressive and elegant way how the reactivity of an active site in an enzyme can be mimicked by small synthetic inorganic complexes (albeit with slower rates and with a different selectivity) by modeling the structural features of this active site as closely as possible. Essentially they succeeded in making a low-molecular-weight copy of the active site of an enzyme.

More recently, the group of Wieghardt and Chaudhuri produced a second catalytic system employing the ligand 2,2'-thiobis(2,4-di-*tert*-butylphenol).^[2] Rather than attempting to reproduce all structural features of the active site of galactose oxidase, they sought with their model to incorporate only those features that are essential to the reactivity in the enzyme. The catalytically active species was recognized as the bis(phenolato)-bridged dicopper(II) complex **1**, in which each copper ion is further coordinated to a phenoxyl radical. In the stoichiometric reaction of **1** with ethanol under anaerobic conditions, a dicopper(II) complex **2** and acetaldehyde is formed [Eq. (2)]. The original complex **1** can be regenerated



by reaction with dioxygen, which is concomitantly converted to hydrogen peroxide. Using catalytic amounts of **1** in tetrahydrofuran under an atmosphere of air at 20°C, ethanol is converted to acetaldehyde in a 63% yield after 12 h of reaction time resulting in 630 turnovers of the catalytic cycle. No further oxidation of the acetaldehyde to acetic acid nor any disproportionation of the formed hydrogen peroxide is detected. But in addition to the acetaldehyde, minor amounts (< 5% each) of 2,3-dihydroxybutane, 3-hydroxy-2-butanone, and 2,3-butanedione are formed. Similar results were observed for the corresponding reaction with benzylalcohol. Secondary alcohols like isopropyl alcohol and diphenylcarbinol are catalytically converted with **1** to the corresponding glycol derivatives in up to 68% yields [Eq. (3)]; formation of the corresponding ketones was not observed. Based on kinetic studies of the reactions, the authors postulated a catalytic reaction cycle for the oxidation of primary alcohols





Scheme 4. Postulated mechanism for the catalytic oxidation of primary alcohols by the dinuclear complex **1**.^[2]

(Scheme 4) in which an alcoholate ion first binds to one of the copper(II) ions at the axial coordination site. After the rate-limiting hydrogen atom-abstraction reaction has taken place, the resulting ketyl radical is converted to the corresponding aldehyde in an intramolecular electron transfer step. Subsequent oxidation of the coordinated phenol ligands by dioxygen to the phenoxyl radicals regenerates the original catalyst. The difference in products resulting from the oxidation of secondary alcohols is explained by an amendment to the postulated reaction mechanism which states that two alcoholate ions instead of one bind to the two copper ions in a *syn*-facial way and that C–C bond formation takes place between the two resulting coordinated ketyl radicals.

The catalytically active species reported by Wieghardt and Chaudhuri distinguishes itself from the active site in galactose oxidase and from the model complexes of Stack et al. in that it is a dinuclear copper(II) complex with two coordinated phenoxyl radicals, that the coordination geometry at each copper(II) ion is presumably square planar, and that no copper(I) intermediate is involved in the catalytic mechanism. In contrast to the mononuclear model complexes, the dicopper compound can catalyze the oxidation of simple aliphatic primary and secondary alcohols to aldehyde and glycol derivatives, respectively. Although the dinuclear catalyst does not bear any close structural resemblance to the active site of galactose oxidase, it displays a reactivity similar to that of the enzyme because the two fundamental attributes of the enzyme for achieving reactivity have been realized in this synthetic copper complex, namely the presence of a stable phenoxyl radical coordinated to a copper(II) ion and the possibility that the complex can carry out two-electron redox chemistry.

The main objective of bioinorganic research is to learn from nature about the basic principles governing reactivity in a

biological system. Chemistry can benefit considerably from this study, since, by applying these principles to small synthetic molecules, novel synthetic methods will be at the disposal of chemists, and new catalysts, which may no longer bear any close structural resemblance to the active site in the enzyme but use the same rationale for the reactivity as the enzyme, can be developed with properties more suitable for practical purposes (e.g. better long-term stability, wider range of application) than the metalloprotein itself. In this context, the study of galactose oxidase will, in my opinion, become a textbook example for how bioinorganic research, working on

a highly interdisciplinary level, can give answers to the question of how nature works on the molecular level, thereby breaking new ground in chemistry. In addition to establishing the novel coordination chemistry of phenoxyl radical, two distinct inorganic complexes which very efficiently catalyze the oxidation of alcohols to aldehyde by dioxygen under mild and environmentally friendly conditions have resulted from this research. This feat provides confidence that similar achievements in the biomimetic studies of the active sites of other metalloproteins will be forthcoming.

German version: *Angew. Chem.* **1999**, *111*, 659–663

Keywords: bioinorganic chemistry • copper • galactose oxidase • oxidations • radicals

- [1] Y. Wang, J. L. DuBois, B. Hedman, K. O. Hodgson, T. P. D. Stack, *Science* **1998**, *279*, 537.
- [2] P. Chaudhuri, M. Hess, U. Flörke, K. Wieghardt, *Angew. Chem.* **1998**, *110*, 2340; *Angew. Chem. Int. Ed.* **1998**, *37*, 2217.
- [3] For recent reviews see: a) J. W. Whittaker in *Metal Ions in Biological Systems*, Vol. 30 (Eds.: H. Sigel, A. Sigel), Marcel Dekker, New York, **1994**, p. 315; b) P. F. Knowles, N. Ito in *Perspectives in Bio-inorganic Chemistry*, Vol. 2, Jai Press, London, **1994**, p. 207; c) J. P. Klinman, *Chem. Rev.* **1996**, *96*, 2541; d) J. Stubbe, W. A. van der Donk, *Chem. Rev.* **1998**, *98*, 705.
- [4] a) N. Ito, S. E. V. Phillips, C. Stevens, Z. B. Ogel, M. J. McPherson, J. N. Keen, K. D. S. Yadav, P. F. Knowles, *Nature* **1991**, *350*, 87; b) N. Ito, S. E. V. Phillips, K. D. S. Yadav, P. F. Knowles, *J. Mol. Biol.* **1994**, *238*, 794.
- [5] M. M. Whittaker, J. W. Whittaker, *J. Biol. Chem.* **1988**, *263*, 6074.
- [6] M. M. Whittaker, J. W. Whittaker, *J. Biol. Chem.* **1990**, *265*, 9610.
- [7] a) M. M. Whittaker, Y.-Y. Chuang, J. W. Whittaker, *J. Am. Chem. Soc.* **1993**, *115*, 10029; b) G. T. Babcock, M. K. El-Deeb, P. O. Sandusky, M. M. Whittaker, J. W. Whittaker, *J. Am. Chem. Soc.* **1992**, *114*, 3727;

- c) G. J. Gerfen, B. F. Bellew, R. G. Griffin, D. J. Singel, C. A. Ekberg, J. W. Whittaker, *J. Phys. Chem.* **1996**, 100, 16739.
- [8] A. Maradufu, G. M. Cree, A. S. Perlin, *Can. J. Chem.* **1971**, 49, 3429.
- [9] a) R. M. Wachter, M. P. Montague-Smith, B. P. Branchaud, *J. Am. Chem. Soc.* **1997**, 119, 7743; b) B. P. Branchaud, M. P. Montague-Smith, D. J. Kosman, F. R. McLaren, *J. Am. Chem. Soc.* **1993**, 115, 798.
- [10] a) M. P. Reynolds, A. J. Baron, C. M. Wilmot, S. E. V. Phillips, P. F. Knowles, M. J. McPherson, *J. Biochem. Soc. Trans.* **1995**, 23, 510S; b) M. M. Whittaker, J. W. Whittaker, *Biophys. J.* **1993**, 64, 762.
- [11] For mononuclear phenoxyl radical complexes with cupric ions see: a) J. A. Halfen, B. Jazdzewski, S. Mahapatra, L. M. Berreau, E. C. Wilkinson, L. Que, Jr., W. B. Tolman, *J. Am. Chem. Soc.* **1997**, 119, 8217; b) A. Sokolowski, H. Leutbecher, T. Weyhermüller, R. Schnepf, E. Bothe, E. Bill, P. Hildebrandt, K. Wieghardt, *J. Biol. Inorg. Chem.* **1997**, 2, 444; c) D. Zurita, I. Gautier-Luneau, S. Menage, J.-L. Pierre, E. Saint-Aman, *J. Biol. Inorg. Chem.* **1997**, 2, 46; d) S. Itoh, S. Takayama, R. Arakawa, A. Furuta, M. Komatsu, A. Ishida, S. Takamuku, S. Fukuzumi, *Inorg. Chem.* **1997**, 36, 1407; e) J. A. Halfen, V. G. Young, W. B. Tolman, *Angew. Chem.* **1996**, 108, 1832; *Angew. Chem. Int. Ed. Engl.* **1996**, 35, 1687.
- [12] For mononuclear phenoxyl radical complexes with non-cupric ions see: a) A. Sokolowski, J. Müller, T. Weyhermüller, R. Schnepf, P. Hildebrandt, K. Hildenbrand, E. Bothe, K. Wieghardt, *J. Am. Chem. Soc.* **1997**, 119, 8889; b) B. Adam, E. Bill, E. Bothe, B. Goerd, H. Haselhorst, K. Hildenbrand, A. Sokolowski, S. Steenken, T. Weyhermüller, K. Wieghardt, *Chem. Eur. J.* **1997**, 3, 308; c) A. Sokolowski, E. Bothe, E. Bill, T. Weyhermüller, K. Wieghardt, *J. Chem. Soc. Chem. Commun.* **1996**, 1671; d) J. Hockertz, S. Steenken, K. Wieghardt, P. Hildebrandt, *J. Am. Chem. Soc.* **1993**, 115, 11222.
- [13] R. Schnepf, A. Sokolowski, J. Müller, V. Bachler, K. Wieghardt, P. Hildebrandt, *J. Am. Chem. Soc.* **1998**, 120, 2352.
- [14] J. Müller, T. Weyhermüller, E. Bill, P. Hildebrandt, L. Ould-Moussa, T. Glaser, K. Wieghardt, *Angew. Chem.* **1998**, 110, 637; *Angew. Chem. Int. Ed.* **1998**, 37, 616.
- [15] Y. Wang, T. D. P. Stack, *J. Am. Chem. Soc.* **1996**, 118, 13097.
- [16] N. Kitajima, K. Whang, Y. Moro-oka, A. Uchida, Y. Sasada, *J. Chem. Soc. Chem. Commun.* **1986**, 1504.

Nonsteroidal Antiinflammatory Drugs: A New Generation of Cyclooxygenase Inhibitors**

Martin Beuck*

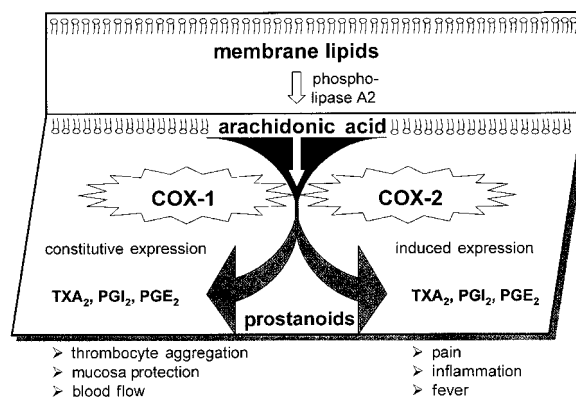
Aspirin®—or acetylsalicylic acid—is synonymous for first aid relief of pain, fever, and inflammation. The 100-year-old and most popular drug is facing new competition. Not simply another compound, but a whole new class with a different spectrum of activities give potential access to indications outside of pain and inflammation.

Therapeutic Basis

The therapeutic effect of acetylsalicylic acid is based on a covalent modification of cyclooxygenase and the inhibition of the first step of prostaglandin synthesis, shown first by Sir John Robert Vane.^[1] Cyclooxygenase (COX) exists in two isoforms, COX-1 and COX-2. Serine residue 530 of COX-1 and serine residue 516 of COX-2 are modified by acetylation. Inhibition of COX-1 or COX-2 leads to very different pharmacological effects. The COX-1 inhibition is predominantly responsible for anti-thrombotic effects, while anti-inflammatory effects are mediated mainly through COX-2.

The cyclooxygenase COX-1 is expressed constitutively in all tissues, and is thus always present and active. As far as it is known, this is the case for COX-2 only in kidney, brain, and ovaries. During inflammatory processes COX-2 is increas-

ingly expressed in affected tissues, and consequently production of the pain-mediating prostaglandins is also increased (Scheme 1).



Scheme 1. Role of COX-1 and COX-2 in arachidonic acid metabolism. COX-1/2: cyclooxygenase-1/2; TXA₂: thromboxan A₂; PGI₂: prostacyclin; PGE₂: prostaglandin E₂.

In contrast to self medication of mild headaches and malaise, therapy of pain, for example that caused by rheumatoid arthritis, was treated with high doses of acetylsalicylic acid in the past. This led to undesirable gastrointestinal side effects. These effects in the gastrointestinal tract were mainly mediated by COX-1. Inhibition of COX-1 impairs the synthesis of prostanoids, which have a protective effect on gastric mucosa.

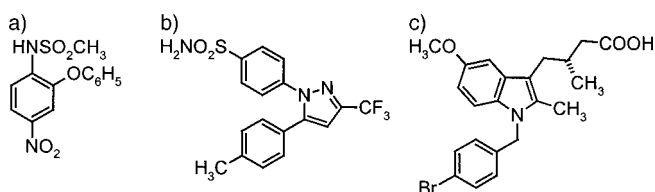
[*] Dr. M. Beuck
Bayer AG, Business Group Pharma, PH-R CSP
Aprather Weg 18a, 42096 Wuppertal (Germany)
Fax: (+49)202-36-4064
E-mail: martin.beuck.mb2@bayer-ag.de

[**] I would like to thank Dr. Dieter Neuser for his support and the fruitful discussions.

Consequently, a strategy to change selectivity towards COX-2-specific inhibitors was followed, leading to novel pain killers without the risk of the known side effects.

New Generations of COX Inhibitors

The currently known COX-2 inhibitors can be divided into three categories:^[2] 1) methanesulfoanilides (e.g. Nimesulide, Scheme 2 a), 2) methylsulfonyl/sulfonamide-substituted tricycles (e.g. Celecoxib, Scheme 2 b), 3) analogues based on nonselective inhibitors (e.g. analogues of indomethacine, Scheme 2 c).



Scheme 2. a) Nimesulide: a first-generation COX-2 inhibitor; b) Celecoxib: a second-generation COX-2 inhibitor; c) the indomethacin analogue L-761,066: a nonselective COX-2 inhibitor.

First concepts for the development of highly specific COX-2 inhibitors for the treatment of rheumatoid arthritis and osteoarthritis are currently being pursued by Monsanto and Merck & Co, and are in advanced stages of clinical development (Table 1). On the market are Meloxicam and in some countries Nimesulide, a COX-2 inhibitor of the first generation which has about a 10- to 20-fold higher affinity for COX-2. The second-generation compounds in clinical development show a 300- to 400-fold (Vioxx/Celebra) higher affinity for COX-2. It is expected that the late followers of second-generation products will have a further 10-fold increased selectivity.

So far clinical studies for arthritis seem to show an equivalent effect. Gastrointestinal side effects were not observed, at least within the very short period of investigation of about a week.

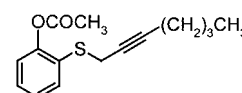
Compounds in clinical development are selective and generally reversibly binding inhibitors of COX-2. Reversibility, however, is limited by the dissociation kinetics of the COX-2 enzyme–inhibitor complex.^[3] After initial binding of the inhibitors to the enzyme a change of conformation in the COX-2 enzyme seems to slow down dissociation of the inhibitor from the enzyme, leading to apparently irreversible binding characteristics.

Table 1. Inhibitors of COX-2 in clinical development.^[a]

COX-2 inhibitor	Company	Status	Indications
Meloxicam	Boehringer Ingelheim	marketed	rheumatoid arthritis, osteoarthritis, spondylitis ankylosans
Nimesulide	Helsinn	marketed	inflammation, fever, rheumatoid arthritis, pain
Celecoxib (Celebra)	Monsanto	phase III	rheumatoid arthritis, osteoarthritis
MK966 (Vioxx)	Merck & Co.	phase III	rheumatoid arthritis, osteoarthritis
JTE522	Japan Tobacco	phase II	rheumatoid arthritis, osteoarthritis
T-614	Toyama	phase II	rheumatoid arthritis
SC-57666	Monsanto	phase I	rheumatoid arthritis
S-2474	Shionogi	phase I	arthritis
GR253035	Glaxo Wellcome	phase I	Alzheimer's disease, chronic inflammatory pain caused by osteoporosis, rheumatoid arthritis

[a] Source: *Pharmaprojects*, PJB Publications, Richmond, Surrey (UK).

The first selective COX-2 inhibitors to show irreversible binding were presented recently by Kalgutkar et al.^[4] They describe a new series of compounds with selectivity for COX-2 in combination with a covalent modification of the enzyme, as observed for acetylsalicylic acid. Chemically these compounds belong to a group of acetoxybenzenes that are substituted with alkyl sulfides. The result of the work is significant, as the best compound shows a 20-fold higher selectivity for COX-2 than for COX-1. This is about the level of first-generation noncovalently binding COX-2 inhibitors. Systematic variation led to *o*-(acetoxyphenyl)heptynyl sulfide (APHS, Scheme 3), the most potent compound of this series. With an IC₅₀ value of 0.8 μM for COX-2 and 17 μM for COX-1, APHS is not yet a highly specific and selective inhibitor. However, it is a starting point, and first results from in vitro and in vivo models confirm this. In a rat inflammation model APHS reduced synthesis of prostaglandin E₂ by 95 % at 5 mg kg⁻¹, while COX-1-mediated synthesis of thromboxan B₂ was not affected.



Scheme 3. *o*-(Acetoxyphenyl)hept-2-ynyl sulfide (APHS):^[4] the first covalently binding COX-2 inhibitor.

New Indications for COX-2 Inhibitors

New studies from the last two years revealed that in addition to arthritis and pain, cancer and neurodegenerative diseases like Alzheimer's disease could potentially be treated with COX-2 inhibitors. In rats^[5] it could be shown that Celecoxib (Monsanto) reduced azoxymethan-induced colon cancer by more than 90 % within the observation period of about a year (50 weeks). Induction of COX-2 expression in these cells was already clear from preceding in vitro experiments.

The molecular mechanism currently under discussion is based on the assumption that COX-2 inhibition leads to a shift in the ratio of cell proliferation and apoptosis. Apoptosis is controlled cell death and can be initiated by *N*-acylsphingosine, which is produced from sphingosine and arachidonic acid. Inhibition of COX-2 results in an enlarged pool of arachidonic acid, thus favoring apoptosis.

Consequently, current studies are designed to show whether Celecoxib is able to reduce formation of colon cancer in humans or to stop further progression of preneoplastic lesions to cancer. If this is a class effect based on the mechanism, one would expect similar results with other COX-2 inhibitors in clinical development. Furthermore, epidemiological studies

suggest that acetylsalicylic acid could also be effective in this indication.^[6]

The relevance of COX-2 in the progression of Alzheimer's disease is also currently being discussed. It is believed that neuronal cells show increased expression of COX-2 upon stress,^[7] and subsequently start the apoptotic process in concert with other highly regulated genes (*c-jun*, *c-fos*, and *fos-B*). It may also be that the effect is mediated through inhibition of other inflammatory components (platelet-activating factor, interleukin-1 β), which are believed to play a role in the development of Alzheimer's disease.

In conclusion, the present models describing the profile of COX-2 inhibitors are not complete. On one hand (cancer) apoptosis is induced by COX-2 inhibition, and on the other hand apoptosis is prevented, like in neuronal cells. Irrespective of the final outcome of molecular pharmacology studies, first of all it is important that this new therapeutic approach gives rise to new prospects for patients. The therapeutical value now needs to be shown in clinical studies.

Conclusion

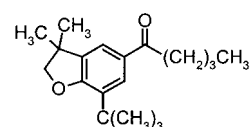
The current paper is focused less on the specific effect of COX-2 inhibitors, but rather on the expectations from this new drug class to achieve a significantly improved profile of side effects. Up to now the clinical results seem to confirm these expectations, at least with respect to the protection of the gastrointestinal mucosa. An exception is treatment of patients with preexisting ulcers. Their healing process is worsened under therapy with COX-2 inhibitors.

We will have to wait and see whether other side effects will show up after long-term therapy. Because COX-2 is expressed constitutively in kidney, brain, and ovaries, toxic effects on kidney, central nervous system (CNS) side effects, and fertility interferences cannot be excluded.

At this point in time it is hard to predict which other additional therapeutic advantages the covalent binding of inhibitors from Kalgutkar et al. might have. This is particularly difficult because of the virtually irreversible binding characteristics of the current COX-2 inhibitors.

Alternative Approaches

Other than COX-2 inhibition there are currently two approaches pursued in order to better control side effects. Procter & Gamble^[8] is following a strategy of dual inhibitors for cyclooxygenase and lipoxygenase. The rationale is that the component with the detrimental effect on gastric mucosa is leukotriene B₄, which is a product of arachidonic acid and 5-lipoxygenase. The lead structures identified belong to a series of 5-substituted dihydromethylbenzofurans (Scheme 4).



Scheme 4. 7-*tert*-Butyl-2,3-dihydro-3,3-dimethyl-5-pentanylbenzofuran:^[2] a dual COX-2 and 5-lipoxygenase inhibitor.

They represent a new class of antiinflammatory and analgesically active compounds. Inhibitory constants for cyclooxygenase are in the sub-micromolar range; the value for 5-lipoxygenase is still in the range of 3–15 μ M. To test the pharmacological concept, improvements of about 10- to 100-fold are necessary.

A second strategy envisages synthesis of NO-acetylsalicylic acid; that is, the acetylsalicylic acid is further substituted with a NO donor group. Release of NO in the gastrointestinal tract would lead to a local relaxation of the blood vessel with lower adhesion of leukocytes. This would improve protection of the mucosa and reduce haemorrhagic effects.^[9] Positive in vitro and in vivo results are available. Further preclinical and clinical investigations will demonstrate the therapeutic benefits, or lack thereof, compared to acetylsalicylic acid.

Outlook

Are COX-2 inhibitors better than Aspirin? The question suggests that these compounds are comparable. However, this is only partially true. Inhibitors of COX-2 represent a new therapeutic principle with prospects for the treatment of severe pain caused by rheumatic diseases or osteoarthritis. They are expected to take a significant part of this market. Already today acetylsalicylic acid is mainly used for myocardial infarct prophylaxis and moderate pain, such as that caused by headache. Dosage is low and gastrointestinal side effects do not play a major role for either indication. The spectrum of effects for acetylsalicylic acid is broader than just inhibition of COX-2. Other indications will potentially be added in the future, like prophylaxis and/or treatment of colon cancer or Alzheimer's disease. Acetylsalicylic acid has a fair chance to compete with COX-2 inhibitors. The advancement of NO-acetylsalicylic acid through clinical studies would be a welcome development indeed. The unique strength of acetylsalicylic acid is its pharmacologically nonselective behavior and lack of specificity for a single target. It is the portfolio of different properties that makes acetylsalicylic acid such a unique drug. In contrast COX-2 inhibitors cover only part of this spectrum and are rather considered to be experts in their respective field.

It is tempting to compare this situation with sports: acetylsalicylic acid would be the favorite in the decathlon, while COX-2 inhibitors would be competitive in two or three disciplines.

German version: *Angew. Chem.* **1999**, *111*, 663–666

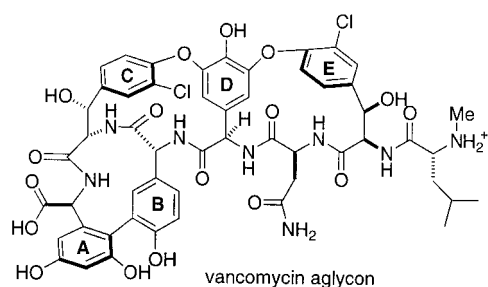
Keywords: acetylsalicylic acid • arthritis • cyclooxygenases • rheumatism

- [1] a) J. R. Vane, *Nature* **1971**, *231*, 232–235; b) J. R. Vane, *Angew. Chem.* **1983**, *95*, 782–794; *Angew. Chem. Int. Ed. Engl.* **1983**, *22*, 741–752.
- [2] J. S. Carter, *Exp. Opin. Ther. Patents* **1997**, *8*, 21–29.
- [3] M. Quillet, *Biochem. J.* **1995**, *305*, 247–251.
- [4] A. S. Kalgutkar, B. C. Crews, S. W. Rowlinson, C. G. Garner, K. Seibert, L. J. Marnett, *Science* **1998**, *280*, 1268–1270.
- [5] T. Kawamori, C. V. Rao, K. Seibert, B. S. Reddy, *Cancer Res.* **1998**, *58*, 409–412.
- [6] M. J. Thun, *Drug Discovery Today* **1996**, *1*, 495–496.
- [7] H. M. Tucker, R. E. Rydel, S. Wright, S. Estus, *J. Neurochemistry* **1998**, *71*, 506–516.
- [8] J. M. Janusz, P. A. Young, J. M. Ridgeway, M. W. Scherz, K. Enzweiler, L. I. Wu, L. Gan, R. Darolia, R. S. Matthews, D. Hennes, D. E. Kellstein, S. A. Green, J. L. Tulich, T. Rosario-Jansen, I. J. Magrisso, K. R. Wehmeyer, D. L. Kuhlbeck, T. H. Eichold, R. L. M. Dobson, S. P. Sirko, R. W. Farmer, *J. Med. Chem.* **1998**, *41*, 1112–1123.
- [9] J. L. Wallace, W. McKnight, T. L. Wilson, P. DelSoldato, G. Cirino, *Am. J. Physiol. Gastrointest. Liver Physiol.* **1997**, *36*, G1246–G1251.

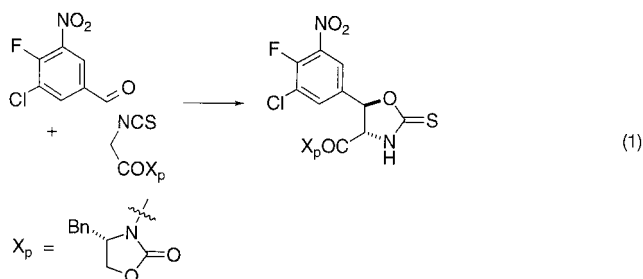
Total Syntheses of Vancomycin**

Alex J. Zhang, and Kevin Burgess*

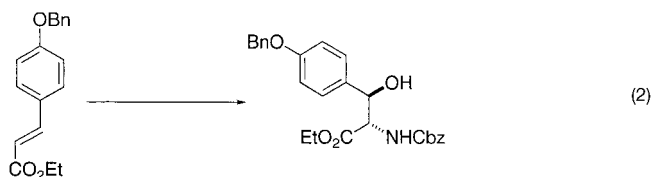
Five consecutive papers in this journal recently described two syntheses of the vancomycin aglycon. D. A. Evans and co-workers developed one route at Harvard University,^[1, 2] while the other stemmed from K. C. Nicolaou's group at the Scripps Research Institute in La Jolla, California.^[3–5] The syntheses represent an amalgamation of synthetic methodologies in schemes that took some of the most skillful bench chemists in academia years to execute. The comparisons and contrasts in the two approaches used are discussed herein.



Stereoselective syntheses of several unnatural amino acids were required to initiate this work. Evans' group used asymmetric reactions of chiral enolates to generate these starting materials [Eq. (1); Bn = benzyl]. In this particular example, an isothiocyanate functionality traps the alcohol of an aldol product giving a thioxazolidinone that provides O- and N-protection in subsequent steps.



Nicolaou's group initiated their project to prepare vancomycin after many routes to the requisite amino acids had been published. They could have made their building blocks by repeating and/or modifying published procedures, but instead chose to develop new approaches or rely on those of colleagues at the Scripps Institute. One such example features Sharpless' aminohydroxylation methodology [Eq. (2); Cbz = carbobenzyloxy = benzyloxycarbonyl].^[6]



A major obstacle to synthesis of the vancomycin aglycon has been construction of the fused macrocyclic ring systems with generation of the correct atropisomers. The two groups overcame this in different ways (Schemes 1 and 2, respectively). Evans' group began by forming the macrocycle encapsulating the **AB** biaryl functionality; for this they used an oxidative coupling developed almost ten years ago.^[7] A S_NAr reaction was then used to form the biaryl ether linkage between rings **C** and **D**, thus for the formation of the **C-O-D** ring.^[8] This cyclization reaction also set one of the amide bonds in the **AB** ring into its required *cis*-orientation.

Scheme 2 indicates that, unlike the Evans' approach, the Nicolaou group constructed the **C-O-D** ring *before* the **AB** system. They used their copper-mediated coupling methodology, involving a triazine ligating group, to form the ether linkage in the first macrocyclization. Unfortunately, this step gave no significant selectivity with respect to the atropisomer formed, hence separation of diastereomeric products was necessary. The precursor to the **AB** ring contained an amino acid with a preformed (Suzuki) **AB** biaryl fragment. Cyclization to form the **AB** ring system was accomplished by a macrolactamization reaction.

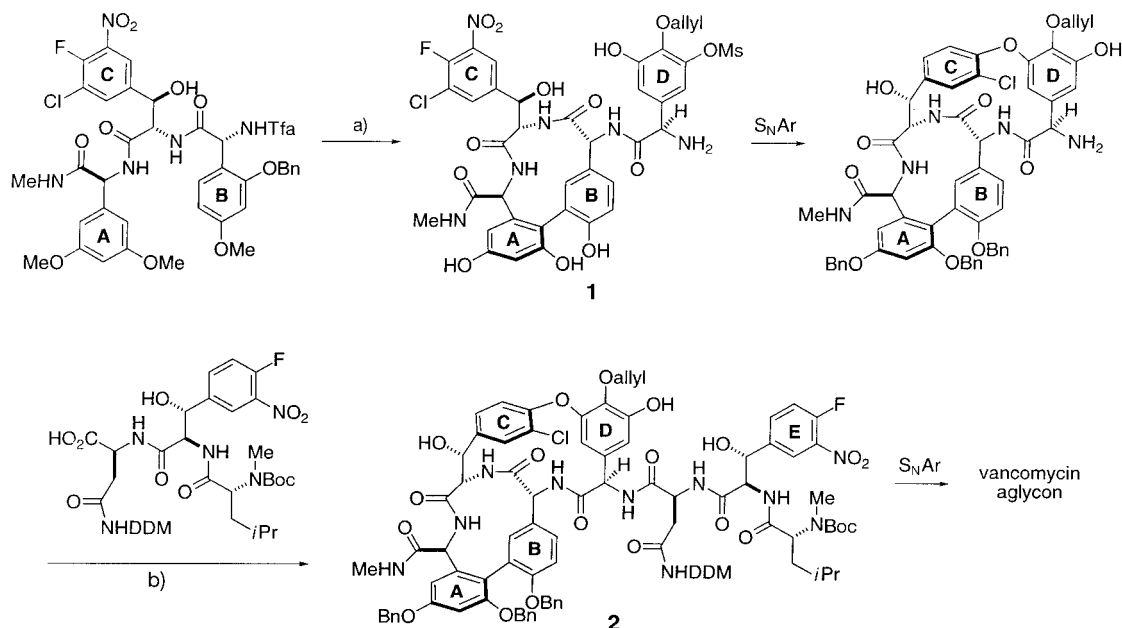
Another significant difference in the two syntheses relates to the C-terminus of the **ABC-O-D** entity, that is at the amino acid precursor fragment attached to aryl ring **A**. The chiral center of this substituent is stereochemically delicate; it epimerized if the C-terminus was an ester, for instance. The Evans group found that the corresponding *N*-methylamide imparted resistance to epimerization at this center making it resilient to subsequent steps in the synthesis, while the Nicolaou group avoided the problem by using a corresponding O-protected alcohol. These strategies necessitated some interesting functional group manipulations towards the end of the synthesis (see below).

Our interpretation of the two synthetic strategies is that the nature of the C-terminus, and the order of construction of the **AB** and **C-O-D** rings, is relatively unimportant, but the latter factor did have significant indirect consequences. Specifically, the Evans group was able to achieve atropisomeric stereoselectivity in their **C-O-D** ring construction process and this might not have been possible if the **AB** ring was not already in place.

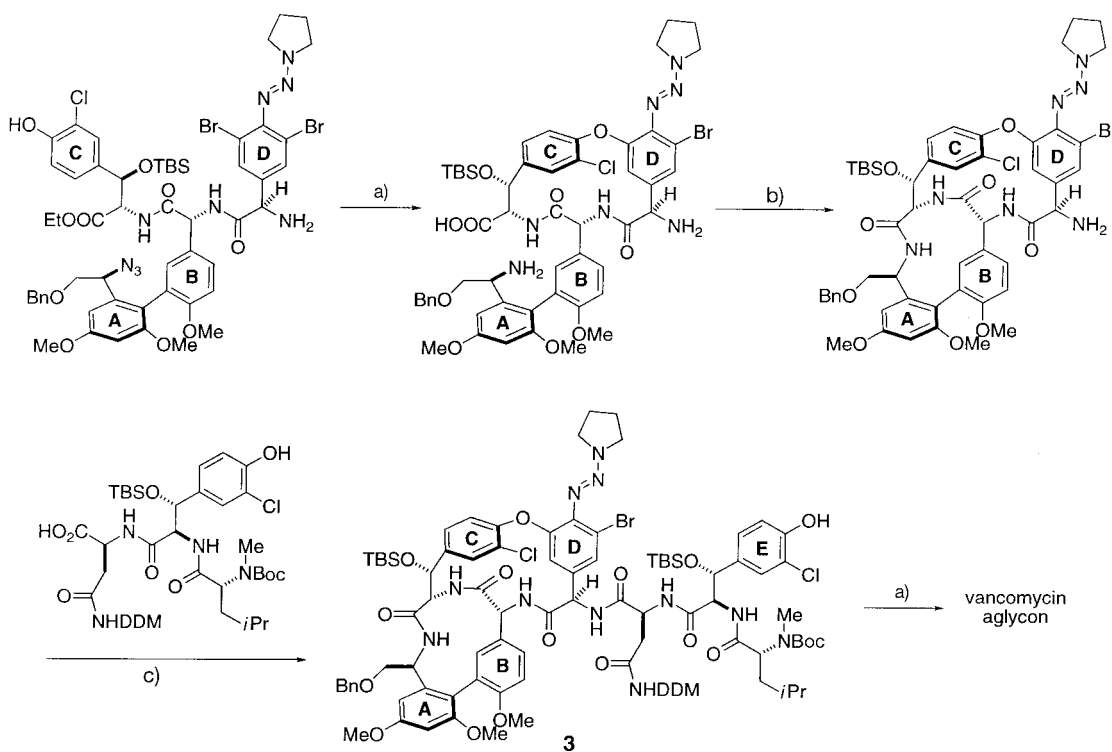
Development of a stereoselective **C-O-D** macrocyclization reaction came about by evaluating a flawed approach to give the **C-O-D** ring, formulating a hypothesis concerning factors governing the stereoselectivity of that process, then adjusting the overall synthetic strategy to accommodate its intrinsic

[*] Prof. K. Burgess, A. J. Zhang
Department of Chemistry, Texas A&M University
Box 30012, College Station, TX 77842-3012 (USA)
Fax: (+1) 409-845-8839
E-mail: burgess@mail.chem.tamu.edu

[**] K.B. thanks The Texas Advanced Research Program and The Robert A. Welch Foundation for support.



Scheme 1. Synthesis of the vancomycin aglycon according to Evans et al.: a) oxidative biaryl coupling. b) Coupling with a preformed tripeptide. Tfa = Trifluoroacetyl; DDM = 4,4'-dimethyloxydiphenylmethyl; Boc = *tert*-butoxycarbonyl.



Scheme 2. Synthesis of the vancomycin aglycon according to Nicolaou et al.: a) copper-mediated coupling. b) Macrolactamization. c) Coupling with a preformed tripeptide. TBS = *tert*-butyldimethylsilyl.

stereochemical bias. Thus Evans' group originally focussed their efforts on an analogue of compound **1** (Scheme 1) without a chlorine atom on ring **C**. Their intent was to replace the **C**-ring nitro group by a chlorine atom. However, a 7:1 atropisomeric selectivity in the undesired sense was achieved under several sets of reaction conditions. Consequently, they accepted the fact that the nitro group was somehow forced into that orientation during the cyclization, and added the

chlorine substituent shown in compound **1**. Their new, and ultimately successful, plan was to substitute the nitro group with a hydrogen after it had served to facilitate the S_NAr process with the desired atropisomeric selectivity. In this way the **C**-**O**-**D** structure was formed with a 5:1 bias in favor of the isomer required for the new approach. The macrocyclization process was also accelerated by the chlorine substituents (reaction time 1.5 h versus 66 h previously) since it increased

the electrophilicity of the neighboring fluorine substituents. In fact, the aryl fluoride was so reactive that the steps leading to formation of compound **1** had to be designed very carefully to avoid premature S_NAr reactions.

Both groups wisely elected to couple their **ABC-O-D** ring intermediates with preformed protected-tripeptides, thus making the synthesis more convergent. As a result, the East and West US-Coast teams entered the end-game with similar intermediates, that is compounds **2** and **3**, respectively.

Only the Evans' team could construct the **D-O-E** ring with selectivity for the desired atropisomer. Their S_NAr macrocyclization approach gave a 5:1 ratio of diastereoisomers, whereas in Nicolaou's group a rather disappointing 1:3 selectivity was obtained. The Nicolaou group was able to recycle the undesired isomer by exploiting observations made by Boger and co-workers.^[9, 10] Thus the undesired atropisomer was heated to 140 °C in DMSO for 4 h; this gave a thermodynamic 1:1 mixture of **D-O-E** ring isomers which was separated to give the desired one. However this discovery must have been a small conciliation for the sour stereochemical twist of fate that afflicted them in this final macrocyclization.

Having formed the **ABC-O-D-O-E** skeleton, both groups were left with the task of functional group manipulations and deprotection steps to form the final product. These seem routine to describe but can be tortuously difficult in practice. Nicolaou's group formed the desired C-terminal acid by a deprotection/oxidation operation on their masked alcohol. Conversion of an N-methyl amide to the corresponding group in the Evans synthesis seems harder, but was in fact accomplished in 68% yield by nitrosation and subsequent treatment with basic peroxide. This transformation was possible since that particular amide functionality is the least hindered of the eight present in this aglycon precursor.

Nicolaou's group approach to the **C-O-D-O-E** framework required that they convert a triazine to a phenolic hydroxy group on ring **D**. This was accomplished in several steps. The triazine was reduced to an amine, and diazotized in the presence of KI to give the corresponding aryl iodide. Unfortunately, 40% of the diazonium compound was reduced ($ArNH_2 \rightarrow ArH$ instead of $ArNH_2 \rightarrow ArI$), and the problem of converting the remaining aryl iodide into a phenol remained. In a very bold step, this iodide was treated with excess $MeMgBr$ and $iPrMgBr$ and the resulting Grignard species was then quenched with trimethylborate to give the aryl boronate. Finally, the phenol was formed by oxidation with basic peroxide.

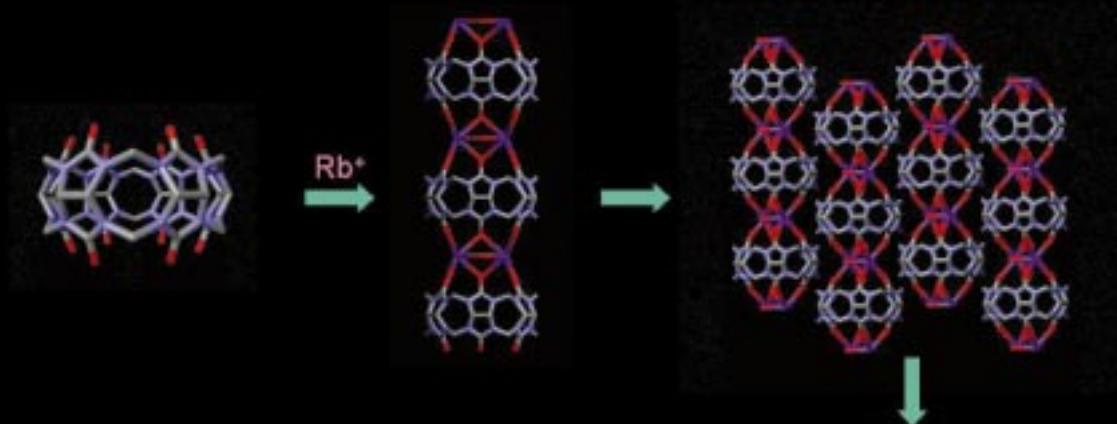
The Nicolaou group entered this area relatively recently, hence it is truly remarkable that they were able to develop a synthesis of the vancomycin aglycon so quickly. However, their route stumbles over the sections that involve atropisomeric selectivity or removal of the triazine. Evans' group synthesis addresses or avoids these problems. It is a more polished effort that took many years and high levels of financial and human resources to develop.

After this contribution was submitted, the Nicolaou group reported the successful transformation of the vancomycin aglycon into vancomycin itself.^[11] Their procedure featured three protection steps, that is silylation of all six hydroxyl groups, formation of a methyl ester at the C-terminus, and N-terminal protection with a benzyloxycarbonyl group. The central phenolic-OH was then unmasked, and sequentially coupled with two monosaccharide units. Finally, deprotection gave the desired product.

German version: *Angew. Chem.* **1999**, *111*, 666–669

Keywords: antibiotics • atropisomerism • nucleophilic aromatic substitutions • total synthesis • vancomycin

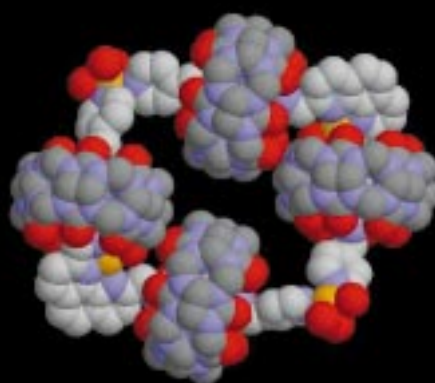
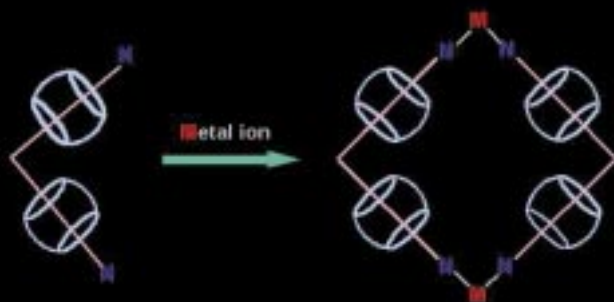
- [1] D. A. Evans, M. R. Wood, B. W. Trotter, T. I. Richardson, J. C. Barrow, J. L. Katz, *Angew. Chem.* **1998**, *110*, 2864–2868; *Angew. Chem. Int. Ed.* **1998**, *37*, 2700–2704.
- [2] D. A. Evans, C. I. Dinsmore, P. S. Watson, M. R. Wood, T. I. Richardson, B. W. Trotter, J. L. Katz, *Angew. Chem.* **1998**, *110*, 2868–2872; *Angew. Chem. Int. Ed.* **1998**, *37*, 2704–2708.
- [3] K. C. Nicolaou, S. Natarajan, H. Li, N. F. Jain, R. Hughes, M. E. Solomon, J. M. Ramanjulu, C. N. C. Boddy, M. Takayanagi, *Angew. Chem.* **1998**, *110*, 2872–2878; *Angew. Chem. Int. Ed.* **1998**, *37*, 2708–2714.
- [4] K. C. Nicolaou, N. F. Jain, W. Natarajan, R. Hughes, M. E. Solomon, H. Li, J. M. Ramanjulu, M. Takayanagi, A. E. Koumbis, T. Bando, *Angew. Chem.* **1998**, *110*, 2879–2881; *Angew. Chem. Int. Ed.* **1998**, *37*, 2714–2716.
- [5] K. C. Nicolaou, M. Takayanagi, N. F. Jain, S. Natarajan, A. E. Koumbis, T. Bando, J. M. Ramanjulu, *Angew. Chem.* **1998**, *110*, 2881–2883; *Angew. Chem. Int. Ed.* **1998**, *37*, 2717–2719.
- [6] D. L. Boger, R. M. Borzilleri, S. Nukui, *J. Org. Chem.* **1996**, *61*, 3561–3565.
- [7] D. A. Evans, J. A. Ellman, K. M. DeVries, *J. Am. Chem. Soc.* **1989**, *111*, 8912–8914.
- [8] J. Zhu, *Synlett* **1997**, 133–44.
- [9] D. L. Boger, O. Loiseleur, S. L. Castle, R. T. Beresis, J. H. Wu, *Bioorg. Med. Chem. Lett.* **1997**, *7*, 3199–3202.
- [10] D. L. Boger, S. Miyazaki, O. Loiseleur, R. T. Beresis, S. L. Castle, J. H. Wu, Q. Jin, *J. Am. Chem. Soc.* **1998**, *120*, 8920–8926.
- [11] K. C. Nicolaou, H. J. Mitchell, N. F. Jain, N. Winssinger, R. Hughes, T. Bando, *Angew. Chem.* **1999**, *111*, 253–257; *Angew. Chem. Int. Ed.* **1999**, *38*, 240–244.



Cucurbituril and rubidium ions form one-dimensional polymers which are arranged in such a way as to produce a honeycomb structure with large linear hexagonal channels.



Like with a string of pearls, four molecular beads are threaded on a molecular rectangle to form a molecular necklace.

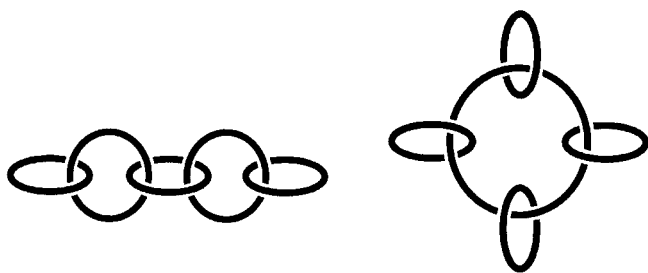


Find out more in the following two papers.

Synthesis of a Five-Membered Molecular Necklace: A 2+2 Approach**

Soo-Gyun Roh, Ki-Min Park, Gil-Jae Park, Shigeru Sakamoto, Kentaro Yamaguchi, and Kimoon Kim*

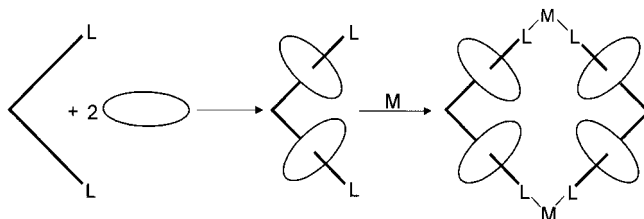
We have been interested in highly efficient syntheses of interlocked structures^[1] such as rotaxanes, polyrotaxanes, and molecular necklaces.^[2] Molecular necklaces (MN) are supramolecular species in which a number of small rings are threaded onto a large ring. They are topological isomers of linear oligocatenanes, where rings are mechanically interlocked in a linear fashion (Scheme 1).^[3] Formation of a



Scheme 1. Schematic representation of a linear [5]catenane (olympiadane; left) and a molecular necklace [5]MN (right).

mixture of molecular necklaces [n]MN ($n = 4-7$), some of which were isolated and characterized by electrospray (ESI) mass spectrometry, was first reported by Sauvage et al.^[4] Recently, we reported a one-pot, nearly quantitative self-assembly of a minimal molecular necklace [4]MN^[5] in which three molecular “beads” are threaded onto a molecular triangle.^[2d] This supramolecular compound is formed from nine species: three molecular beads, three “strings”, and three “angle connectors”. In principle, the same approach can be used for the synthesis of a molecular necklace [5]MN containing four molecular beads threaded onto a molecular square.^[6] However, this method often produces a mixture of [4]MN and [5]MN.^[7] Therefore, we now take another

approach to [5]MN, which we call a “2+2” approach. Using a preorganized, L-shaped molecule, we first synthesize a pseudorotaxane containing two molecular beads and then allow a metal ion (or a metal complex with *cis* vacant coordination sites) to react with the pseudorotaxane to form a [5]MN (Scheme 2). Here we report the synthesis and X-ray crystal structure of a [5]MN prepared by this approach.



Scheme 2. Schematic representation of the 2+2 approach for the synthesis of molecular necklaces [5]MN. The two ends L of the bent building blocks are ligands atoms (such as pyridine nitrogen atoms) that coordinate to a metal center. The ellipsoids symbolize molecular beads, for example cucurbituril (1).


The [5]MN $4 \cdot 14\text{NO}_3^-$ is constructed by threading two equivalents of cucurbituril (1)^[8] with the L-shaped phenanthroline derivative 2 and then allowing the resulting pseudorotaxane $3 \cdot 4\text{NO}_3^-$ to react with $\text{Cu}(\text{NO}_3)_2$ (Scheme 3). The X-ray crystal structure^[9] of $4 \cdot 14\text{NO}_3^-$ reveals that four molecular beads are threaded onto a molecular square in which two copper ions (Cu(1) and Cu(3)) occupy two opposite corners (Figure 1). Each of these copper ions is coordinated by two pyridyl units of 3⁴⁺ and three water molecules in a distorted square pyramidal geometry with the pyridyl units at two adjacent basal positions. Two additional copper ions (Cu(2) and Cu(4)) are bound inside the phenanthroline units making up corners of the square. Each of these copper ions is coordinated by two phenanthroline nitrogen atoms, a secondary amine nitrogen atom, and two oxygen atoms of cucurbituril in a distorted square pyramidal geometry with an oxygen atom (O(201) for Cu(2) and O(401) for Cu(4)) at the apical position. Coordination of the amine nitrogen atoms N(225) and N(425) to the copper ions (Cu(2) and Cu(4), respectively) makes two sides of the molecular square considerably shorter than the other two; therefore, the necklace framework is better described as a rectangle with dimensions of about $19.3 \times 17.0 \text{ \AA}$.^[10] The cucurbituril beads threaded on the longer side of the molecular rectangle are held in place by hydrogen bonds between their carbonyl oxygen atoms and the protonated amine groups of 2. The beads on the shorter side are held in place by such hydrogen-bonding interactions at one end and by coordination to the metal center at the other end (Figure 1). A space-filling representation of the structure of 4⁴⁺ is displayed in Figure 2. The space inside the molecular necklace is filled with nitrate ions and water molecules.

The molecular necklace $4 \cdot 14\text{NO}_3^-$ is soluble in water (and also in acetonitrile when the counterions are exchanged with PF_6^-). Owing to the paramagnetic metal centers, the NMR spectrum of $4 \cdot 14\text{NO}_3^-$ is not informative. Nevertheless, the ESI mass spectrum of $4 \cdot 14\text{PF}_6^-$ is consistent with the

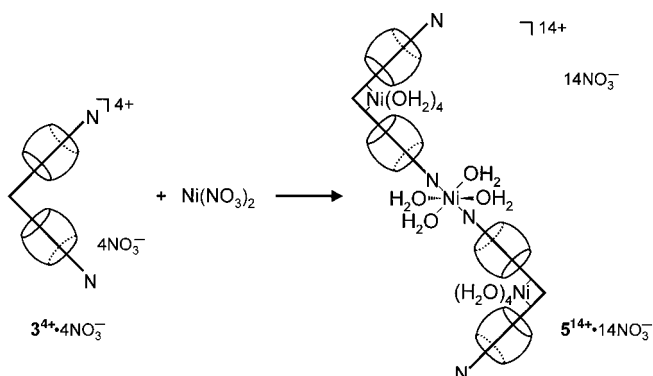
[*] Prof. K. Kim, Dr. S.-G. Roh, Dr. K.-M. Park, G.-J. Park
National Creative Research Initiative Center
for Smart Supramolecules
and
Department of Chemistry
Pohang University of Science and Technology
San 31 Hyojadong, Pohang 790-784 (South Korea)
Fax: (+82) 562-279-8129
E-mail: kkim@postech.ac.kr
Shigeru Sakamoto, Prof. Kentaro Yamaguchi
Chemical Analysis Center, Chiba University
Yayoicho, Inage-ku, Chiba 2638522 (Japan)

[**] This work was supported by the Creative Research Initiative Program of the Korean Ministry of Science and Technology. We thank Professor Jong Hoon Hahn and Ms. Young Ah Kim for low-resolution electrospray ionization mass spectrometry, Mr. Eunsung Lee for technical assistance, and Professor G. V. Smith for helpful comments on the manuscript.

Supporting information for this article is available on the WWW under <http://www.wiley-vch.de/home/angewandte/> or from the author.



639



Scheme 4. Formation of rotaxane 5^{14+} through incorporation of Ni^{2+} ions.

In summary, we present an efficient synthesis of a molecular necklace [5]MN using a preorganized L-shaped pseudorotaxane and a metal ion. Here, as well as in our earlier work,^[2] we demonstrate that such topologically intriguing supramolecular species can be readily assembled from carefully designed organic building blocks and properly chosen metal ions or complexes.

Experimental Section

2: A solution of *N*-(4-pyridylmethyl)-1,4-diaminobutane trihydrobromide (4.50 g, 10.7 mmol) and triethylamine (9 mL) in methanol (60 mL) was added dropwise under argon to a solution containing 1,10-phenanthroline-2,9-dialdehyde^[12] (1.26 g, 5.34 mmol) and anhydrous magnesium chloride (1.01 g, 10.68 mmol) in dry methanol (80 mL), and then stirred for 18 h. At 0 °C sodium borohydride (0.722 g, 19.1 mmol) was added to the solution in small portions (caution: evolution of gas). After 15 h of stirring, water (150 mL) was added, and the mixture was concentrated to 150 mL. After extraction with CH_2Cl_2 (3×100 mL), the combined organic phase was dried over magnesium sulfate and the solvent evaporated. The light red oil was then dissolved in ethanol, and conc. HCl was added slowly to yield **2**·4HCl (yield: 0.80 g, 21 %). M.p. 170 °C (decomp.); 1H NMR (300 MHz, D_2O): δ = 1.92 (8H, brs), 3.33 (8H, m), 4.62 (4H, s), 4.73 (4H, s), 7.93 (4H, d, J = 8.14 Hz), 8.06 (2H, d, J = 6.70 Hz), 8.16 (2H, s), 8.64 (2H, d, J = 8.26 Hz), 8.78 (4H, d, J = 6.76 Hz). The mass spectra were obtained with the free amine **2**, which was generated by treating **2**·4HCl with NaOH. FAB-MS: m/z : 563.2 [$M+H^+$]. The nitrate salt **2**·4HNO₃ was prepared by dissolution of the chloride salt in water and treatment of the solution with 40 % NaOH to adjust the pH to about pH 12 followed by extraction with CH_2Cl_2 , concentration, and addition of ethanol and conc. HNO₃. The NMR spectrum of the nitrate salt is essentially the same as that of the chloride salt. Both salts are very hygroscopic and unstable; therefore, the nitrate salt was used immediately in the synthesis of **3**·4NO₃[−], which is stable.

3·4NO₃[−]: At room temperature a slightly excess amount of **1**·10H₂O (1.79 g, 1.52 mmol) was suspended in a solution of **2**·4HNO₃ (0.59 g; 0.73 mmol) in H₂O (50 mL). After the mixture was stirred for about 16 h, undissolved **1** was filtered off. The filtrate was concentrated, and the product isolated by addition of ethanol. The nearly colorless solid was collected and dried to afford **3**·4NO₃[−] (yield: 1.90 g, 87 %). The 1H NMR spectrum indicates that **3**⁴⁺ contains two molecules of cucurbituril. 1H NMR (300 MHz, D_2O): δ = 0.71 (8H, brs), 2.49 (4H, brs), 2.80 (4H, brs), 4.40 (24H, d, J = 15.70 Hz), 4.62 (4H, s), 4.91 (4H, s), 5.66–5.77 (48H, m), 8.11 (2H, s), 8.15 (4H, d, J = 8.91 Hz), 8.63 (2H, d, J = 8.43 Hz), 8.72 (2H, d, J = 8.37 Hz), 8.79 (2H, m); ESI-MS: m/z : 1425.2 [**3**·2PF₆]²⁺, 901.7 [**3**·PF₆]³⁺, 640.7 [**3**]⁴⁺ (the counterions were exchanged with PF₆[−] for mass spectrometry); elemental analysis calcd for C₁₀₆N₅₆O₂₄H₁₁₈·4NO₃·10H₂O: C 42.60, H 4.65, N 28.12; found: C 42.24, H 4.56, N 28.50.

4·14NO₃[−]: A 3.1×10^{-3} M stock solution of pseudorotaxane **3**·4NO₃[−] (0.196 g; 0.0656 mmol) in H₂O (21 mL) was prepared and divided into seven portions. Each portion was layered over a 0.3 M solution of Cu(NO₃)₂ in H₂O (3 mL) in a diffusion tube to produce in a week sky blue, plate-

shaped crystals of **4**·14NO₃ suitable for an X-ray crystal structure analysis (yield: 32 mg, 13 %). Elemental analysis calcd for Cu₄(C₂₁₂N₁₁₂O₄₈H₂₃₄)(H₂O)₆(NO₃)₁₄·64H₂O: C 33.94, H 5.02, N 23.52; found: C 34.10, H 5.22, N 23.60. The high-resolution ESI mass spectrometry data were obtained with the sample whose counterions had been exchanged with PF₆[−] ions. ESI-MS: positive ion: m/z : 3025.8 (calcd: 3026.2) [(**4**−8H⁺)⁶⁺·4PF₆[−]]²⁺ or [Cu₄(C₂₁₂N₁₁₂O₅₄H₂₃₈)(PF₆)₄]²⁺; negative ion: m/z : 3461.9 (calcd: 3462.1) [(**4**−6H⁺)⁸⁺·10PF₆[−]]^{2−}, 3388.8 (calcd: 3389.1) [(**4**−7H⁺)⁷⁺·9PF₆[−]][−]. The observed isotopic patterns of the ion clusters match the calculated patterns well.

Received: August 25, 1998 [Z12337IE]

German version: *Angew. Chem.* **1999**, *111*, 672–675

Keywords: catenanes • copper • N ligands • rotaxanes • supramolecular chemistry

- Reviews: a) J.-P. Sauvage, *Acc. Chem. Res.* **1990**, *23*, 319; b) D. B. Amabilino, J. F. Stoddart, *Chem. Rev.* **1995**, *95*, 2725; c) D. Philp, J. F. Stoddart, *Angew. Chem.* **1996**, *108*, 1242; *Angew. Chem. Int. Ed. Engl.* **1996**, *35*, 1154; d) H. Gibson, M. C. Bheda, P. T. Engen, *Prog. Polym. Sci.* **1994**, *19*, 843; e) R. Jäger, F. Vögtle, *Angew. Chem.* **1997**, *109*, 966; *Angew. Chem. Int. Ed. Engl.* **1997**, *36*, 930.
- a) Y.-M. Jeon, D. Whang, J. Kim, K. Kim, *Chem. Lett.*, **1996**, 503; b) D. Whang, Y.-M. Jeon, J. Heo, K. Kim, *J. Am. Chem. Soc.* **1996**, *118*, 11333; c) D. Whang, K. Kim, *J. Am. Chem. Soc.* **1997**, *119*, 451; d) D. Whang, K.-M. Park, J. Heo, P. Ashton, K. Kim, *J. Am. Chem. Soc.* **1998**, *120*, 4899.
- Molecular necklaces constitute a subset of catenanes. For a given number of rings, a molecular necklace is uniquely defined. A molecular necklace consisting of a total of n rings ($n-1$ small rings threaded onto one larger ring) is denoted as $[n]$ MN, which is a topological stereoisomer of $[n]$ catenane. For example, the molecular necklace [5]MN described here and olympiadane synthesized by Stoddart and coworkers (D. B. Amabilino, P. R. Ashton, A. S. Reder, N. Spencer, J. F. Stoddart, *Angew. Chem.* **1994**, *106*, 450; *Angew. Chem. Int. Ed. Engl.* **1994**, *33*, 433) are topological stereoisomers. The minimal molecular necklace is [4]MN; the smaller molecular necklaces [2]MN and [3]MN are equivalent to [2]catenane and [3]catenane, respectively.
- a) F. Bitsch, G. Hegy, C. Dietrich-Buchecker, E. Leize, J.-P. Sauvage, A. V. Dorselaer, *J. Am. Chem. Soc.* **1991**, *113*, 4023; b) F. Bitsch, C. O. Dietrich-Buchecker, A.-K. Khemiss, J.-P. Sauvage, A. V. Dorselaer, *New J. Chem.* **1994**, *18*, 801.
- Very recently, Stoddart and co-workers also isolated and characterized a [4]MN in the synthesis of oligocatenanes: D. B. Amabilino, P. R. Ashton, V. Balzani, S. E. Boyd, A. Credi, J. Y. Lee, S. Menzer, J. F. Stoddart, M. Venturi, D. J. Williams, *J. Am. Chem. Soc.* **1998**, *120*, 4295.
- Reviews on molecular squares: a) M. Fujita, K. Ogura, *Bull. Chem. Soc. Jpn* **1996**, *69*, 1471; b) P. J. Stang, B. Olenyuk, *Acc. Chem. Res.* **1997**, *30*, 502.
- J. Heo, K.-M. Park, K. Kim, unpublished results.
- Reviews: a) W. L. Mock in *Comprehensive Supramolecular Chemistry*, Vol. 2 (Ed.: F. Vögtle) Pergamon, Oxford, **1996**, p. 477; b) W. L. Mock, *Top. Curr. Chem.* **1995**, *175*, 1; c) P. Cintas, *J. Incl. Phenom. Molec. Reco. Chem.* **1994**, *17*, 205.
- Crystal data of **4**·14NO₃[−]: [Cu(H₂O)₃[(C₃₄H₄₅N₈)Cu]·(C₃₆H₃₆N₂₄O₁₂)₂](NO₃)₁₄·76H₂O, M_r = 7718.72, triclinic, $P\bar{1}$, a = 23.284(1), b = 25.189(1), c = 29.835(1) Å, α = 100.7458(6), β = 107.8604(7), γ = 93.5909(4)°, V = 16228(2) Å³, Z = 2, ρ_{calcd} = 1.580 g cm^{−3}, T = 188 K, Siemens SMART CCD diffractometer, MoK α (λ = 0.71073), μ = 3.88 cm^{−1}. The structure was solved by Patterson methods. All the alkylamine nitrogen atoms, except the ones (N(225) and N(425)) that are coordinated to the copper ions bound to the phenanthroline units, are protonated, as judged by the difference electron density map and our earlier observations.^[2] The overall charge of the necklace species was therefore assigned to be +14. Of the 14 counterions, 12 nitrate ions behave well during the refinement. One nitrate ion has large thermal parameters, and its structure

deviates considerably from an ideal geometry. One nitrate ion was not found. All non-hydrogen atoms were refined anisotropically. Final block-diagonal matrix least-squares refinement on F^2 with all 46961 reflections and 4611 variables converged to $R1$ ($I > 2\sigma(I)$) = 0.086, $wR2$ (all data) = 0.271, and GOF = 1.07. Crystal data of **5**·14NO₃[−]: [Ni(H₂O)₄](C₃₄H₄₅N₈)Ni(H₂O)₃·(C₃₆H₃₆N₂₄O₁₂)₂](NO₃)₁₄·82H₂O, M_r = 7642.70, triclinic, PI , a = 16.1173(2), b = 21.0397(3), c = 24.2956(2) Å, α = 96.3974(10), β = 103.6400(4), γ = 94.2966(8)°, V = 7912.7(2) Å³, Z = 1, ρ_{calc} = 1.604 g cm^{−3}, T = 188 K, Siemens SMART CCD diffractometer, MoK α (λ = 0.71073), μ = 3.09 cm^{−1}. Full-matrix least-squares refinement on F^2 with all 23393 reflections and 2311 variables converged to $R1$ ($I > 2\sigma(I)$) = 0.144, $wR2$ (all data) = 0.389 and GOF = 1.10. Crystallographic data (excluding structure factors) for the structures reported in this paper have been deposited with the Cambridge Crystallographic Data Center as supplementary publication no. CCDC-102726 (**4**·14NO₃) and CCDC-102727 (**5**·14NO₃). Copies of the data can be obtained free of charge on application to CCDC, 12 Union Road, Cambridge CB21EZ, UK (fax: (+44) 1223-336-033; e-mail: deposit@ccdc.cam.ac.uk).

- [10] The numbers correspond to the distances from the central ring of the phenanthroline to the copper corners.
 [11] Reaction of the metal complexes [Pt(en)(NO₃)₂] and [Pd(en)(NO₃)₂] with **3**·4NO₃[−], as judged by ¹H NMR spectroscopy, yields a mixture from which we have been so far unable to isolate pure compounds (en = ethylenediamine).
 [12] a) U. Lüning, M. Müller, *Liebigs Ann. Chem.* **1989**, 367; b) C. J. Chandler, L. W. Deady; J. A. Reiss, *J. Heterocycl. Chem.* **1981**, 18, 599.

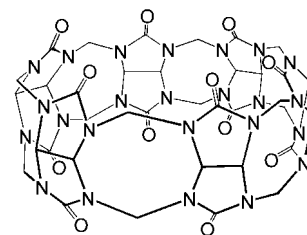
Shape-Induced, Hexagonal, Open Frameworks: Rubidium Ion Complexed Cucurbituril**

Jungseok Heo, Soo-Young Kim, Dongmok Whang, and Kimoon Kim*

Metal-organic solids containing large pores or channels with controlled sizes, shapes, and chemical environments have drawn much attention in recent years because they may have applications in separation, catalysis, and optoelectronics. The “modular” approach has been successfully employed in the construction of metal-organic open-framework materials; various organic building blocks and metal ions have been used to assemble a variety of porous three-dimensional networks.^[1–6] Although these efforts have contributed greatly to our understanding of how to build such solid-state structures, we still need to explore new building blocks and building principles before we are truly able to design and

build specifically engineered solid-state architectures. We present herein a crystal structure that demonstrates a novel way to construct metal-organic open-framework materials with large hexagonal channels using the modular approach.

Cucurbituril^[7, 8] is a macrocyclic cavitand with D_{6h} symmetry, having a hollow core with a diameter of about 5.5 Å and two identical portals surrounded by carbonyl groups (Scheme 1). We recently reported novel molecular container assemblies comprising cucurbituril and alkali metal ions, which are capable of the reversible encapsulation and release



Scheme 1. Cucurbituril.

of guest molecules in solution.^[9] In an effort to understand the host–guest interactions in the molecular container assemblies, we studied their structures in the solid state by X-ray crystallography. In contrast to the case with other alkali metal ions, rubidium and cucurbituril form a one-dimensional coordination polymer in the solid state in which cucurbituril molecules stack atop one another through coordination of their carbonyl groups to the rubidium ions in between. More interestingly, the coordination polymer chains are arranged in such a way as to produce a honeycomb structure with large linear hexagonal channels parallel to the polymer chains.

Vapor diffusion of methanol into an aqueous solution containing cucurbituril and Rb₂SO₄ yields the needle-shaped crystalline product **1**.^[10] The X-ray structure of **1** reveals a one-dimensional coordination polymer of alternating cucurbituril molecules and Rb₂(μ-OH)₂(OH₂)₂ units that extends along the c axis (Figures 1 and 2).^[11] A threefold axis parallel to the c axis passes through the center of the coordination polymer. The Rb₂(μ-OH)₂(OH₂)₂ unit lies on a mirror plane perpendicular to the threefold axis. The two Rb ions are separated by 4.395(5) Å and are related to each other by a twofold symmetry axis passing through the oxygen atoms of the bridging OH groups. Each rubidium ion is coordinated by four portal oxygen atoms of two cucurbituril molecules (two oxygen atoms from each cucurbituril molecule: Rb–O(1) and Rb–O(1′) 2.952(5), Rb–O(2) and Rb–O(2′) 2.938(5) Å), two bridging hydroxide ions (Rb–O(3) 2.93(2), Rb–O(4) 2.94(1) Å), two methanol molecules encapsulated in the cucurbituril molecules (Rb–O(5) and Rb–O(5′) 2.96(1) Å), and a weakly coordinating water molecule (Rb–O(1W) 3.17(1) Å; Figure 1). The coordination geometry of the rubidium ion is best described as a capped square antiprism. The Rb₂(OH)₂ plane is parallel to the plane formed by six oxygen atoms of cucurbituril and separated from it by a mean distance of 2.190(4) Å. The Rb₂(μ-OH)₂(μ-CH₃OH)₂(OH₂)₂ unit is disordered over three sites due to the crystallographically imposed threefold symmetry.

[*] Prof. K. Kim, J. Heo, S.-Y. Kim, Dr. D. Whang
 National Creative Research Initiative Center for Smart Supramolecules
 and
 Department of Chemistry
 Pohang University of Science and Technology
 San 31 Hyojadong, Pohang 790-784 (South Korea)
 Fax: (82) 562-279-8129
 E-mail: kkim@postech.ac.kr

[**] This work was supported by the Creative Research Initiative Program of the Korean Ministry of Science and Technology. We thank Professors M. J. Zaworotko and G. V. Smith for helpful comments on the manuscript.

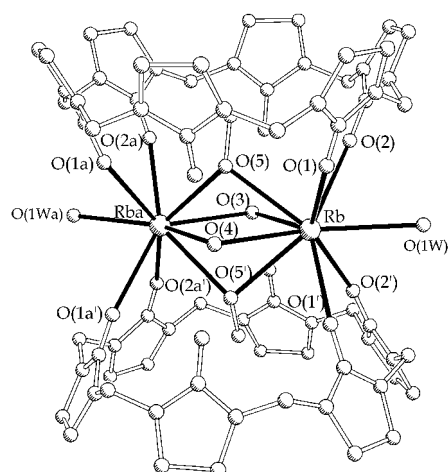


Figure 1. Coordination geometry around the rubidium ions in **1**. The rubidium ions, bridging hydroxide ions, and bound water molecules are disordered over three sites due to the crystallographically imposed threefold symmetry. Only one orientation is depicted. Selected bond lengths [Å]: Rb–O(1) and Rb–O(1') 2.952(5), Rb–O(2) and Rb–O(2') 2.938(5), Rb–O(3) 2.93(2), Rb–O(4) 2.94(1), Rb–O(5) and Rb–O(5') 2.96(1), Rb–O(1W) 3.17(1).

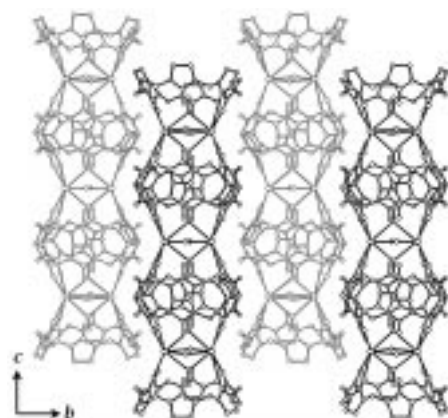


Figure 2. Section of the one-dimensional coordination polymer comprising cucurbituril molecules and $\text{Rb}_2(\mu\text{-OH})_2(\text{OH}_2)_2$ units, and their packing in **1** (view of the bc plane). The neighboring chains are offset by one-half of the repeating unit along the c axis, and by one-half of the cucurbituril unit along the a axis. The $\text{Rb}_2(\mu\text{-OH})_2(\text{OH}_2)_2$ unit is disordered over three sites due to the crystallographically imposed threefold symmetry passing through the center of the coordination polymer along the c axis. Only one orientation is depicted. The weakly coordinating water molecules are also omitted for clarity.

The most interesting feature of the crystal structure is that the coordination polymer chains in **1** are arranged in such a way as to produce a honeycomb structure with linear, hexagonal channels extended along the c axis (Figure 3). The coordination polymer chains are surrounded by three neighboring chains. The chain at the center is offset by one-half of the repeating unit along the c axis so that the “bumps” of the chain fit into “hollows” of the neighboring chains (Figure 2). This structure appears to be stabilized by efficient van der Waals interactions between the coordination polymer chains arising from their self-complementary curvature. The void volume of the channels, whose mean diameter is about 10 Å, is estimated to be around 23 % of the total volume.^[12] The channels are filled with water molecules (34 water

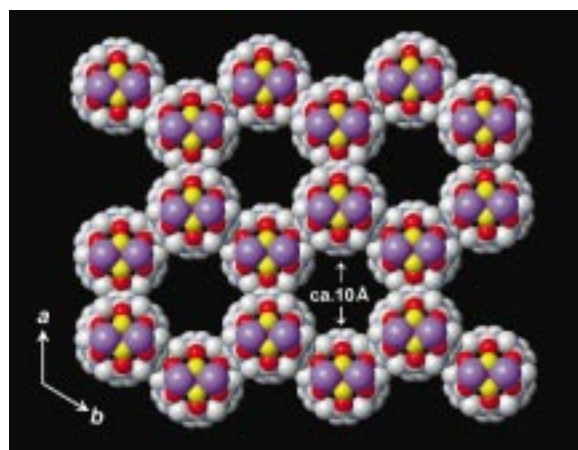
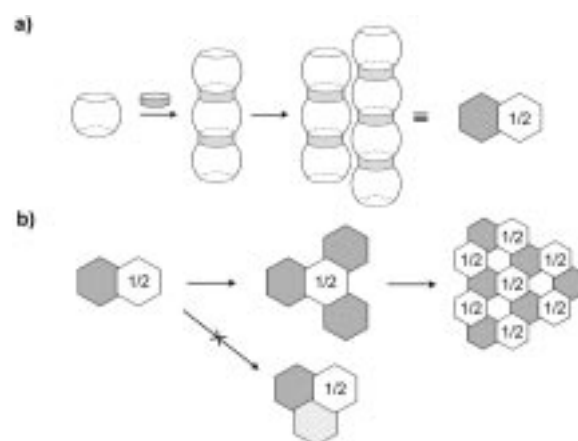


Figure 3. X-ray crystal structure of **1** viewed down the c axis showing large hexagonal channels with a mean diameter of about 10 Å. The $\text{Rb}_2(\mu\text{-OH})_2$ unit is disordered over three sites; only one orientation is depicted. Water molecules in the channels are omitted for clarity. The Rb atoms are purple, the O atoms of the bridging hydroxide ions yellow, the O atoms of cucurbituril red, the N atoms blue, and the C atoms gray.

molecules per unit cell) that form a complicated hydrogen-bonding network among themselves as well as with the water molecules coordinated to the metal centers (O(1W)). Once removed from the mother liquor, however, the crystals quickly lose solvent and crystallinity.^[13] Diffusion of THF or ethylenediamine into an aqueous solution of cucurbituril/ Rb_2SO_4 also produces a rubidium ion complexed cucurbituril with the same honeycomb structure, except that a THF or ethylenediamine molecule is encapsulated in the cavity of cucurbituril.^[14] No organic molecules are found in the channels as in **1**.

Although such large hexagonal channel structures have precedence,^[5, 6a] the way that the present structure is built up is unique (Scheme 2). Here, cucurbituril, a barrel-shaped



Scheme 2. Simplified representation of how the structure of **1** is built up in the crystal.

molecule with D_{6h} symmetry, is used as a bulky, linear, bifunctional building block. The “barrels” are stacked up with metal ion “cement” to form a rigid column with alternating bumps and hollows (Scheme 2a). In the crystal, the next column is offset by one-half of the repeating unit along the column direction to maximize the interactions between the

two columns with a self-complementary curvature by fitting the bumps of one column into hollows of the other. However, placing a third column at the indentation between the two touching columns to achieve a closed-packing structure is not allowed, because the third column cannot be offset by one-half of a unit with respect to both the first and the second columns. Instead, the offset relationship of one-half of a unit between the neighboring columns and the threefold cross-sectional symmetry of the column result in a preferred Y-shaped arrangement of columns, which eventually turns into the hexagonal open-framework structure (Scheme 1b).^[15] This structure not only demonstrates that the shape and symmetry of a building block can induce a specific crystal structure, but also provides a new strategy to open frameworks with linear hexagonal channels. This novel structure and building principle may provide further insight into designing new porous materials as well as other supramolecular architectures.

Received: October 14, 1998 [Z 12528IE]
German version: *Angew. Chem.* **1999**, *111*, 675–678

Keywords: channel structures • coordination polymers • crystal engineering • rubidium • supramolecular chemistry

- [1] a) B. F. Abrahams, B. F. Hoskins, D. M. Michail, R. Robson, *Nature* **1994**, *369*, 727; b) R. Robson in *Comprehensive Supramolecular Chemistry*, Vol. 6 (Eds.: D. D. MacNicol, F. Toda, R. Bishop), Pergamon, Oxford, **1996**, p. 733.
- [2] S. Subramanian, M. J. Zaworotko, *Angew. Chem.* **1995**, *107*, 2295; *Angew. Chem. Int. Ed. Engl.* **1995**, *34*, 2127.
- [3] a) O. M. Yaghi, G. Li, H. Li, *Nature* **1995**, *378*, 703; b) O. M. Yaghi, C. E. Davis, G. Li, H. Li, *J. Am. Chem. Soc.* **1997**, *119*, 2861; c) H. Li, C. E. Davis, T. L. Groy, D. G. Kelley, O. M. Yaghi, *J. Am. Chem. Soc.* **1998**, *120*, 2186.
- [4] M. Fujita, Y. J. Kwon, S. Washizu, K. Ogura, *J. Am. Chem. Soc.* **1994**, *116*, 1151.
- [5] R. E. Norman, N. J. Rose, R. E. Stenkamp, *J. Chem. Soc. Dalton Trans.* **1987**, 2905.
- [6] Representative examples of organic porous materials with hydrogen bonding: a) D. Venkataraman, S. Lee, J. Zhang, J. S. Moore, *Nature* **1994**, *371*, 591; b) P. Brunet, M. Simard, J. D. Wuest, *J. Am. Chem. Soc.* **1997**, *119*, 2737; c) V. A. Russell, C. C. Evans, W. Li, M. D. Ward, *Science* **1997**, *276*, 575.
- [7] a) R. Behrend, E. Meyer, F. Rusche, *Liebigs. Ann. Chem.* **1905**, *339*, 1; b) W. A. Freeman, W. L. Mock, N.-Y. Shih, *J. Am. Chem. Soc.* **1981**, *103*, 7367.
- [8] Reviews: a) W. L. Mock in *Comprehensive Supramolecular Chemistry*, Vol. 2 (Ed.: F. Vogtle), Pergamon, Oxford, **1996**, p. 477; b) W. L. Mock, *Top. Curr. Chem.* **1995**, *175*, 1; c) P. Cintas, *J. Inclusion Phenom. Mol. Recognit. Chem.* **1994**, *17*, 205.
- [9] a) Y.-M. Jeon, J. Kim, D. Whang, K. Kim, *J. Am. Chem. Soc.* **1996**, *118*, 9790; b) D. Whang, J. Heo, J. H. Park, K. Kim, *Angew. Chem.* **1998**, *110*, 83; *Angew. Chem. Int. Ed. Engl.* **1998**, *37*, 78.
- [10] Cucurbituril decahydrate (0.390 g) was added to a saturated solution of Rb_2SO_4 (10 mL). After the mixture was stirred for 1 h, the undissolved cucurbituril was filtered. Methanol vapor was allowed to diffuse into the filtrate at room temperature for a week before the crystalline product **1** was collected, washed with water, and dried in the air. Elemental analysis was performed on the air-dried sample. Elemental analysis (%) calcd for $[(\text{C}_{36}\text{H}_{36}\text{N}_{24}\text{O}_{12})\text{Rb}_2(\text{OH})_2 \cdot (\text{CH}_3\text{OH})_2 \cdot (\text{CH}_3\text{OH})_2] \cdot 3\text{H}_2\text{O}$: C 34.58, H 3.97, N 25.47; found: C 34.36, H 4.28, N 25.71.
- [11] Crystal data of **1**: $[(\text{C}_{36}\text{H}_{36}\text{N}_{24}\text{O}_{12})\text{Rb}_2(\text{OH})_2(\text{H}_2\text{O})_2 \cdot (\text{CH}_3\text{OH})_2] \cdot 17\text{H}_2\text{O}$, $M_r = 1608.23$, hexagonal, space group $P6_3/mmc$, $a = 19.628(6)$, $c = 10.544(3)$ Å, $V = 3518(2)$ Å³, $Z = 2$, $\rho_{\text{calcd}} = 1.518$ g cm⁻³, $T = 188$ K, Siemens SMART CCD diffractometer, MoK_α ($\lambda =$

0.71073 Å), $\mu = 14.95$ cm⁻¹. The structure was solved by Patterson methods (SHELXS-86). All non-hydrogen atoms were refined anisotropically (SHELXL-93). Final full-matrix least-squares refinement on F^2 with all 1049 reflections and 117 variables converged to $R1 = 0.092$ ($I > 2\sigma(I)$), $wR2 = 0.30$ (all data), and $\text{GOF} = 1.12$. Crystallographic data (excluding structure factors) for the structure reported in this paper have been deposited with the Cambridge Crystallographic Data Center as supplementary publication no. CCDC-103350. Copies of the data can be obtained free of charge on application to CCDC, 12 Union Road, Cambridge CB2 1EZ, UK (fax: (+44) 1223-336-033; e-mail: deposit@ccdc.cam.ac.uk).

- [12] The void volume of the channels was estimated by the method described in reference [3b].
- [13] Upon loss of the solvate molecules (water) the open-framework structure collapses to become a denser amorphous material.
- [14] Diffusion of THF into the solution of cucurbituril/ Rb_2SO_4 produces needle-shaped crystals first, which have the same honeycomb structure as **1**. However, the crystals change their morphology slowly to block-shaped crystals which have different cell parameters: monoclinic, space group $C2/m$, $a = 22.8361(4)$, $b = 10.4759(2)$, $c = 19.8560(4)$ Å, $\beta = 113.483(1)$, $V = 4356.7(1)$ Å³. X-ray structural analysis on this crystal is in progress.
- [15] In another way to look at the structure one may consider cucurbituril as a “pseudosphere”. The pseudospheres are forced to line up vertically upon formation of the coordination polymer with the rubidium ions. This vertical lineup prevents the classical hexagonal or cubic closed packing, but leads to the “hexagonal open packing” observed here.

Statistical Investigation into the Structural Complementarity of Natural Products and Synthetic Compounds

Thomas Henkel,* Roger M. Brunne, Hartwig Müller, and Felix Reichel

Natural products represent a rich source of biologically active compounds. They have played a considerable part in the exploration and development of new drugs and crop protection products, which can be informally derived from the retrospective analysis of important commercial products.^[1, 2] This historical point of view does not give any information in regard to the question as to how far the structural properties of natural products differ from the easily accessible synthetic substances. With the entrance of high-throughput-screening (HTS) as well as combinatorial chemistry in the lead-finding process this question however becomes of central importance in defining the future role of natural products in this research area. There is a need to evaluate whether natural products

- [*] Dr. T. Henkel, Dr. H. Müller
Bayer AG, Pharma Forschung
Life Science Center Natural Products (PH-R LSC-NP)
Aprather Weg, D-42096 Wuppertal (Germany)
Fax: (+49) 202-368515
E-mail: thomas.henkel.th@bayer-ag.de
Dr. R. M. Brunne
Bayer AG, Pharma Forschung, Structural Research (PH-R SR)
Dr. F. Reichel
Bayer AG, Zentrale Forschung Wirkstoffforschung (ZF-WFM)

Supporting information for this article is available on the WWW under <http://www.wiley-vch.de/home/angewandte/> or from the author.

represent a structurally unique pool of test substances that can not simply be replaced by synthetic efforts. In this context it is also of interest to determine the specific characteristics of individual natural product sources to provide a possible way of focussing and increasing the efficiency of sample selection.

Herein is a first effort to describe statistically the differences between the structural properties of natural products and synthetic substances so as to derive statements into the complementarity of these pools of structures; therefore two data bases, *DNP* and *BNPD*, which describe the bulk of the published natural products, two chemical data bases, which include available chemicals (*ACD*), and a representative pool of test substances (*Synthetics*), as well as a data base that covers pharmaceutical products/compounds in development (*Drugs*) were used (description in the methods section).

An evaluation of the molecular weight as well as the distribution of heteroatoms from the considered data bases was initially undertaken (see Figures 1–4). On average, natural products have higher molecular weights than the synthetic compounds; the distribution of the *Drugs* and *DNP* pool appear comparable. A lower number of nitrogen, halogen, or sulphur atoms was evident for natural products whereas the content of oxygen is rather increased. *Synthetics* have about 90% of the average highest content of nitrogen.

With regard to topological parameters the natural products (*DNP*) contain a relatively larger fraction of compounds with sp^3 -hybridized bridgehead atoms. Also the average number of rings and chiral centers per molecule is larger (Table 1). As a result natural products can statistically be described as sterically more complex structures.

In regard to the average number of different pharmacophoric groups, for example, amide groups, per molecule natural products (*DNP*, ca. 3.2 pharmacophors/molecule) together with *Synthetics* (ca. 3.3) are positioned between *Drugs* (ca. 3.7) and available chemicals (*ACD*, ca. 2.9). The abundance of certain pharmacophoric groups, however, differs strongly in natural products from those of *Drugs* and *Synthetics* (Figure 5). More distinctly the compounds in the data bases differ in regard to the abundancy of combinations of pharmacophoric groups (Table 2).

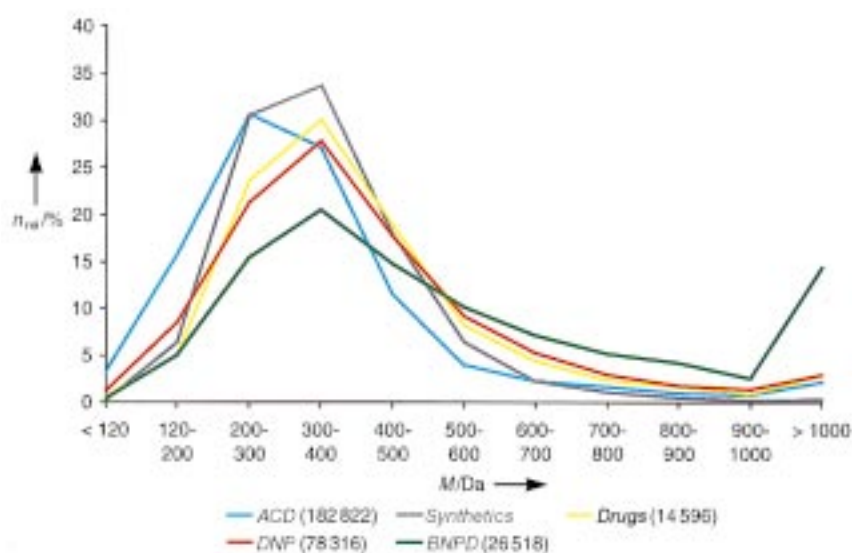


Figure 1. Distribution n of the molecular weights in the five data bases investigated. The numbers in brackets represent the total number of entries processed from the data bases.

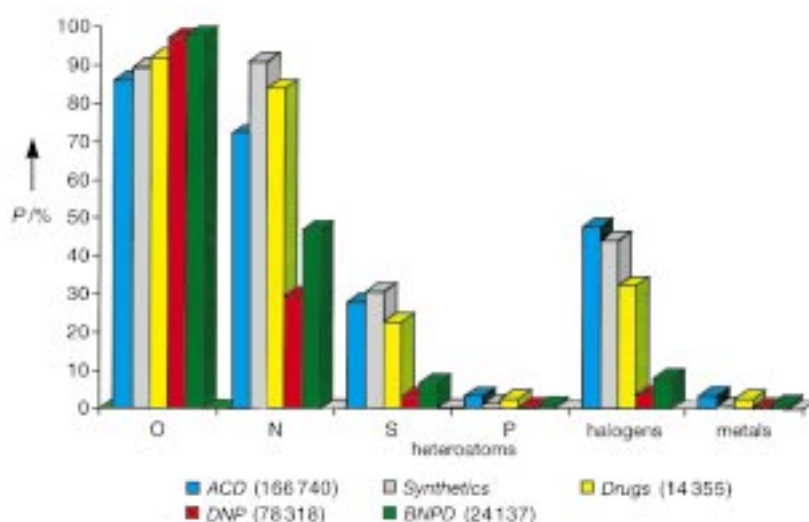


Figure 2. Population P of heteroatoms in the five data bases investigated.

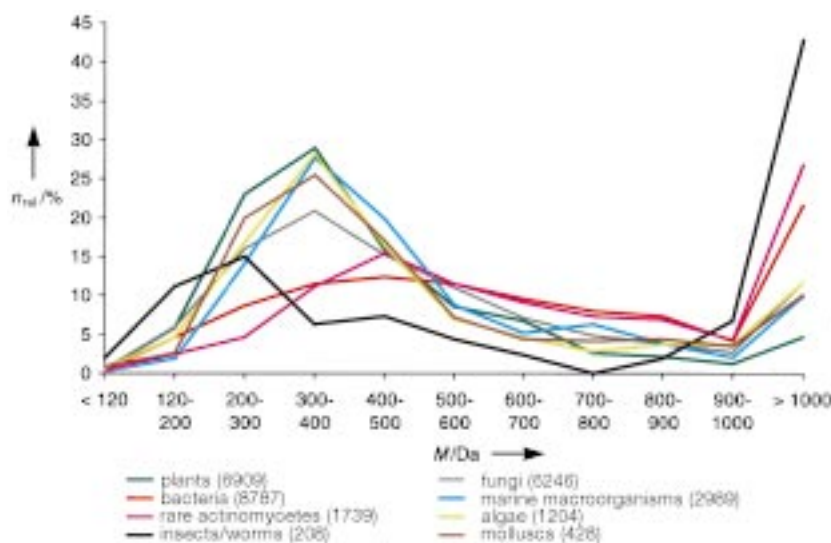


Figure 3. Distribution of the molecular weights of natural products according to producer organism (source: *BNPD*).

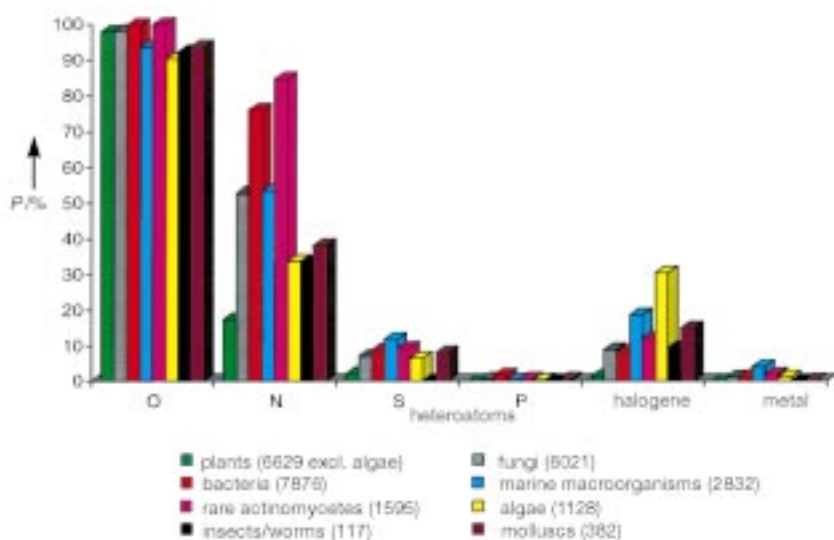


Figure 4. Population *P* of the heteroatoms in the natural products according to producer organisms (source: *BNPD*).

Table 1. Abundance of selected structural properties from all the individual entries of three representative data bases as well as the average number of structural properties per molecule.

Properties	Drugs	Synthetics	DNP
bridgehead atoms with three ring bonds	25 %	9 %	49 %
bridgehead atoms with four ring bonds	4 %	1.4 %	13 %
rotatable C–C bonds	74 %	58 %	66 %
rings per molecule	3.0	2.6	3.3
chiral centers per molecule	1.2	0.1	3.2
rotatable bonds per molecule	10.7	8.0	11.1

Table 2. Combinations of pharmacophoric groups and their abundance.

Pharmacophoric groups	Drugs [%]	Synthetics [%]	DNP [%]
alcohol/ether	19	5	41
alcohol/ester	10	3	30
arene/alcohol	24	13	40
arene/alcohol/ether	12	5	27
amine/arene	50	40	15
arene/amide	31	43	12
amine/arene/amide	20	15	5

The generally known high internal redundancy of natural products—thus the abundance with which at least one structural relative is discoverable for every type of molecule—was determined statistically as 85 % by a computer-based similarity analysis. The *DNP* pool can be reduced from about 80 000 substances to 11 500 structurally diverse types of molecules by excluding this redundancy. By comparison of the structural similarity between compounds in *DNP* with those of *Synthetics* it is evident that about 40 % of the natural products are not represented by synthetic compounds.

The potential of individual natural sources with regard to the structural properties was evaluated initially through comparison of the molecular weight and heteroatom distribution of compounds derived from single producer organisms extracted from *BNPD* (Figures 3 and 4). Significant differences of distribution become evident, for example, the significantly higher molecular weights of natural products from rare actinomycetes and the lower average content of nitrogen in plant substances. A large fraction of terpenes (ca. 35 %) and alkaloids (ca. 20 %) in the *DNP* as well as peptides (ca. 17 %) and alicycles (ca. 19 %) in the *BNPD* pool are found from an analysis of the distribution of the types of structures in the natural product data bases (Figure 6). Significant differences in population can likewise be discovered by dividing these

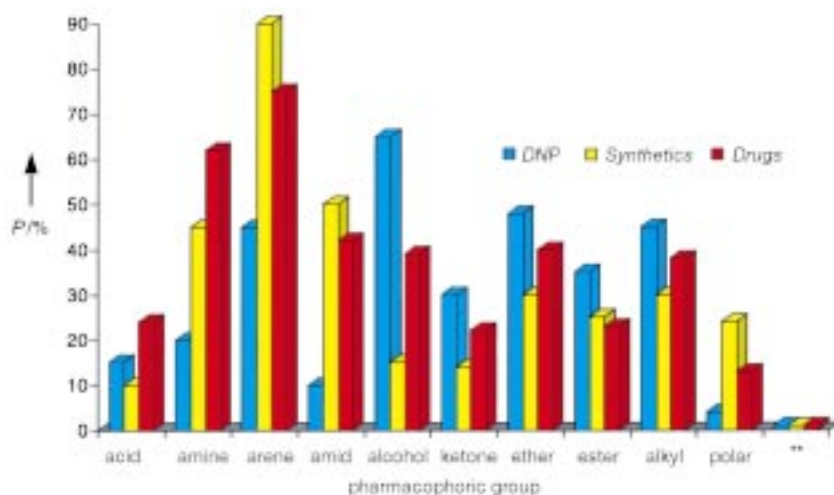


Figure 5. Population *P* of pharmacophore groups analyzed for the *DNP*, *Synthetics*, and *Drugs* data bases, ** = not classified, polar = F, CN, NO₂.

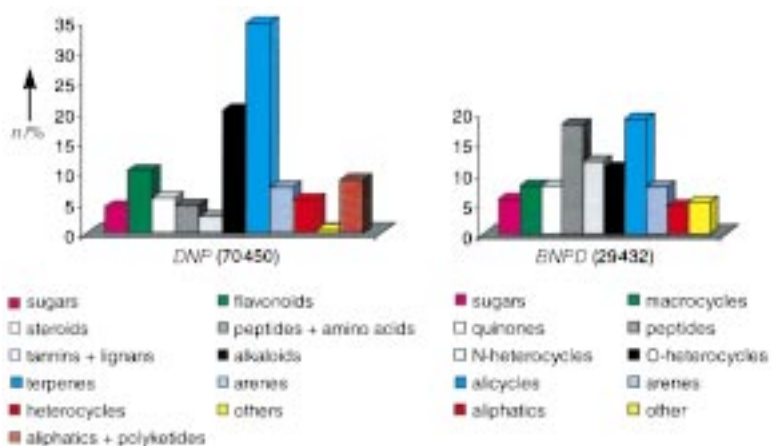


Figure 6. Distribution of structural types in the natural products for the data bases *DNP* and *BNPD* following their assignment in each data base; the data bases are based on different classifications and are listed separately.

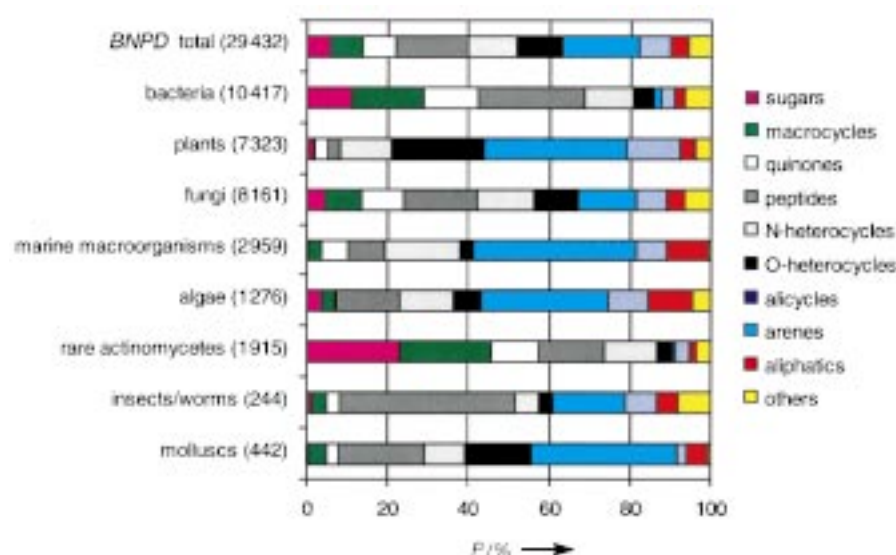


Figure 7. Populations P of the types of structures in the natural products produced by different organisms (source *BNPD*)

distributions in *BNPD* according to producer organisms (Figure 7). In comparison to the total distribution of all bioactive natural products in *BNPD* those of bacteria show an above-average share of macrocycles, which is on the contrary very low in plants. Clearly, a natural product pool that is representative of the types of structures can only be created by consideration of all natural sources. Conversely a supply of individual combinations of preferred types of structures can be obtained.

It can be derived from the number of natural products that have been sorted according to individual sources (Figure 3, 4, 7) that these sources vary in productivity and/or the degree of scientific investigation. More than 10000 bioactive substances from bacteria have been determined as opposed to less than 450 from molluscs. Collectively the origin of approximately 30000 bioactive natural products (*BNPD*) are divided into the four large sources: plants, bacteria, fungi, and animals in 27, 33, 26, and 13%, respectively. The number of bioactive natural products (*BNPD*) described against this background was examined according to year and source (Figure 8). It becomes evident that their number has increased continuously from about 800 between 1960–1965 to more than 5000 between 1990–1995. All the investigated sources contributed, but the numbers for fungi and marine metabolites have increased at a higher rate.

It follows that all the statistical evaluations show a distinct difference in the

considered structural properties of natural products relative to the investigated synthetic compounds. They highlight typical structural elements, which up to now have not been routine targets of synthesis for randomized substance pools. The structural variability of natural products between individual natural sources is conspicuous and should be considered according to certain demands. The potential for new natural products is not exhausted and natural products still represent an important source for the lead-finding process. Hence, the occasionally voiced prepossession that natural products have already been sufficiently examined and therefore no more innovations are to be expected can definitely be rejected for that reason.

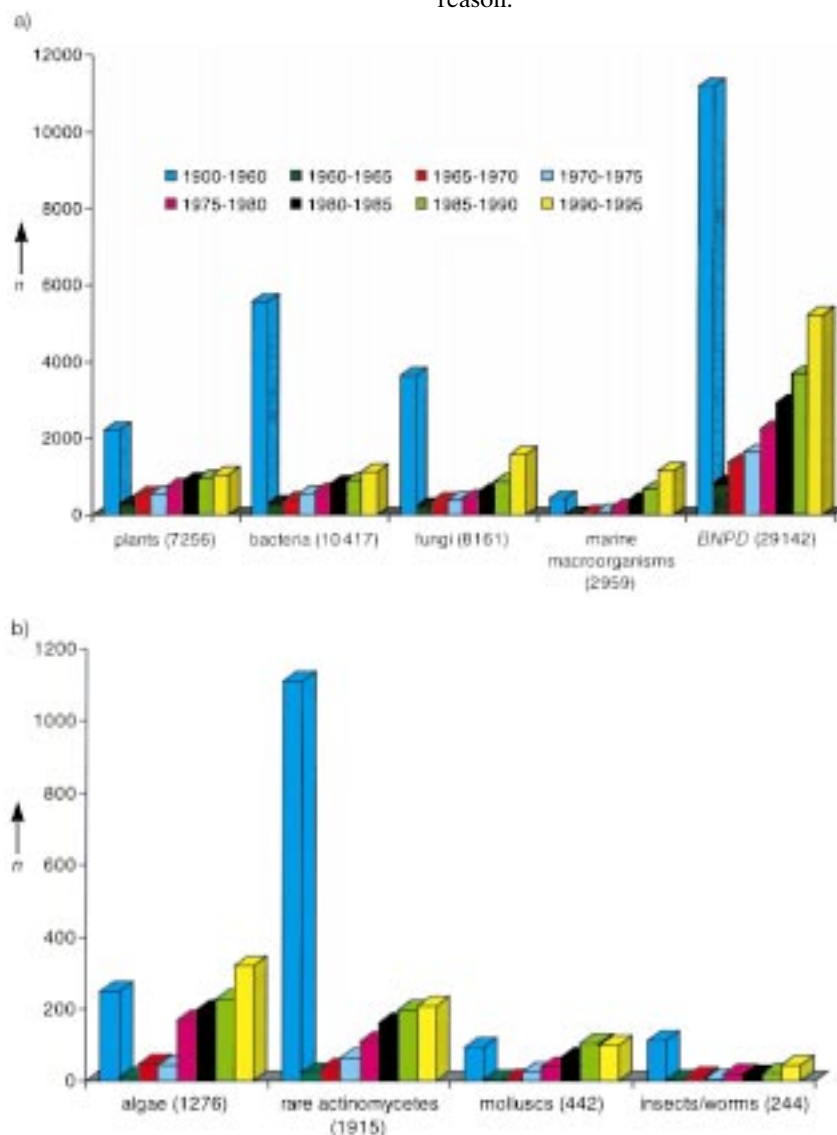


Figure 8. a), b) Time dependency of new entries in *BNPD* according to their biological source.

Method Section:

The data bases taken as the basis were:

- **DNP:** Dictionary of Natural Products on CD-ROM (Chapman&Hall), 78318 structural entries (status: June 96)
- **BNPD:** Bioactive Natural Product Database, Szenzor Management Consulting Company, Budapest, (Hungary) (by Berdy), 29432 entries of natural products with described biological activity (status: July 96)
- **Drugs:** Pharmaceutical products/compounds in development recorded in Pharmaprojects, RDFocus and in the active compounds pool of Bayer AG, 14596 entries (status: June 96)
- **ACD:** Available Chemicals Directory, Version 93.2, from Molecular Design Ltd. Information Systems Inc., San Leandro, CA (USA), 182822 entries
- **Synthetics:** Representative pool of synthetic test compounds from Bayer AG.

The construction of the data bases unavoidably resulted in some peculiarities in the data evaluation, which should be noticed in the detailed inspection of the determined results: *DNP* contains 78318 compounds from which however only 70450 appear as authentic natural products. In some cases it became necessary to use both data sets as a consequence of the restraints applied. *DNP* does not include any identifier for natural product sources, so that an evaluation of producer organisms was limited on *BNPD*. The numbers of investigated compounds in the figures are lower than the total numbers given in the data bases as the data sets are partly incomplete. For a clearer and simplified description only parts of selected data bases are compared in the tables and figures. The data bases were converted in MACCS^[3] and UNITY^[4]-format and analyzed with the available default methods for the evaluations related to structures. The structural similarity analysis between molecules was obtained from the 2D-fingerprint descriptors in the standard definition of UNITY.^[4] The similarity/dissimilarity between pairs of molecules was calculated according to Tanimoto^[5] and discussed in reference to a limiting value of 0.75. The analysis of pharmacophoric groups, predefined from a general chemical understanding, was carried out with software developed by Bayer AG. Full details can be found in the supporting information.

Received: October 7, 1998 [Z12501IE]
German version: *Angew. Chem.* **1999**, *111*, 688–691

Keywords: drug research • molecular diversity • natural products • statistical analysis • structural properties

- [1] a) G. M. Gragg, D. J. Newmann, K. M. Snader, *J. Nat. Prod.* **1997**, *60*, 52–60, and references therein; b) J. P. Pachlatko, *Chimica* **1998**, *52*, 29–47; c) Y.-Z. Shu, *J. Nat. Prod.* **1998**, *61*, 1053–1071.
- [2] PharmaQuant, Ranking of Ethnical Drug Products by Sales Value, Wood Mackenzie, **1998**.
- [3] MACCS-II, Version 2.3., Molecular Design Ltd. Information Systems, **1995**.
- [4] UNITY, Version 2.5., Tripos Inc., St. Louis, MO (USA), **1996**.
- [5] P. Willet, *Similarity and Clustering Systems*, Wiley, New York, **1987**.

Surface-Initiated Polymerization for Amplification of Self-Assembled Monolayers Patterned by Microcontact Printing**

Marc Husemann, David Mecerreyes, Craig J. Hawker,* James L. Hedrick,* Rahul Shah, and Nicholas L. Abbott*

The generation of complex patterns in polymer films is traditionally achieved by combining spin-casting and photolithographic techniques.^[1] Polymer films patterned by this procedure are widely used for the fabrication of microelectronic devices^[2] or as selective barriers to etchants^[3] and redox-active probes.^[4] While successful, the usefulness of these patterned polymer films is restricted by their limited stability with respect to solvents and their tendency to undergo subsequent chemical reactions^[5] as well as by difficulties in their preparation over large areas and complicated topographies.^[6] To address these latter challenges, Whitesides and co-workers have introduced the concept of microcontact printing (μ CP)^[7] for the preparation of patterned self-assembled monolayers (SAMs) on both planar and curved surfaces.^[8] Self-assembled monolayers formed from alkanethiols on gold and silver have been used as barriers to wet chemical etchants.^[9] In this approach, however, the usefulness of SAMs as barriers to etchants is compromised by the susceptibility of monolayer films to formation of defects,^[10] their lack of barrier properties when using dry etchants such as reactive ions, and the conflicting time scales necessary for complete formation of SAMs and for high-resolution patterning.^[11] To address these limitations, we report a first step in a program of research aimed at using polymerization as a tool for chemically amplifying surfaces patterned with organic molecules by microcontact printing into patterned polymer brushes.^[12] The preparation of a macromolecular barrier instead of a molecular one provides a means to mask defects within monolayers and to introduce resistance to a wide range of etchants. We also believe it can provide an avenue to high-resolution patterning of polymers through surface-initiated polymerization to mask incomplete regions of SAMs formed rapidly so as to minimize lateral transport of thiols. The work we report here also represents a general methodology for patterning polymeric films on surfaces.

The basic strategy of this novel process is depicted in Figure 1. Initially a nonreactive SAM formed from CH₃-

[*] Dr. C. J. Hawker, Dr. J. L. Hedrick, M. Husemann, D. Mecerreyes
IBM Almaden Research Center
650 Harry Road, San Jose, CA 95120-6099 (USA)
Fax: (+1) 408-927-3310
E-mail: hedrick@almaden.ibm.com

N. L. Abbott,^[+] R. Shah^[+]
Department of Chemical Engineering and Materials Science
University of California at Davis, Davis, CA (USA)

[+] Present address:
Department of Chemical Engineering
University of Wisconsin, Madison, WI (USA)

[**] We would like to thank the National Science Foundation Materials Research Science and Engineering Center (grant DMR-9400354) for the Center for Polymeric Interfaces and Macromolecular Assemblies and the IBM Corporation for financial support of this work.

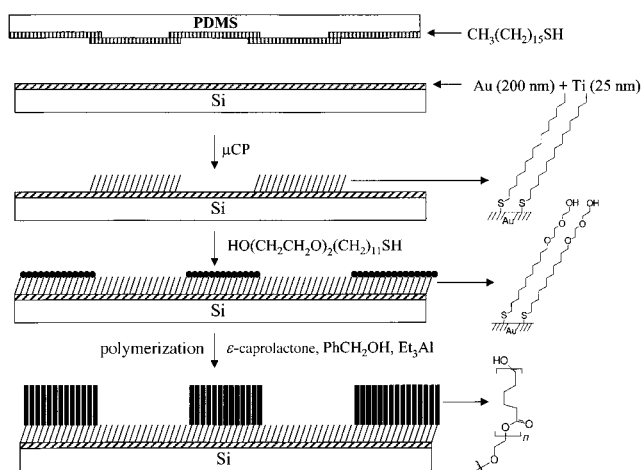


Figure 1. Scheme of strategy for amplification of a patterned SAM prepared by microcontact printing into a patterned polymer brush.

$(\text{CH}_2)_{15}\text{SH}$ is microcontact printed onto a gold surface by standard techniques.^[7] A second functionalized thiol, in this case $\text{HO}(\text{CH}_2\text{CH}_2\text{O})_2(\text{CH}_2)_{11}\text{SH}$ (**1**), is then selectively assembled onto the bare regions of the gold surface by simple immersion into a solution of the functionalized thiol. This procedure results in the formation of a surface patterned with regions of hydroxyl group functionalized SAMs and regions of nonfunctionalized SAMs.^[13] The pattern generated by this technique is, therefore, a direct representation of the original poly(dimethylsiloxane) (PDMS) stamp with the functionalized areas representing a negative image. The selection of the alkanethiol with a terminal di(ethylene glycol) group (**1**) as the initiating moiety was governed by our attempts to use simpler functionalized thiols such as $\text{HO}(\text{CH}_2)_{11}\text{SH}$ (**2**). We observed the surface properties of SAMs formed from **2** to change rapidly with time (Figure 2), and we found these surfaces to be unreliable for the growth of polymers.^[14] In contrast, the surface properties of SAMs formed from **1** were stable over extended periods and provided a highly reliable and reproducible route for the synthesis of hydroxyl group functionalized surfaces.

The final step in this strategy is the surface-initiated ring-opening polymerization (ROP) of ϵ -caprolactone from the functionalized areas of the patterned SAM. The incorporation of reactive hydroxyl groups permits the direct use of these groups, since they are known to be effective initiators for the

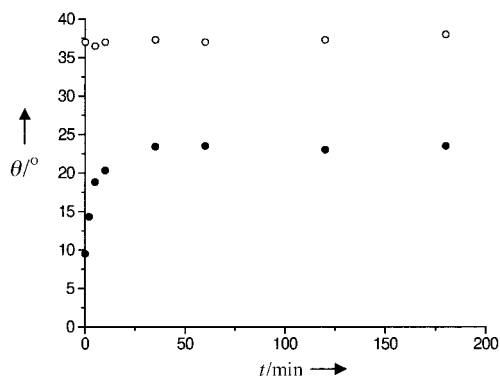


Figure 2. Advancing contact angles of water θ measured as a function of time t on SAMs from **1** (○) or **2** (●).

ROP of cyclic esters such as lactones and lactides in the presence of a suitable organometallic promoter such as aluminum alkoxides.^[15] Initial experiments involved the addition of triethylaluminum to the hydroxyl group containing patterned SAMs followed by addition of ϵ -caprolactone. This procedure resulted in either uncontrolled growth of polymer from the surface or in destruction of the patterned surface. Presumably this is due to the extremely low concentration of initiating sites on the patterned substrate, which leads to susceptibility to trace impurities. Furthermore, extremely large molar ratios of ϵ -caprolactone to the initiating sites leads to no control over the degree of polymerization of the chains grown from the surface. To overcome these difficulties, it was necessary to add a predetermined amount of "free" initiator such as benzyl alcohol to the reaction mixture. Dynamic exchange between the added free initiator and the surface-bound initiators mediates the polymerization, and therefore permits control of the degree of polymerization and thickness of the chains grown from the surface.^[16] This modified procedure resulted in the controlled growth of patterned polymer brushes in less than three hours at 25–30 °C. As can be seen in Figure 3, the thickness of the

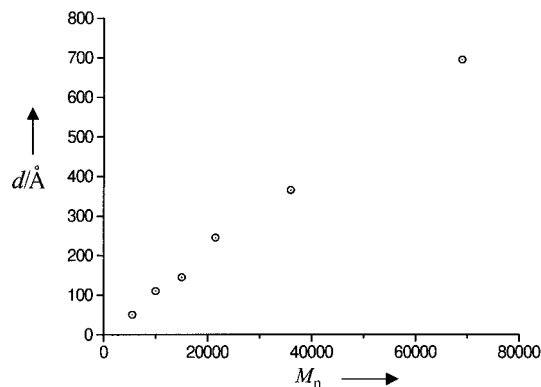


Figure 3. Ellipsometric thicknesses d of brushes of poly(caprolactone) measured as a function of the number-averaged molecular weight M_n of the free polymer formed from the added initiator.

poly(caprolactone) film is a linear function of the degree of polymerization of the polymer formed in solution from the free initiator. The degree of polymerization of the polymer formed in solution is in turn dictated by the initial ratio of benzyl alcohol to caprolactone.^[17] The "soluble" poly(caprolactone) was removed by repeated washing of the gold wafer with toluene and dichloromethane.

Chemical amplification of the patterned hydroxyl group functionalized SAM into spatially localized polymer brushes was confirmed by atomic force microscopy (AFM, Figure 4). The regions of the surface presenting hydroxyl groups were covered by continuous polymer films. Thicknesses of polymer films estimated from AFM images were in close agreement with those measured by ellipsometry. For example, a brush measured to have a thickness of 28 ± 4 nm by AFM was determined to have an ellipsometric thickness of 27 ± 3 nm. High-resolution AFM images reveal internal structure within the polymer films, which may reflect the semicrystalline nature of the poly(caprolactone) brushes.

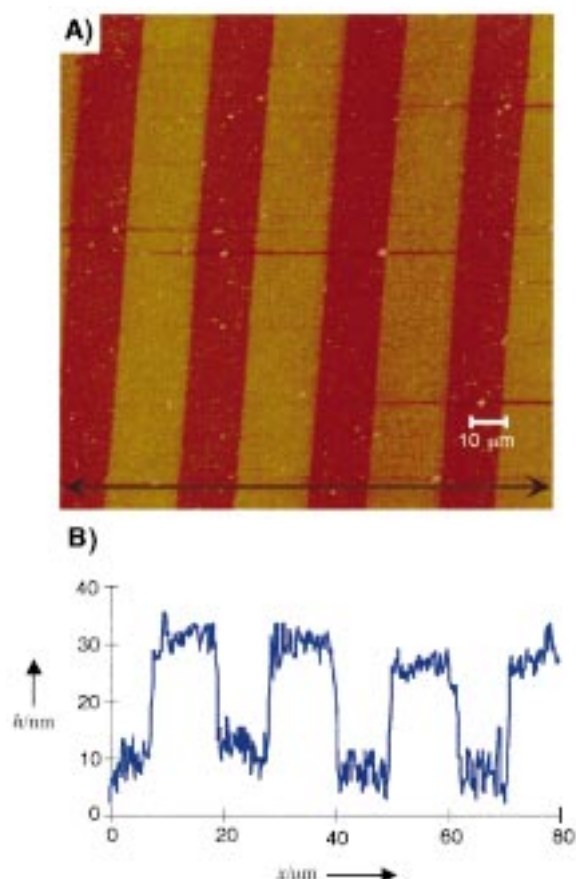


Figure 4. A) Low-resolution contact AFM image and B) cross-sectional profile of patterned brushes formed from poly(caprolactone); h = height of the polymer brush, x = pattern position. The location of the cross-sectional profile is marked in (A) by the double-headed arrow.

In conclusion, we have demonstrated a novel strategy for the preparation of patterned polymer brushes from microcontact printed gold surfaces. The key feature of this approach is the use of surface-initiated polymerization to chemically amplify the patterned SAM into a macromolecular film. This methodology not only leads to formation of patterned polymeric thin films without the need for expensive photolithographic tools, but also uses SAMs in a way that should be tolerant to imperfections within the original monolayer structure. Extension of this strategy to other living and controlled polymerization systems, as well as exploration of the etch and barrier resistance properties of these novel thin films, are under investigation.

Experimental Section

Materials and substrates: Gold films (200 nm) were deposited by electron beam evaporation on glass slides that had been primed with titanium (10–25 nm) to promote adhesion between the glass and gold. The elastomeric stamp was formed by pouring a mixture of PDMS prepolymer and its curing agent Sylgard 184CA (10/1 w/w) onto a clean polystyrene Petri dish. The dish was left at 60 °C for at least 12 h to ensure a complete cure of the polymer mixture. After removal of the master, the elastomeric stamp was rinsed three times with ethanol and dried under a flow of N_2 for 30 s. The thiol derivatives were prepared according to Whitesides et al.^[10]

Microcontact printing: A solution of 3 mM hexadecanethiol in ethanol was used as the ink. The stamp was inked by brushing its surface with a cotton swab soaked in the inking solution. The excess solvent was evaporated from

the stamp by placement of the stamp under a stream of N_2 for 30 s. The stamp was placed by hand onto a polycrystalline gold substrate and withdrawn after a contact period of about 5 s. The stamped gold substrate was washed with ethanol, dried under a flow of N_2 for 30 s, and immersed into a 1 mM solution of **1** in ethanol for 30 min. The slides were then washed with ethanol and dried under a flow of N_2 .

Polymerization: The diethylaluminum alkoxides were prepared in a glove box purged with argon. To a solution of benzyl alcohol (103 μ L, 1.0 mmol) in dry toluene (15 mL) was added dropwise triethylaluminum (0.55 mL of a 2.0 M solution, 1.1 equiv, 1.1 mmol). This solution was vigorously stirred at room temperature for 30 min. Gold films supporting either SAMs formed from **1** or patterned SAMs formed from **1** and hexadecanethiol were then placed into the solution and allowed to stand for 1 h before the toluene was removed under vacuum. Dry toluene (75 mL) was then added followed by ϵ -caprolactone (11.1 mL, 100 mmol), and the polymerization mixture stirred at room temperature for 3 h. To the viscous solution was added acetic acid (5 mL). After the mixture was stirred for 5 min, the gold wafers were removed and washed repeatedly with dichloromethane, toluene, THF, and ethanol. To measure the molecular weight and polydispersity of the polymer grown in solution, the supernatant from the polymerization mixture was precipitated into methanol (500 mL), collected by precipitation, and dried. The polydispersity of these materials were typically between 1.2 and 1.4, and the molecular weights were within 10% of the theoretical value.

Received: September 16, 1998 [Z12421IE]

German version: *Angew. Chem.* **1999**, *111*, 685–687

Keywords: atomic force microscopy • materials science • microcontact printing • polymerizations • polymers

- Q. J. Niu, J. M. J. Fréchet, *Angew. Chem.* **1998**, *110*, 685; *Angew. Chem. Int. Ed.* **1998**, *37*, 667.
- S. A. MacDonald, C. G. Willson, J. M. J. Fréchet, *Acc. Chem. Res.* **1994**, *27*, 151.
- F. P. Zamborini, R. M. Crooks, *Langmuir* **1997**, *13*, 122.
- K. Aoki, J. Osteryoung, *Anal. Chem.* **1981**, *125*, 315.
- R. Zerushalmi-Royen, J. Klein, L. Fetters, *Science* **1994**, *263*, 793.
- N. L. Leon, P. Clem, D. Y. Jung, W. Lin, G. S. Girolami, D. A. Payne, R. G. Nuzzo, *Adv. Mater.* **1997**, *9*, 891; b) N. L. Leon, K. Finnie, K. Branshaw, R. G. Nuzzo, *Langmuir* **1997**, *13*, 3382.
- Review: Y. Xia, G. M. Whitesides, *Angew. Chem.* **1998**, *110*, 568; *Angew. Chem. Int. Ed.* **1998**, *37*, 550.
- R. J. Jackman, J. L. Wilbur, G. M. Whitesides, *Science* **1995**, *269*, 664.
- A. Kumar, H. A. Biebuyck, G. M. Whitesides, *Langmuir* **1994**, *10*, 1498.
- A. Kumar, H. A. Biebuyck, N. L. Abbott, G. M. Whitesides, *J. Am. Chem. Soc.* **1992**, *114*, 9188.
- E. Delamarche, H. Schmid, A. Bietsch, N. B. Larsen, H. Rothuizen, B. Michel, H. A. Biebuyck, *J. Phys. Chem. B* **1998**, *102*, 3324.
- For polymer brushes prepared by surface-initiated free radical polymerization of vinyl monomers, see O. Prucker, J. Rühe, *Macromolecules* **1998**, *31*, 592; for living cationic polymerization of 2-oxazolines, see R. Jordan, A. Ulman, *J. Am. Chem. Soc.* **1998**, *120*, 243; for “living” free radical polymerization of vinyl monomers, see ref. [16].
- An alternate strategy for the patterning of a SAM has been reported: L. Yan, X.-M. Zhao, G. M. Whitesides, *J. Am. Chem. Soc.* **1998**, *120*, 6179; in this case a fully formed SAM is microcontact printed with a reactive derivative which leads to a patterned surface. An alternative approach to patterned polymer brushes has been reported: W. M. Lackowski, P. Ghosh, R. M. Crooks, *J. Am. Chem. Soc.*, in press. ■■
- S. D. Evans, R. Sharma, A. Ulman, *Langmuir* **1991**, *7*, 156.
- P. DuBois, R. Jerome, P. Teyessie, *Makromol. Chem. Makromol. Symp.* **1991**, *42*, 103; b) N. Ropson, P. DuBois, R. Jerome, P. Teyessie, *Macromolecules* **1995**, *28*, 7589.
- C. J. Hawker, J. L. Hedrick, E. E. Malmstrom, D. Benoit, J. Dao, G. G. Barclay, *Polym. Prepr.* **1998**, *39*(1), 626.
- The degree of polymerization is calculated by dividing the number of moles of monomer by the number of moles of free initiator; the overall contribution from the surface groups is small and hence neglected.

Sequence-Specific DNA Alkylation by Hybrid Molecules between Segment A of Duocarmycin A and Pyrrole/Imidazole Diamide**

Zhi-Fu Tao, Tsuyoshi Fujiwara, Isao Saito,* and Hiroshi Sugiyama*

Sequence-specific DNA-alkylating agents have received much current interest due to their significant potential in molecular biology and human medicine.^[1, 2] Duocarmycins, highly potent antitumor antibiotics, are among the most intriguing classes of such molecules that bind to AT-rich sequences and selectively alkylate N3 of adenine (A) at the 3' end of three or more consecutive AT base pairs in DNA.^[2] Duocarmycin A (Duo) has the highest reactivity among the

duocarmycin family and, in some cases, can alkylate N3 of guanine (G).^[3] Recently, we found that the addition of distamycin A (Dist) markedly modulates the Duo alkylation site in DNA fragments where alkylation occurs predominantly at the G residues in GC-rich sequences.^[4] We also demonstrated by NMR spectroscopy that the molecular mechanism of such a G alkylation involves cooperative formation of a heterodimer (Figure 1).^[5]

Polyamides containing *N*-methylimidazole (Im) and *N*-methylpyrrole (Py) developed by Dervan and co-workers as sequence-specific DNA-binding ligands have attracted much current attention.^[6] These polyamides bind cooperatively as an antiparallel dimer to the minor groove of the DNA helix. A simple binary code has been developed to correlate the reading DNA sequence with the side-by-side pairing between

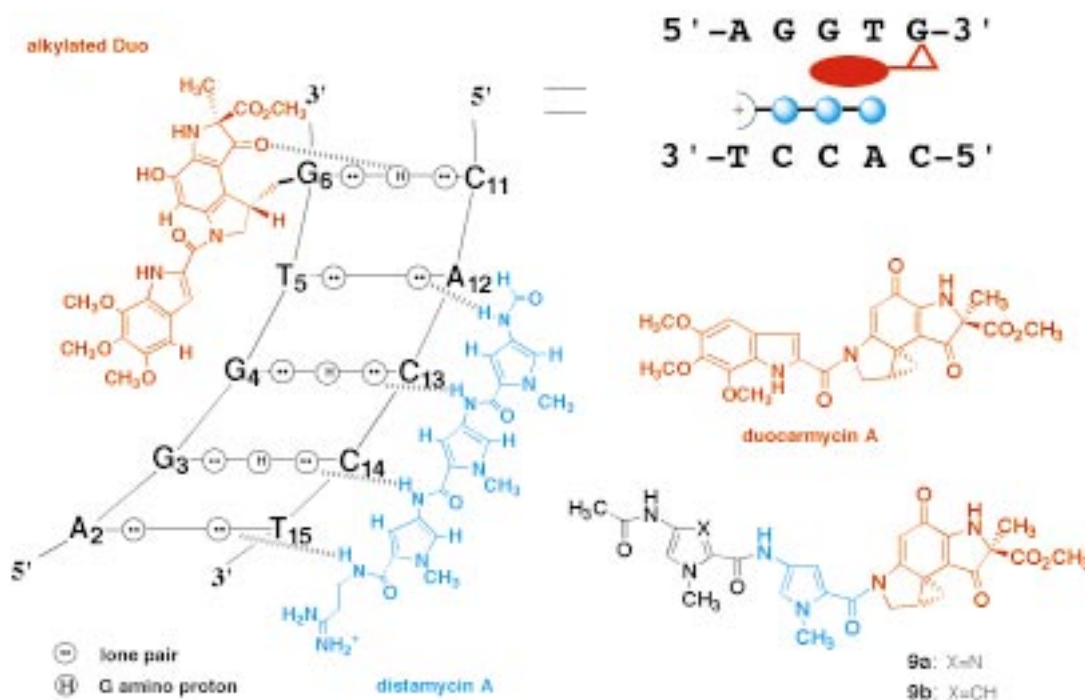


Figure 1. Schematic representation of the heterodimeric binding model of duocarmycin A (Duo) and distamycin A (Dist) to the minor groove of 5'-d(AGGTG)-3'-d(CACCT)-3' as well as the structures of Duo, Dist, and the hybrid compounds **9a** and **9b**. Hydrogen bonds between the drugs and DNA are illustrated by dashed lines.

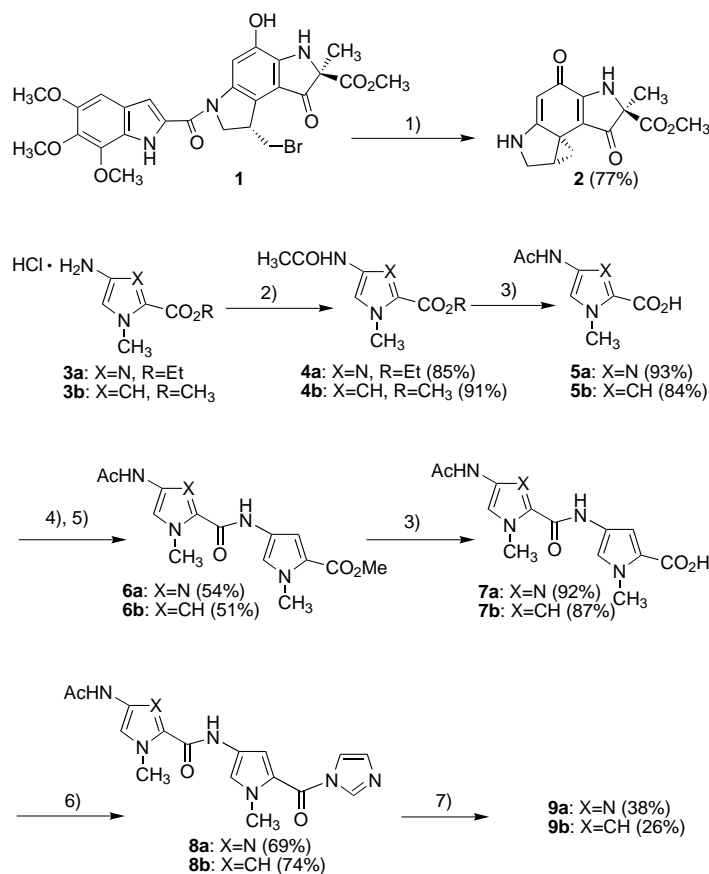
[*] Prof. I. Saito
Department of Synthetic Chemistry and Biological Chemistry
Faculty of Engineering, Kyoto University
Yoshida, Sakyo, Kyoto 606-8501 (Japan)
CREST, Japan Science and Technology Cooperation
Fax: (+81) 75-753-5656
E-mail: saito@sbchem.kyoto-u.ac.jp
Prof. H. Sugiyama, Dr. Z.-F. Tao, Dr. T. Fujiwara
Institute for Medical and Dental Engineering
Tokyo Medical and Dental University
2-3-10 Surugadai, Kanda, Chiyoda, Tokyo 101-0062 (Japan)
CREST, Japan Science and Technology Cooperation
Fax: (+81) 3-5280-8127
E-mail: sugiyama@chem.i-mde.tmd.ac.jp

[**] Duocarmycin B₂ was obtained from Kyowa Hakko through the courtesy of Dr. C. Murakata.

Supporting information for this article is available on the WWW under <http://www.wiley-vch.de/home/angewandte/> or from the author.

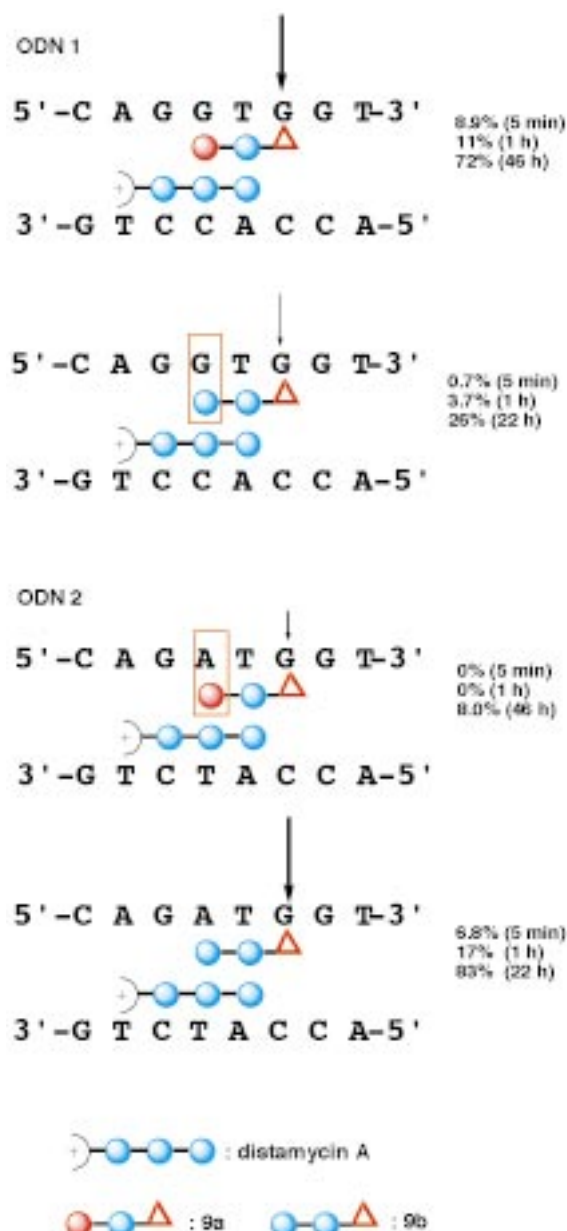
Py and Im carboxamides; that is, Im/Py recognizes GC base pairs and Py/Py recognizes AT base pairs.^[7] Our structure of a Duo-Dist-DNA octamer complex, as determined by NMR spectroscopy, clearly demonstrated that the heterodimer of Duo and Dist precisely binds to the minor groove, in that Dist recognizes the minor groove of one strand according to the binary code of Im/Py polyamides.^[5] In fact, our preliminary studies revealed that substitution of the Py unit of Dist with Im dramatically modulates the sequence specificity of Duo in a predictable manner. Therefore, based on these findings, a new class of tailor-made sequence-specific DNA-alkylating agents can be designed through the incorporation of the Py/Im polyamide subunit into the antitumor antibiotic Duo. Herein we describe the synthesis of novel hybrid molecules between segment A of Duo and Py/Im diamides and their ability to alkylate DNA in the presence and absence of Dist.

Hybrids **9a** and **9b** were prepared by the routes shown in Scheme 1. The hydrolysis of duocarmycin B₂ (**1**) readily produced the segment **2** as reported previously.^[8] Activated amides of the diamides (**8**) were prepared in five steps from amine hydrochloride salts **3**.^[9] The key step was the coupling of the activated amides **8** with the segment **2** to afford target compounds **9a** and **9b**, whose structures were fully characterized by ¹H NMR spectroscopy and high-resolution fast atom bombardment (FAB) mass spectrometry.



Scheme 1. Synthesis of hybrids **9a** and **9b**. 1) NaOMe, MeOH, CH₃CN; 2) pyridine, *N,N*-diisopropylethylamine (DIEA), Ac₂O; 3) NaOH, MeOH, H₂O; 4) dicyclohexyl carbodiimide (DCC), 1-hydroxy-1*H*-benzotriazole (HOBt), DMF; 5) **3b**, DIEA, DMF; 6) 1,1'-carbonyldiimidazole, DMF; 7) NaH, DMF, **2**.

Oligodeoxynucleotides (ODNs) **1** and **2** were initially selected to investigate DNA-alkylation modes of hybrids **9a** and **9b** in the presence and absence of Dist. As shown in Figure 2, ODNs **1** and **2** were match sequences for **9a** and **9b**, respectively. Analysis by HPLC of the reaction mixture of these ODNs incubated with **9a** and **9b** showed no appreciable alkylation products in the absence of Dist even after 46 h. In contrast, these new hybrids alkylated the target G⁶ of their match sequences in the presence of Dist efficiently and with high selectivity. For example, after 46 h of incubation 72% of ODN **1** was alkylated by **9a**, whereas only 8% of ODN **2** was alkylated by **9a** under the same conditions, because A⁴T¹³ of ODN **2** is a mismatch base pair to **9a** (Figure 2). In clear contrast, ODN **2** was smoothly alkylated by **9b**, and ODN **1** was only alkylated to 26% by **9b** after 22 h of incubation. Direct observations of the three- and fourfold negatively



charged ions for **9a**-Dist-ODN1 and **9b**-Dist-ODN2, respectively, by electrospray ionization mass spectrometry indicated that the alkylation occurs through cooperative formation of a heterodimer.^[10]

The sequence-selective alkylation by these hybrids was further confirmed using a TexasRed-labeled 450 base pair DNA fragment. Alkylated DNA fragments were cleaved at the alkylated sites by heating at 90°C, and the cleaved fragments were analyzed with a DNA sequencer.^[11] As shown in Figure 3, in the absence of Dist **9a** and **9b** selectively

alkylated the 3' end of A in AT-rich sequences, although **9b** is much more reactive than **9a**. The narrower the minor groove, the more efficient the alkylation, which is consistent with previously reported alkylation by a monomer.^[12] In contrast, in the presence of Dist, alkylation by **9a** predominantly occurred at the 3' end of guanosine in 5'-GTG-3' sequences within a 450 base pair DNA fragment. These results are in good agreement with the previously reported binary code for base pair recognition by Py/Im polyamides.^[7] The specificity of T over A at the 5' side of the reacting G residue observed in both hybrids can be explained by steric interaction with H5 protons of Duo, as observed in the previous study.^[5] Similarly, the **9b**-Dist heterodimer specifically alkylated the 3' end of G in the 5'-(T/A)TG-3' sequence (Figure 3). These results clearly indicated that the addition of Dist dramatically modulates the sequence selectivity of these hybrid molecules in a predictable manner. This is the first demonstration that the sequence-specific DNA alkylation at a specific atom can be accomplished by Py/Im polyamide ligands that bind DNA.

In conclusion, the present study outlines the preparation of novel hybrid molecules between segment A of Duo and Py/Im diamides. These hybrids primarily alkylate the 3' end of A in AT-rich sequences, as does the parent Duo. More importantly, these hybrids alkylate G residues of predetermined DNA sequences efficiently and with high specificity by formation of a heterodimer with Dist. Recently, Dervan and co-workers have demonstrated that synthetic Py/Im polyamides have a strong affinity and a full range of specificity to DNA sequences which are comparable to that in naturally occurring DNA-binding proteins.^[13] These polyamides are cell-permeable and inhibit transcription of specific genes in cell cultures.^[14] Results from the present investigation suggest a promising approach for developing a new generation of DNA-alkylating agents that can alkylate purine bases at any desired sites.

Received: August 31, 1998 [Z12351 IE]

German version: *Angew. Chem.* **1999**, *111*, 692–695

Keywords: alkylations • antibiotics • antitumor agents • DNA cleavage • DNA recognition

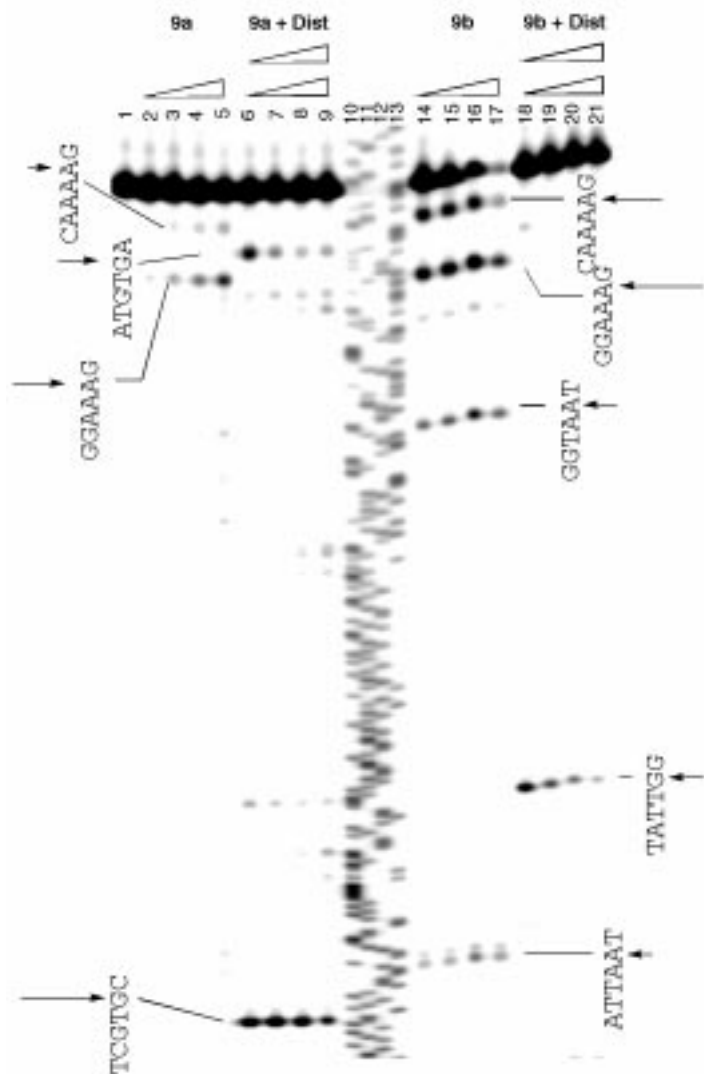


Figure 3. Thermally induced strand cleavage of a 5'-TexasRed-labeled pUC18F378–827 DNA fragment incubated with hybrids **9a** and **9b** in the presence and absence of Dist. Lane 1: DNA control; lanes 2–5: 4, 8, 16, and 32 μM **9a**, respectively; lanes 6–9: 4, 8, 16, and 32 μM **9a** with 8, 16, 32, and 64 μM Dist, respectively; lanes 10–13: Sanger G, C, T, and A sequencing standards; lanes 14–17: 4, 8, 16, and 32 μM of **9b**, respectively; lanes 18–21: 4, 8, 16, and 32 μM **9b** with 8, 16, 32, and 64 μM Dist, respectively. A singly 5'-TexasRed-labeled 450 base pair fragment was prepared by polymerase chain reaction (PCR) using 5'-TexasRed-modified 5'-TGTAACGACGGCCAGT-3' (pUC 18 forward 378–395), and 5'-TGCTGGCCTTTTGCTCACATG-3' (pUC 18 reverse 1861–1881) as primers. The 5'-TexasRed-labeled DNA fragment (75 nm) was alkylated in 8 μL of 12.5 mM Na phosphate buffer (pH 7.0) at room temperature overnight. The reaction was quenched by addition of calf thymus DNA (5 mM, 1 μL) and heated for 5 min at 90°C. DNA was collected by precipitation with ethanol. The pellet was resolved in 8 μL of loading dye (formamide with fushin red) and heated at 94°C for 20 min and then immediately cooled at 0°C. An aliquot (2 μL) was subjected to electrophoresis on 6% denaturing polyacrylamide gel with a 5500-S DNA sequencer.

- [1] For recent examples of sequence-specific DNA-alkylating agents, see a) E. A. Lukhtanov, I. V. Kutayin, V. V. Gorn, M. W. Reed, A. D. Adams, D. D. Lucas, R. B. Meyer, Jr., *J. Am. Chem. Soc.* **1997**, *119*, 6214–6225; b) K. Nakatani, A. Okamoto, I. Saito, *Angew. Chem.* **1997**, *109*, 2881–2883; *Angew. Chem. Int. Ed. Engl.* **1997**, *36*, 2794–2797; c) K. Nakatani, J. Shirai, S. Sando, I. Saito, *J. Am. Chem. Soc.* **1997**, *119*, 7625–7635; d) J. A. Hartley, *Molecular Basis of Specificity in Nucleic Acid–Drug Interaction* (Eds.: B. Pullman, J. Jortner), Kluwer, Dordrecht, **1990**, pp. 513–530; e) B. F. Baker, P. B. Dervan, *J. Am. Chem. Soc.* **1985**, *107*, 8266–8268.
- [2] a) D. L. Boger, D. S. Johnson, *Angew. Chem.* **1996**, *108*, 1542–1580; *Angew. Chem. Int. Ed. Engl.* **1996**, *35*, 1438–1474; b) D. L. Boger, *Acc. Chem. Res.* **1995**, *28*, 20–29; c) D. L. Boger, D. S. Johnson, *Proc. Natl. Acad. Sci. USA* **1995**, *92*, 3642–3649; d) H. Sugiyama, M. Hosoda, I. Saito, A. Asai, H. Saito, *Tetrahedron Lett.* **1990**, *31*, 7197–7200.
- [3] H. Sugiyama, K. Ohmori, K. L. Chan, M. Hosoda, A. Asai, H. Saito, I. Saito, *Tetrahedron Lett.* **1993**, *34*, 2179–2182.
- [4] K. Yamamoto, H. Sugiyama, S. Kawanishi, *Biochemistry* **1993**, *32*, 1059–1066.

- [5] H. Sugiyama, C. Lian, M. Isomura, I. Saito, A. H.-J. Wang, *Proc. Natl. Acad. Sci. USA* **1996**, *93*, 14405–14410.
- [6] Recent reviews: a) D. E. Wemmer, P. B. Dervan, *Curr. Opin. Struct. Biol.* **1997**, *7*, 355–361; b) P. E. Nielsen, *Chem. Eur. J.* **1997**, *3*, 505–508; see also c) J. M. Turner, E. E. Baird, P. B. Dervan, *J. Am. Chem. Soc.* **1997**, *119*, 7636–7644; d) R. P. Lamamie de Clairac, B. H. Geierstanger, M. Mrksinch, P. B. Dervan, D. E. Wemmer, *J. Am. Chem. Soc.* **1997**, *119*, 7909–7916; e) S. E. Swalley, E. E. Baird, P. B. Dervan, *J. Am. Chem. Soc.* **1997**, *119*, 6953–6961; f) X. Chen, B. Ramakrishnan, M. Sundaralingam, *J. Mol. Biol.* **1997**, *267*, 1157–1170; g) M. L. Kapla, D. S. Goodsell, G. W. Han, T. K. Chiu, J. W. Lown, R. E. Dickerson, *Structure* **1997**, *5*, 1033–1046; h) S. E. Swalley, E. E. Baird, P. B. Dervan, *Chem. Eur. J.* **1997**, *3*, 1600–1607; i) C. L. Kielkopf, E. E. Baird, P. B. Dervan, D. C. Rees, *Nat. Struct. Biol.* **1998**, *5*, 104–109.
- [7] a) S. White, E. E. Baird, P. B. Dervan, *Chem. Biol.* **1997**, *4*, 569–578; b) S. White, E. E. Baird, P. B. Dervan, *Biochemistry* **1996**, *35*, 12532–12537.
- [8] T. Yasuzawa, K. Muroi, M. Ichimura, I. Takahashi, T. Ogawa, K. Takahashi, H. Sano, Y. Saitoh, *Chem. Pharm. Bull.* **1995**, *43*, 378–391.
- [9] E. E. Baird, P. B. Dervan, *J. Am. Chem. Soc.* **1996**, *118*, 6141–6146.
- [10] Alkylation by a heterodimer was directly confirmed by electrospray ionization mass spectrometry: **9a**-Dist-ODN 1: calcd: 5863.3, found: 5863.2; **9b**-Dist-ODN 2: calcd: 5861.4, found: 5860.8.
- [11] Subsequent treatment with hot piperidine (90 °C, 20 min) did not further increase the intensity of the cleavage bands, indicating that the present heating condition is sufficient to cleave all alkylated DNA.
- [12] a) A. Abu-Daya, P. M. Brown, K. R. Fox, *Nucleic Acids Res.* **1995**, *23*, 3385–3392; b) C. M. Nun, E. Garman, S. Neidle, *Biochemistry* **1997**, *36*, 4792–4799; c) D. L. Boger, T. Ishizaki, H. Zarrinmayeh, S. A. Munk, P. A. Kitos, O. Suntornwat, *J. Am. Chem. Soc.* **1990**, *112*, 8961–8971.
- [13] a) J. W. Trauger, E. E. Baird, P. B. Dervan, *Nature* **1996**, *382*, 559–561; b) S. White, J. W. Szwedczyk, J. M. Turner, E. E. Baird, P. B. Dervan, *Nature* **1998**, *391*, 468–471.
- [14] J. M. Gottesfeld, L. Neely, J. W. Trauger, E. E. Baird, P. B. Dervan, *Nature* **1997**, *387*, 202–205.

An Open-Framework Germanate with Polycubane-Like Topology**

Hailian Li, Mohamed Eddaoudi, and Omar M. Yaghi*

The ability of germanates to form extended structures with GeO_4 tetrahedra, GeO_5 trigonal bipyramids, and GeO_6 octahedra, coupled with their tendency to adopt a lower M–O–M (M = Ge) minimum angle than that of silicate-based solids, implies that a high number of possible structures with open-framework topologies can be potentially accessed.^[1–3] Unexpectedly, however, only a few porous germanates have been reported thus far.^[4–9] By using synthetic methods analogous to those employed for the production of zeolites and related crystalline materials,^[10] we have synthesized and structurally characterized an open-framework germanate

$[\text{Ge}_9\text{O}_{18}(\text{OH})_4] \cdot 2\text{H}_2\text{ppz} \cdot 0.5\text{H}_2\text{O}$ (ASU-14, ppz = piperazine = $\text{HNC}_4\text{H}_8\text{NH}$), which is constructed from Ge_9 body-centered parallelepiped building blocks. These are linked together at each of their eight vertices to give the rare polycubane topology with an intersecting channel system of ten- and eight-membered rings in which the piperazinium cations and water molecules reside.

ASU-14 was prepared by heating a mixture of germanium dioxide, piperazine, water, pyridine, and HF in the molar ratio 1.0:2.4:31.0:27.7:0.80 to 165 °C for four days. A crystalline colorless solid was recovered in 76% yield (based on germanium dioxide) upon cooling this mixture. Elemental microanalysis performed on a bulk sample of this material gave the composition $[\text{Ge}_9\text{O}_{18}(\text{OH})_4] \cdot (\text{H}_2\text{ppz})_2(\text{H}_2\text{O})_{0.5}$ (calcd: C 8.04, H 2.45, N 4.69, Ge 54.68, F 0.00%; found: C 7.70, H 2.47, N 4.61, Ge 53.06, F 0.19%).

An X-ray diffraction analysis of a single crystal isolated from the reaction product revealed a three-dimensional open framework constructed from the $[\text{Ge}_9\text{O}_{18}(\text{OH})_4]$ units shown in Figure 1. A GeO_6 octahedral germanium center links two Ge_4 units that are related by an inversion center. Each of these

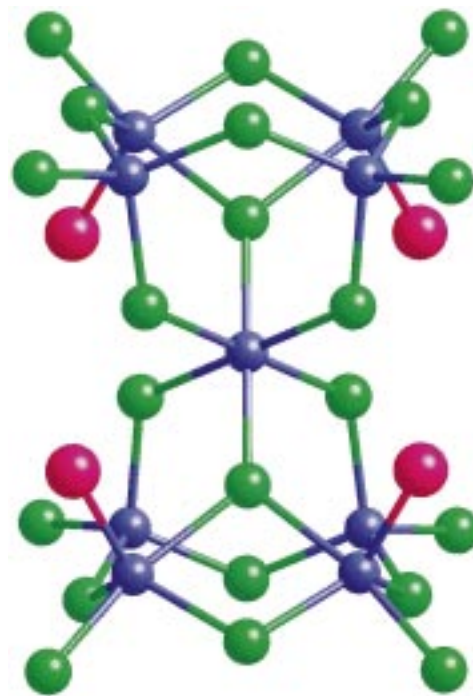


Figure 1. The building block unit present in crystalline $[\text{Ge}_9\text{O}_{18}(\text{OH})_4] \cdot 2\text{H}_2\text{ppz} \cdot 0.5\text{H}_2\text{O}$ (ASU-14), with atoms represented by spheres: blue: Ge, green: O, pink: OH.

units is constructed from a pair of GeO_4 tetrahedra and a pair of $\text{GeO}_4(\text{OH})$ trigonal bipyramids. These are linked together through doubly bridging oxides to yield eight germanium centers that are positioned at what can be considered as the corners of a body-centered parallelepiped building block. The tetrahedral and trigonal bipyramidal Ge atoms are connected to the Ge atom at the center through doubly and triply bridging oxides, respectively. All Ge–O distances for tetrahedral germanium centers (mean: 1.734(9) Å) are similar to those reported for the quartz modification of GeO_2

[*] Prof. O. M. Yaghi, H. Li, M. Eddaoudi
Supramolecular Design and Discovery Group
Department of Chemistry and Biochemistry
Arizona State University, Tempe, AZ 85287–1604 (USA)
Fax: (+1) 602-965-2747
E-mail: oyaghi@asu.edu

[**] This work was supported by the National Science Foundation (CHE-9702131). We thank Prof. M. O’Keeffe for invaluable discussions.

(1.741(3) Å).^[11] The Ge–O distances within the trigonal bipyramidal and octahedral germanium centers vary in the range 1.763(10)–2.005(9) Å, which is in general agreement with those observed in similar compounds.^[4–9] However, each trigonal bipyramidal Ge atom has a terminal hydroxide ligand as evidenced by their slightly elongated Ge–OH contacts (1.779(9) and 1.763(9) Å) relative to other Ge–O(doubly bridging) distances (1.736(8) and 1.734(8) Å) in the structure, and by the presence of a sharp band at 3671 cm^{−1} in the FT-IR spectrum of this material, which is within the expected range for $\tilde{\nu}_{\text{O-H}}$ stretching frequency.^[12] The remaining oxygen atoms, connected to each of the Ge atoms at the corners (one per Ge atom), serve as doubly bridging linkers to neighboring Ge₉ clusters; which thus yields an open framework with an intersecting three-dimensional channel system (Figure 2 top).

The Ge₉ units observed in ASU-14 are closely related to similar parallelepiped building blocks that can be discerned in the germanate [Ge₁₈O₃₈(OH)₄]^{8−}.^[5] Here, instead of having four terminal hydroxide ligands linked to Ge₄ units as observed in the title compound, only two hydroxide groups act as terminal ligands while the remaining two condense to form a doubly bridging oxide that serves to link two different Ge₄ units of the same Ge₉ arrangement.

An instructive way to view the net adopted by ASU-14 involves the recognition that each of the Ge centers at the corners of the parallelepiped building blocks is in fact four coordinate, which leads to an open polycubane-like topology of the composition GeO₂ (Figure 2 bottom). This topology is a rare structural arrangement that was proposed nearly forty years ago, but only achieved recently in the porous structure of the aluminium cobalt phosphate (ACP-1) material.^[13, 14] Here Co(Al)PO₄ cube units are linked at their corners into a cubic body-centered array that leads to pseudo-octagonal micropores with a diameter of 3.8 Å. Larger pores are observed in ASU-14 as a consequence of the larger size of the parallelepiped building blocks. In fact, three intersecting channels run along the crystallographic *a*, *b*, and *c* axes and permeate the framework with ten-, ten-, and eight-membered ring apertures with free pore diameters of nearly 5 × 6, 5 × 6, and 4 × 4 Å, respectively. The foregoing discussion of the structure requires that the framework has a charge of 4−, which is balanced by two diprotonated ppz guests that occupy the channels as confirmed by elemental microanalysis (see above). It should be noted that because of crystallographic disorder of the guests it is difficult to exclude the possibility that small amounts of solvent species such as pyridine are in the pores in addition to piperazinium cations and water. Preliminary thermal gravimetric measurements on a crystalline sample (42.37 mg) of this material showed no mass loss up to 200 °C. A gradual weight loss of 12.6 % is observed in the temperature range 200–330 °C, which is attributed to the decomposition of Hppz and liberation of water from the channels (calculated: 15.5 %). It appears that Hppz is strongly bound to the framework since a lower than expected weight loss is observed upon heating. Consequently, attempts to exchange Hppz with inorganic cations such as Na⁺ and Ag⁺ were not successful.

We believe that germanates offer many possibilities for the formation of cluster building blocks, which are an attractive

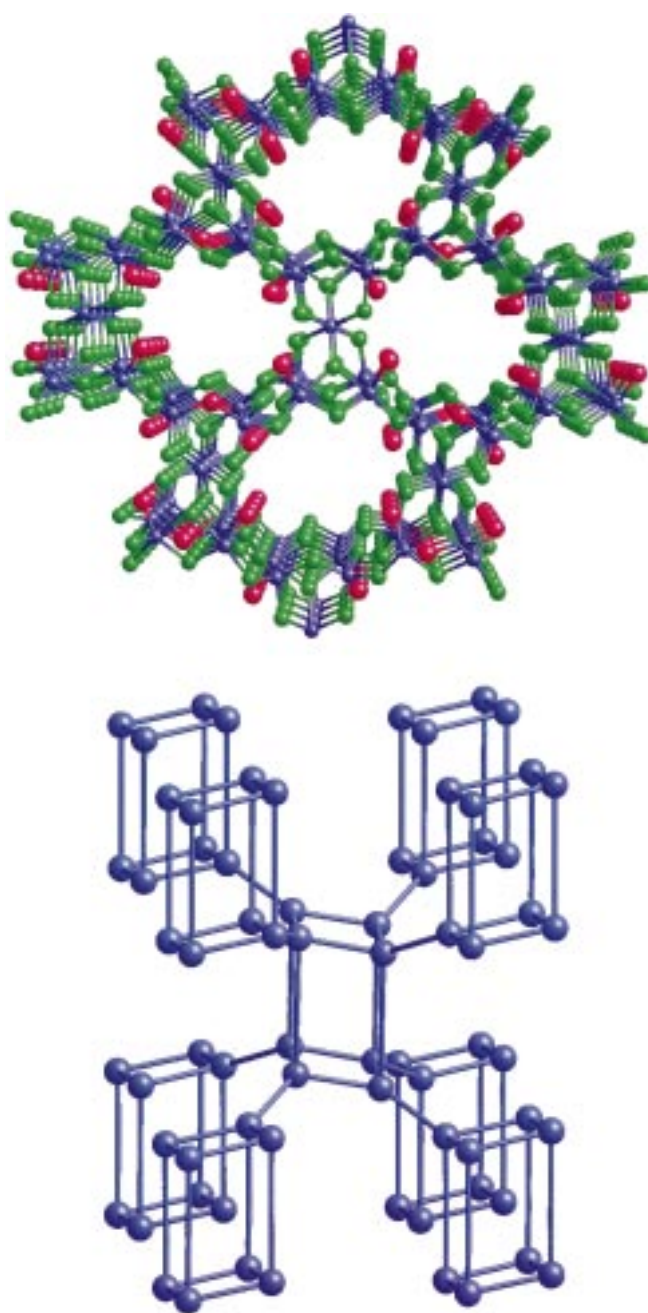


Figure 2. The crystal structure of the three-dimensional porous framework of ASU-14: top: viewed along the crystallographic *b* axis with all guest species omitted for clarity; bottom: a view representing its topology with only the four-coordinate germanium centers shown. The color code is the same as that used in Figure 1.

aspect of this chemistry that is expected to yield a more extensive class of open-frameworks than that of silicate-based compounds.

Experimental Section

X-ray structure analysis: Colorless columnar single crystals of [Ge₉O₁₈(OH)₄] · 2H₂ppz · 0.5H₂O (ASU-14) were analyzed at −155 ± 1 °C, triclinic, space group *P* − 1 (No. 2), *a* = 10.1385(3), *b* = 10.3465(3), *c* = 12.8517(1) Å, *α* = 89.597(1), *β* = 89.291(1), *γ* = 88.923(1)°, *V* = 1347.74(6) Å³, *Z* = 2, ρ_{calcd} = 2.870 g cm^{−3}, $\mu(\text{MoK}\alpha)$ = 99.84 cm^{−1}. A full hemisphere of diffracted intensities (θ = 0.3° counted for a total of 10.0 s per frame) was measured

with graphite-monochromated $\text{MoK}\alpha$ radiation on a Siemens/Bruker SMART CCD single crystal diffraction system. Cell constants and an orientation matrix were obtained from least-squares refinement by using the measured positions of 4386 reflections with $I > 10\sigma$ in the range $3.00 < 2\theta < 45.00^\circ$. The Siemens/Bruker program SHELXTL-PC software package was used to solve the structure by direct methods. All stages of weighted full-matrix least-squares refinement were conducted with F_o^2 data with the SHELXTL-PC Version 5 software package and converged to give $R_1(F) = 0.062$ for 3300 independent absorption-corrected reflections with $2\theta(\text{MoK}\alpha) < 49.5^\circ$ and $I > 2.50\sigma(I)$ and $wR_2(F^2) = 0.069$ with a GOF = 1.70. As a consequence of the twinning found in the crystal some reflections were from the major twin only, and some were measured from both components. At the end of the refinement 87 reflections which had $F_o > F_c$ and $w\Delta F^2 > 5$ were removed from the refinement to allow all of the Ge atoms to refine anisotropically. Crystallographic data (excluding structure factors) for the structure reported in this paper have been deposited with the Cambridge Crystallographic Data Centre as supplementary publication no. CCDC-114519. Copies of the data can be obtained free of charge on application to CCDC, 12 Union Road, Cambridge CB2 1EZ, UK (fax: (+44) 1223-336-033; e-mail: deposit@ccdc.cam.ac.uk).

Received: May 12, 1998

Revised version: October 29, 1998 [Z11848IE]

German version: *Angew. Chem.* **1999**, *111*, 682–685

Keywords: cubanes • germanium • microporosity • solid-state structures • zeolite analogues

- [1] A. F. Wells, *Structural Inorganic Chemistry*, 5th ed, Clarendon, Oxford, **1984**.
- [2] M. O'Keeffe, B. G. Hyde, *Crystal Structures: I. Patterns and Symmetry*, Mineralogical Society of America, Washington, DC (USA), **1996**.
- [3] W. M. Meier, D. H. Olson, Ch. Baerlocher, *Atlas of Zeolite Structure Types*, Elsevier, Boston, MA (USA), **1996**.
- [4] M. A. Roberts, A. N. Fitch, *Z. Kristallogr.* **1996**, *211*, 378–387.
- [5] R. H. Jones, J. Chen, J. M. Thomas, A. George, M. B. Hursthouse, R. Xu, S. Li, Y. Lu, G. Yang, *Chem. Mater.* **1992**, *4*, 808–812.
- [6] J. C. Cheng, R. Xu, G. Yang, *J. Chem. Soc. Dalton Trans.* **1991**, 1537–1540.
- [7] C. Cascales, E. Gutierrez-Puebla, M. A. Monge, C. Ruiz-Valero *Angew. Chem.* **1998**, *110*, 135–138; *Angew. Chem. Int. Ed.* **1998**, *37*, 129–131.
- [8] A. J. C. Wilson, Eds. *Structure Reports, Vol. 11*, Oosthoek-Utrecht, The Netherlands, **1947–1948**, p. 405.
- [9] S. Feng, M. Tsai, M. Greenblatt, *Chem. Mater.* **1992**, *4*, 388–393.
- [10] J. M. Newsam, in *Solid State Chemistry: Compounds* (Eds.: A. K. Cheetham, P. Day), Clarendon, Oxford, **1992**.
- [11] G. S. Smith, P. B. Isaacs, *Acta Cryst.* **1964**, *17*, 842.
- [12] E. A. Knyazev, A. N. Akulov, *Russ. J. Inorg. Chem. (Engl. Transl.)* **1973**, *18*, 139–141.
- [13] R. M. Barrer, F. W. Bultitude, I. S. Kerr, *J. Chem. Soc.* **1959**, 1521–1528.
- [14] P. Feng, X. Bu, G. D. Stucky, *Science* **1997**, *388*, 735–740.

Induced Color Change of Conjugated Polymeric Vesicles by Interfacial Catalysis of Phospholipase A₂**

Sheldon Yoshio Okada, Raz Jelinek, and Deborah Charych*

Conjugated polymers (CPs) such as polydiacetylene (PDA), polythiophene, and polypyrrole display a remarkable array of color transitions that arise from thermal changes (thermochromism),^[1] mechanical stress (mechanochromism),^[2] or ion binding (ionochromism).^[1, 3] The color changes can be ascribed to a change in the effective length of conjugation of the delocalized, π -conjugated polymer backbone.^[4] The application of these “smart” materials for the detection of biological targets (biochromism)^[5–11] is only just beginning to be exploited.

Interfacial catalysis on biomembranes plays a key role in extra- and intracellular processes and covers a range of enzyme classes such as lipolytic enzymes, acyltransferases, protein kinases, and glycosidases. In particular, lipolytic enzymes are involved in important biochemical processes, such as fat digestion and signal transduction. Recent interest in one such enzyme, phospholipase A₂ (PLA₂),^[12, 13] is motivated by its role in the release of arachidonate and lysophospholipids from membranes. These compounds are the precursors for the biosynthesis of eicosanoids (for example, prostaglandins, leukotrienes) that have been implicated in a range of inflammatory diseases such as asthma, ischaemia, and rheumatoid arthritis.^[14–16] Accordingly, the identification of PLA₂ inhibitors is an active area of current research that may lead to novel therapeutics and new biochemical insights into the mechanisms of enzyme activity.^[16–18]

PLA₂ catalyzes the hydrolysis of an acyl ester bond exclusively at the 2-acyl position in glycerophospholipids to

[*] Dr. D. Charych^[+]

Principal Investigator, Center for Advanced Materials
Materials Sciences Division
Lawrence Berkeley National Laboratory, Berkeley, CA 94720 (USA)
S. Y. Okada^[++]
Center for Advanced Materials, Materials Sciences Division
Lawrence Berkeley National Laboratory, Berkeley, CA 94720 (USA)
Prof. R. Jelinek
Department of Chemistry, Ben Gurion University of the Negev
Beer-Sheva 84105 (Israel)

[+] New address:

Chiron Technologies
4560 Horton Avenue, Emeryville, CA 94607 (USA)
Fax: (+1) 510-923-3360
E-mail: deb_charych@cc.chiron.com

[++] New address:

Department of Chemistry
Caltech University
Pasadena, CA (USA)

[**] This work was supported by the Office of Naval Research (Contract No. N0001497F0181) and the Director, Office of Energy Research, Office of Basic Energy Sciences, Division of Materials Sciences, and also by the Division of Energy Bio-Sciences of the U.S. Department of Energy (Contract No. DE-AC03-76SF0098). We thank Professor Mahendra Jain for his kind gift of inhibitor compound MJ33 and for his helpful comments and suggestions. D.C. acknowledges Dr. Mark Alper, Project Director of the Biomolecular Materials Program for his continued support.

yield a free fatty acid and a lysophospholipid. Typical methods for measuring PLA₂ activity include discontinuous radiochemical,^[19] fluorescent,^[20] and spectrophotometric^[21] techniques. Labeled acyl phospholipids are used as substrates in these measurements and enzyme activity is evaluated by the radioactivity, fluorescence, or absorbance of the cleaved fatty acids. Some procedures (particularly radiolabel methods) may require that the cleaved fatty acids be extracted and isolated from the unreacted substrate by thin-layer chromatography or HPLC. The extraction step and the need for synthetic labeled substrates are disadvantages when the rapid analysis of enzyme

activity is considered, for example in high throughput assays that screen potential enzyme inhibitors. Furthermore, phospholipase catalysis is sensitive to the chemical structure of the phospholipid substrate,^[22, 23] therefore the use of nonlabeled, naturally occurring substrates is highly desirable. The biochromic vesicles described herein offer a one-step approach to measuring enzyme activity through detection of a color change of PDA "signaling" lipids that surround the natural enzyme substrate. The strategy does not require additional chemical reagents or post-hydrolysis analytical methods. Furthermore, enzyme inhibitors can be rapidly identified by simply monitoring the color changes of aqueous vesicle suspensions in a standard 96-well microtiter plate.

PLA₂ activity has previously been studied in a variety of model membrane systems such as polymerized vesicles,^[24, 27] micelles,^[21] and monolayers.^[22, 25] The biochromic vesicles^[5, 6, 8] employed here are prepared by probe sonication of a mixture of the polymerizable matrix lipid 10,12-tricosandynoic acid

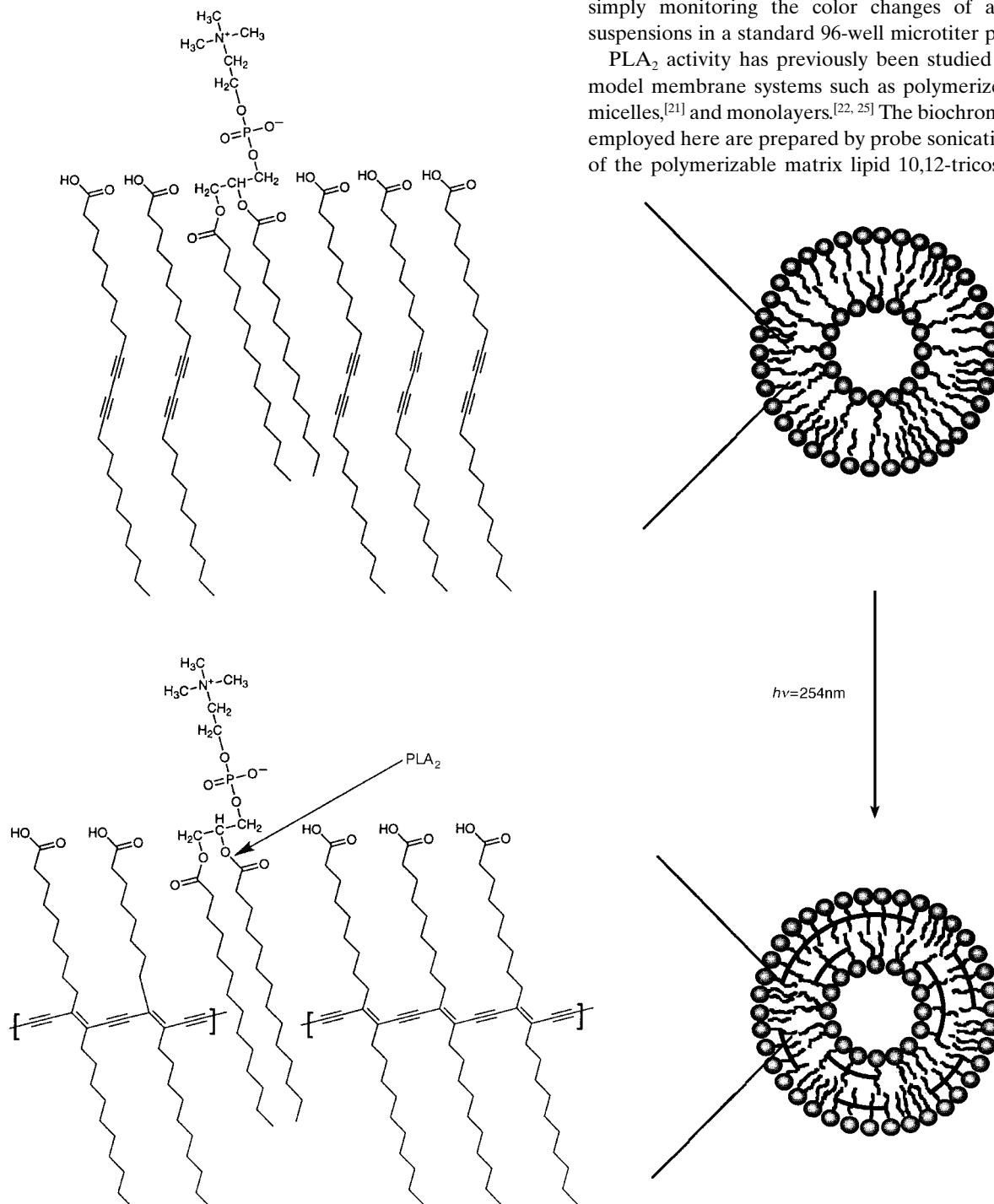


Figure 1. Preparation of biochromic vesicles from polymerizable signaling lipids and the natural lipid DMPC. Below is shown the site of attack by PLA₂. For further information see the text.

and various mole amounts (0–40%) of dimyristoylphosphatidylcholine (DMPC) in water, followed by polymerization with 1.6 mJ cm^{-2} ultraviolet radiation at 254 nm (Figure 1). Analysis of the vesicle solution by transmission electron microscopy indicates an average vesicle size of 100 nm. In their initial state the vesicles appear deep blue to the naked eye and absorb maximally at around 620 nm (Figure 2a). The color of the vesicles arises from the ene-yne conjugated system that comprises the polymer backbone of the polymerized lipid-PDA matrix.^[26] The suspension rapidly turns red (within minutes) upon addition of PLA_2 , and exhibits a

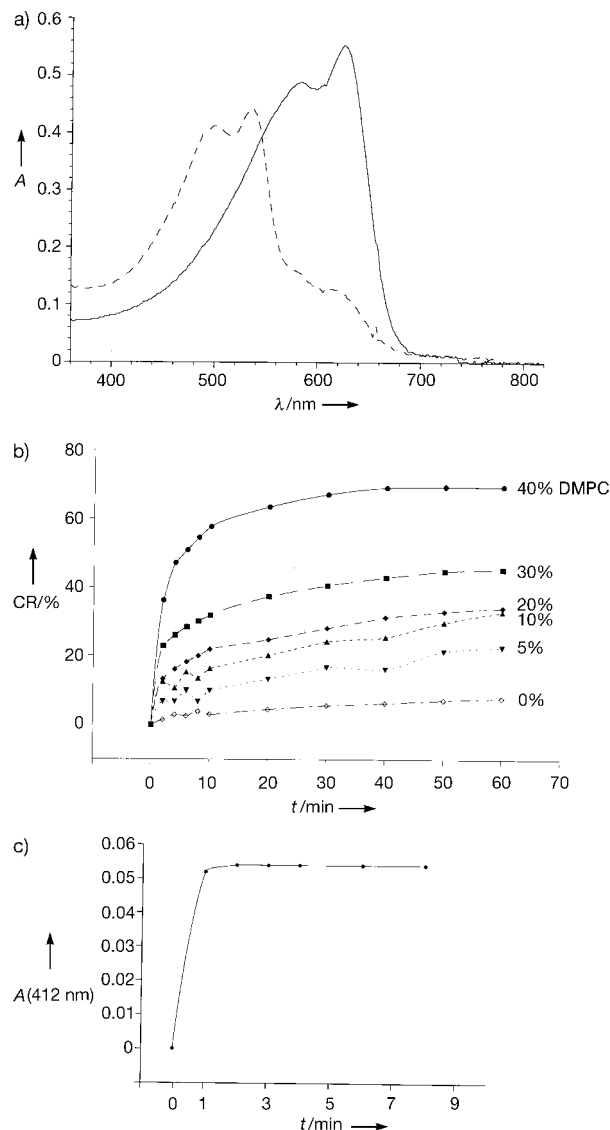


Figure 2. a) Visible absorption of the DMPC/PDA vesicles before (solid line) and after (dashed line) addition of PLA_2 ; b) colorimetric response curves of DMPC/PDA vesicles containing different molar ratios of DMPC upon incubation with PLA_2 ; c) verification of hydrolysis by PLA_2 by using DTPC and DTNB. For further information see the experimental section.

maximum absorption at approximately 540 nm (Figure 2a). A relative color change of 10% or more is observed clearly with the naked eye. The color change is modulated by altering the mole percentage of the natural lipid DMPC in the PDA vesicle and the vesicles that do not contain DMPC remain in their blue phase (Figure 2b).

Biochromic transitions of PDA vesicles and films have been proposed to arise from a perturbation of the extended π overlap of the conjugated polymer backbone. This structural rearrangement, induced in previous studies by multivalent receptor binding or penetration of peptide domains into the PDA matrix, results in absorption at shorter wavelengths (490–540 nm).^[5, 8, 10] The intense color change observed upon the interaction between the enzyme PLA_2 and the mixed DMPC/PDA vesicles indicates, that in this case, chemical modification of the vesicles by interfacial catalysis provides an alternative pathway for inducing the biochromatic transitions.

It has been demonstrated previously that PLA_2 retains its activity at polymerized mixed vesicles composed of poly(dienoyl)lecithin and dipalmitoylphosphatidylcholine (DPPC).^[22, 27] Since the PDA matrix represents a new environment for the enzyme substrate, the PLA_2 activity was independently measured by using a labeled lipid analogue incorporated into the PDA matrix, which allowed the simultaneous measurement of product formation and colorimetric response of the vesicles. The analogue used was the thioester 1,2-bis(*S*-decanoyl)-1,2-dithio-*sn*-glycero-3-phosphocholine (DTPC). Cleavage of DTPC by PLA_2 produces a soluble thiol-modified lipid that readily reacts with 5,5'-dithiobis-2-nitrobenzoic acid (DTNB) to produce a colored product that absorbs characteristically at 412 nm.^[21] Indeed, when PLA_2 was added to mixed vesicles of 40% DTPC in PDA, the hydrolysis products reacted with DTNB to give rise to a significant absorption at 412 nm (Figure 2c). At the same time, the PDA vesicles also changed color, and the suspension exhibited a colorimetric response similar to that of vesicles that contain DMPC (Figure 2b). The differences in the rate of the response between the two methods most likely arises from the lag time in the response of the surrounding polymeric matrix. These results confirm that interfacial catalysis by PLA_2 occurs at the polymerized mixed vesicles.

NMR experiments further verified the occurrence of interfacial catalysis by PLA_2 , and provided information on the fate of the enzymatic reaction products. Figure 3 shows

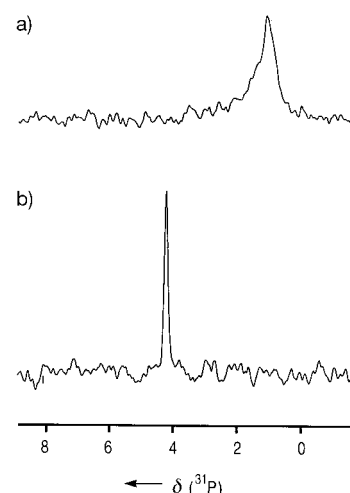


Figure 3. ^{31}P NMR spectra of DMPC/PDA vesicles (0.1 mM total lipid) a) before and b) after addition of PLA_2 . Magnetic parameters: magnetic field: 11.7 Tesla, Bruker DMX500, Block-delay pulse sequence with 2048 acquisition data points, 20000 FIDs in each experiment with two second recycle delays, 0.1 M phosphoric acid used as an external reference.

the ^{31}P NMR spectra of the DMPC/PDA vesicles prior to the addition of PLA_2 (Figure 3a) and after the enzymatic reaction (Figure 3b). The relatively broad, anisotropic ^{31}P resonance from the intact vesicles (Figure 3a) corresponds to the choline head group of DMPC embedded in the PDA vesicles. The ^{31}P anisotropy indicates that the DMPC molecules are immobilized within the vesicle matrix. After addition of PLA_2 the ^{31}P signal is shifted downfield. The position of the ^{31}P resonance in Figure 3b coincides with the shift observed for the water-solubilized lyso-myristoylphosphatidylcholine, the hydrolysis product of DMPC. Furthermore, Figure 3 shows that the ^{31}P resonance observed in the suspension of the enzyme-treated vesicles becomes significantly narrower than the ^{31}P signal from the initial DMPC/PDA vesicles, which indicates a higher mobility of the phosphate groups after PLA_2 catalysis.^[28] This result suggests that dissolution of the lysolipid reaction products occurs. Further support for this hypothesis comes from ^1H NMR data that indicate the appearance of dissolved lipid species after the reaction with PLA_2 .^[29]

The color change of the DMPC/PDA vesicles can be suppressed with known inhibitors to PLA_2 . In the presence of the inhibitor 1-hexadecyl-3-trifluoroethylglycero-2-phosphomethanol (MJ33)^[17, 30] the vesicles remain in their blue phase upon addition of PLA_2 . Figure 4a depicts an image of the PLA_2 /vesicle suspension in the presence (blue) and absence (red) of MJ33 in a 96-well microtiter plate. The absorbance of the wells quantitatively confirms the suppression of the colorimetric response (Figure 4b). The inhibition of the blue to red color change by MJ33 indicates that nonspecific adhesion does not play a role in the biochromic response, and PLA_2 activity is directly responsible for the color change. Inactivation of PLA_2 is also observed upon removal of Ca^{2+} , the catalytic cofactors for PLA_2 ,^[17, 31] from the buffer solution: PLA_2 prepared in buffer containing Zn^{2+} instead of Ca^{2+} ions does not induce a blue to red color change of the vesicles (Figure 4b). The results also suggest that the degree of inhibition of the color change is dependent on the amount of Zn^{2+} added, which is in agreement with earlier viral inhibition experiments of PDA vesicles modified with sialic acid.^[7] Finally, the effect of nonspecific adsorption on the color change was investigated. For example, the vesicles do not change color in the presence of other enzymes such as lysozyme and glucose oxidase, both of which only produce a colorimetric response below 5 % after more than an hour of incubation with the 40 % DMPC/PDA vesicles.

The vesicle color change is ascribed to lipid reorganization and destabilization of the vesicles by hydrolysis of the DMPC embedded in the PDA signaling matrix. In general, the color transitions of PDA-based materials (for example, single crystals, films) are affected by changes in the conformation, packing, and ordering of the pendant alkyl side groups.^[4, 32, 33] Tomioka et al.^[34, 35] demonstrated that the blue to red color change of pure amphiphilic PDA monolayers contained in a Langmuir trough can be induced directly by changes in lateral surface pressure and lipid packing. The effect is believed to arise from a reduction of the effective conjugated length of the ene-yne backbone that is induced by deformation of the alkyl side groups pendant to the polymer backbone. A similar perturbation is brought about in the DMPC/PDA vesicles by

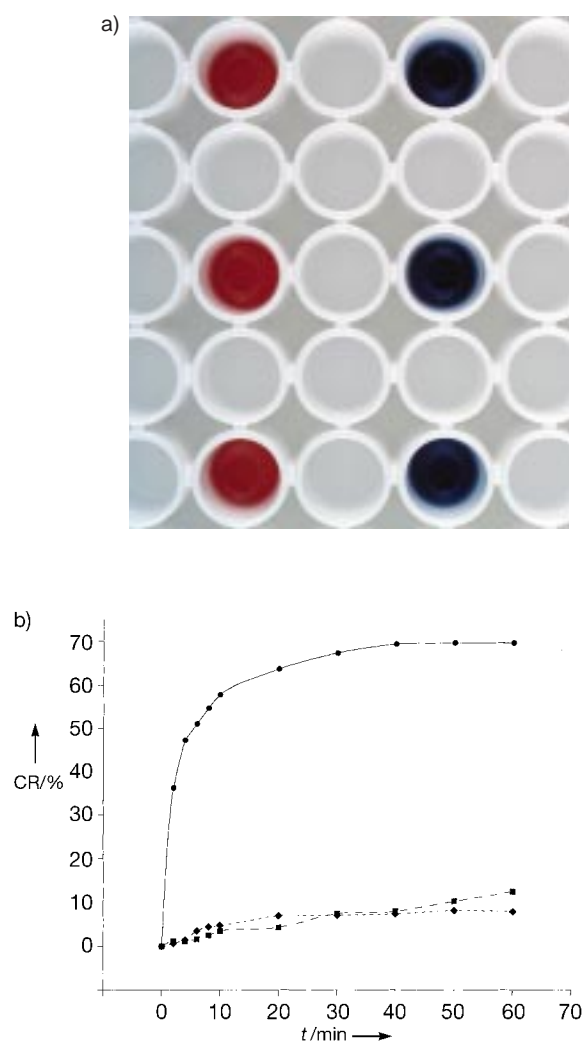


Figure 4. Inhibition of the color response (CR) by a known PLA_2 inhibitor. a) Image of microtiter wells containing a suspension of PLA_2 /vesicles in the presence (blue) and the absence (red) of MJ33 (vesicles: 40 % DMPC/PDA). b) Colorimetric response curves for DMPC/PDA vesicles in the absence (●, max error 1.9 %) and presence of an inhibitor (■ MJ33, max error 6.9 %; ♦, ZnCl_2 , max error 6.5 %). For further information see the experimental section.

alteration of the lipid–lipid packing that is induced by hydrolysis of DMPC. This is supported by previous studies that demonstrate hydrolysis by PLA_2 triggers a significant contraction in the area of Langmuir monolayers containing DMPC.^[22] The extent of contraction reflects quantitative removal of the hydrolysis products from the monolayer. Fluorescence studies have also demonstrated independently that hydrolysis by PLA_2 destabilizes other DMPC-containing vesicles.^[36]

Polymerized mixed vesicles are highly stable against chemical and physical degradation and offer a convenient, economical alternative to enzymatic assays that employ radiolabeled substrates. The vesicle stock solutions described herein have been stored for over six months without affecting the results of the assays. Colorimetric detection of interfacial catalysis by other enzymes such as phospholipase C (PLC) and phospholipase D (PLD) has been achieved also with substrate-modified PDA vesicles,^[29] and suggests that the methodology described here is generally applicable. Both of

these enzymes cleave at the hydrophilic head-group region (phosphate ester) of DMPC. The significance of the detection system described is that it both mimics the natural membrane interface, and also provides a visual reporting component (the conjugated polymer) for the rapid detection of biocatalysis.

The simple, one-step detection method for enzymatic catalysis and inhibition allows convenient adaptation to the high-throughput screening of catalytic inhibitors. In addition, this method may be applied to detect deadly neurotoxins that have enzyme-like activities (for example, β -bungarotoxin). Future efforts are geared towards the study of factors that affect enzyme recognition and activity, parameters that influence reorganization of the conjugated polymer membrane, and adaptation of the colorimetric method to other enzyme systems.

Experimental Section

Figure 2a: The polymerized vesicles composed of 40 % DMPC/60 % PDA, 1 mM total lipid, were diluted 1:10 in 50 mM Tris buffer (pH 7.0) to a final volume of 0.5 mL in a standard cuvette, and the spectra were recorded with a Hewlett Packard Spectrophotometer (model 9153C). Bee venom phospholipase A₂ (Sigma) was dissolved in a buffer (pH 8.9) of 10 mM Tris, 150 mM NaCl, and 5 mM CaCl₂ to yield a final concentration of 1.4 mg mL⁻¹. 50 μ L of this solution was added to the cuvette and the spectrum recorded after 60 min.

Figure 2b: 5 μ L of the 1.4 mg mL⁻¹ solution of PLA₂ was added to 50 μ L of DMPC/DPA vesicles (0.1 mM final total lipid concentration). The experiment was carried out in a standard 96-well plate with a UV_{max} kinetic microplate reader (Molecular Devices). The absorption of the vesicle solution was monitored as a function of time at 620 and 490 nm. The data was then plotted as colorimetric response (CR) versus time to yield the color response curves. Colorimetric response is defined here as the percentage change in the absorption at 620 nm relative to the total absorption maxima.^[6]

Figure 2c: 5 μ L of 40 % DTPC/PDA vesicles diluted with 45 μ L of 50 mM Tris pH 7.0 and 5 μ L of 6 mM DTNB were incubated with 10 μ L of 1.4 mg mL⁻¹ PLA₂. The absorbance at 412 nm was monitored over time.

Figure 4b: MJ33 was added to 5 μ L of unpolymerized 40 % DMPC/PDA vesicles (0.015 mol ratio of MJ33 in the substrate interface) in 40 μ L of 50 mM Tris (pH 7.0) and 5 μ L of a solution of 50 mM Tris, 150 mM NaCl, and 5 mM CaCl₂ (pH 8.9). The mixture was incubated at room temperature for 20 min and polymerized prior to measuring the absorption at 490 and 620 nm. 5 μ L of a 1.4 mg mL⁻¹ solution of PLA₂ was added and the colorimetric response recorded as above. For Zn²⁺ inhibition the enzyme was dissolved in 10 mM Tris, 150 mM NaCl, and 0.1 mM ZnCl₂ at pH 8.9.

Received: July 14, 1998 [Z12143IE]
German version: *Angew. Chem.* **1999**, *111*, 678–682

Keywords: biosensors • conjugation • enzyme catalysis • enzyme inhibitors • vesicles

- [1] I. Levesque, M. Leclerc, *Chem. Mater.* **1996**, *8*, 2843–2849.
- [2] C. Galiotis, R. J. Young, D. N. Batchelder, *J. Polym. Sci. Polym. Phys. Ed.* **1983**, *21*, 2483–2494.
- [3] M. J. Marsella, R. J. Newland, P. J. Carroll, T. M. Swager, *J. Am. Chem. Soc.* **1995**, *117*, 9842–9848.
- [4] H. Tanaka, M. A. Gomez, A. E. Tonelli, M. Thakur, *Macromolecules* **1989**, *22*, 1208–1215.
- [5] D. Charych, Q. Cheng, A. Reichert, G. Kuziemko, M. Stroh, J. O. Nagy, W. Spevak, R. C. Stevens, *Chem. Biol.* **1996**, *3*, 113–120.
- [6] A. Reichert, J. O. Nagy, W. Spevak, D. Charych, *J. Am. Chem. Soc.* **1995**, *117*, 829–830.
- [7] D. H. Charych, J. O. Nagy, W. Spevak, M. D. Bednarski, *Science* **1993**, *261*, 585–588.

- [8] J. Pan, D. Charych, *Langmuir* **1997**, *13*, 1365–1367.
- [9] Q. Cheng, R. C. Stevens, *Chem. Phys. Lipids* **1997**, *87*, 41–53.
- [10] Q. Cheng, R. C. Stevens, *Adv. Mater.* **1997**, *9*, 481–483.
- [11] K. Faid, M. Leclerc, *Chem. Commun.* **1996**, *24*, 2761–2762.
- [12] R. M. Kini, *Venom Phospholipase A₂ Enzymes*, Wiley, Chichester, **1997**.
- [13] M. Waite, *The Phospholipases*, Plenum, New York, **1987**.
- [14] J. S. Bomalaski, M. A. Clark, *Arthritis Rheum.* **1993**, *36*, 190–198.
- [15] F. Ramirez, M. K. Jain, *Proteins Struct. Funct. Genet.* **1991**, *9*, 229–239.
- [16] E. A. Dennis, P. Y. K. Wong, *Phospholipase A₂: Role and Function in Inflammation*, Plenum, New York, **1990**.
- [17] M. H. Gelb, M. K. Jain, O. G. Berg, *FASEB J.* **1994**, *8*, 916–924.
- [18] H.-K. Lin, M. H. Gelb, *J. Am. Chem. Soc.* **1993**, *115*, 3932–3942.
- [19] C. Ehnholm, T. Kuusi, *Methods Enzymol.* **1986**, *129*, 716–738.
- [20] T. Bayburt, B.-Z. Yu, I. Street, F. Ghomashchi, F. Laliberte, H. Perrier, Z. Wang, R. Homan, M. K. Jain, M. H. Gelb, *Anal. Biochem.* **1995**, *232*, 7–23.
- [21] L. J. Reynolds, L. L. Hughes, E. A. Dennis, *Anal. Biochem.* **1992**, *204*, 190–197.
- [22] D. W. Grainger, A. Reichert, H. Ringsdorf, C. Salesse, D. E. Davies, J. B. Lloyd, *Biochim. Biophys. Acta* **1990**, *1022*, 146–153.
- [23] S.-K. Wu, W. Cho, *Anal. Biochem.* **1994**, *221*, 152–159.
- [24] R. Dua, S.-K. Wu, W. Cho, *J. Biol. Chem.* **1995**, *270*, 263–268.
- [25] V. M. Mirsky, C. Krause, K. D. Heckmann, *Thin Solid Films* **1996**, *284*, 939–941.
- [26] G. Wegner, *J. Polym. Sci. Part B* **1971**, *9*, 133–144.
- [27] H. Ringsdorf, B. Schlarb, J. Venzmer, *Angew. Chem.* **1988**, *100*, 117–162; *Angew. Chem. Int. Ed. Engl.* **1988**, *27*, 113–158.
- [28] I. C. P. Smith, I. H. Ekiel, *Phosphorous-31 NMR. Principles and Applications*, Academic Press, Orlando, **1984**.
- [29] R. Jelinek, S. Y. Okada, S. Norvez, D. Charych, *Chem. Biol.* **1998**, *5*, 619–629.
- [30] M. K. Jain, W. Tao, J. Rogers, C. Arenson, H. Eibl, B.-Z. Yu, *Biochemistry* **1991**, *30*, 10256–10268.
- [31] M. Jain, unpublished results.
- [32] M. F. Rubner, D. J. Sandman, C. Velazquez, *Macromolecules* **1987**, *20*, 1296–1300.
- [33] M. Wenzel, G. H. Atkinson, *J. Am. Chem. Soc.* **1989**, *111*, 6123–6127.
- [34] Y. Tomioka, N. Tanaka, S. Imazeki, *J. Chem. Phys.* **1989**, *91*, 5694–5700.
- [35] Y. Tomioka, N. Tanaka, S. Imazeki, *Thin Solid Films* **1989**, *179*, 27–31.
- [36] H. Kitano, N. Kato, N. Ise, *J. Am. Chem. Soc.* **1989**, *111*, 6809–6813.

Practically Perfect Asymmetric Autocatalysis with (2-Alkynyl-5-pyrimidyl)alkanols

Takanori Shibata, Shigeru Yonekubo, and Kenso Soai*

Organic synthesis plays a central role in natural and technical sciences, and the development of organic reactions that proceed with perfect chemo- and stereoselectivity is an important goal for organic chemists.^[1] Reactions that are catalyzed by enzymes in living organisms proceed with extremely high chemo- and stereoselectivities. Enzymes are, however, macromolecules that consist of thousands of amino

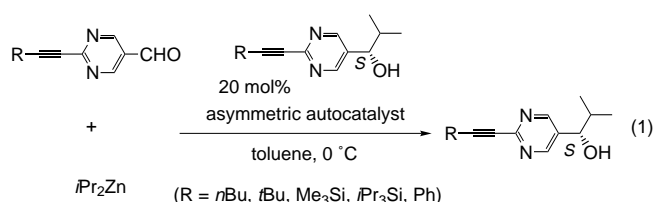
[*] Prof. Dr. K. Soai, Dr. T. Shibata, S. Yonekubo
Department of Applied Chemistry
Faculty of Science, Science University of Tokyo
Kagurazaka, Shinjuku-ku, Tokyo 162–8601 (Japan)
Fax: (+81)3-3235-2214
E-mail: ksoai@ch.kagu.sut.ac.jp

[**] This work was supported by a Grant-in-Aid for Scientific Research from the Ministry of Education, Science, Sports, and Culture, the Kurata Foundation, and the SUT Grant for Research Promotion.

acids. It is a challenging problem in asymmetric synthesis to design a chiral catalyst that exhibits extremely high enantioselectivity.^[2] Although highly enantioselective reactions (>90% *ee*) are known these days, it is much more difficult to develop an enantioselective reaction that gives greater than 99.5% *ee*, even in non-autocatalytic asymmetric synthesis. In general, it is difficult to achieve a reaction with an extremely high *ee* value (>99.5%) because the difference in Gibbs free energy ($\Delta\Delta G^\ddagger$) between the transition states that give the *R* and *S* isomers kinetically increases exponentially with the increase in enantioselectivity.^[3] We have studied asymmetric autocatalysis,^[4, 5] where the catalyst and product have the same structure and configuration.

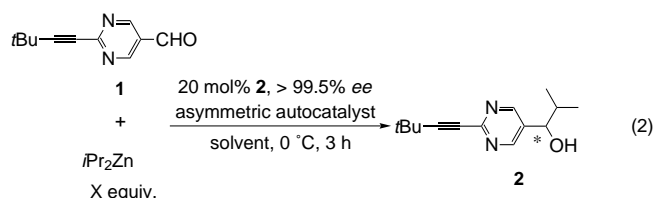
We previously reported the first highly enantioselective autocatalytic reaction,^[5b] but even this reaction did not achieve perfect enantioselectivity: when a pyrimidylalkanol with a high *ee* value was used as an asymmetric autocatalyst, the *ee* value of the resulting pyrimidylalkanol remained at up to 98.2% and the chemical yield was no greater than 80%, as a result of the formation of by-products and the recovery of unreacted aldehyde. We report here an unprecedented practically perfect asymmetric autocatalytic reaction that gives extremely high enantioselectivity (>99.5% *ee*) and almost quantitative chemical yield (>99%).

First, to find a better asymmetric autocatalyst, several 5-pyrimidylalknols that possessed an alkynyl group at their 2-positions were used as asymmetric autocatalysts in the enantioselective alkylation with diisopropylzinc (2.2 equiv) [Eq. (1)]. Differences in selectivity were clarified by the use



of (2-alkynylpyrimidyl)alknols with a low *ee* value. An alkanol, including the catalyst, with 21.2% *ee* was obtained from the use of a pyrimidylalkanol with an *n*-butyl group on the alkyne with 5.8% *ee*. The introduction of a *tert*-butyl or trimethylsilyl group was much more effective (5.5 → 69.6% *ee* for a *tert*-butyl and 8.4 → 74.2% *ee* for a trimethylsilyl group). On the other hand the introduction of a more bulky triisopropylsilyl group reduced the catalytic activity (8.6 → 8.8% *ee*). A phenyl group was also effective (5.9 → 47.3% *ee*), but less than a *tert*-butyl group. These results imply that a moderate electron-withdrawing effect that arises from the alkynyl group and the appropriate bulkiness of the alkyne are indispensable for a practically perfect asymmetric autocatalyst. Thus, 1-(2-*tert*-butylethynyl-5-pyrimidyl)-2-methyl-1-propanol was found to be a very efficient asymmetric autocatalyst.

The enantioselective isopropylation of 2-(*tert*-butylethynyl)pyrimidine-5-carbaldehyde (**1**) with diisopropylzinc (in toluene) and the enantiomerically pure (>99.5% *ee*) (*S*)-pyrimidylalkanol (**S**-**2**) as an asymmetric autocatalyst was performed in toluene [Eq. (2)]. This reaction resulted in the formation of (*S*)-pyrimidylalkanol (**S**-**2**) in 98% yield and



with 99.1% *ee* (Table 1, entry 1). When cumene was used as the solvent instead of toluene the *ee* value increased to 99.3% (entry 2). The *ee* value reached in excess of 99.5% when a cumene solution of diisopropylzinc was used (entry 4). The use of 1.7 equivalents of diisopropylzinc gave (*S*)-**2** with a

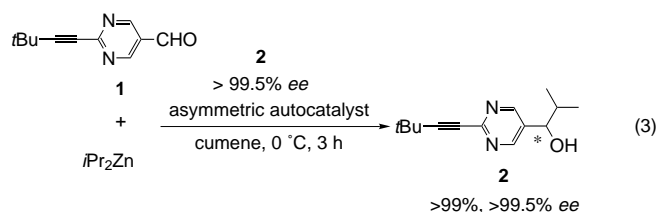
Table 1. Asymmetric autocatalytic reaction as shown in Equation (2) with (*S*)- and (*R*)-**2** with >99.5% *ee*.

Entry	X	Solvent	Asym. autocat. and product <i>ee</i> [%]	Newly formed product yield [%]	<i>ee</i> [%]
1	2.2	toluene ^[a]	99.3 (<i>S</i>)	98	99.1 (<i>S</i>)
2	2.2	cumene ^[a]	99.4 (<i>S</i>)	98	99.3 (<i>S</i>)
3	2.2	<i>tert</i> -butylbenzene ^[a]	99.3 (<i>S</i>)	99	99.1 (<i>S</i>)
4	2.2	cumene ^[b]	> 99.5 (<i>S</i>)	99	> 99.5 (<i>S</i>)
5	1.7	cumene ^[b]	> 99.5 (<i>S</i>)	> 99	> 99.5 (<i>S</i>)
6	1.7	cumene ^[b]	> 99.5 (<i>R</i>)	> 99	> 99.5 (<i>R</i>)

[a] With 1M *i*Pr₂Zn in toluene. [b] With 1M *i*Pr₂Zn in cumene.

greater than 99.5% *ee* and induced a further increase in yield (>99%; entry 5). (*R*)-Pyrimidylalkanol ((*R*)-**2**), with the opposite configuration, is also an extremely efficient asymmetric autocatalyst (entry 6). We ultimately achieved a practically perfect asymmetric autocatalytic reaction in terms of either configurations (>99.5% *ee*, >99% yield).

Under the best reaction conditions (Table 1, entry 5), the reaction was performed successively, with the products of one round serving as the reactants for the next entry (Table 2). Even after ten rounds, all the asymmetric autocatalytic reactions proceeded perfectly (>99%, >99.5% *ee*). In our reaction, the factor by which the amount of (*S*)-**2** multiplied relative to the amount of (*S*)-**2** initially used as an asymmetric



autocatalyst (entry 1) was approximately 10³ in five rounds (entry 5) and approximately 10⁷ in ten rounds (entry 10), with no deterioration of the catalyst. Thus, in the present asymmetric autocatalytic reaction, the factor by which a chiral molecule multiplies is practically unlimited.

In this asymmetric autocatalytic reaction, only one product (catalyst) is obtained. Therefore, if this product can be converted into important chiral synthetic intermediates, the significance of this scheme is surely enhanced. In fact, we previously reported that chiral 5-pyrimidylalknols can be transformed into α -hydroxycarboxylic acid derivatives without racemization.^[6]

Table 2. Consecutive asymmetric autocatalytic reaction^[a] shown in Equation (3). The compounds **2a–k** only distinguish in which round the catalyst is used.

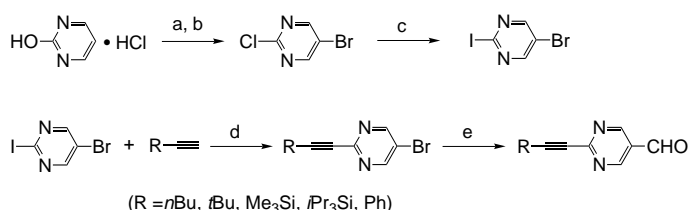
Entry	Asym. Autocat. ee [%]	Product yield [%] ee [%]	Amplified factor ^[b]
1	> 99.5 (2a)	> 99 > 99.5 (2b)	6
2	> 99.5 (2b)	> 99 > 99.5 (2c)	6 ²
3	> 99.5 (2c)	> 99 > 99.5 (2d)	6 ³
4	> 99.5 (2d)	> 99 > 99.5 (2e)	6 ⁴
5	> 99.5 (2e)	> 99 > 99.5 (2f)	6 ⁵ $\approx 8 \times 10^3$
6	> 99.5 (2f)	> 99 > 99.5 (2g)	6 ⁶
7	> 99.5 (2g)	> 99 > 99.5 (2h)	6 ⁷
8	> 99.5 (2h)	> 99 > 99.5 (2i)	6 ⁸
9	> 99.5 (2j)	> 99 > 99.5 (2k)	6 ⁹
10	> 99.5 (2k)	> 99 > 99.5 (2l)	6 ¹⁰ $\approx 6 \times 10^7$

[a] Molar ratio **1**:*i*Pr₂Zn (in cumene):catalyst **2** = 1.0:1.7:0.2. [b] The factor by which the amount of **2** has multiplied based on the amount of **2** used as an asymmetric autocatalyst in entry 1.

Experimental Section

Entry 5, Table 1: A solution of **1** (94.2 mg, 0.50 mmol) in cumene (5.0 mL) was added at 0 °C to a mixture of (*S*)-**2** (23.3 mg, 0.10 mmol, > 99.5 % ee) in cumene (12.0 mL) and *i*Pr₂Zn (0.85 mL of a 1 M solution in cumene, 0.85 mmol) that had been stirred for 15 min at 0 °C. The reaction mixture was stirred for 3 h at 0 °C, then quenched by the addition of 1 M hydrochloric acid (3 mL) and saturated aqueous NaHCO₃ (9 mL) at 0 °C. The mixture was filtered through celite and the filtrate was extracted with ethyl acetate (4 × 15 mL). The extract was dried over anhydrous sodium sulfate and evaporated under reduced pressure. Cumene was removed by flash column chromatography (SiO₂, hexane, then hexane/ethyl acetate, 3/1) to give pure **2** (138.8 mg). HPLC analysis of the obtained **2** on a column with a chiral stationary phase (Daicel Chiralcel OD, eluent 3 % 2-propanol in hexane, flow rate 1.0 mL min⁻¹, 254 nm UV detector, retention time 18.1 min for (*S*)-**2**, 26.9 min for (*R*)-**2**) showed that it had an enantiomeric purity of > 99.5 % ee. The newly formed (*S*)-alcohol (138.8 – 23.3 = 115.5 mg, 99.2 % yield) had an enantiomeric purity of > 99.5 % ee.

Preparation of 2-alkynylpyrimidine-5-carbaldehydes (Scheme 1): Commercially available 2-hydroxypyrimidine hydrochloride was halogenated to form 5-bromo-2-chloropyrimidine by the improved procedure.^[7] Halogen exchange occurred at the 2-position by the reaction with hydroiodic acid to give 5-bromo-2-iodopyrimidine, which was then coupled with alkynes to give 2-alkynyl-5-bromopyrimidines in 80–99 %.^[8] Lithiation of the bromides by *n*- or *tert*-butyllithium and the subsequent formylation^[9] by ethyl formate gave the 2-alkynylpyrimidine-5-carbaldehydes in 25–60 %.



Scheme 1. Synthesis of 2-alkynylpyrimidine-5-carbaldehydes. a) Br₂, H₂O; b) POCl₃, PhNMe₂, 55 % over two steps; c) 57 % HI, CH₂Cl₂, 93 %; d) 1–2 mol % [Pd(PPh₃)₄], 2–4 mol % CuI, *i*Pr₂NH, 80–99 %; e) *n*BuLi or *t*BuLi then HCO₂Et, THF or Et₂O, 25–60 %.

Received: October 15, 1998 [Z 12530 IE]
German version: *Angew. Chem.* **1999**, *111*, 749–751

Keywords: aldehydes • alkylations • asymmetric synthesis • autocatalysis • zinc

- [1] D. Seebach, *Angew. Chem.* **1990**, *102*, 1363–1409; *Angew. Chem. Int. Ed. Engl.* **1990**, *29*, 1320–1367.
- [2] a) *Catalytic Asymmetric Synthesis* (Ed.: I. Ojima), VCH, Weinheim, 1993; b) A. Togni, L. M. Venanzi, *Angew. Chem.* **1994**, *106*, 517–548; *Angew. Chem. Int. Ed. Engl.* **1994**, *33*, 497–526.
- [3] a) J. D. Morrison, H. S. Mosher, *Asymmetric Organic Reaction*, Prentice-Hall, Englewood Cliffs, New Jersey, **1971**, chap. 1, pp. 28–49; b) Y. Izumi, A. Tai, *Stereo-Differentiating Reactions*, Academic Press, New York, **1977**, chap. 7, pp. 178–184.
- [4] Short reviews, see a) K. Soai, T. Shibata, *Yuki Gosei Kagaku Kyokaishi (J. Synth. Org. Chem. Jpn.)* **1997**, *54*, 994–1005; b) C. Bolm, A. Seger, F. Bienewald, *Organic Synthesis Highlights III* (Eds.: J. Mulzer, H. Waldmann), WILEY-VCH, Weinheim, **1998**, pp. 79–83; c) C. Bolm, F. Bienewald, A. Seger, *Angew. Chem.* **1996**, *108*, 1767–1769; *Angew. Chem. Int. Ed. Engl.* **1996**, *35*, 1657–1659.
- [5] a) K. Soai, T. Shibata, H. Morioka, K. Choji, *Nature* **1995**, *378*, 767–777; b) T. Shibata, H. Morioka, T. Hayase, K. Choji, K. Soai, *J. Am. Chem. Soc.* **1996**, *118*, 471–472; c) T. Shibata, K. Choji, H. Morioka, T. Hayase, K. Soai, *Chem. Commun.* **1996**, 751–752; d) T. Shibata, K. Choji, T. Hayase, Y. Aizu, K. Soai, *Chem. Commun.* **1996**, 1235–1236; e) T. Shibata, H. Morioka, S. Tanji, T. Hayase, Y. Kodaka, K. Soai, *Tetrahedron Lett.* **1996**, *37*, 8783–8786; f) T. Shibata, T. Hayase, J. Yamamoto, K. Soai, *Tetrahedron: Asymmetry* **1997**, *8*, 1717–1719.
- [6] a) K. Soai, S. Tanji, Y. Kodaka, T. Shibata, *Enantiomer* **1998**, *3*, 241–243; b) S. Tanji, Y. Kodaka, T. Shibata, K. Soai, *Heterocycles* in press.
- [7] M. Hird, K. J. Toyne, G. W. Gray, *Liq. Cryst.* **1992**, *14*, 741–761.
- [8] J. W. Goodby, M. Hird, R. A. Lewis, K. J. Toyne, *Chem. Commun.* **1996**, 2719–2720.
- [9] T. Rho, Y. F. Abuh, *Synth. Commun.* **1994**, *24*, 253–256.

A Functionalized Heterocubane with Extensive Intermolecular Hydrogen Bonds**

Musa A. Said, Herbert W. Roesky,*
Carsten Rennekamp, Marius Andruh,
Hans-Georg Schmidt, and Mathias Noltemeyer

*Dedicated to Professor Alan H. Cowley
on the occasion of his 65th birthday*

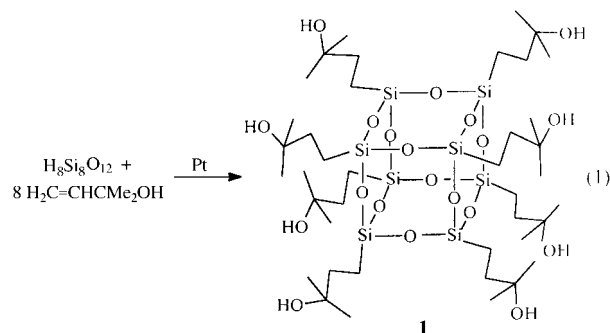
The use of inorganic cage compounds as molecular building blocks for the rational design of materials is an attractive and challenging avenue for the materials chemist. One example is the silicate cage compounds (RSiO_{1.5})_n (R = organic or inorganic group), which are potentially a very useful class of compounds.^[1–6] They have been used as three-dimensional building block units for the synthesis of new materials, such as precursors for ceramics and models in various fields.^[1, 3, 4] In addition, an exciting structural organization of the cubic silicate species [Si₈O₂₀]^{8–} was achieved recently with various

[*] Prof. Dr. H. W. Roesky, Dr. M. A. Said, Dipl.-Chem. C. Rennekamp, Dr. M. Andruh, H.-G. Schmidt, Dr. M. Noltemeyer
Institut für Anorganische Chemie der Universität
Tammannstrasse 4, D-37077 Göttingen (Germany)
Fax: (+49) 551-393-337
E-mail: hroesky@gwdg.de

[**] This work was supported by the Deutsche Forschungsgemeinschaft, the Witco GmbH, and the Volkswagen Foundation. M.A.S. thanks the Alexander-von-Humboldt foundation, Bonn, for a research fellowship. C.R. is grateful to the Fonds der Chemischen Industrie for a fellowship.

cationic surfactants.^[7, 8] This procedure has potential applications as highly ordered mesoporous solids, as organic–inorganic nanocomposites, and as models in the area of biomimetics.^[8]

With an eye towards developing a general methodology for the synthesis of soluble metal-containing siloxane derivatives^[9, 10] and highly functionalized silsesquioxanes to assist the study of silica, we report herein a facile synthesis of $(\text{Si}_8\text{O}_{12})(\text{CH}_2\text{CH}_2\text{CMe}_2\text{OH})_8$ (**1**). Such completely condensed oligosilsesquioxanes (POSS) are quite attractive since they retain reactive $\text{SiCH}_2\text{CH}_2\text{CMe}_2\text{OH}$ functionalities, which allows their exploitation as ligands in a wide variety of complexations with main group and transition metals. Moreover the conventional hydrogen bond is expected to play an essential role in the construction of a new supramolecular network through intermolecular hydrogen bonds. Endo et al. have shown the self-assembly in porous organic structures through formation of hydrogen bonds.^[11] In addition, from a crystal engineering perspective, **1** is a novel solid since the key to the production of materials with predictable crystal structures lies in the engineering of complementary crystal building blocks with hydrogen bond donor/acceptor abilities.^[12]



Despite the fact that a variety of functionalized oligosilsesquioxanes are known, their chemistry has remained undeveloped because of the lack of facile methods for their synthesis in useful quantities in a conveniently short period of time.^[1, 13] The synthesis of **1** has been accomplished in a one-pot reaction in high yield from the readily available hydrosilsesquioxane $\text{H}_8\text{Si}_8\text{O}_{12}$ and an excess of $\text{H}_2\text{C}=\text{CHCMe}_2\text{OH}$ in the presence of a platinum catalyst [Eq. (1)].

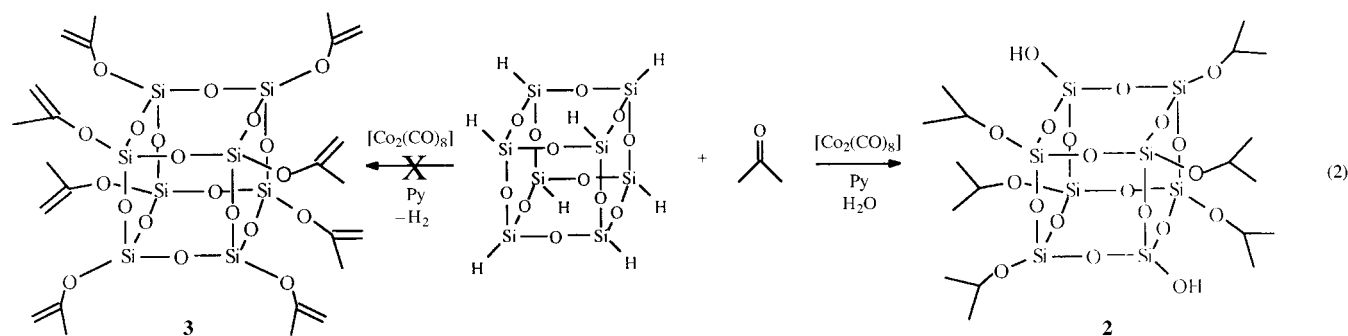
Platinum-catalysed hydrosilylations of $\text{H}_8\text{Si}_8\text{O}_{12}$ provide a variety of functionalized silsesquioxanes.^[6, 14, 15, 16] However, in most cases the products are mixtures of isomers as a

consequence of α and β additions to the alkene. Therefore, increasing the steric bulk at the β position is a useful tool to reduce the number of side products.^[14, 15] In our case, we could suppress the β addition by using a 3,3-substituted α -alkene. Hence treatment of $\text{H}_8\text{Si}_8\text{O}_{12}$ with $\text{H}_2\text{C}=\text{CHCMe}_2\text{OH}$ afforded a high yield of **1**, which spontaneously crystallized from the solution as colorless crystals. The reaction described above could be scaled up to provide much larger quantities of **1**. The easy access of **1** should make it possible to synthesize a wide variety of new hybrid materials.

Herein we also report on the synthesis of $(\text{Si}_8\text{O}_{12})(\text{OCHMe}_2)_6(\text{OH})_2$ (**2**), which was obtained by treatment of $\text{H}_8\text{Si}_8\text{O}_{12}$ with acetone in the presence of a cobalt catalyst and subsequently crystallized in open air from *n*-hexane by slow evaporation (75 %) of the solvent over six weeks [Eq. (2)]. In fact we were planning to synthesize cage compound **3**, which is useful as a tailor-made molecular building block, but compound **2** was formed in a 35 % pure yield. It is important to note that POSS molecules with one or two reactive functionalities are more desirable for the preparation of linear POSS-based polymers.^[17] The slow and total evaporation of the mother liquor of **2** resulted in the formation of a few more crystals along with an oily material. The crystals were identified by elemental analysis as $(i\text{PrO})_8\text{Si}_8\text{O}_{12}$. Clearly complete hydrolysis had not occurred over the six weeks period to give a better yield of **2** from $(i\text{PrO})_8\text{Si}_8\text{O}_{12}$.

Characterization of **1** and **2** was accomplished by ^1H and ^{29}Si NMR spectroscopy as well as IR spectroscopy and elemental analysis. One signal at $\delta = -64.9$ was observed in the ^{29}Si NMR spectrum of **1**, whereas the spectrum of **2** showed two signals at $\delta = -103.3$ and -103.0 . These results are in good agreement with the determined solid state structures. The molecular structures of these two compounds are shown in Figures 1 and 2. The main feature of interest of the octameric cluster **1** is the presence of the hydrogen bonds, which result in the formation of new supramolecular assemblies (Figure 3). The clusters are linked together at each of the vertices to form cavities. As a consequence intramolecular interactions of the $\text{CH}_2\text{CH}_2\text{CMe}_2\text{OH}$ groups of **1** are negligible. In addition, the compensation for the steric demand of the eight $\text{CH}_2\text{CH}_2\text{CMe}_2\text{OH}$ substituents reflects the flexibility of the Si_8O_{12} framework.

Some more of the chemical peculiarities of the structure of **1** should also be emphasized. Two water molecules are introduced from the catalyst ($\text{H}_2[\text{PtCl}_6] \cdot 6\text{H}_2\text{O}$) during the crystallization from a mixture of tetrahydrofuran and *n*-



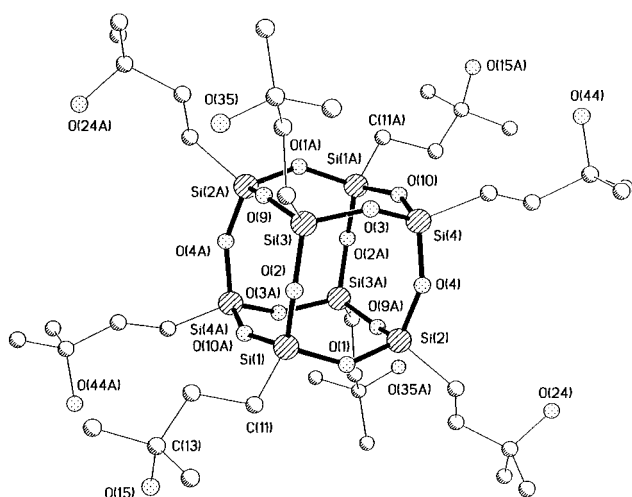


Figure 1. Structure of **1**·THF·2H₂O in the crystal.^[21a] Selected bond lengths [Å] and angles [°]: Si(1)–O(1) 1.626(2), Si(1)–O(2) 1.626(2), O(1)–Si(2) 1.628(2), Si(2)–O(4) 1.621(2), O(2)–Si(3) 1.619(2), Si(3)–O(3) 1.625(2), O(3)–Si(4) 1.625(2), Si(1)–O(4) 1.622(2), Si(1)–C(11) 1.838(2), C(13)–O(15) 1.439(3); Si(1)–O(1)–Si(2) 142.32(10), O(1)–Si(1)–O(2) 109.45(8), O(2)–Si(1)–C(11) 109.84(9). Hydrogen atoms, tetrahydrofuran, and water molecules have been omitted for clarity.

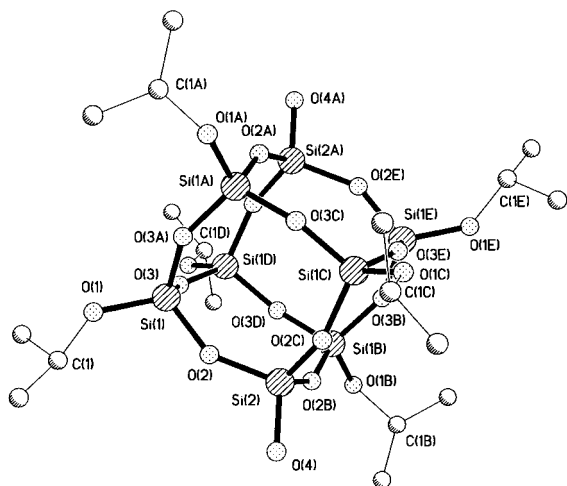


Figure 2. Structure of **2** in the crystal.^[21b] Selected bond lengths [Å] and angles [°]: Si(1)–O(1) 1.599(8), Si(1)–O(3) 1.586(7), Si(1)–O(2) 1.607(7), Si(2)–O(4) 1.553(14), O(1)–C(1) 1.370(2); O(3)–Si(1)–O(2) 107.9(4), C(1)–O(1)–Si(1) 129.0(9), Si(2)–O(2)–Si(1) 148.5(5), O(4)–Si(2)–O(2) 109.6(3). Hydrogen atoms have been omitted for clarity.

hexane. The cavity created through O–H···O bonds acts as a host for two water molecules and a THF molecule, which are kept at different positions by some weak interactions. The guest molecules are not interconnected; the two water molecules are separated from each other by 4 Å, but they are connected to the cage by hydrogen bonds. The cross diameter of the cavities is in the range of 8–9 Å and the effective dimensions are approximately 3 × 3 × 8 Å³. Powder X-ray diffraction investigations showed that heating a sample of compound **1** (130 °C and 0.01 Torr) over a 6 h period resulted in a structural change. Surprisingly such hydrogen bonding is not observed in **2** even though it has two hydroxyl groups at opposite corners of the cube. The orientation of the hydroxyl groups of **2** is such that each hydroxyl group points toward an isopropyl group of the adjacent cluster. The Si–O

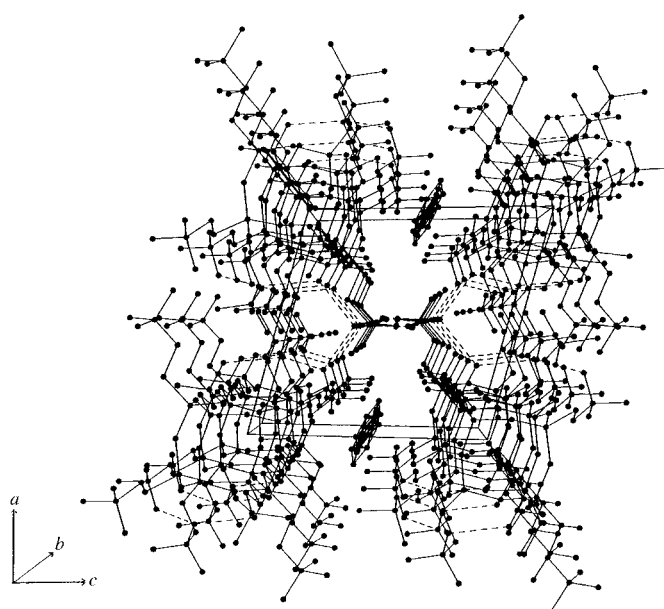


Figure 3. Packing diagram of **1** in the crystal. The O–H···O hydrogen bonds in the crystal of **1** are indicated as dashed lines. Disordered THF molecules are also shown.

and Si–C bond lengths as well as O–Si–O, Si–O–Si, and O–Si–C angles are in accord with values observed for well characterized octameric silsesquioxanes for both the compounds **1** and **2**.^[18–20]

In summary we have developed a straightforward procedure for the synthesis of a hydroxy-substituted silsesquioxane framework. Moreover we have demonstrated the influence of hydrogen bonds in building up new supramolecular assemblies. This result represents an important progress in the development of silsesquioxanes as models for functionalized silica.

Experimental Section

1: The hydrosilsesquioxane O_h-H₈Si₈O₁₂ (0.50 g, 1.18 mmol), 2-methyl-3-buten-2-ol (3 mL, 28.70 mmol), H₂[PtCl₆]·6H₂O (10 mg), and *n*-hexane (20 mL) were added to a glass pressure reactor and heated at 120 °C for 3 h, during which time a white precipitate formed. The reaction mixture was allowed to cool to room temperature and filtered to yield 0.95 g (72 %) of analytically pure **1**. Further purification was achieved by crystallization from a mixture of tetrahydrofuran and *n*-hexane (10:1) to yield 0.80 g (62 %) of **1** as colorless crystals. (Compound **1** can also be obtained from a mixture of acetone and *n*-hexane (1:5) in a similar yield. However the crystals that were grown from this mixture of solvents were not suitable for X-ray diffraction.) M.p. 275 °C; ¹H NMR (200 MHz, (CD₃)₂CO): δ = 0.721 (m, 16H; CH₂CH₂C(CH₃)₂OH), 1.14 (s, 48H; CH₂CH₂C(CH₃)₂OH), 1.57 (m, 16H; CH₂CH₂C(CH₃)₂OH), 3.22 (br, 8H; CH₂CH₂C(CH₃)₂OH); ²⁹Si NMR (50 MHz, (CD₃)₂CO): δ = –64.9; IR (KBr, Nujol): $\tilde{\nu}$ = 3384, 1115.9 cm^{–1}; elemental analysis (after drying in vacuo overnight at 50 °C) calcd for C₄₀H₈₈O₂₀Si₈: C 43.14, H 7.96, Si 20.17; found: C 43.10, H 7.80, Si 19.55.

2: Pyridine (0.012 g, 0.16 mmol) followed by dry acetone (5 mL) was added to O_h-H₈Si₈O₁₂ (0.30 g, 0.71 mmol) and dicobaltoctacarbonyl (0.037 g, 0.11 mmol) in a glass pressure reactor. The mixture was heated at 40 °C for 5 h and finally at 70 °C overnight. The reaction mixture was allowed to cool to room temperature and filtered. Subsequent removal of all volatiles in vacuo gave a residue that was treated with *n*-hexane (15 mL). Compound **2** precipitated as colorless crystals in 35 % yield (0.22 g) over a period of six weeks. M.p. 250 °C; ¹H NMR (200 MHz, C₆D₆): δ = 1.15 (q, 36H; CH(CH₃)₂), 4.28 (sept, 8H; CH(CH₃)₂ and OH); ²⁹Si NMR (50 MHz,

C₆D₆): $\delta = -103.3$ (s, 6 Si, SiOCHMe₂), -103.0 (s, 2 Si, SiOH); IR (KBr, Nujol): $\tilde{\nu} = 3411.3$ cm⁻¹; elemental analysis calcd for C₁₈H₄₄O₂₀Si₈: C 26.84, H 5.47, Si 27.93; found C 26.47, H 5.32, Si 27.85.

Received: July 23

Revised version: December 3 1998 [Z 12195 IE]

German version: *Angew. Chem.* **1999**, *111*, 702–705

Keywords: cage compounds • hydrogen bonds • silicon

- [1] a) P. G. Harrison, R. Kannengiesser, *Chem. Commun.* **1996**, 415; b) P. G. Harrison, *J. Organomet. Chem.* **1997**, 542, 141.
- [2] a) P. A. Agaskar, *J. Chem. Soc. Chem. Commun.* **1992**, 1024; b) P. A. Agaskar, *Inorg. Chem.* **1991**, 30, 2707.
- [3] a) D. Hoebbel, I. Pitsch, D. Heidermann, H. Jancke, W. Hiller, Z. *Anorg. Allg. Chem.* **1990**, 583, 133; b) D. Hoebbel, K. Endres, T. Reinert, I. Pitsch, *J. Non-Cryst. Solids* **1994**, 176, 179; c) M. Wiebcke, D. Hoebbel, *J. Chem. Soc. Dalton Trans.* **1992**, 2451.
- [4] F. J. Feher, T. A. Budzichowski, *Polyhedron* **1995**, 14, 3239.
- [5] F. T. Edelmann, *Angew. Chem.* **1992**, 104, 600; *Angew. Chem. Int. Ed. Engl.* **1992**, 31, 586.
- [6] A. Tsuchida, C. Bolln, F. G. Sernetz, H. Frey, R. Mülhaupt, *Macromolecules* **1997**, 30, 2818.
- [7] C. A. Fyfe, G. Fu, *J. Am. Chem. Soc.* **1995**, 117, 9709.
- [8] A. Firouzi, D. Kumar, L. M. Bull, T. Besier, P. Sieger, Q. Huo, S. A. Walker, J. A. Zasadzinski, C. Glinka, J. Nicol, D. Margolese, G. D. Stucky, B. F. Chmelka, *Science* **1995**, 267, 1138.
- [9] R. Murugavel, A. Voigt, M. G. Walawalkar, H. W. Roesky, *Chem. Rev.* **1996**, 96, 2205.
- [10] R. Murugavel, V. Chandrasekhar, H. W. Roesky, *Acc. Chem. Res.* **1996**, 29, 183.
- [11] a) K. Endo, T. Sawaki, M. Koyanagi, K. Kobayashi, H. Masuda, Y. Aoyama, *J. Am. Chem. Soc.* **1995**, 117, 8341; b) K. Endo, T. Ezuhara, M. Koyanagi, H. Masuda, Y. Aoyama, *J. Am. Chem. Soc.* **1997**, 119, 499.
- [12] a) M. J. Zaworotko, *Chem. Soc. Rev.* **1994**, 23, 283; b) G. R. Desiraju, *Chem. Commun.* **1997**, 1475.
- [13] F. J. Feher, T. A. Budzichowski, *J. Organomet. Chem.* **1989**, 379, 33.
- [14] A. R. Bassindale, T. E. Gentle, *J. Mater. Chem.* **1993**, 3, 1319.
- [15] F. J. Feher, K. D. Wyndham, *Chem. Commun.* **1998**, 323.
- [16] I. Ojima *The Chemistry of Organic Silicon Compounds, part 2* (Eds.: S. Patai, Z. Rappoport), Wiley, New York, **1989**, pp. 1479–1526, and references therein.
- [17] a) J. D. Lichtenhan in *Silsesquioxane-Based Polymers* (Ed.: J. C. Salamone), Wiley, New York, **1996**; b) J. D. Lichtenhan, Y. A. Otonari, M. J. Carr, *Macromolecules* **1995**, 28, 8435; c) J. D. Lichtenhan, *Comments Inorg. Chem.* **1995**, 5, 93.
- [18] C. Bonhomme, P. Tolédano, J. Maquet, J. Livage, L. Bonhomme-Courty, *J. Chem. Soc. Dalton. Trans.* **1997**, 1617.
- [19] G. Calzaferri, R. Imhof, K. W. Törnroos *J. Chem. Soc. Dalton. Trans.* **1994**, 3123.
- [20] G. Koellner, U. Müller, *Acta Crystallogr. Sect. C* **1989**, 45, 1106.
- [21] a) Crystal structure analysis of **1**·THF·2H₂O: C₄₄H₁₀₀O₂₃Si₈, $M_r = 1221.96$, triclinic, space group $P\bar{1}$, $a = 11.865(2)$, $b = 12.251(2)$, $c = 12.322(2)$ Å, $\alpha = 70.471(0)$, $\beta = 74.136(13)$, $\gamma = 81.244(8)^\circ$, $V = 1.6201(5)$ nm³, $Z = 1$, $\rho_{\text{calcd}} = 1.252$ Mg m⁻³, $\mu = 0.234$ mm⁻¹, $F(000) = 660$; total number of reflections measured 6191, of which 5723 were unique ($R_{\text{int}} = 0.0307$) and 5714 observed, 1 restraint, 341 parameters. Data collection range: $3.54 \leq 2\theta \leq 25.08^\circ$. Final R indices: $R1 = \Sigma ||F_o| - |F_c|| / \Sigma |F_o| = 0.0428$, $wR2 = [\Sigma w(F_o^2 - F_c^2)^2 / \Sigma wF_o^4]^{1/2} = 0.1174$ for data with $I > 2\sigma(I)$ and $R1 = 0.0470$, $wR2 = 0.1263$ for all data; GOF = $[\Sigma w(F_o^2 - F_c^2)^2 / \Sigma (n - p)]^{1/2} = 1.071$; max./min. residual electron density 933/–690 e nm⁻³. b) Crystal structure analysis of **2**: C₂₄H₅₆O₂₀Si₈, $M_r = 889.41$, rhombohedral, space group $R\bar{3}$, $a = 15.444(2)$, $b = 15.444(2)$, $c = 16.749(3)$ Å, $\alpha = 90$, $\beta = 90$, $\gamma = 120^\circ$, $V = 3.459.8(10)$ nm³, $Z = 3$, $\rho_{\text{calcd}} = 1.281$ Mg m⁻³, $\mu = 0.298$ mm⁻¹, $F(000) = 1416$; total number of reflections measured 1926, of which 711 were unique ($R_{\text{int}} = 0.0617$) and 709 observed, 0 restraints, 76 parameters. Data collection range: $3.65 \leq 2\theta \leq 19.94^\circ$. Final R indices: $R1 = 0.1014$, $wR2 = 0.2790$ for data with $I > 2\sigma(I)$ and $R1 = 0.1234$,

$wR2 = 0.3502$ for all data; GOF = 1.022; max/min. residual electron density 645/–455 e nm⁻³. c) Colorless single crystals suitable for X-ray diffraction studies were grown from tetrahydrofuran and *n*-hexane for **1** and *n*-hexane for **2**. A suitable crystal of each compound was mounted on a glass fiber and coated with paraffin oil. Diffraction data were collected on a Siemens–Stoe AED2 four-circle instrument (at -150°C for both compounds), with graphite-monochromated MoK α radiation (0.71073 Å). The structures were solved by direct methods with SHELXS-90^[22] and refined against F^2 on all data by full-matrix least-squares with SHELXL-93.^[23] All non-hydrogen atoms were refined anisotropically. Hydrogen atoms were included at geometrically calculated positions and refined using a riding model. Crystallographic data (excluding structure factors) for the structures reported in this paper have been deposited with the Cambridge Crystallographic Data Centre as supplementary publication nos. CCDC-102246 and 102247. Copies of the data can be obtained free of charge on application to CCDC, 12 Union Road, Cambridge CB21EZ, UK (fax: (+44) 1223-336-033; e-mail: deposit@ccdc.cam.ac.uk).

[22] G. M. Sheldrick, *Acta Crystallogr. Sect. A* **1990**, 46, 467.

[23] G. M. Sheldrick, SHELXL-93, program for crystal structure refinement, University of Göttingen Germany, **1993**.

[Zn₂(thf)₂(EtZn)₆Zn₄(μ_4 -O)(*t*BuPO₃)₈]: A Dodecanuclear Zincophosphonate Aggregate with a Zn₄(μ_4 -O) Core**

Yu Yang, Jiri Pinkas, Mathias Noltemeyer, Hans-Georg Schmidt, and Herbert W. Roesky*

Dedicated to Professor Helmut Werner on the occasion of his 65th birthday

Zincophosphates and phosphonates are among the targets of current vigorous research activity aimed at the preparation of novel types of porous structures. These materials could serve as molecular sieves, size/shape selective catalysts, adsorbents, ion exchangers, and matrices for electronic and optical devices. Zincophosphates display a large structural variety and in most cases, they form three-dimensional networks.^[1] Importantly, chiral structures^[2] and large-pore structures with low densities^[3] have also been demonstrated in zincophosphates. Recently, a new family of M₃Zn₄O(PO₄)₃ phases (M = alkali metal) that feature Zn₄(μ_4 -O) centers was reported.^[4] Layered,^[5] chain-like,^[3d, 5a,b, 6] and, in rare cases, even molecular species are also known. Of the two molecular zincophosphates known one features an eight-membered

[*] Prof. Dr. H. W. Roesky, Y. Yang, Dr. J. Pinkas, Dr. M. Noltemeyer, H.-G. Schmidt
Institut für Anorganische Chemie der Universität
Tammannstrasse 4, D-37077 Göttingen (Germany)
Fax: (+49) 551-393-373
E-mail: hroesky@gwdg.de

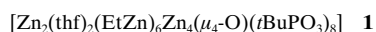
[**] This work was supported by the Deutsche Forschungsgemeinschaft. J.P. thanks the Alexander von Humboldt-Stiftung for a research fellowship.

$[\{\text{Zn}(\mu_2\text{-O})_2\text{PO}_2\}_2]$ ring^[3b] while the other possesses a $[\text{Zn}_4(\mu_4\text{-O})\{(\mu_2\text{-O})_2\text{PO}_2\}_4]$ moiety.^[6b]

The majority of zincophosphonates, on the other hand, have layered structures into which various organic species can intercalate.^[7, 8] However, the dimensionality of the resulting network can be controlled by changing the functionality and steric bulk of the phosphonate R group and through this three-dimensional and chain compounds have been synthesized.^[9]

Oligonuclear zinc complexes have been studied as polymerization catalysts, reagents in organic synthesis, precursors to ZnO-based materials,^[10] and models of active sites in zinc enzymes. The most prevalent species are tetranuclear clusters with an oxygen-centered tetrahedral Zn_4O core.^[11] Other structural types involve Zn_4O_4 cubanes,^[12] a linear Zn_4O_6 chain,^[13] and an eight-membered Zn_4O_4 ring.^[14] However, only a handful of high-nuclearity aggregates have been structurally characterized. The sole example of a hexanuclear aggregate is a drum-like Zn_6O_9 species.^[15] Heptanuclear arrays feature dicubane Zn_7O_8 units,^[16] a Zn_7O_2 double tetrahedron,^[17] and a $\text{Zn}_7\text{O}_{12}\text{N}_{12}$ aggregate in the form of a six-point star.^[18]

Herein we report on the synthesis and the structural and spectroscopic characterization of a large dodecanuclear zincophosphonate aggregate **1** that possesses a $\text{Zn}_4(\mu_4\text{-O})$ core. Reaction of *tert*-butylphosphonic acid in THF with



ZnEt_2 in toluene (in a 1:1.5 ratio) provided compound **1** as colorless crystals in 27% yield. The ^{31}P NMR spectrum of the reaction mixture displayed signals of several products, with **1** being the major species as shown by four signals of the same intensity in the ^{31}P NMR spectrum (Figure 1).

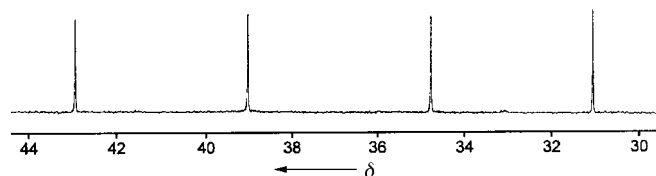


Figure 1. ^{31}P NMR spectrum of **1**.

The four types of chemically inequivalent phosphorus atoms present in the aggregate **1** in solution are also evident in the solid state structure of **1**, which was established by single crystal X-ray diffraction (Figure 2).^[19] The dodecanuclear aggregate consists of a central $\text{Zn}_4(\mu_4\text{-O})$ core and a zincophosphonate “shell”. The molecule **1** has approximate C_2 symmetry with a pseudo- C_2 axis that passes through the $\mu_4\text{-O}3$ atom in the central moiety. There are four pairs of equivalent phosphonate $t\text{BuPO}_3$ groups and six pairs of chemically quite diverse zinc centers. Half of the zinc atoms retained one ethyl group while the other half lost the alkyl substituents completely. Four of these zinc atoms surround the central oxide in a tetrahedral fashion whereas the remaining two complete their coordination sphere by accepting an oxygen atom from the THF ligands. Two zinc atoms reside in a five-coordinate environment and the rest are four coordinate.

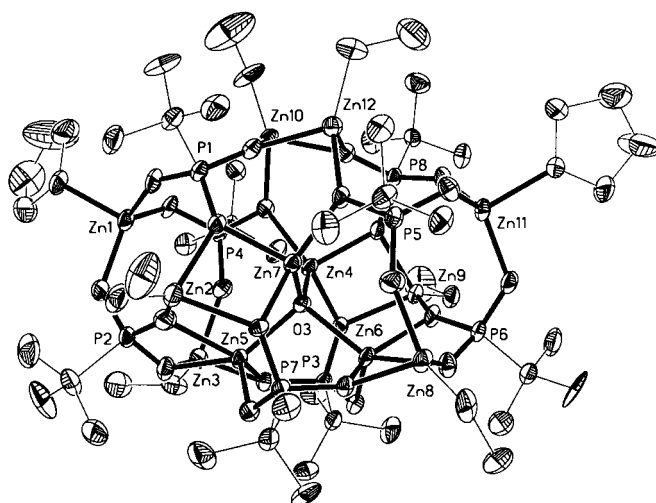


Figure 2. Molecular structure of **1**. Selected bond lengths [Å]: $\text{O}3\text{--Zn}4$ 1.948(4), $\text{O}3\text{--Zn}5$ 2.073(4), $\text{O}3\text{--Zn}6$ 2.072(4), $\text{O}3\text{--Zn}7$ 1.958(4).

Interestingly, the Zn:P ratio in **1** is the same as in the starting reaction mixture ($\text{Zn:P} = 1.5:1$). Thus, **1** contains an excess of zinc with respect to the usual 1:1 ratio that is found in divalent metal phosphonates. This is in turn reflected in the presence of the Zn-O-Zn bonds and, consequently, also of μ_3 - and μ_4 -bridging oxygen atoms.^[20] The bond distances between the phosphorus and μ_2 -O atoms (1.499(5)–1.527(5) Å) and μ_3 -O (1.531(5)–1.569(5) Å) fall in a narrow range, while the corresponding distances with zinc display a wider spread: Zn- μ_2 -O 1.891(5)–1.990(5) Å, Zn- μ_3 -O 1.971(4)–2.291(5) Å, and Zn- μ_4 -O 1.948(4)–2.073(4) Å. The presence of the μ_4 -O atom cannot be attributed to adventitious moisture because of the relatively high yield of **1**. We speculate that its origin can be ascribed to the induced dehydration of phosphonic acid by ZnEt_2 , which resulted in the formation of the phosphonic anhydride $(t\text{BuPO}_2)_3$. A signal observed in the ^{31}P NMR spectrum of the crude reaction mixture at $\delta = 31.18$ supports this notion as it agrees well with the reported value for $(t\text{BuPO}_2)_3$.^[21]

In summary, we have presented the largest zinc oligonuclear aggregate **1** to date, which features several interesting structural motifs that are closely related to zincophosphate and phosphonate frameworks, namely the Zn-O-Zn bonds, three- and four-coordinate oxygen atoms, and a Zn:P ratio of 1.5:1. Moreover, this molecule contains several reactive centers, which may be potentially utilized for the transformation of this precursor into porous materials.

Experimental Section

1: A solution of *tert*-butylphosphonic acid (0.44 g, 3.2 mmol) in THF (10 mL) was added dropwise to a solution of ZnEt_2 (4.3 mL, 1.1 M in toluene) in toluene (10 mL) at -78°C . The resulting solution was slowly warmed to room temperature and stirred for 6 h, and then concentrated to 5 mL. A white precipitate formed overnight and was removed by filtration. The clear solution was allowed to stand at room temperature for two months. Colorless crystals of **1** (0.22 g, 27%) suitable for single crystal X-ray diffraction experiments were formed. M.p. $>270^\circ\text{C}$ decomp; ^1H NMR (250.1 MHz, $\text{C}_6\text{D}_6/[\text{D}_8]\text{THF}$ 1:3): δ = 0.15 (m; ZnCH_2), 0.75 (m; CH_3), 1.14 (m; $t\text{BuP}$) 1.55 (m; THF), 2.14 (s; $\text{CH}_3\text{C}_6\text{H}_5$), 3.44 (m; THF), 7.0 (m; $\text{CH}_3\text{C}_6\text{H}_5$); ^{31}P NMR (101.3 MHz, $\text{C}_6\text{D}_6/[\text{D}_8]\text{THF}$ 1:3): δ = 42.94, 39.04, 34.75, 31.04 (s, 1:1:1:1); IR (nujol): $\tilde{\nu}$ = 1603 vw, 1496 w, 1476 s, 1394 m, 1262

m, 1232 m, 1171 vs, 1139 vs, 1093 vs, 1055 s, 1021 m, 982 s, 955 vs, 921 m, 881 m, 834 s, 802 w, 734 m, 675 vs, 615 s, 586 m, 529 m, 509 m, 465 w, 454 w cm⁻¹; elemental analyses (THF and toluene were removed by drying **1** under vacuum) calcd for C₄₄H₁₀₂O₂₅P₈Zn₁₂ (2063.51): C 25.61, H 4.98; found: C 25.86, H 5.25.

Received: August 5, 1998 [Z12251IE]
German version: *Angew. Chem.* **1999**, *111*, 706–708

Keywords: cage compounds • phosphonate complexes • zinc

- [1] a) X. Bu, P. Feng, T. E. Gier, G. D. Stucky, *J. Solid State Chem.* **1998**, *136*, 210; b) P. Feng, X. Bu, G. D. Stucky, *Angew. Chem.* **1995**, *107*, 1911; *Angew. Chem. Int. Ed. Engl.* **1995**, *34*, 1745; c) T. E. Gier, G. D. Stucky, *Nature* **1991**, *349*, 508; d) T. M. Nenoff, W. T. A. Harrison, T. E. Gier, G. D. Stucky, *J. Am. Chem. Soc.* **1991**, *113*, 378; e) W. T. A. Harrison, T. E. Gier, K. L. Moran, J. M. Nicol, H. Eckert, G. D. Stucky, *Chem. Mater.* **1991**, *3*, 27; f) T. Song, J. Xu, Y. Zhao, Y. Yue, Y. Xu, R. Xu, N. Hu, G. Wei, H. Jia, *J. Chem. Soc. Chem. Commun.* **1994**, 1171.
- [2] W. T. A. Harrison, T. E. Gier, G. D. Stucky, R. W. Broach, R. A. Bedard, *Chem. Mater.* **1996**, *8*, 145.
- [3] a) W. T. A. Harrison, L. Hannooman, *Angew. Chem.* **1997**, *109*, 663; *Angew. Chem. Int. Ed. Engl.* **1997**, *36*, 640; b) W. T. A. Harrison, L. Hannooman, *J. Solid State Chem.* **1997**, *131*, 363; c) W. T. A. Harrison, M. L. F. Phillips, *Chem. Commun.* **1996**, 2771; d) W. T. A. Harrison, M. L. F. Phillips, *Chem. Mater.* **1997**, *9*, 1837.
- [4] W. T. A. Harrison, R. W. Broach, R. A. Bedard, T. E. Gier, X. Bu, G. D. Stucky, *Chem. Mater.* **1996**, *8*, 691.
- [5] a) W. T. A. Harrison, Z. Bircsak, L. Hannooman, *J. Solid State Chem.* **1997**, *134*, 148; b) W. T. A. Harrison, Z. Bircsak, L. Hannooman, Z. Zhang, *J. Solid State Chem.* **1998**, *136*, 93; c) Y. Ortiz-Avila, P. R. Rudolf, A. Clearfield, *Inorg. Chem.* **1989**, *28*, 2137; d) S. Natarajan, M. P. Atfield, A. K. Cheetham, *J. Solid State Chem.* **1997**, *132*, 229.
- [6] a) W. T. A. Harrison, T. M. Nenoff, T. E. Gier, G. D. Stucky, *Inorg. Chem.* **1992**, *31*, 5395; b) C. G. Lugmair, T. D. Tilley, A. L. Rheingold, *Chem. Mater.* **1997**, *9*, 339; c) P. Reinert, N. Z. Logar, J. Patarin, V. Kaucic, *Eur. J. Solid State Inorg. Chem.* **1998**, *35*, 373.
- [7] a) K. J. Martin, P. J. Squattrito, A. Clearfield, *Inorg. Chim. Acta* **1989**, *155*, 7; b) K. J. Frink, R.-C. Wang, J. L. Colon, A. Clearfield, *Inorg. Chem.* **1991**, *30*, 1438; c) D. M. Poojary, A. Clearfield, *J. Am. Chem. Soc.* **1995**, *117*, 11278.
- [8] a) G. Cao, H. Lee, V. M. Lynch, T. E. Mallouk, *Inorg. Chem.* **1988**, *27*, 2781; b) G. Cao, T. E. Mallouk, *Inorg. Chem.* **1991**, *30*, 1434.
- [9] a) S. Drumel, P. Janvier, P. Barboux, M. Bujoli-Doeuff, B. Bujoli, *Inorg. Chem.* **1995**, *34*, 148; b) S. Drumel, P. Janvier, D. Deniaud, B. Bujoli, *J. Chem. Soc. Chem. Commun.* **1995**, 1051; c) F. Fredoueil, V. Penicaud, M. Bujoli-Doeuff, B. Bujoli, *Inorg. Chem.* **1997**, *36*, 4702.
- [10] a) S. Jain, T. T. Kodas, M. Hampden-Smith, *Chem. Vap. Deposition* **1998**, *4*, 51; b) J. Auld, D. J. Houlton, A. C. Jones, S. A. Rushworth, M. A. Malik, P. O'Brien, G. W. Critchlow, *J. Mater. Chem.* **1994**, *4*, 1249.
- [11] F. A. Cotton, L. M. Daniels, L. R. Falvello, J. H. Matonic, C. A. Murillo, X. Wang, H. Zhou, *Inorg. Chim. Acta* **1997**, *266*, 91.
- [12] a) H. M. M. Shearer, C. B. Spencer, *Acta Crystallogr. Sect. B* **1980**, *36*, 2046; b) M. M. Olmstead, P. P. Power, S. C. Shoner, *J. Am. Chem. Soc.* **1991**, *113*, 3379.
- [13] Y. Kai, M. Morita, N. Yasuoka, N. Kasai, *Bull. Chem. Soc. Jpn.* **1985**, *58*, 1631.
- [14] F. H. van der Steen, J. Boersma, A. L. Spek, G. van Koten, *Organometallics* **1991**, *10*, 2467.
- [15] S. Uhlenbrock, R. Wegner, B. Krebs, *J. Chem. Soc. Dalton Trans.* **1996**, 3731.
- [16] a) M. L. Ziegler, J. Weiss, *Angew. Chem.* **1970**, *82*, 931; *Angew. Chem. Int. Ed. Engl.* **1970**, *9*, 905; b) M. Ishimori, T. Hagiwara, T. Tsuruta, Y. Kai, N. Yasuoka, N. Kasai, *Bull. Chem. Soc. Jpn.* **1976**, *49*, 1165.
- [17] a) D. Attanasio, G. Dessy, V. Fares, *J. Chem. Soc. Dalton Trans.* **1979**, 28; b) N. Lalot, C. P. Raptopoulou, A. Terzis, A. E. Aliev, S. P. Perlepes, I. P. Gerotheranassis, E. Manessi-Zoupa, *Chem. Commun.* **1998**, 1513.
- [18] M. Tesmer, B. Mueller, H. Vahrenkamp, *Chem. Commun.* **1997**, 721.
- [19] Crystal data for **1**: C_{62.5}H₁₃₀O₂₇P₈Zn₁₂ (1·1.5C₇H₈), *M*_r = 2345.86, triclinic, space group *P*1̄, *a* = 15.049(10), *b* = 15.178(10), *c* = 24.89(2) Å, *α* = 72.89(2), *β* = 75.54(3), *γ* = 62.51(4)°, *V* = 4777(6) Å³, *Z* = 2, *ρ*_{calcd} = 1.631 g cm⁻³, *F*(000) = 2402, *λ* = 0.71073 Å, *T* = 150 K, *μ*(MoK_α) = 31.51 cm⁻¹, min./max transmission 0.1871/0.3654, crystal dimensions 0.80 × 0.50 × 0.40 mm, 3.59 < *θ* < 25.13°; 16331 data were collected of which 13156 were independent (*R*_{int} = 0.0753). For the final refinement of 1023 parameters no restraints were used. The *R* values were: *R*1 = Σ|*F*_o - *F*_c|/Σ*F*_o = 0.0467 for *I* > 2σ(*I*), and *wR*2 = [Σ*w*(*F*_o² - *F*_c²)/Σ*wF*_o⁴]^{1/2} = 0.1292 for all data; max/min. residual electron density: 0.990/-0.782 e Å⁻³. The unit cell contains two molecules of **1** and three molecules of toluene of crystallization, one of them disordered about the inversion center. Intensity data of **1** were collected on a Siemens-Stoe AED-2 four-circle diffractometer. The crystal was transferred in an inert oil and then flash-cooled in a nitrogen stream.^[22] The structure of **1** was solved with direct methods (SHELXS-97)^[23] and was refined against *F*².^[24] An empirical absorption correction was employed.^[25] All non-hydrogen atoms were refined anisotropically and the riding model was used for the hydrogen atoms. Crystallographic data (excluding structure factors) for the structure reported in this paper have been deposited with the Cambridge Crystallographic Data Centre as supplementary publication no. CCDC-102564. Copies of the data can be obtained free of charge on application to CCDC, 12 Union Road, Cambridge CB21EZ, UK (fax: (+44) 1223-336-033; e-mail: deposit@ccdc.cam.ac.uk).
- [20] a) T. Song, M. B. Hursthouse, J. Chen, J. Xu, K. M. A. Malik, R. H. Jones, R. Xu, J. M. Thomas, *Adv. Mater.* **1994**, *6*, 679; b) X. Bu, P. Feng, G. D. Stucky, *J. Solid State Chem.* **1996**, *125*, 243.
- [21] S. Fuchs, H. Schmidbaur, *Z. Naturforsch. B* **1995**, *50*, 855. However, an AB₂ spin system has also been reported for (tBuPO₂)₃, see K. Diemert, W. Kuchen, W. Poll, F. Sandt, *Eur. J. Inorg. Chem.* **1998**, *1*, 361.
- [22] T. Kottke, D. Stalke, *J. Appl. Crystallogr.* **1993**, *26*, 615.
- [23] G. M. Sheldrick, SHELXS-97, *Program for Structure Solution*, *Acta Crystallogr. Sect. A* **1990**, *46*, 467.
- [24] G. M. Sheldrick, SHELXL-97, *Program for Structure Refinement*, Universität Göttingen, **1997**.
- [25] S. Parkin, B. Moezzi, H. Hope, *J. Appl. Crystallogr.* **1995**, *28*, 53.

Hydrogen-Bonding Cavities about Metal Ions: A Redox Pair of Coordinatively Unsaturated Paramagnetic Co–OH Complexes**

Brian S. Hammes, Victor G. Young, Jr, and Andrew S. Borovik*

Described herein is a synthetic system that uses hydrogen bonds to regulate the chemistry at a coordinatively unsaturated metal center. These regulatory properties are illustrated by the isolation and characterization of monomeric Co–OH complexes, including a five-coordinate paramagnetic Co^{III}–OH complex which, to our knowledge, has not been observed

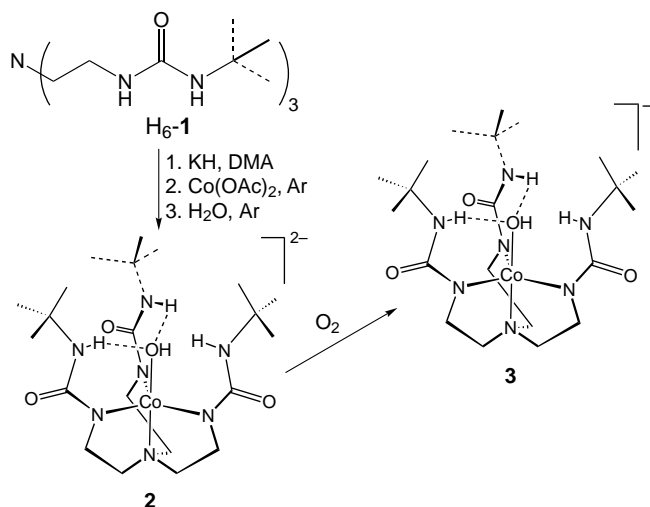
[*] Prof. A. S. Borovik, Dr. B. S. Hammes
Department of Chemistry
University of Kansas
Lawrence, KS 66045 (USA)
Fax: (+1) 785-864-5396
E-mail: aborovik@caco3.chem.ukans.edu
Dr. V. G. Young, Jr.
Department of Chemistry, University of Minnesota (USA)

[**] The NIH (GM50781 to A.S.B.) is acknowledged for financial support of this research.

previously. To accomplish this chemistry the new tripodal ligand $[\text{H}_3\text{-1}]^{3-}$ (see Scheme 1) was synthesized. Metal ion binding to $[\text{H}_3\text{-1}]^{3-}$ yields a cavity structure that can provide up to three intramolecular hydrogen bonds to an external donor atom coordinated to the metal center. To ensure intramolecular hydrogen bonds in these metal complexes, $[\text{H}_3\text{-1}]^{3-}$ is designed so that thermodynamically favored six-membered rings are formed during formation of the hydrogen bonds.^[1]

Hydrogen-bonding interactions are important in influencing the structural and functional properties of metalloproteins.^[2, 3] In several metalloproteins, hydrogen bonds are used in conjunction with metal–ligand covalent bonds to stabilize or control the chemistry of reactive species. This combination of bonding modes is typified by the structure of the active site in oxyhemoglobin, which has, in addition to a covalent Fe–O bond, a hydrogen bond between the distal imidazolyl residue of histidine and the coordinated O_2 molecule.^[4] To model these desirable effects, several synthetic systems have been reported that combined intramolecular covalent and hydrogen bonds to selectively bind and stabilize metal–ligand adducts.^[5] However, few of these systems are structurally characterized to conclusively show that multimode binding is present.^[5e–g,k,l] We have examined how the structures of C_3 -symmetric cavities direct the chemistry of trigonal mono- and bipyramidal complexes.^[6] We now extend our studies to include C_3 -symmetric hydrogen-bonding cavities. X-ray diffraction results confirm that these cavities organize such that hydrogen bonds can form to Co–OH moieties in trigonal-bipyramidal complexes.

$\text{K}_2[\text{CoH}_3\text{-1}(\text{OH})]$ (**K₂-2**) was isolated by a two-step synthesis as shown in Scheme 1. Compound **2** has a quasi-reversible one-electron redox couple at -740 mV (vs. SCE) and can be readily oxidized by O_2 to form $[\text{CoH}_3\text{-1}(\text{OH})]^-$ (**3**).^[7] Labeling studies confirm that water is the source of the OH^- ion in **3**, as no change was observed in the frequency of the $\tilde{\nu}(\text{OH})$ band when $^{18}\text{O}_2$ was used as the oxidant. Moreover,



Scheme 1. Synthesis of **2** and **3**.

the use of H_2^{18}O in the reaction affords $[\text{O}^{18}]\text{-3}$ (IR: $\tilde{\nu}(\text{OH}) = 3616, 3594\text{ cm}^{-1}$; $\tilde{\nu}(\text{OH}) = 3606, 3582\text{ cm}^{-1}$; $\tilde{\nu}(\text{OH})/\tilde{\nu}(\text{OH}) = 1.003$ and 1.003 , respectively, calcd 1.003).

The molecular structures of **K₂-2** and **K-3** were determined by X-ray diffraction methods. The overall structures of **2** and **3** are similar (shown in Figure 1 for **3**), with both complexes having a trigonal-bipyramidal coordination geometry around their cobalt centers.^[8] In **3** the three deprotonated urea

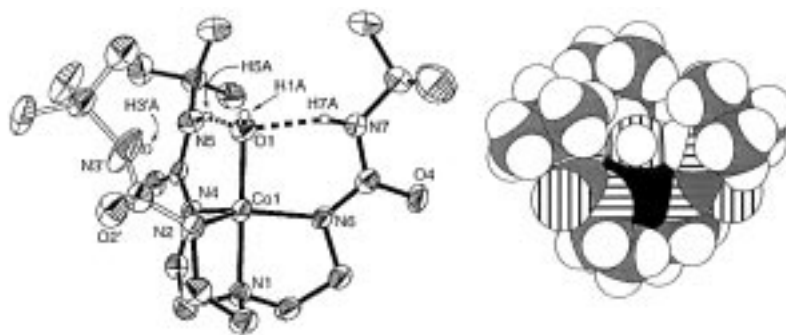


Figure 1. Thermal ellipsoid diagram (left) and a space-filling representation (right) of the structure of **3**. The ellipsoids are drawn at the 50% probability level, and only the urea and hydroxo hydrogen atoms are shown. Only one of the disordered fragments for the arm containing N2 is shown. Selected bond lengths [Å] and angles [°] for **3** (**2**): Co1–N1 1.945(3) (2.190(3)), Co1–N2 1.957(3) (2.042(3)), Co1–N4 1.974(3) (2.090(3)), Co1–N6 1.939(3) (2.085(3)), Co1–O1 1.894(2) (2.072(2)); N2–Co1–N4 108.16(11) (118.34(10)), N2–Co1–N6 132.35(11) (115.92(10)), N4–Co1–N6 116.36(11) (117.70(11)), O1–Co1–N1 175.94(11) (172.67(10)).

nitrogen atoms define the trigonal plane with an average Co1–N_{urea} bond length of 1.957(2) Å. The terminal hydroxo ligand is positioned nearly *trans* to the apical amine nitrogen atom N1; the Co1–O1 and Co1–N1 distances are 1.894(2) and 1.945(3) Å, and the O1–Co1–N1 angle is 175.94(11) Å. The O1–H1A vector is located between the urea arms containing N2 and N6: To accommodate this disposition of the hydroxo ligand the N2–Co1–N6 angle is significantly increased to 132.35(11)° from that expected for trigonal-bipyramidal geometry (120°).

In addition to the covalent Co–OH bond in **2** and **3**, two intramolecular hydrogen bonds to the hydroxo ligand are present between the hydroxo oxygen atom and the urea NH groups. For **3** the heavy atom O1...N5 and O1...N7 distances of 2.748(4) and 2.680(4) Å and the O1–H5A–N5 and O1–H7A–N7 angles of 161(4) and 163(4)° are indicative of strong hydrogen bonds. Similar metrical features are found in **2**.^[9] The NH group of the remaining arm in both complexes is not involved in hydrogen bonding, as it is canted such that the N–H vector is directed away from O1.^[9] In **3**, O2, N3, and C4 exhibit a high degree of anisotropic disorder, causing this portion of the arm to be refined as two fragments, one of which is shown in Figure 1. The presence of distinct urea NH groups in **K₂-2** and **K-3** is supported by solid-state FT-IR studies that show multiple $\tilde{\nu}(\text{NH})$ bands.

The molecular structures of **2** and **3** resemble the structure of a $\text{Cu}^{\text{II}}\text{-OH}$ complex recently reported by Tolman et al. that also has two hydrogen bonds to the hydroxo oxygen atom. However, there are no examples of cobalt complexes where a redox pair has been isolated having the same trigonal-

bipyramidal stereochemistry as shown here for **2** and **3**. Moreover, while Co–OH complexes are known, many are polynuclear species containing bridging hydroxo ligands.^[10] In fact, there are just two reports of structurally characterized monomeric Co–OH complexes:^[11] a low-spin square-pyramidal Co^{II}–OH complex^[12] and the six-coordinate [Co(terpy)(η^2 -CO₃)(OH)] complex (terpy = 2,2':6',2''-terpyridine).^[13] Additionally, Co^{III} complexes are normally diamagnetic, yet **2** and **3** are paramagnetic.^[14] Compound **2** is a high-spin ($S = 3/2$) complex with a room-temperature magnetic moment μ_{eff} of 4.49 μ_{B} and an X-band EPR signal at $g = 3.87$ (77 K). Compound **3** has a room-temperature μ_{eff} value of 3.28(6) μ_{B} , which is consistent with an $S = 1$ ground state.^[15] The unusual spin state in **3** is achieved because the trigonal symmetry around the Co^{III} mandates an intermediate spin ground state for a d⁶ ion. This trigonal-bipyramidal stereochemistry is enforced by the protective hydrogen-bonding cavity of [H₃-1]³⁻, preventing the binding of any additional ligands that would lead to a more common six-coordinate $S = 0$ complex.

The results obtained in this study are reminiscent of the regulatory properties provided by active-site structures in metalloproteins.^[16] The threefold symmetric hydrogen-bonding cavities formed in metal complexes of [H₃-1]³⁻ can control the binding and stabilization of metal–ligand adducts, as demonstrated by the isolation of a unique redox pair of Co–OH complexes.

Experimental Section

K₂-2: A solution of H₆-1 (0.11 g, 0.24 mmol) in anhydrous *N,N*-dimethylacetamide (DMA, 4 mL) was treated with solid KH (0.028, 0.72 mmol) under an Ar atmosphere. After H₂ evolution had ceased, solid Co(OAc)₂ (0.043 g, 0.24 mmol) was added. The resulting solution was stirred for 0.5 h and filtered to remove a small amount of insoluble material (KOAc), which was discarded. H₂O (0.090 g, 0.48 mmol) was added to this filtrate, which caused an immediate color change from blue to violet. The reaction mixture was stirred for 1 h and then filtered. Diethyl ether vapor was allowed to diffuse into the violet filtrate to provide crystalline K₂-2 (0.068 g, 40% yield). Elemental analysis calcd (found) for K₂-2·0.75DMA (C₂₄H_{49.75}CoK₂N_{7.75}O_{4.75}): C 43.67 (43.24), H 7.60 (7.86), N 16.45 (16.30). The presence of DMA was corroborated by IR spectroscopy; IR (Nujol): $\tilde{\nu} = 3227, 3138$ (N–H), 1587 cm⁻¹ (C=O); EPR (X-band, DMA, 77 K): $g = 3.87$; UV/Vis (DMA): $\lambda_{\text{max}}(\epsilon) = 395$ (sh), 474 (sh), 514 (52), 596 (sh), 618 (sh), 681 nm (24); cyclic voltammetry (DMF, 0.1 V s⁻¹): $E_{1/2} = -0.74$ V, $E_{\text{pc}} = 0.39, 0.82$ V; $\mu_{\text{eff}} = 4.49 \mu_{\text{B}}$ (solid, 298 K).

X-ray structure analysis for K₂-2·CH₃CN·DMA (crystals used for X-ray diffraction were grown by diffusing diethyl ether into a DMA/MeCN solution): crystal dimensions, 0.35 × 0.34 × 0.12 mm, monoclinic, space group C2/c, $a = 33.5148(4)$, $b = 12.8140(4)$, $c = 23.2786(4)$ Å; $\beta = 132.464(1)^\circ$; $V = 7374.9(2)$ Å³, $\rho_{\text{calcd}} = 1.302$ Mg m⁻³, $Z = 8$, $3.30 \leq 2\theta \leq 50.00^\circ$; MoK α radiation ($\lambda = 0.71073$ Å), $F(000) = 3080$, $T = 173$ K; of a total of 17 622 reflections collected on a Siemens SMART Platform CCD diffractometer, 6418 were independent ($R_{\text{int}} = 0.0358$), reflection/parameter ratio 6418/453; absorption correction: SADABS (Sheldrick, 1996), max./min. transmission factor 1.000/0.888; structure solution by direct methods (SHELXTL-V5.0), all urea and hydroxo hydrogen atoms were found in the Fourier difference map and refined positionally while holding the U_{eq} values at relative values; refinement by full-matrix least squares on F^2 , $R1 = 0.0513$, $wR2 = 0.0917$ ($I > 2\sigma(I)$), GOF = 1.048, min./max. residual electron density 0.261/–0.301 e Å⁻³.

K-3: A solution of K₂-2 (0.24 mmol) in anhydrous DMA (4 mL) was treated with dry O₂ (0.48 mmol), which caused an immediate color change from violet to dark red. The mixture was stirred for 1 h and evacuated to remove excess O₂. The resulting solution was filtered, and volatile

components were removed under reduced pressure. The complex was crystallized by vapor diffusion of diethyl ether into a solution of K-3 in DMF (0.64 g, 47% yield). Elemental analysis calcd (found) for K-3 (C₂₁H₄₃CoKN₇O₄): C 45.38 (44.93), H 7.81 (7.86), N 17.64 (17.24); IR: $\tilde{\nu} = 3616, 3594$ (O–H), 3366, 3251, 3161 (N–H), 1599, 1581, 1522 cm⁻¹ (C=O); UV/Vis: $\lambda_{\text{max}}(\epsilon) = 288$ (6600), 389 (sh), 474 (3900), 793 nm (480); $\mu_{\text{eff}} = 3.28(6) \mu_{\text{B}}$.

X-ray structure analysis for K-3: crystal dimensions, 0.30 × 0.15 × 0.06 mm, triclinic, space group P $\bar{1}$, $a = 10.7774(3)$, $b = 11.3017(3)$, $c = 11.7250(2)$ Å, $\alpha = 94.319$, $\beta = 95.146(1)$, $\gamma = 98.003(1)^\circ$; $V = 1402.94(6)$ Å³, $\rho_{\text{calcd}} = 1.315$ Mg m⁻³, $Z = 2$, $3.500 \leq 2\theta \leq 50.08^\circ$; MoK α radiation ($\lambda = 0.71073$ Å), $F(000) = 592$, $T = 173(2)$ K; of a total of 8056 reflections collected on a Siemens SMART Platform CCD diffractometer, 4826 were independent ($R_{\text{int}} = 0.0348$), reflection/parameter ratio 4826/365, absorption correction: SADABS (Sheldrick, 1996), max./min. transmission factor 1.000/0.560; the structure was solved by direct methods (SHELXTL-V5.0); all urea and hydroxo hydrogen atoms were found in the Fourier difference map and refined positionally while holding the U_{eq} values at relative values; refinement by full-matrix least squares on F^2 , $R1 = 0.0463$, $wR2 = 0.01055$ ($I > 2\sigma(I)$); GOF = 0.989, 0.500, –0.447 e Å⁻³. For the disordered arm that is not involved in hydrogen bonding, all atoms beyond C3 were split into two fragments and refined with restraints. The refinement led to a 0.48:0.52 ratio in occupancy. In total, 52 SHELXTL SAME and FLAT restraints were applied to atoms of similar nature.

Crystallographic data (excluding structure factors) for the structures reported in this paper have been deposited with the Cambridge Crystallographic Data Centre as supplementary publication no. CCDC-111493 and CCDC-111494 (K₂-2·CH₃CN·DMA and K-3, respectively). Copies of the data can be obtained free of charge on application to CCDC, 12 Union Road, Cambridge CB2 1EZ, UK (fax: (+44) 1223-336-033; e-mail: deposit@ccdc.cam.ac.uk).

Received: August 18, 1998 [Z 12300 IE]

German version: *Angew. Chem.* **1999**, *111*, 744–746

Keywords: cobalt • hydrogen bonds • hydroxo ligands • ligand effects

- [1] A molecule that is similar to H₆-1 has been reported: C. Rapsos, M. Almaraz, M. Martín, V. Weinrich, M. L. Mussóns, V. Alcázar, M. C. Caballero, J. R. Morán, *Chem. Lett.* **1995**, 759–760.
- [2] R. H. Holm, P. Kennepohl, E. I. Solomon, *Chem. Rev.* **1996**, *96*, 2239–2314.
- [3] a) Y. Lu, J. S. Valentine, *Curr. Opin. Struct. Biol.* **1997**, *7*, 495–500; b) L. Regan, *TIBS* **1995**, *20*, 280–285.
- [4] B. A. Springer, S. G. Sligar, J. S. Olsen, G. N. Philips, *Chem. Rev.* **1994**, *94*, 699–714.
- [5] Porphyrin systems: a) G. E. Wuenshell, C. Tetreau, D. Lavalette, C. A. Reed, *J. Am. Chem. Soc.* **1992**, *114*, 3346–3355; b) J. P. Collman, X. Zhang, K. Wong, J. I. Brauman, *J. Am. Chem. Soc.* **1994**, *116*, 6245–6251; c) M. Momenteau, C. A. Reed, *Chem. Rev.* **1994**, *94*, 659–698. d) C. K. Chang, Y. Liang, G. Avilés, S.-M. Peng, *J. Am. Chem. Soc.* **1995**, *117*, 4191–4192; non-heme systems: e) J. E. Kickham, S. J. Loeb, S. L. Murphy, *J. Am. Chem. Soc.* **1993**, *115*, 7031–7032; f) D. M. Rudkevich, W. Verboom, Z. Brzozka, M. J. Palys, W. P. R. V. Stauthamer, G. J. Van Hummel, S. M. Franken, S. Harkema, J. F. J. Engbersen, D. N. Reinhoudt, *J. Am. Chem. Soc.* **1994**, *116*, 4341–4351; g) N. Kitajima, H. Komatsuzaki, S. Hikichi, M. Osawa, Y. Moro-oka, *J. Am. Chem. Soc.* **1994**, *116*, 11 596–11 597; h) P. H. Walton, K. N. Raymond, *Inorg. Chim. Acta* **1995**, *240*, 593–601; i) W. Yao, R. H. Crabtree, *Inorg. Chem.* **1996**, *35*, 3007–3011; j) L. M. Berreau, S. Mahapatra, J. A. Halfen, V. G. Young, W. B. Tolman, *Inorg. Chem.* **1996**, *35*, 6339–6342; k) A. Wada, M. Harata, K. Hasegawa, K. Jitsukawa, H. Masuda, M. Mukai, T. Kitagawa, H. Einaga, *Angew. Chem.* **1998**, *110*, 874–875; *Angew. Chem. Int. Ed. Engl.* **1998**, *37*, 798–799.
- [6] a) M. Ray, G. P. A. Yap, A. L. Rheingold, A. S. Borovik, *Chem. Commun.* **1995**, 1777–1778; b) M. Ray, A. Golombek, M. Hendrich, V. G. Young, A. S. Borovik, *J. Am. Chem. Soc.* **1996**, *118*, 6084–6085;

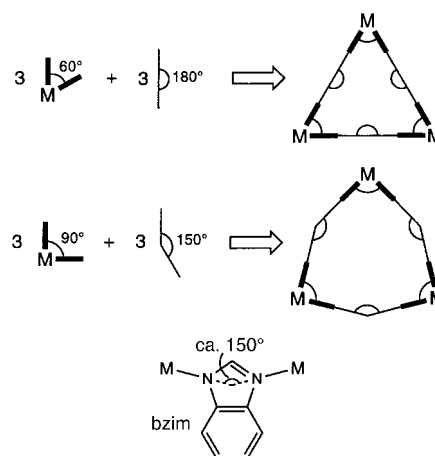
- c) B. S. Hammes, D. Maldonado-Ramos, G. P. A. Yap, L. Liable-Sands, A. L. Rheingold, A. S. Borovik, *Inorg. Chem.* **1997**, *36*, 3210–3211; d) Z. Shirin, V. G. Young, A. S. Borovik, *Chem. Commun.* **1997**, *4*, 1840–1841; e) M. Ray, B. S. Hammes, G. P. A. Yap, A. L. Rheingold, A. S. Borovik, *Inorg. Chem.* **1998**, *37*, 1527–1532.
- [7] The redox potential for the $[\text{CoH}_3\text{-1(OH)}]^-/[\text{CoH}_3\text{-1(OH)}]^{2-}$ redox pair is comparable to that for the $[\text{Co(CN)}_6]^{3-}/[\text{Co(CN)}_6]^{4-}$ pair: N. N. Greenwood, A. Earnshaw, *The Chemistry of the Elements*, Pergamon Press, Oxford, **1984**, pp. 1302–1303.
- [8] The structure of **K₂-2** has a potassium ion (K1) positioned at a distance of 2.798 (3) Å from O1.
- [9] In **2** the O1...N5 and O1...N7 distances are 2.747(4) and 2.779(4) Å, while an O1...N3 distance of 3.019(3) Å is observed for the non-hydrogen-bonded arm.
- [10] D. A. Buckingham, C. R. Clark in *Comprehensive Coordination Chemistry*, Vol. 4 (Eds.: G. Wilkinson, R. D. Guillard, J. A. McCleverty), Pergamon Press, New York, **1987**, pp. 635–900.
- [11] The classical six-coordinate Werner-type complexes $[\text{CoL}_4(\text{H}_2\text{O})(\text{OH})]^{2-}$ have been shown to be dimeric in the solids state with bridging H_3O_2^- ligands: a) M. Ardon, A. Bino, *Inorg. Chem.* **1985**, *24*, 1343–1347; b) M. Ardon, A. Bino, *Polyhedron* **1987**, *6*, 181–187.
- [12] A. Orlandini, L. Sacconi, *Inorg. Chem.* **1976**, *15*, 78–85.
- [13] S. E. Kucharski, B. W. Skelton, A. H. White, *Aust. J. Chem.* **1978**, *31*, 47–51.
- [14] Examples of paramagnetic Co^{III} complexes with trigonal-bipyramidal stereochemistry: a) C. A. McAuliffe, S. M. Godfrey, A. G. Mackie, R. G. Pritchard, *Angew. Chem.* **1992**, *104*, 932–934; *Angew. Chem. Int. Ed. Engl.* **1992**, *31*, 919–921; b) B. S. Jaynes, T. Ren, S. Liu, S. J. Lippard, *J. Am. Chem. Soc.* **1992**, *114*, 9670–9671.
- [15] R. Drago, *Physical Methods in Inorganic Chemistry*, Saunders, Philadelphia, **1977**, chap. 11.
- [16] For examples relevant to M–OH complexes in biology, see I. Bertini, C. Luchinat in *Bioinorganic Chemistry* (Eds.: I. Bertini, H. B. Gray, S. J. Lippard, J. S. Valentine), University Science Books, Mill Valley, **1994**, pp. 37–106.

Self-Assembly of Predesigned Trimetallic Macrocycles Based on Benzimidazole as Nonlinear Bridging Motifs: Crystal Structure of a Luminescent Platinum(II) Cyclic Trimer**

Siu-Wai Lai, Michael Chi-Wang Chan,*
Shie-Ming Peng, and Chi-Ming Che*

Self-assembly of mono- and polycyclic supermolecules is a challenging yet prolific area of research.^[1] In the context of metallomacrocycles with internal cavities, efforts have focused on the design and construction of molecular squares,^[2] while triangular arrays have remained relatively unexplored. In theory, if the building blocks are sufficiently rigid, the

alternating combination of three subunits extending 60° bite angles with three linear linkers would constitute an equilateral triangle (Scheme 1). In practice, the former is difficult to attain at metal centers but is available in a number of bidentate ligands, and thus trimeric assemblies are formed



Scheme 1. Strategies for the synthesis of trimeric macrocycles with metal vertices.

in tandem with linear two-coordinate or *trans*-configured metallic bridges.^[3] Triangular macrocycles bearing metal vertices and supported by 4,4'-bipyridine,^[4] 2,2'-bipyrazine,^[5] 1,3-bis(1-methylbenzimidazol-2-yl)benzene,^[6] and various nucleobases^[7] have been synthesized. However, only moderate selectivities are encountered in these reactions due to the presence of multiple chelating sites and other geometrical factors (ligand flexibility, angle strain at metal center), and mixtures of products are often afforded.

We propose a *ligand-directed* strategy for the fabrication of trimetallic macrocycles by using bzim (bzim = N-anion of benzimidazole) as a rigid nonlinear bridging motif. Coupling of three edges exhibiting 150° angles with right-angled vertices (i.e. *cis* binding sites at metal centers residing in square-planar and octahedral environments) is anticipated to yield a cyclic trimer,^[8] and based on this premise, the predefined geometry and unambiguous binding mode of the bidentate bzim ligand is ideal (Scheme 1). We report herein the highly efficient syntheses of luminescent platinum(II) trimeric assemblies directed by N-deprotonated benzimidazole.

Treatment of the luminescent cyclometalated Pt^{II} precursors $[\text{Pt}(\text{thpy})(\text{Hthpy})\text{Cl}]^{[9a]}$ (Hthpy = 2-(2'-thienyl)pyridine) and $[\text{nBu}_4\text{N}][\text{Pt}(\text{bzqn})\text{Cl}_2]^{[9b]}$ (Hbzqn = 7,8-benzoquinoline) with sodium benzimidazolate afforded $[\text{Pt}(\text{thpy})(\text{bzim})]_3$ (**1**) and $[\text{Pt}(\text{bzqn})(\text{bzim})]_3$ (**2**) as orange and yellow crystalline solids, respectively, in high yields (80–90%). In the FAB mass spectra, the anticipated molecular ion clusters for **1** and **2** are observed at m/z 1417 and 1471, respectively. The trimeric nature of **1** was confirmed by X-ray crystallography.^[10]

The molecular structure of **1** (Figure 1) consists of alternating $[(\text{thpy})\text{Pt}]$ vertices and benzimidazolate edges. The slightly distorted square-planar geometry around each platinum center comprises the N and *ortho*-C atoms of thpy and

[*] Dr. M. C.-W. Chan, Prof. C.-M. Che, S. W. Lai
Department of Chemistry, The University of Hong Kong
Pokfulam Road, Hong Kong (China)
Fax: (+852) 2857 1586
E-mail: cmche@hkucc.hku.hk
mcwchan@hkusub.hku.hk

Prof. S.-M. Peng
Department of Chemistry, National Taiwan University
Taipei (Taiwan)

[**] We are grateful for financial support from The University of Hong Kong (and for a Postdoctoral Fellowship to M.C.W.C.) and the Hong Kong Research Grants Council.

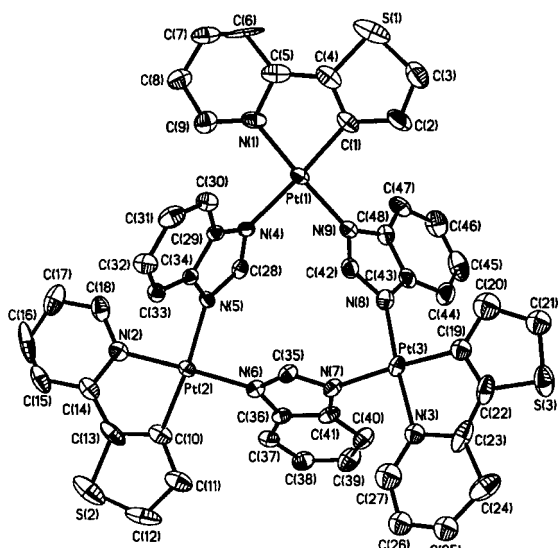


Figure 1. Perspective view of **1** (30% probability ellipsoids. Hydrogen atoms and solvent molecules are omitted for clarity). Selected bond lengths [Å] and angles [°]: Pt(2)–N(2) 2.03(1), Pt(2)–C(10) 2.01(1), Pt(2)–N(5) 2.100(9), Pt(2)–N(6) 2.016(9), N(4)–C(28) 1.33(1), N(5)–C(28) 1.35(1), N(6)–C(35) 1.34(1), N(7)–C(35) 1.32(1), N(8)–C(42) 1.34(1), N(9)–C(42) 1.33(1); N(2)–Pt(2)–C(10) 80.7(5), N(5)–Pt(2)–N(6) 89.0(3), N(7)–Pt(3)–N(8) 88.4(4), N(4)–Pt(1)–N(9) 87.8(3), Pt(1)–N(4)–C(28) 130.3(7), N(4)–C(28)–N(5) 114.6(9), Pt(2)–N(5)–C(28) 132.8(8).

two N atoms of different bzim bridges. The comparable interatomic distances within the N–C–N fragments of the bzim moieties (mean 1.33 Å) imply considerable delocalization after N-deprotonation. The three N–Pt–N angles within the macrocycle (range 87.8(3)–89.0(3)°) show minimal strain, in contrast to Fujita's proposed triangles containing 4,4'-bipyridine.^[4] The Pt–N(bzim) interactions are out of the triplatinum plane (Figure 2) because the bidentate bite angles

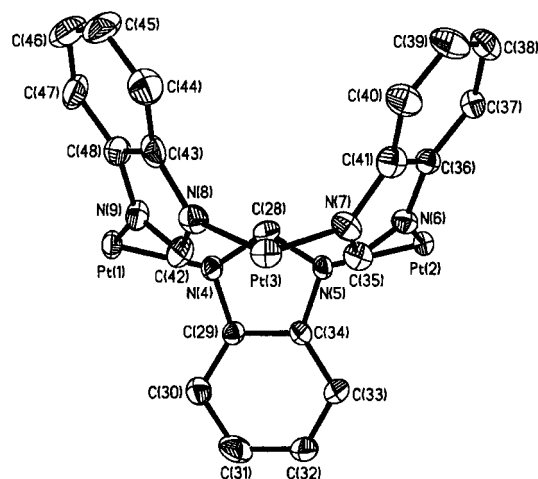


Figure 2. Perspective view of **1** showing orientations of benzimidazolate ligands (thpy groups are omitted for clarity).

exhibited by the bzim anions (range 138–140°) deviate slightly from 150°. This inherent coordination geometry ensures the successful and efficient assembly of the trimeric macrocycles described here. Interestingly, the bzim groups are orientated in a *syn*, *anti*, *anti* (two-up, one-down) fashion to

create an open cavity with different faces, which is reminiscent of the partial cone conformation in calixarenes.^[11] From the mean plane through the platinum atoms, the angle to the *syn* bzim units is 60° (av), while the inclination of the unique bzim is 77°. The opening at the *syn* bzim rim is about 7.4 Å, which narrows considerably towards the core to about 4.7 Å at the imidazole centroids. The Pt...Pt distances are 6.1 Å (av), while the depth of the cavity is approximately 5 Å. This molecular pocket has lower symmetry than previously reported metallomacrocycles,^[2e] and this may have important consequences for future work towards molecular hosts. In addition, π – π interactions are evident between thpy systems in adjacent molecules, with interplanar separations of around 3.5 Å.

The absorption spectrum of **1** in CH₂Cl₂ contains bands at 270–360, 400–430, and 480–560 nm, which can be assigned to spin-allowed ligand-centered (¹LC, $\pi_{\text{thpy}} \rightarrow \pi_{\text{thpy}}^*$ with metal perturbation) and spin-allowed and spin-forbidden metal-to-ligand charge transfer (¹MLCT and ³MLCT, $d_{\text{Pt}} \rightarrow \pi_{\text{thpy}}^*$) transitions, respectively.^[12] The UV/Vis spectrum of **2** is comparable to that of the bis(cyclometalated) derivative [Pt(bzqn)₂].^[13] Complex **1** is emissive at 301 K in CH₂Cl₂, with peak maxima at 560 (sh, 580 nm) and 606 nm (sh, 636 and 661 nm; lifetime, τ = 8 μ s; quantum yield, Φ = 0.016) that are slightly blue-shifted to 557 (sh, 575 nm) and 601 nm (sh, 633 and 656 nm) at 77 K. Based on previous studies^[12, 13] and the observation of minor solvatochromic effects (< 10 nm), these emissions are tentatively assigned as MLCT transitions with LC character. In the crystalline form, multiple emission with λ_{max} at 571, 617, and 664 nm are apparent at 301 K. The substantial red shift of the 664 nm band relative to that observed in the solution state is attributed to excimeric emission arising from π -stacking in the solid state (see above).^[14] In contrast, no emission is observed for **2** in CH₂Cl₂ or in the solid state at room temperature, although weak emission is evident at 77 K in solid state. Hence complex **1** has greater potential for photoinduced energy and electron transfer applications than **2**.

In conclusion, we have described a simple yet efficient methodology for the synthesis of trimeric platinum(II) macrocycles, which are structurally related to calixarenes. We anticipate that this strategy will be applicable to other square-planar and octahedral metal complexes. In view of the established photoluminescence of cyclometalated Pt^{II} species,^[15] this study paves the way for the design of molecular sensors with large cavities^[16] based on suitable nonlinear bidentate ligands with rigid, predefined geometry.

Experimental Section

1: A mixture of benzimidazole (0.05 g, 0.39 mmol) and excess NaH in THF (10 mL) under a N₂ atmosphere was stirred for 20 min until the evolution of hydrogen ceased. The solution was filtered, added to [Pt(thpy)(Hthpy)Cl] (0.20 g, 0.36 mmol) in CH₂Cl₂ (15 mL), and stirred at reflux for 12 h. The resultant orange solution was concentrated to 5 mL and addition of diethyl ether afforded an orange solid. Slow evaporation of an acetone/benzene solution yielded orange crystals (yield 88%). Satisfactory elemental analysis was obtained; ¹H NMR (500 MHz, CD₂Cl₂, 27 °C, TMS): δ = 8.40–6.31 (m); ¹³C NMR (126 MHz, [D₆]DMSO, 27 °C, TMS): δ = 162.6, 150.6–148.3, 144.2–140.3, 133.3–132.7, 128.8–128.1, 123.0–115.5, 110.5; IR (Nujol): $\tilde{\nu}$ = 1605 cm^{–1} (C=N); UV/Vis (CH₂Cl₂): λ_{max} (ϵ) = 277 (47 000),

337 (22000), 357 (18000), 409 (5200), 421 (4800), 480 (110), 494 (110), 512 (110), 535(80), 554 nm (70); FAB-MS: m/z (%): 1417 (100) [M^+], 1300 (30) [$M^+ - \text{bzim}$].

2: As for **1** using benzimidazole (0.04 g, 0.33 mmol), excess NaH, and [$n\text{Bu}_4\text{N}$][Pt(bzqn)Cl₂] (0.20 g, 0.29 mmol). A yellow precipitate was afforded after reflux for 12 h. Slow evaporation of an acetone/benzene solution yielded yellow crystals (yield 84%). Satisfactory elemental analysis was obtained; ¹H NMR (500 MHz, [D₆]DMSO, 27 °C, TMS): δ = 9.26–6.91 (m); ¹³C NMR (126 MHz, [D₆]DMSO, 27 °C, TMS): δ = 156.7, 149.4–148.8, 144.2–138.4, 133.4–115.7, 110.5; IR (Nujol): $\tilde{\nu}$ = 1620, 1610 cm⁻¹ (C=N); UV/Vis (CH₂Cl₂): λ_{max} (ϵ) = 271 (70000), 278 (73000), 358 (14000), 372 (14000), 413 (4000), 469 nm (440); FAB-MS: m/z (%): 1471 (100) [M^+], 1354 (25) [$M^+ - \text{bzim}$].

Received: September 16, 1998 [Z124221E]
German version: *Angew. Chem.* **1999**, *111*, 708–710

Keywords: luminescence • metallomacrocycles • N ligands • platinum • self-assembly

- [1] a) J.-M. Lehn, *Supramolecular Chemistry*, VCH, Weinheim, **1995**; b) V. Balzani, F. Scandola in *Comprehensive Supramolecular Chemistry*, Vol. 10 (Eds.: J. L. Atwood, J. E. D. Davies, D. D. Macnicol, F. Vögtle), Pergamon, Oxford, **1996**, pp. 687–746; c) D. Philp, J. F. Stoddart, *Angew. Chem.* **1996**, *108*, 1242–1286; *Angew. Chem. Int. Ed. Engl.* **1996**, *35*, 1154–1196; d) J.-P. Sauvage, *Acc. Chem. Res.* **1990**, *23*, 319–327.
- [2] a) M. Fujita, K. Ogura, *Bull. Chem. Soc. Jpn.* **1996**, *69*, 1471–1482; b) B. Olenyuk, A. Fechtenkötter, P. J. Stang, *J. Chem. Soc. Dalton Trans.* **1998**, 1707–1728; c) R. V. Slone, J. T. Hupp, C. L. Stern, T. E. Albrecht-Schmitt, *Inorg. Chem.* **1996**, *35*, 4096–4097; d) W. H. Leung, J. Y. K. Cheng, T. S. M. Hun, C. M. Che, W. T. Wong, K. K. Cheung, *Organometallics* **1996**, *15*, 1497–1501; e) C. A. Hunter, *Angew. Chem.* **1995**, *107*, 1181–1183; *Angew. Chem. Int. Ed. Engl.* **1995**, *34*, 1079–1081.
- [3] For example, see: a) H. H. Murray, R. G. Raptis, J. P. Fackler, Jr., *Inorg. Chem.* **1988**, *27*, 26–33; b) J. R. Hall, S. L. Loeb, G. K. H. Shimizu, G. P. A. Yap, *Angew. Chem.* **1998**, *110*, 130–133; *Angew. Chem. Int. Ed.* **1998**, *37*, 121–123.
- [4] M. Fujita, O. Sasaki, T. Mitsuhashi, T. Fujita, J. Yazaki, K. Yamaguchi, K. Ogura, *Chem. Commun.* **1996**, 1535–1536.
- [5] R.-D. Schnebeck, L. Randaccio, E. Zangrando, B. Lippert, *Angew. Chem.* **1998**, *110*, 128–130; *Angew. Chem. Int. Ed.* **1998**, *37*, 119–121.
- [6] a) R. F. Carina, A. F. Williams, G. Bernardinelli, *J. Organomet. Chem.* **1997**, *548*, 45–48; b) S. Rüttimann, G. Bernardinelli, A. F. Williams, *Angew. Chem.* **1993**, *105*, 432–434; *Angew. Chem. Int. Ed. Engl.* **1993**, *32*, 392–394.
- [7] a) H. Chen, M. M. Olmstead, D. P. Smith, M. F. Maestre, R. H. Fish, *Angew. Chem.* **1995**, *107*, 1590–1593; *Angew. Chem. Int. Ed. Engl.* **1995**, *34*, 1514–1517; b) D. P. Smith, E. Baralt, B. Morales, M. M. Olmstead, M. F. Maestre, R. H. Fish, *J. Am. Chem. Soc.* **1992**, *114*, 10647–10649.
- [8] The crystal structure of an imidazolate-bridged trinuclear copper(II) complex has been published: P. Chaudhuri, I. Karpenstein, M. Winter, C. Butzlaff, E. Bill, A. X. Trautwein, U. Flörke, H.-J. Haupt, *J. Chem. Soc. Chem. Commun.* **1992**, 321–322.
- [9] Prepared by modification of published procedures: a) T. J. Giordano, P. G. Rasmussen, *Inorg. Chem.* **1975**, *14*, 1628–1634; b) C. A. Craig, F. O. Garces, R. J. Watts, R. Palmans, A. J. Franks, *Coord. Chem. Rev.* **1990**, *97*, 193–208.
- [10] Crystal structure data for **1**: C₄₈H₃₃N₉Pt₃S₃ · 1.5 C₆H₆; M_r = 1534.47, triclinic, $P\bar{1}$, a = 14.2225(2), b = 15.1095(1), c = 16.0380(2) Å, α = 62.936(1), β = 70.543(1), γ = 71.802(1)°, V = 2840.3(1) Å³, Z = 2, ρ_{calcd} = 1.794 g cm⁻³, μ = 7.524 mm⁻¹, $F(000)$ = 1458, $\lambda(\text{MoK}\alpha)$ = 0.71073 Å, T = 295 K. Orange crystal, dimensions 0.15 × 0.10 × 0.08 mm³. A total of 9954 unique reflections (R_{int} = 0.096) were collected on a Siemens SMART CCD diffractometer (ω scans, $2\theta_{\text{max}}$ = 50°). The structure was solved by direct methods and refined by least-squares treatment on F^2 using the SHELXL-93 program: R = 0.051,

wR = 0.109, GOF = 0.947 for 6219 absorption-corrected (Sadabs, transmission 0.35–0.58) reflections with $I > 2\sigma(I)$ and 570 parameters. The 2-(2'-thienyl)pyridine group chelated to Pt(3) is disordered with 33: 67% occupancy. Crystallographic data (excluding structure factors) for the structures reported in this paper have been deposited with the Cambridge Crystallographic Data Center as supplementary publication no. CCDC-102975. Copies of the data can be obtained free of charge on application to CCDC, 12 Union Road, Cambridge CB21EZ, UK (fax: (+44) 1223-336-033; e-mail: deposit@ccdc.cam.ac.uk).

- [11] C. D. Gutsche, *Calixarenes*, Royal Society of Chemistry, Cambridge, **1989**. A related tetranuclear platinum-incorporated analogue of calix[4]arene [[Pt(en)(uracilate)]₄]⁴⁺ (en = 1,2-diaminoethane) has been reported: H. Rauter, E. C. Hillgeris, A. Erxleben, B. Lippert, *J. Am. Chem. Soc.* **1994**, *116*, 616–624.
- [12] P.-I. Kvam, M. V. Puzyk, V. S. Cotlyr, K. P. Balashev, J. Songstad, *Acta Chem. Scand.* **1995**, *49*, 645–652.
- [13] M. Maestri, D. Sandrini, V. Balzani, L. Chassot, P. Jolliet, A. von Zelewsky, *Chem. Phys. Lett.* **1985**, *122*, 375–379.
- [14] V. H. Houlding, V. M. Miskowski, *Coord. Chem. Rev.* **1991**, *111*, 145–152.
- [15] a) C. W. Chan, T. F. Lai, C. M. Che, S. M. Peng, *J. Am. Chem. Soc.* **1993**, *115*, 11245–11253; b) T. C. Cheung, K. K. Cheung, S. M. Peng, C. M. Che, *J. Chem. Soc. Dalton Trans.* **1996**, 1645–1651; c) H. Q. Liu, T. C. Cheung, C. M. Che, *Chem. Commun.* **1996**, 1039–1040; d) L. Z. Wu, T. C. Cheung, C. M. Che, K. K. Cheung, M. H. W. Lam, *Chem. Commun.* **1998**, 1127–1128.
- [16] A. P. de Silva, H. Q. N. Gunaratne, T. Gunnlaugsson, A. J. M. Huxley, C. P. McCoy, J. T. Rademacher, T. E. Rice, *Chem. Rev.* **1997**, *97*, 1515–1566.

A New Type of Glycosidic Linkage: An Open-Chain Acetal-Linked *N*-Acetylgalactosamine in the Core Part of the Lipopolysaccharides from *Proteus* Microorganisms*

Evgeny Vinogradov and Klaus Bock*

Monosaccharides in natural compounds are usually present in a cyclic hemiacetal form, in which the exocyclic hemiacetal oxygen atom is used for the connection to the aglycon. Herein we report the identification of a new type of linkage between monosaccharides found in the core part of the lipopolysaccharides (LPS) from two serotypes of *Proteus*. LPS is a component of the outer membrane of Gram-negative bacteria, and comprises three regions: the O-antigenic polysaccharide, the lipid A, and the core, a nonrepetitive oligosaccharide linking the O-antigenic polysaccharide to the lipid A.^[1] Normally, core oligosaccharides have complex structures, relatively conserved for each type of bacteria. The biological

[*] Prof. K. Bock, E. Vinogradov
Carlsberg Laboratory, Department of Chemistry
Gamle Carlsberg Vej 10, DK-2500 Copenhagen (Denmark)
Fax: (+45) 3327-4708
E-mail: kbo@crc.dk

[**] We thank Prof. Dr. W. Kaca, Prof. Dr. Z. Sidorchuk, and Prof. Dr. A. Rozalski from The Institute of Microbiology & Immunology of University of Lodz, Lodz, Poland, and Prof. Dr. E. S. Stanislavsky from I. I. Mechnikov Institute of Vaccine and Sera, Russian Academy of Medical Sciences, Moscow, Russia for supplying bacterial cells, and Dr. Jens Ø. Duus for helpful discussions.

functions of the particular core structures are as yet unknown. Partial structural analysis of the core region of LPS has been reported for several strains of *Proteus* bacteria.^[2–7]

In the present work the core oligosaccharides were released from the LPS by mild acid hydrolysis and isolated using gel chromatography and anion exchange chromatography. Analysis of the NMR spectra of the core oligosaccharides from serotypes *Proteus mirabilis* O27 and *Proteus vulgaris* OX2 revealed spin systems of 2-aminoaldoses (units L and L'; lettering is assigned arbitrarily) with an unusual coupling constant pattern (Table 1). The coupling constants do not correspond to values normally observed for pyranosides in chair conformation or equilibria thereof. The absence of low-field carbon signals (Table 2) indicated that these sugars do not possess furanose structures. Intramolecular NOEs observed between either H1 and H3, or H3 and H5, but not from H1 to H5 of

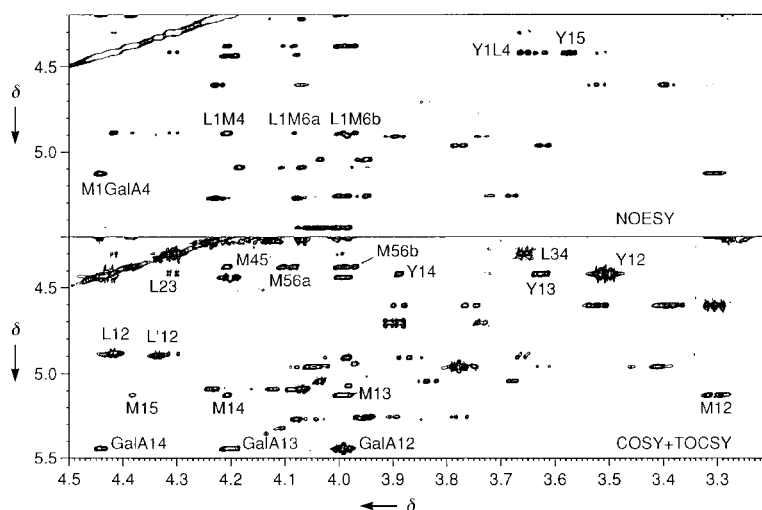


Figure 1. Parts of NOESY (upper trace) and COSY+TOCSY spectra of the core oligosaccharide from *P. vulgaris* OX2. Unit L' is a nonsubstituted residue, which appears in a disaccharide **3** after deamination.

Table 1. ¹H NMR data.^[a]

Unit, compound	H-1	H-2	H-3	H-4	H-5	H-6a	H-6b
S, 1	4.58	3.40	3.49	3.39	3.42	3.94	3.69
S, core O27	4.52	3.28	3.44	3.32	3.41	3.89	3.62
$S J_{n,n+1}$ [Hz]	8	10	10	10	$J_{5,6b}$ 6	$J_{6a,6b}$ 12	$J_{5,6a}$ 2
Y, 2	4.48	3.52	3.64	3.89	3.58	3.64	3.64
Y, core OX2	4.42	3.50	3.63	3.89	3.57	3.74	3.74
$Y J_{n,n+1}$ [Hz]	8	10	3.5	ca. 0	–	–	–
L, 1	4.87	4.34	4.26	3.42	4.08	3.81	3.73
L, core O27	4.84	4.27	4.19	3.36	4.02	3.76	3.67
L, 2	4.87	4.44	4.28	3.67	4.00	3.80	3.66
L, core OX2	4.88	4.41	4.30	3.65	3.99	3.79	3.66
L, 3	4.89	4.36	4.12	3.36	3.93	3.66	3.66
L', core OX2	4.89	4.33	–	–	–	–	–
$L' J_{n,n+1}$ [Hz]	5.5	1.5	10	2	$J_{5,6b}$ 6	$J_{6a,6b}$ 12	$J_{5,6a}$ 7
dM, 1	5.09	3.93	4.39	4.38	4.00	4.16	4.03
M, core O27	5.22	3.58	4.15	4.20	4.39	4.07	3.97
dM, 2	5.09	3.95	4.40	4.40	4.00	4.15	4.02
M, core OX2	5.13	3.30	3.99	4.20	4.38	4.09	3.98
dM, 3	5.09	3.94	4.41	4.40	4.01	4.16	4.03
dM $J_{n,n+1}$ [Hz]	3.5	8	–	–	$J_{5,6b}$ 2	$J_{6a,6b}$ 13	$J_{5,6a}$ < 1

[a] Interresidual NOE: **1**: S1–L5s,6am, L1–dM4s,6bs; core O27: S1–L5s,6am, L1–M4s,5w,6aw,6bs; **2**: Y1–L1w,2m,3w,4s, L1–dM4s,6aw,6bs; core OX2: Y1–L4m, L1–dM4s,6aw,6bs; **3**: L1–M4s,6aw,6bs.

Table 2. ¹³C NMR data.

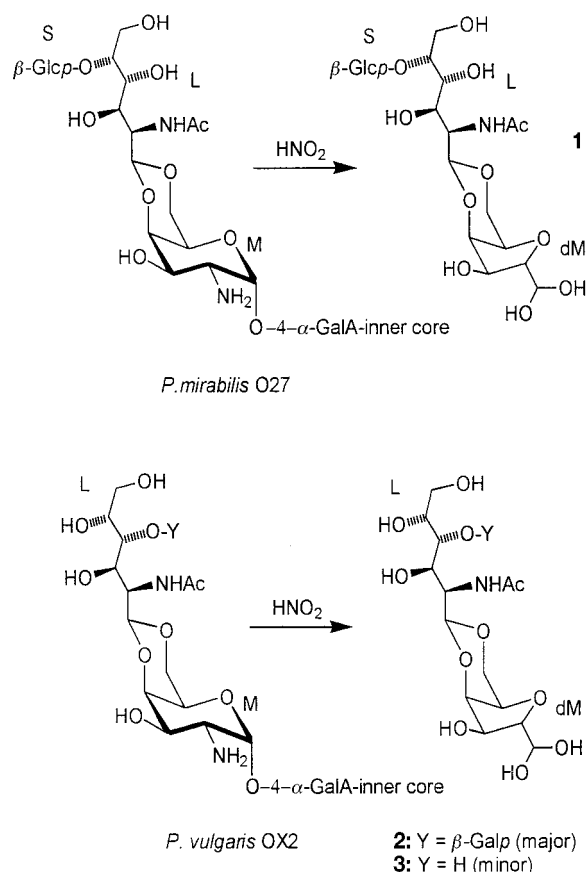
Unit, compound	C1	C2	C3	C4	C5	C6
S, 1	102.8	73.9	76.2	70.4	76.2	61.7
S, core O27	102.9	73.7	75.9	70.1	76.0	61.7
Y, 2	103.6	71.4	73.1	69.0	75.5	61.3
Y, core OX2	103.5	71.3	73.0	68.9	75.4	61.3
L, 1	98.8	52.5	67.9	69.4	78.5	62.0
L, core O27	100.6	52.3	67.8	69.2	78.4	62.2
L, 2	99.1	51.8	67.6	77.1	69.8	62.6
L, core OX2	100.6	51.2	67.4	77.0	69.8	62.5
L, 3	99.0	52.3	68.4	69.7	70.1	63.6
L', core OX2	100.6	51.8	–	–	–	–
dM, 1	90.4	84.0	73.8	76.6	73.4	67.4
M, core O27	96.9	51.2	65.2	75.0	64.1	69.0
dM, 2	90.4	83.8	73.8	76.5	73.3	67.2
M, core OX2	99.6	51.0	67.2	75.3	64.0	69.0
dM, 3	90.5	84.0	73.8	76.5	73.3	67.2

the sugar residue L are difficult to explain by a ring conformation or equilibria thereof. NOE data showed strong correlations between the anomeric L1 proton and protons 4 and 6b of the galactosamine residue M, and a weak signal between L1 and M6a (Table 1, Figure 1). The ¹³C NMR signals of C4 and C6 of the galactosamine residue M were downfield shifted by $\Delta\delta \approx 6–7$ compared to the signals of a nonsubstituted α -galactosamine residue, whereas signals of C3 and C5 were upfield shifted by $\Delta\delta = 3$ and 8, respectively. This indicated simultaneous substitution at O4 and O6.

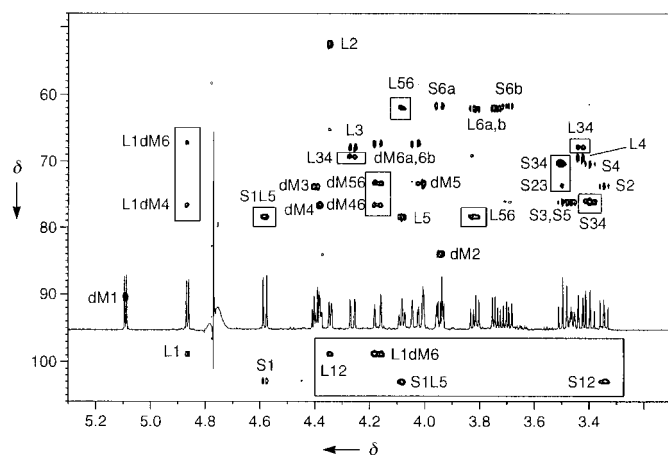
Fragments containing the sugar residue L (compound **1** from O27 serotype, compounds **2** and **3** from OX2 serotype) were isolated after deamination of the core oligosaccharides with sodium nitrite in acetic acid (Scheme 1). MALDI mass spectra of compounds **1** and **2** contained signals of ions $[M+H]^+$ at m/z 528.5 (minor), $[M+H_2O+H]^+$ at m/z 546.5 (major), and $[M+H_2O+Na]^+$ at m/z 568.4. These ions corresponded to trisaccharides built up of two hexoses and one acetamidohexose with an aldehyde group of the reducing 2,5-anhydrotalose (deamination product of galactosamine) present predominantly in the hydrated form.

NMR analysis of compounds **1–3** (Tables 1 and 2) showed that they all contain the above-described fragment L. All coupling constants and other features of the spectra of this residue remained unchanged compared to those of the starting core oligosaccharides. HMBC spectra showed cross peaks from L1 to dM4 and dM6 (Figure 2). Taken together, NOE and HMBC spectra indicated that residue L was linked to both positions 4 and 6 of the 2,5-anhydrotalose residue. Compound **1** contained additionally a β -glucopyranose residue S, attached, according to NOE and HMBC spectra, to O5 of the sugar residue L. In oligosaccharide **2**, the sugar residue L was glycosylated at O4 with a β -galactopyranose residue Y, and a minor product **3** contained only sugar residues L and dM.

The oligosaccharides **1–3** were hydrolyzed (4M HCl, 100 °C, 4 h) and analyzed by using an amino acid analyzer



Scheme 1.


Figure 2. Overlap of ^1H , HSQC, and HMBC (signals in boxes) spectra of the oligosaccharide **1**.

and GC (as alditol acetates). In all cases, galactosamine was detected as well as 2,5-anhydrotalose and glucose (in **1**) or galactose (in **2**). Methylation analysis of oligosaccharides **1–3** (after borohydride reduction) with the identification of the products as alditol acetates by GC-MS confirmed the proposed structures.

Combined together, these data suggest a new type of glycosidic structure with an open-chain *N*-acetylgalactosamine linked as cyclic acetal to positions 4 and 6 of the galactosamine in the α -pyranoside form. NOE correlations

between protons L1 and M4,6 indicate axial orientation of the proton L1, and therefore carbon L1 possesses an (*S*)-configuration. In order to prove that this structure was not an artifact from LPS cleavage under the mild acidic conditions during work-up, the LPS of *P. vulgaris* OX2 was deacylated with anhydrous hydrazine and the product studied by NMR spectroscopy. The fragments Y-L-M and L'-M were identified (differing from the above-described substances by the absence of the *N*-acetyl group in L), and showed the same coupling constants and substitution pattern as for the compounds described here.

The novel type of linkage between sugar residues—open-chain cyclic acetal linkage—is no surprise from a chemical point of view. Nevertheless, it has not been previously reported in natural products and has not even been discussed as a theoretical possibility.^[8] In contrast, cyclic acetals built up of non-sugar oxo compounds, such as pyruvic acid, are common components of bacterial polysaccharides.^[1, 9] The chemical stability of the acetal linkage formed by an *N*-acetylgalactosamine residue does not differ substantially from that of a normal glycosidic linkage, as it survives hydrolysis with acetic acid and methylation analysis, but can be cleaved under the hydrolytic conditions normally used in monosaccharide analysis (2 M HCl, 100 °C). It may therefore be more widely occurring in natural poly- or oligosaccharides but not detected, since conventional analysis of *Proteus* serotype O27 core (monosaccharide analysis, methylation, mass spectrometry) would lead to the identification of terminal glucose, terminal *N*-acetylgalactosamine and 4,6-disubstituted galactosamine instead of the structural fragment described here. We propose the use of the symbol “o” (for “open”) to identify this type of sugar form in abbreviated formulas, thus the formula of the disaccharide **3** could be written as (1*S*)-GaloNac-(1 \rightarrow 4,6)-2,5-anh-Tal. Detailed analysis of the LPS core structures will be reported elsewhere.

Experimental Section

Bacteria were cultivated and lipopolysaccharide was isolated as described previously.^[10, 11]

NMR spectroscopy and general methods: ^1H and ^{13}C NMR spectra were recorded on a Bruker AMX-600 spectrometer in D_2O at 25 °C with acetone as standard ($\delta = 2.225$ for ^1H , $\delta = 31.5$ for ^{13}C) using standard pulse sequences. NOESY spectra were recorded for core oligosaccharides, and ROESY (mixing time 250 ms) for compounds **1–3**. NMR spectra were assigned by using the program Pronto^[12] and NMR, GC, GC-MS, methylation and monosaccharide analysis was performed as previously described.^[13, 14]

Preparation of core oligosaccharides and oligosaccharides **1–3**: LPSs from serotypes O27 and OX2 (200 mg each) were hydrolyzed with 2 % acetic acid (100 °C, 5 h). The resulting precipitate removed by centrifugation, and the supernatant separated on a Sephadex G50 SF gel (Pharmacia) column (2.5 \times 80) using pyridine/acetic acid buffer (4 and 10 mL in 1 L water) and monitoring by Waters differential refractometer. Core fractions were further separated on a TSK-DEAE column (1.5 \times 20 cm) in water, monitored by refractometer, to give several fractions. For the analysis the last fraction eluted was used. Core oligosaccharides (20 mg each) were dissolved in water (2 mL), and NaNO_2 (5 mg) and AcOH (30 μL) were added. After 1 h at 20 °C, the mixtures were desalted by gel filtration chromatography on a TSK HW40(S) gel (Merck) column (1.6 \times 80 cm). Fractions containing oligosaccharides **1–3** (detected by NMR spectroscopy) were separated by ascending paper chromatography (Whatman No

1 paper) in pyridine/butanol/acetic acid/water (1:1:1:1), with alkaline silver nitrate detection. Compounds **1**–**3** were eluted from paper with water.

Received: October 5, 1998 [Z124851E]
German version: *Angew. Chem.* **1999**, *111*, 712–715

Keywords: carbohydrates • glycosides • natural products • NMR spectroscopy

- [1] B. Lindberg, *Adv. Carbohydr. Chem. Biochem.* **1990**, *48*, 279–318.
- [2] J. Radziejewska-Lebrecht, H. Mayer, *Eur. J. Biochem.* **1989**, *183*, 573–581.
- [3] J. Radziejewska-Lebrecht, U. R. Bhat, H. Brade, H. Mayer, *Eur. J. Biochem.* **1988**, *172*, 535–541.
- [4] K. Kotelko, M. Deka, W. Gromska, W. Kaca, J. Radziejewska-Lebrecht, A. Rozalski, *Arch. Immunol. Ther. Exp.* **1983**, *31*, 619–624.
- [5] J. Radziejewska-Lebrecht, U. Feige, M. Jensen, K. Kotelko, H. Friebolin, H. Mayer, *Eur. J. Biochem.* **1980**, *107*, 31–38.
- [6] J. Boll, J. Radziejewska-Lebrecht, C. Warth, D. Krajewska-Pietrasik, H. Mayer, *FEMS Immunol. Med. Microbiol.* **1994**, *8*, 329–342.
- [7] E. V. Vinogradov, J. Thomas-Oates, H. Brade, O. Holst, *J. Endotoxin Res.* **1994**, *1*, 199–206.
- [8] R. A. Laine, *Pure Appl. Chem.* **1997**, *69*, 1867–1873.
- [9] Y. A. Knirel, N. K. Kochetkov, *Biochemistry (Moscow)* **1994**, *59*, 1325–1383.
- [10] E. V. Vinogradov, W. Kaca, A. Rozalski, A. S. Shashkov, M. Cedzynski, Y. A. Knirel, N. K. Kochetkov, *Eur. J. Biochem.* **1991**, *200*, 195–201.
- [11] E. V. Vinogradov, D. Pietrasik, A. S. Shashkov, Y. A. Knirel, N. K. Kochetkov, *Bioorg. Khim.* **1988**, *14*, 1282–1286.
- [12] M. Kjaer, K. V. Andersen, F. M. Poulsen, *Methods Enzymol.* **1994**, *239*, 288–308.
- [13] E. V. Vinogradov, O. Holst, J. Thomas-Oates, K. W. Broady, H. Brade, *Eur. J. Biochem.* **1992**, *210*, 491–498.
- [14] E. V. Vinogradov, K. Bock, B. Petersen, O. Holst, H. Brade, *Eur. J. Biochem.* **1997**, *243*, 122–127.

A Novel Three-Way Chromophoric Molecular Switch: pH and Light Controllable Switching Cycles**

Luca Gobbi, Paul Seiler, and François Diederich*

Dedicated to Professor Fritz Vögtle on the occasion of his 60th birthday

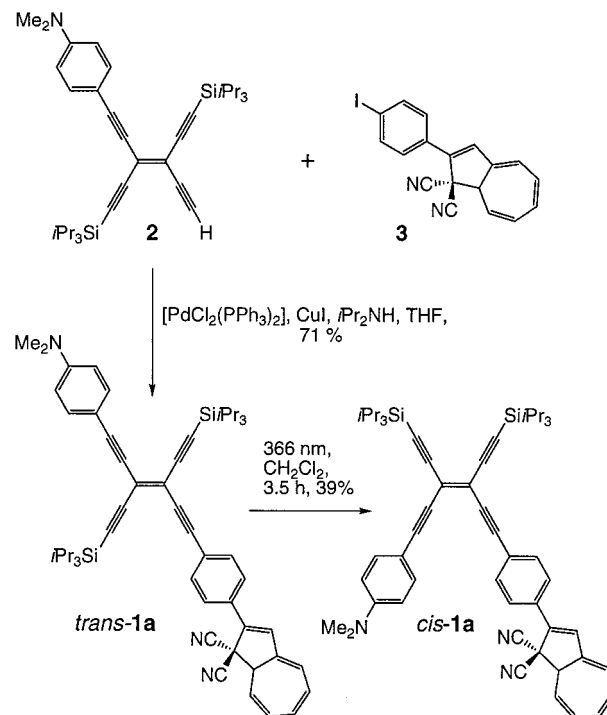
The field of molecular switches has received much attention in recent years.^[1] Of particular interest are photoresponsive systems since the use of light as an external stimulus for the interconversion of two states allows for rapid and clean processes.^[2] Herein we report a molecule with three addressable subunits that can undergo individual, reversible switching cycles.^[3] Compound **1a** (Scheme 1) consists of

[*] Prof. Dr. F. Diederich, Dipl.-Chem. L. Gobbi, P. Seiler
Laboratorium für Organische Chemie, ETH-Zentrum
Universitätsstrasse 16, CH-8092 Zurich (Switzerland)
Fax: (+41) 1-632-1109
E-mail: diederich@org.chem.ethz.ch

[**] This work was supported by the ETH Research Council and a Varon Visiting Professorship at the Weizmann Institute of Science (to F.D.). We thank Dr. M. Gómez-López for useful discussions.

a) a tetraethynylethene (TEE, 3,4-diethynylhex-3-ene-1,5-diyne)^[4] core, which can be reversibly photoisomerized between its *cis* and *trans* forms,^[5] b) a dihydroazulene (DHA) unit, which can be transformed into a vinylheptafulvene (VHF) moiety upon irradiation,^[6] and c) a proton sensitive *N,N*-dimethylanilino (DMA) group.

The target compound *trans*-**1a** (Scheme 1) was prepared by Sonogashira cross-coupling^[7] of TEE **2**^[8] with the aryl iodide **3**.^[9] The X-ray crystal structure analysis of *trans*-**1a**^[10] (Figure 1) shows only minor deviations (ca. 0.1 Å) from



Scheme 1. Synthesis of *trans*-**1a** and *cis*-**1a**.

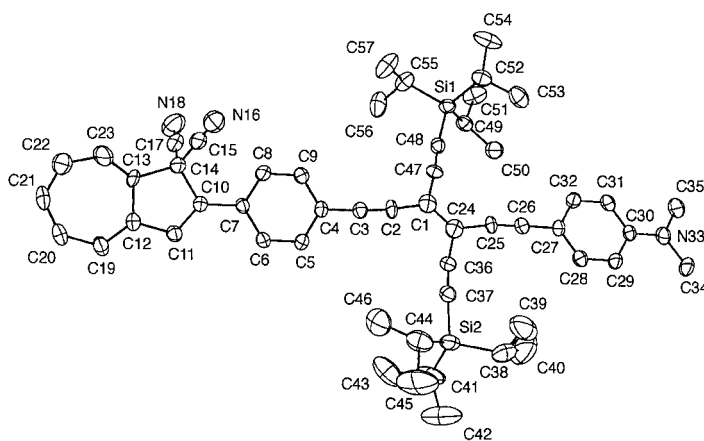


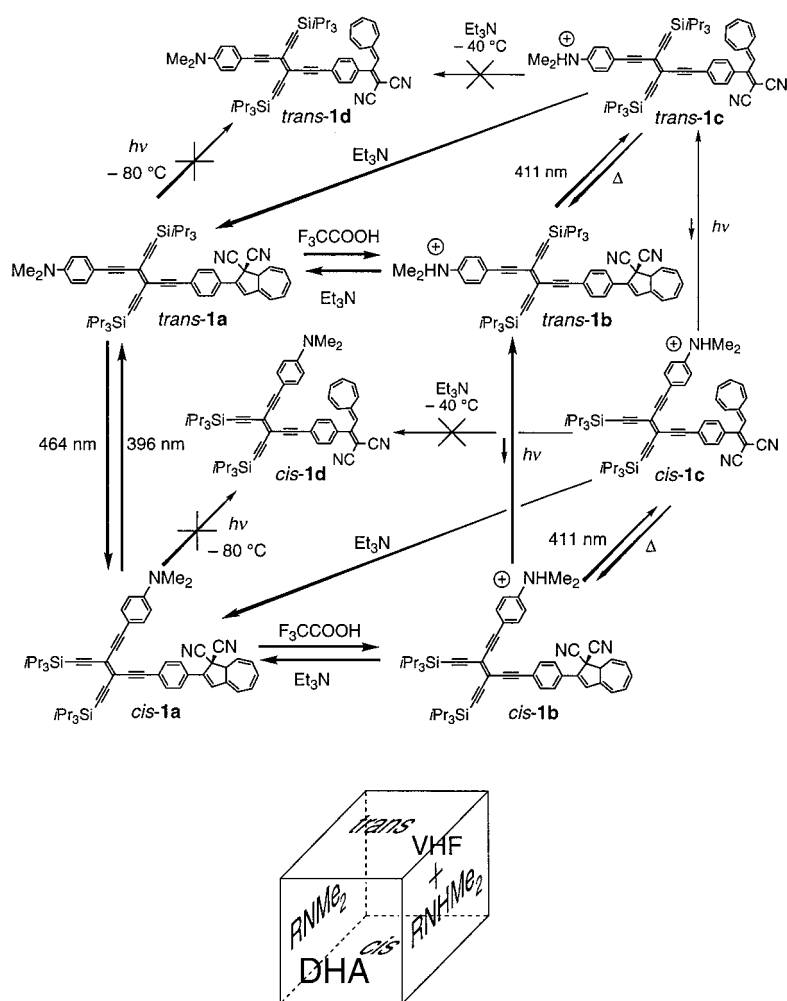
Figure 1. ORTEP plot of *trans*-**1a** in the crystal. The vibrational ellipsoids shown are at the 30% level.

planarity in the diarylated TEE core. The dihydroazulene moiety is slightly turned out of this plane, with the dihedral angle C14–C10–C7–C8 amounting to 13°. The diastereoisomeric *cis*-**1a** was obtained in 39% yield upon photolysis of *trans*-**1a** in CH_2Cl_2 at $\lambda = 366$ nm.

With three possible switching processes, **1** can adopt eight interconvertible states. Such a complex system is best visualized in a three-dimensional representation by a cube with each corner describing one distinct state (*trans*- and *cis*-**1a–d**, Scheme 2). Individual interconversion processes could be cleanly addressed despite this functional complexity, and six of the eight states were detected.

The photochemical, reversible *trans*–*cis* isomerization of arylated TEEs has recently been investigated.^[5] Irradiation at the longest wavelength absorption maximum ($\lambda_{\text{max}} = 464 \text{ nm}$, $\epsilon = 44\,000 \text{ L mol}^{-1} \text{ cm}^{-1}$) of *trans*-**1a** induces rapid conversion into *cis*-**1a**, while irradiation at the wavelength corresponding to the most intense absorption band of the latter ($\lambda_{\text{max}} = 396 \text{ nm}$, $\epsilon = 55\,000 \text{ L mol}^{-1} \text{ cm}^{-1}$) allows the reverse reaction to take place (Figure 2). The ratio of *trans* and *cis* isomers at the photostationary states and the quantum yields for the photoisomerization processes are summarized in Table 1.^[11]

Both *cis*-**1a** and *trans*-**1a** display a strong fluorescence with a maximum at $\lambda = 606 \text{ nm}$. This emission was monitored during several switching cycles to study the resistance of the *cis*–*trans* isomerization process to photofatigue (Figure 3). The intensity of the fluorescence at 606 nm decreases to about 90 % of the initial value after 15 cycles.



Scheme 2. Three-dimensional switching diagram of compound **1**. The eight possible states are shown as the corners of a cube.

Table 1. Physical data for the photochemical *cis*–*trans* isomerization of **1a** in CH_2Cl_2 at 25 °C.

λ ^[a] [nm]	<i>cis</i> ^[b] [%]	<i>trans</i> ^[b] [%]	$\Phi_{c \rightarrow t}$ ^[c]	$\Phi_{t \rightarrow c}$ ^[c]	K_{eq} ^[d]	ϵ_{cis} ^[e] [L mol ^{−1} cm ^{−1}]	ϵ_{trans} ^[e] [L mol ^{−1} cm ^{−1}]
396	35	65	0.19	0.17	1.83	55 000	33 000
464	68	32	0.51	0.37	2.15	26 000	44 000

[a] Irradiation wavelength. [b] Percentile of *cis*- and *trans*-**1a**, respectively, in the photostationary state. [c] Partial quantum yields for the *cis*→*trans* and *trans*→*cis* interconversions, respectively. [d] Photoequilibrium constant, that is, the ratio between the isomers at the photostationary state. [e] Molar extinction coefficients of *cis*-**1a** and *trans*-**1a** at the irradiation wavelength.

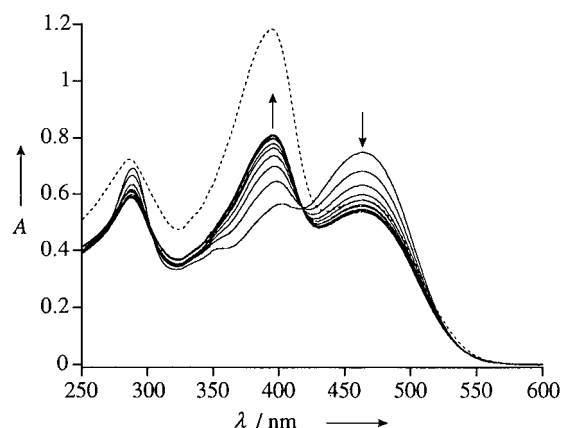


Figure 2. Electronic absorption spectrum in CH_2Cl_2 of pure *cis*-**1a** (---, $c = 2.09 \times 10^{-5} \text{ M}$) and spectra recorded at 10 s intervals during the *trans*→*cis* isomerization process ($\lambda_{\text{irr}} = 464 \text{ nm}$) starting from pure *trans*-**1** ($c = 1.70 \times 10^{-5} \text{ M}$) (—).

Molecular switches that rely on light-triggered electrocyclization and retroelectrocyclization steps have been studied successfully in the past.^[3, 6, 14] The thermally reversible 10-electron photo-retrocyclization of 1,1-dicyano-1,8a-dihydroazulenes (DHA) to 8-(2,2-dicyanovinyl)heptafulvenes (VHF) was first reported by Daub and co-workers.^[6] Compound **1a** bears such a DHA group, but the photoinduced retrocyclization to the VHF form could not be accomplished. However, when the DMA moiety in **1a** was protonated with trifluoroacetic acid—to give **1b** (Scheme 2)—the photochemical ring-opening to the VHF-containing TEE **1c** took place. Protonation of **1a** to give **1b** is clearly indicated by the downfield shifts of the aromatic signals of the DMA group in the ^1H NMR spectrum (from 6.65 and 7.39 ppm to 7.51 and 7.65 ppm for the *trans* isomer and from 6.67 and 7.38 ppm to 7.51 and 7.62 ppm for the *cis* isomer). Yellow solutions of protonated DHA derivatives *cis*-**1b** and *trans*-**1b** in CH_2Cl_2 both showed an absorption maximum of similar intensity at 411 nm and displayed only a weak yellow fluorescence. The VHF-containing compounds *cis*-**1c** and *trans*-**1c** featured a new absorption band at $\lambda_{\text{max}} = 500 \text{ nm}$ in the same solvent, which renders the solution orange-brown. The conversion of *trans*-**1b** into *trans*-

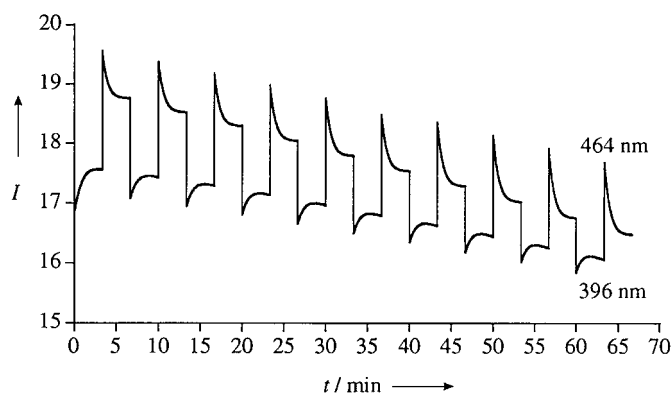


Figure 3. Fluorescence intensity of **1a** ($c = 2.09 \times 10^{-5} \text{ M}$ in CH_2Cl_2) measured at 606 nm at 25 °C for ten switching cycles, starting from *cis*-**1a**. The sample was irradiated at 396 nm (*cis*-**1a** \rightarrow *trans*-**1a**) and at 464 nm (*trans*-**1a** \rightarrow *cis*-**1a**).

1c, upon irradiation at $\lambda = 411 \text{ nm}$, was monitored by both ^1H NMR and UV/Vis spectroscopy (Figure 4). Standard ^1H NMR solutions ($c \approx 10 \text{ mM}$) of *trans*-**1b** are too concentrated to be irradiated and successfully switched. However, when a dilute solution ($c \approx 0.3 \text{ mM}$) of *trans*-**1b** in CDCl_3 was

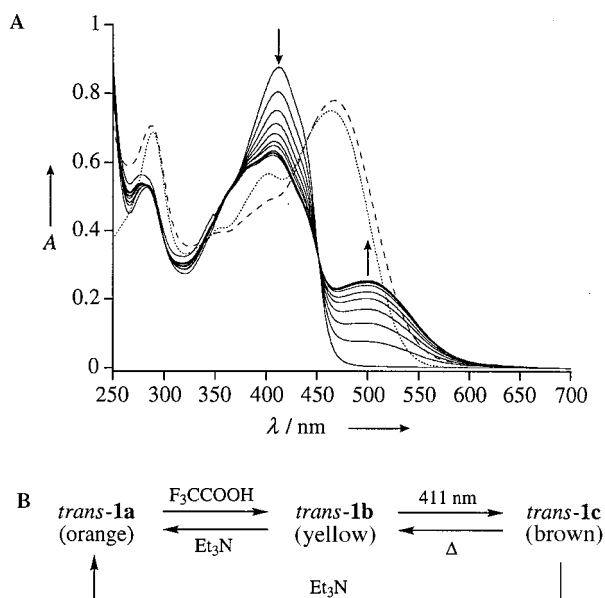


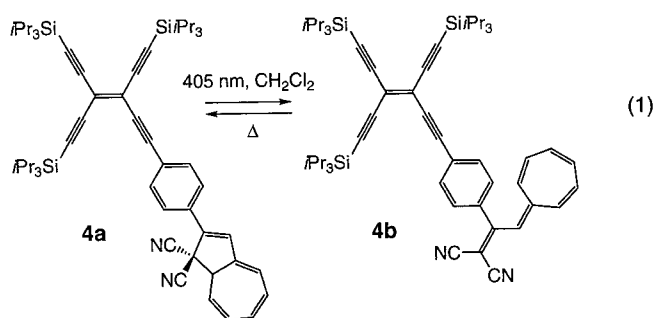
Figure 4. A) Electronic absorption spectra for the *trans*-**1a** \rightarrow *trans*-**1b** \rightarrow *trans*-**1c** \rightarrow *trans*-**1a** switching cycle (B) in CH_2Cl_2 ($c = 1.70 \times 10^{-5} \text{ M}$) at 25 °C. The dotted line corresponds to the initial starting material *trans*-**1a**. The solid lines show the conversion of *trans*-**1b** to *trans*-**1c**, recorded at 1 min intervals during irradiation at $\lambda = 411 \text{ nm}$. The dashed line shows the spectrum of *trans*-**1a** recovered after deprotonation with Et_3N .

irradiated at 411 nm at -50°C , conversion of the DHA-containing starting compound into VHF-containing *trans*-**1c** was observed by ^1H NMR spectroscopy. The VHF-containing compounds **1c** (*trans* or *cis*) readily undergo thermal electrocyclicization back to **1b** ($k_{25^\circ\text{C}} = 7.37 \pm 0.02 \times 10^{-4} \text{ s}^{-1}$, $t_{1/2} = 15.7 \text{ min}$);^[15] therefore, mixtures of **1b** and **1c** were always observed even after long irradiation times at room temperature. The ratio of the DHA and VHF isomers at equilibrium proved to be strongly dependent on the experimental

conditions; in the NMR experiment the final ratio of *trans*-**1c** to *trans*-**1b** was approximately 90:10.

The clean interconversion of *trans*-**1b** and *trans*-**1c** during irradiation at 411 nm, without any isomerization to the *cis* forms, was also evidenced by several isosbestic points in the UV/Vis spectrum (Figure 4). At other wavelengths *trans* \rightarrow *cis* isomerization also occurred.

The switching process of a TEE-linked DHA group into a VHF group was also studied for compound **4** [Equation (1)], in which *trans* \rightarrow *cis* isomerization leads to the same compound. The UV/Vis spectra are very similar and show an absorption



maximum at 405 nm for the DHA-containing **4a** and at 481 nm for the VHF derivative **4b**. However, the thermal electrocyclicization back to **4a** is much slower than in the case of the reaction **1c** \rightarrow **1b** ($k_{25^\circ\text{C}} = 3.917 \pm 0.007 \times 10^{-5} \text{ s}^{-1}$, $t_{1/2} = 4.9 \text{ h}$).^[15]

Treatment of **1c** (a mixture of *cis* and *trans* isomers) with Et_3N causes deprotonation of the amino group and leads directly to the formation of the DHA-containing compound **1a**, as observed by UV/Vis, ^1H and ^{13}C NMR spectroscopy. The VHF-containing donor–acceptor system^[16] **1d** could not be obtained either by deprotonation of **1c**—even at -40°C —or by irradiation of the DMA derivative **1a** at -80°C . These results are attributed to a very fast thermal electrocyclicization of **1d** to **1a**. This seems to indicate that photoinduced electron transfer (PET) or electronic energy transfer (EET) processes that involve the unprotonated DMA group are not responsible for the quenching of the photo-retrocyclization from **1a** to **1b**. These kind of processes have been widely used to construct photoionically-driven fluorescent sensors and switches.^[17]

When a solution of pure *trans*-**1a** in CH_2Cl_2 was treated with CF_3COOH , then irradiated at 411 nm, and finally treated with Et_3N in the dark, only *trans*-**1a** was recovered as shown by UV/Vis (Figure 4) and ^{13}C NMR spectral analysis; no trace of diastereoisomeric *cis*-**1a** could be detected. The reversible conversion of *trans*-**1a** into *trans*-**1b** and then into *trans*-**1c** can be described as an AND logic gate.^[18] The *trans*-**1c** state can only be obtained when both protons and light are present; that is two “inputs” are necessary to generate one “output”. Nondestructive readout of this AND logic gate is ensured by monitoring the appearance of the absorption band of *trans*-**1c** at $\lambda_{\text{max}} = 500 \text{ nm}$ (Figure 4). In contrast, the same cycle, which starts from pure *cis*-**1a**, leads to the recovery of an isomeric mixture that contains mainly the *trans* form. Thus the conversion *cis*-**1a** \rightarrow *cis*-**1b** \rightarrow *cis*-**1c** is not suited for an AND logic gate, as *cis* \rightarrow *trans* isomerization also occurs.

In addition to the described AND logic gate three write/erase processes are present in system **1**, which are not affected by side reactions to other states on the cubic switching diagram if appropriate conditions are used: the reversible *cis*–*trans* photoisomerization between *trans*-**1a** and *cis*-**1a**, and the reversible protonations/deprotonations of the couples *trans*-**1a**/*cis*-**1a** and *trans*-**1b**/*cis*-**1b**. Since the fluorescence enhancement after deprotonation of **1b** amounts to a factor of about 300,^[19] a very efficient nondestructive readout of information for the *cis*-**1a**/**b** and *trans*-**1a**/**b** couples is available by using excitation light of 396 nm for the *cis* and of 464 nm for the *trans* isomer.

The switching system discussed here represents a first step towards multifunctional molecular devices where the performed operation is dependent upon the stimulus that is chosen. The challenge now lies in further development of this system so that it can perform logic operations at a macroscopic level, and thus possess real-life applications.

Received: October 20, 1998 [Z.125441E]
German version: *Angew. Chem.* **1999**, *111*, 740–743

Keywords: fluorescence spectroscopy • molecular devices • optical memory • photochromism • tetraethynylethenes

- [1] For an overview of switchable molecular devices, see a) J.-M. Lehn, *Supramolecular Chemistry*, VCH, Weinheim, **1995**, pp. 124–138; b) M. Ward, *Chem. Ind.* **1997**, 16, 640–645; c) V. Balzani, M. Gómez-López, J. F. Stoddart, *Acc. Chem. Res.* **1998**, *31*, 405–414.
- [2] a) V. Balzani, F. Scandola in *Comprehensive Supramolecular Chemistry*, Vol. 5 (Ed.: D. N. Reinhoudt), Pergamon-Elsevier, Oxford, **1996**, pp. 687–746; b) B. L. Feringa, W. F. Jager, B. de Lange, *Tetrahedron* **1993**, *49*, 8267–8310; c) H. Dürr, *Angew. Chem.* **1989**, *101*, 427–445; *Angew. Chem. Int. Ed. Engl.* **1989**, *28*, 413–431.
- [3] For another example of such a system, see J. Achatz, C. Fischer, J. Salbeck, J. Daub, *J. Chem. Soc. Chem. Commun.* **1991**, 504–507.
- [4] R. R. Tykwinski, F. Diederich, *Liebigs Ann.* **1997**, 649–661.
- [5] R. E. Martin, J. Bartek, F. Diederich, R. R. Tykwinski, E. C. Meister, A. Hilger, H. P. Lüthi, *J. Chem. Soc. Perkin Trans. 2* **1998**, 233–241.
- [6] a) J. Daub, T. Knöchel, A. Mannschreck, *Angew. Chem.* **1984**, *96*, 980–981; *Angew. Chem. Int. Ed. Engl.* **1984**, *23*, 960–961; b) J. Daub, S. Gierisch, U. Klement, T. Knöchel, G. Maas, U. Seitz, *Chem. Ber.* **1986**, *119*, 2631–2646; c) S. Gierisch, J. Daub, *Chem. Ber.* **1989**, *122*, 69–75.
- [7] K. Sonogashira in *Metal-catalyzed Cross-coupling Reactions* (Eds.: F. Diederich, P. J. Stang), WILEY-VCH, Weinheim, **1998**, pp. 203–269.
- [8] R. R. Tykwinski, M. Schreiber, R. Pérez Carlón, F. Diederich, *Helv. Chim. Acta* **1996**, *79*, 2249–2281.
- [9] The photoresponsive dihydroazulene **3** was synthesized according to published methods.^[6c] All new compounds were fully characterized by UV/Vis, fluorescence, IR, ¹H, and ¹³C NMR spectroscopy, FAB-MS, and elemental analysis.
- [10] X-ray crystal structure of *trans*-**1a**; C₅₄H₆₃N₃Si₂ *M_r* = 810.25; triclinic, space group *P* $\bar{1}$ (no. 2), ρ_{calcd} = 1.095 g cm^{−3}, *Z* = 2, *a* = 8.661(4), *b* = 13.259(6), *c* = 22.456(7) Å, α = 94.31(3), β = 93.48(4), γ = 106.36(3)°, *V* = 2458(2) Å³, *T* = 200 K, Nonius CAD4 diffractometer, λ (CuK α) = 1.5418 Å. Single crystals were obtained by slow evaporation of a MeOH solution. The structure was solved by direct methods (*SHELXS-86*) and refined by full-matrix least-squares analysis (*SHELXL-93*), by using an isotropic extinction correction and $w = 1/[\sigma^2(F_o^2) + (0.0999P)^2 + 3.2032P]$, where $P = (F_o^2 + 2F_c^2)/3$. The iPr₃Si groups at Si2 as well as the five- and the seven-membered rings are statically disordered. The disorder within these rings could be resolved for the atoms C13, C22, and C23, that is, two peaks could be located in a difference map and refined isotropically with population parameters of ca. 0.63 and 0.37, respectively. All other heavy atoms were refined

anisotropically (H-atoms isotropic, whereby H positions are based on stereochemical considerations). Final *R*(*F*) = 0.058, *wR*(*F*²) = 0.16 for 566 parameters and 3377 reflections with *I* > 2σ(*I*) and θ < 50°. The disordered seven-membered ring, based on one set of atomic positions, is nearly planar. However, by refining partial atoms as mentioned above, two different conformations are obtained. The one shown in Figure 1 (based on a population parameter of 0.63) is approximately boat shaped, whereas the other (based on a population parameter of 0.37) is less clear. Crystallographic data (without structure factors) for the structure reported in this paper have been deposited with the Cambridge Crystallographic Data Centre as supplementary publication no CCDC-102924. Copies of the data can be obtained free of charge on application to CCDC, 12 Union Road, Cambridge CB2 1EZ (fax: (+44) 1223-336-033; e-mail: deposit@ccdc.cam.ac.uk).

- [11] The quantum yields for both photochemical *cis* → *trans* and *trans* → *cis* isomerization reactions have been determined as described in the literature^[5, 12] from data obtained by following the emission and absorption spectra as a function of the irradiation time. For the isomerization (a) the rate constants *k*_{*c*→*t*} and *k*_{*t*→*c*} were calculated from the overall rate constant *k* [Eq. (b)] and the photoequilibrium constant *K*_{eq} [Eq. (c)]



$$k = k_{t \rightarrow c} + k_{c \rightarrow t} \quad (\text{b})$$

$$K_{\text{eq}} = \frac{k_{c \rightarrow t}}{k_{t \rightarrow c}} = \frac{C_t^{\text{eq}}}{C_c^{\text{eq}}} \quad (\text{c})$$

*K*_{eq} was determined starting from the UV/Vis spectra. *k* for the reaction from *trans* to *cis* was calculated from the electronic absorption spectra from an exponential fit^[12] at the wavelengths of 375, 396, 450, 464 nm [Eq. (d)] where *l* is the length of the cell. *k* for the reaction from *cis* to *trans* was determined from a simple exponential fit of the data of the electronic emission spectra at λ_{em} = 606 nm [Eq. (e)]; the first three curves in Figure 3 for the reaction *cis*-**1a** → *trans*-**1a** were used]. The emission quantum yields are given by Equations (f) and (g).

$$\frac{A_\lambda(t)}{l} = \epsilon_t C_t^{\text{eq}} + \epsilon_c C_c^{\text{eq}} + (\epsilon_t - \epsilon_c) C_c^{\text{eq}} e^{-kt} \quad (\text{d})$$

$$I_\lambda(t) = I_\infty + (I_0 - I_\infty) e^{[k(t_0 - t)]} \quad (\text{e})$$

$$\Phi_{c \rightarrow t} = \frac{k_{c \rightarrow t}}{1000 I_0 [(1 - 10^{-A_\lambda^{\text{eq}}}) / A_\lambda^{\text{eq}}] \epsilon_c} \quad (\text{f})$$

$$\Phi_{t \rightarrow c} = \frac{k_{t \rightarrow c}}{1000 I_0 [(1 - 10^{-A_\lambda^{\text{eq}}}) / A_\lambda^{\text{eq}}] \epsilon_t} \quad (\text{g})$$

The light intensity *I*₀ was determined by the actinometric ferrioxalate method.^[13] An absolute error of about 10% is claimed for the quantum yields.

- [12] J. Polster, *Reaktionskinetische Auswertung spektroskopischer Messdaten*, Vieweg, Braunschweig, **1995**.
- [13] a) C. G. Hatchard, C. A. Parker, *Proc. R. Soc. London A* **1956**, 235, 518–536; b) A. M. Braun, M.-T. Maurette, E. Oliveros, *Photochemical Technology*, Wiley, Chichester, **1991**, pp. 70–106.
- [14] a) M. Irie, O. Miyatake, K. Uchida, *J. Am. Chem. Soc.* **1992**, *114*, 8715–8716; b) M. Hanazawa, R. Sumiya, Y. Horikawa, M. Irie, *J. Chem. Soc. Chem. Commun.* **1992**, 206–207; c) S. L. Gilat, S. H. Kwai, J.-M. Lehn, *Chem. Eur. J.* **1995**, *1*, 275–284; d) S. W. Kwai, S. L. Gilat, R. P. Ponsinet, J.-M. Lehn, *Chem. Eur. J.* **1995**, *1*, 285–293.
- [15] The rate constant for the thermal electrocyclization was determined by an exponential fit of the data obtained by following the decrease in intensity of the absorption band at 500 nm (*trans*-**1c**) and at 481 nm (**4b**) at 25 °C in the dark.
- [16] For donor–acceptor substituted TEEs and their nonlinear optical properties, see R. R. Tykwinski, U. Gubler, R. E. Martin, F. Diederich, C. Bosshard, P. Günter, *J. Phys. Chem. B* **1998**, *102*, 4451–4465.
- [17] a) A. P. de Silva, H. Q. N. Gunaratne, J. Gunlaugsson, A. J. M. Huxley, C. P. McCoy, J. T. Rademacher, T. E. Rice, *Chem. Rev.* **1997**,

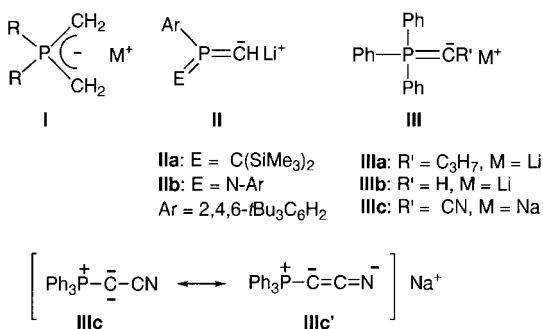
- 97, 1515–1566; b) A. P. de Silva, H. Q. N. Gunaratne, C. P. McCoy, *Nature (London)* **1993**, 364, 42–44; c) R. A. Bissell, A. P. de Silva, H. Q. N. Gunaratne, P. L. M. Lynch, G. E. M. Maguire, K. R. A. S. Sandanayake, *Chem. Soc. Rev.* **1992**, 21, 187–195; d) L. Fabrizzi, M. Licchelli, P. Pallavicini, L. Parodi, *Angew. Chem.* **1998**, 110, 838–841; *Angew. Chem. Int. Ed. Engl.* **1998**, 37, 800–802.
- [18] a) A. P. de Silva, C. P. McCoy, *Chem. Ind.* **1994**, 992–996; b) L. F. Lindoy, *Nature (London)* **1993**, 364, 17–18; c) A. Aviram, *J. Am. Chem. Soc.* **1988**, 110, 5687–5692.
- [19] For systems with large fluorescence enhancement factors, see a) M. E. Huston, K. W. Heider, A. W. Czarnik, *J. Am. Chem. Soc.* **1988**, 110, 4460–4462; b) R. A. Bissell, E. Calle, A. P. de Silva, H. Q. N. Gunaratne, J.-L. Habib-Jiwan, S. L. A. Peiris, R. A. D. D. Rupasinghe, T. K. S. D. Samarasinghe, K. R. A. S. Sandanayake, J.-P. Soumillion, *J. Chem. Soc. Perkin Trans. 2* **1992**, 1559–1564.

Synthetic Utility of Stable Phosphanylcarbenes: Synthesis and Crystal Structure of an α -(Lithiomethylene)phosphorane**

St  phanie Goumri-Magnet, Heinz Gornitzka, Antoine Baceiredo, and Guy Bertrand*

Dedicated to Professor Edgar Niecke on the occasion of his 60th birthday

Alkali metal phosphonium diylides **I** are well-characterized compounds and their properties and molecular structures have been thoroughly investigated.^[1] In contrast, the phosphonium ylides **II** and **III**, which formally feature a dicarbanion center, have been poorly studied (Scheme 1). Niecke et al.^[2] concluded that the stability of the lithium



Scheme 1.

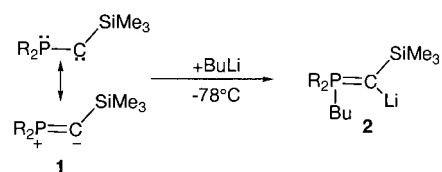
phosphoranylidene ylides **IIa, b** was due to the incorporation of the metalated carbon atom into the heteroallylic π -electron system. The first synthesis of an α -(lithiomethylene)phosphorane (**IIIa**) was proposed by Schlosser et al.^[3] and was based on the reaction of pentaphenylphosphorane with excess

[*] Dr. G. Bertrand, S. Goumri-Magnet, Dr. H. Gornitzka, Dr. A. Baceiredo
Laboratoire de Chimie de Coordination du CNRS
205 route de Narbonne, F-31077 Toulouse cedex (France)
Fax: (+33) 5-61-55-30-03
E-mail: gbertran@lcc-toul.lcc-toulouse.fr

[**] This work was supported by the CNRS. H. G. thanks the Alexander von Humboldt Foundation for a postdoctoral fellowship.

n-butyllithium. Later, Corey et al.^[4] showed that the phosphonium ylide **IIIb** can be prepared at low temperature by direct lithiation of the corresponding ylide, and underwent Wittig reactions even with sterically hindered ketones. The (sodiocyanomethylene)phosphorane **IIIc**^[5] is the only α -(metallomethylene)phosphorane, which has been isolated so far. However, from IR and NMR data, Bestmann et al.^[5] showed that the resonance structure **IIIc'** strongly contributed to the electron distribution in **IIIc** and, therefore, this compound can hardly be considered as a phosphonium ylide. The instability of derivatives **III** and the difficulties associated with the metalation of the starting phosphonium ylides hampered their promising synthetic application.^[6] Here, we propose a new strategy for the one-step synthesis of α -(lithiomethylene)phosphoranes of type **III**, as well as the first single-crystal X-ray diffraction study of such a highly reactive compound.

We have already shown that the stable phosphanyl(silyl)-carbene **1** undergoes formal 1,2-addition reactions with protic reagents (MeOH, Me₂NH, etc.)^[7] as well as with Lewis acids (MeOB(OMe)₂, MeGaMe₂, etc.)^[8] giving rise to the corresponding phosphorus ylides. Thus, we investigated the reaction of **1** with alkyl lithium reagents, in the hope of obtaining the corresponding 1,2-adduct, namely the lithium phosphonium ylide **2** (Scheme 2). Indeed, according to ³¹P NMR



Scheme 2. R = *c*Hex₂N.

spectroscopic results, addition of one equivalent of *n*BuLi (1.6M in hexane) to a solution of carbene **1**^[8b] in pentane at –78 °C instantaneously and quantitatively led to the desired adduct **2**. On warming to room temperature and partial evaporation of the solvent, two equivalents of THF were added. From this solution single crystals, suitable for an X-ray diffraction study,^[9] were obtained at –20 °C. The molecular structure of **2** is shown in Figure 1. In the solid state, **2** is monomeric and features a trigonal-planar coordinated lithium atom (sum of the angles: 359.9°), which is complexed by two molecules of THF. The geometry around the ylidic carbon atom is also planar (sum of the angles: 359.8°), whereas in nonstabilized ylides it is slightly pyramidalized.^[10] The P–C bond length (1.636 Å) is one of the shortest known for a P–C(ylide) bond;^[10a] the Si–C1 bond length is also very short (1.775 Å compared to 1.87–1.91 Å for Si–CH₃), which emphasizes the stabilizing effect of the negative charge by the silyl group.^[11] Significantly, the C–Li bond almost eclipses the P–C(Bu) bond (Li–C1–P–C29 dihedral angle: 17.4(1.0)°). All structural data are in agreement with the results of ab initio calculations^[12] which also predicted that the deprotonation of H₃P=CH₂ to give H₃P=CHLi would induce a rotation about the P–C bond, causing the C–Li bond to eclipse one of the P–H bonds.

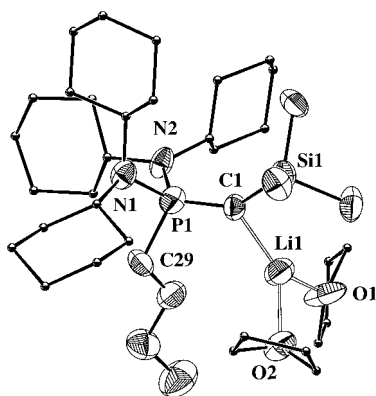
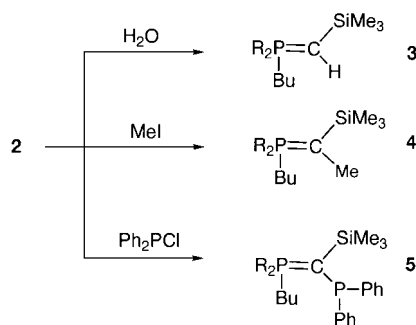


Figure 1. Molecular structure of **2**. Selected bond lengths [Å] and angles [°]: C1–P1 1.636(11), C1–Si1 1.775(10), C1–Li1 2.06(2), P1–N1 1.736(8), P1–N2 1.740(8), P1–C29 1.871(10); P1–C1–Si1 139.0(7), P1–C1–Li1 123.7(8), Si1–C1–Li1 97.1(8), C1–P1–N1 124.2(5), C1–P1–N2 115.7(5), N1–P1–N2 99.9(4), C1–P1–C29 112.6(5), N1–P1–C29 100.5(5), N2–P1–C29 100.4(5).

The ^{31}P NMR spectrum of compound **2** at room temperature showed one broad signal at $\delta = +41$ which, on cooling the sample to -70°C , was resolved into two new signals at $\delta = +47$ and $+32$ (6/4 ratio; coalescence temperature of about -30°C). This is in agreement with the presence of two rotamers of **2** at low temperature. The magnitude of the free energy of activation (35.4 kJ mol^{-1}) is of the order found for a restricted rotation about the P–C bond in phosphonium ylides.^[11] Even at -70°C , only one broad signal was observed at $\delta = +3.9$ in the ^6Li NMR spectrum recorded with a ^6Li -doped sample of **2**. However, selective ^{31}P irradiation experiments showed that the ^6Li signals corresponding to the two rotamers overlapped, and we estimate the $^2J_{\text{PLi}}$ coupling constants to be 1 Hz.

Compound **2** is highly moisture sensitive and is easily transformed into the corresponding phosphonium ylide **3**. It also reacts at low temperature with electrophiles such as methyl iodide and chlorodiphenylphosphane to give the corresponding ylides **4** and **5**, respectively (Scheme 3).



Scheme 3. R = cHex₂N.

Experimental Section

1: In a typical experiment, a solution of the corresponding phosphanyl-(silyl)diazomethane^[8b] (0.1 g, 0.2 mmol) in pentane (1 mL) was irradiated (300 nm) for 8 h. According to ^{31}P NMR spectroscopy the reaction was quantitative and phosphanyl(silyl)carbene **1** was used without any further purification.

3: Yellow oil (0.09 g, 94% yield); $^{31}\text{P}\{^1\text{H}\}$ NMR (C_6D_6): $\delta = 63.5$; $^{13}\text{C}\{^1\text{H}\}$ NMR (C_6D_6): $\delta = 5.3$ (d, $^3J(\text{P,C}) = 3.7\text{ Hz}$, CH_3Si), 8.0 (d, $^1J(\text{P,C}) = 125.7\text{ Hz}$, P=C), 14.6 (s, $\text{P}(\text{CH}_2)_3\text{CH}_3$), 25.2 (d, $^3J(\text{P,C}) = 18.5\text{ Hz}$, $\text{P}(\text{CH}_2)_2\text{CH}_2$), 26.8 (s, NCCCC), 28.1 and 28.3 (s, NCCC), 31.0 (d, $^1J(\text{P,C}) = 87.2\text{ Hz}$, PCH₂), 35.6 and 36.4 (s, NCC), 56.8 (d, $^2J(\text{P,C}) = 5.0\text{ Hz}$, NC); elemental analysis (%) calcd for $\text{C}_{32}\text{H}_{63}\text{N}_2\text{SiP}$: C 71.85; H 11.87; N 5.24; found: C 72.25; H 12.07; N 5.04.

4: Yellow oil (0.09 g, 92% yield); $^{31}\text{P}\{^1\text{H}\}$ NMR (C_6D_6): $\delta = 69.7$; $^{13}\text{C}\{^1\text{H}\}$ NMR (C_6D_6): $\delta = 3.5$ (d, $^3J(\text{P,C}) = 2.6\text{ Hz}$, CH_3Si), 9.2 (d, $^1J(\text{P,C}) = 127.6\text{ Hz}$, P=C), 14.6 (s, $\text{P}(\text{CH}_2)_3\text{CH}_3$), 16.2 (d, $^2J(\text{P,C}) = 1.8\text{ Hz}$, =CCH₃), 25.7 (d, $^3J(\text{P,C}) = 16.2\text{ Hz}$, $\text{P}(\text{CH}_2)_2\text{CH}_2$), 27.1 (s, NCCCC), 27.7 (d, $^2J(\text{P,C}) = 4.1\text{ Hz}$, PCH₂CH₂), 28.5 and 28.6 (s, NCCC), 33.1 (d, $^1J(\text{P,C}) = 84.1\text{ Hz}$, PCH₂), 36.9 (d, $^3J(\text{P,C}) = 3.8\text{ Hz}$, NCC), 37.3 (d, $^3J(\text{P,C}) = 1.0\text{ Hz}$, NCC), 57.2 (d, $^2J(\text{P,C}) = 5.5\text{ Hz}$, NC); elemental analysis (%) calcd for $\text{C}_{33}\text{H}_{65}\text{N}_2\text{SiP}$: C 72.20; H 11.93; N 5.10; found: C 71.95; H 11.65; N 5.24.

5: White crystals (0.12 g, 93% yield); m.p. $185\text{--}186^\circ\text{C}$; $^{31}\text{P}\{^1\text{H}\}$ NMR (C_6D_6): $\delta = 88.6$ [d, $^2J(\text{P,P}) = 183.5\text{ Hz}$, ($\text{R}_2\text{N})_2\text{P}$], 5.3 (d, Ph_2P); $^{13}\text{C}\{^1\text{H}\}$ NMR (C_6D_6): $\delta = 5.7$ (d, $^3J_{\text{PC}} = 2.9\text{ Hz}$, CH_3Si), 12.0 (dd, $^1J(\text{P,C}) = 105.0$ and 21.9 Hz , P=C), 15.8 (s, $\text{P}(\text{CH}_2)_3\text{CH}_3$), 26.6 and 26.8 (s, NCCCC), 27.5, 27.7, 27.8 and 28.1 (s, NCCC), 28.9 (d, $^3J(\text{P,C}) = 24.7\text{ Hz}$, $\text{P}(\text{CH}_2)_2\text{CH}_2$), 35.6 (d, $^3J(\text{P,C}) = 6.2\text{ Hz}$, NCC), 36.2 (d, $^3J(\text{P,C}) = 6.9\text{ Hz}$, NCC), 36.7 and 37.2 (s, NCC), 38.0 (d, $^1J(\text{P,C}) = 93.1\text{ Hz}$, PCH₂), 57.0 (d, $^2J(\text{P,C}) = 4.1\text{ Hz}$, NC), 57.3 (d, $^2J(\text{P,C}) = 8.0\text{ Hz}$, NC), 126.8 (s, C_p), 133.9 (d, $^2J(\text{P,C}) = 18.9\text{ Hz}$, C_q), 137.8 (s, C_m), 145.9 (dd, $^1J(\text{P,C})$ or $^3J(\text{P,C}) = 12.2$ and 8.8 Hz , C_i); elemental analysis (%) calcd for $\text{C}_{44}\text{H}_{72}\text{N}_2\text{SiP}_2$: C 73.49; H 10.09; N 3.90; found: C 73.60; H 10.18; N 4.05.

Received: September 23, 1998 [Z12449IE]

German version: *Angew. Chem.* **1999**, *111*, 710–712

Keywords: carbenes • lithium • phosphorus ylides

- [1] H.-J. Cristau, *Chem. Rev.* **1994**, *94*, 1299–1313.
- [2] T. Baumgartner, B. Schinkels, D. Gudat, M. Nieger, E. Niecke, *J. Am. Chem. Soc.* **1997**, *119*, 12410–12411.
- [3] M. Schlosser, T. Kadibelban, G. Steinhoff, *Angew. Chem.* **1966**, *78*, 1018; *Angew. Chem. Int. Ed. Engl.* **1966**, *5*, 968–969.
- [4] a) E. J. Corey, J. Kang, *J. Am. Chem. Soc.* **1982**, *104*, 4724–4725; b) E. J. Corey, J. Kang, K. Kyler, *Tetrahedron Lett.* **1985**, *26*, 555–558.
- [5] H. J. Bestmann, M. Schmidt, *Angew. Chem.* **1987**, *99*, 64–65; *Angew. Chem. Int. Ed. Engl.* **1987**, *26*, 79–81.
- [6] a) B. Schaub, T. Jenny, M. Schlosser, *Tetrahedron Lett.* **1984**, *25*, 4097–4100; b) B. Schaub, M. Schlosser, *Tetrahedron Lett.* **1985**, *26*, 1623–1626; c) O. I. Kolodiazny, *Russ. Chem. Rev.* **1997**, *66*, 225–254.
- [7] A. Igau, H. Grützmacher, A. Baceiredo, G. Bertrand, *J. Am. Chem. Soc.* **1988**, *110*, 6463–6466.
- [8] a) K. Horchler von Locquenghien, A. Baceiredo, R. Boese, G. Bertrand, *J. Am. Chem. Soc.* **1991**, *113*, 5062–5063; b) G. Alcaraz, R. Reed, A. Baceiredo, G. Bertrand, *J. Chem. Soc. Chem. Commun.* **1993**, 1354–1355; c) A. H. Cowley, F. P. Gabbaï, C. J. Carrano, L. M. Mokry, M. R. Bond, G. Bertrand, *Angew. Chem.* **1994**, *106*, 584–586; *Angew. Chem. Int. Ed. Engl.* **1994**, *33*, 578–580.
- [9] Crystal data for **2**: $\text{C}_{40}\text{H}_{78}\text{LiN}_2\text{O}_2\text{PSi}$, $M_r = 685.04$, triclinic, space group $P\bar{1}$, $a = 10.789(2)$, $b = 13.336(3)$, $c = 15.667(3)\text{ Å}$, $\alpha = 88.88(2)$, $\beta = 89.79(2)$, $\gamma = 69.95(2)^\circ$, $V = 2117.2(7)\text{ Å}^3$, $Z = 2$, $\rho_{\text{calcd}} = 1.075\text{ Mg m}^{-3}$, $F(000) = 760$, $\lambda = 0.71073\text{ Å}$, $T = 173(2)\text{ K}$, $\mu(\text{MoK}\alpha) = 0.126\text{ mm}^{-1}$. Data were collected on a STOE-IPDS diffractometer using an oil-coated, rapidly cooled crystal of dimensions $(0.3 \times 0.2 \times 0.05\text{ mm})$ by the φ -scan method ($4^\circ \leq 2\theta \leq 43^\circ$). Of a total of 17411 collected reflections, 4506 were independent ($R_{\text{int}} = 0.2344$) and were used to refine 518 parameters by using 288 distance and ADP restraints, maximum and minimum of the final difference Fourier synthesis: 257 and -334 e nm^{-3} , $R1(F > 2\sigma(F)) = 0.0704$ and $wR2 = 0.2353$ (all data) with $R1 = \sum ||F_o - F_c|/ \sum |F_o|$ and $wR2 = [\sum w(F_o^2 - F_c^2)^2 / \sum w(F_o^2)^2]^{0.5}$. The structure was solved by direct methods (SHELXS-97)^[13] and refined by full-matrix least-squares procedures on F^2 (SHELXL-97).^[14] The hydrogen atom positions were geometrically idealized and refined by using a riding model. Crystallographic data (excluding structure factors) for the structures reported in this

paper have been deposited with the Cambridge Crystallographic Data Center as supplementary publication no. CCDC-103076. Copies of the data can be obtained free of charge on application to CCDC, 12 Union Road, Cambridge CB21EZ, UK (fax: (+44) 1223-336-033; e-mail: deposit@ccdc.cam.ac.uk).

- [10] a) A. W. Johnson in *Ylides and imines of phosphorus* (Ed.: A. W. Johnson), Wiley-Interscience, New York, **1993**; b) S. M. Bachrach, *J. Org. Chem.* **1992**, 57, 4367–4373.
- [11] a) P. von R. Schleyer, T. Clark, A. J. Kos, G. W. Spitznagel, C. Rohde, D. Arad, K. N. Houk, N. G. Rondan, *J. Am. Chem. Soc.* **1984**, 106, 6467–6475; b) B. Römer, G. G. Gater, M. Zhong, J. I. Brauman, *J. Am. Chem. Soc.* **1998**, 120, 2919–2924.
- [12] a) R. S. McDowell, A. Streitwieser, Jr., *J. Am. Chem. Soc.* **1984**, 106, 4047–4048; b) H. J. Bestmann, A. J. Kos, K. Witzgall, P. von R. Schleyer, *Chem. Ber.* **1986**, 119, 1331–1349.
- [13] G. M. Sheldrick, *Acta Crystallogr. Sect. A* **1990**, 46, 467–473.
- [14] SHELXL; Program for Crystal Structure Refinement; G. M. Sheldrick; University of Göttingen **1997**.

Opposite Orientation of Backbone Inclination in Pyranosyl-RNA and Homo-DNA Correlates with Opposite Directionality of Duplex Properties**

Ronald Micura, Rene Kudick, Stefan Pitsch, and Albert Eschenmoser*

In preceding publications on pyranosyl-RNA (“p-RNA”)^[1a–f] we have emphasized the special importance of interstrand (as opposed to intrastrand) base stacking for the properties of this oligonucleotide base pairing system. Among the properties concerned are the sequence dependence of p-RNA duplex stability,^[1a,e,f] the regioselectivity of the influence of dangling bases on duplex stability,^[1d] and the sequence dependence of the efficiency and selectivity of template-controlled ligation reactions in replication^[1f] and autocatalytic oligomerization.^[1e] The dominance of interstrand over intra-strand base stacking in this pairing system is a consequence of the pronounced inclination between the (approximated) backbone axes relative to the axes of Watson–Crick base pairs in p-RNA duplexes. The orientation and approximate degree of this inclination can be easily inferred from a p-RNA strand’s (idealized) pairing conformation (Figure 1 a, b). This

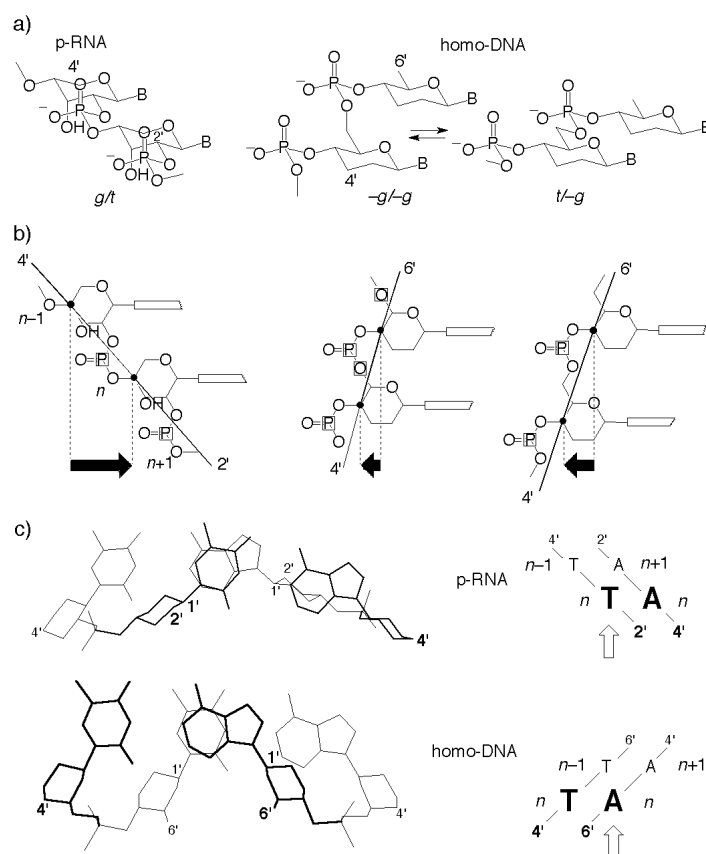


Figure 1. a) Idealized pairing conformations of p-RNA^[1a,c] and homo-DNA.^[2a,c,d] b) Projections of pairing conformations along an axis perpendicular to the mean planes of pyranose chairs, indicating sense and approximate degree of backbone inclination; nucleosidic torsion angle $\sim 120^\circ$. c) Projections perpendicular to the plane of a selected base pair of the p-RNA duplex [pr(CGAATTCC)]₂^[1c] and the homo-DNA duplex [ddGlc(A₅T₅)₂]^[2d] showing upstream interstrand stacking between a pyrimidine and a purine in p-RNA and corresponding downstream interstrand stacking in homo-DNA (taken from references [1c] and [2d]).

conformation has been derived by conformational analysis on the basis of steric repulsion criteria^[1a] and confirmed in a NMR structure determination of the p-RNA duplex [pr(CGAATTCC)]₂^[1c]. In accordance with this analysis, molecular mechanics based modeling of the same duplex shows^[1c] that interstrand base stacking is expected to be effective between purines and purines as well as between purines and pyrimidines, but not between pyrimidines and pyrimidines (Figure 1 c).

The previously studied homo-DNA^[2] is another pairing system with a pronounced backbone inclination. Compared to p-RNA, however, the inclination in homo-DNA is of opposite orientation, as can be deduced from homo-DNA’s two (idealized) pairing conformations^[2a,c] (Figure 1 a, b). The NMR structure analysis of the homo-DNA duplex [ddGlc(A₅T₅)₂] by Otting et al.^[2d] indicates that in at least one of the two pairing conformations, namely *t/g*, interstrand base stacking should dominate over intrastrand stacking to the same extent as it does in p-RNA (Figure 1 c). Whereas in p-RNA interstrand stacking acts in the upstream direction (base *n* stacks with base *n* + 1 of the complementary strand), in homo-DNA it does so in the downstream direction

[*] Prof. Dr. A. Eschenmoser, Dr. R. Micura, Dr. R. Kudick, Dr. S. Pitsch
Laboratorium für Organische Chemie der
Eidgenössischen Technischen Hochschule
Universitätsstrasse 16, CH-8092 Zürich (Switzerland)
Fax: (+41) 1-632-1043
and
The Skaggs Institute for Chemical Biology at The Scripps Research
Institute
10550 North Torrey Pines Road, La Jolla, CA, 92037 (USA)

[**] Chemistry of Pyranosyl-RNA, Part 8. Chemistry of α -Aminonitriles, Part 24. This work was supported by the Ciba-Geigy AG, Basel, and the Schulleitung of the ETH Zürich, as well as the Skaggs Foundation, La Jolla, CA. We thank Dr. H.-V. Hoppe, Dr. N. Windhab, and Dr. C. Miculka, previously Hoechst AG, Frankfurt, for providing us with p-RNA starting materials. R. M. thanks the Austrian Science Fund for a Schrödinger fellowship. Parts 7 and 23: Ref. [1e].

(n stacks with $n - 1$, see Figure 1c). If the postulate is correct that interstrand base stacking is the determinant for the sequence dependence of p-RNA duplex properties, then the sequence dependence of the same type of duplex properties in the homo-DNA series should possess opposite directionality. Therefore, a comparison of relevant properties of selected p-RNA and homo-DNA duplexes offers an opportunity for testing the thesis of the predominant role of interstrand base stacking in oligonucleotide systems with large backbone inclination. With this in mind, we have prepared missing base sequences (particularly of the homo-DNA series) that were required for such a comparison. We find indeed that the sequence dependence of duplex stability in these two pairing systems is, without exception, of opposite directionality. Moreover, we observe the remarkable phenomenon of a quasi-enantiomorphism in the CD spectra of duplexes of a given base sequence in the two systems, even though the sense of chirality of the corresponding sugar units is in both systems the same.

Table 1 gives experimental data concerning the thermal and thermodynamic stabilities of the duplexes investigated, each consisting of antiparallel self-complementary strands. In the p-RNA series, the sequence motif $(py)_n - (PU)_n$ gives rise to higher duplex stability than the inverse motif $(PU)_n - (py)_n$; in the homo-DNA series, the opposite holds (No. 1–6). Analogous behavior is found for the alternating sequence motifs $(py - PU)_n$ and $(PU - py)_n$, provided the base sequences do not allow for frameshifting (No. 13 and 14).^[3] Dangling bases stabilize a duplex in the p-RNA series when located at the 2'-end (and not at the 4'-end);^[1d] again, the opposite is true for the homo-DNA system (No. 13–18). Figure 2 illustrates our working hypothesis for interpreting and predicting relative stabilities of isomeric duplexes based on the type and number of interstrand base stackings.^[4] The coherence observed in this comparison between prediction, based on a single discrim-

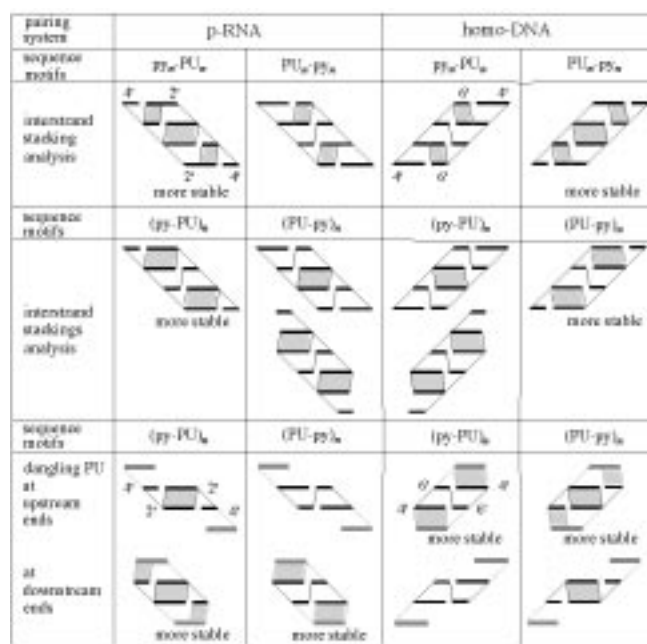


Figure 2. Formal analysis of the relationship between sequence motifs, positions of dangling bases and interstrand stacking in p-RNA and homo-DNA, and correlation with duplex stability. PU = purine, py = pyrimidine.

ination criterion, and experimental observations in the two different oligonucleotide systems with diametrically opposed sequence dependence of duplex stabilities leads us to propose that backbone inclination is a useful new parameter for correlating structure and properties in oligonucleotide systems.^[5]

p-RNA and homo-DNA duplexes with related base sequences show quasi-enantiomorphic CD spectra although the sense of chirality of their pento- and hexopyranosyl sugar units, respectively, is the same. An especially illustrative

Table 1. Melting temperatures T_m (in °C) and thermodynamic parameters (in kcal mol⁻¹) of p-RNA and homo-DNA duplexes.^[a-c]

No.	Self-complementary sequences	T_m	p-RNA duplexes			T_m	homo-DNA duplexes		
			$-\Delta G^0$	$-\Delta H^0$	$-T\Delta S_{25^\circ C}^0$		$-\Delta G^0$	$-\Delta H^0$	$-T\Delta S_{25^\circ C}^0$
1	TTTTAAAA	40	9.8	59.9	50.1	34	8.2	46.9	38.7
2	AAAATTTT	27	7.3	48.1	40.8	38	8.6	43.1	34.5
3	TTTTTAAAAA	54	12.8	67.6	54.8	45	10.3	55.1	44.8
4	AAAAATTTT	43	10.8	71.9	61.1	50	11.4	58.3	46.9
5	CCCGGG	68	13.0	48.5	35.5	49	9.7	39.8	30.1
6	GGGCCC	58	10.8	41.3	30.4	53	10.4	40.9	30.5
7	TATATATA	40	9.3	51.6	42.3	38	8.8	45.4	36.6
8	ATATATAT	38	9.2	58.7	49.5	39	8.7	41.0	32.3
9	ATATATA	38	9.1	54.2	45.1	34	8.0	45.5	37.5
10	TATATAT	29	7.4	43.6	36.2	25	6.8	30.9	24.2
11	CGCGCG	65	12.5	47.9	35.4	55	10.9	40.7	29.8
12	GCGCGC	62	11.3	40.5	29.2	53	10.9	42.7	31.8
13	TACGTA	39	8.7	40.9	32.2	27	7.0	33.6	26.6
14	ATGCAT	29	7.3	36.0	28.7	37	8.1	34.2	26.1
15	TACGTAG	46	10.3	53.1	42.8	23	6.9	34.0	27.1
16	GTACGTA	37	8.3	39.0	30.7	47	10.9	52.0	41.1
17	ATGCATG	51	10.9	51.0	40.1	32	8.0	32.8	24.8
18	GATGCAT	28	7.1	36.6	29.5	43	10.2	54.7	44.5

[a] T_m values refer to an oligomer concentration of 10 μ M, 150 mM NaCl, 10 mM Tris · HCl, pH 7.0; thermodynamic parameters determined from plots of T_m^{-1} vs. $\ln c$; for method see reference [9]; estimated error on $\Delta H^0 \pm 5\%$. [b] For preparation of p-RNA duplexes see reference [1a,b]; for preparation of homo DNA duplexes see reference [2b,e]. [c] p-RNA data of No. 1, 2, 8 from reference [1b,f], of No. 5, 6 from ref. [1f], of No. 11, 12 from reference [1b]; homo-DNA data:^[10] for No. 12 see also ref. [2c]. Tris = Tris(hydroxymethyl)aminomethane.

example is depicted in Figure 3 a, which shows the CD spectra of the self-complementary base sequences TACGTA and ATGCAT, comprising the sequence motifs (py-PU)₃ and (PU-py)₃. In both pairing systems, interstrand base stacking

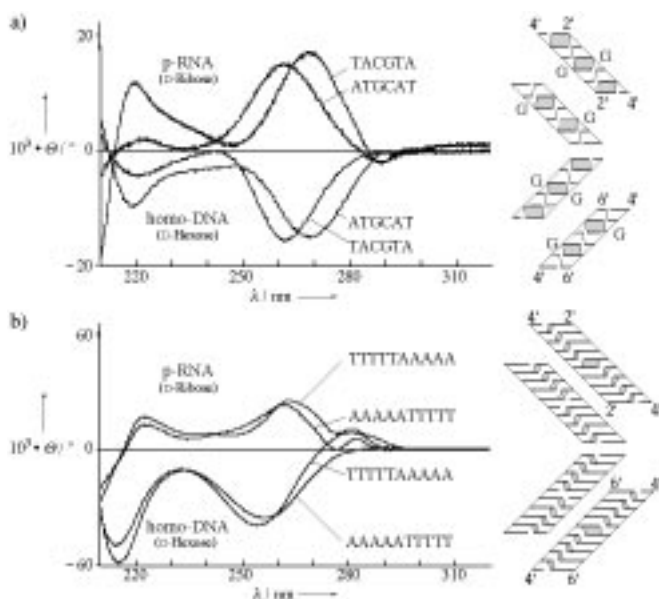


Figure 3. CD spectra of p-RNA and homo-DNA duplexes containing the sequence motifs a) (py-PU)₃ and (PU-py)₃ and b) (py)₅-(PU)₅ and (PU)₅-(py)₅ ($c \approx 10 \mu\text{M}$; in 150 mM NaCl, 10 mM Tris-HCl, pH 7.0, at 20 °C) with illustration of interstrand base stacking analyses.

operates between purines exclusively. The quasi mirror-image-like correspondence of the CD profiles in the two series does not primarily refer to the duplexes of identical base sequence, but rather to the duplexes with identical interstrand base stacking pattern. Thus, the CD profile of the p-RNA duplex TACGTA corresponds to that of the homo-DNA duplex ATGCAT; the base stacking pattern common to both is A/A, G/G, A/A. The spectrum with the bathochromically shifted maximum belongs in both series to the duplex with an additional G/G stacking in the duplex center (Figure 3 a, right), which is considered to be responsible for the higher duplex stability. Mirror-image character of the CD spectra was observed in all p-RNA/homo-DNA-duplex pairs investigated thus far; Figure 3 b depicts an example (duplex No. 3) which is about average with respect to the degree to which duplexes of the two pairing systems show quasi-enantiomorphism of their CD spectra.

Mirror-image character of oligonucleotide CD profiles can, but does not necessarily need to, reflect opposite helicity of twisted duplex structures. In quasi-linear systems with dominating interstrand base stacking, quasi-enantiomorphism of CD spectra may also reflect the fact that in duplexes of opposite backbone inclination a structural subunit comprising two interstrand-stacking bases possesses the opposite sense of chirality (compare Figure 1 c).^[7] Unfortunately, in the present case neither the sense nor the degree of backbone-twisting in duplexes of the p-RNA and homo-DNA series are really established thus far.^[8] Therefore, we have to leave the problem of the origin of the remarkable quasi-enantiomor-

phism of p-RNA and homo-DNA duplexes for further study; a more detailed structural knowledge to be obtained by X-ray crystallography seems indispensable. We do conclude, however, that quasi-linear oligonucleotide systems with strongly inclined backbones represent promising objects of study for detecting and analyzing previously unknown structure-property relationships in nucleic acids.^[5]

Received: October 5, 1998 [Z12484IE]

German version: *Angew. Chem.* **1999**, *111*, 715–718

Keywords: DNA structures • duplex stability • homo-DNA • oligonucleotides • pyranosyl-RNA

- [1] a) S. Pitsch, S. Wendeborn, B. Jaun, A. Eschenmoser, *Helv. Chim. Acta* **1993**, *76*, 2161–2183; b) S. Pitsch, R. Krishnamurthy, M. Bolli, S. Wendeborn, A. Holzner, M. Minton, C. Lesueur, I. Schlönvogt, B. Jaun, A. Eschenmoser, *Helv. Chim. Acta* **1995**, *78*, 1621–1635; c) I. Schlönvogt, S. Pitsch, C. Lesueur, A. Eschenmoser, B. Jaun, R. M. Wolf, *Helv. Chim. Acta* **1996**, *79*, 2316–2345; d) R. Micura, M. Bolli, N. Windhab, A. Eschenmoser, *Angew. Chem.* **1997**, *109*, 899–902; *Angew. Chem. Int. Ed. Engl.* **1997**, *36*, 870–873; e) M. Bolli, R. Micura, A. Eschenmoser, *Chem. Biol.* **1997**, *4*, 309–320; f) M. Bolli, R. Micura, S. Pitsch, A. Eschenmoser, *Helv. Chim. Acta* **1997**, *80*, 1901–1951.
- [2] a) A. Eschenmoser, M. Dobler, *Helv. Chim. Acta* **1992**, *75*, 218–259; b) M. Böhlinger, H.-J. Roth, J. Hunziker, M. Göbel, R. Krishnan, A. Giger, B. Schweizer, J. Schreiber, C. Leumann, A. Eschenmoser, *Helv. Chim. Acta* **1992**, *75*, 1416–1477; c) J. Hunziker, H.-J. Roth, M. Böhlinger, A. Giger, U. Diederichsen, M. Göbel, R. Krishnan, B. Jaun, C. Leumann, A. Eschenmoser, *Helv. Chim. Acta* **1993**, *76*, 259–352; d) G. Otting, M. Billeter, K. Wüthrich, H.-J. Roth, C. Leumann, A. Eschenmoser, *Helv. Chim. Acta* **1993**, *76*, 2701–2756; e) K. Groebke, J. Hunziker, W. Fraser, L. Peng, U. Diederichsen, K. Zimmermann, A. Holzner, C. Leumann, A. Eschenmoser, *Helv. Chim. Acta* **1998**, *81*, 375–474.
- [3] Frameshifts in (PU-py)_n duplexes can lead to the same number of purine-purine interstrand stackings as present in corresponding (py-PU)_n duplexes. This could be the reason for the negligibly small stability differences between the motif pairs No. 7 and 8.^[14] Such an interpretation seems supported by the relative duplex stabilities of No. 9 and 10. In these sequences the (compulsory) frameshifts can occur upstream (in p-RNA) and downstream (in homo-DNA) so that duplex No. 9 with four, as opposed to three, adenine-adenine stackings is the more stable one in both systems (see Figure 2).
- [4] For the assessment of sequence dependence of duplex stabilities in the DNA and RNA series, empirical nearest neighbor parameters are used which do not explicitly differentiate between intra- and interstrand base stacking; see N. Sugimoto, S. Nakano, M. Yoneyama, K. Honda, *Nucleic Acids Res.* **1996**, *24*, 4501–4505; J. SantaLucia, Jr., H. T. Allawi, P. A. Seneviratne, *Biochemistry* **1996**, *35*, 3555–3562, and references therein. On the influence of dangling bases in the DNA and RNA series see N. Sugimoto, R. Kierzek, D. H. Turner, *Biochemistry* **1987**, *26*, 4554–4558; M. Senior, R. A. Jones, K. J. Breslauer, *Biochemistry* **1988**, *27*, 3879–3885.
- [5] In oligonucleotide systems without (or with small) backbone inclination, base stacking is predominately intrastrand; this is the case, for instance, for DNA duplexes of the B-type (but less so for the A-type). The backbone inclination in a strongly helical duplex is not an easily discernible parameter and it is therefore understandable that it has not been used for the classification of DNA and RNA structures (see R. E. Dickerson et al., *Nucleic Acids Res.* **1989**, *17*, 1797–1803). Backbone inclination may nevertheless become a useful parameter for natural nucleic acids when it comes to a detailed structural description of stacking-dependent biological processes such as replication, transcription and codon/anticodon recognition. Local alterations of backbone inclination can arise through corresponding local alterations of nucleosidic torsion angles. Since local strand dissociation

processes may proceed with retention of intrastrand, but must occur with breakage of interstrand stacking, such local structural fluctuations can result in local fluctuations of pairing strength within a duplex. To what extent such effects are significant in biological processes of the type mentioned above is an open, yet interesting, question. The definition of backbone inclination for helical duplexes and the application of this parameter for differentiating DNA and RNA duplex structures will be described in a forthcoming paper together with M. Egli (Northwestern University, Illinois, USA).

- [6] For CD spectroscopy of oligonucleotides of the natural series see W. C. Johnson, Jr. in *Circular Dichroism and the Conformational Analysis of Biomolecules* (Ed.: G. D. Fasman), Plenum Press, New York, **1996**, p. 433–468.
- [7] See for example: I. Jodal, A. Kovacs, J. Ott, G. Snatzke, *Chem. Ber.* **1989**, *122*, 1207–1210.
- [8] The NMR structure analysis of the p-RNA and homo-DNA duplexes described in references [1c, 2d] did not allow the determination of these data.
- [9] L. Marky, K. J. Breslauer, *Biopolymers* **1987**, *26*, 1601–1620.
- [10] Data of the homo-DNA duplexes No. 7, 9, and 10 were determined by S. Guntha (ETH, Zürich).

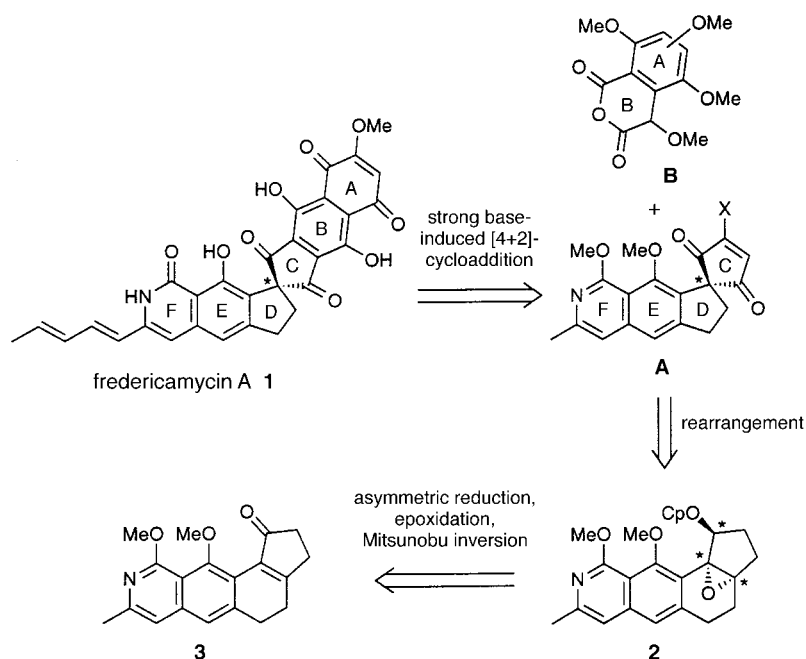
Asymmetric Total Synthesis of Fredericamycin A**

Yasuyuki Kita,* Kazuhiro Higuchi, Yutaka Yoshida, Kiyosei Iio, Shinji Kitagaki, Shuji Akai, and Hiromichi Fujioka

Fredericamycin A (**1**), isolated from *Streptomyces griseus* in 1981, possesses potent antitumor activity against a variety of tumor models (in vivo) such as P388 leukemia, B16 melanoma, and CD8F mammary, and does not show mutagenicity in the Ames test.^[1, 2] Its structure consists of two sets of *peri*-hydroxy tricyclic aromatic moieties connected through a spiro quaternary carbon center, which is made chiral by the presence of a single methoxy group at the farthest position on the A-ring. Its promising biological profile as well as its unprecedented unique structure has made **1** quite attractive as a

lead compound for a novel type of chemotherapeutic drug for human cancers, and hence extensive attention is being focused on its total synthesis. In spite of the enormous efforts towards this goal, including the total syntheses of racemic **1** by five research groups^[3–7] and a recently reported synthesis of optically pure **1** by HPLC separation of a racemic intermediate of **1** using a special chiral column,^[8] no one has so far succeeded in the asymmetric total synthesis of **1**, and its absolute configuration still remains unknown. Most of the reported total syntheses and the related model studies involved the construction of the spiro CD-ring at their final stages, and the lack of sufficient methods for the enantiodifferentiation of the highly symmetrical AB-plane has been the major obstacle in these asymmetric approaches. We present here the first asymmetric total synthesis of **1** with definite absolute configuration of the spiro center, which elucidates the absolute configuration of natural **1** 17 years after its isolation.^[9, 10]

Our synthetic strategy, outlined in Scheme 1, is based on the strong base-induced intermolecular [4+2] cycloaddition of a



Scheme 1. Retrosynthesis of fredericamycin A (**1**).

[*] Prof. Dr. Y. Kita, K. Higuchi, Y. Yoshida, K. Iio, Dr. S. Kitagaki, Dr. S. Akai, Dr. H. Fujioka
Graduate School of Pharmaceutical Sciences, Osaka University
1-6, Yamada-oka, Suita, Osaka 565–0871 (Japan)
Fax: (+81)6-6879-8229
E-mail: kita@phs.osaka-u.ac.jp

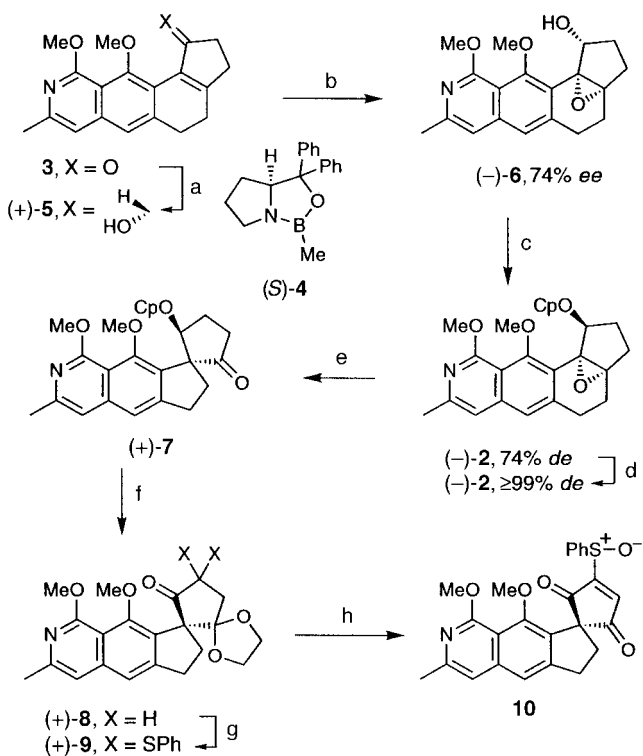
[**] This research was supported by a Grant-in-Aid for Scientific Research from the Ministry of Education, Science, and Culture, Japan, a Special Coordination Funds of the Science and Technology Agency, Japan, and Japan Research Foundation for Optically Active Compounds. We are also grateful to Mr. Keita Matsumoto, Taisho Pharmaceutical Co., Ltd., for X-ray crystallographic analysis and Dr. Hiroshi Hasegawa (SS Pharmaceutical Co., Ltd., Japan) for generously providing an authentic sample of fredericamycin A.

Supporting information for this article is available on the WWW under <http://www.wiley-vch.de/home/angewandte/> or from the author.

suitably functionalized homophthalic anhydride (**B**) to an optically pure dienophile (**A**) corresponding to the CDEF-moiety, in which the regiochemistry during the cycloaddition is known to be controlled by the substituent X on the dienophile.^[11, 12] We envisaged that the cycloaddition of **A** having unambiguous absolute configuration would afford **1** with the retention of the chiral integrity. Since the absolute stereochemistry of **1** is unknown, any synthetic strategy to be developed should be planned in such a way that it allows the synthesis of both enantiomers readily. The dienophile **A** could be prepared from the optically pure *trans*-epoxy camphanate **2** through the stereospecific rearrangement which we have disclosed recently.^[13] As per our previous study, **2** in turn could be prepared from the enone **3** by an asymmetric reduction of

the keto group followed by the epoxidation of the olefin and Mitsunobu inversion of the hydroxy group.

On the basis of this retrosynthesis, we initially examined the transformation of **3**^[14] to **2**. Asymmetric reduction of **3** using the chiral borane (*S*)-**4** and $\text{BH}_3 \cdot \text{Me}_2\text{S}$ as developed by Corey et al.^[15] gave a quantitative yield of the (*R*)-alcohol (+)-**5** with 74% *ee* (Scheme 2).^[16] Sharpless epoxidation of (+)-**5** afforded stereoselectively the *cis*-epoxy alcohol (–)-**6** (81%, 74% *ee*), which was treated with (–)-camphanic acid (>98% *ee*)



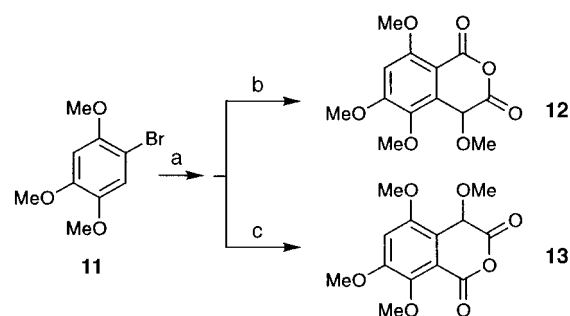
Scheme 2. Synthesis of the dienophile **10**. a) (*S*)-**4**, $\text{BH}_3 \cdot \text{Me}_2\text{S}$, THF, 0 °C, 98%; b) $[\text{VO}(\text{acac})_2]$, $t\text{BuO}_2\text{H}$, C_6H_6 , 0 °C → room temperature, 81%; c) CpOH , Ph_3P , diethyl azodicarboxylate, toluene, 0 °C → room temperature; d) SiO_2 column chromatography, 59% from (–)-**6**; e) $\text{BF}_3 \cdot \text{Et}_2\text{O}$, CH_2Cl_2 , 0 °C, 94%; f) 1. $(\text{CH}_3\text{OTMS})_2$, TMSOTf , CH_2Cl_2 , 0 °C → room temperature, 93%; 2. 10% NaOH , MeOH , room temperature, 97%; 3. Dess–Martin periodinane, CH_2Cl_2 , room temperature, 98%; g) PhSO_2Ph , $\text{LiN}(\text{TMS})_2$, THF, –78 °C → room temperature, 98%; h) 1. 85% aqueous $\text{CF}_3\text{CO}_2\text{H}$, 50 °C, 92%; 2. *m*-CPBA, CH_2Cl_2 , –40 °C → room temperature, 93%. *acac* = acetylacetonate, *Cp* = (–)-camphanyl, *m*-CPBA = *m*-chloroperoxybenzoic acid, *Tf* = trifluoromethanesulfonyl, *TMS* = trimethylsilyl.

under Mitsunobu reaction conditions to give a diastereomeric mixture (74% *de*) of the *trans*-epoxy camphanate [(–)-**2**], from which optically pure (–)-**2** ($\geq 99\%$ *de*, $\geq 99\%$ *ee*) was obtained by SiO_2 -column chromatography.^[16] The absolute configuration of (–)-**2** was determined by X-ray crystallographic analysis.^[17]

The rearrangement reaction of (–)-**2** ($\geq 99\%$ *de*, $\geq 99\%$ *ee*) using $\text{BF}_3 \cdot \text{Et}_2\text{O}$ proceeded at 0 °C with a perfect stereoselectivity to give a 94% yield of the spiro compound (+)-**7** ($\geq 99\%$ *ee*).^[16] Based on our previous results,^[13] the configuration of (+)-**7** was envisaged as depicted in Scheme 2 and finally ascertained by its X-ray crystallographic analysis.^[17] Next, (+)-**7** was transformed to the dienophile **10** while

keeping the chiral integrity by taking into consideration the following two points: 1) To prevent the easy racemization of the spiro keto camphanate (+)-**7** under alkaline conditions (NaOH/MeOH) by retro aldol reaction, acetalization was carried out prior to the alkaline hydrolysis of (+)-**7**. 2) According to our recent study,^[18] a sulfinyl group was introduced as a powerful directing and activating substituent on the dienophile. Thus, α,α -disulfonylation of (+)-**8**, elimination of PhSH by treatment with an acid, and oxidation of sulfide gave **10** as a diastereomeric mixture (ca. 1:1).

The regioisomeric diene parts **12** and **13** were prepared from **11**^[19] with some modifications of the reported method^[12g] (Scheme 3). Reaction of **11** with dimethyl malonate (2.0 equiv), *n*BuLi (3.0 equiv), and tetramethylpiperidine (1.5 equiv) afforded a regioisomeric mixture (3:2) of the



Scheme 3. Synthesis of the diene precursors **12** and **13**. a) Dimethyl malonate, *n*BuLi, 2,2,6,6-tetramethylpiperidine, THF, –78 °C, 3:2 mixture of regioisomers, 58% in total; b) 1. $\text{LiN}(\text{TMS})_2$, NBS, THF, –78 °C, 54%; 2. AgOTf , 2,6-lutidine, MeOH , CH_2Cl_2 , 0 °C, 87%; 3. KOH , $\text{EtOH}/\text{H}_2\text{O}$, reflux, then 10% HCl , 98%; 4. trimethylsilyl(ethoxy)acetylene, CH_2Cl_2 , room temperature, 80%; c) 1. $\text{LiN}(\text{TMS})_2$, NBS, THF, –78 °C, 2. NaOMe , $\text{MeOH}/\text{CH}_2\text{Cl}_2$, –78 °C → room temperature, 60% over 2 steps, 3. KOH , $\text{EtOH}/\text{H}_2\text{O}$, reflux, then $\text{CF}_3\text{CO}_2\text{H}$, 71%; 4. trimethylsilyl(ethoxy)acetylene, CH_2Cl_2 , room temperature, 91%. NBS = *N*-bromosuccinimide.

homophthalates, through a non-regioselective addition of the lithiomalonate to the aryne intermediate. Each regioisomer was readily separated and subjected to sequential bromination, methanolysis, alkaline hydrolysis of the diester, and dehydration of the dicarboxylic acid by using trimethylsilyl(ethoxy)acetylene^[20] to afford the corresponding anhydrides **12** and **13**. The regiochemistry of the products was determined by a nuclear Overhauser effect (NOE) experiment and further confirmed by X-ray crystallographic analysis.^[17]

With both components for the [4+2] cycloaddition in hand, we then examined the intermolecular cycloaddition. Treatment of **12** with NaH (1.15 equiv) generated the anion, to which was added **10** at 0 °C. The reaction mixture was then stirred at room temperature for 7 h, and subsequent treatment with MeI in the presence of K_2CO_3 provided the hexacyclic compound (*R*)-**14** (71%, 90% *ee*). A similar reaction of **13** with **10** afforded the enantiomer (*S*)-**14** (76%, 97% *ee*) (Scheme 4).^[16] Circular dichroism (CD) spectra of both enantiomers of **14** presented a couple of symmetrical curves (Figure 1), among which the CD of the (*S*)-isomer closely resembled that of the fully protected fredericamycin A reported by Boger et al.^[8a] Hence, the following sequence of reactions to obtain **1** was performed on (*S*)-**14**. The F-ring was

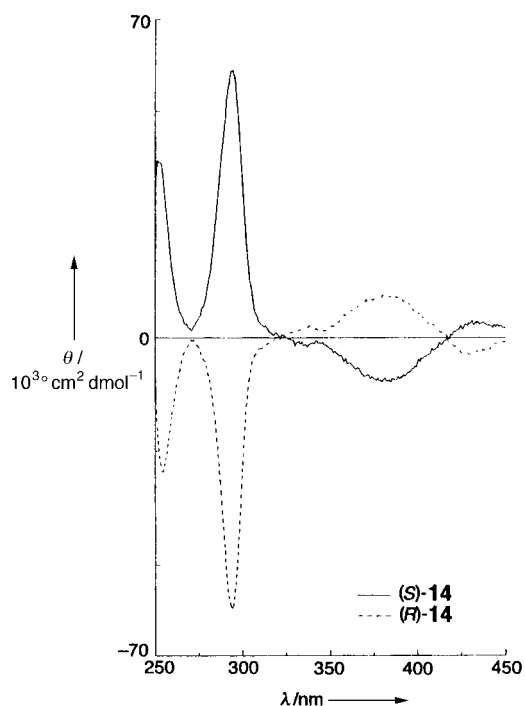
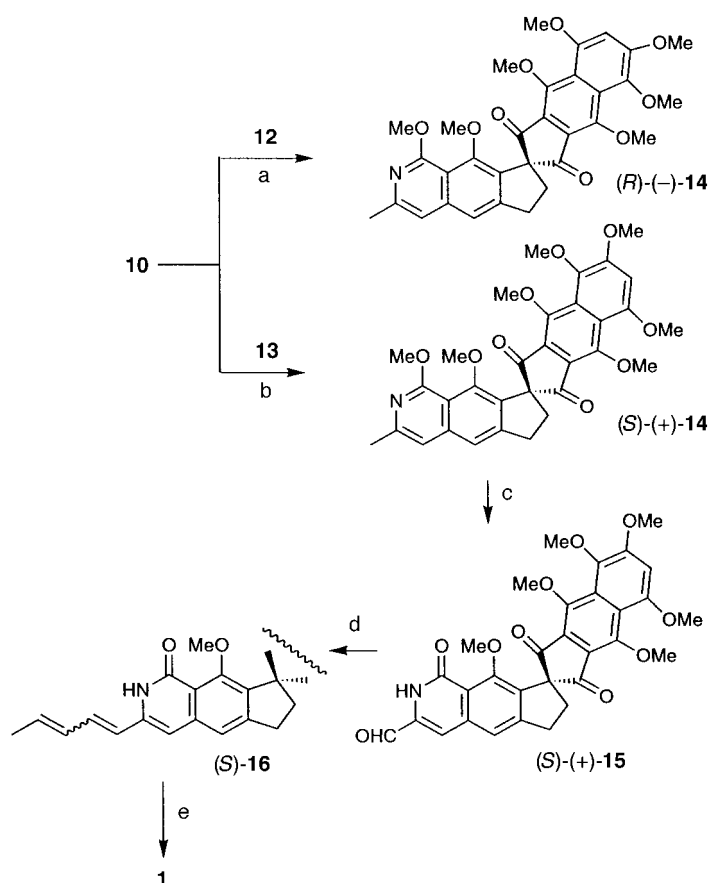


Figure 1. CD spectra of **14** in *i*PrOH.

selectively demethylated with trimethylsilyl iodide (TMSI)^[4b] and the resulting compound was oxidized with SeO₂ to give the aldehyde (*S*)-**15**.^[21] The pentadienyl side chain was introduced by using a standard Wittig reaction^[3] to give a 5:1 mixture of (*E,E*)- and (*E,Z*)-(*S*)-**16** in 46 % yield. Deprotection of this mixture with BBr₃ (12.5 equiv) and subsequent autooxidation afforded a 5:1 mixture of the desired (*E,E*)-isomer (**1**) and its (*E,Z*)-isomer in a total yield of 74 % yield, from which the pure (*E,E*)-isomer **1** was separated by using HPLC column (Jasco Megapak SIL NH2-10, 1 × 25 cm, 800:200:1 CHCl₃/*n*-hexane/acetic acid, 5 mL min⁻¹ flow rate).^[22] The spectral features of synthetic **1** (¹H NMR, IR, UV, CD, and HPLC) were completely identical with those of the isolated natural **1**. Thus, the absolute configuration of natural **1** was ascertained to be *S*.

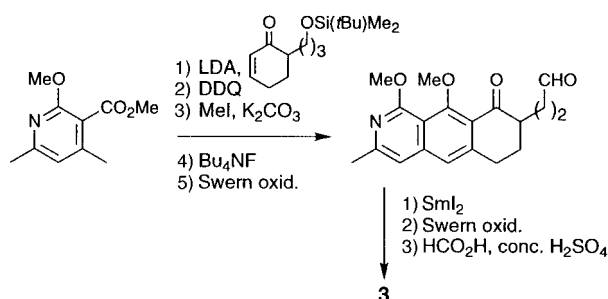
In summary, the asymmetric total synthesis of fredericamycin A (**1**) has been accomplished for the first time and thereby the absolute configuration of its single chiral center established. This success also highlights the efficacy of our protocols; that is, 1) stereospecific rearrangement of the epoxy acylate and 2) the regiocontrolled intermolecular [4+2] cycloaddition of homophthalic anhydrides to dienophiles, for the construction of unique structures such as fredericamycin A (**1**), for which the reported methods are not effective.

Received: August 31, 1998 [Z12357IE]
German version: *Angew. Chem.* **1999**, *111*, 731–734

Keywords: asymmetric synthesis • antitumor agents • cycloadditions • natural products • rearrangements • total synthesis

- [1] Isolation and structure elucidation: see, a) R. C. Pandey, M. W. Toussaint, R. M. Stroschane, C. C. Kalita, A. A. Aszalos, A. L. Garretson, T. T. Wei, K. M. Byrne, R. F. Geoghegan, Jr., R. J. White, *J. Antibiot.* **1981**, *34*, 1389–1401; b) R. Misra, R. C. Pandey, J. V. Silverton, *J. Am. Chem. Soc.* **1982**, *104*, 4478–4479; c) R. Misra, R. C. Pandey, B. D. Hilton, P. P. Roller, J. V. Silverton, *J. Antibiot.* **1987**, *40*, 786–802.
- [2] Studies on biological activity: see, a) D. J. Warnick-Pickle, K. M. Byrne, R. C. Pandey, R. J. White, *J. Antibiot.* **1981**, *34*, 1402–1407; b) B. D. Hilton, R. Misra, J. L. Zweier, *Biochemistry* **1986**, *25*, 5533–5539; c) R. Misra, *J. Antibiot.* **1988**, *41*, 976–981; d) M. D. Latham, C. K. King, P. Gorycki, T. L. Macdonald, W. E. Ross, *Cancer Chemother. Pharmacol.* **1989**, *24*, 167–171; e) N. S. Dalal, X. Shi, *Biochemistry* **1989**, *28*, 748–750.
- [3] a) T. R. Kelly, N. Ohashi, R. J. Armstrong-Chong, S. H. Bell, *J. Am. Chem. Soc.* **1986**, *108*, 7100–7101; b) T. R. Kelly, S. H. Bell, N. Ohashi, R. J. Armstrong-Chong, *J. Am. Chem. Soc.* **1988**, *110*, 6471–6480.
- [4] a) D. L. J. Clive, Y. Tao, A. Khodabocus, Y.-J. Wu, A. G. Angoh, S. M. Bennett, C. N. Boddy, L. Bordeleau, D. Kellner, G. Kleiner, D. S. Middleton, C. J. Nichols, S. R. Richardson, P. G. Vernon, *J. Chem. Soc. Chem. Commun.* **1992**, 1489–1490; b) D. L. J. Clive, Y. Tao, A. Khodabocus, Y.-J. Wu, A. G. Angoh, S. M. Bennett, C. N. Boddy, L. Bordeleau, D. Kellner, G. Kleiner, D. S. Middleton, C. J. Nichols, S. R. Richardson, P. G. Vernon, *J. Am. Chem. Soc.* **1994**, *116*, 11275–11286.
- [5] a) A. V. Rama Rao, A. K. Singh, B. V. Rao, K. M. Reddy, *Tetrahedron Lett.* **1993**, *34*, 2665–2668; b) A. V. Rama Rao, A. K. Singh, B. V. Rao, K. M. Reddy, *Heterocycles* **1994**, *37*, 1893–1912.
- [6] L. Saint-Jalmes, C. Lila, J. Z. Xu, L. Moreau, B. Pfeiffer, G. Eck, L. Pelsez, C. Rolando, M. Julia, *Bull. Soc. Chim. Fr.* **1993**, *130*, 447–449.
- [7] J. A. Wendt, P. J. Gauvreau, R. D. Bach, *J. Am. Chem. Soc.* **1994**, *116*, 9921–9926.
- [8] a) D. L. Boger, O. Hüter, K. Mbiya, M. Zhang, *J. Am. Chem. Soc.* **1995**, *117*, 11839–11849; b) D. L. Boger, *J. Heterocycl. Chem.* **1996**, *33*, 1519–1531.

- [9] We are also investigating a different approach to the total synthesis of **1** based on an intramolecular [4+2] cycloaddition: see a) Y. Kita, R. Okunaka, T. Honda, M. Shindo, O. Tamura, *Tetrahedron Lett.* **1989**, 30, 3995–3998; b) Y. Kita, R. Okunaka, T. Honda, M. Kondo, O. Tamura, Y. Tamura, *Chem. Pharm. Bull.* **1991**, 39, 2106–2114; c) S. Akai, K. Iio, Y. Takeda, H. Ueno, Y. Kita, *Synlett* **1997**, 310–312; d) Y. Kita, S. Akai, H. Fujioka, *Yuki Gosei Kagaku Kyokaiishi* **1998**, 56, 963–974. A similar intramolecular strategy was reported separately: see e) M. Toyota, S. Terashima, *Tetrahedron Lett.* **1989**, 30, 829–832.
- [10] For a study on construction of optically active quaternary carbon in connection with **1**: see W. Trypke, A. Steigel, M. Braun, *Synlett* **1992**, 827–829.
- [11] a) Y. Tamura, M. Sasho, K. Nakagawa, T. Tsugoshi, Y. Kita, *J. Org. Chem.* **1984**, 49, 473–478; b) Y. Tamura, F. Fukata, M. Sasho, T. Tsugoshi, Y. Kita, *J. Org. Chem.* **1985**, 50, 2273–2277; c) Y. Kita, K. Iio, A. Okajima, Y. Takeda, K. Kawaguchi, B. A. Whelan, S. Akai, *Synlett* **1998**, 292–294.
- [12] Application of this method to the total syntheses of *peri*-hydroxy polyaromatic compounds: see reviews, a) Y. Tamura, Y. Kita, *Yuki Gosei Kagaku Kyokaiishi* **1988**, 46, 205–217 [*Chem. Abstr.* **1988**, 109, 129465d]; b) Y. Kita, Y. Takeda, *Kagaku to Kogyo (Osaka)* **1997**, 71, 298–309 [*Chem. Abstr.* **1997**, 127, 190540n]; c) M. Kirihaara, Y. Kita, *Heterocycles* **1997**, 46, 705–726. See also other examples done by other groups, d) F. Matsuda, M. Kawasaki, M. Ohsaki, K. Yamada, S. Terashima, *Tetrahedron* **1988**, 44, 5745–5759; e) J.-F. Lavallée, R. Rej, M. Courchesne, D. Nguyen, G. Attardo, *Tetrahedron Lett.* **1993**, 34, 3519–3522; f) T. Matsumoto, H. Yamaguchi, K. Suzuki, *Synlett* **1996**, 433–434; g) M. D. Shair, T. Y. Yoon, K. K. Mosny, T. C. Chou, S. J. Danishefsky, *J. Am. Chem. Soc.* **1996**, 118, 9509–9525.
- [13] Y. Kita, S. Kitagaki, R. Imai, S. Okamoto, S. Mihara, Y. Yoshida, S. Akai, H. Fujioka, *Tetrahedron Lett.* **1996**, 37, 1817–1820. See also, Y. Kita, S. Kitagaki, Y. Yoshida, S. Mihara, D.-F. Fang, M. Kondo, S. Okamoto, R. Imai, S. Akai, H. Fujioka, *J. Org. Chem.* **1997**, 62, 4991–4997; Y. Kita, S. Kitagaki, Y. Yoshida, S. Mihara, D.-F. Fang, H. Fujioka, *Tetrahedron Lett.* **1997**, 38, 1061–1064.
- [14] The enone **3** was obtained from methyl 2-methoxy-4,6-dimethylpyridine-3-carboxylate as per Scheme 5. The details will be presented in the forthcoming full paper.



Scheme 5. Synthesis of **3**.

- [15] E. J. Corey, R. K. Bakshi, S. Shibata, C.-P. Chen, V. K. Singh, *J. Am. Chem. Soc.* **1987**, 109, 7925–7926.
- [16] Optical purities of the intermediates (**5**, **6**, and **9**) were determined by HPLC using Daicel CHIRALCEL OD (*n*-hexane-*i*PrOH), and those of **2**, **7**, **8**, (*R*)- and (*S*)-**14**, and (*S*)-**15** by Daicel CHIRALPAK AD (*n*-hexane-*i*PrOH).
- [17] Crystallographic data (excluding structure factors) for the structures reported in this paper have been deposited with the Cambridge Crystallographic Data Center as supplementary publication no. CCDC-102892 (for (–)-**2**), CCDC-102893 (for (+)-**7**), and CCDC-102894 [for methyl 2-methoxy-2-[3,4,6-trimethoxy-2-(methoxycarbonyl)phenyl]acetate, a precursor of **13**]. Copies of the data can be obtained free of charge on application to CCDC, 12 Union Road, Cambridge CB2 1EZ, UK (fax: (+44) 1223-336-033; e-mail: deposit@ccdc.cam.ac.uk).
- [18] We have recently elucidated that the dienophiles having sulfinyl group [X = S(O)Ph] are much more reactive for the anionic [4+2] cyclo-

addition to homophthalic anhydrides than the well known halogen-substituted ones.^[11c]

- [19] J. M. Blatchly, J. F. W. McOmie, J. B. Searle, *J. Chem. Soc. C* **1969**, 1350–1353.
- [20] Y. Kita, S. Akai, N. Ajimura, M. Yoshigi, T. Tsugoshi, H. Yasuda, Y. Tamura, *J. Org. Chem.* **1986**, 51, 4150–4158.
- [21] Y. Kita, H. Ueno, S. Kitagaki, K. Kobayashi, K. Iio, S. Akai, *J. Chem. Soc. Chem. Commun.* **1994**, 701–702.
- [22] Extensive research towards complete isomerization of the (*E,Z*)-**16** to its (*E,E*)-isomer by using a catalytic amount of I₂ in the dark under various conditions (in CDCl₃, CHCl₃, or CH₂Cl₂ at room temperature for two days to two weeks) as well as direct demethylation–isomerization by the combined use of I₂ and BBr₃ did not lead to the complete isomerization and, in some cases, caused gradual decomposition. Since **16** is sensitive to visible light leading to decomposition and diene-isomerization, the subsequent steps after chain elongation, that is, demethylation, autooxidation, and HPLC separation, were done immediately. The purified sample (**1**) readily isomerizes in organic solvents containing strong acids such as CF₃COOH.

Regioselective Lactonization of α -(2→8)-Trisialic Acid**

Mou-Chi Cheng, Chun-Hung Lin,* Kay-Hooi Khoo, and Shih-Hsiung Wu*

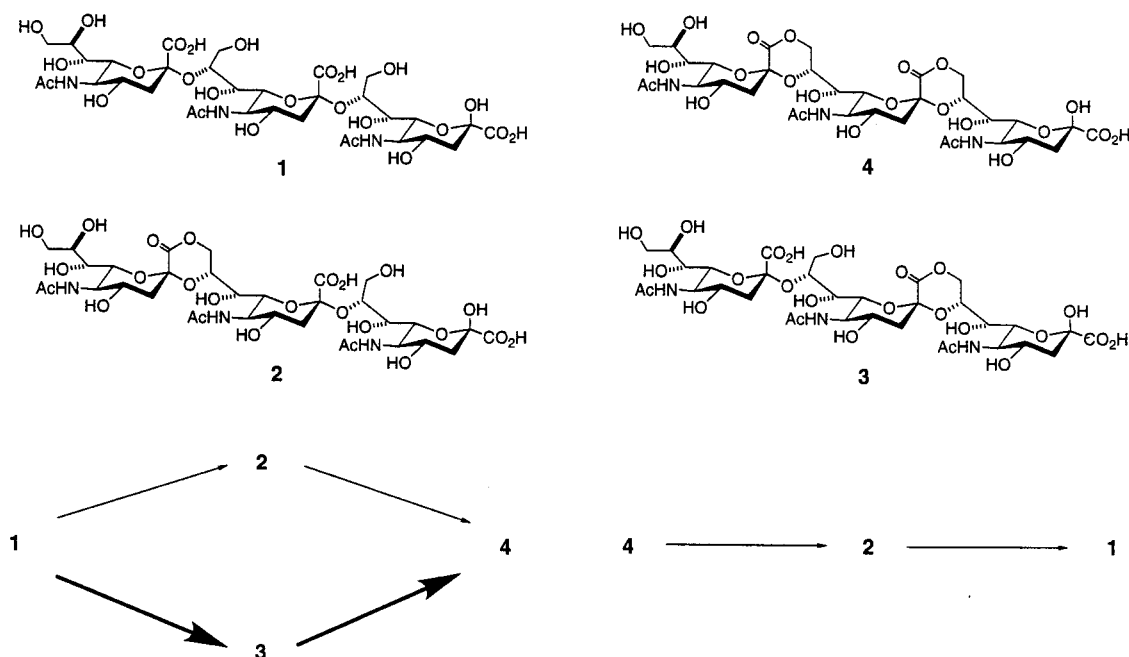
The polymer of α -(2,8)-linked *N*-acetylneuraminic acids (poly(2,8-NeuAc)) is mainly distributed in mammalian cells and bacteria, and associated with many different biological functions.^[1] It has been reported that δ -lactonization, the condensation of the carboxyl group at C-2 of one residue with the hydroxyl group at C-9 of an adjacent residue, is observed in α -2,8-linked polysialic acids at low pH.^[2] Likewise, in gangliosides (glycosphingolipids containing one to three sialic acid moieties), δ -lactone is also formed under acidic conditions.^[3] The δ -lactones of gangliosides have been suggested to be the true immunogens in the preparation of anti-ganglioside antibodies.^[4] Since polysialic acid is a sugar polymer with highly negative charges, lactonization, which reduces the number of carboxylate groups, would influence the charge density. As a consequence, it was proposed that lactone formation may represent an on/off signal of a physiological function.^[5]

Here we report the regioselective lactonization of the α -2,8-linked trisialic acid. There are two lactonized sites in the sialic acid trimer, one at the reducing end and the other at the

[*] Prof. Dr. S.-H. Wu,^[+] Prof. Dr. C.-H. Lin, Prof. Dr. K.-H. Khoo, M.-C. Cheng
Institute of Biological Chemistry, Academia Sinica
National Taiwan University, Taipei (Taiwan)
Fax: (+886) 2-2788-3473
E-mail: shwu@gate.sinica.edu.tw
chunhung@gate.sinica.edu.tw

[+] Additional address:
Institute of Biochemical Sciences
National Taiwan University, Taipei (Taiwan)

[**] Financial support of this work was provided by the National Science Council of Taiwan and Academia Sinica (Taipei, Taiwan).



Scheme 1. Structures of α -2,8-linked sialic acid trimer **1**, 1-monolactone trimer **2**, 2-monolactone trimer **3**, and dilactone trimer **4** as well as the reaction pathway of lactonization (bottom left) and hydrolysis (bottom right).

nonreducing end (Scheme 1). Two different conditions were found under which each of the monolactones was obtained with high regioselectivity. This is the first report that oligosialic acid can undergo regioselective lactonization and delactonization.

The trimer was dissolved in glacial acetic acid at room temperature, and the progress of the lactonization was followed by capillary electrophoresis (CE). As shown in Figure 1, there were four major peaks in the CE spectra corresponding to two monolactones, one dilactone, and the unchanged trimer. Peak A should correspond to the dilactone **4** since it has the lowest charge density. Peak D was identified as belonging to the unchanged trimer **1** by co-injection with an authentic sample. The remaining peaks B and C were assigned to the two monolactonized trimers, which could be identified and distinguished by enzymatic hydrolysis with neuraminidase. Since this enzyme is an exo-glycosidase, it recognizes and releases the sialic acid molecule at the nonreducing terminal, and does not attack the lactonized sialic acid. Peak C, which gradually decreased in intensity during the course of the neuraminidase hydrolysis, is due to the 2-monolactone **3**; the unchanged peak B was assigned to 1-monolactone **2**. Figure 2 shows the time course of enzymatic hydrolysis of the lactonized trimers. The intensities of peaks A and B did not change in the presence of neuraminidase since **2** and **4**, with a lactone ring at the nonreducing end, are resistant to enzymatic hydrolysis. 2-Monolactone **3** (peak C) was hydrolyzed enzymatically into the lactonized dimer (peak a) and sialic acid (peak b), whereas trimer **1** (peak D) was cleaved into the dimer (peak c) and sialic acid. According to Figure 1, lactonization of **1** preferentially occurs first at the reducing terminal under the acidic conditions, so that 2-monolactone **3** is the major product. The mass spectrometry analysis also supported our conclusion that monolactonized

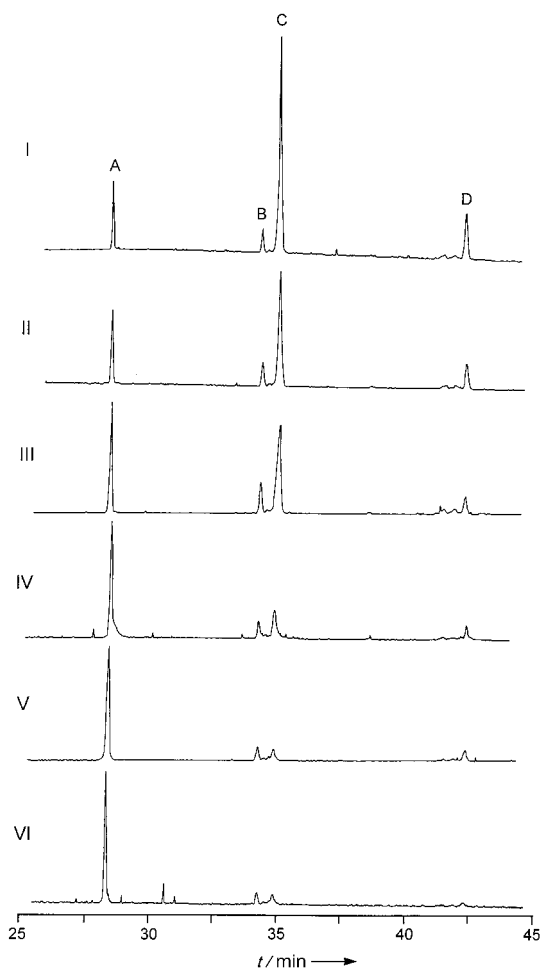


Figure 1. CE spectra of the lactonization of **1** in glacial acetic acid after different reaction times (I: 10 min; II: 20 min; III: 30 min; IV: 1 h; V: 4 h; VI: 8 h).

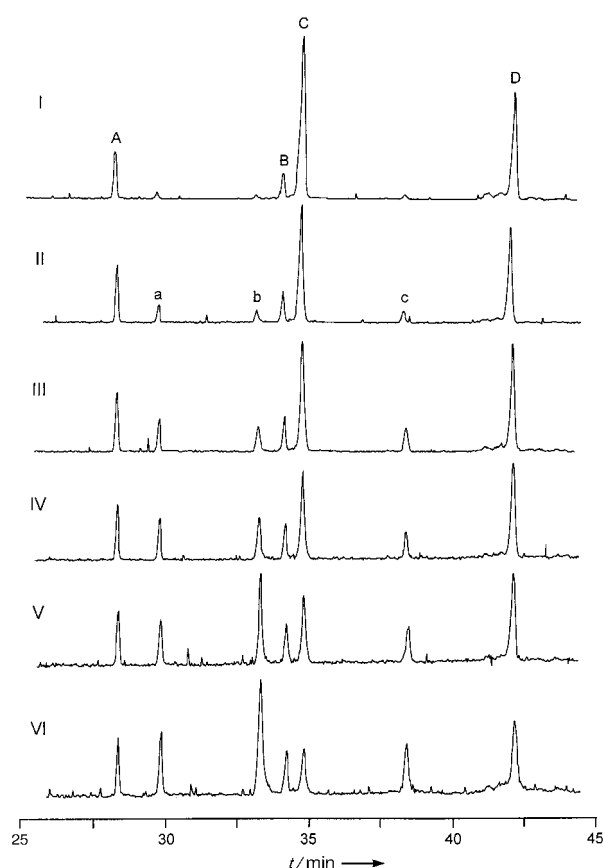


Figure 2. The product mixture obtained from the lactonization of **1** in glacial acetic acid for 10 min was hydrolyzed by neuraminidase and analyzed by CE after different times (I: 0 h; II: 1 h; III: 2 h; IV: 4 h; V: 8 h; VI: 20 h). Peaks A–D were assigned to **4**, **2**, **3**, and **1**, respectively. Peaks a–c are due to lactone dimer, sialic acid monomer, and sialic acid dimer, respectively.

trimers are the major products together with the dilactone and non-lactonized trimers upon treatment with glacial acetic acid for 10 min (Figure 3).

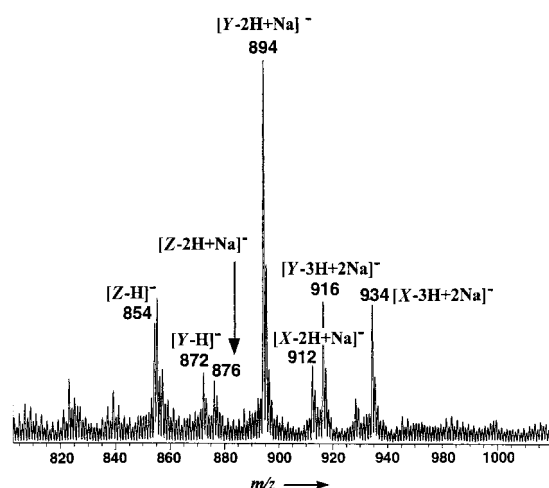


Figure 3. Negative-mode FAB mass spectrum of the sample obtained from the lactonization of α -2,8-linked sialic acid trimer in glacial acetic acid for 10 min. The major signals were assigned and identified as belonging to the molecular ions of the lactonized products and unchanged starting material. X: molecular ion of **1** ($C_{33}H_{53}O_{25}N_3$); Y: molecular ion of **2** and **3** ($C_{33}H_{51}O_{24}N_3$); Z: molecular ion of **4** ($C_{33}H_{49}O_{23}N_3$).

Compound **4** was chemically hydrolyzed in an aqueous solution of 0.1N $(NH_4)_2CO_3$. The CE analysis indicated that **4** was first hydrolyzed to give **2** exclusively and then further hydrolyzed to generate **1** (Figure 4). A co-injection of samples

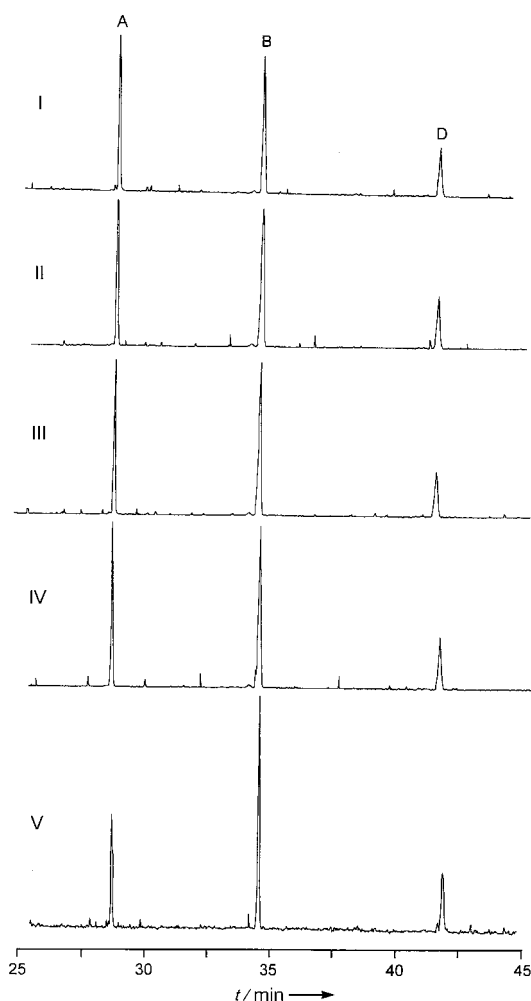


Figure 4. CE spectra of the hydrolysis of **4** under basic conditions after different times (I: 5 min; II: 10 min; III: 20 min; IV: 40 min; V: 80 min).

from both studies (esterification and hydrolysis) verified that peak B in Figure 4 is indeed due to the 1-monolactone **2** and different from the 2-monolactone **3** preferably generated by acidic lactonization (Figure 1).^[6] The assignment of the three peaks in Figure 4 was corroborated by FAB-MS analysis, which afforded the expected molecular ions.

The preferential generation of **3** instead of **2** under the acidic conditions and the exclusive formation of **2** in the alkaline hydrolysis of dilactone trimer **4** is explained by structural differences in each component of the sialic acid trimer. The glycerol side chain at the nonreducing terminal is more flexible. It can interact with the carboxyl group at C-2, so that the formation of **2** is more difficult under acidic conditions. Likewise, similar interaction with the lactone ring at the nonreducing end may prevent its breakdown. The interaction of the sugar side chain with the functional group at the anomeric position has been suggested for a KDO-type molecule (KDO = 2-keto-3-deoxyoctulosonate)^[7] that is

closely related to sialic acid. On the other hand, such an interaction is not possible for the side chains of the other two sugar units since the rigidity is created by the glycosidic linkage fixed at C-8. Other possible explanations cannot be simply ruled out. For example, the different pK_a values of these carboxyl groups^[8] may result in such regioselectivity. However, our speculation waits for the isolation and purification of both monolactone trimers for further NMR studies;^[6] computer modeling is currently in progress.

In conclusion, two different methods are presented to obtain the two possible monolactones of an α -2,8-linked trisialic acid with regioselectivity. The neuraminidase hydrolysis demonstrates a novel way to distinguish both regioisomers from each other. The methods developed here can be further extended and applied to prepare other lactonized oligomers for the investigation of their unknown biological functions.

Experimental Section

Reagents: *N*-Acetylneuraminic acid trimer ($[\rightarrow 8\text{Neu}5\text{Aca}2\rightarrow]_3$) was obtained from NGK Biochemical Ltd. (Handa, Japan) with the help of Prof. Yasuo Inoue. Neuraminidase from *Anthrobacter ureafaciens* was purchased from Sigma (St. Louis, USA). All other reagents for reactions and high-performance capillary electrophoresis (HPCE) were of the highest grade commercially available.

Lactonization of the α -2,8-linked tri-*N*-acetylneuraminic acid: Free trimers of $[\alpha 2\rightarrow 8]$ *N*-acetylneuraminic acid (25 μg) were incubated in glacial acetic acid (1 mL) at room temperature. The reaction mixtures were frozen with liquid nitrogen and then dried immediately by SpeedVac (Savant, USA) to remove acetic acid. Dried samples were dissolved in doubly distilled water, and an aliquot (5 μL) of the mixture was analyzed by HPCE.

Preparation of the dilactone 4: free trimers of $[\alpha 2\rightarrow 8]$ *N*-acetylneuraminic acid (25 μg) were left in glacial acetic acid (1 mL) at room temperature for 8 h, frozen with liquid nitrogen, and then dried immediately by SpeedVac (Savant, USA) to remove acetic acid.

Hydrolysis of 4: A sample of 4 (50 μg) was dissolved in 0.1N $(\text{NH}_4)_2\text{CO}_3$ (500 μL) at 37 °C. After 20, 40, and 80 min an aliquot was removed, frozen with liquid nitrogen, and then dried by SpeedVac (Savant, USA). Dried samples were dissolved in doubly distilled water, and an aliquot (5 μL) of the mixture was analyzed by HPCE.

Chromatographic analysis: Capillary electrophoreses (CE) were performed on a Beckman capillary electrophoresis system (P/ACE 2100) with a fused silica capillary (118 cm \times 75 μm (inner diameter)) at 20 kV and 25 °C. Phosphate buffer (50 mM, pH 8.0) was used as the running buffer. The UV absorption at 200 nm was monitored. Samples were injected into the capillary under a high pressure of nitrogen (1.3 bar) for 3 s. The capillary was regenerated by washing with doubly distilled water for 3 min and then 0.1N NaOH for 5 min.

Neuraminidase hydrolysis: Partially lactonized samples (10 μg) in 100 mM ammonium acetate buffer (pH 5) were digested with neuraminidase (1 mU) from *Anthrobacter ureafaciens* in 20- μL CE vials at room temperature. The progress of hydrolysis was monitored by HPCE at regular time intervals.

Fast atom bombardment (FAB) mass spectrometry: Negative-mode FAB mass spectra of the samples were obtained on an Autospec OA-TOF mass spectrometer (Micromass, UK) fitted with a cesium ion gun operated at 26 kV. Samples were dissolved in Milli Q water for loading on to the probe tip coated with monothiolglycerol as matrix.

Received: July 29, 1998 [Z 12220IE]

German version: *Angew. Chem.* **1999**, *111*, 746–749

Keywords: capillary electrophoresis • lactones • sialic acids

- [1] a) F. A. Troy II, *Glycobiology* **1992**, *2*, 5–23; b) U. Rutishauser, A. Acheson, A. K. Hall, D. M. Mann, J. Sunshine, *Science* **1988**, *240*, 53–57; c) K. Kitajima, S. Inoue, Y. Inoue, F. A. Troy II, *J. Biol. Chem.* **1988**, *263*, 18269–18276; d) C. Zuber, P. M. Lackie, W. A. Caterall, J. Roth, *J. Biol. Chem.* **1992**, *267*, 9965–9971; e) S. Inoue, M. Iwasaki, *Biochem. Biophys. Res. Commun.* **1978**, *83*, 1018–1023; f) J. B. Robbin, G. H. McCracken, Jr., E. C. Gotschlich, F. Ørskov, I. Ørskov, L. A. Hanson, *N. Engl. J. Med.* **1974**, *290*, 1216–1220; g) M. S. Schiffer, E. Oliverira, M. P. Glode, G. H. McCracken, Jr., L. M. Sarff, J. B. Robbin, *Pediatr. Res.* **1976**, *10*, 82–87.
- [2] a) M. R. Lifely, A. S. Gilbert, C. Moreno, *Carbohydr. Res.* **1981**, *94*, 193–203. b) M. R. Lifely, A. S. Gilbert, C. Moreno, *Carbohydr. Res.* **1984**, *134*, 229–243.
- [3] a) L. Riboni, S. Sonnino, D. Acquotti, A. Malesci, R. Ghidoni, H. Egge, S. Mingrino, G. Tettamanti, *J. Biol. Chem.* **1986**, *261*, 8514–8519; b) G. A. Nores, T. Dohi, M. Taniguchi, S. Hakomori, *J. Immunol.* **1989**, *139*, 3171–3176; c) R. Bassi, L. Riboni, S. Sonnino, *Carbohydr. Res.* **1989**, *193*, 141–146.
- [4] S. Ando, R. K. Yu, J. N. Scarsdale, S. Kusunoki, J. H. Prestegard, *J. Biol. Chem.* **1989**, *264*, 3478–3483.
- [5] a) R. K. Yu, T. A. W. Koerner, S. Ando, H. C. Yohe, J. H. Prestegard, *J. Biochem.* **1985**, *98*, 1367–1373; b) B. Maggio, T. Agria, R. K. Yu, *Biochemistry* **1990**, *29*, 8729–8734.
- [6] Based on the results of 2D NMR experiments, the partial assignment of compound **2** is given in the following. The detailed and complete NMR characterizations are currently in progress and will be published in due course. ¹H NMR (500 MHz, HOD): δ = 1.694 (1H, t, J_{3a-3e} = J_{3e-4} = 12 Hz, H-3a[II]), 1.740 (1H, t, J_{3a-3e} = J_{3e-4} = 12 Hz, H-3a[III]), 1.830 (1H, t, J_{3a-3e} = J_{3e-4} = 13 Hz, H-3a[I]), 2.065 (6H, s, 2 acetyl), 2.088 (3H, s, acetyl), 2.229 (1H, dd, J_{3e-3a} = 12, J_{3e-4} = 4.5 Hz, H-3e[I]), 2.254 (1H, dd, J_{3e-3a} = 12, J_{3e-4} = 4.5 Hz, H-3e[III]), 2.814 (1H, dd, J_{3e-3a} = 12, J_{3e-4} = 4.5 Hz, H-3e[II]), 3.625 (1H, m, H-4[II]), 3.651 (1H, m, H-4[III]), 3.802 (1H, m, H-5[III]), 3.895 (1H, m, H-5[I]), 3.973 (1H, m, H-5[II]), 4.022 (1H, m, H-4[I]). [I] is defined as the sugar unit located at the reducing terminal of **2**, and [III] is at the nonreducing end. For this assignment, see also T. Ercégovic, G. Magnusson, *J. Org. Chem.* **1996**, *61*, 179–184; ref. [4].
- [7] a) C.-H. Lin, B. W. Murray, I. R. Ollmann, C.-H. Wong, *Biochemistry* **1997**, *36*, 780–785. b) T. Sugai, C.-H. Lin, G.-J. Shen, C.-H. Wong, *Bioorg. Med. Chem.* **1995**, *3*, 313–320.
- [8] A. E. Manzi, H. H. Higa, S. Diaz, A. Varki, *J. Biol. Chem.* **1994**, *269*, 23617–23624.

Convergent Route to Organometallic Dendrimers Composed of Platinum–Acetylide Units**

Kiyotaka Onitsuka, Masanori Fujimoto, Nobuaki Ohshiro, and Shigetoshi Takahashi*

There is increasing interest in the development of new strategies to synthesize well-defined nanosize macromolecules with specific functions. Dendrimers have a regularly branched architecture and have large, spherical dimensions to meet the requirements for new materials.^[1] One method for the functionalization of dendrimers is the incorporation of

[*] Prof. Dr. S. Takahashi, Dr. K. Onitsuka, M. Fujimoto, N. Ohshiro
The Institute of Scientific and Industrial Research
Osaka University, Mihogaoka, Ibaraki, Osaka 567–0047 (Japan)
Fax: (+81) 6-6879-8459
E-mail: takahashi@sanken.osaka-u.ac.jp

[**] This work was partly supported by a Grant-in-Aid for Scientific Research on Priority Areas (No. 10149228 “Metal-assembled Complexes”) from the Ministry of Education, Science, Sports, and Culture.

transition metals that exhibit some characteristic properties. Most organometallic dendrimers reported previously, however, contain metal atoms either only at the core^[2] or at the surface,^[3] and organometallic dendrimers with transition metals in every generation have so far been less studied.^[4] Since such organometallic dendrimers are built up by successive organometallic reactions, the strategy is severely limited because of the low stability of organometallic complexes relative to organic compounds.

We reported previously the synthesis of platinum–acetylide dendrimers, which utilized triethynylmesitylene as a bridging ligand to build up a heneicosanuclear complex, which is a second generation dendrimer.^[5] Metal–acetylide dendrimers may have potential applicability as new materials, since some metal acetylides are known to show unique properties.^[6] However, it would be difficult to extend the method that we employed previously to synthesize higher generation dendrimers, because of the large effort required to isolate the resulting dendrimers from the reaction mixture when no protecting groups were used. Herein we wish to report an efficient route for the synthesis of an organometallic dendrimer composed of platinum–acetylide units in the main chain by a convergent method. The methodology involves the use of two kinds of trialkylsilyl protecting groups, trimethylsilyl and tri(isopropyl)silyl, of the terminal acetylene unit for the synthesis of platinum–acetylide dendrimers.^[7]

The triethynylbenzene derivatives, which were used as the bridging ligand, were protected as shown in Scheme 1. Treatment of 1,3-dibromo-5-iodobenzene (**1**) with one equiv-

alent of tri(isopropyl)silylacetylene at room temperature in the presence of a $[\text{PdCl}_2(\text{PPh}_3)_2]/\text{CuI}$ catalyst in diethylamine led to the selective formation of the mono(silylethynyl) derivative **2**, which was converted quantitatively into a tri(silylethynyl) derivative **3** by the reaction with excess trimethylsilylacetylene in triethylamine under reflux.^[8] Since a tri(isopropyl)silyl group is less reactive towards a base than a trimethylsilyl group,^[7] selective desilylation of the trimethylsilyl group was performed with K_2CO_3 in acetone to give compound **4**, which had two terminal acetylenic groups in the molecule. *p*-Methoxyphenylethynylplatinum groups, which would eventually become the chain-end groups of our dendrimers, were introduced by the reaction of **4** with two equivalents of the platinum complex **5** in the presence of a CuCl catalyst at room temperature to give the dinuclear acetylide complex **6**.^[9] Removal of the tri(isopropyl)silyl group in **6** by the treatment with Bu_4NF gave the first generation dendron **7**. The molecular structure of **7** was determined by X-ray analysis (Figure 1).^[10] The Pt–C bond distances are in the range of 1.992(9)–2.01(1) Å, which are

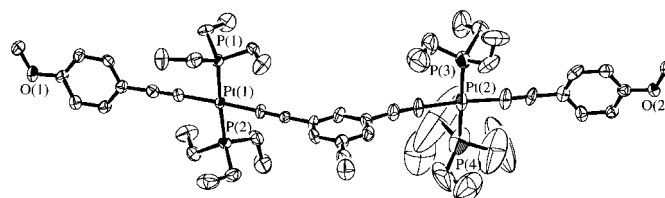
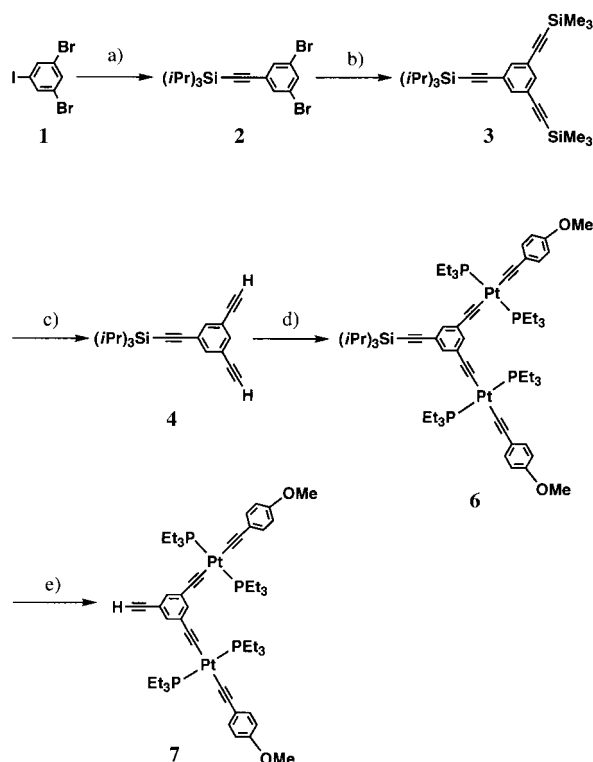


Figure 1. Molecular structure of the first generation dendron **7**. Hydrogen atoms are omitted for clarity.

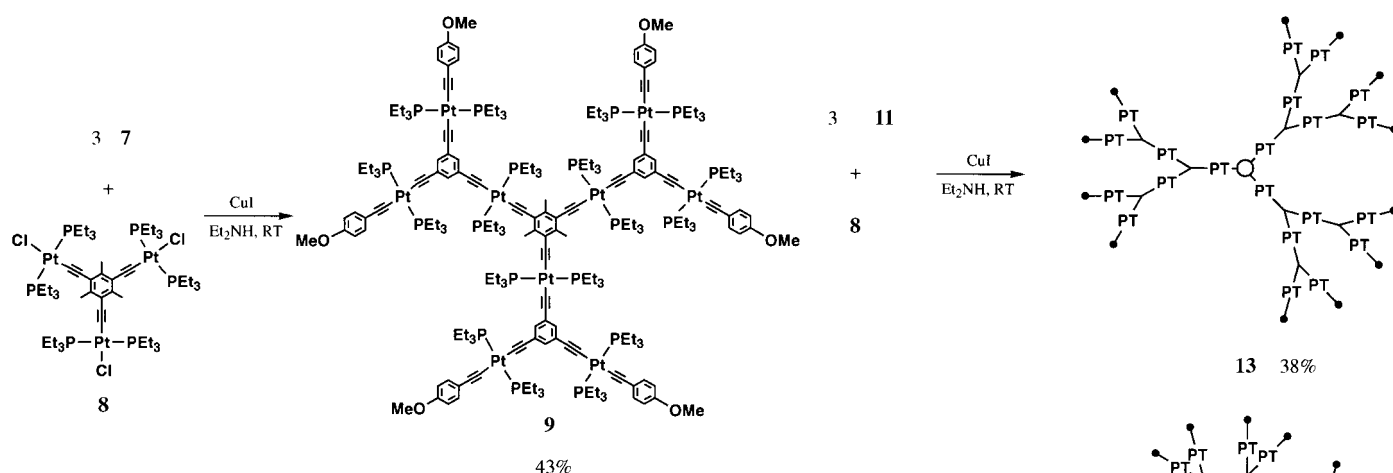


Scheme 1. Synthesis of the first-generation dendron **7**. a) $\text{HC}\equiv\text{CSiPr}_3$, $[\text{Pd}(\text{PPh}_3)_2\text{Cl}_2]$ (cat.), CuI (cat.), Et_2NH , RT, quantitative yield; b) $\text{HC}\equiv\text{CSiMe}_3$, $[\text{Pd}(\text{PPh}_3)_2\text{Cl}_2]$ (cat.), CuI (cat.), Et_3N , benzene, reflux, 90 %; c) K_2CO_3 (aq), acetone, reflux, 95 %; d) $\text{Cl}(\text{Et}_3\text{P})_2\text{Pt}\equiv\text{CC}_6\text{H}_4\text{OMe}$ **5** (2 equiv), CuI (cat.), Et_2NH , RT, 96 %; e) Bu_4NF , THF, $-78^\circ\text{C} \rightarrow \text{RT}$, 95 %.

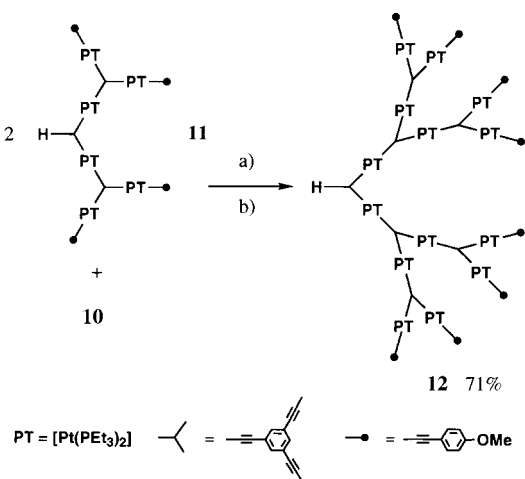
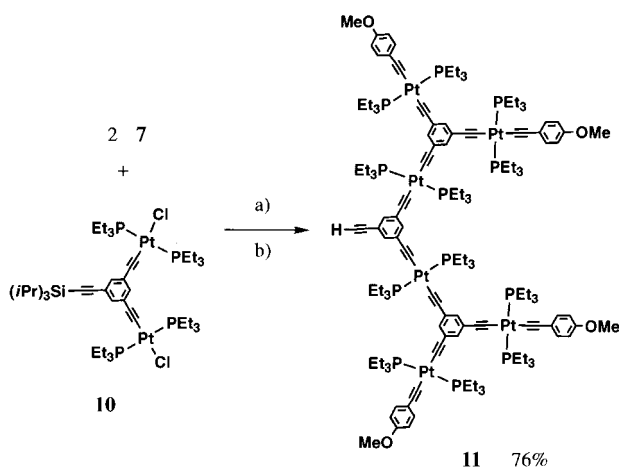
slightly longer than those of the triethynylmesitylene-bridged triplatinum complex **8** because of the strong *trans* influence of an ethynyl group relative to a chloride ligand.^[5] The coordination planes around the Pt atoms in **7** are approximately perpendicular to the aromatic plane of the central bridge and parallel to the aromatic plane of *p*-methoxyphenylethynyl groups, while in **8** the former arrangement has dihedral angles of about 60° .^[5]

The first-generation dendrimer **9**, which contained nine platinum atoms, was prepared by the reaction of **7** with the core complex **8** in a 3:1 molar ratio (Scheme 2). The ^1H NMR spectrum of **9** showed two singlets at $\delta = 2.57$ and 3.78 in a 1:2 integral ratio; the former signal is assignable to the methyl protons of the central mesitylene group and the latter to the methoxy protons of the end group. The $^{31}\text{P}\{^1\text{H}\}$ NMR spectrum of **9** exhibited two singlets at $\delta = 10.88$ ($J_{\text{Pt,P}} = 2381$ Hz) and 11.10 ($J_{\text{Pt,P}} = 2392$ Hz) in a 2:1 integral ratio, which correspond to the phosphane groups bound to the six outer and to three inner platinum atoms, respectively. These data are consistent with the expected structure of **9**, which is also supported by IR and elemental analyses.

The first-generation dendron **7** was successfully grown to a second-generation dendron **11** by the reaction with **10** in a 2:1 molar ratio, followed by desilylation of the tri(isopropyl)silyl group (Scheme 3). The similar reaction of **10** with **11** resulted in the formation of the third generation dendron **12**. Reactions of **11** and **12** with **8** in a 3:1 molar ratio led to the formation of the second and third-generation dendrimers **13**

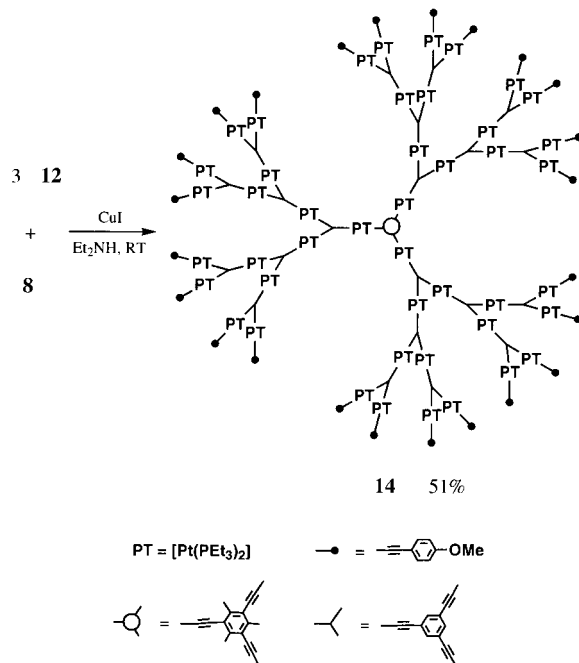


Scheme 2. Synthesis of the first generation dendrimer **9**.



Scheme 3. Synthesis of the second- and third-generation dendrimers **11** and **12**, respectively. a) CuI (cat.), Et₂NH, RT; b) Bu₄NF, THF, −78 °C → RT.

and **14**, respectively (Scheme 4). The ¹H NMR spectrum of **14** (Figure 2) is very simple in spite of it being an extremely large molecule (*M_r* = 25 840), which indicates a highly symmetric structure. Two singlet signals are observed at δ = 2.57 and 3.77 from the central mesitylene group and the methoxy end group, respectively, in a 1:8 integral ratio, which supports the proposed structure of **14**. The ³¹P{¹H} NMR spectrum of **14**



Scheme 4. Synthesis of the second- and third-generation dendrimers **13** and **14**.

showed only two signals at δ = 10.84 (*J_{Pt,P}* = 2381 Hz) and 11.04 (the coupling constant *J_{Pt,P}* could not be determined since the satellite signals were too weak to be detected) in an about 14:1 integral ratio. The latter signal is assigned to the central six phosphanes, and the former to the other eighty four phosphane atoms. To the best of our knowledge **14**, which contains 45 platinum atoms in a molecule, is one of the largest organotransition metal dendrimers and belongs to nanosize materials.

In summary, a methodology for the efficient synthesis of very large platinum–acetylide dendrimers that contain up to 45 platinum atoms has been developed by a convergent method that uses two kinds of trialkylsilyl groups. The method presented here may be applied to the synthesis of metal–acetylide dendrimers other than platinum, since several stable transition metal–acetylide complexes are already known.^[9, 11]

Received: September 9, 1998 [Z 12396 IE]
German version: *Angew. Chem.* **1999**, *111*, 737–739

Keywords: alkyne complexes • dendrimers • platinum

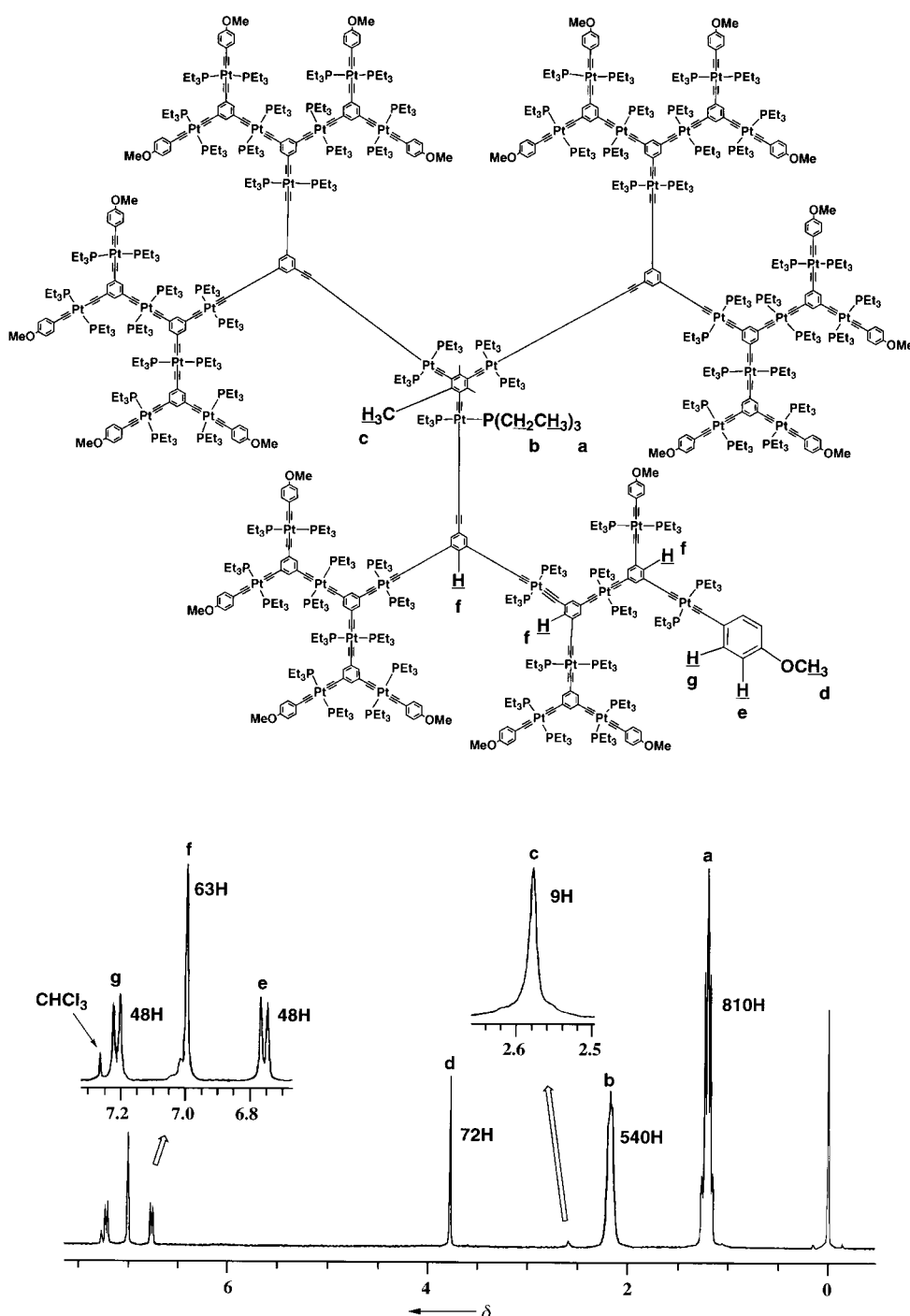


Figure 2. Structure and ^1H NMR spectrum (in CDCl_3) of the third-generation dendrimer **14**.

- [1] For reviews, see a) D. A. Tomalia, A. M. Naylor, W. G. A. Goddard III, *Angew. Chem.* **1990**, *102*, 119; *Angew. Chem. Int. Ed. Engl.* **1990**, *29*, 138; b) J. Issberner, R. Moors, F. Vögtle, *Angew. Chem.* **1994**, *106*, 2507; *Angew. Chem. Int. Ed. Engl.* **1994**, *33*, 2413; c) G. R. Newkome, C. N. Moorefield, F. Vögtle, *Dendritic Molecules. Concepts, Syntheses, Perspectives*, VCH, Weinheim, **1996**; d) H.-F. Chow, T. K.-K. Mong, M. F. Nongrum, C.-W. Wan, *Tetrahedron* **1998**, *54*, 8543; e) M. Fischer, F. Vögtle, *Angew. Chem./Angew. Chem. Int. Ed.* **1999**, in press.
- [2] a) G. R. Newkome, R. Güther, C. N. Moorefield, F. Cardullo, L. Echegoyen, E. Pérez-Cordero, H. Luftmann, *Angew. Chem.* **1995**, *107*, 2159; *Angew. Chem. Int. Ed. Engl.* **1995**, *34*, 2023; b) V. J. Catalano, N. Parodi, *Inorg. Chem.* **1997**, *36*, 537; c) C. B. Gorman, B. L. Parkhurst, W. Y. Su, K.-Y. Chen, *J. Am. Chem. Soc.* **1997**, *119*, 1141; d) C. M. Cardona, A. E. Kaifer, *J. Am. Chem. Soc.* **1998**, *120*, 4023.
- [3] a) J. W. J. Knapen, A. W. van der Made, J. C. de Wilde, P. W. N. M. van Leeuwen, P. Wijkens, D. M. Grove, G. van Koten, *Nature* **1994**, *372*, 659; b) D. Seyferth, T. Kugita, A. L. Rheingold, *Organometallics* **1995**, *14*, 5362; c) Y.-H. Liao, J. R. Moss, *Organometallics* **1996**, *15*, 4307; d) M. Bardaji, M. Kustos, A.-M. Caminade, J.-P. Majoral, B. Chaudret, *Organometallics* **1997**, *16*, 403; e) I. Cuadrado, C. M. Casado, B. Alonso, M. Morán, J. Losada, V. Belsky, *J. Am. Chem. Soc.* **1997**, *119*, 7613.
- [4] a) S. Campagna, G. Denti, S. Serrori, A. Juris, M. Venturi, V. Ricevuto, V. Balzani, *Chem. Eur. J.* **1995**, *1*, 211; b) S. Achar, J. J. Vittal, R. J. Puddephatt, *Organometallics* **1996**, *15*, 43; c) W. T. S. Huck, L. J. Prins, R. H. Fokkens, N. M. M. Nibbering, F. C. J. M. van Veggel, D. N. Reinhoudt, *J. Am. Chem. Soc.* **1998**, *120*, 6240.
- [5] a) N. Ohshiro, F. Takei, K. Onitsuka, S. Takahashi, *Chem. Lett.* **1996**, 871; b) N. Ohshiro, F. Takei, K. Onitsuka, S. Takahashi, *J. Organomet. Chem.* **1998**, *569*, 195.
- [6] a) S. Takahashi, Y. Takai, H. Morimoto, K. Sonogashira, N. Hagihara, *Mol. Cryst. Liq. Cryst.* **1982**, *82*, 139; b) S. Takahashi, Y. Takai, H. Morimoto, K. Sonogashira, *J. Chem. Soc. Chem. Commun.* **1984**, 3; c) T. Kaharu, H. Matsubara, S. Takahashi, *J. Mater. Chem.* **1992**, *2*, 43; d) T. Kaharu, R. Ishii, T. Adachi, T. Yoshida, S. Takahashi, *J. Mater. Chem.* **1995**, *5*, 687.
- [7] a) Y.-F. Lu, C. W. Harwig, A. G. Fallis, *J. Org. Chem.* **1993**, *58*, 4202; b) O. Lavastre, L. Ollivier, P. H. Dixneuf, S. Sibandhit, *Tetrahedron* **1996**, *52*, 5495; c) M. M. Haley, M. L. Bell, J. J. English, C. A. Johnson, T. J. R. Weakley, *J. Am. Chem. Soc.* **1997**, *119*, 2956.
- [8] S. Takahashi, Y. Kuroyama, K. Sonogashira, N. Hagihara, *Synthesis* **1980**, 627.
- [9] K. Sonogashira, T. Yatake, Y. Tohda, S. Takahashi, N. Hagihara, *J. Chem. Soc. Chem. Commun.* **1977**, 291.
- [10] Crystallographic data for **7**: $\text{C}_{54}\text{H}_{78}\text{O}_2\text{P}_4\text{Pt}_2$ ($M_r = 1273.28$), monoclinic, space group $P2_1/c$ (No. 14), $a = 24.461(3)$, $b = 10.286(3)$, $c = 22.814(4)$ Å, $\beta = 106.50(1)^\circ$, $V = 5503(1)$ Å³, $Z = 4$, $\rho_{\text{calcd}} = 1.536$ g cm⁻³, $\mu(\text{MoK}\alpha) = 52.10$ cm⁻¹, -75°C , ω - 2θ scan, $6 < 2\theta < 55^\circ$, R (R_w) = 0.051 (0.061) determined by full-matrix least-squares method for 559 parameters against 6391 reflections with $I > 3.0\sigma(I)$ from 12 638 unique reflections ($R_{\text{int}} = 0.037$), GOF = 1.07. Crystallographic data (excluding structure factors) for the structure reported in this paper have been deposited with the Cambridge Crystallographic Data Centre as supplementary publication no. CCDC-102875. Copies of the data can be obtained free of charge on application to CCDC, 12 Union Road, Cambridge CB2 1EZ, UK (fax: (+44) 1223-336-011; e-mail: deposit@ccdc.cam.ac.uk).
- [11] M. I. Bruce, M. G. Humphrey, J. G. Matisons, S. K. Roy, A. G. Swincer, *Aust. J. Chem.* **1984**, *37*, 1955.

$\text{Ln}_2\text{Al}_3\text{Si}_2$ (Ln = Ho, Er, Tm): New Silicides from Molten Aluminum—Determination of the Al/Si Distribution with Neutron Crystallography and Metamagnetic Transitions**

Xian-Zhong Chen, Bradley Sieve, Robert Henning, Arthur J. Schultz, Paul Brazis, Carl R. Kannewurf, Jerry A. Cowen, Richard Crosby, and Mercouri G. Kanatzidis*

Silicides are both scientifically and technologically important, and have been extensively studied during the past several decades.^[1] Various topics and review articles can be found regarding their preparation, properties, crystal chemistry,^[2] thermodynamics,^[3] applications in silicon technology,^[4] and materials aspects for advanced technologies.^[5] Silicides are typically synthesized by direct reaction of the elements with heating to over 1000 °C and often with the necessary use of an arc-welder or induction furnace. Although single crystals can sometimes be obtained by annealing or quenching the product, in most situations only powder samples are formed with these traditional methods. This can complicate structure determinations and limit proper characterization. Recently, we have initiated exploratory synthetic investigations of silicides using metal fluxes and find that many new aluminum silicides form, most with novel structure types.^[6] These compounds usually decompose rapidly upon contact with acid, but they can be easily separated from the excess Al flux with aqueous sodium hydroxide solution. The products often consist of many single crystals with nice shapes. Here we present our results for the Ln/Al/Si systems (Ln = Ho, Er, Tm). There are few examples of rare earth aluminum silicides in the literature.^[7] Most of them were synthesized as powders, and their crystal structures have not been determined or refined. As for Ho, Er, and Tm, only $\text{Ln}_6\text{Al}_3\text{Si}$ (Ln = Ho, Tm)^[8] and Er_4AlSi_3 ^[9] have been described. Here we report on the new aluminum silicides $\text{Ln}_2\text{Al}_3\text{Si}_2$ (Ln = Ho, Er, Tm) synthesized in Al metal flux.

The black compounds $\text{Ln}_2\text{Al}_3\text{Si}_2$ ^[10] (Ln = Ho, Er, Tm) are stable in the air, water, and aqueous NaOH solution, but decompose instantaneously in aqueous HCl to release a gas which ignites upon contact with air. Mass spectrometry showed that the gas contains disilane (Si_2H_6) with a small amount of SiH_4 and there are no trisilanes or higher silanes detected. The lanthanides Ho, Er, and Tm behave differently from others in the series. For example La, Ce, Pr, Nd, and Sm give LnAlSi ,^[11] whereas La, Sm, Tb, and Yb give LnAl_2Si_2 .^[11] Neither of these two types of compounds has been found for Ho, Er, and Tm so far. Instead, the $\text{Ln}_2\text{Al}_3\text{Si}_2$ and LnAl_2Si ^[12] families seems to be more stable.

The three $\text{Ln}_2\text{Al}_3\text{Si}_2$ compounds are isostructural ($\text{Y}_2\text{Al}_3\text{Si}_2$ -type^[13]); they possess an $[\text{Al}_3\text{Si}_2]^{6-}$ framework filled with rare earth cations (Figure 1). The positions of Al and Si, which are

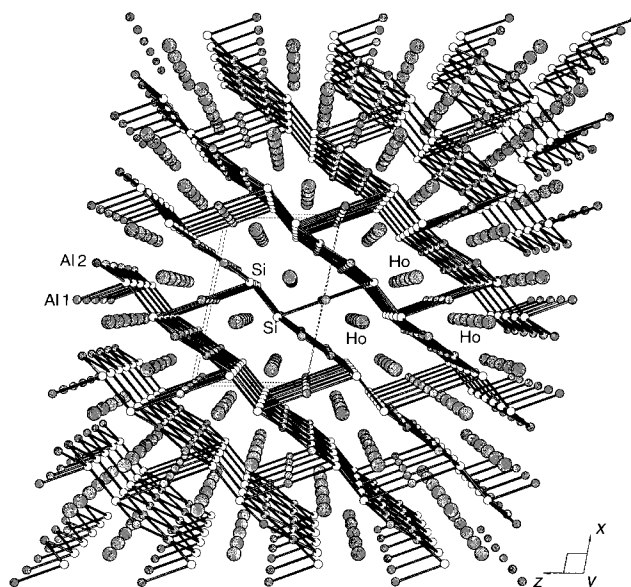


Figure 1. Perspective view of the structure of $\text{Ln}_2\text{Al}_3\text{Si}_2$ (Ln = Ho, Er, Tm).

almost impossible to determine on the basis of X-ray diffraction studies only, were decided on the basis of reasonableness of bond lengths around Al and Si. This choice was validated by the results of a neutron diffraction study (see below). In the $[\text{Al}_3\text{Si}_2]^{6-}$ framework, parallel Al–Al zigzag chains (by Al2) along the *b* direction are bridged by Si–Si dimers to form Al_2Si_2 layers perpendicular to the *ac* plane (Figure 2 A). The distances Al2–Al2, Al2–Si, and Si–Si are 2.768, 2.600, and 2.369 Å, respectively. Within the Al_2Si_2 layer, chairlike hexagonal rings that are formed by Si and Al2 atoms and edge-sharing along the *b* direction can also be seen. These layers are linked together by Al1 atoms, through linear Si–Al–Si bonds with a Si–Al distance of 2.721 Å, to form a three-dimensional structure. The structure shows parallel tunnels along the *b* direction, and two rows of rare earth atoms sit in each tunnel. Within each tunnel, the Ln–Ln distances are 4.027 (Ln = Ho), 4.018 (Ln = Er), and 4.005 Å (Ln = Tm), respectively, in each row and 3.765 (Ln = Ho), 3.754 (Ln = Er), and 3.749 Å (Ln = Tm), respectively, between the two rows. The shortest Ln–Ln distances, however, of 3.670, 3.648, and 3.628 Å for Ln = Ho, Er, and Tm, respectively, are found

- [*] Prof. Dr. M. G. Kanatzidis, Dr. X.-Z. Chen, B. Sieve
Department of Chemistry
Michigan State University
East Lansing, Michigan 48823 (USA)
Fax: (+1) 517-353-1793
E-mail: kanatzid@argus.cem.msu.edu
- R. Henning, Dr. A. J. Schultz
Argonne National Laboratory, IPNS, Bldg. 360
Argonne, IL 60439-4814
- P. Brazis, Prof. C. R. Kannewurf
Department of Electrical Engineering and Computer Science
Northwestern University, Evanston, IL 60208 (USA)
- Prof. J. A. Cowen, R. Crosby
Department of Physics and Center for Fundamental Materials Research
Michigan State University, East Lansing, MI 48824-1322
- [**] M.G.K. is a Camille and Henry Dreyfus Teacher Scholar 1993–1998. This work made use of the SEM facilities of the Center for Electron Optics at Michigan State University. Work at Argonne National Laboratory is sponsored by the Department of Energy, Office of Basic Energy Sciences (contract no. W-31-109-ENG-38).

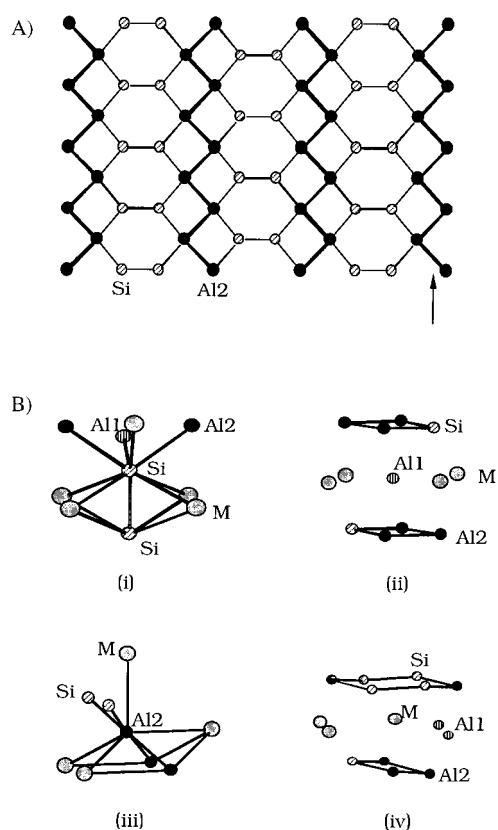


Figure 2. A) The structure of the Al_2Si_2 layer with atom labeling. The Al zigzag chains are marked with an arrow. B) The coordination environments of each atom in $\text{Ln}_2\text{Al}_3\text{Si}_2$ ($\text{Ln} = \text{Ho}, \text{Er}, \text{Tm}$).

between Ln atoms in adjacent tunnels and right above and below the Si–Si dimers. The presence of Si–Si dimers in the structure is consistent with mass spectrometry experiments which indicate the release of disilane upon treatment with acid. No trisilanes or higher silanes were detected. The coordination environments for different atoms are shown in Figure 2B.

To unequivocally determine the correct Al and Si positions in the structure, we performed a single-crystal neutron crystallographic analysis on $\text{Ho}_2\text{Al}_3\text{Si}_2$.^[14] The scattering neutron cross-sections of Al and Si differ by about 25%, which is enough to distinguish them from one another.^[15] Tables 1 and 2 show the atomic coordinates and selected bond distances obtained with this analysis, and they are in excellent agreement with those obtained from X-ray diffraction studies. This suggests that using expected bond lengths as a criterion for assigning Si and Al positions may be appropriate in most aluminum silicides, although the criterion will probably fail when high coordination numbers (>6) are involved.

The electrical conductivity and thermopower data on single crystals of the compounds indicate a p-type metallic behavior

Table 1. Atomic positions for $\text{Ho}_2\text{Al}_3\text{Si}_2$ as determined from the neutron diffraction data.

Atom	<i>x</i>	<i>y</i>	<i>z</i>	<i>U</i> / <i>U</i> _c × 100
Ho	0.61981(8)	0	0.32319(12)	0.46
Si	0.90690(16)	0	0.36033(23)	0.75
Al1	0	0	0	1.19
Al2	0.30502(21)	0	0.13414(29)	0.97

Table 2. Selected bond lengths [Å] for $\text{Ho}_2\text{Al}_3\text{Si}_2$ as determined from the neutron diffraction data.

Ho–Ho	3.6667(16)	Si–Si	2.3706(30)
Ho–Ho	3.7543(13)	Si–Al1	2.7129(15)
Ho–Si	2.8708(18)	Si–Al2	2.5983(15)
Ho–Si	2.9934(13)	Al1–Al2	3.0471(20)
Ho–Si	2.9459(12)	Al1–Al2	3.0646(15)
Ho–Al1	3.0117(7)	Al2–Al2	2.7688(25)
Ho–Al2	3.5077(20)		
Ho–Al2	3.1628(16)		

for all three compounds (see Figure 3 for data on $\text{Ho}_2\text{Al}_3\text{Si}_2$). The room-temperature conductivity of all compounds is very high at about $40\,000\text{ S cm}^{-1}$, while the corresponding thermopower is lower than $+3\text{ }\mu\text{V K}^{-1}$. Magnetic susceptibility data for $\text{Ho}_2\text{Al}_3\text{Si}_2$ are presented in Figure 4A. $\text{Tm}_2\text{Al}_3\text{Si}_2$ and $\text{Ho}_2\text{Al}_3\text{Si}_2$ show an antiferromagnetic (AF) transition with a

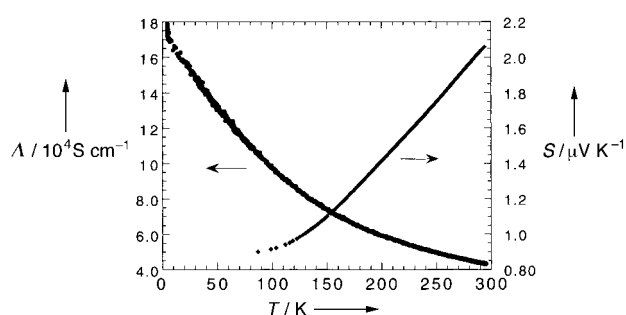


Figure 3. A) Temperature-dependent, four-probe electrical conductivity λ and thermopower data S for a single crystal of $\text{Ho}_2\text{Al}_3\text{Si}_2$.

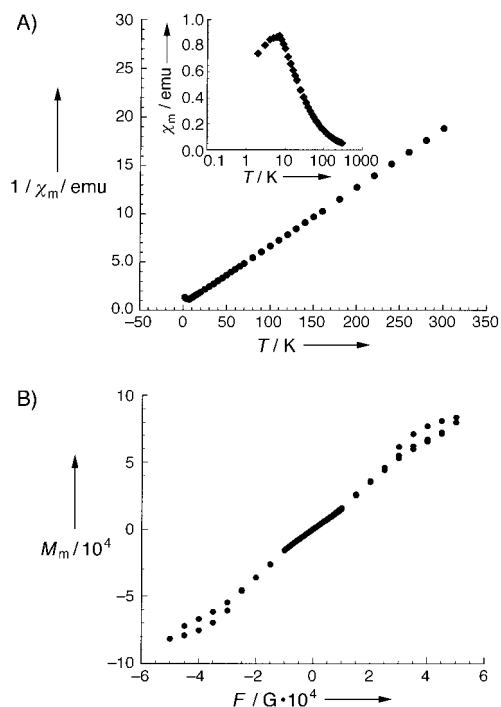


Figure 4. A) Plots of molar magnetic susceptibility χ_m [emu mol^{-1}] and $1/\chi_m$ [mol emu^{-1}] versus temperature [K] for $\text{Ho}_2\text{Al}_3\text{Si}_2$. Inset: an enlargement of the AF transition ($\lg T$ scale). B) Molar magnetization M_m of $\text{Ho}_2\text{Al}_3\text{Si}_2$ as a function of field strength F (hysteresis at 2.5 K). The magnetic susceptibilities were measured on ground crystals with a Quantum Design SQUID magnetometer between 2 and 300 K.

Néel temperature T_N of 7 K. Above this temperature, the data for both compounds follow the Curie–Weiss law, with Curie temperatures $\theta = -10.5$ and 4 K for $\text{Ho}_2\text{Al}_3\text{Si}_2$ and $\text{Tm}_2\text{Al}_3\text{Si}_2$, respectively. The AF transition for $\text{Er}_2\text{Al}_3\text{Si}_2$ occurs below 4 K. The measured effective magnetic moment at 300 K is $11.2 \mu_B$ for $\text{Ho}_2\text{Al}_3\text{Si}_2$ and $7.58 \mu_B$ for $\text{Tm}_2\text{Al}_3\text{Si}_2$; these values are close to the theoretical μ_{eff} for Ln^{3+} ($10.61 \mu_B$ for Ho^{3+} and $7.56 \mu_B$ for Tm^{3+}). Well below the AF transition temperature, the hysteresis, $M(H)$, curves taken on powder samples of the Tm and Ho compounds exhibit an inflection point at a critical field of about 6 kG with an increase in slope at higher fields. Such behavior is characteristic of the “spin-flop” transition in an antiferromagnet when the field is applied along the direction of sublattice magnetization. The magnetization of powder samples of the Ho compound has a similar inflection point at about 30 kG, which is characteristic of a metamagnetic transition. Data on single-crystal samples are necessary for the complete understanding of the magnetic properties of these isostructural compounds.^[16]

Three new rare earth aluminum silicides $\text{Ln}_2\text{Al}_3\text{Si}_2$ (Ln = Ho, Er, Tm) have been synthesized in molten Al.^[17] The Al flux acts as a good carrier for Si by solubilizing it and making it available for reaction, without forming a binary Al/Si compound. In the absence of Si, such reactions yield a variety of novel aluminides.^[18, 19] The compounds $\text{Ln}_2\text{Al}_3\text{Si}_2$ show an antiferromagnetic transition at low temperature and undergo “spin-flop” metamagnetic transitions upon the application of strong magnetic fields.

Experimental Section

Synthesis: In a N_2 -filled box, Ln metal (Ln = Ho, Er, Tm), Si, and Al were mixed in a vial in several different molar ratios with a large excess of Al and transferred into alumina containers, which were flame sealed in silica tubes under high vacuum. The samples were heated to 1000°C for 3 d, and then cooled to 300°C at -7.3°h^{-1} and finally to room temperature. The products were isolated as shiny black crystals after treatment with aqueous NaOH.

Single-crystal X-ray diffraction data were collected at room temperature with a Rigaku 4-circle diffractometer with MoK_α radiation ($\lambda = 0.71073 \text{ \AA}$). Empirical absorption corrections, based upon ψ scans, were applied to the data. The structures were solved by direct methods. All calculations including structural refinements were performed by using the TEXSAN^[20] crystallographic software package. As in all Al- and Si-containing intermetallic compounds, Al and Si are difficult to distinguish. The current model gives the lowest R values, the best temperature factors, and a composition that is most consistent with the elemental analysis determined by energy-dispersive spectroscopy (EDS). As expected, the Ln–Si (Ln = Ho, Er, Tm) distances are shorter than the Ln–Al distances, and the Si–Al distances are longer than the Si–Si distance. More significantly, the bond distances clearly reveal the correct positions of the Al and Si atoms, and this is supported by the results of neutron diffraction experiments.

Received: March 2, 1998

Revised version: October 29, 1998 [Z11541 IE]

German version: *Angew. Chem.* **1999**, *111*, 695–698

Keywords: aluminum • conducting materials • lanthanides • magnetic properties • silicon

- [1] A. Szytuda, J. Leciejewicz in *CRC Handbook of Crystal Structures and Magnetic Properties of Rare Earth Intermetallics*, CRC Press, Boca Raton, FL, **1994**, p. 110, and references therein.
- [2] B. Aronsson, T. Lundström, S. Rundqvist in *Borides, Silicides and Phosphides*, Methuen, London, **1965**.

- [3] a) M. E. Schlesinger, *Chem. Rev.* **1990**, *90*, 607–628; b) T. G. Chart, *A Critical Assessment of Thermochemical Data for Transition Metal-Silicon Systems*, National Physical Laboratory, Teddington (UK), **1972** (NPL report on Chemistry 18).
- [4] A. H. Reader, A. H. Vanommen, P. J. W. Weijss, R. A. M. Wolters, D. J. Oostra, *Rep. Prog. Phys.* **1993**, *56*(11), 1397–1467.
- [5] K. Maex, *Appl. Surf. Sci.* **1991**, *53*, 328–337.
- [6] X. Z. Chen, S. Sportouch, B. Sieve, J. Cowen, C. R. Kannewurf, P. Brazis, M. G. Kanatzidis, *Chem. Mater.* **1998**, *10*, 3202–3211.
- [7] There exist several older reports on the production of binary compounds such as LnSi_2 , ThSi_2 , MoSi_2 , and WSi_2 with the use of molten aluminum. However, most of these materials are in fact metal aluminum silicides (e.g. LnAlSi) rather than metal silicides: X. Z. Chen, B. Sieve, M. Zhuravleva, P. Brazis, C. R. Kannewurf, M. G. Kanatzidis, unpublished results; a) O. Höningschmid, *Monatshefte Chemie* **1906**, *27*, 1069; b) G. Brauer, A. Mitius, *Z. Anorg. Allg. Chem.* **1942**, *249*, 325–339; c) G. Brauer, H. Haag, *Z. Anorg. Allg. Chem.* **1952**, *267*, 198–212.
- [8] I. S. Dubenko, A. A. Evdokimov, Yu. N. Titov, *Russ. J. Inorg. Chem. Engl. Transl.* **1985**, *30*(11), 1707–1708.
- [9] A. Raman, *Inorg. Chem.* **1968**, *7*, 973–976.
- [10] Single-crystal X-ray diffraction data were collected at room temperature with a Rigaku four-circle diffractometer with MoK_α radiation ($\lambda = 0.71073 \text{ \AA}$). Crystal data for $\text{Ln}_2\text{Al}_3\text{Si}_2$ (Ln = Ho, Er, Tm): crystal sizes $0.10 \times 0.07 \times 0.35$ (Ln = Ho), $0.14 \times 0.08 \times 0.40$ (Ln = Er), $0.10 \times 0.06 \times 0.10$ (Ln = Tm); $a = 10.126(1)$, $b = 4.0266(9)$, $c = 6.5812(8) \text{ \AA}$, $\beta = 100.93(1)^\circ$, $V = 263.48(7) \text{ \AA}^3$ (Ln = Ho); $a = 10.083(3)$, $b = 4.0175(9)$, $c = 6.566(1) \text{ \AA}$, $\beta = 100.73(2)^\circ$, $V = 261.3(1) \text{ \AA}^3$ (Ln = Er); $a = 10.043(2)$, $b = 4.0050(8)$, $c = 6.550(3) \text{ \AA}$, $\beta = 100.54(3)^\circ$, $V = 259.0(1) \text{ \AA}^3$ (Ln = Tm); space group $C2/m$, $Z = 2$; $\mu = 30.968$ (Ln = Ho), 33.127 (Ln = Er), 35.204 mm^{-1} (Ln = Tm); total reflections: 1408 (Ln = Ho), 1754 (Ln = Er), 1720 (Ln = Tm); unique: 343 [$R(\text{int}) = 0.036$, Ln = Ho], 434 [$R(\text{int}) = 0.033$, Ln = Er], 430 [$R(\text{int}) = 0.077$, Ln = Tm]; observed ($I > 3\sigma$): 338 (Ln = Ho), 429 (Ln = Er), 418 (Ln = Tm); index ranges $-13 \leq h \leq 13$, $-5 \leq k \leq 5$, $-9 \leq l \leq 9$ (Ln = Ho), $-14 \leq h \leq 14$, $-6 \leq k \leq 6$, $-9 \leq l \leq 9$ (Ln = Er), $-14 \leq h \leq 14$, $-6 \leq k \leq 6$, $-9 \leq l \leq 9$ (Ln = Tm); $R/wR(I > 3\sigma)$ and GOF: 0.039/0.043 and 2.76 (Ln = Ho), 0.027/0.034 and 2.10 (Ln = Er), 0.026/0.032 and 1.43 (Ln = Tm), where $R = \Sigma ||F_o| - |F_c|| / \Sigma |F_o|$ and $wR = [(\Sigma w(|F_o| - |F_c|)^2) / \Sigma wF_o^2]^{1/2}$.
- [11] X. Z. Chen, M. Zhuravleva, P. Small, C. R. Kannewurf, P. Brazis, J. A. Cowen, R. Crosby, M. G. Kanatzidis, unpublished results.
- [12] P. Small, M. Zhuravleva, B. Sieve, M. G. Kanatzidis, unpublished results.
- [13] T. I. Yanson, M. B. Manyakov, O. I. Bodak, R. E. Gladyshevskii, R. Cerny, K. Yvon, *Acta Crystallogr. Sect. C* **1994**, *50*, 1377.
- [14] A single crystal ($1 \times 1 \times 2 \text{ mm}^3$) of $\text{Ho}_2\text{Al}_3\text{Si}_2$ was mounted on an aluminum pin and placed on the SCD diffractometer at the Intense Pulsed Neutron Source (IPNS) at Argonne National Laboratory. A position-sensitive area detector was used to obtain time-of-flight Laue data with a wavelength range of $0.7 - 4.2 \text{ \AA}$ for 25 settings of the crystal to cover two octants of reciprocal space. The details of the data collection and analysis procedures have been described previously.^[14a] A wavelength-dependent spherical absorption correction was applied.^[14b] Since extinction is strongly dependent on wavelength, symmetry-related reflections were not averaged. The structural refinement was performed using the GSAS program.^[14c] Since the ordering of the aluminum and silicon atoms needed to be determined, several models were refined with the anions in various positions. The lowest R value was obtained with the original model (determined from bond distance arguments), while the R value was at least 1.5% higher when the anions were switched. The anisotropic thermal parameters also suggested that the original model was correct. The fractional occupancies of the aluminum and silicon positions were also refined in each model to see if any mixing occurs on the sites. The occupancies of the aluminum and silicon in the original model obtained from X-ray diffraction refined to unity within 3σ , while the occupancies in the other models refined to 0.18(1) with aluminum on a silicon site and 0.82(1) with silicon on an aluminum site. These values are consistent with fully occupied silicon and aluminum positions. The neutron data confirm that the X-ray diffraction model is correct and that no disorder occurs between the aluminum and silicon positions.

- a) A. J. Schultz, K. Srinivasan, R. G. Teller, J. M. Williams, C. M. Lukehart, *J. Am. Chem. Soc.* **1984**, *106*, 999; b) R. A. J. Jacobson, *Appl. Crystallogr.* **1986**, *19*, 283; c) A. C. Larson, R. B. Von Dreele, *GSAS-General Structure Analysis System*, Los Alamos National Laboratory, **1994**.
- [15] Radiation: neutrons, $\lambda = 0.7\text{--}4.2\text{ \AA}$; data collection by the time-of-flight Laue technique with a position-sensitive area detector; $i(\theta)$ [cm^{-1}] = $0.195 + 0.550\theta$; extinction parameter g [rad^{-1}] = $2.1(1) \times 10^{-5}$; number of reflections in the final least-squares refinement with $F_o^2 > 3\sigma(F_o^2)$ 841; number of unique reflections 728; variables 48; minimized function $\sum w(F_o - F_c)^2$; $R_w(F_o^2) = 0.110$, $R(F^2) = 0.112$, $R_w(F) = 0.054$, $R(F) = 0.064$, GOF = 5.87.
- [16] B. Sieve, J. A. Cowen, M. G. Kanatzidis, unpublished results.
- [17] Recently we discovered that $\text{Dy}_2\text{Al}_3\text{Si}_2$ is isostructural to the compounds reported here, and it too exhibits a metamagnetic transition.
- [18] a) S. Niemann, W. Jeitschko, *J. Solid State Chem.* **1995**, *114*, 337–341; b) S. Niemann, W. Jeitschko, *Z. Kristallogr.* **1995**, *210*, 338–341; c) S. Niemann, W. Jeitschko, *J. Solid State Chem.* **1995**, *116*, 131–135; d) S. Niemann, W. Jeitschko, *J. Alloys Compd.* **1995**, *221*, 235–239.
- [19] P. C. Canfield, Z. Fisk, *Philos. Mag. B* **1992**, *65*, 1117–1123.
- [20] "TEXSAN—TEXRAY Structure Analysis Package", Molecular Structure Corporation, The Woodlands, TX, **1992**.

Functional Molecular Thin Films: Topological Templates for the Chemoselective Ligation of Antigenic Peptides to Self-Assembled Monolayers**

Lukas Scheibler, Pascal Dumy, Mila Boncheva, Kirsten Leufgen, Hans-Jörg Mathieu, Manfred Mutter, and Horst Vogel*

The study of molecular thin films for use in the controlled design of interfacial properties^[1] that have important implications in many different fields ranging from research on friction, lubrication and wetting,^[2] development of micro- and nanoscale devices^[3] to biocompatible surfaces, has attracted considerable interest.^[4] Most of the work has concentrated on

self-assembled monolayers (SAMs), in particular on the self-assembly of sulfur-bearing molecules such as thioalkanes^[5] and lipids^[6] on the surface of gold, or suitable silanes to hydroxylated surfaces (usually silicon oxide or glass).^[7] Self-assembled molecular thin films that comprise biopolymers are most interesting for the development of novel analytical techniques.^[8] Several novel micropatterning techniques have opened the possibility for the creation of multiarray sensor devices on the level of SAMs.^[9] In particular in the latter case, a generally applicable method for the design and synthesis of complex functional peptides suitable for the integration into SAMs is still a demanding task. We have shown recently that tethering template-assembled synthetic proteins (TASP) that expose metal or antigenic binding sites to SAMs results in highly sensitive and selective functional surfaces.^[10, 11] Here we elaborate novel strategies based on the template concept for the regioselective functionalization of SAMs on gold surfaces. In particular, regioselectively addressable functional templates (RAFT) that feature differentially reactive, spatially distinguishable domains in combination with chemoselective ligation procedures are used for the covalent attachment of antigenic peptides to SAMs. The formation of the SAM, its functionalization by several consecutive surface chemistry reactions, and the final binding of antibodies to the tethered TASP, were monitored and controlled by surface plasmon resonance (SPR), time-of-flight secondary-ion mass spectrometry (TOF-SIMS), and Fourier transform infrared (FTIR) spectroscopy. These methods are capable of measuring molecular reactions on gold surfaces: SPR delivers direct and continuous information on the mean concentration of the molecules on the surface during the formation of monomolecular films, TOF-SIMS allows the direct analysis of the chemical composition of SAMs, FTIR spectra carry information on both the presence of specific functional groups and the conformation of the molecules on the gold surface. The FTIR spectra were obtained by a recently developed attenuated total reflection (ATR) technique where the ATR crystal was covered by a gold film that is thin enough to be transparent for the infrared light but thick enough to serve as a continuous gold surface for the formation of SAMs by thioalkanes.^[12]

As a representative example of this general approach of functionalizing SAMs we covalently coupled a derivative of the antigenic (NANP)₃ peptide to a SAM of topological templates. This peptide was chosen because of its relevance to the immune response against malaria parasites; in another context it has been immobilised on gold surfaces by thioalkane linkers.^[13] As the RAFT molecule we used a cyclic peptide of the sequence $c[(\text{K}(\text{Boc})\text{K}(\text{Boc})\text{PGK}(\text{Alloc}))_2]$ **1**, which features orthogonally protected attachment sites on opposite faces of the cycle.^[14] Carboxythioalkanes were attached in bulk solution to the lower face of the deprotected K(Alloc) side chains of the template **1**, followed by the coupling of serines to the remaining deprotected K(Boc) sites of the serine groups. Subsequently, the RAFT molecule **2** was self-assembled on a gold surface through the thioalkane linkers. The hydroxyl groups on the four serine side chains that are on the upper face of the template were oxidized to aldehyde functions (Figure 1). Finally, the aminooxyacetyl-containing antigenic peptide **4** was ligated to the surface-

[*] Prof. H. Vogel, Dr. M. Boncheva,^[+] Dr. K. Leufgen
LCPPM, Institute of Physical Chemistry
Swiss Federal Institute of Technology Lausanne (EPFL)
CH-1015 Lausanne (Switzerland)
Fax: (+41)21-693-6190
E-mail: horst.vogel@epfl.ch

Prof. M. Mutter, Dr. L. Scheibler,^[++] Prof. P. Dumy^[+++]
Institute of Organic Chemistry, University of Lausanne
(Switzerland)

Prof. H.-J. Mathieu
LMCH, Institute of Material Sciences, EPFL (Switzerland)

[+] Current address:
Chalmers University of Technology
Department of Physical Chemistry, Göteborg (Sweden)

[++] Current address:
Harvard Institute of Medicine
Division of Bone and Mineral Metabolism, Boston (USA)

[+++] Current address:
LEDSS, Université J. Fourier, Grenoble, (France)

[**] This work was financially supported by the Board of the Swiss Federal Institutes of Technology (MINAST: 7.06).

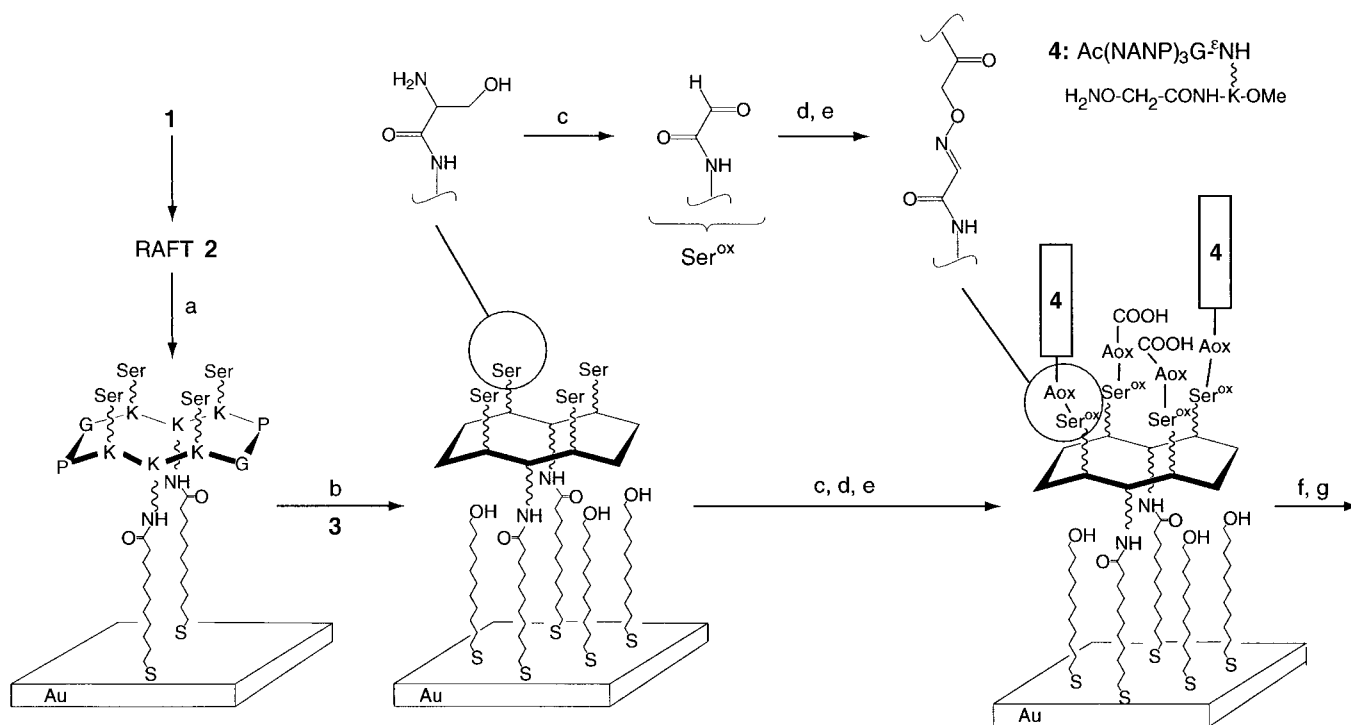


Figure 1. Individual reaction steps of the TASP synthesis on a gold surface: a) Self-assembly of **2** on the surface, b) blocking of the remaining bare gold surfaces (gaps and defects in the SAM) by 11-sulfanylundecanol (**3**), c) oxidation of N-terminal serine residues, d) chemoselective ligation of peptide **4** to the surface, e) blocking of the remaining terminal aldehyde groups. The thus functionalized gold surface comprises receptor sites for the selective binding of the monoclonal antibody (f), which can finally be displaced from the surface under controlled conditions by the application of excess free antigen Ac-(NANP)₃G-OH to the bulk solution (g). Steps (a)–(f) were observed by ATR–FTIR spectroscopy (Figure 2), steps (c) and (e) by TOF–SIMS (Figure 3), steps (a)–(g) by SPR measurements (Figure 4). The amino acid residues are given in one letter code except for serine so that it can be distinguished from the terminal sulfur atom attached to the gold surface.

assembled RAFT by formation of oxime bonds.^[15] The resulting monomolecular film on the gold surface contained functionalities for the selective and reversible binding of the monoclonal antibody Sp3E9, which is directed against the NANP peptide. The whole sequence of surface reactions comprises seven individual steps:

a) A SAM was formed by adsorption of **2** from a methanolic solution onto a gold surface. A resonance angle shift of $\Delta\theta = 0.37^\circ$ was observed by SPR, which corresponds to a mean surface area of 240 \AA^2 for an individual molecule of **2**. This value is somewhat higher than expected from the template geometry, possibly as a consequence of the bulkiness of the carboxythioalkane chains and serine residues attached to the template. The FTIR spectrum of **2** on gold shows the amide I and II bands at similar wavenumbers and with similar shapes (Figure 2, (a)–Au) as their counterparts in the bulk material on ATR plates.

b) The remaining bare gold surfaces that result from gaps and defects in the SAM of **2** were filled by adsorption of 11-sulfanylundecanol (**3**) from a solution in ethanol/water (1/1). This modification resulted in the appearance of an OH-bending band at 1640 cm^{-1} in the FTIR spectrum (Figure 2, (b)–(a)). The SPR resonance angle was shifted by $\Delta\theta = 0.18^\circ$.

c) The serine-terminated template monolayers were oxidized by a solution of NaIO_4 in citric acid/sodium phosphate buffer (pH 3.3) for 20 min. As a result of the small change of the molecular mass this reaction was not detectable by SPR;

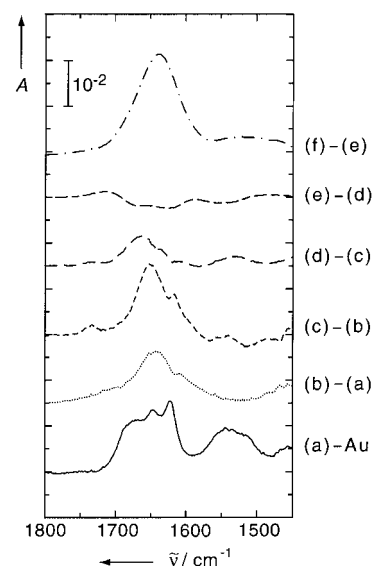


Figure 2. ATR–FTIR difference spectra of the monomolecular layers at gold surfaces for the consecutive reaction steps (a) to (f) (see text and Figure 1).

however, a new band at 1660 cm^{-1} in the FTIR spectrum could be attributed to the formation of aldehyde groups in the template (Figure 2, (c)–(b)). This was confirmed in the TOF–SIMS spectrum (Figure 3A) by a signal at m/z 1702, which corresponds to the molecular ion of the template oxidized at all four serine residues.

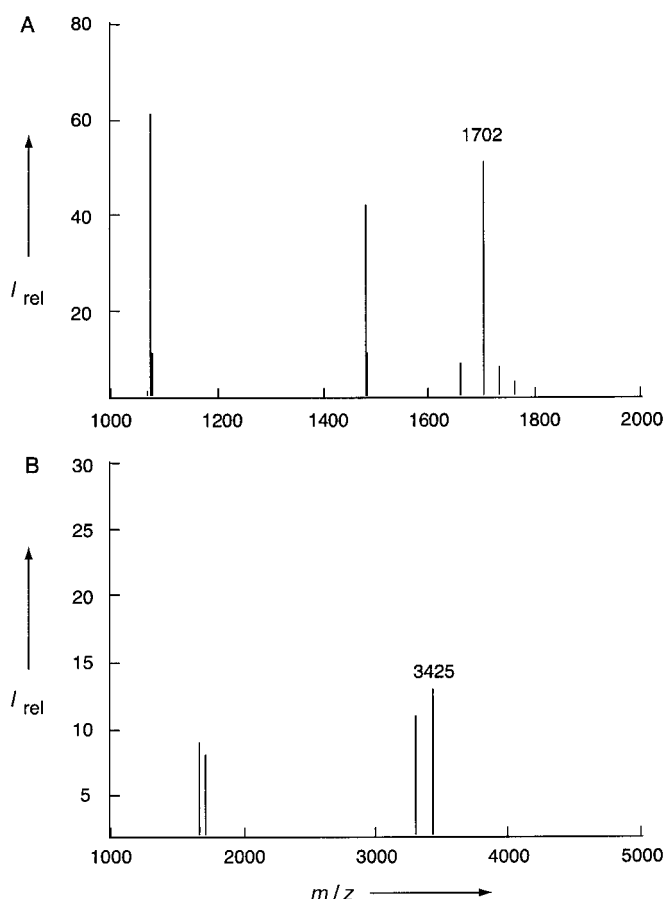


Figure 3. TOF-SIMS spectra of negative secondary ions recorded A) after step (c) and B) after step (e) of the reaction scheme shown in Figure 1.

d) The coupling of peptide **4** to the modified RAFT molecule was performed overnight at room temperature, again in the citric acid/sodium phosphate buffer. Two new bands appeared at 1657 and 1528 cm^{-1} in the FTIR spectrum (Figure 2, (d)–(c)). These bands correspond to the amide I and II bands of the peptide **4**, which were observed at similar positions in the bulk peptide sample. An SPR resonance angle shift of $\Delta\theta = 0.50^\circ$ was finally obtained; this corresponds to the condensation of about two molecules of **4** (mean surface area of 115 \AA^2) to each of the adsorbed RAFT molecules. Incomplete oxidation of the serine residues on the template can be excluded as the origin of this partial saturation of the attachment sites on **2** by **4**, as a prolonged oxidation (step c) did not result in a higher surface density of **4** as measured by SPR. In accordance with earlier observations,^[13b] peptide **4** seems to be sterically saturated at the surface of the monomolecular film. In contrast to the situation at the SAM surface, all ligation sites of **2** can be selectively functionalized in solution.

e) The unchanged terminal aldehyde functions at the monolayer were modified by treatment with excess aminoxyacetic acid. This step affected neither the SPR nor the FTIR spectra (Figure 2, (e)–(d)), but the corresponding reaction products were clearly visible in the TOF-SIMS spectrum (Figure 3B): The peak at m/z 425 corresponds to a RAFT molecule with one molecule of **4** and three serine

residues modified by aminoxyacetic acid. The lack of a peak corresponding to RAFT molecules with two or more peptide molecules per template might be a result of the low desorption and transmission probability of this extremely high mass secondary ion.

f) The activity of the tethered TASP layer was assayed by antibody binding experiments: the functionalized monolayer at the gold surface was incubated with a $4.7 \times 10^{-7} \text{ M}$ solution of the antibody in PBS buffer. This produced an intense amide I band at 1640 cm^{-1} (Figure 2, (f)–(e)) in quantitative agreement with the FTIR spectrum of the bulk antibody sample. Concomitant SPR measurements showed a shift in the resonance angle of $\Delta\theta = 1.10^\circ$ (Figure 4).

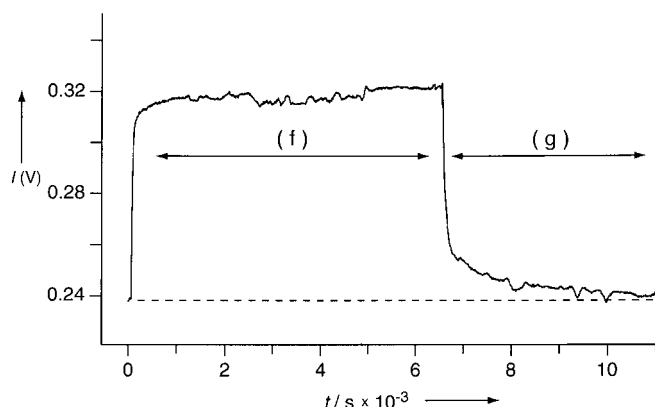


Figure 4. On-line SPR measurement of the antibody binding to the tethered TASP on the gold surface (step (f) in Figure 1), and subsequent antibody displacement upon incubation of the monolayer with excess free antigen in the bulk solution (step (g)). $I(V)$ is the electrical signal of the photodiode, which is proportional to the reflected light intensity.

g) Addition of a suitably high concentration (10^{-4} M) of the antigenic peptide Ac-(NANP)₃G-OH to the bulk aqueous buffer solution displaced the monoclonal antibody from the monolayer surface as indicated by the SPR resonance angle shift of $\Delta\theta = -1.03^\circ$ (Figure 4). This demonstrates the reversibility of the antibody binding to the functionalized surface.

In conclusion, chemical ligation methods in combination with regioselective addressable templates have allowed the preparation of well defined, complex monomolecular films tethered to gold surfaces. The supramolecular monolayers exposed artificial recognition sites, here for monoclonal antibodies. SPR, FTIR spectroscopies, and TOF-SIMS were ideally suited surface sensitive techniques to enable the essential control of the individual reaction steps. The concept presented here for the functionalization of gold surfaces may be easily applied to other supporting materials such as glass(like) surfaces, it is certainly not limited to peptides but can be equally well extended to proteins and other biopolymers such as polynucleotides (DNA or RNA). This approach can be extended, in conjunction with methodologies, for chemoselective ligation and orthogonal protection techniques^[16] to the construction of multifunctional surfaces with interesting potential in bioanalytics.^[9, 17]

Experimental Section

Amino acids were obtained from Nova Biochem (Switzerland) or Bachem (Switzerland), all other reagents were obtained from Fluka (Switzerland). Template **2** was synthesized according to published protocols.^[10] Peptide **4** was synthesized according to a convergent strategy: The linear peptide Ac-(NANP)₃G-OH was assembled on a Sasrin resin and, after cleavage and HPLC purification, coupled to Boc-NOCH₂CO-Lys-OMe with PyBOP. Boc removal and HPLC purification resulted in **4** with an overall yield of 61 %. The chemical integrity was confirmed by HPLC, ESI-MS, and amino acid analysis. Compound **3** was supplied by A. Heusler (EPFL) and the monoclonal antibody Sp3E9 by Dr. G. Corradin (University of Lausanne).

SPR experiments were performed on a home-made apparatus as described previously.^[18] The consecutive surface synthesis steps were performed by incubating a glass slide covered by a 40-nm thick gold film in the corresponding reaction solutions. The particular reaction was finally terminated by washing the gold surface with the corresponding solvent. Modification of the gold surface was monitored continuously on line by measuring the reflected intensity slightly off the SPR resonance angle. Surface adsorption of organic molecules shift the resonance curve to higher angles, which causes an increase in the reflected intensity (see Figure 4 as an example). In addition, angle scans were performed, which yielded the optical film thickness of the particular monolayers (details for evaluating the SPR data are given by Boncheva et al.^[8c]).

FTIR spectra were recorded on a Bruker IFS 28 spectrometer equipped with a HgCdTe detector as described in detail by Liley et al.^[12] One face of a Zn/Se trapezoidal ATR plate (angle of incidence 45°) was coated with a thin layer (ca 10 nm) of gold by thermal evaporation. This face was pressed against a teflon cell to form a water-tight seal. After each chemical modification of the gold surface, the ATR plate was washed with the corresponding solvent and dried under a flow of nitrogen. For each spectrum 1000 scans were recorded at 1 cm⁻¹ resolution and the water vapor bands subtracted from the spectra.

TOF-SIMS spectra were recorded in triplicate on a TOF-SI mass spectrometer TRIFT^[19] designed by Ch. Evans & Comp. A liquid-metal ion source pulsed at 5 kHz was used for the production of the gallium primary ions (15 kV) with a pulse width of 8 ns. The total ion dose required for one spectrum was less than 10¹¹ cm⁻², that is, within the static regime limits of SIMS. Charge compensation was performed by injecting one low energy electron (20 eV) at every eighth ion pulse.

Received: September 21, 1998 [Z12433IE]

German version: *Angew. Chem.* **1999**, *111*, 699–702

Keywords: IR spectroscopy • molecular recognition • surface chemistry • template synthesis • thin films

Imaging and Visualization (Ed. A. T. Hubbard), Boca Raton, CRC Press, FL, **1995**, pp. 713–732.

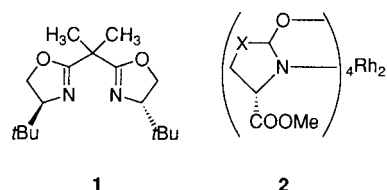
- [6] a) M. Stelzle, G. Weismüller, E. Sackmann, *J. Phys. Chem.* **1993**, *97*, 2974–2981; b) E.-L. Florin, H. E. Gaub, *Biophys. J.* **1993**, *64*, 375–383; c) A. L. Plant, *Langmuir* **1993**, *9*, 2764–2767; d) H. Lang, C. Duschl, H. Vogel, *Langmuir* **1994**, *10*, 197–210; e) C. Steinem, A. Janshoff, W.-P. Ulrich, M. Sieber, H.-J. Galla, *Biochim. Biophys. Acta* **1996**, *1279*, 169–180.
- [7] a) M. E. McGovern, K. M. R. Kallury, M. Thompson, *Langmuir* **1994**, *10*, 3607–3614; b) S. Heyse, H. Vogel, M. Sängler, H. Sigrüst, *Protein Sci.* **1995**, *4*, 2532–2544.
- [8] a) E. Sackmann, *Science* **1996**, *271*, 43–48; b) A. Bardea, E. Katz, A. F. Bückmann, I. Willner, *J. Am. Chem. Soc.* **1997**, *119*, 9114–9119; c) M. Boncheva, H. Vogel, *Biophys. J.* **1997**, *73*, 1056–1072; d) “Affinity Biosensing: Techniques and Protocols”: B. Liedberg, K. Johansen in *Methods in Biotechnology*, Vol 7: (Eds.: K. R. Rogers, A. Mulchadani, J.), Humana Press, New York, **1998**, pp. 31–53; e) T. Stora, S. Heyse, E. Schmid, J. H. Lakey, H. Vogel, *Biochim. Biophys. Acta* **1998**, *85507*, 319–338.
- [9] a) C. Duschl, M. Liley, H. Vogel, *Angew. Chem.* **1994**, *106*, 1361–1364; *Angew. Chem. Int. Ed. Engl.* **1994**, *33*, 1274–1276; b) M. Mrksich, G. M. Whitesides, *Trends Biotechnol.* **1995**, *13*, 228–235; c) L. A. Chrisley, C. E. O’Ferrall, B. J. Spargo, C. S. Dulcey, J. M. Calvert, *Nucl. Acids Res.* **1996**, *24*, 3040–3047; d) P. Heiduschka, W. Göpel, W. Beck, W. Kraas, S. Kienle, G. Jung, *Chem. Eur. J.* **1996**, *2*, 667–672; e) J. T. Groves, N. Ulman, S. Boxer, *Science* **1997**, *275*, 651–653.
- [10] L. Scheibler, P. Dumy, D. Stamou, C. Duschl, H. Vogel, M. Mutter, *Tetrahedron* **1998**, *54*, 3725–3734.
- [11] L. Scheibler, PhD Thesis, University of Lausanne, **1998**.
- [12] M. Liley, T. A. Keller, C. Duschl, H. Vogel, *Langmuir* **1997**, *13*, 4190–4192.
- [13] a) D. J. van den Heuvel, R. P. H. Koyman, J. W. Drijfhout, G. W. Welling, *Anal. Biochem.* **1993**, *215*, 223–230; b) C. Duschl, A. F. Sevin-Landais, H. Vogel, *Biophys. J.* **1996**, *70*, 1985–1995.
- [14] P. Dumy, I. Eggleston, S. Cervigni, U. Sila, X. Sun, M. Mutter, *Tetrahedron Lett.* **1995**, *36*, 1255–1258.
- [15] K. Rose, *J. Am. Chem. Soc.* **1994**, *116*, 30–33.
- [16] a) P. E. Dawson, S. B. H. Kent, *J. Am. Chem. Soc.* **1993**, *115*, 7263–7266; b) A. Nefzi, X. Sun, M. Mutter, *Tetrahedron Lett.* **1995**, *36*, 229–230; c) L. E. Canne, A. R. Ferredamare, S. K. Burley, S. B. H. Kent, *J. Am. Chem. Soc.* **1995**, *117*, 2998–3007; d) J. Shao, J. Tam, *J. Am. Chem. Soc.* **1995**, *117*, 3893–3899; e) T. W. Muir, *Structure* **1995**, *3*, 649–652; f) T. W. Muir, M. J. Williams, M. H. Ginsberg, S. B. H. Kent, *Biochemistry* **1994**, *33*, 7701–7708.
- [17] C. Duschl, M. Liley, G. Corradin, H. Vogel, *Biophys. J.* **1994**, *67*, 1229–1237.
- [18] S. Terrettaz, T. Stora, C. Duschl, H. Vogel, *Langmuir* **1993**, *9*, 1361–1369.
- [19] B. Schueler, *Microsc. Microanal. Microstruct.* **1992**, *3*, 119–139.

- [1] a) A. Ulman, *An Introduction to Ultrathin Organic Films: From Langmuir-Blodgett to Self-Assembly*, Academic Press, San Diego, CA, **1991**; b) J. H. Fendler, *Membrane-Mimetic Approach to Advanced Materials*, Springer, Berlin, **1994**; c) D. K. Schwartz, *Surface Science Reports* **1997**, *27*, 241–334; d) *Biomolecular Self-Assembling Materials: Scientific and Technological Frontiers* (National Research Council), National Academy Press, Washington DC, **1996**.
- [2] a) A. Kumar, G. M. Whitesides, *Science* **1994**, *263*, 60–62; b) M. Liley, D. Gourdon, D. Stamou, U. Meseth, T. M. Fischer, C. Lautz, H. Stahlberg, H. Vogel, N. A. Burnham, C. Duschl, *Science* **1998**, *280*, 273–275.
- [3] a) K. E. Drexler *Nanosystems: Molecular Machinery, Manufacturing, and Computation*, Wiley-Interscience, New York, **1992**; b) *Nanoparticles and Nanostructured Films* (Ed.: J. H. Fendler), WILEY-VCH, Weinheim, **1998**.
- [4] M. Mrksich, G. M. Whitesides, *Annu. Rev. Biophys. Biomol. Struct.* **1996**, *25*, 55–78.
- [5] a) L. H. Dubois, R. G. Nuzzo, *Annu. Rev. Phys. Chem.* **1992**, *43*, 437–463; b) G. M. Whitesides, C. B. Gorman in *Handbook of Surface*

Macrocyclic Cyclopropenes by Highly Enantioselective Intramolecular Addition of Metal Carbenes to Alkynes**

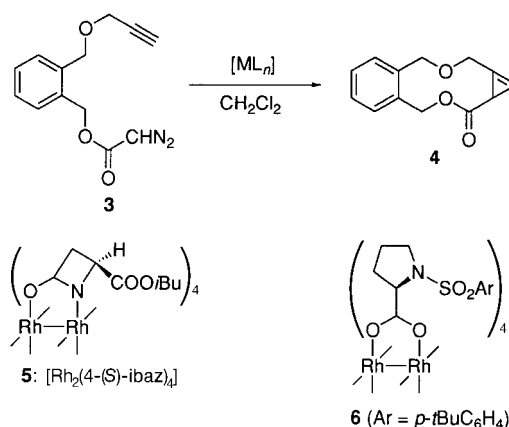
Michael P. Doyle,* Doina G. Ene, Chad S. Peterson, and Vince Lynch

Cyclopropenes that are formed by intermolecular carbene addition to a carbon–carbon triple bond are generally stable to self-decomposition,^[1] and many of these compounds have well-defined biological effects.^[2] Intramolecular cyclopropanation has been investigated with similar intensity,^[3] but, in those cases where ring strain is further increased, the cyclopropene products are unstable and, in the presence of transition metal catalysts employed for their formation, rapidly decompose to vinyl carbenes which have their own characteristic chemistry.^[3, 4] We have previously reported that [Cu(MeCN)₄]PF₆ in combination with chiral bis-oxazoline **1** was an effective catalyst for enantioselective (87–91 % *ee*) intramolecular cyclopropanation that resulted in the formation of 10- to 15-membered ring cyclopropane-fused lactones; chiral dirhodium(II) carboxamate catalysts of the type **2** were appreciably less effective for enantioselective synthesis (< 50 % *ee*).^[5] We now report that macrocyclic cyclopropanation occurs in even higher yields and enantiocontrol, but that selectivity in these processes is highly dependent on the catalyst.



- a, X = CH₂ : [Rh₂(5-(*S*)-mepy)₄]
 b, X = O : [Rh₂(4-(*S*)-meox)₄]
 c, X = NCOCH₂CH₂Ph : [Rh₂(4-(*S*)-mppim)₄]

Catalytic diazo decomposition of **3** in CH₂Cl₂ caused by the action of a broad array of chiral catalysts resulted in the formation of **4** as the sole product, which was isolated in yields ranging from 62 to 92 %. The X-ray crystal structure of **4** was determined, and an ORTEP diagram of the structure is



provided in Figure 1.^[6] Of the catalysts employed, [Rh₂(4-(*S*)-ibaz)₄] (**5**)^[7] exhibited the highest enantiocontrol at 92 % *ee*, the next best catalyst was CuPF₆/**1** at 80 % *ee*. Other chiral

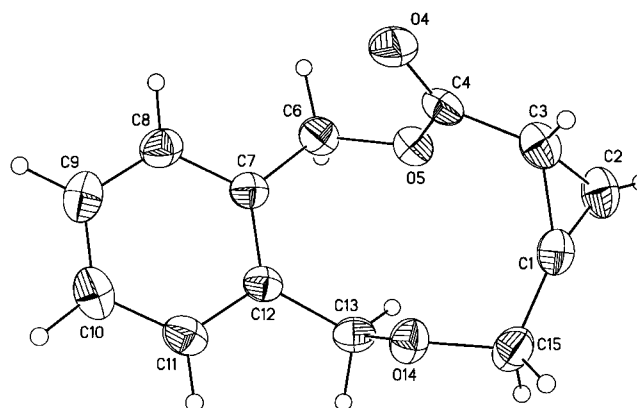


Figure 1. Crystal structure of (*S*)-**4** with selected bond lengths [Å] and angles [°]: C1–C3 1.514(3), C2–C3 1.506(3), C1–C2 1.265(3), C3–H3 0.88(2), C2–H2 0.93(3); C2–C3–C1 49.5(2), C1–C2–C3 65.5(2), C2–C1–C3 64.9(2), O5–C4–C3 111.0(2).

dirhodium carboxamides showed a lower degree of enantiocontrol, but the chiral dirhodium prolinates (**6**)^[8] was basically unselective. The absolute configuration of **4** formed by the *S*-configured dirhodium(II) catalyst **5** was established by hydrogenolysis/hydrogenation catalyzed by 5 % Pd(OH)₂/C in ethanol to the known (1*R*,5*S*)-3-oxabicyclo[3.1.0]hexan-2-one.^[9] Thus, in the presence of catalytic amounts of **5**, **3** yielded (1*R*)-**4** in 92 % *ee*.

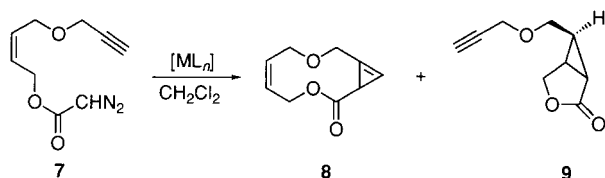
Since dirhodium(II) carboxamides exhibited a high selectivity for allylic cyclopropanation,^[9] compared with addition to a remote double bond, while CuPF₆/**1** favored addition to the terminal site,^[5] we expected the same outcome for the propargyl analogue **7**. Instead we found that, although with dirhodium carboxamides of type **2** compound **9** was formed highly selectively, [Rh₂(4-(*S*)-ibaz)₄] (**5**) had the inverse selectivity along with exceptional enantiocontrol. In contrast, use of CuPF₆/**1** gave a 1:2 mixture of **8** and **9** with unexpectedly unimpressive enantiocontrol.

That macrocyclic cyclopropanation of **3** and **7** is not merely a function of the geometry of the reactants is evident in results obtained with the propargyl diazoacetate **10** having a 1,4-

[*] Prof. M. P. Doyle, Dr. D. G. Ene, Dr. C. S. Peterson
 Department of Chemistry
 University of Arizona
 Tucson, AZ 85721-0041 (USA)
 Fax: (+1) 520-621-8407
 E-mail: mdoyle@u.arizona.edu

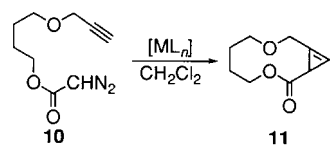
Dr. V. Lynch
 Department of Chemistry and Biochemistry
 University of Texas
 Austin, TX 78712 (USA)
 Fax: (+1) 512-471-8696
 E-mail: vmlynch@mail.utexas.edu

[**] This work was supported by grants from the Robert A. Welch Foundation, the National Science Foundation, and the National Institutes of Health.



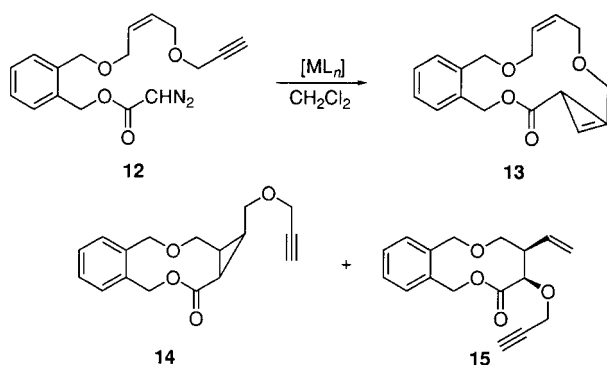
[ML _n]	yield [%]	8:9	ee (8) [%]	ee (9) [%]
CuPF ₆ /1	54	31:69	75	46
2a	76	4:96	–	96
5	80	84:16	97	88
6	87	96:4	12	20

butanediol linker. With yields of isolated products in the range 73–92 %, [Rh₂(4-(*S*)-ibaz)₄] gave **11** with ≥ 99 % *ee*, whereas enantioselectivities with other catalysts were: 82 % *ee* (CuPF₆/1), 78 % *ee* (2a), and 17 % *ee* (2c). Once again [Rh₂(4*S*-ibaz)₄] exhibited exceptional enantiocontrol.

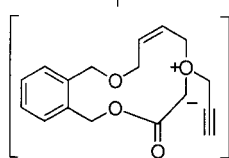


A defining test of chemoselectivity/enantiocontrol is found in the diazo decomposition of

12 from which three reaction pathways are possible: cyclopropanation yielding the 15-membered ring **13**, cyclopropanation yielding the 10-membered ring **14**, and ylide generation/[2,3]-sigmatropic rearrangement^[10] forming **15**. All three products were obtained with CuPF₆/1 as the catalyst, but the formation of **13** was virtually the exclusive outcome of reactions with chiral dirhodium carboxamidates, although with diminished enantiocontrol from that obtained for the formation of **4**, **8**, or **11**. Cyclopropene **13** was relatively unstable and, therefore, was treated with 1,3-diphenylisobenzofuran to form its stable *exo*-Diels–Alder adduct;^[11] the % *ee* of **13** was obtained following selective hydrogenation of the cyclopropene with diimide.^[12] The ylide derived product **15** that was a major outcome of the CuPF₆/1 catalyzed reaction was formed in only 18 % *ee*.



[ML _n]	yield [%]	13:14:15	ee (13) [%]
CuPF ₆ /1	85	57:12:31	79
2a	59	95:3:2	35
5	70	99:1:–	65



The chiral dirhodium(II) azetidinone-carboxylate **5** is clearly superior to all other catalysts examined for enantio- and chemoselective cyclopropanation. In contrast to prior results from intermolecular cyclopropanation,^[12] the CuPF₆/1 combination is an effective catalyst,^[13] although not sufficiently selective to be of synthetic value. With product yields averaging 80 % for the formation of 10-membered ring-fused cyclopropenes, without the need for high-dilution techniques, this methodology is one of the most effective for the enantioselective synthesis of large ring compounds.

Experimental Section

In a typical procedure, [Rh₂(4*S*-ibaz)₄] (8.8 mg, 10 μmol, 1.0 mol %) was added to an oven-dried two-neck round-bottom flask fitted with a reflux condenser and a rubber septum. To this flask was added freshly distilled CH₂Cl₂ (5 mL), and the homogeneous solution was stirred at reflux for 5 min. Diazoacetate **3** (244 mg, 1.00 mmol) dissolved in anhydrous CH₂Cl₂ (10 mL) was added to the refluxing solution of catalyst through a syringe pump at a rate of 1.0 mL h^{−1}. Upon completion of addition, the reaction solution was passed through a plug of silica gel, and the solvent was removed under reduced pressure. The resulting solid material was purified by flash chromatography on silica gel (8:1 CH₂Cl₂:ethyl acetate) to provide pure **4** (119 mg; 62 %) as a white solid, m.p. 98–100 °C. The product mixture was hydrogenolyzed in the presence of 5 % Pd(OH)₂/C in ethanol to (1*R*,5*S*)-3-oxabicyclo[3.1.0]hexan-2-one in 93 % yield: 92 % *ee* by GC analysis (Chiraldex G-TA, 90 °C; Altech and Assoc., Inc.). [α]_D²⁵ = −84.0 (*c* = 1.07 in CH₂Cl₂).

Received: September 11, 1998 [Z 12406 IE]

German version: *Angew. Chem.* **1999**, *111*, 722–724

Keywords: asymmetric synthesis • carbene complexes • homogeneous catalysis • macrocycles • rhodium

- Reviews: M. S. Baird, *Top. Curr. Chem.* **1988**, *144*, 137–209; P. Binger, H. M. Buch, *Top. Curr. Chem.* **1987**, *135*, 77–151; M. N. Protopopova, E. A. Shapiro, *Russ. Chem. Rev.* **1989**, *58*, 667–681; T. Ye, M. A. McKerver, *Chem. Rev.* **1994**, *94*, 1091–1160.
- Reviews: C. Djerassi, C. J. Silva, *Acc. Chem. Res.* **1991**, *24*, 371–378; J. Salaun, M. S. Baird, *Fr. Curr. Med. Chem.* **1995**, *2*, 511–542; A. A. Andrianaivo-Rafehivolo, E. E. Gaydou, L. H. Rakotovo, *Oleagineux* **1994**, *49*, 177–188.
- Reviews: A. Padwa, M. D. Weingarten, *Chem. Rev.* **1996**, *96*, 223–269; M. P. Doyle, M. A. McKerver, T. Ye, *Modern Catalytic Methods for Organic Synthesis with Diazo Compounds*, Wiley, New York, **1998**, chap. 5.
- T. R. Hoye, J. R. Vyvyan, *J. Org. Chem.* **1995**, *60*, 4184–4195; P. Müller, C. Gränicer, *Helv. Chim. Acta* **1995**, *78*, 129–144.
- M. P. Doyle, C. S. Peterson, D. L. Parker, Jr., *Angew. Chem.* **1996**, *108*, 1439–1440; *Angew. Chem. Int. Ed. Engl.* **1996**, *35*, 1334–1336.
- Crystal data for **4**: C₁₃H₁₂O₃, *M*_r = 216.23, tetragonal, space group P4₂,2 with *a* = 8.388(1), *c* = 31.804(2) Å, *V* = 2237.7(7) Å³, *Z* = 8, ρ_{calcd} = 1.28 g cm^{−3}, *F*(000) = 912. Colorless triangular prism (0.24 × 0.42 × 0.78 mm) cut from larger crystal. Data were collected out to 2θ = 55° by the ω-scan technique (1.2° ωscan) on a Siemens P4 diffractometer at 25 °C using graphite-monochromatized MoK_α radiation (λ = 0.71073 Å). A total of 6225 reflections were measured, of which 2578 reflections were unique [*R*_{int}(*F*²) = 0.049]. The structure was solved by direct methods and refined by full-matrix least-squares on *F*² with anisotropic displacement parameters for the non-hydrogen atoms. The hydrogen atom positions were observed in a Δ*F* map and refined with isotropic displacement parameters. The final *R*_w(*F*²) = 0.0856 with a goodness of fit = 1.032 for refining 194 parameters. The conventional *R*(*F*) = 0.0454 for 1540 reflections with *F*_o > 4σ(*F*_o). Data reduction, decay correction, structure solution, and refinement were done using the SHELXTL/PC software package (G. M. Shel-

drick, SHELXTL/PC, Version 5.03, Siemens Analytical X-ray Instruments, Inc., Madison, WI, (USA)). b) Crystallographic data (excluding structure factors) for the structures reported in this paper have been deposited with the Cambridge Crystallographic Data Center as supplementary publication no. CCDC-103167. Copies of the data can be obtained free of charge on application to CCDC, 12 Union Road, Cambridge CB2 1EZ, UK (fax: (+44) 1223-336-033; e-mail: deposit@ccdc.cam.ac.uk).

- [7] M. P. Doyle, Q.-L. Zhou, S. H. Simonsen, V. Lynch, *Synlett* **1996**, 697–698.
- [8] a) H. M. L. Davies, P. R. Bruzinski, D. H. Lake, N. Kong, M. J. Fall, *J. Am. Chem. Soc.* **1996**, *118*, 6897–6907; b) M. Kennedy, M. A. McKerver, A. R. Maguire, G. H. P. Roos, *J. Chem. Soc. Chem. Commun.* **1990**, 361–362.
- [9] M. P. Doyle, R. E. Austin, A. S. Bailey, M. P. Dwyer, A. B. Dyatkin, A. V. Kalinin, M. M. Y. Kwan, S. Liras, C. J. Oalman, R. J. Pieters, M. N. Protopopova, C. E. Raab, G. H. P. Roos, Q.-L. Zhou, S. F. Martin, *J. Am. Chem. Soc.* **1995**, *117*, 5763–5775.
- [10] a) M. P. Doyle, D. C. Forbes, M. M. Vasbinder, C. S. Peterson, *J. Am. Chem. Soc.* **1998**, *120*, 7653–7654; b) M. P. Doyle, C. S. Peterson, *Tetrahedron Lett.* **1997**, *38*, 5265–5268.
- [11] P. Müller, G. Bernardinelli, J. Pfyffer, D. Rodriguez, J.-P. Schaller, *Helv. Chimica Acta* **1988**, *71*, 544–550.
- [12] M. P. Doyle, M. Protopopova, P. Müller, D. Ene, E. A. Shapiro, *J. Am. Chem. Soc.* **1994**, *116*, 8492–8498.
- [13] In the presence of $\text{CuPF}_6/\mathbf{1}$, addition of ethyl diazoacetate to propargyl methyl ether formed the product from cyclopropene in 81 % *ee* (60 % yield).

A Novel Method for the Demetalation of Tricarbonyliron – Diene Complexes by a Photolytically Induced Ligand Exchange Reaction with Acetonitrile**

Hans-Joachim Knölker,* Helmut Goesmann, and Rüdiger Klauss

Tricarbonyl(η^4 -1,3-diene)iron complexes are a useful class of organometallic compounds with versatile applications to organic synthesis.^[1] The coordination of the conjugated diene to the transition metal fragment leads to a significant alteration of its reactivity. Therefore, the tricarbonyliron fragment has been used for the stabilization of labile hydrocarbons and as a protecting group for dienes.^[1] After the desired transformations at the ligand of the tricarbonyl(η^4 -1,3-diene)iron complex a demetalation is required to provide the free diene. This decomplexation of tricarbonyliron complexes is usually achieved under strong oxidizing reaction conditions,

for example with ferric chloride,^[2] ceric ammonium nitrate,^[3] trimethylamine *N*-oxide (TMANO),^[4] cupric chloride,^[5] or hydrogen peroxide/sodium hydroxide.^[6] In connection with investigations of the iron-mediated [2+2+1] cycloaddition^[7, 8] and our studies directed towards the application of tricarbonyliron complexes to the synthesis of alkaloids^[9] we required a method for demetalation of tricarbonyliron complexes by using extremely mild reaction conditions. Herein we describe a novel procedure for the demetalation of tricarbonyliron – diene complexes using a photolytically induced exchange of the carbonyl ligands by acetonitrile at low temperature and subsequent demetalation in the air.

Although the iron-mediated [2+2+1] cycloaddition has been known for four decades,^[10] only a few very limited applications were reported because of the difficulties associated with the demetalation of the resulting tricarbonyl(η^4 -cyclopentadienone)iron complexes. We recently demonstrated that selective demetalation is feasible using trimethylamine *N*-oxide by careful control of the reaction conditions.^[7a,b] However, the yields in some cases were only moderate. Therefore, we set out to develop a novel demetalation procedure in which the bonding of the metal fragment to the diene becomes labile by exchange of the carbon monoxide ligands. Acetonitrile ligands appeared to be promising candidates for such a transformation in the coordination sphere of the metal since they are rather poor acceptors. Thus, their introduction should result in a decreased back donation of electrons from the filled iron d orbitals to the ligand and the resulting complexes should be more easily oxidized.

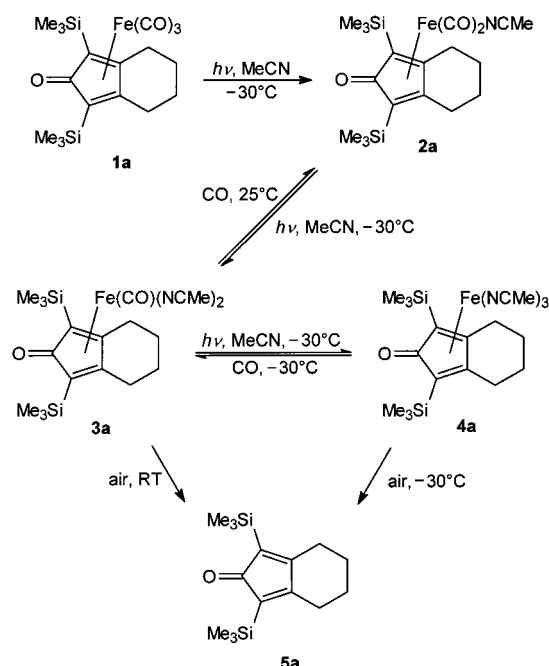
The tricarbonyliron complex **1a**^[7a] is stable at room temperature in the air. No acetonitrile complexes are observed on refluxing a solution of **1a** in acetonitrile for 29 h in the dark. However, exposure to daylight at room temperature results in a very slow formation of the monoacetonitrile complex **2a** along with the demetalated cyclopentadienone **5a**. Irradiation of a solution of complex **1a** in acetonitrile under argon atmosphere using a medium-pressure mercury lamp accelerates the ligand exchange dramatically and leads to a stepwise exchange of all three carbonyl ligands (Scheme 1, Table 1).

Photolysis of **1a** in acetonitrile at -30°C afforded after 1 h the diacetonitrile complex **3a** in 76 % as dark red crystals. Injection of argon into the solution during the photolysis provided a purple solution of the triacetonitrile complex **4a**. The addition of the third acetonitrile ligand is reversible even at -30°C . Therefore, the complexes **3a** or **4a** can be prepared selectively. In order to prove the reversibility of the ligand exchange carbon monoxide was injected at -30°C into the purple solution of complex **4a** in acetonitrile. Within 30 min the color changed to red and the diacetonitrile complex **3a** was isolated in 65 % yield based on **1a**. On warming the mixture, the exchange of the second acetonitrile ligand becomes reversible too. By injection of carbon monoxide at room temperature the red solution turned orange and the monoacetonitrile complex **2a** was obtained in 61 % yield based on **1a**. Related ligand exchange reactions at the cationic complex $[\eta^5\text{-CpFe}(\text{CO})_3]^+\text{PF}_6^-$ were previously described by Astruc et al.^[11] However, the cationic CpFe complexes with acetonitrile ligands reported therein are fairly stable compared to those of cyclopentadienones.

[*] Prof. Dr. H.-J. Knölker, Dr. R. Klauss
Institut für Organische Chemie der Universität
Richard-Willstätter-Allee, D-76131 Karlsruhe (Germany)
Fax: (+49) 721-698-529
E-mail: knoe@ochhades.chemie.uni-karlsruhe.de

Dr. H. Goesmann
Institut für Anorganische Chemie der Universität
Engesserstrasse, D-76128 Karlsruhe (Germany)

[**] Transition Metal Complexes in Organic Synthesis, Part 48. This work was supported by the Deutsche Forschungsgemeinschaft (Gerhard-Hess-Förderpreis) and the Fonds der Chemischen Industrie. We are grateful to the BASF AG, Ludwigshafen, for a generous gift of pentacarbonyliron. Part 47: ref. [9c].



Scheme 1. Photolytically induced ligand exchange reactions at complex **1a** with acetonitrile and demetalation of the resulting acetonitrileiron complexes **3a** and **4a**.

Table 1. Demetalation of the (cyclopentadienone)iron complexes **1a–4a** by stirring of an acetonitrile solution in the air.

Complex	$\bar{\nu}_{\text{C=O}}$ [cm^{-1}]	Reaction conditions	1a , Yield [%]	2a , Yield [%]	5a , Yield [%]
1a	1606	25 °C, 3 h	96	1	2
1a	1606	25 °C, 70 h	87	5	5
2a	1589	25 °C, 24 h	–	60	39
3a	1544	25 °C, 1 h	–	–	100
4a	1510	–30 °C, 1–2 min ^[a]	–	–	(quant.)

[a] Demetalation by injection of air into the solution of complex **4a** without isolation.

The structural assignments of the complexes **2a** and **3a** are based on their spectral data^[12] and an X-ray crystal structure determination of **3a** (Figure 1).^[13] A characteristic structural

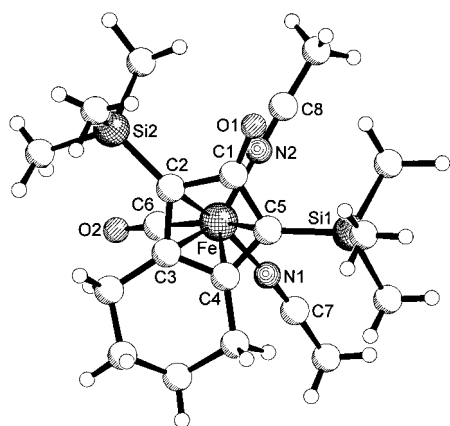


Figure 1. Molecular structure of **3a** in the crystal. Selected bond lengths [\AA]: Fe–C2 2.114(9), Fe–C3 2.057(9), Fe–C4 2.053(9), Fe–C5 2.131(9), Fe–C6 1.758(11), Fe–N1 1.942(9), Fe–N2 1.940(8), C1–O1 1.237(10), C6–O2 1.155(10), N1–C7 1.147(12), N2–C8 1.145(12).

feature of the diacetonitrile complex **3a** is the loss of symmetry caused by exchange of the second carbonyl ligand. In contrast the complexes **1a**^[7a] and **2a** are symmetrical. The ^1H and ^{13}C NMR spectra show the unsymmetrical arrangement of the coligands of complex **3a** in solution by the loss of C_s symmetry. The X-ray analysis confirms the conformation of the metal fragment for the solid state with tetragonal-pyramidal coordination of the iron atom and one acetonitrile ligand in the apical position (Figure 1). The ^{13}C NMR spectrum in deuterated $[\text{D}_8]$ dioxane at room temperature exhibits sharp signals for all carbon atoms indicating that the preferred conformation is frozen under these conditions. Stepwise increase of the temperature using $[\text{D}_{10}]p$ -xylene as solvent leads to coalescence of the two signals for the trimethylsilyl (TMS) groups in the ^1H NMR spectrum at 400 MHz. The activation barrier for this fluxional process caused by basal–apical ligand exchange was determined (Figure 2).^[14] The free enthalpies of activation for related turnstile rotations of several tricarbonyliron–diene complexes were previously reported.^[15] The

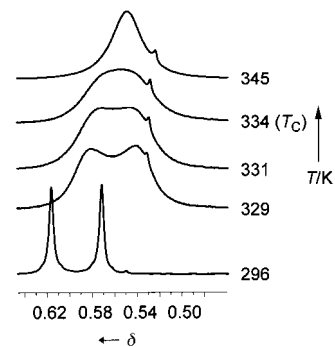


Figure 2. Dynamic ^1H NMR spectra of complex **3a** in the TMS region (400 MHz, $[\text{D}_{10}]p$ -xylene).

activation barrier for the intramolecular ligand exchange at the present (diacetonitrile)carbonyliron fragment of **3a** was found to be $\Delta G^\ddagger = 17.0 \pm 0.3 \text{ kcal mol}^{-1}$ ($T_c = 334 \pm 5 \text{ K}$, $\Delta\nu = 18 \text{ Hz}$). This value is significantly higher than observed for the tricarbonyliron complexes of cyclohexa-1,3-diene ($\Delta G^\ddagger = 8.7 \pm 0.3 \text{ kcal mol}^{-1}$),^[15c] buta-1,3-diene ($\Delta G^\ddagger = 10.5 \pm 0.5 \text{ kcal mol}^{-1}$),^[15c] and even 1-azabuta-1,3-dienes ($\Delta G^\ddagger = 13.5–14.7 \pm 0.3 \text{ kcal mol}^{-1}$),^[15e] and indicates a reduced back bonding from the iron atom to the acetonitrile coligands. On the other hand, the stretching frequency for the carbonyl band of the carbon monoxide ligand of complex **3a** at 1926 cm^{-1} is much lower than for the corresponding tricarbonyliron complex **1a**,^[7a] which is significant of an increased back donation of electrons from iron d orbitals into the LUMO of the carbonyl ligand. Due to its high sensitivity the triacetonitrile complex **4a** could be characterized only by FT-IR spectroscopy.^[12] The IR spectra show decreasing stretching frequencies for the carbonyl bands of the cyclopentadienone with increasing donor substitution at the metal (Table 1). A similar shift is observed for the $\text{C}\equiv\text{N}$ bands of the complexes **3a** and **4a**.

We next investigated the demetalation behavior of the complexes **1a–4a**. The orange yellow complex **2a** is stable at room temperature and the crystals can be handled even in the air. A solution of **2a** undergoes a selective demetalation in the air to provide the free ligand **5a** (see Table 1). However, even after 24 h there is still 60 % of complex **2a** unchanged. The diacetonitrile complex **3a** can be stored at room temperature under inert gas atmosphere. Injection of air into the solution of **3a** in acetonitrile at -30°C does not lead to

demetalation. However, on stirring the solution of complex **3a** in the air at room temperature the red color disappears completely within 1 h and the cyclopentadienone **5a** can be isolated quantitatively. The triacetonitrile complex **4a** is extremely air sensitive. Solutions of complex **4a** in acetonitrile are stable only under argon atmosphere at temperatures below -20°C . Warming the cold solution of **4a** leads to decomposition. However, the solid compound can be handled at room temperature under an argon atmosphere for a short period of time. On injection of air into a solution of **4a** in acetonitrile at -30°C the purple color of the triacetonitrile complex disappears instantaneously and the free ligand **5a** is obtained in excellent yield. The differences of the complexes **3a** and **4a** with respect to their stability in the air can be utilized for a chemoselective demetalation which was monitored by FT-IR spectroscopy (Figure 3). Photolysis of **1a** in acetonitrile at -30°C with injection of argon into the solution, evaporation of the solvent at -20°C , and washing of the residue with hexane provides the triacetonitrile complex **4a** along with the diacetonitrile complex **3a** as minor product. Brief contact of the solid complexes to the air leads to instantaneous demetalation of **4a** to the free ligand **5a** (IR band at 1678 cm^{-1}), while **3a** is stable under these conditions.

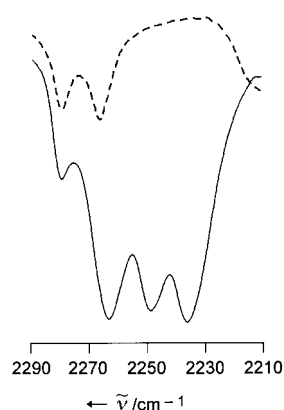
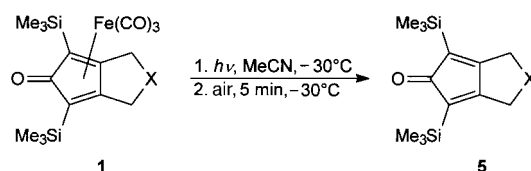


Figure 3. IR spectrum of the triacetonitrileiron complex **4a** containing the diacetonitrileiron complex **3a** (solid line); IR spectrum after contact with air for 3 s (dotted line).

The feasibility to focus the reaction on **3a** or **4a**, respectively, offers two alternative pathways for the demetalation by photolytically induced ligand exchange. Method A: photolysis of **1a** in acetonitrile at -30°C with injection of argon into the solution for 45 min and subsequent demetalation of the intermediate triacetonitrile complex **4a** by injection of air at -30°C . Method B: photolysis of **1a** in acetonitrile at -30°C under argon atmosphere (but without injection of argon into the solution!) for 60 min and demetalation of the intermediate diacetonitrile complex **3a** by injection of air with simultaneous warming to room temperature. The cyclopentadienone **5a** was provided in 89% yield by method A and in 88% yield by method B. The demetalation of a series of bicyclic tricarbonyl(η^4 -cyclopentadienone)iron complexes **5** was carried out using method A with individual optimization of the irradiation time if necessary (Scheme 2, Table 2). The yields for the free ligands **5a–d**, previously prepared by using TMANO,^[7b] were considerably improved (83–91%). The cyclopentadienone **5e** could be obtained for the first time by the present method.^[16] Treatment of **5e** with TMANO led to the known thiophene derivative by twofold double-bond isomerization and proto-desilylation. This result provides direct evidence for the sequence of steps involved in the demetalation of **1e** with TMANO.^[7b]



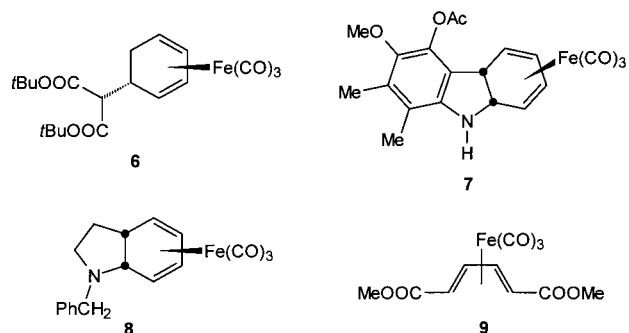
Scheme 2. Photolysis of the tricarbonyliron complexes **1** in acetonitrile with subsequent demetalation of the intermediate triacetonitrileiron complexes by injection of air.

Table 2. Demetalation of the bicyclic tricarbonyl(η^4 -cyclopentadienone)iron complexes **1** via the intermediate triacetonitrile complexes **4** (method A).

1	X	Irradiation time [min]	5 , Yield [%]
a	(CH ₂) ₂	45	89
a	(CH ₂) ₂	60	88 ^[a]
b	CH ₂	45	91
c	C(COOMe) ₂	45	86
d	O	60	83
e	S	30	56

[a] Method B: Demetalation via the diacetonitrile complex **3a**.

Moreover, the novel demetalation procedure was also applied to the tricarbonyl(η^4 -cyclohexa-1,3-diene)iron complexes **6–8**^[17] and the (η^4 -buta-1,3-diene)tricarbonyliron complex **9**. The irradiation time for the cyclohexadiene and



butadiene complexes was increased to 90 min in order to achieve a complete ligand exchange. Using method B via the intermediate diacetonitrile complexes the free dienes **6a–9a** were obtained in high yields (80–85%). The reaction sequence for the demetalation of tricarbonyliron complexes of cyclohexa-1,3-dienes and buta-1,3-dienes is most likely the same as described above for cyclopentadienone complexes. However, the acetonitrileiron complexes of simple dienes are much more labile than their cyclopentadienone analogues. Photolysis of complex **6** in acetonitrile at -30°C led to the exchange of two carbonyl ligands. The resulting diacetonitrile complex was characterized by IR spectroscopy by the two bands in the $\text{C}\equiv\text{N}$ region (2310 and 2282 cm^{-1}) and demetalated within a few minutes on contact with air. Method A via an intermediate triacetonitrile complex provided a better result for the demetalation of the cyclohexadiene complex **6** (yield of **6a**: 87%). The demetalation of **7** to **7a**^[18] by photolytically induced ligand exchange using method B provided the first example of a 4a,9a-dihydro-9H-carbazole unsubstituted at the nitrogen atom which is not coordinated to a metal atom.^[19]

In conclusion, we developed a novel procedure for the demetalation of tricarbonyl(η^4 -1,3-diene)iron complexes under very mild reaction conditions. It could be demonstrated that the present procedure provides access to free ligands not available by previous methods.

Experimental Section

General procedure for the demetalation of the bicyclic tricarbonyl(η^4 -cyclopentadienone)iron complexes **1** by photolytically induced ligand exchange (method A): A solution of complex **1** (0.239 mmol) in acetonitrile (120 mL) was photolyzed using a 150 W medium-pressure mercury lamp (Heraeus TQ 150, Pyrex filter) at -30°C for 30–60 min (see Table 2) with concomitant injection of argon into the solution. Then air was injected into the cold purple solution for 5 min. Filtration through a short path of Celite, evaporation of the solvent, and flash chromatography of the residue on silica gel provided the free ligand **5**.

Received: September 28, 1998 [Z12459IE]
German version: *Angew. Chem.* **1999**, *111*, 727–731

Keywords: diene complexes • iron • photochemistry • synthetic methods

- [1] A. J. Pearson, *Acc. Chem. Res.* **1980**, *13*, 463; R. Grée, *Synthesis* **1989**, 341; A. J. Pearson, *Iron Compounds in Organic Synthesis*, Academic Press, London, **1994**, chap. 4 and 5; C. Iwata, Y. Takemoto, *Chem. Commun.* **1996**, 2497; H.-J. Knölker in *Transition Metals for Fine Chemicals and Organic Synthesis, Vol. 1*, (Eds.: C. Bolm, M. Beller), WILEY-VCH, Weinheim, **1998**, chap. 3.13, p. 534.
- [2] R. Pettit, G. Emerson, J. Mahler, *J. Chem. Educ.* **1963**, *40*, 175; G. F. Emerson, J. E. Mahler, R. Kochhar, R. Pettit, *J. Org. Chem.* **1964**, *29*, 3620.
- [3] J. D. Holmes, R. Pettit, *J. Am. Chem. Soc.* **1963**, *85*, 2531; L. Watts, J. D. Fitzpatrick, R. Pettit, *J. Am. Chem. Soc.* **1965**, *87*, 3253.
- [4] Y. Shvo, E. Hazum, *J. Chem. Soc. Chem. Commun.* **1974**, 336; H.-J. Knölker, *J. Prakt. Chem.* **1996**, 338, 190.
- [5] D. J. Thompson, *J. Organomet. Chem.* **1976**, *108*, 381.
- [6] M. Franck-Neumann, M. P. Heitz, D. Martina, *Tetrahedron Lett.* **1983**, *24*, 1615; M. Franck-Neumann in *Organometallics in Organic Synthesis* (Eds.: A. de Meijere, H. tom Dieck), Springer, Berlin, **1988**, p. 247.
- [7] a) H.-J. Knölker, J. Heber, C. H. Mahler, *Synlett* **1992**, 1002; b) H.-J. Knölker, J. Heber, *Synlett* **1993**, 924; c) H.-J. Knölker, E. Baum, J. Heber, *Tetrahedron Lett.* **1995**, *36*, 7647.
- [8] A. J. Pearson, R. J. Shively, R. A. Dubbert, *Organometallics* **1992**, *11*, 4096; A. J. Pearson, R. J. Shively, *Organometallics* **1994**, *13*, 578; A. J. Pearson, X. Yao, *Synlett* **1997**, 1281.
- [9] Reviews: a) H.-J. Knölker, *Synlett* **1992**, 517; b) H.-J. Knölker in *Advances in Nitrogen Heterocycles, Vol. 1*, (Ed.: C. J. Moody), JAI Press, Greenwich (CT), **1995**, p. 173; c) H.-J. Knölker, *Chem. Soc. Rev.* **1999**, *28*, in press.
- [10] E. Weiss, W. Hübel, *J. Inorg. Nucl. Chem.* **1959**, *11*, 42; E. Weiss, R. Merényi, W. Hübel, *Chem. Ber.* **1962**, *95*, 1170.
- [11] D. Catheline, D. Astruc, *J. Organomet. Chem.* **1983**, *248*, C9; D. Catheline, D. Astruc, *J. Organomet. Chem.* **1984**, *272*, 417; see also: T. P. Gill, K. R. Mann, *Inorg. Chem.* **1983**, *22*, 1986.
- [12] Spectral data of the mono-, di-, and triacetonitrileiron complexes **2a**, **3a**, and **4a**. **2a**: Diffuse reflectance infrared Fourier transform (DRIFT)-IR: $\tilde{\nu}$ = 2944, 2899, 2865, 1987, 1932, 1589, 1441, 1394, 1374, 1367, 1342, 1261, 1244 cm^{-1} ; ^1H NMR (400 MHz, C_6D_6): δ = 0.45 (s, 18H), 0.86 (s, 3H), 1.26 (m, 4H), 2.09 (m, 2H), 2.35 (m, 2H); ^{13}C NMR and DEPT (100 MHz, CDCl_3): δ = -0.12 (6 CH_3), 4.46 (CH_3), 22.30 (2 CH_2), 24.82 (2 CH_2), 69.92 (2 C), 106.57 (2 C), 126.07 ($\text{C}\equiv\text{N}$), 180.09 ($\text{C}=\text{O}$), 212.83 (2 CO); elemental analysis calcd for $\text{C}_{19}\text{H}_{29}\text{FeNO}_3\text{Si}_2$ (%): C 52.89, H 6.77, N 3.25; found: C 52.86, H 6.67, N 2.90. **3a**: DRIFT-IR: $\tilde{\nu}$ = 3823, 2950, 2279, 2266, 1926, 1544, 1443, 1406, 1370, 1300, 1267, 1239, 1071 cm^{-1} ; ^1H NMR (400 MHz, C_6D_6): δ = 0.53 (s, 9H), 0.55 (s, 9H), 0.69 (s, 3H), 1.27 (s, 3H), 1.52 (m, 1H), 1.64 (m, 2H), 1.74 (m, 1H), 1.89 (m, 1H), 2.12–2.27 (m, 2H), 2.67 (m, 1H); ^{13}C NMR and DEPT (125 MHz, $[\text{D}_8]\text{dioxane}$): δ = 0.19 (3 CH_3), 0.65 (3 CH_3), 3.46 (CH_3), 3.75 (CH_3), 23.41 (CH_2), 23.65 (CH_2), 25.20 (CH_2), 25.80 (CH_2), 46.29 (C), 70.47 (C), 98.16 (C), 102.53 (C), 127.05 ($\text{C}\equiv\text{N}$), 129.15 ($\text{C}\equiv\text{N}$), 178.41 ($\text{C}=\text{O}$), 218.74 (CO); elemental analysis calcd for $\text{C}_{20}\text{H}_{32}\text{FeN}_2\text{O}_2\text{Si}_2$ (%): C 54.04, H 7.26, N 6.30; found: C 53.83, H 7.20, N 6.15. **4a**: DRIFT-IR: $\tilde{\nu}$ = 2263, 2249, 2236, 1510 cm^{-1} .
- [13] X-ray crystal structure analysis of **3a**: $\text{C}_{20}\text{H}_{32}\text{FeN}_2\text{O}_2\text{Si}_2$, orthorhombic, space group *Pbca*, a = 9.583(6), b = 18.102(14), c = 27.40(2) Å, V = 4753(6) Å³, Z = 8, T = 200(2) K, ρ_{calcd} = 1.242 g cm^{-3} , μ = 0.751 mm^{-1} , λ = 0.71073 Å, θ range: 2.25–20.00°; 2205 independent reflections; refinement method: full-matrix least squares on F^2 ; final R indices [$I > 2\sigma(I)$]: R_1 = 0.0674, wR_2 = 0.0960, maximal residual electron density: 0.378 e Å^{-3} . Programs: G. M. Sheldrick, SHELXS-86 (Göttingen **1986**), SHELXL-93 (Göttingen **1993**); E. Keller, SCHAKAL-97 (Freiburg i.Br., **1997**). Crystallographic data (excluding structure factors) for the structure reported in this paper have been deposited with the Cambridge Crystallographic Data Centre as supplementary publication no. CCDC-103176. Copies of the data can be obtained free of charge on application to CCDC, 12 Union Road, Cambridge CB2 1EZ, UK (fax: (+44) 1223-336-033; e-mail: deposit@ccdc.cam.ac.uk).
- [14] H. Günther, *NMR-Spektroskopie*, 3rd ed., Thieme, Stuttgart, **1992**, p. 310.
- [15] a) J.-Y. Lallemand, P. Laszlo, C. Muzette, A. Stockis, *J. Organomet. Chem.* **1975**, *91*, 71; b) D. Leibfritz, H. tom Dieck, *J. Organomet. Chem.* **1976**, *105*, 255; c) L. Kruczynski, J. Takats, *Inorg. Chem.* **1976**, *15*, 3140; d) Ö. Gonzáles-Blanco, V. Branchadell, *Organometallics* **1997**, *16*, 475; e) H.-J. Knölker, G. Baum, N. Foitzik, H. Goesmann, P. Gonser, P. G. Jones, H. Röttele, *Eur. J. Inorg. Chem.* **1998**, 993.
- [16] **5e**: m.p. 89–90°C; ^1H NMR (500 MHz, CDCl_3): δ = 0.18 (s, 18H), 3.71 (s, 4H); ^{13}C NMR and DEPT (125 MHz, CDCl_3): δ = -0.83 (6 CH_3), 30.40 (2 CH_2), 125.21 (2 C), 173.32 (2 C), 211.96 ($\text{C}=\text{O}$); elemental analysis calcd for $\text{C}_{13}\text{H}_{22}\text{OSSI}_2$ (%): C 55.26, H 7.85; found: C 55.21, H 7.84.
- [17] The tricarbonyliron-cyclohexadiene complexes were taken from ongoing research projects in our group and prepared by using standard procedures. **6**: A. J. Pearson, M. Chandler, *J. Chem. Soc. Perkin Trans. 1* **1982**, 2641; H.-J. Knölker, M. Graf, U. Mangei, *J. Prakt. Chem.* **1998**, *340*, 530; H.-J. Knölker, D. Herzberg, unpublished results. **7**: H.-J. Knölker, M. Bauermeister, *Helv. Chim. Acta*, **1993**, *76*, 2500; H.-J. Knölker, W. Fröhner, unpublished results. **8**: H.-J. Knölker, A.-A. El-Ahl, G. Weingärtner, *Synlett* **1994**, 194.
- [18] **7a**: m.p. 113°C; ^1H NMR (500 MHz, CDCl_3): δ = 2.03 (s, 3H), 2.15 (s, 3H), 2.35 (s, 3H), 3.59 (br s, 1H), 3.67 (s, 3H), 4.12 (br d, J = 12.0 Hz, 1H), 4.50 (dd, J = 12.0, 4.8 Hz, 1H), 5.70 (ddt, J = 9.7, 3.3, 0.9 Hz, 1H), 5.81 (ddd, J = 9.7, 4.8, 0.9 Hz, 1H), 5.90 (m, 1H), 6.00 (ddd, J = 9.7, 5.2, 0.4 Hz, 1H); ^{13}C NMR and DEPT (125 MHz, CDCl_3): δ = 12.38 (CH_3), 13.90 (CH_3), 20.62 (CH_3), 40.25 (CH), 55.16 (CH), 61.00 (CH_3), 117.16 (C), 120.85 (C), 121.66 (CH), 124.07 (CH), 124.36 (CH), 125.98 (CH), 129.74 (C), 138.78 (C), 143.42 (C), 145.32 (C), 169.05 ($\text{C}=\text{O}$); elemental analysis calcd for $\text{C}_{17}\text{H}_{19}\text{NO}_3$ (%): C 71.56, H 6.71, N 4.91; found: C 71.47, H 6.80, N 4.87.
- [19] D. B. Grotjahn, K. P. C. Vollhardt, *J. Am. Chem. Soc.* **1986**, *108*, 2091; H.-J. Knölker, P. G. Jones, J.-B. Pannek, A. Weinkauff, *Synlett* **1991**, 147; H.-J. Knölker, G. Baum, J.-B. Pannek, *Tetrahedron* **1996**, *52*, 7345.

Biphasic Synthesis of Hydrogen Peroxide from Carbon Monoxide, Water, and Oxygen Catalyzed by Palladium Complexes with Bidentate Nitrogen Ligands

Daniele Bianchi,* Rossella Bortolo, Rino D'Aloisio, and Marco Ricci*

Hydrogen peroxide is a commercially important chemical used in large volumes for bleaching and a wide variety of chemical oxidations. In recent years H₂O₂ has become more and more popular as an environmentally friendly reagent, mainly because it produces water as its only by-product.^[1] Industrially, hydrogen peroxide is produced primarily by the alternate oxidation and reduction of alkylanthraquinone derivatives.^[2] Since this method is quite complex, extensive studies have been carried out in an effort to find a direct route, such as the synthesis from carbon monoxide, oxygen, and water in the presence of a palladium triphenylphosphane catalyst disclosed in 1979 by Yermakov et al. [Eq. (1)].^[3]



Despite the favorable thermodynamics of this reaction ($\Delta G^0 = -134 \text{ kJ mol}^{-1}$), the catalyst was quite inefficient and a turnover number (TON, moles of hydrogen peroxide per mole of palladium) of only 5 was achieved. The rapid inactivation of the catalyst was mainly due to the oxidation of the phosphane ligand and the resulting precipitation of palladium metal. A moderate improvement of the catalyst lifetime (TON up to 87) was achieved by using the more stable triphenylarsane as the palladium ligand;^[4] however, the process was still not suitable for practical applications.

In the last fifteen years, nitrogen ligands have proved to be valuable substitutes of more traditional phosphorus ligands in a number of homogeneously catalyzed reactions.^[5] As part of research aimed at developing a new industrial process for the production of hydrogen peroxide, we have therefore investigated a series of palladium complexes containing bidentate nitrogen ligands **1–8**. Herein we describe an effective and stable catalyst for the synthesis of hydrogen peroxide from oxygen, carbon monoxide, and water, the productivity of which is quite comparable to that of commercial processes.

1,10-phenanthroline	1
2,2'-bipyridine	2
4,7-diphenyl-1,10-phenanthroline	3
2,9-dimethyl-1,10-phenanthroline	4
2,9-di- <i>n</i> -butyl-1,10-phenanthroline	5
2,9-diphenyl-1,10-phenanthroline	6
2,9-dichloro-1,10-phenanthroline	7
2,9-dimethyl-4,7-diphenyl-1,10-phenanthroline	8

The reaction was carried out in a biphasic system in which the catalyst is soluble in the organic phase and the produced

hydrogen peroxide is soluble in the aqueous phase. The biphasic system minimizes the ligand oxidation by reducing the contact with hydrogen peroxide and facilitates the separation and recycling of the catalyst by simple decantation. After screening a wide variety of organic solvents, we found that the reaction was accelerated significantly by the presence of a water-insoluble tertiary alcohol, which possibly plays an active role in the reaction mechanism by acting as ligand. Primary and secondary alcohols were also effective but, under the reaction conditions employed, they were oxidized to some extent (2% conversion was found after 10 h) to the corresponding carbonyl derivatives.^[6] A mixture of 2-methyl-2-butanol, 1,2,4-trichlorobenzene (a hydrophobic solvent added in order to improve the phase separation), and water was selected as the reaction medium for the comparison of the catalysts.

Each of the catalysts were generated in situ from Pd(acetate)₂, four equivalents of the appropriate ligand **1–8**, and 40 equivalents of an acid with a weakly coordinating anion as cocatalyst. In the case of the more hydrophilic ligands such as **1**, **2**, and **4**, which afforded complexes soluble in the aqueous phase, the catalysts were transferred into the organic phase by using a highly hydrophobic acid cocatalyst (perfluorooctanoic acid), which functioned as a phase transfer anion (e.g. the partition of the complex with ligand **4** in the organic layer was <1% and >99% with trifluoroacetate and perfluorooctanoate anion, respectively).

All the reactions were performed at 70 °C and at a total pressure 7100 kPa ($p_{\text{CO}} = 600 \text{ kPa}$; $p_{\text{O}_2} = 6500 \text{ kPa}$). An excess of oxygen was used in order to prevent the precipitation of palladium metal, which becomes predominant under reductive conditions. We observed three different reactivities, depending on the nature of the substitution at the 2,9-position of the ligand (Table 1). The unsubstituted ligands **1**, **2**, and **3**, in presence of CO, led to the formation of stable red complexes,^[7] which proved ineffective for the synthesis of hydrogen peroxide.

Ligands bearing bulky substituents, such as **5** and **6**, did not form binuclear species due to the steric hindrance adjacent to the N-donor function, but instead gave unstable soluble Pd⁰

Table 1. Effect of ligand on the synthesis of hydrogen peroxide by palladium catalysis.^[a]

Ligand	Acid	TOF [h ⁻¹] ^[b]
1	C ₇ F ₁₅ COOH	0 ^[c]
6	CF ₃ COOH	0 ^[c]
2	C ₇ F ₁₅ COOH	0 ^[c]
7	CF ₃ COOH	39
3	CF ₃ COOH	0 ^[c]
8	CF ₃ COOH	527
4	CF ₃ COOH	0 ^[d]
8	C ₇ F ₁₅ COOH	578
4	C ₇ F ₁₅ COOH	124
8	Tol-SO ₃ H	256
5	CF ₃ COOH	0 ^[e]

[a] Ligand/acid/Pd molar ratio: 4/40/1; solvent: trichlorobenzene/2-methyl-2-butanol/water 35/25/40 (v/v/v); temperature: 70 °C; $p_{\text{CO}} = 600 \text{ kPa}$; $p_{\text{O}_2} = 6500 \text{ kPa}$. [b] Turnover number frequency (calculated as moles of hydrogen peroxide per mole of palladium per hour). [c] The formation of red dimeric complexes was observed. [d] The complex was soluble in the aqueous phase. [e] The precipitation of palladium metal was observed.

[*] Dr. D. Bianchi, Dr. R. Bortolo, R. D'Aloisio, Dr. M. Ricci
EniChem S.p.A. - Centro Ricerche Novara "Istituto G. Donegani"
Via Fauser 4, I-28100 Novara (Italy)
Fax: (+390) 321-447378
E-mail: Daniele_Bianchi@hq.eni-chem.geis.com

complexes that quickly dissociated, leading to the formation of palladium metal. The best results in palladium-catalyzed synthesis of hydrogen peroxide were obtained with the ligands **4** and **8**. The lower turnover frequency (TOF) obtained for catalysts with the ligand **7** indicates that such electron-withdrawing substituents have a severe negative effect on the catalytic activity. In the case of ligand **4**, the water-soluble complex was active only if it was transferred into the organic phase by using the hydrophobic perfluorooctanoate anion.

The kinetic profiles of the reaction carried out using [Pd(**8**)X₂] as catalyst in a halogenated environment (X: C₇F₁₅COO⁻; solvent: 1,2,4-trichlorobenzene/2-methyl-2-butanol/water) or in a halogen-free environment (X: toluene-4-sulfonate, solvent: toluene/2-methyl-2-butanol/water) are shown in Figure 1.

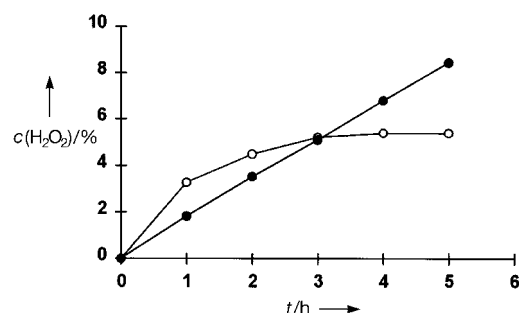


Figure 1. Effect of solvent on the synthesis of hydrogen peroxide by palladium catalysis: (○) Catalyst: [Pd(**8**)(C₇F₁₅COO)₂]; solvent: 1,2,4-trichlorobenzene/2-methyl-2-butanol/water; (●) catalyst: [Pd(**8**)(Tol-SO₃)₂]; solvent: toluene/2-methyl-2-butanol/water.

In spite of their strong accelerating effect on the synthesis of hydrogen peroxide, and their stabilizing effect with regard to the formation of palladium metal,^[8] chlorinated solvents are not the most appropriate reaction media since they can also undergo undesired side reactions, such as the palladium-catalyzed reduction in the presence of CO and water [Eq. (2)].^[9] The hydrochloric acid generated in this way, even at a low concentration (molar ratio Cl/Pd ≥ 4/1), can act as a strongly coordinating ligand of palladium, leading to the formation of unreactive complexes and thus to inactivation of the catalyst.^[10]



Much better results in terms of catalyst stability were obtained by operating in a halogen-free solvent and by adding only sufficient hydrochloric acid (molar ratio Cl/Pd = 1/1) to prevent the precipitation of palladium metal. Under these conditions it was possible to achieve high TONs and produce hydrogen peroxide aqueous solutions up to 8% w/w concentration. The catalyst, which is quantitatively distributed in the organic phase, could be easily recovered and reused in several consecutive reactions, without appreciable loss of activity.

Although detailed mechanistic information is not currently available, the reaction is likely to involve the reduction of Pd^{II} species by carbon monoxide to form a Pd⁰ complex via a hydride intermediate.^[11] The subsequent oxidation of the Pd⁰

species to afford a Pd^{II} peroxy species and eventually, under acidic conditions, hydrogen peroxide, is known.^[12, 13]

In conclusion, complexation of palladium with a suitable bidentate nitrogen ligand provides an efficient catalyst for the synthesis of hydrogen peroxide from carbon monoxide, oxygen, and water. The structure of the ligand as well as the nature of the weakly coordinating anion and the solvent play a key role in determining the catalytic activity and the operational stability of the complexes; catalytic systems were developed that displayed far better catalytic activity and operational stability than in palladium-based catalytic systems described to date. The development of a continuous operation process, more suitable for an industrial application, is presently under consideration.

Experimental Section

Ligands **1–4** and **8** were purchased from Aldrich, and **5–7** were synthesized according to literature methods.^[14, 15]

General procedure for the synthesis of hydrogen peroxide: Pd(OAc)₂ (0.07 mmol), CF₃COOH or C₇F₁₅COOH (2.8 mmol), and one of the ligands **1–8** (0.28 mmol) were dissolved in a mixture of 1,2,4-trichlorobenzene (40 mL) and 2-methyl-2-butanol (60 mL), and stirred for 6 h at 25 °C. The resulting solution was added to water (80 mL) to form a biphasic system and poured into an autoclave containing a glass liner. The reactor was then pressured to 6500 kPa partial pressure of O₂ and 600 kPa partial pressure of CO to form a nonflammable gas mixture. The reactions were carried out for one hour at 70 °C; the mixture was stirred by a magnetically driven impeller. After the reactor was depressurized, the hydrogen peroxide concentration in the aqueous solution was measured by titration with potassium permanganate.

Kinetics measurements: Pd(OAc)₂ (2.5 mmol), C₇F₁₅COOH (60 mmol), and **8** (20 mmol) were dissolved in a mixture of 1,2,4-trichlorobenzene (85 mL) and 2-methyl-2-butanol (15 mL), and stirred for 6 h at 25 °C. A second catalytic system was prepared in the same way by using toluene-4-sulfonic acid and toluene instead of C₇F₁₅COOH and 1,2,4-trichlorobenzene, respectively. The resulting solutions were added to water (80 mL) to form a biphasic system. The comparison between the two catalysts was carried out in the same reactor as described above equipped with an automatic system to maintain both the inlet pressure and the inlet composition of the gas mixture at constant values. The reactions were carried out at 70 °C and 8100 kPa of total pressure (*p*_{CO} = 600 kPa; *p*_{O₂} = 7500 kPa). The hydrogen peroxide concentration in the aqueous phase was determined periodically during the course of each run by temporarily stopping the gas flow for one minute, which allowed the liquid phases to separate, withdrawing a measured volume of aqueous phase, and pumping an equal volume of deionized water back into the reactor.

Received: June 24, 1998

Revised version: October 29, 1998 [Z12045 IE]

German version: *Angew. Chem.* **1999**, *111*, 734–736

Keywords: hydrogen peroxide • N ligands • palladium

- [1] G. Strukul in *Catalytic Oxidations with Hydrogen Peroxide as Oxidant* (Ed.: G. Strukul), Kluwer, Dordrecht, **1992**, pp. 1–11.
- [2] G. Goor in *Catalytic Oxidations with Hydrogen Peroxide as Oxidant* (Ed.: G. Strukul), Kluwer, Dordrecht, **1992**, pp. 13–43.
- [3] V. N. Zudin, V. A. Likhonov, Y. I. Yermakov, *Kinet. Katal.* **1979**, *20*, 1559–1600.
- [4] F. E. Jacobson (BOC) US-A 4711772, **1987** [*Chem. Abstr.* **1988**, *108*, 40590x].
- [5] A. Togni, L. M. Venanzi, *Angew. Chem.* **1994**, *106*, 517–547; *Angew. Chem. Int. Ed. Engl.* **1994**, *33*, 497–526.
- [6] Y. Tamaru, Y. Yamada, K. Inoue, Y. Yamamoto, Z. Yoshida, *J. Org. Chem.* **1983**, *48*, 1286–1292.

- [7] V. V. Grushin, *Chem. Rev.* **1996**, 96, 2011–2033.
 [8] F. Ragaini, S. Cenini, *J. Mol. Catal. A* **1996**, 109, 1–25.
 [9] By using 1,2,4-trichlorobenzene as a solvent, a progressive accumulation of mono- and dichlorobenzenes was detected in the reaction mixture.
 [10] A. Bontempi, E. Alessio, G. Chanos, G. Mestroni, *J. Mol. Catal.* **1987**, 42, 67–80.
 [11] A. Yamamoto, *Organotransition Metal Chemistry. Fundamental Concepts and Applications*, Wiley, New York, **1986**, p. 280, 343.
 [12] G. Wilke, H. Schott, P. Heimbach, *Angew. Chem.* **1967**, 79, 62; *Angew. Chem. Int. Ed. Engl.* **1967**, 6, 92–93.
 [13] S. Muto, H. Ogata, Y. Kamiya, *Chem. Lett.* **1975**, 8, 809–812.
 [14] C. O. Dietrich-Buchecker, P. A. Marnot, J. P. Savage, *Tetrahedron Lett.* **1982**, 50, 5291–5294.
 [15] M. Yamada, Y. Nakamura, S. Kuroda, I. Shimao, *Bull. Chem. Soc. Jpn.* **1990**, 63, 2710–2712.

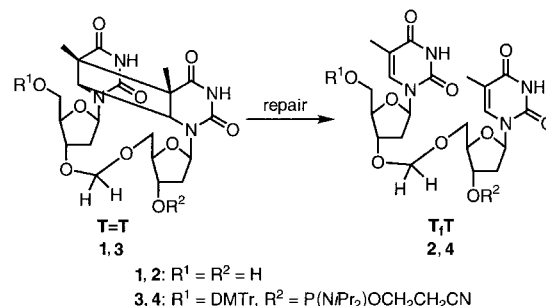
“Base Flipping”: Photodamaged DNA–RNA Duplexes Are Poor Substrates for Photoreactivating DNA-Repair Enzymes**

Jens Butenandt, Lars T. Burgdorf, and Thomas Carell*

cis-syn Cyclobutane pyrimidine dimers (photodimers) are the main DNA lesions formed on irradiation of cells with UV light.^[1] They are responsible for cell death, the development of various skin cancers, and therefore represent a severe threat to all organisms that are exposed to sunlight.^[2] All organisms have developed DNA repair processes,^[1–3] in order to remove UV-induced lesions from the genome and to overcome DNA damage. The observation that certain genome sites are repaired with greatly reduced efficiency, giving rise to mutation hot spots,^[3a, 4] has shifted the investigation of the factors that determine the effectiveness of lesion recognition into the center of DNA repair research. It is currently believed that lesion-specific repair enzymes recognize structural alterations of the normal DNA duplex which are maybe caused by weakened hydrogen bonds and π -stacking interactions around a DNA lesion. Crystallographic data show that many repair enzymes subsequently “flip” the damaged base out of the DNA duplex for repair.^[5] This process could be influenced by the DNA packing, which may shield DNA lesions,^[6] and by the local DNA sequence and conformation.^[7] A first indication that DNA repair might be influenced by the duplex conformation, stems from the discovery that dsDNA-specific repair enzymes remove lesions from DNA–RNA

hybrids,^[8] which are in an atypical A-like conformation, with reduced efficiency.^[9]

In order to learn if and to what extent the duplex conformation is able to influence the DNA-photolyase repair process, depicted schematically in Scheme 1, we investigated the extent to which A- and B-type double strands are



Scheme 1. The starting material **1** and **2** of the phosphamidite building blocks **3** and **4**, which were used for the synthesis of lesion-containing DNA single and DNA–DNA and DNA–RNA double strands. The repair occurs under cleavage of the cyclobutane ring catalyzed by photolyase DNA-repair enzymes.

destabilized by a photolesion, which has been incorporated site-specifically into the DNA strand. The repair was probed with a DNA-photolyase, which is believed to recognize the *cis-syn* photolesions in an extrahelical, “flipped-out” conformation.^[5d] The presented thermodynamic data reveal that photodimers significantly destabilize a B-duplex but decrease the stability of an A-like duplex only to a small extent. The low destabilization was found to correlate with less efficient repair, which indicates that the local DNA conformation might modulate the DNA lesion “flipping” process.

In order to allow the preparation of oligonucleotides with a site-specific *cis-syn* photolesion in sufficient amounts for this investigation, all studies were performed with the recently introduced formacetal-linked^[10] *cis-syn* photodimer analogue **1** (Scheme 1), which is readily available in gram quantities.^[11] This compound was shown to be a good photolyase substrate since DNA photolyases ignore the central intradimer phosphodiester moiety during the repair process.^[12] Compound **1** and the reference compound **2** were converted into the phosphamidites **3** and **4**, respectively, and incorporated into the GC-rich 12mer and the AT-rich 14mer oligonucleotides **5–8** (Table 1) using previously published procedures.^[11] The oligonucleotides were annealed with 1.0 equivalent (1.3 equivalents for the enzymatic studies) of the complementary DNA or RNA strand to give the DNA–DNA duplexes **9–12** (B-conformation) and the DNA–RNA duplexes **13–16** (A-like conformation).^[8] The reference duplexes **9**, **11**, **13**, and **15** were prepared for comparison.

Circular dichroism (CD) studies with all duplexes were performed to investigate their conformations in solution.^[13] The CD spectra were recorded at 25 °C ($c_{\text{oligo}} = 5 \mu\text{M}$) and represent an average of two independent measurements (Figure 1). The CD spectrum of the reference DNA–DNA duplex **9** and of the photodimer-containing DNA–DNA duplex **10** are very similar and feature all the characteristics of

[*] Dr. T. Carell, Dipl.-Chem. L. T. Burgdorf, Dipl.-Chem. J. Butenandt
 Laboratorium für Organische Chemie, ETH-Zentrum
 Universitätsstrasse 16, CH-8092, Zürich (Switzerland)
 Fax: (+41) 1-632-1109
 E-mail: tcarell@org.chem.ethz.ch

[**] This work was supported by the Schweizer Nationalfond and by the Boehringer Ingelheim Fonds (Stipend to J. B.). We thank Prof. F. Diederich for his generous support, Dr. S. Pitsch for many helpful discussions, Dr. L. Cox for a careful inspection of the manuscript, and Dr. A. P. M. Eker for providing the *A. nidulans* photolyase. The crude RNA strands were kindly provided by Xeragon, Zurich.

Table 1. Melting temperatures T_m [°C], free energies $\Delta G_{15^\circ\text{C}}^\circ$ [kJ mol⁻¹],^[18] enthalpies ΔH° [kJ mol⁻¹] and Entropies ΔS° [kJ K⁻¹ mol⁻¹] for DNA–DNA and DNA–RNA duplex formation derived from van't Hoff plots.

	Sequence	T_m [°C] ^[a]	$\Delta G_{15^\circ\text{C}}^\circ$ [kJ mol ⁻¹] ^[b]	ΔH° [kJ mol ⁻¹]	ΔS° [kJ K ⁻¹ mol ⁻¹]
5	5'd(CGACGT _T TGCAGC)3'	–	–	–	–
6	5'd(CGTATT _T TATTCTGC)3'	–	–	–	–
7	5'd(CGACGT = TGCAGC)3'	–	–	–	–
8	5'd(CGTATT = TATTCTGC)3'	–	–	–	–
B-type DNA duplexes					
9	5'd(CGACGT _T TGCAGC)3' 3'd(GCTGCA ACGTCG)5'	58.2	– 81	– 367	– 0.99
10	5'd(CGACGT = TGCAGC)3' 3'd(GCTGCA ACGTCG)5'	51.0	– 69	– 321	– 0.88
11	5'd(CGTATT _T TATTCTGC)3' 3'd(GCATAA ATAAGACG)5'	46.8	– 78	– 458	– 1.32
12	5'd(CGTATT = TATTCTGC)3' 3'd(GCATAA ATAAGACG)5'	41.2	– 68	– 417	– 1.21
A-type DNA duplexes					
13	5'd(CGACGT _T TGCAGC)3' 3'r(GCTGCA ACGTCG)5'	54.9	– 78	– 371	– 1.02
14	5'd(CGACGT = TGCAGC)3' 3'r(GCTGCA ACGTCG)5'	51.5	– 72	– 344	– 0.95
15	5'd(CGTATT _T TATTCTGC)3' 3'r(GCATAA ATAAGACG)5'	46.3	– 75	– 427	– 1.22
16	5'd(CGTATT = TATTCTGC)3' 3'r(GCATAA ATAAGACG)5'	45.6	– 73	– 412	– 1.18

[a] Conditions: 150 mM NaCl, 10 mM Tris/HCl,^[18] pH 7.4, $c_{\text{oligo}} = 4.0 \mu\text{M}$. Error in T_m : $\pm 0.3^\circ\text{C}$. [b] Obtained by plotting $1/T_m$ vs $\ln c_T$. Data from at least five concentrations and of two to three independent measurements were used; error estimate at $\pm 5\%$.

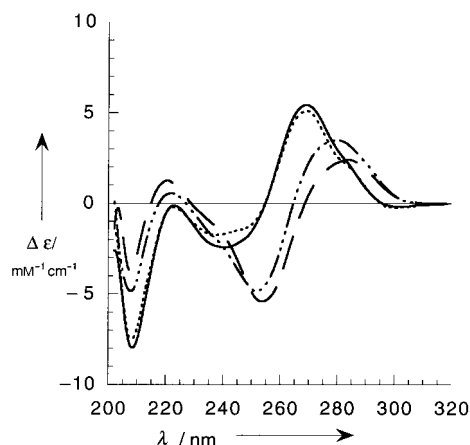


Figure 1. CD spectra of the oligonucleotide at 25°C in 150 mM NaCl, 10 mM Tris/HCl (Tris = tris(hydroxymethyl)aminomethane),^[18] pH 7.4, $c_{\text{oligo}} = 5 \mu\text{M}$. --- **9**, **10**, **13**, — **14**. Similar results were obtained for the series **11**, **12** and **15**, **16**.

a B-type double helix. Incorporation of the photodimer analogue **1** does consequently not affect the overall B-structure. The CD spectra of the DNA–RNA duplexes **13** and **14** reveal an A-type duplex structure.^[8, 13] Both CD spectra of **13** and **14** were found to be mostly identical, indicating that the photolesion does not affect the A-like conformation as well.

Melting temperature studies were carried out to quantify the destabilizing effect of a photodimer lesion in an A- and B-type duplex environment (Table 1). Thermodynamic parameters (15°C) were determined from van't Hoff plots with at least five different concentrations (0.5–8.0 μM) each.^[14] Under the described conditions, the two reference DNA–DNA duplexes **9** and **11** have a T_m (4 μM) of 58.2°C and

46.8°C (Table 1). Incorporation of the photodimer model results in a significant destabilization of the duplexes **10** and **12**, which possess T_m values (4 μM) of 51.0°C (**10**) and 41.2°C (**12**). Such a destabilization has been previously ascribed to a local disruption of the π -stacking and hydrogen-bonding interactions of the dimer in the DNA duplex,^[15] although NMR investigations^[15c, 16] and calculations^[17] suggest that the dimer lesion is still positioned within the duplex.

The control DNA–RNA heteroduplexes **13** and **15** melt at $T_m = 54.9^\circ\text{C}$ and 46.3°C , respectively (4 μM). Incorporation of the photodimer unit in these A-like duplex structures causes a significantly smaller destabilization of the duplex: the melting points decrease to a much smaller extent yielding a T_m value of 51.5°C for **14** and of 45.6°C for **16** (4 μM). These values are only 3.4°C and 0.7°C lower than those for the reference compounds **13** and **15**, respectively. The diminished destabilization of the damaged DNA–RNA hybrids is supported by the thermodynamic data (Table 1). Incorporation of the dimer unit into the DNA–DNA duplexes (**10**, **12**) reduced their stability by +12 and +10 kJ mol⁻¹ compared to that of **9** and **11**. Within the A-type DNA–RNA series, however, the reduction of the stability is two to four times smaller, yielding $\Delta(\Delta G) = +6$ kJ mol⁻¹ between **13** and **14**, and only +2 kJ mol⁻¹ between **15** and **16**.

If the DNA lesion recognition process is influenced by the duplex conformation and the amount of duplex destabilization, we would expect an increased repair rate for **1** in the strongly destabilized B duplex. In order to test the hypothesis we compared the repair efficiency of **1**-containing DNA–DNA and DNA–RNA duplexes using a DNA-photolyase (*A. nidulans*).^[19] Footprinting data showed that these enzymes recognize only a few phosphodiester groups directly adjacent to the dimer unit, almost exclusively in the lesion-containing

strand.^[12] In order to verify this result we initially investigated the repair of DNA single strands (**7** and **8**) and DNA–DNA double strands (**10** and **12**). We observed, however, identical repair efficiencies, which underlines that photolyases repair *cis-syn* photolesions, at the used concentrations, largely independent of the counter strand (Figure 2).^[3d] The final

duplex through the major groove we argue, that the special A-like conformation, with its narrow and deep major groove, hinders the “flipping” of lesions out of the A-like duplex.

Received: October 2, 1998 [Z12482IE]

German version: *Angew. Chem.* **1999**, *111*, 718–721

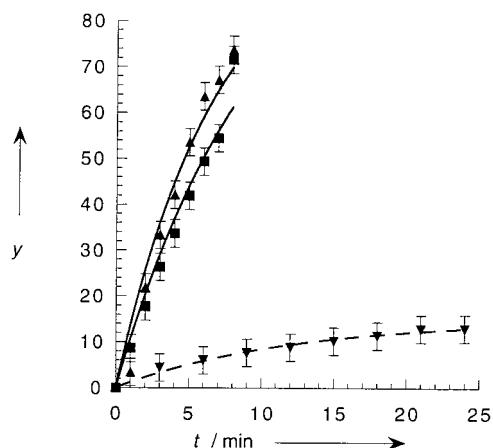


Figure 2. The repair kinetics measured with the lesion-1-containing single strand (**7**, ■), the lesion-1-containing DNA–DNA duplex (**10**, ▲), and the DNA–RNA duplex (**14**, ▼). Similar results were obtained for the series **8**, **12**, and **16**. All photolyase measurements were performed at least twice with two different oligonucleotide concentrations ($c_{\text{oligo}} = 10^{-6}\text{M}$ and 10^{-7}M , $c_{\text{enzyme}} = 5 \times 10^{-8}\text{M}$). y: Amount of repaired oligonucleotide in %.

repair data obtained for the DNA–DNA and DNA–RNA duplexes are presented in Figure 2 for the oligonucleotide series **7**, **10** and **14**. Measurement of the dimer repair in the A-like DNA–RNA environment (**14** and **16**) revealed in agreement with the hypothesis dramatically reduced repair efficiencies (Figure 2). Under all circumstances we observed a repair rate that was reduced by a factor of almost 10(!). Addition of noncomplementary RNA during repair experiments did not influence the repair efficiency, which excludes the possibility that RNA inhibits the photolyase enzyme. Although we cannot fully exclude that the 2'OH group of the RNA in the DNA–RNA duplexes affects the lesion recognition step, the RNA control experiments and the single strand results indicate that the influence of the 2'OH group is limited.

The thermodynamic data show that one of the major environmentally induced DNA photolesions destabilizes a duplex in an A-like conformation to a significantly smaller extent compared to a duplex in standard B-conformation. The DNA-photolyase-catalyzed repair of the same lesion-1-containing DNA strand, if paired with a RNA counter strand (DNA–RNA hybrid), is strongly reduced in comparison to the corresponding DNA–DNA duplex. Although neither the supposed photolyase-induced “lesion-flipping” nor the question to which extent the 2'OH groups of the RNA counter strand effects the photolyase binding are yet fully understood our data provide clear evidence that conformational factors modulate the destabilization affect of DNA lesion and influences the DNA repair efficiency. Based on our data and the knowledge that photolyases approach the DNA

Keywords: DNA repair • DNA structures • DNA–RNA hybrids • photolyases • UV-photolesions

- [1] a) T. Lindahl, *Nature* **1993**, *362*, 709–715; b) P. F. Heelis, R. F. Hartman, S. D. Rose, *Chem. Soc. Rev.* **1995**, 289–297; c) T. P. Begley, *Acc. Chem. Res.* **1994**, *27*, 394–401; d) T. Carell, *Chimia* **1995**, *49*, 365–373; e) T. Carell, *Angew. Chem.* **1995**, *107*, 2697–2700; *Angew. Chem. Int. Ed. Engl.* **1995**, *34*, 2491–2494.
- [2] a) H. W. Thielmann, *Recent Results in Cancer Research: Skin Carcinogenesis in Man and in Experimental Models*, Vol. 128, Springer, Heidelberg, **1993**; b) J.-S. Taylor, *J. Chem. Educ.* **1990**, *67*, 835–841; c) J.-S. Taylor, *Acc. Chem. Res.* **1994**, *27*, 76–82.
- [3] a) E. C. Friedberg, G. C. Walker, W. Siede, *DNA Repair and Mutagenesis*, ASM Press, Washington, DC, **1995**; b) A. Sancar, *Science* **1994**, *266*, 1954–1956; c) A. Sancar, *J. Biol. Chem.* **1995**, *270*, 15915–15918; d) A. Sancar, *Biochemistry* **1994**, *33*, 2–9.
- [4] a) L. Daya-Grosjean, N. Dumaz, A. Sarasin, *J. Photochem. Photobiol. B* **1995**, *28*, 115–124; b) A. J. Nataraj, J. C. Trent II, H. N. Ananthaswamy, *Photochem. Photobiol.* **1995**, *62*, 218–230; c) S. Tornaletti, G. P. Pfeifer, *Science* **1994**, *263*, 1436–1438.
- [5] a) R. S. Lloyd, X. Cheng, *Curr. Opin. Chem. Biol.* **1998**, *4*, 139–151; b) R. J. Roberts, *Cell* **1995**, *82*, 9–12; c) G. L. Verdine, S. D. Bruner, *Chem. Biol.* **1997**, *4*, 329–334; d) evidence for base flipping with photolyases see reference [19] and: B. J. van de Berg, G. B. Sancar, *J. Biol. Chem.* **1998**, *273*, 20276–20284; D. Ramaiah, Y. Kan, T. Koch, H. Ørsum, G. B. Schuster, *Proc. Natl. Acad. Sci. USA* **1998**, *95*, 12902–12905.
- [6] a) B. Suter, M. Livingstone-Zatchej, F. Thoma, *EMBO J.* **1997**, *16*, 2150–2160; b) R. E. Wellinger, F. Thoma, *EMBO J.* **1997**, *16*, 5056–5056.
- [7] Z. Livneh, O. Cohen-Fix, R. Skaliter, T. Elizur, *Crit. Rev. Biochem. Mol. Biol.* **1993**, *28*, 465–513.
- [8] Such hybrid duplexes are biologically relevant during DNA transcription, DNA replication, and RNA reverse transcription. For a detailed investigation of their conformation see for example: a) M. Egli, N. Usman, A. Rich, *Biochemistry* **1993**, *32*, 3221–3237; b) M. Egli, N. Usman, S. Zhang, A. Rich, *Proc. Natl. Acad. Sci. USA* **1992**, *89*, 534–538. In solution DNA–RNA hybrids form a globally more A-like duplex in which the deoxyribose adopts a C_2' -endo- and the ribose a C_3' -endo conformation. See for example: a) L. Ratmeyer, R. Vinayak, Y. Y. Zhong, G. Zon, W. D. Wilson, *Biochemistry* **1994**, *33*, 5298–5304; b) J. I. Gyi, G. L. Conn, A. N. Lane, T. Brown, *Biochemistry* **1996**, *36*, 12538–12548.
- [9] A. S. Kamath-Loeb, A. Hizi, J. Tabone, M. S. Solomon, L. A. Loeb, *Eur. J. Biochem.* **1997**, *250*, 492–501. Other repair systems show also increased activity with increasing duplex instability. See for example: a) C. P. Selby, A. Sancar, *Science* **1993**, *260*, 53–58; b) X. Zhao, J. Liu, D. S. Hsu, S. Zhao, J.-S. Taylor, A. Sancar, *J. Biol. Chem.* **1997**, *272*, 32580–32590; c) D. Mu, M. Tursun, D. R. Duckett, J. T. Drummond, P. Modrich, A. Sancar, *Mol. Cell. Biol.* **1997**, *17*, 760–789; d) M. T. Hess, U. Schwitter, M. Petretta, B. Giese, H.-P. Nägeli, *Proc. Natl. Acad. Sci. USA* **1997**, *94*, 6663–6669; e) D. L. Svoboda, C. A. Smith, J.-S. A. Taylor, A. Sancar, *J. Biol. Chem.* **1993**, *268*, 10694–10700.
- [10] a) J. M. Veal, X. Gao, F. K. Brown, *J. Am. Chem. Soc.* **1993**, *115*, 7139–7145; b) X. Gao, F. K. Brown, P. Jeffs, N. Bischofberger, K. Y. Lin, A. Pipe, S. A. Noble, *Biochemistry* **1992**, *31*, 6228–6236.
- [11] J. Butenandt, A. P. M. Eker, T. Carell, *Chem. Eur. J.* **1998**, *4*, 642–653.
- [12] a) I. Husain, G. B. Sancar, S. R. Holbrook, A. Sancar, *J. Biol. Chem.* **1987**, *262*, 13188–13197; b) S.-T. Kim, A. Sancar, *Biochemistry* **1991**, *30*, 8623–8630; c) a small effect of the counter strand on the binding by photolyases was reported by: A. Kiener, I. Husain, A. Sancar, C.

- Walsh, *J. Biol. Chem.* **1989**, *264*, 13880–13887; d) the DNA sequence slightly effects the binding (K_d) of photolyases to a DNA–DNA double strand: D. L. Svoboda, C. A. Smith, J.-S. Taylor, A. Sancar, *J. Biol. Chem.* **1993**, *258*, 10694–10700.
- [13] a) K. B. Hall, L. W. McLaughlin, *Biochemistry* **1991**, *30*, 10606–10613; b) L. Ratmeyer, R. Vinayak, Y. Y. Zhong, G. Zon, W. D. Wilson, *Biochemistry* **1994**, *33*, 5298–5304; c) J. I. Gyi, G. L. Conn, A. N. Lane, T. Brown, *Biochemistry* **1996**, *35*, 12538–12548.
- [14] L. A. Marky, K. J. Breslauer, *Biopolymers* **1987**, *26*, 1601–1620.
- [15] a) F. N. Hayes, D. L. Williams, R. L. Ratliff, A. J. Varghese, C. S. Rupert, *J. Am. Chem. Soc.* **1971**, *93*, 4940–4942; b) F. Barone, A. Bonincontro, F. Mazzei, A. Minoprio, F. Pedone, *Photochem. Photobiol.* **1995**, *61*, 61–67; c) J.-S. Taylor, D. S. Garrett, I. R. Brockie, D. L. Svoboda, J. Telser, *Biochemistry* **1990**, *29*, 8858–8866.
- [16] a) J. Kemmink, R. Boelens, T. Koning, G. A. van der Marel, J. H. van Boom, R. Kaptein, *Nucleic Acids Res.* **1987**, *15*, 4645–4653; b) J. Kemmink, R. Boelens, T. M. G. Koning, R. Kaptein, G. A. van der Marel, J. H. van Boom, *Eur. J. Biochemistry* **1987**, *162*, 37–43; c) J.-K. Kim, D. Patel, B.-S. Choi, *Photochem. Photobiol.* **1995**, *62*, 44–50.
- [17] a) T. I. Spector, T. E. Cheatham III, P. A. Kollman, *J. Am. Chem. Soc.* **1997**, *119*, 7095–7104; b) M. G. Cooney, J. H. Miller, *Nucleic Acids Res.* **1997**, *25*, 1432–1436; c) H. Yamaguchi, D. M. F. van Aalten, M. Pinak, A. Furukawa, R. Osman, *Nucleic Acids Res.* **1998**, *26*, 1939–1946; d) K. Miaskiewicz, J. Miller, M. Cooney, R. Osman, *J. Am. Chem. Soc.* **1996**, *118*, 9156–9163.
- [18] All thermodynamic experiments were performed in Tris/HCl buffer. ΔG is reported at 15 °C. This allows the thermodynamic data to be compared more directly with the enzymatic repair kinetics, which were performed in a phosphate buffer (pH 7.0) at 15 °C.
- [19] For X-ray structures see: a) H.-W. Park, S.-T. Kim, A. Sancar, J. Deisenhofer, *Science* **1995**, *268*, 1866–1872; b) T. Tamada, K. Kitadokoro, Y. Higuchi, K. Inaka, A. Yasui, P. E. de Ruiter, A. P. M. Eker, K. Miki, *Nature Struct. Biol.* **1997**, *11*, 887–891.

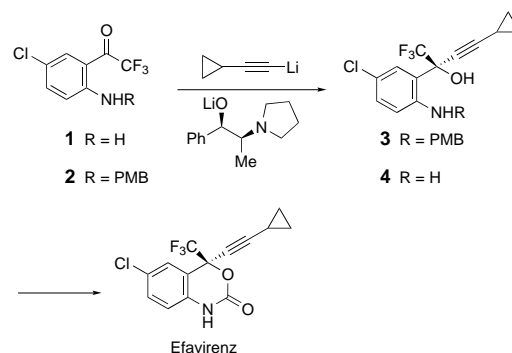
A Novel, Highly Enantioselective Ketone Alkynylation Reaction Mediated by Chiral Zinc Aminoalkoxides

Lushi Tan,* Cheng-yi Chen, Richard D. Tillyer, Edward J. J. Grabowski, and Paul J. Reider

Stereocontrolled nucleophilic addition to carbonyl compounds is an important synthetic method. While the enantioselective alkylation of carbonyl compounds has been widely studied,^[1] nucleophilic alkynylation has enjoyed only very limited success. A few examples of enantioselective alkynylation of aldehydes by organometallic compounds in combination with chiral modifiers have been reported.^[2, 3] For example, Soai and Niwa showed that the addition of dialkynylzinc and alkylalkynylzinc reagents to benzaldehyde in the presence of amino alcohols provides propargyl alcohols with an *ee* of less than 50%.^[2c] Recently, Corey and Cimprich reported the addition of alkynylboranes to aldehydes with promotion by substoichiometric quantities of proline-derived oxazaborolidines to give propargyl alcohols with up to 97% *ee* at low temperature.^[3] We report here a novel, highly enantio-

selective, and practical alkynylation (up to 99.2% *ee*) of a prochiral ketone by alkynyllithium and alkynylmagnesium reagents with mediation by chiral zinc aminoalkoxides.

Efavirenz is a potent nonnucleosidal HIV reverse transcriptase inhibitor which has just been approved by the US FDA for treatment of AIDS.^[4] The importance of this compound prompted us to seek an efficient and scalable synthesis that would allow the installation of the quaternary carbon atom with absolute stereocontrol. A recently reported asymmetric synthesis of this compound is based on a highly enantioselective addition of lithium cyclopropylacetylide to the PMB-protected ketoaniline **2** (Scheme 1).^[5] The reactive

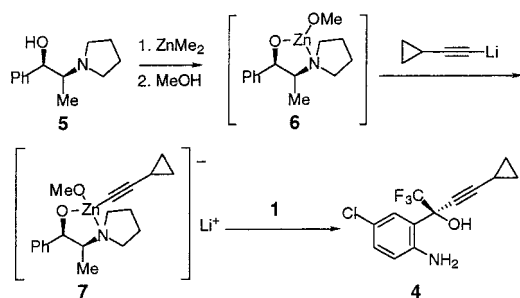


Scheme 1. Synthesis of efavirenz. PMB = *p*-methoxybenzyl.

species responsible for the strong chiral induction in this reaction was well characterized on the basis of ^6Li NMR data.^[6] The chiral addition step, which proceeds with greater than 98% *ee*, requires the use of 2.2 equivalents of lithium cyclopropylacetylide, 2.2 equivalents of (1*R*,2*S*)-*N*-pyrrolidinylnorephedrine alkoxide as chiral controller, and low temperatures (–60 °C). In addition, the success of the reaction relies on the protection of the aniline moiety, and this makes a protection/deprotection step necessary. The most straightforward and efficient asymmetric synthesis of efavirenz would involve the direct enantioselective alkynylation of the unprotected ketoaniline **1**^[5] to afford amino alcohol **4**. Addition of lithium cyclopropylacetylide to **1** by the reported method,^[5] however, suffered from low conversion and low enantioselectivity. Furthermore, the strongly basic conditions eventually led to decomposition of the product.

We reasoned that the inefficiency of the reaction between lithium cyclopropylacetylide and **1** is due to the strong basicity of the lithium reagent, which deprotonates the aniline group. It was proposed that complexation of a zinc alkoxide $\text{Zn}(\text{OR})_2$ with the lithium acetylide would lower the basicity while maintaining the nucleophilicity of the acetylide. In addition, a chiral alkoxide could serve as a mediator for asymmetric induction. This conceptually simple approach proved to be highly effective for the asymmetric alkynylation of the unprotected ketoaniline **1**. The reaction of dimethylzinc with one equivalent of (1*R*,2*S*)-*N*-pyrrolidinylnorephedrine (**5**)^[7] followed by one equivalent of methanol generated the chiral zinc alkoxide **6** (Scheme 2).^[8a] The zinc reagent **6** was then treated with lithium cyclopropylacetylide, which presumably generates the zincate **7**.^[8] Reaction of **7** with **1**

[*] Dr. L. Tan, C. Chen, R. D. Tillyer, E. J. J. Grabowski, P. J. Reider
Department of Process Research
Merck Research Laboratories
P.O. Box 2000, RY80E-108
Rahway, New Jersey 07065 (USA)
Fax: (+1) 732-594-8360
E-mail: lushi_tan@merck.com



Scheme 2. Preparation of the zinc complex and its reaction with ketone **1**.

(toluene/THF, 25 °C, 7 h) afforded the amino alcohol **4** with 83 % yield of isolated product and 83 % *ee*.^[9] This result prompted a systematic study of the reaction to improve the enantioselectivity and yield.

As anticipated, the chiral auxiliary has a dramatic influence on the enantioselectivity. Other chiral auxiliaries such as cinchona alkaloids, binaphthol, and tartaric acid derivatives gave very poor selectivity. The initial success with (1*R*,2*S*)-*N*-pyrrolidinylnorephedrine as chiral auxiliary led us to focus our attention on norephedrine derivatives for improving the selectivity (Table 1). (1*R*,2*S*)-Ephedrine and (1*R*,2*S*)-norephedrine gave only moderate selectivities (entries 1 and 2),

Table 1. Effect of the chiral auxiliary and the counteranion on the selectivity.^[a]

Entry	M	Ephedrine auxiliary (OR)	<i>ee</i> of 4 [%]
1	Li	(1 <i>R</i> ,2 <i>S</i>)-ephedrine	28.2
2	Li	(1 <i>R</i> ,2 <i>S</i>)-norephedrine	41.6
3	Li	(1 <i>R</i> ,2 <i>S</i>)- <i>N</i> -methylephedrine	81.0
4	Li	(1 <i>R</i> ,2 <i>S</i>)- <i>N</i> -pyrrolidinylnorephedrine	83.0
5	MgCl	(1 <i>R</i> ,2 <i>S</i>)- <i>N</i> -pyrrolidinylnorephedrine	87.0
6	MgBr	(1 <i>R</i> ,2 <i>S</i>)- <i>N</i> -pyrrolidinylnorephedrine	53.6
7	MgI	(1 <i>R</i> ,2 <i>S</i>)- <i>N</i> -pyrrolidinylnorephedrine	50.6

[a] All reactions were carried out at 25 °C in THF/toluene with 1 equivalent each of chiral auxiliary, methanol, dimethylzinc, and cyclopropylacetylide, and 0.83 equivalents of **1**.

and the best results were obtained with (1*R*,2*S*)-*N*-pyrrolidinylnorephedrine and (1*R*,2*S*)-*N*-methylephedrine (entries 3 and 4). The counteranion also had a significant effect on the enantioselectivity. For example, with the chloromagnesium acetylide, **4** was obtained with 87 % *ee* (entry 5), but only about 50 % *ee* was obtained with the bromo- and iodomagnesium acetylides.

Interestingly, variation of the achiral additive has a profound influence on the enantioselectivity of the alkynylation reaction (Table 2). At 25 °C with complexes derived from (1*R*,2*S*)-*N*-pyrrolidinylnorephedrine and chloromagnesium cyclopropylacetylide, the use of ethanol as achiral auxiliary gave **4** with 55 % *ee* (entry 2), while neopentyl alcohol (entry 3) and methanol (entry 1) gave 96 and 87 % *ee*, respectively. These results suggested that the achiral alcohol

Table 2. Effect of the achiral auxiliary (HX) on the selectivity.^[a]

Entry	Auxiliary	<i>ee</i> of 4 [%]
1	CH ₃ OH	87.0
2	CH ₃ CH ₂ OH	55.0
3	(CH ₃) ₃ CCH ₂ OH	95.6
4	CH ₂ =CHCH ₂ OH	90.0
5	PhCH ₂ OH	89.0
6	CF ₃ CH ₂ OH	95.7
7	CF ₃ CO ₂ H	89.4
8	(CH ₃) ₃ CCO ₂ H	71.6
9	4-NO ₂ PhOH	89.0

[a] All reactions were carried out at 25 °C in THF/toluene with 1 equivalent each of chiral auxiliary, methanol, dimethylzinc, and cyclopropylacetylide, and 0.83 equivalents of **1**.

might exert a steric effect on the stereoselectivity. However, the increase in enantioselectivity from 55 % to about 96 % when 2,2,2-trifluoroethanol was used instead of ethanol indicates a possible significant inductive effect. Good enantioselectivities were also obtained with carboxylic acids and phenols as auxiliaries.

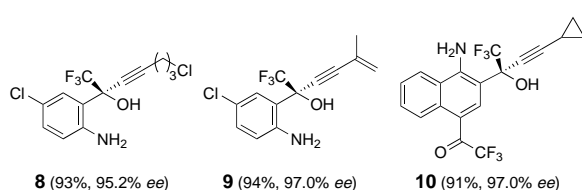
Further optimization of this reaction was carried out with neopentyl alcohol or 2,2,2-trifluoroethanol as achiral auxiliary. We found that dimethyl- and diethylzinc were equally effective, and the chiral zinc reagent could be prepared by mixing the chiral auxiliary, the achiral auxiliary and the dialkylzinc reagent in any order without affecting the conversion and selectivity of the reaction. However, the ratio of chiral to achiral additive does affect the efficiency of the reaction. The enantioselectivity increased to 97.5 % when 1.2 equivalents of (1*R*,2*S*)-*N*-pyrrolidinylnorephedrine and 0.8 equivalents of neopentyl alcohol were used to prepare the zinc alkoxide (Table 3). Further increase in the ratio of chiral to achiral auxiliary did not lead to significant improvement in stereoselectivity. For instance, the zinc alkoxide derived from two equivalents of (1*R*,2*S*)-*N*-pyrrolidinylnorephedrine gave **4** with 95.8 % *ee* but only 50 % conversion. Similar results were obtained with 2,2,2-trifluoroethanol. The enantioselectivity was only slightly dependent on the reaction temperature. Reactions with the zinc alkoxide derived from (1*R*,2*S*)-*N*-pyrrolidinylnorephedrine and 2,2,2-trifluoroethanol gave **4** with 99.2 % *ee* at 0 °C and 94.0 % *ee* at 40 °C.

Table 3. Effect of the amount of chiral auxiliary on the selectivity.^[a]

Entry	Equiv of chiral auxiliary ^[b]	<i>ee</i> of 4 [%]
1	0.8	58.8
2	1	95.6
3	1.1	95.8
4	1.2	97.5
5	1.5	97.7
6	2	95.8

[a] All reactions were carried out at 25 °C in THF/toluene with neopentyl alcohol as the achiral auxiliary, (1*R*,2*S*)-*N*-pyrrolidinylnorephedrine as the chiral auxiliary, and (CH₃)₂CHC≡CMgCl as the nucleophile. [b] Relative to ZnMe₂.

The scope of this new alkynylation reaction was briefly examined. The reaction is applicable to other acetylenes such as 5-chloropentyne and 2-methyl-1-buten-3-yne, which gave **8**^[11] and **9**^[12] in high yield and enantioselectivity. The presence of the unprotected amino group in the ketoaniline seems to be important for the efficiency of the reaction. Under similar conditions only 45 % *ee* was obtained with the PMB-protected ketoaniline **2**, and essentially no reaction was observed when the nitrogen center was protected with a bulky group such as trityl. Interestingly, alkynylation of 1-[1-amino-4-(2,2,2-trifluoroacetyl)naphth-2-yl]-2,2,2-trifluoroethan-1-one under the same conditions resulted in exclusive addition at the carbonyl group flanking the aniline moiety and provided **10**^[13] in 91 % yield with 97 % *ee*. This result clearly demonstrates that the presence of an unprotected aniline group adjacent to the carbonyl group in the substrate is important for the reactivity (and probably selectivity).



We have developed a novel, highly efficient, and practical asymmetric alkynylation of the ketoaniline **1**. The reaction has been carried out successfully and reliably on a multi-kilogram scale and is now the cornerstone of the most efficient synthesis of efavirenz^[5] to date. The degree of stereocontrol with a chiral zinc aminoalkoxide is remarkable. The reaction mechanism and extension of the method to other carbonyl compounds are currently under investigation.

Experimental Section

In a typical experiment, THF (240 mL, dried over molecular sieves), 2,2,2-trifluoroethanol^[10] (19.2 g, 0.19 mol), and (1*R*,2*S*)-*N*-pyrrolidinylnorephedrine (59.1 g, 0.29 mol) were mixed under nitrogen. The mixture was cooled to 0 °C, and diethylzinc (1.1M in toluene, 218 mL, 0.24 mol) was added slowly enough to keep the temperature below 30 °C. A solution of chloromagnesium cyclopropylacetylide was prepared by reaction of cyclopropylacetylene (15.9 g, 0.24 mol) and *n*-butylmagnesium chloride (2.0M in THF, 120 mL, 0.24 mol) at 0 °C for 1 h. The solution was then transferred to the zinc reagent by cannula with THF (100 mL) as a wash. The mixture was cooled to 0 °C, and **1** (44.7 g, 0.20 mol) was added. The reaction mixture was quenched with 1M citric acid (400 mL) after 15 h. The two layers were separated. The aqueous layer was saved for recovery of (1*R*,2*S*)-*N*-pyrrolidinylnorephedrine. The organic layer (assay of this solution indicated 99.2 % *ee*^[9]) was washed with water (200 mL) and concentrated to about 180 mL. Toluene (100 mL) was added and the solution was again concentrated to about 180 mL to remove all THF. Heptane (240 mL) was added slowly. The mixture was cooled to 0 °C, and the solid was collected by filtration, washed with heptane (ca. 50 mL), and dried to give 55.2 g (95.3 % yield, 99.2 % *ee*) of analytically pure **4** as a white solid. M.p. 139–141 °C; ¹H NMR (CDCl₃, 300 MHz): δ = 7.52 (d, *J* = 2.4 Hz, 1H), 7.12 (dd, *J* = 2.4, 8.7 Hz, 1H), 6.61 (d, *J* = 8.7 Hz, 1H), 4.70 (s, 1H), 4.39 (s, 2H), 1.39 (m, 1H), 0.85 (m, 4H); ¹³C NMR (CDCl₃, 75.5 MHz): δ = 143.21, 130.44, 130.04, 123.94, 123.93 (q), 121.11, 120.81, 93.51, 74.80 (q), 70.58, 8.59, –0.85; elemental analysis calcd for C₁₅H₁₁NOCIF₃ (%): C 53.80, H 3.77, N 4.72; found: C 53.71, H 3.75, N 4.64.

Received: September 28, 1998 [Z 124621E]
German version: *Angew. Chem.* **1999**, *111*, 724–727

Keywords: alkynylations • amino alcohols • ketones • nucleophilic additions • zinc

- [1] a) R. Noyori, M. Kitamura, *Angew. Chem.* **1991**, *103*, 34–55; *Angew. Chem. Int. Ed. Engl.* **1991**, *30*, 49–69; b) K. Soai, S. Niwa, *Chem. Rev.* **1992**, *92*, 833–856; c) R. O. Duthaler, A. Hafner, *Chem. Rev.* **1992**, *92*, 807–832; d) D. A. Evans, *Science* **1989**, *240*, 420; e) T. Shibata, H. Morioka, T. Hayase, K. Choji, K. Soai, *J. Am. Chem. Soc.* **1996**, *118*, 471–472, and references therein.
- [2] a) T. Mukaiyama, K. Suzuki, K. Soai, T. Sato, *Chem. Lett.* **1979**, 447–448; b) T. Mukaiyama, K. Suzuki, *Chem. Lett.* **1980**, 255–256; c) S. Niwa, K. Soai, *J. Chem. Soc. Perkin Trans. 1* **1990**, 937–943; d) G. M. R. Tombo, E. Didier, B. Loubinoux, *Synlett* **1990**, 547–548; e) M. Ishizaki, O. Hoshino, *Tetrahedron: Asymmetry* **1994**, *5*, 1901–1904.
- [3] E. J. Corey, K. A. Cimprich, *J. Am. Chem. Soc.* **1994**, *116*, 3151–3152.
- [4] a) S. D. Young, S. F. Britcher, L. O. Tran, L. S. Payne, W. C. Lumma, T. A. Lyle, J. R. Huff, P. S. Anderson, D. B. Olsen, S. S. Carrol, D. J. Pettibone, J. A. O'Brien, R. G. Ball, S. K. Balani, J. H. Lin, I.-W. Chen, W. A. Schleif, V. V. Sardana, W. J. Long, V. W. Byrnes, E. A. Emini, *Antimicrob. Agents Chemother.* **1995**, *39*, 2602; b) D. Mayers, S. Riddler, M. Bach, D. Stein, M. D. Havlir, J. Kahn, N. Ruiz, D. F. Labriola, and the DMP-266 clinical development team, Clinical data presented at the ICAAC meeting (Toronto) **1997**, 1-175, Durable Clinical Anti-HIV-1 Activity and Tolerability for DMP-266 in Combination with Indinavir (IDV) at 24 Weeks.
- [5] A. S. Thompson, E. G. Corley, M. F. Huntington, E. J. J. Grabowski, *Tetrahedron Lett.* **1995**, *36*, 8937–8940.
- [6] a) A. S. Thompson, E. G. Corley, M. F. Huntington, E. J. J. Grabowski, J. F. Remenar, D. B. Collum, *J. Am. Chem. Soc.* **1998**, *120*, 2028–2038; b) Feng Xu (Merck), personal communication.
- [7] D. Zhao, C.-Y. Chen, F. Xu, L. Tan, R. D. Tillyer, M. E. Pierce, J. R. Moore, *Org. Synth.*, submitted.
- [8] a) A similar species has been reported: D. Enders, J. Zhu, G. Raabe, *Angew. Chem.* **1996**, *108*, 1827; *Angew. Chem. Int. Ed. Engl.* **1996**, *35*, 1725–1728; b) Preliminary ¹H and ¹³C NMR studies of the solution showed a very complicated system. The observed chiral amplification supported the formation of dimer or higher order aggregates: the enantiomeric excess of the product was 97.5, 94.4, and 79.6%, respectively, when (1*R*,2*S*)-*N*-pyrrolidinylnorephedrine with 100, 80, and 50% *ee* was used for the reaction at room temperature.
- [9] The enantiomeric excess was determined by HPLC assay on a chiralcel-AD column (hexane/isopropyl alcohol, 3/1)
- [10] Trifluoroethanol is preferred to neopentyl alcohol because it gives a faster reaction.
- [11] ¹H NMR (CDCl₃, 300 MHz): δ = 7.53 (d, *J* = 2.4 Hz, 1H), 7.12 (dd, *J* = 2.4, 8.7 Hz, 1H), 6.62 (d, *J* = 8.7 Hz, 1H), 4.68 (brs, 3H), 3.69 (m, 2H), 2.57 (m, 2H), and 2.06 (m, 2H); ¹³C NMR (CDCl₃, 75.5 MHz): δ = 143.18, 130.37, 130.28, 130.21, 125.60(q), 122.16, 121.09, 88.49, 76.65 (q), 74.74, 43.42, 30.62, 16.18; elemental analysis calcd for C₁₃H₁₂NOCIF₃ (%): C 47.88, H 3.71, N 4.29; found: C 48.14, H 3.39, N 4.15.
- [12] ¹H NMR (CD₃CN, 300 MHz): δ = 7.47 (d, *J* = 2.4 Hz, 1H), 7.11 (dd, *J* = 2.4, 8.7 Hz, 1H), 6.66 (d, *J* = 8.7 Hz, 1H), 5.48 (m, 2H), 5.00 (brs, 3H), 1.95 (m, 3H); ¹³C NMR (CD₃CN, 75.5 MHz): δ = 147.19, 131.09, 130.39, 126.32, 125.54, 125.40(q), 121.27, 120.04, 119.06, 90.75, 84.02, 75.08 (q), 22.94; elemental analysis calcd for C₁₃H₁₁NOCIF₃ (%): C 53.80, H 3.77, N 4.72; found: C 53.67, H 3.80, N 4.67.
- [13] ¹H NMR (CD₃CN, 400 MHz): δ = 9.29 (d, *J* = 9.2 Hz, 1H), 8.60 (brs, 1H), 7.85 (d, *J* = 8.7 Hz, 1H), 7.69 (dd, *J* = 9.0, 9.2 Hz, 1H), 7.59 (dd, *J* = 8.7, 9.0 Hz, 1H), 6.35 (brs, 2H), 3.40 (brs, 1H), 1.41 (m, 1H), 0.90 (m, 4H); ¹³C NMR (CDCl₃, 100.6 MHz): δ = 179.0 (q), 150.4, 138.9, 133.5, 130.5, 126.5, 126.4, 125.3 (q), 123.2, 122.5 (q), 120.8, 113.5, 108.3, 95.4, 76.5 (q), 70.1, 8.5, 8.4, –0.8; elemental analysis calcd for C₁₉H₁₃F₆NO₂ (%): C 56.87, H 3.27, N 3.49; found: C 56.99, H 2.98, N 3.42.

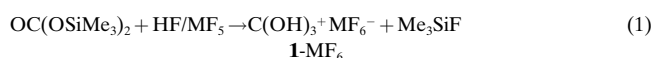
Trihydroxycarbenium Hexafluorometalates: Salts of Protonated Carbonic Acid

Rolf Minkwitz* and Stefan Schneider

Dedicated to Professor Wolfgang Sawdony on the occasion of his 65th birthday

The work of G. A. Olah on the feasibility of protonation of extremely weak bases has stimulated interest in this area of research, as highlighted recently by T. S. Sorensen.^[1]

The trihydroxycarbenium ion, $\text{C}(\text{OH})_3^+$ (**1**), which is isoelectronic with orthoboric acid, was up to now only confirmed by NMR spectroscopy as a compound of the reaction mixture of the protonation of carbonates or hydrogen carbonates with the superacid $\text{FSO}_3\text{H}/\text{SbF}_5$.^[2] Since carbonic acid is not available as a reactant,^[3, 4] we used, as for the synthesis of protonated hydrogen peroxide,^[5] carbonic acid bis(trimethylsilyl) ester for the reaction with the superacids HF/MF_5 ($\text{M} = \text{As}, \text{Sb}$) according to Equation (1).



The NMR spectra (in HF at -60°C : $\delta(^1\text{H}) = 11.7$, $\delta(^{13}\text{C}) = 166.8$)^[2, 7] confirm that the trimethylsilyl groups are removed leading to the formation of compound **1**. Whereas the $\text{HSO}_3\text{F}/\text{SbF}_5$ system contains no readily volatile components, in this case the excess HF, which also serves as solvent, as well as the Me_3SiF which is formed in the reaction can be removed at -78°C under vacuum. The moisture-sensitive salts decompose quantitatively into CO_2 and $\text{H}_3\text{O}^+ \text{MF}_6^-$ above -16°C in the case of **1**- AsF_6 and above -4°C in the case of **1**- SbF_6 . The decomposition proceeds by removal of water from **1**. This

requires a 1,3 proton shift, for which a remarkable energy barrier of 238 kJ mol^{-1} was calculated.^[8] The surprising stability of the trihydroxycarbenium ions was already explained by resonance stabilization via onium ions.^[2]

The vibrational spectra of the salts of **1** are congruent with the spectra of the isoelectronic boric acid (Table 1, Figure 1).^[9] In the Raman spectra, unlike in the IR spectra, the vibrations of the cations can only be observed at very low intensities. By assuming C_{3h} symmetry for **1** all vibrational frequencies can be

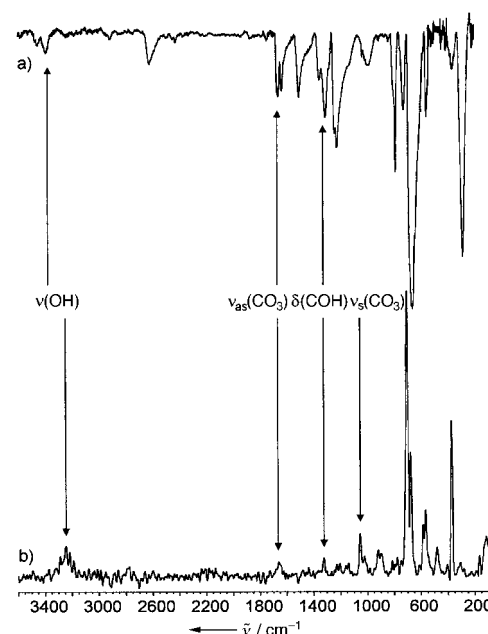


Figure 1. a) IR spectrum of **1**- SbF_6 (-40°C) and b) Raman spectrum of **1**- AsF_6 (-70°C) of the solid compounds.

Table 1. Vibrational frequencies [cm^{-1}] of $\text{C}(\text{OX})_3^+$ ($\text{X} = \text{H}, \text{D}$) and assignment.^[a]

$\text{B}(\text{OX})_3^{[11]}$		$\text{C}(\text{OH})_3^+$		$\text{C}(\text{OD})_3^+$		Assignment	
$\text{X} = \text{H}$	$\text{X} = \text{D}$	SbF_6^-	AsF_6^-	SbF_6^-	AsF_6^-	$(\text{X} = \text{H}, \text{D})$	
		Raman	IR	Raman	IR	Raman	IR
3245	2434		3457 vw		3409 b		2496 m
3220	2400		3390 vw				2486 w
3168	2377	n.o.		3254 wb			
1440	1415		1663 w	1661 vw	1661 w		1633 w
1365	1225		1635 w		1629 w		1611 w
1185	910		1352 w	1330 vw	1349 w		1199 w
1163	1013	1310 vw	1307 w		1309 w		1182 w
1077	835	1232 vw	1238 w	1235 vw			1258 vw
878	832	1055 m		1056 m			1197 w
818	650		1037 vw	1028 w	1035 vw		1138 w
808	560		989 wb		991 wb		1065 m
625	665		804 w				1032 vw
538	510		786 m	787 vw	785 m		1035 vw
498	460	721 m	728 w				982 w
		650 vs		698 vs			928 w
			661 vs		704 vs		987 w
		570 m		573 m			801 w
			283 s		380 s		790 m
		285 s		374 s			724 w
							722 w
							656 vs
							665 vs
							698 vs
							567 m
							389 s
							293 m
							374 s

[a] Vibrations of the anions are not listed; vw: very weak, w: weak, m: medium, s: strong, vs: very strong, b: broad, sh: shoulder, n.o.: not observed.

[*] Prof. Dr. R. Minkwitz, Dipl.-Chem. S. Schneider
 Fachbereich Chemie der Universität
 D-44221 Dortmund (Germany)
 Fax: (+49) 231-755-3797
 E-mail: Minkwitz@citrin.chemie.uni-dortmund.de

assigned in analogy to those of the boric acid; however, owing to the positive charge of **1** the vibrational frequencies are shifted on average by 200 cm^{-1} to higher wavenumbers, in comparison to those of boric acid. The symmetric C–O

stretching vibration, characteristic for ion **1**, is observed in the region between 1055 and 1065 cm^{-1} . According to the vibrational spectra, no reduction in the symmetry of the octahedral hexafluorometalate anions is found; three Raman-active and two IR-active vibrations can be assigned in accordance with O_h symmetry.

The spectroscopic studies of the salts of **1** were complemented by the single-crystal X-ray structure investigation of **1-AsF₆** (Table 2).^[10] The cation **1** shows C_3 symmetry in the solid. The C–O bond lengths of 123.1(4) pm are comparable

Table 2. Selected bond lengths [pm] and angles [°] of **1-AsF₆**.

As(1)–F(2)	168.2(3)	F(2d)–As(1)–F(2)	91.7(2)
As(1)–F(1)	171.6(3)	F(2)–As(1)–F(1)	89.6(2)
C(1)–O(1)	123.1(4)	F(2c)–As(1)–F(1)	177.6(2)
O(1)–H(1)	88.7	O(1a)–C(1)–O(1)	119.9(1)
O...F	273.7(4)	C(1)–O(1)–H(1)	108.6

with those found in the structure of protonated formic acid (125.5(5) and 123.9(6) pm).^[11] In contrast in neutral formic acid the C–O double bond is 122.2(2) pm and the C–O single bond is 130.8(2) pm.^[12] This leads to the conclusion that the bond order of the C–O bonds in **1** is 1.5, and the positive charge is delocalized over the whole cation. Short interionic contacts (273.7(6) pm) to fluorine atoms of three adjacent anions are made through the oxygen atoms (Figure 2). The hydrogen atoms are also localized along these O...F axes. These contacts between cations and anions lead to the formation of a three-dimensional network (Figure 3).

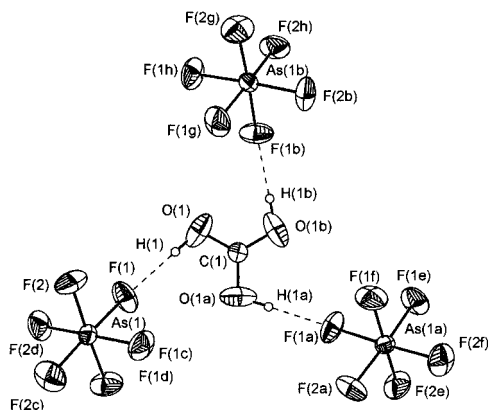


Figure 2. Structure of **1-AsF₆** in the crystal with interionic contacts and atom labels.

Experimental Section

(Me₃SiO)₂CO was prepared according to reference [6]. AsF₅ was prepared by reaction of the elements and was condensed fractionally, SbF₅ was distilled fractionally, and HF and DF were dried with fluorine.

In a KEL-F reactor^[13] MF₅ (3 mmol; M = As, Sb) was dissolved in HF/DF (5 g). After the solution had been frozen, MF₅ (3 mmol; M = As, Sb) was added at –196 °C under an inert atmosphere (N₂). The reaction mixture was slowly allowed to warm to –60 °C. Subsequently the volatile compounds (HF/DF/Me₃SiF) were removed at –60 °C under dynamic vacuum. C(OX)₃⁺MF₆[–] (X = H, D; M = As, Sb) remained as a colorless solid.

Alternatively NaOCO₂SiMe₃ was used as the starting material. Under identical conditions the reaction mixture was kept at –78 °C for 12 h. The alkali metal hexafluorometalates accumulate at the bottom of the reactor. After removal of the volatile components, crystalline **1-AsF₆** formed on the walls of the vessel.

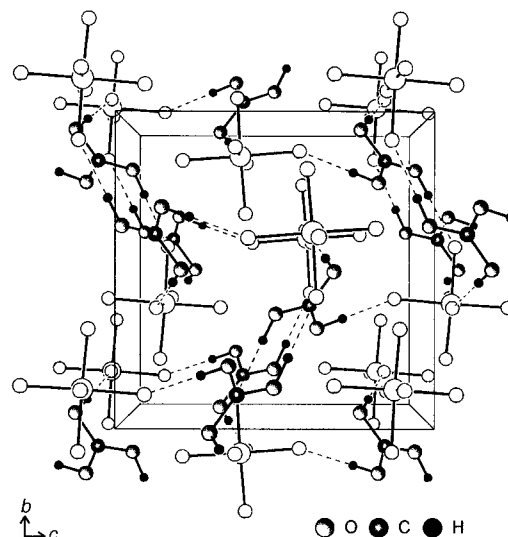


Figure 3. Section of the crystal packing of **1-AsF₆**.

Equipment: Raman: Bruker FT-Spektrometer IF66 with Raman accessory, FRA 106 Neodym-YAG-laser ($\lambda = 1064 \text{ nm}$); IR: Bruker IFS 113v; NMR: Bruker DPX300; X-ray diffractometer, Nonius-Kappa CCD (1152 × 1242 pixel).

Received: September 11, 1998 [Z 12403 IE]

German version: *Angew. Chem.* **1999**, *111*, 752–754

Keywords: carbenium ions • carbonic acid • vibrational spectroscopy • superacidic systems • trihydroxycarbenium salts

- [1] T. S. Sorensen, *Angew. Chem.* **1998**, *110*, 623–624; *Angew. Chem. Int. Ed.* **1998**, *37*, 603–604.
- [2] G. A. Olah, A. M. White, *J. Am. Chem. Soc.* **1968**, *90*, 1884–1889.
- [3] A. G. Galinos, A. A. Carotti, *J. Am. Chem. Soc.* **1961**, *83*, 752.
- [4] G. Gattow, U. Gerwarth, *Angew. Chem.* **1965**, *77*, 132–133; *Angew. Chem. Int. Ed. Engl.* **1965**, *4*, 149–150.
- [5] R. Minkwitz, H. Hartl, C. Hirsch, *Angew. Chem.* **1998**, *110*, 1776–1779; *Angew. Chem. Int. Ed.* **1998**, *37*, 1681–1684.
- [6] R. Minkwitz, S. Schneider, *Z. Naturforsch. B* **1998**, *53*, 849–852.
- [7] G. Rasul, V. P. Reddy, L. Z. Zdunek, G. K. S. Prakash, G. A. Olah, *J. Am. Chem. Soc.* **1993**, *115*, 2236–2238.
- [8] H. Egsgaard, L. Carlseb, *J. Chem. Soc. Faraday Trans. 1* **1989**, *85*, 3403–3411.
- [9] J. R. Durig, W. H. Green, A. L. Marston, *J. Mol. Spectr.* **1968**, *2*, 19–37.
- [10] Crystal structure investigation of **1-AsF₆**: crystals obtained from HF, cubic, space group $P2_13$ (no. 198), $a = 860.0(1) \text{ pm}$, $Z = 4$, $V = 636.0(1) \times 10^6 \text{ pm}^3$; $\rho_{\text{calc}} = 2.631 \text{ g cm}^{-3}$, crystal dimensions $0.18 \times 0.18 \times 0.18 \text{ mm}^3$, $\text{MoK}\alpha$ radiation ($\lambda = 71.069 \text{ pm}$), $2\theta/\omega$ scans, $2\theta_{\text{max}} = 51.0^\circ$, $T = 173(2) \text{ K}$; 3410 measured reflections, 384 independent reflections, σ -limit 2.0; $\mu(\text{MoK}\alpha) = 5.433 \text{ mm}^{-1}$, structure solution: Patterson, difference Fourier synthesis; SHELXS-86, SHELXL-93, PARST, PLATON, MISSYM, DENZO, SCALEPACK, 35 free parameters, hydrogen atoms not determined from ΔF , $R = 0.0283$, $wR = 0.0659$, $R = \Sigma ||F_o| - |F_c|| / \Sigma |F_o|$, refinement method: full-matrix least-squares fit against F^2 , min./max. residual electron density = $-0.332/0.343 \text{ e } \text{\AA}^{-3}$. Further details of the crystal structure investigation can be obtained from the Fachinformationszentrum Karlsruhe, D-76344 Eggenstein-Leopoldshafen, Germany (fax: (+49) 7247-808-666; e-mail: crysdata@fiz-karlsruhe.de), on quoting the depositary number CSD-410089.
- [11] R. Minkwitz, H. Hartl, S. Schneider, M. Seifert, *Z. Anorg. Allg. Chem.* **1996**, *622*, 1404–1410.
- [12] I. Nahringerbauer, *Acta Crystallogr. Sect. B* **1978**, *34*, 315–318.
- [13] A. Werner, Thesis, Universität Dortmund **1988**.